Background Papers—
Suramin, the Cell Danger Response, Autism Spectrum Disorder, Chronic Fatigue Syndrome, ALS, Epigenetics, Purinergic Signaling, and Healing

Robert K. Naviaux, MD, PhD
Professor of Medicine, Pediatrics, Pathology, and Genetics
University of California, San Diego School of Medicine
IRB Project #150134, IND #118212
Email: rnaviaux@health.ucsd.edu
2020

A new disorder of purine metabolism with behavioral manifestations

Hyperuricemia has been observed in a 3-year-old boy with mental retardation, dysplastic teeth, failure to cry with tears, absence of speech, and unusual, autistic behavior. Increased synthesis of purines de novo was documented by a rate of conversion of glycine to uric acid that was seven times that of control. The activity of the enzyme hypoxanthine guanine phosphoribosyl transferase was normal, while that of adenine phosphoribosyl transferase was increased. These observations are interpreted to reflect a distinct disease productive of hyperuricemia very early in life.

William L. Nyhan, M.D., Ph.D., John A. James, M.D., Annabel J. Teberg, M.D., Lawrence Sweetman, B.S., and Leslie G. Nelson, M.D.

MIAMI, FLA., AND LOS ANGELES, CALIF.

A DISORDER OF purine metabolism has recently been reported[1, 2] in which overproduction of uric acid has accompanied a severe disturbance in cerebral function. Involved patients have had mental retardation, athetoid cerebral palsy, and aggressive, self-mutilating behavior. The disease is transmitted as an X-linked recessive trait.[3] Activity of the enzyme, hypoxanthine guanine phosphoribosyl transferase, has been found to be absent in this condition,[4] and this enzyme defect has been thought to be responsible for the disordered purine metabolism observed.

We have recently studied a boy in whom hyperuricemia was documented early in infancy. He lacked most of the features of the children studied previously but had mild developmental retardation, dysplastic teeth, and absence of tears when he cried. He was found to have marked overproduction of uric acid. The activity of hypoxanthine guanine phosphoribosyl transferase in his erythrocytes was normal. The findings in this patient appear to represent an inborn error of purine metabolism responsible for hyperuricemia in childhood distinct from

From Departments of Pediatrics and Biochemistry, University of Miami School of Medicine, and the Department of Pediatrics, University of Southern California School of Medicine and the Los Angeles County–University of Southern California Medical Center.

This investigation was supported by United States Public Health Service Research Grants No. HD 02609 from the National Institute of Child Health and Human Development and No. FR 00261 from the General Clinical Research Centers Branch, Division of Research Facilities and Resources, National Institutes of Health, and by Public Health Service Training Grant No. T1 HD 76 from the National Institute of Child Health and Human Development, National Institutes of Health.

those in which hypoxanthine guanine phosphoribosyl transferase is abnormal.

CASE REPORT

S. M. was born after an uneventful 36 week gestation. The delivery, labor, and neonatal course were unremarkable. The birth weight was 5 pounds, 8 ounces; the length was 20¾ inches. A glandular hypospadias was present. The infant fed poorly and gained weight slowly during the first 3 months.

First admission. When the patient was 2 months old, it was noted that his urine was persistently pink. He was admitted to the hospital at the age of 4 months for investigation of hematuria and correction of hypospadias. Physical examination revealed an irritable, rather poorly nourished infant, weighing 10 pounds, 10 ounces. The liver and spleen were palpable 3.5 cm. below the costal margins. The developmental progress was considered slow for a 4-month-old infant; he had head lag, general irritability, and muscular hypertonicity. Roentgenograms of the skull, chest, and extremities revealed no abnormalities, nor did an intravenous pyelogram and a voiding cystogram. Electroencephalography revealed generalized slowing with spindle activity over the right hemisphere.

The hemoglobin was 14.5 Gm. per 100 ml. The urine contained a trace of protein, 30 to 35 red cells per high-power field, and many crystals with the appearance of uric acid. The bone marrow was normal. The bladder was normal in tone and capacity, but full of golden-yellow crystals. A first-stage hypospadias repair was carried out and an indwelling Foley catheter inserted. The concentration of uric acid in the serum on the day after the operation was 23.5 mg. per 100 ml. After cystoscopy, the fever rose to 102° F.; 200 mg. of tetracycline was given daily for 19 days.

After the baby had been discharged from the hospital, intermittent hematuria and crystalluria persisted. Sodium bicarbonate was given (3 mEq. per kilogram per day). Weight gain remained slow.

Second admission. The patient was readmitted for evaluation at 8 months of age. At this time the weight was 15 pounds, 10 ounces; the length was 26 inches. There were 2 maxillary and 6 mandibular teeth; the latter were small and dysplastic. The liver was palpable 1 cm. below the right costal margin; the spleen was not palpable. The concentration of uric acid in the serum ranged from 8.5 to 11.4 mg. per 100 ml. It decreased to a range of 5.4 to 6.2 mg. per 100 ml. during treatment with probenecid in a dose of 270 mg. daily for 3 days. Uric acid excretion increased from a mean of 43 mg. per kilogram to 69 mg. per kilogram during this period. The patient was discharged without treatment.

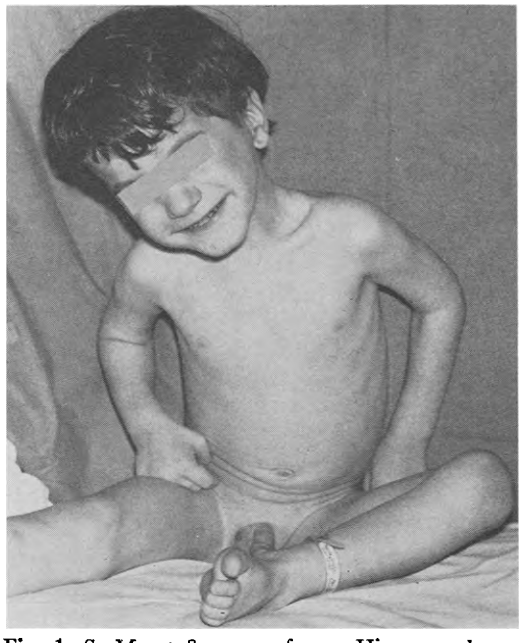

Fig. 1. S. M. at 3 years of age. His general appearance and characteristic odd grin are illustrated.

Third admission. The baby was readmitted for study at the age of 16 months (Fig. 1). In the interim he had continued to pass blood and crystals intermittently in the urine. It was noted by his foster mother that he never shed tears when he cried. Erupting teeth had continued to be hypoplastic and had a yellow discoloration which appeared fluorescent under ultraviolet illumination. The concentration of uric acid in the plasma was 11.6 mg. per 100 ml. The cerebrospinal fluid concentration of uric acid was 0.14 mg. per 100 ml. Treatment was begun with 50 mg. of allopurinol* twice daily.

The subsequent clinical course has been relatively uneventful. The dose of allopurinol was lowered to 50 mg. a day until the boy was 3½ years old, after which the serum concentration of uric acid increased and the dose was raised to

*Allopurinol (Zyloprim) was obtained through the courtesy of Drs. George Hitchings and Stanley Bloomfield of Burroughs-Wellcome and Co., Tuckahoe, N. Y.

100 mg. daily. No toxic effects of the drug have been observed. He still has no tears when he cries. Intradermal injection of 0.3 ml. of 1:1000 histamine resulted in a wheal and flare. Methacholine, 2.5 per cent instilled into the conjunctival sac, did not result in pupillary constriction. Normal numbers of fungiform papillae were present over the tip of the tongue. Sweat chloride concentration was 28 mEq. per liter. Growth has been steady along the third percentile for both height and weight. At the time of report at 3 years and 7 months, he was 37½ inches tall and weighed 28 pounds.

Family history. The mother was a 21-year-old unmarried Caucasian primigravida. Both the mother and father were in good health. Nothing is known of their previous medical or family history.

Developmental evaluations. At 8 months of age, the baby was alert and responsive, and he performed within the lower limits of normal when allowance was made for his gestational age. He had smiled at 6 weeks, cooed at 8 to 9 weeks, and reached for and grasped objects at 6 months. He had been placed at 5 days of age with a foster mother, who seemed genuinely interested in his well-being. There were no other children in the home. There was generalized muscular hypotonia (in contrast to the hypertonia noted at 4 months of age), but no evidence of neurologic abnormality.

At 16½ months of age, he appeared frail, irritable, and mildly apprehensive. His performance seemed mechanical and his manner apathetic. No language was noted; the nurses reported that he would say "mama" and "dada," but these sounds were not felt to be specific words. He was generally hypotonic. His developmental quotient (D. Q.) was estimated at 70 to 75.

By 2½ years of age, his foster home situation had been changed, and he had been in a family with 3 natural children for a year. The social worker felt this to be a good placement. At this time, his behavior seemed very disturbed and autistic. He seemed totally oblivious to people around him. He hummed and growled as he manipulated toys, making no contact with the examiner. He had no understandable speech but had a D. Q. of 60 to 65 when all language items were excluded.

At 34 months of age, his performance was characterized by wide and inappropriate mood swings—from giddy behavior to inconsolable frustration. He was able to relate to persons in his environment. Language consisted of growling and humming.

At 42 months, his over-all behavior and performance remained much the same. When frustrated, he was noted to pick at his eyes and cheeks and to tear up laundry. He was in a new foster home with a placid, kindly appearing woman who attempted to frustrate him as little as possible. He still had no speech but followed simple directions. His developmental level remained at 60 to 65.

MATERIALS AND METHODS

Metabolic studies were carried out in the Clinical Research Center of the Los Angeles County–University of Southern California Medical Center. During this period the patient was fed a diet virtually free of exogenous purine.[1] Methods employed for the assay of uric acid and the other oxypurines and for the incorporation of ^{14}C-labeled glycine into uric acid have been described previously.[1, 5] The method for hypoxanthine guanine phosphoribosyl transferase and that for adenine phosphoribosyl transferase were modifications of the method described by Flaks,[6] which will be published elsewhere.

RESULTS

Concentrations of uric acid in the plasma and its excretion in the urine. Increased concentrations of uric acid in the plasma were documented repeatedly from the age of 6 weeks. Values obtained at the age of 16 months during a period of rigid restric-

Table I. Uric acid in the plasma and urine

	Urine			
		Uric acid		
Day	*Creatinine (mg./24 hr.)*	*Mg./24 hr.*	*Mg./mg. creatinine*	*Plasma uric acid (mg./100 ml.)*
1	34	112	3.26	
2	31	85	2.79	11.6
3	79	210	2.68	
4	108	254	2.36	
5	127	233	1.84	
6	52	125	2.39	
7	69	205	2.97	9.6
8	37	112	3.03	
9	52	147	2.82	9.5

tion of purine intake varied from 9.5 to 11.6 mg. per 100 ml. (Table I). The excretion of uric acid in the urine was also markedly increased. Variations encountered in the total amounts of uric acid in the urine were interpreted to reflect variation in the completeness of 24 hour collections, because the urine volume and excretion of creatinine varied concomitantly. There was much less variation in the uric acid/creatinine ratio. The 24 hour uric acid excretion appeared to approximate 200 mg. per 24 hr. The patient weighed 9 kilograms at the time of the study. The mean excretion of uric acid during days of complete collection was 25 mg. per kilogram of body weight. The mean uric acid/creatinine ratio for the 9 days of study was 2.75. These values are similar to those of patients with the syndrome previously described.[1-3] They are considerably larger than those of controls, who seldom exceed 10 mg. per kilogram per 24 hr. or 1.0 mg. per milligram of creatinine.[1]

Conversion of ^{14}C-labeled glycine to uric acid. The synthesis of purine *de novo* was studied by the injection of 2 μc per kilogram of glycine-U-^{14}C on the third day of the study (illustrated in Table I). The specific activities of the uric acid isolated from the urine are shown in Fig. 2. The shape of the curve indicates the very rapid conversion of glycine to uric acid with a peak in the first 12 hours after injection. This was earlier than in patients with the self-destructive syndrome previously studied, in whom peak specific activities were found in the second 24 hours; distinct peaks were not obtained in controls.[1] Peak specific activities were similar to those of hyperuricemic children studied previously.

The cumulative percentage of the isotope of administered glycine that was recovered as uric acid is illustrated in Fig. 3. In the patient this value approximated 0.7 per cent in the studied 7 day period. In contrast, those of controls approximated 0.1 per cent. These observations clearly indicate an overproduction of purine.

The effect of allopurinol. The response to administration of 100 mg. of allopurinol a day is shown in Fig. 4. The excretion of uric acid in the urine fell within the first 24 hours of treatment to 0.52 mg. per milligram of creatinine, and was maintained in this range. The concentration of uric acid in the plasma varied from 2.4 to 3.1 mg. per 100 ml.

The patient has been treated with allopurinol for the past 2$\frac{4}{12}$ years. During most

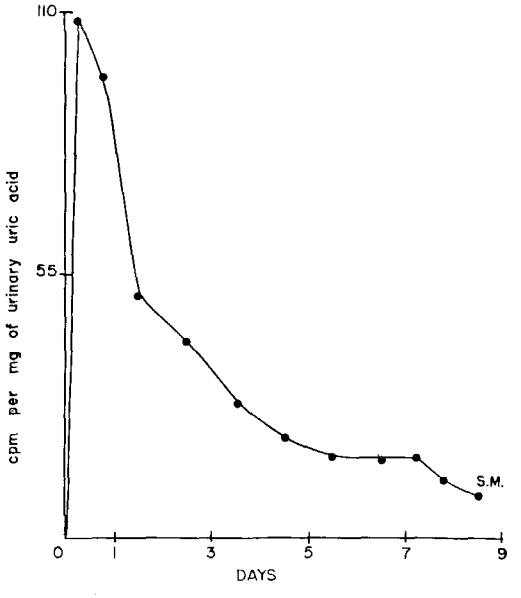

Fig. 2. Specific activities of urinary uric acid following the injection of glycine-U-^{14}C.

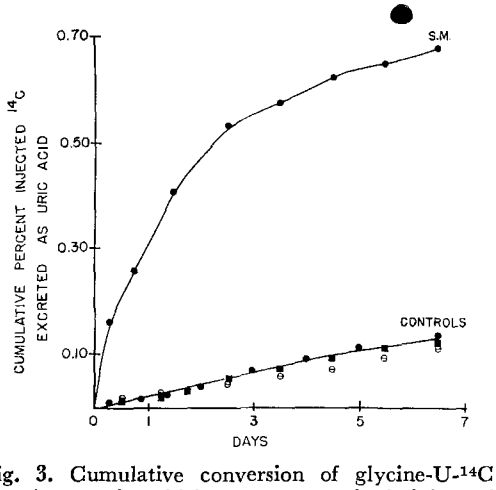

Fig. 3. Cumulative conversion of glycine-U-^{14}C to urinary uric acid in percentage of administered dose. Control children were those previously reported upon.[1]

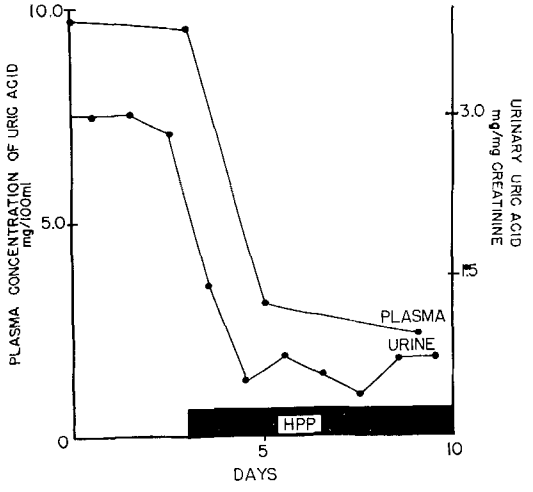

Fig. 4. Effect of allopurinol on the concentration of uric acid in the plasma and on the excretion of uric acid in the urine. The abbreviation HPP is employed for allopurinol (4-hydroxypyrazolo-[3,4-*d*]-pyrimidine).

of this period he has been given 50 mg. a day. Plasma concentrations have been maintained between 3.9 and 7.5 mg. per 100 ml., and usually within the range of 5.5 to 6.0 mg. per 100 ml.

The influence of the drug on the excretion of xanthine and hypoxanthine is indicated in Table II. The total quantities of purine excreted as xanthine, hypoxanthine, and uric acid were relatively constant in the absence of treatment, amounting to over 3 mg. per milligram of creatinine excreted. Most of this was excreted as uric acid. The administration of allopurinol increased the amounts of the other oxypurines in the urine while decreasing the amounts of uric acid; however, the total amounts of oxypurines excreted after treatment were definitely decreased.

The data in Table II were obtained by the enzymatic method, which gives the sum of xanthine and hypoxanthine as milligrams of uric acid formed in the presence of xanthine oxidase and subsequently assayed spectrophotometrically with uricase. The purine from samples 9 and 17 were also separated by cation exchange chromatography and assayed individually. In the absence of treatment, the patient excreted 4.9 mg. of hypoxanthine and 1.9 mg. of xanthine. With treatment, he excreted 16.2 mg. of hypoxanthine and 52.8 mg. of xanthine. Expressed as milligrams of uric acid for comparison with the data of Table II, the total of xanthine plus hypoxanthine was 8.1 mg. before treatment and 78.3 mg. after, demonstrating close agreement between the values obtained by the two different methods. The molar ratio of hypoxanthine to xanthine was 2.9 in the control state and 0.34 in the presence of 100 mg. per day of allopurinol.

Enzyme activity. Assays of the activity of enzymes in erythrocytes which form nucleotides from free purines are indicated in Table III. One enzyme catalyzes the reaction of 5-phosphoribosyl-1-pyrophosphate with hypoxanthine or guanine to yield inosinic acid or guanylic acid (E.C. 2-4-2-8). A separate enzyme catalyzes the formation of adenylic acid from adenine and 5-phosphoribosyl-1-pyrophosphate (E.C. 2-4-2-7). Hypoxanthine guanine phosphoribosyltransferase, the former enzyme, was tested with both substrates. In the human erythrocyte, the activity of this enzyme with guanine was considerably greater than with hypoxanthine. Heat stability of this enzyme was tested in patient S. M. and in a control (L. S.) by carrying out the reaction at 37° C. as well as at 60° C., and by preheating the enzyme preparation for 5 minutes at 80° C. before assaying for enzyme activity at 60° C. No differences were found between patient and control.

The activity of adenine phosphoribosyl transferase is increased to approximately 170 per cent in patients with defective hypoxanthine guanine phosphoribosyl transferase activity. The activity of this enzyme was found to be increased to the same degree in patient S. M.

DISCUSSION

Hyperuricemia is an essential feature of gout. If present over a number of years, it leads to acute attacks of arthritis, tophaceous deposits, and nephropathy. Patients who ex-

Table II. Effect of allopurinol on the excretion of oxypurines*

Sample No.	*Allopurinol (mg./day)*	*Xanthine plus hypoxanthine (mg./24 hr.)*	*Uric acid (mg./24 hr.)*	*Creatinine (mg./24 hr.)*	*Total oxypurines (mg./mg. creatinine)*
8	0	12.3	204.5	68.9	3.15
9	0	7.6	111.5	36.8	3.24
16	100	40.7	19.5	53.0	1.14
17	100	76.8	30.7	41.7	2.58

*The oxypurines hypoxanthine plus xanthine are expressed in milligrams of uric acid equivalents, which permits summation of the total oxypurines in the presence and absence of allopurinol.

Table III. Phosphoribosyl transferase activity in erythrocytes

	Phosphoribosyl transferase activity (d.p.m./μl packed RBC)		
*Subject**	*Hypoxanthine*	*Guanine*	*Adenine*
Patient S. M.	24,642	64,764	26,144
Control G. A.	23,592	69,680	15,502
Control L. S.	26,364	70,266	15,332
Patient R. S.	0	32	26,977

*S. M. was the subject of this report. R. S. was a patient with hyperuricemia and cerebral dysfunction previously reported.[2] In each instance, the reaction was run for 20 minutes at 60° C. The concentration of each substrate tested was 1.8×10^{-4}M, containing 0.4 μc, or 888,000 d.p.m., of ^{14}C.

crete large amounts of urate in the urine are particularly likely to have hematuria, crystalluria, urinary tract stones, and infections, as well as renal damage due to deposits of urate in the kidneys. Hyperuricemia or gout occurring in childhood has been reported infrequently. A review of the literature from 1823 to 1964[1] yielded only 15 patients younger than 10 years of age. On the other hand, the description of the disorder of uric acid metabolism in which patients also have cerebral dysfunction and self-mutilating behavior[1] led to the recognition of a relatively large number of hyperuricemic children in a short period of time. We now have information on over 70 of these patients and have studied 21 in some detail. The observation that such patients have a defect in hypoxanthine guanine phosphoribosyl transferase[4] now makes it possible to distinguish among hyperuricemic patients those with and without a defect in that enzyme.

The patient described in this report differs in a number of respects from those studied previously and is felt to represent a distinct disease which causes hyperuricemia very early in life. Clinical characteristics include below-average growth in length and weight, dysplastic teeth, failure to produce tears with crying, and mild mental retardation. In the absence of similar cases, it is not possible to decide whether or not these clinical characteristics are related to the metabolic abnormality. Fluorescent staining was noted on the teeth, but the dysplasia of the teeth appeared out of proportion to that seen with tetracycline and the period of known tetracycline administration was not consistent with the abnormalities seen. Undocumented tetracycline administration during pregnancy is of course possible, but there was no history that was even suggestive of this possibility. The association between abnormal behavior and abnormal purine metabolism in hypoxanthine guanine phosphoribosyl transferase deficiency suggests the possibility that the unusual behavior observed in this patient may also be related to a metabolic abnormality. His behavior has not been unusually aggressive. He has appeared autistic and at almost 4 years of age has still had no speech. These features could, of course, be related to his environment, but they have not been observed in others in the same homes and they are certainly out of proportion to his degree of retardation. Failure to produce tears may occur with absence of or infiltration in the lacrimal glands or with lesions of the facial nerve. However, the eyes were normally moist. These features are virtually pathog-

nomonic of dysautonomia. However, such patients, unlike ours, have a marked miotic response to conjunctival methacholine, an absent flare response to intradermal histamine, and absence of visible fungiform papillae.

The amounts of uric acid produced in this patient appeared to be somewhat less than those observed previously in hyperuricemic children. Plasma concentrations were the same. Urinary excretion of uric acid is greater in younger than older children, whether expressed per kilogram of body weight or per milligram of creatinine excreted.[7] Excretion of urate in the patient at a level of 25 mg. per kilogram per day is about twice that found in controls but less than the 45 mg. per kilogram per day[1] or 58 mg. per kilogram per day[2] reported in somewhat older hyperuricemic children with self mutilation. Similarly, studies of the cumulative formation of uric acid from ^{14}C-glycine documented an overproduction of purine that was 7 times the rates observed in controls but about a third of the rates found in the previously studied group of children.[1-3] These findings indicate the presence of a different metabolic defect and that is consistent with the results of enzyme assay.

The excretion of xanthine and hypoxanthine also revealed some distinctive features. In the untreated state there was more hypoxanthine than xanthine in the urine; a molar ratio of hypoxanthine/xanthine of 2.9 is similar to that found in other hyperuricemic children.[5] Ratios of less than 1.0 found in control children and adults with gout have suggested the possibility that under ordinary conditions xanthine which is formed from sources other than hypoxanthine, such as guanine or xanthylic acid, is the major precursor of urinary urate. Allopurinol reduces this ratio in all patients. However, the magnitude of reduction in this patient to 0.34 reflected a pattern of urinary oxypurines similar to allopurinol-treated controls, whereas the ratio seldom decreased below 1.0 in hyperuricemic children.[5]

The effect of allopurinol on the total excretion of oxypurines is a significant decrease in most individuals with or without gout.[5, 8, 9] However, in patients with deficient activity of hypoxanthine guanine phosphoribosyl transferase, total excretion of oxypurine does not fall after allopurinol.[5, 9] The most likely explanation of these data is that, in the presence of normal activity of the enzyme, hypoxanthine is readily reutilized by conversion to its nucleotide. Enhanced utilization of exogenous hypoxanthine with allopurinol in man[8] and enhancement by allopurinol of incorporation of hypoxanthine into nucleic acids in mice[10] are consistent with this hypothesis. The normal decrease in total oxypurine excretion with allopurinol in our patient is in keeping with the normal activity of hypoxanthine guanine phosphoribosyl transferase.

The activity of adenine phosphoribosyl transferase is regularly increased in patients with decreased activity of hypoxanthine guanine phosphoribosyl transferase.[4, 9] However, it was not found to be increased in four adults with overproduction of purine and normal activity of hypoxanthine guanine phosphoribosyl transferase. The elevation of this enzyme in our patient was to the same degree as that observed in patients with defective hypoxanthine guanine phosphoribosyl transferase. These observations suggest the existence of mechanisms of control over the synthesis of enzymes involved in purine utilization. These mechanisms are not dependent simply on elevated concentrations of uric acid, overproduction of purine, or the activity of one enzyme. Elucidation of the metabolic abnormality in this patient could contribute to understanding of these and other mechanisms of interrelations in purine metabolism.

SUMMARY

A 3-year-old boy was described in whom hyperuricemia has been associated with mild developmental retardation, dysplastic teeth, absence of tears with crying, no speech, and odd, autistic behavior. Increased amounts of uric acid were excreted in the urine, and the formation of uric acid from ^{14}C-labeled

glycine was seven times that of controls. Treatment with allopurinol decreased the amounts of uric acid in the blood and urine. With allopurinol there was a concomitant increase in the excretion of hypoxanthine and xanthine but the total amounts of oxypurine in the urine fell normally, as did the molar ratio of hypoxanthine to xanthine. The activity of the enzyme hypoxanthine guanine phosphoribosyl transferase in the patient's erythrocytes was normal, but that of adenine phosphoribosyl transferase was increased.

We acknowledge the assistance of Mrs. Goldie Lieberman, P.H.N., and Dr. Daniel Ivler in the completion of these studies.

REFERENCES

1. Lesch, M., and Nyhan, W. L.: A familial disorder of uric acid metabolism and central nervous system function, Am. J. Med. **36:** 561, 1964.
2. Nyhan, W. L., Oliver, W. J., and Lesch, M.: A familial disorder of uric acid metabolism and central nervous system function. II. J. PEDIAT. **67:** 257, 1965.
3. Nyhan, W. L., Pesek, J., Sweetman, L., Carpenter, D. G., and Carter, C. H.: Genetics of an X-linked disorder of uric acid metabolism and cerebral function, Pediat. Res. **1:** 5, 1967.
4. Seegmiller, J. E., Rosenbloom, F. M., and Kelley, W. N.: Enzyme defect associated with a sex-linked human neurological disorder and excessive purine synthesis, Science **155:** 1682, 1967.
5. Sweetman, L., and Nyhan, W. L.: Excretion of hypoxanthine and xanthine in a genetic disease of purine metabolism, Nature **215:** 859, 1967.
6. Flaks, J. G.: Guanosine 5′-phosphate and inosine 5′-phosphate pyrophosphorylase, *in* Colowick, S. P., and Kaplan, N. O., Editors: Methods in enzymology, New York, 1963, Academic Press, Inc., vol. 6, p. 144.
7. Nyhan, W. L.: Purine metabolism as reflected in uric acid excretion, *in* Cheek, D. B., Editor: Human growth, body composition, cell growth, energy, and intelligence, Philadelphia, 1968, Lea & Febiger, Publishers, pp. 417-423.
8. Rundles, R. W.: Metabolic effects of allopurinol and alloxanthine, Ann. Rheumat. Dis. **25:** 615, 1966.
9. Kelley, W. N., Rosenbloom, F. M., Miller, J., and Seegmiller, J. E.: An enzymatic basis for variation in response to allopurinol, New England J. Med. **278:** 287, 1968.
10. Pomales, R., Bieber, S., Friedman, R., and Hitchings, G. H.: Augmentation of the incorporation of hypoxanthine into nucleic acids by the administration of an inhibitor of xanthine oxidase, Biochim. et biophys. acta **72:** 119, 1963.

CHAPTER

2.5

Mitochondria and Autism Spectrum Disorders

Robert K. Naviaux

The Mitochondrial and Metabolic Disease Center, Departments of Medicine, Pediatrics, Pathology, University of California, San Diego School of Medicine, San Diego, CA, USA

OUTLINE

THE BIRTH OF MITOCHONDRIAL MEDICINE

The first clinical and biochemical description of mitochondrial disease was reported by Rolf Luft in 1962 (Luft et al., 1962). Only two patients with Luft disease have been described to date (DiMauro et al., 1976). Both were interesting examples of intellectually normal adults (both women) with a rare form of mitochondrial over-function associated with high oxygen consumption rates, hypermetabolism, heat intolerance, resting tachycardia, hyperhidrosis, and death in middle age from respiratory muscle failure. Although mitochondria were first reported to contain their own DNA in 1963 by Margit and Sylvan Nass (Nass and Nass, 1963), it was another 25 years before the first DNA mutations were found that caused mitochondrial disease. We date the dawn of the molecular age of mitochondrial medicine to 1988, when Doug Wallace and colleagues reported the first mitochondrial DNA (mtDNA) mutations that cause disease (Wallace et al., 1988a, b). In the same year, Holt (1988) and Zeviani (1988) and their colleagues reported the first disease-associated deletions in mtDNA. Today, we know of more than 300 clinically, biochemically, or molecularly distinct forms of mitochondrial disease (Naviaux, 2004).

WHAT IS DEFINITE MITOCHONDRIAL DISEASE?

Mitochondrial disorders are among the most difficult diseases to diagnose in all of medicine. They constitute a large group of clinically heterogeneous disorders that have defied all efforts to find a universal biomarker

The Neuroscience of Autism Spectrum Disorders.
http://dx.doi.org/10.1016/B978-0-12-391924-3.00012-0

or universal symptom. In most cases, a child with mitochondrial disease is completely healthy at birth, but develops symptoms in a step-wise fashion, weeks to years later. In rare cases, symptoms may not appear until 70 years of age (Weiss and Saneto, 2010). New symptoms typically appear over time, so that at any one time early in the disease, not all symptoms are present. This makes early diagnosis challenging or impossible. Mitochondrial diseases share the one fact that they are fundamentally bioenergetic and metabolic disorders that result from defects (under-function) in oxidative phosphorylation – the ability to make ATP in mitochondria from electrons, hydrogen, and oxygen. This clinical heterogeneity has led to the widely quoted axiom that mitochondrial disease can produce any symptom, in any organ, at any age (Munnich et al., 1996).

Mitochondrial under-function and over-function disorders are clinically distinct. Historically, the field of mitochondrial medicine has focused on the disorders of under-function. The disorders of over-function will be addressed later in this chapter. Mitochondrial under-function diseases can be divided into primary and secondary forms. Primary mitochondrial diseases are genetic disorders caused by mutations in either nuclear or mitochondrial DNA that affect the proteins of the mitochondrial respiratory chain. For this reason, they are sometimes call respiratory chain (RC) disorders. Secondary mitochondrial diseases are ecogenetic disorders that result from a combination of environmental and genetic factors. The distinction between primary and secondary mitochondrial disorders is clinically important because it carries implications for genetic counseling. Primary disorders are monogenic and carry recurrence risks associated with known Mendelian and maternal patterns of genetic transmission. Secondary disorders are rarely monogenic and require exposure to one or more environmental factors such as a drug, toxicant, or viral infection. Counseling for recurrence risks of secondary mitochondrial and other ecogenetic disorders is empiric.

When a single biomarker, sign, or symptom is unable to establish a disease diagnosis in a deterministic manner, medicine has historically developed probabilistic methods for diagnosis. The modified Walker criteria (Bernier et al., 2002) have been widely adopted to group or stratify patients according to the likelihood of genetic forms of mitochondrial disease. Using these criteria, patients are given a diagnosis of definite, probable, or possible mitochondrial disease (Table 2.5.1). If a causal DNA mutation is not found, a muscle biopsy is typically required to confirm a definite diagnosis of mitochondrial disease. The criteria for 'definite' mitochondrial disease have been used

TABLE 2.5.1 Modified Walker Criteria for the Diagnosis of Mitochondrial Disease*

Mitochondrial disease diagnosis	**Diagnostic requirements**
Definite	≥ 2 major, or 1 major + 2 minor criteria
Probable	1 major + 1 minor, or ≥ 3 minor criteria
Possible	1 major, or 1 minor clinical + 1 other minor criterion
Major criteria	**Minor criteria**
Clinical: Classic multisystem mitochondrial phenotype with progressive clinical course, or positive family history	Clinical: Incomplete mitochondrial phenotype
Histology: ≥ 2% Ragged-red fibers (RRF)	Histology: 1–2% RRF if 30–50 years old, or any RRF if < 30 years, or widespread ultrastructural abnormalities
Enzymology: ≥ 2% COX-negative fibers if < 50 yrs old; or ≥ 5% COX-negative fibers if ≥ 50 yrs old; or < 20% any respiratory chain (RC) enzyme or polarographic activity; or < 30% in cell culture, or 20–30% in ≥ 2 different tissues	Enzymology: Antibody-based demonstration of defective RC subunit expression, or 20–30% RC activity in a tissue, or 30–40% RC activity in a cell line, or 30–40% RC activity in ≥ 2 tissues
Functional: Fibroblast ATP synthesis ≥ 3 SD below the mean	Functional: Fibroblast ATP synthesis 2–3 SD below the mean, or unable to grow in galactose
Molecular: Pathogenic mtDNA or nuclear DNA abnormality	Molecular: mtDNA or nuclear DNA abnormality of probable pathogenicity
	Metabolic: ≥ 1 Abnormal metabolic indicator of RC function (eg., lactate, 31P-MRS)

* *Tables summarized from Bernier et al., 2002.*

to determine the epidemiology of mitochondrial disease.

EPIDEMIOLOGY OF MITOCHONDRIAL DISEASE

The epidemiology of mitochondrial disease has evolved rapidly over the past 15 years. The first estimates of its prevalence were as low as 1:33,000 (Applegarth et al., 2000). These lower estimates were hampered by the absence of consistent standards for diagnosis and early stages of the rapidly growing awareness of the clinical heterogeneity of mitochondrial diseases. Most children with mitochondrial disease before the year 2000 died without a proper diagnosis. The best figures now available are that 1 in 2,000 children born each year in the US will develop definite mitochondrial disease in their lifetimes. About half of these children (1:4,000) will develop symptoms in the first 10 years of life (Naviaux, 2004). The other half (1:4,000) will remain healthy, without any symptoms until after age 10. Many adult mitochondrial disorders do not manifest until 20–50 years of age, and in rare cases not until the 70s (Weiss and Saneto, 2010). About half of adult mitochondrial disease is caused by mtDNA mutations and half by nuclear DNA mutations. A recent study of mitochondrial disease among adults in the UK found about 1 in 4,000 adults (25.7 per 100,000) had or were at risk for mtDNA-based disease (Schaefer et al., 2008). The growing awareness that mutations in nuclear DNA can lead to many different adult mitochondrial disorders with many different symptoms (Cohen and Naviaux, 2010; Saneto and Naviaux, 2010) means that the prevalence figures for adult mitochondrial disorders may continue to rise over the next few years.

About 15% of pediatric mitochondrial disease is caused by mtDNA mutations (Rotig et al., 2004) and 85% is caused by nuclear DNA mutations that are inherited in a Mendelian fashion. Most of these are inherited as autosomal recessive disorders, but X-linked and dominant forms are also well known. Over 200 point mutations and 400 deletion break points have been described in mitochondrial DNA that lead to disease (DiMauro et al., 2006) and over 60 nuclear genes have been identified with well over 500 disease-causing mutations (Falk, 2010; Haas et al., 2008; Wong, 2010). Excellent diagnostic algorithms have recently been published to assist physicians in choosing which genes to select for DNA testing to best explain a particular clinical presentation (Wong, 2010; Wong et al., 2010). When an mtDNA mutation is suspected, full mitochondrial DNA sequencing by NextGen methods is now available and recommended (Kauffman et al., 2012). When a Mendelian pattern of transmission is identified in a pedigree and the probability of finding one of the more common nuclear gene causes is low, exome capture and NextGen sequencing of 362 to 524 nuclear mitochondrial genes is available (Shen et al., 2011; Vasta et al., 2009).

DEFINITE MITOCHONDRIAL DISEASE IS A RARE CAUSE OF AUTISM SPECTRUM DISORDERS

The first evidence of a mitochondrial DNA mutation that could cause autism spectrum disorders (ASD) was published in 2000 (Graf et al., 2000). In this report, the authors found a heteroplasmic point mutation in the mitochondrial tRNA for lysine (G8362A) that was the cause of Leigh syndrome in a 6-year-old girl with a history of normal development in the first year of life, with the onset of ataxia and myoclonus at 15 months of age. She had classic, symmetric T2 signal abnormalities in the basal ganglia and brain stem, characteristic of Leigh syndrome. Her speech and language were normal except for dysarthria and moderate intellectual impairment. The mtDNA mutation was associated with a respiratory chain defect in muscle complex IV. Her younger brother was diagnosed with ASD after developmental regression at 1.5–2 years of age. By 3.5 years of age, he had no functional speech or language, was hyperactive, and displayed bouts of self-injurious behavior. He carried the same tRNA lysine mutation as his older sister, but at lower level of heteroplasmy (61% vs. 86%). In sharp contrast to his older sister with Leigh syndrome, the muscle biopsy of the brother with autism showed a paradoxical hyperactivity in complex I that was 250% of normal (200.6 vs. 81; SD of 29.4; normalized for citrate synthase activity) (Graf et al., 2000). Recently, a group of children with hyperactivity of complex IV and autism has been described (Frye and Naviaux, 2011). Some patients with complex IV hyperactivity and autism have been found to have a mutation in the mitochondrial calcium-regulated aspartate-glutamate carrier (AGC1) (Palmieri et al., 2010).

In March 2008, the connection between mitochondria and autism was catapulted into the national spotlight when news media picked up the story of Hannah Poling (Stobbe, 2008; Wallis, 2008), a little girl who had mitochondrial disease and developed an ASD within weeks of receiving several immunizations at 1.5 years of age in 2000 (Poling et al., 2006). In June 2008, the US National Institute of Mental Health (NIMH), National Institute of Child Health and Human Development (NICHD), Centers for Disease Control and Prevention (CDC), and Food and Drug Administration (FDA) rapidly organized a public, special topic symposium on Mitochondrial Disease and Autism in Indianapolis, IN, in conjunction

with the annual meeting of the United Mitochondrial Disease Foundation (UMDF) (Gorski, 2008). This case is unusual for definite forms of mitochondrial diseases, which typically do not show regression after routine immunizations (Verity et al., 2010; 2011).

Now, in 2012, the connection between mitochondrial dysfunction and ASD (Haas, 2010; Rossignol and Frye, 2011) remains one of the freshest new leads in nearly 70 years of autism research since autism was first identified as a childhood disease by Leo Kanner in 1943 (Kanner, 1943). However, as evidenced in an epidemiological study in mainland Portugal and the Azores, only 5% of children with ASD have definite forms of mitochondrial disease (Oliveira et al., 2007), and this estimate would benefit from replication in independent epidemiological cohorts. The classic forms of primary mitochondrial disease have a very different clinical character to that found in children with ASD. Mitochondrial disease patients often have devastating, multi-organ system disorders with mortalities as high as 10–50% per year after the onset of the first symptoms (Cohen and Naviaux, 2010; Naviaux, 1997; Rahman et al., 1996). This mortality far exceeds the rate of 0.2% deaths per year (26 of 342 ASD patients studied over 36 years) observed in ASD (Mouridsen et al., 2008). In addition, children with mitochondrial disease are often found to have decreased sensitivity to sound, touch, and light, decreased muscle strength, decreased activity, with normal social engagement. Hyperactivity and repetitive movements are rare in definite mitochondrial disease. These symptoms are in sharp contrast to those found in children with ASD.

The weight of the evidence collected since 2000 now points to a more subtle connection between mitochondrial function and ASD. Simple mitochondrial under-function does not cause either narrowly defined autism or ASD, with rare exceptions (Shoffner et al., 2010; Weissman et al., 2008). Several cases of mitochondrial respiratory chain over-function and ASD have now been described (Frye and Naviaux, 2011; Graf et al., 2000). This is likely to be an under-reported phenomenon, since most specialists in mitochondrial medicine dismiss respiratory chain enzyme hyperactivity ($\geq$ 165% of controls) as incidental, or as compensation for another, often unmeasured, defect. In either case, respiratory chain over-function is not a cause of primary mitochondrial disease. The relative proportions and overlaps between children with autism and mitochondrial disease are summarized in Figure 2.5.1.

MITOCHONDRIAL DISEASE AND AUTISM RESPOND DIFFERENTLY TO THE SAME TREATMENTS

If two diseases have the same cause, they should respond similarly to the same treatments. The fact that this is not the case with definite mitochondrial disease and ASD is further evidence that these disorders should not be lumped together. Table 2.5.2 lists four cases that distinguish mitochondrial disease on the one hand and ASD on the other. Valproic acid (depakote, divalproex) is an 8-carbon branched-chain fatty acid that is widely used to treat seizures and other disorders in ASD (Hollander et al., 2010), but is known to produce mitochondrial toxicity in the large majority of patients with mitochondrial disease (Saneto et al., 2010). The only case of mitochondrial disease in which valproic acid therapy is usually well tolerated and effective is in MERRF (myoclonus, epilepsy, with

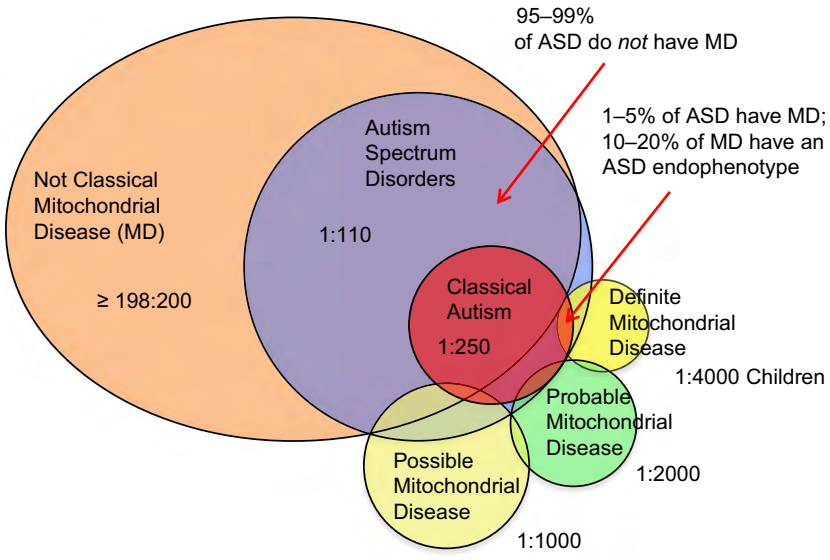

FIGURE 2.5.1 The majority of children with autism do not have classic forms of mitochondrial disease (MD). Epidemiologic studies show that fewer than 5% of children with autism spectrum disorders have classical mitochondrial disease. Other forms of mitochondrial dysfunction, such as a persistent danger response, or segmental over-function of certain mitochondrial functions in innate immunity, may be more common and impair cellular communication by effects on metabolism. These non-oxidative-phosphorylation functions of mitochondria are not routinely measured in the evaluation of children for classic forms of mitochondrial disease.

TABLE 2.5.2 Definite Mitochondrial Disease and Autism Respond Differently to the Same Treatments

Treatment or feature	Definite mitochondrial disease	Autism spectrum disorders	Reference
Valproate	Deterioration (except MERRF)	71% improved	Hollander et al., 2010
Fever	Deterioration (fade response)	83% improved	Curran et al., 2007
Hyperbaric O_2	Deterioration	30–80% improved, or no net benefit	Jepson et al., 2011; Rossignol et al., 2009
Recovery (spontaneous or therapy-associated)	Very rare (LHON, reversible COX tRNA-Glu)	3–25%	Helt et al., 2008

LHON = Leber's hereditary optic neuropathy.

ragged-red fibers) when given with L-carnitine supplementation. This is a form of mitochondrial disease that is characterized by massive mitochondrial proliferation and may have some symptoms that result from an element of metabolic hyperfunction, in addition to the known oxidative phosphorylation deficiency.

The response to fever is also different in mitochondrial disease patients and most patients with ASD. Infections and fever caused over 70% of the neurodegenerative events observed in children with mitochondrial disease (Edmonds et al., 2002). However, in a prospective study of 30 children with autism and 30 controls, Andy Zimmerman and his colleagues at the Kennedy Krieger Institute found that 83% (25 of 30) of the children with ASD improved in at least one area related to hyperactivity, stereotypy, or speech, although lethargy scores were worse (Curran et al., 2007) (Table 2.5.2). The curious 'awakening' of ASD during fever is short-lived, as the children returned to their previous state with the resolution of the infection and fever. Infection and fever are also known to produce transient improvements in some patients with schizophrenia. The history of the role of fever, cytokines, and innate immunity in the pathogenesis of disease has been reviewed (Patterson, 2009). How can fever be involved both in the cause of autism and in its transient improvement? We will return to this question later in this chapter in the sections on innate immunity and mitochondrial hormesis.

Hyperbaric oxygen treatment was shown to have neutral (Jepson et al., 2011) or beneficial (Rossignol et al., 2009) effects on children with ASD. This would be in sharp contrast to the experience of definite mitochondrial disease patients who can suffer catastrophic neurodegeneration and sometimes death associated with hyperbaric oxygen therapy (Table 2.5.2). The question of hyperbaric oxygen therapy for mitochondrial disease was addressed by the scientific advisory board of the United Mitochondrial Disease Foundation in 2007 (UMDF, 2007). Classic mitochondrial disease is caused by an inherited inability of the cell to use oxygen. The forcible delivery of increased levels of oxygen in classic forms of mitochondrial disease does not improve mitochondrial function. Instead, it results in a deleterious increase in damaging reactive oxygen species (ROS), which can further damage mitochondrial membranes, enzymes, and DNA and lead to neurodegeneration. This difference in the clinical response to hyperbaric oxygen further differentiates the major mechanisms of pathogenesis that underlie ASD and mitochondrial disease and underscores the risk of hyperbaric oxygen in ASD unless mitochondrial disease is ruled out.

Recovery or partial recovery has been reported in 3–25% of children with ASD (Helt et al., 2008) (Table 2.5.2). In most cases this has occurred in association with intensive behavioral and/or biomedical therapy. Recoveries in mitochondrial disease are virtually unheard of. There are two rare exceptions that in total constitute less than 1% of all mitochondrial disease. These are spontaneous or treatment-associated recovery of vision in certain forms of Leber's hereditary optic neuropathy (LHON) (Sadun et al., 2011) and spontaneous recovery in a rare form of cytochrome oxidase deficiency (Mimaki et al., 2010). In all other cases of mitochondrial disease, the natural history typically involves step-wise or gradual deterioration over months to years after the onset of symptoms. In many cases, this leads to early death. Multiple organ systems eventually become involved.

Single-gene defects cause the classic forms of mitochondrial disease. In contrast, most ASD is thought to be multifactorial, with genes of major and minor effect interacting with environmental and additional factors (see other chapters in this section). Where genes meet the environment is metabolism, and mitochondria are the hub of the wheel of metabolism. The remainder of this chapter focuses on the metabolic functions of mitochondria that are involved in innate immunity. Cellular defense is one of the most ancient functions of mitochondria. By considering the responses of genes and

metabolic processes to danger signals in the environment, we can get a little closer to understanding the complex link between mitochondria and ASD.

NUCLEAR MITOCHONDRIAL GENOCARTOGRAPHY AND CNVS

The mitochondrial proteome consists of about 1,500 proteins (Pagliarini et al., 2008) encoded by over 1,000 nuclear genes (Figure 2.5.2) and 13 proteins made by mtDNA. Every one of the 10^{14} cells of the body contains different mitochondria, that are specialized to meet the metabolic demands of that cell. Therefore, there is a different mitochondrial network, with a different proteome, with different post-translational modifications for every different cell in the body. This remarkable feat is accomplished by regulating both nuclear and mitochondrial gene expression in tissue-specific ways (Johnson et al., 2007), and by making dozens of post-translational modifications in proteins that fine-tune metabolism according to the time of day, availability of nutrients, toxin exposure, microbial infection, and even the season of the year (Staples and Brown, 2008; Zhao et al., 2011). The chromosomal location of each of these 1,500 proteins can be mapped. On average, each of our 23 chromosomes contains about 20–70 mitochondrial genes (Figure 2.5.2).

Recent studies have shown that about 4% of children with autism have rare DNA copy number variations (CNVs) that might contribute to disease, compared to just 2% of typically developing, age-matched controls (e.g., Pinto et al., 2010; see also Chapters 2.1 and 2.2). Most of these CNVs were duplications, not deletions, although there is good evidence that deletions are more likely associated with ASD and other neurodevelopmental disorders. Interestingly, the same CNVs found to be associated with ASD have also been found to be enriched in patients with schizophrenia (e.g., Guilmatre et al., 2009; see also Chapters 2.1 and 2.2), suggesting that disruption of brain development by CNV can contribute to a myriad of neurodevelopmental disorders, likely in concert with other genetic or environmental factors (see Chapter 2.1). Analysis of the genes affected by recurrent CNVs and single-gene defects in ASD highlights the complex etiology of ASD with

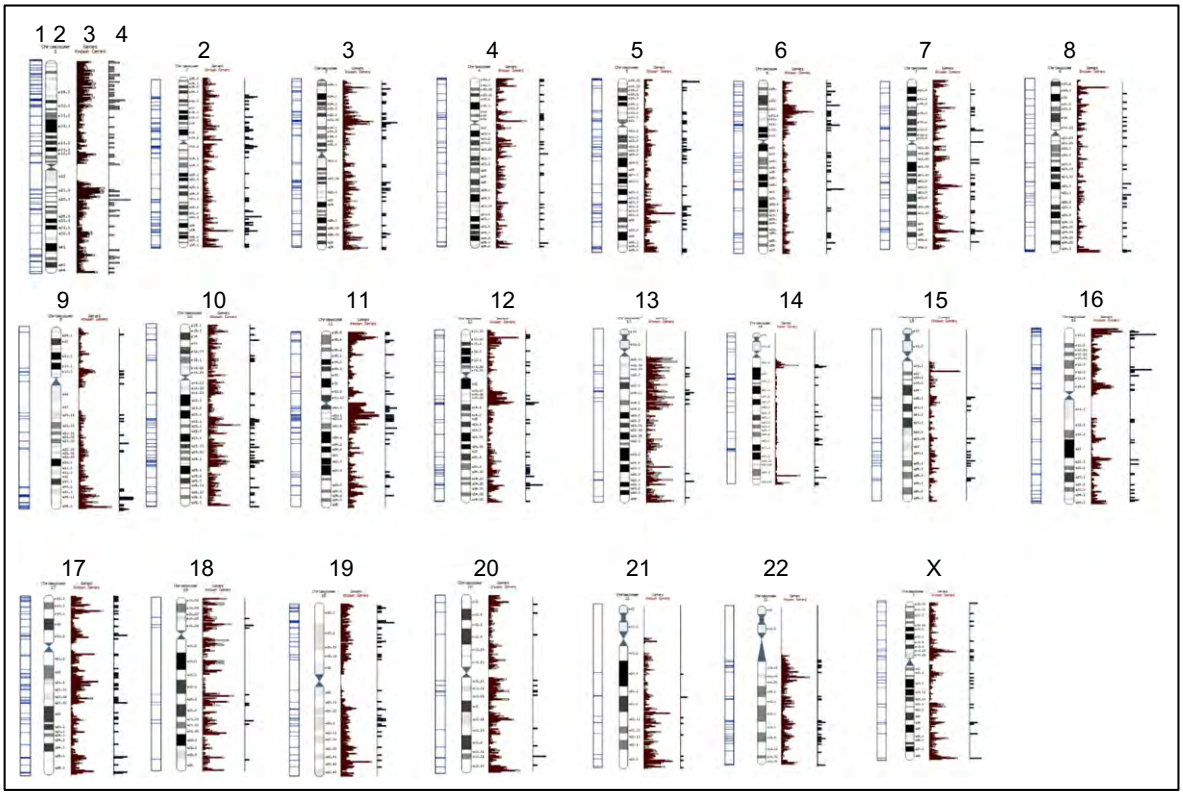

FIGURE 2.5.2 Mitochondrial genocartography. Each of the 23 human chromosomes illustrated is associated with four vertical bars (labeled 1–4 over chromosome 1). Bar #1 in blue illustrates the number and position of nuclear mitochondrial genes. Over 1,000 of these are known. Bar #2 illustrates the conventional G-banding pattern of each chromosome. Bar #3 illustrates the density of non-mitochondrial genes on the chromosome. Bar #4 illustrates the density of mitochondrial genes on the chromosome. Each chromosome contains 20–70 mitochondrial genes. When copy number variations (CNVs) occur, the mitochondrial genes in the affected areas are also varied, leading to gene dose effects that can alter any of over 500 bioenergetic and metabolic functions of mitochondria in the cell.

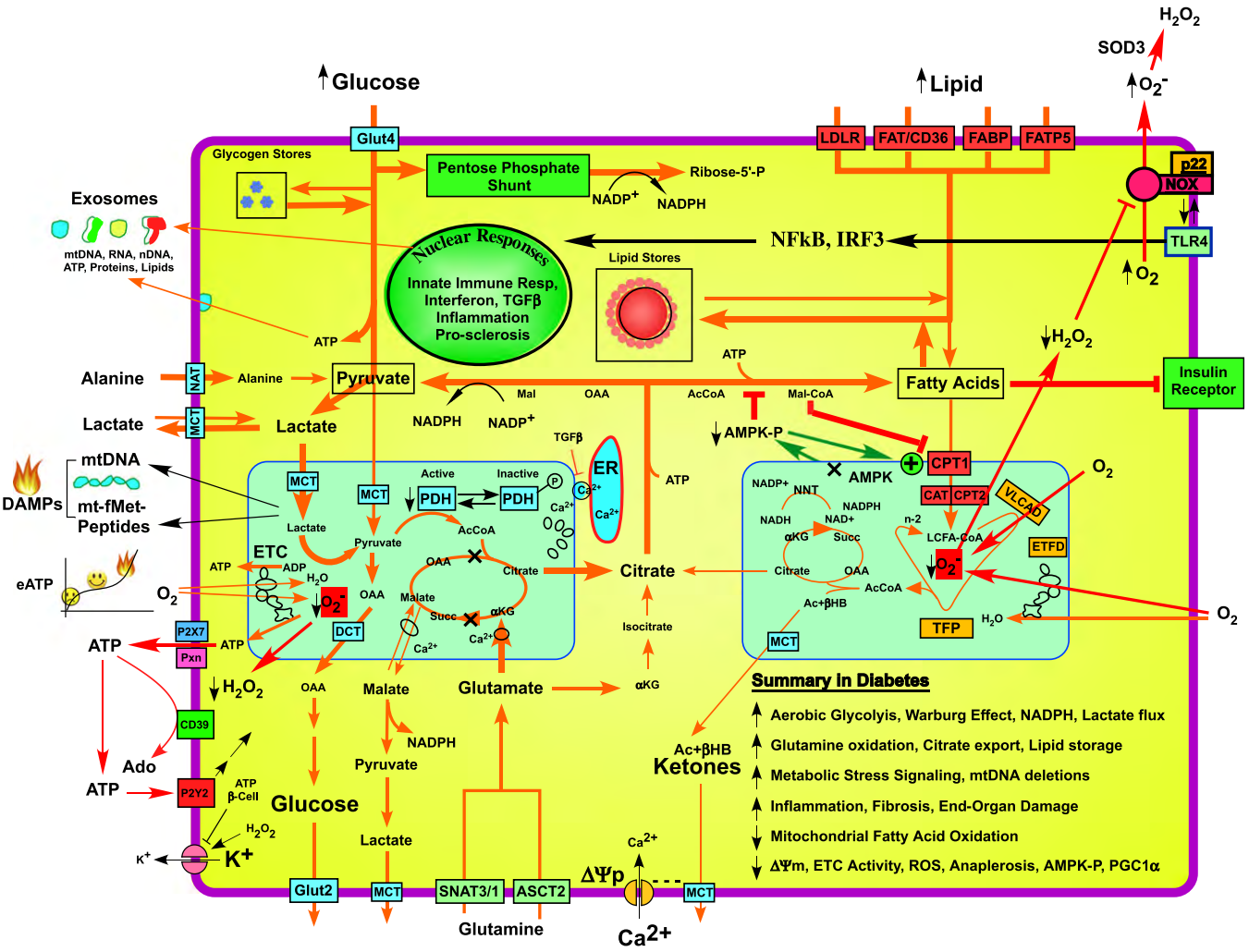

FIGURE 2.5.3 The language of the cell is metabolism. Cells communicate with neighboring and distant cells in the body by exchanging small molecule metabolites like nucleotides, organic acids, amino acids, and lipids. This ancient language of the cell is still largely untranslated. New methods in mass spectrometry are revealing how cells communicate messages about stress, danger, health, and disease. The cell above is a liver cell adapting to nutrient excess in diabetes. Mitochondria are illustrated as the two blue boxes in the center, receiving pyruvate on the left and fatty acids on the right. Cells in affected tissues of patients with autism speak a different message but use the same vocabulary of chemical words. The most common developmental and chronic diseases in medicine can be understood as disorders of cellular communication.

multiple organelles and systems implicated (Chapter 2.1). The interpretation of duplication CNVs is complicated, because typically developing children can have the same CNVs, consistent with reduced impact and/or penetrance of duplications (Pinto et al., 2010).

MITOCHONDRIA AND THE CONTROL OF CNVs, DNA INSTABILITY, AND REPAIR

Gene duplication and deletion events are regulated by cross-over events that lead to mitotic recombination (Matos et al., 2011). It is known that changes in mitochondrial DNA copy number have dramatic effects on nuclear DNA repair and genomic instability (Singh et al., 2005). What are some of the factors that control mtDNA copy number in cells? TLR4 signaling after LPS signaling associated with bacterial infection leads to mtDNA damage and depletion (Suliman et al., 2005). Significant amounts of free fatty acids can also act as endogenous ligands of the TLR4 receptor during periods of metabolic mismatch associated with disorders like diabetes (Schaeffler et al., 2009). Interferon released during infections activates the cellular RNAse L that can traffic to mitochondria and destroy mitochondrial RNA (Chandrasekaran et al., 2004). Even certain viruses, like herpes simplex virus, encode a special DNAse (UL12.5) that travels to mitochondria and produces mitochondrial DNA damage and depletion (Corcoran et al., 2009). It turns out that many infectious agents target mitochondria in an effort to downregulate oxygen consumption, which inhibits DNA synthesis and replication.

A spectrum of environmental neurotoxicants such as bisphenol A (BPA), polychlorinated biphenyls (PCBs) (Jolous-Jamshidi et al., 2010), and certain polybrominated diphenyl ethers (PBDEs) (Ashwood et al., 2009), known to cause autism-like behaviors in mouse and rat models, also can regulate mitochondrial function either directly or indirectly via alterations in cellular calcium handling (Coburn et al., 2008). Although it has not yet been experimentally verified, it seems plausible that infection, environmental neurotoxicants, and/or metabolic stress can each produce changes in mitochondrial function that might alter the somatic control of mitotic recombination and CNV formation rates during embryogenesis and early childhood development. Acutely this can produce a transient increase in somatic CNV formation.

MITOCELLULAR HORMESIS

Chronically, mitochondria are known to help the cell adapt to past metabolic stresses by producing long-term changes in cellular reactivity in a process called mitochondrial hormesis (Ristow and Zarse, 2010). When both mitochondrial and cellular mechanisms adapt, the result is mitocellular hormesis. Mitocellular hormesis in response to xenobiotics produces long-term up-regulation of cellular oxidation, inactivation, and excretion pathways like cytochrome P450, sulfation, and glucuronidation (Xu et al., 2005). Mitocellular hormesis in response to infectious or inflammatory agents activates innate immune pathways that increase reactive oxygen species (ROS) production, activate cell signaling and cytokine responses, alter folate, B12, and other vitamin metabolism, and change the gene expression and epigenetic programs of the cell. The response to cellular stress is invariably biphasic. First there is an acute inhibition, followed by long-term adaptation, much like the metabolic memory response associated with exercise (Ji et al., 2006). When the triggering stimulus is inhibitory, or surpasses the mitochondrial capacity to process the resulting metabolites, then mitochondrial proliferation and hyperfunction results (Sano and Fukuda, 2008). If proliferation and mitochondrial hyperfunction occur in neurons or microglia in the brain, then persistent low-level excitotoxicity and neuroinflammation can result. What is the final common denominator that maintains this cycle of metabolic innate immune activation, excitotoxicity, and inflammation?

MITOCHONDRIAL FUNCTIONS IN METABOLISM

Mitochondria are located at the hub of the wheel of metabolism. They perform over 500 different functions in the cell. Respiratory chain proteins constitute about 10–20% of the mitochondrial proteome (Pagliarini et al., 2008). The other 80–90% of mitochondrial proteins play roles in hundreds of other pathways, including in innate immunity, cellular defense, amino acid transport, calcium metabolism, iron metabolism, copper metabolism, reductive and oxidative stress metabolism, hydrogen sulfide and nitric oxide metabolism, fuel sensing, translation, protein folding and assembly, autophagy, microtubule association, folate metabolism, porphyrin metabolism, steroid metabolism, glycolate metabolism, and DNA repair. None of these non-oxidative phosphorylation functions is routinely measured when a child is evaluated for mitochondrial disease. Therefore, a large part of mitochondrial function has never been systematically measured in children with ASD because it relates to functions outside the respiratory chain, and produces symptoms that are not characteristic of definite mitochondrial disease.

It can be stated simply that metabolism is the language of the cell. Figure 2.5.2 illustrates some of the metabolic pathways that characterize a liver cell. The methods of mass spectrometry and metabolomics have allowed investigators to 'eavesdrop' on the collective conversation of cells in ASD. These early studies have identified abnormalities in glutathione (James et al., 2004), taurine, glutamate, hippurate (Yap et al., 2010), and polyunsaturated phospholipid metabolism (Pastural et al., 2009). The language of metabolism is spoken using small molecule metabolites as the words. This is a universal language of life on Earth, with many dialects that reflect the specialization of organisms adapting to their environment. Despite its universal usage, this language of metabolism is still largely untranslated. Future studies using the tools of mass spectrometry will help expand our lexicon of metabolites and their meanings, and help us to interpret the conversation of metabolism in children with ASD.

MITOCHONDRIAL FUNCTIONS IN INNATE IMMUNITY

One of the most ancient functions of mitochondria is in cell defense. I have called this the 'secret life of mitochondria' because it is largely separate from oxidative phosphorylation. When a cell is attacked by a virus, a cascade of events is initiated that is designed to protect the cell from injury, limit viral replication, and warn neighboring cells of the intrusion. Healthy cells can increase or decrease their response to a given infection or inflammatory stimulus by a process of priming. Primed cells have adopted a more defensive set-point,

sacrificing certain differentiated cell functions for the ability to respond rapidly to an attack. When this happens in the brain, excitotoxicity and inflammation can result. When it happens in gut-associated lymphoid tissue (GALT), then abnormally aggressive responses to the normal gut microbiome can result. If a cell is injured or broken in the attack, then a large number of molecules are released into the extracellular space as 'danger' signals. Many of these are present in high concentrations within mitochondria. These danger signals are collectively called damage-associated molecular patterns (DAMPS). ATP is a DAMP (Zhang et al., 2010). Inside the cell, ATP concentrations range from 1–5 mM depending on the cell type. Each cell maintains a pericellular halo of ATP in the 1–5 μM range that interacts with a family of ancient cell-surface proteins called purinergic receptors. The possible role of purinergic signaling in ASD will be discussed in a later section.

Another reason that a number of mitochondrial molecules act as DAMPs is the evolutionary origin of mitochondria as the ancestors of ancient, free-living gram-negative bacteria (Cavalier-Smith, 2006). Mitochondrial DNA itself contains unmethylated CpG dinucleotides that resemble bacterial DNA and activate TLR9. Proteins synthesized in mitochondria start with a bacteria-like formyl-methionine. *N*-formyl-methionine-containing peptides from mitochondria bind the formyl peptide receptor (FPR1, and FPRL1) and activate innate immunity (West et al., 2011). The regulation of intracellular calcium release from the endoplasmic reticulum to mitochondria through the IP3 receptor and ryanodine receptor channel is a crucial point of regulation of the metabolic response to infection and stress (Zecchini et al., 2007). Recent studies have suggested that abnormalities in mitochondrial calcium handling (Gellerich et al., 2010) may be a common denominator in ASD (Napolioni et al., 2011).

REGRESSION

Regression is common in mitochondrial disease in response to infection. The first report to quantify the risk of neurodegeneration with infection in definite mitochondrial disease was published in 2002 (Edmonds et al., 2002). The authors of this paper found that 60% of children with mitochondrial disease suffered neurodegenerative events (regressions). A total of 72% of the regression events were associated with infections that occurred within two weeks before the onset of regression. None of the regression events in children with mitochondrial disease were associated with childhood immunizations. A total of 28% of the regressions occurred spontaneously, with no identifiable trigger. Regressions occurred at any age, and were not confined to the first two to three years of life. The form of regression was one of a 'fade' response that occurred 2–10 days after the peak fever associated with the illness. Most often the neurodegeneration occurred during an otherwise normal recovery period after a common childhood infectious illness. Over a period of a few days, the child became obtunded or encephalopathic, or experienced a stroke-like episode, new-onset seizures, or lost the ability to walk or talk, lost vision, developed swallowing problems or gastrointestinal dysmotility, or lost other developmental milestones. In most cases, the child was able to make a slow and sometimes complete recovery over several months, but often there were residual deficits. In less common cases, there was a slow progression to encephalopathy, coma, and death over two to three months.

Regression is less common in ASD and more subject to large differences in estimates of its prevalence based on small differences in the definition of regression. Regression occurred in 15% of 333 children 2–5 years of age with ASD reported by Hansen et al. (2008). The criteria for regression were loss of both language and social skills. The loss of social skills was found to be a more sensitive indicator for regression and 26% of children had either language loss or loss of social skills. 59% percent of the 333 children in this CHARGE study had no history of regression. The severity of the neurological regressions in ASD was much less, and their character was different to those in mitochondrial disease. Strokes and permanent weakness are rare in ASD, and no deaths were reported.

The role of mitochondrial dysfunction as a risk factor for regression in a subgroup of children with ASD was recently highlighted in a paper by Shoffner et al. (2010). A group of 28 children with both mitochondrial respiratory chain disease and ASD were selected for retrospective analysis. The authors found that 61% had a history of a neurodegenerative episode that eventually grew into the features of ASD. 39% of children developed ASD gradually, without a history of regression. When regression occurred, 71% happened within two weeks of a fever of over 101°F. These proportions were similar to those originally reported by Edmonds et al. in children without autism (Edmonds et al., 2002). In four children (14% of the 28), the fever occurred after routine vaccination. In the remaining eight children, fever came with a routine infection or was a fever of unknown origin. This study emphasizes the fragile nature of children with mitochondrial disease. The observation that four children regressed after immunization is rare in mitochondrial disease in general. Most children with classic forms of mitochondrial disease tolerate immunization well.

TABLE 2.5.3 Careful Attention to the Timing and Symptoms of an Adverse Reaction After Infection or Immunization Provides Insights into the Underlying Cause

	Character of the adverse reaction		
	STORM	**FLARE**	**FADE**
Timing	2–12 hrs, or 2–6 days after exposure	Peaks at 48–72 hrs – coincides with peak symptoms of infection	Peaks at 2–10 days after peak symptoms of infection
Symptoms	Fever, HA, abd/low back pain, T-cell activation, widespread apoptosis, TNFα/IFNγ synergy, +/− ADCC, complement C5a, shock, histamine, DIC, hemorrhage	Stereotyped 'sickness behavior'; or high fever ≥ 10°2F, hyper-irritability, inconsolability, intermittent high-pitched screaming, delirium, opisthotonous, GI hypermotility with diarrhea	No fever or low-grade fever, ataxia, gastroparesis, aphasia or hypophasia, stroke-like episodes, change in muscle tone (hypo- or transient hypertonia 2° to CNS hypofunction)
Sequelae	Death in 4–14 days; or slow recovery over 2–6 months, sometimes with permanent disability	Self-limited course, normal vaccination conversion rate; or loss of milestones, with appearance of autism spectrum behaviors over 3–6 months. May improve transiently with fever later.	Self-limited neurodegeneration, poor vaccination conversion rate, slow recovery; or progressive complications and multi-organ system dysfunction, leading to death in 1–4 months
Mechanism	Anamnestic response	Exaggerated innate immune response, possible mitochondrial hyperfunction	Mitochondrial failure
Examples	Jesse Gelsinger (Wilson, 2009); Dengue shock (Pang et al., 2007)	Hannah Poling (Poling et al., 2006)	Reye syndrome (Partin, 1994) Definite mitochondrial disease after infection (Edmonds et al., 2002)

Abd = abdominal; CNS = central nervous system; GI = gastrointestinal; IFN = interferon; TNF = tumor necrosis factor.

STORM, FLARE, AND FADE RESPONSES

Careful attention to the timing and character of an adverse reaction to infection or immunization can provide crucial insight into the cellular mechanisms involved. Table 2.5.3 illustrates the three classes of adverse response. The cytokine 'storm' response requires prior immunization with the triggering antigen. Perhaps the most famous example is the tragic case of Jesse Gelsinger who developed a cytokine storm within hours of receiving gene therapy with an adenovirus vector and died two days later (Wilson, 2009). Another widely recognized example of a perfect storm of cytokines occurs with Dengue shock syndrome (Pang et al., 2007), in which a second exposure to Dengue virus produces a severe memory, or anamnestic, response that can lead to shock and death.

When children with the common forms of mitochondrial disease suffer a regression, it is most often a 'fade' response (Table 2.5.3). The fade response is typically delayed for 2–10 days *after* a fever resolves (Edmonds et al., 2002), similar to the time course found in Reye syndrome in the 1980s (Partin, 1994). In the case of Reye syndrome, the early metabolic profile of highly elevated short chain fatty acids that are normally fully metabolized in mitochondria is evidence that mitochondria are catastrophically downregulated early in the disease process. Recovery from Reye syndrome was associated with the removal of short chain fatty acids like propionate, isobutyrate, and isovalerate (Trauner et al., 1977) indicating that mitochondrial function was restored. Parents of children with mitochondrial disease will typically report that their child was getting better from their cold or flu, when, suddenly, their consciousness fades. The child can become difficult to fully awaken, or will stop walking, stop talking, stiffen or lose muscle tone, or have a seizure, or a stroke-like episode. The fade response involves an energy failure, and can lead to a series of neurodegenerative events and even death over the next two to three months, or to a self-limited event like a stroke-like episode that gradually gets better.

In contrast, autistic regression that is associated with unrecognized mitochondrial dysfunction appears to be more of a 'flare' response, similar to that suffered by Hannah Poling and described in the scientific literature (Poling et al., 2006). A flare response typically occurs early, at the peak of the fever and inflammatory response, within two to three days of infection (Table 2.5.3). During a flare response, there is a high fever, often over 102°F, with hyper-irritablilty, crying, inconsolability, a disrupted sleep-wake cycle, and a refusal to walk in children who might otherwise appear to be physically able to walk, choosing rather to crawl (Poling et al.,

2006). Following a flare response, there can be a gradual evolution of other problems from persistent gastrointestinal problems and diarrhea, a gradual loss of language over two to three months, with the onset of repetitive movements, to gaze and social avoidance (Poling et al., 2006). It must be emphasized that a flare response is not simply a high fever, or even a dramatic reaction to a high fever, like a febrile seizure. It is a multisystem inflammatory response that carries a risk of autistic regression in genetically susceptible children. Is it possible that an unusually high fever is because of a primed state of innate immunity associated with an element of mitochondrial hyperfunction? Mutations in the ryanodine receptor known to cause calcium release and mitochondrial heat production by uncoupling in malignant hyperthermia result from induction of primed mitochondria (Yuen et al., 2012). Systemic inflammation not only triggers calcium release, but is a known trigger of excitotoxic amounts of ATP in the brain (Gourine et al., 2007).

THE POSSIBLE ROLE OF PURINERGIC SIGNALING IN AUTISM SPECTRUM DISORDERS

How might all of the facts about the complex connection between mitochondria and ASD be integrated into a unified theory of pathogenesis? One possibility might be called a purinergic theory of autism. The metabolism of a child adjusts dynamically during development to match the changing environment by the process of metabolic matching. Changes in nutrition, infectious agents, environmental toxicants, and activity each cause metabolic mismatch that permits the cells and tissues to adapt to the current environment, and to strengthen the response to future encounters. Rebound growth after transient metabolic inhibition can result in changes in the time-dependent choreography of brain development. Mitocellular hormesis to severe stress can produce a chronic and pathological increase in many components of mitochondrial metabolism, and to an increase in extracellular ATP (eATP). eATP is a damage-associated molecular pattern (DAMP) that binds to purinergic receptors (P2X and P2Y) on all cells, triggering innate immunity and inflammation, alters brain synapse formation, and contributes to neurochemically mediated excitotoxicity. When this happens during vulnerable periods of brain development, between the late first trimester and the first two years of life, the risk of ASD might be increased.

Several excellent reviews on extracellular nucleotide signaling via purinergic receptors have recently appeared (Abbracchio et al., 2009; Burnstock and Verkhratsky, 2009; Surprenant and North, 2009). P2X receptors are ATP-gated cation channels that regulate calcium conductance. These are known as the ionotropic purinergic receptors. P2Y receptors are G-protein coupled receptors (GPCRs), collectively called the metabotropic purinergic receptors. In humans, there are seven subclasses of P2X receptor, designated P2X1–7. There are eight subclasses of P2Y receptor,

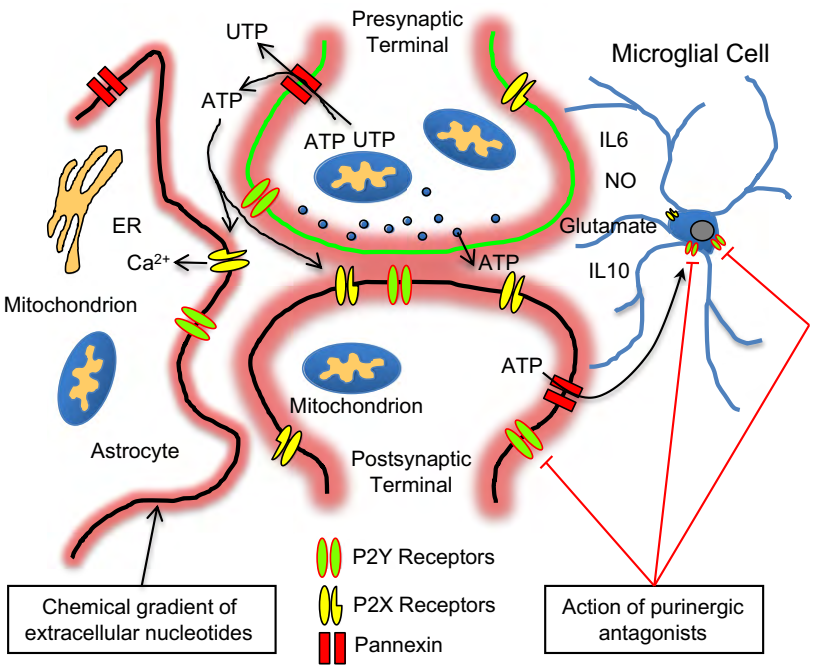

FIGURE 2.5.4 Purinergic regulation of synaptogenesis. ATP is a co-neurotransmitter at every synapse studied to date. Mitochondria are the ultimate source of extracellular ATP (eATP). The activity and usage of each synapse regulates that concentration of eATP surrounding the synaptic junction. Microglial cells monitor synaptic activity and respond to eATP to either stabilize or inhibit synapse formation. Excitotoxicity results in excessive eATP that binds to microglial purinergic receptors and stimulates neuroinflammation. ER = endoplasmic reticulum; IL = interleukin; NO = nitric oxide.

designated P2Y1, 2, 4, 6, 11, 12, 13, and 14 (P2Y 3, 5, 7, 8, 9, and 10 were subsequently removed from the list) (Jacobson and Boeynaems, 2010). P2X receptors are all ATP-gated. P2Y agonists differ according to subtype. ATP, UTP, ADP, UDP, and UDP-glucose are used selectively by different subtypes. EC_{50}s are typically in the micromolar range. Nucleotide signaling via P2X and P2Y receptors mediates a large number of biological phenomena of relevance to autism. These include normal synaptogenesis and brain development (Abbracchio et al., 2009), regulation of the PI3K/AKT pathway (Franke et al., 2009), control of immune responses and chronic inflammation (Pelegrin, 2008), gut motility (Gallego et al., 2008), gut permeability (Matos et al., 2007), taste chemosensory transduction (Surprenant and North, 2009), sensitivity to food allergies (Leng et al., 2008), hearing (Housley et al., 2002), innate immune signaling, neuroinflammation, antiviral signaling, microglial activation, neutrophil chemotaxis, autophagy, and chronic pain syndromes (Abbracchio et al., 2009). Figure 2.5.4 illustrates the role of purinergic receptors in the types of cell which play a role in normal synapse formation. The role of purinergic signaling in ASD has not yet been reported but is under active investigation in the author's laboratory. From the perspective of brain development and function, purinergic signaling represents an important new area for study in ASD as it has direct effects on pathways implicated in ASD (see Section 4).

SUMMARY

Recently, the connections between mitochondria and ASD have become increasingly clear. The nature of this connection is more complex than previously thought. Simple reduction in mitochondrial function does not cause ASD. A small, but informative, fraction of autism is caused by single-gene defects or DNA copy number variations. The large majority of ASD is the result of variation in hundreds of genes and loci interacting with environmental and other factors. The crossroads of genes and environment is metabolism. Mitocellular hormesis is the adaptation of cellular and mitochondrial metabolism to environmental change. Changes in nutrition, infectious agents, environmental toxicants, intellectual attention, and physical activity each play a role in mitocellular hormesis during children's development. Definite mitochondrial disease is responsible for as much as 5% of ASD. However, pathological disturbances in mitochondrial metabolism leading to excitotoxicity may lie at the heart of a larger proportion of ASD and this is an important area for future studies.

ACKNOWLEDGMENTS

RKN thanks the UCSD Christini Fund, the Wright Foundation, the Lennox Foundation, the Jane Botsford Johnson Foundation, and the Hailey's Wish Foundation for their support. RKN thanks Roman Sasik, Gary Hardiman, and Narimene Lakmine for assistance in creating the chromosomal map of mitochondrial proteins.

References

Abbracchio, M.P., Burnstock, G., Verkhratsky, A., Zimmermann, H., 2009. Purinergic signalling in the nervous system: An overview. Trends In Neurosciences 32, 19–29.

Applegarth, D.A., Toone, J.R., Lowry, R.B., 2000. Incidence of inborn errors of metabolism in British Columbia, 1969-1996. Pediatrics 105, e10.

Ashwood, P., Schauer, J., Pessah IN, Van de Water, J., 2009. Preliminary evidence of the in vitro effects of BDE-47 on innate immune responses in children with Autism spectrum disorders. Journal of Neuroimmunology 208, 130–135.

Bernier, F.P., Boneh, A., Dennett, X., Chow, C.W., Cleary, M.A., Thorburn, D.R., 2002. Diagnostic criteria for respiratory chain disorders in adults and children. Neurology 59, 1406–1411.

Burnstock, G., Verkhratsky, A., 2009. Evolutionary origins of the purinergic signalling system. Acta Physiologica (Oxford) 195, 415–447.

Cavalier-Smith, T., 2006. Origin of mitochondria by intracellular enslavement of a photosynthetic purple bacterium. Proceedings Biological Sciences 273, 1943–1952.

Chandrasekaran, K., Mehrabian, Z., Li, X.L., Hassel, B., 2004. RNase-L regulates the stability of mitochondrial DNA-encoded mRNAs in mouse embryo fibroblasts. Biochemical and Biophysical Research Communications 325, 18–23.

Coburn, C.G., Curras-Collazo, M.C., Kodavanti, P.R., 2008. In vitro effects of environmentally relevant polybrominated diphenyl ether (PBDE) congeners on calcium buffering mechanisms in rat brain. Neurochemical Research 33, 355–364.

Cohen, B.H., Naviaux, R.K., 2010. The clinical diagnosis of POLG disease and other mitochondrial DNA depletion disorders. Methods 51, 364–373.

Corcoran, J.A., Saffran, H.A., Duguay, B.A., Smiley, J.R., 2009. Herpes simplex virus UL12.5 targets mitochondria through a mitochondrial localization sequence proximal to the N terminus. Journal of Virology 83, 2601–2610.

Curran, L.K., Newschaffer, C.J., Lee, L.C., Crawford, S.O., Johnston, M.V., Zimmerman, A.W., 2007. Behaviors associated with fever in children with Autism spectrum disorders. Pediatrics 120, e1386–1392.

DiMauro, S., Bonilla, E., Lee, C.P., Schotland, D.L., Scarpa, A., Conn H., Jr., et al., 1976. Luft's disease: Further biochemical and ultrastructural studies of skeletal muscle in the second case. Journal of the Neurological Sciences 27, 217–232.

DiMauro, S., Hirano, M., Schon, E.A., 2006. Mitochondrial Medicine. Informa Healthcare.

Edmonds, J.L., Kirse, D.J., Kearns, D., Deutsch, R., Spruijt, L., Naviaux, R.K., 2002. The otolaryngological manifestations of mitochondrial disease and the risk of neurodegeneration with infection. Archives of Otolaryngology 128, 355–362.

Falk, M.J., 2010. Neurodevelopmental manifestations of mitochondrial disease. Journal of Developmental and Behavioral Pediatrics 31, 610–621.

Franke, H., Sauer, C., Rudolph, C., Krugel, U., Hengstler, J.G., Illes, P., 2009. P2 receptor-mediated stimulation of the PI3-K/Akt-pathway in vivo. Glia 57, 1031–1045.

Frye, R.E., Naviaux, R.K., 2011. Autistic disorder with complex IV overactivity: A new mitochondrial syndrome. Journal of Pediatric Neurology 9, 427–434.

Gallego, D., Vanden Berghe, P., Farre, R., Tack, J., Jimenez, M., 2008. P2Y1 receptors mediate inhibitory neuromuscular transmission and enteric neuronal activation in small intestine. Neurogastroenterology and Motility 20, 159–168.

Gellerich, F.N., Gizatullina, Z., Trumbeckaite, S., Nguyen, H.P., Pallas, T., Arandarcikaite, O., et al., 2010. The regulation of OXPHOS by extramitochondrial calcium. Biochimica et Biophysica Acta 1797, 1018–1027.

Gorski, C., 2008. Dialogue about the potential links between mitochondrial disease and Autism spectrum disorders begins at Indy. UMDF News Release, June 17.

Gourine, A.V., Dale, N., Llaudet, E., Poputnikov, D.M., Spyer, K.M., Gourine, V.N., 2007. Release of ATP in the central nervous system during systemic inflammation: Real-time measurement in the hypothalamus of conscious rabbits. Journal of Physiology 585, 305–316.

Graf, W.D., Marin-Garcia, J., Gao, H.G., Pizzo, S., Naviaux, R.K., Markusic, D., et al., 2000. Autism associated with the mitochondrial DNA G8363A transfer RNA(Lys) mutation. Journal of Child Neurology 15, 357–361.

Guilmatre, A., Dubourg, C., Mosca, A.L., Legallic, S., Goldenberg, A., Drouin-Garraud, V., et al., 2009. Recurrent rearrangements in synaptic and neurodevelopmental genes and shared biologic pathways in schizophrenia, Autism and mental retardation. Archives of General Psychiatry 66, 947–956.

Haas, R.H., 2010. Autism and mitochondrial disease. Developmental Disabilities Research Reviews 16, 144–153.

Haas, R.H., Parikh, S., Falk, M.J., Saneto, R.P., Wolf, N.I., Darin, N., et al., 2008. The in-depth evaluation of suspected mitochondrial disease. Molecular Genetics and Metabolism.

Hansen, R.L., Ozonoff, S., Krakowiak, P., Angkustsiri, K., Jones, C., Deprey, L.J., et al., 2008. Regression in Autism Prevalence and associated factors in the CHARGE Study. Ambulatory Pediatrics 8, 25–31.

Helt, M., Kelley, E., Kinsbourne, M., Pandey, J., Boorstein, H., Herbert, M., et al., 2008. Can children with Autism recover? If so, how? Neuropsychology Review 18, 339–366.

Hollander, E., Chaplin, W., Soorya, L., Wasserman, S., Novotny, S., Rusoff, J., et al., 2010. Divalproex sodium vs placebo for the treatment of irritability in children and adolescents with Autismspectrum disorders. Neuropsychopharmacology 35, 990–998.

Holt, I.J., Harding, A.E., Morgan-Hughes, J.A., 1988. Deletions of muscle mitochondrial DNA in patients with mitochondrial myopathies. Nature 331, 717–719.

Housley, G.D., Jagger, D.J., Greenwood, D., Raybould, N.P., Salih, S.G., Jarlebark, L.E., et al., 2002. Purinergic regulation of sound transduction and auditory neurotransmission. Audiology and Neurotology 7, 55–61.

Jacobson, K.A., Boeynaems, J.M., 2010. P2Y nucleotide receptors: Promise of therapeutic applications. Drug Discovery Today 15, 570–578.

James, S.J., Cutler, P., Melnyk, S., Jernigan, S., Janak, L., Gaylor, D.W., et al., 2004. Metabolic biomarkers of increased oxidative stress and impaired methylation capacity in children with Autism. The American Journal of Clinical Nutrition 80, 1611–1617.

Jepson, B., Granpeesheh, D., Tarbox, J., Olive, M.L., Stott, C., Braud, S., et al., 2011. Controlled evaluation of the effects of hyperbaric oxygen therapy on the behavior of 16 children with Autism spectrum disorders. Journal of Autism and Developmental Disorders 41, 575–588.

Ji, L.L., Gomez-Cabrera, M.C., Vina, J., 2006. Exercise and hormesis: Activation of cellular antioxidant signaling pathway. Annals of the New York Academy of Sciences 1067, 425–435.

Johnson, D.T., Harris, R.A., Blair, P.V., Balaban, R.S., 2007. Functional consequences of mitochondrial proteome heterogeneity. American Journal of Physiology - Cell Physiology 292, C698–C707.

Jolous-Jamshidi, B., Cromwell, H.C., McFarland, A.M., Meserve, L.A., 2010. Perinatal exposure to polychlorinated biphenyls alters social behaviors in rats. Toxicology Letters 199, 136–143.

Kanner, L., 1943. Autistic distubances of affective contact. The Nervous Child 2, 217–250.

Kauffman, M.A., Gonzalez-Moron, D., Consalvo, D., Westergaard, G., Vazquez, M., Mancini, E., et al., 2012. Diagnosis of mitochondrial disorders applying massive pyrosequencing. Molecular Biology Reports.

Leng, Y., Yamamoto, T., Kadowaki, M., 2008. Alteration of cholinergic, purinergic and sensory neurotransmission in the mouse colon of food allergy model. Neuroscience Letters 445, 195–198.

Luft, R., Ikkos, D., Palmieri, G., Ernster, L., Afzelius, B., 1962. A case of severe hypermetabolism of nonthyroid origin with a defect in the maintenance of mitochondrial respiratory control: A correlated clinical, biochemical, and morphological study. Journal of Clinical Investigation 41, 1776–1804.

Matos, J., Blanco, M.G., Maslen, S., Skehel, J.M., West, S.C., 2011. Regulatory control of the resolution of DNA recombination intermediates during meiosis and mitosis. Cell 147, 158–172.

Matos, J.E., Sorensen, M.V., Geyti, C.S., Robaye, B., Boeynaems, J.M., Leipziger, J., 2007. Distal colonic Na(+) absorption inhibited by luminal P2Y(2) receptors. Pflügers Arch 454, 977–987.

Mimaki, M., Hatakeyama, H., Komaki, H., Yokoyama, M., Arai, H., Kirino, Y., et al., 2010. Reversible infantile respiratory chain deficiency: A clinical and molecular study. Annals of Neurology 68, 845–854.

Mouridsen, S.E., Bronnum-Hansen, H., Rich, B., Isager, T., 2008. Mortality and causes of death in Autism spectrum disorders: An update. Autism 12, 403–414.

Munnich, A., Rotig, A., Chretien, D., Cormier, V., Bourgeron, T., Bonnefont, J.P., et al., 1996. Clinical presentation of mitochondrial disorders in childhood. Journal of Inherited Metabolic Disease 19, 521–527.

Napolioni, V., Persico, A.M., Porcelli, V., Palmieri, L., 2011. The mitochondrial aspartate/glutamate carrier AGC1 and calcium homeostasis: Physiological links and abnormalities in Autism. Molecular Neurobiology 44, 83–92.

Nass, M.M., Nass, S., 1963. Intramitochondrial fibers with DNA characteristics. I. Fixation and electron staining reactions. The Journal of Cell Biology 19, 593–611.

Naviaux, R.K., 1997. The spectrum of mitochondrial disease. In: Mitochondrial and metabolic disorders: a primary care physcian's guide. Psy-Ed Corporation, Oradell, NJ, pp. 3–10.

Naviaux, R.K., 2004. Developing a systematic approach to the diagnosis and classification of mitochondrial disease. Mitochondrion 4, 351–361.

Oliveira, G., Ataide, A., Marques, C., Miguel, T.S., Coutinho, A.M., Mota-Vieira, L., et al., 2007. Epidemiology of Autismspectrum disorder in Portugal: Prevalence, clinical characterization, and medical conditions. Developmental Medicine & Child Neurology 49, 726–733.

Pagliarini, D.J., Calvo, S.E., Chang, B., Sheth, S.A., Vafai, S.B., Ong, S.E., et al., 2008. A mitochondrial protein compendium elucidates complex I disease biology. Cell 134, 112–123.

Palmieri, L., Papaleo, V., Porcelli, V., Scarcia, P., Gaita, L., Sacco, R., et al., 2010. Altered calcium homeostasis in Autismspectrum

disorders: Evidence from biochemical and genetic studies of the mitochondrial aspartate/glutamate carrier AGC1. Molecular Archives of General 15, 38–52.

Pang, T., Cardosa, M.J., Guzman, M.G., 2007. Of cascades and perfect storms: The immunopathogenesis of Dengue haemorrhagic fever-Dengue shock syndrome (DHF/DSS). Immunology & Cell Biology 85, 43–45.

Partin, J.C., 1994. Reye's Syndrome. In: Suchy, F. (Ed.), Liver Disease in Children. Mosby, St. Louis, MO, pp. 653–671.

Pastural, E., Ritchie, S., Lu, Y., Jin, W., Kavianpour, A., Khine Su-Myat, K., et al., 2009. Novel plasma phospholipid biomarkers of Autism: Mitochondrial dysfunction as a putative causative mechanism. Prostaglandins Leukot Essent Fatty Acids 81, 253–264.

Patterson, P.H., 2009. Immune involvement in schizophrenia and Autism: Etiology, pathology and animal models. Behavioural Brain Research 204, 313–321.

Pelegrin, P., 2008. Targeting interleukin-1 signaling in chronic inflammation: Focus on P2X(7) receptor and Pannexin-1. Drug News Perspect 21, 424–433.

Pinto, D., Pagnamenta, A.T., Klei, L., Anney, R., Merico, D., Regan, R., et al., 2010. Functional impact of global rare copy number variation in Autism spectrum disorders. Nature 466, 368–372.

Poling, J.S., Frye, R.E., Shoffner, J., Zimmerman, A.W., 2006. Developmental regression and mitochondrial dysfunction in a child-with Autism. Journal of Child Neurology 21, 170–172.

Rahman, S., Blok, R.B., Dahl, H.H., Danks, D.M., Kirby, D.M., Chow, C.W., et al., 1996. Leigh syndrome: Clinical features and biochemical and DNA abnormalities. Annals of Neurology 39, 343–351.

Ristow, M., Zarse, K., 2010. How increased oxidative stress promotes longevity and metabolic health: The concept of mitochondrial hormesis (mitohormesis). Experimental Gerontology 45, 410–418.

Rossignol, D.A., Frye, R.E., 2011. Mitochondrial dysfunction in Autism spectrum disorders: A systematic review and meta-analysis. Molecular Psychiatry.

Rossignol, D.A., Rossignol, L.W., Smith, S., Schneider, C., Logerquist, S., Usman, A., et al., 2009. Hyperbaric treatment for children with Autism A multicenter, randomized, double-blind, controlled trial. BMC Pediatrics 9, 21.

Rotig, A., Lebon, S., Zinovieva, E., Mollet, J., Sarzi, E., Bonnefont, J.P., et al., 2004. Molecular diagnostics of mitochondrial disorders. Biochimica et Biophysica Acta 1659, 129–135.

Sadun, A.A., La Morgia, C., Carelli, V., 2011. Leber's Hereditary Optic Neuropathy. Current Treatment Options in Neurology 13, 109–117.

Saneto, R.P., Naviaux, R.K., 2010. Polymerase gamma disease through the ages. Developmental Disabilities Research Reviews 16, 163–174.

Saneto, R.P., Lee, I.C., Koenig, M.K., Bao, X., Weng, S.W., Naviaux, R.K., et al., 2010. POLG DNA testing as an emerging standard of care before instituting valproic acid therapy for pediatric seizure disorders. Seizure 19, 140–146.

Sano, M., Fukuda, K., 2008. Activation of mitochondrial biogenesis by hormesis. Circulation Research 103, 1191–1193.

Schaefer, A.M., McFarland, R., Blakely, E.L., He, L., Whittaker, R.G., Taylor, R.W., et al., 2008. Prevalence of mitochondrial DNA disease in adults. Annals of Neurology 63, 35–39.

Schaeffler, A., Gross, P., Buettner, R., Bollheimer, C., Buechler, C., Neumeier, M., et al., 2009. Fatty acid-induced induction of Toll-like receptor-4/nuclear factor-kappaB pathway in adipocytes links nutritional signalling with innate immunity. Immunology 126, 233–245.

Shen, P., Wang, W., Krishnakumar, S., Palm, C., Chi, A.K., Enns, G.M., et al., 2011. High-quality DNA sequence capture of 524 disease candidate genes. Proceedings of the National Academy of Sciences USA 108, 6549–6554.

Shoffner, J., Hyams, L., Langley, G.N., Cossette, S., Mylacraine, L., Dale, J., et al., 2010. Fever plus mitochondrial disease could be risk factors for autistic regression. Journal of Child Neurology 25, 429–434.

Singh, K.K., Kulawiec, M., Still, I., Desouki, M.M., Geradts, J., Matsui, S., 2005. Inter-genomic cross talk between mitochondria and the nucleus plays an important role in tumorigenesis. Gene 354, 140–146.

Staples, J.F., Brown, J.C., 2008. Mitochondrial metabolism in hibernation and daily torpor: A review. Journal of Comparative Physiology B. Biochemical, Systemic, and Environmental Physiology 178, 811–827.

Stobbe, M., 2008. Parents Speak Out on Vaccine Settlement. In: Washington Post, March 6. Associated Press, Washington, DC.

Suliman, H.B., Welty-Wolf, K.E., Carraway, M.S., Schwartz, D.A., Hollingsworth, J.W., Piantadosi, C.A., 2005. Toll-like receptor 4 mediates mitochondrial DNA damage and biogenic responses after heat-inactivated E. coli. FASEB Journal 19, 1531–1533.

Surprenant, A., North, R.A., 2009. Signaling at purinergic P2X receptors. Annual Review of Physiology 71, 333–359.

Trauner, D., Sweetman, L., Holm, J., Kulovich, S., Nyhan, W.L., 1977. Biochemical correlates of illness and recovery in Reye's syndrome. Annals of Neurology 2, 238–241.

UMDF, 2007. United Mitochondrial Disease Foundation (UMDF) Scientific & Medical Advisory Board statement on hyperbaric oxygen Therapy. Mitochondrial News 12, 1–20.

Vasta, V., Ng, S.B., Turner, E.H., Shendure, J., Hahn, S.H., 2009. Next generation sequence analysis for mitochondrial disorders. Genome Medicine 1, 100.

Verity, C.M., Stellitano, L.S., Winstone, A.M., 2011. The PIND study found no association between vaccination and Autismin mitochondrial disease – correction. Developmental Medicine & Child Neurology 53, 477.

Verity, C.M., Winstone, A.M., Stellitano, L., Krishnakumar, D., Will, R., McFarland, R., 2010. The clinical presentation of mitochondrial diseases in children with progressive intellectual and neurological deterioration: A national, prospective, population-based study. Developmental Medicine & Child Neurology 52, 434–440.

Wallace, D.C., Singh, G., Lott, M.T., Hodge, J.A., Schurr, T.G., Lezza, A.M., et al., 1988. Mitochondrial DNA mutation associated with Leber's hereditary optic neuropathy. Science 242, 1427–1430.

Wallace, D.C., Zheng, X.X., Lott, M.T., Shoffner, J.M., Hodge, J.A., Kelley, R.I., et al., 1988. Familial mitochondrial encephalomyopathy (MERRF): Genetic, pathophysiological, and biochemical characterization of a mitochondrial DNA disease. Cell 55, 601–610.

Wallis C (2008) Case Study: Autismand Vaccines Time Magazine, March 10. Available at: <http://www.time.com/time/health/article/0, 8599, 1721109,00.html> (accessed 24.05.12).

Weiss, M.D., Saneto, R.P., 2010. Sensory ataxic neuropathy with dysarthria and ophthalmoparesis (SANDO) in late life due to compound heterozygous POLG mutations. Muscle and Nerve 41, 882–885.

Weissman, J.R., Kelley, R.I., Bauman, M.L., Cohen, B.H., Murray, K.F., Mitchell, R.L., et al., 2008. Mitochondrial disease in Autismspectrum disorder patients: A cohort analysis. PLoS ONE 3, e3815.

West, A.P., Shadel, G.S., Ghosh, S., 2011. Mitochondria in innate immune responses. Nature Reviews Immunology 11, 389–402.

Wilson, J.M., 2009. Lessons learned from the gene therapy trial for ornithine transcarbamylase deficiency. Molecular Genetics and Metabolism 96, 151–157.

Wong, L.J., 2010. Molecular genetics of mitochondrial disorders. Developmental Disabilities Research Reviews 16, 154–162.

Wong, L.J., Scaglia, F., Graham, B.H., Craigen, W.J., 2010. Current molecular diagnostic algorithm for mitochondrial disorders. Molecular Genetics and Metabolism 100, 111–117.

Xu, C., Li, C.Y., Kong, A.N., 2005. Induction of phase I, II and III drug metabolism/transport by xenobiotics. Archives of Pharmacal Research 28, 249–268.

Yap, I.K., Angley, M., Veselkov, K.A., Holmes, E., Lindon, J.C., Nicholson, J.K., 2010. Urinary metabolic phenotyping differentiates children with Autismfrom their unaffected siblings and age-matched controls. Journal of Proteomic Research 9, 2996–3004.

Yuen, B., Boncompagni, S., Feng, W., Yang, T., Lopez, J.R., Matthaei, K.I., et al., 2012. Mice expressing T4826I-RYR1 are viable but exhibit sex- and genotype-dependent susceptibility to malignant hyperthermia and muscle damage. FASEB Journal 26, 1311–1322.

Zecchini, E., Siviero, R., Giorgi, C., Rizzuto, R., Pinton, P., 2007. Mitochondrial calcium signalling: Message of life and death. The Italian Journal of Biochemistry 56, 235–242.

Zeviani, M., Moraes, C.T., DiMauro, S., Nakase, H., Bonilla, E., Schon, E.A., et al., 1988. Deletions of mitochondrial DNA in Kearns-Sayre syndrome. Neurology 38, 1339–1346.

Zhang, Q., Raoof, M., Chen, Y., Sumi, Y., Sursal, T., Junger, W., et al., 2010. Circulating mitochondrial DAMPs cause inflammatory responses to injury. Nature 464, 104–107.

Zhao, X., Leon, I.R., Bak, S., Mogensen, M., Wrzesinski, K., Hojlund, K., et al., 2011. Phosphoproteome analysis of functional mitochondria isolated from resting human muscle reveals extensive phosphorylation of inner membrane protein complexes and enzymes. Molecular & Cellular Proteomics 10, M110.000299.

1521-0103/12/3423-608–618$25.00
THE JOURNAL OF PHARMACOLOGY AND EXPERIMENTAL THERAPEUTICS
Vol. 342, No. 3
192120/3789468

JPET 342:608–618, 2012

Perspectives in Pharmacology

Oxidative Shielding or Oxidative Stress?

Robert K. Naviaux

The Mitochondrial and Metabolic Disease Center, Departments of Medicine, Pediatrics, and Pathology, University of California San Diego School of Medicine, San Diego, California

Received March 2, 2012; accepted June 8, 2012

ABSTRACT

In this review I report evidence that the mainstream field of oxidative damage biology has been running fast in the wrong direction for more than 50 years. Reactive oxygen species (ROS) and chronic oxidative changes in membrane lipids and proteins found in many chronic diseases are not the result of accidental damage. Instead, these changes are the result of a highly evolved, stereotyped, and protein-catalyzed "oxidative shielding" response that all eukaryotes adopt when placed in a chemically or microbially hostile environment. The machinery of oxidative shielding evolved from pathways of innate immunity designed to protect the cell from attack and limit the spread of infection. Both oxidative and reductive stress trigger oxidative shielding. In the cases in which it has been studied explicitly, functional and metabolic defects occur in the cell before the increase in ROS and oxidative changes. ROS are the response to disease, not the cause. Therefore, it is not the oxidative changes that should be targeted for therapy, but rather the metabolic conditions that create them. This fresh perspective is relevant to diseases that range from autism, type 1 diabetes, type 2 diabetes, cancer, heart disease, schizophrenia, Parkinson's disease, and Alzheimer disease. Research efforts need to be redirected. Oxidative shielding is protective and is a misguided target for therapy. Identification of the causal chemistry and environmental factors that trigger innate immunity and metabolic memory that initiate and sustain oxidative shielding is paramount for human health.

Nothing in biology makes sense except in the light of evolution.
—Theodosius Dobzhansky (Dobzhansky, 1973)

Introduction

An alternative title for this review might be, "Oxidative stress or oxidative shielding: can 50 years of research be wrong?" To understand why cells might choose to defend themselves from harm by intentionally making reactive oxygen species (ROS), such as superoxide and hydrogen peroxide, and by stiffening the cell membrane to make it less permeable and less vulnerable to attack, we need to start at the beginnings of life on our planet. The great evolutionary pulses of metabolic and structural innovation of life on Earth can be correlated with changes in environmental oxygen (Holland, 2006). In the beginning, all life on Earth was anaerobic and oxygen was toxic. The first cells to emerge in the Precambrian seas were anaerobic bacteria that made ATP by anoxygenic photosynthesis. This life chemistry dates to approximately 3.5 billion years ago (GYA) (Cavalier-Smith, 2006). Most of the pathways of intermediary metabolism that we know today were developed during this anaerobic epoch of life's history on Earth. Isoprenyl and ubiquinol synthesis, fatty acid oxidation and synthesis, iron-sulfur cluster synthesis, glycolysis, carotenoid synthesis, the pentose phosphate pathway, the glyoxylate cycle, pyruvate dehydrogenase, cobalamin synthesis, heme synthesis, cytochromes, glutathione metabolism, electron transport, chemiosmotic proton-coupling for ATP synthesis, and both reductive and oxidative (reverse and forward) Krebs cycles all were present in the oldest bacteria known, the green sulfur bacteria (Tang and Blankenship, 2010). These and other bacterial primary producers fixed carbon from CO_2, fertilized the seas with organic molecules that later became food, and created the genetic tool

R.K.N. is supported by the University of California San Diego Christini Fund, the Wright Foundation, the Lennox Foundation, the Jane Botsford-Johnson Foundation, and the Hailey's Wish Foundation.
Article, publication date, and citation information can be found at http://jpet.aspetjournals.org.
http://dx.doi.org/10.1124/jpet.112.192120.

ABBREVIATIONS: ROS, reactive oxygen species; GYA, giga (10^9) years ago; Torr, millimeters of mercury pressure (mm Hg); GSH, glutathione; GSSG, GSH disulfide; CI, confidence interval; ER, endoplasmic reticulum; pO_2, oxygen partial pressure.

kit for intermediary metabolism on which all later life was based.

Oxygen came late on the scene. Beginning approximately 2.4 billion years ago, cyanobacteria started producing oxygen from photosynthesis in sufficient quantities to ventilate shallow seas and raise atmospheric oxygen levels to approximately 2 to 4% (Rasmussen et al., 2008; Hohmann-Marriott and Blankenship, 2011). This value of 2 to 4% oxygen [0.02–0.04 atm; 2–4 kilopascals; 15–30 Torr (mm Hg partial pressure) assuming an atmospheric pressure of 760 Torr at sea level] corresponds to approximately 20 to 40 μM dissolved oxygen in shallow, well mixed Precambrian seas. This is very close to the partial pressure of oxygen of most mammalian tissues at the end of capillary beds today and is also very close to the saturation midpoint of hemoglobin A of 28 Torr (Winslow, 2007). The first single-celled eukaryotes with mitochondria may have emerged as early as 1.7 to 1.1 GYA (Knoll et al., 2006; Brinkmann and Philippe, 2007). The saturation midpoint of modern mitochondria for oxygen in state 4 respiration is 0.2 Torr (0.025 kilopascals) or approximately 0.3 μM (Gnaiger et al., 1995). This creates a natural 150-fold oxygen gradient from ambient concentrations of 30 Torr outside the cell to 0.2 Torr at the site of oxygen consumption by the enzyme cytochrome *c* oxidase in each mitochondrion. These ancestral plant and animal cells were dispersed by the winds and tides as plankton, finding chemically unique niches, specializing, and sharing the Precambrian seas with bacteria and viruses. This rich ecology coevolved for a billion years before multicellularity took hold and expanded during the Cambrian approximately 0.54 GYA. The ability of cells to use oxygen to make ATP today, to detoxify it, and to release it as ROS for purposes of cell signaling and defense were developed during this pivotal Precambrian epoch. The free radical theory of aging was proposed by Harman (1956).

Self-defense is Nature's oldest law.
—John Dryden, "Absalom and Achitophel," (1681)

Mitochondria, Innate Immunity, and Cellular Defense

In this review I present evidence that one of the most ancient functions of mitochondria was cellular defense. Today we call this metabolic response to cellular attack or injury "innate immunity." Mitochondria play a central role in innate immunity today (West et al., 2011). This is the direct result of the role that bacterial ancestors or mitochondria played in the Earth's early oceans. The complex ecology of the Precambrian seas was replete with viruses and predatory intracellular bacteria (Wichels et al., 1998). No cells without effective defenses survived. The biochemical signature of an attack is a metabolic "steal" or diversion of electrons and resources such as nitrogen, phosphorus, iron, and copper. When limiting cellular resources are used by predators and parasites, those resources are not available to the host cell. Mitochondria are uniquely equipped to detect and respond to this metabolic steal. When the local chemistry of the cell provides nutrients and resources in concentrations that are matched to mitochondrial metabolism, mitochondria will create a normal oxygen gradient of approximately 30 outside the cell to 0.2 Torr in the mitochondrial matrix (Gnaiger et al., 1995) (see above). When cellular resources are consumed by a parasite, a "metabolic mismatch" is produced.

Mitochondria have a proteome of approximately 1500 proteins (Pagliarini et al., 2008). Nearly 1000 of these proteins have catalytic functions in cell metabolism, such as citrate synthase or malate dehydrogenase. Under normal physiologic conditions, the concentrations of thousands of nutrients and metabolic substrates in mitochondria are closely governed by the collective kinetic constants (K_m, K_{cat}, V_{max}, Hill coefficient, etc.) of all the enzymes responsible for transforming those metabolites. This has recently been computationally modeled in the Recon 1 and BiGG reconstructions of cell and organ metabolism (Schellenberger et al., 2010; Rolfsson et al., 2011). Only the primary structure of an enzyme is genetically determined. The activity of an enzyme at any instant in time is determined by ambient metabolic conditions. For example, the K_m of citrate synthase for oxaloacetate is approximately 2 μM, but the enzyme is allosterically inhibited by ATP, NADH, acetyl-CoA, palmitoyl-CoA, and the product citric acid, so the rate of converting oxaloacetate to citrate is changing minute to minute according to the condition of the cell (Shepherd and Garland, 1969). When the concentrations of substrates are perturbed by viral or microbial infection, disease, toxin, or nutritional excess, mitochondria sense this as a metabolic mismatch between the optimum concentration of those metabolites for a given tissue and the actual concentration.

This metabolic mismatch diverts electron flow away from mitochondria in the cell and decreases intramitochondrial electron flow, and mitochondrial oxygen consumption falls. When mitochondrial oxygen consumption (extraction) falls and the cell is still surrounded by 30 Torr (2–4%) oxygen supplied by capillaries, the concentration of oxygen in the cell rises sharply. When cellular oxygen rises, the redox of the cell rises, and the chemistry of polymer assembly (DNA, RNA, lipid, protein, and carbohydrate synthesis) is ultimately stopped because the NADPH/$NADP^+$ ratio falls as the change in Gibbs chemical free energy of synthetic reactions becomes less negative (more positive changes in Gibbs chemical free energy are thermodynamically less favorable). Under these more oxidizing conditions, electrons are no longer available for carbon-carbon bond formation to build biomass for viral or intracellular bacterial replication. Electrons are instead abstracted by the rising tide of intracellular oxygen to make superoxide, other ROS, and reactive nitrogen species and form bonds between free thiols in amino acids, such as cysteine, and peptides, such as glutathione, to make disulfides, such as cystine and the glutathione disulfide (GSSG). The rising tide of intracellular oxygen also oxidizes iron-sulfur clusters and redox-responsive sites in many proteins, inactivating proteins for macromolecular synthesis and activating proteins that shield the cell membrane from further attack. These include lipoxygenases and NF-κB (Serezani et al., 2011), NADPH oxidases (Jiang et al., 2011), redox-sensitive signaling systems in innate immunity such as the purinergic receptors (Hillmann et al., 2009), and transcriptional regulators such as Keap1/NRF2, and sirtuin-FOXO (Speciale et al., 2011). The net result of oxidative shielding in innate immunity is to limit the replication and prevent the exit of the invading pathogen.

Oxidative Shielding

Oxidative shielding is a stereotyped response to cellular injury or attack. To better understand the fundamental differences between the oxidative stress and the oxidative shielding perspectives it is helpful to ask and answer a few questions from the viewpoint of these two different schools of thought. This approach is similar to Galileo's dialog (Galileo, 2001) between adherents of Ptolemaic and Copernican systems as a method of showcasing their relative strengths and weaknesses.

What Triggers the Production of Superoxide, Hydrogen Peroxide, and Other ROS? Hostile, damaging, or unhealthy conditions surrounding the cell trigger the production of superoxide, hydrogen peroxide, and other ROS. Both stress and shielding schools agree with this answer.

Where Do the ROS Come From? ROS come from mitochondria and specialized enzyme systems in the cell. Both stress and shielding schools agree with this answer.

What Is the Function or Purpose of ROS? The shielding school holds that the function of ROS is, first, to protect the cell if possible, both as signaling molecules and by physically decreasing the cellular uptake, release, and exchange of potentially toxic pathogens or chemicals from and with the environment; and second, to actively kill the cell by apoptosis or necrosis when the local environmental conditions threaten to spread to neighboring cells and jeopardize the survival of host. ROS are an effect of disease, not the prime cause. In the shielding school, the organism is considered the ultimate unit of Darwinian selection. The fitness of an individual, in terms of its ability to reproduce, can be substantially increased by rapidly cutting off resources, walling off, or actively killing damaged or infected cells in a part of the body to save the whole.

The stress school holds that the function of ROS is to cause cell damage and disease.

What Is the Target of Effective Therapy in Diseases Associated with Increased ROS and ROS-Related Damage? The shielding school holds that because the prime cause of disease can ultimately be traced back to toxic exposure, microbial pathogen, unhealthy nutritional practices, nutrient loading, or unhealthy patterns of exercise and activity therapy should be directed at eliminating these causal factors. ROS production will naturally fall back to normal levels when physiologic balance is restored.

The stress school holds that because ROS are the prime cause of disease therapy should be directed at eliminating or normalizing ROS and ROS-related cell damage.

Randomized Clinical Trials

The scientific literature is rife with cell culture and animal experiments showing apparent benefits of antioxidant therapy and opinion papers that advocate antioxidants for treating everything from diabetes to cancer and Alzheimer's disease. However, the gold standard of proof in medicine is the randomized clinical trial. When antioxidants are put to the test in randomized clinical trials they generally fail or, worse, show evidence of unexpected harm. For example, in a meta-analysis of nine clinical trials that evaluated the benefit of treating type 2 diabetes with antioxidants such as α-tocopherol (vitamin E) there was no benefit (Suksomboon et al., 2011). Like many purified antioxidant vitamins, vitamin E is a two-edged sword. The reasons for this are not entirely clear, but may relate to the fact that therapeutic dosing of purified micronutrients and antioxidants intervenes in regulatory pathways that produce biochemical symptoms associated with cell defense, but are not the actual cause of disease. Vitamin E supplementation, alone or in combination with β-carotene, was shown to increase the risk of lung cancer in smokers (The Alpha-Tocopherol, Beta Carotene Cancer Prevention Study Group, 1994). Vitamin C supplementation was found to double the risk of cancer death in nonobese women [relative risk (RR) = 2.0; 95% CI = 1.12–3.58], while having no effect in obese women (Lin et al., 2009). The SELECT clinical trial of vitamin E and selenium was terminated early because of an apparent increase in the risk of new onset diabetes in the selenium group and a 1.6-fold increased risk in prostate cancer in the vitamin E group (Lippman et al., 2009; Klein et al., 2011). If ROS are at the heart of cancer, diabetes, and heart disease, why are antioxidants so ineffective at preventing or treating these diseases?

Other data that may prove helpful in weighing the merits of the schools of oxidative shielding versus oxidative stress are the results of clinical trials in which a therapy recommended by the shielding school, for example, diet and exercise (which is known to stimulate ROS; Niess and Simon, 2007), is directly compared with conventional medical intervention. When this is done in type 2 diabetes and its prodromal metabolic syndrome, diet and exercise are categorically superior to the best drug intervention. A recent meta-analysis of 13 clinical trials involving 3907 subjects found that the odds ratio for disease improvement with diet and exercise was 3.8 (95% CI = 2.5–5.9), but the odds ratios for disease improvement with drug treatment was 1.6 (95% CI = 1.0–2.5) (Dunkley et al., 2012). Diet and exercise can actually cure early type 2 diabetes while simultaneously reducing the risk of heart disease. In contrast, common drug interventions such as the thiazolidinedione insulin-sensitizing drug rosiglitazone will decrease diabetes, but increase the risk of heart failure (DREAM Trial Investigators et al., 2008).

Evolutionary Conservation of the Oxidative Shielding Response

The stereotyped oxidative shielding response to danger and metabolic mismatch can be identified in all aerobic forms of life on Earth. Even bacteria have it. For example, *Escherichia coli* rapidly generates superoxide and hydrogen peroxide in a manner reminiscent of mitochondria, by partially reducing oxygen at the site of NADH dehydrogenases and quinone acceptor sites along the inner membrane (Cabiscol et al., 2000). The magnitude of the response is regulated by nutrient availability, environmental toxin, and infection exposure (González-Flecha and Demple, 1997). It is noteworthy that ROS production by bacteria is highest under conditions of nutrient loading, similar to increased ROS production under nutrient loading in diabetes. Inhibitors of NADH dehydrogenase activity, such as the pesticides paraquat or rotenone, produce a rapid increase in ROS and mutation rates in the stressed bacteria (Cabiscol et al., 2000). Antioxidant defenses in aerobic bacteria are coordinately up-regulated by endogenously produced ROS by redox-reactive thiols on cys-

teines of peroxide-responsive OxyR and superoxide-sensitive SoxR transcription factors.

Plant cell ROS production leads to cross-linking of tyrosine-rich proteins in the cell wall (Bradley et al., 1992). Animal cells use many mechanisms including the use of another tyrosine-rich protein, melanin, and the production of collagen scar tissue to wall off the chronically disturbed or injured collection of cells. The initiating rise in intracellular oxygen that is caused by the failure of mitochondria to reduce oxygen to water is the hallmark of a metabolic "fever" or mismatch.

Why is it important to make the distinction between oxidative shielding and oxidative damage? When an oxidative shielding response is beneficial to the cell or the organism, then antioxidant treatments designed to block or reverse it will have two effects: 1) there will be no effect on the primary cause of the cellular toxicity, e.g., the viral infection, toxic exposure, or metabolic mismatch causing the cellular oxidative response, and 2) chronic treatment may ultimately prove harmful because it inhibits the highly evolved protective and hormetic functions of protein-catalyzed oxidative shielding.

Apoptosis, Cellular Altruism, and the Seductive Clarity of Cell Culture

Cell culture experiments have proved to be highly successful over the years in answering genetic questions. However, cell culture experiments have not been as reliable and are often misleading, in answering metabolic questions when the experiment is aimed at answering a question about multicellular development, organ function, or a whole animal phenotype. This happens because of four major differences between the metabolic conditions of cell culture and tissues. These can be briefly stated as the apoptosis, hyperoxia, cycling cell NADPH, and multicellularity problems.

Apoptosis: Bad for Cells in Culture, Good for the Species

Mitochondria are the principal regulators of apoptosis (Karbowski, 2010). This process lies at the heart of the developmental program of plants and animals that permits embryos to grow and remove cells that are no longer needed. Another essential function of apoptosis is the physical containment of injury or infection. Cells that become infected by viruses, or other microbial pathogens, initiate the program of apoptotic cell death to prevent the spread of infection. Many viruses and other microbes devote substantial genetic resources to thwart the infected cell's effort to commit suicide (Galluzzi et al., 2008). Evolution has preserved and refined the apoptotic program because it confers an increased fitness to the plant or animal during development and under attack. This can be seen as a form of cellular altruism without intent, in which the death and removal of a few infected, injured, or obsolete cells increases the likelihood of survival of the organism. Protein-catalyzed ROS production and membrane and protein oxidation events precede the commitment to apoptosis in most cell types. These genetic and metabolic pathways have been selected over evolutionary time to increase the fitness of the organism. Ultimately, the oxidative shielding response confers evolutionary advantage for the organism. This advantage cannot be seen in cell culture because the death of cells in culture occurs without reference to the survival of the whole organism.

Hyperoxia: The Uniquely Oxidizing Environment of the Culture Dish

Cells in culture are typically grown under ambient oxygen tensions of approximately 100 Torr that result from diffusion from a 21% oxygen atmosphere at sea level. They are not usually grown at the 2 to 4% oxygen (15–30 Torr) that is normal in tissues. Because all of the proteins involved in antioxidant defense evolved under physiologic conditions of 15 to 30 Torr oxygen, they typically have K_m values for oxygen in the 15- to 30-Torr range. Cell culture hyperoxia in the 30- to 100-Torr range will naturally activate antioxidant and pro-oxidant proteins that would otherwise be quiescent and substrate-limited. This makes the interpretation of oxidative changes in cell culture seductively clear. The measurement of a myriad of reactive oxygen species such as superoxide and hydrogen peroxide and biomarkers of oxidation such as lipid peroxidation is technically simple in cultured cells. However, the judgment that these changes are deleterious in the context of the whole organism is biologically unsound.

NADPH: The Electron Carrier for Biomass Synthesis, Not for Cell Work

Cycling cells have higher NADPH/$NADP^+$ ratios than postmitotic cells (Attene-Ramos et al., 2005). Cultured cells must double their biomass each day in preparation for division. Postmitotic cells in tissues do not. Postmitotic cells direct electrons to NADH for cellular work, not NADPH for biomass production. This essential difference between growing and nongrowing cells must be grasped before the different roles of mitochondria in growing and nongrowing cells can be understood. The synthesis of lipids, proteins, DNA, and RNA requires the use of electrons carried by NADPH to make new carbon-carbon and other chemical bonds. NADPH is made in large amounts by the pentose phosphate pathway in which glucose 6-phosphate is used before entering glycolysis to make ribose for DNA and RNA synthesis and NADPH for macromolecular synthesis and glutathione metabolism (Wamelink et al., 2008). When incoming electrons from glucose and other nutrients are directed to NADPH, those electrons are not available for NADH used in mitochondrial oxidative phosphorylation. The combined effect of increased NADPH and hyperoxia (21% O_2) in cell culture conspires to amplify superoxide and hydrogen peroxide production by NADPH oxidases, making the study of more subtle factors such as regulation of the pentose phosphate pathway by nitric oxide (Bolaños et al., 2008) and compartmental redox regulation during differentiation challenging or impossible.

Multicellularity and Metabolic Complementarity: The Autonomy of Cells in Culture

In cell culture, investigators necessarily remove the normal connectedness of cells in tissues. As a consequence, single cells in culture must be cell-autonomous, that is, they must synthesize everything they need for growth without

reliance on supplies from other cells. This is not the case in somatic tissues. In tissues, distant and neighboring cells adopt complementary metabolic functions. It is wasteful for photoreceptor cells in the eye, for example, to express genes that are used to produce muscle contraction in the heart. Likewise, it is wasteful and potentially toxic for all somatic cells to make a particular hormone such as insulin or testosterone. In another example, the cells of the liver lobule clearly differentiate along the gradient of oxygen established between the high oxygen present in the vicinity of the hepatic artery in the portal triads where ornithine transcarbamoylase is expressed and the low oxygen present in center of the lobule surrounding the portal vein where ornithine aminotransferase is expressed (Naviaux and McGowan, 2000). Somatic cells epigenetically silence unused genes by DNA methylation and other processes. The process of DNA methylation is regulated by folate, B12, and *S*-adenosylmethionine metabolism, which are also controlled by mitochondria (Naviaux, 2008). The natural metabolic cooperativity among differentiated cells in the body is lost in cell culture. No longer is there any selective pressure for cells to cooperate as they do in tissues and organs. No longer can the death of a few cells be clearly identified in the context of its evolutionary function to decrease the probability of death of the organism under stress. It is easy to see how an investigator studying cells in a dish might think that active cell processes that cause cell death, such as apoptosis and necrosis, are "bad." However, it is the pathway's oxidative shielding, and occasionally cell death, that permits the organism to live on and reproduce under the ever-changing conditions of life on Earth.

Tug at a single thread in Nature and you will find it connected to the rest of the Universe.
—modified from John Muir (1911) (Muir 1911)

Cell Metabolism Is Like an Ecosystem

The chemical reactions of the cell take place in a myriad of discrete locations and compartments within the cell that are maintained in thermodynamic disequilibrium. Natural redox boundaries and oxygen gradients are maintained by proteins and membranes in each of these compartments. Cell metabolism can be visualized intuitively as a coral reef ecosystem. The metabolic products of one compartment in the cell are used as resources by other compartments, just as one species of coral can provide resources for another species in the reef. Metabolism is a complex trophic web that stabilizes or destabilizes the differentiated function of the cell. Ultimately, the end products of metabolism are released from the cell into the blood and excreted in the urine, back into the external ecosystem. In both the coral reef and the microcosm of the cell, small-molecule metabolites and signaling molecules drive changes in gene expression, not the reverse. The success of transgenic and gene knockout experiments over the past 20 years has given scientists the impression that genes drive the evolution of metabolism. This is wrong. Rather, it is environmental nutrients and the small molecules of metabolism that drive the evolution of genes.

Over evolutionary time, genes and gene expression patterns evolved to handle the resources provided by the environment. Over shorter time periods of minutes to hours, and weeks to months, nutrients such as glucose, fats, and amino acids, and small molecules of metabolism are the forcing variables that induce the changes in enzyme activity and gene expression associated with feeding, fasting, and seasonal variations in nutrient availability. The amino acid leucine plays a central role in stimulating the master fuel regulator mammalian target of rapamycin (mTOR) and inhibiting AMP kinase and autophagy (Han et al., 2012).

Many intermediary metabolites act differently inside and outside the cell. Inside the cell they act as carbon skeletons for fat, protein, carbohydrate, DNA, and RNA synthesis. Outside the cell they act as signaling molecules that bind cell receptors and alter gene expression. For example, ATP is an energy-carrying molecule inside the cell. Outside the cell, ATP is a "mitokine" and damage-associated molecular pattern (Zhang et al., 2010) that binds ionotropic and metabotropic purinergic receptors, activating innate immunity and inflammatory pathways (Marques-da-Silva et al., 2011). Succinate is a Krebs cycle intermediate inside the cell, but binds the G protein-coupled receptor 91 (GPRC91) on the cell surface that can reverse the antiplatelet activity of aspirin (Spath et al., 2012). In another example, citric acid inside the cell is the namesake of the "citric acid cycle," known more commonly as the Krebs cycle. Outside the cell, citrate is a mobile carbon source and barometer of nutrient availability. Citrate is taken into cells via a cell surface transporter called INDY (for "I'm Not Dead Yet") that when mutated leads to cellular citrate depletion and mimics the life-extending effects of caloric restriction (Birkenfeld et al., 2011). These genetic manipulations illustrate the role of small-molecule metabolites as being prime regulators of cell gene expression. The literature on this topic of metabolic regulation of gene expression is extensive (for a recent review see Buchakjian and Kornbluth, 2010).

Metabolic Consequences of Nutrient Excess

In 1929, Herbert Crabtree used mouse cancer cells to show that when glucose was added to a medium oxygen consumption decreased (Crabtree, 1929). Mitochondria were not yet identified as the oxygen-consuming particles. Otto Warburg coined the term the "Atmungsferment," the iron and cytochrome-containing respiratory catalyst, to describe the site of oxygen consumption in cells (Warburg and Negelein, 1928) later discovered to be mitochondria. The Crabtree effect has been called the inverted Pasteur effect, because in the Pasteur effect exposure to oxygen was found to inhibit anaerobic glycolysis. The magnitude of the respiratory inhibition by glucose caused by the Crabtree effect varies between 5 and 50% (Ibsen, 1961) depending on the cell type and the concentration of glucose added. The Crabtree effect plays an important role in many conditions, including diabetes, in which persistently high levels of calories and glucose produce a relative decrease in mitochondrial oxygen consumption. There are several biochemical mechanisms that combine to produce the Crabtree effect under conditions of nutrient loading (Sussman et al., 1980). The most significant is the inhibitory effect of the cytosolically produced [ATP]/[ADP][Pi] ratio on mitochondrial ATP synthesis. This happens because mitochondrial oxidative phosphorylation requires cytosolic ADP and Pi to make ATP. When cytosolic ATP rises and ADP falls, ADP becomes limiting in mitochondria, and the ex-

cesses of cytosolic ATP inhibits the forward action of mitochondrial ATP synthase (complex V) by classic mechanisms of product inhibition. This induces a chemiosmotic backpressure of protons in the mitochondrial inner membrane space and hyperpolarizes the mitochondrial membrane, i.e., makes the mitochondrial membrane potential ($\Delta\psi_m$) more negative. Excess electrons that enter mitochondria under these conditions cannot be used to make ATP because of the backpressure. The partial reduction of oxygen to superoxide and peroxide serves as a "pressure release valve" (Fisher-Wellman and Neufer, 2012) that permits excess electrons to be dissipated and excess oxygen to be exported from the cell in the form of soluble hydrogen peroxide. All of these biophysical and thermodynamic consequences of nutrient loading result in a net decrease in mitochondrial oxygen consumption that we call the Crabtree effect.

Because mitochondria create the oxygen sink for the cell, when mitochondrial extraction of oxygen is decreased, cell and tissue oxygen levels rise, and the tissue extraction of oxygen from the blood falls. This is observed clinically as a decrease in the arteriovenous difference in pO_2. Physiologically, this is interpreted as "wasted" oxygenation. Ultimately, it results in the pruning of capillary beds and reductions in tissue vascularity, i.e., peripheral vascular disease. Over time, this leads to chronic tissue hypoxia, ischemia, and loss of organ function, to heart and kidney failure, and chronic neurodegenerative disease.

Tissue Hypoxia and Ocean Hypoxia: Universal Metabolic Response to Nutrient Loading

There is an ocean-scale analog to the cellular Crabtree effect. When excessive amounts of nutrients are concentrated in agricultural fertilizer runoff and urban waste and carried downriver to the ocean, the metabolism of plankton in the sea is changed. Ultimately, this process creates seasonal and persistent "dead zones" of ocean hypoxia (Diaz and Rosenberg, 2008) that cannot support coral, fish, shellfish, or any eukaryotic life larger than a nematode or a few small snails. Repopulating these lost ecosystems can take years of concerted remediation. Excessive "calories" and nutrients injected into the ocean trigger an ecosystem-scale Crabtree effect, in a biphasic process that is similar to type II diabetes. First, there is an inhibition of aerobic metabolism and a rapid increase in algal and cyanobacterial oxygenic photosynthesis to create plankton blooms. This occurs for the same metabolic reasons as in nutrient-loaded human cells; excess nutrients exceed the oxidative capacity of the cells and redirect these excess electrons to NADPH and biomass synthesis. Nonphotosynthetic cells also shift to this more fermentative metabolism to facilitate rapid conversion of the new nutrient resources to biomass. In diabetes, this shift to biosynthesis leads to organ hypertrophy and the accumulation of adipose tissue and intracellular fat. The net result in the ocean is a transient increase in water oxygen because of photosynthesis and decreased oxygen utilization by heterotrophs. This metabolic shift is quantified by biological oceanographers as an increase in bacterial growth efficiency (Azam and Malfatti, 2007). This first stage of hyperoxia is short-lived and rarely measured. This is similar to the situation in diabetic tissues exposed to excessive nutrients. The second stage of the response to nutrient loading is a decrease in water oxygen. In the ocean this occurs because the excess plankton biomass produced by the blooms dies and becomes fuel for other bacteria that extract oxygen from the water to process the dead biomass. Hypoxia results. In tissues, chronic nutrient excess leads to tissue hypoxia because of capillary pruning that results from decreased mitochondrial oxygen consumption as described above, and from decreased arteriovenous differences in pO_2. Initially, the tissue hypoxia from excess nutrient load is patchy, resulting in localized areas of ischemia and segments of dysfunction. Later, the patches of organ hypoxia begin to merge and significant organ dysfunction occurs.

Redox Compartments and Oxygen Gradients in the Cell

The intracellular "ecosystem" of the eukaryotic cell is comprised of at least eight different organellar compartments, each with its own redox poise (Fig. 1). These include: lysosomes (Gille and Nohl, 2000), smooth ER, rough ER (Hwang et al., 1992), the Golgi (Navas et al., 2010), the cytosol (Go and Jones, 2008), peroxisomes (Yano et al., 2010), the nucleus (Go and Jones, 2011), and the mitochondrial matrix (Go and Jones, 2008). These compartments are not in equilibrium because the proteins that maintain the redox in each compartment, and the membranes that separate them, are not diffusible (Jones, 2010). The standard redox potentials of each of these compartments with regard to the glutathione couple (GSH/GSSG) have been measured (Table 1).

In contrast to sharp boundaries of redox poise that define the different organelles of the cell, the concentration of oxygen at any point in the cell is determined by oxygen diffusion along its gradient from the capillary to the mitochondrial matrix. With a little imagination, one can imagine that each organelle "swims" to a point in the cellular ecosystem that best meets its need for oxygen and nutrients. The oxygen partial pressure of 40 Torr in venous plasma, 30 Torr in the pericellular space (Pittman, 2011), and 0.02 to 0.2 Torr (25–250 nM) in mitochondria (Scandurra and Gnaiger, 2010) can be conceptualized in an "oxygen well" or "target diagram" of the cell (Fig. 2A). When the measured glutathione redox couple is plotted against the log of the partial pressure of oxygen in Torr, a linear regression can be calculated. The formula for this line is: GSH/GSSG redox (in mV) = 82.6 × Log(oxygen in Torr) − 272 (Fig. 2B). This connection between oxygen concentration at every point along the oxygen diffusion gradient and compartmental redox helps explain the profound effect that small changes in mitochondrial oxygen consumption, leading to increased dissolved oxygen concentrations in throughout the extramitochondrial compartments of the cell, can have on the metabolic and work performance of the cell. Indeed, the cell cycle has been characterized as a redox cycle (Burhans and Heintz, 2009).

Cellular Thermodynamics and Work

Ilya Prigogine described the mathematics of dissipative systems in which physical work and the capacity for self-organization can be extracted from the environment by maintaining a compartmentalized, collective chemical "distance" from thermodynamic equilibrium (Prigogine, 1984). Mito-

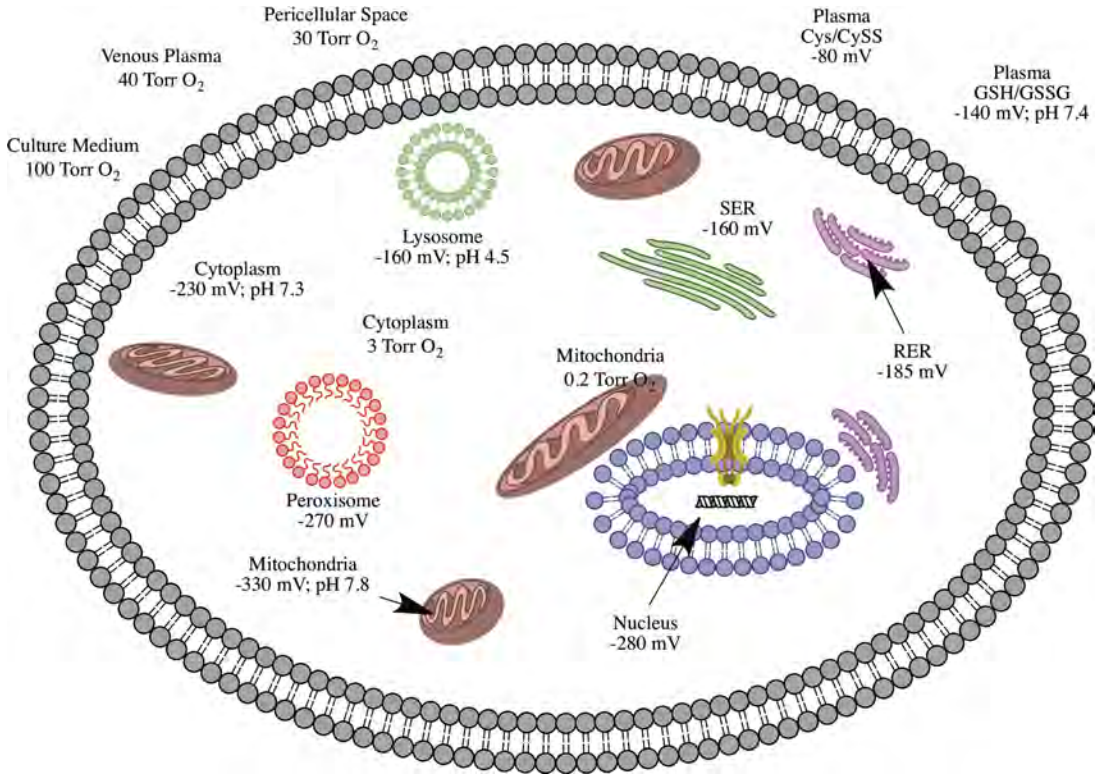

Fig. 1. Redox boundaries and oxygen tensions in the organellar compartments of the cell. Values of oxygen concentration, glutathione redox potential, pH, and associated references are listed in Table 1. Cys/CySS, cysteine/cystine; GSH/GSSG, glutathione/oxidized glutathione homodimer; SER, smooth endoplasmic reticulum; RER, rough endoplasmic reticulum.

TABLE 1

Compartmental redox and oxygen tension in mammalian cells

Glutathione redox potentials vary between 10 and 15% according to growth conditions in single cells and vary up to 20% in different cell types. Plasma redox potentials vary between 5 and 10% in a diurnal cycle and become up to 20 mV more oxidizing with age and disease (Go and Jones, 2011).

Compartment	pH	Glutathione Redox, GSH/GSSG	Dissolved Oxygen
		mV	*Torr*
Mitochondrial matrix	7.8–8.0	−330 (Go and Jones, 2008)	0.2 (Gnaiger et al., 1995; Scandurra and Gnaiger, 2010)
Nucleus	7.6	−280 (Go and Jones, 2011)	0.8*
Peroxisomes	7.6	−270 (Yano et al., 2010)	1*
Cytoplasm	7.3	−230 (Jones, 2010)	3*
Rough ER	7.3	−185 (Hwang et al., 1992)	11*
Smooth ER	7.3	−160 (Jones, 2010)	23*
Golgi	5.0 (Navas et al., 2010)	−160	23*
Lysosomes	4.5	−160 (Gille and Nohl, 2000)	23*
Pericellular space	7.4	−150	30 (Copp et al., 2009)
Venous plasma	7.3	−140 (Go and Jones, 2008)	40 (West, 2000)

* Estimated from the regression equation: $\text{Log}(pO_2 \text{ in Torr}) = (\text{mV redox} + 272) \div 82.6$.

chondria set a limit on the maximum free energy available for work by a cell by consuming oxygen and transforming metabolites. Highly aerobic mitochondria produce a deep oxygen gradient (Fig. 3) of nearly 150-fold, from 30 Torr in the pericellular space to 0.2 Torr (Scandurra and Gnaiger, 2010) at the site of cytochrome *c* oxidase in the inner mitochondrial membrane. The depth of the oxygen sink creates the potential energy that acts like a coiled spring to drive the living clockwork of metabolism, development, differentiation, and organ function.

Less active mitochondria maintain more shallow oxygen gradients and have a lower work capacity, but greater proliferative capacity. This is illustrated in Fig. 3, left. This occurs because electrons in the cytosol are redirected to NADPH and macromolecular synthesis and away from usage as NADH in mitochondria when oxygen consumption rates are lower (Fig. 3). The ultimate energy currency of the cell is electrons that enter the cell in the form of the chemical bonds in the carbon skeletons of nutrients such as glucose, amino acids, and fatty acids. Mitochondrial oxygen consumption determines the depth of the oxygen sink and ultimately tips the redox balance of the cell either toward growth and proliferation or to differentiation and work.

Metabolic Memory and Exercise

Short-duration physical or chemical stimuli produce long-term cellular effects by inducing kinetically linked chains of events that can be measured metabolically and by protein changes. This phenomenon is called metabolic memory. It is the result of post-translational activation and inhibition and transcriptional activation and inhibi-

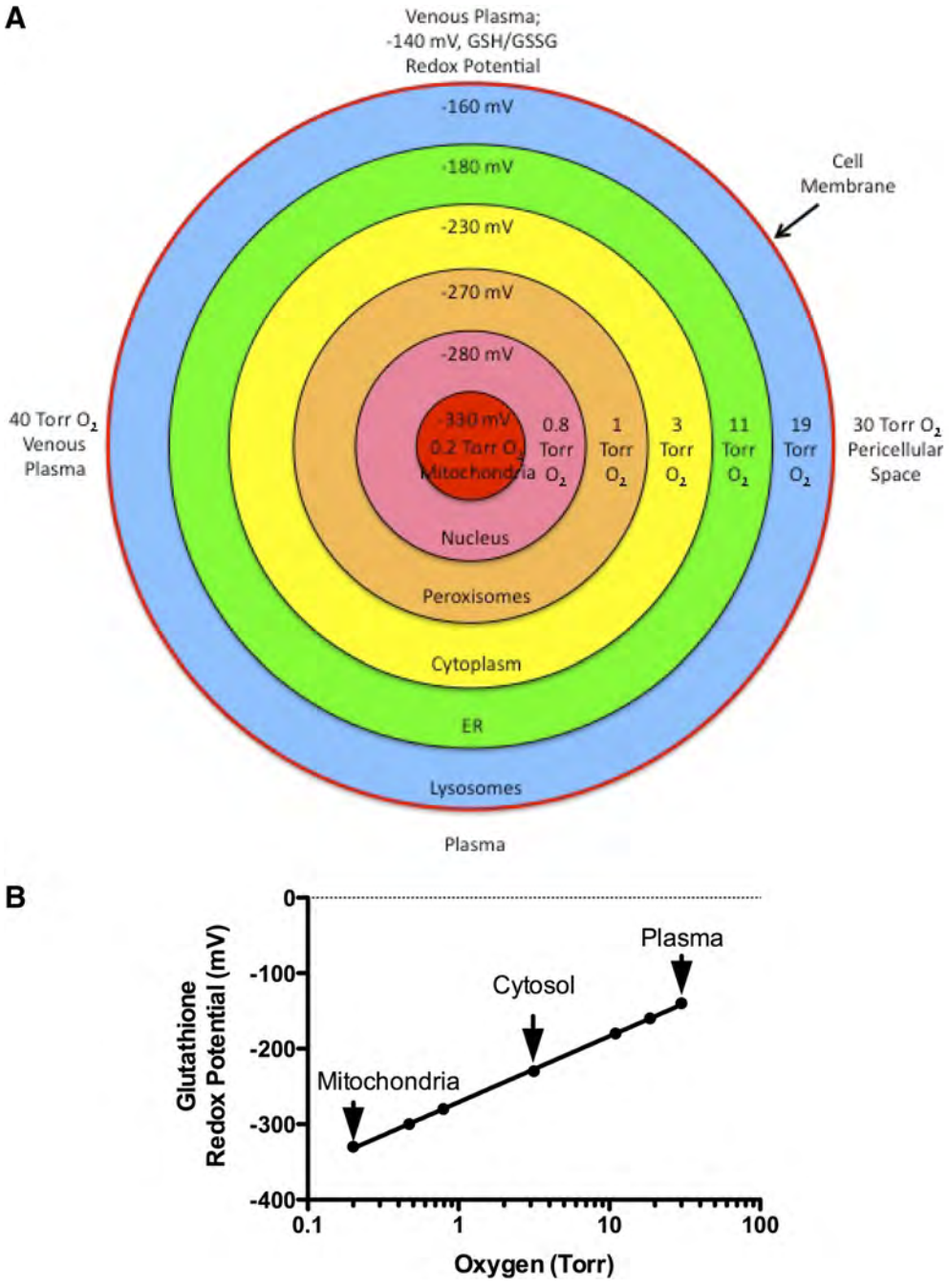

Fig. 2. Conceptualized oxygen well and redox diagram of the cell. A, oxygen well diagram and redox zones of the cell. This is a schematic that illustrates the measured standard redox potential of the glutathione couple (GSH/GSSG) in six compartments of the cell. B, semilog plot of the partial pressure of oxygen shows a linear correlation with compartmental redox potential. GSH/GSSG redox (in mV) = 82.6 × Log(oxygen in Torr) − 272.

tion events that are initiated by the short-duration stimulus. Many examples are known. The most widely reported example is the long-term effect of short-term, strict metabolic management in patients with diabetes. Even after the management of diabetes is relaxed long-term metabolic changes in insulin sensitivity and decreased incidence of vascular complications and end-organ disease are observed (Cooper, 2009).

Physical exercise is perhaps the best-known method of inducing metabolic memory. Even a single session of exercise will produce an increase in basal metabolic rate for hours after the session (LaForgia et al., 2006). Adaptive strength and cardiovascular benefits can be measured over days. Regular resistance training produces metabolic memory and reverses age-related changes in skeletal muscle over months (LaForgia et al., 2006). The mechanisms of these adaptive changes to exercise seem to require the transient pulses of ROS that are produced (Niess and Simon, 2007).

Antioxidant Therapy Inhibits the Benefits of Exercise

What happens if the normal amounts of superoxide and hydrogen peroxide produced during exercise are inhibited by treatment with antioxidants? In a ground-breaking study in 2009, Ristow et al. (2009) studied the effect of antioxidant supplements (vitamin C at 1000 mg/day; vitamin E at 400 IU/day) on insulin sensitivity and markers

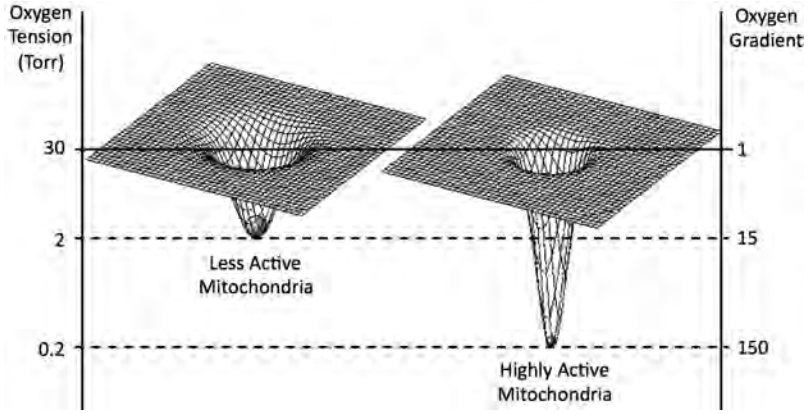

Fig. 3. Mitochondria create the oxygen gradient that generates the thermodynamic potential energy that drives metabolism and cellular work. Right, highly active mitochondria create a deep oxygen sink of 150-fold (30–0.2 Torr) that is highly electrophilic, attracting electrons in the form of NADH like iron to a magnet. This potential energy is harnessed like a coiled spring to power the functional capacity of the cell and provide metabolic reserves that are made available under times of stress. Left, less active mitochondria produce a shallower gradient of 15-fold in this example (30/2 Torr) and have a lower work capacity and less oxidative reserve, but are able to divert electrons more efficiently to NADPH for biosynthesis and cell proliferation.

such as plasma adiponectin and the master mitochondrial biogenesis regulator peroxisome proliferator-activated receptor-γ coactivator 1α (PGC1α) after 1 month of exercise. They found that the subjects who exercised and did not take antioxidant supplements had significant improvements in insulin sensitivity, adiponectin, and PGC1α. Antioxidants inhibited these metabolic benefits of exercise. Ristow et al. proposed that mitochondrial hormesis, or beneficial adaptation to stress, requires transient oxidative stress to induce the downstream changes in nuclear gene expression that promote health and longevity (Ristow and Schmeisser, 2011).

Antioxidant Treatment Decreases Tissue Perfusion

Experimental work has also been conducted to study the effects of vitamin C and the antioxidant tempol on skeletal muscle performance. When antioxidants were provided acutely, Copp et al. (2009) showed that spinotrapezius muscle contractile force was decreased 25%. Muscle blood flow was also reduced, and the resting oxygen tension in the skeletal muscle was reduced 14%, from 29.9 to 25.6 Torr (Copp et al., 2009). Copp et al. report that optimum blood flow and optimum contractile force depend on the redox state of skeletal muscle. Therefore, antioxidant therapy resulted in decreased muscle perfusion and contractile performance measured acutely (Copp et al., 2009) and interfered with the beneficial effects of exercise such as increased insulin sensitivity when measured after 1 month of supplementation (Ristow and Schmeisser, 2011).

Phytonutrients and Xenohormesis

Plants and animals that share an ecosystem coevolve. Many plants depend on mammals and birds for seed dispersal. Therefore, the survival of these plants depends on the survival of the mammals and birds that facilitate the dispersal of their seeds. If the coevolving animals do not survive a drought or other seasonal hardship, the plants also perish. Plants have developed secondary metabolites and small-molecule stress hormones such as resveratrol that not only help the plant survive, but also activate molecules such as the sirtuins in animal cells that produce a metabolic shift that improves drought and heat tolerance in the animals. Resveratrol is a polyphenol that activates the lysine-deacetylase activity of sirtuin 1 under conditions of caloric restriction that promote a high NAD+/NADH ratio. The principal health benefits of fruits and vegetables lie not just in the vitamins, minerals, and fiber they provide, but in the dozens to hundreds of phytonutrients such as the polyphenols, flavonoids, terpenoids, and quinones that have evolved to activate mammalian cellular targets such as sirtuins, cytoskeleton, tyrosine protein kinases, phosphoinositide 3 kinase, mitogen-activated protein kinases, and transcription factors such as Keap1 and NRF2 (Murakami and Ohnishi, 2012). Animals that consume foliage from stressed plants redirect energy resources away from reproductive pathways. This results in a decrease in fecundity. However, the animals benefit directly from an increase in their own heat and drought tolerance. This phenomenon in which coevolving plants produce signaling molecules that benefit ecologically connected animals is called "xenohormesis" (Howitz and Sinclair, 2008).

An important fact has emerged in the study of the antioxidant properties of plants. Just as in the response to exercise, the durable antioxidant effects of botanicals occur because of their acute, but transient, pro-oxidant (electrophilic and/or ROS-generating) effects (Speciale et al., 2011). Electrophiles abstract electrons from (oxidize) other molecules. Metabolically, this is similar to the action of intracellular microbial pathogens that "steal" electrons to make carbon-carbon bonds and replicate the parasite biomass at the expense of the cell. For this reason, the stereotyped metabolic responses antioxidant defenses and innate immunity are activated similarly by electrophiles and certain microbial pathogens. Potent phytonutrients such as curcumin in turmeric, quercetin in onions, sulforaphane in broccoli, and epigallocatechingallate in green tea produce their antioxidant effects by acting acutely as pro-oxidants in the cell and inducing metabolic hormesis. The electrophilic chemical nature of these compounds up-regulates Keap1/NRF2-mediated transcription of dozens of antioxidant defense genes that contain antioxidant response elements (electrophile response elements). These include enzymes for glutathione synthesis and metabolism (γ-glutamylcysteine synthetase, glutathione peroxidase, glutathione reductase, sulforedoxin, and thioredoxin), stress proteins such as heme oxygenase-1, and drug detoxification enzymes such as glutathione transferase and NADPH-quinone oxidoreductase, and cytokines such as interleukin-6 (Speciale et al., 2011).

Conclusions

ROS and oxidative changes in chronic disease are the symptoms of disease and not the cause. Indeed, transient and

regular stimulation of ROS production is required for mitochondrial hormesis and the beneficial physiologic adaptations associated with exercise and a diet rich in fruits and vegetables. Membrane lipid peroxidation, fibrosis, protein oxidation, and hundreds of other markers that were formerly cataloged as oxidative damage need to be understood as cellular oxidative shielding. The conserved pathways of oxidative shielding are protein-catalyzed reactions that evolved as the first steps in innate immunity. They evolved to protect the cell from chemical and microbial threats in the environment. Both oxidative and reductive stress will trigger cellular oxidative shielding. Oxidative shielding takes many forms in different bacterial, plant, and animal phyla. All forms ultimately increase membrane rigidity, decrease membrane permeability, and inhibit cell division. Systemwide conditions such as calorie restriction or nutrient loading modify the cellular response to stress. When stress coincides with dietary nutrient excess, cellular electrons are transferred preferentially to NADPH and not NADH, glycolytically synthesized ATP inhibits mitochondrial oxygen consumption via the Crabtree effect, and chronic inflammation results.

Research efforts need to be redirected. Catalogs of the many forms of oxidative changes that are found in 100 chronic diseases provide no insight into the underlying pathogenesis of disease. Treatment of oxidative changes in chronic disease with antioxidants is similar to treating a fever with aspirin instead of treating the pneumonia. If the clinical outcome selected for monitoring the disease is the fever, then aspirin will be "clinically proven" to be effective at improving the "disease." However, the untreated pneumonia might still kill the patient. It is better to "treat" the fever by treating the bacterial cause of the pneumonia. Certain antioxidants might be shown to decrease oxidative markers such as nitrotyrosine. However, nitrotyrosine-modified proteins are a symptom, not the disease. More patients will benefit when the true cause of the fever, the cause of the disease, is identified and treated.

New methods of targeted and untargeted metabolomics will help decode the language of metabolism in disease (Tautenhahn et al., 2011; Yanes et al., 2011) and assist physicians in providing personalized medical treatment. NextGen treatments will need to restore the normal "ecology" of metabolism. Complex diseases such as autism, autoimmune disease, diabetes, cancer, and kidney and cardiovascular disease do not have simple causes that are true for every patient. Personalized causes must be sought and new diagnostic tools developed. Identification of the causal chemistry and environmental factors that trigger innate immunity and metabolic memory that initiate and sustain oxidative shielding will lead to fresh new therapies for old diseases.

References

Alpha-Tocopherol, Beta Carotene Cancer Prevention Study Group (1994) The effect of vitamin E and beta carotene on the incidence of lung cancer and other cancers in male smokers. *N Eng J Med* **330:**1029–1035.

Attene-Ramos MS, Kitiphongspattana K, Ishii-Schrade K, and Gaskins HR (2005) Temporal changes of multiple redox couples from proliferation to growth arrest in IEC-6 intestinal epithelial cells. *Am J Physiol Cell Physiol* **289:**C1220–C1228.

Azam F and Malfatti F (2007) Microbial structuring of marine ecosystems. *Nat Rev Microbiol* **5:**782–791.

Birkenfeld AL, Lee HY, Guebre-Egziabher F, Alves TC, Jurczak MJ, Jornayvaz FR, Zhang D, Hsiao JJ, Martin-Montalvo A, Fischer-Rosinsky A, et al. (2011) Deletion of the mammalian INDY homolog mimics aspects of dietary restriction and protects against adiposity and insulin resistance in mice. *Cell Metab* **14:**184–195.

Bolaños JP, Delgado-Esteban M, Herrero-Mendez A, Fernandez-Fernandez S, and Almeida A (2008) Regulation of glycolysis and pentose-phosphate pathway by nitric oxide: impact on neuronal survival. *Biochim Biophys Acta* **1777:**789–793.

Bradley DJ, Kjellbom P, and Lamb CJ (1992) Elicitor- and wound-induced oxidative cross-linking of a proline-rich plant cell wall protein: a novel, rapid defense response. *Cell* **70:**21–30.

Brinkmann H and Philippe H (2007) The diversity of eukaryotes and the root of the eukaryotic tree. *Adv Exp Med Biol* **607:**20–37.

Buchakjian MR and Kornbluth S (2010) The engine driving the ship: metabolic steering of cell proliferation and death. *Nat Rev Mol Cell Biol* **11:**715–727.

Burhans WC and Heintz NH (2009) The cell cycle is a redox cycle: linking phase-specific targets to cell fate. *Free Radic Biol Med* **47:**1282–1293.

Cabiscol E, Piulats E, Echave P, Herrero E, and Ros J (2000) Oxidative stress promotes specific protein damage in *Saccharomyces cerevisiae*. *J Biol Chem* **275:**27393–27398.

Cavalier-Smith T (2006) Cell evolution and Earth history: stasis and revolution. *Philos Trans R Soc Lond B Biol Sci*, **361:**969–1006.

Cooper ME (2009) Metabolic memory: implications for diabetic vascular complications. *Pediatr Diabetes* **10:**343–346.

Copp SW, Ferreira LF, Herspring KF, Hirai DM, Snyder BS, Poole DC, and Musch TI (2009) The effects of antioxidants on microvascular oxygenation and blood flow in skeletal muscle of young rats. *Exp Physiol* **94:**961–971.

Crabtree HG (1929) Observations on the carbohydrate metabolism of tumours. *Biochem J* **23:**536–545.

Diaz RJ and Rosenberg R (2008) Spreading dead zones and consequences for marine ecosystems. *Science* **321:**926–929.

Dobzhansky T (1973) Nothing in biology makes sense except in the light of evolution. *Am Biol Teacher* **35:**125–129.

DREAM Trial Investigators, Dagenais GR, Gerstein HC, Holman R, Budaj A, Escalante A, Hedner T, Keltai M, Lonn E, McFarlane S, et al. (2008) Effects of ramipril and rosiglitazone on cardiovascular and renal outcomes in people with impaired glucose tolerance or impaired fasting glucose: results of the Diabetes REduction Assessment with ramipril and rosiglitazone Medication (DREAM) trial. *Diabetes Care* **31:**1007–1014.

Dunkley AJ, Charles K, Gray LJ, Camosso-Stefinovic J, Davies MJ, and Khunti K (2012) Effectiveness of interventions for reducing diabetes and cardiovascular disease risk in people with metabolic syndrome: systematic review and mixed treatment comparison meta-analysis. *Diabetes Obes Metab* **14:**616–625.

Fisher-Wellman KH and Neufer PD (2012) Linking mitochondrial bioenergetics to insulin resistance via redox biology. *Trends Endocrinol Metab* **23:**142–153.

Galileo G (2001) *Dialogue Concerning the Two Chief World Systems: Ptolemaic and Copernican (English translation of the original Italian)*. Modern Library, New York.

Galluzzi L, Brenner C, Morselli E, Touat Z, and Kroemer G (2008) Viral control of mitochondrial apoptosis. *PLoS Pathog* **4:**e1000018.

Gille L and Nohl H (2000) The existence of a lysosomal redox chain and the role of ubiquinone. *Arch Biochem Biophys* **375:**347–354.

Gnaiger E, Steinlechner-Maran R, Méndez G, Eberl T, and Margreiter R (1995) Control of mitochondrial and cellular respiration by oxygen. *J Bioenerg Biomembr* **27:**583–596.

Go YM and Jones DP (2008) Redox compartmentalization in eukaryotic cells. *Biochim Biophys Acta* **1780:**1273–1290.

Go YM and Jones DP (2011) Cysteine/cystine redox signaling in cardiovascular disease. *Free Radic Biol Med* **50:**495–509.

González-Flecha B and Demple B (1997) Transcriptional regulation of the *Escherichia coli* oxyR gene as a function of cell growth. *J Bacteriol* **179:**6181–6186.

Han JM, Jeong SJ, Park MC, Kim G, Kwon NH, Kim HK, Ha SH, Ryu SH, and Kim S (2012) Leucyl-tRNA synthetase is an intracellular leucine sensor for the mTORC1-signaling pathway. *Cell* **149:**410–424.

Harman D (1956) Aging: a theory based on free radical and radiation chemistry. *J Gerontol* **11:**298–300.

Hillmann P, Ko GY, Spinrath A, Raulf A, von Kügelgen I, Wolff SC, Nicholas RA, Kostenis E, Höltje HD, and Müller CE (2009) Key determinants of nucleotide-activated G protein-coupled P2Y(2) receptor function revealed by chemical and pharmacological experiments, mutagenesis and homology modeling. *J Med Chem* **52:**2762–2775.

Hohmann-Marriott MF and Blankenship RE (2011) Evolution of photosynthesis. *Annu Rev Plant Biol* **62:**515–548.

Holland HD (2006) The oxygenation of the atmosphere and oceans. *Philos Trans R Soc Lond B Biol Sci* **361:**903–915.

Howitz KT and Sinclair DA (2008) Xenohormesis: sensing the chemical cues of other species. *Cell* **133:**387–391.

Hwang C, Sinskey AJ, and Lodish HF (1992) Oxidized redox state of glutathione in the endoplasmic reticulum. *Science* **257:**1496–1502.

Ibsen KH (1961) The Crabtree effect: a review. *Cancer Res* **21:**829–841.

Jiang F, Zhang Y, and Dusting GJ (2011) NADPH oxidase-mediated redox signaling: roles in cellular stress response, stress tolerance, and tissue repair. *Pharmacol Rev* **63:**218–242.

Jones DP (2010) Redox sensing: orthogonal control in cell cycle and apoptosis signalling. *J Intern Med* **268:**432–448.

Karbowski M (2010) Mitochondria on guard: role of mitochondrial fusion and fission in the regulation of apoptosis. *Adv Exp Med Biol* **687:**131–142.

Klein EA, Thompson IM Jr, Tangen CM, Crowley JJ, Lucia MS, Goodman PJ, Minasian LM, Ford LG, Parnes HL, Gaziano JM, et al. (2011) Vitamin E and the risk of prostate cancer: the Selenium and Vitamin E Cancer Prevention Trial (SELECT). *JAMA* **306:**1549–1556.

Knoll AH, Javaux EJ, Hewitt D, and Cohen P (2006) Eukaryotic organisms in Proterozoic oceans. *Philos Trans R Soc Lond B Biol Sci* **361:**1023–1038.

LaForgia J, Withers RT, and Gore CJ (2006) Effects of exercise intensity and duration on the excess post-exercise oxygen consumption. *J Sports Sci* **24:**1247–1264.

Lin J, Cook NR, Albert C, Zaharris E, Gaziano JM, Van Denburgh M, Buring JE, and Manson JE (2009) Vitamins C and E and beta carotene supplementation and cancer risk: a randomized controlled trial. *J Natl Cancer Inst* **101:**14–23.
Lippman SM, Klein EA, Goodman PJ, Lucia MS, Thompson IM, Ford LG, Parnes HL, Minasian LM, Gaziano JM, Hartline JA, et al. (2009) Effect of selenium and vitamin E on risk of prostate cancer and other cancers: the Selenium and Vitamin E Cancer Prevention Trial (SELECT). *JAMA* **301:**39–51.
Marques-da-Silva C, Burnstock G, Ojcius DM, and Coutinho-Silva R (2011) Purinergic receptor agonists modulate phagocytosis and clearance of apoptotic cells in macrophages. *Immunobiology* **216:**1–11.
Murakami A and Ohnishi K (2012) Target molecules of food phytochemicals: food science bound for the next dimension. *Food Funct* **3:**462–476.
Muir J (1911) *My First Summer in the Sierra*, Houghton Mifflin, Boston, MA.
Navas P, Sun I, Crane FL, Morré DM, and Morré DJ (2010) Monoascorbate free radical-dependent oxidation-reduction reactions of liver Golgi apparatus membranes. *J Bioenerg Biomembr* **42:**181–187.
Naviaux RK (2008) Mitochondrial control of epigenetics. *Cancer Biol Ther* **7:**1191–1193.
Naviaux RK and McGowan KA (2000) Organismal effects of mitochondrial dysfunction. *Hum Reprod* **15 (Suppl 2):**44–56.
Niess AM and Simon P (2007) Response and adaptation of skeletal muscle to exercise–the role of reactive oxygen species. *Front Biosci* **12:**4826–4838.
Pagliarini DJ, Calvo SE, Chang B, Sheth SA, Vafai SB, Ong SE, Walford GA, Sugiana C, Boneh A, Chen WK, et al. (2008) A mitochondrial protein compendium elucidates complex I disease biology. *Cell* **134:**112–123.
Pittman RN (2011) Oxygen gradients in the microcirculation. *Acta Physiol (Oxf)* **202:**311–322.
Prigogine I (1984) *Order Out of Chaos.* Bantam, New York.
Rasmussen B, Fletcher IR, Brocks JJ, and Kilburn MR (2008) Reassessing the first appearance of eukaryotes and cyanobacteria. *Nature* **455:**1101–1104.
Ristow M and Schmeisser S (2011) Extending life span by increasing oxidative stress. *Free Radic Biol Med* **51:**327–336.
Ristow M, Zarse K, Oberbach A, Klöting N, Birringer M, Kiehntopf M, Stumvoll M, Kahn CR, and Blüher M (2009) Antioxidants prevent health-promoting effects of physical exercise in humans. *Proc Natl Acad Sci U S A* **106:**8665–8670.
Rolfsson O, Palsson BØ, and Thiele I (2011) The human metabolic reconstruction Recon 1 directs hypotheses of novel human metabolic functions. *BMC Syst Biol* **5:**155.
Scandurra FM and Gnaiger E (2010) Cell respiration under hypoxia: facts and artefacts in mitochondrial oxygen kinetics. *Adv Exp Med Biol* **662:**7–25.
Schellenberger J, Park JO, Conrad TM, and Palsson BØ (2010) BiGG: a Biochemical Genetic and Genomic knowledgebase of large scale metabolic reconstructions. *BMC Bioinformatics* **11:**213.
Serezani CH, Lewis C, Jancar S, and Peters-Golden M (2011) Leukotriene B4 amplifies NF-κB activation in mouse macrophages by reducing SOCS1 inhibition of MyD88 expression. *J Clin Invest* **121:**671–682.
Shepherd D and Garland PB (1969) The kinetic properties of citrate synthase from rat liver mitochondria. *Biochem J* **114:**597–610.
Spath B, Hansen A, Bokemeyer C, and Langer F (2012) Succinate reverses in-vitro platelet inhibition by acetylsalicylic acid and P2Y receptor antagonists. *Platelets* **23:**60–68.
Speciale A, Chirafisi J, Saija A, and Cimino F (2011) Nutritional antioxidants and adaptive cell responses: an update. *Curr Mol Med* **11:**770–789.
Suksomboon N, Poolsup N, and Sinprasert S (2011) Effects of vitamin E supplementation on glycaemic control in type 2 diabetes: systematic review of randomized controlled trials. *J Clin Pharm Ther* **36:**53–63.
Sussman I, Erecińska M, and Wilson DF (1980) Regulation of cellular energy metabolism: the Crabtree effect. *Biochim Biophys Acta* **591:**209–223.
Tang KH and Blankenship RE (2010) Both forward and reverse TCA cycles operate in green sulfur bacteria. *J Biol Chem* **285:**35848–35854.
Tautenhahn R, Patti GJ, Kalisiak E, Miyamoto T, Schmidt M, Lo FY, McBee J, Baliga NS, and Siuzdak G (2011) metaXCMS: second-order analysis of untargeted metabolomics data. *Anal Chem* **83:**696–700.
Wamelink MM, Struys EA, and Jakobs C (2008) The biochemistry, metabolism and inherited defects of the pentose phosphate pathway: a review. *J Inherit Metab Dis* **31:**703–717.
Warburg OH and Negelein E (1928) Über den Einfluss der Wellenlänge auf die Verteilung des Atmungsferments. (Absorptionsspektrum des Atmungsferments.) (On the influence of wavelength on the activity of the respiratory ferment [in the presence of carbon monoxide] .). *Biochemische Zeitschrift* **193:**339–346.
West AP, Shadel GS, and Ghosh S (2011) Mitochondria in innate immune responses. *Nat Rev Immunol* **11:**389–402.
West JB (2000) *Respiratory Physiology: The Essentials.* Lippincott, Philadelphia, PA.
Wichels A, Biel SS, Gelderblom HR, Brinkhoff T, Muyzer G, and Schütt C (1998) Bacteriophage diversity in the North Sea. *Appl Environ Microbiol* **64:**4128–4133.
Winslow RM (2007) The role of hemoglobin oxygen affinity in oxygen transport at high altitude. *Respir Physiol Neurobiol* **158:**121–127.
Yanes O, Tautenhahn R, Patti GJ, and Siuzdak G (2011) Expanding coverage of the metabolome for global metabolite profiling. *Anal Chem* **83:**2152–2161.
Yano T, Oku M, Akeyama N, Itoyama A, Yurimoto H, Kuge S, Fujiki Y, and Sakai Y (2010) A novel fluorescent sensor protein for visualization of redox states in the cytoplasm and in peroxisomes. *Mol Cell Biol* **30:**3758–3766.
Zhang Q, Raoof M, Chen Y, Sumi Y, Sursal T, Junger W, Brohi K, Itagaki K, and Hauser CJ (2010) Circulating mitochondrial DAMPs cause inflammatory responses to injury. *Nature* **464:**104–107.

Address correspondence to: Robert K. Naviaux, University of California San Diego School of Medicine, 214 Dickinson St., Bldg CTF, Rm C102, San Diego, CA 92103-8467. E-mail: naviaux@ucsd.edu

Mitochondrion 16 (2014) 7–17

Contents lists available at ScienceDirect

Mitochondrion

journal homepage: www.elsevier.com/locate/mito

Metabolic features of the cell danger response

Robert K. Naviaux *

The Mitochondrial and Metabolic Disease Center, Departments of Medicine, Pediatrics, and Pathology, University of California, San Diego School of Medicine, 214 Dickinson St., Bldg CTF, Rm C102, San Diego, CA 92103-8467, USA
Veterans Affairs Center for Excellence in Stress and Mental Health (CESAMH), La Jolla, CA, USA

ARTICLE INFO

Available online 24 August 2013

Keywords:
Oxidative stress
Oxidative shielding
Innate immunity
Inflammation
Purinergic signaling
Mitochondria

ABSTRACT

The cell danger response (CDR) is the evolutionarily conserved metabolic response that protects cells and hosts from harm. It is triggered by encounters with chemical, physical, or biological threats that exceed the cellular capacity for homeostasis. The resulting metabolic mismatch between available resources and functional capacity produces a cascade of changes in cellular electron flow, oxygen consumption, redox, membrane fluidity, lipid dynamics, bioenergetics, carbon and sulfur resource allocation, protein folding and aggregation, vitamin availability, metal homeostasis, indole, pterin, 1-carbon and polyamine metabolism, and polymer formation. The first wave of danger signals consists of the release of metabolic intermediates like ATP and ADP, Krebs cycle intermediates, oxygen, and reactive oxygen species (ROS), and is sustained by purinergic signaling. After the danger has been eliminated or neutralized, a choreographed sequence of anti-inflammatory and regenerative pathways is activated to reverse the CDR and to heal. When the CDR persists abnormally, whole body metabolism and the gut microbiome are disturbed, the collective performance of multiple organ systems is impaired, behavior is changed, and chronic disease results. Metabolic memory of past stress encounters is stored in the form of altered mitochondrial and cellular macromolecule content, resulting in an increase in functional reserve capacity through a process known as mitocellular hormesis. The systemic form of the CDR, and its magnified form, the purinergic life-threat response (PLTR), are under direct control by ancient pathways in the brain that are ultimately coordinated by centers in the brainstem. Chemosensory integration of whole body metabolism occurs in the brainstem and is a prerequisite for normal brain, motor, vestibular, sensory, social, and speech development. An understanding of the CDR permits us to reframe old concepts of pathogenesis for a broad array of chronic, developmental, autoimmune, and degenerative disorders. These disorders include autism spectrum disorders (ASD), attention deficit hyperactivity disorder (ADHD), asthma, atopy, gluten and many other food and chemical sensitivity syndromes, emphysema, Tourette's syndrome, bipolar disorder, schizophrenia, post-traumatic stress disorder (PTSD), chronic traumatic encephalopathy (CTE), traumatic brain injury (TBI), epilepsy, suicidal ideation, organ transplant biology, diabetes, kidney, liver, and heart disease, cancer, Alzheimer and Parkinson disease, and autoimmune disorders like lupus, rheumatoid arthritis, multiple sclerosis, and primary sclerosing cholangitis.

1. Introduction

Cells have a limited number of ways they can respond to threat. An important consequence of this is that evolutionary selection preserves similar cellular responses to diverse forms of threat. The cell danger response (CDR) is an evolutionarily conserved cellular metabolic response that is activated when a cell encounters a chemical, physical, or microbial threat that could injure or kill the cell. Common microbial threats are viruses, bacteria, fungi, and parasites. Physical threats include heat, salt, or pH shock, or UV or ionizing radiation. Chemical forms of danger include heavy and trace metals like lead, mercury, cadmium, arsenic, and nickel, certain electrophilic aromatic chemicals like the plasticizer bisphenol A, the chemical flame retardants like the brominated diphenyl ethers (BDEs), and certain halogenated pesticides like chlorpyrifos and DDT. Psychological trauma, particularly during childhood, can also activate the cell danger response, produce chronic inflammation, and increase the risk of many disorders (Ehlert, 2013). Mixtures of these factors and susceptible genotypes have synergistic effects. The total load of triggers is integrated by metabolism and regulates the CDR. Mitochondria are evolved to sense all of these threats according to the induced changes in electron flow available for normal metabolism. This review will emphasize communication between mitochondria

* The Mitochondrial and Metabolic Disease Center, University of California, San Diego School of Medicine, 214 Dickinson St., Bldg CTF, Rm C102, San Diego, CA 92103-8467, USA. Tel.: +1 619 543 2105; fax: +1 619 543 7868.
E-mail address: Naviaux@ucsd.edu.

1567-7249
http://dx.doi.org/10.1016/j.mito.2013.08.006

and the nucleus, and show how many pathways of extracellular, cell–cell communication are ultimately traceable to mitochondrial metabolism. The cell danger response is coordinated in the brain via chemosensory integration of whole body and microbiome metabolism. Abnormal persistence of the CDR ultimately leads to altered organ function and behavior, and results in chronic disease.

Small molecule nutrients and metabolites are the prime movers of the CDR. Protein, glycan, RNA, epigenetic, and genetic changes are essential, but secondary, and can only be understood with reference to the prime drivers in metabolism. Readers interested in the mitochondria-associated proteins (Arnoult et al., 2011), glycans (Angata et al., 2012), microRNAs, genetics, and epigenetics (Knight, 2013) of innate immunity and inflammation that are associated with the CDR are referred to recent reviews on those topics.

2. Historical foundations

The concept of the cell danger response described in this review has evolved from a confluence of six rivers of scholarship that have developed in relative isolation over the past 60 years. Briefly these are: 1) the recognition that inherited disorders in purine and pyrimidine metabolism produce distinct behavioral and immunologic phenotypes that are not explained by current concepts in neuropharmacology and immunology, 2) the recognition that extracellular purines and pyrimidines like ATP, ADP, UTP, and UDP bind to ubiquitous ion channels and G-protein coupled receptors (GPCRs) to control everything from neurotransmission, to cortisol production, inflammation, chronic pain signaling, and control of the autonomic nervous system, 3) the recognition that immunologic systems have evolved not to distinguish self from non-self, but rather to respond to threats that result in cellular injury, 4) the recognition from the field of virology that the most adaptive strategy is a co-evolutionary negotiation between virus and host, that the pre-exposure condition of the host determines a large fraction of the pathology of infection, and that across virtually all classes of animal cell viruses studied, considerable genetic reserves are expended to target the host mitochondrial "danger alarm system", 5) the recognition within the field of mitochondrial medicine of that extracellular nucleotides are ultimately traceable to mitochondria and that one of the most ancient functions of mitochondria is cellular defense—the detection and response to cellular danger as a fundamental component of innate immunity, and 6) the concept that humans and all other animals are ecosystems of cooperating cells, and that even the most complex ecosystems on Earth can be understood and made more resilient with attention to the relevant forcing variables of physical habitat, resource availability, complementary biodiversity, elimination of invasive species, and the recycling and removal of metabolic end products.

2.1. Biochemical genetics

Biochemical genetics is a mature medical subspecialty that dates to the publication of Sir Archibald Garrod's report of the Mendelian inheritance of alkaptonuria in 1902 (Garrod, 1902), and has been dedicated to the care of children and adults with inborn errors of metabolism since the 1960s. William Nyhan is one of the fathers of the field of biochemical genetics and a mentor to many leaders in the field today. Dr. Nyhan published the first example of an inherited defect in purine metabolism that profoundly altered behavior known as Lesch–Nyhan Disease (Lesch and Nyhan, 1964). Just a few years later he published the first example of a child with autism-like behaviors resulting from an inherited increase in purine synthesis known as phosphoribosylpyrophosphate synthase (PRPPS) super activity syndrome (Nyhan et al., 1969). Both disorders resulted in a profound increase in de novo purine biosynthesis. The complex behavioral and immunologic syndromes produced by inherited defects in purine and pyrimidine metabolism have recently been reviewed (Micheli et al., 2011; Nyhan, 2005). Although the fact that purine and pyrimidine disturbances produce these syndromes is well established, no unifying mechanistic theory exists to explain the development of these complex neuroimmuno-developmental disorders.

2.2. Purinergic signaling

Purinergic signaling was pioneered by Geoffrey Burnstock in the early 1970s, when he described the first examples of non-adrenergic, non-cholinergic (NANC) signaling mediated by the stimulated release of ATP (Burnstock et al., 1972). Skepticism was high in the early days that extracellular ATP could actually be a neurotransmitter. With the cloning of 19 different purinergic receptors that are widely distributed in every neural and non-neural tissue of the body, this early skepticism has been soundly extinguished (Burnstock and Verkhratsky, 2009; Burnstock et al., 2010, 2011). Today, the role of purinergic signaling continues to expand virtually into every fundamental cell communication, stress response, autonomic, vestibular, and sensory integration pathway known (Bours et al., 2011; Burnstock, 2012; Choo et al., 2013; Halassa, 2011; Junger, 2011; Pimentel et al., 2013).

2.3. Immunologic cell danger

Polly Matzinger and Ephraim Fuchs developed the cell danger model of tolerance and immunoreactivity in the early 1990s to explain why effective adaptive immune responses are best mounted under conditions of cell danger and injury (Dreifus, 1998; Matzinger, 1994). This danger theory of immunology has produced many fruitful insights over the past 20 years ranging from contributions to tumor immunology, to graft versus host disease, allergy, asthma, and next generation adjuvants (Fuchs and Matzinger, 1996; Matzinger and Kamala, 2011; Seong and Matzinger, 2004).

2.4. Virology

Since the polio epidemics of the 1950s, we've learned that the vast majority of infections do not kill or permanently disable the host. In the case of polio, just 1 in 150 to 1 in 1800 people infected develops paralytic disease (Nathanson and Kew, 2010). More than 99% of poliovirus infections are either silent, or lead to self-limited upper respiratory tract infections ("colds"), or flu-like abdominal symptoms. Malnutrition and innate immune status are major factors that determine the probability that exposure to poliovirus will result in paralytic disease. Darwin went further. He recognized that many indigenous people were ravaged by disease that was brought by European explorers aboard ships where no disease was evident. Native people had an innate susceptibility to disease that did not affect the European explorers. He noted this phenomenon during his visit to Australia in 1836:

> *It is certainly a fact, which cannot be controverted, that most of the diseases that have raged in the islands during my residence there, have been introduced by ships; and what renders this fact remarkable is that there might be no appearance of the disease among the crew of the ship which conveyed this destructive importation* (Darwin, 1839).

The comprehensive study of viral gene structure since the 1990s has revealed that virtually every class of animal virus has incorporated into its genome the machinery to thwart, suppress, neutralize, or evade the mitochondrial "danger alarm system" (Corcoran et al., 2009; Ohta and Nishiyama, 2011; Scott, 2010). This genetic insight has cast a bright light on the role of mitochondria in antiviral signaling, and cellular defense. In this review, the role of mitochondria in the initiation and maintenance of the cell danger response is placed in context of coordinated changes in whole cell, and whole body metabolism, that together lead to changes in neurodevelopment, behavior, and to chronic disease.

2.5. Mitochondrial medicine

For many years, the treatment of inborn errors in mitochondrial oxidative phosphorylation was directed at trying to restore cellular ATP production, with limited success. At one memorable meeting in Melbourne, Australia in 1998, the distinguished yeast geneticist, biochemist, and mitochondrial biologist Dr. Anthony Linnane stood up and commented (to paraphrase), "If we are intellectually honest, we must discard old ideas and look for new paradigms to explain the cause of symptoms in a disease if we test a rationally designed therapy in patients with the disease, but it fails repeatedly." Mitochondria are located at the hub of the wheel of metabolism, contain 1500 proteins tailored to meet the needs of each different cell type, and catalyze over 500 different chemical reactions in metabolism. The connection between neurodegenerative episodes and infection in mitochondrial disease was recognized and quantified in the early 2000s (Edmonds et al., 2002). With the discovery that mitochondria represented the front lines in cellular defense and innate immunity, this connection between neurological setbacks and infection began to be understood (Seth et al., 2005; West et al., 2011). Ultimately, all the phosphorylated nucleotides of the cell are traceable to reactions in mitochondria. This makes mitochondria fundamental sources of nucleotides for purinergic signaling.

2.6. Ecology and medicine

Even the most complex ecosystem dynamics can be understood as a function of a discrete set of forcing variables that include the physical habitat, resources, complementary biodiversity, disruptive biodiversity (invasive species), and the recycling and removal of metabolic end products. Metabolism, and indeed, whole body function and development can be considered as a complex web of interconnected and interdependent pathways that change in an orderly pattern from conception to old age. Ecologists focus on the identification of drivers, forcing variables, or state variables that can alter the state of an ecosystem, preserve resilience, or drive succession. Drivers are discrete physical, chemical, or biological entities that when changed a small amount, produce large changes in the interaction and performance of the ecosystem as a whole. For example, factors like sunlight, ocean temperature, pH, CO_2, and dissolved oxygen concentration produce dramatic changes in the health of coral reef ecosystems (Riegl et al., 2009).

As we reduce the scale of analysis to the level of the cell, the details of chemistry become more important, and the time constants of response shorten from years in terrestrial ecosystems, to seconds to months in metabolism. Physical habitats are established in complementary microhabitats in each organ, like interdependent structures in the brain. Species become differentiated cell types in tissues that develop complementary and interdependent metabolisms. Within a cell, specialized proteins and enzymes are organized in complementary and interdependent compartments or microhabitats called organelles, and trophic layers in a network. These intracellular trophic layers distinguish proteins needed for the recycling of nutrients, from proteins required for the synthesis of secondary metabolites and polymers—larger structures from smaller building blocks. Resources in the cell are the chemical building blocks of proteins, fats, carbohydrates, and nucleic acids. More generally, the traffic flow patterns of resources and electrons within a cell determine its state of health, alarm, or disease.

What are the state variables in metabolism? In metabolism, pH, CO_2, and oxygen are also important state variables. However, metabolic intermediates like alpha-ketoglutarate (AKG), and cofactors and vitamins are also state variables. Deficiencies in vitamin C produce defects in collagen proline hydroxylation and neurotransmitter metabolism known as scurvy. Deficiencies in thiamine produce defects in glucose, pyruvate, and amino acid metabolism that cause Beriberi and Wernicke–Korsakoff syndrome. Other drivers or state variables in metabolism will be discovered by the systematic application of advanced mass spectrometry and metabolomics methods in each complex disease state, before and after successful treatment.

In ecology, an ecosystem can fail or become unhealthy for many reasons. The field of restoration ecology concerns itself both with identifying the governing dynamics of the complex system, and with the identification of the discrete factors that can be modified to restore health and resilience to the system (Gunderson, 2000). The same is true in medicine. An important forcing variable in the control of chronic inflammation and the cell danger response is purinergic signaling.

3. The cell danger response

When ATP synthesis, nucleotide metabolism, and associated purinergic signaling are disturbed, a coordinated set of cellular responses is triggered that evolved to help the cell defend itself from microbial attack or physical harm. Elements of this cell danger response (CDR) have been given many names that reflect the level and tools of analysis used to study it. The CDR includes the endoplasmic reticulum (ER) stress response (Liu et al., 2008), the unfolded protein response (Lee and Glimcher, 2009), the mitochondrial unfolded protein response (Haynes et al., 2013), the heat shock protein response (Kim et al., 2006), the integrated cell stress response (Silva et al., 2009), the oxidative stress response (Lushchak, 2010), the oxidative shielding response (Naviaux, 2012), innate immunity (West et al., 2011), and inflammation (Zhou et al., 2011). These can be understood as a unified, and functionally coordinated response by considering the CDR in its most fundamental and most ancient role; to improve cell and host survival after viral attack. The acute CDR produces at least 8 functional changes: 1) it shifts cellular metabolism from net polymer synthesis to monomer synthesis to prevent the hijacking and assembly of cellular resources by intracellular pathogens, 2) it stiffens the membranes of the cell and circumscribes an area of damage to limit pathogen egress, 3) releases antiviral and antimicrobial chemicals into the pericellular environment, 4) increases autophagy and mitochondrial fission to remove intracellular pathogens, 5) changes DNA methylation and histone modification to alter gene expression, 6) mobilizes endogenous retroviruses and other mobile genetic elements like the long interspersed nuclear elements (LINEs) to produce genetic variations, 7) warns neighboring cells and distant effector cells of the danger, and 8) alters the behavior of the host to prevent the spread of infection to kin and sleep patterns to facilitate healing (Fig. 1).

3.1. Ancient and modern triggers of the CDR

In the Precambrian seas, the only cells that could transmit their DNA to the next generation were cells that had successfully survived infection by viruses and other microbial pathogens, and exposure to a wide array of chemical and physical forces that were fixtures of the young biosphere. Early cells synthesized ATP and other nucleotides for a diverse array of metabolic functions in addition to RNA and DNA synthesis. The concentration of ATP inside of single cells is typically about 1–5 mM—nearly one million times more than in the extracellular environment (<5–10 nM). When a cell was injured or lysed by a virus, ATP and other nucleotides and metabolites were released into the surrounding area, creating a bright chemical "flare" warning other cells of the danger and the presence of a pathogen.

Before a cell is broken or lysed, mitochondria in an infected eukaryotic cell sense the presence of an intruding microbe by detecting the diversion of electrons (as NADH and NADPH) and carbon to viral biogenesis centers for polymer synthesis to make viral RNA, protein, and DNA from building blocks in the host cell. This "electron steal" is sensed as a voltage drop, or decrease in electron flow available within the cell for oxidative phosphorylation in mitochondria. The metabolic consequences are nearly instantaneous. Mitochondria rapidly decrease their oxygen consumption, which is coupled to electron flow. The dissolved oxygen concentration in the cell begins to rise because mitochondria

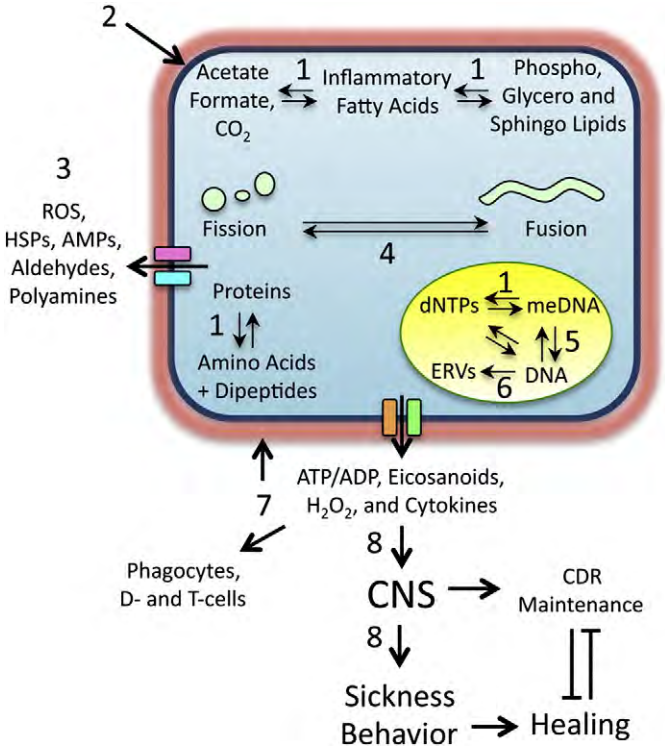

Fig. 1. Functions of the acute cell danger response. The acute CDR includes 8 functional changes in cell structure, physiology, metabolism, and gene expression. These are: 1) shift cellular metabolism from polymer to monomer synthesis to prevent the hijacking and assembly of cellular resources by intracellular pathogens, 2) stiffen the cell membranes to limit superinfection and pathogen egress, 3) release antiviral and antimicrobial chemicals into the pericellular environment, 4) increase autophagy, mitochondrial fission, and mitophagy to facilitate removal of intracellular pathogens and biogenesis centers, 5) change DNA methylation and histone modification to alter gene expression, 6) mobilize endogenous retroviruses and LINEs to produce genetic variations, 7) warn neighboring cells and distant effector cells of the danger with extracellular nucleotides, H_2O_2, eicosanoids, metabolites, and cytokines, and 8) alter the behavior of the host to prevent the spread of infection to kin, and sleep patterns to facilitate healing. *Abbreviations*: HSPs: heat shock proteins; AMPs: antimicrobial peptides; D-cells: Dendritic Cells; ERVs: endogenous retroviruses; LINEs: long interspersed nuclear elements; meDNA: methylated DNA; dNTPs: deoxynucleoside triphosphates; CNS: central nervous system.

are the oxygen sink in every eukaryotic cell. This makes the cellular redox chemistry more oxidizing (Naviaux, 2012). Highly oxidizing environments strongly inhibit the assembly of monomeric building blocks into polymers, and rapidly decrease the efficiency of RNA, protein, and DNA synthesis by the infecting virus. Oxidizing conditions also result in the oxidation of sulfur in methionine, and thiols like cysteine, homocysteine, and glutathione, and the disassembly of iron–sulfur clusters in many enzyme systems, and decrease the availability of the thiol of coenzyme A that is essential for intermediary metabolism.

The ability of mitochondria to monitor electron flow and sulfur oxidation makes them ideally suited as generalized cell "danger alarms". Their rapid metabolism makes mitochondria the "canaries in the coal mine" for the cell. Any trace or heavy metal that acts as an electrophile or sulfurophile in the cell will trigger a mitochondrial response that is similar to that of a viral infection, because metal electrophiles and replicating pathogens both divert and consume electrons. Likewise, a large number of molecules have been synthesized since the 1850s as dyes, pesticides, drugs, and industrial chemicals. Many are polyaromatic and halogenated. These modern chemicals with conjugated ring systems, multiple double bonds, and delocalized π orbital electron clouds are highly electrophilic and will produce an electron steal within the cell that can also activate the CDR. The CDR is a generic, but highly evolved response that often complicates more specific molecular effects that occur when a synthetic molecule binds to a receptor, or competes with and disrupts normal metabolic or hormone signaling. Mixtures of chemical and biological threats can have synergistic effects, and the total load of danger triggers can influence the magnitude and form of the CDR. When danger is detected, mitochondria alter cellular metabolism to help shield the cell from further injury. This is accomplished by stiffening cell membranes, activating the production of reactive oxygen species (ROS), and producing changes in many different pathways in intermediary metabolism that have the effect of limiting pathogen replication and limiting the spread of danger (Naviaux, 2012). These pathways are immature in newborns and growing children (Wood et al., 2010), leading to effects that are not limited to inflammation and innate immunity in peripheral tissues, but can also alter neurodevelopment (Landrigan et al., 2012) and increase the risk of other chronic childhood diseases.

3.2. Summer and winter metabolism

Large trends in the seasonal variation of metabolism can be placed in context by considering the evolutionary forces that have acted on our ancestors. Seasonal changes in calorie availability were the rule. Summer was a time of plenty, when the environment provided abundant calories, which were harvested with physical exercise. This was a natural time for cell growth, during which building blocks were polymerized to produce new cells and increase biomass. Physical exercise ensured that the added biomass was functionally efficient. The master fuel sensor in the cell during summer is mTOR (mammalian target of rapamycin) (Yang and Ming, 2012). mTOR facilitates protein synthesis and growth using new materials taken in from the environment. mTOR inhibits the internal recycling of used or damaged cellular resources by autophagy. The pathways supported by mTOR are Janus faced. In cells capable of dividing, mTOR promotes rapid growth with net polymer synthesis, without inflammation. Used or damaged proteins, lipids, glycans, RNA, and DNA are diluted by new synthesis from fresh building blocks obtained from rich summer ecosystems. In differentiated cells that cannot dispose of excess calories without hypertrophy, mTOR excess results in the accumulation of old and damaged macromolecules like oxidized or aggregated proteins, and produces chronic inflammation—oxidizing conditions that act as a thermodynamic break on the inexorable accumulation of intracellular polymers like lipids, proteins, glycogen, and nucleic acids from their monomer building blocks.

Winter was a time of caloric restriction and a time when resources stored in the summer and fall had to be used with great efficiency if survival was to be assured. The master fuel sensor in the winter is AMPK (AMP activated protein kinase) (Salminen and Kaarniranta, 2012). AMPK optimizes energy efficiency and stimulates the recycling of cellular materials in autophagy. This cycle occurs to a lesser extent each night and during fasting. The pathways activated by AMPK support regeneration and are anti-inflammatory because they work to break down damaged proteins, lipids, glycans, RNA, and DNA. AMPK facilitates the resynthesis of these macromolecules from newly synthesized monomers and refreshed building blocks. Monomer synthesis and polymer synthesis are balanced for winter maintenance. Historically, before the 1980s, most human nutrition research was focused on disorders of deficiency. After the 1980s, much of human nutrition research has been redirected to disorders of caloric excess. Indeed many of the genes that have been found to guard against age-related diseases like diabetes, cancer, and heart disease are found to be "winter genes" coordinated by AMPK, while the "summer genes" coordinated by mTOR lead to chronic disease and inflammation when combined with caloric excess and physical inactivity. Technological progress and industrial scale farming practices have been a double-edge sword for the health of populations around the world. Many developed nations now experience an "endless summer" of calorie availability, decreased physical exercise, and an absence of the historical norm of winter caloric restriction. This has led to

modern epidemics of obesity in both adults and children, and to a growing tide of chronic disease traceable to cellular inflammation.

4. Metabolic features of the CDR

The following section is designed to be read with close reference to Fig. 2. Panels A and B illustrate 21 branch points in metabolism that are normally tipped in the direction of "healthy development", reducing conditions, polymer synthesis and renewal (upward in the figure). However, when a cell is infected by a virus or other microbial pathogen, metabolism is shifted to innate immunity, inflammation, oxidizing conditions, and monomer synthesis to oppose the efforts of the pathogen to parasitize resources and replicate itself by assembling polymers. The shift in metabolism during this cell danger response (CDR) is indicated in the downward direction in the Figure. When these changes occur in the context of cell division and the distribution of accumulated biomass to daughter cells during growth, then inflammation is avoided unless accompanied by significant cell damage. Problems arise when these conditions are activated in post-mitotic tissues that have a limited capacity for growth. The list of metabolic branch points in Fig. 2AB is not intended to be comprehensive, and not all metabolic fates of the branch-point metabolites are discussed. The reader is referred to topical reviews of each of the branch point metabolites of interest for more comprehensive discussion.

4.1. Mitochondria

Mitochondria fragment under conditions of the CDR leading to ineffective control and propagation of intracellular calcium transients (Eisner et al., 2010). When cells are injured and mitochondrial proteins are released to the extracellular space, formyl-methionine initiated mitochondrial proteins can stimulate inflammation via the formyl-peptide receptor (Rabiet et al., 2005). Extracellular mitochondrial DNA activates innate immunity via the TLR9 receptor (West et al., 2011), and is specifically released during infection by eosinophils as an antimicrobial net (Yousefi et al., 2008).

4.2. Oxygen

When mitochondrial oxygen consumption decrease, dissolve cytoplasmic oxygen rises and activates reactive oxygen species (ROS) production by many enzyme systems including NOX4 (Hecker et al., 2009). Increased dissolved oxygen, superoxide and hydrogen peroxide activate many proteins including the central inflammatory regulator NFkB (Lluis et al., 2007) and the multifunctional transglutaminase 2 (Caccamo et al., 2012). Although ROS are sometimes considered intrinsically inflammatory, it is interesting to note that one of the most destructive genetic forms of chronic inflammatory disease is one that cannot produce ROS in response to infection. Chronic granulomatous disease (CGD) is caused by the genetic deficiency of subunits of phagocyte NADPH oxidase 2 (NOX2) that makes the child unable to produce significant amounts of superoxide, hydrogen peroxide, and hypochlorous acid for antibacterial and antifungal defense (Kuijpers and Lutter, 2012). In another example, ROS are protective, and now recognized as important inhibitors of inflammation in autoimmune disorders like rheumatoid arthritis, multiple sclerosis, thyroiditis, and type 1 diabetes (Hultqvist et al., 2009).

4.3. ATP

Purinergic signaling nucleotides like ATP, ADP, UTP, and UDP are released in increased amounts from cells under stress and activate inflammation (Xia et al., 2012). Cells need not be broken or lysed to increase the release of ATP, other nucleotides, and metabolites. ATP and sodium urate crystals are activators of NLRP3 inflammasome assembly (Riteau et al., 2012). Purinergic signaling via ATP directly stimulates cortisol synthesis and release from the adrenal cortex, independent of ACTH stimulation (Kawamura et al., 1991).

4.4. Cysteine and sulfur

Sulfur metabolism is shifted such that glutathione is consumed in glutathionylation regulatory (McLain et al., 2013) and liver phase II detoxification reactions (Zamek-Gliszczynski et al., 2006), and cysteine is diverted to H_2S, taurine, and sulfate excretion (Stipanuk and Ueki, 2011). As an important compensation, the increased plasma oxidation state of the CDR favors cysteine oxidation to cystine (CySSCy), which is used to transport needed cysteine across the blood–brain barrier to the brain (Bridges et al., 2012; Lewerenz et al., 2013), and into macrophages for glutathione synthesis (Kobayashi et al., 2012).

4.5. Vitamin D

In the face of normal body stores of calcium and phosphorus, vitamin D metabolism is altered significantly by the CDR. A mitochondrial P450 enzyme, the 1α hydroxylase, in the kidney is required to activate 25-Hydroxyvitamin D to hormonally active, 1,25-Dihydroxyvitamin D. Another mitochondrial enzyme, the 24α-hydroxylase, is used to inactivate vitamin D. The 24α-hydroxylase is increased by cell danger threats like endotoxin (Shanmugasundaram and Selvaraj, 2012). This decreases the concentration of active vitamin D and contributes to the CDR by increasing inflammation, but also increases the risk of developing of autoantibodies that may include anti-thyroid antibodies (Kivity et al., 2011), and may contribute to the development of other autoantibodies like anti-folate receptor antibodies.

4.6. Folate and B12 metabolism

The metabolism of folic acid and vitamin B12 is tightly interconnected with mitochondrial function, sulfur metabolism, glycine, serine, nucleotide synthesis, and DNA and histone methylation (Naviaux, 2008). Out of over 2700 enzymes encoded by the human genome (Romero et al., 2005) only two require B12, but no fewer than 15 proteins are dedicated to the absorption, transport, and metabolism of B12 (Nielsen et al., 2012). One of the two enzymes is methylmalonyl CoA mutase. It is located in mitochondria and uses the adenosyl form of B12, adenosylcobalamin to convert methylmalonyl-CoA to succinyl-CoA for import into the Krebs cycle. The other B12-dependent enzyme, methionine synthase (MS), is located in the cytosol and uses the methyl form of B12, methylcobalamin, to synthesize methionine from homocysteine. Methionine can be used to initiate protein synthesis, or as a precursor for S-adenosyl methionine (SAM) synthesis. Ultimately the flux through alternative pathways of folate, glutathione, and methionine metabolism is determined by cellular redox poise. Under oxidizing conditions of the CDR, SAM is directed preferentially to polyamine synthesis to assist with ROS and antiviral and antimicrobial polyamine aldehyde synthesis and release (Bachrach, 2007). This lowers the SAM/SAH ratio, while simultaneously decreasing net availability of SAM for DNA methylation reactions. Gene- and cell type-specific demethylation of histones is stimulated by oxidizing conditions of the CDR by the Jumonji histone demethylases, increasing expression of pro-inflammatory cytokines like TNFα (Kruidenier et al., 2012). In addition, the oxidizing conditions of the CDR increase the ratio of formyl-tetrahydrofolate to methyl-tetrahydrofolate (fTHF/mTHF) and the ratio of methylene-THF to mTHF. This favors the de novo synthesis of nucleotides like IMP and dTMP that require 1-carbon donation from fTHR and methylene-THF, respectively. The resulting increase in IMP synthesis can be used to make purine nucleotides like ATP for purinergic signaling. The oxidizing conditions of the CDR ensure that the resulting nucleotides will be used preferentially as monomers for metabolic and signaling purposes, since assembly into polymers of RNA and DNA is chemically unfavorable.

4.7. SAM

S-adenosyl methionine (SAM) is used as a universal methyl donor for DNA, histone, and neurotransmitter methylation reactions. After decarboxylation by SAM decarboxylase, dcSAM is used as an essential aminopropyl donor for polyamine and methylthioadenosine (MTA) synthesis (Fontecave et al., 2004). When the CDR is activated, a larger portion of SAM is diverted to the synthesis of polyamines like

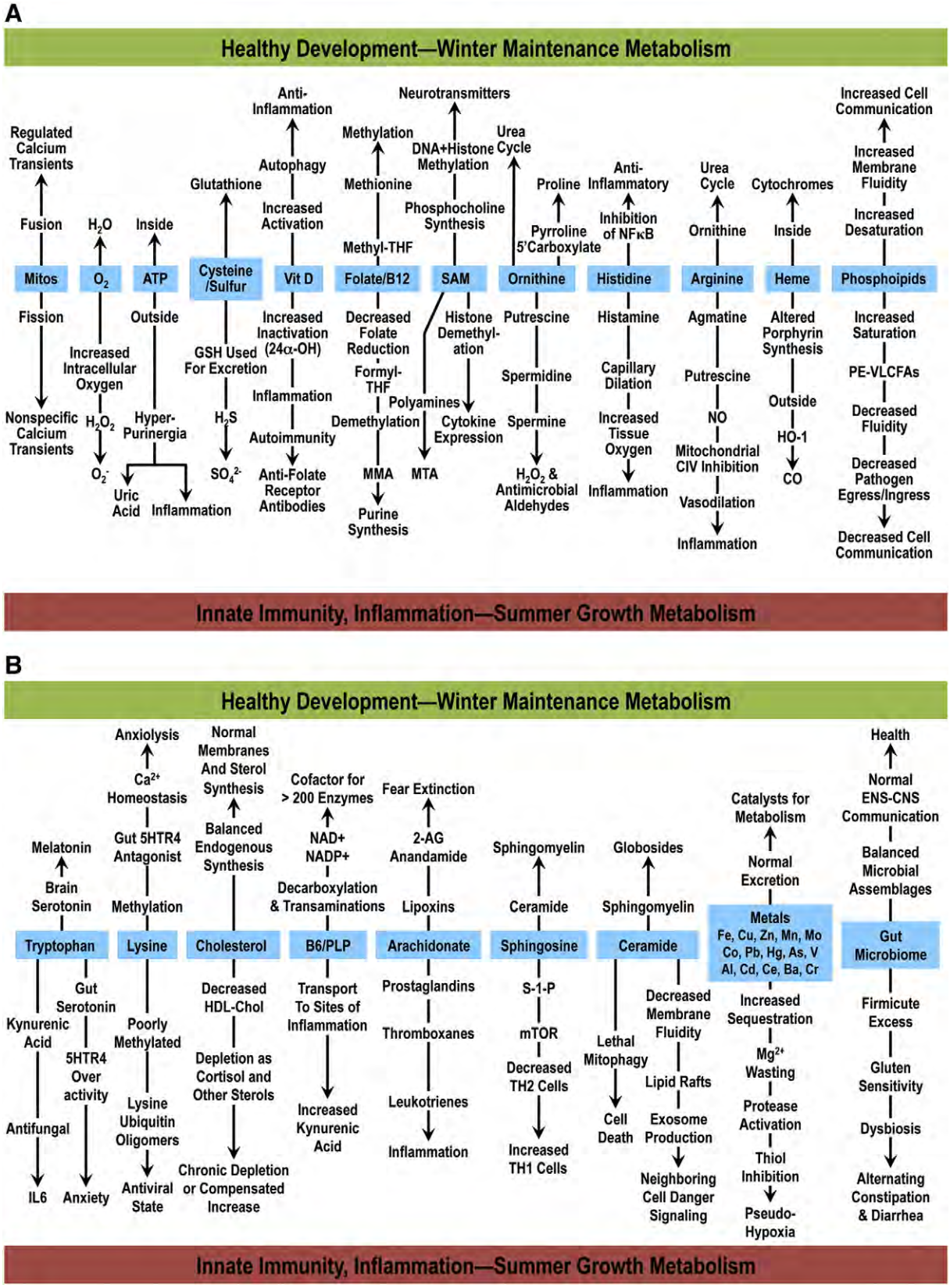

spermidine and spermine, which can be used to synthesize hydrogen peroxide and potent antimicrobial aldehydes like 3-aminopropanal, and 3-acetoaminopropanal (Cervelli et al., 2012). SAM can be usurped by invading pathogens as a methyl donor for the maturation of pathogen mRNAs. S-adenosylhomocysteine (SAH) is a potent feedback inhibitor of SAM-mediated methylation reactions. By decreasing the SAM/SAH ratio, the CDR further consolidates an intracellular environment that is unfavorable for pathogen replication. Adenosine and several purine nucleosides and nucleotides help to maintain a low SAM/SAH ratio by inhibiting SAH hydrolase (SAHH), a key enzyme known to be the target of several synthetic antiviral drugs (De Clercq, 2009).

4.8. Ornithine

Ornithine is a non-proteogenic amino acid synthesized from arginine by arginase I in the liver, and arginase II in many other tissues. When the CDR is activated, ornithine is decarboxylated by the B6-dependent enzyme ornithine decarboxylase (ODC) to putrescine, the polyamine used for all higher molecular weight polyamines like spermidine and spermine. Sustained activation of ODC contributes to increased inflammation and the development of autoantibodies in animal models of lupus erythematosis (Hsu et al., 1994).

4.9. Histidine

Acute activation of the CDR stimulates the B6-dependent enzyme histidine decarboxylase to yield histamine. Histamine is a potent vasodilator that facilitates the delivery of increased oxygen and immune effector cells to sites of inflammation. Histamine is also critical for mast cell and eosinophil function in allergy and the anti-parasite limb of innate immunity (Fulkerson and Rothenberg, 2013).

4.10. Arginine

Arginine has several fates in metabolism. It is a substrate for the tetrahydrobiopterin-dependent nitric oxide synthase. The resulting nitric oxide (NO) gas is a potent and reversible inhibitor of mitochondrial cytochrome c oxidase, also known as complex IV (Forstermann and Sessa, 2012). Arginine can also be decarboxylated to synthesize agmatine, a natural anti-depressant neurotransmitter (Bernstein et al., 2012). Under conditions of the CDR, agmatine is hydrolyzed to produce urea and the antiviral polyamine, putrescine (Bernstein et al., 2012).

4.11. Heme

Heme is abundant in erythrocyte hemoglobin, but is also present as an important prosthetic group in the mitochondrial cytochromes of respiratory chain complexes II, III, and IV (Kim et al., 2012). In a sequence of events that activates the CDR, red cell and mitochondrial heme centers are released from damaged cells. In the extracellular space, heme is metabolized by heme oxygenase I (HO-1) to produce carbon monoxide (CO), releasing iron and biliverdin. Like NO, CO is a potent inhibitor of mitochondrial complex IV. In non-erythroid cells, heme is a feedback inhibitor of porphyrin biosynthesis (Ajioka et al., 2006).

4.12. Phospholipids

The membranes of all eukaryotic cells are composed largely of phospholipids. Most of these are phosphoglycerolipids that are comprised of a glycerol backbone, two fatty acid side chains, and a phosphate-containing polar head group. The fluidity of the cell membrane is a biophysical consequence of thermal packing of the fatty acid side chains. In general, the shorter and more polyunsaturated (more cis double bonds) the side chain, the more fluid the membrane. Reciprocally, the longer the carbon side chain, and the more saturated, the stiffer the membranes become. In the plasma, phosphoethanolamine-containing saturated very long chain fatty acids (PE-VLCFAs) are more abundant (Pastural et al., 2009). Under conditions of cell danger, both Jumonji demethylases (Liu et al., 2012) and heme oxygenase I (Nie et al., 2013) upregulate lipoxygenase expression. The double bonds of fatty acids in the membrane are targets for peroxidation by lipoxygenases. Under conditions of the CDR, the cell membrane is stiffened by progressive replacement of shorter polyunsaturated lipids with longer, more saturated lipids. The activation of phospholipase D2 leads to coupling of G-protein activation (Mahankali et al., 2011) and release of the potent signaling lipids as phosphatidic acid (Peng and Frohman, 2012). Since a large number of purinergic and other innate immune signaling receptors are G-protein coupled receptors, the early translocation of PLD2 to the membrane has the effect of priming purinergic signaling in the early steps of the CDR.

4.13. Tryptophan

The many metabolic fates of tryptophan make it an important molecule in both the early and late stages of the CDR. Tryptophan can be metabolized either to serotonin and melatonin via the hydroxylation (tryptophan hydroxylase) pathway, or to kynurenic acid, quinolinic acid, niacin, and the pyridine nucleotides (NAD+, NADP+) via the dioxygenase (indoleamine 2,3-dioxygenase, IDO) pathway. About 90% of the total body stores of serotonin are synthesized in gut enterochromaffin cells, and transported in platelets in the form of dense, δ-granules, which also contain ADP, ATP, histamine and calcium. Gut microbial metabolism of tryptophan results in the synthesis of a large family of indoles, several of which can also be metabolized to kynurenine. Kynurenic acid acts as an endogenous ligand for the aryl hydrocarbon receptor and synergistic inducer of IL6 (DiNatale et al., 2010), stimulates the innate immune functions like the anti-fungal activity of neutrophils, and stimulates TH2 cells, while attenuating adaptive immunity by the stimulation of TH1-inhibitory, regulatory T cells (T_{reg}) (Mandi and Vecsei, 2012).

4.14. Lysine

The antiviral CDR is strongly regulated by the post-translational state of lysines on histones and immune effector proteins like the double strand RNA binding protein known as RIG1 (retinoic acid inducible gene 1), and the mitochondrial antiviral sensor (MAVS) (Jiang et al., 2012). Lysine ubiquitination facilitates oligomerization of RIG1, which is required for efficient binding to MAVS and interferon induction. SAM-mediated lysine methylation stabilizes proteins, inhibits ubiquitination, and works to oppose increased proteasome-mediated protein turnover that is part of the CDR. Dietary lysine is an antagonist of the gut

Fig. 2. Metabolic features of the cell danger response. A. Twelve branch-point metabolites from mitochondria to phospholipids. Each of the metabolites and effectors indicated can be metabolized in two or more alternative pathways. The pathways indicated in the upward direction in the figure are characteristic of healthy development. They are also active during conditions of caloric restriction, such as those that occurred historically during the winter, during which the maintenance and preservation of limiting resources and energy is essential. The metabolic pathways indicated in the bottom half of the Figure are active during periods of unrestricted nutrient and resource availability, as is characteristic of the abundance of summer. When cell division can occur, healthy growth without inflammation results. However, when cell division cannot occur readily, as is the case in many differentiated tissues like the brain, and physical exercise is limited, innate immune disease and chronic inflammation result. B. Nine branch-point metabolites and effectors from tryptophan to the gut microbiome. The reactions illustrated in the bottom half of the Figure are characteristic of the CDR. The list of CDR metabolites and their metabolic fates illustrated in panels A and B is not intended to be complete. Other metabolites, effectors, and metabolic fates also exist and are coordinately regulated with those indicated, and tailored by metabolic memory to help defend the cell during danger. When the CDR persists pathologically, chronic disease results.

serotonin receptor 4 (5HTR4), is anxiolytic (Smriga and Torii, 2003), and opposes the CDR.

4.15. Cholesterol

Unesterified cholesterol increases the shear-stress resistance and activation of neutrophils (Zhang et al., 2011). Low cholesterol inhibits calcium activation and oxidative burst in neutrophils (Kannan et al., 2007). High cholesterol also makes neuronal cells more resistant to the cytotoxic effects of amyloid beta peptides (AβP) (Arispe and Doh, 2002). The plasma membrane of many eukaryotic cells consists of nearly 50 mol% unesterified cholesterol, which acts as an intramembrane space filler, with a small polar head group (a single hydroxyl), to help solubilize phospholipids. Cholesterol accumulates with GM1 ganglioside in microdomains called caveolae that continuously sample the pericellular environment. When the cell is activated, GM1 and cholesterol concentrate to form lipid rafts, which cause many proteins to patch and concentrate into the rafts for more efficient anti-microbial defense. CDR proteins like the formyl peptide receptor and NADPH oxidase (NOX) are assembled in lipid rafts for efficient ROS production (Jin and Zhou, 2009).

4.16. Vitamin B6

Low plasma levels of the active metabolite of vitamin B6, pyridoxal 5′-phosphate (PLP) are a common feature of inflammation and the CDR (Paul et al., 2013). PLP is a cofactor in 4 reactions in the dioxygenase (IDO) pathway of tryptophan metabolism, after the formation of kynurenine, leading to the synthesis of quinolinic acid and NAD+ and NADP+. PLP is also required by the enzyme S1P lyase for inactivating the lymphocyte chemoattractant sphingosine-1-phosphate (S1P). Low systemic levels of PLP have the effect of increasing the kynurenine/tryptophan ratio, and increase S1P in inflamed tissues, thereby sustaining an active CDR.

4.17. Arachidonate

Cells that are especially rich in mitochondria, like brain, nerve, and epithelial cells, are also rich in plasmalogen lipids, which contain arachidonic acid in the sn-2 position. This is the preferred substrate for phospholipase A2 (PLA2) isoforms for the release of arachidonate for prostaglandin, leukotriene, and other inflammatory lipid synthesis (Ong et al., 2010) during an active CDR.

4.18. Sphingosine

Several intracellular pathogens have evolved mechanisms to either inhibit the synthesis and translocation of sphingosine 1-phosphate (S1P) (Thompson et al., 2005), or stimulate its degradation in mitochondria (Degtyar et al., 2009). S1P is a phosphorylated sphingolipid that contains a single fatty acid linked to a phosphoserine head group. Intracellular S1P traffics to phagosomes where it facilitates calcium-dependent acidification during autophagy and the elimination of intracellular parasites and modulates histone acetylation in the nucleus (Lucki and Sewer, 2012). Extracellular S1P binds to 5 G-protein linked receptors, acts to inhibit apoptosis, prevents lymphocyte egress from sites of production as well as sites of inflammation (Takabe et al., 2008), and is essential for normal development of hearing and vestibular function (MacLennan et al., 2006). S1P opposes the immunomodulatory effects of kynurenine by inhibiting T_{regs}, stimulating TH1, and activating mTOR (Liu et al., 2010).

4.19. Ceramide

Ceramide is the precursor to GM1 ganglioside, sphingosine, and S1P. Ceramide both requires mitochondria for synthesis (Novgorodov and Gudz, 2011), and targets mitochondria under conditions that lead to cell death (Sentelle et al., 2012). The cell death or cell survival result of the CDR depends in part on the balance between S1P and ceramide.

4.20. Metals

Normal metabolism depends critically on the presence of a large number of metals like Mg^{2+}, Ca^{2+}, Fe^{2+}, Cu^{+}, Zn^{2+}, Mn^{2+}, Mo^{4+}, Se^{2+}, and Co^{2+} that interact with nucleotides and other metabolites, and with proteins to stabilize structure and create organometallic reaction centers. Many other metals like Pb, Hg, As, V, Ni, Al, Cd, Ce, and Cr are toxic. Under reducing redox conditions of cell health, these toxic metals are not accumulated because excretion normally exceeds exposure. When the CDR is activated, the oxidizing intracellular conditions favor sequestration, toxic amounts of trace and heavy metals can be accumulated, and are not easily mobilized. Many toxic metals act not only as electrophiles because of their positive charge, but are also sulfurophiles—they readily form sulfides with free thiols of cysteine, and glutathione. This makes free thiols unavailable for normal metabolic reactions and can create a condition known as pseudohypoxia in which intrapeptide cysteine residues of redox-sensing proteins remain uncrosslinked, disulfide bonds cannot form normally, and the three dimensional structure of the reduced form of the protein is favored under normal oxygen concentrations that would otherwise stabilize disulfide bonding. In addition to these effects, the more specific neurotoxic effects of metals like lead and mercury are well known (Ibrahim et al., 2006). When functional vitamin D is decreased by a chronically active CDR, subclinical renal wasting of magnesium can occur (Sutton and Domrongkitchaiporn, 1993).

4.21. Gut microbiome

Healthy metabolism acts as a survival engine that computes the optimum chemical solution for fitness based on the developmental history, current environmental conditions, and the genetic resources available to the individual. When we sample blood or urine, we are actually sampling the collective metabolism of the host-microbiome system. This collective metabolism also controls the epigenetic modification of DNA in somatic cells that creates long-term changes in gene expression (Naviaux, 2008). The human metabotype consists of a dynamically regulated core vocabulary of about 400–1200 chemical words that cells use to communicate. These are small molecule metabolites with a mass less than 2000 Da in size. The stoichiometric proportions of these metabolites are a reflection of our state of health at the time of sampling. The adult human body consists of about 10^{14} human cells and 10^{15} bacterial cells that act as a living shield to help protect us from opportunistic pathogens and keep us healthy. About 99% of our microbiome is in our gut. The biomass of our microbiome is about 1.5 kg, or about 2% of our body weight. Collectively, the bacteria, archaea, rare fungi, protists, and invertebrate metazoans that constitute the 3000 to 30,000 species in our gut microbiome contain a genetic complexity of about 4.5×10^{11} Gb—about 150 fold more genetic information than in the human haploid genome. This is evidence that the metabolic diversity in the gut microbiome far exceeds that of the human host.

The composition and function of the microbiome are best considered as an ecosystem that is continuously shaped by the developmental history, diet, health, and activity of the host. As with any ecosystem, the health and species composition of the microbiome are determined by a discrete set of forcing variables that include the physical habitat, resources, complementary biodiversity, disruptive biodiversity (invasive species), and the recycling and removal of metabolic end products. When the host is sick, the microbiome is also sick. The chronic activation of the CDR alters both the physical habitat of the distal bowel and the availability of resources in the form of dietary nutrients. For example, in children with autism spectrum disorders (ASD), the expression of

intestinal disaccharidases is decreased so that the microbiota of the distal bowel receives a larger number of simple disaccharides like sucrose, lactose, and maltose (Williams et al., 2011). In addition, the increase in oxidizing conditions associated with the CDR in cells lining the intestine leads to changes in the uptake, intracellular processing, and folding of the proline and glutamine-rich, processed gliadin 33-mer peptide (Oguma et al., 2007), and to an increase in gluten sensitivity (Jacobs, 2007). These and other factors combine to alter the permeability and species composition in the gut. Among children with ASD, this commonly leads to dysbiosis and alternating bouts of constipation and diarrhea. It also leads to changes in behavior that are a result of communication abnormalities between the enteric nervous system (ENS) that monitors the health and function of the microbiome, and the central nervous system (CNS). Restoring a sick microbiome is not as simple as adding back missing or underrepresented species. Both the physical habitat of the gut and the nutrient resources delivered must be durably changed in order to produce a durable change in the complex microbial ecosystem.

5. Resolution of the CDR

Once the danger has been eliminated or neutralized, two things happen naturally. First, a choreographed sequence of anti-inflammatory and regenerative pathways is activated that helps replace lost cells and restore normal organ function (Heber-Katz and Stocum, 2013). Next, a metabolic memory of the exposure that led to the CDR is stored in a way similar to the way the brain stores memories, in the form of durable changes in mitochondrial biomass, and cellular protein, lipid and other macromolecule content, cell structure, and gene expression via somatic epigenetic modifications (Naviaux, 2008). This metabolic memory is also called mitocellular hormesis (Naviaux, 2012). Under conditions that are determined by a mixture of host genotype, and the character, developmental timing, magnitude, and frequency of exposure, a dysfunctional form of the CDR can persist that leads to chronic disease. Because the CDR is initially adaptive and coordinated by the close interplay of mitochondria and the cell, but becomes maladaptive once the environmental danger is gone, this can be referred to as "anachroadaptive mitocellular dysfunction".

6. Disease implications and summary

When the CDR fails to resolve, chronic disease results. Beginning in the first trimester, the brainstem is responsible for the chemosensory integration of whole body metabolism with neurodevelopment. After birth, the trajectory of normal development can be altered if the CDR and its attendant metabolic changes persist. Some of the diseases that result from a pathological persistence of the CDR include: autism spectrum disorders (ASD), attention deficit hyperactivity disorder (ADHD), food allergies, asthma, atopy, emphysema, Tourette's syndrome, bipolar disorder, schizophrenia, post-traumatic stress disorder (PTSD), traumatic brain injury (TBI), chronic traumatic encephalopathy (CTE), suicidal ideation, ischemic brain injury, spinal cord injury, diabetes, kidney, liver, and heart disease, cancer, Alzheimer and Parkinson disease, and autoimmune disorders like lupus, rheumatoid arthritis, multiple sclerosis, and primary sclerosing cholangitis. Pathological persistence of the CDR can occur after the inciting agent has gone. This can be the result of hormesis and metabolic memory, somatic epigenetic changes (Blumberg et al., 2013), or both. Purinergic signaling appears to play an important role in sustaining the multifaceted metabolic features of the CDR. This observation led to the successful correction of all 16 of 16 multi-system, autism-like features in a classic animal model of ASD using antipurinergic therapy (APT) (Naviaux et al., 2013).

The chronic CDR disorders listed above produce abnormalities in a broad range of target tissues and cell types. The genotype and health of the host, and the developmental timing and the nature of the exposure determine the risk of developing a particular disease. In many cases, it appears that mixtures of cell danger exposures are required. When the abnormalities appear later in childhood or young adult life, and have not persisted long enough to produce structural abnormalities, there is a chance that many disorders currently thought to be static, irreversible, and poorly responsive to treatment, or even degenerative, might actually be dynamic functional states that respond well to anti-CDR treatments. Many of the disorders named above have already shown response to APT in animal models (Table 1). An important caveat to APT is that if the physical, chemical, or biological trigger of the CDR has not been eliminated or neutralized, treatments designed to inhibit a persistent CDR may have mixed effects. For example, if the CDR is a response to perinatal exposure to PBDE flame retardants (Blumberg et al., 2013), but the PBDEs have not been removed from living space of an affected child, then a persistent CDR can be adaptive and not anachroadaptive. APT under these conditions may cause net harm.

Table 1
Disorders corrected or improved by antipurinergic therapy.

Disease	Species	Antipurinergic drug	Reference
Autism	Mice	Suramin	Naviaux et al. (2013)
Spinal cord injury	Rats	Brilliant Blue G	Peng et al. (2009)
Traumatic brain injury	Rats and Mice	MRS2179	Choo et al. (2013)
Ischemic brain injury	Rats	Suramin	Kharlamov et al. (2002)
Glutamate excitotoxicity	Rats	Suramin	Bezvenyuk et al. (2000)
Epilepsy	Mice	A438079	Engel et al. (2012)
Rheumatoid arthritis	Rats	Suramin	Sahu et al. (2012))
Chronic pain	Rats	P2X3-15h	Cantin et al. (2012)
Multiple sclerosis	Mice	Suramin	Novales-Li (1996)
Lupus erythematosis	Mice	Suramin	Ballok and Sakic (2008)
Restenosis after angioplasty	Rabbits	Suramin	Gray et al. (1999)
Duchenne cardiomyopathy	Mice	Suramin	de Oliveira Moreira et al. (2013)
Heart failure	Rats	Apyrase	Marina et al. (2013)
Alcoholic liver disease/cirrhosis	Rats	Suramin	He et al. (2013))
Asthma	Guinea Pigs	Suramin	Oguma et al. (2007)
Emphysema	Mice	Suramin	Cicko et al. (2010)
Diabetic kidney disease	Rats	Suramin	Korrapati et al. (2012)

Each of the metabolic features of the CDR illustrated in Figs. 1 and 2AB can be addressed individually with specific treatments, or more globally with a combination of supplements, dietary and activity changes, or with adaptogen therapies (Panossian and Wikman, 2009). However, since the CDR appears to be a functional response that is coordinated by purinergic signaling, a new chapter in complex disease therapeutics can be imagined in which the pharmacology of purinergic antagonists is expanded, natural products are sought, and new anti-inflammatory drugs are developed that selectively target one or more of the 19 known classes of purinergic receptors.

Acknowledgments

RKN thanks Jane Naviaux, Will Alaynick, Jim Adams, Steve Edelson, Kate Crowley, and Vicki Kobliner for helpful comments on the manuscript. This work was made possible by support from the UCSD Christini Fund, the Jane Botsford Johnson Foundation, the Wright Foundation, the Lennox Foundation, the It Takes Guts Foundation, the UCSD Mitochondrial Disease Research Foundation, and the Hailey's Wish Foundation.

Conflict of interest

None.

References

Ajioka, R.S., Phillips, J.D., Kushner, J.P., 2006. Biosynthesis of heme in mammals. Biochim. Biophys. Acta 1763, 723–736.

Angata, T., Fujinawa, R., Kurimoto, A., Nakajima, K., Kato, M., Takamatsu, S., Korekane, H., Gao, C.X., Ohtsubo, K., Kitazume, S., Taniguchi, N., 2012. Integrated approach toward the discovery of glyco-biomarkers of inflammation-related diseases. Ann. N. Y. Acad. Sci. 1253, 159–169.

Arispe, N., Doh, M., 2002. Plasma membrane cholesterol controls the cytotoxicity of Alzheimer's disease AbetaP (1–40) and (1–42) peptides. FASEB J. 16, 1526–1536.

Arnoult, D., Soares, F., Tattoli, I., Girardin, S.E., 2011. Mitochondria in innate immunity. EMBO Rep. 12, 901–910.

Bachrach, U., 2007. Antiviral activity of oxidized polyamines. Amino Acids 33, 267–272.

Ballok, D.A., Sakic, B., 2008. Purine receptor antagonist modulates serology and affective behaviors in lupus-prone mice: evidence of autoimmune-induced pain? Brain Behav. Immun. 22, 1208–1216.

Bernstein, H.G., Stich, C., Jager, K., Dobrowolny, H., Wick, M., Steiner, J., Veh, R., Bogerts, B., Laube, G., 2012. Agmatinase, an inactivator of the putative endogenous antidepressant agmatine, is strongly upregulated in hippocampal interneurons of subjects with mood disorders. Neuropharmacology 62, 237–246.

Bezvenyuk, Z., Suuronen, T., Salminen, A., Solovyan, V., 2000. Protective effect of suramin against cell death in rat cerebellar granular neurons and mouse neuroblastoma cells. Neurosci. Lett. 292, 111–114.

Blumberg, S.J., Bramlett, M.D., Kogan, M.D., Schieve, L.A., Jones, J.R., Lu, M.C., 2013. Changes in prevalence of parent-reported autism spectrum disorder in school-aged U.S. children: 2007 to 2011–2012. Natl. Health Stat. Report 65, 1–12.

Bours, M.J., Dagnelie, P.C., Giuliani, A.L., Wesselius, A., Di Virgilio, F., 2011. P2 receptors and extracellular ATP: a novel homeostatic pathway in inflammation. Front Biosci. (Schol Ed) 3, 1443–1456.

Bridges, R.J., Natale, N.R., Patel, S.A., 2012. System xc(−) cystine/glutamate antiporter: an update on molecular pharmacology and roles within the CNS. Br. J. Pharmacol. 165, 20–34.

Burnstock, G., 2012. Targeting the visceral purinergic system for pain control. Curr. Opin. Pharmacol. 12, 80–86.

Burnstock, G., Verkhratsky, A., 2009. Evolutionary origins of the purinergic signalling system. Acta Physiol. (Oxf) 195, 415–447.

Burnstock, G., Dumsday, B., Smythe, A., 1972. Atropine resistant excitation of the urinary bladder: the possibility of transmission via nerves releasing a purine nucleotide. Br. J. Pharmacol. 44, 451–461.

Burnstock, G., Fredholm, B.B., North, R.A., Verkhratsky, A., 2010. The birth and postnatal development of purinergic signalling. Acta Physiol (Oxf) 199, 93–147.

Burnstock, G., Krugel, U., Abbracchio, M.P., Illes, P., 2011. Purinergic signalling: from normal behaviour to pathological brain function. Prog. Neurobiol. 95, 229–274.

Caccamo, D., Curro, M., Ferlazzo, N., Condello, S., Ientile, R., 2012. Monitoring of transglutaminase 2 under different oxidative stress conditions. Amino Acids 42, 1037–1043.

Cantin, L.D., Bayrakdarian, M., Buon, C., Grazzini, E., Hu, Y.J., Labrecque, J., Leung, C., Luo, X., Martino, G., Pare, M., Payza, K., Popovic, N., Projean, D., Santhakumar, V., Walpole, C., Yu, X.H., Tomaszewski, M.J., 2012. Discovery of P2X3 selective antagonists for the treatment of chronic pain. Bioorg. Med. Chem. Lett. 22, 2565–2571.

Cervelli, M., Amendola, R., Polticelli, F., Mariottini, P., 2012. Spermine oxidase: ten years after. Amino acids 42, 441–450.

Choo, A.M., Miller, W.J., Chen, Y.C., Nibley, P., Patel, T.P., Goletiani, C., Morrison III, B., Kutzing, M.K., Firestein, B.L., Sul, J.Y., Haydon, P.G., Meaney, D.F., 2013. Antagonism of purinergic signalling improves recovery from traumatic brain injury. Brain 136, 65–80.

Cicko, S., Lucattelli, M., Muller, T., Lommatzsch, M., De Cunto, G., Cardini, S., Sundas, W., Grimm, M., Zeiser, R., Durk, T., Zissel, G., Boeynaems, J.M., Sorichter, S., Ferrari, D., Di Virgilio, F., Virchow, J.C., Lungarella, G., Idzko, M., 2010. Purinergic receptor inhibition prevents the development of smoke-induced lung injury and emphysema. J. Immunol. 185, 688–697.

Corcoran, J.A., Saffran, H.A., Duguay, B.A., Smiley, J.R., 2009. Herpes simplex virus UL12.5 targets mitochondria through a mitochondrial localization sequence proximal to the N terminus. J. Virol. 83, 2601–2610.

Darwin, C.R., 1839. Journal and remarks, 1832–1836. In: Nicholas, F.W., Nicholas, J.M. (Eds.), Charles Darwin in Australia. Cambridge University Press, Cambridge, pp. 30–31.

De Clercq, E., 2009. Another ten stories in antiviral drug discovery (part C): "old" and "new" antivirals, strategies, and perspectives. Med. Res. Rev. 29, 611–645.

de Oliveira Moreira, D., Pereira, J.A., Taniguti, A.P., Matsumura, C.Y., Ramos, L.A., Areas, M.A., Neto, H.S., Marques, M.J., 2013. Suramin attenuates dystrophin-deficient cardiomyopathy in the mdx mouse model of Duchenne muscular dystrophy. Muscle Nerve.

Degtyar, E., Zusman, T., Ehrlich, M., Segal, G., 2009. A Legionella effector acquired from protozoa is involved in sphingolipids metabolism and is targeted to the host cell mitochondria. Cell. Microbiol. 11, 1219–1235.

DiNatale, B.C., Murray, I.A., Schroeder, J.C., Flaveny, C.A., Lahoti, T.S., Laurenzana, E.M., Omiecinski, C.J., Perdew, G.H., 2010. Kynurenic acid is a potent endogenous aryl hydrocarbon receptor ligand that synergistically induces interleukin-6 in the presence of inflammatory signaling. Toxicol. Sci. 115, 89–97.

Dreifus, C., 1998. A Conversation With Polly Matzinger; Blazing an Unconventional Trail to a New Theory of Immunity. The New York Times, Science. June 16, 1998.

Edmonds, J.L., Kirse, D.J., Kearns, D., Deutsch, R., Spruijt, L., Naviaux, R.K., 2002. The otolaryngological manifestations of mitochondrial disease and the risk of neurodegeneration with infection. Arch. Otolaryngol. Head Neck Surg. 128, 355–362.

Ehlert, U., 2013. Enduring psychobiological effects of childhood adversity. Psychoneuroendocrinology (Electronic publication ahead of print).

Eisner, V., Parra, V., Lavandero, S., Hidalgo, C., Jaimovich, E., 2010. Mitochondria fine-tune the slow Ca(2+) transients induced by electrical stimulation of skeletal myotubes. Cell Calcium 48, 358–370.

Engel, T., Gomez-Villafuertes, R., Tanaka, K., Mesuret, G., Sanz-Rodriguez, A., Garcia-Huerta, P., Miras-Portugal, M.T., Henshall, D.C., Diaz-Hernandez, M., 2012. Seizure suppression and neuroprotection by targeting the purinergic P2X7 receptor during status epilepticus in mice. FASEB J. 26, 1616–1628.

Fontecave, M., Atta, M., Mulliez, E., 2004. S-adenosylmethionine: nothing goes to waste. Trends Biochem. Sci. 29, 243–249.

Forstermann, U., Sessa, W.C., 2012. Nitric oxide synthases: regulation and function. Eur. Hear. J. 33, 829–837.

Fuchs, E.J., Matzinger, P., 1996. Is cancer dangerous to the immune system? Semin. Immunol. 8, 271–280.

Fulkerson, P.C., Rothenberg, M.E., 2013. Targeting eosinophils in allergy, inflammation and beyond. Nat. Rev. Drug Discov. 12, 117–129.

Garrod, A.E., 1902. The incidence of alkaptonuria: a study in chemical individuality. Lancet 12, 1616–1620.

Gray, T.J., Strauss, B.H., Hinek, A., 1999. Inhibitory mechanisms by which suramin may attenuate neointimal formation after balloon angioplasty. J. Cardiovasc. Pharmacol. 33, 960–971.

Gunderson, L.H., 2000. Ecological resilience — in theory and application. Annu. Rev. Ecol. Syst. 31, 425–439.

Halassa, M.M., 2011. Thalamocortical dynamics of sleep: roles of purinergic neuromodulation. Semin. Cell Dev. Biol. 22, 245–251.

Haynes, C.M., Fiorese, C.J., Lin, Y.F., 2013. Evaluating and responding to mitochondrial dysfunction: the mitochondrial unfolded-protein response and beyond. Trends Cell Biol. 23, 311–318.

He, S., Rehman, H., Shi, Y., Krishnasamy, Y., Lemasters, J.J., Schnellmann, R.G., Zhong, Z., 2013. Suramin decreases injury and improves regeneration of ethanol-induced steatotic partial liver grafts. J. Pharmacol. Exp. Ther. 344, 417–425.

Heber-Katz, E., Stocum, D.L., 2013. New Perspectives in Regeneration. Springer, New York, NY.

Hecker, L., Vittal, R., Jones, T., Jagirdar, R., Luckhardt, T.R., Horowitz, J.C., Pennathur, S., Martinez, F.J., Thannickal, V.J., 2009. NADPH oxidase-4 mediates myofibroblast activation and fibrogenic responses to lung injury. Nat. Med. 15, 1077–1081.

Hsu, H.C., Seibold, J.R., Thomas, T.J., 1994. Regulation of ornithine decarboxylase in the kidney of autoimmune mice with the lpr gene. Autoimmunity 19, 253–264.

Hultqvist, M., Olsson, L.M., Gelderman, K.A., Holmdahl, R., 2009. The protective role of ROS in autoimmune disease. Trends Immunol. 30, 201–208.

Ibrahim, D., Froberg, B., Wolf, A., Rusyniak, D.E., 2006. Heavy metal poisoning: clinical presentations and pathophysiology. Clin. Lab. Med. 26, 67–97 (viii).

Jacobs, S.A., 2007. Celiac sprue is primarily a disease of blocked cellular recognition. Med. Hypotheses 68, 308–313.

Jiang, X., Kinch, L.N., Brautigam, C.A., Chen, X., Du, F., Grishin, N.V., Chen, Z.J., 2012. Ubiquitin-induced oligomerization of the RNA sensors RIG-I and MDA5 activates antiviral innate immune response. Immunity 36, 959–973.

Jin, S., Zhou, F., 2009. Lipid raft redox signaling platforms in vascular dysfunction: features and mechanisms. Curr. Atheroscler. Rep. 11, 220–226.

Junger, W.G., 2011. Immune cell regulation by autocrine purinergic signalling. Nat. Rev. Immunol. 11, 201–212.

Kannan, K.B., Barlos, D., Hauser, C.J., 2007. Free cholesterol alters lipid raft structure and function regulating neutrophil Ca2+ entry and respiratory burst: correlations with calcium channel raft trafficking. J. Immunol. 178, 5253–5261.

Kawamura, M., Matsui, T., Niitsu, A., Kondo, T., Ohno, Y., Nakamichi, N., 1991. Extracellular ATP stimulates steroidogenesis in bovine adrenocortical fasciculata cells via P2 purinoceptors. Jpn. J. Pharmacol. 56, 543–545.

Kharlamov, A., Jones, S.C., Kim, D.K., 2002. Suramin reduces infarct volume in a model of focal brain ischemia in rats. Exp. Brain Res. 147, 353–359.

Kim, H.P., Morse, D., Choi, A.M., 2006. Heat-shock proteins: new keys to the development of cytoprotective therapies. Expert Opin. Ther. Targets 10, 759–769.

Kim, H.J., Khalimonchuk, O., Smith, P.M., Winge, D.R., 2012. Structure, function, and assembly of heme centers in mitochondrial respiratory complexes. Biochim. Biophys. Acta 1823, 1604–1616.

Kivity, S., Agmon-Levin, N., Zisappl, M., Shapira, Y., Nagy, E.V., Danko, K., Szekanecz, Z., Langevitz, P., Shoenfeld, Y., 2011. Vitamin D and autoimmune thyroid diseases. Cell. Mol. Immunol. 8, 243–247.

Knight, J.C., 2013. Genomic modulators of the immune response. Trends Genet. 29, 74–83.

Kobayashi, S., Kuwata, K., Sugimoto, T., Igarashi, K., Osaki, M., Okada, F., Fujii, J., Bannai, S., Sato, H., 2012. Enhanced expression of cystine/glutamate transporter in the lung caused by the oxidative-stress-inducing agent paraquat. Free Radic. Biol. Med. 53, 2197–2203.

Korrapati, M.C., Shaner, B.E., Neely, B.A., Alge, J.L., Arthur, J.M., Schnellmann, R.G., 2012. Diabetes-induced renal injury in rats is attenuated by suramin. J. Pharmacol. Exp. Ther. 343, 34–43.

Kruidenier, L., Chung, C.W., Cheng, Z., Liddle, J., Che, K., Joberty, G., Bantscheff, M., Bountra, C., Bridges, A., Diallo, H., Eberhard, D., Hutchinson, S., Jones, E., Katso, R., Leveridge, M., Mander, P.K., Mosley, J., Ramirez-Molina, C., Rowland, P., Schofield, C.J., Sheppard, R.J., Smith, J.E., Swales, C., Tanner, R., Thomas, P., Tumber, A., Drewes, G., Oppermann, U., Patel, D.J., Lee, K., Wilson, D.M., 2012. A selective jumonji H3K27 demethylase inhibitor modulates the proinflammatory macrophage response. Nature 488, 404–408.

Kuijpers, T., Lutter, R., 2012. Inflammation and repeated infections in CGD: two sides of a coin. Cell Mol. Life Sci. 69, 7–15.

Landrigan, P., Lambertini, L., Birnbaum, L., 2012. A research strategy to discover the environmental causes of autism and neurodevelopmental disabilities. Environ. Heal. Perspect. 120, a258–a260.

Lee, A.H., Glimcher, L.H., 2009. Intersection of the unfolded protein response and hepatic lipid metabolism. Cell Mol. Life Sci. 66, 2835–2850.

Lesch, M., Nyhan, W.L., 1964. A familial disorder of uric acid metabolism and central nervous system function. Am. J. Med. 36, 561–570.

Lewerenz, J., Hewett, S.J., Huang, Y., Lambros, M., Gout, P.W., Kalivas, P.W., Massie, A., Smolders, I., Methner, A., Pergande, M., Smith, S.B., Ganapathy, V., Maher, P., 2013. The cystine/glutamate antiporter system x(c)(−) in health and disease: from molecular mechanisms to novel therapeutic opportunities. Antioxid. Redox Signal. 18, 522–555.

Liu, G., Sun, Y., Li, Z., Song, T., Wang, H., Zhang, Y., Ge, Z., 2008. Apoptosis induced by endoplasmic reticulum stress involved in diabetic kidney disease. Biochem. Biophys. Res. Commun. 370, 651–656.

Liu, G., Yang, K., Burns, S., Shrestha, S., Chi, H., 2010. The S1P(1)-mTOR axis directs the reciprocal differentiation of T(H)1 and T(reg) cells. Nat. Immunol. 11, 1047–1056.

Liu, C., Xu, D., Han, H., Fan, Y., Schain, F., Xu, Z., Claesson, H.E., Bjorkholm, M., Sjoberg, J., 2012. Transcriptional regulation of 15-lipoxygenase expression by histone h3 lysine 4 methylation/demethylation. PLoS One 7, e52703.

Lluis, J.M., Buricchi, F., Chiarugi, P., Morales, A., Fernandez-Checa, J.C., 2007. Dual role of mitochondrial reactive oxygen species in hypoxia signaling: activation of nuclear factor-{kappa}B via c-SRC and oxidant-dependent cell death. Cancer Res. 67, 7368–7377.

Lucki, N.C., Sewer, M.B., 2012. Nuclear sphingolipid metabolism. Annu. Rev. Physiol. 74, 131–151.

Lushchak, V.I., 2010. Adaptive response to oxidative stress: bacteria, fungi, plants and animals. Comp. Biochem. Physiol. C Toxicol. Pharmacol. 153, 175–190.

MacLennan, A.J., Benner, S.J., Andringa, A., Chaves, A.H., Rosing, J.L., Vesey, R., Karpman, A.M., Cronier, S.A., Lee, N., Erway, L.C., Miller, M.L., 2006. The S1P2 sphingosine 1-phosphate receptor is essential for auditory and vestibular function. Hear. Res. 220, 38–48.

Mahankali, M., Peng, H.J., Henkels, K.M., Dinauer, M.C., Gomez-Cambronero, J., 2011. Phospholipase D2 (PLD2) is a guanine nucleotide exchange factor (GEF) for the GTPase Rac2. Proc. Natl. Acad. Sci. U. S. A. 108, 19617–19622.

Mandi, Y., Vecsei, L., 2012. The kynurenine system and immunoregulation. J. Neural Transm. 119, 197–209.

Marina, N., Tang, F., Figueiredo, M., Mastitskaya, S., Kasimov, V., Mohamed-Ali, V., Roloff, E., Teschemacher, A.G., Gourine, A.V., Kasparov, S., 2013. Purinergic signalling in the rostral ventro-lateral medulla controls sympathetic drive and contributes to the progression of heart failure following myocardial infarction in rats. Basic Res. Cardiol. 108, 317.

Matzinger, P., 1994. Tolerance, danger, and the extended family. Annu. Rev. Immunol. 12, 991–1045.

Matzinger, P., Kamala, T., 2011. Tissue-based class control: the other side of tolerance. Nat. Rev. Immunol. 11, 221–230.

McLain, A.L., Cormier, P.J., Kinter, M., Szweda, L.I., 2013. Glutathionylation of alpha-ketoglutarate dehydrogenase: the chemical nature and relative susceptibility of the cofactor lipoic acid to modification. Free Radic. Biol. Med. 61C, 161–169.

Micheli, V., Camici, M., Tozzi, M.G., Ipata, P.L., Sestini, S., Bertelli, M., Pompucci, G., 2011. Neurological disorders of purine and pyrimidine metabolism. Curr. Top Med. Chem. 11, 923–947.

Nathanson, N., Kew, O.M., 2010. From emergence to eradication: the epidemiology of poliomyelitis deconstructed. Am. J. Epidemiol. 172, 1213–1229.

Naviaux, R.K., 2008. Mitochondrial control of epigenetics. Cancer Biol. Ther. 7, 1191–1193.

Naviaux, R.K., 2012. Oxidative shielding or oxidative stress? J. Pharmacol. Exp. Ther. 342, 608–618.

Naviaux, R.K., Zolkipli, Z., Wang, L., Nakayama, T., Naviaux, J.C., Le, T.P., Schuchbauer, M.A., Rogac, M., Tang, Q., Dugan, L.L., Powell, S.B., 2013. Antipurinergic therapy corrects the autism-like features in the poly(IC) mouse model. PLoS One 8, e57380.

Nie, X., Hui, Y., Shi, S., Ma, J., Wang, S., Qiu, Z., Song, S., Pan, Z., Li, Q., Gao, X., Zhu, D., 2013. Heme oxygenase-1 induces 15-lipoxygenase expression during hypoxia-induced pulmonary hypertension. Int. J. Biochem. Cell Biol. 45, 964–972.

Nielsen, M.J., Rasmussen, M.R., Andersen, C.B., Nexo, E., Moestrup, S.K., 2012. Vitamin B12 transport from food to the body's cells — a sophisticated, multistep pathway. Nat. Rev. Gastroenterol. Hepatol. 9, 345–354.

Novales-Li, P., 1996. Suramin exerts in vivo cytokine modulatory properties on splenocytes from experimental allergic encephalomyelitis-induced SJL mice: implications for autoimmune disease therapy. Immunopharmacology 35, 155–162.

Novgorodov, S.A., Gudz, T.I., 2011. Ceramide and mitochondria in ischemic brain injury. Int. J. Biochem. Mol. Biol. 2, 347–361.

Nyhan, W.L., 2005. Disorders of purine and pyrimidine metabolism. Mol. Genet. Metab. 86, 25–33.

Nyhan, W.L., James, J.A., Teberg, A.J., Sweetman, L., Nelson, L.G., 1969. A new disorder of purine metabolism with behavioral manifestations. J. Pediatr. 74, 20–27.

Oguma, T., Ito, S., Kondo, M., Makino, Y., Shimokata, K., Honjo, H., Kamiya, K., Kume, H., 2007. Roles of P2X receptors and Ca2+ sensitization in extracellular adenosine triphosphate-induced hyperresponsiveness in airway smooth muscle. Clin. Exp. Allergy 37, 893–900.

Ohta, A., Nishiyama, Y., 2011. Mitochondria and viruses. Mitochondrion 11, 1–12.

Ong, W.Y., Farooqui, T., Farooqui, A.A., 2010. Involvement of cytosolic phospholipase A(2), calcium independent phospholipase A(2) and plasmalogen selective phospholipase A(2) in neurodegenerative and neuropsychiatric conditions. Curr. Med. Chem. 17, 2746–2763.

Panossian, A., Wikman, G., 2009. Evidence-based efficacy of adaptogens in fatigue, and molecular mechanisms related to their stress-protective activity. Curr. Clin. Pharmacol. 4, 198–219.

Pastural, E., Ritchie, S., Lu, Y., Jin, W., Kavianpour, A., Khine Su-Myat, K., Heath, D., Wood, P.L., Fisk, M., Goodenowe, D.B., 2009. Novel plasma phospholipid biomarkers of autism: mitochondrial dysfunction as a putative causative mechanism. Prostaglandins Leukot. Essent. Fat. Acids 81, 253–264.

Paul, L., Ueland, P.M., Selhub, J., 2013. Mechanistic perspective on the relationship between pyridoxal 5′-phosphate and inflammation. Nutr. Rev. 71, 239–244.

Peng, X., Frohman, M.A., 2012. Mammalian phospholipase D physiological and pathological roles. Acta Physiol (Oxf) 204, 219–226.

Peng, W., Cotrina, M.L., Han, X., Yu, H., Bekar, L., Blum, L., Takano, T., Tian, G.F., Goldman, S.A., Nedergaard, M., 2009. Systemic administration of an antagonist of the ATP-sensitive receptor P2X7 improves recovery after spinal cord injury. Proc. Natl. Acad. Sci. U. S. A. 106, 12489–12493.

Pimentel, V.C., Zanini, D., Cardoso, A.M., Schmatz, R., Bagatini, M.D., Gutierres, J.M., Carvalho, F., Gomes, J.L., Rubin, M., Morsch, V.M., Moretto, M.B., Colino-Oliveira, M., Sebastiao, A.M., Schetinger, M.R., 2013. Hypoxia-ischemia alters nucleotide and nucleoside catabolism and Na+, K+-ATPase activity in the cerebral cortex of newborn rats. Neurochem. Res. 38, 886–894.

Rabiet, M.J., Huet, E., Boulay, F., 2005. Human mitochondria-derived N-formylated peptides are novel agonists equally active on FPR and FPRL1, while Listeria monocytogenes-derived peptides preferentially activate FPR. Eur. J. Immunol. 35, 2486–2495.

Riegl, B., Bruckner, A., Coles, S.L., Renaud, P., Dodge, R.E., 2009. Coral reefs: threats and conservation in an era of global change. Ann. N. Y. Acad. Sci. 1162, 136–186.

Riteau, N., Baron, L., Villeret, B., Guillou, N., Savigny, F., Ryffel, B., Rassendren, F., Le Bert, M., Gombault, A., Couillin, I., 2012. ATP release and purinergic signaling: a common pathway for particle-mediated inflammasome activation. Cell Death Dis. 3, e403.

Romero, P., Wagg, J., Green, M.L., Kaiser, D., Krummenacker, M., Karp, P.D., 2005. Computational prediction of human metabolic pathways from the complete human genome. Genome Biol. 6, R2.

Sahu, D., Saroha, A., Roy, S., Das, S., Srivastava, P.S., Das, H.R., 2012. Suramin ameliorates collagen induced arthritis. Int. Immunopharmacol. 12, 288–293.

Salminen, A., Kaarniranta, K., 2012. AMP-activated protein kinase (AMPK) controls the aging process via an integrated signaling network. Ageing Res. Rev. 11, 230–241.

Scott, I., 2010. The role of mitochondria in the mammalian antiviral defense system. Mitochondrion 10, 316–320.

Sentelle, R.D., Senkal, C.E., Jiang, W., Ponnusamy, S., Gencer, S., Selvam, S.P., Ramshesh, V.K., Peterson, Y.K., Lemasters, J.J., Szulc, Z.M., Bielawski, J., Ogretmen, B., 2012. Ceramide targets autophagosomes to mitochondria and induces lethal mitophagy. Nat. Chem. Biol. 8, 831–838.

Seong, S.Y., Matzinger, P., 2004. Hydrophobicity: an ancient damage-associated molecular pattern that initiates innate immune responses. Nat. Rev. Immunol. 4, 469–478.

Seth, R.B., Sun, L., Ea, C.K., Chen, Z.J., 2005. Identification and characterization of MAVS, a mitochondrial antiviral signaling protein that activates NF-kappaB and IRF 3. Cell 122, 669–682.

Shanmugasundaram, R., Selvaraj, R.K., 2012. Vitamin D-1alpha-hydroxylase and vitamin D-24-hydroxylase mRNA studies in chickens. Poult. Sci. 91, 1819–1824.

Silva, J.M., Wong, A., Carelli, V., Cortopassi, G.A., 2009. Inhibition of mitochondrial function induces an integrated stress response in oligodendroglia. Neurobiol. Dis. 34, 357–365.

Smriga, M., Torii, K., 2003. L-Lysine acts like a partial serotonin receptor 4 antagonist and inhibits serotonin-mediated intestinal pathologies and anxiety in rats. Proc. Natl. Acad. Sci. U. S. A. 100, 15370–15375.

Stipanuk, M.H., Ueki, I., 2011. Dealing with methionine/homocysteine sulfur: cysteine metabolism to taurine and inorganic sulfur. J. Inherit. Metab. Dis. 34, 17–32.

Sutton, R.A., Domrongkitchaiporn, S., 1993. Abnormal renal magnesium handling. Miner. Electrolyte Metab. 19, 232–240.

Takabe, K., Paugh, S.W., Milstien, S., Spiegel, S., 2008. "Inside-out" signaling of sphingosine-1-phosphate: therapeutic targets. Pharmacol. Rev. 60, 181–195.

Thompson, C.R., Iyer, S.S., Melrose, N., VanOosten, R., Johnson, K., Pitson, S.M., Obeid, L.M., Kusner, D.J., 2005. Sphingosine kinase 1 (SK1) is recruited to nascent phagosomes in human macrophages: inhibition of SK1 translocation by *Mycobacterium tuberculosis*. J. Immunol. 174, 3551–3561.

West, A.P., Shadel, G.S., Ghosh, S., 2011. Mitochondria in innate immune responses. Nat. Rev. Immunol. 11, 389–402.

Williams, B.L., Hornig, M., Buie, T., Bauman, M.L., Cho Paik, M., Wick, I., Bennett, A., Jabado, O., Hirschberg, D.L., Lipkin, W.I., 2011. Impaired carbohydrate digestion and transport and mucosal dysbiosis in the intestines of children with autism and gastrointestinal disturbances. PLoS One 6, e24585.

Wood, J.H., Partrick, D.A., Johnston Jr., R.B., 2010. The inflammatory response to injury in children. Curr. Opin. Pediatr. 22, 315–320.

Xia, J., Lim, J.C., Lu, W., Beckel, J.M., Macarak, E.J., Laties, A.M., Mitchell, C.H., 2012. Neurons respond directly to mechanical deformation with pannexin-mediated ATP release and autostimulation of P2X7 receptors. J. Physiol. 590, 2285–2304.

Yang, Z., Ming, X.F., 2012. mTOR signalling: the molecular interface connecting metabolic stress, aging and cardiovascular diseases. Obes. Rev. 13 (Suppl. 2), 58–68.

Yousefi, S., Gold, J.A., Andina, N., Lee, J.J., Kelly, A.M., Kozlowski, E., Schmid, I., Straumann, A., Reichenbach, J., Gleich, G.J., Simon, H.U., 2008. Catapult-like release of mitochondrial DNA by eosinophils contributes to antibacterial defense. Nat. Med. 14, 949–953.

Zamek-Gliszczynski, M.J., Hoffmaster, K.A., Nezasa, K., Tallman, M.N., Brouwer, K.L., 2006. Integration of hepatic drug transporters and phase II metabolizing enzymes: mechanisms of hepatic excretion of sulfate, glucuronide, and glutathione metabolites. Eur. J. Pharm. Sci. 27, 447–486.

Zhang, X., Hurng, J., Rateri, D.L., Daugherty, A., Schmid-Schonbein, G.W., Shin, H.Y., 2011. Membrane cholesterol modulates the fluid shear stress response of polymorphonuclear leukocytes via its effects on membrane fluidity. Am. J. Physiol. Cell Physiol. 301, C451–C460.

Zhou, R., Yazdi, A.S., Menu, P., Tschopp, J., 2011. A role for mitochondria in NLRP3 inflammasome activation. Nature 469, 221–225.

Mitochondrion xxx (xxxx) xxx–xxx

Contents lists available at ScienceDirect

Mitochondrion

journal homepage: www.elsevier.com/locate/mito

Review

Antipurinergic therapy for autism—An in-depth review

Robert K. Naviaux

University of California, San Diego School of Medicine, 214 Dickinson St., Bldg CTF, Rm C102, MC #8467, San Diego, CA 92103, United States

ARTICLE INFO

Keywords:
M1 mitochondria
M2 mitochondria
Purinergic signaling
Cell danger response
Ecogenetics
Ecoalleles
Epigenetics
Metabolism
Nucleotides
Antipurinergic therapy
Suramin

ABSTRACT

Are the symptoms of autism caused by a treatable metabolic syndrome that traces to the abnormal persistence of a normal, alternative functional state of mitochondria? A small clinical trial published in 2017 suggests this is possible. Based on a new unifying theory of pathogenesis for autism called the cell danger response (CDR) hypothesis, this study of 10 boys, ages 5–14 years, showed that all 5 boys who received antipurinergic therapy (APT) with a single intravenous dose of suramin experienced improvements in all the core symptoms of autism that lasted for 5–8 weeks. Language, social interaction, restricted interests, and repetitive movements all improved. Two children who were non-verbal spoke their first sentences. None of these improvements were observed in the placebo group. Larger and longer studies are needed to confirm this promising discovery. This review introduces the concept of M2 (anti-inflammatory) and M1 (pro-inflammatory) mitochondria that are polarized along a functional continuum according to cell stress. The pathophysiology of the CDR, the complementary functions of M1 and M2 mitochondria, relevant gene-environment interactions, and the metabolic underpinnings of behavior are discussed as foundation stones for understanding the improvements in ASD behaviors produced by antipurinergic therapy in this small clinical trial.

1. Background

In over 20 years of modern clinical trial efforts (McPheeters et al., 2011) and 75 years since the first description of autism (Kanner, 1943), no drug has been FDA approved to treat the core symptoms of autism spectrum disorder (ASD). I believe this is because the root cause of ASD is not yet understood. This has made it impossible to develop a unifying theory of pathogenesis that might help to guide new drug development.

2. The cell danger response hypothesis

The Suramin Autism Treatment 1 (SAT1) study (Naviaux et al., 2017) was the first clinical trial to test a new unifying theory for the root cause and a new treatment of autism. The cell danger response hypothesis represents a paradigm shift in how scientists think about the cause of autism. Instead of focusing on a particular behavior, cell type, genes, the microbiome, synapses, or the connectivity of neural circuits in the brain, the cell danger hypothesis states that the root cause of autism is a universal cellular response to stress that shifts normal cell function to a new state. Severe and/or prolonged stress forces a reallocation of cellular resources for survival. This universal response to stress traces to mitochondria and is called the cell danger response (CDR) (Naviaux, 2014). Aspects of the CDR are also referred to as the integrated stress response (Green et al., 2011; Nikkanen et al., 2016; Silva et al., 2009). The CDR gives the appearance of mitochondrial dysfunction, but is actually a normal, necessary, and *highly regulated change* in mitochondrial function from oxidative phosphorylation to cellular defense. This shift is needed to respond to a threat, and to heal after an injury. Mitochondria that defend the cell in danger can no longer function the same as they do under unstressed conditions (Naviaux et al., 2009). This programmed change in mitochondrial function is needed for innate immunity and inflammation (West, 2017), which in turn are required for establishing the adaptive immune response and healing.

3. M1 and M2 mitochondria

To emphasize the importance and dynamic nature of this programmed change in mitochondrial function, I have designated these as M1 and M2 mitochondria (Fig. 1). M1 and M2 mitochondria represent two poles on a functional continuum (Sander and Garaude, 2017) regulated by the CDR. M2 mitochondria are devoted to oxphos and are anti-inflammatory. In contrast, M1 mitochondria are pro-inflammatory. M1 mitochondria are specialized for creating the oxidative shielding response (Naviaux, 2012b). M1 mitochondria are tasked for cellular defense and increase cellular redox (are pro-oxidants) and perform dozens of other functions needed for anti-viral and anti-microbial defense. The shift from M2 to M1 mitochondrial functions is an intrinsic feature of an activated CDR. Within a given cell, this shift creates a spectrum from 100% M2 mitochondria when stress is minimum, to

E-mail address: Naviaux@ucsd.edu.

https://doi.org/10.1016/j.mito.2017.12.007
Received 15 September 2017; Received in revised form 11 December 2017; Accepted 14 December 2017

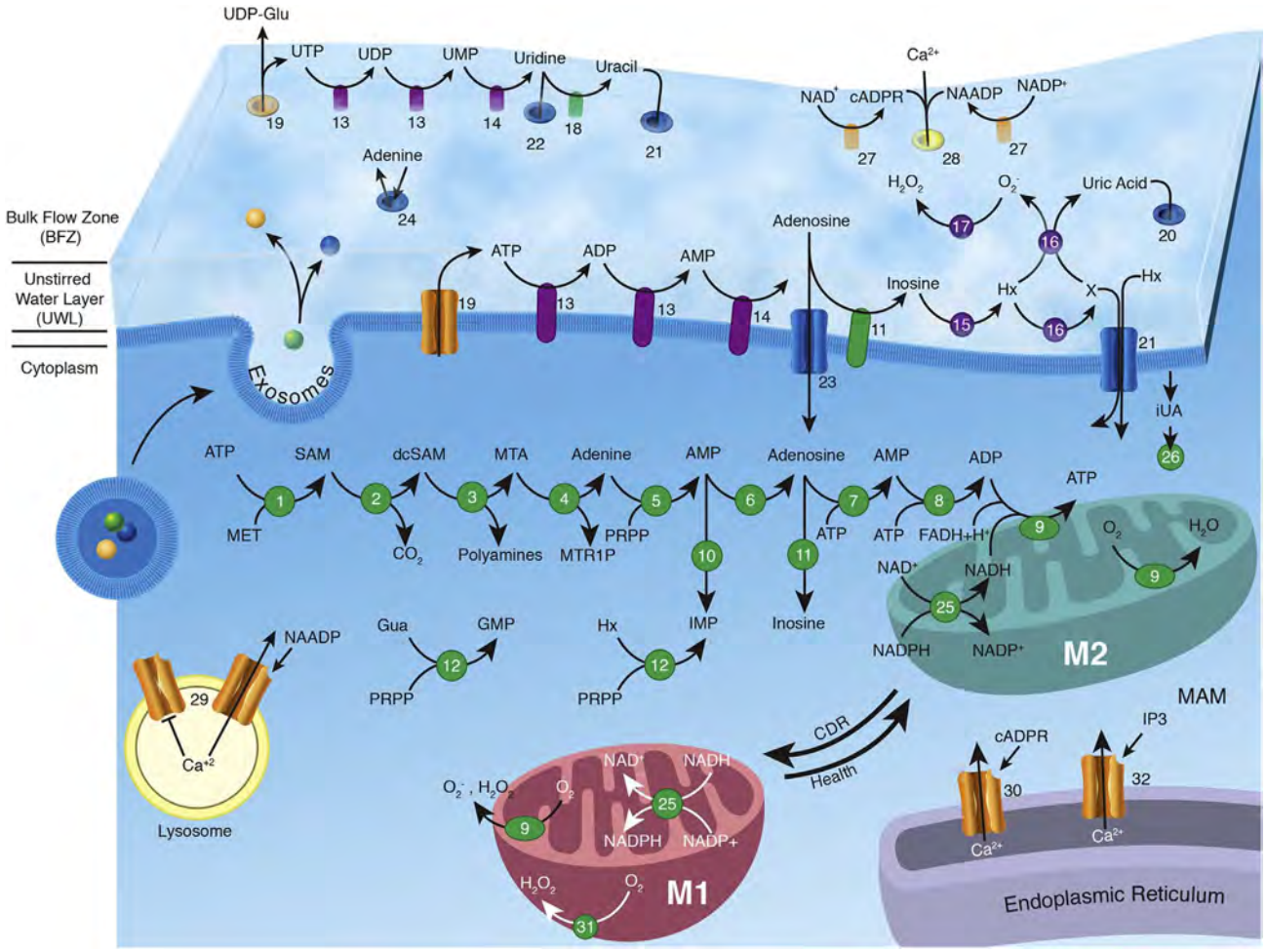

Fig. 1. Metabolic control of purinergic signaling. The availability of purinergic effectors in the unstirred water layer where receptors and ligands meet is controlled by a suite of metabolic proteins and solute channels. A simplified summary of their actions, and the dynamic capacity for mitochondrial functional changes that are associated with the CDR are illustrated.
Cellular zones: Bulk flow zone (BFZ), unstirred water layer (UWL), cell membrane, cytoplasm, ER-mitochondria-associated membranes (MAMs).
Organelles: M1 mitochondria are pro-inflammatory and dedicated to helping to orchestrate the cell danger response (CDR). M2 mitochondria are anti-inflammatory and dedicated to oxidative phosphorylation (oxphos). Lysosomes contain an acidic pool of calcium gated by NAADP acting on TCP. Endoplasmic reticulum (ER) contains a neutral pool of calcium gated by cADPR acting on the ryanodine receptor (RyR). Exosomes are sphingolipid-enriched nanovesicles that are used for cell-cell signaling and the removal and exchange of intracellular materials.
Proteins: Integral Membrane-associated enzymes (purple), Non-Integral membrane enzymes (green), Receptors and Ligand-gated channels (orange), and Non-ligand-gated Transport Channels (blue). 1—MAT: methionine adenosyl transferase. 2—SAMdc: S-Adenosylmethionine (SAM) decarboxylase. 3—dcSAM aminopropyltransferases; spermidine synthase and spermine synthase. 4—MTAP: methylthioadenosine phosphorylase. 5—APRT: adenine phosphoribosyl transferase. 6—5NT: 5′-nucleotidase. 7—ADOK: adenosine kinase. 8—ADK; adenylate kinase (also known as myokinase). 9—The mitochondrial electron transport chain (ETC), consisting of mitochondrial respiratory chain complexes I, II, III, IV, and V. 10—AMPD2: AMP deaminase 2. 11—ADA: adenosine deaminase. 12—HGPRT: hypoxanthine-guanine phosphoribosyl transferase. 13—CD39: ectonucleoside triphosphate diphosphohydrolase (also called ENTPD1), 14—CD73: ecto-5′-nucleotidase (also called NT5E). 15—PNP: purine nucleoside phosphorylase. 16—XO: xanthine oxidase. 17—SOD3: copper-zinc dependent ecto-superoxide dismutase 3. 18—Upase: uridine phosphorylase. 19—Pannexin/P2X7 Porin; activated by oxidation and ATP, and blocked by suramin. 20—GLUT9a/SLC2A9: cytokine regulated uric acid transporter. 21—SNBT1/SLC23A4: sodium-dependent, concentrative nucleobase transporter 1. 22—ENTI/SLC29A1: equilibrative nucleoside transporter 1. 23—ENT2/SLC29A2: equilibrative nucleoside transporter 2. 24—ENBT1/SLC43A3: equilibrative nucleobase transporter 1. 25—NNT: nicotinamide-nucleotide transhydrogenase. 26—NLRP3 inflammasome assembly. 27—CD38: cyclic ADP ribose hydrolase. 28—TRPM2: transient receptor potential cation channel, subfamily M, member 2. 29—TPC: two pore channel. 30—RyR: ryanodine receptor. 31—NOX4: NADPH oxidase 4. 32—IP3R: inositol trisphosphate receptor.
Metabolites: Met: methionine. ATP: Adensoine triphosphate. ADP: adenosine diphosphate. AMP: adenosine monophosphate (also called adenylate or adenylic acid). SAM: S-adenosyl methionine. dcSAM: decarboxyl-SAM. Polyamines: spermidine, spermine. MTA: methylthioadenosine. MTR1P: methylthioribose-1-phosphate. PRPP: phosphoribosylpyrophosphate. Hx: hypoxanthine. Gua: guanine. X: xanthine. eUA: extracellular uric acid. iUA: intracellular uric acid. UTP: uridine triphosphate. UDP: uridine disphosphate. UMP: uridine monophosphate (also called uridylate or uridylic acid). UDP-Glu: UDP-glucose. NADH: nicotinamide adenine dinucleotide (reduced form). NADPH: Nicotinamide adenine dinucleotide phosphate (reduced form). cADPR: cyclic ADP ribose. NAADP: nicotinic acid adenine dinucleotide phosphate. IP3: inositol trisphosphate.

50:50 M1:M2 and intermediate forms at medium-stress conditions, up to 100% M1 when the survival of the cell is threatened. When the fusion-fission cycle of mitochondria in a particular cell type is rapid (minutes to hours), as occurs in rapidly dividing cells in the bone marrow and gut epithelium, this transition comes to a new steady-state within minutes to hours. When the fusion-fission cycle of mitochondria is slow (for example, it is 2 weeks in the cardiac myocytes of adult mice (Song and Dorn II, 2015)), the M2 to M1 transition occurs more slowly, and the M1 state lasts longer after the danger has passed. Other differentiation states of mitochondria exist. For example, the mitochondria in brown adipose tissue (BAT) and beige/bright cells in white adipose tissue (WAT) have distinct developmental origins (Kajimura and Saito, 2014). Pluripotential M0 mitochondria are present in stem cells (Folmes et al., 2012) and primary oocytes (Van Blerkom, 2011).

The shift from M2 (anti-inflammatory) to M1 (pro-inflammatory) mitochondria that occurs when a cell becomes threatened is not unlike the analogous shift in the functional state of macrophages from resting

M0 or polarized M2, to M1. The M1 phenotype of macrophages is pro-inflammatory and needed for cell defense, while M2 macrophages are anti-inflammatory and needed to facilitate the resolution of inflammation and healing. This cellular polarization is strongly correlated with oxidative phenotype of the mitochondria within macrophages (Chen et al., 2017). When the choreographed sequence of metabolic steps in the healing cycle encounters a roadblock for any reason, a persistent form of the CDR results, and M1 pro-inflammatory mitochondria persist past the time they are needed. This changes the trajectory of child development, and can lead to ASD and several other disorders.

4. ASD genetics, the CDR, and inflammation

Each of the common genes known to strongly increase the risk of ASD can be shown to play a role in CDR signaling or maintenance. Fragile X is just one of several examples. The Fragile X gene FMR1 encodes a protein that normally inhibits the translation of proinflammatory cytokines like TNFα (Garnon et al., 2005). Decreased expression of the Fragile X protein results in persistent activation of the CDR in the form of a low-grade inflammatory response in the brain (Di Marco et al., 2016). Could therapy directed at the CDR be effective in Fragile X, and other genetic causes of ASD? Antipurinergic therapy (APT) directed at the CDR has already proven effective in correcting ASD-like behaviors in the Fragile X mouse model (Naviaux et al., 2015).

Rett syndrome is another example of a genetic cause of autism spectrum disorder that is tied to the cell danger response and inflammation (Cortelazzo et al., 2014). Most cases of Rett syndrome trace to new mutations in the MeCP2 gene, which codes for a methyl-CpG binding protein. Mutations in MeCP2 alter chromatin structure and lead to retroelement mobilization (Muotri et al., 2010), genetic instability, and profound changes in the innate immune response (Derecki et al., 2012). The CDR coordinates retroelement mobilization and innate immunity (Naviaux, 2014). Animal models of Rett syndrome are an important reminder that even in some genetic causes of autism, the core behavioral features of ASD are not permanent. Behaviors can be reversed by treating the cell danger response that underlies oxidative changes and inflammation (Derecki et al., 2013).

Other examples include Angelman and Smith-Magenis syndrome. Angelman syndrome is usually caused by a *de novo* maternal deletion or mutation of a gene called ubiquitin-protein ligase E3A (UBE3A) located on chromosome15q11-q13. UBE3A is involved in the unfolded protein response. Mutations in UBE3A result in the accumulation of unfolded proteins (Mishra et al., 2009), which are in turn known to activate the CDR (Smith, 2014). Smith-Magenis syndrome is usually caused by chromosomal copy number variation (CNV) resulting in a deletion of a patch of DNA on chromosome 17p11.2 containing the retinoic acid induced 1 (RAI1) gene (Huang et al., 2016). This is not to be confused with the retinoic acid induced gene 1 (RIG1), a helicase on chromosome 9. Defects in RAI1 result in increased childhood infections and immunologic abnormalities (Perkins et al., 2017) that result in repeated activation of the CDR. Future studies will be required to test therapies directed at the CDR in children with Fragile X, Rett, Angelman, and Smith-Magenis syndromes.

5. Cellular order, metabolism, defense, and immunity

5.1. Mitochondria and the CDR

The daily operations of the cell require protein-protein and many other macromolecular interactions that rely critically on cellular spatial order—packing—for efficient function. When order is disrupted, function suffers. Any kind of physical or biological injury to the cell decreases electrons shuttled from nutrients to mitochondria. Mitochondrial electron flow acts as a barometer of cellular health. When mitochondrial electron transfer is disrupted a cellular metabolic syndrome is produced. This new cellular metabolic state is needed for healing. This starts locally at the site of injury, but propagates to neighboring cells as they adopt a change in function to contain the injury. If the injury cannot be contained locally, systemic signals are sent by neuroendocrine and autonomic nervous systems that ultimately produce changes in systemic metabolism and behavior. Disruptions in molecular order or the organization of cytoskeleton and organelles within cells is perhaps one of the most fundamental signals of danger. Increasing cellular disorder is the biologic equivalent of increasing thermodynamic entropy.

5.2. The importance of water

The decrease in the ordered state of macromolecules and solutes forces a change in the distribution, behavior, and thermodynamic properties of water molecules (H_2O) in and around cells (Chaplin, 2006; Pollack, 2013; Prigogine and Nicolis, 1971). The partial positive and negative charge on a molecule of water, and other forces, constrain its movement by interacting with the surface charges around proteins, membranes, and cytoskeleton creating a fraction of bound or “vicinal” water that covers all biological surfaces. The more polymers or membranes in solution, the greater the fraction of bound to unbound water. The net effect of increased acidity and increased dissolved oxygen in cells and tissues is to inhibit macromolecular (polymer) synthesis reactions. Polymer synthesis reactions include the condensation of amino acids to make proteins and nucleotides to make RNA and DNA. This decreases the differentiated functional capacity of the cell, but is required to initiate healing after injury. Mitochondrial fusion-fission dynamics shift toward fission to permit increased quality control under stress (Youle and van der Bliek, 2012). Metabolic synapses between mitochondria and the endoplasmic reticulum known as mitochondrial-associated membranes (MAMs) also change under stress, further altering the ordered intracellular structure of organellar networks. MAMs regulate calcium, phospholipid, sphingolipid exchange, and many other key physiologic processes (Sano et al., 2009). Changes in mitochondrial dynamics during cell stress in tissues link increasing cytoplasmic disorder with increasing disorder of water molecules, and an increase in CDR-associated functions. The monitoring of cellular disorder is fundamental for normal immune system function (Cunliffe, 1997).

6. The CDR, redox, M1 mitochondria, and ASD

Oxidative changes in autism have been well-studied (James et al., 2006; Rose et al., 2017). Single cells make reactive oxygen species (ROS) to harden themselves when they come under attack by pathogenic organisms or environmental stress (Naviaux, 2012b). Indeed, the mitochondria in cells make the very ROS that inhibit their own bioenergetic functions. This seems self-destructive, but it is not. The adaptive function of the ROS-response cannot be understood within a single-cell frame of reference. The relevant frame of reference is the host considered as a collective system of many cells and tissues. Local ROS are responsible for activating a normal, but latent, alternative function of mitochondria in threatened cells. Under baseline conditions, tissue mitochondria exist mostly in an M2, or anti-inflammatory state dedicated to oxphos. When ROS are increased, mitochondria take on a new job. They become polarized to M1 mitochondria, become an important source of ROS themselves, increase the rate of damaged organelle removal via intracellular quality control methods, and become the initiators and coordinators of the antiviral response (Seth et al., 2005) and cellular defense (West et al., 2011). To do this, mitochondria must temporarily drop their “day job” as the hub of oxidative phosphorylation served by their M2 polarized state. The cell-autonomous inhibition of mitochondrial oxphos by ROS decreases both the production of cellular building blocks and the exchange of building blocks with other cells. The ROS-response and M1 polarization of mitochondria is adaptive because it decreases the chances that a virus, or pathogenic

organism, or damage from a traumatic or chemical injury or toxin can spread to kill the host. A line of cells in which mitochondrial oxphos is decreased, and lactic acid and ROS are increased, creates the cellular equivalent of sealing the bulkheads that separate the compartments on a damaged ship or submarine to prevent the spread of more water to undamaged sections. Furthermore, when the metabolic rate of a single cell is decreased relative to neighboring cells, the local clock of biological time within that cell slows, permitting it to resist maturation and outlast the cells unable to use fewer resources for survival. For this and other reasons, the author favors the term "oxidative shielding" instead of "oxidative stress" (Naviaux, 2012b). The host benefits strongly from the ability of single cells to shift nimbly from peacetime M2 metabolism to defensive M1 metabolism needed for damage containment in response to environmental stress. When viewed contextually, it can be understood that this is not "mitochondrial dysfunction". The M1 state is an adaptive, new function of mitochondria that is produced when cells come under stress. Chronic disease results when this cell danger response cannot be turned off when its job is done.

7. The CDR, exosomes, and the immune response in ASD

Stressed cells increase the number and diversity of lipid nanovesicles called exosomes that they release into the extracellular space (Fig. 1) (Nemeth et al., 2017). Exosomes are enriched in stress- and danger-signaling sphingolipids, self-antigens that include metabolic enzymes from internal compartments of the cell, micro-RNAs, mitochondrial DNA (mtDNA), and partially processed materials from the mitophagy and autophagy pathways (Pellegrino and Haynes, 2015). Exosomes help to remove non-infectious aggregates of proteins like β-amyloid, α-synuclein, and tau that might otherwise accumulate inside the cell and become toxic (Rajendran et al., 2006; Wang et al., 2017; Yang et al., 2017). Exosomes are also critical for many forms of cell-cell communication involved in fundamental biological processes like fertilization (Machtinger et al., 2016) and neurotransmission (Lachenal et al., 2011). Viruses and microbial pathogens are known to hijack exosomes for cell-to-cell transmission. To combat this, certain interferon-induced genes like ISG15 have evolved that decrease total cell protein synthesis and exosome release from infected cells. This creates a reduction in cell-to-cell communication through exosome release, but permits more efficient disposal of pathogens within the cell by fusion with lysosomes (Villarroya-Beltri et al., 2017).

Another function of exosomes is to permit the export and recycling of biochemical building blocks produced during normal cell function (Fig. 1). Exosome release and reuptake into neighboring or distant cells occurs naturally during the turnover of billions of cells that occurs daily by apoptosis. Naturally occurring molecules like mtDNA, α-galactosylceramide in lipid rafts, formyl-methionine containing mitochondrial peptides, released ATP and UTP, and other molecules can stimulate toll-like receptors (TLRs) and related stress-sensing receptors on B1 cells and support the production of naturally occurring, low-affinity, IgM antibodies. These natural autoantibodies (NAAs) are present from birth, are produced by T-cell independent, TLR-stimulated B1 cells, and have potent anti-inflammatory effects (Lobo, 2017). Low-titer IgM antibodies to self-antigens are increased after surgery and other traumas (Raad et al., 2014) because of increased release of material from stressed or damaged cells (Oka et al., 2012). These natural autoantibodies play an important protective role, limiting inflammation (Andaluz-Ojeda et al., 2013). Once the trauma or cellular damage is healed, exosome production, and other cellular sources of antigens are diminished, and autoantibody production is returned to background levels. If antigen presentation continues because of ongoing stress or infection, then high-affinity IgG antibodies can be stimulated, selected, and amplified.

Autoantibodies to the folate receptor (Frye et al., 2016a), and maternal antibodies to brain proteins (Edmiston et al., 2017) are associated with ASD risk. Complex neuroimmune syndromes like pediatric acute-onset neuropsychiatric syndrome (PANS), pediatric autoimmune neuropsychiatric disorder associated with streptococcal infections (PANDAS), and autonomic disturbances like postural orthostatic tachycardia syndrome (POTS) are also risks in ASD. The chronically activated CDR can also lead to sleep disturbances, seizures, leaky gut, gut inflammation, and dysmotility. Thyroid abnormalities reflected by an increase in the rT3 also occur (Frye et al., 2017). This may be a consequence of stress induction of the selenoproteins, deiodinases 2 and 3 (DIO2 and 3), that are responsible for inactivating T4 and producing reverse T3 (rT3) (Lamirand et al., 2008). The CDR also regulates Th17 cells through purinergic signaling (Sullivan et al., 2014). Th17 cells and Th17 receptor expression on monocytes play several important roles in regulating breaches in immune tolerance (Pfeifle et al., 2017), and inflammation in autism (Nadeem et al., 2017).

8. The CDR, natural infections, and vaccinations

The CDR is a normal and universal feature of any stress. This means that it is normally activated by both natural infections and vaccination. The CDR is needed to establish cellular and humoral immunity. Since the large majority of children and adults who receive vaccinations, or are exposed to common natural viral infections like Epstein Barr Virus (EBV), are able to recover without incident, the biological question is, "Why are some children and adults unable to moderate or turn off the CDR when its job is done and immunity is established?" We do not have an answer to this question yet. However, relatively simple measures like distributing vaccinations over time, instead of giving a large number at once would decrease the chances of triggering an excessive CDR in individual children deemed to be at increased risk. In addition, future research into the metabolomic phenotypes of children before and after vaccinations may begin to shine some light on differences in natural metabolic and physiologic states, that might permit us to predict the risk and develop treatments to prevent the rare complications like post-immunization, febrile seizures (MacDonald et al., 2014).

9. Gene-environment interactions in ASD

9.1. Managing environmental risks

The CDR is triggered by both genes and environmental factors. Genes, and the proteins they make, can be thought of as providing adaptive resilience, like stretch in a homeostatic safety net, to a large number of stressors. When new, more frequent, or more severe exposures are encountered, the adaptive and healing capacity of cells can be pushed to, and beyond its homeostatic limits. This creates roadblocks to healing that result in a persistent form of the CDR. Environmental factors that can test the resilience of any given genotype include physical, chemical, nutritional, microbial, and psychological traumas. Infections during pregnancy (Zerbo et al., 2013), prenatal maternal psychological stress (Kinney et al., 2008; Ronald et al., 2010), early life stress (Cameron et al., 2017; Heun-Johnson and Levitt, 2016; Rutter et al., 2001), and exposure to a variety of toxins (Braun et al., 2014), metals (Kalkbrenner et al., 2014; Palmer et al., 2009), or traffic-related air pollution (Volk et al., 2011; Volk et al., 2013) have each been shown to contribute to ASD risk. Combinations of all these factors in a particular home, neighborhood, city, or rural environment contribute to the concept of total toxic load (Herbert et al., 2013). If the exposure happens during critical periods in early child development, ASD and several other childhood disorders can result (Landrigan et al., 2012). When avoidable risks are managed, pregnancy outcomes and child health can be improved (Adams et al., 2016; Schmidt et al., 2011).

9.2. Ecogenetics, ecoalleles, and ASD

Recent twin studies show that environmental factors are responsible for about 60% (mean = 58%; 95% CI = 30–80%) of ASD. The collective contribution of all genes was about 40% (mean = 37%; 95% CI

8–84%) (Hallmayer et al., 2011), but no single gene accounts for more than 1–2% of all of ASD (Talkowski et al., 2014). The term ecogenetics describes the interaction between genes and environment. Many genes show strong differences in function depending on exposure to different environmental factors. These "ecoalleles" are common gene variants—polymorphisms with allelic frequencies of about 2%–50%—in enzymes, receptors, transporters, and transcription factors that have different activities depending on environmental factors. Some of these environmental factors include seasonal and diurnal temperature fluctuations, or the availability of calories, fats or carbohydrates, trace metals, redox, critical cofactors like thiamine (B1), niacin (B3), riboflavin (B2), folic acid (B9), B12, lipoic acid, tetrahydrobiopterin (BH4), biotin, pantothenic acid, vitamin D, C, or pyridoxine (B6), or exposure to drugs, pesticides, or toxins.

The prevalence of ecoalleles in different populations around the world differs significantly according to different climatic, dietary, infectious disease, and cultural conditions. For example, the ecoallele c.677T in methylene tetrahydrofolate reductase (MTHFR) is rare in populations from sub-Saharan Africa (5%), but more common in Mexican, Italian, and Ashkenazi Jewish populations where it has an allelic frequency of about 50% (Karban et al., 2016). The risk of disease associated with the c.677T ecoallele is context dependent. Despite being more common in Ashkenazi Jewish populations, the c.677T allele in MTHFR was a risk factor for autism, inflammatory bowel disease, and certain other diseases in non-Ashkenazi populations but not in Ashkenazi populations (Frye and James, 2014; Karban et al., 2016). If ecoalleles were always harmful in all world contexts at all ages, they would eventually be removed from the ancestral gene pool, or reduced to frequencies well below 1%. Alleles that cause disease in post-reproductive adults can be maintained by advantages to children or young adults. In the case of MTHFR, it has been hypothesized that the c.677T variant confers resistance to malaria (Meadows et al., 2014). In sub-Saharan Africa, the sickle-cell hemoglobin trait became the most common genetic form of resistance to malaria. In other regions where different ecological and nutritional factors played a role in the selection of mechanisms of pathogen resistance that were not limited to malaria, MTHFR variants became more widespread, as in historical populations in southern Europe and Mexico.

Other ecoalleles include variants of cystathionine beta synthase (CBS), catechol-O-methyl transferase (COMT), monoamine oxidase A (MAO-A), amine oxidase, copper-containing 1 (AOC1; also known as diamine oxidase, DAO, and amiloride binding protein, ABP), histamine N-methyl transferase (HNMT), N-acetyltransferase 2 (NAT2), sulfotransferase 1A1 (SULT1A1), glucose-6-phosphate dehydrogenase (G6PD), extracellular super oxide dismutase 3 (SOD3), deiodinase 2 (DIO2), chitinase 1 (CHIT1), solute carrier 19A1 (SLC19A1, also called the reduced folate carrier 1, RFC1), methionine adenosyltransferase 1 (MAT1), sphingomyelinase phosphodiesterase 1 (SMPD1, also called acid sphingomyelinase, ASM), endothelial nitric oxide synthase (eNOS, also called NOS3), hemochromatosis (HFE), glutathione peroxidase 1 (GPX1), glutathione-S-transferase pi-1 (GSTP1), and serum paraoxonase/arylesterase 1 (PON1). Evolutionary selection maintains the prevalence of ecoalleles at frequencies of about 2%-50% because they have environment- and context-dependent fitness advantages, sometimes manifested only as the heterozygote carrier genotype.

9.3. The CDR activates the moonlighting functions of ecoalleles

As discussed above, M1 mitochondria use ROS to activate their latent/moonlighting function as coordinators of the cell danger response under conditions of environmental stress. Many metabolic enzymes also have moonlighting functions that are induced by new environmental conditions (Sriram et al., 2005). These moonlighting functions often seem self-destructive unless understood in terms of the cell danger response (CDR) (Naviaux, 2014). One important example is the mitochondrial enzyme dihydrolipoamide dehydrogenase (DLD), also known as the E3 protein. This protein is shared by 5 different mitochondrial enzyme systems that are critical for regulating cellular bioenergetics, redox, and amino acid metabolism. The enzyme systems catalyze NAD^+ dependent, oxidative decarboxylation reactions. They are: pyruvate dehydrogenase complex (PDH), alpha-keto glutarate dehydrogenase (AKDH, also known as 2-OGDH), branched chain ketoacid dehydrogenase complex (BCKDH), 2-oxoadipate dehydrogenase (2-OADH), and the glycine cleavage system. Each of these 5 key enzyme systems can be affected when DLD changes from its canonical function to its moonlighting function under conditions of environmental stress. This leads to CDR-associated chromatin remodeling because alpha ketoglutarate released from mitochondria is an essential cofactor for Jumonji histone demethylases (Kang et al., 2017), and NAD^+ build-up activates histone deacetylation and DNA transcriptional silencing by sirtuins (Simoneau et al., 2016). The net result is to slow gene expression and metabolism in stressed cells. Over 90 DNA variants of DLD are currently listed in ClinVar (https://www.ncbi.nlm.nih.gov/clinvar?term=238331 [MIM]). Thirty-one of 92 variants (34%) are currently classified as benign or likely benign. Some of these may in fact be ecoalleles of DLD that have not yet been fully characterized. Several DLD variants are strongly inhibited by valproate, creating an ecogenetic risk for drug-induced liver toxicity (Kudin et al., 2017).

Under conditions of low mitochondrial matrix pH produced by ischemia-reperfusion, high salt concentration, and other stresses, DLD changes from its normal dimeric conformation and adopts an oligomeric or monomeric structure. The normal DLD activity is lost as the moonlighting functions of the E3 protein are activated by stress. The first new activity to emerge is reactive oxygen species (ROS) production (Ambrus and Adam-Vizi, 2017) using NADH and oxygen for oxidative shielding in response to microbial infection or other stress (Naviaux, 2012b). This accompanies the shift from M2 anti-inflammatory to M1 pro-inflammatory mitochondria. Progressive stress leads to the transformation to monomer configuration and unmasks a cryptic protease activity. The emergent E3 protease cleaves several mitochondrial substrates, including the iron-sulfur cluster biogenesis protein frataxin (Babady et al., 2007). This leads to a prolonged shift from M2 to M1 mitochondria after transient but severe stress (Klyachko et al., 2005). Disruptions in iron-sulfur cluster assembly can have profound affects on dozens of proteins in key pathways of the cell danger response. Among these are viperin and ABCE1 used in the antiviral response, aconitase in the Krebs cycle, subunits of the mitochondrial respiratory chain complexes I, II, and III needed for energy production, and DNA repair proteins like XPD and FANCJ (Braymer and Lill, 2017).

9.4. Emergent phenotypes, epigenetics, and metabolic treatments

Mixtures of ecoalleles, with and without moonlighting functions, produce new phenotypes and patterns of disease risk and resilience that represent latent traits that are revealed by exposure to specific environmental triggers. While single ecoalleles can have predictable consequences like common pharmacogenomic variants (Schuck and Grillo, 2016), mixtures of ecoalleles are conditional and have emergent phenotypes that cannot be predicted from genomic analysis alone. Ecoalleles create resilience in the homeostatic safety net that helps life manage environmental infections, toxins, famine, vascular and tissue injury, and other stressors. The combined effect of unique mixtures of ecoalleles is to create metabolic phenotypes that are key targets for natural selection and evolution. Emergent metabolic traits are the result of real-time interaction of genes and environment. Their fitness depends on the environmental context. What permits survival under harsh conditions may slow reproduction or development under mild conditions.

When environmental conditions change over the course of child development, and harsh conditions alternate with mild, or harsh conditions begin to be more common than mild, recovery from the survival or defensive cellular state can be delayed or persist. Some of the

Table 1
Metabolic disturbances in autism spectrum disorder.

No.	Metabolic abnormality	Authors	Dates	References
1	Decreased tryptophan conversion to serotonin; increased kynurenine pathway	H. Eldon Sutton	1958	Sutton and Read (1958)
2	Increased tryptophan and platelet serotonin	Daniel Freedman	1961	Mulder et al. (2004); Schain and Freedman (1961)
3	Increased purine metabolism	William Nyhan, Mary Coleman	1969, 2000	Nyhan et al. (1969); Page and Coleman (2000)
4	Pyridoxine metabolism	Bernard Rimland James Adams	1978, 2006	Adams et al. (2006); Rimland et al. (1978)
5	Increased sphingolipids and gangliosides	Chris Gillberg	1998	Nordin et al. (1998); Schengrund et al. (2012)
6	Decreased sulfation, and plasma sulfate; Increased plasma cysteine, urine sulfate	Rosemary Waring	1999	Alberti et al. (1999)
7	Mitochondrial DNA mutations	William Graf, Robert Naviaux, Richard Haas	2000	Graf et al. (2000)
8	Mitochondrial respiratory chain complex overactivity	William Graf et al. Luigi Palmieri and Tony Persico Richard Frye and Robert Naviaux Shannon Rose, Richard Frye,Jill James	2000 2010 2011 2014	Frye and Naviaux (2011); Graf et al. (2000); Palmieri et al. (2010); Rose et al. (2014a); Rose et al. (2014b)
9	Decreased cholesterol/sterols	Elaine Tierney, Richard Kelley	2000	Tierney et al. (2000)
10	Microbiome dysbiosis	Richard Sandler, Sydney Finegold	2000, 2002	Finegold et al. (2002); Sandler et al. (2000)
11	1-Carbon and folate metabolism	Jill James	2004	James et al. (2004)
12	Cysteine, glutathione, SAM/SAH	Jill James	2006	James et al. (2006)
13	Reactive oxygen metabolism	Jill James	2006	Frustaci et al. (2012); James et al. (2006)
14	Pyrimidines—increased uridine, BAIB	W. Brussel, James Adams	2006, 2011	Adams et al. (2011)Brussel et al. (2006); Micheli et al. (2011)
15	Creatine deficiency	V. Leuzzi, Sylvia Stoeckler-Ipsiroglu	2002, 2006	Leuzzi (2002); Mercimek-Mahmutoglu et al. (2006)
16	Mitochondrial control of epigenetics	Robert Naviaux, Keshav Singh, Doug Wallace	2008, 2010	Naviaux (2008); Smiraglia et al. (2008); Wallace and Fan (2010)
17	Vitamin D insufficiency	John Cannell, Chris Gillberg	2008, 2012	Cannell (2008); Kočovská et al. (2012)
18	Increased VLCFA PE lipids	Dayan Goodenowe	2009	Pastural et al. (2009)
19	Decreased biopterin	Richard Frye	2010	Frye et al. (2010)
20	Decreased plasma biotin	James Adams	2011	Adams et al. (2011)
21	Decreased plasma ATP, increased adenosine	James Adams	2011	Adams et al. (2011)
22	Increased plasma glutamate	James Adams	2011	Adams et al. (2011)
23	Decreased branched chain amino acids	James Adams Rabindra Tirouvanziam Joe Gleeson	2011, 2012	Adams et al. (2011)Novarino et al. (2012)Tirouvanziam et al. (2012)
24	Increased plasma and urine oxalate	Jerzy Konstantynowicz	2012	Konstantynowicz et al. (2012)
25	Propiogenic amino acid metabolism	Derrick MacFabe, M. Al-Owain	2007, 2012	Al-Owain et al. (2013); MacFabe et al. (2007)
26	Decreased carnitine synthesis	Art Beaudet	2012	Celestino-Soper et al. (2012)
27	Eicosanoids	Afaf El-Ansary	2012	Beaulieu (2013); El-Ansary and Al-Ayadhi (2012); Gorrindo et al. (2013)
28	Oxidative shielding and metabolic memory	Robert Naviaux	2012	Naviaux (2012b)
29	Decreased fatty acid oxidation	Richard Frye	2013	Frye et al. (2013b)
30	Decreased plasma choline and betaine	Jill James	2013	Hamlin et al. (2013)
31	Increased rT3/TSH	Richard Frye	2017	Frye et al. (2017)
32	Cell danger response metabolism	Robert Naviaux	2012 2013 2014 2015 2017	Naviaux et al. (2014); Naviaux et al. (2015); Naviaux (2012a, 2014); Naviaux et al. (2017); Naviaux et al. (2013)

persistence of these traits can be driven by durable epigenetic changes that trace to mitochondrial function (Minocherhomji et al., 2012; Naviaux, 2008; Wallace and Fan, 2010), but produce changes in gene expression that can persist beyond their utility because of time lags between frequent activation in a harsh environment, and recovery. Under these changing environmental conditions, mixtures of ecoalleles and epigenetic changes that were once advantageous may become a disadvantage. When this happens in ASD, cofactor and metabolic therapies directed at ecoallele-driven phenotypes in ASD can help strengthen resilience in the homeostatic safety net and improve behavioral symptoms (Frye et al., 2013a, 2016b).

10. Metabolism and ASD behavior

The idea that behaviors in autism are caused by a change in metabolism is not new. The first organic abnormalities reported in ASD were metabolic (Rimland, 1964; Sutton and Read, 1958) (Table 1). Several genetic disorders of purine and pyrimidine (Micheli et al., 2011; Nyhan et al., 1969; Page and Coleman, 2000) and energy metabolism (Stockler-Ipsiroglu and van Karnebeek, 2014) are associated with autistic behaviors. Bernie Rimland, the founder of the Autism Research Institute (ARI), pioneered the metabolic approach to treatment in the first clinical trial of pyridoxine in children with ASD (Rimland et al., 1978). When cells detect genetic or environmental threats, mitochondrial function changes in a predictable way. These changes produce the CDR and act as a two-edged sword. On the one hand, the change in cell metabolism allows threatened cells surrounding the injury to better survive dangerous conditions. On the other hand, when these changes become widespread and occur during pregnancy or the first 3 years of life, and are severe or sustained, they can alter the trajectory of normal

child development. The CDR produces effects on purinergic signaling that change how neural circuits are selected and how synapses are formed and pruned in the brain (Sipe et al., 2016). Many other organ systems are also affected by the CDR. These include the immune system, the gut microbiome, and the autonomic nervous system. Each of these is documented to be dysfunctional in autism.

Over 30 metabolic abnormalities have been described in ASD over the past 60 years (Table 1). All are known markers of the cell danger response (Naviaux, 2014; Naviaux et al., 2016). Interestingly, this set of about 30 different metabolic pathways is shared with the conserved cellular response to danger or threat regardless of whether the trigger was a virus (Wikoff et al., 2009), a bacterium (Degtyar et al., 2009), genetic forms of mitochondrial disease (Nikkanen et al., 2016), or neurodevelopmental disorders with complex gene-environment pathogenic mechanisms like autism (James et al., 2004). The hopeful message behind the CDR hypothesis is that the root cause of the communication difficulties, social anxiety, sensory abnormalities, GI problems, seizures, allergies, and many other comorbidities in autism, is a treatable metabolic syndrome. This means that contrary to classical teaching in medical schools around the world for the past 70 years, autism may not be permanent in some children. By treating the root cause, the CDR hypothesis gives hope that longstanding roadblocks to development can be removed and the children can make remarkable progress, despite a great heterogeneity in the causes of ASD. Future clinical trials will be needed to test this hypothesis rigorously.

11. Purinergic signaling and ASD

11.1. Purinergic signaling maintains the CDR

If the CDR is the problem, what is the cellular signal that keeps it turned on after it is no longer needed for healing? To answer this question, researchers had to weave together several apparently unrelated threads. These threads included research on mitochondria and healing (Naviaux et al., 2009), genetic forms of mitochondrial dysfunction in autism (Graf et al., 2000), genetic forms of autism associated with increased purine metabolism (Nyhan et al., 1969), and the paradoxical improvement with fever that proved that the core behaviors of autism could be dynamically regulated by metabolism (Curran et al., 2007). The author hypothesized that the root cause of pathological persistence of the CDR was continued excessive or unbalanced purinergic signaling, called hyperpurinergia (Naviaux et al., 2013), and dyspurinergia, respectively.

Hyperpurinergia is a universal and normal feature of the immediate and subacute cellular response to injury. Stressed cells release ATP and other small molecules less than about 800 Da in size through specialized membrane channels. The pannexin/P2X7 porin is an example of one of these stress-gated channels (Burnstock and Knight, 2017; Naviaux, 2012b). This phenomenon is illustrated in the whiteboard animation available at: https://www.youtube.com/watch?v=zIdUufy8Lks. When ATP, UTP, and other mitokines (signaling molecules traceable to mitochondria) are released through the stress-gated channels in the cell membrane, they bind to receptors on the cell surface to signal danger. Nineteen (19) purinergic receptors have been cloned. There are 8 P2Y receptors, 7 P2X receptors, and 4 P1 (adenosine) receptors. Extracellular ATP, ADP, adenosine, and UDP-glucose are important regulators of mast cell degranulation (Lazarowski and Harden, 2015; Osipchuk and Cahalan, 1992), neutrophils and T-cell function (Ledderose et al., 2015). Many different disease processes are regulated by purinergic signaling (Burnstock, 2014). Once the danger has passed, the release of ATP decreases, the CDR turns off, cells can complete the healing cycle, and return to normal “peacetime” function. Mixtures of CDR triggers can be synergistic. This contributes to the concept of total toxic load. Sequential exposures during critical developmental windows can stack to create a “perfect storm” of events that can derail the healing process and lead to pathological persistence of the CDR.

11.2. Nucleotide metabolism regulates purinergic signaling

In principle, hyperpurinergia can be produced by increased release of ATP and related receptor ligands, increased nucleotide dwell time caused by decreased metabolism or inactivation of purinergic effectors, a failure of receptors to desensitize once their job is done, or a combination of each. The dwell time of extracellular nucleotides in the pericellular halo is tightly regulated by cell-specific expression of CD39 (ectonucleoside triphosphate diphosphohydrolase 1) and CD73 (ecto-5′-nucleotidase) on the cell membrane. These proteins convert extracellular ATP and ADP to AMP (CD39), and AMP to adenosine (CD73) in calcium- and magnesium-dependent reactions (Antonioli et al., 2013) (Fig. 1). Adenosine is then either taken up by the cell through the equilibrative nucleoside transporter 1 (ENT1, SLC29A1), or metabolized to inosine by adenosine deaminase (ADA). Inosine is hydrolyzed to yield hypoxanthine and ribose-1-phospate by purine nucleoside phosphorylase (PNP). PNP does not accept adenosine as a substrate and is not a source of adenine. Adenine base can be produced by methylthioadenosine phosphorylase (MTAP) during polyamine synthesis and methionine salvage (Mavrakis et al., 2016). Free adenine can be released or taken up by cells via the equilibrative nucleobase transporter (ENBT1, SLC43A3). When taken up, adenine is used for salvage synthesis of AMP by adenine phosphoribosyl transferase (APRT). Hypoxanthine can be taken up by cells for salvage synthesis of purines via membrane transporters like the concentrative sodium-dependent nucleobase transporter 1 (SNBT1, SLC23A4), then condensed with phosphoribosylpyrophosphate (PRPP) by the enzyme hypoxanthine guanine phosphoribosyl transferase (HGPRT) to make IMP. Hypoxanthine can also be oxidized in the extracellular space to xanthine and uric acid, with the production of superoxide (O_2^{-}) by the molybdenum-dependent flavoprotein xanthine oxidase (XO). Extracellular superoxide is converted to hydrogen peroxide (H_2O_2) by the copper and zinc-dependent, extracellular superoxide dismutase (SOD3). Extracellular and intracellular NAD^+ and $NADP^+$ are converted by CD38 to cADPR and NAADP, respectively. Both cADPR and NAADP activate calcium influx via the TRPM2 membrane channels. Inside the cell, cADPR releases calcium from the ER through the ryanodine receptor (RyR), and NAADP releases acidic calcium stores from lysosomes through the two pore channel (TPC) proteins. In anti-inflammatory, M2 polarized mitochondria the flux of NAD^+ and NADPH through the nicotinamide nucleotide transhydrogenase (NNT) favors NADH and $NADP^+$ production. In M1 (pro-inflammatory) mitochondria, the flux through NNT favors NADPH and NAD^+. NADPH and oxygen are then used by mitochondrial outer membrane-associated NADPH oxidase 4 (NOX4) to produce H_2O_2. Uric acid is transported into the cell by the cytokine-regulated uric acid transporter SLC2A9 (So and Thorens, 2010) and can stimulate inflammation directly by triggering the assembly of the NLRP3 inflammasome (Ghaemi-Oskouie and Shi, 2011) (Fig. 1).

UTP, UDP, and UDP-glucose are also released from cells under stress and act as signaling molecules that bind to purinergic receptors. CD39 and CD73 can also dephosphorylate UTP and UDP to produce extracellular uridine. Uridine can be metabolized by uridine phosphorylase (UPase) to produce the free nucleobase uracil and ribose-1-phosphate. Uracil can be imported as a free nucleobase into the cell by SNBT1. Uridine is transported into the cell through ENT1. Inside the cell, uridine is salvaged by phosphorylation by uridine-cytidine kinase 1 and 2 (UCK1/2). By regulating the relative expression of CD39, CD73, ADA, ENT1, SNBT1, ENBT1, PNP, XO, SOD3, CD38, TRPM2, APRT, HGPRT, SLC2A9, and UCK1/2, the nuanced informational content of the unstirred water layer (UWL) produced by the release of extracellular ATP and UTP can be precisely calibrated in accordance with the functional states of each responding cell type (Fig. 1).

11.3. Purinergic signaling, the CDR, and the symptoms of ASD

When healing is incomplete, cells can be left in a state of hyper- or hypo-responsiveness to new threats. Chronic changes in purinergic signaling alter pain perception (Magni et al., 2017), and the processing of other sensory stimuli (Breza and Travers, 2016; Dietz et al., 2012). This is not unlike a cellular form of post-traumatic stress disorder (PTSD) resulting in durable changes in behavior after exposure to a transient, but serious stress. Cells cannot heal if a significant fraction of ATP is exported for purposes of signaling danger instead of being kept in the cell for normal energy metabolism. The use of antipurinergic drugs like suramin to treat a misfiring CDR has been called "molecular armistice therapy" because it sends a signal that "the war is over". This decreases losses of ATP through stress-gated membrane channels, and decreases purinergic autocrine and paracrine signaling of danger (https://www.youtube.com/watch?v=zIdUufy8Lks) so cells and mitochondria can return to peacetime metabolism needed for healing and development. The concept that purinergic signaling abnormalities are involved in ASD and can alter behavior is not just theoretical. Evidence of purinergic signaling abnormalities was found in children with ASD in a recent gene expression study (Ginsberg et al., 2012). Purinergic signaling has been shown to regulate a number of the cellular comorbidities and functional abnormalities associated with ASD (Table 2).

12. Preclinical studies of antipurinergic therapy

The idea that purinergic signaling might be involved in autism was born in 2008 (Naviaux research supported by Mr. Dan Wright). In 2010, the Naviaux Lab received a "Trailblazer" award from Autism Speaks (https://autismspeaksblog.wordpress.com/tag/mitochondria/) to test this idea. Suramin has many actions (Liu and Zhuang, 2011; Voogd et al., 1993). One of its most studied actions is as a non-selective purinergic antagonist (Burnstock, 2006a). The 2013 paper (Naviaux et al., 2013) describing the results of the first suramin treatment studies in ASD mouse models showed that abnormal persistence of extracellular ATP signaling could cause ASD-like behaviors. It also produced excitoxicity that led to the death of Purkinje cells in the cerebellum. Rebalancing the CDR with suramin restored normal behavior and prevented the loss of these cells (Naviaux et al., 2013). Two additional studies confirmed that antipurinergic therapy with the non-selective purinergic inhibitor suramin improved both the core behaviors and the metabolic syndrome underlying autism-like symptoms in both the Fragile X genetic model and the environmental maternal immune activation (MIA) models (Naviaux et al., 2014; Naviaux et al., 2015). The mouse models also showed that high doses were not necessary. Low-dose suramin that produced blood levels of just 5–15 μM was both safe and effective in treating the symptoms of autism in these models.

13. Results of the SAT1 clinical trial

13.1. Metabolic abnormalities in ASD were improved by low-dose suramin

Using mass spectrometry, the metabolic pathways that were disturbed at baseline and changed by suramin were characterized in two mouse models of ASD-like behavior. Suramin treatment improved 17 of 18 (94%) biochemical pathways that were abnormal in the MIA mouse model (Naviaux et al., 2014) and 20 of 20 (100%) pathways disturbed in the Fragile X mouse model (Naviaux et al., 2015). Metabolomic analysis was also performed in the 10 children with ASD in the SAT1 study (Naviaux et al., 2017). This study showed that 21 of 28 (75%) of the pathways disturbed in children with autism were also abnormal in the mouse models. These included improvements in purines, 1-carbon/folate, S-adenosylmethionine (SAMe), glutathione, microbiome, branched chain amino acids, fatty acid metabolism, and others (Naviaux et al., 2017) (Fig. 2). These improvements in metabolism were associated with similar improvements in each of the core symptoms of autism. There was a flowering of interest in social communication, new language, new social activities on the playground like playing tag, and at home like playing catch and other games with neurotypical siblings. The half-life of suramin after a single-dose was 14.7 ± 0.7 days. Studies in African sleeping sickness have shown that the plasma half-life of suramin can increase to 1 or 2 months after multiple doses (Hawking, 1940). As the single dose of suramin in the SAT1 study gradually wore off over 5–8 weeks, metabolism drifted back toward baseline, and most of the behavioral gains were lost. It is not yet known if regular suramin given every month or so could support continued developmental gains. These studies strongly underscore the hopeful message that the symptoms of autism might be caused by a treatable metabolic syndrome and that antipurinergic therapy with low-dose suramin is a powerful tool in treating these fundamental metabolic abnormalities.

Table 2
Cellular comorbidities and functional abnormalities in autism spectrum disorder regulated by purinergic signaling.

No.	Feature	References
1	Innate immunity, allergies, and inflammation	West et al. (2011)
2	Autoimmunity	Savio and Coutinho-Silva (2016)
3	Microglial and astroglial activation	Butt (2011)
4	T-cell proliferation	Yu et al. (2010)
5	Th17 cells	Sullivan et al. (2014)
6	Treg cells	Cortes-Garcia et al. (2016)
7	NK cells	Raskovalova et al. (2005)
8	Mast cell activation	Feng et al. (2004)
9	Eosinophil activation	Ferrari et al. (2006)
10	Neuronal migration	Liu et al. (2008)
11	Brain injury and repair	Burnstock (2016)
12	Glutathione, ROS, and redox	Zhang et al. (2005)
13	Nitric oxide synthesis	Silva et al. (2006)
14	Apoptosis	Dawicki et al. (1997)
15	Gliovascular coupling	Pelligrino et al. (2011)
16	Synaptogenesis and neuronal plasticity	Pankratov et al. (2009)
17	cMet/mTor signaling	Gerasimovskaya et al. (2005)
18	PI3/AKT signaling	Katz et al. (2011)
19	Sensory perception and sensory integration	Pain (Burnstock, 2006b) Sight (Housley et al., 2009) Sound (Housley et al., 2002) Touch (Wang et al., 2010) Taste (Huang et al., 2009) Smell (Housley et al., 2009) Vestibular (Lee et al., 2001)
20	Epilepsy and the seizure threshold	Dona et al. (2009)
21	Oxytocin and vasopressin secretion	Song et al. (2009)
22	Obsessive compulsive behaviors	Mastrangelo et al. (2012)
23	Depression and affect	Sperlagh et al. (2012)
24	Cortisol secretion and the HPA axis	Bjelobaba et al. (2015)
25	Appetite and feeding behaviors	Stojilkovic (2009)
26	Anxiety and retention of aversive memories	Campos et al. (2014)
27	Self-injurious behavior	Mastrangelo et al. (2012)
28	Gut Inflammation and the microbiome	Estrela and Abraham (2011)
29	Gut permeability	Matos et al. (2007)
30	Food allergen reactivity	Leng et al. (2008)
31	GI motility, constipation, diarrhea, irritable bowel	Jimenez et al. (2014)
32	Parasympathetic autonomic nervous system	Passamani et al. (2011)
33	Blood pressure control	Pijacka et al. (2016)
34	Sleep	Halassa (2011)
35	Stem cell development	Burnstock and Ulrich (2011)

13.2. Core symptoms of ASD were improved by low-dose suramin

Low-dose of suramin used in the SAT1 study (Naviaux et al., 2017) improved the core symptoms of ASD measured by ADOS2 (autism diagnostic observation schedule, 2nd edition) score by 1.6 ± 0.55 points in 6 weeks ($p < 0.0028$; Fig. 3). Language, social interaction,

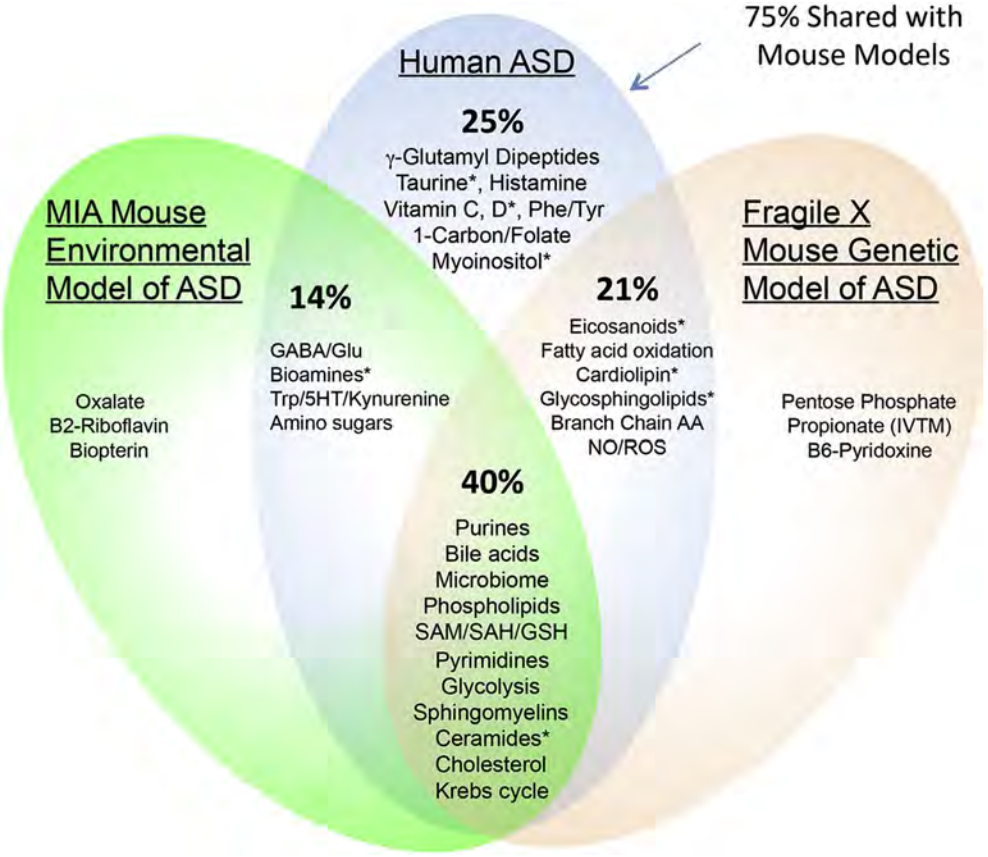

Fig. 2. Biochemical abnormalities of autism were improved by low-dose suramin. The figure lists the pathways that were improved by anti-purinergic therapy with suramin in children with ASD in the SAT1 study. Twenty-one of 28 (75%) of the metabolic pathway abnormalities were also improved by suramin in the maternal immune activation (MIA) and Fragile X mouse models of autism. Each of these pathways is known to play a role in the cell danger response (CDR). The observation that the core symptoms of ASD were improved with the metabolic pathways known to be associated with the CDR, supports the hypothesis that the behavioral symptoms of autism may be caused by a treatable metabolic syndrome.
Adapted from (Naviaux et al., 2017).

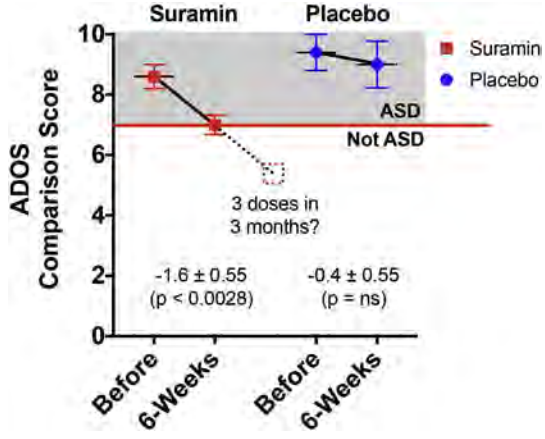

Fig. 3. A single dose of suramin Improved ADOS scores by 1.6 points in 6 weeks. ADOS2 comparison scores of 7–10 (gray box) are used as a gold standard for the diagnosis of autism spectrum disorder (ASD) and classical autism. A single dose of suramin resulted in a 1.6 ± 0.55 point improvement in ADOS scores, from a mean of 8.6 ± 0.9, to 7.0 ± 0.7 ($p < 0.0028$) when measured after 6 weeks. If a few doses of suramin given over 3 months produce improvements at the same rate of 1 point/month, then some children would be able to come off the autism spectrum (dotted red box), and those with more severe forms of autism might improve significantly. [Data from the SAT1 study (Naviaux et al., 2017); N = 5 per group.]

restricted interests, and repetitive movements all improved. Two children who were previously non-verbal spoke their first sentences. Suramin treatment was synergistic with regular school, educational enrichment programs, applied behavioral analysis (ABA), speech, and occupational therapy. None of these improvements were observed in the placebo group. The authors reported that the maximum benefit from a single dose of suramin occurred after 3 weeks then decreased slowly. Even after 6 weeks, three children had improved by 2 points and two children improved by 1 point, compared to baseline. No children were unimproved in the treatment group. In comparison, three children who received placebo were unchanged, and two improved by 1 point each. This gave rise to an estimate of the placebo effect of 0.4 ± 0.55 points (Fig. 3; p = 0.18; ns). ADOS comparison scores of 7–9 are used as a gold standard for the diagnosis of autism spectrum disorder (ASD). An ADOS score of 10 meets criteria for classical autism. If a few doses of suramin given over 3 months produce improvements at the same rate of 1 point per month, then children with symptoms that were initially severe enough to be on the spectrum (ASD = ADOS comparison scores of 7–9), might be able to come off the autism spectrum (dotted red box), and those with more severe forms of autism might improve significantly (Fig. 3). Does this mean suramin might be the first effective drug treatment for autism in nearly 75 years of research efforts? It is too early to say. Some biomedical treatments of ASD show benefits for a few weeks or months, then lose effectiveness over time. There is no evidence this could happen with suramin, but more clinical trials are needed. We need to know if a few doses given over a few months are safe and are able to maintain the same rates of ADOS score improvement of about 1 point per month of treatment. If this is true, then we are one step closer to the goal.

13.3. Low-dose suramin safety

Low-dose suramin that produced blood levels of just 5–15 μM, was safe and produced significant improvement in ASD symptoms at 6 weeks in the SAT1 trial (Naviaux et al., 2017) (Fig. 4). This low dose of suramin has never been studied before. The side effect profile of high-dose suramin (150–270 μM) is known from cancer chemotherapy studies (Stein, 1993). One author has expressed concern about the safety of high-dose suramin (Theoharides, 2013) citing a review of cancer studies (Kaur et al., 2002) that used prolonged exposure to high-doses of suramin that produced 25-times higher blood levels than those needed

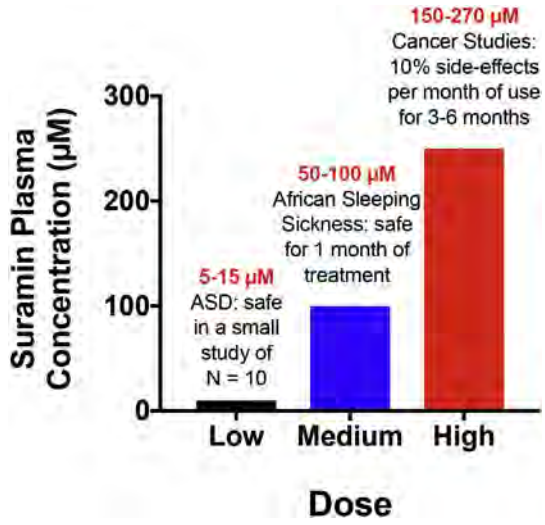

Fig. 4. Low-dose suramin was safe in children with autism spectrum disorder (ASD). The safety and toxicity of suramin are dose-dependent. Definitions: Low-dose suramin (5–15 μM) as antipurinergic therapy of ASD, Medium-dose (50–100 μM) as antimicrobial therapy for trypanosomiasis, high-dose (150–270 μM) as anticancer adjunct therapy.

to treat autism (Naviaux et al., 2017). Cancer studies typically used a dose and schedule of suramin designed produced blood levels of 250 μM compared to 10 μM used in the SAT1 study. High doses of most drugs have toxicities that are not seen at lower doses. The safety and side effect profile from medium-dose suramin (50–100 μM) is well known from nearly 100 years of study in African sleeping sickness (Hawking, 1940, 1978). This work showed that when a cumulative dose of 2.5–3 g/m^2 was divided into five, weekly intravenous infusions over a month, the elimination half-life increased from 2 weeks to 1.5–2 months, and suramin concentrations ≥ 4 μM (≥ 5 mg/L; MW = 1297 g/mol) were safely maintained for at least 6 months. About 10% of patients treated were rapid excretors and did not maintain these concentrations for as long (Hawking, 1978). These studies were done in Africa before the era of pharmacogenomics, so future studies in more ethnically diverse patient populations may reveal genetic differences in the handling and response to suramin that cannot yet be predicted. The side effect profile of low-dose suramin, given for several months is unknown. Future studies are needed to answer four big questions: 1) Do all children with ASD benefit, or just a fraction? 2) Does suramin lose effectiveness after a few months, or do children continue to benefit for as long as the drug levels in the blood are above 5 μM? 3) Does suramin need to be given for life, or are 4–8 doses over 6–12 months sufficient for normal child development to become self-sustaining? and 4) How long can low-dose suramn be used safely?

14. Sparking a Renaissance in drug development

14.1. Suramin as the first antipurinergic drug

Like the first antibiotic, or first beta-blocker for high blood pressure, suramin is the first antipurinergic drug (APD). APDs represent a class of medicines that is completely new to the world's pharmacopeia. Soon other drugs that work like suramin will be developed (Jacobson and Müller, 2016). Eventually, the goal of this new Renaissance would be to create a shelf-full of APDs, each with slightly different pharmacologic properties that would allow doctors to pick and choose the best match for each patient. The recent discovery that suramin prevents Zika, Ebola, Chikungunya, Coxsackievirus A16, and Enterovirus A71 (Albulescu et al., 2017; Henss et al., 2016; Ren et al., 2017) from infecting cells may prompt additional clinical trials and further interest in APD development. Currently however, suramin is the only non-selective APD available for human use. Research into the role of purinergic signaling in autism is so new that we do not yet know which of the 19 purinergic receptors are most relevant. Suramin is a broad-spectrum inhibitor of most purinergic signaling systems.

Several P2Y12-selective antagonists like Plavix (clopidogrel) are used as antiplatelet agents to prevent blood clots, strokes, and heart attacks. However, their safety and activity in autism is unknown. Brilliant Blue G (BBG) is a P2X7 inhibitor and protein binding dye that has been used successfully in animal models to prevent excessive inflammation after spinal cord injury (Peng et al., 2009), Parkinson disease (Ferrazoli et al., 2017), and acetaminophen-associated liver injury (Abdelaziz et al., 2017). BBG is also widely used by ophthalmologists during retinal surgery (Azuma et al., 2016). Several experimental APDs are in clinical trials for rheumatoid arthritis and pain that target the P2X7 receptor, but none are yet available to prescribing physicians. It is likely that novel antipurinergic activities will be found in herbs, fungi, and other natural products distributed throughout the biosphere (Faria et al., 2012; Soares-Bezerra et al., 2013). Some may already be in use but their essential pharmacologic action as purinergic inhibitors is not yet known. Alternatively, knowledge of the synthetic chemical additives in our food chain that activate or inhibit purine and pyrimidine signaling (Ferreira et al., 2016), may shed new light on why some food colorings and additives are a problem in some children (Weiss, 2012).

14.2. Current clinical trials of antipurinergic drugs

In 2017, a search of the keyword "purinergic" among interventional trials in clinicaltrials.gov returned 418 studies in the US. Currently, over 90% of these studies are focused on platelets and heart disease. However, the broad involvement of purinergic signaling in nearly every chronic disease in which it has been studied (Burnstock, 2017) suggests great potential for the development of this new class of medications.

15. Conclusions

Over $1 billion has been spent on genetic research in autism over the past 10 years by the NIH, Autism Speaks, and the Simons Foundation. This work has shown that hundreds of genes play a role in different children, and that no single gene accounts for more than 1–2% of autism (Talkowski et al., 2014). While most genetic studies conclude that each genetic cause of ASD must be treated differently, the CDR hypothesis suggests that one mechanism—a unified cellular response—might be at the root of all the different causes of autism. In addition, the CDR hypothesis comes with a detailed molecular mechanism and a treatment. This new theory has already been rigorously tested in the lab since 2011 and found successful in classical animal models of autism. It also showed promise in 10 children with ASD as a unifying theory of pathogenesis in the SAT1 clinical trial (Naviaux et al., 2017).

15.1. The economic impact of a treatment for ASD

The average family caring for a child with ASD in the US spends over $17,000 annually in extra costs not covered by the health care and educational systems (Lavelle et al., 2014). About 3.5 million Americans today live with ASD (Buescher et al., 2014). Using the current estimates of 1 in 68 (Developmental Disabilities Monitoring Network Surveillance Year Principal et al., 2014) to 1 in 45 (Zablotsky et al., 2015) children in the US with ASD and a birthrate of 4 million children per year, about 75,000 ± 15,000 children will be diagnosed with ASD this year in the United States. The national economic cost of autism in the US is estimated to be $268 billion annually, or close to $75,000 per year per patient with ASD. This could rise to $461 billion by 2025 if the rising prevalence of ASD is not stopped (Leigh and Du, 2015). If a new treatment could help just 10% of patients come off the autism spectrum, it would bring back over $26 billion into the US economy each year ($268 billion × 10% = $26.8 billion). The financial return from this

discovery in a single year would be enough to support over 100 years of autism research funded by the National Institutes of Health (NIH). The 2016 budget for autism research projects at NIH was $232 million (https://report.nih.gov/categorical_spending.aspx;$26.8 billion saved ÷ $0.232 billion/year NIH budget = 115 years).

15.2. Human impact

If autism is proven to be a treatable metabolic syndrome in some children, it means that some children now living with disabling forms of ASD, whose parents fear might never be able to live independently, could have a chance for independence and live happy, self-reliant lives. In addition, ASD often affects children who have shown early gifts and might otherwise grow up to become some of the best and brightest of their generation. If new science can lift their disabling symptoms without touching the unique gifts that make them special, the children with ASD today could grow up to become the young men and women of tomorrow who can think creatively to crack the problems that no one else can—to solve our technological problems, to ease social unrest, protect the environment, and help create a healthier future for us all.

16. Special note from the author

Until recently, the public has not heard the name of a new drug until it has been approved by the FDA to treat a particular disorder and it is ready to be marketed by its manufacturer. This has the beneficial effect of protecting patients from asking for, or trying a drug that has not yet been proven safe and effective for their disease. A growing number of drugs are experiencing new interest as researchers discover new uses for old drugs. This is called “drug repurposing”. Drug repurposing is not as simple as using an old drug “off-label” to treat a new disorder. Many drugs are not safe or effective when used this way. Many times the dose and schedule, and even the fundamental pharmacology, like the half-life and volume of distribution, of a drug are different in different patient populations. Careful clinical trials are needed to establish safety and efficacy for each new indication.

Suramin is approved to treat African sleeping sickness (trypanosomiasis). It is not approved for the treatment of autism. There is currently no approved use of suramin in the United States. It is illegal to import suramin into the US for human use without FDA approval. Like many intravenous drugs, when administered improperly by untrained personnel, at the wrong dose and schedule, without careful measurement of drug levels and monitoring for toxicity, suramin can cause harm. Careful clinical trials will be needed over several years at several sites to learn how to use low-dose suramin safely in autism, and to identify drug-drug interactions and rare side effects that cannot currently be predicted. The author strongly cautions against the unauthorized use of suramin. Ultimately, clinical trials may show that suramin is not the final answer for autism. Its effects may be limited to a small number of children, or they may not last, or side effects may emerge. However, the discovery that the cell danger response and purinergic signaling are fundamental features of ASD is now stimulating new research around the world. New antipurinergic drugs, and the rediscovery of old ones, will not be far behind.

Funding

All funding for these studies was philanthropic. This work was supported in part by gifts from the UCSD Christini Fund, the William Wright Family Foundation, the Autism Research Institute (ARI), the Lennox Foundation, the Gupta Family and Satya Fund, the Agrawal Family, Linda Clark, the N of One Autism Research Foundation, the Rodakis Family, the It Takes Guts Foundation, the UCSD Mitochondrial Disease Research Fund, Dr. Elizabeth Mumper Cooper, the Daniel and Kelly White Family, the Brent Kaufman Family, Fred and Sylvia Fogel, the David Cannistraro Family, Ian and Rochelle Yankwitt, George and Caryn Harb, the Francis Clougherty Charitable Trust, and the Heritage Youth Foundation. Funding for the mass spectrometers was provided by a gift from the Jane Botsford Johnson Foundation.

Conflicts of interest

RKN is a scientific advisory board member for the Autism Research Institute (ARI) and the Open Medicine Foundation (OMF), a consultant for Stealth Biotherapeutics, and has submitted a technology disclosure to UCSD describing antipurinergic therapy for autism and related spectrum disorders.

Acknowledgements

RKN thanks Danielle Sternberg for creating the visualization of nucleotide metabolism and transport illustrated in Fig. 1. RKN thanks Mr. Dan Wright for his support of the MRL mouse studies on healing that created the foundation for the CDR hypothesis, and for the phone call one winter day in January 2008 that began a new trail of discovery in mitochondrial medicine and autism, and John Green, Steve Edelson, Nancy O’Hara, Neil Nathan, and A. Taylor Bright for comments on the manuscript, and Richard Haas, Eric Gordon, Paul Hardy, Vicki Kobliner, Maya Shetreat-Klein, Mauro Lins, and Caio Scocco for helpful discussions. RKN thanks the United Mitochondrial Disease Foundation (UMDF) and NIH for a conference grant in 2010 that first brought together investigators to focus their interests on the crossroads of mitochondria and autism. RKN also thanks the Autism Research Institute (ARI) for their invitation to many high-level scientific, medical, and family conferences, think tanks, and topical focus groups over the years. These events, the professional collaborations that they fostered, and many families and children affected by autism around the world, have helped to refine the concepts of the CDR, purinergic signaling, and new approaches to treatment discussed in this review.

References

Abdelaziz, H.A., Shaker, M.E., Hamed, M.F., Gameil, N.M., 2017. Repression of acetaminophen-induced hepatotoxicity by a combination of celastrol and brilliant blue G. Toxicol. Lett. 275, 6–18.

Adams, J.B., George, F., Audhya, T., 2006. Abnormally high plasma levels of vitamin B6 in children with autism not taking supplements compared to controls not taking supplements. J. Altern. Complement. Med. 12, 59–63.

Adams, J.B., Audhya, T., McDonough-Means, S., Rubin, R.A., Quig, D., Geis, E., Gehn, E., Loresto, M., Mitchell, J., Atwood, S., Barnhouse, S., Lee, W., 2011. Nutritional and metabolic status of children with autism vs. neurotypical children, and the association with autism severity. Nutr. Metab. 8, 34.

Adams, J.B., Dietert, R., Freedenfeld, S., Frye, R.E., Green, J., Hamilton, D., Heilbrun, L., Huberty, J., Kobliner, V., Laake, D., Lein, P.J., Lipski, E., McDonough-Means, S., Mitchell, J., Naviaux, R.K., O'Hara, N., Palmer, R., Records, K., Kenney, L., Willhite, C., 2016. The Healthy Child Guide. Neurological Health Foundation, Dallas, TX.

Alberti, A., Pirrone, P., Elia, M., Waring, R.H., Romano, C., 1999. Sulphation deficit in “low-functioning” autistic children: a pilot study. Biol. Psychiatry 46, 420–424.

Albulescu, I.C., Kovacikova, K., Tas, A., Snijder, E.J., van Hemert, M.J., 2017. Suramin inhibits Zika virus replication by interfering with virus attachment and release of infectious particles. Antivir. Res. 143, 230–236.

Al-Owain, M., Kaya, N., Al-Shamrani, H., Al-Bakheet, A., Qari, A., Al-Muaigl, S., Ghaziuddin, M., 2013. Autism spectrum disorder in a child with propionic acidemia. JIMD Rep. 7, 63–66.

Ambrus, A., Adam-Vizi, V., 2017. Human dihydrolipoamide dehydrogenase (E3) deficiency: novel insights into the structural basis and molecular pathomechanism. Neurochem. Int. http://dx.doi.org/10.1016/j.neuint.2017.05.018. (E-pub ahead of print. PMID: 28579060).

Andaluz-Ojeda, D., Iglesias, V., Bobillo, F., Nocito, M., Loma, A.M., Nieto, C., Ramos, E., Gandia, F., Rico, L., Bermejo-Martin, J.F., 2013. Early levels in blood of immunoglobulin M and natural killer cells predict outcome in nonseptic critically ill patients. J. Crit. Care 28 (1110 e1117–1110 e1110).

Antonioli, L., Pacher, P., Vizi, E.S., Hasko, G., 2013. CD39 and CD73 in immunity and inflammation. Trends Mol. Med. 19, 355–367.

Azuma, K., Noda, Y., Hirasawa, K., Ueta, T., 2016. BRILLIANT BLUE G-ASSISTED INTERNAL LIMITING MEMBRANE PEELING FOR MACULAR HOLE: a systematic review of literature and meta-analysis. Retina 36, 851–858.

Babady, N.E., Pang, Y.P., Elpeleg, O., Isaya, G., 2007. Cryptic proteolytic activity of dihydrolipoamide dehydrogenase. Proc. Natl. Acad. Sci. U. S. A. 104, 6158–6163.

Beaulieu, M.A., 2013. Linking the Fragile X mental retardation protein to the lipoxygenase pathway. Med. Hypotheses 80, 289–291.

Bjelobaba, I., Janjic, M.M., Stojilkovic, S.S., 2015. Purinergic signaling pathways in endocrine system. Auton. Neurosci. 191, 102–116.
Braun, J.M., Kalkbrenner, A.E., Just, A.C., Yolton, K., Calafat, A.M., Sjodin, A., Hauser, R., Webster, G.M., Chen, A., Lanphear, B.P., 2014. Gestational exposure to endocrine-disrupting chemicals and reciprocal social, repetitive, and stereotypic behaviors in 4- and 5-year-old children: the HOME study. Environ. Health Perspect. 122, 513–520.
Braymer, J.J., Lill, R., 2017. Iron-sulfur cluster biogenesis and trafficking in mitochondria. J. Biol. Chem. 292, 12754–12763.
Breza, J.M., Travers, S.P., 2016. P2X2 Receptor Terminal Field Demarcates a "Transition Zone" for Gustatory and Mechanosensory Processing in the Mouse Nucleus Tractus Solitarius. Chem. Senses 41, 515–524.
Brussel, W., van Kuilenburg, A.B., Janssens, P.M., 2006. A neonate with recurrent vomiting and generalized hypotonia diagnosed with a deficiency of dihydropyrimidine dehydrogenase. Nucleosides Nucleotides Nucleic Acids 25, 1099–1102.
Buescher, A.V., Cidav, Z., Knapp, M., Mandell, D.S., 2014. Costs of autism spectrum disorders in the United Kingdom and the United States. JAMA Pediatr. 168, 721–728.
Burnstock, G., 2006a. Pathophysiology and therapeutic potential of purinergic signaling. Pharmacol. Rev. 58, 58–86.
Burnstock, G., 2006b. Purinergic P2 receptors as targets for novel analgesics. Pharmacol. Ther. 110, 433–454.
Burnstock, G., 2014. The Paton Lecture: purinergic signalling: from discovery to current developments. Exp. Physiol. 99, 16–34.
Burnstock, G., 2016. An introduction to the roles of purinergic signalling in neurodegeneration, neuroprotection and neuroregeneration. Neuropharmacology 104, 4–17.
Burnstock, G., 2017. The therapeutic potential of purinergic signalling. Biochem. Pharmacol. http://dx.doi.org/10.1016/j.bcp.2017.07.016. (E-pub ahead of print. PMID: 28735873).
Burnstock, G., Knight, G.E., 2017. Cell culture: complications due to mechanical release of ATP and activation of purinoceptors. Cell Tissue Res. 370 (1), 1–11.
Burnstock, G., Ulrich, H., 2011. Purinergic signaling in embryonic and stem cell development. Cell. Mol. Life Sci. 68, 1369–1394.
Butt, A.M., 2011. ATP: a ubiquitous gliotransmitter integrating neuron-glial networks. Semin. Cell Dev. Biol. 22, 205–213.
Cameron, J.L., Eagleson, K.L., Fox, N.A., Hensch, T.K., Levitt, P., 2017. Social Origins of Developmental Risk for Mental and Physical Illness. J. Neurosci. 37, 10783–10791.
Campos, R.C., Parfitt, G.M., Polese, C.E., Coutinho-Silva, R., Morrone, F.B., Barros, D.M., 2014. Pharmacological blockage and P2X7 deletion hinder aversive memories: reversion in an enriched environment. Neuroscience 280, 220–230.
Cannell, J.J., 2008. Autism and vitamin D. Med. Hypotheses 70, 750–759.
Celestino-Soper, P.B., Violante, S., Crawford, E.L., Luo, R., Lionel, A.C., Delaby, E., Cai, G., Sadikovic, B., Lee, K., Lo, C., Gao, K., Person, R.E., Moss, T.J., German, J.R., Huang, N., Shinawi, M., Treadwell-Deering, D., Szatmari, P., Roberts, W., Fernandez, B., Schroer, R.J., Stevenson, R.E., Buxbaum, J.D., Betancur, C., Scherer, S.W., Sanders, S.J., Geschwind, D.H., Sutcliffe, J.S., Hurles, M.E., Wanders, R.J., Shaw, C.A., Leal, S.M., Cook Jr., E.H., Goin-Kochel, R.P., Vaz, F.M., Beaudet, A.L., 2012. A common X-linked inborn error of carnitine biosynthesis may be a risk factor for nondysmorphic autism. Proc. Natl. Acad. Sci. U. S. A. 109, 7974–7981.
Chaplin, M., 2006. Do we underestimate the importance of water in cell biology? Nat. Rev. Mol. Cell Biol. 7, 861–866.
Chen, W., Sandoval, H., Kubiak, J.Z., Li, X.C., Ghobrial, R.M., Kloc, M., 2017. The phenotype of peritoneal mouse macrophages depends on the mitochondria and ATP/ADP homeostasis. Cell Immunol. http://dx.doi.org/10.1016/j.cellimm.2017.11.003. (Epub ahead of print: PMID: 29129293).
Cortelazzo, A., De Felice, C., Guerranti, R., Signorini, C., Leoncini, S., Pecorelli, A., Zollo, G., Landi, C., Valacchi, G., Ciccoli, L., Bini, L., Hayek, J., 2014. Subclinical inflammatory status in Rett syndrome. Mediat. Inflamm. 2014, 480980.
Cortes-Garcia, J.D., Lopez-Lopez, C., Cortez-Espinosa, N., Garcia-Hernandez, M.H., Guzman-Flores, J.M., Layseca-Espinosa, E., Portales-Cervantes, L., Portales-Perez, D.P., 2016. Evaluation of the expression and function of the P2X7 receptor and ART1 in human regulatory T-cell subsets. Immunobiology 221, 84–93.
Cunliffe, J., 1997. Morphostasis: an evolving perspective. Med. Hypotheses 49, 449–459.
Curran, L.K., Newschaffer, C.J., Lee, L.C., Crawford, S.O., Johnston, M.V., Zimmerman, A.W., 2007. Behaviors associated with fever in children with autism spectrum disorders. Pediatrics 120, e1386–1392.
Dawicki, D.D., Chatterjee, D., Wyche, J., Rounds, S., 1997. Extracellular ATP and adenosine cause apoptosis of pulmonary artery endothelial cells. Am. J. Phys. 273, L485–494.
Degtyar, E., Zusman, T., Ehrlich, M., Segal, G., 2009. A Legionella effector acquired from protozoa is involved in sphingolipids metabolism and is targeted to the host cell mitochondria. Cell. Microbiol. 11, 1219–1235.
Derecki, N.C., Cronk, J.C., Lu, Z., Xu, E., Abbott, S.B., Guyenet, P.G., Kipnis, J., 2012. Wild-type microglia arrest pathology in a mouse model of Rett syndrome. Nature 484, 105–109.
Derecki, N.C., Cronk, J.C., Kipnis, J., 2013. The role of microglia in brain maintenance: implications for Rett syndrome. Trends Immunol. 34, 144–150.
Developmental Disabilities Monitoring Network Surveillance Year Principal, I., Centers for Disease, C., Prevention, 2014. Prevalence of autism spectrum disorder among children aged 8 years - autism and developmental disabilities monitoring network, 11 sites, United States, 2010. MMWR Surveill. Summ. 63, 1–21.
Di Marco, B., Bonaccorso, C.M., Aloisi, E., D'Antoni, S., Catania, M.V., 2016. Neuro-inflammatory mechanisms in developmental disorders associated with intellectual disability and autism spectrum disorder: a neuro-immune perspective. CNS Neurol. Disord. Drug Targets 15, 448–463.
Dietz, B., Jovanovic, S., Wielsch, B., Nerlich, J., Rubsamen, R., Milenkovic, I., 2012. Purinergic modulation of neuronal activity in developing auditory brainstem. J. Neurosci. 32, 10699–10712.
Dona, F., Ulrich, H., Persike, D.S., Conceicao, I.M., Blini, J.P., Cavalheiro, E.A., Fernandes, M.J., 2009. Alteration of purinergic P2X4 and P2X7 receptor expression in rats with temporal-lobe epilepsy induced by pilocarpine. Epilepsy Res. 83, 157–167.
Edmiston, E., Ashwood, P., Van de Water, J., 2017. Autoimmunity, Autoantibodies, and Autism Spectrum Disorder. Biol. Psychiatry 81, 383–390.
El-Ansary, A., Al-Ayadhi, L., 2012. Lipid mediators in plasma of autism spectrum disorders. Lipids Health Dis. 11, 160.
Estrela, A.B., Abraham, W.R., 2011. Adenosine in the inflamed gut: a Janus faced compound. Curr. Med. Chem. 18, 2791–2815.
Faria, R., Ferreira, L., Bezerra, R., Frutuoso, V., Alves, L., 2012. Action of natural products on p2 receptors: a reinvented era for drug discovery. Molecules 17, 13009–13025.
Feng, C., Mery, A.G., Beller, E.M., Favot, C., Boyce, J.A., 2004. Adenine nucleotides inhibit cytokine generation by human mast cells through a Gs-coupled receptor. J. Immunol. 173, 7539–7547.
Ferrari, D., la Sala, A., Panther, E., Norgauer, J., Di Virgilio, F., Idzko, M., 2006. Activation of human eosinophils via P2 receptors: novel findings and future perspectives. J. Leukoc. Biol. 79, 7–15.
Ferrazoli, E.G., de Souza, H.D., Nascimento, I.C., Oliveira-Giacomelli, A., Schwindt, T.T., Britto, L.R., Ulrich, H., 2017. Brilliant Blue G, But Not Fenofibrate, Treatment Reverts Hemiparkinsonian Behavior and Restores Dopamine Levels in an Animal Model of Parkinson's Disease. Cell Transplant. 26, 669–677.
Ferreira, L.G., Faria, R.X., Ferreira, N.C., Soares-Bezerra, R.J., 2016. Brilliant blue dyes in daily food: how could purinergic system be affected? Int J Food Sci 2016, 7548498.
Finegold, S.M., Molitoris, D., Song, Y., Liu, C., Vaisanen, M.L., Bolte, E., McTeague, M., Sandler, R., Wexler, H., Marlowe, E.M., Collins, M.D., Lawson, P.A., Summanen, P., Baysallar, M., Tomzynski, T.J., Read, E., Johnson, E., Rolfe, R., Nasir, P., Shah, H., Haake, D.A., Manning, P., Kaul, A., 2002. Gastrointestinal microflora studies in late-onset autism. Clin. Infect. Dis. 35, S6–S16.
Folmes, C.D., Dzeja, P.P., Nelson, T.J., Terzic, A., 2012. Metabolic plasticity in stem cell homeostasis and differentiation. Cell Stem Cell 11, 596–606.
Frustaci, A., Neri, M., Cesario, A., Adams, J.B., Domenici, E., Dalla Bernardina, B., Bonassi, S., 2012. Oxidative stress-related biomarkers in autism: systematic review and meta-analyses. Free Radic. Biol. Med. 52, 2128–2141.
Frye, R.E., James, S.J., 2014. Metabolic pathology of autism in relation to redox metabolism. Biomark. Med 8, 321–330.
Frye, R.E., Naviaux, R.K., 2011. Autistic disorder with complex IV overactivity: A new mitochondrial syndrome. J. Pediatr. Neurol. 9, 427–434.
Frye, R.E., Huffman, L.C., Elliott, G.R., 2010. Tetrahydrobiopterin as a novel therapeutic intervention for autism. Neurotherapeutics 7, 241–249.
Frye, R.E., Melnyk, S., Fuchs, G., Reid, T., Jernigan, S., Pavliv, O., Hubanks, A., Gaylor, D.W., Walters, L., James, S.J., 2013a. Effectiveness of methylcobalamin and folinic acid treatment on adaptive behavior in children with autistic disorder is related to glutathione redox status. Autism Res. Treat. 2013, 609705.
Frye, R.E., Melnyk, S., Macfabe, D.F., 2013b. Unique acyl-carnitine profiles are potential biomarkers for acquired mitochondrial disease in autism spectrum disorder. Transl. Psychiatry 3, e220.
Frye, R.E., Delhey, L., Slattery, J., Tippett, M., Wynne, R., Rose, S., Kahler, S.G., Bennuri, S.C., Melnyk, S., Sequeira, J.M., Quadros, E., 2016a. Blocking and binding folate receptor alpha autoantibodies identify novel autism spectrum disorder subgroups. Front. Neurosci. 10, 80.
Frye, R.E., Slattery, J., Delhey, L., Furgerson, B., Strickland, T., Tippett, M., Sailey, A., Wynne, R., Rose, S., Melnyk, S., Jill James, S., Sequeira, J.M., Quadros, E.V., 2016b. Folinic acid improves verbal communication in children with autism and language impairment: a randomized double-blind placebo-controlled trial. Mol. Psychiatry. http://dx.doi.org/10.1038/mp.2016.168. (Epub ahead of print: PMID: 27752075).
Frye, R.E., Wynne, R., Rose, S., Slattery, J., Delhey, L., Tippett, M., Kahler, S.G., Bennuri, S.C., Melnyk, S., Sequeira, J.M., Quadros, E.V., 2017. Thyroid dysfunction in children with autism spectrum disorder is associated with folate receptor alpha autoimmune disorder. J. Neuroendocrinol. 29.
Garnon, J., Lachance, C., Di Marco, S., Hel, Z., Marion, D., Ruiz, M.C., Newkirk, M.M., Khandjian, E.W., Radzioch, D., 2005. Fragile X-related protein FXR1P regulates proinflammatory cytokine tumor necrosis factor expression at the post-transcriptional level. J. Biol. Chem. 280, 5750–5763.
Gerasimovskaya, E.V., Tucker, D.A., Weiser-Evans, M., Wenzlau, J.M., Klemm, D.J., Banks, M., Stenmark, K.R., 2005. Extracellular ATP-induced proliferation of adventitial fibroblasts requires phosphoinositide 3-kinase, Akt, mammalian target of rapamycin, and p70 S6 kinase signaling pathways. J. Biol. Chem. 280, 1838–1848.
Ghaemi-Oskouie, F., Shi, Y., 2011. The role of uric acid as an endogenous danger signal in immunity and inflammation. Curr. Rheumatol. Rep. 13, 160–166.
Ginsberg, M.R., Rubin, R.A., Falcone, T., Ting, A.H., Natowicz, M.R., 2012. Brain transcriptional and epigenetic associations with autism. PLoS One 7, e44736.
Gorrindo, P., Lane, C.J., Lee, E.B., McLaughlin, B., Levitt, P., 2013. Enrichment of elevated plasma F2t-isoprostane levels in individuals with autism who are stratified by presence of gastrointestinal dysfunction. PLoS One 8, e68444.
Graf, W.D., Marin-Garcia, J., Gao, H.G., Pizzo, S., Naviaux, R.K., Markusic, D., Barshop, B.A., Courchesne, E., Haas, R.H., 2000. Autism associated with the mitochondrial DNA G8363A transfer RNA(Lys) mutation. J. Child Neurol. 15, 357–361.
Green, D.R., Galluzzi, L., Kroemer, G., 2011. Mitochondria and the autophagy-inflammation-cell death axis in organismal aging. Science 333, 1109–1112.
Halassa, M.M., 2011. Thalamocortical dynamics of sleep: roles of purinergic neuromodulation. Semin. Cell Dev. Biol. 22, 245–251.
Hallmayer, J., Cleveland, S., Torres, A., Phillips, J., Cohen, B., Torigoe, T., Miller, J., Fedele, A., Collins, J., Smith, K., Lotspeich, L., Croen, L.A., Ozonoff, S., Lajonchere, C., Grether, J.K., Risch, N., 2011. Genetic heritability and shared environmental factors among twin pairs with autism. Arch. Gen. Psychiatry 68, 1095–1102.
Hamlin, J.C., Pauly, M., Melnyk, S., Pavliv, O., Starrett, W., Crook, T.A., James, S.J.,

2013. Dietary intake and plasma levels of choline and betaine in children with autism spectrum disorders. Autism Res. Treat. 2013, 578429.
Hawking, F., 1940. Concentration of Bayer 205 (Germanin) in human blood and cerebrospinal fluid after treatment. Trans. R. Soc. Trop. Med. Hyg. 34, 37–52.
Hawking, F., 1978. Suramin: with special reference to onchocerciasis. Adv. Pharmacol. Chemother. 15, 289–322.
Henss, L., Beck, S., Weidner, T., Biedenkopf, N., Sliva, K., Weber, C., Becker, S., Schnierle, B.S., 2016. Suramin is a potent inhibitor of Chikungunya and Ebola virus cell entry. Virol. J. 13, 149.
Herbert, M., Herbert, M.R., Weintraub, K., 2013. The Autism Revolution: Whole-Body Strategies for Making Life All It Can Be. Ballantine Books.
Heun-Johnson, H., Levitt, P., 2016. Early-life stress paradigm transiently alters maternal behavior, dam-pup interactions, and offspring vocalizations in mice. Front. Behav. Neurosci. 10, 142.
Housley, G.D., Jagger, D.J., Greenwood, D., Raybould, N.P., Salih, S.G., Jarlebark, L.E., Vlajkovic, S.M., Kanjhan, R., Nikolic, P., Munoz, D.J., Thorne, P.R., 2002. Purinergic regulation of sound transduction and auditory neurotransmission. Audiol. Neurootol. 7, 55–61.
Housley, G.D., Bringmann, A., Reichenbach, A., 2009. Purinergic signaling in special senses. Trends Neurosci. 32, 128–141.
Huang, Y.A., Dando, R., Roper, S.D., 2009. Autocrine and paracrine roles for ATP and serotonin in mouse taste buds. J. Neurosci. 29, 13909–13918.
Huang, W.H., Guenthner, C.J., Xu, J., Nguyen, T., Schwarz, L.A., Wilkinson, A.W., Gozani, O., Chang, H.Y., Shamloo, M., Luo, L., 2016. Molecular and neural functions of Rai1, the causal gene for smith-magenis syndrome. Neuron 92, 392–406.
Jacobson, K.A., Müller, C.E., 2016. Medicinal chemistry of adenosine, P2Y and P2X receptors. Neuropharmacology 104, 31–49.
James, S.J., Cutler, P., Melnyk, S., Jernigan, S., Janak, L., Gaylor, D.W., Neubrander, J.A., 2004. Metabolic biomarkers of increased oxidative stress and impaired methylation capacity in children with autism. Am. J. Clin. Nutr. 80, 1611–1617.
James, S.J., Melnyk, S., Jernigan, S., Cleves, M.A., Halsted, C.H., Wong, D.H., Cutler, P., Bock, K., Boris, M., Bradstreet, J.J., Baker, S.M., Gaylor, D.W., 2006. Metabolic endophenotype and related genotypes are associated with oxidative stress in children with autism. Am. J. Med. Genet. B Neuropsychiatr. Genet. 141B, 947–956.
Jimenez, M., Clave, P., Accarino, A., Gallego, D., 2014. Purinergic neuromuscular transmission in the gastrointestinal tract; functional basis for future clinical and pharmacological studies. Br. J. Pharmacol. 171, 4360–4375.
Kajimura, S., Saito, M., 2014. A new era in brown adipose tissue biology: molecular control of brown fat development and energy homeostasis. Annu. Rev. Physiol. 76, 225–249.
Kalkbrenner, A.E., Schmidt, R.J., Penlesky, A.C., 2014. Environmental chemical exposures and autism spectrum disorders: a review of the epidemiological evidence. Curr. Probl. Pediatr. Adolesc. Health Care 44, 277–318.
Kang, M.K., Mehrazarin, S., Park, N.H., Wang, C.Y., 2017. Epigenetic gene regulation by histone demethylases: emerging role in oncogenesis and inflammation. Oral Dis. 23 (6), 709–720. http://dx.doi.org/10.1111/odi.12569. (Epub ahead of print: 2016/08/16, PubMed PMID: 27514027; PMCID: PMC5493521).
Kanner, L., 1943. Autistic disturbances of affective contact. Nervous Child 2, 217–250.
Karban, A., Feldman, T., Waterman, M., Leiba, R., Efrati, E., 2016. The association of the MTHFR C677T polymorphism with inflammatory bowel diseases in the Israeli Jewish population: an example of genetic heterogeneity. Medicine (Baltimore) 95, e5611.
Katz, S., Ayala, V., Santillan, G., Boland, R., 2011. Activation of the PI3K/Akt signaling pathway through P2Y(2) receptors by extracellular ATP is involved in osteoblastic cell proliferation. Arch. Biochem. Biophys. 513, 144–152.
Kaur, M., Reed, E., Sartor, O., Dahut, W., Figg, W.D., 2002. Suramin's development: what did we learn? Investig. New Drugs 20, 209–219.
Kinney, D.K., Miller, A.M., Crowley, D.J., Huang, E., Gerber, E., 2008. Autism prevalence following prenatal exposure to hurricanes and tropical storms in Louisiana. J. Autism Dev. Disord. 38, 481–488.
Klyachko, N.L., Shchedrina, V.A., Efimov, A.V., Kazakov, S.V., Gazaryan, I.G., Kristal, B.S., Brown, A.M., 2005. pH-dependent substrate preference of pig heart lipoamide dehydrogenase varies with oligomeric state: response to mitochondrial matrix acidification. J. Biol. Chem. 280, 16106–16114.
Kočovská, E., Fernell, E., Billstedt, E., Minnis, H., Gillberg, C., 2012. Vitamin D and autism: clinical review. Res. Dev. Disabil. 33, 1541–1550.
Konstantynowicz, J., Porowski, T., Zoch-Zwierz, W., Wasilewska, J., Kadziela-Olech, H., Kulak, W., Owens, S.C., Piotrowska-Jastrzebska, J., Kaczmarski, M., 2012. A potential pathogenic role of oxalate in autism. Eur. J. Paediatr. Neurol. 16, 485–491.
Kudin, A.P., Mawasi, H., Eisenkraft, A., Elger, C.E., Bialer, M., Kunz, W.S., 2017. Mitochondrial liver toxicity of valproic acid and its acid derivatives is related to inhibition of α-lipoamide dehydrogenase. Int. J. Mol. Sci. 18.
Lachenal, G., Pernet-Gallay, K., Chivet, M., Hemming, F.J., Belly, A., Bodon, G., Blot, B., Haase, G., Goldberg, Y., Sadoul, R., 2011. Release of exosomes from differentiated neurons and its regulation by synaptic glutamatergic activity. Mol. Cell. Neurosci. 46, 409–418.
Lamirand, A., Pallud-Mothre, S., Ramauge, M., Pierre, M., Courtin, F., 2008. Oxidative stress regulates type 3 deiodinase and type 2 deiodinase in cultured rat astrocytes. Endocrinology 149, 3713–3721.
Landrigan, P., Lambertini, L., Birnbaum, L., 2012. A research strategy to discover the environmental causes of autism and neurodevelopmental disabilities. Environ. Health Perspect. 120 (7), e258–e260.
Lavelle, T.A., Weinstein, M.C., Newhouse, J.P., Munir, K., Kuhlthau, K.A., Prosser, L.A., 2014. Economic burden of childhood autism spectrum disorders. Pediatrics 133, e520–e529.
Lazarowski, E.R., Harden, T.K., 2015. UDP-sugars as extracellular signaling molecules: cellular and physiologic consequences of P2Y14 receptor activation. Mol. Pharmacol. 88, 151–160.
Ledderose, C., Bao, Y., Zhang, J., Junger, W.G., 2015. Novel method for real-time monitoring of ATP release reveals multiple phases of autocrine purinergic signalling during immune cell activation. Acta Physiol. (Oxford) 213, 334–345.
Lee, J.H., Chiba, T., Marcus, D.C., 2001. P2X2 receptor mediates stimulation of parasensory cation absorption by cochlear outer sulcus cells and vestibular transitional cells. J. Neurosci. 21, 9168–9174.
Leigh, J.P., Du, J., 2015. Brief Report: forecasting the Economic Burden of Autism in 2015 and 2025 in the United States. J. Autism Dev. Disord. 45, 4135–4139.
Leng, Y., Yamamoto, T., Kadowaki, M., 2008. Alteration of cholinergic, purinergic and sensory neurotransmission in the mouse colon of food allergy model. Neurosci. Lett. 445, 195–198.
Leuzzi, V., 2002. Inborn errors of creatine metabolism and epilepsy: clinical features, diagnosis, and treatment. J. Child Neurol. 17 (Suppl. 3) (3S89–3S97; discussion 83S97).
Liu, N., Zhuang, S., 2011. Tissue protective and anti-fibrotic actions of suramin: new uses of an old drug. Curr. Clin. Pharmacol. 6, 137–142.
Liu, X., Hashimoto-Torii, K., Torii, M., Haydar, T.F., Rakic, P., 2008. The role of ATP signaling in the migration of intermediate neuronal progenitors to the neocortical subventricular zone. Proc. Natl. Acad. Sci. U. S. A. 105, 11802–11807.
Lobo, P.I., 2017. Role of natural IgM autoantibodies (IgM-NAA) and IgM anti-leukocyte antibodies (IgM-ALA) in regulating inflammation. Curr. Top. Microbiol. Immunol. 408, 89–117.
MacDonald, S.E., Dover, D.C., Simmonds, K.A., Svenson, L.W., 2014. Risk of febrile seizures after first dose of measles-mumps-rubella-varicella vaccine: a population-based cohort study. CMAJ 186, 824–829.
MacFabe, D.F., Cain, D.P., Rodriguez-Capote, K., Franklin, A.E., Hoffman, J.E., Boon, F., Taylor, A.R., Kavaliers, M., Ossenkopp, K.P., 2007. Neurobiological effects of intraventricular propionic acid in rats: possible role of short chain fatty acids on the pathogenesis and characteristics of autism spectrum disorders. Behav. Brain Res. 176, 149–169.
Machtinger, R., Laurent, L.C., Baccarelli, A.A., 2016. Extracellular vesicles: roles in gamete maturation, fertilization and embryo implantation. Hum. Reprod. Update 22, 182–193.
Magni, G., Riccio, D., Ceruti, S., 2017. Tackling chronic pain and inflammation through the purinergic system. Curr. Med. Chem. http://dx.doi.org/10.2174/0929867324666170710110630. (Epub ahead of print: PMID: 28699505).
Mastrangelo, L., Kim, J.E., Miyanohara, A., Kang, T.H., Friedmann, T., 2012. Purinergic signaling in human pluripotent stem cells is regulated by the housekeeping gene encoding hypoxanthine guanine phosphoribosyltransferase. Proc. Natl. Acad. Sci. U. S. A. 109, 3377–3382.
Matos, J.E., Sorensen, M.V., Geyti, C.S., Robaye, B., Boeynaems, J.M., Leipziger, J., 2007. Distal colonic Na(+) absorption inhibited by luminal P2Y(2) receptors. Pflugers Arch. Eur. J. Physiol. 454, 977–987.
Mavrakis, K.J., McDonald 3rd, E.R., Schlabach, M.R., Billy, E., Hoffman, G.R., deWeck, A., Ruddy, D.A., Venkatesan, K., Yu, J., McAllister, G., Stump, M., deBeaumont, R., Ho, S., Yue, Y., Liu, Y., Yan-Neale, Y., Yang, G., Lin, F., Yin, H., Gao, H., Kipp, D.R., Zhao, S., McNamara, J.T., Sprague, E.R., Zheng, B., Lin, Y., Cho, Y.S., Gu, J., Crawford, K., Ciccone, D., Vitari, A.C., Lai, A., Capka, V., Hurov, K., Porter, J.A., Tallarico, J., Mickanin, C., Lees, E., Pagliarini, R., Keen, N., Schmelzle, T., Hofmann, F., Stegmeier, F., Sellers, W.R., 2016. Disordered methionine metabolism in MTAP/CDKN2A-deleted cancers leads to dependence on PRMT5. Science 351, 1208–1213.
McPheeters, M.L., Warren, Z., Sathe, N., Bruzek, J.L., Krishnaswami, S., Jerome, R.N., Veenstra-Vanderweele, J., 2011. A systematic review of medical treatments for children with autism spectrum disorders. Pediatrics 127, e1312–1321.
Meadows, D.N., Pyzik, M., Wu, Q., Torre, S., Gros, P., Vidal, S.M., Rozen, R., 2014. Increased resistance to malaria in mice with methylenetetrahydrofolate reductase (Mthfr) deficiency suggests a mechanism for selection of the MTHFR 677C > T (c.665C > T) variant. Hum. Mutat. 35, 594–600.
Mercimek-Mahmutoglu, S., Stoeckler-Ipsiroglu, S., Adami, A., Appleton, R., Araujo, H.C., Duran, M., Ensenauer, R., Fernandez-Alvarez, E., Garcia, P., Grolik, C., Item, C.B., Leuzzi, V., Marquardt, I., Muhl, A., Saelke-Kellermann, R.A., Salomons, G.S., Schulze, A., Surtees, R., van der Knaap, M.S., Vasconcelos, R., Verhoeven, N.M., Vilarinho, L., Wilichowski, E., Jakobs, C., 2006. GAMT deficiency: features, treatment, and outcome in an inborn error of creatine synthesis. Neurology 67, 480–484.
Micheli, V., Camici, M., Tozzi, M.G., Ipata, P.L., Sestini, S., Bertelli, M., Pompucci, G., 2011. Neurological disorders of purine and pyrimidine metabolism. Curr. Top. Med. Chem. 11, 923–947.
Minocherhomji, S., Tollefsbol, T.O., Singh, K.K., 2012. Mitochondrial regulation of epigenetics and its role in human diseases. Epigenetics 7.
Mishra, A., Godavarthi, S.K., Maheshwari, M., Goswami, A., Jana, N.R., 2009. The ubiquitin ligase E6-AP is induced and recruited to aggresomes in response to proteasome inhibition and may be involved in the ubiquitination of Hsp70-bound misfolded proteins. J. Biol. Chem. 284, 10537–10545.
Mulder, E.J., Anderson, G.M., Kema, I.P., de Bildt, A., van Lang, N.D., den Boer, J.A., Minderaa, R.B., 2004. Platelet serotonin levels in pervasive developmental disorders and mental retardation: diagnostic group differences, within-group distribution, and behavioral correlates. J. Am. Acad. Child Adolesc. Psychiatry 43, 491–499.
Muotri, A.R., Marchetto, M.C., Coufal, N.G., Oefner, R., Yeo, G., Nakashima, K., Gage, F.H., 2010. L1 retrotransposition in neurons is modulated by MeCP2. Nature 468, 443–446.
Nadeem, A., Ahmad, S.F., Attia, S.M., Bakheet, S.A., Al-Harbi, N.O., Al-Ayadhi, L.Y., 2018. Activation of IL-17 receptor leads to increased oxidative inflammation in peripheral monocytes of autistic children. Brain Behav. Immun. 67, 335–344. http://dx.doi.org/10.1016/j.bbi.2017.09.010. (Epub ahead of print: 2017/09/25, PubMed PMID: 28935156).

Naviaux, R.K., 2008. Mitochondrial control of epigenetics. Cancer Biol. Ther. 7, 1191–1193.
Naviaux, R.K., 2012a. Mitochondria and autism. In: Buxbaum, J.D., Hof, P.R. (Eds.), The Neuroscience of Autism Spectrum Disorders. Academic Press, Elsevier, Waltham, MA, pp. 179–193.
Naviaux, R.K., 2012b. Oxidative shielding or oxidative stress? J. Pharmacol. Exp. Ther. 342, 608–618.
Naviaux, R.K., 2014. Metabolic features of the cell danger response. Mitochondrion 16, 7–17.
Naviaux, R.K., Le, T.P., Bedelbaeva, K., Leferovich, J., Gourevitch, D., Sachadyn, P., Zhang, X.M., Clark, L., Heber-Katz, E., 2009. Retained features of embryonic metabolism in the adult MRL mouse. Mol. Genet. Metab. 96, 133–144.
Naviaux, R.K., Zolkipli-Cunningham, Z., Nakayama, T., Naviaux, J.C., Le, T., Wang, L., Schuchbauer, M., Rogac, M., Li, Q., Dugan, L.L., Powell, S., 2013. Antipurinergic Therapy Corrects the Autism-Like Features in the Poly(IC) Mouse Model. PLoS One 8, e57380.
Naviaux, J.C., Schuchbauer, M.A., Li, K., Wang, L., Risbrough, V.B., Powell, S.B., Naviaux, R.K., 2014. Reversal of autism-like behaviors and metabolism in adult mice with single-dose antipurinergic therapy. Transl. Psychiatry 4, e400.
Naviaux, J.C., Wang, L., Li, K., Bright, A.T., Alaynick, W.A., Williams, K.R., Powell, S.B., Naviaux, R.K., 2015. Antipurinergic therapy corrects the autism-like features in the Fragile X (Fmr1 knockout) mouse model. Mol. Autism 6, 1.
Naviaux, R.K., Naviaux, J.C., Li, K., Bright, A.T., Alaynick, W.A., Wang, L., Baxter, A., Nathan, N., Anderson, W., Gordon, E., 2016. Metabolic features of chronic fatigue syndrome. Proc. Natl. Acad. Sci. U. S. A. 113, E5472–5480.
Naviaux, R.K., Curtis, B., Li, K., Naviaux, J.C., Bright, A.T., Reiner, G.E., Westerfield, M., Goh, S., Alaynick, W.A., Wang, L., Capparelli, E.V., Adams, C., Sun, J., Jain, S., He, F., Arellano, D.A., Mash, L.E., Chukoskie, L., Lincoln, A., Townsend, J., 2017. Low-dose suramin in autism spectrum disorder: a small, phase I/II, randomized clinical trial. Ann. Clin. Transl. Neurol. 4, 491–505.
Nemeth, A., Orgovan, N., Sodar, B.W., Osteikoetxea, X., Paloczi, K., Szabo-Taylor, K.E., Vukman, K.V., Kittel, A., Turiak, L., Wiener, Z., Toth, S., Drahos, L., Vekey, K., Horvath, R., Buzas, E.I., 2017. Antibiotic-induced release of small extracellular vesicles (exosomes) with surface-associated DNA. Sci. Rep. 7, 8202.
Nikkanen, J., Forsstrom, S., Euro, L., Paetau, I., Kohnz, R.A., Wang, L., Chilov, D., Viinamaki, J., Roivainen, A., Marjamaki, P., Liljenback, H., Ahola, S., Buzkova, J., Terzioglu, M., Khan, N.A., Pirnes-Karhu, S., Paetau, A., Lonnqvist, T., Sajantila, A., Isohanni, P., Tyynismaa, H., Nomura, D.K., Battersby, B.J., Velagapudi, V., Carroll, C.J., Suomalainen, A., 2016. Mitochondrial DNA replication defects disturb cellular dNTP pools and remodel one-carbon metabolism. Cell Metab. 23, 635–648.
Nordin, V., Lekman, A., Johansson, M., Fredman, P., Gillberg, C., 1998. Gangliosides in cerebrospinal fluid in children with autism spectrum disorders. Dev. Med. Child Neurol. 40, 587–594.
Novarino, G., El-Fishawy, P., Kayserili, H., Meguid, N.A., Scott, E.M., Schroth, J., Silhavy, J.L., Kara, M., Khalil, R.O., Ben-Omran, T., Ercan-Sencicek, A.G., Hashish, A.F., Sanders, S.J., Gupta, A.R., Hashem, H.S., Matern, D., Gabriel, S., Sweetman, L., Rahimi, Y., Harris, R.A., State, M.W., Gleeson, J.G., 2012. Mutations in BCKD-kinase lead to a potentially treatable form of autism with epilepsy. Science 338, 394–397.
Nyhan, W.L., James, J.A., Teberg, A.J., Sweetman, L., Nelson, L.G., 1969. A new disorder of purine metabolism with behavioral manifestations. J. Pediatr. 74, 20–27.
Oka, T., Hikoso, S., Yamaguchi, O., Taneike, M., Takeda, T., Tamai, T., Oyabu, J., Murakawa, T., Nakayama, H., Nishida, K., Akira, S., Yamamoto, A., Komuro, I., Otsu, K., 2012. Mitochondrial DNA that escapes from autophagy causes inflammation and heart failure. Nature 485, 251–255.
Osipchuk, Y., Cahalan, M., 1992. Cell-to-cell spread of calcium signals mediated by ATP receptors in mast cells. Nature 359, 241–244.
Page, T., Coleman, M., 2000. Purine metabolism abnormalities in a hyperuricosuric subclass of autism. Biochim. Biophys. Acta 1500, 291–296.
Palmer, R.F., Blanchard, S., Wood, R., 2009. Proximity to point sources of environmental mercury release as a predictor of autism prevalence. Health Place 15, 18–24.
Palmieri, L., Papaleo, V., Porcelli, V., Scarcia, P., Gaita, L., Sacco, R., Hager, J., Rousseau, F., Curatolo, P., Manzi, B., Militerni, R., Bravaccio, C., Trillo, S., Schneider, C., Melmed, R., Elia, M., Lenti, C., Saccani, M., Pascucci, T., Puglisi-Allegra, S., Reichelt, K.L., Persico, A.M., 2010. Altered calcium homeostasis in autism-spectrum disorders: evidence from biochemical and genetic studies of the mitochondrial aspartate/glutamate carrier AGC1. Mol. Psychiatry 15, 38–52.
Pankratov, Y., Lalo, U., Krishtal, O.A., Verkhratsky, A., 2009. P2X receptors and synaptic plasticity. Neuroscience 158, 137–148.
Passamani, L.M., Pedrosa, D.F., Mauad, H., Schenberg, L.C., Paton, J.F., Sampaio, K.N., 2011. Involvement of the purinergic system in central cardiovascular modulation at the level of the nucleus ambiguus of anaesthetized rats. Exp. Physiol. 96, 262–274.
Pastural, E., Ritchie, S., Lu, Y., Jin, W., Kavianpour, A., Khine Su-Myat, K., Heath, D., Wood, P.L., Fisk, M., Goodenowe, D.B., 2009. Novel plasma phospholipid biomarkers of autism: mitochondrial dysfunction as a putative causative mechanism. Prostaglandins Leukot. Essent. Fat. Acids 81, 253–264.
Pellegrino, M.W., Haynes, C.M., 2015. Mitophagy and the mitochondrial unfolded protein response in neurodegeneration and bacterial infection. BMC Biol. 13, 22.
Pelligrino, D.A., Vetri, F., Xu, H.L., 2011. Purinergic mechanisms in gliovascular coupling. Semin. Cell Dev. Biol. 22, 229–236.
Peng, W., Cotrina, M.L., Han, X., Yu, H., Bekar, L., Blum, L., Takano, T., Tian, G.F., Goldman, S.A., Nedergaard, M., 2009. Systemic administration of an antagonist of the ATP-sensitive receptor P2X7 improves recovery after spinal cord injury. Proc. Natl. Acad. Sci. U. S. A. 106, 12489–12493.
Perkins, T., Rosenberg, J.M., Le Coz, C., Alaimo, J.T., Trofa, M., Mullegama, S.V., Antaya, R.J., Jyonouchi, S., Elsea, S.H., Utz, P.J., Meffre, E., Romberg, N., 2017. Smith-magenis syndrome patients often display antibody deficiency but not other immune pathologies. J. Allergy Clin. Immunol. Pract. 5 (1344–1350), e1343.
Pfeifle, R., Rothe, T., Ipseiz, N., Scherer, H.U., Culemann, S., Harre, U., Ackermann, J.A., Seefried, M., Kleyer, A., Uderhardt, S., Haugg, B., Hueber, A.J., Daum, P., Heidkamp, G.F., Ge, C., Bohm, S., Lux, A., Schuh, W., Magorivska, I., Nandakumar, K.S., Lonnblom, E., Becker, C., Dudziak, D., Wuhrer, M., Rombouts, Y., Koeleman, C.A., Toes, R., Winkler, T.H., Holmdahl, R., Herrmann, M., Bluml, S., Nimmerjahn, F., Schett, G., Kronke, G., 2017. Regulation of autoantibody activity by the IL-23-TH17 axis determines the onset of autoimmune disease. Nat. Immunol. 18, 104–113.
Pijacka, W., Moraes, D.J., Ratcliffe, L.E., Nightingale, A.K., Hart, E.C., da Silva, M.P., Machado, B.H., McBryde, F.D., Abdala, A.P., Ford, A.P., Paton, J.F., 2016. Purinergic receptors in the carotid body as a new drug target for controlling hypertension. Nat. Med. 22, 1151–1159.
Pollack, G.H., 2013. The Fourth Phase of Water: Beyond Solid, Liquid, and Vapor. Ebner & Sons, Seattle, WA.
Prigogine, I., Nicolis, G., 1971. Biological order, structure and instabilities. Q. Rev. Biophys. 4, 107–148.
Raad, M., Nohra, E., Chams, N., Itani, M., Talih, F., Mondello, S., Kobeissy, F., 2014. Autoantibodies in traumatic brain injury and central nervous system trauma. Neuroscience 281, 16–23.
Rajendran, L., Honsho, M., Zahn, T.R., Keller, P., Geiger, K.D., Verkade, P., Simons, K., 2006. Alzheimer's disease beta-amyloid peptides are released in association with exosomes. Proc. Natl. Acad. Sci. U. S. A. 103, 11172–11177.
Raskovalova, T., Huang, X., Sitkovsky, M., Zacharia, L.C., Jackson, E.K., Gorelik, E., 2005. Gs protein-coupled adenosine receptor signaling and lytic function of activated NK cells. J. Immunol. 175, 4383–4391.
Ren, P., Zheng, Y., Wang, W., Hong, L., Delpeyroux, F., Arenzana-Seisdedos, F., Altmeyer, R., 2017. Suramin interacts with the positively charged region surrounding the 5-fold axis of the EV-A71 capsid and inhibits multiple enterovirus A. Sci. Rep. 7, 42902.
Rimland, B., 1964. Infantile Autism: The Syndrome and Its Implications for a Neural Theory of Behavior. Appleton-Century-Crofts, New York, NY.
Rimland, B., Callaway, E., Dreyfus, P., 1978. The effect of high doses of vitamin B6 on autistic children: a double-blind crossover study. Am. J. Psychiatry 135, 472–475.
Ronald, A., Pennell, C.E., Whitehouse, A.J., 2010. Prenatal maternal stress associated with ADHD and autistic traits in early childhood. Front. Psychol. 1, 223.
Rose, S., Frye, R.E., Slattery, J., Wynne, R., Tippett, M., Melnyk, S., James, S.J., 2014a. Oxidative stress induces mitochondrial dysfunction in a subset of autistic lymphoblastoid cell lines. Transl. Psychiatry 4, e377.
Rose, S., Frye, R.E., Slattery, J., Wynne, R., Tippett, M., Pavliv, O., Melnyk, S., James, S.J., 2014b. Oxidative stress induces mitochondrial dysfunction in a subset of autism lymphoblastoid cell lines in a well-matched case control cohort. PLoS One 9, e85436.
Rose, S., Bennuri, S.C., Wynne, R., Melnyk, S., James, S.J., Frye, R.E., 2017. Mitochondrial and redox abnormalities in autism lymphoblastoid cells: a sibling control study. FASEB J. 31, 904–909.
Rutter, M.L., Kreppner, J.M., O'Connor, T.G., English, Romanian Adoptees study, t, 2001. Specificity and heterogeneity in children's responses to profound institutional privation. Br. J. Psychiatry J. Ment. Sci. 179, 97–103.
Sander, L.E., Garaude, J., 2017. The mitochondrial respiratory chain: A metabolic rheostat of innate immune cell-mediated antibacterial responses. Mitochondrion. http://dx.doi.org/10.1016/j.mito.2017.10.008. (Epub ahead of print: PMID: 29054472).
Sandler, R.H., Finegold, S.M., Bolte, E.R., Buchanan, C.P., Maxwell, A.P., Vaisanen, M.L., Nelson, M.N., Wexler, H.M., 2000. Short-term benefit from oral vancomycin treatment of regressive-onset autism. J. Child Neurol. 15, 429–435.
Sano, R., Annunziata, I., Patterson, A., Moshiach, S., Gomero, E., Opferman, J., Forte, M., d'Azzo, A., 2009. GM1-ganglioside accumulation at the mitochondria-associated ER membranes links ER stress to Ca(2 +)-dependent mitochondrial apoptosis. Mol. Cell 36, 500–511.
Savio, L.E., Coutinho-Silva, R., 2016. Purinergic signaling in infection and autoimmune disease. Biom. J. 39, 304–305.
Schain, R.J., Freedman, D.X., 1961. Studies on 5-hydroxyindole metabolism in autistic and other mentally retarded children. J. Pediatr. 58, 315–320.
Schengrund, C.L., Ali-Rahmani, F., Ramer, J.C., 2012. Cholesterol, GM1, and autism. Neurochem. Res. 37, 1201–1207.
Schmidt, R.J., Hansen, R.L., Hartiala, J., Allayee, H., Schmidt, L.C., Tancredi, D.J., Tassone, F., Hertz-Picciotto, I., 2011. Prenatal vitamins, one-carbon metabolism gene variants, and risk for autism. Epidemiology 22, 476–485.
Schuck, R.N., Grillo, J.A., 2016. Pharmacogenomic Biomarkers: an FDA Perspective on Utilization in Biological Product Labeling. AAPS J. 18, 573–577.
Seth, R.B., Sun, L., Ea, C.K., Chen, Z.J., 2005. Identification and characterization of MAVS, a mitochondrial antiviral signaling protein that activates NF-kappaB and IRF 3. Cell 122, 669–682.
Silva, G., Beierwaltes, W.H., Garvin, J.L., 2006. Extracellular ATP stimulates NO production in rat thick ascending limb. Hypertension 47, 563–567.
Silva, J.M., Wong, A., Carelli, V., Cortopassi, G.A., 2009. Inhibition of mitochondrial function induces an integrated stress response in oligodendroglia. Neurobiol. Dis. 34, 357–365.
Simoneau, A., Ricard, E., Weber, S., Hammond-Martel, I., Wong, L.H., Sellam, A., Giaever, G., Nislow, C., Raymond, M., Wurtele, H., 2016. Chromosome-wide histone deacetylation by sirtuins prevents hyperactivation of DNA damage-induced signaling upon replicative stress. Nucleic Acids Res. 44, 2706–2726.
Sipe, G.O., Lowery, R.L., Tremblay, M.E., Kelly, E.A., Lamantia, C.E., Majewska, A.K., 2016. Microglial P2Y12 is necessary for synaptic plasticity in mouse visual cortex. Nat. Commun. 7, 10905.
Smiraglia, D.J., Kulawiec, M., Bistulfi, G.L., Gupta, S.G., Singh, K.K., 2008. A novel role for mitochondria in regulating epigenetic modification in the nucleus. Cancer Biol. Ther. 7, 1182–1190.
Smith, J.A., 2014. A new paradigm: innate immune sensing of viruses via the unfolded

protein response. Front. Microbiol. 5, 222.
So, A., Thorens, B., 2010. Uric acid transport and disease. J. Clin. Invest. 120, 1791–1799.
Soares-Bezerra, R.J., Calheiros, A.S., da Silva Ferreira, N.C., da Silva Frutuoso, V., Alves, L.A., 2013. Natural products as a source for new anti-inflammatory and analgesic compounds through the inhibition of purinergic P2X receptors. Pharmaceuticals (Basel) 6, 650–658.
Song, M., Dorn II, G.W., 2015. Mitoconfusion: noncanonical functioning of dynamism factors in static mitochondria of the heart. Cell Metab. 21, 195–205.
Song, Z., Gomes, D.A., Stevens, W., 2009. Role of purinergic P2Y1 receptors in regulation of vasopressin and oxytocin secretion. Am. J. Physiol. Regul. Integr. Comp. Physiol. 297, R478–484.
Sperlagh, B., Csolle, C., Ando, R.D., Goloncser, F., Kittel, A., Baranyi, M., 2012. The role of purinergic signaling in depressive disorders. Neuropsychopharmacol. Hung 14, 231–238.
Sriram, G., Martinez, J.A., McCabe, E.R., Liao, J.C., Dipple, K.M., 2005. Single-gene disorders: what role could moonlighting enzymes play? Am. J. Hum. Genet. 76, 911–924.
Stein, C.A., 1993. Suramin: a novel antineoplastic agent with multiple potential mechanisms of action. Cancer Res. 53, 2239–2248.
Stockler-Ipsiroglu, S., van Karnebeek, C.D., 2014. Cerebral creatine deficiencies: a group of treatable intellectual developmental disorders. Semin. Neurol. 34, 350–356.
Stojilkovic, S.S., 2009. Purinergic regulation of hypothalamopituitary functions. Trends Endocrinol Metab 20, 460–468.
Sullivan, J.A., Jankowska-Gan, E., Shi, L., Roenneburg, D., Hegde, S., Greenspan, D.S., Wilkes, D.S., Denlinger, L.C., Burlingham, W.J., 2014. Differential requirement for P2X7R function in IL-17 dependent vs. IL-17 independent cellular immune responses. Am. J. Transplant. 14, 1512–1522.
Sutton, H.E., Read, J.H., 1958. Abnormal amino acid metabolism in a case suggesting autism. AMA J. Dis. Child 96, 23–28.
Talkowski, M.E., Minikel, E.V., Gusella, J.F., 2014. Autism spectrum disorder genetics: diverse genes with diverse clinical outcomes. Harv. Rev. Psychiatry 22, 65–75.
Theoharides, T.C., 2013. Extracellular mitochondrial ATP, suramin, and autism? Clin. Ther. 35, 1454–1456.
Tierney, E., Nwokoro, N.A., Kelley, R.I., 2000. Behavioral phenotype of RSH/Smith-Lemli-Opitz syndrome. Ment. Retard. Dev. Disabil. Res. Rev. 6, 131–134.
Tirouvanziam, R., Obukhanych, T.V., Laval, J., Aronov, P.A., Libove, R., Banerjee, A.G., Parker, K.J., O'Hara, R., Herzenberg, L.A., Herzenberg, L.A., Hardan, A.Y., 2012. Distinct plasma profile of polar neutral amino acids, leucine, and glutamate in children with Autism Spectrum Disorders. J. Autism Dev. Disord. 42, 827–836.
Van Blerkom, J., 2011. Mitochondrial function in the human oocyte and embryo and their role in developmental competence. Mitochondrion 11, 797–813.
Villarroya-Beltri, C., Guerra, S., Sanchez-Madrid, F., 2017. ISGylation - a key to lock the cell gates for preventing the spread of threats. J. Cell Sci. 130 (18), 2961–2969.
Volk, H.E., Hertz-Picciotto, I., Delwiche, L., Lurmann, F., McConnell, R., 2011. Residential proximity to freeways and autism in the CHARGE study. Environ. Health Perspect. 119, 873–877.
Volk, H.E., Lurmann, F., Penfold, B., Hertz-Picciotto, I., McConnell, R., 2013. Traffic-related air pollution, particulate matter, and autism. JAMA Psychiatry 70, 71–77.
Voogd, T.E., Vansterkenburg, E.L., Wilting, J., Janssen, L.H., 1993. Recent research on the biological activity of suramin. Pharmacol. Rev. 45, 177–203.
Wallace, D.C., Fan, W., 2010. Energetics, epigenetics, mitochondrial genetics. Mitochondrion 10, 12–31.
Wang, Y., Zhang, X., Guo, Q.L., Zou, W.Y., Huang, C.S., Yan, J.Q., 2010. Cyclooxygenase inhibitors suppress the expression of P2X(3) receptors in the DRG and attenuate hyperalgesia following chronic constriction injury in rats. Neurosci. Lett. 478, 77–81.
Wang, Y., Balaji, V., Kaniyappan, S., Kruger, L., Irsen, S., Tepper, K., Chandupatla, R., Maetzler, W., Schneider, A., Mandelkow, E., Mandelkow, E.M., 2017. The release and trans-synaptic transmission of Tau via exosomes. Mol. Neurodegener. 12, 5.
Weiss, B., 2012. Synthetic food colors and neurobehavioral hazards: the view from environmental health research. Environ. Health Perspect. 120, 1–5.
West, A.P., 2017. Mitochondrial dysfunction as a trigger of innate immune responses and inflammation. Toxicology 391, 54–63.
West, A.P., Shadel, G.S., Ghosh, S., 2011. Mitochondria in innate immune responses. Nat. Rev. Immunol. 11, 389–402.
Wikoff, W.R., Kalisak, E., Trauger, S., Manchester, M., Siuzdak, G., 2009. Response and recovery in the plasma metabolome tracks the acute LCMV-induced immune response. J. Proteome Res. 8, 3578–3587.
Yang, Y., Qin, M., Bao, P., Xu, W., Xu, J., 2017. Secretory carrier membrane protein 5 is an autophagy inhibitor that promotes the secretion of alpha-synuclein via exosome. PLoS One 12, e0180892.
Youle, R.J., van der Bliek, A.M., 2012. Mitochondrial fission, fusion, and stress. Science 337, 1062–1065.
Yu, T., Junger, W.G., Yuan, C., Jin, A., Zhao, Y., Zheng, X., Zeng, Y., Liu, J., 2010. Shockwaves increase T-cell proliferation and IL-2 expression through ATP release, P2X7 receptors, and FAK activation. Am. J. Phys. Cell Physiol. 298, C457–464.
Zablotsky, B., Black, L.I., Maenner, M.J., Schieve, L.A., Blumberg, S.J., 2015. Estimated prevalence of autism and other developmental disabilities following questionnaire changes in the 2014 national health interview survey. Natl. Health Stat. Rep. 1–20.
Zerbo, O., Iosif, A.M., Walker, C., Ozonoff, S., Hansen, R.L., Hertz-Picciotto, I., 2013. Is maternal influenza or fever during pregnancy associated with autism or developmental delays? results from the CHARGE (CHildhood Autism Risks from Genetics and Environment) Study. J. Autism Dev. Disord. 43, 25–33.
Zhang, Y., Handy, D.E., Loscalzo, J., 2005. Adenosine-dependent induction of glutathione peroxidase 1 in human primary endothelial cells and protection against oxidative stress. Circ. Res. 96, 831–837.

Mitochondrion 46 (2019) 278–297

Contents lists available at ScienceDirect

Mitochondrion

journal homepage: www.elsevier.com/locate/mito

Metabolic features and regulation of the healing cycle—A new model for chronic disease pathogenesis and treatment

Robert K. Naviaux

The Mitochondrial and Metabolic Disease Center, Departments of Medicine, Pediatrics, and Pathology, University of California, San Diego School of Medicine, 214 Dickinson St., Bldg CTF, Rm C102, MC#8467, San Diego, CA 92103, United States

ARTICLE INFO

Keywords:
Cell danger response
Healing cycle
Mitochondrial nexus
Metabolic addiction
Metabolic memory
Purinergic signaling
Metabokines
Antipurinergic therapy
M0, M1 and M2 mitochondria
Ecoalleles
Ecogenetics
Allostasis
Allostatic load
Integrated stress response

ABSTRACT

Without healing, multicellular life on Earth would not exist. Without healing, one injury predisposes to another, leading to disability, chronic disease, accelerated aging, and death. Over 60% of adults and 30% of children and teens in the United States now live with a chronic illness. Advances in mass spectrometry and metabolomics have given scientists a new lens for studying health and disease. This study defines the healing cycle in metabolic terms and reframes the pathophysiology of chronic illness as the result of metabolic signaling abnormalities that block healing and cause the normal stages of the cell danger response (CDR) to persist abnormally. Once an injury occurs, active progress through the stages of healing is driven by sequential changes in cellular bioenergetics and the disposition of oxygen and carbon skeletons used for fuel, signaling, defense, repair, and recovery. > 100 chronic illnesses can be organized into three persistent stages of the CDR. One hundred and two targetable chemosensory G-protein coupled and ionotropic receptors are presented that regulate the CDR and healing. Metabokines are signaling molecules derived from metabolism that regulate these receptors. Reframing the pathogenesis of chronic illness in this way, as a systems problem that *maintains* disease, rather than focusing on remote trigger(s) that *caused* the initial injury, permits new research to focus on novel signaling therapies to *unblock* the healing cycle, and restore health when other approaches have failed.

1. Introduction

Much of modern Western medicine is based on the principles of acute interventions for poisoning, physical injury, or infection. These principles trace to historical figures like Paracelsus (1493–1541), Ambroise Paré (1510–1590), and Louis Pasteur (1822–1895). These acute care interventions are now widely used in the modern fields of pharmacology, toxicology, urgent care, emergency medicine, and surgery. When caring for acute disruptions in health, the careful identification of the trigger, or cause of the problem, and the anatomical location of the defect, is an important part of good medical care. However, when dealing with chronic illness, treatments based on the rules of acute care medicine have proven less helpful, and can even cause harm by producing unwanted side-effects (Qato et al., 2018).

In chronic illness, the original triggering event is often remote, and may no longer be present. Emerging evidence shows that most chronic illness is caused by the biological *reaction* to an injury, and not the initial injury, or the agent of injury itself. For example, melanoma can be caused by sun exposure that occurred decades earlier, and post-traumatic stress disorder (PTSD) can occur months or years after a bullet wound has healed. If healing is incomplete between injuries, more severe disease is produced. If a new head injury is sustained before complete healing of an earlier concussion, the clinical severity of the second injury is amplified, and recovery is prolonged. This occurs even when the energy of the second impact was less than the first. Progressive dysfunction with recurrent injury after incomplete healing occurs in all organ systems, not just the brain. Chronic disease then results when cells are caught in a repeating loop of incomplete recovery and re-injury, unable to fully heal. This biology is at the root of virtually every chronic illness known, including susceptibility to sequential or recurrent infections, autoimmune diseases like rheumatoid arthritis, diabetic heart and kidney disease, asthma and chronic obstructive pulmonary disease (COPD), autism spectrum disorder (ASD), chronic fatigue syndrome (CFS), cancer, affective disorders, psychiatric illnesses, Alzheimer dementia, and many more.

Great strides have been made since the 1940s in the treatment of

Abbreviations: TOGLEs, transporters Opsins G protein-coupled receptors ligands and effectors; CDR, cell danger response; ASD, autism spectrum disorder; CFS, chronic fatigue syndrome; DAMPs, damage-associated molecular patterns; DARMs, damage-associated reactive metabolites; PTSD, post-traumatic stress disorder; M0, uncommitted; M1, pro-inflammatory; M2, anti-inflammatory mitochondrial polarization

E-mail address: Naviaux@ucsd.edu.

https://doi.org/10.1016/j.mito.2018.08.001
Received 25 April 2018; Accepted 2 August 2018
Available online 09 August 2018

acute illness. This success has decreased infant mortality, lowered mortality from infections and trauma, and has improved survival after heart attacks, strokes, and cancer. However, this success has led to a sea change in medicine. Instead of spending the majority of time treating acute illness, physicians and health care workers in 2018 now spend the majority of time and effort caring for patients with chronic disease. Over $2.5 trillion is spent every year in the US to care for patients with chronic illness (Burke, 2015). While it has been tempting to treat this rising tide of chronic disease by using the principles that have proven so successful in acute care medicine, a growing literature supports the conclusion that every chronic disease is actually a whole body disease—a *systems problem*—that cannot be solved using the old paradigm. For example, autism, bipolar disorder, schizophrenia, Parkinson, and Alzheimer disease each affect the brain, but are also characterized by whole-body metabolic abnormalities that are measureable in the blood and urine (Gevi et al., 2016; Han et al., 2017; He et al., 2012; Varma et al., 2018; Yoshimi et al., 2016). Rheumatoid arthritis affects the joints, but also has metabolic abnormalities in the blood that show an activated cell danger response (CDR) (Naviaux, 2014) for several years before the onset of clinical joint disease (Surowiec et al., 2016). Coronary artery disease affects the heart, but is the result of long-standing abnormalities in metabolism called "the metabolic syndrome" (Mottillo et al., 2010).

All chronic diseases produce systems abnormalities that either block communication (signaling), or send alarm signals between cells and tissues. Cells that cannot communicate normally with neighboring or distant cells are stranded from the whole, cannot reintegrate back into normal tissue and organ function, and are functionally lost to the tissue, even when they are surrounded by a normal mosaic of differentiated cells. As this process continues, two different outcomes are produced, depending on age. If the block in cell-cell communication occurs in a child, then the normal trajectory of development can be changed, leading to alterations in brain structure and function, and changes in long-term metabolic adaptations of other organs like liver, kidney, microbiome, and immune system. If the communication block occurs in adults, then organ performance is degraded over time, more and more cells with disabled or dysfunctional signaling accumulate, and age-related deterioration of organ function, senescence, or cancer occurs.

Blocked communication and miscommunication inhibit progress through the healing cycle, and prevent normal energy-, information-, and resource-coordination with other organ systems (Wallace, 2010). This predisposes to additional damage and disease. When chronic disease is seen as a systems problem in which the healing system is blocked by key metabolites that function as signaling molecules—metabokines—new therapeutic approaches become apparent that were hidden before. What follows is a description of our best current model of the metabolic features of the healing cycle. Future research will be needed to flesh out additional details.

2. Materials and methods

2.1. Bioinformatic analysis of P2Y1R-related proteins

A TBLASTN search of the human genome was conducted using the P2Y1R protein (Uniprot P47900, ENSP00000304767) as the reference. The top 156 matching sequences were recovered. After removal of pseudogenes, partial, and duplicate sequences, the top 91 unique genes recovered ranged from 257 to 388 amino acids in length, shared a 22%–42% identity with P2Y1R, had blast scores of 70–740, and e-values of 8×10^{-10} to 2×10^{-66}. TAS2R46, a bitter taste receptor, encoded by the *T2R46* gene, was used as an outgroup for tree construction. Sequence alignments were performed using the clustal w method in MegAlign (Lasergene v15.1, DNAStar Inc., Madison, WI). Tree analysis and visualizations were performed using FigTree v1.4.3 (http://tree.bio.ed.ac.uk/software/figtree/).

2.2. Bioinformatic analysis of P2X1R-related proteins

A TBLASTN search of the human genome was conducted using the P2X1R protein (Uniprot P51575, ENSP00000225538) as the reference. The only related genes found were the other 6 known P2X receptors. A BLASTP search of related proteins recovered 46 splice variants of the 7 known ionotropic P2X receptors. The 7 top sequences were 352–399 amino acids in length, sharing 38%–52% identity with P2XR1, and had blast scores of 291–831, and e-scores of 3×10^{-91} to 5×10^{-149}.

2.3. Gene ontology

A gene ontology analysis of the 91 P2Y1R-related genes was performed using the online gene list analysis tools available on the Panther Gene Ontology website (http://www.pantherdb.org/). The top 6 pathways had gene enrichments > 3 times the expected threshold, explained 98% of the connections, and had false discovery rates from 0.02 to 2.7×10^{-65}.

3. Need for a systems biology of healing

The classical signs of inflammation that begin the process of wound healing have been known since before the time of Hippocrates (c. 460–370 BCE). Medical students today still learn the classical Latin terms for the signs of inflammation as *rubor*, *tumor*, *calor*, *dolor*, and *functio laesa* (redness, swelling, heat, pain, and loss of function). In United States, the curriculum at most medical schools does not yet include a specific course on the molecular systems biology of healing. The descriptive elements of injury and healing are taught in traditional courses like pathology, histology, and during clinical service on the surgical and burn wards. However, a dedicated systems biology course, describing our current understanding of the choreographed changes in cell metabolism, biochemistry, gene expression, cell structure, cell function, and pathophysiology that occur after injury and during healing, is missing. The rapidly growing fields of Integrative (Rakel, 2018), Functional (Baker et al., 2010), and Natural (Pizzorno and Murray, 2013) Medicine devote considerable attention to the broader, multi-dimensional study of whole-body healing as it applies to the treatment of chronic illness. However, a modern synthesis of functional and traditional medicine with state-of-the-art medical technology directed at the molecular aspects of healing has not yet been achieved.

4. Metabolomics—A new lens for chronic disease medicine

The newest "omics" technologies to be added to the systems biology toolbox are metabolomics (Jang et al., 2018) and lipidomics (Harkewicz and Dennis, 2011). Rapid advances in these emergent technologies were made possible by technological advancements in mass spectrometry that have occurred since about 2012. In 2018, we are still at least 10 years behind the technical sophistication of genomics, but a flood of new publications using metabolomics has revealed the first outlines of a missing link that connects the genes and disease. Whole-body *chemistry* appears to be this link (Fiehn, 2002).

5. Metabolites as both matter and information

Chemistry provides the link between genotype and phenotype in two ways: (1) cell metabolism is the direct result of gene-environment interactions (G × E = metabolism), and (2) chemicals (metabolites) made by and processed by the cell have a dual biology as both *matter* and *information*. Metabolites have a well-known function as *matter*; metabolites are the physical building blocks used for cell growth, structure, function, repair, and as energy and electron carriers. In ecosystem theory, this metabolic matter represents resources for system structure, function and growth, and for energy to support ecosystem connectivity and resilience to purturbation (Bernhardt and Leslie,

2013). Many metabolites also have a lesser-known function as *information*; they bind specific receptors to change behavior, regulate fetal and child development, shape the microbiome, activate neuroendocrine and immune systems, and regulate the autonomic and enteric nervous systems.

Metabolites like ATP, S-adenosylmethionine (SAMe), acetyl-CoA, NAD+, and others are used to modify DNA and histones directly to alter gene expression through epigenetics (Naviaux, 2008; Nieborak and Schneider, 2018; Wallace and Fan, 2010). Other metabolites like α-ketoglutarate, succinate, fumarate, iron, FAD, and oxygen act as essential cofactors for epigenetic modifications. These metabolites, and others like propionyl-CoA, butyryl-CoA, succinyl-CoA, myristoyl-CoA, farnesyl-diphosphate, and UDP-glucose, also alter the function of other proteins by post-translational modifications of nuclear transcription factors and enzymes throughout the cell as a function of real-time changes in metabolism. Finally, dozens of metabolites act as signaling molecules called metabokines, by binding to dedicated cell surface receptors.

6. The healing cycle

The healing process is a dynamic circle that starts with injury and ends with recovery. This process becomes less efficient as we age (Gosain and Dipietro, 2004), and reciprocally, incomplete healing results in cell senescence and accelerated aging (Valentijn et al., 2018). Reductions in mitochondrial oxidative phosphorylation and altered mitochondrial structure are fundamental features of aging (Kim et al., 2018). The changes in aging are similar to programmed changes that occur transiently during the stages of the cell danger response needed for healing (Naviaux, 2014) (Fig. 1). Although the circular nature of healing seems obvious from daily experience with cuts, scrapes, and the common cold, the extension of this notion to a unified theory to explain the pathophysiology of chronic complex disease has only recently become possible. Technological advancements in mass spectrometry and metabolomics have permitted the characterization of 4 discrete stages in the healing cycle (Fig. 1). The first of these is the health cycle, which requires wakeful activity alternating with periods of restorative sleep. The health cycle will be discussed after first reviewing the 3 stages of the cell danger response: CDR1, CDR2, and CDR3. Aspects of the CDR include the integrated stress response (ISR) (Lu et al., 2004) and the mitochondrial ISR (Khan et al., 2017; Nikkanen et al., 2016; Silva et al., 2009). While all aspects of the CDR are coordinated by nuclear-mitochondrial cross-talk, the precise controls of the transitions between the stages of the CDR are largely unknown.

The following is a current model based on evidence drawn from many experimental studies. As such, the details must be considered provisional. The 3 stages of the CDR are energetically and metabolically distinct. The smooth transition from one step to the next is choreographed by metabolic signaling and regulated by 3 sequential quality control checkpoints, CP1, CP2, and CP3 (Fig. 1). The checkpoints appear to interrogate mitochondrial and cellular function. The completion of each stage of the CDR appears to be decided largely on a cell-by-cell basis. These checkpoints are not regulated by a single, deterministic signaling molecule. Checkpoints are better considered as gates controlled by the synergistic effects of multiple permissive and inhibitory signals. The concentration of a particular signaling molecule is determined in part by the total number of cells in a tissue in each stage of the CDR. Both local and systemic signals are used. As such, the checkpoints that regulate progress through the healing cycle are probability gates. Based on real-time chemical signals and

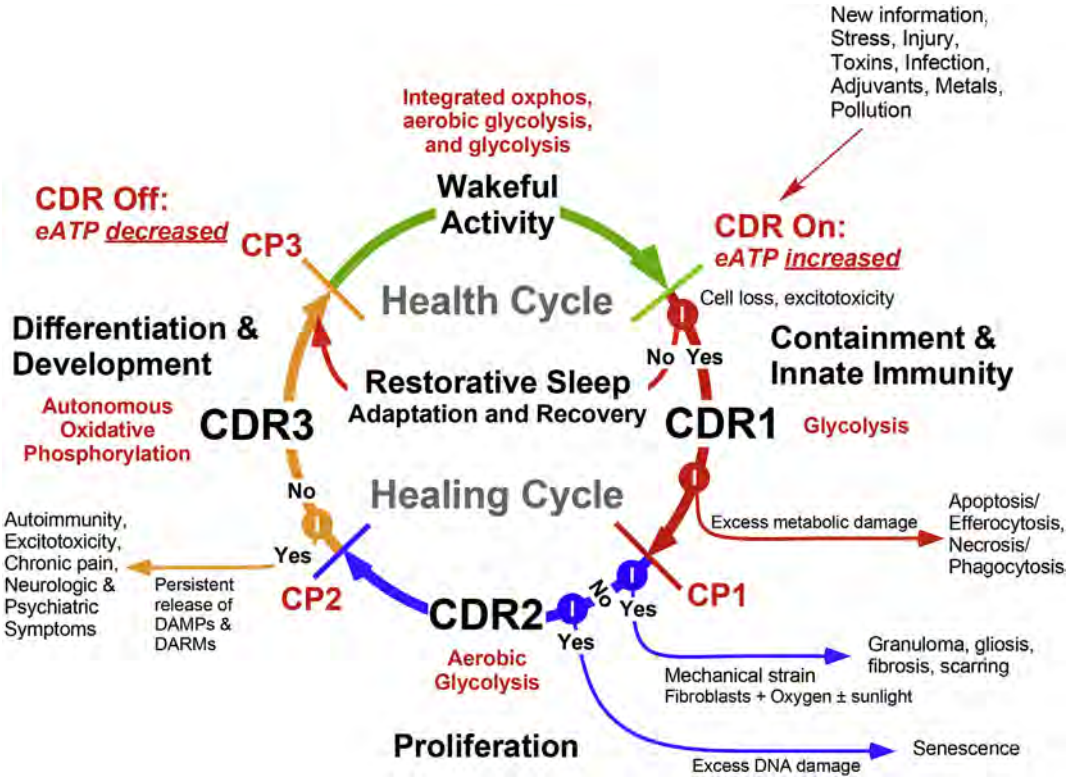

Fig. 1. A metabolic model of the health and healing cycles. Health is a dynamic process that requires regular cycling of wakeful activity and restorative sleep. The healing or damage cycle is activated when the cellular stress exceeds the capacity of restorative sleep to repair damage and restore normal cell-cell communication. CDR1 is devoted to damage control, innate immunity, inflammation, and clean up. CDR2 supports cell proliferation for biomass replacement, and blastema formation in tissues with augmented regeneration capacity. CDR3 begins when cell proliferation and migration have stopped, and recently mitotic cells can begin to differentiate and take on organ-specific functions. **Abbreviations**: eATP; extracelllular ATP; CP1–3: checkpoints 1–3; DAMPs: damage-associated molecular patterns; DARMs: damage-associated reactive metabolites.

Table 1
Provisional classification of stage-specific healing cycle disorders.*

CDR1 Disorders	CDR2 Disorders	CDR3 Disorders
Innate Immune Disorders	**Proliferative Disorders**	**Differentiation Disorders**
–HPA Axis, ATP, Lipids, mtDNA	–mTOR, p21, HIF, PHDs	–DARMs, Mito Polarization
Systemic Inflammatory Response Syndromes (SIRS)	Dyslipidemia	Autism spectrum disorder
Multiple Organ Dysfunction Syndrome (MODS),	Hyperuricemia	Chronic Fatigue Syndrome
Septic shock	Diabetes	Post-traumatic stress disorder
Acute Respiratory Distress Syndrome (ARDS)	Diabetic retinopathy	Fibromyalgia, Chronic pain syndromes, Allodynia
Allergies, asthma, atopy	Hypertension	Neuropathic pain syndromes
Chronic infections (fungal, bacteria, viral, parasitic)	Heart disease	Complex regional pain syndromes
Gulf War Illness (GWI)	Peripheral vascular disease	Obsessive Compulsive Disorder
Tinea pedis, Tinea versicolor, Tinea corporis, Tinea barbae	Cerebral vascular disease	Generalized Anxiety Disorder
Histoplasmosis, Coccidiomycosis	Inflammatory bowel disease	Major depressive disorder
Aspergillosis, Chronic mucocutaneous Candidiasis,	(Crohn's, Ulcerative colitis)	Bipolar disorder
Sporotrichosis, Cryptococcosis,	Non-alcoholic steatohepatitis	Migraine headaches
Sarcoidosis, Chronic granulomatous disease,	(NASH), Cirrhosis	New daily persistent headaches
Chlamydia, Listeriosis,	Idiopathic pulmonary fibrosis	POTS, PANS, PANDAS
Toxoplasmosis, Bartonellosis,	Benign prostatic hyperplasia	Schizophrenia, acute psychosis
Syphilis, Helicobacter, Neisseria,	Keloid formation	Parkinson, Alzheimer
Vibrio cholerae, Tuberculosis,	Subacute spinal cord injury	Multiple sclerosis, Tourette's
Non-tuberculous mycobacteria infections, Leprosy, Lyme,	Dermal vasculitis,	Dystonia syndromes, Lupus Selected epilepsies, Behcet's
Typhoid, Malaria, Leishmaniasis,	Temporal arteritis,	Scleroderma, Sjögren's,
Onchocerciasis, Schistosomiasis	Kawasaki coronary arteritis	Polymyalgia rheumatica
Trypanosomiasis, Filariasis	Cancers and Leukemias	Ankylosing spondylitis
		Amyotrophic lateral sclerosis
Ecosystem disorders		Chronic traumatic encephalopathy
Coral reef fungal infections (*Aspergillus*),		Traumatic brain injury
Coral bleaching disorder (*Vibrio*),		Selected post-stroke syndromes
Shrimp black gill disease (*Hyalophysa*),		Wakeful delta wave activity (EEG)
Microsporidial gill disease in fish,		Hashimoto's thyroiditis
Colony collapse disorder in honey bees,		Psoriasis, eczema
White nose disease in bats (*Geomycosis*),		Alopecia areata, vitiligo
Chytridiomycosis in frogs and salamanders,		Autoantibodies to intrinsic factor
Potato plague (*Phytophthera*),		Rheumatoid arthritis
Sudden Oak Death (*Phytophthera*),		Osteoarthritis
Tea leaf blister,		Macular degeneration
Coffee rust,		Presbyopia, presbycusis
Cacao tree witch's broom fungus,		Diabetic neuropathy
White pine blister rust (*Cronartium)*,		Diabetic nephropathy
Sudden Aspen Decline (*Cytospora*)		Irritable bowel syndrome
		Adaptive Energy Conservation and Survival States
		Dauer, diapause, torpor, estivation
		Hibernation, Persister cells
		Plant seed embryo formation
		Caloric restriction metabolism
		Longevity metabolism

* Subdivisions occur within each of the 3 main stages of the CDR.

mitochondrial function, each cell has a certain probability of entering the next stage of healing. This probability is 0%–100% based on cell-specific metabolism and the net effect of all the metabokines in the millieu around the cell. For any given cell, one step in the healing cycle cannot be entered until the previous step has been completed and mitochondrial function in that cell is ready for the next step. Restoration of normal communication between neighboring and distant cells is the last step of the healing cycle and is monitored by checkpoint 3 (Fig. 1). Some of the chronic illnesses and ecosystem disruptions that result from stage-specific interruptions in the healing cycle are listed in Table 1. Further studies will be needed to refine this provisional classification.

7. CDR1—Glycolysis, M1 mitochondria

The function of CDR1 is the activation of innate immunity, intruder and toxin detection and removal, damage control, and containment (Fig. 1). The level of inflammation produced in CDR1 is adjusted according to need. A major trigger of CDR1 appears to be a fundamental change in cellular organization or order, generalized as thermodynamic entropy (Cunliffe, 1997). Physical disruption of gap junctions that connect and coordinate cell function in tissues can activate the CDR. Other triggers include bacteria, viruses, fungi, protozoa, or exposure to biological or chemical toxins. In all cases, extracellular ATP and other metabokines are released from the cell to signal danger. This happens through stress-gated pannexin/P2X7 channels in the membrane and through an increase in vesicular export of ATP through SLC17A9, the vesicular nucleotide transporter (VNUT), and related transporters (Sakaki et al., 2013).

Mitochondria change their function rapidly under stress. Within minutes, the normal anti-inflammatory M2 form of mitochondria that is specialized to meet the metabolic needs of the differentiated cell, is polarized toward pro-inflammatory, M1 mitochondria (Naviaux, 2017) (Fig. 2). This initiates the oxidative shielding response needed for damage control and containment (Naviaux, 2012). When less oxygen is consumed by mitochondria for energy production by oxphos, more oxygen becomes available for synthesis of oxylipin signaling molecules (Gabbs et al., 2015) and reactive oxygen species (ROS) for defense. The incorporation of oxidized nucleotides produced during the oxidative shielding response that occurs during CDR1 into newly synthesized mitochondrial DNA, and the release of small fragments of this new oxy-

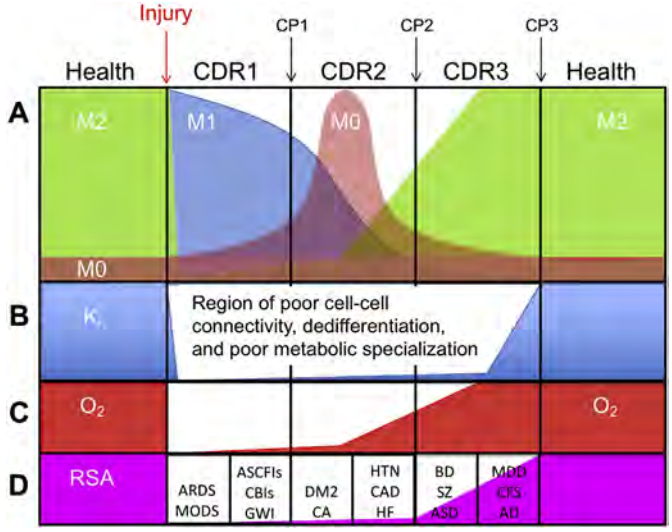

Fig. 2. Systems coordination during the healing cycle. **A.** Functional polarization of mitochondria. **B.** Connectivity (K_i): tissue and cellular responsiveness to circadian, autonomic, and neuroendocrine coordination. **C.** Tissue oxygen consumption and delivery (O_2). **D.** Ventral Vagal Complex (myelinated parasympathetic) Tone (RSA; respiratory sinus arrhythmia). Examples of chronic illnesses within subdivisions of the CDR are provisional. **Abbreviations**: M2—anti-inflammatory mitochondria specialized for oxidative phosphorylation. M1—pro-inflammatory mitochondria specialized for cellular defense in cells that use glycolysis for ATP synthesis. M0—uncommitted mitochondria adapted for rapid cellular growth and aerobic glycolysis. CP1–3: checkpoints 1–3. K_i—inter-organ, intercellular, intracellular, inter-organellar connectivity and communication. RSA: respiratory sinus arrhythmia. ARDS—acute respiratory distress syndrome. MODS—multiorgan dysfunction of sepsis. ASCFIs—Acute Staphylococcal and chronic fungal infections. CBIs—chronic bacterial infections (TB, Helicobacter, Lyme, etc). GWI—Gulf War Illness. DM2—Type 2 Diabetes. CA—cancer. HTN—hypertension. CAD—coronary artery disease. HF—heart failure. BD—Bipolar Disorder. SZ—schizophrenia. ASD—autism spectrum disorder. MDD—Major Depressive Disorder. CFS—chronic fatigue syndrome. AD—Alzheimer dementia.

mtDNA into the cytosol is required for NLRP3 inflammasome activation (Zhong et al., 2018). Release of newly synthesized double-stranded mitochondrial RNA into the cytosol also helps defend the cell during CDR1 by activating type I interferons and the antiviral response (Dhir et al., 2018).

A useful metaphor for communicating this transformation to lay audiences is as a change from powerplants to battleships. The powerplant function of M2 mitochondria is adapted for oxidative phosphorylation. The battleship function of M1 mitochondria is adapted for ROS (peroxides, superoxide, and singlet oxygen), reactive nitrogen species (RNS: nitric oxide and peroxynitrite), and reactive aliphatic hydrocarbons (RAHs: epoxides, acyl-, and amine-aldehyde) production. With M1 polarization, energy-coupled mitochondrial oxygen consumption drops, and cellular energy production switches to glycolysis and lactate production. This switch in bioenergetics is protective to cells when capillaries have been disrupted and the availability of oxygen for aerobic metabolism is compromised. Ischemic preconditioning exposes cells to a transient, sublethal stress that increases ROS and induces HIF1α and TIGAR (TP53-induced glycolysis and apoptosis regulator) for 1–3 days (Semenza, 2011; Zhou et al., 2016). This treatment causes cells to enter CDR1, decreasing mitochondrial oxidative phosphorylation and increasing glycolysis. The result is a dramatic reduction in cell death when preconditioned cells in CDR1 are exposed to potentially lethal insults within the 1–3 day window of protection. If no cells are lost, preconditioned cells return directly to CDR3 and the health cycle via the direct stress-response track that is used regularly during restorative sleep (Fig. 1).

A cell that adopts the CDR1 phenotype must functionally disconnect many lines of communication with neighboring cells. This is needed to make the metabolic and physical changes needed for cellular defense under threat. Communication with neighboring cells during this time is dramatically decreased and changed. The decrease in, and restructuring of cell-cell communication represents a kind of cellular autism that is not just beneficial, but required to initiate the healing process. However, because organs require tight cell-cell communication and coordination for optimum function, this disconnection of cells from the whole comes at a cost; normal organ function is temporarily decreased while cells pass through the steps of healing (Fig. 1). This contributes to the "*functio laesa*", loss of function, described as a canonical feature of early wound repair and inflammation. Removal of debris and damaged cells is accomplished by the combined actions of polymorphonuclear and mononuclear phagocytes recruited to the site, venous, and lymphatic drainage. This loss of function can last for weeks or months after an injury before recovery occurs. One well-studied example is the stunned myocardium that can occur after acute myocardial infarction. After injury, a segment of heart muscle can remain alive and perfused, but non-contractile for months. When recovery occurs, it is accompanied by a shift in metabolism from glycolysis (CDR1), through a blended transition phase of aerobic glycolysis (CDR2), back to oxidative phosphorylation (CDR3) (Figs. 1 and 2). This sequence is associated with an increase in mitochondrial fusion proteins and normal fatty acid oxidation (Holley et al., 2015; van der Vusse, 2011; Vogt et al., 2003), and a restoration of normal cell-cell communication needed for electromechanical coupling. CDR1 ends with passage through checkpoint 1 (CP1, Figs. 1 and 2). CP1 requires the creation of a less-oxidizing and less inflammatory extracellular environment that is conducive for shifting the thermodynamic balance from monomer to polymer synthesis needed for rebuilding RNA, DNA, proteins and membranes, and for the recruitment of previously quiescent satellite and stem cells into cell division in CDR2.

8. CDR2—Aerobic glycolysis, M0 mitochondria

The function of CDR2 is biomass replacement (Fig. 1). Every organ and tissue has an optimum number and distribution of differentiated cell types that are needed for healthy organ function. When cells are lost, they must be replaced or organ function cannot be fully restored. Once the damage associated with the initial injury, infection, or toxin exposure has been cleared or contained in CDR1, the cells that were lost need to be replaced. In CDR2, stem cells are recruited to replace the lost biomass. Stem cells are present in all tissues throughout life. When activated, they will enter the cell cycle. The mitochondria in stem cells and their immediate daughter cells exist in a youthful, metabolically uncommitted state called "M0" (Fig. 2A). M0 mitochondria help to facilitate aerobic glycolysis, also known as Warburg metabolism, which is needed for rapidly growing cells. During aerobic glycolysis, ATP is synthesized by glycolysis. However, M0 mitochondria still consume oxygen and electrons. Instead of using the potential energy gradient for synthesizing ATP by oxidative phosphorylation, M0 mitochondria dissipate the energy gradient by releasing metabolic intermediates needed for polymer synthesis and cell growth. For example, mitochondria are needed for de novo pyrimidine synthesis. The mitochondrial inner membrane protein, dihydroorotate dehydrogenase (DHODH) is required for the 4th step in de novo pyrimidine synthesis to make orotic acid. Orotic acid is needed to make UMP, which is then used to make all the Us, Cs, and Ts the cell needs for RNA and DNA synthesis, and for activated intermediates like UDP-glucose for receptor glycoprotein synthesis and glycogen synthesis, and CDP-choline for phosphatidylcholine synthesis. M0 mitochondria also supply succinyl-CoA and glycine for delta-amino levulinic acid (δ-ALA, also known as 5-ALA), porphyrin, and heme synthesis needed for cytochromes and hemoglobin. M0 mitochondria also synthesize and release citric acid, which can be used either in the cytosol or nucleus by ATP-citrate lyase

Table 2
Functional characteristics of the CDR and health cycle.

Feature	CDR1	CDR2	CDR3	Health Cycle
Cell Metabolism	Glycolysis	Aerobic glycolysis	Oxidative phosphorylation	Balanced oxphos, glycolysis, and aerobic glycolysis
Cellular Autonomy[1]	High	High	Decreasing	Low
Ventral Vagal[2] **Autonomic Tone**	Low	Low	Increasing	High, with diet and activity-related cyclic variations under circadian and seasonal control
Function	Containment, pathogen removal, toxin sequestration, Innate Immunity, clean-up	Proliferation, Biomass Restoration, Blastema Formation*	Differentiation, Cell-cell communication, Metabolic Memory, Adaptive Immunity, Detoxification	Cell-cell communication, Metabolic complementarity, Development, Learning, Fitness, Restorative sleep, Healthy Aging, Cancer suppression, neuroendocrine systems integration
Diseases	Chronic Infections, allergies, MODS, SIRS, ARDS	Diabetes, Heart disease, Cancer, Fibrosis	Pain, Autonomic, Affective, Psychiatric, Neurologic, Immune/Autoimmune, and Microbiome dysfunction, other target organ dysfunction	n/a
CDR Gene Examples	NRF2, CRF2, IDO1, NOXs, NFkB, HO1, PARs, REXO2, eIF2α, STAT1/2, MMP9, IRF1, IRF3/4, SP1, IFNα/β, IL1β, UMP-CMPK2, TNFα	mTOR, HIF1α, AhR, p53, p21, $p16^{INK4A}$, c-myc, PHDs, BRCA1/2, ATR, other DNA repair enzymes, Nanog*, Sox2*, Oct4*, Isl1*	AMPK, FOXO, PPARs, BCL2, P1, P2Y, P2X, CD38, RXRs, CD38, CD39, CD73, IL6, FXR, IFNγ, IL17, IL4, TGF, Iron-sulfur cluster proteins, Mfn1/2, Opa1, Intestinal disaccharidases	n/a

Abbreviations: MODS—multiple organ system dysfunction in sepsis; SIRS—systemic inflammatory response syndrome; ARDS—acute respiratory distress syndrome; NOXs—NADPH oxidases; PARs—protease activated receptors (F2R/PAR1, F2RL1/PAR2, F2RL2/PAR3); IRF1—interferon regulatory factor 1; PHDs—HIF1α-targeting prolyl hydroxylase domain proteins; PPARs—peroxisome proliferator activated receptors; RSA—respiratory sinus arrhythmia; HRV—heart rate variability. [1]Cell autonomy is associated with cellular disconnection, whole body stress, and activation of the HPA axis. [2]Ventral vagal tone via myelinated fibers from the *nucleus ambiguus*, measured by RSA and/or HRV. *For embryonic development and multilineage regeneration in some animals.

(ACYL) as a mobile source of acetyl-CoA. In the cytosol, the acetyl-CoA can be used to make fatty acids, triacylglycerol for energy reserves, and phospholipids for new cell membranes. In the nucleus, the acetyl-CoA is used by histone acetyl transferases (HATs) to place epigenetic marks on chromatin to regulate new gene expression and DNA repair (Sivanand et al., 2017). CDR2 is a stage in which cells with too much DNA damage exit the cell cycle and can adopt an irreversible senescence phenotype, with secretion of exosomes, inflammatory cytokines, growth factors, and proteases (He and Sharpless, 2017).

CDR2 is also the stage in which fibroblasts and myofibroblasts are recruited to help close wounds or "wall-off" an area of damage or infection with scar tissue that could not be completely cleared in CDR1 (Fig. 1). CDR2 is also when blastema formation occurs in certain aquatic organisms like the Mexican salamander (eg, *Axolotl)*, flatworms (eg, *Planaria),* and *Hydra* that display the capacity for multi-lineage tissue regeneration after injury (Heber-Katz and Messersmith, 2018). Less extensive blastema formation is seen as a feature of healing and multi-lineage regeneration in the MRL mouse, a strain of laboratory mouse with remarkable healing abilities (Heber-Katz, 2017; Naviaux et al., 2009).

Recent studies have begun to target metabolic enzymes that regulate CDR2. A class of proline hydroxylase domain proteins (PHDs) that mark HIF1α for proteasome degradation acts as a tissue oxygen sensor. Drug inhibition of a PHD increased HIF1α stability and expression in the presence of normal oxygen, permitted blastema formation, and improved epimorphic regeneration in strains of mice that cannot otherwise fully regenerate after injury (Zhang et al., 2015). During CDR2, dividing and migrating cells are unable to establish long-term metabolic cooperation between cells because their location within tissues is continuously changing. Only after cells have stopped growing and migrating can they begin to establish long-term symbiotic relationships with neighboring cells that build physiologic reserve capacity, provide resistance to re-exposure to a similar environmental danger, and benefit the whole. Once cells exit the cell cycle and establish durable cell-cell contacts through gap junctions and other structural connections, they can exit CDR2 and enter CDR3 (Figs. 1 and 2).

9. CDR3—Cell autonomous oxphos, M2 mitochondria

The functions of CDR3 include cellular differentiation, tissue remodeling, adaptive immunity, detoxification, metabolic memory, sensory and pain modulation, and sleep architecture tuning (Fig. 1). Cells that enter CDR3 stop dividing and establish cell-cell connections with their neighbors. Newly-born cells, that were generated during cell growth from satellite or stem cells in CDR2, must undergo a process of cellular education that involves adjustments in gene expression, cell structure and metabolism, to best adapt to existing tissue conditions before they can take on the role of a fully-differentiated cell in the mature organ and tissue. Healing remains incomplete in CDR3 until newly-born cells differentiate by receiving metabolic instructions and materials from older, neighboring cells that carry the metabolic memories and programming from before the time of the tissue injury that activated the CDR.

Mitochondria in CDR3 cells repolarize from M0 to M2 organelles (Fig. 2). Most remaining M1 mitochondria also repolarize to the M2, anti-inflammatory phenotype needed for differentiated cell function and oxidative phosphorylation (oxphos). This is accomplished in part by re-establishing permanent access to oxygen and nutritional resources, while permitting free release of metabolites and waste products to neighboring capillaries and lymphatics. Oxygen, iron, and sulfur delivery are differentiating and promote mitochondrial biogenesis of iron-sulfur clusters. Iron-sulfur clusters are needed for differentiated cell functions like oxidative phosphorylation, the anti-viral response, protein translation, genome integrity maintenance, and organ-specific physiologic functions (Braymer and Lill, 2017). Outer mitochondrial membrane fusion proteins like mitofusin 1 and 2, and the inner membrane fusion protein Opa1 are also needed to achieve normal mitochondrial network morphology and fully differentiated tissue function (Cao et al., 2017; Del Dotto et al., 2017) (Table 2).

As differentiation proceeds, cells also reestablish connections with the autonomic nervous system and tissue lymphatics. All blood vessels and most tissues receive innervation from the sympathetic and parasympathetic nervous systems. Metabolite and waste product removal helps to provide remote information to and from organs like the brain, liver, intestines, and kidney. Each of these organs participates in regulating whole-body absorption, secretion, metabolism, function, and behavior according to chemical signals that are circulated in the blood. Tissue-specific detoxification restarts in CDR3 and continues through the health cycle. A major regulator of checkpoint 3 is purinergic signaling. The health cycle cannot be reentered until extracellular levels of ATP and related ligands decrease. A decrease in eATP at the completion of CDR3 is a permissive signal that facilitates new and old cells to reestablish the physical, autonomic, and neuroendocrine contact needed for health (Fig. 1, Table 2). In many instances, the completion of CDR3 results in improved baseline physiogic performance and extended reserve capacity compared to before the stress or injury. At a cellular level, this is called hormesis (Fig. 3) and lies at the heart of adaptive improvements in both baseline performance and reserve capacities in response to many forms of stress. These stresses can range from exercise to radiation or chemical toxin exposure, drug tachyphylaxis, to stimuli that result in long-term memory (Calabrese and Baldwin, 2003; Chen et al., 2013; Ristow, 2014).

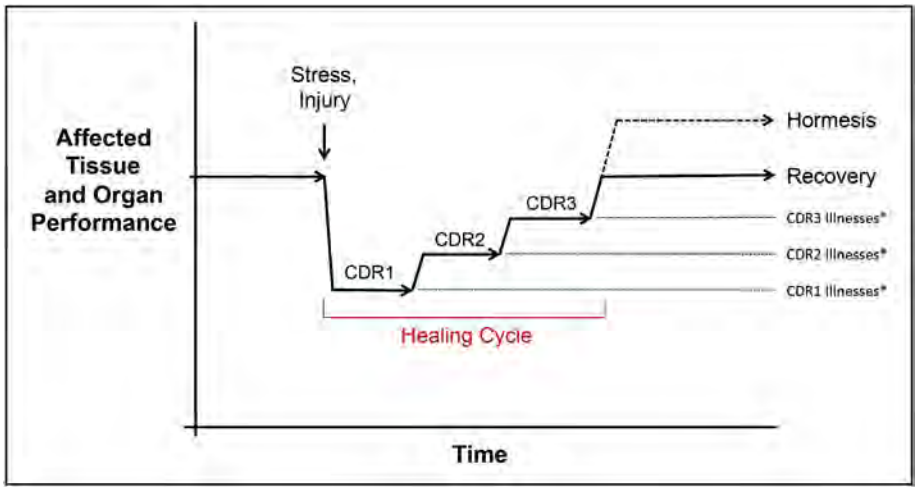

Fig. 3. Timeline of the healing cycle and hormesis. Despite a cascade of events triggered by injury, and hundreds of molecular abnormalities that can be measured in each stage of the healing cycle, the arrow of time is not reversed to heal damage and normalize abnormal functions. The metabolic stages of the healing cycle proceed sequentially forward in time. Healing follows a similar path regardless of the mechanism of injury. *Once a chronic illness occurs, there is little practical difference between the severities possible for CDR1, 2, or 3 disorders. With rare exceptions, each can produce a spectrum from mild disability to death.

10. The health cycle—Harmonized and periodized bioenergetics

The function of the health cycle is to promote wakeful activity, restorative sleep, normal child development, adaptive fitness, and healthy aging. The health cycle is characterized by the balanced, integrated, and periodized usage of all three bioenergetics programs; glycolysis, aerobic glycolysis, and oxidative phosphorylation (Fig. 1). Health requires brain integration and coordination of organ function and whole body metabolism using neuroendocrine and autonomic controls. Wakeful activity and a varied, seasonally-appropriate diet that is sourced from local ecosystems and consumed during daytime hours helped select the gene pools that humans received from their ancestors, up until about the last 200 years. Disruptions in this pattern of seasonal food availability, the increasing prevalence of night shift work, and the decline of traditionally active outdoor lifestyles, have led to new selection pressures on our inherited gene pool. Modern mass spectrometry and metabolomics have helped us achieve a more detailed understanding of the importance of dietary cycling that occurs naturally with the seasons and periodically with occasional short fasts that promote health throughout the year (Mattson et al., 2018).

Cruciferous vegetables in a healthy diet contain isothiocyanates like sulforaphane that act rapidly as chemical pro-oxidants to transiently decrease the amount of intracellular glutathione. This short-term pro-oxidant effect produces a long-term increase in antioxidant defenses by blocking KEAP1 and Cullin 3-dependent ubiquitination, and permitting the translocation of NRF2 (nuclear factor 2 erythroid related factor 2) to the nucleus. In the nucleus, NRF2 acts as a transcription factor to up-regulate over a dozen different cytoprotective proteins like glutamate-cysteine ligase (GCL) to increase glutathione synthesis, glutathione-S-transferase (GST) for xenobiotic detoxification, and heme oxygenase 1 (HO1) for local synthesis of carbon monoxide (CO) at sites of heme extravasation to attenuate M1-polarized mitochondrial pro-inflammatory effects. While oxygen inhibits the stability of HIF1α, the same conditions increase the stability and support the transcriptional activity of NRF2. Acute stress leads to a normal, NRF2 activation response. In contrast, chronic activation by stress ultimately desensitizes and decreases NRF2 activation, and permits long-term increases in inflammation-associated NFkB activation (Djordjevic et al., 2015). The normal health cycle requires the daily modulation of these cycles of increased and decreased oxygen-related redox stress associated with wakeful activity and restorative sleep (Figs. 1 and 2).

11. Exercise and healthy aging

Exercise is medicine. Wakeful activity is essential for the health cycle (Fig. 1) and healthy aging. Regular exercise appears to be the single most important habit known that mitigates the degenerative effects of aging. Moderate exercise creates a natural stimulus that facilitates restorative sleep and repair by creating balanced activation of all the stages of the healing cycle. In many important metabolic ways, exercise “reminds” the body how to heal and promotes disease-free health throughout life. Exercise is adaptogenic (Panossian, 2017). Exercise increases physiologic reserve capacity and resilience to periodic exposure to stress or acute illness. Organ reserve capacity diminishes with age (Atamna et al., 2018). Exercise combats this loss. Even just 15 min of moderate-to-vigorous exercise per day each week lowers all-cause mortality by 22%. Older adults who completed > 30 min/day for 5 days each week had a 35% decrease in mortality over 7–10 years (Hupin et al., 2015; Saint-Maurice et al., 2018).

12. Slow wave sleep and healing

Sleep is medicine. Slow wave sleep (SWS) and the associated increase in parasympathetic autonomic tone are important for healing and recovery during rapid growth in childhood (Takatani et al., 2018). Disruptions in SWS and parasympathetic tone during sleep are risk factors for many chronic illnesses (Carney et al., 2016; Rissling et al., 2016). Delta waves in an electroencephalogram (EEG) are defined as high amplitude (100–300 μV) slow waves (0.5–2 Hz). Delta waves are a normal feature of the deep stages 3 and 4 of sleep. Rapid growth and recovery after high-intensity exercise are associated with an increase SWS in children (Dworak et al., 2008; McLaughlin Crabtree and Williams, 2009). In classical mitochondrial diseases like Alpers syndrome, the need for brain repair is so great that delta waves are seen in the EEG even while awake (Naviaux et al., 1999). Wakeful delta wave activity (slow wave activity) has also proven to be a useful biomarker in studies of traumatic brain injury (Huang et al., 2016). Reciprocally, new methods are being developed to promote wakeful delta waves as therapy in patients with traumatic brain injury (Huang et al., 2017).

13. Metabokines and their receptors

13.1. Metabokines, neurotransmitters, and immune regulators

While it is clear that both exercise and sleep influence metabolism, how does the cell leverage changes in metabolism to influence progression through the healing cycle? Metabolites have long been known to act as signaling molecules in neuroscience. All the classical neurotransmitters are technically metabokines. Molecules like serotonin, melatonin, acetylcholine, glutamate, aspartate, glycine, D-serine, GABA, dopamine, norepinephrine, epinephrine, histamine, anandamide, and adenosine are all products of metabolism that act as signaling molecules by binding to cellular receptors. There are even circulating classes of memory T-cells that contain the enzyme choline acetyl transferase (ChAT) and release acetylcholine in response to vagal nerve stimulation to activate important anti-inflammatory macrophages expressing the nicotinic acetylcholine 7 alpha subunit (nAch7α) (Baez-Pagan et al., 2015; Rosas-Ballina et al., 2011). This signaling function of metabolites has not been widely incorporated into discussions of metabolic control of cellular functions and development. Metabolites act directly as informational molecules by acting as ligands for specific G-protein coupled and ionotropic receptors. Secreted metabokines alter the informational content of the extracellular millieu in many ways. One of these is through a process called *exosignalling* (Pincas et al., 2014), which can prime cells for contextually-dependent, non-linear quantitative and qualitative responses to hormones and other signaling molecules. Purinergic receptors respond to adenine and uracil nucleotides and nucleosides (Verkhratsky and Burnstock, 2014). Nineteen (19) purinergic receptors are present in the human genome (Fig. 4). Four P1 receptors are 7-transmembrane G-protein coupled receptors (GPCRs) that respond to adenosine (ADORA1, 2A, 2B, and 3). Eight GPCRs are single-exon, P2Y receptors (1, 2, 4, 6, 11, 12, 13, and 14) that respond to ATP, ADP, UTP, UDP, and UDP-glucose (Fig. 4A). Seven are multi-exon, ionotropic P2X receptors (1–7) that respond to extracellular ATP and act as ion channels for calcium and potassium (Fig. 4B).

13.2. Dendrogram and gene ontology analysis

To investigate the number of receptor systems that are related to the release of ATP and other nucleotides from stressed and damaged cells, a TBLASTN search was performed of human proteins related to the P2Y1 receptor, a prototypic purinergic receptor. The P2Y1R is a conventional, single exon, metabotropic, G-protein coupled receptor with 7 transmembrane domains. A dendrogram of the top 91 P2YR1-related proteins revealed a possibility of 6 groupings according to amino acid sequence and function in the healing cycle (Fig. 5A). These are: A) hemostasis, pH monitoring, cannabinoid, Krebs cycle, leukotriene, and purinergic signaling, B) lysophospholipid, sphingolipid, cannabinoid, and metabolite signaling, C) eicosanoid, lactate, niacin, short chain fatty acid (acetate, propionate, butyrate, and the ketone body β-hydroxybutyrate), and protease signaling, D) viral co-receptors, glucose/sucrose signaling, pro-inflammatory and anti-inflammatory peptides E)

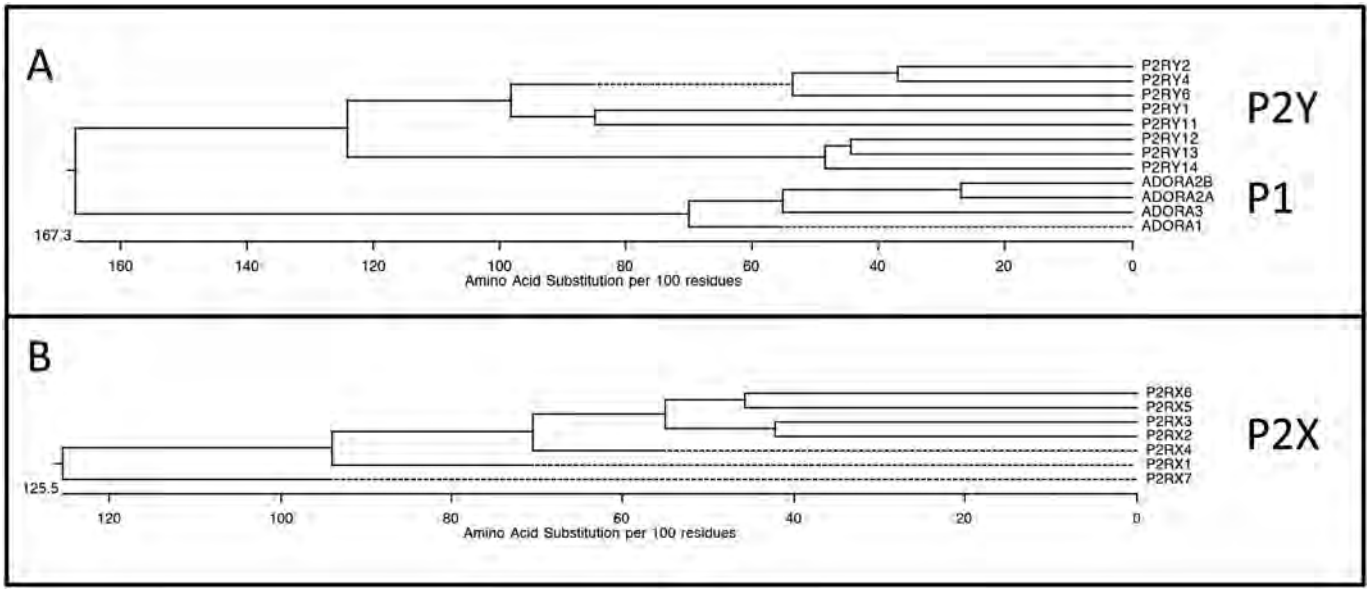

Fig. 4. Purinergic receptors. **A.** Metabotropic G-Protein Coupled Purinergic Receptors, P2Y receptors respond to ATP, ADP, UTP, UDP, UDP-glucose, and/or Ap4A (diadenosine tetraphosphate). P1 receptors respond to adenosine receptor A (ADORA1, 2A, 2B, and 3). **B.** Ionotropic Purinergic Receptors. P2X receptors respond to ATP and/or Ap4A.

neuropeptides and other peptide hormones, and F) chemokines. A gene ontology analysis of the pathways that were enriched in this set of 91 proteins showed that about 50% of the pathways were involved in calcium signaling, 20% with cell movement, and the remainder divided among molecular regulation, immune response, apoptosis, and sensory processing (Fig. 5B).

13.3. Ligand analysis

The ligands that bind to the 91 P2YR1-related proteins differ in size. Eight of the 91 related receptors in Fig. 5A use nucleotides, eg, ATP, ADP, UTP, UDP etc., as their canonical ligand. Another 35 of the receptors use other common metabolites and neurotransmitters like lactic acid, succinate, alpha-ketoglutarate, glutamate, short chain fatty acids, long chain fatty acids, eicosanoids, cannabinoids, sphingolipids, lysophospholipids, serotonin, and melatonin. A total of 43 of 91 (47%) receptors respond to metabokines less than about 400 Da in size. Twenty-four (26%) use peptides 4 to about 80 amino acids long (400–8000 Da), often released by proteolytic activation from an inactive precursor. Twenty-one (22%) respond to chemokines that are 8000 to 10,000 Da in size. Among these are receptors that are essential for innate immunity and for healing and regeneration after injury. For example, the CXCR4 binds to the chemokine CXCL12, also known as stromal derived factor 1 (SDF1), which negatively regulates multilineage regeneration (Heber-Katz, 2017). Four (4%) of the 91 GPCRs related to P2YR1 are constitutively active, or have ligands that are not yet known (Table S1).

14. The TOGLEs that regulate metabolism

Transporters, opsins, G protein-coupled receptors, and their ligands and effectors (TOGLEs) are a diverse group of proteins that share a common evolutionary origin (Saier Jr. et al., 2016; Yee et al., 2013). The single, most diverse superfamily of genes found in metagenomic surveys of ocean picoplankton (bacteria) are the bacterial rhodopsins (Venter et al., 2004). Interestingly, the opsins are related to a group of phosphate, sulfur, cystine, heavy metal, organic acid, salt, and sugar transporters that share similar structures and transmembrane topologies. Difficulties in sensing, handling, or responding to many of these molecules have been documented in complex diseases like autism spectrum disorder (ASD) (Adams et al., 2011). These transporters and opsins are related to G-protein coupled receptors (GPCRs) that constitute over 800 genes in the human genome (Gether, 2000). The functional tie that binds all the TOGLEs together is their role in monitoring the cellular environment for signs of nutrient resources, recognizing friends, signaling danger, and facilitating social and reproductive behaviors. The very receptors that now permit cells to monitor minute changes in the chemical environment are descended from ancestral genes for color vision, smell, and taste (Liman, 2012).

15. Hormone target resistance and axis suppression by the CDR

End organ resistance to hormone signaling is an intrinsic part of the CDR. Once a tissue suffers injury, a shift to dependence on local chemical cues and paracrine signaling is essential. Remote decision-making by endocrine glands cannot provide “boots on the ground”, real-time instructions to injured cells when bidirectional lines of communication are disrupted. A shift from fully integrated and periodized metabolism to cell-autonomous metabolism is an obligate feature of CDR stages 1 and 2 (Figs. 1 and 2, Table 2). *Re*-establishment of hormone sensitivity begins during CDR3, and is required for re-entry into the health cycle (Fig. 1, Table 2). All known mechanisms of hormone resistance have been cataloged. Hormone release, target cell hormone metabolism (Incollingo Rodriguez et al., 2015), and intracellular hormone signaling can each be attenuated by the CDR. End organ resistance during the CDR can affect all the major endocrine systems. Thyroid, adrenal cortical glucocorticoid and mineralocorticoid, and renin-angiotensin system attenuation states are common in patients with chronic fatigue syndrome (CFS). The most common forms of stimulus-response dysregulation lead to complex endocrine syndromes that do not fit classical medical definitions of deficiency or failure because residual hormone production can usually be shown by physiologic stimulation, but is suppressed. These complex disorders have sometimes been called thyroid or adrenal exhaustion syndromes. On the other side of the intracellular energy spectrum, insulin resistance associated with caloric excess and inactivity can lead to type 2 diabetes mellitus (DM2). In all these end-organ resistance states, the treatments that have been most effective are metabolic, diet, and lifestyle interventions that restore normal bidirectional function of the endocrine system. In contrast, chronic treatment with the hormone in question typically leads to

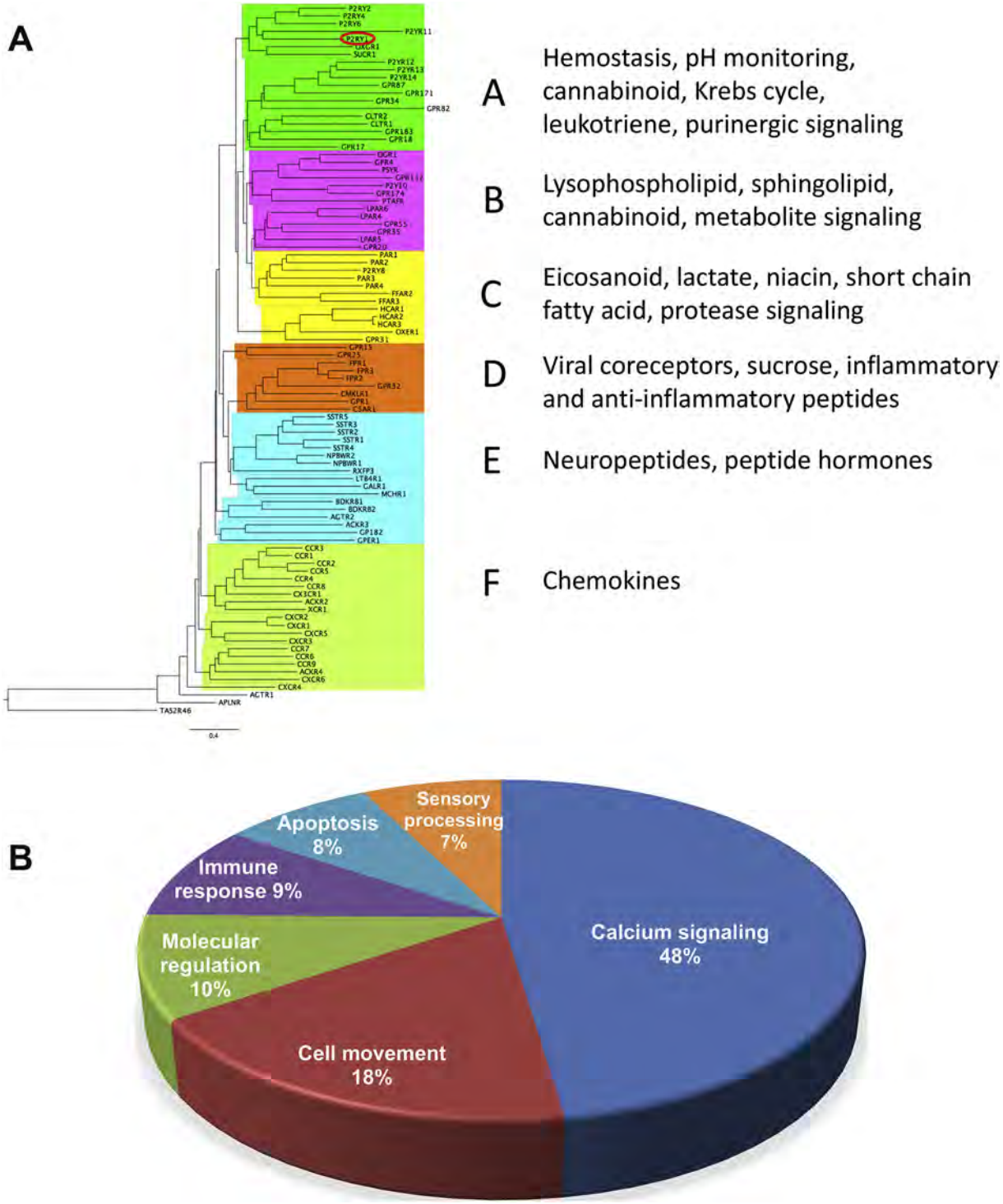

Fig. 5. P2Y1R-related GPCR genes in the human genome. **A.** Dendrogram analysis. P2RY1 is circled to indicate the reference protein used in the TBLASTN search that recovered the 91 proteins analyzed. Colored functional groupings were loosely associated with sequence similarity. **B.** Gene ontology pathway enrichment analysis. (N = 91 P2Y1R-related genes; PANTHER analysis).

iatrogenic side-effects, and dependence on the exogenous hormone. Knowledge of the cell autonomy requirement of the CDR helps reframe the causal mechanisms behind these previously unconnected syndromes (Figs. 1–3, and Table 2).

16. Vagal target resistance and axis suppression by the CDR

The activity of the parasympathetic nervous system measured along a gradient of environmental safety is U-shaped. The ventral vagus complex (VVC) is comprised of myelinated fibers from the *nucleus ambiguus* to the vagus nerve. The VVC is most active under conditions of social attachment, caloric security, and physical safety. At the other extreme is the dorsal vagal complex (DVC). The DVC is also called the dorsal motor nucleus of the 10th cranial nerve (DMNX). The DMNX sends unmyelinated fibers to the vagus nerve. The DMNX is most active acutely under life-threatening conditions, and periodically in synchrony with the VVC during predictable changes in physiology associated with feeding, sleep, and reproduction. Since the majority of wakeful activity

occurs between these two extremes of absolute safety and absolute danger, a large part of life is spent at the bottom of the "U", poised between the neurophysiologic and neuroendocrine commitment to one or the other. A shift to the left on the U-curve is in the direction of health and fitness (Lucas et al., 2018). A shift to the right leads to chronic illness, disability, and death. When the CDR is chronically activated, the coordination between the two limbs of the vagus is disrupted. This results in disinhibiting the sympathetic nervous system and the hypothalamic-pituitary-adrenal (HPA), which dominate during illness (Fig. 2, Table 2).

Disruption of cellular communication, and the associated increase in cell-autonomous and paracrine signaling by metabokines during the CDR is tightly associated with either a disruption in normal parasympathetic tone from the VVC, or end-organ resistance to cholinergic signals. This is typically quantified by measurements of respiratory sinus arrhythmia (RSA) and heart rate variability (HRV) (Porges, 2007). Substages of the CDR occur during the transition between a fully active ventral vagus complex in health, its rapid inhibition by CDR1, and its gradual return in CDR3. The return of oxygen utilization by healing tissues during CDR2 and CDR3 is associated with increases in RSA and HRV (Fig. 2, Panel D). Increased RSA and HRV are also known to be associated with endurance exercise and aerobic health (De Meersman, 1992, 1993).

When the normal cyclic variations in vagal outflow are disrupted during the CDR, a number of autonomic abnormalities occur. These include postural orthostatic tachycardia syndrome (POTS), and autoimmune disorders like pediatric autoimmune neuropsychiatric syndrome (PANS), and pediatric autoimmune neuropsychiatric disorders associated with streptococcal infections (PANDAS). All three of these disorders have autoimmune components that appear tied to a decrease or absence of normal anti-inflammatory signaling by the vagus. Vagal efferents mobilize T-cells from gut associated lymphoid tissue (GALT) in the GI tract. The T-cells then induce the anti-inflammatory M2 macrophage phenotype through nicotinic acetylcholine 7 alpha (nAch7α) receptors (Baez-Pagan et al., 2015). Vagal efferents also inhibit cysteinyl leukotriene release by mast cells via nicotinic cholinergic signaling (Mishra et al., 2010). Cysteinyl leukotrienes C4, D4, and E4 are also called the slow reacting substances of anaphylaxis, and bind to receptors closely related to P2Y receptors (CTLR1 and 2 in Fig. 5A). Additional support for the important role played by cholinergic signaling from the vagus comes from the use of nicotinic cholinergic antagonists for neuromuscular blockade (NMBA) during anesthesia. Drugs like suxamethonium and atracurium are used for NMBA, and block nicotinic cholinergic signaling everywhere receptors exist, not just at the neuromuscular junction. These drugs are associated with a risk for anesthesia-induced allergic and non-allergic immediate type hypersensitivity reactions, especially in patients with known allergies and mast cell hypersensitivity (Laroche et al., 2017). Even POTS has recently been shown to be associated with autoantibodies to the angiotensin II receptor (Yu et al., 2018).

17. Tissue mosaics and cellular dyssynchrony in healing

Healing is necessarily heterogeneous and dyssynchronous at the cellular level. This occurs for three reasons: 1) all differentiated tissues and organs are mosaics of metabolically specialized cells with differing gene expression profiles that permit the metabolic complementarity needed for optimum organ performance, 2) physical injury, poisoning, infection, or stress do not affect all cells equally within a tissue, and 3) once a tissue is injured, cells that have not yet completed the healing cycle have not yet reintegrated back into the tissue mosaic, creating chinks or weaknesses in tissue defenses from the old injuries that makes a tissue more vulnerable to new injuries. This process gradually decreases organ function and cellular functional reserve capacity as we age.

Severe threats or injuries cause cells to disconnect from neighboring cells. The initial stages of healing require cell-autonomous actions. If a an entire organ or tissue is threatened, millions of cells will activate the cell danger response (CDR) program in an effort to survive, at the expense of their normal differentiated cell functions. If injury, or the threat of injury, is severe enough, signals are sent from the brain to alter organismal behavior to limit the chances of worsening injury, or the chance of spreading contagion to family or community members. The brain coordinates this stereotyped sickness behavior during activation of the CDR (Dantzer and Kelley, 2007; Naviaux, 2014). The rate at which cells are able to progress through the healing cycle differs according to the local severity of the danger and the ability of the host to mount protective defenses. Metabolic memory of past exposures primes the cellular response to future exposures, even when the original trigger or stress is no longer present.

18. Genes, drugs, and devices that regulate stages of the CDR

To date, the only drug that has been tried explicitly as a treatment for a blocked CDR to promote healing is suramin (Naviaux et al., 2014; Naviaux et al., 2015; Naviaux et al., 2017; Naviaux et al., 2013). A recent study of a device for pulse-based transcranial electrical stimulation to stimulate restorative, wake-time delta wave activity and to improve the quality of sleep has shown promise in the treatment of traumatic brain injury (TBI) (Huang et al., 2017). Brain delta waves are associated with a shift in metabolism that facilitates brain and body repair, recovery, and healing. Once the healing cycle (Figs. 1 and 2) is understood in greater detail, many other drugs and treatments may emerge that are designed to provide novel approaches to treating CDR-associated chronic diseases (Table 1). While increased ATP release from cells is a part of each of the 3 stages of the CDR (Fig. 1), other metabolites and genes play more selective roles. By studying the metabolites, genes, and cell types involved in each stage, more selective therapies can be developed. For example, the NRF2 and hypothalamic-pituitary-adrenal (HPA) axis appear to be involved early in CDR1 and do not require the physical loss of cells as a decision point indicated by the "I" for "information" in Fig. 1.

Organisms have the capacity to mount a similar metabolomic response to stress, regardless of whether the triggering event is neuropsychiatric (Picard et al., 2015), or physical cell damage (Nishi et al., 2013). In both cases, mitochondria are the pivotal organelle (Picard et al., 2017). In both cases extracellular ATP is released by stressed cells as a first alarm for entering CDR1 and the healing cycle (Fig. 1) and intracellular calcium handling is regulated (Schmunk et al., 2017). When glucocorticoids are directly released by ATP stimulation of the adrenal cortex by stressed or damaged cells, hypothalamic corticotrophin releasing factor (CRF) and pituitary ACTH are decreased by feedback inhibition. On the other hand, childhood or adult neuropsychological stress can lead to direct stimulation of CRF. In addition to CRF receptors in the brain, peripheral CRF receptors exist in the GI tract and other organs (Buckinx et al., 2011). Peripheral metabolic responses to stress appear to be regulated in part by urocortin acting on peripheral CRF2 receptors in the kidneys and GI tract (Lovejoy et al., 2014). Drugs and supplements directed at NRF2 or CRF2 signaling may have broad-reaching effects since they will affect the entry and completion of the earliest stage of the cell danger response (Fig. 1, Table 2).

HIF1α (hypoxia induced factor 1α), mTOR (mammalian target of rapamycin), and the arylhydrocarbon receptor (AhR) are important for CDR2-associated cell proliferation (Figs. 1 and 2, Table 2). Because CDR2 involves cell growth and proliferation, the risk for side-effects and iatrogenic complications of CDR2-modulating therapies is high. The drug 1,4-DPCA has been used to target proline hydroxylase domain (PHD) proteins. By inhibiting PHDs, HIF1α is stabilized even under normal oxygen levels. This creates a metabolic state of pseudohypoxia and facilitates tissue regeneration after injury (Zhang et al., 2015).

mTOR and its partners are needed to help coordinate anabolic cell growth. Phosphatidic acid that is newly synthesized from fatty acids

Table 3
Stress-response systems regulated by the mitochondrial CDR.

No.	Stress response system	References
1	Apoptosis and anti-apoptosis	(Portt et al., 2011)
2	NRF2 activation	(Esteras et al., 2016; Naviaux, 2012)
3	Sirtuins and epigenetics	(Lin et al., 2018)
4	Scar formation	(Kuehl and Lagares, 2018)
5	Autophagy	(Boya et al., 2018)
6	Mitophagy	(Zimmermann and Reichert, 2017)
7	Exosomes and secretion	(Claude-Taupin et al., 2017; Saeed-Zidane et al., 2017)
8	Lipid raft formation	(Sorice et al., 2012)
9	Efferocytosis	(Wang et al., 2017)
10	Endoplasmic reticulum (ER) stress	(Carreras-Sureda et al., 2018)
11	Proteostasis and the unfolded protein response	(Murao and Nishitoh, 2017)
12	Transglutaminase activation	(Nurminskaya and Belkin, 2012)
13	DNA damage and repair	(Prates Mori and de Souza-Pinto, 2017)
14	Sensory processing	(Kann, 2016)
15	Allodynia, fibromyalgia, chronic pain	(Gerdle et al., 2013)
16	Hypothalamic-Pituitary-Adrenal (HPA) axis	(Lapp et al., 2018)
17	Liver xenobiotic detoxification	(Jeske et al., 2017)
18	Renal tubular secretion and reabsorption	(Kim et al., 2012)
19	Autonomic nervous system dynamics	(Ford et al., 2015)
20	Innate immunity, inflammation, allergies, autoimmunity	(Hoffmann and Griffiths, 2018; Mills et al., 2017)
21	Energy, glucose, and lipid metabolism	(Anupama et al., 2018)
22	Hypertension and cardiovascular stress responses	(Lahera et al., 2017)

and glycerol-3-phosphate, binds mTOR, alters metabolism, and stimulates growth (Menon et al., 2017). Rapamycin and other mTOR inhibitors have antiproliferative and immunomodulatory effects and have been used to treat a mouse model of a mitochondrial disease called Leigh syndrome (Johnson et al., 2015), but side-effects like delayed wound healing, stomatitis, hypercholesterolemia, and susceptibility to viral infections, may complicate broad extension to CDR-related chronic diseases in humans.

The AhR connects many pathways in CDR2. These include effects on redox signaling and HIF1α, circadian rhythm regulation through BMAL, and immune function via T_{reg} cells (Gutierrez-Vazquez and Quintana, 2018). Indoles from food and the microbiome, and kynurenine from the inflammatory arm of tryptophan metabolism, are natural ligands for the AhR. These effectors act through AhR to facilitate anti-inflammatory T cell and macrophage responses to prevent runaway inflammation during CDR2.

The differentiated functions of cells begin to appear again as cells leave the cell cycle of CDR2 and enter CDR3 (Figs. 1 and 2). Cells become integrated intro the extracellular matrix and 3-dimensional structure of tissues once they have stopped growing in CDR3. Genes important for CDR3 function include AMPK (AMP-activated protein kinase), PPARs (peroxisome proliferator activated receptors α, β/δ, γ), RXRs (retinoid × receptors), BCL2, iron-sulfur cluster proteins, FXR (farnesoid × receptor; also called the BAR: bile acid receptor), and mitochondrial fusion proteins (Table 2). The literature on each of these genes and gene families is extensive. Each plays a role in facilitating mitochondrial polarization from M0 and M1 in CDR2 to M2 organelles adapted for oxidative phosphorylation and the beginnings of metabolic complementarity and differentiated cell function in CDR3 (Fig. 2).

19. Dangers of tonic, single-stage, CDR interventions

Many drugs have mitochondrial toxicity (Will and Dykens, 2018). These drugs can benefit some people, but lead to catastrophic side effects in others. Predicting the mitochondrial risk has proven difficult. The reason for this may lie in the fact that different drugs target mitochondrial functions in different stages of the healing cycle. Visualization of the healing cycle permits a conceptual understanding of how these drugs and certain genetic polymorphisms called ecoalleles (Naviaux, 2017), can have a beneficial effect on one class of aging-related disorders, while having a detrimental effect on others. For example, mitochondrial DNA variants that increase the risk of Parkinson disease (a CDR3-associated disease) also decrease the risk of prostate cancer (a CDR2-associated disease). This amphitropic effect of CDR-selective factors is seen in both genes and drugs. It is likely that chronic treatments directed at any one of the checkpoints governing the healing cycle, will increase the risk of disease caused by unbalanced accumulation of cells in another stage of the CDR. For example, certain treatments of cancer (a CDR2 disease) will increase the risk of Alzheimer dementia (a CDR3 disease) (Driver, 2014). Or a treatment for cardiovascular disease and hypertension (CDR2 disorders) will increase the risk of autoimmune disorders (CDR3). Evidence for this includes data on statin-associated polymyalgia rheumatica (de Jong et al., 2012), and drug-associated Lupus. Likewise, it is theoretically possible, although not yet demonstrated, that chronic preventive therapy for dementia (CDR3), will increase the risk of certain cancers (CDR2) by decreasing excitotoxicity and the removal of mutant cells by immune surveillance. Chronic treatments for pain and inflammation syndromes associated with CDR1 disease may increase the risk of diabetes and cardiovascular disease (CDR2-assoicated disorders), and/or autoimmune disease (CDR3-associated disorders) (Chang and Gershwin, 2011). Subdivisions within each of the CDR stages are likely to exist. For example, the fact that statin treatment for cardiovascular disease increases the risk of diabetes (Chrysant, 2017) suggests that these two disorders belong to functionally separate subdivisions within CDR2 (Table 1, Fig. 2). Further resolution of subdivisions within each stage of the CDR, and corrections of any errors in this first version of the model will require future research. However, without an understanding of the pathophysiology of the healing cycle (Figs. 1 and 2), there is no unified framework for predicting the complex side-effects of old and new treatments for chronic disease.

20. Evolutionary origins

It is no accident that the stages of healing recapitulate the chemical evolution of animal cells. The Precambrian Earth had an atmosphere that was largely devoid of oxygen. When capillaries, lymphatics, or glymphatics in the brain (Plog and Nedergaard, 2018) are torn by injury or decreased by disease, oxygen delivery and waste removal are impaired. An alternative method of energy production must occur if cells experiencing hypoxia are to survive. Under conditions of impaired oxygen delivery, oxidative phosphorylation is handicapped and glycolysis becomes a more reliable source of energy. Once the damage is contained, aerobic glycolysis provides a way of removing excess oxygen, which is genotoxic, to protect against DNA damage, while permitting rapid cell growth needed for biomass replacement. This patterned sequence of metabolic transitions needed for orderly wound repair, tissue regeneration, and differentiation has been studied recently in a classic model of healing and regeneration in flatworms (*Planaria)* (Osuma et al., 2018).

21. Allostasis and the mitochondrial nexus

Allostasis is a concept that was introduced in the late 1980s by Sterling and Eyer (Sterling and Eyer, 1988). The authors gave credit to Professor Charles Kahn at the University of Pennsylvania for suggesting the term. Allostasis literally means “stability through change”. Brain control of metabolism was a fundamental principle described in this paper. Allostasis embodied the idea that all body functions need to be adjusted dynamically according to continuously changing environmental conditions to achieve maximum fitness for long-term survival

and reproduction. While the concept of "homeostasis" taught in medical schools today describes the idea that every measureable parameter in the body has an "optimum set-point" that is continuously defended based on local signals, allostasis points out that all physiologic parameters vary within large dynamic limits according to recent, current, and anticipated future environmental conditions based on brain coordination of the needed physiologic adjustments.

The range of variation for any given parameter is very large in the young, but the capacity to achieve the same dynamic highs and lows decreases with age. This decline is associated with an age-related decrease in the physiologic reserve capacity of every organ system. In an example given by the authors, when blood pressure was measured continuously for 24 h in a young man, values of 110/70 were maintained for several hours during the day. It dropped to 90/55 for an hour when he fell asleep during a lecture. Preparing for work in the morning produced a value of 140/80 for 2 h, while dropping to 70/40 for 6 h at night during sleep, and to 50/30 for 1 h during deep sleep (Sterling and Eyer, 1988). The point of allostasis is that each of these blood pressures is "normal" for the conditions during which they occurred. Over time, if higher blood pressure is maintained, the smooth muscle lining of blood vessels becomes thickened and even higher blood pressures are required to maintain the same resting blood flow. Sterling and Eyer point out that under conditions of unpredictable environmental stress, the brain becomes "addicted" to systems and signaling molecules (hormones, neurotransmitters, cytokines, and metabokines) needed to produce rapid arousal states, and the anticipatory stress responses become the norm. This complicates treatment. Some therapies can result in "withdrawal" symptoms, making a return to a healthy ground state difficult to maintain without a persistent change in diet and lifestyle.

McEwen and Stellar introduced the concept of allostatic load (AL) in the early 1990s (McEwen and Stellar, 1993). Under this concept, when homeostasis fails in the face of multiple types of environmental stress, many different types of disease can result. Recent multivariate analysis of 23 measurable parameters, reporting on 7 physiologic systems that regulate the stress response concluded that AL was a valid construct for operationalizing the components of variance contributed by many different stressors (Wiley et al., 2016). Interestingly, all the metabolic, inflammatory, neuroendocrine, and gene expression changes that occur in response to stress are regulated by mitochondria (Picard et al., 2015). McEwen and coworkers have recently incorporated the idea of mitochondria as the nexus for regulating the biomarkers of AL and chronic disease (Picard et al., 2017). Mitochondria help coordinate the large majority of stress response systems that become activated by allostatic load (Table 3).

Under the healing cycle model for chronic disease, allostatic load initiates the CDR and the healing cycle. In most cases of persistent chronic illness lasting for > 3–6 months, mitochondria are not dysfunctional. They are just stuck in a developmental stage that was intended to be temporary, unable to complete the healing cycle. The healing cycle requires a *programmed change* in mitochondrial function—a shift from M2, to M1, to M0 organelles, and back to M2 (Figs. 1 and 2). When the programmed change becomes fixed and is unable to cycle normally, chronic illness results (Table 1). Over time, sustained changes in mitochondrial function can lead to structural changes in tissues and organs that can make full recovery more difficult.

22. The dauer failsafe response in humans—ME/CFS

Myalgic encephalomyelitis/chronic fatigue syndrome (ME/CFS) is an energy conservation program—a suite of metabolic and gene expression changes—that permits persistence under harsh environmental conditions at the expense of reduced functional capacity, chronic suffering, and disability (Naviaux et al., 2016). A formal animal model for ME/CFS has not yet been developed. However, several energy conservation states are known that are activated by harsh environmental conditions. One of these is called dauer, the German word for persistence, or to endure. When dauer is triggered by harsh conditions, the life expectancy of a classical genetic model system, the 1 mm long worm *Caenorhabditis elegans,* is extended from 2 to 3 weeks to up to 4 months. Animals that fail to enter dauer under harsh conditions die at an increased rate. In this sense, the metabolic program activated by dauer is a failsafe mechanism that increases the chances of survival in a harsh and unpredictable environment.

Interestingly, the genes involved in inhibiting and promoting dauer have been a rich resource for the study of longevity (Uno and Nishida, 2016). Many DAF (dauer associated factor) genes are also regulated by caloric restriction, a common environmental stress known to increase life expectancy in mammals and many other animals. Despite the fact that dauer worms live longer than unstressed animals, it is not a fully functional life. Mitochondria polarize toward a hardened M1 configuration that is adapted for inducible reactive oxygen species (ROS) production, metabolic energy production shifts toward increased usage of glycolysis, which allows dauer animals to survive in reduced oxygen environments (Hand et al., 2011). Some fatty acid oxidation is still conducted by the newly-polarized mitochondria to permit stored fat reserves to be used for energy, while peroxisomes use very long chain fatty acids to synthesize a glycolipid pheromone (a daumone) needed to induce and maintain the dauer state (Joo et al., 2009). Behavioral responses become "brittle", such that small stimuli produce large responses in otherwise docile animals. Dauer animals are also more resistant to cold-stress (Hu et al., 2015), ultraviolet (UV) light (Murakami and Johnson, 1996), and salt stress. Significant changes in circadian rhythm regulation (Driver et al., 2013), innate immunity (Holt, 2006), behavior (Lee et al., 2017), and sensory processing (Chen and Chalfie, 2014) also accompany the dauer phenotype. Overall, the dauer state and other hypometabolic states permit survival under harsh conditions, but at a high price of much-altered and much-restricted normal function.

The good news is that the dauer state in the worm model is completely reversible. If dauer is a good model for ME/CFS, then there is hope that by studying the molecular controls of the dauer phenotype, new treatments might be discovered rationally to help stimulate the exit from the dauer-like state and begin the process of recovery. The following is a summary of a plausible sequence of pathogenesis for ME/CFS. All stressed cells leak ATP through stress-gated pannexin/P2X7 and other channels. Extracellular ATP (eATP) signals danger and CDR1 is initiated (Fig. 1). If the acute cell danger response and healing cycle fail to eliminate the stress and stop the ATP leak by successful completion of CDR3, then an energy conservation program is activated. Normal cell activation pathways utilize lipid rafts and sphingolipid microdomains on the cell membrane to facilitate metabokine- and cytokine-receptor binding and signaling by receptor subunit dimerization. Sphingolipids are downregulated in most cases of ME/CFS (Naviaux et al., 2016) and may facilitate an energy conservation state.

The dauer-like energy conservation program in mammals may also involve a ligand-receptor desensitization process, decreasing the ability of cells to release intracellular calcium when needed. Calcium stimulates mitochondrial oxidative phosphorylation. When stimulated by ATP and related nucleotides, IP3-gated calcium release is decreased (Schmunk et al., 2017), and mitochondrial and whole cell reserve capacity is reduced. Other mechanisms for downregulating mitochondrial energy production can contribute to this energy conservation state. A multifactorial reduction in mitochondrial pyruvate dehydrogenase complex activity in ME/CFS has been described (Fluge et al., 2016). Upregulation of ectonucleotidases like CD39 and CD73 can increase the conversion of ATP and ADP to AMP and adenosine. Both AMP and adenosine bind adenosine receptors (Fig. 4A) and produce a reversible hypometabolic state in mice that is protective against many environmental stresses, including lethal irradiation (Ghosh et al., 2017). Continued leakage of ATP to the extracellular space for CDR signaling also creates a source for the hypometabolic signaling molecules AMP and adenosine, while depleting intracellular reserves of ATP. Although not

yet tested in a clinical trial in patients with ME/CFS, the ATP and UTP leak might be stopped by blocking the efflux of nucleotides through the pannexin/P2X7 channel with an antipurinergic drug, thereby unblocking the healing cycle (Fig. 1) and permitting recovery to begin. This is similar to a strategy recently tested in a clinical trial in autism spectrum disorder (Naviaux et al., 2017) and illustrated in a whiteboard animation available at: https://www.youtube.com/watch?v=zIdUufy8Lks.

23. Reversibility of chronic illness

If a chronic illness occurs because of a change in function associated with blocks in the CDR, and not a change in structure or loss of cells, that illness is theoretically reversible, ie, curable. When the healing cycle is unblocked, a full recovery is possible. Because the path leading to healing and recovery is different from, and not the reverse of the path that led originally to the disease (Fig. 3), the term "reversibility" is technically incorrect. This point is expanded in Section 29 below. Even when there is some cell loss, scarring, calcification, or other structural change, some healing is still possible by tissue remodeling, but a full recovery becomes more difficult to achieve. Autism spectrum disorder (ASD) can be classified as a CDR3 disorder (Table 1), characterized by both functional and brain structural changes that can vary significantly in severity. In a mouse model of autism, when treatment was delayed until the human biological age-equivalent of 30 years old, the core functional abnormalities in behavior and metabolism in ASD could still be completely corrected with antipurinergic therapy (APT) with suramin, but the gait abnormalities associated with the structural loss of cerebellar Purkinje cells were not reversed (Naviaux et al., 2014).

In the case of cancer, cardiovascular disease, and other proliferative disorders associated with CDR2 diseases (Table 1), metabolic, innate immune, and adaptive immunity can reduce the burden of abnormal cells by removing them. Successful reactivation of CDR1 in the surrounding normal cells, followed by entry into CDR2 for biomass replacement and CDR3 to facilitate tissue remodeling, may result in functional cures for the major symptoms of some CDR2 disorders, even if some limitations remain because of imperfect biomass replacement and tissue remodeling. In the case of CDR3 diseases like autism, treatments directed at unblocking the healing cycle and rebooting metabolism may lead to remarkable clinical improvements (Naviaux et al., 2017).

24. The tempo of physiologic change

The tempo of chronic disease is slower than many people might think. Like a new exercise program, and shifts in metabolism after making an abrupt change in diet, new metabolism and physiology take at least 3 weeks in young adults to settle in to the "new normal". The temporal parallel between disease, diet, and exercise is no accident. The ability to shift metabolism according to seasonal changes and new patterns of food availability within a few weeks of migration to a new location was key to the survival of our ancestors. This timing is built into our genes. It takes 3–4 days before new patterns of gene expression begin to consolidate, and about 3 weeks for new physiologic patterns to "reset" to a new normal after a change in diet, exercise, and other environmental conditions. It takes more time to fully commit to the change. Ultimately, it takes a season of about 3 months or more to fully commit to new foods, physical activities, and environmental exposures (sun, monsoons, droughts, hard freezes, etc) of the season. Three months is also the average minimum time needed to demonstrate synaptic remodeling with exercise or meditation (Thomas and Baker, 2013). A similar tempo might be needed to "reboot" and reset metabolism to a new normal after starting a new treatment for a chronic disease.

25. Metabolic addiction

Once the CDR is unblocked and the healing cycle rebooted, the simplest form of the CDR model predicts that recovery will follow naturally, and health will persist because the genes inherited from our ancestors will defend health in preference to disease and disability. Clinical experience suggests this is not always true. Many patients tend to drift back to the old disease state unless they continue to take measures to actively prevent relapse. This phenomenon may be metabolically similar to addiction. Addiction is a physiologic condition characterized by a baseline physiologic arousal or anxiety state that is temporarily quenched or relieved by a particular behavior or drug. A large body of research has shown that the predisposition to addiction is conditioned by genetics, epigenetics, environmental chemicals, and life stress (Yuan et al., 2016). The most successful alcohol and drug rehabilitation programs teach that recovery is a lifelong process. An addict is never "cured". They are taught to identify themselves as a "recovering alcoholic" or "recovering gambling addict" for life to strengthen resilience and decrease the risk of relapse.

The concept of metabolic addiction suggests that the increased risk of relapse after recovery from chronic illness is the result of a physiologic dependence on the endogenous chemical state produced by a particular stage of the CDR. For example, once a person has suffered from an episode of major depressive disorder (MDD) and recovered, the risk of recurrence is 3–6 times greater than the background population risk (Hoertel et al., 2017). This latent risk suggests that predisposing genetic and/or metabolic factors persist that facilitate a drift back to chronic illness, even after predisposing environmental risks are removed. New studies using metabolomics methods will be needed to test this hypothesis directly.

26. The brain controls metabolism and exit from the CDR

The last step in the healing cycle, CDR3, is ended when the brain reestablishes bidirectional neuroendocrine and autonomic communication with each organ system. Only after the brain re-integrates metabolism over the periodized course of wakeful activity and restorative sleep can the health cycle be re-established. The vagus nerve plays and important role in communicating information from tissues to the CNS. Vagal mechanoreceptors and chemoreceptors monitor organ physiology (Powley et al., 2011). Eighty percent of vagus nerve fibers are made up of sensory fibers returning information from all organ systems to the brain. Among the chemoreceptors are vanilloid (TPRV1) and the purinergic P2X3 receptors responding to noxious stimuli, and extracellular ATP, respectively (Hermes et al., 2016). Vagal afferents terminate in excitatory glutamatergic synapses in the *nucleus tractus solitarius* (NTS). From the NTS, extracranial sensory information is transduced and distributed widely throughout the brain. NTS fibers project back to the ventral vagal complex of the *nucleus ambiguus* and the dorsal vagal complex of the dorsal motor nucleus of the 10th cranial nerve (DMNX) as feedback to the vagus. Feedback to the *nucleus ambiguus* modulates signals conducted along myelinated motor fibers to the vagus nerve for rapid changes in cardiorespiratory and vasomotor function, swallowing, speech, and hearing that occur with stress and well-being (Porges, 2011). The NTS also projects to the locus coeruleus in the reticular activating system to regulate behavioral responses to stress and panic, and to the amygdala in the limbic system, and the paraventricular nuclei of the hypothalamus to regulate physiologic and neuroendocrine responses to stress.

Brain neuroendocrine and autonomic systems function as bidirectional circuits. When CDR stages 1 and 2, or the first parts of CDR3 are active in the periphery, this information is carried to the brain along three channels; endocrine feedback, autonomic afferents, and chemosensory neurons. When this information is received, the brain initiates sickness behavior and sends pro-inflammatory, pro-stress, pro-arousal endocrine and autonomic efferent signals to the periphery. Sleep

structure is also altered to facilitate recovery and promote survival. The default state in both the brain and peripheral tissues is CDR activation. In the absence of additional information, danger and threat are assumed. Healing is an active process that requires positive reinforcement with non-danger, safety and security signals from the brain. Brain inflammation can last for a lifetime after physical injury (Johnson et al., 2013) or early life stress (ELS) and psychological trauma (Cameron et al., 2017). In addition, peripheral pain syndromes and organ inflammation are common after brain or spinal cord injury (Irvine et al., 2018) or brain death (Esmaeilzadeh et al., 2017; Jafari et al., 2018). Unresolved CDR activation by adverse childhood experiences (ACEs) and socioeconomic factors may also play a role in many other adult illnesses like heart disease, cancer, and stroke (Cassel, 1976; Hughes et al., 2017). Once the CNS efferent and local tissue CDR signals are effective, metabokines in the blood return to normal, cell danger signals diminish, and non-danger, pro-resolving, and pro-healing signals predominate.

Metabokines like purines, pyrimidines, amino acids, bioamines, fatty acids, eicosanoids, sphingolipids, phosphatidic acids, lysophospholipids, and many others, in addition to critical blood chemistry information like sodium and osmolality are independently monitored by chemosensory neurons in the 8 circumventricular organs (CVOs) of the brain (Siso et al., 2010). These chemosensory neurons lack a blood brain barrier and provide continuous sensory information that is independent of endocrine feedback and autonomic afferents. One of the well-known CVOs is the *area postrema* (AP) located at the floor of the 4th ventricle that contains the chemoreceptor trigger zone and regulates nausea and vomiting. The AP sends fibers that project to the *nucleus tractus solitarius* (NTS) to modulate the response to vagal sensory information (Hay and Bishop, 1991). Once blood chemistry starts returning to normal, chemosensory neurons of the CVO system communicate this information to neuroendocrine and autonomic systems to gradually shift efferent information back to anti-inflammatory, anxiolytic, pro-resolving, and pro-social signals. This shift in outflowing information from the brain marks the last stages of CDR3 and is required for re-entry into the health cycle of wakeful activity and restorative sleep (Fig. 1, Table 2).

27. Deterministic health and stochastic disease

While it is not possible to predict when and how an injury will happen, the chance that injuries and infections will happen is a certainty for all life on Earth. Without a way to heal after these injuries, any species would go extinct. The genetic program that facilitates recovery from any injury has been highly selected and tuned over evolutionary time. We now know that the healing cycle activates discrete sets of genes in a predictable sequence after injury. While injury is random, recovery and health are deterministic. Recovery is the programed result of the healing cycle (Fig. 1). Recovery occurs in the large majority of cases when the healing cycle is activated. Yet, why is it that some individuals get sick from common exposures, and cannot complete the healing cycle? For example, Epstein-Barr virus (EBV) is a risk factor for ME/CFS. In the US, 82% of people have been exposed to EBV by the time they are 19 years old (Dowd et al., 2013). If EBV is "the" cause, why do fewer than 1% of the US population have ME/CFS? Clinicians have documented dozens of other risk factors that can contribute to the chances of developing ME/CFS. An interesting point about chronic disease is that every non-infectious, chronic illness is caused by a perfect storm of several factors, not by one factor. The chances that this perfect storm of factors for a particular disease will occur for any one patient in a population of millions is small. But once disease strikes, the small initial probability rises to 100% certainty for that person. Therefore, as the environmental factors like pollution and food chain contamination start to increase, more people are exposed to risk, and more individuals will develop chronic illness. Reducing the environmental factors that contribute to risk will reduce the incidence of chronic illness.

So is chronic illness deterministic or stochastic? Scientists are most comfortable with deterministic, linear chains of logic. If cause "A" leads to disease "B" in 100% of people exposed and disease "B" never occurs without an exposure to cause "A", then there is little room for debate. Cause "A" is necessary and sufficient to produce disease "B". The problem is that literally none of the top 10, non-infectious chronic illnesses in the world has a single cause that produces the disease in every person exposed. Heart disease, diabetes, stroke, dementia, cancer, arthritis, autism, ADHD, depression, and schizophrenia all have dozens of risk factors, but no single "cause". By reducing the exposure to the risk factors, a nation can prevent a large percentage of all chronic illness in its citizens. Chronic illness is best modeled as a stochastic process, with an incidence that is modifiable by increasing or decreasing risk factors. This means that in large populations like the 325 million people in the United States, the management of even small chemical risk factors by a proactive government can produce dramatic changes in the incidence of chronic illness and its ripple effects in society. For example, if a hypothetical chemical were ubiquitous and synergized with the background mix of factors to increase the risk of mental illness leading to gun violence in just 0.001% of the population, removal of that chemical from the environment would result in 3250 (0.001% × 325 million) fewer cases of mental illness and gun violence each year.

28. A new pharmacology

In the past, student physicians and pharmacologists have been taught that drugs work by mechanisms that are the same in health and disease. While this was true for drugs designed to treat acute illneses, the treatment of chronic disease forces a revision of the old teaching. The health cycle and the healing cycle represent different biological states that have different bioenergetics, and different governing dynamics (Fig. 1, Table 2). *Biology* and *pathobiology* are qualitatively distinct states of function. Both are normal. However, the functional state associated with *pathobiology* (the healing cycle) is only normal when it occurs transiently. Pathological persistence of the stages of the healing cycle lead to chronic illness and the inability to heal. Drugs that will work best for treating chronic illness will target receptors like those illustrated in Fig. 5A that play key roles in the healing cycle, but remain virtually unused, or are used differently in health.

Personalized pharmacogenomics will help refine the new pharmacology as it has the old (Caudle et al., 2016), once the best targets in the healing cycle have been identified. A goal of the new pharmacology will be to discover new treatments for chronic illness that have targets that are active in disease, but are dormant in health, and therefore have little or no effect in healthy children and adults. Like Paul Ehrlich's magic bullet (Tan and Grimes, 2010), the new drugs will have fewer side effects because once the disease is cured and the patient has recovered, the target of the drug will have disappeared, and the bullet can pass without causing harm. The need for chronic drug use is then eliminated. While the simile is evocative, it is important to remember that "magic" bullets are not really magic. They just work by scientific mechanisms that have not yet been discovered, or are not yet well understood.

29. Failures of failure analysis

A fundamental difference between living and inanimate systems is that living systems can heal and inanimate systems cannot. When a machine or other manmade object of technology fails, the analysis of the mechanism of failure has proven to be a logical and effective way to discover a fix for the problem. For example, once the defect in the optics of the Hubble Space Telescope was precisely characterized, a solution was engineered to compensate for the defect, thereby fixing the problem. This same engineering logic is often applied successfully to "fix" acute illnesses in living systems. In contrast to acute illnesses, many

chronic disorders are self-sustaining alternative performance or failure states that limit the potential for independence in a child and reduce the quality of life in children and adults for years.

New tools in systems biology like genomics, RNAseq, proteomics, and metabolomics have created the ability to minutely characterize the way a system has failed in any one of the complex disorders listed in Table 1. The same tools can be applied to individuals with any given chronic disease as part of a precision medicine effort to phenotype that patient at the molecular level. The results of this precision medicine analysis have shown that chronic illnesses are characterized by hundreds of molecular differences from healthy control states. Historically, the pharmaceutical industry has systematically analyzed the molecular paths that lead to a recognizable disease state and have cataloged the defects present once that disease state becomes persistent. This information was then used to identify drugable targets. This approach to treat chronic disease in living systems has failed to produce cures because it is more like engineering than biology. Living systems engage the same evolutionarily conserved path to cellular recovery after injury—the same healing cycle with minor modifications—regardless of the mechanism of injury (Fig. 1). Biological healing in a living system does not involve the precise identification and point-for-point correction of each of the hundreds of defects present in chronic illness. Living systems do not turn back the arrow of time to retrace the path that led to the injury and illness. They move forward along a new path in order to heal (Fig. 3), eliminating hundreds of abnormalities in step with progress through each stage of the CDR. Each step in healing represents a concerted regime change in metabolism and gene expression, like the rapid succession of cellular ecosystems that return the system back to optimum integrated performance. For these reasons, treating a unique target for each individual disease may not be necessary. The path that permits a patient to exit any given disease state, i.e., to recover from chronic illness, may be the same for hundreds of diseases. A new generation of drugs and devices designed to unblock the healing cycle may turn out to be able to treat many diseases. Only time, and good clinical trials, will tell if this hypothesis is true.

30. Conclusions

30.1. Beginning a 2nd book of medicine

Much of western medical teaching in the US in 2018 is based on principles that were developed historically to treat acute illnesses from poisoning, physical injury, and infections. These principles have been incorporated into the books and literature used to train modern physicians and health care workers. Philosophically, this corpus of knowledge can be thought of as "the 1st book of medicine". When treatments developed to treat acute causes and specific organ system dysfunction are applied to chronic illness, they produce marginal improvements, almost never cure a chronic disease, and must be given for life. This is good from the point of view of a drug company that manufactures a drug, but not for patients, and not for a nation whose economic health is tied to the health of its citizens.

Healing is a biologically active, energy-requiring process that is intrinsic to all life. Healing chronic illness cannot occur without engaging, unblocking, and actively supporting this universal system. "The 2nd book of medicine" will focus on the prevention of chronic illness and the care and recovery of patients with chronic disease. This book will introduce the concept that many treatments for chronic illness will be directed at the processes that block the healing cycle. These new treatments may only need to be given for a short period of time to cure or improve a chronic illness. This might be functionally similar to applying a cast to promote the healing of a broken leg. Treatment only needs to be given for a period of time needed for tissues to complete the healing cycle. When the cast is removed, the limb is weak, but after a period of time needed for reconditioning, the muscles have recovered, and the bone that was once broken is actually stronger at the point of injury than it was before. New drug treatments for chronic disorders like autism or PTSD, may only need to be given for a few months at a time, until the healing cycle can be completed, or the process of recovery, building strength, fitness, and resilience can be started and become self-sustaining again. Individuals may need occasional "tune-ups" to maintain recovery over the years, since genetic predispositions, environmental conditions, and metabolic memories of past exposures may cause health to drift back to the previous disease pattern, but the majority of time might be spent without the need for chronic treatment, or the limitations caused by chronic illness.

30.2. Potential economic impact

Eighty-six percent (86%) of the $3.3 trillion spent annually on medical costs in the US is spent to care for chronic conditions (CDC.gov, 2017). The cost of health care is predicted to rise to $5.5 trillion by 2025 because of chronic disease. This will require nearly 20% of the GDP of the US, estimated to be about $27 trillion (CMS.gov, 2017), if the trend of relentlessly growing chronic disease is not reversed. Today, 30% of children under 12 years have a chronic disease, and another 20% will develop a serious mental illness in their teens (HHS, 2018). Sixty percent of adult US citizens 18–64 years have a chronic disease, 90% of people over age 65 have at least one chronic illness, and 81% over 65 have 2 or more chronic conditions (CDC.gov, 2017). Shifting healthcare insurance policies from multi-payer to single-payer or back will have little effect on this cost. The fact that more Americans are getting sick, and not small variations in insurance policies, is driving the lion's share of rising costs. If just 10% of people now suffering with chronic illness could be cured by new methods directed at the healing cycle, more than $250 billion (10% × $2.5 trillion) would be saved annually. The savings in a single year would be more than the annual budgets of the National Institutes of Health (NIH; $37 billion), Environmental Protection Agency (EPA; $8.7 billion), Food and Drug Administration (FDA; $5.1 billion), and the US Department of Agriculture (USDA; $151 billion) combined.

31. Summary

Interruptions in the molecular stages of the healing cycle may be at the root of many complex, chronic illnesses. Three stages of the cell danger response (CDR1, 2, and 3) comprise the healing cycle. These stages are triggered by stress or injury and controlled by changes in mitochondrial function and metabolism (Figs. 1 and 2, Table 2). Many metabolites are metabokines that bind to dedicated receptors and signal when a cell is ready to enter the next stage of healing (Figs. 4 and 5). Purinergic signaling from the release and metabolism of extracellular nucleotides plays an important role in all stages of the healing cycle (Fig. 1). Programmed changes in the differentiation state of mitochondria, known as M0, M1, and M2-polarized organelles, and corresponding changes in cellular redox and the repurposing of cellular energy for cell defense and healing, also play fundamental roles (Fig. 2, Table 3) (Naviaux, 2017). When a stage of the healing cycle cannot be completed, dysfunctional cells accumulate that contain developmentally inappropriate forms of mitochondria, organ function is compromised, and chronic illness results (Fig. 3). Over 100 chronic illnesses can be classified according to the stage of the CDR that is blocked (Table 1). Unblocking therapies directed at stimulating the completion of the healing cycle by regulating metabokine signaling hold promise as a new approach to treatment. A small clinical trial of the antipurinergic drug suramin in autism spectrum disorder (ASD) has shown promise for this approach (Naviaux, 2017; Naviaux et al., 2017). Metabolic addiction to the chemistry produced by different stages of the CDR can occur. When this happens, it can create a life-long risk of relapse or slow return to chronic illness if diet and lifestyle interventions are not maintained.

Prevention and treatment of chronic illness require distinctly

different, but complementary approaches. New cases of chronic illness can be *prevented* by reducing the environmental risks that trigger the damage cycle of the CDR, and by promoting exercise, nutritional and life-style changes that promote resilience and maintain the health cycle (Fig. 1). However, once illness has occurred in a given patient, the opportunity for prevention is lost, and a perfect storm of multiple triggers can usually be identified. Many triggers are remote and no longer present. Once any remaining triggers have been identified and removed, and any symptoms or primed sensitivities caused by the metabolic memory of those triggers have been treated, a new approach to *treatment* is required to improve the chances of completing the healing cycle and achieving a full recovery. By shifting the focus away from the *initial causes*, to the metabolic factors and signaling pathways that *maintain* chronic illness by blocking progress through the healing cycle, new research will be stimulated and novel treatments will follow.

Supplementary data to this article can be found online at https://doi.org/10.1016/j.mito.2018.08.001.

Acknowledgements

RKN thanks the many families with primary mitochondrial disease, autism spectrum disorder (ASD), and myalgic encephalitis/chronic fatigue syndrome (ME/CFS) who have helped make this research possible. He thanks Neil Nathan, Eric Gordon, John Green, A.Taylor Bright, Elizabeth Mumper, David Sarfatti, Ellen Heber-Katz, Jon Berner, John Rodakis, Nancy O'Hara, Johanna Assies, and Stuart Sealfon for helpful discussions and/or comments on the manuscript, and Jonathan Monk and Mindi Summers for assistance with the gene sequence alignments.

Funding sources

This work was funded in part by philanthropic gifts from the UCSD Christini Fund, the Lennox Foundation, Malone Family Foundation, N of One Autism Research Foundation, the UCSD Mitochondrial Disease Research Fund, the JMS Fund, and gifts in memory of Wayne Riggs, and from Linda Clark, Jeanne Conrad, Jeff Ansell, Josh Spears, David Cannistraro, the Kirby and Katie Mano Family, Simon and Evelyn Foo, Wing-kun Tam, Gita Gupta, and the Daniel and Kelly White Family. Funding for the mass spectrometers was provided by a gift from the Jane Botsford Johnson Foundation. RKN wishes to thank over 2000 individuals who have each provided gifts in the past year to support Naviaux Lab research.

Conflicts of interest

RKN is a scientific advisory board member for the Autism Research Institute and the Open Medicine Foundation, and has submitted a patent application for the use of antipurinergic therapy in autism and related disorders.

References

Adams, J.B., Audhya, T., McDonough-Means, S., Rubin, R.A., Quig, D., Geis, E., Gehn, E., Loresto, M., Mitchell, J., Atwood, S., Barnhouse, S., Lee, W., 2011. Nutritional and metabolic status of children with autism vs. neurotypical children, and the association with autism severity. Nutr. Metabol. 8, 34.

Anupama, N., Sindhu, G., Raghu, K.G., 2018. Significance of mitochondria on cardiometabolic syndromes. Fundam. Clin. Pharmacol. 32 (4), 346–356.

Atamna, H., Tenore, A., Lui, F., Dhahbi, J.M., 2018. Organ reserve, excess metabolic capacity, and aging. Biogerontology 19, 171–184.

Baez-Pagan, C.A., Delgado-Velez, M., Lasalde-Dominicci, J.A., 2015. Activation of the macrophage alpha7 nicotinic acetylcholine receptor and control of inflammation. J. Neuroimmune Pharmacol. Official J. Soc. NeuroImmune Pharmacol. 10, 468–476.

Baker, S., Bennett, P., Bland, J., Galland, L., Hedaya, R., Houston, M., Hyman, M., Lombard, J., Roundtree, R., Vasquez, A., 2010. Textbook of Functional Medicine. The Institute for Functional Medicine, Gig Harbor, WA.

Bernhardt, J.R., Leslie, H.M., 2013. Resilience to climate change in coastal marine ecosystems. Annu. Rev. Mar. Sci. 5, 371–392.

Boya, P., Codogno, P., Rodriguez-Muela, N., 2018. Autophagy in stem cells: repair, remodelling and metabolic reprogramming. Development 145.

Braymer, J.J., Lill, R., 2017. Iron-sulfur cluster biogenesis and trafficking in mitochondria. J. Biol. Chem. 292, 12754–12763.

Buckinx, R., Adriaensen, D., Nassauw, L.V., Timmermans, J.P., 2011. Corticotrophin-releasing factor, related peptides, and receptors in the normal and inflamed gastrointestinal tract. Front. Neurosci. 5, 54.

Burke, J., 2015. In: Thorpe, K. (Ed.), Partnership to Fight Chronic Disease. Emory University, Atlanta, GA. https://www.fightchronicdisease.org/latest-news/130-million-americans-chronic-disease-cost-more-25-trillion-annually.

Calabrese, E.J., Baldwin, L.A., 2003. Hormesis: the dose-response revolution. Annu. Rev. Pharmacol. Toxicol. 43, 175–197.

Cameron, J.L., Eagleson, K.L., Fox, N.A., Hensch, T.K., Levitt, P., 2017. Social origins of developmental risk for mental and physical illness. J. Neurosci. 37, 10783–10791.

Cao, Y.L., Meng, S., Chen, Y., Feng, J.X., Gu, D.D., Yu, B., Li, Y.J., Yang, J.Y., Liao, S., Chan, D.C., Gao, S., 2017. MFN1 structures reveal nucleotide-triggered dimerization critical for mitochondrial fusion. Nature 542, 372–376.

Carney, R.M., Freedland, K.E., Steinmeyer, B.C., Rubin, E.H., Stein, P.K., Rich, M.W., 2016. Nighttime heart rate predicts response to depression treatment in patients with coronary heart disease. J. Affect. Disord. 200, 165–171.

Carreras-Sureda, A., Pihan, P., Hetz, C., 2018. Calcium signaling at the endoplasmic reticulum: fine-tuning stress responses. Cell Calcium 70, 24–31.

Cassel, J., 1976. The contribution of the social environment to host resistance: the Fourth Wade Hampton Frost Lecture. Am. J. Epidemiol. 104, 107–123.

Caudle, K.E., Gammal, R.S., Whirl-Carrillo, M., Hoffman, J.M., Relling, M.V., Klein, T.E., 2016. Evidence and resources to implement pharmacogenetic knowledge for precision medicine. Am. J. Health Syst. Pharm. 73, 1977–1985.

Cdc.Gov, 2017. Chronic Disease Overview. National Center for Chronic Disease Prevention and Health Promotion. Atlanta, GA. https://www.cdc.gov/chronicdisease/overview/index.htm#ref17.

Chang, C., Gershwin, M.E., 2011. Drug-induced lupus erythematosus: incidence, management and prevention. Drug Saf. 34, 357–374.

Chen, X., Chalfie, M., 2014. Modulation of C. elegans touch sensitivity is integrated at multiple levels. J. Neurosci. 34, 6522–6536.

Chen, J., Tan, Z., Zeng, L., Zhang, X., He, Y., Gao, W., Wu, X., Li, Y., Bu, B., Wang, W., Duan, S., 2013. Heterosynaptic long-term depression mediated by ATP released from astrocytes. Glia 61, 178–191.

Chrysant, S.G., 2017. New onset diabetes mellitus induced by statins: current evidence. Postgrad. Med. 129, 430–435.

Claude-Taupin, A., Jia, J., Mudd, M., Deretic, V., 2017. Autophagy's secret life: secretion instead of degradation. Essays Biochem. 61, 637–647.

CMS.gov, 2017. 2016–2025 Projections of national health expenditures data released. In: M.M, C.f. (Ed.), Services, Baltimore, MD. https://www.cms.gov/Newsroom/MediaReleaseDatabase/Press-releases/2017-Press-releases-items/2017-02-15-2.html.

Cunliffe, J., 1997. Morphostasis: an evolving perspective. Med. Hypotheses 49, 449–459.

Dantzer, R., Kelley, K.W., 2007. Twenty years of research on cytokine-induced sickness behavior. Brain Behav. Immun. 21, 153–160.

de Jong, H.J., Saldi, S.R., Klungel, O.H., Vandebriel, R.J., Souverein, P.C., Meyboom, R.H., Passier, J.L., van Loveren, H., Cohen Tervaert, J.W., 2012. Statin-associated polymyalgia rheumatica. An analysis using WHO global individual case safety database: a case/non-case approach. PloS one 7, e41289.

De Meersman, R.E., 1992. Respiratory sinus arrhythmia alteration following training in endurance athletes. Eur. J. Appl. Physiol. Occup. Physiol. 64, 434–436.

De Meersman, R.E., 1993. Heart rate variability and aerobic fitness. Am. Heart J. 125, 726–731.

Del Dotto, V., Mishra, P., Vidoni, S., Fogazza, M., Maresca, A., Caporali, L., McCaffery, J.M., Cappelletti, M., Baruffini, E., Lenaers, G., Chan, D., Rugolo, M., Carelli, V., Zanna, C., 2017. OPA1 isoforms in the hierarchical organization of mitochondrial functions. Cell Rep. 19, 2557–2571.

Dhir, A., Dhir, S., Borowski, L.S., Jimenez, L., Teitell, M., Rötig, A., Crow, Y.J., Rice, G.I., Duffy, D., Tamby, C., Nojima, T., Munnich, A., Schiff, M., Ribeiro De Almeida, C., Rehwinkel, J., Dziembowski, A., Szczesny, R.J., Proudfoot, N.J., 2018. Mitochondrial double-stranded RNA triggers antiviral signalling in humans. Nature (Epub ahead of print).

Djordjevic, J., Djordjevic, A., Adzic, M., Mitic, M., Lukic, I., Radojcic, M.B., 2015. Alterations in the Nrf2-Keap1 signaling pathway and its downstream target genes in rat brain under stress. Brain Res. 1602, 20–31.

Dowd, J.B., Palermo, T., Brite, J., McDade, T.W., Aiello, A., 2013. Seroprevalence of Epstein-Barr virus infection in U.S. children ages 6–19, 2003–2010. PLoS One 8, e64921.

Driver, J.A., 2014. Inverse association between cancer and neurodegenerative disease: review of the epidemiologic and biological evidence. Biogerontology 15, 547–557.

Driver, R.J., Lamb, A.L., Wyner, A.J., Raizen, D.M., 2013. DAF-16/FOXO regulates homeostasis of essential sleep-like behavior during larval transitions in C. elegans. Curr. Biol. 23, 501–506.

Dworak, M., Wiater, A., Alfer, D., Stephan, E., Hollmann, W., Struder, H.K., 2008. Increased slow wave sleep and reduced stage 2 sleep in children depending on exercise intensity. Sleep Med. 9, 266–272.

Esmaeilzadeh, M., Sadeghi, M., Galmbacher, R., Daniel, V., Knapp, J., Heissler, H.E., Krauss, J.K., Mehrabi, A., 2017. Time-course of plasma inflammatory mediators in a rat model of brain death. Transpl. Immunol. 43–44, 21–26.

Esteras, N., Dinkova-Kostova, A.T., Abramov, A.Y., 2016. Nrf2 activation in the treatment of neurodegenerative diseases: a focus on its role in mitochondrial bioenergetics and function. Biol. Chem. 397, 383–400.

Fiehn, O., 2002. Metabolomics–the link between genotypes and phenotypes. Plant Mol. Biol. 48, 155–171.

Fluge, O., Mella, O., Bruland, O., Risa, K., Dyrstad, S.E., Alme, K., Rekeland, I.G., Sapkota,

D., Rosland, G.V., Fossa, A., Ktoridou-Valen, I., Lunde, S., Sorland, K., Lien, K., Herder, I., Thurmer, H., Gotaas, M.E., Baranowska, K.A., Bohnen, L.M., Schafer, C., McCann, A., Sommerfelt, K., Helgeland, L., Ueland, P.M., Dahl, O., Tronstad, K.J., 2016. Metabolic profiling indicates impaired pyruvate dehydrogenase function in myalgic encephalopathy/chronic fatigue syndrome. JCI Insight 1, e89376.
Ford, A.P., Undem, B.J., Birder, L.A., Grundy, D., Pijacka, W., Paton, J.F., 2015. P2X3 receptors and sensitization of autonomic reflexes. Auton. Neurosci. 191, 16–24.
Gabbs, M., Leng, S., Devassy, J.G., Monirujjaman, M., Aukema, H.M., 2015. Advances in our understanding of oxylipins derived from dietary PUFAs. Adv. Nutr. 6, 513–540.
Gerdle, B., Forsgren, M.F., Bengtsson, A., Leinhard, O.D., Soren, B., Karlsson, A., Brandejsky, V., Lund, E., Lundberg, P., 2013. Decreased muscle concentrations of ATP and PCR in the quadriceps muscle of fibromyalgia patients–a 31P-MRS study. Eur. J. Pain 17, 1205–1215.
Gether, U., 2000. Uncovering molecular mechanisms involved in activation of G protein-coupled receptors. Endocr. Rev. 21, 90–113.
Gevi, F., Zolla, L., Gabriele, S., Persico, A.M., 2016. Urinary metabolomics of young Italian autistic children supports abnormal tryptophan and purine metabolism. Mol. Autism 7, 47.
Ghosh, S., Indracanti, N., Joshi, J., Ray, J., Indraganti, P.K., 2017. Pharmacologically induced reversible hypometabolic state mitigates radiation induced lethality in mice. Sci. Rep. 7, 14900.
Gosain, A., Dipietro, L.A., 2004. Aging and wound healing. World J. Surg. 28, 321–326.
Gutierrez-Vazquez, C., Quintana, F.J., 2018. Regulation of the immune response by the aryl hydrocarbon receptor. Immunity 48, 19–33.
Han, W., Sapkota, S., Camicioli, R., Dixon, R.A., Li, L., 2017. Profiling novel metabolic biomarkers for Parkinson's disease using in-depth metabolomic analysis. Mov. Disord. 32, 1720–1728.
Hand, S.C., Menze, M.A., Borcar, A., Patil, Y., Covi, J.A., Reynolds, J.A., Toner, M., 2011. Metabolic restructuring during energy-limited states: insights from Artemia franciscana embryos and other animals. J. Insect Physiol. 57, 584–594.
Harkewicz, R., Dennis, E.A., 2011. Applications of mass spectrometry to lipids and membranes. Annu. Rev. Biochem. 80, 301–325.
Hay, M., Bishop, V.S., 1991. Interactions of area postrema and solitary tract in the nucleus tractus solitarius. Am. J. Phys. 260, H1466–H1473.
He, S., Sharpless, N.E., 2017. Senescence in health and disease. Cell 169, 1000–1011.
He, Y., Yu, Z., Giegling, I., Xie, L., Hartmann, A.M., Prehn, C., Adamski, J., Kahn, R., Li, Y., Illig, T., Wang-Sattler, R., Rujescu, D., 2012. Schizophrenia shows a unique metabolomics signature in plasma. Transl. Psychiatry 2, e149.
Heber-Katz, E., 2017. Oxygen, metabolism, and regeneration: lessons from mice. Trends Mol. Med. 23, 1024–1036.
Heber-Katz, E., Messersmith, P., 2018. Drug delivery and epimorphic salamander-type mouse regeneration: a full parts and labor plan. Adv. Drug Deliv. Rev. 129, 254–261.
Hermes, S.M., Andresen, M.C., Aicher, S.A., 2016. Localization of TRPV1 and P2X3 in unmyelinated and myelinated vagal afferents in the rat. J. Chem. Neuroanat. 72, 1–7.
HHS, U.S., 2018. United States Adolescent Mental Health Facts.
Hoertel, N., Blanco, C., Oquendo, M.A., Wall, M.M., Olfson, M., Falissard, B., Franco, S., Peyre, H., Lemogne, C., Limosin, F., 2017. A comprehensive model of predictors of persistence and recurrence in adults with major depression: results from a national 3-year prospective study. J. Psychiatr. Res. 95, 19–27.
Hoffmann, M.H., Griffiths, H.R., 2018. The dual role of ROS in autoimmune and inflammatory diseases: evidence from preclinical models. Free Radic. Biol. Med (Epub ahead of print).
Holley, C.T., Long, E.K., Butterick, T.A., Duffy, C.M., Lindsey, M.E., Stone, L.H., McFalls, E.O., Kelly, R.F., 2015. Mitochondrial fusion proteins in revascularized hibernating hearts. J. Surg. Res. 195, 29–36.
Holt, S.J., 2006. Staying alive in adversity: transcriptome dynamics in the stress-resistant dauer larva. Funct. Integr. Genomics 6, 285–299.
Hu, J.P., Xu, X.Y., Huang, L.Y., Wang, L.S., Fang, N.Y., 2015. Freeze-thaw Caenorhabditis elegans freeze-thaw stress response is regulated by the insulin/IGF-1 receptor daf-2. BMC Genet. 16, 139.
Huang, M., Risling, M., Baker, D.G., 2016. The role of biomarkers and MEG-based imaging markers in the diagnosis of post-traumatic stress disorder and blast-induced mild traumatic brain injury. Psychoneuroendocrinology 63, 398–409.
Huang, M.X., Swan, A.R., Quinto, A.A., Matthews, S., Harrington, D.L., Nichols, S., Bruder, B.J., Snook, C.C., Huang, C.W., Baker, D.G., Lee, R.R., 2017. A pilot treatment study for mild traumatic brain injury: neuroimaging changes detected by MEG after low-intensity pulse-based transcranial electrical stimulation. Brain Inj. 31, 1951–1963.
Hughes, K., Bellis, M.A., Hardcastle, K.A., Sethi, D., Butchart, A., Mikton, C., Jones, L., Dunne, M.P., 2017. The effect of multiple adverse childhood experiences on health: a systematic review and meta-analysis. Lancet Public Health 2, e356–e366.
Hupin, D., Roche, F., Gremeaux, V., Chatard, J.C., Oriol, M., Gaspoz, J.M., Barthelemy, J.C., Edouard, P., 2015. Even a low-dose of moderate-to-vigorous physical activity reduces mortality by 22% in adults aged > /=60 years: a systematic review and meta-analysis. Br. J. Sports Med. 49, 1262–1267.
Incollingo Rodriguez, A.C., Epel, E.S., White, M.L., Standen, E.C., Seckl, J.R., Tomiyama, A.J., 2015. Hypothalamic-pituitary-adrenal axis dysregulation and cortisol activity in obesity: a systematic review. Psychoneuroendocrinology 62, 301–318.
Irvine, K.A., Sahbaie, P., Liang, D.Y., Clark, D., 2018. TBI disrupts pain signaling in the brainstem and spinal cord. J. Neurotrauma 35 (13), 1495–1509.
Jafari, R., Aflatoonian, R., Falak, R., Pourmand, G., Dehghani, S., Mortazavi, M., Adelipour, A., Rezaei, A., Tajik, N., 2018. Down-regulation of inflammatory signaling pathways despite up-regulation of Toll-like receptors; the effects of corticosteroid therapy in brain-dead kidney donors, a double-blind, randomized, controlled trial. Mol. Immunol. 94, 36–44.
Jang, C., Chen, L., Rabinowitz, J.D., 2018. Metabolomics and isotope tracing. Cell 173, 822–837.
Jeske, J., Bitter, A., Thasler, W.E., Weiss, T.S., Schwab, M., Burk, O., 2017. Ligand-dependent and -independent regulation of human hepatic sphingomyelin phosphodiesterase acid-like 3A expression by pregnane X receptor and crosstalk with liver X receptor. Biochem. Pharmacol. 136, 122–135.
Johnson, V.E., Stewart, J.E., Begbie, F.D., Trojanowski, J.Q., Smith, D.H., Stewart, W., 2013. Inflammation and white matter degeneration persist for years after a single traumatic brain injury. Brain J. Neurol. 136, 28–42.
Johnson, S.C., Yanos, M.E., Bitto, A., Castanza, A., Gagnidze, A., Gonzalez, B., Gupta, K., Hui, J., Jarvie, C., Johnson, B.M., Letexier, N., McCanta, L., Sangesland, M., Tamis, O., Uhde, L., Van Den Ende, A., Rabinovitch, P.S., Suh, Y., Kaeberlein, M., 2015. Dose-dependent effects of mTOR inhibition on weight and mitochondrial disease in mice. Front. Genet. 6, 247.
Joo, H.J., Yim, Y.H., Jeong, P.Y., Jin, Y.X., Lee, J.E., Kim, H., Jeong, S.K., Chitwood, D.J., Paik, Y.K., 2009. Caenorhabditis elegans utilizes dauer pheromone biosynthesis to dispose of toxic peroxisomal fatty acids for cellular homoeostasis. Biochem. J. 422, 61–71.
Kann, O., 2016. The interneuron energy hypothesis: implications for brain disease. Neurobiol. Dis. 90, 75–85.
Khan, N.A., Nikkanen, J., Yatsuga, S., Jackson, C., Wang, L., Pradhan, S., Kivela, R., Pessia, A., Velagapudi, V., Suomalainen, A., 2017. mTORC1 regulates mitochondrial integrated stress response and mitochondrial myopathy progression. Cell Metab. 26 (419–428), e415.
Kim, S.M., Kim, Y.G., Jeong, K.H., Lee, S.H., Lee, T.W., Ihm, C.G., Moon, J.Y., 2012. Angiotensin II-induced mitochondrial Nox4 is a major endogenous source of oxidative stress in kidney tubular cells. PLoS One 7, e39739.
Kim, Y., Zheng, X., Ansari, Z., Bunnell, M.C., Herdy, J.R., Traxler, L., Lee, H., Paquola, A.C.M., Blithikioti, C., Ku, M., Schlachetzki, J.C.M., Winkler, J., Edenhofer, F., Glass, C.K., Paucar, A.A., Jaeger, B.N., Pham, S., Boyer, L., Campbell, B.C., Hunter, T., Mertens, J., Gage, F.H., 2018. Mitochondrial aging defects emerge in directly reprogrammed human neurons due to their metabolic profile. Cell Rep. 23, 2550–2558.
Kuehl, T., Lagares, D., 2018. BH3 mimetics as anti-fibrotic therapy: unleashing the mitochondrial pathway of apoptosis in myofibroblasts. Matrix Biol. 68-69, 94–105.
Lahera, V., de Las Heras, N., Lopez-Farre, A., Manucha, W., Ferder, L., 2017. Role of mitochondrial dysfunction in hypertension and obesity. Curr. Hypertens. Rep. 19, 11.
Lapp, H.E., Ahmed, S., Moore, C.L., Hunter, R.G., 2018. Toxic stress history and hypothalamic-pituitary-adrenal axis function in a social stress task: genetic and epigenetic factors. Neurotoxicol. Teratol (Epub ahead of print).
Laroche, D., Leturgie, P., Mariotte, D., Ollivier, Y., Hanouz, J.L., Le Mauff, B., Parienti, J.J., 2017. In vivo cysteinyl leukotriene release in allergic and nonallergic immediate hypersensitivity reactions during anesthesia. Anesthesiology 126, 834–841.
Lee, D., Lee, H., Kim, N., Lim, D.S., Lee, J., 2017. Regulation of a hitchhiking behavior by neuronal insulin and TGF-beta signaling in the nematode Caenorhabditis elegans. Biochem. Biophys. Res. Commun. 484, 323–330.
Liman, E.R., 2012. Changing senses: chemosensory signaling and primate evolution. Adv. Exp. Med. Biol. 739, 206–217.
Lin, S., Xing, H., Zang, T., Ruan, X., Wo, L., He, M., 2018. Sirtuins in mitochondrial stress: indispensable helpers behind the scenes. Ageing Res. Rev. 44, 22–32.
Lovejoy, D.A., Chang, B.S., Lovejoy, N.R., del Castillo, J., 2014. Molecular evolution of GPCRs: CRH/CRH receptors. J. Mol. Endocrinol. 52, T43–T60.
Lu, P.D., Harding, H.P., Ron, D., 2004. Translation reinitiation at alternative open reading frames regulates gene expression in an integrated stress response. J. Cell Biol. 167, 27–33.
Lucas, A.R., Klepin, H.D., Porges, S.W., Rejeski, W.J., 2018. Mindfulness-based movement: a polyvagal perspective. Integr. Cancer Ther. 17, 5–15.
Mattson, M.P., Moehl, K., Ghena, N., Schmaedick, M., Cheng, A., 2018. Intermittent metabolic switching, neuroplasticity and brain health. Nat. Rev. Neurosci. 19, 63–80.
McEwen, B.S., Stellar, E., 1993. Stress and the individual. Mechanisms leading to disease. Arch. intern. Med. 153, 2093–2101.
McLaughlin Crabtree, V., Williams, N.A., 2009. Normal sleep in children and adolescents. Child Adolesc. Psychiatr. Clin. N. Am. 18, 799–811.
Menon, D., Salloum, D., Bernfeld, E., Gorodetsky, E., Akselrod, A., Frias, M.A., Sudderth, J., Chen, P.H., DeBerardinis, R., Foster, D.A., 2017. Lipid sensing by mTOR complexes via de novo synthesis of phosphatidic acid. J. Biol. Chem. 292, 6303–6311.
Mills, E.L., Kelly, B., O'Neill, L.A.J., 2017. Mitochondria are the powerhouses of immunity. Nat. Immunol. 18, 488–498.
Mishra, N.C., Rir-sima-ah, J., Boyd, R.T., Singh, S.P., Gundavarapu, S., Langley, R.J., Razani-Boroujerdi, S., Sopori, M.L., 2010. Nicotine inhibits Fc epsilon RI-induced cysteinyl leukotrienes and cytokine production without affecting mast cell degranulation through alpha 7/alpha 9/alpha 10-nicotinic receptors. J. Immunol. 185, 588–596.
Mottillo, S., Filion, K.B., Genest, J., Joseph, L., Pilote, L., Poirier, P., Rinfret, S., Schiffrin, E.L., Eisenberg, M.J., 2010. The metabolic syndrome and cardiovascular risk a systematic review and meta-analysis. J. Am. Coll. Cardiol. 56, 1113–1132.
Murakami, S., Johnson, T.E., 1996. A genetic pathway conferring life extension and resistance to UV stress in Caenorhabditis elegans. Genetics 143, 1207–1218.
Murao, N., Nishitoh, H., 2017. Role of the unfolded protein response in the development of central nervous system. J. Biochem. 162, 155–162.
Naviaux, R.K., 2008. Mitochondrial control of epigenetics. Cancer Biol. Ther. 7, 1191–1193.
Naviaux, R.K., 2012. Oxidative shielding or oxidative stress? J. Pharmacol. Exp. Ther. 342, 608–618.
Naviaux, R.K., 2014. Metabolic features of the cell danger response. Mitochondrion 16, 7–17.
Naviaux, R.K., 2017. Antipurinergic therapy for autism-an in-depth review. Mitochondrion.

Naviaux, R.K., Nyhan, W.L., Barshop, B.A., Poulton, J., Markusic, D., Karpinski, N.C., Haas, R.H., 1999. Mitochondrial DNA polymerase gamma deficiency and mtDNA depletion in a child with Alpers' syndrome. Ann. Neurol. 45, 54–58.
Naviaux, R.K., Le, T.P., Bedelbaeva, K., Leferovich, J., Gourevitch, D., Sachadyn, P., Zhang, X.M., Clark, L., Heber-Katz, E., 2009. Retained features of embryonic metabolism in the adult MRL mouse. Mol. Genet. Metab. 96, 133–144.
Naviaux, R.K., Zolkipli-Cunningham, Z., Nakayama, T., Naviaux, J.C., Le, T., Wang, L., Schuchbauer, M., Rogac, M., Li, Q., Dugan, L.L., Powell, S., 2013. Antipurinergic therapy corrects the autism-like features in the poly(IC) mouse model. PLoS One 8, e57380.
Naviaux, J.C., Schuchbauer, M.A., Li, K., Wang, L., Risbrough, V.B., Powell, S.B., Naviaux, R.K., 2014. Reversal of autism-like behaviors and metabolism in adult mice with single-dose antipurinergic therapy. Transl. Psychiatry 4, e400.
Naviaux, J.C., Wang, L., Li, K., Bright, A.T., Alaynick, W.A., Williams, K.R., Powell, S.B., Naviaux, R.K., 2015. Antipurinergic therapy corrects the autism-like features in the Fragile X (Fmr1 knockout) mouse model. Mol. Autism 6, 1.
Naviaux, R.K., Naviaux, J.C., Li, K., Bright, A.T., Alaynick, W.A., Wang, L., Baxter, A., Nathan, N., Anderson, W., Gordon, E., 2016. Metabolic features of chronic fatigue syndrome. Proc. Natl. Acad. Sci. U. S. A. 113, E5472–E5480.
Naviaux, R.K., Curtis, B., Li, K., Naviaux, J.C., Bright, A.T., Reiner, G.E., Westerfield, M., Goh, S., Alaynick, W.A., Wang, L., Capparelli, E.V., Adams, C., Sun, J., Jain, S., He, F., Arellano, D.A., Mash, L.E., Chukoskie, L., Lincoln, A., Townsend, J., 2017. Low-dose suramin in autism spectrum disorder: a small, phase I/II, randomized clinical trial. Ann. Clin. Transl. Neurol. 4, 491–505.
Nieborak, A., Schneider, R., 2018. Metabolic intermediates – Cellular messengers talking to chromatin modifiers. Mol. Metab (Epub ahead of print).
Nikkanen, J., Forsstrom, S., Euro, L., Paetau, I., Kohnz, R.A., Wang, L., Chilov, D., Viinamaki, J., Roivainen, A., Marjamaki, P., Liljenback, H., Ahola, S., Buzkova, J., Terzioglu, M., Khan, N.A., Pirnes-Karhu, S., Paetau, A., Lonnqvist, T., Sajantila, A., Isohanni, P., Tyynismaa, H., Nomura, D.K., Battersby, B.J., Velagapudi, V., Carroll, C.J., Suomalainen, A., 2016. Mitochondrial DNA replication defects disturb cellular dNTP pools and remodel one-carbon metabolism. Cell Metab. 23, 635–648.
Nishi, H., Arai, H., Momiyama, T., 2013. NCI-H295R, a human adrenal cortex-derived cell line, expresses purinergic receptors linked to Ca(2)(+)-mobilization/influx and cortisol secretion. PLoS One 8, e71022.
Nurminskaya, M.V., Belkin, A.M., 2012. Cellular functions of tissue transglutaminase. Int. Rev. Cell Mol. Biol. 294, 1–97.
Osuma, E.A., Riggs, D.W., Gibb, A.A., Hill, B.G., 2018. High throughput measurement of metabolism in planarians reveals activation of glycolysis during regeneration. Regeneration (Wiley) 5, 78–86.
Panossian, A., 2017. Understanding adaptogenic activity: specificity of the pharmacological action of adaptogens and other phytochemicals. Ann. N. Y. Acad. Sci. 1401, 49–64.
Picard, M., McManus, M.J., Gray, J.D., Nasca, C., Moffat, C., Kopinski, P.K., Seifert, E.L., McEwen, B.S., Wallace, D.C., 2015. Mitochondrial functions modulate neuroendocrine, metabolic, inflammatory, and transcriptional responses to acute psychological stress. Proc. Natl. Acad. Sci. U. S. A. 112, E6614–E6623.
Picard, M., Juster, R.P., Sloan, R.P., McEwen, B.S., 2017. Mitochondrial nexus to allostatic load biomarkers. Psychosom. Med. 79, 114–117.
Pincas, H., Choi, S.G., Wang, Q., Jia, J., Turgeon, J.L., Sealfon, S.C., 2014. Outside the box signaling: secreted factors modulate GnRH receptor-mediated gonadotropin regulation. Mol. Cell. Endocrinol. 385, 56–61.
Pizzorno, J.E., Murray, M.T., 2013. Textbook of Natural Medicine, 4th Edition, 4th ed. Elsevier Health Sciences.
Plog, B.A., Nedergaard, M., 2018. The glymphatic system in central nervous system health and disease: past, present, and future. Annu. Rev. Pathol. 13, 379–394.
Porges, S.W., 2007. The polyvagal perspective. Biol. Psychol. 74, 116–143.
Porges, S.W., 2011. The Polyvagal Theory: Neurophysiological Foundations of Emotions, Attachment, Communication, and Self-Regulation. W. W. Norton & Company, New York, NY.
Portt, L., Norman, G., Clapp, C., Greenwood, M., Greenwood, M.T., 2011. Anti-apoptosis and cell survival: a review. Biochim. Biophys. Acta 1813, 238–259.
Powley, T.L., Spaulding, R.A., Haglof, S.A., 2011. Vagal afferent innervation of the proximal gastrointestinal tract mucosa: chemoreceptor and mechanoreceptor architecture. J. Comp. Neurol. 519, 644–660.
Prates Mori, M., de Souza-Pinto, N.C., 2017. Role of mitochondrial dysfunction in the pathophysiology of DNA repair disorders. Cell Biol. Int. 42 (6), 643–650.
Qato, D.M., Ozenberger, K., Olfson, M., 2018. Prevalence of prescription medications with depression as a potential adverse effect among adults in the United States. JAMA J. Am. Med. Assoc. 319, 2289–2298.
Rakel, D., 2018. Integrative Medicine, 4th edition. Elsevier, Philadelphia, PA.
Rissling, M.B., Dennis, P.A., Watkins, L.L., Calhoun, P.S., Dennis, M.F., Beckham, J.C., Hayano, J., Ulmer, C.S., 2016. Circadian contrasts in heart rate variability associated with posttraumatic stress disorder symptoms in a young adult cohort. J. Trauma. Stress. 29, 415–421.
Ristow, M., 2014. Unraveling the truth about antioxidants: mitohormesis explains ROS-induced health benefits. Nat. Med. 20, 709–711.
Rosas-Ballina, M., Olofsson, P.S., Ochani, M., Valdes-Ferrer, S.I., Levine, Y.A., Reardon, C., Tusche, M.W., Pavlov, V.A., Andersson, U., Chavan, S., Mak, T.W., Tracey, K.J., 2011. Acetylcholine-synthesizing T cells relay neural signals in a vagus nerve circuit. Science 334, 98–101.
Saeed-Zidane, M., Linden, L., Salilew-Wondim, D., Held, E., Neuhoff, C., Tholen, E., Hoelker, M., Schellander, K., Tesfaye, D., 2017. Cellular and exosome mediated molecular defense mechanism in bovine granulosa cells exposed to oxidative stress. PLoS One 12, e0187569.
Saier Jr., M.H., Reddy, V.S., Tsu, B.V., Ahmed, M.S., Li, C., Moreno-Hagelsieb, G., 2016. The transporter classification database (TCDB): recent advances. Nucleic Acids Res. 44, D372–D379.
Saint-Maurice, P.F., Troiano, R.P., Matthews, C.E., Kraus, W.E., 2018. Moderate-to-vigorous physical activity and all-cause mortality: do bouts matter? J. Am. Heart Assoc. 7.
Sakaki, H., Tsukimoto, M., Harada, H., Moriyama, Y., Kojima, S., 2013. Autocrine regulation of macrophage activation via exocytosis of ATP and activation of P2Y11 receptor. PLoS One 8, e59778.
Schmunk, G., Nguyen, R.L., Ferguson, D.L., Kumar, K., Parker, I., Gargus, J.J., 2017. High-throughput screen detects calcium signaling dysfunction in typical sporadic autism spectrum disorder. Sci. Rep. 7, 40740.
Semenza, G.L., 2011. Hypoxia-inducible factor 1: regulator of mitochondrial metabolism and mediator of ischemic preconditioning. Biochim. Biophys. Acta 1813, 1263–1268.
Silva, J.M., Wong, A., Carelli, V., Cortopassi, G.A., 2009. Inhibition of mitochondrial function induces an integrated stress response in oligodendroglia. Neurobiol. Dis. 34, 357–365.
Siso, S., Jeffrey, M., Gonzalez, L., 2010. Sensory circumventricular organs in health and disease. Acta Neuropathol. 120, 689–705.
Sivanand, S., Rhoades, S., Jiang, Q., Lee, J.V., Benci, J., Zhang, J., Yuan, S., Viney, I., Zhao, S., Carrer, A., Bennett, M.J., Minn, A.J., Weljie, A.M., Greenberg, R.A., Wellen, K.E., 2017. Nuclear acetyl-CoA production by ACLY promotes homologous recombination. Mol. Cell 67 (252–265), e256.
Sorice, M., Garofalo, T., Misasi, R., Manganelli, V., Vona, R., Malorni, W., 2012. Ganglioside GD3 as a raft component in cell death regulation. Anti Cancer Agents Med. Chem. 12, 376–382.
Sterling, P., Eyer, J., 1988. Allostasis: a new paradigm to explain arousal pathology. In: Fisher, S., Reason, J. (Eds.), Handbook of Life Stress, Cognition, and Health. John Wiley & Sons, Inc., New York, NY, pp. 629–649.
Surowiec, I., Arlestig, L., Rantapaa-Dahlqvist, S., Trygg, J., 2016. Metabolite and lipid profiling of biobank plasma samples collected prior to onset of rheumatoid arthritis. PLoS One 11, e0164196.
Takatani, T., Takahashi, Y., Yoshida, R., Imai, R., Uchiike, T., Yamazaki, M., Shima, M., Nishikubo, T., Ikada, Y., Fujimoto, S., 2018. Relationship between frequency spectrum of heart rate variability and autonomic nervous activities during sleep in newborns. Brain and Development 40, 165–171.
Tan, S.Y., Grimes, S., 2010. Paul Ehrlich (1854–1915): man with the magic bullet. Singap. Med. J. 51, 842–843.
Thomas, C., Baker, C.I., 2013. Teaching an adult brain new tricks: a critical review of evidence for training-dependent structural plasticity in humans. NeuroImage 73, 225–236.
Uno, M., Nishida, E., 2016. Lifespan-regulating genes in *C. elegans*. NPJ. Aging Mech. Dis. 2, 16010.
Valentijn, F.A., Falke, L.L., Nguyen, T.Q., Goldschmeding, R., 2018. Cellular senescence in the aging and diseased kidney. J Cell Commun Signal 12, 69–82.
van der Vusse, G.J., 2011. The fascinating and elusive life of cardiac fatty acids. Cardiovasc. Res. 92, 363–364.
Varma, V.R., Oommen, A.M., Varma, S., Casanova, R., An, Y., Andrews, R.M., O'Brien, R., Pletnikova, O., Troncoso, J.C., Toledo, J., Baillie, R., Arnold, M., Kastenmueller, G., Nho, K., Doraiswamy, P.M., Saykin, A.J., Kaddurah-Daouk, R., Legido-Quigley, C., Thambisetty, M., 2018. Brain and blood metabolite signatures of pathology and progression in Alzheimer disease: a targeted metabolomics study. PLoS Med. 15, e1002482.
Venter, J.C., Remington, K., Heidelberg, J.F., Halpern, A.L., Rusch, D., Eisen, J.A., Wu, D., Paulsen, I., Nelson, K.E., Nelson, W., Fouts, D.E., Levy, S., Knap, A.H., Lomas, M.W., Nealson, K., White, O., Peterson, J., Hoffman, J., Parsons, R., Baden-Tillson, H., Pfannkoch, C., Rogers, Y.H., Smith, H.O., 2004. Environmental genome shotgun sequencing of the Sargasso Sea. Science 304, 66–74.
Verkhratsky, A., Burnstock, G., 2014. Biology of purinergic signalling: its ancient evolutionary roots, its omnipresence and its multiple functional significance. BioEssays News Rev. Mol. Cellular Dev. Biol. 36, 697–705.
Vogt, A.M., Elsasser, A., Nef, H., Bode, C., Kubler, W., Schaper, J., 2003. Increased glycolysis as protective adaptation of energy depleted, degenerating human hibernating myocardium. Mol. Cell. Biochem. 242, 101–107.
Wallace, D.C., 2010. Colloquium paper: bioenergetics, the origins of complexity, and the ascent of man. Proc. Natl. Acad. Sci. U. S. A. 107 (Suppl. 2), 8947–8953.
Wallace, D.C., Fan, W., 2010. Energetics, epigenetics, mitochondrial genetics. Mitochondrion 10, 12–31.
Wang, Y., Subramanian, M., Yurdagul Jr., A., Barbosa-Lorenzi, V.C., Cai, B., de Juan-Sanz, J., Ryan, T.A., Nomura, M., Maxfield, F.R., Tabas, I., 2017. Mitochondrial fission promotes the continued clearance of apoptotic cells by macrophages. Cell 171 (331–345), e322.
Wiley, J.F., Gruenewald, T.L., Karlamangla, A.S., Seeman, T.E., 2016. Modeling multisystem physiological dysregulation. Psychosom. Med. 78, 290–301.
Will, Y., Dykens, J.A., 2018. Mitochondrial Dysfunction Caused by Drugs and Environmental Toxicants. John Wiley & Sons, Inc., Hoboken, NJ, USA.
Yee, D.C., Shlykov, M.A., Vastermark, A., Reddy, V.S., Arora, S., Sun, E.I., Saier Jr., M.H., 2013. The transporter-opsin-G protein-coupled receptor (TOG) superfamily. FEBS J. 280, 5780–5800.
Yoshimi, N., Futamura, T., Kakumoto, K., Salehi, A.M., Sellgren, C.M., Holmen-Larsson, J., Jakobsson, J., Palsson, E., Landen, M., Hashimoto, K., 2016. Blood metabolomics analysis identifies abnormalities in the citric acid cycle, urea cycle, and amino acid metabolism in bipolar disorder. BBA Clin. 5, 151–158.
Yu, X., Li, H., Murphy, T.A., Nuss, Z., Liles, J., Liles, C., Aston, C.E., Raj, S.R., Fedorowski, A., Kem, D.C., 2018. Angiotensin II type 1 receptor autoantibodies in postural tachycardia syndrome. J. Am. Heart Assoc. 7.
Yuan, T.F., Li, A., Sun, X., Ouyang, H., Campos, C., Rocha, N.B.F., Arias-Carrion, O.,

Machado, S., Hou, G., So, K.F., 2016. Transgenerational inheritance of paternal neurobehavioral phenotypes: stress, addiction, ageing and metabolism. Mol. Neurobiol. 53, 6367–6376.
Zhang, Y., Strehin, I., Bedelbaeva, K., Gourevitch, D., Clark, L., Leferovich, J., Messersmith, P.B., Heber-Katz, E., 2015. Drug-induced regeneration in adult mice. Sci. Transl. Med. 7, 290ra292.
Zhong, Z., Liang, S., Sanchez-Lopez, E., He, F., Shalapour, S., Lin, X.-J., Wong, J., Ding, S., Seki, E., Schnabl, B., Hevener, A.L., Greenberg, H.B., Kisseleva, T., Karin, M., 2018. New mitochondrial DNA synthesis enables NLRP3 inflammasome activation. Nature (Epub ahead of print).
Zhou, J.H., Zhang, T.T., Song, D.D., Xia, Y.F., Qin, Z.H., Sheng, R., 2016. TIGAR contributes to ischemic tolerance induced by cerebral preconditioning through scavenging of reactive oxygen species and inhibition of apoptosis. Sci. Rep. 6, 27096.
Zimmermann, M., Reichert, A.S., 2017. How to get rid of mitochondria: crosstalk and regulation of multiple mitophagy pathways. Biol. Chem. 399, 29–45.

biology

MDPI

Review

Incomplete Healing as a Cause of Aging: The Role of Mitochondria and the Cell Danger Response

Robert K. Naviaux

The Mitochondrial and Metabolic Disease Center, Departments of Medicine, Pediatrics, Pathology, University of California, San Diego School of Medicine, San Diego, CA 92103, USA; Naviaux@ucsd.edu; Tel.: +1-619-993-2904

Received: 9 January 2019; Accepted: 20 February 2019; Published: 11 May 2019

Abstract: The rate of biological aging varies cyclically and episodically in response to changing environmental conditions and the developmentally-controlled biological systems that sense and respond to those changes. Mitochondria and metabolism are fundamental regulators, and the cell is the fundamental unit of aging. However, aging occurs at all anatomical levels. At levels above the cell, aging in different tissues is qualitatively, quantitatively, and chronologically distinct. For example, the heart can age faster and differently than the kidney and vice versa. Two multicellular features of aging that are universal are: (1) a decrease in physiologic reserve capacity, and (2) a decline in the functional communication between cells and organ systems, leading to death. Decreases in reserve capacity and communication impose kinetic limits on the rate of healing after new injuries, resulting in dyssynchronous and incomplete healing. Exercise mitigates against these losses, but recovery times continue to increase with age. Reinjury before complete healing results in the stacking of incomplete cycles of healing. Developmentally delayed and arrested cells accumulate in the three stages of the cell danger response (CDR1, 2, and 3) that make up the healing cycle. Cells stuck in the CDR create physical and metabolic separation—buffer zones of reduced communication—between previously adjoining, synergistic, and metabolically interdependent cells. Mis-repairs and senescent cells accumulate, and repeated iterations of incomplete cycles of healing lead to progressively dysfunctional cellular mosaics in aging tissues. Metabolic cross-talk between mitochondria and the nucleus, and between neighboring and distant cells via signaling molecules called metabokines regulates the completeness of healing. Purinergic signaling and sphingolipids play key roles in this process. When viewed against the backdrop of the molecular features of the healing cycle, the incomplete healing model provides a new framework for understanding the hallmarks of aging and generates a number of testable hypotheses for new treatments.

Keywords: cell danger response; healing cycle; mitochondria; purinergic signaling; metabokines; sphingolipids; integrated cell stress response; de-emergence; crabtree effect; pasteur effect

1. Introduction

Some of the oldest [1], and the most recent [2,3] scientific publications on the biology of aging have focused on nutrition and metabolism as prime drivers. Mitochondria are located at the hub of the wheel of cellular metabolism. The mitochondrial proteome is transcriptionally and post-transcriptionally regulated according to tissue-specific needs [4], consists of about 1300 proteins [5], responds to injury [6], food quality [7], exercise [8], environmental pollution [9], and coordinates the cell danger response (CDR) [10]. The CDR is a term that was coined in 2014 [10], but includes elements of inflammation and healing that have been studied since before the time of Hippocrates (c. 460–370 BCE) [11]. The CDR is an evolutionarily conserved, multi-system response of multicellular organisms that is used to manage and heal from threat or injury. The CDR is a graded response that consists of nested layers that range

from the molecular control of electron utilization and cellular oxygen consumption, through changes in the microbiome, mast cells and immune system, to the autonomic nervous system, enteric nervous system, and neuroendocrine circuits that are needed for whole-body integration of the response. When analyzed at the molecular and single-cell level, a widely-studied component of the CDR is known as the integrated cell stress response (ICSR) [12–14].

2. Defining Cellular Stress

In this paper, the word "stress" has a specific scientific meaning. Stress is any force, condition, chemical, pathogen or other stimulus that acts to perturb cellular function, requiring the expenditure of energy and resources to return the cell to its pre-stimulus or to a new steady state. Remarkably, psychological stresses, particularly early life stresses (ELS), regulate some of the same metabolic and gene expression networks used to defend the cell from microbial pathogens, physical injury, poisoning, and adversity of many other types [15–17]. In the case of major depressive disorder, innate immune/pro-inflammatory gene expression is increased, while adaptive immune/anti-inflammatory/pro-resolving gene expression is decreased [18]. Greater stresses stimulate proportionately more nucleotide and metabolite release through cell membrane channels [19], leading to greater metabokine and purinergic signaling [20,21]. Learning and development emerge from both conscious stresses and subconscious chemical stresses encountered throughout life. Stresses lead to metabolic memories that help cells and tissues improve future responses to previously encountered conditions [22]. Transient increases in the mitochondrial and cellular sources of reactive oxygen species (ROS) such as superoxide and hydrogen peroxide, reactive nitrogen species (RNS) such as nitric oxide (NO) and peroxynitrite (ONO_2^-), reactive aldehydes (RAs), and dissolved oxygen itself, help to regulate cellular redox. Redox, in turn, regulates the efflux of metabolites from the cell via membrane channels and transporters that contain redox-responsive cysteine disulfide residues [23]. Pulses of dissolved oxygen occur with a carbohydrate-rich meal because of the transient inhibitory effect of glucose on mitochondria produced by the Crabtree effect [24]. ROS, insulin, and IL1β are also stimulated naturally by every meal and can vary in magnitude according to the nutrient content of the meal [25]. As the dissolved oxygen concentration rises within the cell, glycolysis becomes inhibited by the Pasteur effect, creating a natural brake on an unchecked inhibition of mitochondrial oxphos from the meal-associated glucose and the Crabtree effect. However, glucose, oxygen, ROS, RNS, and RAs are only a part of the multi-faceted metabolic signaling network that is used to control cellular reactivity, epigenetic marking, and gene expression. Over 100 chemosensory G-protein coupled receptors respond to metabokines and peptides released after stress and injury and regulate the healing cycle [11].

3. The Healing Cycle

The mitochondrial responses that initiate and maintain the CDR are used to control cellular bioenergetics, oxygen utilization, redox signaling, and metabolism needed for healing [6] and regeneration [26] after injury or threat. The stages of the CDR are illustrated in Figure 1. Wakeful activity with nutrient intake, followed by restorative sleep are essential parts of health. These activities stimulate an integrated mix of three metabolic states that are controlled locally by metabolic signaling, and systemically by the central nervous system (CNS). Healthy whole-body function requires the coordination and use of cell-specific (1) glycolysis, (2) aerobic glycolysis, and (3) oxidative phosphorylation for energy and metabolism (Figure 1). Chemical activity associated with nutrient intake, brain activity, and basal metabolism, and added physical activity from natural child play or adult exercise lead to the graded release of extracellular ATP and related nucleotides, and to glutamate release [27,28] through stress-gated P2X7-pannexin and other channels in the cell membrane [19]. Once outside the cell, ATP and related nucleotides participate in purinergic signaling. Receptor binding to ATP and ADP leads to IP3-gated intracellular calcium release [29] and contextual changes in gene expression through autocrine and paracrine signaling pathways [30]. After extracellular metabolism by CD73 and CD39, ATP is converted to ADP, AMP, and to adenosine that acts to inhibit

excess chemical stimulation and plays a key role in initiating and maintaining sleep by binding to P1/Adenosine /ADORA A2AR and A1R receptors [31]. This is illustrated as the restorative sleep cycle in Figure 1.

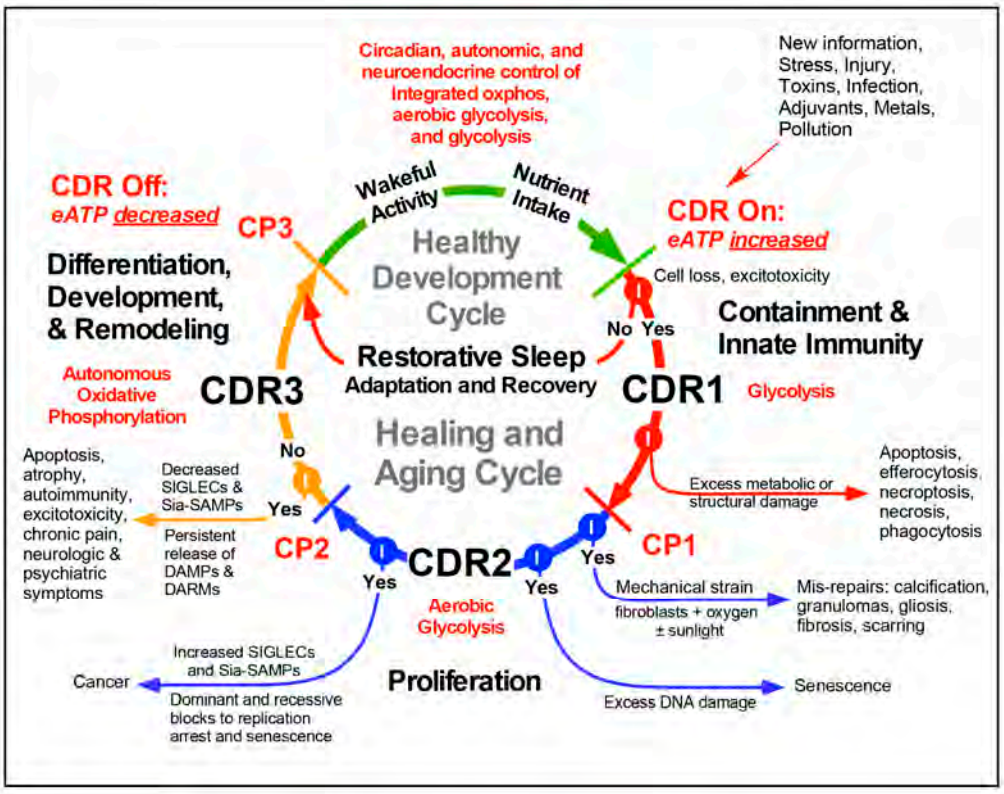

Figure 1. The metabolic features of the health and healing cycles. Abbreviations: CDR—cell danger response, eATP—extracellular ATP, CP1-3—checkpoints 1, 2, and 3, DAMP—damage-associated molecular pattern, DARM—damage-associated reactive metabolites, SIGLEC—sialic acid binding immunoglobulin-type lectin, e.g., CD33-related SIGLECs (CD33r-SIGLECs), Sia-SAMP—sialoglycan self-associated molecular pattern.

When the stress is of sufficient magnitude to cause cell death, more ATP is released and acts as a pro-inflammatory damage-associated molecular pattern (DAMP). Increased extracellular ATP triggers entry into the CDR1 stage of the healing cycle (Figure 1). Once the CDR is triggered, three different metabolic stages must be activated in sequence to heal. Healing cannot occur without activation of this metabolically-controlled cycle. CDR1 is characterized by the upregulation of anaerobic glycolysis and a reallocation of cellular resources for defense, damage containment, innate immunity, and repair at the expense of normal differentiated tissue function. Gap junctions between cells are decreased or lost as the tissue structure is disrupted by injury, and cell-autonomous functions become primary and metabolic cooperation between neighboring cells is decreased or suspended. Platelets and neutrophils are recruited to sites of injury or infection. CDR2 uses aerobic glycolysis to support stem cell recruitment and cell division needed for biomass replacement of cells lost in CDR1. If cell loss is not replaced, then age-related atrophy and sarcopenia occur. If excessive DNA damage is sustained by a cell in CDR2, replicative senescence occurs [32]. If the blocks to senescence are broken, then cancer can occur. If oxygen levels are high and significant mechanical strain is present, tissue fibrosis or wound scarring is stimulated (Figure 1). Fibrosis is one of several different types of mis-repairs that contribute to the symptoms of aging [33–35] (Figures 1–3).

In CDR3, cell-autonomous, aerobic metabolism by mitochondrial oxidative phosphorylation is gradually restored as new cells born in CDR2 take up residence in the recovering tissue and establish new tissue-specific contacts and gap junctions needed to extinguish the gene expression programs used

for defense and growth in CDR1 and CDR2, and to restore normal differentiated cell, tissue, and organ function. If damage-associated molecular pattern (DAMP) and damage-associated reactive metabolite (DARM) release persists [36] or if ROS production is extinguished prematurely [37], autoimmunity can develop [38]. The adaptive immune response is regulated in CDR3. Persistent DAMP and DARM release can stimulate excitotoxicity in cells still in the CDR1 and CDR2 stages within a dyssynchronous mosaic of healing cells. With the completion of CDR3, the concentration of metabokines and DAMPS in the extracellular space is actively reduced to levels compatible with restoration of cell specialization and reintegration of cells back into a metabolically optimized cellular network. Re-integration and re-specialization are necessary for cells that have recently exited the CDR in order to re-establish their responsiveness to circadian patterns of wakeful activity and restorative sleep (Figure 1).

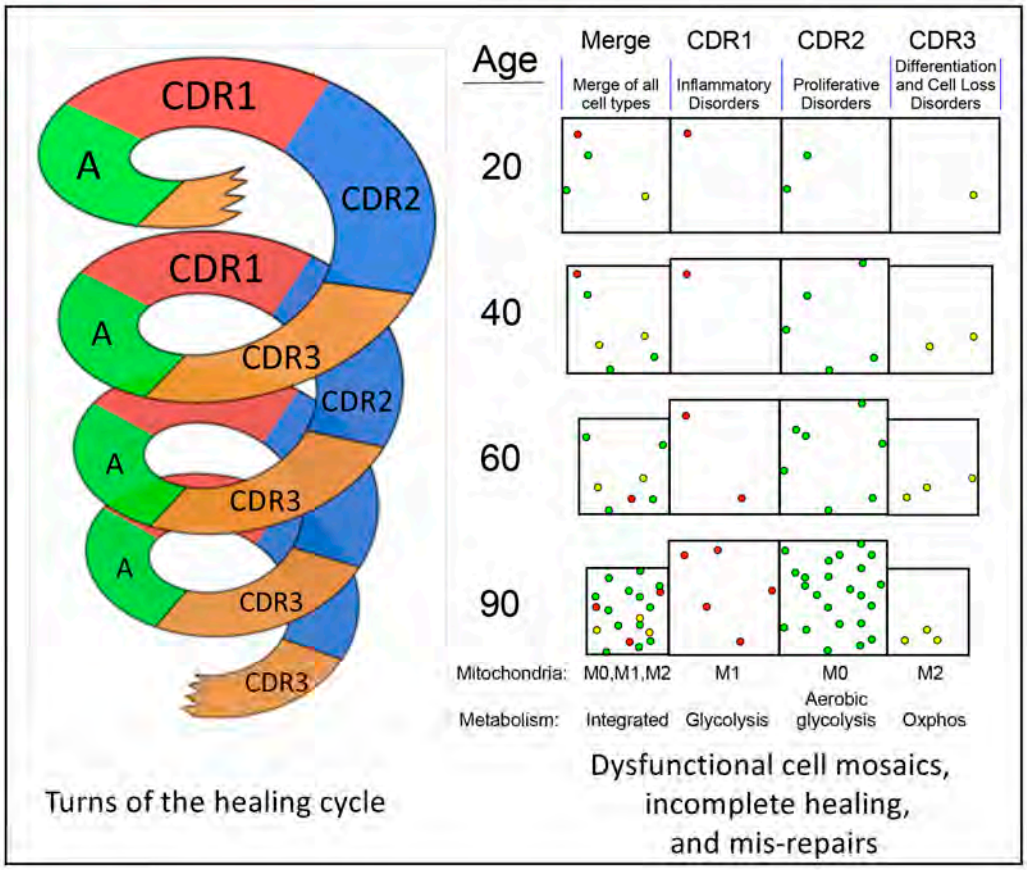

Figure 2. Repeated cycles of incomplete healing lead to aging and age-related disease. The spiral represents sequential turns of the healing cycle throughout life. Colored cells in the boxes on the right represent cells that have been delayed or arrested in a stage of the healing cycle. The decreased size of some boxes represents the loss in tissue volume from cell loss and atrophy. In this example, most arrested or delayed cells in the merge on the right after 60 and 90 years are in CDR2 (green). This will create an increased risk of proliferative disorders such as diabetes, heart disease, and cancer. Color code: CDR1 cells—red; CDR2 cells—green; CDR3 cells—yellow. Abbreviations: A—wakeful activity and nutrient intake. M1—mitochondria adapted for cell defense, reactive oxygen, nitrogen, and aldehyde production; M0—mitochondria adapted for cell growth and Warburg metabolism; M2—mitochondria adapted for oxidative phosphorylation (oxphos).

The sequence and stages of the healing cycle are highly conserved and tightly choreographed. Once pathological stress or cell death occurs, the same stages of the healing cycle are activated and restore normal function after any recoverable injury (Figure 2). Inevitably, some cells fail to complete the healing cycle and are left behind with each turn of the cycle. These arrested or delayed cells are unable to return to a normal metabolism and the gene expression pattern that is needed for peak

differentiated cell and organ function (Figure 2). As non-specialized cells and mis-repairs such as fibrosis accumulate in incomplete stages of the healing cycle, the peak performance of tissues is degraded over time, and the risk for age-related disease is increased.

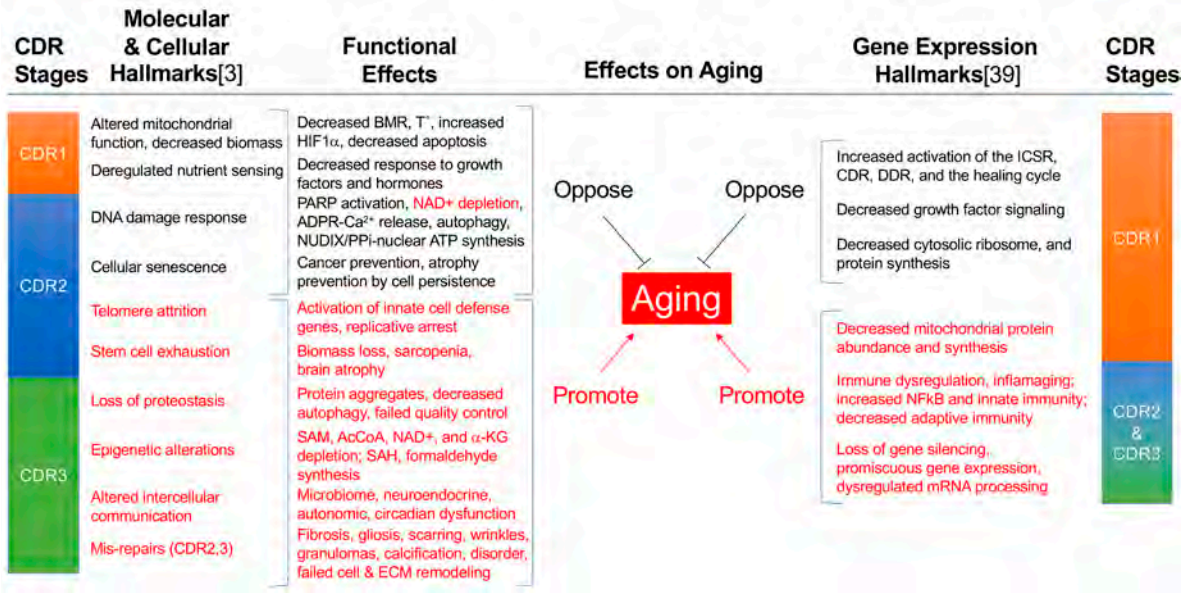

Figure 3. The hallmarks of aging as natural products of incomplete healing and the cell danger response [3,39]. Black font: hallmarks that oppose aging. Red font: hallmarks that promote aging. Abbreviations: CDR—cell danger response, ICSR—integrated cell stress response, DDR—DNA damage response, BMR—basal metabolic rate, T°—basal body temperature, HIF1α—hypoxia inducible factor 1α, PARP—poly ADP ribose polymerase, NAD+—nicotinamide adenine dinucleotide, ADPR—adenosine diphosphate ribose, SAM—S-adenosyl methionine, AcCoA—acetyl CoA, α-KG—alpha ketoglutarate, SAH—S-adenosyl homocysteine, PPi—pyrophosphate, NUDIX—nucleoside diphosphate X hydrolases, e.g., NUDT5, ECM—extracellular matrix.

4. Three Functionally-Polarized Forms of Mitochondria Are Used by the CDR

For over 60 years, mitochondria have been thought of as "damaged" or "dysfunctional" if they shift from energy production by oxidative phosphorylation to ROS production or shift from burning carbon skeletons to CO_2 and water to synthesizing new carbon skeletons for export as building blocks needed for cell growth. Yet mitochondria shift regularly and necessarily between these states throughout life. A simplified way of understanding the alternative differentiation states of mitochondria is to see the organelles as the metabolic gate-keepers of the electrons harvested by breaking down the carbon–carbon bonds in food. In this scheme, electrons can be used in mitochondria: (1) to fully reduce oxygen (O_2) to water (H_2O) while capturing the released chemical energy to make ATP by oxidative phosphorylation in the third stage of the cell danger response, CDR3 and in health, (2) to partially reduce oxygen to superoxide radicals (O_2^-) and hydrogen peroxide (H_2O_2) while relying on anaerobic glycolysis for ATP synthesis in CDR1 and cell defense, or (3) to use the electrons to synthesize new carbon–carbon bonds to produce and export building blocks such as citrate for cell membrane lipid synthesis or orotic acid for pyrimidine synthesis, while still consuming oxygen to make water and making ATP by aerobic glycolysis in CDR2 and cell growth (Figure 1).

A new nomenclature was introduced in 2017 to describe these three, functionally-polarized forms of mitochondria of the CDR [11,29]. All three "species" of mitochondria co-exist in different proportions in cells throughout development and aging in all multicellular organisms. The transition between states is determined by the interaction between nutrition and metabolism, the developmental and chronological age of the organism, the recent state of cell danger signaling and healing, and ambient environmental conditions. The naming of the differentiation states of mitochondria was based on the

recognition that the pro-inflammatory state of macrophages known as M1 macrophages corresponded with the ROS producing capacity of their mitochondria and energy production by glycolysis [40]. The anti-inflammatory/pro-resolving M2 macrophages were found to contain mitochondria adapted for oxidative phosphorylation (oxphos). M0 macrophages are not yet committed to a fully M1 or M2 phenotype and contain mitochondria that are intermediate between M1 and M2. In the healing cycle, three different mitochondrial differentiation states are used to meet the specialized needs of each stage of the CDR. M1 mitochondria are used in CDR1. M0 mitochondria are used in CDR2, and M2 mitochondria are used in CDR3 (Figures 1 and 2, Table 1).

In vitro protocols have recently been developed that distinguish between M1, M0, and M2 macrophages experimentally based on mitochondrial phenotypes [41]. M1 mitochondria consume small amounts of oxygen, have a low spare respiratory capacity (SRC, or physiologic reserve capacity), can use fatty acids for ROS production and NLRP3 assembly [42], are not dependent on glutamine, and the cells containing M1 mitochondria produce large amounts of lactic acid. In contrast, M2 mitochondria consume more oxygen at baseline, can use both glucose oxidized to pyruvate and fatty acids for oxphos, have a higher SRC, are dependent on glutamine for the fully differentiated phenotype, and the cells produce small amounts of acid. M0, uncommitted or multipotential mitochondria have a low basal oxygen consumption similar to M1, shunt some glucose down the pentose phosphate pathway (PPP) for NADPH and building block production, have an SRC that is intermediate between M2 and M1 organelles, and produce small amounts of extracellular acid, similar to M2 [41] (Table 1).

Table 1. Phenotypic characteristics of animal cell mitochondria.

No.	Trait	Mitochondrial Phenotype [40,41,43]		
		M0	**M1**	**M2**
1	Cellular energy metabolism	Aerobic glycolysis	Glycolysis	Oxidative phosphorylation
2	Mitochondrial DNA copy number	Intermediate	Low	High
3	Predominant morphology	Intermediate	Punctate	Filamentous
4	Cell replicative potential	High (Warburg)	Intermediate	Low
5	Cell multilineage regenerative potential	High	Low	Low
6	Cell differentiation potential	Low	Intermediate	High
7	Cell cancer potential	High	Intermediate	Low
8	Inflammatory potential	Intermediate	High	Low
9	Cell susceptibility to killing by apoptosis	Low	Intermediate	High
10	Inducible organellar quality control	Intermediate	Low	High
11	Baseline oxygen consumption	Low	Low	High
12	Stressed (uncoupled) oxygen consumption above baseline (spare respiratory capacity)	Intermediate	Low	High
13	ROS production	Intermediate	High	Low
14	NLRP3 inflammasome assembly	Low	High	Low
15	Lactate release from cells	Intermediate	High	Low
16	Pentose phosphate pathway (PPP)	High—NADPH for biosynthesis and cell growth	Intermediate—NADPH for NOX	Intermediate—NADPH for redox

Table 1. *Cont.*

No.	Trait	Mitochondrial Phenotype [40,41,43]		
		M0	**M1**	**M2**
17	Use of fatty acid oxidation (FAO)	Fatty acid synthesis for growth > FAO	For ROS and NLRP3 activation	For oxphos
18	Use of glucose	Glycolysis and PPP	Glycolysis and lactate release	PPP and pyruvate for oxphos
19	Use of glutamine	High: citrate for ATP citrate lyase and Acetyl-CoA	Low	High: oxphos via alpha-ketoglutarate
20	Stage of greatest use in the healing cycle and cell danger response	CDR2	CDR1	CDR3

M0, M1, and M2 mitochondrial phenotypes also occur in solid tissues and can be recognized in part by morphological criteria. Mitochondria can be described informally as being distributed along a spaghetti (filamentous) and meatball (punctate) gradient. M2 mitochondria are filamentous and interconnected, and predominate in post-mitotic or slowly regenerating tissues. M1 mitochondria are punctate, and M0 mitochondria are intermediate in form, with both short filaments and punctate organelles reminiscent of the coccobacillary forms of their proteobacterial ancestors [44]. Mitochondrial fusion–fission dynamics naturally regulate the balance between fused and elongated mitochondria, and fragmented/fissioned mitochondria according the growth and metabolic characteristics of the cell [45]. M0, uncommitted, or stem-like mitochondria predominate in cells that survive after exposure to chemotherapeutic agents or toxins [46]. M2 mitochondria under these conditions are depleted by DRP1-dependent fission/fragmentation, and conversion to M1 organelles prior to cell removal by apoptosis. Similar transitions in mitochondrial structure and function are readily demonstrated in brain astroglia before and after treatment with pro-inflammatory triggers such as lipopolysaccharide (LPS) and interferon gamma (IFN-γ) [43].

The total mitochondrial biomass is decreased naturally after triggering the cell danger response (CDR) with toxins [46], physical injury [6], infection, or any trigger that activates the healing cycle [11]. Mitochondrial biomass can also be reduced experimentally by the dominant-negative expression of the D1135A allele of the mitochondrial polymerase gamma (POLG1) to deplete mitochondrial DNA copy numbers by about 50% [47]. This mouse model mimics the mitochondrial defects that are a well-established hallmark of aging [48]. The phenotypes of aging found in this model included increased NFkB and matrix metalloproteinase 9 (MMP9) expression, increased inflammation, age spots, wrinkled skin, and premature hair loss. These transcriptional and anatomical signs of aging were reversed within 1 month of treatment in mice by unblocking mtDNA synthesis and restoring normal mtDNA copy numbers [47].

5. The Importance of Nucleotides and Purinergic Signaling

Of an estimated 1300 mitochondrial protein coding genes, 1158 are catalogued in MitoCarta v2.0 [5]. Only 13 mitochondrial proteins are encoded by mitochondrial DNA (mtDNA). The remaining 1145 are encoded by nuclear genes that are subject to tissue-specific gene expression programs. At least 789 mitochondrial proteins (68% of 1158) are enzymes with catalytic functions that have been assigned enzyme commission (EC) numbers, or encode subunits of multi-protein enzyme complexes such as those in respiratory chain complexes I, II, III, IV, and V, or are transporters, or kinases that use ATP (Table S1). At least 433 (55% of 789) of these proteins are regulated by the availability of purine and pyrimidine nucleotides such as ATP, GTP, UTP, NAD(P)+, or FAD either as substrates, or as allosteric regulators (Table S1). No other single class of molecules regulates more of the mitochondrial proteome than the nucleotides. In addition, an unknown fraction of nuclear mitochondrial genes is regulated

transcriptionally and post-transcriptionally by purinergic signaling via the 12 G-protein coupled receptors (GPCRs; 4 P1R and 8 P2YR) and seven ionotropic receptors (P2XR) that are widely distributed in all tissues [49]. Some purinergic receptors are also expressed in intracellular compartments such as mitochondria, lysosomes, and the nucleus [50]. For example, P2X6 receptors are translocated to the nucleus in an age-dependent manner, interact with mRNA splicing factor 3A1, decrease mRNA processing, and contribute to aging [51].

6. The Importance of Nutrition in Healing and Aging

Different stages in child development, human aging, and athletic performance have different specific nutrients and calories that produce the best outcomes at each stage [52–54]. Based on measured differences in mitochondrial substrate preferences between M1, M0, and M2 organelles (Table 1), it is hypothesized that each stage of the healing cycle—CDR 1, 2, and 3 in Figure 1, and even certain chronic illnesses stuck in one of the three stages of the CDR [11]—will also have different stage-specific nutritional needs for optimal outcomes. Both chemical mass action from substrate supply and metabolite signaling via metabokines [11] are likely to be important mechanistically. Some of the broadest clues that connect nutrition with aging, mitochondria, and healing come from studies of caloric restriction [3]. Natural aging results in a reduction in the rate of turnover of mitochondria (mitochondrial biogenesis, or "mitochondriogenesis"), and a decrease in mitochondrial protein synthesis, standing mitochondrial biomass, respiratory reserve capacity, and oxphos function [55] (Figure 3). Caloric restriction, on the other hand, stimulates mitochondrial turnover through pathways associated with AMPK-stimulated autophagy and mitophagy [56]. This leads to improved mitochondrial quality control, oxphos function, and reserve capacity, but does not increase overall mitochondrial biomass measured as mtDNA copy number [57]. Caloric restriction also leads to a decrease in circulating thyroid hormone, decreased resting energy expenditure (REE), and a decrease in circulating anabolic hormones such as IGFI, insulin, human growth hormone, and testosterone [58]. From an evolutionary point of view, this hypometabolic response allows fewer calories to be consumed while opposing weight loss during periods of seasonal hardship.

Caloric restriction is a classical trigger of a reversible, stress-resistant, non-reproductive stage in the nematode *Caenorhabditis elegans* called dauer. Dauer has been the source of discovery of many longevity genes and has stimulated a productive discussion of the difference between lifespan and healthspan extension [59]. Dauer permits animals to live for up to 4 months under harsh conditions instead of their normal lifespan of 2 weeks. However, longevity in dauer comes at the cost of much reduced function and many changes associated with altered sensory anatomy [60], repetitive behaviors [61] and metabolism [62]. When calories are restored to animals in dauer, they exit the stage and re-enter their normal life-cycle, picking up where they left off, as if little or no biological aging had occurred during the time they spent in dauer [63].

More specific changes in nutrient supply also play an important role in aging and healing. Dietary supplementation with branch chain amino acids at a level of 1.5 g/kg/day, corresponding to about 1% of daily calorie intake in mice, has been shown to extend lifespan by about 10% [64]. This effect required normal production of nitric oxide (NO) by endothelial nitric oxide synthase (eNOS) [64]. The selective addition of a stoichiometric mix of essential amino acids (EAAs) including branch chain amino acids, also has anti-cancer effects by promoting growth inhibition and apoptosis in transformed but not in normal cells [65]. EAAs also promoted wound healing by moderating inflammation in the early stages, and maintaining TGFβ needed for tissue remodeling in the later stages of healing [66]. This later effect is in what would be called CDR3 in the model presented here (Figure 1). Interestingly, TGF β (DAF-7) signaling also plays a key role in recovery from dauer and the re-establishment of normal development in *C. elegans* [67].

7. Progressively Dysfunctional Cellular Mosaics

The number of nucleated cells in a 70-kg adult male is about 5×10^{12}. Non-nucleated red blood cells are 5-times more abundant (2.5×10^{13}), but make up just 6.5% of the total mass of an adult [68]. The total number of human cells in an adult is 3.0×10^{13}. There are also 3.8×10^{13} bacterial cells in a typical adult body [68]. Cells die every day and must be replaced. It is estimated that an adult turns over about 1×10^{10} (10 billion; about 10 grams of) cells/day by apoptosis [69]. This is equivalent to about 1 in 500 nucleated cells/day removed by apoptosis. The distribution of cell turnover is highly heterogeneous. Most spontaneous, or physiologic cell death with replacement occurs in short-lived cells such as those in bone marrow, intestines, skin, and hair follicles whose function is tolerant to spatial changes in tissue architecture produced by continuous cell growth and use-dependent removal or exit of cells from the compartment of origin. These rapidly dividing and structurally malleable tissues can turn over several times per year, with nearly 100% of the cells in these compartments turning over in a few days to weeks or months. Other tissues turn over more slowly. Adipose tissue is replaced at a rate of 10% of the cells per year [70], turning over completely in about 10 years. Skeletal muscle turns over at a rate of 6.6% per year [71]. Muscle fiber loss accelerates after age 60, leading to sarcopenia [72]. The kidneys weigh about 150 grams each, shed about 1.7×10^6 epithelial cells/day into the urine [73], and replace this loss and other losses by cell division and remodeling from recruited stem cells [74]. The adult liver weighs about 1400 grams and consists of about 2.4×10^{11} cells and replaces about 1.8% per year as a young adult, but fewer as liver size decreases with age [75]. Heart cells are replaced at a rate of 1% per year at age 25, falling to 0.45% per year at age 75 [76], and pancreatic islet β-cells are long-lived and not replaced after age 30 years [77].

Exposure to physical injury, toxins, or infection adds pathological cell death to the basal level of physiologic cell death described above. When a cell dies physiologically by apoptosis, the inflammatory reactions associated with CDR1 are avoided. Instead, the tissue skips to CDR2 and CDR3 to replace the lost cell and restore normal metabolism and tissue-specific gene expression patterns (Figure 1). The number of cells that die pathologically during a typical viral or bacterial infection will be dependent on the type of microbial pathogen and the severity of the infection, but the exact cell numbers lost in the course of a typical infection are not known. An average child has 5–6 recognized viral or bacterial infections each year for the first 5 years of life, then 2–3 per year throughout adult life [78]. Pathological cell death caused by infection, toxins, or injury will trigger inflammation and entry into the healing cycle by activating CDR1. As a thought experiment, one can imagine a systemic viral infection that might kill 1×10^{10} cells (about 10 grams, or 2 teaspoons), a number equal to the basal loss per day by apoptosis. Somatic DNA mutation rates are about 2.7×10^{-5} per typical 10,000 bp, protein-coding locus per cell division [79]. In this example, one turn of the healing cycle would result in 270,000 cells (10^{10} cells replaced $\times$ 2.7×10^{-5} mutations/gene/division = 270,000 cells) sustaining a mutation that marks that cell as different from neighboring cells in the tissue. Mitotic recombination errors and chromosomal microaneuploidy [80], mobilization of retroelements [81] and endogenous retroviruses [82] in recruited stem cells, and reactivation and suppression cycles of latent DNA virus infections [83] will contribute to genetic variation produced by repetitive activation of the CDR over a lifetime. In addition to DNA mutations, there will also be an even larger number of induced and stochastic changes in transcription, post-transcriptional, and metabolic features that lead to changes in cell development.

With each turn of the healing cycle, cells such as neutrophils move out of capillaries and into tissues, releasing ROS via activated NADPH oxidases such as NOX2. Over time, this cyclic process creates tides of reactive oxygen, metabolic, innate immune, and inflammatory defenses that rise with injury and fall during wellness, ebbing and flowing with each turn of the healing cycle. Sialic acid binding immunoglobulin-type lectins (SIGLECs) include the CD33-related molecules expressed on neutrophils, natural killer (NK), macrophages, and T-cells that modulate ROS production, innate immune cell, and adaptive T-cell activity upon binding to sia-SAMPs (sialoglycan self-associated molecular patterns) [84]. Across species, the number of CD33r-SIGLEC genes is associated with

healthy aging in the "wellderly", and decreased numbers accelerate age-related symptoms in mouse models [85]. Many cancers emerge from hypersialated cellular fields that have the effect of dampening the immune response by engaging inhibitory SIGLECs such as Siglec-9 [86]. The ceaseless tides or waves of innate immune cell migration into and out of tissue compartments continues throughout life with each turn of the healing cycle (Figures 1 and 2), and contributes to the progressively dysfunctional mosaics illustrated in Figure 2.

In the brain, a compensatory system of glial–lymphatic (glymphatic) tidal flows occurs by regulated changes in cell volume that are controlled by circadian changes in metabolism [87]. This daily cycle of glympahtic flow helps to remove aggregates of tau and beta amyloid that would otherwise accumulate as the byproducts of CDR activation both from normal learning and from microglial and synaptosomal innate immune activation that increase progressively with aging. Interestingly, a number of molecules that regulate mTOR and other metabolic aspects of the CDR, have recently been found to slow the aging process and extend longevity, while simultaneously protecting against age-related markers of Alzheimer dementia in animal models [88]. These "geroneuroprotecting" drugs were plant-based natural products similar to curcumin and polyphenols such as fisetin. The healing cycle-promoting properties of these drugs prevented the accumulation of tau and beta amyloid markers of Alzheimer dementia even though the drugs were not directed at the protein markers specifically [88].

The importance of innate immune activation and healing in aging is underscored by a recent discovery in Werner syndrome. Werner syndrome is a recessively inherited adult progeria syndrome caused by mutations in the Werner helicase (WRN). In addition to genomic instability caused by WRN mutations, the protein was recently found to play a key role in innate immunity as a transcriptional coactivator of the NFkB-dependent expression of the chemokine IL8 [89]. Werner mutations inhibit NFkB- and IL8-dependent ROS production. ROS production is not only an essential component of an effective CDR1 (Figure 1), but is important for NRF2 induction of long-term anti-oxidant and detoxification defenses [90]. In addition, the WRN protein is important for HIF1 stabilization [91] needed for tissue regeneration [26] during CDR2 (Figure 1).

With each turn of the healing cycle, the induced combination of transcriptional and metabolic changes and the DNA damage response will result in some injured and newly replaced cells being unable to complete the normal stages of the cycle. Perhaps 0.1–1 million cells of the 10^{10} cells that must be replaced after pathological cell death may be left behind, stuck or delayed in one of the three stages, CDR1, CDR2, and CDR3. An even larger number of cells whose function was transiently changed by injury, but were not killed, will contribute to the cells that are left behind in stages of the healing cycle. This process is illustrated as progressively dysfunctional mosaics on the right of the spiral in Figure 2. The ecogenetic interaction of inherited genotype of a given individual with the particular environmental insult (nutritional stress, pathogen, toxin, or physical injury) will determine how many cells are delayed or lost in the three different stages of the CDR. Examples of aging cellular mosaics are illustrated at age 20, 40, 60, and 90 years (Figure 2). Delayed and arrested cells that are incompletely differentiated create physical and metabolic separation—buffer zones—that act like control rods in a nuclear reactor that absorb signals and inhibit communication between previously adjoining, synergistic, and metabolically interdependent cells. Loss of cellular connectivity through functional gap junctions decreases the physiologic reserve capacity and increases vulnerability to stress-related cell death [92].

The propagation of calcium waves from cell to cell in a tissue via the inositol trisphosphate (IP3)-gated release of intracellular calcium stores is a common example of the cooperative response to neuroendocrine signaling, and is highly dependent on fully differentiated mitochondrial function [93]. CD38 increases with age [94] and is used by the cell to synthesize cyclic adenosine diphosphate ribose (cADPR) from NAD+ and nicotinic acid adenine dinucleotide phosphate (NAADP) from NADP+ as IP3-responsive calcium signaling declines [95]. cADPR and NAADP are intracellular ligands that stimulate IP3-independent release of calcium from the endoplasmic reticulum (ER) and lysosomes, respectively [29]. NAD+ and NADP+ are depleted by CD38 in the course of aging [94].

Cellular depletion of NAD+ and NADH leads to a decrease in mitonuclear communication [96], and to progressive declines in mitochondrial electron transport that contribute to aging [97]. Supplementation with the NAD+ precursor, nicotinamide riboside (NR), in animal models improves cell differentiation, restores laminin scaffolding and a more normal cellular mosaic in tissues, attenuates senescent cell formation, and increases longevity by about 10% [98]. In a recent study of the effect of transplanted senescent cells, the authors found that ≥ 1 senescent cell among 10,000 total cells in the body (0.01%), or ≥ 1 in 350 normal cells in a specific tissue (≥0.28%) was enough to produce a dysfunctional cellular mosaic and measurable functional defects such as decreased grip strength and exercise capacity [99].

8. De-Emergence as a Cause of Dysfunction

Complex living systems are comprised of at least seven discrete subsystems: (1) molecules; monomers, metabolites, and other building blocks, (2) polymers requiring energy for synthesis, such as proteins, polysaccharides, nucleic acids, and lipids made of amino acid, monosaccharide, nucleotide, acetyl and isoprene monomers, respectively, (3) polymers that assemble spontaneously such as charged and neutral lipids and hydrophobic proteins that form membranes, lipid droplets, and other lowered free energy structures in aqueous matrices, (4) organelles, (5) cells, (6) tissues, (7) organs. Many of the phenotypes associated with normal development, health, disease, and aging are emergent properties that depend on the function, arrangement, and interaction of the subsystems, but are qualitatively, quantitatively, and chronologically distinct from any single subsystem. For example, long-term memory is an emergent property that requires new protein synthesis that alters several aspects of all the subsystems that make up the brain, but knowledge of any one of the subsystems is insufficient to explain long-term memory. Other emergent properties of health include the ability to walk, talk, think, eat, excrete, mount an immune response, reproduce, detect and respond to a toxin or injury, and to heal. Aging degrades each of these abilities. If health is thought of as a collection of emergent phenotypes, then illness and aging can be thought of the gradual fading away, or de-emergence of the emergent properties that results from the degradation of metabolic and cellular order and the interactions of the subsystems that define health and resilience to environmental change. The images of progressively dysfunctional cellular mosaics shown in Figure 2 illustrate just one level—the cellular level—of the problem. Dysfunctional mosaics occur in every one of the seven subsystems, and mis-repairs accumulate at each level with each turn of the healing cycle.

9. The Hallmarks of Aging Emerge as a Result of Incomplete Healing

The molecular, cellular [2,3,48] and gene expression hallmarks [39] of aging can be organized according to their usage during the healing cycle and the stages of the multisystem CDR [10,11,29] (Figure 3). These hallmarks have been identified in studies of aging that have led naturally to an improved molecular understanding of mitochondrial stress [13,17,100], the integrated cell stress response (ICSR) [12,101,102], and the CDR [10,11,29,103]. Each trait associated with these hallmarks arises naturally from the activation of a molecular feature needed in the healing cycle, followed by the failure to extinguish this normal function or gene expression state of the CDR once it is no longer needed. Persistence of an aging hallmark after a turn of the healing cycle (Figure 2) can also occur in five other ways: (1) when a cell sustains too much genetic damage and becomes senescent, (2) when a cell that has been removed is not replaced and leads to tissue atrophy, (3) when a cell is replaced but fails to re-specialize according to the differentiated needs of the tissue, (4) when a mis-repair such as fibrosis or scarring [104] cannot be removed by remodeling, and (5) when genetic and metabolic changes bypass senescence and lead to cancer (Figure 1). The legacy of each of these events is to add to the dysfunctional mosaic illustrated in Figure 2.

Brain, muscle, nerve, and endocrine tissues are particularly susceptible to the incomplete replacement of lost cells once they have died and have been removed because of their limited regeneration capacity and the high degree of spatial organization required for optimal organ function. The function of these tissues is highly dependent on the spatial organization and metabolic

complementarity of the cellular mosaic. This complementarity can only be achieved through cell specialization and chemical cooperativity between neighboring cells, which in turn, depends on the relative position and architecture of layers and columns of cells that must remain fixed over long periods of time. The cost of removing a cell from a chain of connected cells in the cerebral cortex or any other part of the brain has a high price that cannot easily be repaid by recruiting stem cells from another location. However, the cost of converting a cell to the hypersecretory phenotype of a senescent cell [105] is even higher, since just one senescent cell in 350 normal cells is enough to decrease the function of a tissue [99]. The smaller collective volume of cells that occurs in most tissues with age is illustrated in Figure 2. The decreasing volume of tissues in the columns labeled "Merge" and "CDR3" represents the effect of cell loss (atrophy) that occurs with incomplete progress through the healing cycle (Figures 1 and 2). In the example illustrated in Figure 2, more cells have accumulated in CDR2 (illustrated in green) by the ages of 60 and 90 years. Accumulation of cells in CDR2 will increase the risk of diseases such as diabetes, heart disease, and cancer because cells arrested or delayed in CDR2 maintain their proliferative capacity [11] (Figure 1). Proliferative capacity is maintained in part because cells in CDR2 contain more multipotential M0 mitochondria adapted for Warburg metabolism (Table 1). Inherited mutations in the RECQL4 helicase, which interacts with p53 and POLG in mitochondria, increase aerobic glycolysis associated with CDR2, lead to an increased risk of cancer, and to a form of progeria known as Rothmund–Thomson syndrome [106–108].

10. Conclusions

A new model is presented that reframes aging as the result of repeated cycles of incomplete healing. In this model, cycles of incomplete healing stack over time, leading to cellular mosaics that become progressively dysfunctional with age (Figure 2). Cells that accumulate in one of the three stages of the cell danger response (CDR) lead to specific risks of age-related disease. The accumulation of cells in CDR1 leads to chronic inflammatory and pain syndromes, and to susceptibility to chronic viral, bacterial, and fungal infections that require adaptive T-cell immunity for eradication [11]. The accumulation of cells in CDR2 leads to diabetes, heart disease, congestive heart failure, peripheral vascular disease, fibrotic disorders, and cancer risk. The accumulation of cells in CDR3 leads to autoimmune disorders, immune suppression or deficiency, neuropathic pain syndromes, behavioral and mental health disorders, or neurodevelopmental and neurodegenerative disease [11]. It is currently unknown what drugs, devices, or procedures can unblock arrested cells in the mosaic and permit the completion of the healing cycle. However, specific nutritional interventions such as nicotinamide riboside or essential amino acids have been found to facilitate healing [66], longevity [98] or both [64,66] in animal models. A prediction of the incomplete healing model is that differentiation checkpoints exist at each stage of the CDR (Figure 1) and that the molecular signals that are used naturally by cells to facilitate completion of healing may provide fresh clues for both preventing and treating age-related symptoms and disease. One procedure that is well-known to improve physical and psychological well-being, decrease mortality, and decrease the risk of age-related disease, is exercise [109,110]. The effects of exercise are multifaceted, but the increase in autophagy and remodeling of the mitochondrial network, leading to adaptive improvements in quality control and increased reserve capacity, may play key roles [111]. The search for geroneuroprotectants [88] and chemical exercise mimetics [112] has already begun. However, a deeper understanding of the role of natural metabolites as signaling molecules—metabokines [11]—and molecules regulated by exercise—exerkines and exosomes [113–115]—that regulate the completion of the healing cycle holds promise for preventing, slowing, and perhaps reversing [47] some of the effects of aging. Interventions that exploit purinergic [20] and sphingolipid [116] signaling pathways may be particularly powerful since over half of all mitochondrial proteins are regulated by ATP, NAD+, and related nucleotides (Table S1), and many of the molecular hallmarks of aging trace to or regulate the interplay between purines, mitochondria, sphingolipids [117,118], and the nucleus [119].

Supplementary Materials: The following are available online at http://www.mdpi.com/2079-7737/8/2/27/s1, Table S1: The mitochondrial proteome and nucleotide regulation.

Funding: This work was funded in part by philanthropic gifts from the UCSD Christini Fund, the Lennox Foundation, Malone Family Foundation, the Aloe family, the Harb family, Marc Spilo and all the others who contributed to the Aloe family autism research fund, the N of One Autism Research Foundation, the UCSD Mitochondrial Disease Research Fund, the JMS Fund, gifts in memory of Wayne Riggs, and from Linda Clark, Jeanne Conrad, Jeff Ansell, Josh Spears, David Cannistraro, the Kirby and Katie Mano Family, Simon and Evelyn Foo, Wing-kun Tam, Gita and Anurag Gupta, the Brent Kaufman Family, and the Daniel and Kelly White Family. RKN wishes to thank over 2000 individuals who have each provided gifts in the past year to support Naviaux Lab research.

Acknowledgments: RKN thanks the many families with primary mitochondrial disease, autism spectrum disorder (ASD), and myalgic encephalomyelitis/chronic fatigue syndrome (ME/CFS) who have helped make this research possible. RKN thanks Scott McAvoy from the UCSD Digital Media Lab for preparing the art work for the healing spiral in Figure 2, and Vamsi Mootha, Sarah Calvo, and Jonathan Monk for the bioinformatic analysis of mitochondrial proteins and enzymes.

Conflicts of Interest: RKN is an unpaid scientific advisory board member for the Autism Research Institute (ARI) and the Open Medicine Foundation (OMF). Financial supporters for this study had no role in data analysis, interpretation, writing, or publication of this work.

References

1. McCay, C.M.; Crowell, M.F. Prolonging the life span. *Sci. Mon.* **1934**, *39*, 405–414.
2. Finkel, T. The metabolic regulation of aging. *Nat. Med.* **2015**, *21*, 1416–1423. [CrossRef] [PubMed]
3. Lopez-Otin, C.; Galluzzi, L.; Freije, J.M.P.; Madeo, F.; Kroemer, G. Metabolic Control of Longevity. *Cell* **2016**, *166*, 802–821. [CrossRef]
4. Pagliarini, D.J.; Calvo, S.E.; Chang, B.; Sheth, S.A.; Vafai, S.B.; Ong, S.E.; Walford, G.A.; Sugiana, C.; Boneh, A.; Chen, W.K.; et al. A mitochondrial protein compendium elucidates complex I disease biology. *Cell* **2008**, *134*, 112–123. [CrossRef]
5. Calvo, S.E.; Clauser, K.R.; Mootha, V.K. MitoCarta2.0: An updated inventory of mammalian mitochondrial proteins. *Nucleic Acids Res.* **2016**, *44*, D1251–D1257. [CrossRef] [PubMed]
6. Naviaux, R.K.; Le, T.P.; Bedelbaeva, K.; Leferovich, J.; Gourevitch, D.; Sachadyn, P.; Zhang, X.M.; Clark, L.; Heber-Katz, E. Retained features of embryonic metabolism in the adult MRL mouse. *Mol. Genet. Metab.* **2009**, *96*, 133–144. [CrossRef] [PubMed]
7. Ma, S.; Huang, Q.; Tominaga, T.; Liu, C.; Suzuki, K. An 8-Week Ketogenic Diet Alternated Interleukin-6, Ketolytic and Lipolytic Gene Expression, and Enhanced Exercise Capacity in Mice. *Nutrients* **2018**, *10*, 1696. [CrossRef]
8. Ogborn, D.I.; McKay, B.R.; Crane, J.D.; Safdar, A.; Akhtar, M.; Parise, G.; Tarnopolsky, M.A. Effects of age and unaccustomed resistance exercise on mitochondrial transcript and protein abundance in skeletal muscle of men. *Am. J. Physiol. Regul. Integr. Comp. Physiol.* **2015**, *308*, R734–R741. [CrossRef] [PubMed]
9. Winckelmans, E.; Nawrot, T.S.; Tsamou, M.; Den Hond, E.; Baeyens, W.; Kleinjans, J.; Lefebvre, W.; Van Larebeke, N.; Peusens, M.; Plusquin, M.; et al. Transcriptome-wide analyses indicate mitochondrial responses to particulate air pollution exposure. *Environ. Health A Glob. Access Sci. Source* **2017**, *16*, 87. [CrossRef] [PubMed]
10. Naviaux, R.K. Metabolic features of the cell danger response. *Mitochondrion* **2014**, *16*, 7–17. [CrossRef]
11. Naviaux, R.K. Metabolic features and regulation of the healing cycle-A new model for chronic disease pathogenesis and treatment. *Mitochondrion* **2018**. [CrossRef] [PubMed]
12. Quiros, P.M.; Prado, M.A.; Zamboni, N.; D'Amico, D.; Williams, R.W.; Finley, D.; Gygi, S.P.; Auwerx, J. Multi-omics analysis identifies ATF4 as a key regulator of the mitochondrial stress response in mammals. *J. Cell Biol.* **2017**, *216*, 2027–2045. [CrossRef] [PubMed]
13. Nikkanen, J.; Forsstrom, S.; Euro, L.; Paetau, I.; Kohnz, R.A.; Wang, L.; Chilov, D.; Viinamaki, J.; Roivainen, A.; Marjamaki, P.; et al. Mitochondrial DNA Replication Defects Disturb Cellular dNTP Pools and Remodel One-Carbon Metabolism. *Cell Metab.* **2016**, *23*, 635–648. [CrossRef]
14. Silva, J.M.; Wong, A.; Carelli, V.; Cortopassi, G.A. Inhibition of mitochondrial function induces an integrated stress response in oligodendroglia. *Neurobiol. Dis.* **2009**, *34*, 357–365. [CrossRef]

15. Cameron, J.L.; Eagleson, K.L.; Fox, N.A.; Hensch, T.K.; Levitt, P. Social Origins of Developmental Risk for Mental and Physical Illness. *J. Neurosci. Off. J. Soc. Neurosci.* **2017**, *37*, 10783–10791. [CrossRef] [PubMed]
16. Fredrickson, B.L.; Grewen, K.M.; Algoe, S.B.; Firestine, A.M.; Arevalo, J.M.; Ma, J.; Cole, S.W. Psychological well-being and the human conserved transcriptional response to adversity. *PLoS ONE* **2015**, *10*, e0121839. [CrossRef] [PubMed]
17. Picard, M.; McManus, M.J.; Gray, J.D.; Nasca, C.; Moffat, C.; Kopinski, P.K.; Seifert, E.L.; McEwen, B.S.; Wallace, D.C. Mitochondrial functions modulate neuroendocrine, metabolic, inflammatory, and transcriptional responses to acute psychological stress. *Proc. Natl. Acad. Sci. USA* **2015**, *112*, E6614–E6623. [CrossRef] [PubMed]
18. Leday, G.G.R.; Vertes, P.E.; Richardson, S.; Greene, J.R.; Regan, T.; Khan, S.; Henderson, R.; Freeman, T.C.; Pariante, C.M.; Harrison, N.A.; et al. Replicable and Coupled Changes in Innate and Adaptive Immune Gene Expression in Two Case-Control Studies of Blood Microarrays in Major Depressive Disorder. *Biol. Psychiatry* **2018**, *83*, 70–80. [CrossRef] [PubMed]
19. Burnstock, G.; Knight, G.E. Cell culture: Complications due to mechanical release of ATP and activation of purinoceptors. *Cell Tissue Res.* **2017**. [CrossRef]
20. Burnstock, G. The therapeutic potential of purinergic signalling. *Biochem. Pharmacol.* **2018**, *151*, 157–165. [CrossRef]
21. Burnstock, G. Short- and long-term (trophic) purinergic signalling. *Philos. Trans. R. Soc. Lond.* **2016**, *371*, 20150422. [CrossRef]
22. De la Fuente, I.M. Elements of the cellular metabolic structure. *Front. Mol. Biosci.* **2015**, *2*, 16. [CrossRef] [PubMed]
23. Jindrichova, M.; Kuzyk, P.; Li, S.; Stojilkovic, S.S.; Zemkova, H. Conserved ectodomain cysteines are essential for rat P2X7 receptor trafficking. *Purinergic Signal.* **2012**, *8*, 317–325. [CrossRef] [PubMed]
24. Sussman, I.; Erecinska, M.; Wilson, D.F. Regulation of cellular energy metabolism: The Crabtree effect. *Biochim. Biophys. Acta* **1980**, *591*, 209–223. [CrossRef]
25. Dror, E.; Dalmas, E.; Meier, D.T.; Wueest, S.; Thevenet, J.; Thienel, C.; Timper, K.; Nordmann, T.M.; Traub, S.; Schulze, F.; et al. Postprandial macrophage-derived IL-1beta stimulates insulin, and both synergistically promote glucose disposal and inflammation. *Nat. Immunol.* **2017**, *18*, 283–292. [CrossRef]
26. Heber-Katz, E. Oxygen, Metabolism, and Regeneration: Lessons from Mice. *Trends Mol. Med.* **2017**, *23*, 1024–1036. [CrossRef] [PubMed]
27. Barros-Barbosa, A.R.; Oliveira, A.; Lobo, M.G.; Cordeiro, J.M.; Correia-de-Sa, P. Under stressful conditions activation of the ionotropic P2X7 receptor differentially regulates GABA and glutamate release from nerve terminals of the rat cerebral cortex. *Neurochem. Int.* **2018**, *112*, 81–95. [CrossRef]
28. Xiong, Y.; Teng, S.; Zheng, L.; Sun, S.; Li, J.; Guo, N.; Li, M.; Wang, L.; Zhu, F.; Wang, C.; et al. Stretch-induced Ca(2+) independent ATP release in hippocampal astrocytes. *J. Physiol.* **2018**, *596*, 1931–1947. [CrossRef]
29. Naviaux, R.K. Antipurinergic therapy for autism-An in-depth review. *Mitochondrion* **2017**. [CrossRef]
30. Sakaki, H.; Tsukimoto, M.; Harada, H.; Moriyama, Y.; Kojima, S. Autocrine regulation of macrophage activation via exocytosis of ATP and activation of P2Y11 receptor. *PLoS ONE* **2013**, *8*, e59778. [CrossRef] [PubMed]
31. Huang, Z.L.; Zhang, Z.; Qu, W.M. Roles of adenosine and its receptors in sleep-wake regulation. *Int. Rev. Neurobiol.* **2014**, *119*, 349–371. [PubMed]
32. He, S.; Sharpless, N.E. Senescence in Health and Disease. *Cell* **2017**, *169*, 1000–1011. [CrossRef] [PubMed]
33. Wang-Michelitsch, J.; Michelitsch, T.M. Misrepair accumulation theory: A theory for understanding aging, cancer development, longevity, and adaptation. *arXiv* **2015**, arXiv:1505.07016.
34. Wang-Michelitsch, J.; Michelitsch, T.M. Tissue fibrosis: A principal proof for the central role of Misrepair in aging. *arXiv* **2015**, arXiv:1505.01376.
35. Wang, J.; Michelitsch, T.; Wunderlin, A.; Mahadeva, R. Aging as a consequence of misrepair–a novel theory of aging. *arXiv* **2009**, arXiv:0904.0575.
36. Zhao, R.; Liang, D.; Sun, D. Blockade of Extracellular ATP Effect by Oxidized ATP Effectively Mitigated Induced Mouse Experimental Autoimmune Uveitis (EAU). *PLoS ONE* **2016**, *11*, e0155953. [CrossRef]
37. Hultqvist, M.; Olsson, L.M.; Gelderman, K.A.; Holmdahl, R. The protective role of ROS in autoimmune disease. *Trends Immunol.* **2009**, *30*, 201–208. [CrossRef]

38. Alvarez, K.; Vasquez, G. Damage-associated molecular patterns and their role as initiators of inflammatory and auto-immune signals in systemic lupus erythematosus. *Int. Rev. Immunol.* **2017**, *36*, 259–270. [CrossRef] [PubMed]
39. Frenk, S.; Houseley, J. Gene expression hallmarks of cellular ageing. *Biogerontology* **2018**, *19*, 547–566. [CrossRef]
40. Chen, W.; Sandoval, H.; Kubiak, J.Z.; Li, X.C.; Ghobrial, R.M.; Kloc, M. The phenotype of peritoneal mouse macrophages depends on the mitochondria and ATP/ADP homeostasis. *Cell. Immunol.* **2018**, *324*, 1–7. [CrossRef] [PubMed]
41. Liu, P.S.; Ho, P.C. Determining Macrophage Polarization upon Metabolic Perturbation. *Methods Mol. Biol.* **2019**, *1862*, 173–186. [PubMed]
42. Van den Bossche, J.; O'Neill, L.A.; Menon, D. Macrophage Immunometabolism: Where Are We (Going)? *Trends Immunol.* **2017**, *38*, 395–406. [CrossRef] [PubMed]
43. Motori, E.; Puyal, J.; Toni, N.; Ghanem, A.; Angeloni, C.; Malaguti, M.; Cantelli-Forti, G.; Berninger, B.; Conzelmann, K.K.; Gotz, M.; et al. Inflammation-induced alteration of astrocyte mitochondrial dynamics requires autophagy for mitochondrial network maintenance. *Cell Metab.* **2013**, *18*, 844–859. [CrossRef]
44. Roger, A.J.; Munoz-Gomez, S.A.; Kamikawa, R. The Origin and Diversification of Mitochondria. *Curr. Biol.* **2017**, *27*, R1177–R1192. [CrossRef] [PubMed]
45. Chen, H.; Chan, D.C. Mitochondrial Dynamics in Regulating the Unique Phenotypes of Cancer and Stem Cells. *Cell Metab.* **2017**, *26*, 39–48. [CrossRef] [PubMed]
46. Giedt, R.J.; Fumene Feruglio, P.; Pathania, D.; Yang, K.S.; Kilcoyne, A.; Vinegoni, C.; Mitchison, T.J.; Weissleder, R. Computational imaging reveals mitochondrial morphology as a biomarker of cancer phenotype and drug response. *Sci. Rep.* **2016**, *6*, 32985. [CrossRef]
47. Singh, B.; Schoeb, T.R.; Bajpai, P.; Slominski, A.; Singh, K.K. Reversing wrinkled skin and hair loss in mice by restoring mitochondrial function. *Cell Death Dis.* **2018**, *9*, 735. [CrossRef] [PubMed]
48. Atamna, H.; Tenore, A.; Lui, F.; Dhahbi, J.M. Organ reserve, excess metabolic capacity, and aging. *Biogerontology* **2018**, *19*, 171–184. [CrossRef] [PubMed]
49. Verkhratsky, A.; Burnstock, G. Biology of purinergic signalling: Its ancient evolutionary roots, its omnipresence and its multiple functional significance. *BioEssays News Rev. Mol. Cell. Dev. Biol.* **2014**, *36*, 697–705. [CrossRef]
50. Burnstock, G. Intracellular expression of purinoceptors. *Purinergic Signal.* **2015**, *11*, 275–276. [CrossRef] [PubMed]
51. Diaz-Hernandez, J.I.; Sebastian-Serrano, A.; Gomez-Villafuertes, R.; Diaz-Hernandez, M.; Miras-Portugal, M.T. Age-related nuclear translocation of P2X6 subunit modifies splicing activity interacting with splicing factor 3A1. *PLoS ONE* **2015**, *10*, e0123121. [CrossRef]
52. Dietz, W.H. Critical periods in childhood for the development of obesity. *Am. J. Clin. Nutr.* **1994**, *59*, 955–959. [CrossRef]
53. Das, J.K.; Salam, R.A.; Thornburg, K.L.; Prentice, A.M.; Campisi, S.; Lassi, Z.S.; Koletzko, B.; Bhutta, Z.A. Nutrition in adolescents: Physiology, metabolism, and nutritional needs. *Ann. N. Y. Acad. Sci.* **2017**, *1393*, 21–33. [CrossRef]
54. Desbrow, B.; Burd, N.A.; Tarnopolsky, M.; Moore, D.R.; Elliott-Sale, K.J. Nutrition for Special Populations: Young, Female, and Masters Athletes. *Int. J. Sport Nutr. Exerc. Metab.* **2019**, 1–8. [CrossRef]
55. Lopez-Lluch, G.; Irusta, P.M.; Navas, P.; de Cabo, R. Mitochondrial biogenesis and healthy aging. *Exp. Gerontol.* **2008**, *43*, 813–819. [CrossRef] [PubMed]
56. Weir, H.J.; Yao, P.; Huynh, F.K.; Escoubas, C.C.; Goncalves, R.L.; Burkewitz, K.; Laboy, R.; Hirschey, M.D.; Mair, W.B. Dietary Restriction and AMPK Increase Lifespan via Mitochondrial Network and Peroxisome Remodeling. *Cell Metab.* **2017**, *26*, 884–896 e885. [CrossRef]
57. Rabol, R.; Svendsen, P.F.; Skovbro, M.; Boushel, R.; Haugaard, S.B.; Schjerling, P.; Schrauwen, P.; Hesselink, M.K.; Nilas, L.; Madsbad, S.; et al. Reduced skeletal muscle mitochondrial respiration and improved glucose metabolism in nondiabetic obese women during a very low calorie dietary intervention leading to rapid weight loss. *Metabolism* **2009**, *58*, 1145–1152. [CrossRef]

58. Muller, M.J.; Enderle, J.; Pourhassan, M.; Braun, W.; Eggeling, B.; Lagerpusch, M.; Gluer, C.C.; Kehayias, J.J.; Kiosz, D.; Bosy-Westphal, A. Metabolic adaptation to caloric restriction and subsequent refeeding: The Minnesota Starvation Experiment revisited. *Am. J. Clin. Nutr.* **2015**, *102*, 807–819. [CrossRef] [PubMed]
59. Ewald, C.Y.; Castillo-Quan, J.I.; Blackwell, T.K. Untangling Longevity, Dauer, and Healthspan in Caenorhabditis elegans Insulin/IGF-1-Signalling. *Gerontology* **2018**, *64*, 96–104. [CrossRef] [PubMed]
60. Albert, P.S.; Riddle, D.L. Developmental alterations in sensory neuroanatomy of the Caenorhabditis elegans dauer larva. *J. Comp. Neurol.* **1983**, *219*, 461–481. [CrossRef] [PubMed]
61. Lee, D.; Lee, H.; Kim, N.; Lim, D.S.; Lee, J. Regulation of a hitchhiking behavior by neuronal insulin and TGF-beta signaling in the nematode Caenorhabditis elegans. *Biochem. Biophys. Res. Commun.* **2017**, *484*, 323–330. [CrossRef] [PubMed]
62. Lant, B.; Storey, K.B. An overview of stress response and hypometabolic strategies in Caenorhabditis elegans: Conserved and contrasting signals with the mammalian system. *Int. J. Biol. Sci.* **2010**, *6*, 9–50. [CrossRef] [PubMed]
63. Androwski, R.J.; Flatt, K.M.; Schroeder, N.E. Phenotypic plasticity and remodeling in the stress-induced Caenorhabditis elegans dauer. *Wiley Interdiscip. Rev. Dev. Biol.* **2017**, *6*, e278. [CrossRef]
64. D'Antona, G.; Ragni, M.; Cardile, A.; Tedesco, L.; Dossena, M.; Bruttini, F.; Caliaro, F.; Corsetti, G.; Bottinelli, R.; Carruba, M.O.; et al. Branched-chain amino acid supplementation promotes survival and supports cardiac and skeletal muscle mitochondrial biogenesis in middle-aged mice. *Cell Metab.* **2010**, *12*, 362–372. [CrossRef]
65. Bonfili, L.; Cecarini, V.; Cuccioloni, M.; Angeletti, M.; Flati, V.; Corsetti, G.; Pasini, E.; Dioguardi, F.S.; Eleuteri, A.M. Essential amino acid mixtures drive cancer cells to apoptosis through proteasome inhibition and autophagy activation. *FEBS J.* **2017**, *284*, 1726–1737. [CrossRef] [PubMed]
66. Corsetti, G.; Romano, C.; Pasini, E.; Marzetti, E.; Calvani, R.; Picca, A.; Flati, V.; Dioguardi, F.S. Diet enrichment with a specific essential free amino acid mixture improves healing of undressed wounds in aged rats. *Exp. Gerontol.* **2017**, *96*, 138–145. [CrossRef]
67. Fielenbach, N.; Antebi, A.C. elegans dauer formation and the molecular basis of plasticity. *Genes Dev.* **2008**, *22*, 2149–2165. [CrossRef]
68. Sender, R.; Fuchs, S.; Milo, R. Revised Estimates for the Number of Human and Bacteria Cells in the Body. *PLoS Biol.* **2016**, *14*, e1002533. [CrossRef]
69. Renehan, A.G.; Booth, C.; Potten, C.S. What is apoptosis, and why is it important? *BMJ* **2001**, *322*, 1536–1538. [CrossRef]
70. Spalding, K.L.; Arner, E.; Westermark, P.O.; Bernard, S.; Buchholz, B.A.; Bergmann, O.; Blomqvist, L.; Hoffstedt, J.; Naslund, E.; Britton, T.; et al. Dynamics of fat cell turnover in humans. *Nature* **2008**, *453*, 783–787. [CrossRef]
71. Spalding, K.L.; Bhardwaj, R.D.; Buchholz, B.A.; Druid, H.; Frisen, J. Retrospective birth dating of cells in humans. *Cell* **2005**, *122*, 133–143. [CrossRef] [PubMed]
72. Doherty, T.J. Invited review: Aging and sarcopenia. *J. Appl. Physiol.* **2003**, *95*, 1717–1727. [CrossRef]
73. Prescott, L.F. The normal urinary excretion rates of renal tubular cells, leucocytes and red blood cells. *Clin. Sci.* **1966**, *31*, 425–435. [PubMed]
74. Rinkevich, Y.; Montoro, D.T.; Contreras-Trujillo, H.; Harari-Steinberg, O.; Newman, A.M.; Tsai, J.M.; Lim, X.; Van-Amerongen, R.; Bowman, A.; Januszyk, M.; et al. In vivo clonal analysis reveals lineage-restricted progenitor characteristics in mammalian kidney development, maintenance, and regeneration. *Cell Rep.* **2014**, *7*, 1270–1283. [CrossRef] [PubMed]
75. Kim, I.H.; Kisseleva, T.; Brenner, D.A. Aging and liver disease. *Curr. Opin. Gastroenterol.* **2015**, *31*, 184–191. [CrossRef] [PubMed]
76. Bergmann, O.; Bhardwaj, R.D.; Bernard, S.; Zdunek, S.; Barnabe-Heider, F.; Walsh, S.; Zupicich, J.; Alkass, K.; Buchholz, B.A.; Druid, H.; et al. Evidence for cardiomyocyte renewal in humans. *Science* **2009**, *324*, 98–102. [CrossRef]
77. Perl, S.; Kushner, J.A.; Buchholz, B.A.; Meeker, A.K.; Stein, G.M.; Hsieh, M.; Kirby, M.; Pechhold, S.; Liu, E.H.; Harlan, D.M.; et al. Significant human beta-cell turnover is limited to the first three decades of life as determined by in vivo thymidine analog incorporation and radiocarbon dating. *J. Clin. Endocrinol. Metab.* **2010**, *95*, E234–E239. [CrossRef] [PubMed]

78. Fox, J.P.; Hall, C.E.; Cooney, M.K.; Luce, R.E.; Kronmal, R.A. The Seattle virus watch. II. Objectives, study population and its observation, data processing and summary of illnesses. *Am. J. Epidemiol.* **1972**, *96*, 270–285. [CrossRef] [PubMed]
79. Milholland, B.; Dong, X.; Zhang, L.; Hao, X.; Suh, Y.; Vijg, J. Differences between germline and somatic mutation rates in humans and mice. *Nat. Commun.* **2017**, *8*, 15183. [CrossRef]
80. Peterson, S.E.; Westra, J.W.; Paczkowski, C.M.; Chun, J. Chromosomal mosaicism in neural stem cells. *Methods Mol. Biol.* **2008**, *438*, 197–204.
81. Muotri, A.R.; Chu, V.T.; Marchetto, M.C.; Deng, W.; Moran, J.V.; Gage, F.H. Somatic mosaicism in neuronal precursor cells mediated by L1 retrotransposition. *Nature* **2005**, *435*, 903–910. [CrossRef]
82. Romer, C.; Singh, M.; Hurst, L.D.; Izsvak, Z. How to tame an endogenous retrovirus: HERVH and the evolution of human pluripotency. *Curr. Opin. Virol.* **2017**, *25*, 49–58. [CrossRef]
83. Harris, S.A.; Harris, E.A. Herpes Simplex Virus Type 1 and Other Pathogens are Key Causative Factors in Sporadic Alzheimer's Disease. *J. Alzheimer's Dis. JAD* **2015**, *48*, 319–353. [CrossRef]
84. Bornhofft, K.F.; Goldammer, T.; Rebl, A.; Galuska, S.P. Siglecs: A journey through the evolution of sialic acid-binding immunoglobulin-type lectins. *Dev. Comp. Immunol.* **2018**, *86*, 219–231. [CrossRef]
85. Schwarz, F.; Pearce, O.M.; Wang, X.; Samraj, A.N.; Laubli, H.; Garcia, J.O.; Lin, H.; Fu, X.; Garcia-Bingman, A.; Secrest, P.; et al. Siglec receptors impact mammalian lifespan by modulating oxidative stress. *Elife* **2015**, *4*. [CrossRef]
86. Stanczak, M.A.; Siddiqui, S.S.; Trefny, M.P.; Thommen, D.S.; Boligan, K.F.; von Gunten, S.; Tzankov, A.; Tietze, L.; Lardinois, D.; Heinzelmann-Schwarz, V.; et al. Self-associated molecular patterns mediate cancer immune evasion by engaging Siglecs on T cells. *J. Clin. Investig.* **2018**, *128*, 4912–4923. [CrossRef]
87. Bower, N.I.; Hogan, B.M. Brain drains: New insights into brain clearance pathways from lymphatic biology. *J. Mol. Med.* **2018**, *96*, 383–390. [CrossRef]
88. Schubert, D.; Currais, A.; Goldberg, J.; Finley, K.; Petrascheck, M.; Maher, P. Geroneuroprotectors: Effective Geroprotectors for the Brain. *Trends Pharmacol. Sci.* **2018**, *39*, 1004–1007. [CrossRef]
89. Mizutani, T.; Ishizaka, A.; Furuichi, Y. The Werner Protein Acts as a Coactivator of Nuclear Factor kappaB (NF-kappaB) on HIV-1 and Interleukin-8 (IL-8) Promoters. *J. Biol. Chem.* **2015**, *290*, 18391–18399. [CrossRef]
90. Huang, Y.; Li, W.; Su, Z.Y.; Kong, A.N. The complexity of the Nrf2 pathway: Beyond the antioxidant response. *J. Nutr. Biochem.* **2015**, *26*, 1401–1413. [CrossRef]
91. Li, B.; Iglesias-Pedraz, J.M.; Chen, L.Y.; Yin, F.; Cadenas, E.; Reddy, S.; Comai, L. Downregulation of the Werner syndrome protein induces a metabolic shift that compromises redox homeostasis and limits proliferation of cancer cells. *Aging Cell* **2014**, *13*, 367–378. [CrossRef]
92. Blanc, E.M.; Bruce-Keller, A.J.; Mattson, M.P. Astrocytic gap junctional communication decreases neuronal vulnerability to oxidative stress-induced disruption of Ca2+ homeostasis and cell death. *J. Neurochem.* **1998**, *70*, 958–970. [CrossRef] [PubMed]
93. Duchen, M.R. Mitochondria and calcium: From cell signalling to cell death. *J. Physiol.* **2000**, *529 Pt 1*, 57–68. [CrossRef]
94. Camacho-Pereira, J.; Tarrago, M.G.; Chini, C.C.S.; Nin, V.; Escande, C.; Warner, G.M.; Puranik, A.S.; Schoon, R.A.; Reid, J.M.; Galina, A.; et al. CD38 Dictates Age-Related NAD Decline and Mitochondrial Dysfunction through an SIRT3-Dependent Mechanism. *Cell Metab.* **2016**, *23*, 1127–1139. [CrossRef]
95. Igwe, O.J.; Filla, M.B. Aging-related regulation of myo-inositol 1,4,5-trisphosphate signal transduction pathway in the rat striatum. *Brain Res. Mol. Brain Res.* **1997**, *46*, 39–53. [CrossRef]
96. Gomes, A.P.; Price, N.L.; Ling, A.J.; Moslehi, J.J.; Montgomery, M.K.; Rajman, L.; White, J.P.; Teodoro, J.S.; Wrann, C.D.; Hubbard, B.P.; et al. Declining NAD(+) induces a pseudohypoxic state disrupting nuclear-mitochondrial communication during aging. *Cell* **2013**, *155*, 1624–1638. [CrossRef]
97. Chini, C.C.S.; Tarrago, M.G.; Chini, E.N. NAD and the aging process: Role in life, death and everything in between. *Mol. Cell. Endocrinol.* **2017**, *455*, 62–74. [CrossRef] [PubMed]
98. Zhang, H.; Ryu, D.; Wu, Y.; Gariani, K.; Wang, X.; Luan, P.; D'Amico, D.; Ropelle, E.R.; Lutolf, M.P.; Aebersold, R.; et al. NAD(+) repletion improves mitochondrial and stem cell function and enhances life span in mice. *Science* **2016**, *352*, 1436–1443. [CrossRef] [PubMed]
99. Xu, M.; Pirtskhalava, T.; Farr, J.N.; Weigand, B.M.; Palmer, A.K.; Weivoda, M.M.; Inman, C.L.; Ogrodnik, M.B.; Hachfeld, C.M.; Fraser, D.G.; et al. Senolytics improve physical function and increase lifespan in old age. *Nat. Med.* **2018**, *24*, 1246–1256. [CrossRef] [PubMed]

100. Go, Y.M.; Fernandes, J.; Hu, X.; Uppal, K.; Jones, D.P. Mitochondrial network responses in oxidative physiology and disease. *Free Radic. Biol. Med.* **2018**, *116*, 31–40. [CrossRef]
101. Salminen, A.; Kaarniranta, K.; Kauppinen, A. Integrated stress response stimulates FGF21 expression: Systemic enhancer of longevity. *Cell Signal.* **2017**, *40*, 10–21. [CrossRef] [PubMed]
102. Pakos-Zebrucka, K.; Koryga, I.; Mnich, K.; Ljujic, M.; Samali, A.; Gorman, A.M. The integrated stress response. *EMBO Rep.* **2016**, *17*, 1374–1395. [CrossRef] [PubMed]
103. Naviaux, R.K. Oxidative shielding or oxidative stress? *J. Pharmacol. Exp. Ther.* **2012**, *342*, 608–618. [CrossRef] [PubMed]
104. Wang-Michelitsch, J.; Michelitsch, T. Aging as a process of accumulation of Misrepairs. *arXiv* **2015**, arXiv:1503.07163.
105. Hernandez-Segura, A.; de Jong, T.V.; Melov, S.; Guryev, V.; Campisi, J.; Demaria, M. Unmasking Transcriptional Heterogeneity in Senescent Cells. *Curr. Biol.* **2017**, *27*, 2652–2660 e2654. [CrossRef] [PubMed]
106. Kumari, J.; Hussain, M.; De, S.; Chandra, S.; Modi, P.; Tikoo, S.; Singh, A.; Sagar, C.; Sepuri, N.B.; Sengupta, S. Mitochondrial functions of RECQL4 are required for the prevention of aerobic glycolysis-dependent cell invasion. *J. Cell Sci.* **2016**, *129*, 1312–1318. [CrossRef] [PubMed]
107. Gupta, S.; De, S.; Srivastava, V.; Hussain, M.; Kumari, J.; Muniyappa, K.; Sengupta, S. RECQL4 and p53 potentiate the activity of polymerase gamma and maintain the integrity of the human mitochondrial genome. *Carcinogenesis* **2014**, *35*, 34–45. [CrossRef]
108. Croteau, D.L.; Singh, D.K.; Hoh Ferrarelli, L.; Lu, H.; Bohr, V.A. RECQL4 in genomic instability and aging. *Trends Genet.* **2012**, *28*, 624–631. [CrossRef]
109. Hupin, D.; Roche, F.; Gremeaux, V.; Chatard, J.C.; Oriol, M.; Gaspoz, J.M.; Barthelemy, J.C.; Edouard, P. Even a low-dose of moderate-to-vigorous physical activity reduces mortality by 22% in adults aged >/=60 years: A systematic review and meta-analysis. *Br. J. Sports Med.* **2015**, *49*, 1262–1267. [CrossRef]
110. Gries, K.J.; Raue, U.; Perkins, R.K.; Lavin, K.M.; Overstreet, B.S.; D'Acquisto, L.J.; Graham, B.; Finch, W.H.; Kaminsky, L.A.; Trappe, T.A.; et al. Cardiovascular and Skeletal Muscle Health with Lifelong Exercise. *J. Appl. Physiol.* **2018**. [CrossRef]
111. Radak, Z.; Torma, F.; Berkes, I.; Goto, S.; Mimura, T.; Posa, A.; Balogh, L.; Boldogh, I.; Suzuki, K.; Higuchi, M.; et al. Exercise effects on physiological function during aging. *Free Radic. Biol. Med.* **2019**, *132*, 33–41. [CrossRef]
112. Fan, W.; Evans, R.M. Exercise Mimetics: Impact on Health and Performance. *Cell Metab.* **2017**, *25*, 242–247. [CrossRef]
113. Yu, M.; Tsai, S.F.; Kuo, Y.M. The Therapeutic Potential of Anti-Inflammatory Exerkines in the Treatment of Atherosclerosis. *Int. J. Mol. Sci.* **2017**, *18*, 1260. [CrossRef]
114. Whitham, M.; Parker, B.L.; Friedrichsen, M.; Hingst, J.R.; Hjorth, M.; Hughes, W.E.; Egan, C.L.; Cron, L.; Watt, K.I.; Kuchel, R.P.; et al. Extracellular Vesicles Provide a Means for Tissue Crosstalk during Exercise. *Cell Metab.* **2018**, *27*, 237–251 e234. [CrossRef]
115. Safdar, A.; Tarnopolsky, M.A. Exosomes as Mediators of the Systemic Adaptations to Endurance Exercise. *Cold Spring Harb. Perspect. Med.* **2018**, *8*, a029827. [CrossRef]
116. Jesko, H.; Stepien, A.; Lukiw, W.J.; Strosznajder, R.P. The Cross-Talk Between Sphingolipids and Insulin-Like Growth Factor Signaling: Significance for Aging and Neurodegeneration. *Mol. Neurobiol.* **2018**. [CrossRef]
117. Trayssac, M.; Hannun, Y.A.; Obeid, L.M. Role of sphingolipids in senescence: Implication in aging and age-related diseases. *J. Clin. Investig.* **2018**, *128*, 2702–2712. [CrossRef]
118. Jazwinski, S.M. Mitochondria to nucleus signaling and the role of ceramide in its integration into the suite of cell quality control processes during aging. *Ageing Res. Rev.* **2015**, *23*, 67–74. [CrossRef]
119. Fakouri, N.B.; Hansen, T.L.; Desler, C.; Anugula, S.; Rasmussen, L.J. From powerhouse to perpetrator—mitochondria in health and disease. *Biology* **2019**, (in press).

cells

MDPI

Review

Regulation of Microglial Functions by Purinergic Mechanisms in the Healthy and Diseased CNS

Peter Illes [1,2,*], Patrizia Rubini [2], Henning Ulrich [3], Yafei Zhao [4] and Yong Tang [2,4]

1 Rudolf Boehm Institute for Pharmacology and Toxicology, University of Leipzig, 04107 Leipzig, Germany
2 International Collaborative Centre on Big Science Plan for Purine Signalling, Chengdu University of Traditional Chinese Medicine, Chengdu 610075, China; patrizia.rubini@cdutcm.edu.cn (P.R.); tangyong@cdutcm.edu.cn (Y.T.)
3 Department of Biochemistry, Institute of Chemistry, University of São Paulo, São Paulo 748, Brazil; henning@iq.usp.br
4 Acupuncture and Tuina School, Chengdu University of Traditional Chinese Medicine, Chengdu 610075, China; zhaoyafei@stu.cdutcm.edu.cn
* Correspondence: peter.illes@medizin.uni-leipzig.de; Tel.: +49-34-1972-46-14

Received: 17 March 2020; Accepted: 27 April 2020; Published: 29 April 2020

Abstract: Microglial cells, the resident macrophages of the central nervous system (CNS), exist in a process-bearing, ramified/surveying phenotype under resting conditions. Upon activation by cell-damaging factors, they get transformed into an amoeboid phenotype releasing various cell products including pro-inflammatory cytokines, chemokines, proteases, reactive oxygen/nitrogen species, and the excytotoxic ATP and glutamate. In addition, they engulf pathogenic bacteria or cell debris and phagocytose them. However, already resting/surveying microglia have a number of important physiological functions in the CNS; for example, they shield small disruptions of the blood–brain barrier by their processes, dynamically interact with synaptic structures, and clear surplus synapses during development. In neurodegenerative illnesses, they aggravate the original disease by a microglia-based compulsory neuroinflammatory reaction. Therefore, the blockade of this reaction improves the outcome of Alzheimer's Disease, Parkinson's Disease, multiple sclerosis, amyotrophic lateral sclerosis, etc. The function of microglia is regulated by a whole array of purinergic receptors classified as P2Y12, P2Y6, P2Y4, P2X4, P2X7, A2A, and A3, as targets of endogenous ATP, ADP, or adenosine. ATP is sequentially degraded by the ecto-nucleotidases and 5′-nucleotidase enzymes to the almost inactive inosine as an end product. The appropriate selective agonists/antagonists for purinergic receptors as well as the respective enzyme inhibitors may profoundly interfere with microglial functions and reconstitute the homeostasis of the CNS disturbed by neuroinflammation.

Keywords: surveying microglia; amoeboid microglia; P2X receptors; P2Y receptors; P1 receptors; CD39; CD73; microglia-neuron crosstalk; phagocytosis; microglial products; neuroinflammation

1. Introduction

The human central nervous system (CNS) consists of neuronal and non-neuronal cells in approximately a 1:1 relationship [1,2]. Glia constitute most of the non-neuronal cell population, but other cell types such as pericytes and endothelial cells are also part of it. On the basis of morphological criteria, in the human neocortex, oligodendrocytes (including oligodendrocyte precursor cells, NG2 glia) account for about 50–75% of the total glial population, astrocytes for 20–40%, and microglia for 5–10% [3,4]. Microglial cells are resident macrophages and the most important effectors of the brain's innate immunity [5,6]. The origin of microglia has been the subject of a long-standing debate, which reached an end a couple of years ago with the recognition that in spite of their similarity to peripheral

macrophages, these cells are of different genetic origin. Macrophages are continuously produced in the bone marrow during the post-natal stage, whereas microglia are derived from yolk-sac progenitors migrating into the CNS by starting at embryonic day 8.5 and continuing this migration until the blood–brain barrier is formed [7]. Lineage-specific genes (e.g., *Pu.1, Irf8*) define the microglial transcriptional network and distinguish it from that of tissue-resident macrophages [8].

Microglia exist in a highly ramified form under resting conditions but get activated by changes in brain homeostasis [9]. This leads eventually to polarization into an amoeboid form which is able to phagocytose pathogenic bacteria and releases a number of bioactive molecules such as pro-inflammatory cytokines (interleukin-1β (IL-1β), tumor necrosis factor (TNF-α), chemokines, proteases, reactive oxygen/nitrogen species, and probably also the excitotoxic ATP and glutamate by vesicular exocytosis) [10]. In addition to this classically activated M1 microglial/macrophage phenotype, typically releasing the mentioned destructive pro-inflammatory mediators, the alternatively activated M2-phenotype clears cellular debris through phagocytosis and releases numerous protective factors (IL-4, IL-13, nerve growth factor (NGF), fibroblast growth factor (FGF)) [11]. Whereas M1 microglia are supposed to participate in immunological defense mechanisms of the CNS, M2 microglia are involved in regenerative mechanisms accompanying long-lasting neurodegeneration in, e.g., Alzheimer's Disease (AD) or Parkinson's Disease (PD). In addition to the differential release of inflammatory and protective factors from M1 and M2 microglia, respectively, the two phenotypes are characterized by different cell surface markers (e.g., M1: CD11b, CD16; M2: CD163, CD206) [12,13]. Further, in vitro treatment of microglia with lipopolysaccharide (LPS) induces transformation to M1 microglia, whereas treatment with the autocrine cytokine IL-4 induces transformation to M2 microglia [14].

However, recent evidence indicates that the M1/M2 dichotomy is an oversimplified conceptual framework that only represents two extreme activation states. Firstly, M2 microglia/macrophages are divided into three major types based on their roles (M2a, M2b, M2c) [15,16], and secondly, a mixture of M1/M2 phenotypes have been also reported [17]. It is now clear that there is not either a single nor a discrete number of microglial reactive states but a diversity of phenotypes that are determined by a fine detection of environmental cues, which allows microglial cells to perform specific functions in different physiological and pathological conditions [16]. In spite of these limitations, the M1/M2 concept is generally accepted as a working model used to describe microglial phenotypic appearances.

After having conveyed some useful general knowledge on microglial cells, we will discuss the physiological/pathophysiological functions of microglia.

2. Physiological Roles of Microglia

2.1. Comparability of Results Obtained on Microglia Under In Vivo and In Vitro Conditions

Mechanical damage inflicted upon brain tissue during the preparation of primary cell cultures activates resting microglia; therefore, results from cell cultures should be interpreted with caution (microglia has morphological and functional properties different from the in vivo situation); results obtained from the superficial layers of brain slice preparations may also supply properties only relevant for activated microglia (in deeper layers, the conditions are more comparable to the in vivo situation) [16]. Because we deal in this review article with purinergic receptors of microglia and the (patho)physiological effects mediated by them, it is important to find out whether these effects are comparable in cultured preparations and synaptically wired in vitro experimental systems.

Microglia respond to neurotransmitter release and neuronal activity at nearby synapses, although, in contrast to isolated/cultured microglia [18], these cells, when located in brain slices or in the intact brain, are largely devoid of receptors for most neurotransmitters [19]. However, they exhibit a plethora of P2X and P2YR subtypes which may be activated by ATP released from neurons following the stimulation of their receptors by other neurotransmitters [2]. Purinergic receptors, as well as ATP release mechanisms participating in neuron–astrocyte–microglia cross-talk, are illustrated in Figure 1 (see also Section 5).

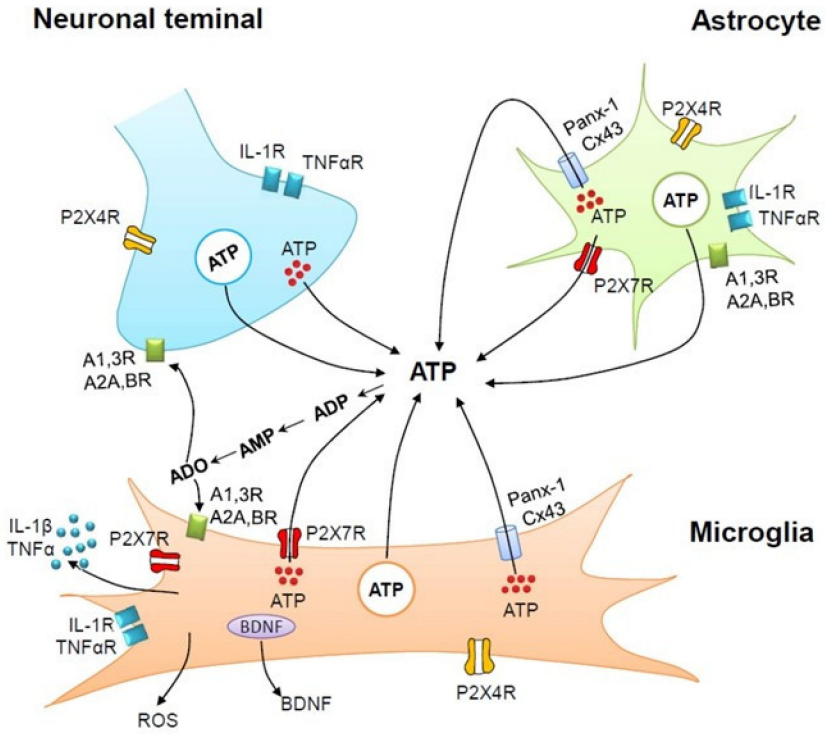

Figure 1. Purinergic receptors as well as ATP release mechanisms participating in neuron-astrocyte-microglia cross-talk. Microglia possess the ligand-gated P2X4 and P2X7 receptor subtypes as well as all subtypes of the G protein-coupled P1 (A1, A2A, A2B, A3) receptors. In addition, microglia release ATP from synaptic/lysosomal vesicles via exocytosis but also via connexin (mainly Cx43) channels and pannexin (Panx-1) hemichannels. P2X4 receptor (R) activation induces the vesicular release of brain-derived neurotrophic factor (BDNF), which causes neuropathic pain in the dorsal horn spinal cord. P2X7R activation results in the outward blebbing of the microglial plasma membrane and the production of extracellular vesicles containing interleukin-1β (IL-1β). The pro-inflammatory cytokines IL-1β and tumor necrosis factor-α (TNFα) bind to their receptors IL-1R and TNFαR, respectively. P2X7R activation induces the diffusion of reactive oxygen species (ROS) through the plasma membrane. All these microglial products cause neuroinflammation and neurodegeneration. Exocytotic, Ca^{2+}-dependent, vesicular release occurs from neurons, astrocytes, and microglia. The vesicular release of ATP from neurons is much faster than that from astrocytes or microglia, although the vesicular proteins involved in exocytosis are relatively similar in the three cell types. ATP is rapidly degraded by ecto-nucleotidases to ADP, AMP, and eventually by 5′-nucleotidase to the bioactive adenosine (ADO). Artwork by Dr. Haiyan Yin.

The group of Helmut Kettenmann noticed as early as 1993 that cultured microglial cells prepared from the mouse brain respond to ATP at the resting membrane potential with an early inward cationic current and a late outward K^+ current [20,21]. The cultured cells were slightly elongated but process-free, thereby exhibiting morphological characteristics of amoeboid microglia [20]. The non-selective cationic current was considered to be due to the activation of P2X, and the late K^+ current to the activation of P2Y receptors (Rs). These effects of ATP could be reproduced in microglial cells of acute brain slices identified by staining with Texas Red-coupled tomato lectin [22,23]. In mouse corpus callosum slices, the cells recorded from showed the typical morphology of resting, process-bearing microglia [23].

Somewhat later, a similar situation was observed to occur in rat cortical astrocytes. both in cell culture and in brain slices. The highly plastic astrocytes exhibited, instead of their typical process-bearing shape, a confluent, background layer of flat cells on the base of the culture dish [24], while in brain slices prepared from the rat prefrontal cortex, fluorescence microscopy of Lucifer Yellow-filled astrocytes showed cells surrounded by dense processes extending several micrometers

around the somata [25]. Nonetheless, the P2X7R currents recorded from microglia in primary cultures and brain slices could not be discriminated from each other either by physiological (reversal potential measurement) nor pharmacological (selective agonists and antagonists) means.

Based on these and similar observations, we tentatively suggest that whereas cultured microglia/astrocytes may only incompletely model the in vivo situation for a variety of CNS signalling molecules, ATP/ADP and even adenosine effects are much more stable at different levels of synaptic organization or their absence (primary cell cultures, acutely isolated cells, brain slice preparations, intact brain). The reason for this phenomenon may be that ATP/ADP/adenosine are primitive signalling molecules appearing very early in phylo- and ontogenesis and being quite enduring in their functional properties [26,27]. Therefore, we decided to indicate only in a few cases when tissue cultures were used for investigations.

2.2. Microglial Process Motility

In order to investigate microglial cells in their natural environment, transgenic mice (CX3CR1-EGFP; [28]) were used which showed specific expression of enhanced green fluorescent protein (EGFP) in resident microglia of the CNS. CX3CR1 (R stands for receptor) is a chemokine receptor highly specific to microglia; the chemokine fractalkine (CX3CL1; L stands for ligand) is present in neurons and signals to microglia via this receptor [29]. Time-lapse imaging experiments were acquired transcranially by using thinned-skull preparations in vivo. The somata of microglial cells remained fixed for rather long periods of time, while the microglial processes were remarkably motile. These processes rapidly approached a small laser ablation caused by the two-photon laser [30] or disruption of the blood–brain barrier and provoked a shielding of the injured site [31]. It was most interesting to notice that the release of ATP via astrocytic hemichannels may be a chemoattractant to induce site-directed movement of microglial processes [30]. It was concluded that resting microglia continuously survey the parenchymal environment within non-overlapping territories with a multitude of fine, exceptionally motile processes/protrusions and sense tissue abnormalities [32,33].

2.3. Microglia–Neuron Crosstalk at Synaptic Structures

Microglia are well-positioned to monitor neuronal firing and synaptic function; in response to neuronal activity, microglia steer their processes towards active synapses [34,35]. In adult mouse visual cortex, dynamic interactions between highly motile microglial processes and synaptic structures were observed under non-pathological conditions by two-photon imaging [34]. In this study, microglial processes were found to interact with axon terminals and dendritic spines in a transient manner. Reducing neural activity by enucleating both eyes induced retraction of microglial processes.

The ‘tripartite synapse’ hypothesis suggests that presynaptic neuronal elements, postsynaptic dendritic specializations, and astrocytic processes that contact or even enwrap the synapse, together form a mutually interacting unit influenced by neuro- and glio-transmitters [36]. The realization that microglial processes also contact synaptic structures and thereby establish a dynamic crosstalk between astrocytes, microglia, and neurons broadened this concept to the idea of a ‘quadpartite synapse’ [37]. It has been shown that neuronal ATP may modulate the microglial secretion of certain cytokines [38]. In return, microglia influence and modulate neuronal functions by the release of cytokines, prostaglandins, and neurotrophic factors [37]. In accordance with this assumption, microglia could regulate the basal glutamatergic and GABAergic synaptic transmission [39].

2.4. Microglial Phagocytosis

It has been known for a long time that neuronal damage leads to the activation of ramified microglia through several steps transforming them by multiple factors, such as colony-stimulating factor, LPS, and interferon-γ, into the amoeboid morphology [40,41]. More recently, it became generally accepted that macrophage/microglia activation is not an all-or-none process; it may be partially reversible and depends on the pathological context, the nature and strength of the stimuli, and the

settings in which these stimuli appear [16,42]. With these limitations in mind, the reader should forgive us for illustrating microglial activation because of didactic reasons in Figure 2 as a linear process.

Complement receptors appear to steer microglial phagocytosis. It was shown that C1q, the initiating protein in the classical complement cascade, is expressed by postnatal neurons and is localized to synapses throughout the CNS [43]. Mice deficient in complement protein C1q or the downstream complement protein C3 exhibit large sustained defects in CNS synapse elimination, leading to abnormal neuronal function. In conclusion, it is hypothesized that unwanted synapses are tagged by complement and are subsequently eliminated by microglial activity induced by the binding of this complement to its microglial pattern recognition receptor CR3.

In fact, microglia engulf presynaptic inputs in the reticulogeniculate system of the visual pathway, and engulfment is dependent upon neuronal activity as well as the microglia-specific phagocytic signal transduction [44]. This was shown by the use of mice lacking functional CR3 or mice deficient in the CR3 ligand C3; the knockout animals did not show the microglial reactions aimed at eliminating synapses. Hence, it was concluded that based on the perception of synaptic activity, microglia are able to remove excess synapses by synaptic pruning and thereby shape postnatal neuronal circuits [44].

Further evidence for microglial phagocytosis was obtained from investigations of the fractalkine (CX3CL1) pathway (see Section 2.2). Young CX3CR1 knockout mice show a significant reduction in the density of microglia during the postnatal period and exhibit transient defects in synaptic connectivity and plasticity in the postnatal hippocampus [45]. These mice reveal an increase in dendritic spine density and postsynaptic density protein 25 (PSD-95) immunoreactivity, enhanced hippocampal long-term depression, and decreased duration of latency to pentylenetetrazol-induced seizure responses, characteristically associated with less mature synapses. It was considered that synaptic pruning by microglia is targeted to both pre- and postsynaptic elements and is necessary for normal brain development which is absent in these knockout animals [45].

In contrast to the idea of microglial 'phagocytosis' of entire synapses, it was reported that only 'trogocytosis' (synaptic nibbling) occurs [46]. This means elimination of presynaptic boutons and axons, with no evidence for elimination of postsynaptic material. Intriguingly, microglia contacts at postsynaptic sites frequently elicited transient filopodia, most of which originated from mature spines. It is quite possible that the neuronal damage is preferentially presynaptic [44], with some denervation-type secondary changes on the postsynaptic side [45].

In addition to synaptic pruning, microglia may sculpt neuronal circuits during development by selective phagocytosis of neural stem cells (NSCs) [47,48]. Neurons of the adult cerebral cortex are generated in the ventricular and subventricular zones during prenatal development [49]. Phagocytosis of overtly produced cells by microglia is essential, especially at the end stages of cortical neurogenesis [48]. Unrestrained cell production during prenatal brain development would have profoundly negative consequences for brain organization and function. Not only surplus NSCs, but freshly generated redundant neurons may also be killed and eliminated by microglial apoptosis and subsequent phagocytosis [50,51].

3. Pathological Roles of Microglia-activation Processes

As previously mentioned, microglia get activated in response to changes in brain homeostasis. These cells acquire phagocytic properties and the ability to release a number of pro-inflammatory molecules. The ATP-sensitive P2X7R, which is a subtype of the ligand-gated P2XR family (see Sections 4.1 and 4.2.4), is a major driver of inflammation [52]. This receptor is stimulated by large concentrations of ATP outpouring from CNS cells under noxious conditions during both acute injury (e.g., trauma, hypoxia/ischemia or epilepsy-induced seizures) and chronic neurodegenerative illnesses (e.g., AD, PD, amyotrophic lateral sclerosis, and multiple sclerosis) [53].

In the CNS, P2X7Rs are preferentially localized on microglial cells [54]. Microglia are equipped with a battery of pattern recognition receptors that stereotypically recognize pathogen-associated molecules (PAMPs) that warn of the presence of exogenous material such as components of the bacterial

cell wall (e.g., lipopolysaccharide (LPS) acting on toll-like receptor TLR4) or repeats of bacterial or viral nucleic acids [55]. Microglia also possess a wide range of surface molecules sensing danger-associated molecular patterns (DAMPs), such as scavenger [56], purine P2X7 [57], and cytokine/chemokine receptors; the stimulation by PAMPs/DAMPs results in the activation of resting microglia [58].

The activation process can be traced by bulk RNA [59] and single-cell RNA [60] sequencing, as well as by epigenetic [61] and proteomic analyses [16,62]. These investigations lend further support to the most heterogeneous nature of this process in microglial cells. Based on single-cell RNA sequencing data, homeostatic microglia adopt distinct disease-associated microglia (DAM) profiles in amyloid β (Aβ) protein plaques of AD brains [60,63]. Aβ is one of the neurodegeneration-associated molecular patterns (NAMPs) that are commonly present in various pathogenous CNS conditions and are recognized by receptors constitutively expressed on microglia triggering their transition/activation into DAM [64]. In conclusion, DAM microglia have been identified as a subpopulation of microglial cells in experimental models of neurodegenerative illnesses such as AD, frontotemporal dementia, and amyotrophic lateral sclerosis [64].

4. P1 and P2 Purinergic Receptors Involved in Microglial Functions

4.1. Receptors and Inactivation Mechanisms for ATP/ADP and Adenosine

ATP not only supports energy storage within cells but is also a transmitter/signalling molecule that serves intercellular communication [65]. Receptors for ATP have been classified into two types, the ligand-gated cationic channel P2X (seven mammalian subtypes: P2X1, 2, 3, 4, 5, 6, and 7) and the G protein-coupled P2YRs (eight mammalian subtypes: P2Y1, 2, 4, 6, 11, 12, 13, and 14) [66]. P2XRs consist of assemblies of three identical or divergent subunits, thereby forming homo- or heteromeric channels [67]. The P2X7R is unique in occurring only as a homotrimer and causing, in addition to immediate effects, molecular changes on a much longer time scale, such as proliferation and apoptosis [68]. Numerous detailed review articles discuss evidence for the presence of P2X/P2YRs on microglia and the functional consequences of their activation (e.g., [69–71]); this information will be updated in the present overview.

P2R signalling is terminated by the conversion of ATP/ADP to adenosine within the extracellular compartment by the activity of ecto-nucleotidases. The four main groups of ectonucleotidases are the ecto-nucleoside triphosphate diphosphohydrolases (NTPDases), ecto-5′-nucleotidase, ectonucleotide pyrophosphatase/phosphodiesterases, and alkaline phosphatases [72,73]. The degradation of ATP/ADP to adenosine generates an agonist with multiple, sometimes opposite, effects to those of its mother molecules. Adenosine may act at four types of receptors, termed A1, A2A, A2B, and A3 [74]. All adenosine receptors are G protein-coupled; A1/A3Rs inhibit adenylate cyclase activity via coupling to Gi/o, while A2A/A2BRs stimulate this enzyme via $G_{s/olf}$. The effect of adenosine is terminated by enzymatic degradation to the only slightly active inosine by adenosine deaminase [75] or by enzymatic conversion to AMP by adenosine kinase [76]. However, extracellular adenosine is also rapidly taken up into the surrounding tissue by the equilibrative nucleoside transporter isoenzymes ENT1-4 [77].

All these receptors and enzyme systems form a complex network sometimes called the ‘purinome’ [78]. Within this network, the enzymatic pathways generate agonists for a wide range of receptors, which results in a huge diversity of sometimes even contradictory responses. In the present review article, we will concentrate on those receptors which are important for the regulation of microglial functions (Figure 2). It has to be mentioned that depending on the activation state of microglia, the densities as well as the agonist sensitivities of their purinergic receptors become modified [19,79,80].

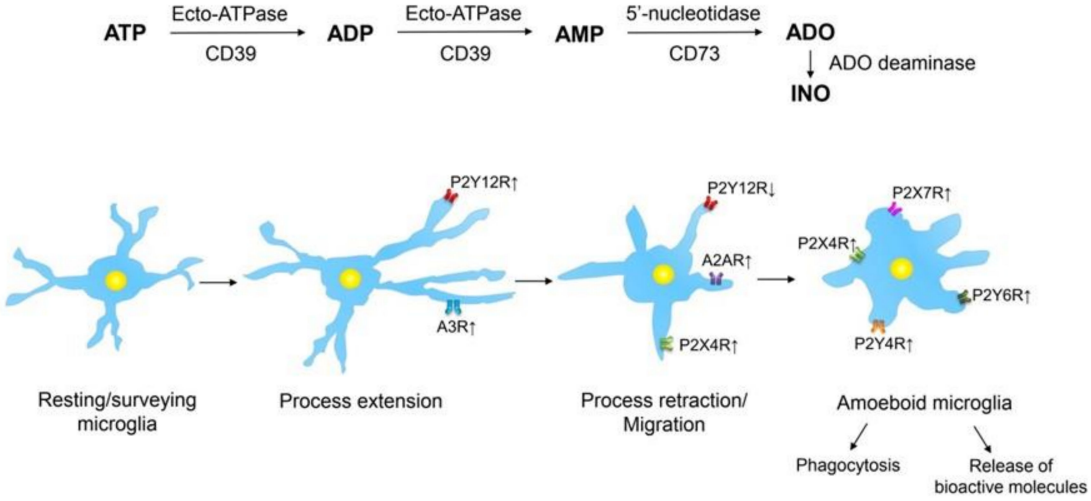

Figure 2. Purinergic receptors at microglial cells exemplifying their different activation states. ATP is sequentially dephosphorylated by an enzymatic cascade to AMP by ecto-ATPase (NPDase-1; CD39) through the intermediary product ADP. AMP is further degraded to adenosine (ADO) by 5′-nucleotidase (CD73). Finally, adenosine is almost inactivated by adenosine deaminase to inosine (INO). Resting/ramified microglia extend and retrieve processes, thereby scanning their territories, non-overlapping with those of the neighboring microglial cells. When ATP is released/outpoured into the extracellular space from damaged CNS cells, as a first step of microglial activation, these cells extend their processes towards the site of injury triggered by stimulation of P2Y12 receptors (Rs). Both P2Y12 and A3Rs are upregulated in consequence of CNS damage, and they co-operate in steering the microglial process extension. Subsequently, these processes retract due to the downregulation of P2Y12Rs and the upregulation A2ARs; the migratory activity of this microglia is controlled by the interaction of P2Y12 and P2X4Rs. After the complete retraction of the microglial processes, an amoeboid phenotype is evolving. On this microglia, phagocytosis and pinocytosis are induced by P2Y6R and P2Y4R activation, respectively. P2X4Rs mediate the secretion of brain-derived neurotrophic factor (BDNF) in spinal cord microglia. P2X7Rs may initiate multiple secretory processes such as the release of pro-inflammatory cytokines, chemokines, growth factors, proteases, reactive oxygen/nitrogen species, cannabinoids, and probably also the excitotoxic ATP and glutamate. Upwardly directed arrows beside receptors indicate their upregulation or increased activation by agonists, while downwardly directed arrows indicate their downregulation or decreased activation by agonists. For further details, see [19,79,80]. Artwork by Dr. Haiyan Yin.

4.2. Regulation of Physiological and Pathological Functions of Microglia by ATP/ADP, UTP/UDP, and Adenosine; Chemotaxis and Secretory Properties

4.2.1. P2Y12 and P2Y13 Receptors

As mentioned earlier, resting/surveying microglia continuously scan a given territory of their parenchymal environment with a multitude of fine and exceptionally motile processes/protrusions and record tissue abnormalities (see Section 2.1). While one of the original reports on this phenomenon already delivered convincing proofs for the participation of ATP/ADP in the motility of the microglial processes [30], a more recent publication characterized the receptor involved as belonging to the ADP-sensitive P2Y12-type [81]. The P2Y12R was initially identified on blood platelets, where it regulates their conversion from the inactive to the active state during the blotting process [82]. The molecular changes triggered by P2Y12R activation appear to be similar in platelets and microglia, but of course with different functional consequences. Protruding microglial processes may shield minor sites of endothelial/astrocytic/neuronal damage in the CNS [31]. More massive disturbances of CNS homeostasis, however, result in strong activation of microglia, adapting an amoeboid morphology; this causes migration of the microglial cell body towards the source of released ATP [83].

We discussed already that microglial processes contact synaptic structures and thereby establish a dynamic cross-talk with neurons [37]. However, a recent publication raised an alternative, most interesting hypothesis [84]. The authors of this study identified the site of interaction between microglial processes and cortical layer 2/3 neurons at the cell body rather than at synaptic elements, including axonal boutons and dendritic spines, in the adult brain of CRXCR1-GFP transgenic mouse. Metabolic activity of neuronal mitochondria was linked by the production of ATP and its somatic, vesicular release, with the rapid formation of microglial junctions. In consequence, the protrusion of microglial processes was an immediate reaction to neuronal activation and was blocked by inhibition of P2Y12Rs.

Microglial process extension, and as a non-obligatory second step, the transition of resting to amoeboid microglia and its migratory movement, is due to the P2Y12R-induced activation of phosphatidylinositol 3′-kinase (PI3K) and phospholipase C (PLC) signalling pathways [85]. It was reported that the PLC-mediated increase in intracellular Ca^{2+} concentration-triggered proteinkinase B (Akt) activation was also involved in the second-messenger mechanisms of P2Y12Rs [85]. Eventually, P2Y12Rs initiate an adhesive interaction with the surrounding extracellular matrix through integrins [86].

Nerve-injury-activated microglia engulf myelinated axons in the spinal cord dorsal horn in a P2Y12R-triggered and p38 mitogen-activated protein kinase signalling dependent manner; this reaction is causally involved in the pathogenesis of neuropathic pain [87]. Further, P2Y12Rs contribute to the neuronal damage in brain ischemia [88,89] and multiple sclerosis [90].

P2Y12 and P2Y13R mRNA and protein both occur in microglia in considerable amounts; accordingly, P2Y13Rs markedly potentiate the P2Y12R-mediated chemotaxis response [91]. In addition, microglia in P2Y13R-deficient mice were less ramified than in the wild-type controls, suggesting the participation of these receptors in the regulation of microglial morphology.

4.2.2. P2Y6 and P2Y4 Receptors

Whereas P2Y12 is an ADP-sensitive receptor, the agonist rank order at P2Y6Rs, the nucleotide with the highest agonist potency is UDP (UDP > UTP > ADP), and at P2Y4Rs, UTP (UTP > ATP = UDP; human) or UTP = ATP (rat, mouse) [92]. It was reported that binding of the endogenous agonist UDP to metabotropic P2Y6Rs triggers microglial phagocytosis [93]. P2Y6Rs of microglia are upregulated when neurons become damaged and send diffusible UDP signals to microglia to initiate phagocytosis and the clearing of neuronal debris. It is interesting to mention that during metabolic damage caused by mesial temporal lobe epilepsy, large concentrations of ATP are released, which may blind microglia to the ATP microgradients released by apoptotic cells as 'find me' signals; this causes a decreased phagocytic activity of microglia [94] (see also Section 5). Hence, UDP and ATP signalling may affect phagocytosis in opposite manners.

Pinocytosis, the internalization of fluid-phase materials, is regulated by P2Y4 rather than P2Y6Rs [95]. Another function of UDP via P2Y6R stimulation is to block the ATP-dependent migration of microglia, most likely by a shift from its migratory phenotype to a phagocytic one [96].

4.2.3. P2X4 Receptors

P2X4 and *P2X7* genes in humans are located on chromosome 12 in close proximity, indicating a tight relationship [97]. The overlapping expression of the receptor proteins has been documented in peripheral macrophages and microglia [98]. The reason for this co-expression may be the involvement of both receptors in inflammatory processes [99]. The binding affinities largely differ between P2X4 and P2X7Rs; while the former one is activated by ATP in the micromolar range, the latter one responds to ATP in the millimolar range [100]. The two receptors do not form a heteromeric receptor but appear to mutually influence each other on the molecular level and may become activated over a wide range of ATP concentrations as a P2X4-P2X7R multiprotein complex [101].

In addition to their discrimination by selective pharmacological ligands, the two related receptors exhibit at least threefold functional difference: (1) in neuronal tissue, P2X4Rs can be found in astrocytes and microglia as well as in neurons; by contrast, P2X7Rs appear to be localized in all types of glial cells, but not in neurons [102]; (2) unlike P2X7Rs, P2X4Rs are predominantly located intracellularly in lysosomal compartments of microglia [103], from where they traffic to the cell membrane under the influence of inflammatory stimuli [104]; and (3) both P2X7 and P2X4Rs form on long-lasting-activation large cytolytic pores, allowing the transmembrane passage of molecules larger than the diameter of their intrinsic channel proteins [105]. However, as opposed to P2X7Rs, the pores formed by P2X4Rs fail to induce cytoskeletal rearrangements and do not lead to cell death [105].

P2X4Rs may increase both migration and secretory properties of microglia. It was found that this receptor interacts with the P2Y12R in regulating chemotaxis; the downregulation or pharmacological blockade of P2X4Rs protracted microglial site-directed migration [83]. Spinal microglia may secrete on activation brain-derived neurotrophic factor (BDNF), causing an altered transmembrane gradient of Cl^- in a subpopulation of dorsal horn lamina I neurons, presumably through the downregulation of the neuronal chloride transporter KCC2 [106,107]. This in turn reverses in these neurons the polarity of GABA and glycine effects to depolarization instead of hyperpolarization, resulting in an excitability increase. Such an excitability increase manifests itself on the systemic level as neuropathic pain, with the cardinal symptoms of spontaneous pain, hyperalgesia, and tactile allodynia. Although these early investigations suffered under the low selectivity of the antagonist trinitrophenyl-ATP (TNP-ATP) for P2X4Rs versus P2X1 and P2X3Rs, the simultaneous use of antisense oligodeoxynucleotides and P2X4R-deleted mice strengthened the conclusions. It is noteworthy that, in the meantime, we have several highly selective P2X4R antagonists/negative allosteric modulators at our disposal [108].

Mechanical injury of the L4 spinal nerve induces the production of the chemokine CCL21 and its transportation via the dorsal root ganglion to the spinal cord dorsal horn, where it increases the membrane expression of intracellular P2X4Rs [109]. The extracellular matrix protein fibronectin also stimulates the upregulation of P2X4Rs in microglial cells [110]. Fibronectin acts through the activation of Lyn, a member of the Src tyrosine kinase family [111].

Microglia have been shown to shape the function of oligodendrocyte precursor cells (OPCs), the brain cells which differentiate into myelin-forming cells [112]. In consequence, microglia participated both in myelin injury and remyelination during multiple sclerosis, depending on the release of the lipid components of extracellular vesicles released from microglial cell surfaces (see also Section 4.2.4). Further, blockade of P2X4R signalling exacerbated clinical signs in the experimental autoimmune encephalomyelitis (EAE) model of multiple sclerosis; this blockade also favored microglia activation to a pro-inflammatory phenotype and inhibited myelin phagocytosis [113]. Conversely, potentiation of P2X4R signalling by the positive allosteric modulator ivermectin favored a switch in microglia to an anti-inflammatory phenotype and promoted remyelination.

In a model of kainate-induced status epilepticus (SE), SE was associated with an induction of P2X4R expression in the hippocampus, mostly localized in activated microglial cells [114]. In P2X4R-deficient mice, behavioral responses to kainate-induced SE were unaltered, but some specific features of microglial activation (cell recruitment, upregulation of voltage-dependent K^+ channels) were impaired. Therefore, the CA1 area of the hippocampus was protected from SE-induced neuronal death in the P2X4R knockout (KO) animals when compared with their wild-type controls.

4.2.4. P2X7 Receptors

The expression of P2X7R mRNA and protein in the brain is highest in microglia, with much lower quantities in astrocytes [115]. Because of its well-known low sensitivity to ATP, this receptor becomes activated only by high concentrations of ATP released/outpouring from CNS cells under pathological conditions. It was suggested about twenty years ago that some P2XR channels (P2X2, P2X4, P2X7) exhibit progressive dilation during repetitive or long-lasting stimulation by ATP and that the generated pore is permeable to high molecular weight cationic dyes [116,117]. However, it was later

shown that this interpretation of the experimental data obtained by reversal potential measurements is probably misleading [101,118], especially because patch-clamp recordings failed to document a change in single-channel current amplitudes or permeation characteristics during continuous ATP application [119]. Nonetheless, convincing experimental evidence proves the opening of a gateway for the entry of large molecules (e.g., Yo-Pro) into the cell interior after P2X7R stimulation, probably via the associated protein pannexin-1 forming a hemichannel [120].

The P2X7R pore is believed to be involved in the release of neuroinflammatory cytokines. Activation of microglia stimulates the release of IL-1β in a two-step process: the first being the occupation of TLR4 by LPS, leading to accumulation of cytoplasmic pro-IL-1β, and the second one being the ATP-dependent stimulation of P2X7Rs, promoting nucleotide-binding, leucine-rich repeat, pyrin domain containing 3 (NLRP3), inflammasome-mediated caspase-1 activation, and eventually secretion of IL-1β [121]. Caspase-1 generates IL-1β from pro-IL-1β by enzymatic degradation. It is important to note that the decrease of intracellular K^+ is a major stimulus for P2X7R-dependent NLRP3 inflammasome activation [122]. Although the maturation and release of IL-1β and IL-18 are initiated by the co-stimulation of TLR4 and P2X7Rs, activated microglia may secrete also further pro-inflammatory cytokines, such as IL-6 and TNFα by other mechanisms [123]. It is important to note that the loss of intracellular K^+ through the P2X7Rs themselves [52,116], or via two-pore domain K^+ channels [124], is a major stimulus for P2X7R-dependent NLRP3 inflammasome activation.

IL-1β is released from microglia, packed in extracellular vesicles of variable shape/size generated by the outward blebbing of the microglial plasma membrane [125,126]. Several lines of evidence indicate that P2X7R activation by ATP is the initiating factor of blebbing, which is furthermore dependent upon p38 mitogen-activated protein kinase; it also requires rho-associated protein kinase (ROCK) activation, causing disassembly of the cytoskeletal elements, and is associated with the P2X7R C-terminus [127].

It was reported for a mouse embryonic spinal cord preparation that the ability of microglia to proliferate depends on the presence of wild-type P2X7Rs; microglia prepared from P2X7R-deficient mice showed only moderate proliferation [128]. This suggests that the physiological proliferation of microglia observed at day 13.5 in the spinal cord motoneuron area, when microglia phagocytize dying motoneurons, is regulated by P2X7Rs [128,129]. In enriched microglial cultures, only the pore-forming variant of P2X7R was able to promote proliferation [130,131]. In the case of a point mutation in the *N*-terminus of this receptor (P2X7R-G345Y), the pore-forming and proliferation-inducing capacities were lost, although the channel function remained intact. It was also reported that the ability of P2X7Rs to drive microglial proliferation appears to depend on the release of IL-1β [130].

Microglial phagocytosis is executed in the first line by P2Y6Rs, but P2X7Rs are also involved in this cellular reaction. However, ATP inhibited rather than fostered microglial phagocytic activity in rat primary microglial cultures through the stimulation of P2X7Rs [132]. The knockdown or pharmacological blockade of P2X7Rs restored phagocytosis by ATP-treated microglia. In apparent contradiction to this finding, neural progenitor cells and neuroblasts of human fetal telencephalon could clear apoptotic cells by innate phagocytosis mediated by their P2X7Rs [133]. It was astonishing that this scavenger activity was not prevented/reversed by pharmacological P2X7R antagonists [134]. The involvement of authentic P2X7Rs in the phagocytic process was suggested among others by its typical low sensitivity to ATP and by molecular biology methods.

The loss of important cell ingredients through the P2X7R pore and the release of pro-inflammatory cytokines and chemokines with their subsequent deleterious effects may cause necrotic death of both the microglia itself ('suicide receptor'; [135,136]), and the targeted CNS neurons by the accompanying neuroinflammation evolving during neurodegenerative illnesses (AD, [137]; PD, [138]). In addition, P2X7Rs are involved in apoptotic reactions via the activation of the caspase cascade [139]. However, the P2X7R-mediated release of TNFα (causing not only apoptosis but also proliferation) may cause neuroprotection and in consequence favors neuroregeneration, observed during long-lasting neurodegenerative illnesses [140,141].

There is a high number of recent review articles available on the involvement of microglia [8,142] and especially their P2X7Rs in neurodegenerative diseases [143–145]. The reader is requested to consult these reviews instead of expecting a detailed discussion of such effects in our present overview. It should be mentioned, however, that irrespective of the pathophysiology of the specific neurodegenerative disease, there is always a superimposed neuroinflammatory component that heavily depends on the overstimulation of microglial P2X7Rs. This explains the demonstrated beneficial effect of P2X7R antagonists in various in vivo and in vitro experimental models of neurodegenerative illnesses such as AD [146,147], PD [148,149], amyotrophic lateral sclerosis [150,151], multiple sclerosis [152,153], epilepsy [154,155], and ischemia [156].

4.2.5. A2A and A2B Receptors

As pointed out repeatedly, microglia survey brain tissue by motile cell processes. The movement of these processes is guided by the local release of the chemoattractant ATP/ADP acting via P2Y12R stimulation. The ADP-driven process extension was reversed to process retraction during inflammation by A2A adenosine receptor upregulation coincident with P2Y12R downregulation [157]. Process retraction is indicative of the shaping of resting to amoeboid microglia and the development of a neuroinflammatory state characterized by microglial phagocytosis and the release of bioactive molecules. It was proposed that the enzymatic degradation of the originally released ATP to adenosine is causally involved in this process.

A2ARs have multiple effects in the CNS: (1) they increase the release of the excytotoxic glutamate from the respective nerve terminals, and (2) they increase the activation state of microglial cells [158]. Pharmacological blockade of A2ARs has emerged as an efficient therapeutic manipulation in various animal models of neurodegenerative disorders [146]. However, the agonistic stimulation of A2ARs may under certain circumstances also be beneficial [159]. In the following, we discuss a few examples of the predominantly neuroprotective effects of A2AR antagonists.

A2AR antagonists are effective as an adjuvant therapy to complement dopamine D2R agonistic drugs to treat PD [160]. The drug targets are supposed to be neuronal A2ARs situated at medium spiny neurons in the striatum, giving rise to the so-called indirect striatopallidal projections [53]. At the cell bodies of these neurons, A2A and D2Rs are co-localized and interact antagonistically. Thus, blockade of A2ARs enforces the effect of the diminished D2R-induced stimulation by pathologically low dopaminergic innervation from the damaged substantia nigra pars compacta. Microglia in the midbrain/substantia nigra display a higher degree of activation in patients with PD in post mortem samples and assessed with PET imaging [161], as well as in animal models of the disease [162]. Thus, A2AR antagonists certainly act at neuronal targets but also restore the activated/amoeboid, neuroinflammatory microglia to its resting/surveying state in an MPTP (selective dopaminergic neurotoxin) model of PD [163]. The consequence of this dual effect is a stronger D2R-mediated stimulation of the medium spiny neurons and additionally less degeneration of the neuronal pathways of the extrapyramidal system.

The enhancement of neuroinflammatory reactions after perinatal brain injury was observed in rats due to A2AR activation and the consequent upregulation of M1 microglial markers (IL-β, IL-6, TNF-α); an antagonist of A2ARs was beneficial under these conditions [164]. Developmental risk factors, such as the exposure to high levels of glucocorticoids, may contribute to the pathogenesis of anxiety disorders [165]. The perinatal exposure to dexamethasone of the prefrontal cortex of male rats caused hyper-ramification and increased length of microglial processes. A2AR antagonists were able to ameliorate the microglial process alterations and the accompanying anxiety behavior. Similarly, intracerebroventricular injection of an A2AR antagonist attenuated the LPS-induced increase in the level of inflammatory cytokines such as IL-1β, confirming the potentiation of neuroinflammation by A2AR agonists [166].

A2AR antagonists have been shown to protect retinal ganglion cells from microglia-induced damage in experimental models of glaucoma and ischemic retinal diseases [167]. This was shown

to be due to the reversal of microglia-mediated neuroinflammation. Eventually, A2BRs augmented the production of cytokines from microglia, irrespective of their pro-inflammatory (IL-6 [168]) or anti-inflammatory nature (IL-10 [169]).

4.2.6. A1 and A3 Receptors

In the CNS, A1Rs are highly expressed on microglia and as opposed to microglial A2ARs, do not induce cytoskeletal rearrangements [170,171]. In mouse microglia kept in primary culture, ATP caused, via the activation of P2X4 and P2X7Rs, a rounder cellular shape with ruffled borders; selective A1R agonists inhibited the morphological activation of microglia, probably by depressing the ATP-induced Ca^{2+} entry into these cells [171]. Similarly, the presence of A1Rs appeared to depress microglial responses to experimental traumatic brain injury (TBI; [172]) and EAE, a model of multiple sclerosis [173]. Evidence for this assumption was supplied by comparing the microglial response and neuronal damage to TBI, as well as the extent of the pro-inflammatory reactions accompanying EAE (microglial activation, demyelination, axonal injury, inflammatory gene expression) in the wild-type and KO animals. Agonists and antagonists for A1Rs confirmed the assumption that the stimulation of these receptors restricts activation of microglia during CNS injury or disease.

Microglial P2Y12Rs and A3Rs ensure a synergistic interaction between ATP and adenosine on process extension and migratory properties of this cell type [83]. Further, A3Rs attenuate neuropathic pain by suppressing the activation of microglia in the spinal cord dorsal horn [174].

4.2.7. NTPDase1 (CD39) and Ecto-5′-Nucleotidase (CD73)

Microglia have been shown to release ATP, which, either by itself or after degradation to adenosine, acts on microglial receptors in a feed-back manner [175,176]. The release machinery was attributed to lysosomes endowed with a vesicular nucleotide transporter (VNUT) which transports cytosolic ATP using the proton-mediated membrane potential as a driving force [176]. Local microinjection of the relatively stable non-selective P2R agonist ATP-γ-S into a rat microglial culture caused the release of ATP through lysosomal exocytosis [175]. It was suggested that this may provide a positive feedback mechanism to generate a long-range extracellular signal for attracting distant microglia to migrate towards and accumulate at the site of ATP release being a marker for local injury.

We mentioned earlier that ATP is degraded to AMP (mainly NTPDase1) and then to adenosine (5′-nucleotidase) by a cascade of enzymes (see Section 4.1). Three related family members of NTPDase are expressed in mammalian brain [177]. NPTDase1 (CD39) hydrolyses nucleoside 5′-triphosphates and -diphosphates equally well, NTPDase3 has a threefold preference to nucleoside 5′-triphosphates over -diphosphates, and NTPDase2 hydrolyses nucleoside 5′-diphosphates only to a marginal extent. NTPDase1 has been identified as a prominent ecto-nuleotidase in the nervous tissue and had specific expression in microglia and vascular tissue [178]. It has been reported that microglial cultures prepared from CD39 KO mice exhibited low migration rates towards ATP because there was no major degradation of this ATP to ADP and eventually to adenosine on the microglial plasma membrane [179]. In other words, the ADP-sensitive P2Y12R appeared to develop its full chemoattractant activity only under co-stimulation with adenosine A3Rs [79]. Similarly, microglia in acute brain slices of CD39 KO mice had increased constitutive phagocytic activity which could not be enhanced by ATP in contrast to control animals [180]. Whereas CD39 may block the enzymatic degradation of UTP to UDP, which is an agonist to the phagocytosis regulating P2Y6Rs, it is of no surprise that ATP had no effect in this system [79].

Constitutive deletion of CD39 and CD73 or both (lower endogenous ADP and adenosine concentrations) caused an inhibition of the microglial ramified phenotype in the mouse brain with a reduction in the length of microglial processes, branching frequency, and number of intersections [181]. By contrast, the elevation of extracellular adenosine levels by inhibition of adenosine uptake by dipyridamole, the application of exogenous adenosine, and the degradation of ATP/ADP by injected apyrase, facilitated the transformation of $CD39^{-/-}$ and $CD73^{-/-}$ microglia into a

ramified process-bearing phenotype. In conclusion, the modification of the agonist concentrations of ADP (P2Y12) and adenosine (A2A, A1/A3) receptors in the biophase around microglia by the ATP/adenosine-degrading enzymes CD39/CD73 regulated the neuroinflammation-relevant microglial functions.

CD73-derived A2AR signalling appeared to modulate microglial immunoresponses and morphological dynamics in mice [80]. The genetic inactivation of CD73 attenuated LPS-induced pro-inflammatory responses in microglia, but enhanced microglia process extension, movement, and morphological transformation in the laser injury and acute MPTP-induced Parkinson's disease models. These findings unequivocally support the notion that A2AR activation during Parkinson's disease may contribute to the deleterious dysbalance of A2A-D2Rs at the medium spiny output neurons in the striatum (see Section 4.2.5).

5. Interactions Between Microglia, Astrocytes, and Neurons via ATP/ADP and Adenosine

As mentioned previously, the extension of the 'tripartite synapse' hypothesis to the so-called 'quadpartite synapse' hypothesis states a tight interaction between neurons, astrocytes, and microglia with each other by means of neuro-/gliotransmitters and microglial-signalling molecules [37] (see Section 2.3). In the following, we enumerate further arguments supporting this interaction primarily by ATP.

In an ex vivo retinal explant system, morphological parameters and process motility of microglia were increased by ionotropic glutamatergic transmission and were decreased by ionotropic GABAergic transmission [182]. Neither glutamate nor GABA caused direct current responses on microglia, suggesting that the effects are indirect, probably via the release of ATP. In fact, the pannexin channel blocker probenecid and the wide-spectrum P2R antagonist suramin both inhibited the effects of the glutamatergic or GABAergic agonists on microglial morphology and process extension/retrieval.

In support of this idea, in hippocampal slices of mice, the application of *N*-Methyl-D-Aspartate (NMDA) triggered transient microglial process outgrowth which was blocked by the P2R antagonist reactive blue 2 and the pannexin channel inhibitor probenecid [183]. Nonetheless probenecid did not act via the blockade of pannexin channels, because a more selective inhibitor, carbenoxolone, was without effect, and genetic deletion of pannexin channels also failed to alter the NMDA-induced microglial process propulsion. The involvement of P2Y12Rs in this process was confirmed by the use of P2Y12R$^{-/-}$ mice [184]. It was also reported that a widespread ATP release during massive neuronal hyperactivity in a mouse model of mesial temporal lobe epilepsy resulted in a 'blinding' of microglia, otherwise reacting to ATP gradients by the phagocytotic clearance of apoptotic neural progenitor cells in the hippocampal subgranular zone [94]. ATP release from LPS-challenged microglia differentially modulated synaptic transmission and short-term plasticity at dentate gyrus-CA3 synapses in hippocampal slices by acting on presynaptic P2X4Rs or after degradation of ATP to adenosine, on A1Rs [185].

There are also further examples of a microglia–neuron interaction by the mediation of astrocytes. Repetitive action potentials in individual layer 2/3 pyramidal neurons elicited swelling of axons, but not dendrites, which was accompanied by a large sustained depolarization of the membrane potential [186]. Microglial processes extended to these swollen axons in a mechanism involving ATP release. This extension was followed by microglial wrapping of axons that induced a soma repolarization causing neuroprotection. In another series of experiments, LPS-activated microglia released ATP, which stimulated astrocytes to release glutamate, modulating neuronal activity through the occupation of metabotropic glutamate receptors [2,187]. This was recorded as an increase in the frequency of miniature excitatory postsynaptic currents in CA1 pyramidal neurons of hippocampal brain slices. Further, when exposed to the neurotoxic methylmercury, microglia exocytosed ATP. This ATP stimulated astrocytic P2Y1Rs releasing IL-6, protecting neurons against methylmercury [188]. In fact, a bidirectional astrocyte-microglia cross-talk via ATP and inflammatory cytokines was repeatedly demonstrated [189].

Aberrant astrocyte signalling to neurons plays an important role in producing network hyperexcitability as a cause of epilepsy [190]. TNFα, possibly of microglial origin, may trigger glutamate release from astrocytes, which drives abnormal synaptic activity in the hippocampus. This chain of events was dependent on the autocrine activation of P2Y1Rs by ATP co-released with glutamate from astrocytes.

6. Conclusions

Microglia are definitely more than the 'garbage man' of the CNS, phagocyting pathogenic microorganisms and cellular debris [191]. They have important physiological and pathophysiological functions serving the homeostasis of the CNS parenchyma and the intactness of the blood–brain barrier. In contrast to primary microglial cultures, microglial cells do not appear to possess diversified receptors for all types of neurotransmitters but are instead endowed with a large array of purinergic receptors of the P2X, P2Y, and P1-classes. ATP released from nerve terminals and cell somata by vesicular mechanisms are sequentially degraded at first to ADP, then to the bioactive adenosine, and eventually to the only slightly active inosine, by an enzymatic cascade. In addition to the neurotransmitter ATP, various classic neurotransmitters such as glutamate and GABA have been shown to release ATP from astrocytes, which then may stimulate microglial cells. Thereby, a neuron/astrocyte/microglia crosstalk is operational with the participation of purinergic neuro/gliotransmitters and their respective receptors.

Microglia have important functions in neuroinflammation accompanying neurodegenerative illnesses (AD, PD, multiple sclerosis, amyotrophic lateral sclerosis, neuropathic pain, epilepsy, and ischemia). In all these illnesses, the core pathogenetic mechanism is different, but the simultaneously occurring chronic neuroinflammation is a superimposed exacerbating factor. Especially, P2X4, P2X7, and A2AR antagonists may be valuable tools to improve these conditions. However, it is noteworthy that whereas the M1 phenotype of microglia is typically releasing a host of pro-inflammatory mediators, the M2 phenotype clears cellular debris through phagocytosis and releases numerous protective factors. Whereas M1 microglia are supposed to participate in immunological defense mechanisms of the CNS, M2 microglia are involved in regenerative mechanisms going along with long-lasting neurodegeneration. Hence, microglia are by no way unequivocally injurious for the CNS.

In summary, microglia as interacting partners of neurons and neuroglial cells (astrocytes, oligodendrocytes) shape the CNS reactions to preserve homeostasis.

Author Contributions: P.I. drafted the first version of the manuscript; P.R., H.U., Y.Z., and Y.T. reviewed the manuscript, critically revised it including re-interpretation of some results, and contributed additional data. All authors have read and agreed to the published version of the manuscript.

Funding: Our work was made possible by a generous grant ('The Project First-Class Disciplines Development'; CZYHW1901) of the Chengdu University of Traditional Chinese Medicine to P.I. and Y.T. in order to build up 'International Collaborative Centre on Big Science Plan for Purine Signalling', and grants of the Sichuan Provincial Administration of Foreign Affairs to support the stays of P.I. and P.R. in Chengdu (SZD201731, SZD201846).

Acknowledgments: We are grateful to Hayan Yin for expert drawing of the figures.

Conflicts of Interest: All authors declare no conflicts of interest.

Abbreviations

AD	Alzheimer's disease
BDNF	brain-derived neurotrophic factor
CD39	NTPDase-1
CD73	ecto-5′-nucleotidase
DAMPs	danger-associated molecular patterns
EGFP	enhanced green fluorescence protein
FGF	fibroblast growth factor
IL-1β	interleukin-1β
KO	knockout

LPS	lipopolysaccharide
NGF	nerve growth factor
NLRP3	nucleotide-binding, leucine-rich repeat, pyrin domain containing 3
NTPDases	ecto-nucleoside triphosphate diphosphohydrolases
OPC	oligodendrocyte precursor cells
PAMPs	pathogen-associated molecules
PD	Parkinson's disease
PI3K	phosphatidylinositol 3′-kinase
PLC	phospholipase C
PSD-95	postsynaptic density protein 25
R	receptor
SE	status epilepticus
TLR4	toll-like receptor 4
TNF-α	TNF-α, tumor necrosis factor-α

References

1. Azevedo, F.A.; Carvalho, L.R.; Grinberg, L.T.; Farfel, J.M.; Ferretti, R.E.; Leite, R.E.; Jacob, F.W.; Lent, R.; Herculano-Houzel, S. Equal numbers of neuronal and nonneuronal cells make the human brain an isometrically scaled-up primate brain. *J. Comp. Neurol.* **2009**, *513*, 532–541. [CrossRef] [PubMed]
2. Illes, P.; Burnstock, G.; Tang, Y. Astroglia-Derived ATP Modulates CNS Neuronal Circuits. *Trends Neurosci.* **2019**, *42*, 885–898. [CrossRef] [PubMed]
3. Pelvig, D.P.; Pakkenberg, H.; Stark, A.K.; Pakkenberg, B. Neocortical glial cell numbers in human brains. *Neurobiol. Aging* **2008**, *29*, 1754–1762. [CrossRef] [PubMed]
4. Verkhratsky, A.; Nedergaard, M. Physiology of Astroglia. *Physiol. Rev.* **2018**, *98*, 239–389. [CrossRef]
5. Kreutzberg, G.W. Microglia: A sensor for pathological events in the CNS. *Trends Neurosci.* **1996**, *19*, 312–318. [CrossRef]
6. Tronel, C.; Largeau, B.; Santiago Ribeiro, M.J.; Guilloteau, D.; Dupont, A.C.; Arlicot, N. Molecular Targets for PET Imaging of Activated Microglia: The Current Situation and Future Expectations. *Int. J. Mol. Sci.* **2017**, *18*, E802. [CrossRef]
7. Gomez, P.E.; Schulz, C.; Geissmann, F. Development and homeostasis of "resident" myeloid cells: The case of the microglia. *Glia* **2013**, *61*, 112–120. [CrossRef]
8. Salter, M.W.; Stevens, B. Microglia emerge as central players in brain disease. *Nat. Med.* **2017**, *23*, 1018–1027. [CrossRef]
9. Hanisch, U.K.; Kettenmann, H. Microglia: Active sensor and versatile effector cells in the normal and pathologic brain. *Nat. Neurosci.* **2007**, *10*, 1387–1394. [CrossRef]
10. Kigerl, K.A.; Gensel, J.C.; Ankeny, D.P.; Alexander, J.K.; Donnelly, D.J.; Popovich, P.G. Identification of two distinct macrophage subsets with divergent effects causing either neurotoxicity or regeneration in the injured mouse spinal cord. *J. Neurosci.* **2009**, *29*, 13435–13444. [CrossRef]
11. Kettenmann, H.; Kirchhoff, F.; Verkhratsky, A. Microglia: New roles for the synaptic stripper. *Neuron* **2013**, *77*, 10–18. [CrossRef] [PubMed]
12. Geloso, M.C.; Corvino, V.; Marchese, E.; Serrano, A.; Michetti, F.; D'Ambrosi, N. The Dual Role of Microglia in ALS: Mechanisms and Therapeutic Approaches. *Front. Aging Neurosci.* **2017**, *9*, 242. [CrossRef] [PubMed]
13. Subramaniam, S.R.; Federoff, H.J. Targeting Microglial Activation States as a Therapeutic Avenue in Parkinson's Disease. *Front. Aging Neurosci.* **2017**, *9*, 176. [CrossRef] [PubMed]
14. Franco, R.; Fernandez-Suarez, D. Alternatively activated microglia and macrophages in the central nervous system. *Prog. Neurobiol.* **2015**, *131*, 65–86. [CrossRef] [PubMed]
15. Martinez, F.O.; Sica, A.; Mantovani, A.; Locati, M. Macrophage activation and polarization. *Front. Biosci.* **2008**, *13*, 453–461. [CrossRef]
16. Hirbec, H.; Rassendren, F.; Audinat, E. Microglia Reactivity: Heterogeneous Pathological Phenotypes. *Methods Mol. Biol.* **2019**, *2034*, 41–55.
17. Casella, G.; Garzetti, L.; Gatta, A.T.; Finardi, A.; Maiorino, C.; Ruffini, F.; Martino, G.; Muzio, L.; Furlan, R. IL4 induces IL6-producing M2 macrophages associated to inhibition of neuroinflammation in vitro and in vivo. *J. Neuroinflammation.* **2016**, *13*, 139. [CrossRef]

18. Kettenmann, H.; Hanisch, U.K.; Noda, M.; Verkhratsky, A. Physiology of microglia. *Physiol. Rev.* **2011**, *91*, 461–553. [CrossRef]
19. Domercq, M.; Vazquez-Villoldo, N.; Matute, C. Neurotransmitter signaling in the pathophysiology of microglia. *Front. Cell Neurosci.* **2013**, *7*, 49. [CrossRef]
20. Walz, W.; Ilschner, S.; Ohlemeyer, C.; Banati, R.; Kettenmann, H. Extracellular ATP activates a cation conductance and a K^+ conductance in cultured microglial cells from mouse brain. *J. Neurosci.* **1993**, *13*, 4403–4411. [CrossRef]
21. Kettenmann, H.; Banati, R.; Walz, W. Electrophysiological behavior of microglia. *Glia* **1993**, *7*, 93–101. [CrossRef] [PubMed]
22. Haas, S.; Brockhaus, J.; Verkhratsky, A.; Kettenmann, H. ATP-induced membrane currents in ameboid microglia acutely isolated from mouse brain slices. *Neuroscience* **1996**, *75*, 257–261. [CrossRef]
23. Boucsein, C.; Zacharias, R.; Farber, K.; Pavlovic, S.; Hanisch, U.K.; Kettenmann, H. Purinergic receptors on microglial cells: Functional expression in acute brain slices and modulation of microglial activation in vitro. *Eur. J. Neurosci.* **2003**, *17*, 2267–2276. [CrossRef] [PubMed]
24. Norenberg, W.; Schunk, J.; Fischer, W.; Sobottka, H.; Riedel, T.; Oliveira, J.F.; Franke, H.; Illes, P. Electrophysiological classification of P2X7 receptors in rat cultured neocortical astroglia. *Br. J. Pharmacol.* **2010**, *160*, 1941–1952. [CrossRef]
25. Oliveira, J.F.; Riedel, T.; Leichsenring, A.; Heine, C.; Franke, H.; Krugel, U.; Norenberg, W.; Illes, P. Rodent cortical astroglia express in situ functional P2X7 receptors sensing pathologically high ATP concentrations. *Cereb. Cortex* **2011**, *21*, 806–820. [CrossRef] [PubMed]
26. Burnstock, G.; Verkhratsky, A. Evolutionary origins of the purinergic signalling system. *Acta Physiol. Oxf.* **2009**, *195*, 415–447. [CrossRef] [PubMed]
27. Burnstock, G.; Fredholm, B.B.; North, R.A.; Verkhratsky, A. The birth and postnatal development of purinergic signalling. *Acta Physiol. Oxf.* **2010**, *199*, 93–147. [CrossRef]
28. Jung, S.; Aliberti, J.; Graemmel, P.; Sunshine, M.J.; Kreutzberg, G.W.; Sher, A.; Littman, D.R. Analysis of fractalkine receptor CX3CR1 function by targeted deletion and green fluorescent protein reporter gene insertion. *Mol. Cell Biol.* **2000**, *20*, 4106–4114. [CrossRef]
29. Ransohoff, R.M.; Perry, V.H. Microglial physiology: Unique stimuli, specialized responses. *Annu. Rev. Immunol.* **2009**, *27*, 119–145. [CrossRef]
30. Davalos, D.; Grutzendler, J.; Yang, G.; Kim, J.V.; Zuo, Y.; Jung, S.; Littman, D.R.; Dustin, M.L.; Gan, W.B. ATP mediates rapid microglial response to local brain injury in vivo. *Nat. Neurosci.* **2005**, *8*, 752–758. [CrossRef]
31. Nimmerjahn, A.; Kirchhoff, F.; Helmchen, F. Resting microglial cells are highly dynamic surveillants of brain parenchyma in vivo. *Science* **2005**, *308*, 1314–1318. [CrossRef] [PubMed]
32. Salter, M.W.; Beggs, S. Sublime microglia: Expanding roles for the guardians of the CNS. *Cell* **2014**, *158*, 15–24. [CrossRef] [PubMed]
33. Szepesi, Z.; Manouchehrian, O.; Bachiller, S.; Deierborg, T. Bidirectional Microglia-Neuron Communication in Health and Disease. *Front. Cell Neurosci.* **2018**, *12*, 323. [CrossRef] [PubMed]
34. Wake, H.; Moorhouse, A.J.; Jinno, S.; Kohsaka, S.; Nabekura, J. Resting microglia directly monitor the functional state of synapses in vivo and determine the fate of ischemic terminals. *J. Neurosci.* **2009**, *29*, 3974–3980. [CrossRef]
35. Li, Y.; Du, X.F.; Liu, C.S.; Wen, Z.L.; Du, J.L. Reciprocal regulation between resting microglial dynamics and neuronal activity in vivo. *Dev. Cell* **2012**, *23*, 1189–1202. [CrossRef] [PubMed]
36. Araque, A.; Parpura, V.; Sanzgiri, R.P.; Haydon, P.G. Tripartite synapses: Glia, the unacknowledged partner. *Trends Neurosci.* **1999**, *22*, 208–215. [CrossRef]
37. Schafer, D.P.; Lehrman, E.K.; Stevens, B. The "quad-partite" synapse: Microglia-synapse interactions in the developing and mature CNS. *Glia* **2013**, *61*, 24–36. [CrossRef] [PubMed]
38. Fazio, F.; Ulivieri, M.; Volpi, C.; Gargaro, M.; Fallarino, F. Targeting metabotropic glutamate receptors for the treatment of neuroinflammation. *Curr. Opin. Pharmacol.* **2018**, *38*, 16–23. [CrossRef] [PubMed]
39. Bezzi, P.; Domercq, M.; Brambilla, L.; Galli, R.; Schols, D.; De Clercq, E.; Vescovi, A.; Bagetta, G.; Kollias, G.; Meldolesi, J.; et al. CXCR4-activated astrocyte glutamate release via TNFα: Amplification by microglia triggers neurotoxicity. *Nat. Neurosci.* **2001**, *4*, 702–710. [CrossRef]
40. Illes, P.; Norenberg, W.; Gebicke-Haerter, P.J. Molecular mechanisms of microglial activation. B. Voltage- and purinoceptor-operated channels in microglia. *Neurochem. Int.* **1996**, *29*, 13–24.

41. Gebicke-Haerter, P.J.; van Calker, D.; Norenberg, W.; Illes, P. Molecular mechanisms of microglial activation. A. Implications for regeneration and neurodegenerative diseases. *Neurochem. Int.* **1996**, *29*, 1–12. [PubMed]
42. Murray, P.J.; Allen, J.E.; Biswas, S.K.; Fisher, E.A.; Gilroy, D.W.; Goerdt, S.; Gordon, S.; Hamilton, J.A.; Ivashkiv, L.B.; Lawrence, T.; et al. Macrophage activation and polarization: Nomenclature and experimental guidelines. *Immunity* **2014**, *41*, 14–20. [CrossRef] [PubMed]
43. Stevens, B.; Allen, N.J.; Vazquez, L.E.; Howell, G.R.; Christopherson, K.S.; Nouri, N.; Micheva, K.D.; Mehalow, A.K.; Huberman, A.D.; Stafford, B.; et al. The classical complement cascade mediates CNS synapse elimination. *Cell* **2007**, *131*, 1164–1178. [CrossRef] [PubMed]
44. Schafer, D.P.; Lehrman, E.K.; Kautzman, A.G.; Koyama, R.; Mardinly, A.R.; Yamasaki, R.; Ransohoff, R.M.; Greenberg, M.E.; Barres, B.A.; Stevens, B. Microglia sculpt postnatal neural circuits in an activity and complement-dependent manner. *Neuron* **2012**, *74*, 691–705. [CrossRef] [PubMed]
45. Paolicelli, R.C.; Bolasco, G.; Pagani, F.; Maggi, L.; Scianni, M.; Panzanelli, P.; Giustetto, M.; Ferreira, T.A.; Guiducci, E.; Dumas, L.; et al. Synaptic pruning by microglia is necessary for normal brain development. *Science* **2011**, *333*, 1456–1458. [CrossRef]
46. Weinhard, L.; di Bartolomei, G.; Bolasco, G.; Machado, P.; Schieber, N.L.; Neniskyte, U.; Exiga, M.; Vadisiute, A.; Raggioli, A.; Schertel, A.; et al. Microglia remodel synapses by presynaptic trogocytosis and spine head filopodia induction. *Nat. Commun.* **2018**, *9*, 1228. [CrossRef]
47. Sierra, A.; Encinas, J.M.; Deudero, J.J.; Chancey, J.H.; Enikolopov, G.; Overstreet-Wadiche, L.S.; Tsirka, S.E.; Maletic-Savatic, M. Microglia shape adult hippocampal neurogenesis through apoptosis-coupled phagocytosis. *Cell Stem Cell* **2010**, *7*, 483–495. [CrossRef]
48. Cunningham, C.L.; Martinez-Cerdeno, V.; Noctor, S.C. Microglia regulate the number of neural precursor cells in the developing cerebral cortex. *J. Neurosci.* **2013**, *33*, 4216–4233. [CrossRef]
49. Rakic, P. Evolution of the neocortex: A perspective from developmental biology. *Nat. Rev. Neurosci.* **2009**, *10*, 724–735. [CrossRef]
50. Marin-Teva, J.L.; Cuadros, M.A.; Martin-Oliva, D.; Navascues, J. Microglia and neuronal cell death. *Neuron Glia Biol.* **2011**, *7*, 25–40. [CrossRef]
51. Mosser, C.A.; Baptista, S.; Arnoux, I.; Audinat, E. Microglia in CNS development: Shaping the brain for the future. *Prog. Neurobiol.* **2017**, *149–150*, 1–20. [CrossRef] [PubMed]
52. Di Virgilio, F.; Dal, B.D.; Sarti, A.C.; Giuliani, A.L.; Falzoni, S. The P2X7 Receptor in Infection and Inflammation. *Immunity* **2017**, *47*, 15–31. [CrossRef] [PubMed]
53. Burnstock, G.; Krugel, U.; Abbracchio, M.P.; Illes, P. Purinergic signalling: From normal behaviour to pathological brain function. *Prog. Neurobiol.* **2011**, *95*, 229–274. [CrossRef] [PubMed]
54. Sperlagh, B.; Illes, P. P2X7 receptor: An emerging target in central nervous system diseases. *Trends Pharmacol. Sci.* **2014**, *35*, 537–547. [CrossRef]
55. Bianchi, M.E. DAMPs, PAMPs and alarmins: All we need to know about danger. *J. Leukoc. Biol.* **2007**, *81*, 1–5. [CrossRef]
56. Husemann, J.; Loike, J.D.; Anankov, R.; Febbraio, M.; Silverstein, S.C. Scavenger receptors in neurobiology and neuropathology: Their role on microglia and other cells of the nervous system. *Glia* **2002**, *40*, 195–205. [CrossRef]
57. Young, C.N.J.; Gorecki, D.C. P2RX7 Purinoceptor as a Therapeutic Target-The Second Coming? *Front. Chem.* **2018**, *6*, 248. [CrossRef]
58. Castellano, B.; Bosch-Queralt, M.; Almolda, B.; Villacampa, N.; Gonzalez, B. Purine Signaling and Microglial Wrapping. *Adv. Exp. Med. Biol.* **2016**, *949*, 147–165.
59. Beins, E.; Ulas, T.; Ternes, S.; Neumann, H.; Schultze, J.L.; Zimmer, A. Characterization of inflammatory markers and transcriptome profiles of differentially activated embryonic stem cell-derived microglia. *Glia* **2016**, *64*, 1007–1020. [CrossRef]
60. Orre, M.; Kamphuis, W.; Osborn, L.M.; Jansen, A.H.P.; Kooijman, L.; Bossers, K.; Hol, E.M. Isolation of glia from Alzheimer's mice reveals inflammation and dysfunction. *Neurobiol. Aging* **2014**, *35*, 2746–2760. [CrossRef]
61. Cheray, M.; Joseph, B. Epigenetics Control Microglia Plasticity. *Front. Cell Neurosci.* **2018**, *12*, 243. [CrossRef]
62. Sharma, K.; Schmitt, S.; Bergner, C.G.; Tyanova, S.; Kannaiyan, N.; Manrique-Hoyos, N.; Kongi, K.; Cantuti, L.; Hanisch, U.K.; Philips, M.A.; et al. Cell type- and brain region-resolved mouse brain proteome. *Nat. Neurosci.* **2015**, *18*, 1819–1831. [CrossRef]

63. Keren-Shaul, H.; Spinrad, A.; Weiner, A.; Matcovitch-Natan, O.; Dvir-Szternfeld, R.; Ulland, T.K.; David, E.; Baruch, K.; Lara-Astaiso, D.; Toth, B.; et al. A Unique Microglia Type Associated with Restricting Development of Alzheimer's Disease. *Cell* **2017**, *169*, 1276–1290. [CrossRef] [PubMed]
64. Deczkowska, A.; Keren-Shaul, H.; Weiner, A.; Colonna, M.; Schwartz, M.; Amit, I. Disease-Associated Microglia: A Universal Immune Sensor of Neurodegeneration. *Cell* **2018**, *173*, 1073–1081. [CrossRef] [PubMed]
65. Burnstock, G. Purinergic nerves. *Pharmacol. Rev.* **1972**, *24*, 509–581. [PubMed]
66. Kennedy, C.; Burnstock, G. Evidence for two types of P2-purinoceptor in longitudinal muscle of the rabbit portal vein. *Eur. J. Pharmacol.* **1985**, *111*, 49–56. [CrossRef]
67. North, R.A. Molecular physiology of P2X receptors. *Physiol. Rev.* **2002**, *82*, 1013–1067. [CrossRef] [PubMed]
68. Surprenant, A.; Rassendren, F.; Kawashima, E.; North, R.A.; Buell, G. The cytolytic P2Z receptor for extracellular ATP identified as a P2X receptor (P2X7). *Science* **1996**, *272*, 735–738. [CrossRef]
69. Sperlagh, B.; Illes, P. Purinergic modulation of microglial cell activation. *Purinergic. Signal.* **2007**, *3*, 117–127. [CrossRef]
70. Calovi, S.; Mut-Arbona, P.; Sperlagh, B. Microglia and the Purinergic Signaling System. *Neuroscience* **2019**, *405*, 137–147. [CrossRef]
71. Farber, K.; Kettenmann, H. Purinergic signaling and microglia. *Pflugers Arch.* **2006**, *452*, 615–621. [CrossRef] [PubMed]
72. Zimmermann, H.; Zebisch, M.; Strater, N. Cellular function and molecular structure of ecto-nucleotidases. *Purinergic. Signal.* **2012**, *8*, 437–502. [CrossRef] [PubMed]
73. Yegutkin, G.G. Enzymes involved in metabolism of extracellular nucleotides and nucleosides: Functional implications and measurement of activities. *Crit. Rev. Biochem. Mol. Biol.* **2014**, *49*, 473–497. [CrossRef] [PubMed]
74. Fredholm, B.B.; IJzerman, A.P.; Jacobson, K.A.; Linden, J.; Muller, C.E. International Union of Basic and Clinical Pharmacology. LXXXI. Nomenclature and classification of adenosine receptors—An update. *Pharmacol. Rev.* **2011**, *63*, 1–34. [CrossRef] [PubMed]
75. Eltzschig, H.K.; Faigle, M.; Knapp, S.; Karhausen, J.; Ibla, J.; Rosenberger, P.; Odegard, K.C.; Laussen, P.C.; Thompson, L.F.; Colgan, S.P. Endothelial catabolism of extracellular adenosine during hypoxia: The role of surface adenosine deaminase and CD26. *Blood* **2006**, *108*, 1602–1610. [CrossRef]
76. Morote-Garcia, J.C.; Rosenberger, P.; Kuhlicke, J.; Eltzschig, H.K. HIF-1-dependent repression of adenosine kinase attenuates hypoxia-induced vascular leak. *Blood* **2008**, *111*, 5571–5580. [CrossRef]
77. Sheth, S.; Brito, R.; Mukherjea, D.; Rybak, L.P.; Ramkumar, V. Adenosine receptors: Expression, function and regulation. *Int. J. Mol. Sci.* **2014**, *15*, 2024–2052. [CrossRef]
78. Dos Santos-Rodrigues, A.; Grane-Boladeras, N.; Bicket, A.; Coe, I.R. Nucleoside transporters in the purinome. *Neurochem. Int.* **2014**, *73*, 229–237. [CrossRef]
79. Koizumi, S.; Ohsawa, K.; Inoue, K.; Kohsaka, S. Purinergic receptors in microglia: Functional modal shifts of microglia mediated by P2 and P1 receptors. *Glia* **2013**, *61*, 47–54. [CrossRef] [PubMed]
80. Meng, F.; Guo, Z.; Hu, Y.; Mai, W.; Zhang, Z.; Zhang, B.; Ge, Q.; Lou, H.; Guo, F.; Chen, J.; et al. CD73-derived adenosine controls inflammation and neurodegeneration by modulating dopamine signalling. *Brain* **2019**, *142*, 700–718. [CrossRef]
81. Haynes, S.E.; Hollopeter, G.; Yang, G.; Kurpius, D.; Dailey, M.E.; Gan, W.B.; Julius, D. The P2Y12 receptor regulates microglial activation by extracellular nucleotides. *Nat. Neurosci.* **2006**, *9*, 1512–1519. [CrossRef]
82. Hollopeter, G.; Jantzen, H.M.; Vincent, D.; Li, G.; England, L.; Ramakrishnan, V.; Yang, R.B.; Nurden, P.; Nurden, A.; Julius, D.; et al. Identification of the platelet ADP receptor targeted by antithrombotic drugs. *Nature* **2001**, *409*, 202–207. [CrossRef] [PubMed]
83. Ohsawa, K.; Irino, Y.; Nakamura, Y.; Akazawa, C.; Inoue, K.; Kohsaka, S. Involvement of P2X4 and P2Y12 receptors in ATP-induced microglial chemotaxis. *Glia* **2007**, *55*, 604–616. [CrossRef] [PubMed]
84. Cserep, C.; Posfai, B.; Lenart, N.; Fekete, R.; Laszlo, Z.I.; Lele, Z.; Orsolits, B.; Molnar, G.; Heindl, S.; Schwarcz, A.D.; et al. Microglia monitor and protect neuronal function through specialized somatic purinergic junctions. *Science* **2020**, *367*, 528–537. [CrossRef]
85. Irino, Y.; Nakamura, Y.; Inoue, K.; Kohsaka, S.; Ohsawa, K. Akt activation is involved in P2Y12 receptor-mediated chemotaxis of microglia. *J. Neurosci. Res.* **2008**, *86*, 1511–1519. [CrossRef] [PubMed]

86. Ohsawa, K.; Irino, Y.; Sanagi, T.; Nakamura, Y.; Suzuki, E.; Inoue, K.; Kohsaka, S. P2Y12 receptor-mediated integrin-β1 activation regulates microglial process extension induced by ATP. *Glia* **2010**, *58*, 790–801.
87. Kobayashi, K.; Yamanaka, H.; Fukuoka, T.; Dai, Y.; Obata, K.; Noguchi, K. P2Y12 receptor upregulation in activated microglia is a gateway of p38 signaling and neuropathic pain. *J. Neurosci.* **2008**, *28*, 2892–2902. [CrossRef]
88. Webster, C.M.; Hokari, M.; McManus, A.; Tang, X.N.; Ma, H.; Kacimi, R.; Yenari, M.A. Microglial P2Y12 deficiency/inhibition protects against brain ischemia. *PLoS ONE* **2013**, *8*, e70927. [CrossRef]
89. Gelosa, P.; Lecca, D.; Fumagalli, M.; Wypych, D.; Pignieri, A.; Cimino, M.; Verderio, C.; Enerback, M.; Nikookhesal, E.; Tremoli, E.; et al. Microglia is a key player in the reduction of stroke damage promoted by the new antithrombotic agent ticagrelor. *J. Cereb. Blood Flow Metab.* **2014**, *34*, 979–988. [CrossRef]
90. Amadio, S.; Montilli, C.; Magliozzi, R.; Bernardi, G.; Reynolds, R.; Volonte, C. P2Y12 receptor protein in cortical gray matter lesions in multiple sclerosis. *Cereb. Cortex* **2010**, *20*, 1263–1273. [CrossRef]
91. Kyrargyri, V.; Madry, C.; Rifat, A.; Arancibia-Carcamo, I.L.; Jones, S.P.; Chan, V.T.T.; Xu, Y.; Robaye, B.; Attwell, D. P2Y13 receptors regulate microglial morphology, surveillance, and resting levels of interleukin 1β release. *Glia* **2020**, *68*, 328–344. [CrossRef] [PubMed]
92. Von Kugelgen, I.; Harden, T.K. Molecular pharmacology, physiology, and structure of the P2Y receptors. *Adv. Pharmacol.* **2011**, *61*, 373–415. [PubMed]
93. Koizumi, S.; Shigemoto-Mogami, Y.; Nasu-Tada, K.; Shinozaki, Y.; Ohsawa, K.; Tsuda, M.; Joshi, B.V.; Jacobson, K.A.; Kohsaka, S.; Inoue, K. UDP acting at P2Y6 receptors is a mediator of microglial phagocytosis. *Nature* **2007**, *446*, 1091–1095. [CrossRef] [PubMed]
94. Abiega, O.; Beccari, S.; Diaz-Aparicio, I.; Nadjar, A.; Laye, S.; Leyrolle, Q.; Gomez-Nicola, D.; Domercq, M.; Perez-Samartin, A.; Sanchez-Zafra, V.; et al. Neuronal Hyperactivity Disturbs ATP Microgradients, Impairs Microglial Motility, and Reduces Phagocytic Receptor Expression Triggering Apoptosis/Microglial Phagocytosis Uncoupling. *PLoS Biol.* **2016**, *14*, e1002466. [CrossRef] [PubMed]
95. Li, H.Q.; Chen, C.; Dou, Y.; Wu, H.J.; Liu, Y.J.; Lou, H.F.; Zhang, J.M.; Li, X.M.; Wang, H.; Duan, S. P2 receptor-mediated pinocytosis contributes to amyloid beta-induced self-uptake by microglia. *Mol. Cell Biol.* **2013**, *33*, 4282–4293. [CrossRef]
96. Bernier, L.P.; Ase, A.R.; Boue-Grabot, E.; Seguela, P. Inhibition of P2X4 function by P2Y6 UDP receptors in microglia. *Glia* **2013**, *61*, 2038–2049. [CrossRef]
97. Suurvali, J.; Boudinot, P.; Kanellopoulos, J.; Ruutel, B.S. P2X4: A fast and sensitive purinergic receptor. *Biomed. J.* **2017**, *40*, 245–256. [CrossRef]
98. Dubyak, G.R. Go it alone no more—P2X7 joins the society of heteromeric ATP-gated receptor channels. *Mol. Pharmacol.* **2007**, *72*, 1402–1405. [CrossRef] [PubMed]
99. Hung, S.C.; Choi, C.H.; Said-Sadier, N.; Johnson, L.; Atanasova, K.R.; Sellami, H.; Yilmaz, O.; Ojcius, D.M. P2X4 assembles with P2X7 and pannexin-1 in gingival epithelial cells and modulates ATP-induced reactive oxygen species production and inflammasome activation. *PLoS ONE* **2013**, *8*, e70210. [CrossRef]
100. Kaczmarek-Hajek, K.; Lorinczi, E.; Hausmann, R.; Nicke, A. Molecular and functional properties of P2X receptors–recent progress and persisting challenges. *Purinergic. Signal.* **2012**, *8*, 375–417. [CrossRef]
101. Illes, P.; Verkhratsky, A.; Tang, Y. Pathological ATPergic Signaling in Major Depression and Bipolar Disorder. *Front. Mol. Neurosci.* **2019**, *12*, 331. [CrossRef] [PubMed]
102. Illes, P.; Khan, T.M.; Rubini, P. Neuronal P2X7 Receptors Revisited: Do They Really Exist? *J. Neurosci.* **2017**, *37*, 7049–7062. [CrossRef] [PubMed]
103. Qureshi, O.S.; Paramasivam, A.; Yu, J.C.; Murrell-Lagnado, R.D. Regulation of P2X4 receptors by lysosomal targeting, glycan protection and exocytosis. *J. Cell Sci.* **2007**, *120*, 3838–3849. [CrossRef] [PubMed]
104. Raouf, R.; Chabot-Dore, A.J.; Ase, A.R.; Blais, D.; Seguela, P. Differential regulation of microglial P2X4 and P2X7 ATP receptors following LPS-induced activation. *Neuropharmacology* **2007**, *53*, 496–504. [CrossRef] [PubMed]
105. Bernier, L.P.; Ase, A.R.; Boue-Grabot, E.; Seguela, P. P2X4 receptor channels form large noncytolytic pores in resting and activated microglia. *Glia* **2012**, *60*, 728–737. [CrossRef]
106. Tsuda, M.; Shigemoto-Mogami, Y.; Koizumi, S.; Mizokoshi, A.; Kohsaka, S.; Salter, M.W.; Inoue, K. P2X4 receptors induced in spinal microglia gate tactile allodynia after nerve injury. *Nature* **2003**, *424*, 778–783. [CrossRef]

107. Coull, J.A.; Beggs, S.; Boudreau, D.; Boivin, D.; Tsuda, M.; Inoue, K.; Gravel, C.; Salter, M.W.; De Konninck, Y. BDNF from microglia causes the shift in neuronal anion gradient underlying neuropathic pain. *Nature* **2005**, *438*, 1017–1021. [CrossRef]
108. Donnelly-Roberts, D.; McGaraughty, S.; Shieh, C.C.; Honore, P.; Jarvis, M.F. Painful purinergic receptors. *J. Pharmacol. Exp. Ther.* **2008**, *324*, 409–415. [CrossRef]
109. Biber, K.; Tsuda, M.; Tozaki-Saitoh, H.; Tsukamoto, K.; Toyomitsu, E.; Masuda, T.; Boddeke, H.; Inoue, K. Neuronal CCL21 up-regulates microglia P2X4 expression and initiates neuropathic pain development. *EMBO J.* **2011**, *30*, 1864–1873. [CrossRef]
110. Nasu-Tada, K.; Koizumi, S.; Tsuda, M.; Kunifusa, E.; Inoue, K. Possible involvement of increase in spinal fibronectin following peripheral nerve injury in upregulation of microglial P2X4, a key molecule for mechanical allodynia. *Glia* **2006**, *53*, 769–775. [CrossRef]
111. Tsuda, M.; Tozaki-Saitoh, H.; Masuda, T.; Toyomitsu, E.; Tezuka, T.; Yamamoto, T.; Inoue, K. Lyn tyrosine kinase is required for P2X4 receptor upregulation and neuropathic pain after peripheral nerve injury. *Glia* **2008**, *56*, 50–58. [CrossRef] [PubMed]
112. Lombardi, M.; Parolisi, R.; Scaroni, F.; Bonfanti, E.; Gualerzi, A.; Gabrielli, M.; Kerlero de Rosbo, N.; Uccelli, A.; Giussani, P.; Viani, P.; et al. Detrimental and protective action of microglial extracellular vesicles on myelin lesions: Astrocyte involvement in remyelination failure. *Acta Neuropathol.* **2019**, *138*, 987–1012. [CrossRef]
113. Zabala, A.; Vazquez-Villoldo, N.; Rissiek, B.; Gejo, J.; Martin, A.; Palomino, A.; Perez-Samartin, A.; Pulagam, K.R.; Lukowiak, M.; Capetillo-Zarate, E.; et al. P2X4 receptor controls microglia activation and favors remyelination in autoimmune encephalitis. *EMBO Mol. Med.* **2018**, *10*, e8743. [CrossRef] [PubMed]
114. Ulmann, L.; Levavasseur, F.; Avignone, E.; Peyroutou, R.; Hirbec, H.; Audinat, E.; Rassendren, F. Involvement of P2X4 receptors in hippocampal microglial activation after status epilepticus. *Glia* **2013**, *61*, 1306–1319. [CrossRef] [PubMed]
115. Illes, P.; Verkhratsky, A.; Burnstock, G.; Franke, H. P2X receptors and their roles in astroglia in the central and peripheral nervous system. *Neuroscientist* **2012**, *18*, 422–438. [CrossRef]
116. Di Virgilio, F.; Schmalzing, G.; Markwardt, F. The Elusive P2X7 Macropore. *Trends Cell Biol.* **2018**, *28*, 392–404. [CrossRef]
117. Virginio, C.; MacKenzie, A.; Rassendren, F.A.; North, R.A.; Surprenant, A. Pore dilation of neuronal P2X receptor channels. *Nat. Neurosci.* **1999**, *2*, 315–321. [CrossRef]
118. Li, M.; Toombes, G.E.; Silberberg, S.D.; Swartz, K.J. Physical basis of apparent pore dilation of ATP-activated P2X receptor channels. *Nat. Neurosci.* **2015**, *18*, 1577–1583. [CrossRef]
119. Riedel, T.; Lozinsky, I.; Schmalzing, G.; Markwardt, F. Kinetics of P2X7 receptor-operated single channels currents. *Biophys. J.* **2007**, *92*, 2377–2391. [CrossRef]
120. Pelegrin, P.; Surprenant, A. Pannexin-1 mediates large pore formation and interleukin-1β release by the ATP-gated P2X7 receptor. *EMBO J.* **2006**, *25*, 5071–5082. [CrossRef]
121. Perregaux, D.G.; Gabel, C.A. Post-translational processing of murine IL-1: Evidence that ATP-induced release of IL-1 alpha and IL-1β occurs via a similar mechanism. *J. Immunol.* **1998**, *160*, 2469–2477.
122. Munoz-Planillo, R.; Kuffa, P.; Martinez-Colon, G.; Smith, B.L.; Rajendiran, T.M.; Nunez, G. K^+ efflux is the common trigger of NLRP3 inflammasome activation by bacterial toxins and particulate matter. *Immunity* **2013**, *38*, 1142–1153. [CrossRef] [PubMed]
123. Shieh, C.H.; Heinrich, A.; Serchov, T.; van Calker, D.; Biber, K. P2X7-dependent, but differentially regulated release of IL-6, CCL2, and TNF-α in cultured mouse microglia. *Glia* **2014**, *62*, 592–607. [CrossRef]
124. Madry, C.; Kyrargyri, V.; Arancibia-Carcamo, I.L.; Jolivet, R.; Kohsaka, S.; Bryan, R.M.; Attwell, D. Microglial Ramification, Surveillance, and Interleukin-1β Release Are Regulated by the Two-Pore Domain K^+ Channel THIK-1. *Neuron* **2018**, *97*, 299–312. [CrossRef] [PubMed]
125. Bianco, F.; Pravettoni, E.; Colombo, A.; Schenk, U.; Moller, T.; Matteoli, M.; Verderio, C. Astrocyte-derived ATP induces vesicle shedding and IL-1β release from microglia. *J. Immunol.* **2005**, *174*, 7268–7277. [CrossRef] [PubMed]
126. Prada, I.; Furlan, R.; Matteoli, M.; Verderio, C. Classical and unconventional pathways of vesicular release in microglia. *Glia* **2013**, *61*, 1003–1017. [CrossRef]
127. Turola, E.; Furlan, R.; Bianco, F.; Matteoli, M.; Verderio, C. Microglial microvesicle secretion and intercellular signaling. *Front. Physiol.* **2012**, *3*, 149. [CrossRef]

128. Rigato, C.; Swinnen, N.; Buckinx, R.; Couillin, I.; Mangin, J.M.; Rigo, J.M.; Legendre, P.; Le, C.H. Microglia proliferation is controlled by P2X7 receptors in a Pannexin-1-independent manner during early embryonic spinal cord invasion. *J. Neurosci.* **2012**, *32*, 11559–11573. [CrossRef]
129. Rigato, C.; Buckinx, R.; Le-Corronc, H.; Rigo, J.M.; Legendre, P. Pattern of invasion of the embryonic mouse spinal cord by microglial cells at the time of the onset of functional neuronal networks. *Glia* **2011**, *59*, 675–695. [CrossRef]
130. Monif, M.; Reid, C.A.; Powell, K.L.; Drummond, K.J.; O'Brien, T.J.; Williams, D.A. Interleukin-1β has trophic effects in microglia and its release is mediated by P2X7R pore. *J. Neuroinflammation* **2016**, *13*, 173. [CrossRef]
131. Monif, M.; Reid, C.A.; Powell, K.L.; Smart, M.L.; Williams, D.A. The P2X7 receptor drives microglial activation and proliferation: A trophic role for P2X7R pore. *J. Neurosci.* **2009**, *29*, 3781–3791. [CrossRef] [PubMed]
132. Fang, K.M.; Yang, C.S.; Sun, S.H.; Tzeng, S.F. Microglial phagocytosis attenuated by short-term exposure to exogenous ATP through P2X receptor action. *J. Neurochem.* **2009**, *111*, 1225–1237. [CrossRef]
133. Lovelace, M.D.; Gu, B.J.; Eamegdool, S.S.; Weible, M.W.; Wiley, J.S.; Allen, D.G.; Chan-Ling, T. P2X7 receptors mediate innate phagocytosis by human neural precursor cells and neuroblasts. *Stem Cells* **2015**, *33*, 526–541. [CrossRef] [PubMed]
134. Ou, A.; Gu, B.J.; Wiley, J.S. The scavenger activity of the human P2X7 receptor differs from P2X7 pore function by insensitivity to antagonists, genetic variation and sodium concentration: Relevance to inflammatory brain diseases. *Biochim. Biophys. Acta Mol. Basis. Dis.* **2018**, *1864*, 1051–1059. [CrossRef]
135. Ferrari, D.; Chiozzi, P.; Falzoni, S.; Dal Susino, M.; Collo, G.; Buell, G.; Di Virgilio, F. ATP-mediated cytotoxicity in microglial cells. *Neuropharmacology* **1997**, *36*, 1295–1301. [CrossRef]
136. He, Y.; Taylor, N.; Fourgeaud, L.; Bhattacharya, A. The role of microglial P2X7: Modulation of cell death and cytokine release. *J. Neuroinflammation* **2017**, *14*, 135. [CrossRef] [PubMed]
137. Faivre, E.; Coelho, J.E.; Zornbach, K.; Malik, E.; Baqi, Y.; Schneider, M.; Cellai, L.; Carvalho, K.; Sebda, S.; Figeac, M.; et al. Beneficial Effect of a Selective Adenosine A2A Receptor Antagonist in the APPswe/PS1dE9 Mouse Model of Alzheimer's Disease. *Front. Mol. Neurosci.* **2018**, *11*, 235. [CrossRef] [PubMed]
138. Crabbe, M.; Van der Perren, A.; Bollaerts, I.; Kounelis, S.; Baekelandt, V.; Bormans, G.; Casteels, C.; Moons, L.; Van Laere, K. Increased P2X7 Receptor Binding Is Associated With Neuroinflammation in Acute but Not Chronic Rodent Models for Parkinson's Disease. *Front. Neurosci.* **2019**, *13*, 799. [CrossRef] [PubMed]
139. Savio, L.E.B.; de Andrade, M.P.; da Silva, C.G.; Coutinho-Silva, R. The P2X7 Receptor in Inflammatory Diseases: Angel or Demon? *Front. Pharmacol.* **2018**, *9*, 52. [CrossRef] [PubMed]
140. Suzuki, T.; Hide, I.; Ido, K.; Kohsaka, S.; Inoue, K.; Nakata, Y. Production and release of neuroprotective tumor necrosis factor by P2X7 receptor-activated microglia. *J. Neurosci.* **2004**, *24*, 1–7. [CrossRef]
141. Masuch, A.; Shieh, C.H.; van Rooijen, N.; van Calker, D.; Biber, K. Mechanism of microglia neuroprotection: Involvement of P2X7, TNFα, and valproic acid. *Glia* **2016**, *64*, 76–89. [CrossRef]
142. Song, W.M.; Colonna, M. The identity and function of microglia in neurodegeneration. *Nat. Immunol.* **2018**, *19*, 1048–1058. [CrossRef]
143. Bhattacharya, A.; Biber, K. The microglial ATP-gated ion channel P2X7 as a CNS drug target. *Glia* **2016**, *64*, 1772–1787. [CrossRef]
144. Bartlett, R.; Stokes, L.; Sluyter, R. The P2X7 receptor channel: Recent developments and the use of P2X7 antagonists in models of disease. *Pharmacol. Rev.* **2014**, *66*, 638–675. [CrossRef] [PubMed]
145. De Marchi, E.; Orioli, E.; Dal Ben, D.; Adinolfi, E. P2X7 Receptor as a Therapeutic Target. *Adv. Protein Chem. Struct. Biol.* **2016**, *104*, 39–79. [PubMed]
146. Chen, J.F.; Sonsalla, P.K.; Pedata, F.; Melani, A.; Domenici, M.R.; Popoli, P.; Geiger, J.; Lopes, L.V.; de Mendonca, A. Adenosine A2A receptors and brain injury: Broad spectrum of neuroprotection, multifaceted actions and "fine tuning" modulation. *Prog. Neurobiol.* **2007**, *83*, 310–331. [CrossRef] [PubMed]
147. Illes, P.; Rubini, P.; Huang, L.; Tang, Y. The P2X7 receptor: A new therapeutic target in Alzheimer's disease. *Expert. Opin. Ther. Targets* **2019**, *23*, 165–176. [CrossRef] [PubMed]
148. Carmo, M.R.; Menezes, A.P.; Nunes, A.C.; Pliassova, A.; Rolo, A.P.; Palmeira, C.M.; Cunha, R.A.; Canas, P.M.; Andrade, G.M. The P2X7 receptor antagonist Brilliant Blue G attenuates contralateral rotations in a rat model of Parkinsonism through a combined control of synaptotoxicity, neurotoxicity and gliosis. *Neuropharmacology* **2014**, *81*, 142–152. [CrossRef]

149. Wang, X.H.; Xie, X.; Luo, X.G.; Shang, H.; He, Z.Y. Inhibiting purinergic P2X7 receptors with the antagonist brilliant blue G is neuroprotective in an intranigral lipopolysaccharide animal model of Parkinson's disease. *Mol. Med. Rep.* **2017**, *15*, 768–776. [CrossRef]
150. Apolloni, S.; Amadio, S.; Parisi, C.; Matteucci, A.; Potenza, R.L.; Armida, M.; Popoli, P.; D'Ambrosi, N.; Volonte, C. Spinal cord pathology is ameliorated by P2X7 antagonism in a SOD1-mutant mouse model of amyotrophic lateral sclerosis. *Dis. Model. Mech.* **2014**, *7*, 1101–1109. [CrossRef]
151. Fabbrizio, P.; Amadio, S.; Apolloni, S.; Volonte, C. P2X7 Receptor Activation Modulates Autophagy in SOD1-G93A Mouse Microglia. *Front. Cell Neurosci.* **2017**, *11*, 249. [CrossRef] [PubMed]
152. Sharp, A.J.; Polak, P.E.; Simonini, V.; Lin, S.X.; Richardson, J.C.; Bongarzone, E.R.; Feinstein, D.L. P2x7 deficiency suppresses development of experimental autoimmune encephalomyelitis. *J. Neuroinflammation* **2008**, *5*, 33. [CrossRef] [PubMed]
153. Domercq, M.; Matute, C. Targeting P2X4 and P2X7 receptors in multiple sclerosis. *Curr. Opin. Pharmacol.* **2019**, *47*, 119–125. [CrossRef] [PubMed]
154. Engel, T.; Gomez-Villafuertes, R.; Tanaka, K.; Mesuret, G.; Sanz-Rodriguez, A.; Garcia-Huerta, P.; Miras-Portugal, M.T.; Henshall, D.C.; Diaz-Hernandez, M. Seizure suppression and neuroprotection by targeting the purinergic P2X7 receptor during status epilepticus in mice. *FASEB J.* **2012**, *26*, 1616–1628. [CrossRef]
155. Beamer, E.; Fischer, W.; Engel, T. The ATP-Gated P2X7 Receptor As a Target for the Treatment of Drug-Resistant Epilepsy. *Front. Neurosci.* **2017**, *11*, 21. [CrossRef]
156. Melani, A.; Amadio, S.; Gianfriddo, M.; Vannucchi, M.G.; Volonte, C.; Bernardi, G.; Pedata, F.; Sancesario, G. P2X7 receptor modulation on microglial cells and reduction of brain infarct caused by middle cerebral artery occlusion in rat. *J. Cereb. Blood Flow Metab.* **2006**, *26*, 974–982. [CrossRef]
157. Orr, A.G.; Orr, A.L.; Li, X.J.; Gross, R.E.; Traynelis, S.F. Adenosine A2A receptor mediates microglial process retraction. *Nat. Neurosci.* **2009**, *12*, 872–878. [CrossRef]
158. Dai, S.S.; Zhou, Y.G. Adenosine 2A receptor: A crucial neuromodulator with bidirectional effect in neuroinflammation and brain injury. *Rev. Neurosci.* **2011**, *22*, 231–239. [CrossRef]
159. Reece, T.B.; Tribble, C.G.; Okonkwo, D.O.; Davis, J.D.; Maxey, T.S.; Gazoni, L.M.; Linden, J.; Kron, I.L.; Kern, J.A. Early adenosine receptor activation ameliorates spinal cord reperfusion injury. *J. Cardiovasc. Med. Hagerstown.* **2008**, *9*, 363–367. [CrossRef]
160. Pinna, A. Novel investigational adenosine A2A receptor antagonists for Parkinson's disease. *Expert. Opin. Investig. Drugs* **2009**, *18*, 1619–1631. [CrossRef]
161. Gerhard, A.; Pavese, N.; Hotton, G.; Turkheimer, F.; Es, M.; Hammers, A.; Eggert, K.; Oertel, W.; Banati, R.B.; Brooks, D.J. In vivo imaging of microglial activation with [11C](R)-PK11195 PET in idiopathic Parkinson's disease. *Neurobiol. Dis.* **2006**, *21*, 404–412. [CrossRef] [PubMed]
162. Tansey, M.G.; Goldberg, M.S. Neuroinflammation in Parkinson's disease: Its role in neuronal death and implications for therapeutic intervention. *Neurobiol. Dis.* **2010**, *37*, 510–518. [CrossRef] [PubMed]
163. Gyoneva, S.; Shapiro, L.; Lazo, C.; Garnier-Amblard, E.; Smith, Y.; Miller, G.W.; Traynelis, S.F. Adenosine A2A receptor antagonism reverses inflammation-induced impairment of microglial process extension in a model of Parkinson's disease. *Neurobiol. Dis.* **2014**, *67*, 191–202. [CrossRef] [PubMed]
164. Colella, M.; Zinni, M.; Pansiot, J.; Cassanello, M.; Mairesse, J.; Ramenghi, L.; Baud, O. Modulation of Microglial Activation by Adenosine A2a Receptor in Animal Models of Perinatal Brain Injury. *Front. Neurol.* **2018**, *9*, 605. [CrossRef]
165. Caetano, L.; Pinheiro, H.; Patricio, P.; Mateus-Pinheiro, A.; Alves, N.D.; Coimbra, B.; Baptista, F.I.; Henriques, S.N.; Cunha, C.; Santos, A.R.; et al. Adenosine A2A receptor regulation of microglia morphological remodeling-gender bias in physiology and in a model of chronic anxiety. *Mol. Psychiatry* **2017**, *22*, 1035–1043. [CrossRef] [PubMed]
166. Rebola, N.; Simoes, A.P.; Canas, P.M.; Tome, A.R.; Andrade, G.M.; Barry, C.E.; Agostinho, P.M.; Lynch, M.A.; Cunha, R.A. Adenosine A2A receptors control neuroinflammation and consequent hippocampal neuronal dysfunction. *J. Neurochem.* **2011**, *117*, 100–111. [CrossRef]
167. Liu, X.; Huang, P.; Wang, J.; Yang, Z.; Huang, S.; Luo, X.; Qi, J.; Shen, X.; Zhong, Y. The Effect of A2A Receptor Antagonist on Microglial Activation in Experimental Glaucoma. *Investig. Ophthalmol. Vis. Sci.* **2016**, *57*, 776–786. [CrossRef]

168. Merighi, S.; Bencivenni, S.; Vincenzi, F.; Varani, K.; Borea, P.A.; Gessi, S. A2B adenosine receptors stimulate IL-6 production in primary murine microglia through p38 MAPK kinase pathway. *Pharmacol. Res.* **2017**, *117*, 9–19. [CrossRef]
169. Koscso, B.; Csoka, B.; Selmeczy, Z.; Himer, L.; Pacher, P.; Virag, L.; Hasko, G. Adenosine augments IL-10 production by microglial cells through an A2B adenosine receptor-mediated process. *J. Immunol.* **2012**, *188*, 445–453. [CrossRef]
170. Johnston, J.B.; Silva, C.; Gonzalez, G.; Holden, J.; Warren, K.G.; Metz, L.M.; Power, C. Diminished adenosine A1 receptor expression on macrophages in brain and blood of patients with multiple sclerosis. *Ann. Neurol.* **2001**, *49*, 650–658. [CrossRef]
171. Luongo, L.; Guida, F.; Imperatore, R.; Napolitano, F.; Gatta, L.; Cristino, L.; Giordano, C.; Siniscalco, D.; Di Marzo, V.; Bellini, G.; et al. The A1 adenosine receptor as a new player in microglia physiology. *Glia* **2014**, *62*, 122–132. [CrossRef] [PubMed]
172. Haselkorn, M.L.; Shellington, D.K.; Jackson, E.K.; Vagni, V.A.; Janesko-Feldman, K.; Dubey, R.K.; Gillespie, D.G.; Cheng, D.; Bell, M.J.; Jenkins, L.W.; et al. Adenosine A1 receptor activation as a brake on the microglial response after experimental traumatic brain injury in mice. *J. Neurotrauma* **2010**, *27*, 901–910. [CrossRef] [PubMed]
173. Tsutsui, S.; Schnermann, J.; Noorbakhsh, F.; Henry, S.; Yong, V.W.; Winston, B.W.; Warren, K.; Power, C. A1 adenosine receptor upregulation and activation attenuates neuroinflammation and demyelination in a model of multiple sclerosis. *J. Neurosci.* **2004**, *24*, 1521–1529. [CrossRef] [PubMed]
174. Terayama, R.; Tabata, M.; Maruhama, K.; Iida, S. A3 adenosine receptor agonist attenuates neuropathic pain by suppressing activation of microglia and convergence of nociceptive inputs in the spinal dorsal horn. *Exp. Brain Res.* **2018**, *236*, 3203–3213. [CrossRef]
175. Dou, Y.; Wu, H.J.; Li, H.Q.; Qin, S.; Wang, Y.E.; Li, J.; Lou, H.F.; Chen, Z.; Li, X.M.; Luo, Q.M.; et al. Microglial migration mediated by ATP-induced ATP release from lysosomes. *Cell Res.* **2012**, *22*, 1022–1033. [CrossRef]
176. Imura, Y.; Morizawa, Y.; Komatsu, R.; Shibata, K.; Shinozaki, Y.; Kasai, H.; Moriishi, K.; Moriyama, Y.; Koizumi, S. Microglia release ATP by exocytosis. *Glia* **2013**, *61*, 1320–1330. [CrossRef]
177. Zimmermann, H.; Braun, N. Ecto-nucleotidases—molecular structures, catalytic properties, and functional roles in the nervous system. *Prog. Brain Res.* **1999**, *120*, 371–385.
178. Braun, N.; Sevigny, J.; Robson, S.C.; Enjyoji, K.; Guckelberger, O.; Hammer, K.; Di Virgilio, F.; Zimmermann, H. Assignment of ecto-nucleoside triphosphate diphosphohydrolase-1/cd39 expression to microglia and vasculature of the brain. *Eur. J. Neurosci.* **2000**, *12*, 4357–4366.
179. Farber, K.; Markworth, S.; Pannasch, U.; Nolte, C.; Prinz, V.; Kronenberg, G.; Gertz, K.; Endres, M.; Bechmann, I.; Enjyoji, K.; et al. The ectonucleotidase cd39/ENTPDase1 modulates purinergic-mediated microglial migration. *Glia* **2008**, *56*, 331–341. [CrossRef]
180. Bulavina, L.; Szulzewsky, F.; Rocha, A.; Krabbe, G.; Robson, S.C.; Matyash, V.; Kettenmann, H. NTPDase1 activity attenuates microglial phagocytosis. *Purinergic. Signal.* **2013**, *9*, 199–205. [CrossRef]
181. Matyash, M.; Zabiegalov, O.; Wendt, S.; Matyash, V.; Kettenmann, H. The adenosine generating enzymes CD39/CD73 control microglial processes ramification in the mouse brain. *PLoS ONE* **2017**, *12*, e0175012. [CrossRef] [PubMed]
182. Fontainhas, A.M.; Wang, M.; Liang, K.J.; Chen, S.; Mettu, P.; Damani, M.; Fariss, R.N.; Li, W.; Wong, W.T. Microglial morphology and dynamic behavior is regulated by ionotropic glutamatergic and GABAergic neurotransmission. *PLoS ONE* **2011**, *6*, e15973. [CrossRef] [PubMed]
183. Dissing-Olesen, L.; LeDue, J.M.; Rungta, R.L.; Hefendehl, J.K.; Choi, H.B.; MacVicar, B.A. Activation of neuronal NMDA receptors triggers transient ATP-mediated microglial process outgrowth. *J. Neurosci.* **2014**, *34*, 10511–10527. [CrossRef] [PubMed]
184. Eyo, U.B.; Peng, J.; Swiatkowski, P.; Mukherjee, A.; Bispo, A.; Wu, L.J. Neuronal hyperactivity recruits microglial processes via neuronal NMDA receptors and microglial P2Y12 receptors after status epilepticus. *J. Neurosci.* **2014**, *34*, 10528–10540. [CrossRef] [PubMed]
185. George, J.; Cunha, R.A.; Mulle, C.; Amedee, T. Microglia-derived purines modulate mossy fibre synaptic transmission and plasticity through P2X4 and A1 receptors. *Eur. J. Neurosci.* **2016**, *43*, 1366–1378. [CrossRef]
186. Kato, G.; Inada, H.; Wake, H.; Akiyoshi, R.; Miyamoto, A.; Eto, K.; Ishikawa, T.; Moorhouse, A.J.; Strassman, A.M.; Nabekura, J. Microglial Contact Prevents Excess Depolarization and Rescues Neurons from Excitotoxicity. *eNeuro* **2016**, *3*, ENEURO.0004-16.2016. [CrossRef]

187. Pascual, O.; Ben, A.S.; Rostaing, P.; Triller, A.; Bessis, A. Microglia activation triggers astrocyte-mediated modulation of excitatory neurotransmission. *Proc. Natl. Acad. Sci. USA* **2012**, *109*, E197–E205. [CrossRef]
188. Shinozaki, Y.; Nomura, M.; Iwatsuki, K.; Moriyama, Y.; Gachet, C.; Koizumi, S. Microglia trigger astrocyte-mediated neuroprotection via purinergic gliotransmission. *Sci. Rep.* **2014**, *4*, 4329. [CrossRef]
189. Verderio, C.; Matteoli, M. ATP mediates calcium signaling between astrocytes and microglial cells: Modulation by IFN-γ. *J. Immunol.* **2001**, *166*, 6383–6391. [CrossRef]
190. Nikolic, L.; Shen, W.; Nobili, P.; Virenque, A.; Ulmann, L.; Audinat, E. Blocking TNFα-driven astrocyte purinergic signaling restores normal synaptic activity during epileptogenesis. *Glia* **2018**, *66*, 2673–2683. [CrossRef]
191. Kettenmann, H. Neuroscience: The brain's garbage men. *Nature* **2007**, *446*, 987–989. [CrossRef] [PubMed]

Cell

ATP Synthase c-Subunit Leak Causes Aberrant Cellular Metabolism in Fragile X Syndrome

Graphical Abstract

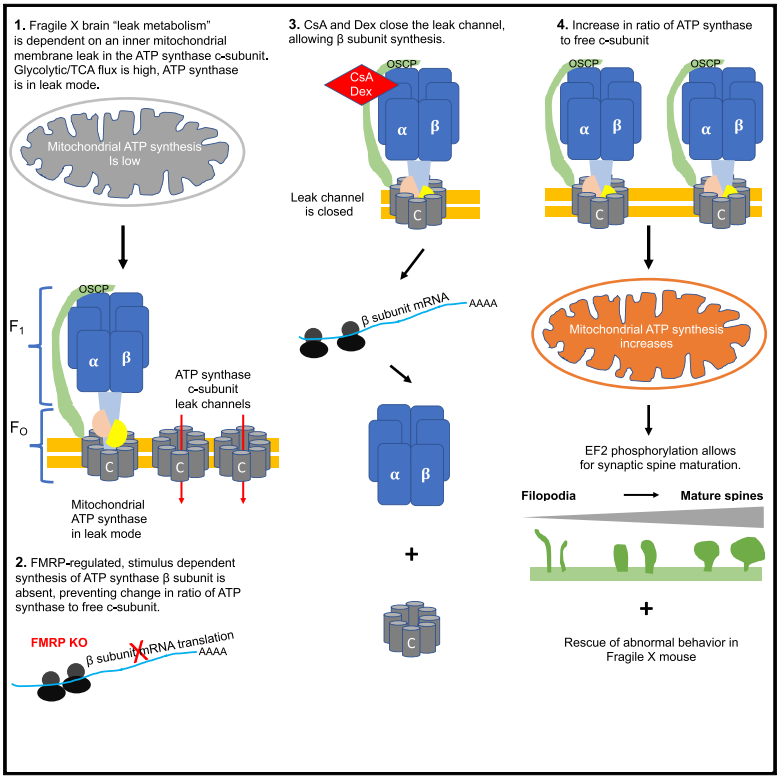

Highlights

- ATP synthase c-subunit leak in Fragile X causes aberrant metabolism
- Changes in ATP synthase component stoichiometry regulate protein synthesis rate
- Inhibition of the leak normalizes synaptic spine morphology and Fragile X behavior

Authors

Pawel Licznerski, Han-A Park, Harshvardhan Rolyan, ..., Valentin K. Gribkoff, Richard J. Levy, Elizabeth A. Jonas

Correspondence

pawel.licznerski@yale.edu (P.L.), elizabeth.jonas@yale.edu (E.A.J.)

In Brief

Lack of FMRP in Fragile X neurons is associated with a leak in the ATP synthase, the blockade of which normalizes cellular and behavioral disease phenotypes.

Licznerski et al., 2020, Cell *182*, 1–16
September 3, 2020
https://doi.org/10.1016/j.cell.2020.07.008

Please cite this article in press as: Licznerski et al., ATP Synthase c-Subunit Leak Causes Aberrant Cellular Metabolism in Fragile X Syndrome, Cell (2020), https://doi.org/10.1016/j.cell.2020.07.008

Cell

CellPress

Article

ATP Synthase c-Subunit Leak Causes Aberrant Cellular Metabolism in Fragile X Syndrome

Pawel Licznerski,[1,*] Han-A Park,[1,5] Harshvardhan Rolyan,[1] Rongmin Chen,[1] Nelli Mnatsakanyan,[1] Paige Miranda,[1] Morven Graham,[2] Jing Wu,[1] Nicole Cruz-Reyes,[4] Nikita Mehta,[4] Sana Sohail,[4] Jorge Salcedo,[4] Erin Song,[4] Charles Effman,[4] Samuel Effman,[4] Lucas Brandao,[6] Gulan N. Xu,[1] Amber Braker,[1] Valentin K. Gribkoff,[1,4] Richard J. Levy,[3] and Elizabeth A. Jonas[1,4,7,*]

[1]Department of Internal Medicine, Section of Endocrinology, Yale University School of Medicine, New Haven, CT 06511, USA
[2]Department of Cell Biology, Yale University School of Medicine, New Haven, CT 06520, USA
[3]Department of Anesthesiology, Columbia University Medical Center, New York, NY 10032, USA
[4]Marine Biological Laboratory, Woods Hole, MA 02543, USA
[5]Department of Human Nutrition and Hospitality Management, College of Human Environmental Sciences, The University of Alabama, Tuscaloosa, AL 35487, USA
[6]Department of Biology, Clark University, Worcester, MA 01610, USA
[7]Lead Contact
*Correspondence: pawel.licznerski@yale.edu (P.L.), elizabeth.jonas@yale.edu (E.A.J.)
https://doi.org/10.1016/j.cell.2020.07.008

SUMMARY

Loss of the gene (*Fmr1*) encoding Fragile X mental retardation protein (FMRP) causes increased mRNA translation and aberrant synaptic development. We find neurons of the *Fmr1*$^{-/y}$ mouse have a mitochondrial inner membrane leak contributing to a "leak metabolism." In human Fragile X syndrome (FXS) fibroblasts and in *Fmr1*$^{-/y}$ mouse neurons, closure of the ATP synthase leak channel by mild depletion of its c-subunit or pharmacological inhibition normalizes stimulus-induced and constitutive mRNA translation rate, decreases lactate and key glycolytic and tricarboxylic acid (TCA) cycle enzyme levels, and triggers synapse maturation. FMRP regulates leak closure in wild-type (WT), but not FX synapses, by stimulus-dependent ATP synthase β subunit translation; this increases the ratio of ATP synthase enzyme to its c-subunit, enhancing ATP production efficiency and synaptic growth. In contrast, in FXS, inability to close developmental c-subunit leak prevents stimulus-dependent synaptic maturation. Therefore, ATP synthase c-subunit leak closure encourages development and attenuates autistic behaviors.

INTRODUCTION

Fragile X syndrome (FXS) is a devastating X-linked genetic disorder and the most common inherited cause of intellectual disability (Dölen et al., 2010; Wijetunge et al., 2013). It results from a CGG repeat expansion within the *Fmr1* gene that leads to loss of expression of Fragile X mental retardation protein (FMRP). The FX phenotype is characterized by constitutively increased mRNA translation rates, morphological immaturity of synapses and dendritic spines (Dölen et al., 2007), aberrant synaptic plasticity (Bear et al., 2004), excitotoxicity (Dölen et al., 2007, 2010), and enhanced excitability (Brown et al., 2010; Deng et al., 2013; El-Hassar et al., 2019; McCullagh et al., 2020; Strumbos et al., 2010; Zhang et al., 2012). The structural and functional deficiencies in FX neurons correlate with loss of normal learning patterns and an increase in autistic behaviors (Santos et al., 2014) in rodents and humans (Zoghbi and Bear, 2012). Despite the fact that FMRP has been well described as an RNA-binding protein (Darnell, 2011; Darnell et al., 2011), there have been, to date, no effective therapies for the disorder.

Prior work found that depletion of *Fmr1* and its homolog *Fxr2* reduces fat deposits in mutant mice and leads to higher food intake, increased oxygen consumption, and CO_2 production, suggesting uncoupled oxidative phosphorylation (Lumaban and Nelson, 2015). In human autism spectrum disorder patients, elevated lactate levels, indicative of glycolysis driven by mitochondrial dysfunction, have been described (Dhillon et al., 2011; Goh et al., 2014). Hippocampal neurons of the *Fmr1* CGG repeat knockin (KI) mouse (FMRP levels decreased by 42.6%) have small mitochondria with reduced mobility, high O_2 uptake, and a large proton leak (Kaplan et al., 2012). In a recent report, *Drosophila fmr1* was found to alter the metabolome of the flies such that the *dfmr1* mutants had decreased carbohydrate and lipid stores, were hypersensitive to starvation stress, hyperphagic, and had reduced NAD^+/NADH ratio (Weisz et al., 2018). This was related to a defect in mitochondria producing an increase in maximal respiratory capacity. A recent report also found that, in *Fmr1*$^{-/y}$ mouse brains, electron transport complexes run at high rates even though ATP production is low, suggesting inner membrane inefficiency (H^+ ion leak) (D'Antoni et al.,

Please cite this article in press as: Licznerski et al., ATP Synthase c-Subunit Leak Causes Aberrant Cellular Metabolism in Fragile X Syndrome, Cell (2020), https://doi.org/10.1016/j.cell.2020.07.008

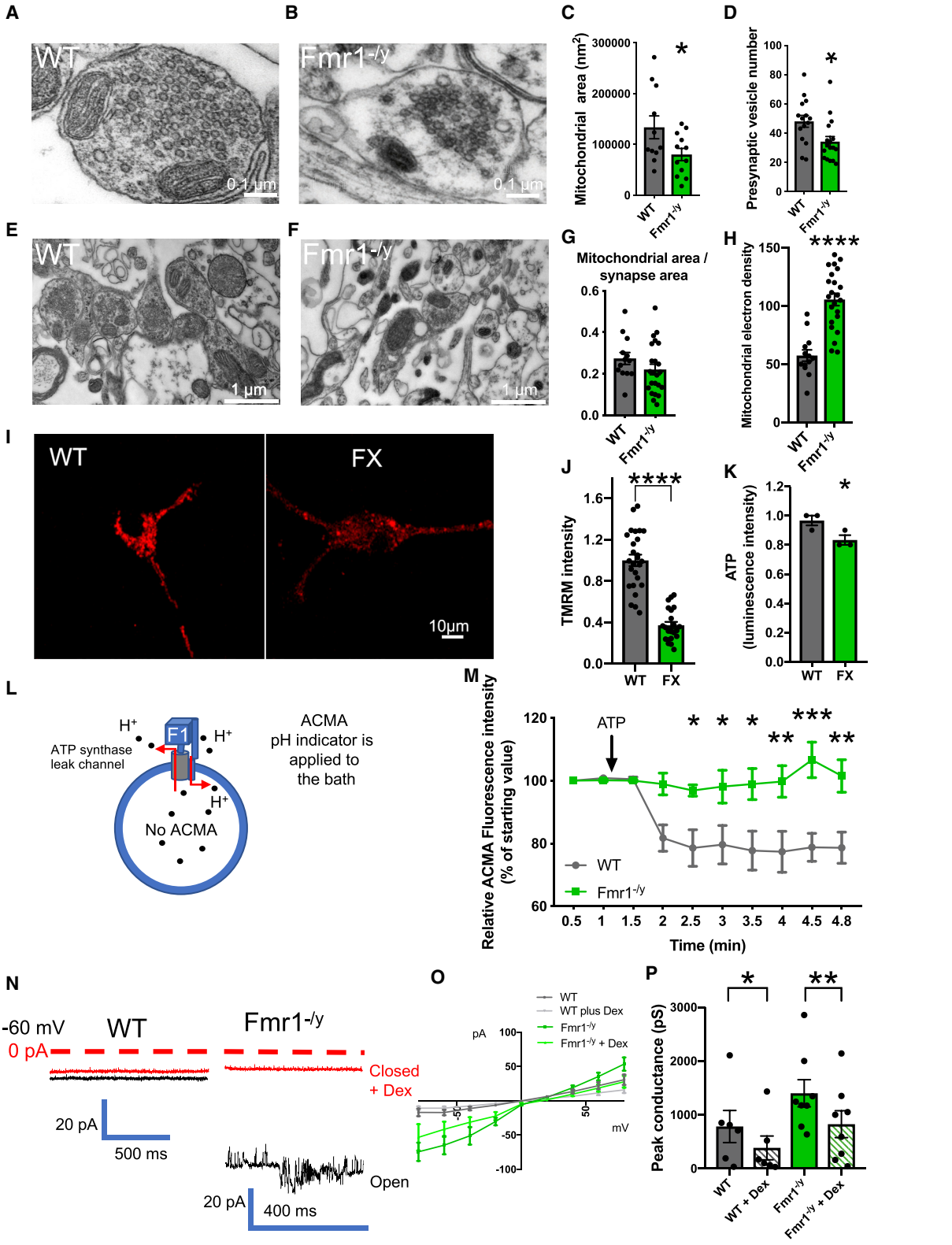

Figure 1. *Fmr1*$^{-/y}$ Mitochondria Have an Inner Mitochondrial Membrane Leak

(A and B) Representative electron microscopy images of brain slices show smaller synapses within the CA1 region of the mouse *Fmr1*$^{-/y}$ hippocampus compared to WT.

(legend continued on next page)

Please cite this article in press as: Licznerski et al., ATP Synthase c-Subunit Leak Causes Aberrant Cellular Metabolism in Fragile X Syndrome, Cell (2020), https://doi.org/10.1016/j.cell.2020.07.008

2020). Our group's recent report shows that mitochondria from the *Fmr1*$^{-/y}$ mouse brains have inefficient thermogenic respiration due to a futile coenzyme Q-regulated proton leak, leading to synaptic spine and behavioral abnormalities (Griffiths et al., 2020). Although these findings suggest that FMRP and related proteins might be required in general for normal developmental mitochondrial function, they also highlight the possibility that FX mitochondria are uncoupled and have an inner membrane leak that makes the mitochondria inefficient, burning fuel instead of saving energy.

The mitochondrial abnormalities could be emblematic of neuronal immaturity. Several findings indicate that FX neurons are underdeveloped (Bassell and Warren, 2008; Bhattacharya et al., 2012; Pyronneau et al., 2017). They have redundant postsynaptic spines with a thin, long filopodial shape that has failed to change to a mushroom shape characteristic of mature synapses (Bagni and Greenough, 2005). FX mitochondria are also small (Kaplan et al., 2012). The possibility that this structural immaturity throughout brain development is related to the delay of a metabolic shift during development is suggested by reports on cardiac development in the early wild-type (WT) embryo. At embryonic day (E) 9.5 profound inner mitochondrial membrane leak accompanies a lack of respiration (Hom et al., 2011). The leak closes between E11.5 and E13.5 at the onset of oxidative phosphorylation (Hom et al., 2011) and respiration becomes coupled to phosphorylation. This normal developmental process is related to closure of the cell death channel that spans the mitochondrial inner membrane, known as the permeability transition pore (mPTP), and development is hastened by the mPTP inhibitor cyclosporine A (CsA) (Beutner et al., 2014, 2017).

We have reported previously that certain proteins and pharmacological reagents regulate directly mitochondrial inner membrane efficiency by binding to the ATP synthase enzymatic (F_1) portion (Alavian et al., 2011, 2015; Chen et al., 2011, 2019). Our work indicates that a leak that regulates inner membrane ATP production efficiency resides within the membrane-embedded c-subunit ring of the ATP synthase (Alavian et al., 2014). We have further suggested that the c-subunit ring may form or contribute significantly to the CsA regulated mPTP (Alavian et al., 2014; Bernardi and Di Lisa, 2015; Bonora et al., 2013; Mnatsakanyan et al., 2019; Neginskaya et al., 2019; Rasola and Bernardi, 2014). We have shown recently that the mPTP is aberrantly active in *Fmr1*$^{-/y}$ mitochondria (Griffiths et al., 2020).

We now suggest that the mitochondrial inner membrane leak of FX neurons and cells is caused by abnormally high levels of ATP synthase c-subunit. We find that the c-subunit leak causes persistence of an immature metabolic phenotype associated specifically with mitochondrial leak, termed here "leak metabolism." The c-subunit leak aberrantly elevates protein synthesis; a decrease in c-subunit level or specific pharmacological inhibition of ATP synthase leak reduces protein synthesis rates and decreases the leak metabolism in the neurons. In keeping with the c-subunit leak as causative of abnormally delayed neuronal development, we find that inhibition of the ATP synthase leak allows for the maturation of synapses and normalizes autistic behaviors in a mouse model of FX.

RESULTS

Mitochondrial Morphology and Function Are Altered in FX Mouse Neurons

Mitochondria are necessary for normal synapse formation and thus mitochondria themselves undergo developmental plasticity; large changes in mitochondrial structure and function occur during development (Brandt et al., 2017; McCarron et al., 2013). We therefore examined mitochondria in *Fmr1*$^{-/y}$ neurons and compared them to mitochondria of WT neurons of the same age. Electron micrographs taken of hippocampal CA1 brain slices prepared from 2-month-old mice revealed that presynaptic vesicle pools were smaller in *Fmr1*$^{-/y}$ synapses than those of WT synapses as previously described (Figures 1A, 1B, and 1D) (Klemmer et al., 2011). The mitochondria within *Fmr1*$^{-/y}$ synapses also had a decreased area compared to WT synapses (Figures 1A–1C), but the ratio of mitochondrial area to synapse area was similar in *Fmr1*$^{-/y}$ versus WT synapses (Figures 1E–1G), suggesting that mitochondrial size was scaled to

(C) Group data show a decrease in mitochondrial area in *Fmr1*$^{-/y}$ compared to WT (-n = 15 for *Fmr1*$^{-/y}$ and –n = 17 micrographs for WT, *p = 0.043).
(D) The vesicle number in presynaptic boutons is reduced in *Fmr1*$^{-/y}$ (n= 11 micrographs of each condition; *p = 0.0143).
(E and F) Example electron micrographs of synapses from the CA1 region of the mouse hippocampus slices show that *Fmr1*$^{-/y}$ synapses contain electron dense mitochondria not present in WT synapses.
(G) Mitochondrial area/synapse area is unchanged comparing WT to *Fmr1*$^{-/y}$ (n = 13 micrographs for WT and 23 for *Fmr1*$^{-/y}$).
(H) Group data show electron density is increased in *Fmr1*$^{-/y}$ compared to WT (n= 23 micrographs for *Fmr1*$^{-/y}$ and 13 for WT; *p = 0.0114).
(I) Representative images of mitochondrial membrane potential indicator TMRM fluorescence in isolated cortical neurons.
(J) Group data show TMRM intensity is reduced in FX compared to WT (n= 20–24 neurons each condition, 4 independent cultures; ****p < 0.0001).
(K) Cytosolic ATP levels of isolated cortical neurons are reduced in FX compared to WT (n = 3 wells for each, *p < 0.05).
(L) Illustration of method of measurement of bath H^+ ion concentration using the H^+ sensitive indicator ACMA. SMVs are illustrated with mitochondrial ATP synthase F_1 facing toward the bath. ATP hydrolysis causes H^+ ion sequestration into the lumen of the vesicles. Vesicles are impermeant to the pH indicator. Red arrows show paths of H^+ pumping (at the side of the c-subunit) and H^+ leak (through the center of the c-subunit).
(M) Lack of sequestration of H^+ ions into *Fmr1*$^{-/y}$ SMVs during ATP hydrolysis by the ATP synthase (n = 3 samples per condition).
(N) Representative patch clamp recordings of SMVs of *Fmr1*$^{-/y}$ and WT at the indicated holding potential. Black trace indicates open channel. Red trace shows the relatively closed channel in the same recording after Dex exposure.
(O) Current voltage relationship for the group of SMV recordings shown in (P).
(P) Group data of peak conductances of the independent recordings (n= 6 for WT and WT+Dex; n = 8 for *Fmr1*$^{-/y}$ and *Fmr1*$^{-/y}$ +Dex) measured from 0 pA (*p = 0.0449 comparing WT to WT+Dex; **p = 0.0064 comparing *Fmr1*$^{-/y}$ to *Fmr1*$^{-/y}$+Dex). Linear current voltage relationship was assumed for calculation of peak conductance. In (C), (D), (G), (H), (J), and (K), unpaired two-tailed Student's t test was used. In (M), two-way repeated-measures ANOVA followed by Sidak's multiple comparison test was used. In (P), paired two-way Student's t test was used. Data are represented as mean ± SEM (*p < 0.05; **p < 0.01; ***p < 0.001; ****p < 0.0001).

Please cite this article in press as: Licznerski et al., ATP Synthase c-Subunit Leak Causes Aberrant Cellular Metabolism in Fragile X Syndrome, Cell (2020), https://doi.org/10.1016/j.cell.2020.07.008

the smaller synaptic size in *Fmr1*$^{-/y}$. The mitochondria of *Fmr1*$^{-/y}$ synapses had no apparent disturbance of cristae structure, although there was a marked increase in matrix density relative to that of controls (Figures 1E, 1F, and 1H), possibly reflecting a high protein amount within the matrix compartment.

To examine mitochondrial function at an earlier stage of development, we prepared cortical neurons from mice at postnatal days (P) 1–2 and studied them at the time when synapses are forming rapidly (DIV14). Mitochondrial inner membrane polarization is indicative of appropriate use of the electron transport chain. Using the membrane potential indicator tetramethylrhodamine methyl ester (TMRM), we determined that FX mitochondria generated less than half the membrane potential of the mitochondria of WT neurons (Figures 1I and 1J). Lack of membrane potential can arise from rapid ATP production caused by inability to keep up with increased energy demand or from depolarization caused by a mitochondrial inner membrane leak. In either case, ATP levels may be decreased. In fact, ATP levels in FX neurons were slightly decreased compared to WT control neurons (Figure 1K), suggesting that FX neurons fall behind in their combined mitochondrial and glycolytic ATP production.

Fmr1$^{-/y}$ Mitochondria Have a Large Conductance Inner Membrane Leak

In the setting of increased energy demand, H^+ ions move across the mitochondrial ATP synthase and cause a conformational change in the ATP synthase molecular complex that results in ATP production. The enzyme can also hydrolyze ATP to provide energy to translocate H^+ ions across the inner mitochondrial membrane in reverse mode. The 9-amino-6-chloro-2-methoxyacridine (ACMA) assay measures the ATP synthase enzymatic rate using this reverse mode (Figure 1L) (Caviston et al., 1998). To perform this assay, mitochondrial inner membrane remnants that are relatively enriched in ATP synthase (submitochondrial vesicles [SMVs]) are prepared (Chan et al., 1970; Chen et al., 2004; Ko et al., 2003). In these SMVs, the F_1 or enzymatic portion of the ATP synthase is exposed to the medium, which contains a membrane impermeant H^+ indicator. SMVs prepared from WT brain readily sequestered H^+ ions in response to the addition of ATP to the bath. In contrast, *Fmr1*$^{-/y}$ SMVs failed to sequester H^+ ions in response to ATP addition (Figure 1M), indicating either failure of the enzyme to translocate H^+ or an H^+ leak in the SMV membranes. To detect directly an inner mitochondrial membrane leak, we analyzed patch clamp recordings of *Fmr1*$^{-/y}$ brain SMVs. We found a large multi-conductance, voltage-dependent channel activity not present in WT brain SMVs (Figures 1N–1P), indicating that lack of sequestration of H^+ ions in the ACMA assay was due to loss of the H^+ ions through an open channel in the SMV membranes.

Our previous reports demonstrated an effect of an ATP synthase modulator, dexpramipexole (Dex) on inner mitochondrial membrane leak channel activity (Alavian et al., 2015). It had been described previously that Dex, which is the R(+) enantiomer of the widely used Parkinson's drug, Pramipexole, has no significant dopaminergic efficacy, is not a CsA analog, and it readily crosses the blood brain barrier (Bozik et al., 2010; Cudkowicz et al., 2011). We reported that radiolabeled Dex binds to ATP synthase F_O subunit b and F_1 subunit oligomycin sensitivity conferring protein (OSCP), closing an inner membrane leak in patch clamp recordings, enhancing ATP production efficiency and decreasing cell death and oxygen consumption with modest potency (Alavian et al., 2015). To test if ATP synthase leak was the cause of the open channel in *Fmr1*$^{-/y}$ SMVs, we applied Dex during the recordings. Dex decreased small conductance activity of the WT SMVs and decreased large conductance channel activity in the *Fmr1*$^{-/y}$ SMVs as measured by change in peak conductance (Figured 1N and 1P). This suggests that at least some of the leak in *Fmr1*$^{-/y}$ mitochondrial inner membranes is produced by increased activity of the ATP synthase leak channel, although a resistant fraction of the leak could be produced by uncomplexed c-subunit or by other channels.

ATP synthase contains a highly regulated, multi-conductance channel that is contained within the c-subunit ring of the main membrane bound (F_O) portion (Alavian et al., 2014; Mnatsakanyan et al., 2019). Pathological opening of the channel may occur upon conformational change of the ATP synthase including loss of an inhibitory structure in its cavity (Gerle, 2016; Gu et al., 2019; Mnatsakanyan and Jonas, 2020; Vlasov et al., 2019), separation of the F_1 from the F_O (Alavian et al., 2014), or loss of F_1 (Chen et al., 2019). We hypothesized, based on these previous findings and the channel recording data, that the ratio of c-subunit (F_O) to F_1 might be altered such that *Fmr1*$^{-/y}$ mitochondria could have an unopposed (uncoupled to F_1) c-subunit that would readily leak ions across the inner mitochondrial membrane in a voltage-dependent manner. We found, in *Fmr1*$^{-/y}$, that ATP synthase β-subunit (a major part of the soluble enzyme or F_1 component) level was markedly elevated above that measured in control mitochondria (Figure 2A), but the level of c-subunit (F_O) was elevated to an even greater degree (Figure 2A). To determine if this resulted in free c-subunit in the mitochondrial membrane, we subjected mitochondrial proteins to non-denaturing Native-PAGE electrophoresis (Figure 2B). These immunoblots showed that, although total amounts of assembled ATP synthase monomer plus dimer were not significantly elevated in *Fmr1*$^{-/y}$ compared to WT, level of free c subunit was markedly elevated compared to WT controls. We analyzed the blots in two ways. In the same blot, we compared the level of *Fmr1*$^{-/y}$ fully assembled ATP synthase (monomer plus dimer) to the WT controls and the level of *Fmr1*$^{-/y}$ free c-subunit to the WT controls (left set of histograms). In the right histogram, we calculated the ratio of free c-subunit to its own assembled ATP synthase within the same lane. Both analyses showed that free c-subunit is markedly elevated in *Fmr1*$^{-/y}$ compared to WT controls.

We next carried out experiments to determine if the increase in β and c subunit levels in *Fmr1*$^{-/y}$ mitochondria can be attributed directly to FMRP-regulated mRNA translation. Many of the nuclear-encoded mRNAs for components of the ATP synthase have been found to bind FMRP in crosslinking immunoprecipitation experiments, and mRNA for the ATP synthase β subunit is the 87th most represented on the list of over 800 mRNAs (Darnell et al., 2011). To confirm the binding of FMRP to ATP synthase β-subunit mRNA, we immunoprecipitated FMRP from synaptoneurosomal (hereafter synaptosomal) lysates and performed PCR on the cDNA synthesized from the immunoprecipitate. We confirmed that FMRP binds β subunit mRNA. By reverse transcription PCR (RT-PCR), ATP5G2 was found to be by far

Please cite this article in press as: Licznerski et al., ATP Synthase c-Subunit Leak Causes Aberrant Cellular Metabolism in Fragile X Syndrome, Cell (2020), https://doi.org/10.1016/j.cell.2020.07.008

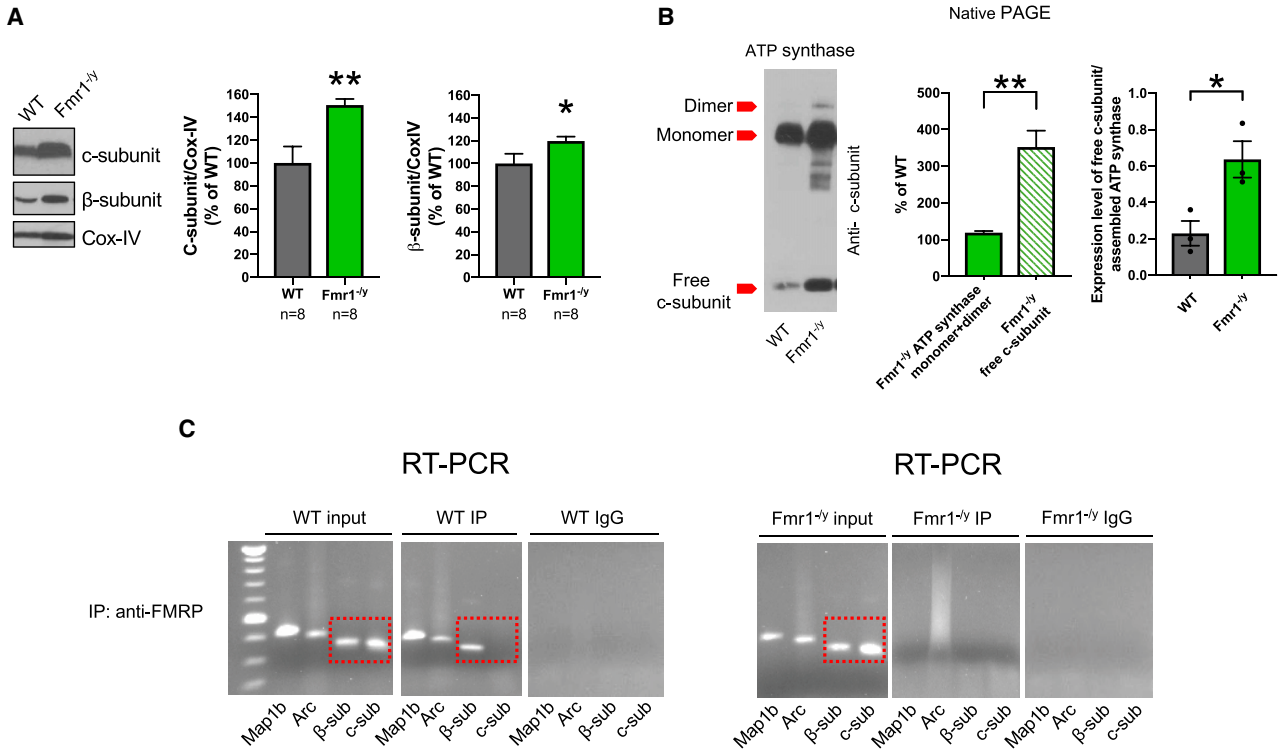

Figure 2. Expression of ATP Synthase Subunits Causing Inner Membrane Leak Is Increased in *Fmr1*$^{-/y}$ Mitochondria

(A) c- and β-subunit protein expression levels are higher in *Fmr1*$^{-/y}$ brain mitochondria compared to those of WT (n = 8 independent samples for each, **p = 0.0083 and *p = 0.031).

(B) An example of three independent experiments of non-denaturing Native-PAGE electrophoresis of isolated brain mitochondria. Immunoblotting performed with anti-c-subunit antibody. The abundance of the free c-subunit is higher in *Fmr1*$^{-/y}$ mitochondria compared to WT. Left histograms: level of fully assembled ATP synthase (monomer plus dimer) and the level of free c-subunit in *Fmr1*$^{-/y}$ as a percent of WT control. Right histograms: ratio of free c-subunit to its own assembled ATP synthase within the same lane. n = 3 for each condition.

(C) FMRP immunoprecipitation from isolated synaptosomes pulls down ATP synthase β-subunit mRNA but not ATP synthase c-subunit mRNA (ATP5G2) as detected by RT-PCR (shown is one of n= 3 independent immunoprecipitation experiments). All experiments in this figure used unpaired Student's t test, data are represented as mean ± SEM (*p < 0.05; **p < 0.01; ***p < 0.001; ****p < 0.0001).

See also Figure S1 and Table S2.

the dominant c-subunit gene, but we failed to detect binding of FMRP to any of the three c-subunit gene products (only ATP5G2 is shown in Figure 2C). In *Fmr1*$^{-/y}$ synapses, quantitative real-time PCR (qRT-PCR) of the synaptosomes (Figure S1), performed to detect total expression of ATP synthase β subunit and ATP5G2 c-subunit mRNA, showed that these mRNAs were elevated compared to those of WT synapses. Therefore, although loss of FMRP may lead to enhanced transcription of both ATP synthase β and c-subunit mRNAs, in contrast only β subunit, but not c-subunit, translation is likely to be regulated by FMRP. Taken together, these results suggest a role for FMRP in ATP synthase assembly during activity-dependent synaptic development (see Figure 5D).

FX Neurons Have a Mitochondrial Leak-Dependent Metabolic Phenotype

Despite the leaky inner membrane, ATP levels were only slightly decreased in FX neurons compared to controls (Figure 1K), suggesting that glycolytic ATP might contribute to the overall ATP level in the neuronal cytoplasm. To determine the metabolic phenotype of the neurons, we labeled newly synthesized proteins with puromycin and immunoprecipitated with an anti-puromycin antibody. We then evaluated the newly synthesized proteome by liquid chromatography with tandem mass spectrometry (LC-MS/MS) (Figures 3A and 3B; Table S1). This study revealed that FX neurons have an increase in certain glycolytic enzymes including hexokinase II, pyruvate kinase M2 variant and lactate dehydrogenase, and also in enzymes required for tricarboxylic acid (TCA) cycle and NAD^+/NADH metabolism, including enzymes of the malate/aspartate shunt and isocitrate dehydrogenase (Dayton et al., 2016; Li et al., 2016; Roberts and Miyamoto, 2015; Vander Heiden et al., 2009; Zheng et al., 2016). Because these data suggested an increase in activity of glycolytic enzymes, we measured lactate levels and found that they were markedly increased in the FX culture media (Figure 3 C). High glycolytic activity and lactate production, but also increases in TCA cycle enzymes, are hallmark features of immature and developing cells (Fame et al., 2019). Although puromycin incorporation into newly translating proteins provided us with an estimate of the high translation rate of metabolic enzymes, it did not

Please cite this article in press as: Licznerski et al., ATP Synthase c-Subunit Leak Causes Aberrant Cellular Metabolism in Fragile X Syndrome, Cell (2020), https://doi.org/10.1016/j.cell.2020.07.008

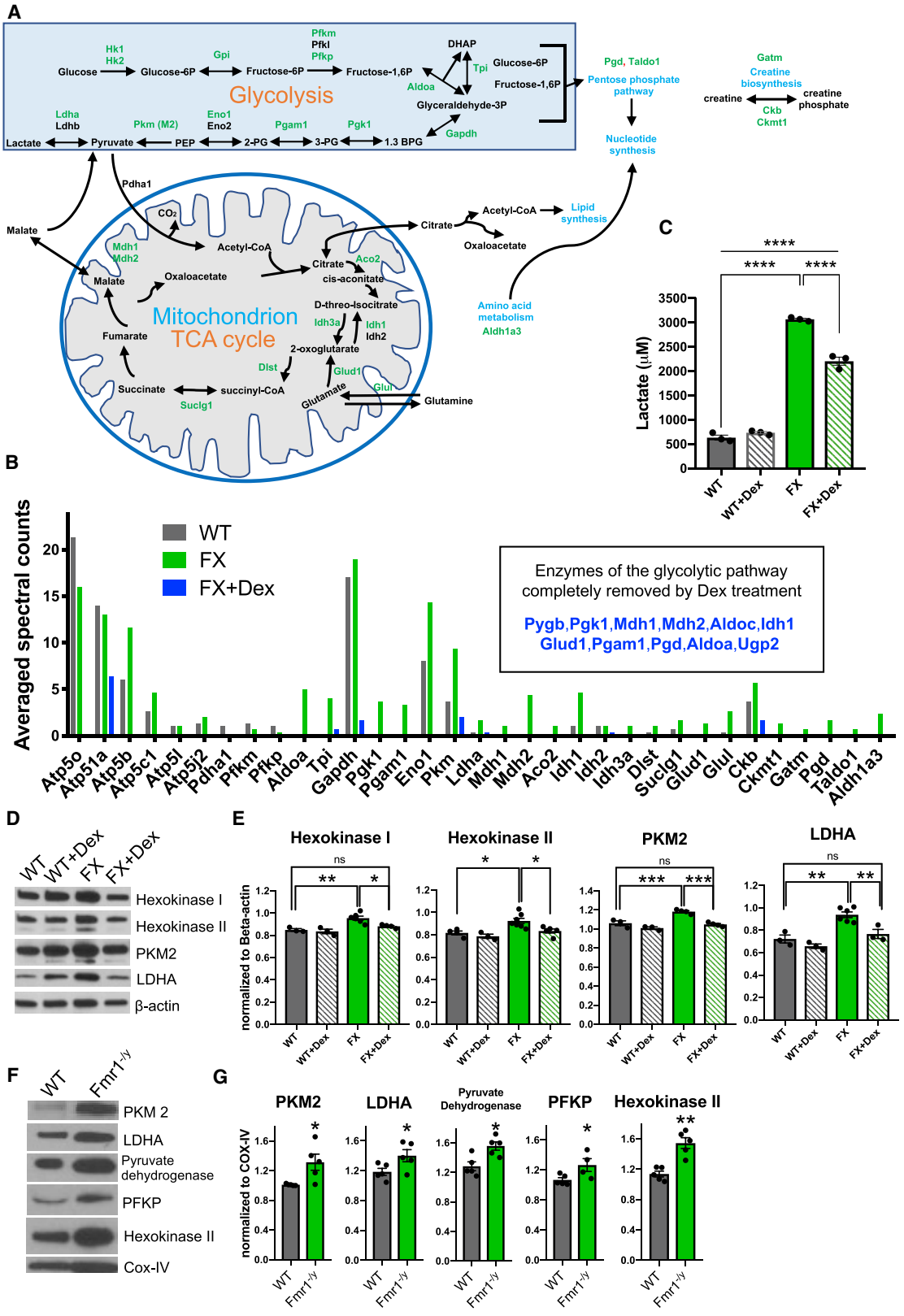

(legend on next page)

Please cite this article in press as: Licznerski et al., ATP Synthase c-Subunit Leak Causes Aberrant Cellular Metabolism in Fragile X Syndrome, Cell (2020), https://doi.org/10.1016/j.cell.2020.07.008

tell us about the steady state levels of these enzymes. To test if specific enzymes are elevated in FX, we performed immunoblots on WT and FX neuronal cultures and brain mitochondria. These showed that the levels of certain key enzymes are elevated in FX (Figures 3D–3G), including hexokinase and pyruvate dehydrogenase, suggestive not only of enhanced glycolytic flux but also of enhanced TCA cycle function, supporting the idea that increased flux through the FX mitochondria is caused by the mitochondrial inner membrane leak. Because Dex closed the mitochondrial inner membrane leak in patch clamp recordings, and we reported previously that Dex enhances the efficiency of oxidative phosphorylation (Alavian et al., 2015), we tested if Dex treatment of the FX neuronal cultures would eliminate the increased flux of the leak metabolic phenotype. We found that Dex effectively decreased the lactate levels in FX neurons; it also reversed the abnormally high levels of glycolytic and TCA enzymes (Figures 3B–3D). These results are consistent with increased flux through glycolytic and TCA pathways caused by the inner membrane leak in FX. Dex normalizes the aberrant leak metabolism of FX neurons through its actions to close the ATP synthase leak.

Genetic or Pharmacological Modulation of ATP Synthase Leak Decreases Abnormally Elevated Protein Synthesis Rates in FX

Previous work has shown that the anti-apoptotic protein Bcl-xL acts on the ATP synthase to close the mitochondrial inner membrane leak (Alavian et al., 2011; Chen et al., 2011), but whether this is tied to changes in protein synthesis rate was not known. Both translation of the reporter Dendra (Figures S2A and S2B), and puromycin incorporation assays (Figures 4E–4H) demonstrated that rates of mRNA translation in general are elevated in FX neurons compared to WT, as has been described previously (Bear et al., 2004; Dölen et al., 2007; Jacquemont et al., 2018; Muscas et al., 2019; Udagawa et al., 2013). We found that rates of Dendra translation or puromycin incorporation were similarly elevated in WT neurons by exposure to the selective Bcl-xL inhibitor ABT-737 (Figures S2C–S2E), and in contrast, these rates were reduced by Bcl-xL protein transfection into synapses (Figures S2F and S2G). These findings are consistent with the hypothesis that opening of the ATP synthase leak (Alavian et al., 2011) increases overall mRNA translation rates in developing neurons. The pertinent pharmacological reagents (Dex and CsA) and Bcl-xL all bind in the soluble portion (F_1) of the ATP synthase, not within the membrane embedded portion. Therefore, to determine if membrane-embedded ATP synthase c-subunit leak channel directly modulates mRNA translation rate, we depleted c-subunit protein by small interfering RNA (siRNA) or increased c-subunit protein level by overexpression in human FX fibroblasts and measured protein synthesis rates by puromycin incorporation. We found that mild depletion of c-subunit decreased protein synthesis rate (Figure 4A) and, in contrast, c-subunit overexpression increased the rate of protein synthesis (Figure 4B), directly implicating c-subunit leak in regulation of protein synthesis rate in human FX cells. In FX cortical neurons, the ATP synthase leak inhibitor Dex also decreased protein synthesis rates in a concentration-dependent manner (Figures 4C and 4D), consistent with Dex effects on decreasing the open probability of the ATP synthase leak channel. Application of Dex also decreased protein synthesis in brain slices (Figures 4E and 4F). We then tested a well-known and more potent inhibitor of the ion channel conductance of the ATP synthase that also inhibits the mPTP, CsA (Baines et al., 2005; Nakagawa et al., 2005). CsA prevents binding of cyclophilin D to ATP synthase subunit OSCP (Giorgio et al., 2009, 2013). In FX neuronal cultures, small concentrations of CsA readily reversed the aberrantly increased mRNA translation rate (Figures 4G and 4H), but had no effect on mRNA translation in WT neurons (Figures 4G and 4H), suggesting that the CsA-sensitive leak is larger in FX compared to WT neuronal mitochondria (see Figures 1N–1P).

We also carried out electron microscopy to visualize the effects of CsA on the protein synthetic machinery in the CA1 region of hippocampal slices from *Fmr1*$^{-/y}$ and WT mice. Slices were treated with CsA or vehicle for 2.5 h then fixed for processing. Our studies showed a large increase in the number of actively translating ribosomal assemblies (rosettes) in *Fmr1*$^{-/y}$ CA1 neurons, consistent with an enhancement in mRNA translation over that seen in WT neurons (Figures 4I–4N). Strikingly, CsA greatly reduced the number of rosettes in the contralateral half of the same coronal brain slice, suggesting that its effects on mitochondrial inner membrane leak rapidly decreased the rate of mRNA translation in *Fmr1*$^{-/y}$ CA1 neurons.

Figure 3. Metabolic Profile of FX Cortical Neurons Shows Enhancement of Glycolysis/TCA Flux in FX Compared to WT

(A) Glycolysis and tricarboxylic acid (TCA) cycle schematics illustrating enzymes involved in both pathways. Enzymes increased in FX > WT in at least 2 of 3 independent cultures are labeled in green.

(B) Averaged spectral counts of metabolic peptides expressed in WT and FX cortical neuron cultures. Puromycin immunoprecipitates were analyzed by LC-MS/MS after cortical neuronal cultures (DIV14) were exposed to puromycin for 15 min. Shown in blue are the enzymes decreased by Dex treatment in at least 2 out of 3 FX cultures (n = 3 independent cultures of each condition). Metabolic peptides completely removed by Dex treatment are indicated above the graph in blue lettering.

(C) Lactate levels are elevated in the culture media collected from FX primary neurons compared to those of WT. Exposure of FX neurons to Dex significantly decreases lactate levels in the media.

(D) Representative immunoblots of WT and FX cortical cultures exposed to vehicle or Dex.

(E) Quantification of blots shown in (D). At least 3 independent cultures were used. A set of 4 key enzymes is elevated in FX compared to WT. Dex treatment normalizes the protein levels of all enzymes in the set.

(F) Representative immunoblots of WT and *Fmr1*$^{-/y}$ mitochondria isolated from brain.

(G) Quantification of blots shown in (F). At least three animals per condition. Glycolytic enzymes and pyruvate dehydrogenase protein levels are elevated in *Fmr1*$^{-/y}$ mitochondrial fractions. In (C) and (E), two-way ANOVA followed by Tukey's multiple comparisons test was used. In (G), unpaired two-tailed Student's t test was used. Data are represented as mean ± SEM (*$p < 0.05$; **$p < 0.01$; ***$p < 0.001$; ****$p < 0.0001$).

See also Table S1.

Please cite this article in press as: Licznerski et al., ATP Synthase c-Subunit Leak Causes Aberrant Cellular Metabolism in Fragile X Syndrome, Cell (2020), https://doi.org/10.1016/j.cell.2020.07.008

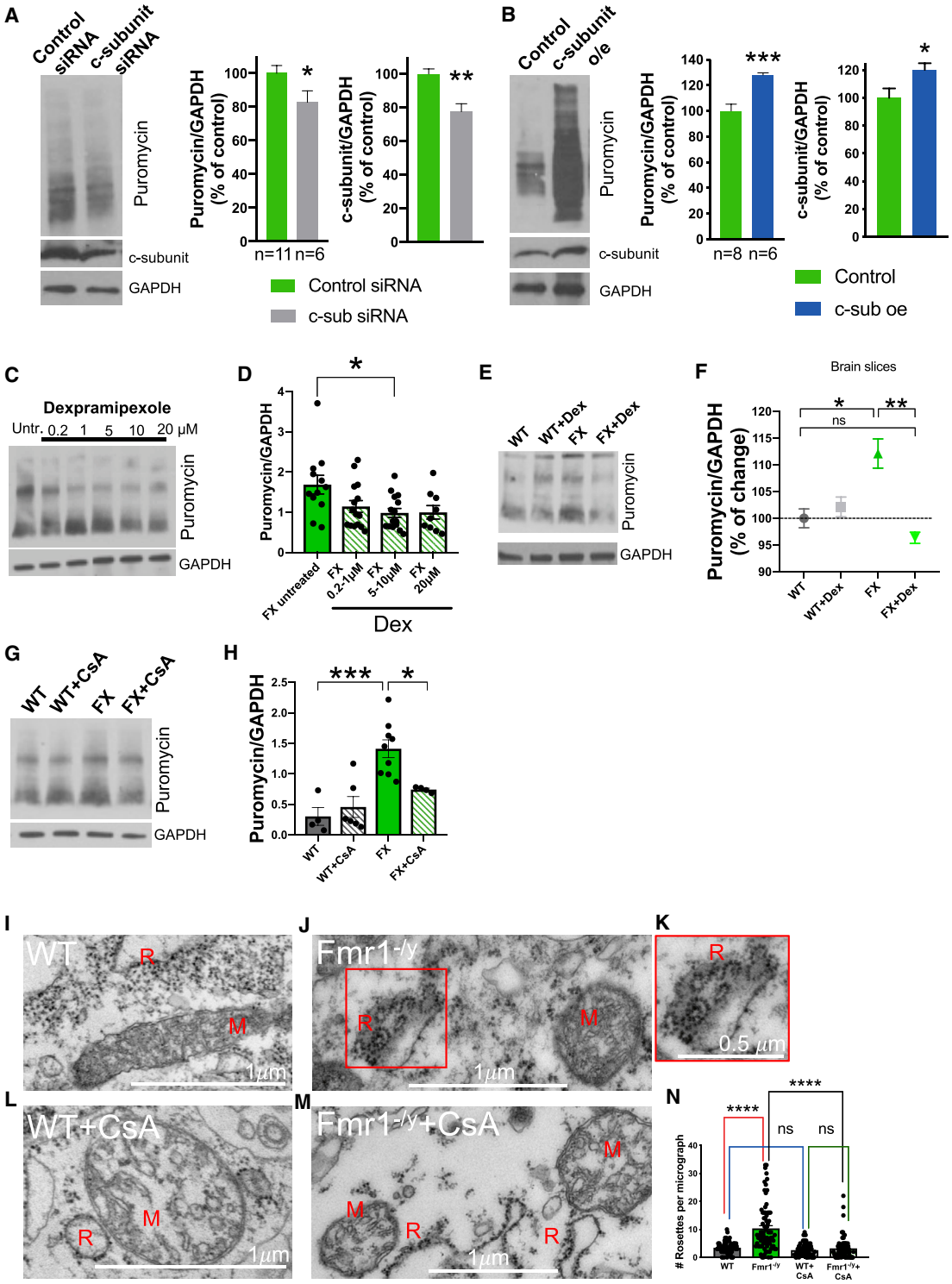

Figure 4. Inhibition of the Mitochondrial Inner Membrane Leak Decreases Protein Synthesis in FX

(A) c-subunit depletion in human FX fibroblasts decreases the rate of protein synthesis. Representative puromycin (top), c-subunit immunoblots (middle), and protein controls (bottom) are shown at left. Quantification of the immunoblots is shown at right.

(B) c-subunit overexpression in human FX fibroblasts increases the rate of protein synthesis. Representative blots of puromycin and c-subunit are shown at left as in (A). Quantification of the immunoblots is shown at right.

(legend continued on next page)

Please cite this article in press as: Licznerski et al., ATP Synthase c-Subunit Leak Causes Aberrant Cellular Metabolism in Fragile X Syndrome, Cell (2020), https://doi.org/10.1016/j.cell.2020.07.008

Abnormally Enhanced Mitochondrial Inner Membrane Leak Prevents Stimulus-Dependent Protein Synthesis

FX neuronal synapses have abnormal stimulus-dependent synaptic plasticity and ineffective synapse maturation (Pfeiffer and Huber, 2009; Sidorov et al., 2013). We considered that inefficient ATP production by mitochondria in FX synapses could compromise stimulation-dependent phosphorylation events of the protein synthesis machinery, thereby affecting synaptic growth. The translation of mRNAs for synaptic proteins during long term changes in synaptic plasticity is regulated by an increase in phosphorylation of elongation factor 2 (EF2) ~5 min after neuronal stimulation (Autry and Monteggia, 2012; Gildish et al., 2012; Park et al., 2008; Scheetz et al., 2000; Um et al., 2013). We found that stimulation of WT synaptosomes using the NMDA glutamate receptor co-agonist D-serine led to robust phosphorylation of EF2 at 5 min followed by increased protein synthesis at 30 min, as has been reported previously (Figures 5A–5C) (Scheetz et al., 2000). Strikingly, both EF2 phosphorylation and protein synthesis changes failed to occur following synaptic stimulation in *Fmr1*$^{-/y}$ synapses (Figures 5A–5C). If the mitochondrial membrane leak were responsible for the failure of phosphorylation of EF2 during synaptic stimulation, then this specific phosphorylation event would be rescued by closing the leak. Indeed, application of low dose CsA completely rescued EF2 phosphorylation and restored the normal pattern of protein synthesis upon synaptic stimulation in *Fmr1*$^{-/y}$ synapses (Figures 5A–5C), confirming that this phosphorylation event and subsequent changes in protein synthesis rate are sensitive to ATP synthase leak modulation.

One potential mechanism by which FMRP could regulate the leak across the inner mitochondrial membrane is by controlling the translation of FMRP-bound mRNA coding for the ATP synthase β subunit. A stimulus-induced increase in protein levels of β subunit would decrease the level of free c-subunit by assembling the full F_1F_O ATP synthase. To test this, we measured β subunit protein levels in the same stimulated synaptosomes that were used for determination of p-EF2 levels and puromycin incorporation (Figure 5D). These studies showed that levels of ATP synthase β subunit protein are increased 30 min after stimulation of WT synaptosomes but are unchanged after stimulation of *Fmr1*$^{-/y}$ synaptosomes. Moreover, CsA treatment of the *Fmr1*$^{-/y}$ synaptosomes restored the normal stimulus-induced increase in β subunit protein (Figure 5D). Comparing column 3 to column 2 (in the last panel of Figure 5D) we find there is a markedly enhanced rate of *de novo* synthesis of β subunit protein at 30 min after peak EF2 phosphorylation, suggesting a rapid change in ATP synthase stoichiometry upon synaptic stimulation.

ATP Synthase Modulation Enhances Synaptic Plasticity

A number of studies have reported that FXS produces abnormalities in dendritic spines, including an increase in the number of spines and delays in their morphological maturity (for review, see He and Portera-Cailliau, 2013). To determine if ATP synthase leak closure rescues dendritic spine abnormalities, we carried out analyses of dendritic spine morphology in WT and FX neuronal cultures exposed to Dex or vehicle. In vehicle-treated WT cultures (at DIV 20), mushroom (mature) spines contributed ~50% of the total spine count, whereas in the FX cultures, mushroom spines represented only 10%. Dex treatment caused a 3-fold increase in the mature spines in FX cultures that increased the mature spines to 25% of the total spine count (Figures 6A–6F).

Dex, in addition to CsA, increases the efficiency in ATP production by ATP synthase (Alavian et al., 2015), which should phosphorylate targets such as EF2 during synaptic stimulation. To determine if local ATP levels are affected by stimulation in FX synapses, we measured ATP levels in living neurons using an ATP-fluorescence resonance energy transfer (FRET) construct (Imamura et al., 2009). We found that at 1 h after synaptic stimulation, ATP levels were decreased in FX synapses compared to WT. In contrast, treatment with Dex restored post-stimulation levels of ATP in FX synapses to those of WT (Figure 6G).

Dex Rescues Autistic Behaviors in the *Fmr1*$^{-/y}$ Mice

Developmental synaptic plasticity is required for normal mammalian behavior (Citri and Malenka, 2008). *Fmr1*$^{-/y}$ mice exhibit abnormal behaviors that can be measured by various paradigms. For example, they are more likely to engage in repetitive behaviors including grooming and shredding their nestlets (Angoa-Pérez et al., 2013; Kalueff et al., 2016; Kane et al., 2012; Silverman et al., 2010). *Fmr1*$^{-/y}$ mice are also hyperactive compared to WT mice, as measured by overall locomotor

(C) Dex decreases protein synthesis rate in FX neurons. Representative blot of puromycin incorporation in FX cortical cultures is shown in the presence of different concentrations of Dex. Cultures were treated with Dex for 2–24 h.
(D) Group data for experiments shown in (C). The group data for WT translation rates are shown in (H). n= samples from at least 3 independent cultures.
(E) Puromycin incorporation into WT and *Fmr1*$^{-/y}$ after incubation of mouse brain slices with 10 μM Dex or vehicle for 2.5 h.
(F) Group data of experiments shown in (E). n = 3–6 brain slices for each condition, at least three animals per condition.
(G) Representative immunoblot of puromycin incorporation showing that the rate of protein synthesis in FX cortical neurons is increased over WT neurons; exposure to 0.2 μM CsA for 7 days reduced the rate of puromycin incorporation in FX neurons.
(H) Quantification of the data shown in (G) n = samples from at least 3 independent cultures.
(I–M) Increase in rosettes (indicating actively translating ribosomes) in *Fmr1*$^{-/y}$ over WT brains is shown in these panels. The increase in rosettes is normalized in the *Fmr1*$^{-/y}$ brain to WT levels by CsA exposure. Representative electron micrographs of the CA1 region of hippocampal brain slices of *Fmr1*$^{-/y}$ mouse is shown and compared to WT and CsA exposed slices (R, ribosomal rosettes; M, mitochondria). (K) A higher magnification of the actively translating ribosomes (rosettes) shown in (J). Parallel slices from the corresponding hemisphere were incubated in 0.2 μM CsA or vehicle for 2.5 h. Scale bars as indicated.
(N) Group data of 65–76 micrographs analyzed per condition. (A) and (B) used unpaired two-tailed Student's t test. In (D), one-way ANOVA followed by Tukey's multiple comparisons test was used. For (F), (H), and (N), two-way ANOVA followed by Tukey's multiple comparisons test was used. Data are represented as mean ± SEM (*$p < 0.05$; **$p < 0.01$; ***$p < 0.001$; ****$p < 0.0001$).
See also Figure S2 and Table S2.

Please cite this article in press as: Licznerski et al., ATP Synthase c-Subunit Leak Causes Aberrant Cellular Metabolism in Fragile X Syndrome, Cell (2020), https://doi.org/10.1016/j.cell.2020.07.008

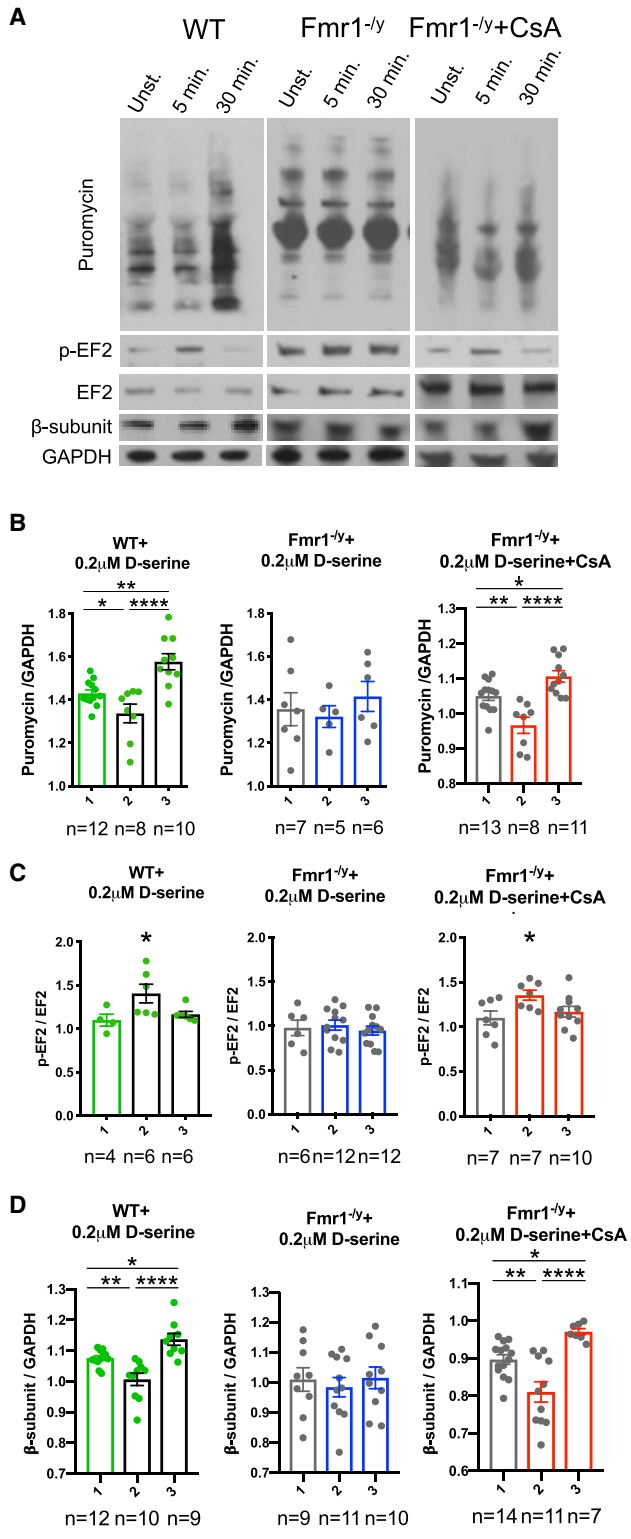

Figure 5. The Time Course of Synaptic Stimulation-Induced Changes in Protein Synthesis and EF2 Phosphorylation Is Disrupted in *Fmr1*$^{-/y}$ Synaptosomes, Normalized by ATP Synthase Leak Inhibition

(A) Representative immunoblots of synaptosomal samples harvested at the indicated time points before and after 0.2 μM D-serine stimulation. Top panels: puromycin incorporation; middle panels: p-EF2 and EF2; bottom panels: ATP synthase β subunit and protein loading control (GAPDH). CsA restores the normal pattern of response to stimulation in *Fmr1*$^{-/y}$ synaptosomes.

(B–D) Group data for experiments shown in (A): (B) for puromycin incorporation, (C) p-EF2/EF2 protein levels, and (D) ATP synthase β subunit protein levels. One-way ANOVA followed by Tukey's multiple comparisons test was used for all panels in the figure. Synaptosomes were prepared from at least three independent animals per condition. n= samples. Data are represented as mean ± SEM (*p < 0.05; **p < 0.01; ***p < 0.001; ****p < 0.0001).

See also Figure S1.

activity (Baker et al., 2010; Dolan et al., 2013; Tranfaglia, 2011). To determine if ATP synthase leak closure rescues these behavioral abnormalities, we injected 2-month-old mice with Dex over 2 days and tested their repetitive behaviors and locomotor activity. Although Dex did not significantly alter repetitive behaviors in WT mice, it markedly reduced the time spent grooming and the number of attempts made at grooming in *Fmr1*$^{-/y}$ animals (Figures 6H and 6I). Dex also decreased the abnormal nestlet shredding behavior measured in *Fmr1*$^{-/y}$ mice, suggesting that inhibiting the ATP synthase leak normalizes certain types of autistic behaviors (Figure 6J). Dex also markedly reduced the hyperactivity of *Fmr1*$^{-/y}$ mice (Figure 6K). The amelioration of these behavioral patterns by Dex suggests that ATP synthase leak inhibition is required for the development of normal mammalian behaviors.

DISCUSSION

We have found that the mitochondrial inner membrane leak of FX neurons and cells is caused by abnormal levels of ATP synthase c-subunit. The c-subunit leak causes persistence of a mitochondrial leak metabolic phenotype characterized by high glycolytic flux, high lactate levels, and increased levels of glycolytic and TCA enzymes. The leak also aberrantly elevates overall and specific protein synthesis; a decrease in c-subunit level or pharmacological inhibition of the ATP synthase leak reduces protein synthesis rates and decreases the levels of leak metabolism enzymes. In *Fmr1*$^{-/y}$ synapses, stimulation-dependent protein synthesis is absent. This is correlated with a lack of stimulus-induced EF2 phosphorylation and a lack of synthesis of the ATP synthase β-subunit. These abnormalities are readily reversed by ATP synthase leak inhibitors, suggesting that leak closure is required for the ATP-dependent phosphorylation of EF2 adjacent to mitochondria. EF2 phosphorylation may regulate the change in subsets of proteins synthesized and may be correlated with- the overabundant synthesis of enzymes supporting a high flux glycolytic/TCA cycle "leak" metabolism indicative of metabolic immaturity. Consistent with the hypothesis that the c-subunit leak is also a major cause of synapse immaturity, we find that inhibition of the ATP synthase leak allows the maturation of synapses and normalizes autistic behaviors.

ATP Synthase Leak Closure Regulates Metabolic and Synaptic Maturation in an FMRP-Dependent Manner

Our findings highlight the complex metabolic scenario of FMRP-deficient neurons. Normally there is an increase in synaptic/neuronal activity during early neuronal development (Bailey

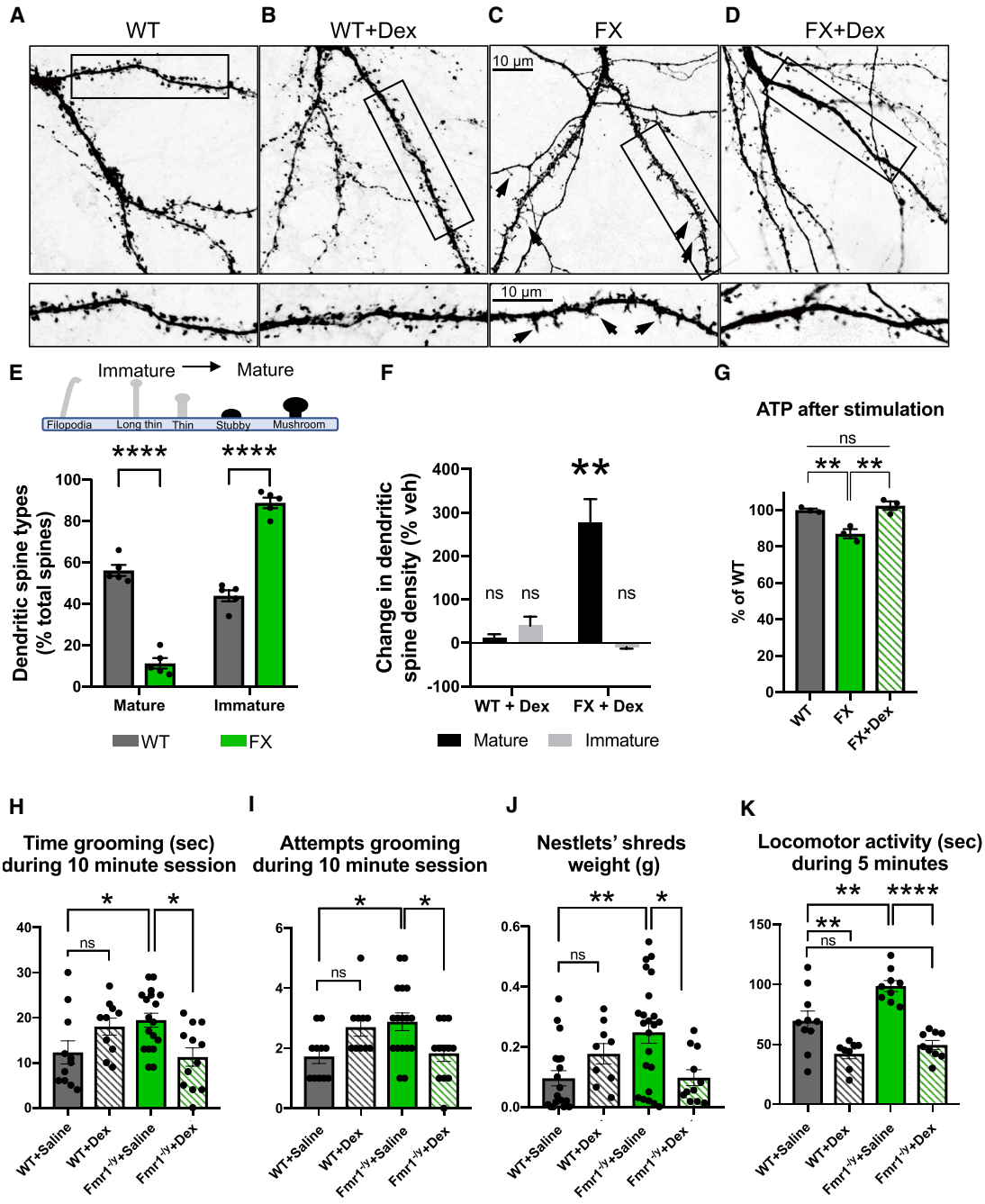

Figure 6. ATP Synthase Leak Inhibition Enhances Synaptic Plasticity

(A–D) Representative micrographs of primary neurons show the differences in synaptic spine morphology between FX and WT neurons. FX neurons (panel C) have fewer mature, mushroom-like spines compared to WT (panel A) but this is normalized by Dex (panel D). WT spine morphologies are unaffected by Dex (panel B). Insets show details of dendritic shafts.

(E) Dendritic spines were categorized according to their morphology into mature and immature spines. Illustration depicts subtypes of spines analyzed. Histograms show FX neurons have a reduced percentage of mature spines and an increased percentage of immature spines compared to WT. The types of spines are graphed as a percent of the total number of spines counted per unit length. n= 5 neurons per condition from at least 2 independent cultures.

(F) 5 μM Dex treatment each day for 6 consecutive days (DIV 15–20) caused an increase in the percent of mature dendritic spines / total spines per unit length in FX neurons. Dex treatment had no effect on WT neuron spine density. n= 5 neurons per condition from at least 2 independent cultures.

(G) Dex normalizes dendritic ATP levels in stimulated FX neurons. ATP levels were measured in neurons at DIV 20 using FRET-based ATP reporter ATeam YEMK. Neurons were stimulated for 3 min with 10 μM D-serine and ATP values were recorded at 1 h after stimulation. Histogram shows ATP values at 1 h after stimulation as a percentage of WT at 1 h after stimulation. n= 3 neurons per condition; 15–30 ROIs measured per neuron.

(legend continued on next page)

Please cite this article in press as: Licznerski et al., ATP Synthase c-Subunit Leak Causes Aberrant Cellular Metabolism in Fragile X Syndrome, Cell (2020), https://doi.org/10.1016/j.cell.2020.07.008

et al., 2015; Watson et al., 2016) accompanied by a change in metabolism from glycolytic to oxidative phosphorylation (Fame et al., 2019; Zheng et al., 2016). Our findings suggest persistence of a glycolytic/TCA cycle leak metabolic phenotype at the time of synapse formation in the FX neuronal cultures. Although it has been previously shown and is well-accepted that FMRP binds to synaptic mRNAs, the specific mRNAs that regulate synapse development are not known and how they contribute to development in an FMRP-dependent manner is not fully understood. The present results suggest that FMRP binds to ATP synthase β subunit mRNA to regulate the timing of metabolic maturation from a leak phenotype toward oxidative phosphorylation. It is not likely that the change in levels of glycolytic/TCA enzymes occurs by direct FMRP binding to the enzyme mRNAs. Only Hexokinase I is a possible FMRP target out of the group of metabolic enzymes that we find elevated by immunoblot (Darnell et al., 2011). Instead, when synaptic stimulation increases ATP synthase β subunit levels in an FMRP-dependent manner and closes the c-subunit leak, this may change the probability of translation of a subset of mRNAs waiting near the mitochondria, thereby changing levels of metabolic enzymes required for efficient oxidative phosphorylation and decreasing those needed for the leak metabolism. Of course, it is also possible that stimulation might release FMRP from a metabolic transcriptional regulator (Fame et al., 2019), thereby coordinating the decrease in glycolytic/TCA enzymes with the increase in ATP synthase enzyme components. Future analysis will discover which scenario is tractable.

ATP Synthase c-Subunit Leak Channel Regulates the Rate of Protein Synthesis in FX Neurons and Fibroblasts

One of the key findings of this study is that the ATP synthase c-subunit leak channel level activity regulates the rate of protein synthesis. We demonstrate that knock down or overexpression of the c-subunit directly regulates the rate of protein synthesis measured by puromycin incorporation. Pharmacological reagents Dex and CsA that bind within the ATP synthase F_1 to reduce c-subunit leak channel activity (Alavian et al., 2011, 2015; Chen et al., 2011; Giorgio et al., 2009; Szabó and Zoratti, 1991) also reduce overall protein synthesis. Finally, Bcl-xL, a protein that we have reported previously to bind to the F_1 (Alavian et al., 2011; Chen et al., 2011), reduces protein synthesis, suggesting that Bcl-xL or another endogenous ATP synthase leak modulator (Stefely and Pagliarini, 2017) could also assist in the stimulus-dependent changes in protein synthesis (Figures S2F–S2H). We find that the reason the leak is so important for regulation of the rate of protein synthesis is because the increase in mitochondrial ATP produced by leak closure is used in phosphorylating local translation targets. We identified EF2, because its rapid phosphorylation after high intensity glutamate receptor stimulation (Scheetz et al., 2000) suggested it as a candidate to produce a change in synaptic plasticity. Indeed, we found that there was no phosphorylation of EF2 or change in rate of protein synthesis in *Fmr1*$^{-/y}$ synapses after glutamate receptor stimulation. In contrast, the stimulus-dependent phosphorylation event was rescued by closing the ATP synthase leak with CsA (Giorgio et al., 2009; Szabó and Zoratti, 1991).

Mitochondrial Inner Membrane Leak Closure Decreases "Leak" Metabolism, Favoring More Efficient Oxidative Phosphorylation during Synaptogenesis

Immature cells prefer a metabolism favoring glycolytic production of ATP over mitochondrial ATP production (Warburg, 1956; Zheng et al., 2016), but the idea that a shift toward oxidative phosphorylation could occur during synaptogenesis has not been shown previously. Recent reports in cardiomyocytes support this developmental shift. Cardiomyocytes change their metabolism (from glycolytic to oxidative) over several days during embryonic development (Hom et al., 2011). The respiratory complexes aggregate into a "supercomplex" (Beutner et al., 2017). These events occur earlier in cells that have been exposed to CsA (Hom et al., 2011). Studies also support a similar scenario in early neuronal differentiation from stem cells (Fame et al., 2019; Zheng et al., 2016). Our previous work has suggested that oxidative changes in synapses during development are regulated by increases in expression of the anti-apoptotic protein Bcl-xL. Bcl-xL levels peak during periods of synaptogenesis in the developing brain, then remain elevated in adulthood (Krajewska et al., 2002). We have reported that overexpression of Bcl-xL enhances synapse formation and maturity in hippocampal neurons (Li et al., 2008). Bcl-xL supports both mitochondrial biogenesis and movement of mitochondria closer to synaptic sites during synaptic enlargement (Berman et al., 2009; Li et al., 2008). Accompanying this change is an improvement in the efficiency of oxidative phosphorylation as Bcl-xL interacts directly with the ATP synthase F_1 to improve enzymatic function and close the inner membrane leak (Alavian et al., 2011; Chen et al., 2011).

Unlike for cardiomyocytes as described above, at the same embryonic dates (~E9), oxygen consumption is high in the developing nervous system yet accompanied by high glycolytic flux. Different from the heart, oxygen consumption then actually decreases upon neuronal maturation as oxidative phosphorylation takes over as the main metabolic phenotype (Fame et al., 2019). Recent accounts have highlighted that metabolic phenotypes are much more complex than simply "glycolytic" versus "oxidative," and mitochondria are not always silent when glycolytic metabolism is favored (Li et al., 2016; Vander Heiden et al., 2009; Zheng et al., 2016). On the contrary, mitochondrial metabolism is often enhanced in that use of the TCA cycle for anabolism is increased; this includes upregulation of enzymes needed for lipid biosynthesis, protein synthesis and deoxy- and ribonucleic acid biosynthesis. Hallmarks of this state are the upregulation of enzymes involved in glutaminolysis (Wise et al., 2008),

(H–K) Abnormal behavior in *Fmr1*$^{-/y}$ mice is rescued by Dex. Two-month-old mice were given 3 intraperitoneal injections of 10 mg/kg Dex or saline over 40 h prior to behavioral testing. Repetitive behaviors (grooming and nestlet shredding, H–I) were normalized by Dex in *Fmr1*$^{-/y}$ mice. Hyperactivity (K) as measured by locomotor activity was normalized by Dex in *Fmr1*$^{-/y}$ mice. In (E) and (F), unpaired two-tailed Student's t test was used. For (G), one-way ANOVA followed by Tukey's multiple comparisons test was used. For (H)–(K), two-way ANOVA followed by Tukey's multiple comparisons test was used. Data are represented as mean ± SEM (*$p < 0.05$; **$p < 0.01$; ***$p < 0.001$; ****$p < 0.0001$).

malate aspartate shuttle (Li et al., 2016), the re-supply of NAD^+, alteration of the NAD^+/NADH ratio (Magni et al., 2008), and changes in pyruvate metabolism (Dayton et al., 2016). Enzymes upregulated for this form of metabolism include lactate dehydrogenase, malate dehydrogenase, glutamate dehydrogenase, isocitrate dehydrogenase, and PKM2 (Dayton et al., 2016). In our current study, the list of enzymes that are upregulated in FX versus WT neurons and synapses includes all the pathways mentioned above. Most strikingly, these are rapidly downregulated in FX neurons following Dex treatment, suggesting high metabolic flexibility in early developing neurons and synapses. These results also suggest that inner membrane leak may be upregulated early in development to enhance electron transport so that NAD^+ can be reformed from NADH. In addition, the TCA cycle may run faster in the presence of an inner membrane leak to synthesize components of developing cells/synapses. It is likely that this "leak" metabolic phenotype is advantageous to FX neurons, because they require increased protein synthesis and may need enhanced lipid supply for membrane remodeling. This is supported by several recent reports including in *dfmr1* mutant mitochondria in which it was described that mitochondria have significantly increased maximum electron transport system (ETS) capacity accompanied by high oxygen consumption, reduced carbohydrate and lipid stores and hyperphagia, suggestive of an inner mitochondrial membrane leak (Weisz et al., 2018). NAD^+/NADH ratio was also significantly lower in the *dfmr1* mutants relative to controls (Weisz et al., 2018), suggesting the requirement for upregulation of enzymes that resupply NAD^+. A recent report on *Fmr1*$^{-/y}$ mouse brains shows that electron transport complexes run at high rates even though mitochondrial ATP production is low, suggesting inner membrane inefficiency (D'Antoni et al., 2020). Our recent findings confirm that mitochondria from the *Fmr1*$^{-/y}$ mouse brains have inefficient and membrane potential-dependent enhancement in oxygen consumption caused by an inner membrane leak sensitive to coenzyme Q and CsA (Griffiths et al., 2020). Therefore, the "leak" metabolism of neuronal immaturity in our analysis of these examples is characterized by high glycolytic/TCA flux and high electron transport with an increase, not a decrease, in oxygen consumption.

Although we have been concentrating on the leak as the abnormality in this study, the ATP synthase is only one part of a complex inner mitochondrial membrane structure (Cogliati et al., 2016; Davies et al., 2012). Changes in cristae morphology at the onset of oxidative metabolism contribute to the enhanced efficiency of ATP production (Esparza-Perusquía et al., 2017). These alterations in mitochondrial inner membrane architecture may occur during normal synaptic maturation, suggesting other ways in which mitochondrial plasticity may be required for mature synapse formation.

STAR★METHODS

Detailed methods are provided in the online version of this paper and include the following:

SUPPLEMENTAL INFORMATION

Supplemental Information can be found online at https://doi.org/10.1016/j.cell.2020.07.008.

ACKNOWLEDGMENTS

The Q-Exactive Plus mass spectrometer located at the Yale/Keck MS & Proteomics Resource where the mass spectrometry work was carried out was funded in part by NIH SIG from the Office of The Director, NIH (S10OD018034). The content is solely the responsibility of the authors and does not necessarily represent the official views of the NIH. We also would like to thank Weiwei Wang and Jean Kanyo for assistance with mass spectrometry, sample preparation and data collection; and Dr. TuKiet Lam for his help with interpreting the data. Human FX and WT cell lines were kindly shared by Dr. Gary J. Bassell laboratory (Emory University, Atlanta, GA) and Dr. Elizabeth Berry-Kravis (Rush University Medical Center, Chicago, IL). We also thank Dr. Leonard K. Kaczmarek (Yale University, New Haven, CT) for sharing FVB and FMRP KO mice and for insightful scientific discussion. FRET constructs were kindly provided by Dr. Imamura and Dr. Noji (Imamura et al., 2009).

This study was supported by FRAXA, Simons Foundation, NIH NS112706 and NIH NS045876 (to E.A.J.), NIA (K01AG054734 to N. Mnatsakanyan),

Beavers Award and NSF Research Experiences for Undergraduates (REU) (to L.B.), Yale College First-Year Summer Research Fellowship in the Sciences and Engineering (to G.N.X.), Yale College STARS I Summer Research Program (to A.B.), NSF REU (to N.C.-R.), METCALF Internship from the University of Chicago (to N. Mehta, S.S., J.S., and E.S.).

AUTHOR CONTRIBUTIONS

P.L. and E.A.J. conceived the project, designed experiments, interpreted the data and prepared the manuscript. P.L., H.P., H.R., R.C., P.M., N. Mnatsakanyan, M.G., J.W., N.C.-R., N. Mehta, S.S., J.S., E.S., C.E., S.E., L.B., G.N.X., A.B., V.K.G., and E.A.J. performed experiments. V.K.G. and R.J.L. provided scientific discussion and intellectual contributions.

DECLARATION OF INTERESTS

The authors declare no competing interests.

Received: November 14, 2018
Revised: March 4, 2020
Accepted: July 10, 2020
Published: August 13, 2020

REFERENCES

Alavian, K.N., Li, H., Collis, L., Bonanni, L., Zeng, L., Sacchetti, S., Lazrove, E., Nabili, P., Flaherty, B., Graham, M., et al. (2011). Bcl-xL regulates metabolic efficiency of neurons through interaction with the mitochondrial F1FO ATP synthase. Nat. Cell Biol. *13*, 1224–1233.

Alavian, K.N., Beutner, G., Lazrove, E., Sacchetti, S., Park, H.A., Licznerski, P., Li, H., Nabili, P., Hockensmith, K., Graham, M., et al. (2014). An uncoupling channel within the c-subunit ring of the F1FO ATP synthase is the mitochondrial permeability transition pore. Proc. Natl. Acad. Sci. USA *111*, 10580–10585.

Alavian, K.N., Dworetzky, S.I., Bonanni, L., Zhang, P., Sacchetti, S., Li, H., Signore, A.P., Smith, P.J., Gribkoff, V.K., and Jonas, E.A. (2015). The mitochondrial complex V-associated large-conductance inner membrane current is regulated by cyclosporine and dexpramipexole. Mol. Pharmacol. *87*, 1–8.

Angoa-Pérez, M., Kane, M.J., Briggs, D.I., Francescutti, D.M., and Kuhn, D.M. (2013). Marble burying and nestlet shredding as tests of repetitive, compulsive-like behaviors in mice. J. Vis. Exp. (82), 50978.

Autry, A.E., and Monteggia, L.M. (2012). Brain-derived neurotrophic factor and neuropsychiatric disorders. Pharmacol. Rev. *64*, 238–258.

Bagni, C., and Greenough, W.T. (2005). From mRNP trafficking to spine dysmorphogenesis: the roots of fragile X syndrome. Nat. Rev. Neurosci. *6*, 376–387.

Bailey, C.H., Kandel, E.R., and Harris, K.M. (2015). Structural Components of Synaptic Plasticity and Memory Consolidation. Cold Spring Harb. Perspect. Biol. *7*, a021758.

Baines, C.P., Kaiser, R.A., Purcell, N.H., Blair, N.S., Osinska, H., Hambleton, M.A., Brunskill, E.W., Sayen, M.R., Gottlieb, R.A., Dorn, G.W., et al. (2005). Loss of cyclophilin D reveals a critical role for mitochondrial permeability transition in cell death. Nature *434*, 658–662.

Baker, K.B., Wray, S.P., Ritter, R., Mason, S., Lanthorn, T.H., and Savelieva, K.V. (2010). Male and female Fmr1 knockout mice on C57 albino background exhibit spatial learning and memory impairments. Genes Brain Behav. *9*, 562–574.

Bassell, G.J., and Warren, S.T. (2008). Fragile X syndrome: loss of local mRNA regulation alters synaptic development and function. Neuron *60*, 201–214.

Bear, M.F., Huber, K.M., and Warren, S.T. (2004). The mGluR theory of fragile X mental retardation. Trends Neurosci. *27*, 370–377.

Beaudoin, G.M., 3rd, Lee, S.H., Singh, D., Yuan, Y., Ng, Y.G., Reichardt, L.F., and Arikkath, J. (2012). Culturing pyramidal neurons from the early postnatal mouse hippocampus and cortex. Nat. Protoc. *7*, 1741–1754.

Berman, S.B., Chen, Y.B., Qi, B., McCaffery, J.M., Rucker, E.B., 3rd, Goebbels, S., Nave, K.A., Arnold, B.A., Jonas, E.A., Pineda, F.J., and Hardwick, J.M. (2009). Bcl-x L increases mitochondrial fission, fusion, and biomass in neurons. J. Cell Biol. *184*, 707–719.

Bernardi, P., and Di Lisa, F. (2015). The mitochondrial permeability transition pore: Molecular nature and role as a target in cardioprotection. J. Mol. Cell. Cardiol. *78*, 100–106.

Beutner, G., Eliseev, R.A., and Porter, G.A., Jr. (2014). Initiation of electron transport chain activity in the embryonic heart coincides with the activation of mitochondrial complex 1 and the formation of supercomplexes. PLoS ONE *9*, e113330.

Beutner, G., Alanzalon, R.E., and Porter, G.A., Jr. (2017). Cyclophilin D regulates the dynamic assembly of mitochondrial ATP synthase into synthasomes. Sci. Rep. *7*, 14488.

Bhattacharya, A., Kaphzan, H., Alvarez-Dieppa, A.C., Murphy, J.P., Pierre, P., and Klann, E. (2012). Genetic removal of p70 S6 kinase 1 corrects molecular, synaptic, and behavioral phenotypes in fragile X syndrome mice. Neuron *76*, 325–337.

Bonora, M., Bononi, A., De Marchi, E., Giorgi, C., Lebiedzinska, M., Marchi, S., Patergnani, S., Rimessi, A., Suski, J.M., Wojtala, A., et al. (2013). Role of the c subunit of the FO ATP synthase in mitochondrial permeability transition. Cell Cycle *12*, 674–683.

Bozik, M.E., Kramer, W.G., Gribkoff, V.K., and Ingersoll, E.W. (2010). Safety, Tolerability, and Pharmacokinetics of KNS-760704 (Dexpramipexole) in Healthy Adult Subjects. J. Clin. Pharmacol. https://doi.org/10.1177/0091270010379412.

Bozik, M.E., Mather, J.L., Kramer, W.G., Gribkoff, V.K., and Ingersoll, E.W. (2011). Safety, tolerability, and pharmacokinetics of KNS-760704 (dexpramipexole) in healthy adult subjects. J. Clin. Pharmacol. *51*, 1177–1185.

Brandt, T., Mourier, A., Tain, L.S., Partridge, L., Larsson, N.G., and Kühlbrandt, W. (2017). Changes of mitochondrial ultrastructure and function during ageing in mice and *Drosophila*. eLife *6*, e24662.

Brown, M.R., Sullivan, P.G., Dorenbos, K.A., Modafferi, E.A., Geddes, J.W., and Steward, O. (2004). Nitrogen disruption of synaptoneurosomes: an alternative method to isolate brain mitochondria. J. Neurosci. Methods *137*, 299–303.

Brown, M.R., Kronengold, J., Gazula, V.R., Chen, Y., Strumbos, J.G., Sigworth, F.J., Navaratnam, D., and Kaczmarek, L.K. (2010). Fragile X mental retardation protein controls gating of the sodium-activated potassium channel Slack. Nat. Neurosci. *13*, 819–821.

Caviston, T.L., Ketchum, C.J., Sorgen, P.L., Nakamoto, R.K., and Cain, B.D. (1998). Identification of an uncoupling mutation affecting the b subunit of F1F0 ATP synthase in Escherichia coli. FEBS Lett. *429*, 201–206.

Chan, T.L., Greenawalt, J.W., and Pedersen, P.L. (1970). Biochemical and ultrastructural properties of a mitochondrial inner membrane fraction deficient in outer membrane and matrix activities. J. Cell Biol. *45*, 291–305.

Chen, C., Ko, Y., Delannoy, M., Ludtke, S.J., Chiu, W., and Pedersen, P.L. (2004). Mitochondrial ATP synthasome: three-dimensional structure by electron microscopy of the ATP synthase in complex formation with carriers for Pi and ADP/ATP. J. Biol. Chem. *279*, 31761–31768.

Chen, Y.B., Aon, M.A., Hsu, Y.T., Soane, L., Teng, X., McCaffery, J.M., Cheng, W.C., Qi, B., Li, H., Alavian, K.N., et al. (2011). Bcl-xL regulates mitochondrial energetics by stabilizing the inner membrane potential. J. Cell Biol. *195*, 263–276.

Chen, R., Park, H.A., Mnatsakanyan, N., Niu, Y., Licznerski, P., Wu, J., Miranda, P., Graham, M., Tang, J., Boon, A.J.W., et al. (2019). Parkinson's disease protein DJ-1 regulates ATP synthase protein components to increase neuronal process outgrowth. Cell Death Dis. *10*, 469.

Citri, A., and Malenka, R.C. (2008). Synaptic plasticity: multiple forms, functions, and mechanisms. Neuropsychopharmacology *33*, 18–41.

Cogliati, S., Enriquez, J.A., and Scorrano, L. (2016). Mitochondrial Cristae: Where Beauty Meets Functionality. Trends Biochem. Sci. *41*, 261–273.

Cudkowicz, M., Bozik, M.E., Ingersoll, E.W., Miller, R., Mitsumoto, H., Shefner, J., Moore, D.H., Schoenfeld, D., Mather, J.L., Archibald, D., et al. (2011). The effects of dexpramipexole (KNS-760704) in individuals with amyotrophic lateral sclerosis. Nat. Med. *17*, 1652–1656.

D'Antoni, S., de Bari, L., Valenti, D., Borro, M., Bonaccorso, C.M., Simmaco, M., Vacca, R.A., and Catania, M.V. (2020). Aberrant mitochondrial bioenergetics in the cerebral cortex of the Fmr1 knockout mouse model of fragile X syndrome. Biol. Chem. *401*, 497–503.

Darnell, J.C. (2011). Defects in translational regulation contributing to human cognitive and behavioral disease. Curr. Opin. Genet. Dev. *21*, 465–473.

Darnell, J.C., Van Driesche, S.J., Zhang, C., Hung, K.Y., Mele, A., Fraser, C.E., Stone, E.F., Chen, C., Fak, J.J., Chi, S.W., et al. (2011). FMRP stalls ribosomal translocation on mRNAs linked to synaptic function and autism. Cell *146*, 247–261.

Davies, K.M., Anselmi, C., Wittig, I., Faraldo-Gómez, J.D., and Kühlbrandt, W. (2012). Structure of the yeast F1Fo-ATP synthase dimer and its role in shaping the mitochondrial cristae. Proc. Natl. Acad. Sci. USA *109*, 13602–13607.

Dayton, T.L., Jacks, T., and Vander Heiden, M.G. (2016). PKM2, cancer metabolism, and the road ahead. EMBO Rep. *17*, 1721–1730.

Deng, P.Y., Rotman, Z., Blundon, J.A., Cho, Y., Cui, J., Cavalli, V., Zakharenko, S.S., and Klyachko, V.A. (2013). FMRP regulates neurotransmitter release and synaptic information transmission by modulating action potential duration via BK channels. Neuron *77*, 696–711.

Dhillon, S., Hellings, J.A., and Butler, M.G. (2011). Genetics and mitochondrial abnormalities in autism spectrum disorders: a review. Curr. Genomics *12*, 322–332.

Dolan, B.M., Duron, S.G., Campbell, D.A., Vollrath, B., Shankaranarayana Rao, B.S., Ko, H.Y., Lin, G.G., Govindarajan, A., Choi, S.Y., and Tonegawa, S. (2013). Rescue of fragile X syndrome phenotypes in Fmr1 KO mice by the small-molecule PAK inhibitor FRAX486. Proc. Natl. Acad. Sci. USA *110*, 5671–5676.

Dölen, G., Osterweil, E., Rao, B.S., Smith, G.B., Auerbach, B.D., Chattarji, S., and Bear, M.F. (2007). Correction of fragile X syndrome in mice. Neuron *56*, 955–962.

Dölen, G., Carpenter, R.L., Ocain, T.D., and Bear, M.F. (2010). Mechanism-based approaches to treating fragile X. Pharmacol. Ther. *127*, 78–93.

El-Hassar, L., Song, L., Tan, W.J.T., Large, C.H., Alvaro, G., Santos-Sacchi, J., and Kaczmarek, L.K. (2019). Modulators of Kv3 Potassium Channels Rescue the Auditory Function of Fragile X Mice. J. Neurosci. *39*, 4797–4813.

Esparza-Perusquía, M., Olvera-Sánchez, S., Pardo, J.P., Mendoza-Hernández, G., Martínez, F., and Flores-Herrera, O. (2017). Structural and kinetics characterization of the F_1F_0-ATP synthase dimer. New repercussion of monomer-monomer contact. Biochim. Biophys. Acta Bioenerg. *1858*, 975–981.

Fame, R.M., Shannon, M.L., Chau, K.F., Head, J.P., and Lehtinen, M.K. (2019). A concerted metabolic shift in early forebrain alters the CSF proteome and depends on MYC downregulation for mitochondrial maturation. Development *146*, dev182857.

Gerle, C. (2016). On the structural possibility of pore-forming mitochondrial FoF1 ATP synthase. Biochim. Biophys. Acta *1857*, 1191–1196.

Gildish, I., Manor, D., David, O., Sharma, V., Williams, D., Agarwala, U., Wang, X., Kenney, J.W., Proud, C.G., and Rosenblum, K. (2012). Impaired associative taste learning and abnormal brain activation in kinase-defective eEF2K mice. Learn. Mem. *19*, 116–125.

Giorgio, V., Bisetto, E., Soriano, M.E., Dabbeni-Sala, F., Basso, E., Petronilli, V., Forte, M.A., Bernardi, P., and Lippe, G. (2009). Cyclophilin D modulates mitochondrial F0F1-ATP synthase by interacting with the lateral stalk of the complex. J. Biol. Chem. *284*, 33982–33988.

Giorgio, V., von Stockum, S., Antoniel, M., Fabbro, A., Fogolari, F., Forte, M., Glick, G.D., Petronilli, V., Zoratti, M., Szabó, I., et al. (2013). Dimers of mitochondrial ATP synthase form the permeability transition pore. Proc. Natl. Acad. Sci. USA *110*, 5887–5892.

Glass, L.N., Swapna, G., Chavadi, S.S., Tufariello, J.M., Mi, K., Drumm, J.E., Lam, T.T., Zhu, G., Zhan, C., Vilchéze, C., et al. (2017). Mycobacterium tuberculosis universal stress protein Rv2623 interacts with the putative ATP binding cassette (ABC) transporter Rv1747 to regulate mycobacterial growth. PLoS Pathog. *13*, e1006515.

Goh, S., Dong, Z., Zhang, Y., DiMauro, S., and Peterson, B.S. (2014). Mitochondrial dysfunction as a neurobiological subtype of autism spectrum disorder: evidence from brain imaging. JAMA Psychiatry *71*, 665–671.

Griffiths, K.K., Wang, A., Wang, L., Tracey, M., Kleiner, G., Quinzii, C.M., Sun, L., Yang, G., Perez-Zoghbi, J.F., Licznerski, P., et al. (2020). Inefficient thermogenic mitochondrial respiration due to futile proton leak in a mouse model of fragile X syndrome. FASEB J. *34*, 7404–7426.

Gu, J., Zhang, L., Zong, S., Guo, R., Liu, T., Yi, J., Wang, P., Zhuo, W., and Yang, M. (2019). Cryo-EM structure of the mammalian ATP synthase tetramer bound with inhibitory protein IF1. Science *364*, 1068–1075.

He, C.X., and Portera-Cailliau, C. (2013). The trouble with spines in fragile X syndrome: density, maturity and plasticity. Neuroscience *251*, 120–128.

Hom, J.R., Quintanilla, R.A., Hoffman, D.L., de Mesy Bentley, K.L., Molkentin, J.D., Sheu, S.S., and Porter, G.A., Jr. (2011). The permeability transition pore controls cardiac mitochondrial maturation and myocyte differentiation. Dev. Cell *21*, 469–478.

Imamura, H., Nhat, K.P., Togawa, H., Saito, K., Iino, R., Kato-Yamada, Y., Nagai, T., and Noji, H. (2009). Visualization of ATP levels inside single living cells with fluorescence resonance energy transfer-based genetically encoded indicators. Proc. Natl. Acad. Sci. USA *106*, 15651–15656.

Jacquemont, S., Pacini, L., Jønch, A.E., Cencelli, G., Rozenberg, I., He, Y., D'Andrea, L., Pedini, G., Eldeeb, M., Willemsen, R., et al. (2018). Protein synthesis levels are increased in a subset of individuals with fragile X syndrome. Hum. Mol. Genet. *27*, 2039–2051.

Kaech, S., and Banker, G. (2006). Culturing hippocampal neurons. Nat. Protoc. *1*, 2406–2415.

Kalueff, A.V., Stewart, A.M., Song, C., Berridge, K.C., Graybiel, A.M., and Fentress, J.C. (2016). Neurobiology of rodent self-grooming and its value for translational neuroscience. Nat. Rev. Neurosci. *17*, 45–59.

Kane, M.J., Angoa-Peréz, M., Briggs, D.I., Sykes, C.E., Francescutti, D.M., Rosenberg, D.R., and Kuhn, D.M. (2012). Mice genetically depleted of brain serotonin display social impairments, communication deficits and repetitive behaviors: possible relevance to autism. PLoS ONE *7*, e48975.

Kaplan, E.S., Cao, Z., Hulsizer, S., Tassone, F., Berman, R.F., Hagerman, P.J., and Pessah, I.N. (2012). Early mitochondrial abnormalities in hippocampal neurons cultured from Fmr1 pre-mutation mouse model. J. Neurochem. *123*, 613–621.

Klemmer, P., Meredith, R.M., Holmgren, C.D., Klychnikov, O.I., Stahl-Zeng, J., Loos, M., van der Schors, R.C., Wortel, J., de Wit, H., Spijker, S., et al. (2011). Proteomics, ultrastructure, and physiology of hippocampal synapses in a fragile X syndrome mouse model reveal presynaptic phenotype. J. Biol. Chem. *286*, 25495–25504.

Ko, Y.H., Delannoy, M., Hullihen, J., Chiu, W., and Pedersen, P.L. (2003). Mitochondrial ATP synthasome. Cristae-enriched membranes and a multiwell detergent screening assay yield dispersed single complexes containing the ATP synthase and carriers for Pi and ADP/ATP. J. Biol. Chem. *278*, 12305–12309.

Krajewska, M., Mai, J.K., Zapata, J.M., Ashwell, K.W., Schendel, S.L., Reed, J.C., and Krajewski, S. (2002). Dynamics of expression of apoptosis-regulatory proteins Bid, Bcl-2, Bcl-X, Bax and Bak during development of murine nervous system. Cell Death Differ. *9*, 145–157.

Li, H., Chen, Y., Jones, A.F., Sanger, R.H., Collis, L.P., Flannery, R., McNay, E.C., Yu, T., Schwarzenbacher, R., Bossy, B., et al. (2008). Bcl-xL induces Drp1-dependent synapse formation in cultured hippocampal neurons. Proc. Natl. Acad. Sci. USA *105*, 2169–2174.

Li, H., Alavian, K.N., Lazrove, E., Mehta, N., Jones, A., Zhang, P., Licznerski, P., Graham, M., Uo, T., Guo, J., et al. (2013). A Bcl-xL-Drp1 complex regulates synaptic vesicle membrane dynamics during endocytosis. Nat. Cell Biol. *15*, 773–785.

Li, C., Zhang, G., Zhao, L., Ma, Z., and Chen, H. (2016). Metabolic reprogramming in cancer cells: glycolysis, glutaminolysis, and Bcl-2 proteins as novel therapeutic targets for cancer. World J. Surg. Oncol. *14*, 15.

Lumaban, J.G., and Nelson, D.L. (2015). The Fragile X proteins Fmrp and Fxr2p cooperate to regulate glucose metabolism in mice. Hum. Mol. Genet. *24*, 2175–2184.

Magni, G., Orsomando, G., Raffelli, N., and Ruggieri, S. (2008). Enzymology of mammalian NAD metabolism in health and disease. Front. Biosci. *13*, 6135–6154.

McCarron, J.G., Wilson, C., Sandison, M.E., Olson, M.L., Girkin, J.M., Saunter, C., and Chalmers, S. (2013). From structure to function: mitochondrial morphology, motion and shaping in vascular smooth muscle. J. Vasc. Res. *50*, 357–371.

McCullagh, E.A., Rotschafer, S.E., Auerbach, B.D., Klug, A., Kaczmarek, L.K., Cramer, K.S., Kulesza, R.J., Jr., Razak, K.A., Lovelace, J.W., Lu, Y., et al. (2020). Mechanisms underlying auditory processing deficits in Fragile X syndrome. FASEB J. *34*, 3501–3518.

Mnatsakanyan, N., and Jonas, E.A. (2020). ATP synthase c-subunit ring as the channel of mitochondrial permeability transition: Regulator of metabolism in development and degeneration. J. Mol. Cell. Cardiol. *144*, 109–118.

Mnatsakanyan, N., Llaguno, M.C., Yang, Y., Yan, Y., Weber, J., Sigworth, F.J., and Jonas, E.A. (2019). A mitochondrial megachannel resides in monomeric F_1F_O ATP synthase. Nat. Commun. *10*, 5823.

Muscas, M., Louros, S.R., and Osterweil, E.K. (2019). Lovastatin, not Simvastatin, Corrects Core Phenotypes in the Fragile X Mouse Model. eNeuro *6*, ENEURO.0097-19.2019.

Muzzi, M., Gerace, E., Buonvicino, D., Coppi, E., Resta, F., Formentini, L., Zecchi, R., Tigli, L., Guasti, D., Ferri, M., et al. (2018). Dexpramipexole improves bioenergetics and outcome in experimental stroke. Br. J. Pharmacol. *175*, 272–283.

Nakagawa, T., Shimizu, S., Watanabe, T., Yamaguchi, O., Otsu, K., Yamagata, H., Inohara, H., Kubo, T., and Tsujimoto, Y. (2005). Cyclophilin D-dependent mitochondrial permeability transition regulates some necrotic but not apoptotic cell death. Nature *434*, 652–658.

Neginskaya, M.A., Solesio, M.E., Berezhnaya, E.V., Amodeo, G.F., Mnatsakanyan, N., Jonas, E.A., and Pavlov, E.V. (2019). ATP Synthase C-Subunit-Deficient Mitochondria Have a Small Cyclosporine A-Sensitive Channel, but Lack the Permeability Transition Pore. Cell Rep. *26*, 11–17.

Ofengeim, D., Chen, Y.B., Miyawaki, T., Li, H., Sacchetti, S., Flannery, R.J., Alavian, K.N., Pontarelli, F., Roelofs, B.A., Hickman, J.A., et al. (2012). N-terminally cleaved Bcl-xL mediates ischemia-induced neuronal death. Nat. Neurosci. *15*, 574–580.

Park, S., Park, J.M., Kim, S., Kim, J.A., Shepherd, J.D., Smith-Hicks, C.L., Chowdhury, S., Kaufmann, W., Kuhl, D., Ryazanov, A.G., et al. (2008). Elongation factor 2 and fragile X mental retardation protein control the dynamic translation of Arc/Arg3.1 essential for mGluR-LTD. Neuron *59*, 70–83.

Pfeiffer, B.E., and Huber, K.M. (2009). The state of synapses in fragile X syndrome. Neuroscientist *15*, 549–567.

Pyronneau, A., He, Q., Hwang, J.Y., Porch, M., Contractor, A., and Zukin, R.S. (2017). Aberrant Rac1-cofilin signaling mediates defects in dendritic spines, synaptic function, and sensory perception in fragile X syndrome. Sci. Signal. *10*, eaan0852.

Rasola, A., and Bernardi, P. (2014). The mitochondrial permeability transition pore and its adaptive responses in tumor cells. Cell Calcium *56*, 437–445.

Roberts, D.J., and Miyamoto, S. (2015). Hexokinase II integrates energy metabolism and cellular protection: Akting on mitochondria and TORCing to autophagy. Cell Death Differ. *22*, 364.

Sacchetti, S., Alavian, K.N., Lazrove, E., and Jonas, E.A. (2013). F1FO ATPase vesicle preparation and technique for performing patch clamp recordings of submitochondrial vesicle membranes. J. Vis. Exp. (75), e4394.

Santos, A.R., Kanellopoulos, A.K., and Bagni, C. (2014). Learning and behavioral deficits associated with the absence of the fragile X mental retardation protein: what a fly and mouse model can teach us. Learn. Mem. *21*, 543–555.

Scheetz, A.J., Nairn, A.C., and Constantine-Paton, M. (2000). NMDA receptor-mediated control of protein synthesis at developing synapses. Nat. Neurosci. *3*, 211–216.

Schmidt, E.K., Clavarino, G., Ceppi, M., and Pierre, P. (2009). SUnSET, a nonradioactive method to monitor protein synthesis. Nat. Methods *6*, 275–277.

Sidorov, M.S., Auerbach, B.D., and Bear, M.F. (2013). Fragile X mental retardation protein and synaptic plasticity. Mol. Brain *6*, 15.

Silverman, J.L., Yang, M., Lord, C., and Crawley, J.N. (2010). Behavioural phenotyping assays for mouse models of autism. Nat. Rev. Neurosci. *11*, 490–502.

Stefely, J.A., and Pagliarini, D.J. (2017). Biochemistry of Mitochondrial Coenzyme Q Biosynthesis. Trends Biochem. Sci. *42*, 824–843.

Strumbos, J.G., Brown, M.R., Kronengold, J., Polley, D.B., and Kaczmarek, L.K. (2010). Fragile X mental retardation protein is required for rapid experience-dependent regulation of the potassium channel Kv3.1b. J. Neurosci. *30*, 10263–10271.

Szabó, I., and Zoratti, M. (1991). The giant channel of the inner mitochondrial membrane is inhibited by cyclosporin A. J. Biol. Chem. *266*, 3376–3379.

Tranfaglia, M.R. (2011). The psychiatric presentation of fragile x: evolution of the diagnosis and treatment of the psychiatric comorbidities of fragile X syndrome. Dev. Neurosci. *33*, 337–348.

Udagawa, T., Farny, N.G., Jakovcevski, M., Kaphzan, H., Alarcon, J.M., Anilkumar, S., Ivshina, M., Hurt, J.A., Nagaoka, K., Nalavadi, V.C., et al. (2013). Genetic and acute CPEB1 depletion ameliorate fragile X pathophysiology. Nat. Med. *19*, 1473–1477.

Um, J.W., Kaufman, A.C., Kostylev, M., Heiss, J.K., Stagi, M., Takahashi, H., Kerrisk, M.E., Vortmeyer, A., Wisniewski, T., Koleske, A.J., et al. (2013). Metabotropic glutamate receptor 5 is a coreceptor for Alzheimer aβ oligomer bound to cellular prion protein. Neuron *79*, 887–902.

Vander Heiden, M.G., Cantley, L.C., and Thompson, C.B. (2009). Understanding the Warburg effect: the metabolic requirements of cell proliferation. Science *324*, 1029–1033.

Vlasov, A.V., Kovalev, K.V., Marx, S.H., Round, E.S., Gushchin, I.Y., Polovinkin, V.A., Tsoy, N.M., Okhrimenko, I.S., Borshchevskiy, V.I., Büldt, G.D., et al. (2019). Unusual features of the c-ring of F_1F_O ATP synthases. Sci. Rep. *9*, 18547.

Warburg, O. (1956). On respiratory impairment in cancer cells. Science *124*, 269–270.

Watson, D.J., Ostroff, L., Cao, G., Parker, P.H., Smith, H., and Harris, K.M. (2016). LTP enhances synaptogenesis in the developing hippocampus. Hippocampus *26*, 560–576.

Weisz, E.D., Towheed, A., Monyak, R.E., Toth, M.S., Wallace, D.C., and Jongens, T.A. (2018). Loss of Drosophila FMRP leads to alterations in energy metabolism and mitochondrial function. Hum. Mol. Genet. *27*, 95–106.

Wijetunge, L.S., Chattarji, S., Wyllie, D.J., and Kind, P.C. (2013). Fragile X syndrome: From targets to treatments. Neuropharmacology *68*, 83–96.

Wise, D.R., DeBerardinis, R.J., Mancuso, A., Sayed, N., Zhang, X.Y., Pfeiffer, H.K., Nissim, I., Daikhin, E., Yudkoff, M., McMahon, S.B., and Thompson, C.B. (2008). Myc regulates a transcriptional program that stimulates mitochondrial glutaminolysis and leads to glutamine addiction. Proc. Natl. Acad. Sci. USA *105*, 18782–18787.

Zhang, Y., Brown, M.R., Hyland, C., Chen, Y., Kronengold, J., Fleming, M.R., Kohn, A.B., Moroz, L.L., and Kaczmarek, L.K. (2012). Regulation of neuronal excitability by interaction of fragile X mental retardation protein with slack potassium channels. J. Neurosci. *32*, 15318–15327.

Zheng, X., Boyer, L., Jin, M., Mertens, J., Kim, Y., Ma, L., Ma, L., Hamm, M., Gage, F.H., and Hunter, T. (2016). Metabolic reprogramming during neuronal differentiation from aerobic glycolysis to neuronal oxidative phosphorylation. eLife *5*, e13374.

Zoghbi, H.Y., and Bear, M.F. (2012). Synaptic dysfunction in neurodevelopmental disorders associated with autism and intellectual disabilities. Cold Spring Harb. Perspect. Biol. *4*, a009886.

Please cite this article in press as: Licznerski et al., ATP Synthase c-Subunit Leak Causes Aberrant Cellular Metabolism in Fragile X Syndrome, Cell (2020), https://doi.org/10.1016/j.cell.2020.07.008

STAR★METHODS

KEY RESOURCES TABLE

REAGENT or RESOURCE	SOURCE	IDENTIFIER
Antibodies		
Mouse anti-FMRP 7G1-1	Developmental Studies Hybridoma Bank	https://dshb.biology.uiowa.edu/7G1-1; RRID:AB_528251
Rabbit anti-FMRP	Cell Signaling	Cat. #4317; RRID: AB_1903978
Rabbit anti-Bcl-xL (54H6)	Cell Signaling	Cat. #2764; RRID:AB_2228008
Mouse anti-Puromycin [3RH11]	Kerafast	Cat. #Equation 0001; RRID:AB_2620162
Mouse anti-GAPDH (6C5)	Santa Cruz Biotech.	Cat. #sc-32233; RRID:AB_627679
Rabbit anti-PSD-95	Cell Signaling	Cat. #2507; RRID:AB_561221
Rabbit anti-p-EF2 (Thr56)	Cell Signaling	Cat.#2331; RRID:AB_10015204
Mouse anti-EF2 (F-9)	Santa Cruz Biotech.	Cat. #sc-166409; RRID:AB_2262106
Rabbit anti-ATP5G1/G2/G3 [EPR13908]	abcam	Cat. #ab180149
Mouse anti-ATPB [3D5]	abcam	Cat. #ab14730; RRID:AB_301438
Rabbit anti-COX IV	Cell Signaling	Cat. #4844; RRID:AB_2085427
Mouse anti-Beta-actin [C4]	Santa Cruz Biotech.	Cat. #sc-47778; RRID:AB_626632
Glycolysis Antibody Sampler Kit	Cell Signaling	Cat. #8337; RRID:AB_10897509
Chicken anti-GFP	abcam	Cat. #ab13970; RRID:AB_300798-
Anti-mouse IgG HRP-linked	Cell Signaling	Cat. #7076; RRID:AB_330924
Anti-rabbit IgG HRP-linked	Cell Signaling	Cat. #7074; RRID:AB_2099233
ChromPure mouse IgG, whole molecule	Jackson ImmunoResearch	Cat. #015-000-003; RRID:AB_2337188
ChromPure rabbit IgG, whole molecule	Jackson ImmunoResearch	Cat. #011-000-003; RRID: AB_2337118
Bacterial and Virus Strains		
One Shot TOP10 chemically competent *Escherichia coli*	Invitrogen	Cat. #C404010
Chemicals, Peptides, and Recombinant Proteins		
ABT-737	Selleck Chemicals	Cat. #S1002
Dexpramipexole Dihydrochloride	Sigma-Aldrich	Cat. #SML0392
ACMA (9-amino-6-chloro-2-methoxyacridine)	Sigma-Aldrich	Cat. #A5806
TMRM tetramethylrhodamine, methyl ester	Invitrogen	Cat. #T668
Puromycin Dihydrochloride from *Streptomyces alboniger*	Sigma-Aldrich	Cat. #P8833
D-serine	Sigma-Aldrich	Cat. #S4250
Cyclosporin A	Cell Signaling	Cat. #9973
Lipofectamine 3000 transfection reagent	Thermo Fisher	Cat. #L3000001
Lipofectamine 2000 transfection reagent	Thermo Fisher	Cat. #11668030
EZview Red Anti-FLAG M2 affinity gel	Millipore Sigma	Cat. #F2426
Protein G agarose	Roche	Cat. #11719416001
Protein A/G PLUS agarose	Santa Cruz Biotech.	Cat. #sc-2003
cOmplete, Mini, EDTA-free Protease Inhibitor Cocktail	Roche	Cat. #11836170001
Protector RNase inhibitor	Roche	Cat. #3335399001
RIPA buffer (10x)	Cell Signaling	Cat. #9806
Recombinant Flag-tagged Bcl-xL	This paper	N/A
Critical Commercial Assays		
ATPlite Luminescence Assay System	PerkinElmer	Cat. #6016943
iScript cDNA Synthesis Kit	Bio-Rad	Cat. #1708890

(*Continued on next page*)

Please cite this article in press as: Licznerski et al., ATP Synthase c-Subunit Leak Causes Aberrant Cellular Metabolism in Fragile X Syndrome, Cell (2020), https://doi.org/10.1016/j.cell.2020.07.008

Continued

REAGENT or RESOURCE	SOURCE	IDENTIFIER
TaqMan Gene expression Assays: mouse ATP5G1	Thermo Fisher	Probe ID: Mm02601566_g1
TaqMan Gene expression Assays: mouse ATP5G2	Thermo Fisher	Probe ID: Mm00848143_g1
TaqMan Gene expression Assays: mouse ATP5G3	Thermo Fisher	Probe ID: Mm01334541_g1
TaqMan Gene expression Assays: mouse ATP5B	Thermo Fisher	Probe ID: Mm01160389_g1
TaqMan Gene expression Assays: mouse ActB	Thermo Fisher	Probe ID: Mm02619580_g1
L-lactate Assay Kit I	Eton Bioscience	Cat. #120001 100A
Qproteome Mitochondria Isolation Kit	QIAGEN	Cat. #37612
RNeasy Plus Mini Kit	QIAGEN	Cat. #74134
Deposited Data		
LC/MS/MS full dataset	This Paper	Table S1
Experimental Models: Cell Lines		
Human Embryonic Kidney HEK293	Millipore Sigma	Cat. #12022001
Human WT fibroblast lines sc-173 and sc-176	Dr. Gary J. Bassell	https://www.cores.emory.edu/escc/about/who%20we%20are/gary.html
Human FX fibroblast lines CH095 and sc-128	Dr. Gary J. Bassell	https://www.cores.emory.edu/escc/about/who%20we%20are/gary.html
Human FX fibroblast lines S001, S002, S005	Dr. Elizabeth Berry-Kravis	https://www.rushu.rush.edu/research/departmental-research/pediatrics-research/laboratory-elizabeth-berry-kravis-md-phd
Experimental Models: Organisms/Strains		
Mouse: FVB.129P2-*Pde6b*$^{+}$*Tyr*$^{c\text{-}ch}$/*AntJ*	The Jackson Laboratory	Stock #004828
Mouse: Fmr1$^{-/y}$ (FVB.129P2-*Fmr1*^{tm1Cgr}/*J*	The Jackson Laboratory	Stock #004624
Oligonucleotides		
Please refer to Table S2.	N/A	N/A
Recombinant DNA		
Plasmid: FRET based ATP reporter ATeam YEMK	Imamura et al., 2009	N/A
Plasmid: c-subunit expression	Alavian et al., 2014	N/A
Plasmid: Bcl-xL expression	Li et al., 2013	N/A
Plasmid: Dendra translation indicator	Dr. Deanna Benson	https://icahn.mssm.edu/profiles/deanna-l-benson
Software and Algorithms		
Prism 8.0.0 (131)	GraphPad Software, Inc.	https://www.graphpad.com
ImageJ	NIH	https://imagej.nih.gov/ij/
Scaffold4 proteome software	Proteome Software Inc.	http://www.proteomesoftware.com/products/scaffold/

RESOURCE AVAILABILITY

Lead Contact

Further information and requests for resources and reagents should be directed to and will be fulfilled by the Lead Contact, Elizabeth A. Jonas (elizabeth.jonas@yale.edu).

Materials Availability

All unique/stable reagents generated in this study are available from the Lead Contact without restriction. For reagents please contact Elizabeth A. Jonas (lead contact) (elizabeth.jonas@yale.edu).

Please cite this article in press as: Licznerski et al., ATP Synthase c-Subunit Leak Causes Aberrant Cellular Metabolism in Fragile X Syndrome, Cell (2020), https://doi.org/10.1016/j.cell.2020.07.008

Data and Code Availability

The published article includes all datasets generated or analyzed during this study. Original data for the LC/MS/MS dataset are included in this manuscript in Table S1. LC/MS/MS source files are available from Pawel Licznerski (pawel.licznerski@yale.edu) on request without restrictions.

EXPERIMENTAL MODEL AND SUBJECT DETAILS

Mice

Wild-type (WT) (FVB.129P2-*Pde6b*$^{+}$*Tyr*$^{c\text{-}ch}$/*Ant*) and Fmr1$^{-/y}$ (FVB.129P2-*Fmr1*^{tm1Cgr}/*J*) mice were purchased from Jackson Laboratories (Bar Harbor, MA). All procedures were performed in accordance with the NIH Guidelines for the Care and Use of Laboratory Animals and approved by Yale University's Institutional Animal Care and Use Committee (IACUC).

Human fibroblast lines

Human FX and WT cell lines were kindly shared by Dr. Gary J. Bassell laboratory (Emory University, Atlanta, GA) and Dr. Elizabeth Berry-Kravis (Rush University Medical Center, Chicago, IL).

Cells were cultured in high glucose DMEM supplemented with 10% v/v FBS, 100 U/ml penicillin, 100 μg/ml streptomycin (all from GIBCO).

METHOD DETAILS

Mice hippocampal primary cultures

Primary hippocampal neurons were prepared from mouse embryos (WT or FX male and female pups at E19), as described previously (Beaudoin et al., 2012; Kaech and Banker, 2006; Li et al., 2008). Briefly, after isolation of hippocampi from prenatal brains, neurons were dissociated and plated (0.15×10^6 cells/ 35mm plate) in plating medium with 5% FBS. After 2-4 hr incubation, plating medium was changed to neurobasal medium supplemented with B-27, glutamine, and antibiotics (Invitrogen GIBCO life technologies, Carlsbad, CA). Neurons were grown at 37°C in a 5% CO_2 and 20% O_2 humidified incubator.

Mouse cortical primary cultures

Cortical cultures were prepared from P0-P2 FVB (WT control) and FMRP KO pups as described in Beaudoin et al. (2012).

Dendra translation indicator

Plasmid coding for Dendra embedded in the 5′ and 3′ UTR of beta-actin was kindly shared by Dr. Deanna Benson (Icahn School of Medicine at Mount Sinai, New York, NY). Cells were transfected using Lipofectamine 2000 (Invitrogen) and experiments were performed at DIV14-21. When Dendra is translated *in vitro*, it emits green fluorescent light. Green fluorescence is photoconverted to red fluorescence by exposure to fluorescent light 400-490 nm for 2 min., after which the newly developing green fluorescence represents newly translated actin reporter. Measurements were obtained at 5 min. after photoconversion, using a Zeiss Axiovert 200 microscope and analyzed for fluorescence intensity (center of the soma) using ImageJ software.

ABT-737 treatment

A stock solution of ABT-737 (Selleckchem, Houston, TX) was prepared in dimethyl sulfoxide (DMSO). ABT-737 (1 μM) or the same volume of DMSO was added into the culture dishes for mRNA translation studies.

Cyclosporine A

Cyclosporine A (CsA) was purchased from Cell Signaling and stock solution was prepared in dimethyl sulfoxide (DMSO). Primary neuronal cortical cultures at DIV 14-16 were treated with 0.2 to 0.5 μM CsA (final concentration) or DMSO as a control for 6 hours, harvested, lysed and processed for further analysis.

Dexpramipexole

A dose of Dex for *in vivo* treatment was chosen by searching the literature and analyzing previous reports on Dex metabolism (Bozik et al., 2011; Cudkowicz et al., 2011; Muzzi et al., 2018). A stock solution of Dexpramipexole dihydrochloride (SIGMA-ALDRICH, St. Louis, MO) was prepared in sterile dH_2O and used at different concentrations described in the manuscript.

DNA plasmid transfections

All neuronal cultures were transfected at day 5-7 DIV (days *in vitro*) using Lipofectamine 2000 reagent (Invitrogen), according to the manufacturer's specifications. The same reagent was used to transfect human fibroblast lines. Vector for c-subunit expression was the same as previously used and described by Alavian et al. (2014).

siRNA

DsiRNA (Integrated DNA Technologies, USA) stocks were prepared according to the manufacturer's protocol. Transfections of siRNA (final concentration: 25 pmol per well) were performed using Lipofectamine 2000 reagent (Invitrogen). Cell lysates were prepared 20-24 hours post transfection.

Control DsiRNA:

Sense: CGUUAAUCGCGUAUAAUACGCGUAT
Antisense: AUACGCGUAUUAUACGCGAUUAACGAC
c-subunit DsiRNA (hs.Ri.ATP5G1.13.1):
Sense: CCAGUGAAUUCAUCUAAACAGCCTT
Antisense: CGGGUCACUUAAGUAGAUUUGUCGGAA

Purification of recombinant Bcl-xL

Flag-tagged Bcl-xL (Li et al., 2013) was immunoprecipitated from HEK293T cell lysates using the EZview Red ANTI-FLAG M2 Affinity Gel (Sigma-Aldrich) according to the manufacturer's protocol. The purified protein samples were examined by western blot.

Puromycin incorporation for measurement of protein synthesis

Puromycin (Puromycin dihydrochloride, SIGMA-ALDRICH) labeling was performed as previously described (Schmidt et al., 2009). Briefly, cells or synaptosomes were incubated in puromycin containing media (10 μg/ml) for 15 minutes, washed twice with cold PBS, lysed in 1xRIPA buffer (Cell Signaling) containing proteinase inhibitors (Roche, Indianapolis, Indiana) and phosphatase inhibitors PhosSTOP (Roche Diagnostics GmbH, Mannheim, Germany).

For *in vivo* studies adult (2 month or older) mice were injected (IP) with (30 mg/kg) puromycin (SIGMA ALDRICH). After 2.5 hr animals were sacrificed and brain and liver samples were harvested and homogenized in 1xRIPA buffer (Cell Signaling) containing proteinase inhibitors (Roche, Indianapolis, Indiana) and phosphatase inhibitors PhosSTOP (Roche Diagnostics GmbH, Mannheim, Germany) and processed for western blot analysis. Alternatively, adult mice were sacrificed and 200 μm brain slices containing prefrontal cortex were incubated in hippocampal recording buffer (with 95% O_2 and 5% CO_2) containing (in nmol): 125 mM NaCl, 25 mM $NaHCO_3$, 2.5 mM KCl, 25 mM glucose, 1.25 mM NaH_2PO_4, 1 mM $MgCl_2$, 2 mM $CaCl_2$ bubbled with 95%O_2, 5% CO_2, for 2.5 hr. with Dexpramipexole (final concentration 10 μM). For the last 15 minutes of incubation puromycin was added to the bath (final 10 μg/ml). Next, brain slices were homogenized in 1xRIPA buffer (Cell Signaling) containing proteinase inhibitors (Roche, Indianapolis, Indiana) and phosphatase inhibitors PhosSTOP (Roche Diagnostics GmbH, Mannheim, Germany) and processed for western blot analysis.

Immunoprecipitation of puromycin labeled peptides

Isolated synaptosomes or P0-P2 FVB or FX DIV14-16 cortical cultures were treated for 15 min. with puromycin. 50-100 μg of protein from cell lysate, was incubated at 4°C overnight with 1 μg of anti-puromycin antibody (Kerafast). Next, 50 μL of protein G agarose (Roche Diagnostics GmbH) was added to samples for an overnight incubation at 4°C. Beads were washed 3 times with 1x RIPA buffer (Cell Signaling) and processed for mass spectrometry analysis. For experiments with Dexpramipexole, cortical cultures were treated with 10 μM Dex for 2-24 hours prior to puromycin treatment and then processed for western blot.

Co-immunoprecipitation of FMRP and the beta- and c-subunit of the ATP synthase

WT and FX purified synaptosomal lysates were incubated at 4°C overnight with 10 μg of mouse anti-FMRP 7G1-1 (developed by Stephen T. Warren, this antibody was obtained from the Developmental Studies Hybridoma Bank developed under the auspices of NICHD and maintained by the University of Iowa, Department of Biological Sciences, Iowa City IA 55242) or 10 μg of mouse IgG. Next, immunoprecipitates were immobilized on A/G agarose beads (Santa-Cruz Biotechnology) at 4°C overnight and washed 4-5x15 minutes with 1x RIPA lysis buffer (Cell Signaling) with 40 U/ml protector RNase inhibitor (Roche) and 1x Complete EDTA-free protease inhibitor cocktail tablet (Roche). mRNA was purified from beads using the quickRNA purification kit (QIAGEN) according to the manufacturer's protocol. RNAs were then reverse transcribed using a cDNA reverse transcription kit (Biorad) according to the manual. Next, a standard PCR reaction was run using the following primers:

GGCAAGATGGGGTATAGAGA; Map1b forward primer
CCCACCTGCTTTGGTCTTTG; Map1b reverse primer
AAGCTGGAGAACAACTTGGAC; Arc forward primer
CCCCCAAGACTGATATTGCTGAG, Arc reverse primer

Primer sequences above have been published by Brown et al. (2010).

GCCAGAGACTATGCGGCGCAG; mATP5B forward primer
GGACCTCTCTCATCAATAGG; mATP5B reverse primer

GGCCTGTGTCTGCCTCCCTCC; mATP5G1 forward primer
GGCGACCATCAAACAGAAGAG; mATP5G1 reverse primer
GAGCACCTCTCAGCTGCTGAGTCG; mATP5G2 forward primer
GGCCTCTGAGAGGGCAAAGCC; mATP5G2 reverse primer
GTTCGCCTGCGCCAAGCTCGC; mATP5G3 forward primer
GTGAAGGGTTTCAGCACCAG; mATP5G3 reverse primer

Western blot analysis

Brain tissue or primary neuronal culture lysates or mitochondrial lysates were prepared using RIPA lysis buffer (Cell Signaling) containing proteinase inhibitors (Roche, Indianapolis, Indiana) and phosphatase inhibitors PhosSTOP (Roche Diagnostics GmbH, Mannheim, Germany). The protein concentration was measured using a BCA kit (Pierce, Rockford, Illinois). Then, protein samples were electrophoretically separated on an SDS-PAGE gel (4%–20% gradient gel, Bio-Rad, USA) and transferred overnight to PVDF membranes (0.2 μm pores, Bio-Rad, USA). The membranes were incubated in 2% BSA (Tris-buffered saline (TBS), 0.1% Tween 20) for 1 h and then incubated at 4°C overnight with primary anti-Bcl-xL (1:1000, Cell Signaling), anti-puromycin (1:1000, Kerafast), anti-GAPDH (1:1000, Santa Cruz Biotechnology), anti-PSD-95 (1:1000, Cell Signaling), anti-p-EF2 (1:1000, Cell Signaling), anti-EF2 (1:1000, Santa Cruz Biotechnology), anti-ATP5g1/2/3 (1:1000, abcam), anti-ATPb (1:1000, abcam), anti-beta-actin (1:1000, Cell Signaling), anti-FMRP (1:1000, Cell Signaling). Antibodies for glycolytic enzyme detection were supplied by Glycolysis Antibody Sampler Kit #8337, Cell Signaling and used at 1:1000 dilution. After 3 × 15 min washes membranes were incubated for 1 h with secondary, horseradish peroxidase (HRP) conjugated antibodies (1:5000, Cell Signaling) and developed using a chemilluminescence kit (Pierce, Rockford, Illinois).

Blue Native Page Electrophoresis

Protein complexes from 20 μg (verified by BCA assay) of mitochondria (per lane) were separated on Bis-Tris 3%–12% Native gels. Samples were solubilized on ice for 20 minutes with 4 μg digitonin/μg protein. After separation the protein complexes were wet-transferred onto a polyvinylidene fluoride (PVDF) membrane, which was probed with anti-ATP5G1,2,3 antibody for ATP synthase c-subunit.

Isolation of mitochondria

Mitochondria were isolated and purified from mouse brain as previously described (Ofengeim et al., 2012; Sacchetti et al., 2013). In brief, brain tissue was homogenized in isolation buffer (250mM sucrose, 20mM HEPES, 1mM EDTA, 0.5% BSA). After a series of centrifugations, the nuclear material, cytosolic fraction and the mitochondrial pellet containing synaptosomes were separated. Synaptosomes were disrupted by applying 1200 psi pressure for 10min and mitochondria were separated by ultracentrifugation (Brown et al., 2004) . To isolate mitochondria from human fibroblasts, a Qproteome^{TM} Mitochondria isolation kit was used (QIAGEN, Cat.37612), according to the manufacturer's protocol.

Isolation of SMVs from mouse brain

FVB or FMRP KO mouse brain tissue (without cerebellum) was homogenized in ice-cold isolation buffer (250 mM sucrose, 20 mM HEPES (pH 7.2), 1 mM EDTA, and 0.5% BSA). After a brief centrifugation at 1,500 g, the supernatants were centrifuged at high-speed (16,000 × g) for 10 min at 4°C. The crude pellets were re-suspended in isolation buffer and a pressure of 1,200psi was applied for 10min, followed by rapid decompression. The pure mitochondrial fraction was then pelleted in a ficoll density gradient by centrifugation and washed with isolation buffer. Non-ionic detergents (digitonin and Lubrol-PX) were used to further solubilize and stabilize membrane-bound protein complexes, and the sub mitochondrial vesicles (SMVs) were isolated by a final 2 hr ultracentrifugation (Chan et al., 1970; Sacchetti et al., 2013). Freshly prepared SMV protein amount was quantified using the Bradford protein assay

Preparation of synaptosomal fractions

Synaptosomal fractions were prepared as previously described (Alavian et al., 2011). Briefly, cultured neurons were homogenized in isotonic mitochondrial buffer and centrifuged at 600 x g for 10 min at 4 °C. The pellet, containing the nuclear and unbroken cells, was discarded and the supernatant, containing the mitochondrial, synaptosomal and cytosolic fractions, was centrifuged at 10,000 g for 30 min at 4 °C. The supernatant, containing the cytosolic fraction, was separated from the pellet. The pellet containing the mitochondrial and synaptosomal fractions was resuspended in 100 μL isolation buffer and layered onto a 7.5%–10% Ficoll gradient. After 30 min ultracentrifugation at 90,000 g, 4 °C, the mitochondrial pellet and the middle layer, containing synaptoneurosomes (hereafter called synaptosomes) were removed. The synaptosomal layer was resuspended in isolation buffer and centrifuged for 10 min at 20,000 g, resulting in a crude synaptosomal pellet.

D-serine stimulation of synaptosomes

Synaptosomal samples purified from FVB and FMRP KO mice and were stimulated with D-serine (final concentration 0.2 μM), supplied in extracellular (EC) recording buffer without magnesium (120mM NaCl, 4mM KCl, 2mM $CaCl_2$, 10mM HEPES, 10mM

D-Glucose, pH = 7.4). 1 μg of puromycin was also added to measure protein synthesis. EC buffer lacking D-serine was added to unstimulated control samples. Samples were harvested and lysed in 1xRIPA at 3, 5, 15 and 30 minutes post stimulation.

Quantitative Real Time RT-PCR

Total RNA was extracted from FVB and FX synaptosomes using RNeasy Plus Mini Kit according to the manufacturer's protocol (QIAGEN). Next, extracted RNA was reverse transcribed using Bio-Rad iScript first cDNA synthesis kit. TaqMan® Gene Expression Assays (Thermo Fisher Scientific, USA) was used to quantify mRNA levels. Data were analyzed using the $2^{-\Delta\Delta CT}$ method using beta-actin as the normalizing endogenous control. The following probes were used: mATP5G1 (Mm02601566_g1), mATP5G2 (Mm00848143_g1), mATP5G3 (Mm01334541_g1), mATP5B (Mm01160389_g1), mActB (Mm02619580_g1).

Measurement of ATP levels in Figure 1

Primary cortical neurons were seeded onto 96 well plates (0.015×10^6 neurons/ well). After 1-2 weeks incubation, cells were treated as stated in relevant figure legends. ATP production was measured by using ATPlite™ Luminescence Assay System (PerkinElmer, Waltham, MA) according to the manufacturer's protocol. Cells were washed with sterile PBS, lysed and incubated with substrate (luciferin) for 15 min. The reaction between ATP, luciferase and luciferin produced bioluminescence. ATP-induced-luminescence was measured with a VICTOR^3 multilabel reader (PerkinElmer, Waltham, MA).

Measurement of mitochondrial potential ($\Delta\psi$)

Mitochondrial membrane potential ($\Delta\psi$) was measured using the fluorescent lipophilic cationic dye tetramethylrhodamine methyl ester (TMRM, Invitrogen, Molecular Probes, Carlsbad, CA, USA), which accumulates within mitochondria in a membrane potential-dependent manner. Primary hippocampal neurons were stained with 5 nM TMRM for 30 min at 37°C in the dark. Images were taken using a Zeiss LSM 710 confocal scanning microscope and TMRM fluorescence densitometry was analyzed using ZEN software (Carl Zeiss Microscopy GmbH, Jena, Germany).

ACMA assay

ACMA (9-amino-6-chloro-2-methoxyacridine, Sigma A5806) fluorescence quenching was measured as previously described (Alavian et al., 2011) with some modifications. In brief, 2μM ACMA and 50 μg of the isolated mouse brain submitochondrial vesicles (SMVs), were used. SMV suspension fluorescence was measured at 490 nm using a PerkinElmer VICTOR3 (PerkinElmer, Waltham, MA) multilabel plate reader.

Lactate assay

Growth media were collected at DIV20 from WT and FX neuronal primary cultures treated with either 5 μM Dex or vehicle daily from DIV15 to DIV20. Lactate levels in the growth medium samples were calculated using the L-Lactate assay Kit I (Eton Bioscience, Charlestown, MA) according to the manual provided.

SMV ion channel recordings

SMV recordings were made by forming giga-ohm seals onto SMVs in intracellular solution (120 mM KCl, 8 mM NaCl, 0.5 mM EGTA, 10 mM, HEPES (pH 7.3)) using an Axopatch 200B amplifier (Axon Instruments) at room temperature (22–25°C). Recording electrodes were pulled from borosilicate glass capillaries (WPI) with a final resistance in the range of 50–120 MΩ. Signals were filtered at 5 kHz using the amplifier circuitry. Data were analyzed using pClamp 10.0 software (Axon Instruments). Membrane currents under different experimental conditions were assessed by measuring peak membrane current (in pA). All current measurements were adjusted for the holding voltage assuming a linear current-voltage relationship: The resulting conductances are expressed in pS according to the equation G = I/V where G is conductance in pS, V is the membrane holding voltage in mV, and I is the peak membrane current in pA. Group data were quantified in terms of conductance. All population data were expressed as mean ± SEM.

Brain Electron microscopy

Brain slices from FVB (WT) and FMRP KO adult mice (over 2 month-old) were incubated in artificial cerebral spinal fluid (ACSF) containing (in mM): 125 mM NaCl, 25 mM $NaHCO_3$, 2.5 mM KCl, 25 mM glucose, 1.25 mM NaH_2PO_4, 1 mM $MgCl_2$, 2 mM $CaCl_2$ bubbled with 95%O_2, 5% CO_2 with vehicle or 0.2 μM Cyclosporin A for 2 hr 45 min. Samples were fixed in 4% paraformaldehyde in 0.25M HEPES for 1 hour. Samples were rinsed in PBS and re-suspended in 10% gelatin, chilled and trimmed to smaller blocks and placed in cryoprotectant of 2.3M sucrose overnight on a rotor at 4°C. They were transferred to aluminum pins and frozen rapidly in liquid nitrogen. The frozen block was trimmed on a Leica Cryo-EMUC6 UltraCut and 65-75nm thick sections were collected using the Tokoyasu method. The frozen sections were collected on a drop of sucrose, thawed and placed on a nickel formvar/carbon coated grid and floated in a dish of PBS ready for immunolabeling. Grids were placed section side down on drops of 0.1M ammonium chloride to quench untreated aldehyde groups, then blocked for nonspecific binding on 1% fish skin gelatin in PBS. All grids were rinsed in PBS, fixed using 1% glutaraldehyde for 5mins, rinsed and transferred to a UA/methylcellulose drop, then dried for viewing. Samples were viewed FEI Tencai Biotwin TEM at 80Kv. Images were taken using Morada CCD and iTEM (Olympus) software. Analysis of electron micrographs was performed using ImageJ software (NIH).

Please cite this article in press as: Licznerski et al., ATP Synthase c-Subunit Leak Causes Aberrant Cellular Metabolism in Fragile X Syndrome, Cell (2020), https://doi.org/10.1016/j.cell.2020.07.008

Dendritic spine density analysis and ATP measurement

Hippocampal neurons were isolated from E18.5-19 FMRP KO and WT mice using enzymatic digestion with Trypsin EDTA (GIBCO) followed by mechanical trituration and then cultured in Neurobasal media with 1 X B27 supplement (GIBCO). Half of the medium was replaced with fresh medium every week. Cells were transfected at DIV1 with the ATeam ATP reporter construct (Imamura et al., 2009) (kindly provided by Dr. Imamura and Dr. Noji from Osaka University, Osaka, Japan) using Lipofectamine 3000 (Thermo Fisher) as per manufacturer's recommendations. Cells were treated with 5 μm Dexpramipexole additively for 6 consecutive days from DIV 15 – DIV 20. At DIV 20 conditioned medium was collected for measurement of lactate levels.

For quantification of dendritic spines, cells were fixed at DIV 20 with 4% buffered formalin and immuno-stained with anti-GFP antibody (Abcam, ab13970). Images were acquired with a Zeiss 880 Airyscan microscope. Dendritic spines were accessed visually on the basis on their morphology; mature spines were identified by their mushroom-like shape; all other spines were considered immature (see illustration in Figure 6).

ATP levels were measured in neurons at DIV 20 using the well characterized FRET based ATP reporter ATeam YEMK (Imamura et al., 2009a) in a HEPES (10 mM) based buffer containing NaCl (125 mM), KCl (3 mM), $CaCl_2$ (2 mM), $MgCl_2$ (2 mM) and D-Glucose (5 mM). For LTP stimulation of neurons, 10 μM D-Serine was applied in the same buffer but lacking $MgCl_2$ for 5 min. FRET measurements were performed with a Zeiss 710 confocal microscope equipped with a controlled atmosphere cabinet at 25°C. Measurements of changes in pH using a pH sensitive indicator were performed separately and did not show any significant changes in pH before or after stimulation during the times of acquisition of ATP signal.

Mass Spectrometry

Following separation of protein complexes in one-dimension by SDS-PAGE, protein bands of interest were excised for bottom-up protein identification by LC/MS/MS. Gel bands were prepared as described (Glass et al., 2017). Briefly, excised gel bands in 1.5 Eppendorf tubes are washed 4 times; first with 500 μL 60% acetonitrile containing 0.1%TFA and then with 5% acetic acid, then with 250 μL 50% H_2O/50% acetonitrile followed by a 250 μL 50% CH_3CN/ 50 mM NH_4HCO_3, and a final wash with 250 μL 50% CH_3CN/10 mM NH_4HCO_3 prior to removal of wash and complete drying of gel pieces in a Speed Vac. 10 μL of a 0.1 mg/mL stock solution of trypsin (Promega Trypsin Gold MS grade) in 5mM acetic acid is freshly diluted into a 140 μL solution of 10mM NH_4HCO_3 to make the working digestion solution. 124 μL of the working digestion solution is added to the dried gels pieces (additional 10 mM NH_4HCO_3 was added to ensure gel pieces are completely submerged in the digestion solution) and incubated at 37°C overnight. Sample is then stored at −20°C until analysis. Tryptic peptides were separated on a nanoAcquity UPLC column (Waters) coupled to a Q-Exactive Plus mass spectrometer. High resolution tandem LC MS/MS data were collected by Higher-Energy Collisional Dissociation (HCD) with a 1.4 Da window followed by normalized collision energy of 32%. Resulting LC MS/MS data were analyzed and processed through Proteome Discoverer (v.2.2 and linked to MASCOT search engine v.2.4) and further integrated with Scaffold (v.4.8, Proteome Software Inc.).

Behavioral experiments

Male FVB (WT) and $Fmr1^{-/y}$ mice 2 months of age were used for all experiments. All animal procedures were in accordance with US National Institutes of Health standards and approved by the Yale University Institutional Animal Care and Use Committee. Prior to behavioral testing mice were handled individually by the investigator to decrease anxiety. Next, mice received 3 IP injections of Dex (10 mg/kg) over the course of 40 hours: two injections separated by 24 hour period and the third 16 hours after the second injection. Behavioral testing started 2-3 hours after the last (third) injection. For repetitive behaviors (grooming and nestlet shredding) (Angoa-Pérez et al., 2013; Silverman et al., 2010) mice were placed in a new, empty home cage and their behavior was monitored during 10 minute sessions, video recorded and scored manually. Grooming was identified as body licking or stroking, scratching of the head or body with the two forelimbs. Attempts at grooming were defined as a total number of grooming events during the 10 minute session. For nestlet shredding mice were placed in a new empty home cage without bedding with one cotton nestlet and recorded for 10 minutes. Nestlet shreds were collected and weighed. Exploratory locomotion (total time moving, walking plus running) was assessed during a 5 minute session, recorded and scored manually (Baker et al., 2010; Dolan et al., 2013). The investigator was blinded as to the genetic variant during scoring.

QUANTIFICATION AND STATISTICAL ANALYSIS

Statistical analysis was performed using Prism 8 (GraphPad Software, San Diego, CA). Data are presented as mean ± SEM. Paired or unpaired Student's two-tailed t test was used for two group comparisons. For multiple comparisons, one-way or two-way ANOVA test with Tukey post hoc test was used. Statistical details and methods used in each experiment can be found in figures and in the figure legends. $p < 0.05$ is considered statistically significant. *p* values are provided in figure legends (*$p < 0.05$; **$p < 0.01$; ***$p < 0.001$; ****$p < 0.0001$).

Supplemental Figures

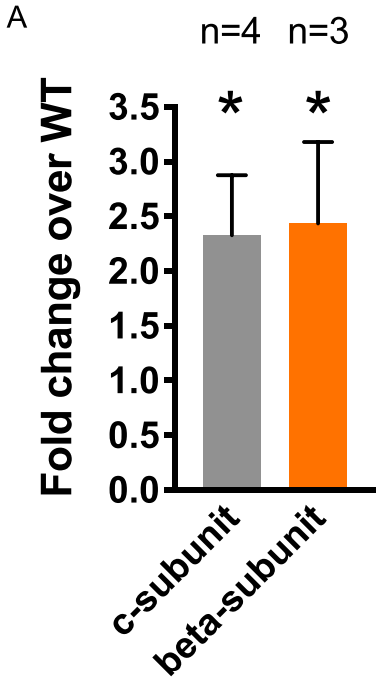

Figure S1. qRT-PCR Expression Profile of c-Subunit (ATP5G2) and β-Subunit mRNA from Synaptosomes, Related to Figures 2 and 5

Shown is fold change of *Fmr1*$^{-/y}$ over WT (n = 4 and 3 different animals, *p < 0.05). Unpaired two-tailed Student's t test was used. Data are represented as mean ± SEM (*p < 0.05; **p < 0.01; ***p < 0.001; ****p < 0.0001)

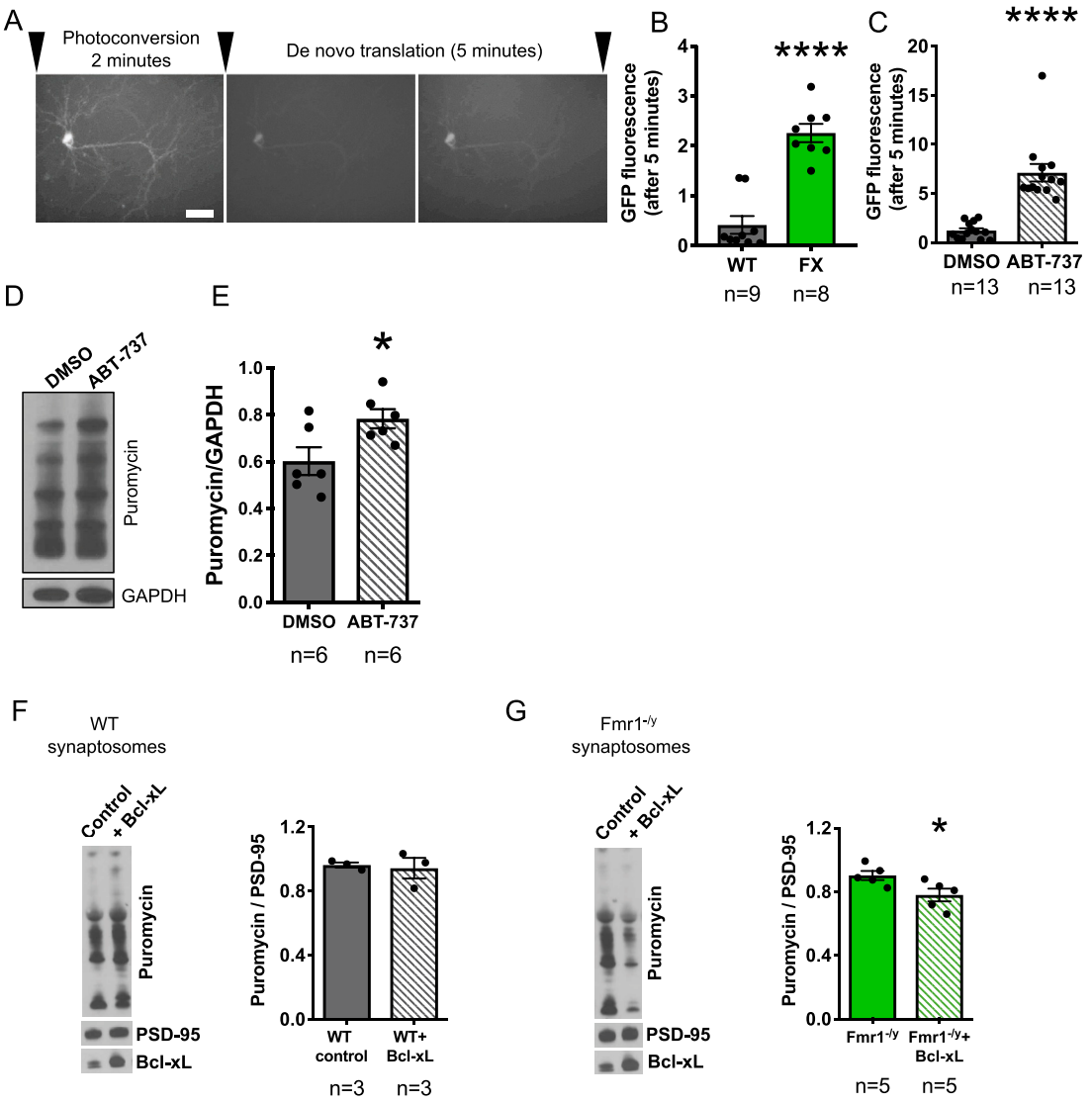

Figure S2. Protein Synthesis Rate Is Elevated in FX Neurons, Related to Figure 4

(A) Representative images of Dendra in isolated cortical neurons before, just after, and 5 minutes after photoconversion (see methods). (B) The rate of translation of Dendra during 5 min after photoconversion in WT and FX mouse neurons. (C) The rate of translation of Dendra in WT neurons exposed to vehicle (DMSO) or 1 μM Bcl-xL inhibitor, ABT-737 for 20 min. (D, E) Puromycin incorporation over 15 minutes in WT cortical neurons exposed to 1 μM ABT-737 or vehicle control (DMSO) for 1 hour prior to puromycin application. (F, G) Example of puromycin assay before and after transfection of recombinant Bcl-xL protein (0.045-0.79 mg/ml) into synaptosomes. Bcl-xL represses protein translation in FX but not in WT. (F) Group data for puromycin incorporation for WT control samples. (G) Group data for puromycin incorporation for FX samples from at least three different animals (*p = 0.037). Unpaired two-tailed Student's t test. Data are represented as mean ± SEM (*p < 0.05; **p < 0.01; ***p < 0.001; ****p < 0.0001)

Mitochondrion 51 (2020) 40–45

Contents lists available at ScienceDirect

Mitochondrion

journal homepage: www.elsevier.com/locate/mito

Perspective: Cell danger response Biology—The new science that connects environmental health with mitochondria and the rising tide of chronic illness

Robert K. Naviaux

Professor of Genetics, Departments of Medicine, Pediatrics, and Pathology, University of California, San Diego School of Medicine, 214 Dickinson Street, Building CTF, Room C107, San Diego, CA 92103, USA

A B S T R A C T

This paper is written for non-specialists in mitochondrial biology to provide access to an important area of science that has broad implications for all people. The cell danger response (CDR) is a universal response to environmental threat or injury. Once triggered, healing cannot be completed until the choreographed stages of the CDR are returned to an updated state of readiness. Although the CDR is a cellular response, it has the power to change human thought and behavior, child development, physical fitness and resilience, fertility, and the susceptibility of entire populations to disease. Mitochondria regulate the CDR by monitoring and responding to the physical, chemical, and microbial conditions within and around the cell. In this way, mitochondria connect cellular health to environmental health. Over 7,000 chemicals are now made or imported to the US for industrial, agricultural, and personal care use in amounts ranging from 25,000 to over 1 million pounds each year, and plastic waste now exceeds 83 billion pounds/year. This chemical load creates a rising tide of manmade pollutants in the oceans, air, water, and food chain. Fewer than 5% of these chemicals have been tested for developmental toxicity. In the 1980s, 5–10% of children lived with a chronic illness. As of 2018, 40% of children, 50% of teens, 60% of adults under age 65, and 90% of adults over 65 live with a chronic illness. Several studies now report the presence of dozens to hundreds of manmade chemicals and pollutants in placenta, umbilical cord blood, and newborn blood spots. New methods in metabolomics and exposomics allow scientists to measure thousands of chemicals in blood, air, water, soil, and the food chain. Systematic measurements of environmental chemicals can now be correlated with annual and regional patterns of childhood illness. These data can be used to prepare a prioritized list of molecules for congressional action, ranked according to their impact on human health.

"When a deep injury is done to us, we never heal until we forgive."
Nelson Mandela (1918–2013)

1. Introduction

Mitochondria sense and respond to changes in the cellular environment. By sensing safety and danger, mitochondria act as fundamental regulators of the cell danger response (CDR) (Naviaux, 2014). The CDR is an ancient and universal response to threat, stress, or injury. Mitochondria are uniquely suited to monitor the environmental and genetic conditions, and the gene-environment (ecogenetic) interactions that regulate the CDR. The mitochondrial proteome consists of about 1300 proteins (Calvo et al., 2016) that are transcriptionally and post-translationally regulated according to tissue-specific needs (Pagliarini et al., 2008), injury (Naviaux et al., 2009), infection (Wang et al., 2011), and presence or absence of environmental pollution (Winckelmans et al., 2017). Chemical, physical, and microbial changes that surround all multicellular life on Earth are translated into changes in mitochondrial structure and function. These changes in mitochondria are used to signal safety or danger in the cell, alter gene expression, trigger the healing response, and adjust fitness and susceptibility to chronic illness (Naviaux, 2019b). These changes even help to adjust the rate of aging in response to environmental stress (Naviaux, 2019a). The term CDR was originally coined to include all levels of the organismal response to stress, including inflammation, immunity, metabolism, microbiome, epigenetics, behavior and memory (Naviaux, 2014). Some aspects of the CDR are studied independently and called the integrated stress response (ISR) (Lu et al., 2004) and the mitochondrial ISR (Khan et al., 2017; Nikkanen et al., 2016; Silva et al., 2009).

When the CDR is triggered, the priorities of a multicellular organism are reset to optimize survival. The CDR is so fundamental to the survival of all living things, that the same core defenses of metabolism, inflammation, immunity, microbiome, brain function, sleep pattern and behavioral changes are activated by many different kinds of threats. These threats can be as diverse as an infection, poisoning, physical, or psychological trauma, and still trigger the same stereotyped sickness behavior (Shattuck and Muehlenbein, 2015). This stereotyped response to danger includes withdrawal from social contact, activation of innate immunity, decreased speech, fragmented sleep, head, muscle and abdominal aches, changes in the gut microbiome, and the increased

E-mail address: rnaviaux@health.ucsd.edu.

https://doi.org/10.1016/j.mito.2019.12.005
Received 2 November 2019; Received in revised form 11 December 2019; Accepted 16 December 2019
Available online 23 December 2019

sensitivity to touch, sound, and light that many people experience when they have the flu, or are recovering from a serious injury. It is the CDR that produces these familiar signs and symptoms (Naviaux, 2012, 2019b). At a cellular level, the cell danger response cannot be turned off until the cell receives the final "all clear" signal. Until then, the CDR remains stuck in a repeating loop that blocks further healing in an attempt to eradicate perceived danger. This can lead to long-term suffering, disability and chronic disease. Only when a cell perceives safety can it heal completely.

The concepts of cellular perception and reactivity are critical. Danger can be real or imagined. From the time we take our first breath, our genes are hard-wired to treat the world as a dangerous place, to anticipate a struggle to survive. When conditions become extreme, one cell can defend itself with powerful chemical weapons, while another may sacrifice itself to save its neighbors by activating a single-cell "self-destruct" sequence. The threshold for cellular reactivity is set by past environmental experience. The perception of safety leads to calm. Perception of danger leads to hypersensitivity.

2. Cellular safety

Organismal safety starts with cellular safety—a condition determined by access to adequate shelter and nutrients for growth and repair, effective management of intercurrent infections, absence of chemical, physical, and psychological trauma, and ample opportunities for healthy play. Sending a clear message of child safety early in life is essential for adult health. At a cellular level, anxiety is created when safety is not assured—when there is uncertainty about nutrient resources and support from neighboring cells, or about protection from exposure to a toxin or alarm signal. When cells are threatened, they behave the way nations do when they go to war. They harden their borders and don't trust their neighbors. The biophysical properties of membranes of cells undergoing the cell danger response change dramatically, leading to aggregation of patches of sphingolipids and cholesterol (Lingwood et al., 2008), membrane hardening, and the release of cellular ATP to signal danger and recruit cells needed to fight infection and heal (Burnstock, 2016). Cellular calm is created when environmental uncertainties are removed and the signals of health and safety are restored. It is now well known that a child raised in neglect or extreme adversity carries a lifelong risk of chronic illness and mental health struggles (Cameron et al., 2017). Social adversity can result in physical changes in brain development and other organs that can permanently change the trajectory of child development and can injure a child for life. What is only recently becoming known is that a rising tide of manmade chemicals and other changes to our environment are creating a similar impact on lifelong illness and mental health by threatening cellular safety. Children with chronic illness grow up to be adults with chronic illness. In the past 40 years, the fraction of children living with chronic disease in the United States has risen from approximately 5–10 percent in the 1980s, to 40 percent today. Rising teen depression, suicidal ideation, anxiety and behavioral mental health disorders add another 10–20 percent so that 50% of teens struggle with a chronic illness (Bethell et al., 2011). Sixty percent of adults under 65, and 90 percent of those over 65, now live with a chronic illness, a number that has doubled since the 1980s, and continues to grow (CDC.gov, 2017) (Fig. 1).

3. The economic cost of chronic illness

The United States now spends $2.8 trillion annually on medical care for children and adults with chronic conditions. This represents 86 percent of the $3.3 trillion US budget for health care. If the rising tide of chronic illness over the past 30 years continues unabated, the cost of health care in the US is projected to exceed $5.5 trillion by 2025, creating adverse effects that will derail economic prosperity not just in this country, but in many nations around the world (CDC.gov, 2017; CMS.gov, 2017; Khazan, March 15, 2019). What if a new approach to medicine were able to alleviate the suffering and the need for expensive medical care for just 10 percent of people with a chronic disorder? This new approach would return $280 billion (10 percent times $2.8 trillion) back into the US economy each year. This savings in a single year would surpass the annual budgets of the National Institutes of Health (NIH; $37 billion), the Environmental Protection Agency (EPA; $8.7 billion), the Food and Drug Administration (FDA; $5.1 billion) and the US Department of Agriculture (USDA; $151 billion) combined.

4. Chronic disease and the chemical World—the mixtures that make up the chemosphere

When viewed from far in space, Carl Sagan pointed out that the Earth appears as a pale blue dot (Sagan, 1997). A little closer, when viewed from the orbit of the International Space Station, the totality of livable space on our planet appears as a wispy thin layer of atmosphere, land, and ocean that scientists call the biosphere. Invisibly extending through and beyond the biosphere are the chemicals that make up both the living and non-living parts of the Earth. These chemicals are mingled with every drop of water, every breath of air in the skies, and adsorbed to particles of soil and sediments on land and sea. The chemical world on Earth is called the chemosphere.

The vast majority of the chemosphere is invisible to human eyes, tasteless, and odorless. The majority of what we "sense" of the chemosphere is through subconscious cellular responses to this invisible world that surrounds us. Tens of thousands of chemicals in the chemosphere are manmade and many are toxic even at low doses. Ultimately, the total load (Herbert and Weintraub, 2013)—the collective mixture—of both manmade and natural chemicals in the chemosphere, and other stresses in the biosphere helps determine the population risk of chronic illness. Recent studies have established that mixtures of chemicals can have deleterious effects on metabolism even when no single chemical is present in concentrations defined as "toxic" (Bonvallot et al., 2018). These findings have underscored a need for government agencies to revisit the guiding concepts in environmental toxicology called the "no observed adverse effect level" (NOAEL) and "lowest observed adverse effect level" (LOAEL), since low-level exposures to real-world mixtures of manmade chemicals can be toxic and produce chronic illness even at concentrations well below NOAEL.

Within every population there are sensitive and resistant individuals, and risk of harm is a probability, not a certainty for any given person. Resistant individuals can remain healthy despite exposure at one particular time, but then become vulnerable in another season or after a predisposing event at another time. In sensitive children and adults, whose cell danger response has been primed by a perfect storm of previous chemical, microbial, physical, and/or psychological stresses, the same levels of chemical or biotoxin burden produce pathological and prolonged metabolic, epigenetic, and physiologic responses. This hypersensitive response has two major effects: 1) it leads to disability and chronic illness, and 2) it interferes with the body's natural efforts to heal (Naviaux, 2019b).

5. Slow DNA and fast industries

The DNA of *Homo sapiens* changes slowly, and requires generations to adapt to the chemical changes around us. Common new diseases are not the result of mutations in our DNA, but the result of an environment that is changing faster than our genes can adapt. Although important, not even the rapid epigenetic changes regulated by mitochondria (Smiraglia et al., 2008) can fully rescue us from this problem. By evolutionary default, the cellular response to anything unknown or new is to first treat it as a threat. Repetitive activation of the cell danger response can lead to cellular mosaics in which healing has been slowed or incomplete (Naviaux, 2019a, b). In a rapidly changing world, our cells respond to so many chemicals that are new and threatening that it is

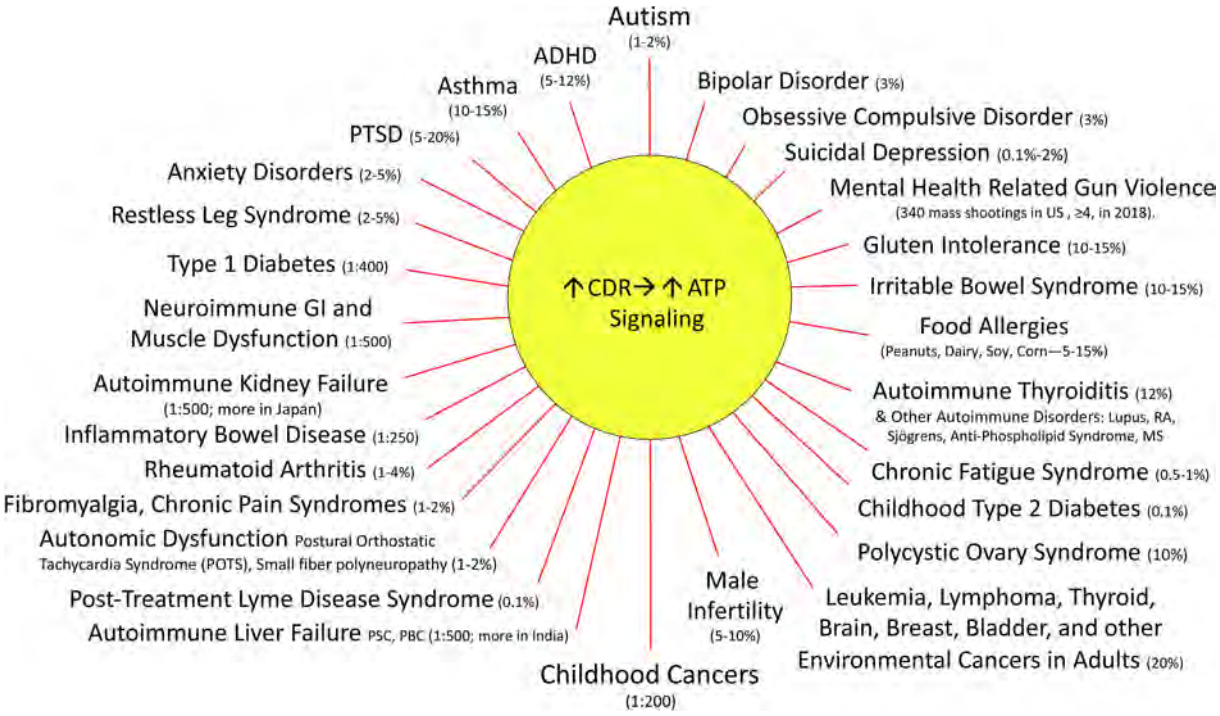

Fig. 1. Chronic Health Disorders that have Increased 2-100 times since the 1980s. Forty percent of children born in the US today and 60 percent of adults under 65 live with at least one chronic illness. ATP signaling is also known as purinergic signaling (Burnstock, 2018; Naviaux, 2018). **Abbreviations**: CDR, cell danger response; ATP, adenosine triphosphate; ASD, autism spectrum disorder; ADHD, attention deficit hyperactivity disorder; PTSD, post-traumatic stress disorder. Numbers reflect the population prevalence of each illness in the United States in 2018.

becoming increasingly difficult to heal completely after any common injury caused by the common cold, the flu, accidental poisoning, allergens or physical trauma. In much the same way that repeatedly ripping the scab from a skinned knee delays healing and leaves a scar, repeated exposure to a toxic world means that cellular safety and "all clear" signals are becoming harder to sustain. The absence of safety signals leaves a mark. Children and many adults are left in a state of primed hypersensitivity. New pesticides, plasticizers, antibiotics, food additives, dyes, solvents and other pollutants that our genome and our microbiomes have not yet evolved mechanisms to detoxify are entering our food chain, water supply and air like an invisible but poisonous chemical tide—a miasma of our own making.

6. Generational transmission

A study conducted by the Environmental Working Group in 2005 found that the umbilical cord blood of newborn babies in the United States already contained an average of 287 pesticides, pollutants and other environmental chemicals (Houlihan et al., 2005). The methods used at that time allowed the authors to look for 413 molecules from 9 different chemical classes. Other studies that have looked for a smaller number of pesticides or persistent organic pollutants have documented the presence of dozens of pollutants in newborn blood samples from around the world (Cabrera-Rodriguez et al., 2019; Silver et al., 2015). Similar pollutant loads have been documented in the placenta and found to change mitochondrial DNA content (Vriens et al., 2017). These studies show that when a child is born, they inherit a sample of their parents' chemical exposure history. Many chemicals are biomagnified in fat, bone and reproductive organs, accumulating over years of exposure to levels that can be hundreds of times higher than the concentration in any given environmental source of air, water or food (Drouillard et al., 2001). Many banned pesticides like DDT and industrial chemicals like PCBs can still be found in people decades later (Montano et al., 2013). If a child is born today with a burden of 300 manmade chemicals, in 25 years that child will add to their inherited burden by accumulating new toxic chemicals from their environment as they grow to reproductive maturity. As adults, they will then pass on a new sample of both their inherited and their newly-accumulated environmental chemicals to their children. If a net increase of 50 environmental pollutants occurs in the umbilical cord blood with each generation, and is added to the current number of 300, the toxic chemicals passed on to our children will soon have more devastating effects on human health than any mutation in DNA, leading to escalating infertility rates, miscarriages, childhood and adult chronic disease.

7. Increasing human impacts on the chemosphere and biosphere

The problem of environmental accumulation of toxic chemicals has been noted since the beginning of the industrial revolution in the 1700s, but has been accelerating since the rise of industrial scale farming and other large-scale industries since World War II. Rachel Carson was the first to call attention to the ecological effects of this accumulation in her landmark book *Silent Spring* (Carson, 1962), which first appeared in 1962. The title of her book referred to the decrease in the songs of birds in the spring because of pesticide accumulation in their food chain. Since that time, 30% of all birds in North America have been lost (Rosenberg et al., 2019). In 1962, the world's human population was 3.1 billion people. Today, the population is 7.7 billion and is growing at a rate of about 1% per year—about one billion people every decade. To glimpse the sheer magnitude of the ecological footprint of humans on the Earth, we need only look to the north Pacific Ocean to find a garbage patch of plastics and other manmade debris now twice the size of Texas, the exponential increase in plastic deposits in ocean floor sediments that has occurred since World War II (Brandon et al., 2019), or to the dying swaths of coral in the Great Barrier Reef (Kroon et al., 2016) the size of cities. The hopeful message is that by cleaning up pollution from the environment, the next generation can begin to off-load their inherited burden at a rate faster than they accumulate new toxins.

8. Canaries in the coal mine

Children are most susceptible to this menacing tide because their cells are growing rapidly and their metabolism, brain and endocrine systems are more sensitive to disruption. Children are like canaries in the coal mine—the first responders to environmental change. Many chemicals pass safely through adults, but strike our children during their periods of rapid growth in the womb and first few years of life, leaving them with chronic illnesses like asthma, attention deficit hyperactivity disorder (ADHD) and autism spectrum disorder (ASD). In the case of ASD, the prevalence has risen from 1 in 5000 (20 in 100,000) in the 1970s to 1 in 59 (1700 in 100,000; an 84-times increase) in 2014 (Baio and Investigators, 2018). It has been calculated that 60% of the apparent increase can be explained by changes in the diagnostic criteria for ASD over the past 40 years (Hansen et al., 2015). However, even with this conservative correction, the adjusted prevalence of ASD of 1 in 59 children today represents an absolute increase of 34 times ($84 \times 0.4 = 34$) from the 1970s (Fig. 1).

Chemical exposures in childhood can have many other lifelong effects, even when the same exposures in adults produce no obvious effect. A *Lancet* Commission study from 2016 reported that 940,000 children die each year around the world as the result of manmade pollution (Landrigan et al., 2018; Landrigan et al., 2019). This report also found that pollution was responsible for 9 million premature deaths each year—a number that continues to grow (Fuller et al., 2018; Martin and Landrigan, 2017). In addition to the deaths, which occur in only 1–10 percent of those exposed, it can be estimated that ten to hundred times these numbers—nearly 1 billion people around the world—are sickened annually from exposure to manmade pollution. For many, the illnesses caused by exposure to pollution will remain with them for the rest of their lives.

The persistent cell danger response caused by environmental chemical exposure has the power to change human thought and behavior. Because the brain controls metabolism (Naviaux et al., 2017; Naviaux et al., 2016; Naviaux et al., 2019), the persistent CDR that was originally triggered by mitochondria and reached the brain, feeds back on peripheral mitochondria using neuroendocrine and autonomic circuits from the brain, to amplify the cellular response to environmental change in an attempt to eradicate danger and restore safety. If the danger is not successfully eradicated, persistence of an activated CDR creates a cellular form of anxiety that can bubble up to create psychological anxiety and fear of change. In many people, the anxiety translates to a fear of strangers, outbursts of anger and violence, repetitive and obsessive-compulsive behaviors, and rigid imposition of past rules regardless of current circumstances in an effort to preserve the safety associated with earlier times. In others, the pervasive anxiety can lead to chronic pain, suffering, and drug addiction. I believe the rising tide of depression, suicide, gun violence, mental health issues, chronic pain and the opioid crisis reflects the changing set-point for the CDR in America. This new set-point creates a loss of past resilience to disease. The new set-point of the CDR is primed to react to smaller and smaller threats that arise by repeated exposures to a toxic mix of manmade chemicals, and acoustic and electromagnetic pollution in our increasingly industrialized cities, food chain, water and air.

9. A Second Book of Medicine

To treat the rising tide of chronic disease, a *Second Book of Medicine* is needed (Naviaux, 2019b). The *First Book of Medicine* contains the corpus of medical knowledge from the past 5,000 years of written history. From the *First Book of Medicine*, doctors learned how to treat acute illnesses caused by infections, poisonings and physical injuries. Typical acute illnesses last less than six months. The topic of the *Second Book of Medicine* will be the cause and treatment of chronic diseases that last longer than six months. In this book, a new chapter in pharmacology will be needed. A new class of medicines that might be called "armistice therapies" can now be developed (Naviaux, 2018). This new class of medicines will help doctors adjust the set-point of the CDR so it is no longer hypersensitive to chemicals and other threats that are below the threshold required to cause harm. The new medicines will help send the chemical message that the "war is over," allowing a child or adult struggling with a chronic illness to return to the "peace time" activities that permit healing, recovery and health. This new class of medicines will have fewer side effects than drugs from the *First Book of Medicine* because the new medicines will target biological processes that are most active under conditions of illness, when healing is incomplete. Once the illness or injury has healed, armistice medicines of the *Second Book of Medicine* will become inert because their targets will have receded or disappeared once health has been restored, and the use of adaptogens can help maintain and strengthen resilience (Panossian, 2017).

10. Environmental health for human health

Unfortunately, unless the environment can be cleaned up, and the repeated exposures to chemical, acoustic and electromagnetic triggers of the CDR are reduced, modern medicine will not be able to completely cure most chronic illnesses. Regular efforts to rejuvenate and heal by reconnecting with the natural world through walks in the park, or in a forest as is now prescribed in Japan as preventive medical care in the practice known as *shinrin yoku (*Miyazaki, 2018*)*, are steps in the right direction, but will not be able to hold back the tide. Incomplete healing occurs in part because many environmental chemicals block the body's ability to heal. Without restoring the environment, chronic illnesses will not heal completely, but will instead become relapsing-remitting disorders. Instead of putting a condition like a broken leg in the past—cast off, leg good as new—many people with chronic illness will remain at risk for recurrence throughout life. For example, a person who has recovered from diabetes would become a "recovering diabetic" for life, and someone with post-traumatic stress disorder (PTSD) who has been successfully treated and has recovered full function would still be at risk of relapse for the rest of their life.

Precision medicine will soon be able to use personal genome and serial metabolomic analysis to identify points of vulnerability in each person that might be strengthened with supplements, drugs, diet, exercise, restorative sleep and other measures. However, these advanced tools will only identify weak links in the personalized chain under tension. Ultimately, every chain has a breaking point. The ongoing accumulation of manmade changes in the environment is like a hydraulic winch that steadily adds tension to the chain of every citizen. Some chains will break before others, but ultimately, all living organisms are affected.

11. Toward sustainable health

Just as the body resets its priorities to face new threats that activate the cell danger response, nations of the world in the 21st century must reset their priorities to respond to new threats to our health caused by the changing chemistry and climate of our planet. Individual health must be given priority over corporate profit. Both are possible if both are valued equally and measures are taken to protect all the stakeholders. As part of this effort, it has been recommended that a portion of all land and ocean habitats be set aside in its natural state to preserve the biodiversity needed to recycle and purify the planet's water and air (Wilson, 2016). Without such actions, both profits and nations will fall as citizens sicken. New legislation is needed to regulate technological and industrial practices that promote safety and sustainability. The over-extraction and over-consumption of the Earth's resources and the discharge of pollutants into the environment can no longer be written off as economic "externalities" by industry and agriculture. Both resource usage and waste production need to be tracked with the same assiduous attention now paid to monetary profits. Governments of the

21st century must find ways to encourage all farms and businesses to comply with pollution-prevention standards to create a greener economy, and to financially reward businesses with the best sustainability practices.

Environmental protection agencies around the world must reinvigorate their mandate to monitor, record and remediate the crushing impact of the human footprint upon Earth's ecosystems, and minimize or prevent future impacts. If this doesn't happen, the consequences of political apathy, ignorance, or economic short-sightedness will be well-engrained, and Earth-scale processes thus set in motion will develop unstoppable momentum before we can finally agree there is a problem and can unite to make a change. In 2014, a study published in the *Proceedings of the National Academy of Sciences (USA)* found that 42 percent of lakes and rivers in Europe were already contaminated with enough chemicals to cause chronic illness in freshwater animals (Malaj et al., 2014). A similar study of waterways in the US has not yet been conducted. This failure to act has occurred in America despite early wakeup calls like the Cuyahoga river near Cleveland, Ohio catching fire several times from 1952 to 1969 because of industrial pollution, tap water igniting in Pennsylvania because of fracking (Tollefson, 2013), and harmful algal blooms from farm and city runoffs that create dead zones in rivers, lakes, and ocean fisheries that are decimating local economies (Diaz and Rosenberg, 2008; Grattan et al., 2016), making people sick, and are occurring more frequently each year.

Plastic waste in the US now exceeds 83 billion pounds/year (38 million metric tonnes) (Ritchie and Roser, 2018) and produces toxicity and impacts on human health by several mechanisms (Barboza et al., 2018; Wright and Kelly, 2017). Over 3,000 chemicals are made in or imported to the US in amounts over 1 million pounds per year (Landrigan and Landrigan, 2018). Another 4,000 are made in amounts over 25,000 lb per year. The rate of production of manmade pollutants now exceeds the rate at which the Earth can recycle them. This has led to a toxic rising tide that is entering ground water, soil, lakes, rivers, oceans, and the air. Fewer than 5% of these chemicals have been tested for their long-term effects on child development and health. Still thousands more are made in amounts less than 25,000 lb per year. These include widely-prescribed antibiotics, pharmaceuticals, hormones, and chemicals found in personal care products that are being found increasingly in our ground water and food chain (Bacanli and Basaran, 2019; Peng et al., 2014). Many of these manmade chemicals are biomagnified over years of exposure in our fat, bones, and reproductive organs to levels far above the concentration found in any single environmental source. If systematic scientific monitoring and recording, and regular reassessment of the chemistry of both people and the environment are not done, we will not have the tools to ward off the future of looming poor health. People around the world will fall prey to chronic illness in greater numbers; the land and seas will become disease-causing waste dumps; our faltering immune systems will make us vulnerable to untreatable microbial infections and disabling autoimmune diseases; new chronic and degenerative diseases will emerge; and the costs from illness and threats to our social fabric will bankrupt communities, states and nations.

12. The right to be born into a healthy environment

We often take for granted the freedoms afforded to us by good health. This must change, or thriving health will become rare, and plagues, wars and mental health struggles will become the new normal. If the activities of a nation poison its own people, then those activities must be changed. What is more important to the health of a nation than the health of its citizens? This question has motivated a call for a new constitutional amendment to invest each citizen with a new right: the right to be born and live in an environment that does not cause chronic disease. Readers can learn more at: http://naviauxlab.ucsd.edu/the-28th-amendment-project/.

Dedication

This work is dedicated to Olivia, a young lady with ASD whose spirit and imagination shine as a bright light of hope for children and families around the world.

Funding

This work was supported by foundation gifts from the UCSD Christini Fund, the Lennox Foundation, the UCSD Mitochondrial Research Fund, the JMS Fund, the N of One Foundation, the Autism Research Institute, the Open Medicine Foundation, the Khosla Foundation, the Westreich Foundation, and the Malone Foundation, and philanthropic support from Aloe family, the Harb family, Marc Spilo and contributors to the Aloe Family Autism Research Fund, Linda Clark, Jeanne Conrad, Josh Spears, David Cannistraro, the Kirby and Katie Mano Family, Simon and Evelyn Foo, Wing-kun Tam, Gita and Anurag Gupta, the Brent Kaufman Family, the Daniel and Kelly White Family, and grassroots support from over 2000 individuals from around the world who have each provided gifts in the past year to support Naviaux Lab research. Funding for the mass spectrometers was provided by a gift from the Jane Botsford Johnson Foundation.

Acknowledgments

RKN thanks the many families with primary mitochondrial disease, autism spectrum disorder (ASD), myalgic encephalomyelitis/chronic fatigue syndrome (ME/CFS), and healthy control volunteers who have helped make this research possible. RKN also thanks Neil Nathan, Eric Gordon, Liz Mumper, Nancy O'Hara, Scott Lafee, John Green, David Kaufman, John Rodakis, Christabelle Yeoh, and Maya Shetreat-Klein for comments on the manuscript.

Conflicts of Interest

RKN is an unpaid scientific advisory board member for the Autism Research Institute (ARI), the Open Medicine Foundation (OMF), and Yuva Biosciences. Financial supporters for this study had no role in the design, data analysis, interpretation, writing, or publication of this work.

References

Bacanli, M., Basaran, N., 2019. Importance of antibiotic residues in animal food. Food Chem. Toxicol. 125, 462–466.

Baio, J., Investigators, D.D.M.N.S.Y.P., 2018. Prevalence of Autism Spectrum Disorder Among Children Aged 8 Years — Autism and Developmental Disabilities Monitoring Network, 11 Sites, United States, 2014. MMWR CDC Surveill Summ 67, pp. 1–28.

Barboza, L.G.A., Dick Vethaak, A., Lavorante, B., Lundebye, A.K., Guilhermino, L., 2018. Marine microplastic debris: an emerging issue for food security, food safety and human health. Mar. Pollut. Bull. 133, 336–348.

Bethell, C.D., Kogan, M.D., Strickland, B.B., Schor, E.L., Robertson, J., Newacheck, P.W., 2011. A national and state profile of leading health problems and health care quality for US children: key insurance disparities and across-state variations. Acad. Pediatr. 11, S22–S33.

Bonvallot, N., Canlet, C., Blas, Y.E.F., Gautier, R., Tremblay-Franco, M., Chevolleau, S., Cordier, S., Cravedi, J.P., 2018. Metabolome disruption of pregnant rats and their offspring resulting from repeated exposure to a pesticide mixture representative of environmental contamination in Brittany. PloS one 13, e0198448.

Brandon, J.A., Jones, W., Ohman, M.D., 2019. Multidecadal increase in plastic particles in coastal ocean sediments. Sci. Adv. 5, eaax0587.

Burnstock, G., 2016. An introduction to the roles of purinergic signalling in neurodegeneration, neuroprotection and neuroregeneration. Neuropharmacology 104, 4–17.

Burnstock, G., 2018. The therapeutic potential of purinergic signalling. Biochem. Pharmacol. 151, 157–165.

Cabrera-Rodriguez, R., Luzardo, O.P., Almeida-Gonzalez, M., Boada, L.D., Zumbado, M., Acosta-Dacal, A., Rial-Berriel, C., Henriquez-Hernandez, L.A., 2019. Association between prenatal exposure to multiple persistent organic pollutants (POPs) and growth indicators in newborns. Environ. Res. 171, 285–292.

Calvo, S.E., Clauser, K.R., Mootha, V.K., 2016. MitoCarta2.0: an updated inventory of mammalian mitochondrial proteins. Nucleic Acids Res. 44, D1251–D1257.

Cameron, J.L., Eagleson, K.L., Fox, N.A., Hensch, T.K., Levitt, P., 2017. Social origins of

developmental risk for mental and physical illness. J. Neurosci. 37, 10783–10791 The official journal of the Society for Neuroscience.
Carson, R., 1962. Silent Spring. Houghton Mifflin Company, New York, NY.
CDC.gov, 2017. Chronic Disease Overview. National Center for Chronic Disease Prevention and Health Promotion, Atlanta, GA.
CMS.gov, 2017. 2016–2025 projections of national health expenditures data released. In: Services, C.f.M.M. (Ed.), Baltimore, MD.
Diaz, R.J., Rosenberg, R., 2008. Spreading dead zones and consequences for marine ecosystems. Science 321, 926–929.
Drouillard, K.G., Fernie, K.J., Smits, J.E., Bortolotti, G.R., Bird, D.M., Norstrom, R.J., 2001. Bioaccumulation and toxicokinetics of 42 polychlorinated biphenyl congeners in American kestrels (Falco sparverius). Environ. Toxicol. Chem. 20, 2514–2522.
Fuller, R., Rahona, E., Fisher, S., Caravanos, J., Webb, D., Kass, D., Matte, T., Landrigan, P.J., 2018. Pollution and non-communicable disease: time to end the neglect. Lancet Planet Health 2, e96–e98.
Grattan, L.M., Holobaugh, S., Morris Jr., J.G., 2016. Harmful algal blooms and public health. Harmful Algae 57, 2–8.
Hansen, S.N., Schendel, D.E., Parner, E.T., 2015. Explaining the increase in the prevalence of autism spectrum disorders: the proportion attributable to changes in reporting practices. JAMA Pediatr. 169, 56–62.
Herbert, M., Weintraub, K., 2013. The Autism Revolution: Whole-Body Strategies for Making Life All It Can Be. Ballantine Books.
Houlihan, J., Kropp, T., Wiles, R., Gray, S., Campbell, C., 2005. Body Burden—The Pollution in Newborns a Benchmark Investigation of Industrial Chemicals, Pollutants, and Pesticides in Umbilical Cord Blood. Environmental Working Group, Washington, DC.
Khan, N.A., Nikkanen, J., Yatsuga, S., Jackson, C., Wang, L., Pradhan, S., Kivela, R., Pessia, A., Velagapudi, V., Suomalainen, A., 2017. mTORC1 regulates mitochondrial integrated stress response and mitochondrial myopathy progression. Cell Metab. 26 (419–428), e415.
Khazan, O., March 15, 2019. Americans are going bankrupt from getting sick. The Atlantic, Washington, DC.
Kroon, F.J., Thorburn, P., Schaffelke, B., Whitten, S., 2016. Towards protecting the Great Barrier Reef from land-based pollution. Glob. Chang. Biol. 22, 1985–2002.
Landrigan, P.J., Fuller, R., Acosta, N.J.R., Adeyi, O., Arnold, R., Basu, N.N., Balde, A.B., Bertollini, R., Bose-O'Reilly, S., Boufford, J.I., Breysse, P.N., Chiles, T., Mahidol, C., Coll-Seck, A.M., Cropper, M.L., Fobil, J., Fuster, V., Greenstone, M., Haines, A., Hanrahan, D., Hunter, D., Khare, M., Krupnick, A., Lanphear, B., Lohani, B., Martin, K., Mathiasen, K.V., McTeer, M.A., Murray, C.J.L., Ndahimananjara, J.D., Perera, F., Potocnik, J., Preker, A.S., Ramesh, J., Rockstrom, J., Salinas, C., Samson, L.D., Sandilya, K., Sly, P.D., Smith, K.R., Steiner, A., Stewart, R.B., Suk, W.A., van Schayck, O.C.P., Yadama, G.N., Yumkella, K., Zhong, M., 2018. The Lancet Commission on pollution and health. Lancet 391, 462–512.
Landrigan, P.J., Fuller, R., Fisher, S., Suk, W.A., Sly, P., Chiles, T.C., Bose-O'Reilly, S., 2019. Pollution and children's health. Sci. Total Environ, 650, 2389–2394.
Landrigan, P.J., Landrigan, M.M., 2018. Children and Environmental Toxins—What Everyone Needs to Know. Oxford University Press, New York, NY.
Lingwood, D., Ries, J., Schwille, P., Simons, K., 2008. Plasma membranes are poised for activation of raft phase coalescence at physiological temperature. Proc. Natl. Acad. Sci. U.S.A 105, 10005–10010.
Lu, P.D., Harding, H.P., Ron, D., 2004. Translation reinitiation at alternative open reading frames regulates gene expression in an integrated stress response. J. Cell Biol. 167, 27–33.
Malaj, E., von der Ohe, P.C., Grote, M., Kuhne, R., Mondy, C.P., Usseglio-Polatera, P., Brack, W., Schafer, R.B., 2014. Organic chemicals jeopardize the health of freshwater ecosystems on the continental scale. Proc. Natl. Acad. Sci. U.S.A 111, 9549–9554.
Martin, K., Landrigan, P.J., 2017. Healthy people, healthy ecosystems. Ann. Glob. Health 83, 1–2.
Miyazaki, Y., 2018. Shinrin Yoku—The Japanese Art of Forest Bathing. Timber Press, Portland, OR.
Montano, M., Gutleb, A.C., Murk, A.J., 2013. Persistent toxic burdens of halogenated phenolic compounds in humans and wildlife. Environ. Sci. Technol. 47, 6071–6081.
Naviaux, R.K., 2012. Oxidative shielding or oxidative stress? J. Pharmacol. Exp. Ther. 342, 608–618.
Naviaux, R.K., 2014. Metabolic features of the cell danger response. Mitochondrion 16, 7–17.
Naviaux, R.K., 2018. Antipurinergic therapy for autism-An in-depth review. Mitochondrion 43, 1–15.
Naviaux, R.K., 2019a. Incomplete healing as a cause of aging: the role of mitochondria and the cell danger response. Biology (Basel) 8, 8.
Naviaux, R.K., 2019b. Metabolic features and regulation of the healing cycle-A new model for chronic disease pathogenesis and treatment. Mitochondrion 46, 278–297.
Naviaux, R.K., Curtis, B., Li, K., Naviaux, J.C., Bright, A.T., Reiner, G.E., Westerfield, M., Goh, S., Alaynick, W.A., Wang, L., Capparelli, E.V., Adams, C., Sun, J., Jain, S., He, F., Arellano, D.A., Mash, L.E., Chukoskie, L., Lincoln, A., Townsend, J., 2017. Low-dose suramin in autism spectrum disorder: a small, phase I/II, randomized clinical trial. Ann. Clin. Transl. Neurol. 4, 491–505.
Naviaux, R.K., Le, T.P., Bedelbaeva, K., Leferovich, J., Gourevitch, D., Sachadyn, P., Zhang, X.M., Clark, L., Heber-Katz, E., 2009. Retained features of embryonic metabolism in the adult MRL mouse. Mol. Genet. Metab. 96, 133–144.
Naviaux, R.K., Naviaux, J.C., Li, K., Bright, A.T., Alaynick, W.A., Wang, L., Baxter, A., Nathan, N., Anderson, W., Gordon, E., 2016. Metabolic features of chronic fatigue syndrome. Proc. Natl. Acad. Sci. U.S.A. 113, E5472–E5480.
Naviaux, R.K., Naviaux, J.C., Li, K., Wang, L., Monk, J.M., Bright, A.T., Koslik, H.J., Ritchie, J.B., Golomb, B.A., 2019. Metabolic features of Gulf War illness. PloS one 14, e0219531.
Nikkanen, J., Forsstrom, S., Euro, L., Paetau, I., Kohnz, R.A., Wang, L., Chilov, D., Viinamaki, J., Roivainen, A., Marjamaki, P., Liljenback, H., Ahola, S., Buzkova, J., Terzioglu, M., Khan, N.A., Pirnes-Karhu, S., Paetau, A., Lonnqvist, T., Sajantila, A., Isohanni, P., Tyynismaa, H., Nomura, D.K., Battersby, B.J., Velagapudi, V., Carroll, C.J., Suomalainen, A., 2016. Mitochondrial DNA replication defects disturb cellular dNTP pools and remodel one-carbon metabolism. Cell Metab. 23, 635–648.
Pagliarini, D.J., Calvo, S.E., Chang, B., Sheth, S.A., Vafai, S.B., Ong, S.E., Walford, G.A., Sugiana, C., Boneh, A., Chen, W.K., Hill, D.E., Vidal, M., Evans, J.G., Thorburn, D.R., Carr, S.A., Mootha, V.K., 2008. A mitochondrial protein compendium elucidates complex I disease biology. Cell 134, 112–123.
Panossian, A., 2017. Understanding adaptogenic activity: specificity of the pharmacological action of adaptogens and other phytochemicals. Ann. N.Y. Acad. Sci. 1401, 49–64.
Peng, X., Ou, W., Wang, C., Wang, Z., Huang, Q., Jin, J., Tan, J., 2014. Occurrence and ecological potential of pharmaceuticals and personal care products in groundwater and reservoirs in the vicinity of municipal landfills in China. Sci. Total Environ. 490, 889–898.
Ritchie, H., Roser, M., 2018. Plastic pollution. https://ourworldindata.org/plastic-pollution.
Rosenberg, K.V., Dokter, A.M., Blancher, P.J., Sauer, J.R., Smith, A.C., Smith, P.A., Stanton, J.C., Panjabi, A., Helft, L., Parr, M., 2019. Decline of the North American avifauna. Science eaaw1313.
Sagan, C., 1997. Pale Blue Dot: A Vision of the Human Future in Space. Random House Digital Inc.
Shattuck, E.C., Muehlenbein, M.P., 2015. Human sickness behavior: ultimate and proximate explanations. Am. J. Phys. Anthropol. 157, 1–18.
Silva, J.M., Wong, A., Carelli, V., Cortopassi, G.A., 2009. Inhibition of mitochondrial function induces an integrated stress response in oligodendroglia. Neurobiol. Dis. 34, 357–365.
Silver, M.K., Shao, J., Chen, M., Xia, Y., Lozoff, B., Meeker, J.D., 2015. Distribution and predictors of pesticides in the umbilical cord blood of Chinese newborns. Int. J. Environ. Res. Public Health 13.
Smiraglia, D.J., Kulawiec, M., Bistulfi, G.L., Gupta, S.G., Singh, K.K., 2008. A novel role for mitochondria in regulating epigenetic modification in the nucleus. Cancer Biol. Ther. 7, 1182–1190.
Tollefson, J., 2013. Gas drilling taints groundwater. Nature 498, 415–416.
Vriens, A., Nawrot, T.S., Baeyens, W., Den Hond, E., Bruckers, L., Covaci, A., Croes, K., De Craemer, S., Govarts, E., Lambrechts, N., Loots, I., Nelen, V., Peusens, M., De Henauw, S., Schoeters, G., Plusquin, M., 2017. Neonatal exposure to environmental pollutants and placental mitochondrial DNA content: a multi-pollutant approach. Environ. Int. 106, 60–68.
Wang, C., Liu, X., Wei, B., 2011. Mitochondrion: an emerging platform critical for host antiviral signaling. Exp. Opin. Ther. Targets 15, 647–665.
Wilson, E.O., 2016. Half-Earth: Our Planet's Fight for Life. WW Norton & Company.
Winckelmans, E., Nawrot, T.S., Tsamou, M., Den Hond, E., Baeyens, W., Kleinjans, J., Lefebvre, W., Van Larebeke, N., Peusens, M., Plusquin, M., Reynders, H., Schoeters, G., Vanpoucke, C., de Kok, T.M., Vrijens, K., 2017. Transcriptome-wide analyses indicate mitochondrial responses to particulate air pollution exposure. Environ. Health: Global Access Sci. Source 16, 87.
Wright, S.L., Kelly, F.J., 2017. Plastic and human health: a micro issue? Environ. Sci. Technol. 51, 6634–6647.

[Cancer Biology & Therapy 7:8, 1191-1193; August 2008]; ©2008 Landes Bioscience

Commentary

Mitochondrial control of epigenetics

Robert K. Naviaux

The Mitochondrial and Metabolic Disease Center; University of California; San Diego, California USA

Key words: mitochondrial DNA copy number, mtDNA depletion, DNA methylation, cancer epigenetics, folate metabolism, S-Adenosyl methionine (SAM) metabolism

It has become increasingly clear in recent years that a complete knowledge of the sequence of DNA in the germline of an individual is insufficient to predict the gene expression pattern and metabolism found in somatic cells. Within 5–10 years, DNA sequencing technologies will have advanced to the point that the full 6 x 10^9 base pairs of diploid nuclear DNA (nDNA), in addition to the 16,569 base pairs of inherited mitochondrial DNA (mtDNA), can be determined for an individual in just a few days. Yet this information will not allow us to predict why certain genes are expressed and regulated for example, in a cardiac myocyte, and not in a skin fibroblast, or not in any of the other roughly 350 different somatic cell types.

Several types of epigenetic characteristics are known that distinguish somatic cells. Two of these are nuclear DNA methylation and mtDNA copy number. The first occurs in the nucleus and is qualitative. The second occurs in the cytoplasm—in mitochondria—and is quantitative. Over 150 tissue-specific nuclear DNA methylation sites have been identified.[1] The quantity of mitochondrial DNA per cell (the mtDNA copy number) is regulated in a tissue-specific manner and can be as high as 6970 copies per cell in the heart,[2] and as low as 120 copies per cell in a skin fibroblast.[3]

Until now, no experimental evidence existed that linked these two classes of epigenetic change. The fields of nuclear DNA methylation and mitochondrial DNA copy number regulation evolved along independent paths for nearly 20 years. Both produce tissue-specific differences in nuclear gene expression,[4,5] and both help to set the metabolic phenotype of the cell.[6,7] Both are clinically relevant. Epigenetic changes in nuclear DNA correlate with poor cancer survival.[8] And low copy numbers of mtDNA in breast cancer correlate with poor survival.[9] The communication between mitochondria and the nucleus is bidirectional. The genetic elements of the signaling pathways from mitochondria to the nucleus are called the retrograde response.[10]

Correspondence to: Robert K. Naviaux; The Mitochondrial and Metabolic Disease Center; University of California; San Diego; 214 Dickinson St.; Bldg. CTF; Rm. C103; San Diego, California 92103-8467 USA; Tel.: 619.543.2904; Email: naviaux@ucsd.edu

Submitted: 06/27/08; Accepted: 08/04/08

Previously published online as a *Cancer Biology & Therapy* E-publication: http://www.landesbioscience.com/journals/cbt/article/6741

Commentary to: Smiraglia DJ, Kulawiec M, Bistulfi GL, Gupta SG, Singh KK. A novel role for mitochondria in regulating epigenetic modification in the nucleus. Can Biol Ther 2008; This Issue.

Mitochondria and Nuclear Gene Methylation

The role of mtDNA copy number as a component of retrograde signaling from mitochondria to the nucleus as now been addressed in a paper by Smiraglia, et al. in this issue of *Cancer Biology & Therapy.*[11] This paper brings into sharp focus the finding that mtDNA copy number strongly influences nuclear DNA methylation patterns. The authors report their observations in four cell types; a breast epithelial cell line and three different cancer cell lines from melanoma, breast and bone cancers, and their respective daughter cell lines derived by the removal of mtDNA. Cells that lack mtDNA are called rho zero (ρ^0) cells. Rho zero cells have mitochondria, but lack the 13 polypeptides, 22 tRNAs, and 2 rRNAs normally produced by mtDNA and required for aerobic energy metabolism by mitochondrial oxidative phosphorylation. Rho zero cells are readily grown glycolytically in glucose-containing media supplemented with pyruvate and uridine. The ρ^0 cell requirement for uridine (uridine auxotrophy) occurs because the 4th step of de novo pyrimidine synthesis requires the enzyme dihydroorotate CoQ10 oxidoreductase (DHO-QO, EC 1.3.99.11), also known as dihydroorotate dehydrogenase (DHOD, EC 1.3.3.1). This enzyme is located on the outer leaflet of the inner mitochondrial membrane in animal cells.[12] It is a widely underappreciated fact of mitotic cell metabolism that all de novo synthesis of pyrimidines—all the rUs and rCs for RNA synthesis and other reactions, and all the dTs and dCs for DNA synthesis—require a functional mitochondrial electron transport chain to provide the oxidized form of CoQ10 needed to accept electrons from dihydroorotate (DHO) as it is oxidized by DHOD to synthesize orotic acid. Orotic acid is converted to UMP by UMP synthase, and UMP is the ultimate source of all de novo pyrimidines.

Another important contribution of mitochondria to the cell is folate metabolism and regulation of the metabolic switch between S-adenosyl methionine (SAM) synthesis and nucleotide synthesis. This dance between mitochondrial and cytosolic folate metabolism is called the One-Carbon Cycle (Fig. 1).[13] The behavior of this highly coordinated metabolic network and its connection to glutathione metabolism has recently been modeled.[14,15] The mitochondrial bifunctional enzyme (MBE, Fig. 1) is turned off in differentiated cells.[16] This has the effect of increasing methylene tetrahydrofolate (methylene-THF) pools and diverting one-carbon units away from formate and nucleotide synthesis and toward SAM and glutathione synthesis. SAM is required as a methyl donor for nearly a dozen different methylation reactions, including athe epigenetic methylation of cytosine residues in CpG islands of nuclear DNA. In embryonic cells and cancer, MBE remains active and one-carbon

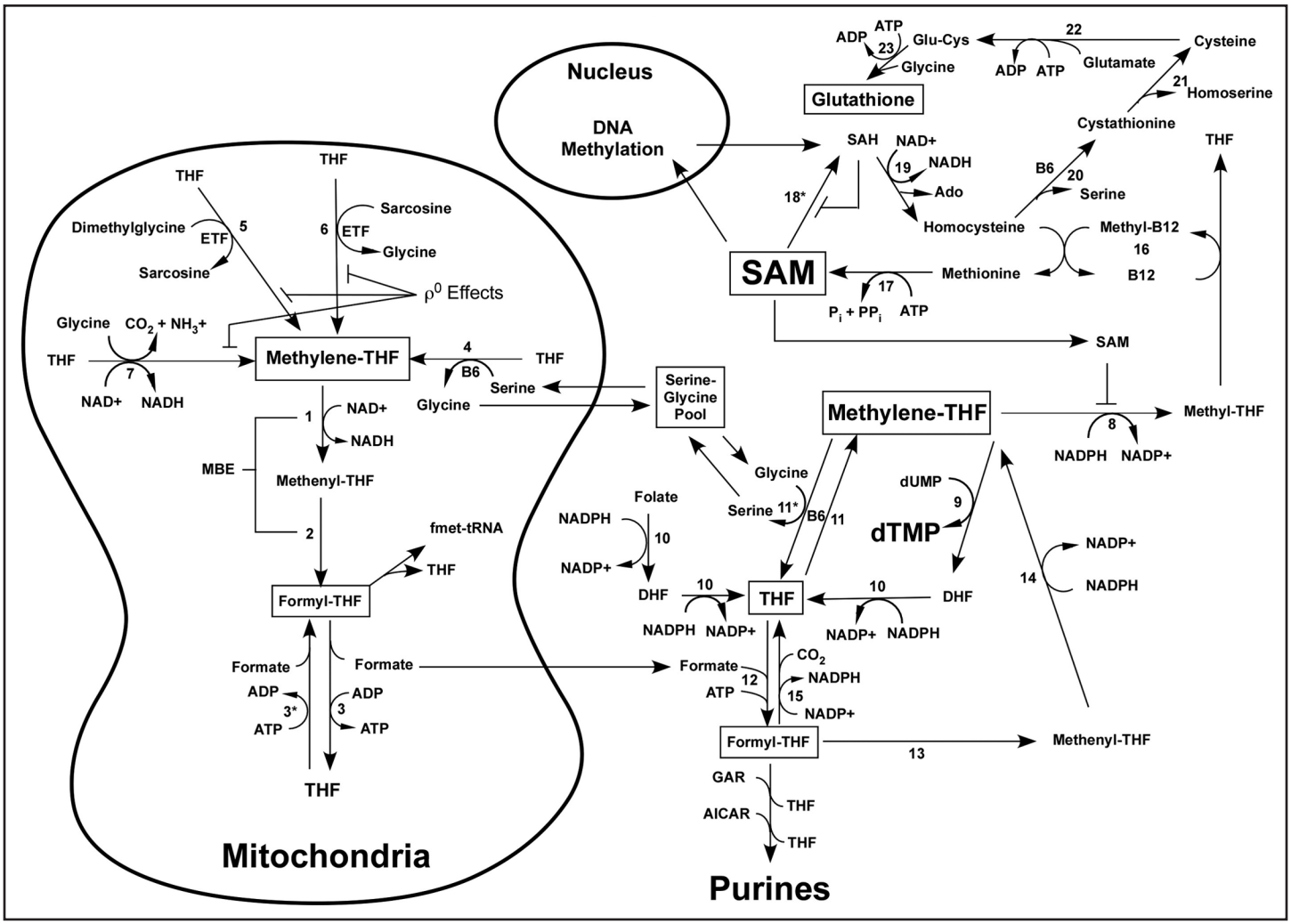

Figure 1. The Connection Between Mitochondrial Folate Metabolism, Redox, and Nuclear DNA Methylation. In cancer and embryonic cells, MBE (enzyme activities #1 and 2 are present in a single polypeptide) is expressed and one-carbon units are efficiently converted to Formyl-THF and formate for cytosolic nucleotide synthesis. Under these conditions, fewer one-carbon units are available for SAM synthesis and DNA methylation. Mitochondrial DNA (mtDNA) depletion has a similar effect, but one that is redox-coupled. When mtDNA is reduced or removed, as in rho zero cells and some cancers, the redox-dependent steps in mitochondria (enzymes 5, 6 and 7) are slowed. This leads to reduced SAM synthesis and reduced DNA methylation (see text). When MBE is turned off in differentiated cells, less mitochondrial formate is produced, and one-carbon units are directed through Methylene-THF toward increased SAM synthesis and increased DNA methylation. Abbreviations: 1/2–Mitochondrial Bifunctional Enzyme–MBE (1–NAD+ Dependent Methylene Tetrahydrofolate Reductase, 2–Methenyl-THF Cyclohydrolase), 3–Formyl-THF Synthase (FTS), 3*–FTS can reverse directions in differentiated cells when MBE is turned off, 4–Mitochondrial Serine Hydroxymethyl Transferase (mSHMT), 5–Dimethylglycine Dehydrogenase, ETF–Electron Transfer Flavoprotein, 6–Sarcosine Dehydrogenase, 7–Glycine Cleavage System, 8–Methylene-THF Reductase (MTFR), 9–Thymidylate Synthase, 10–Dihydrofolate Reductase (DHFR), 11–Cytosolic Serine Hydroxymethyl Transferase (cSHMT), 11*–cSHMT reverse reaction, 12/13/14–Cytosolic Trifunctional Enzyme (12–Formyl-THF Synthase, 13–Methenyl-THF Cyclohydrolase, 14–NADPH-dependent Methylene-THF Dehydrogenase), 15–Formyl-THF Dehydrogenase, 16–Homocysteine Methyl Transferase (Methionine Synthase), 17–Methionine Adenosyl Transferase (MAT), 18*–Multiple DNA-, RNA-, Protein–, and Other Methyltransferase reactions in the nucleus, cytosol, and mitochondria, 19–S-Adenosyl Homocysteine Hydrolase (SAHH), 20–Cystathionine β-Synthase (CBS), 21–Cystathionase, 22–γ-Glutamylcysteine Synthase (GCS), 23–Glutathione Synthase, GAR–Glycinamide Ribonucleotide, AICAR–Aminoimidazole Carboxamide Ribonucleotide, Ado–Adenosine.

units are diverted to nucleotide synthesis, with fewer carbons being used for SAM synthesis. MBE is also active in ρ^0 cells, however, the flux of one-carbon units is strongly influenced by the propagating redox effect produced by the removal of mitochondrial DNA.

The removal of mtDNA causes a decrease in mitochondrial NADH oxidation to NAD^+, and a decrease in the oxidation of ETF, while stimulating cytosolic glycolysis and lactate production. The increased NADH/NAD^+ ratio limits the redox-coupled conversion of THF to methylene-THF by mitochondrial dehydrogenases (enzymes 5, 6 and 7 in Fig. 1) and increases the flux of serine through the non-redox-coupled mitochondrial serine hydroxymethyl transferase (mSHMT, enzyme 4, Fig.1) in order to meet the mitochondrial demand for methylene-THF. This has two propagating effects in the cytosol. The first is to draw cytosolic serine into mitochondria and slow the normal forward reaction rate of the cytosolic form of SHMT (enzyme 11, Fig. 1). This leads to increased pools of cytosolic THF. The second effect of the increased mitochondrial NADH/NAD^+ ratio is a cascading effect to increase the

NADH/NAD+ and NADPH/NADP+ ratios in the cytoplasm, drawing one-carbon units away from Methyl-THF and SAM synthesis, and toward THF and Formyl-THF for nucleotide synthesis (Fig. 1). The increased NADH/NAD+ ratio in the cytosol will also limit the conversion of S-Adenosyl Homocysteine (SAH) to homocysteine by the NAD+ dependent SAH-hydrolase (SAHH, enzyme 19, Fig. 1). SAH is a potent feedback inhibitor of many methyl-transferases, and would be expected to further limit DNA methylation under these more reducing cytosolic conditions. The unutilized SAM is a feedback inhibitor of its own synthesis via carbon entry at the Methylene-THF Reductase step (enzyme 8, Fig. 1). This scheme illustrates how mitochondria are at the heart of a metabolic switch between cell differentiation, DNA methylation, reduced de novo nucleotide synthesis, and cell cycle arrest on the one hand, and dedifferentiation, demethylation, increased de novo nucleotide synthesis, and cell cycle entry on the other (Fig. 1).

Smiraglia, et al. use the technique of Restriction Landmark Genome Scanning (RLGS)[17] with the methylation-sensitive enzyme NotI, which recognizes the sequence GCGGCCGC, to show that up to 64 sites of hypomethylation and 50 sites of hypermethylation are produced by the removal of mtDNA from the four different cell lines. The methylation changes affected 2–9% of the CpG regions surveyed. This is comparable to the 2–5% changes in methylation that distinguish the epigenomes of different tissues.[1,4] In a control set of experiments, Smiraglia, et al. reintroduced the original mtDNA into the 143B osteosarcoma ρ^0 cells to create a cybrid line for examining the reversibility of the 22 epigenetic changes that were found after the removal of mtDNA and subsequent selection. When mtDNA was removed, hypomethylation events outnumbered hypermethylation events 3-to-1, similar to the loss of imprinting (LOI) events associated in increased tumorigenesis.[18] Seventeen ρ^0 sites became hypomethylated, and five sites became methylated. After replacement of mtDNA, all five of the newly-methylated sites remained methylated, and 12 of 17 (70%) of the hypomethylated sites remained hypomethylated. Only 5 of the 17 hypomethylated sites (30%) were remethylated after the reintroduction of mtDNA.

These data show that the epigenetic changes produced by reduction or loss of mitochondrial DNA in cancer cells are complex, widespread, and only partially reversible with the reintroduction of mtDNA. This latter observation suggests that the arrow of molecular evolution and selection in these types of cancer is largely unidirectional, and punctuated by steps with cascading effects before a new steady-state is achieved. The relative irreversibility of time's arrow, and of the myriad metabolic, genetic and epigenetic changes produced by mtDNA copy number reduction in cancer cells captures at the cellular level, the principle of Dollo's Law of irreversibility in evolutionary biology first published in 1893.[19] Dollo's Law reflects the statistical fact that when the historical contingencies of time, variation and selection produce a myriad of coordinated changes, each with cascading effects, the probability of exactly retracing the steps that led to the current steady-state of life is astronomically remote.

Conclusion

Smiraglia, et al. bring the importance of mitochondrial DNA copy number into crisp relief, showing that mtDNA copy number changes have a profound effect on the methylation pattern of nuclear genes.

Acknowledgements

R.K.N. thanks Dr. Fred Nijhout and Dr. Bob Mackenzie for helpful comments.

References

1. Song F, et al. Association of tissue-specific differentially methylated regions (TDMs) with differential gene expression. Proc Natl Acad Sci USA 2005; 102:3336-41.
2. Miller FJ, Rosenfeldt FL, Zhang C, Linnane AW and Nagley P. Precise determination of mitochondrial DNA copy number in human skeletal and cardiac muscle by a PCR-based assay: Lack of change of copy number with age. Nucleic Acids Res 2003; 31:61.
3. Chabi B, Mousson de Camaret B, Duborjal H, Issartel JP and Stepien G. Quantification of mitochondrial DNA deletion, depletion and overreplication: Application to diagnosis. Clin Chem 2003; 49:1309-17.
4. Kitamura E, et al. Analysis of tissue-specific differentially methylated regions (TDMs) in humans. Genomics 2007; 89:326-37.
5. Delsite R, Kachhap S, Anbazhagan R, Gabrielson E and Singh KK. Nuclear genes involved in mitochondria-to-nucleus communication in breast cancer cells. Mol Cancer 2002; 1:6.
6. Devaskar SU and Thamotharan M. Metabolic programming in the pathogenesis of insulin resistance. Rev Endocr Metab Disord 2007; 8:105-13.
7. King MP and Attardi G. Isolation of human cell lines lacking mitochondrial DNA. Methods in Enzymology 1996; 264:304-13.
8. Munot K, et al. Pattern of expression of genes linked to epigenetic silencing in human breast cancer. Hum Pathol 2006; 37:989-99.
9. Yu M, et al. Reduced mitochondrial DNA copy number is correlated with tumor progression and prognosis in Chinese breast cancer patients. IUBMB Life 2007; 59:450-7.
10. Liao X and Butow RA. RTG1 and RTG2: Two yeast genes required for a novel path of communication from mitochondria to the nucleus. Cell 1993; 72:61-71.
11. Smiraglia D, Kulawiec M, Bistulfi GL, Ghoshal S and Singh KK. A novel role for mitochondria in regulating epigenetic modification in the nucleus. Cancer Biol Ther 2008; 7:1182-90.
12. Rawls J, Knecht W, Diekert K, Lill R and Loffler M. Requirements for the mitochondrial import and localization of dihydroorotate dehydrogenase. Eur J Biochem 2000; 267:2079-87.
13. Depeint F, Bruce WR, Shangari N, Mehta R and O'Brien PJ. Mitochondrial function and toxicity: role of B vitamins on the one-carbon transfer pathways. Chem Biol Interact 2006; 163:113-32.
14. Reed MC, et al. A mathematical model of glutathione metabolism. Theor Biol Med Model 2008; 5:8.
15. Nijhout HF, et al. In silico experimentation with a model of hepatic mitochondrial folate metabolism. Theor Biol Med Model 2006; 3:40.
16. Christensen KE and MacKenzie RE. Mitochondrial one-carbon metabolism is adapted to the specific needs of yeast, plants and mammals. Bioessays 2006; 28:595-605.
17. Costello JF, Smiraglia DJ and Plass C. Restriction landmark genome scanning. Methods 2002; 27:144-9.
18. Feinberg AP, Ohlsson R and Henikoff S. The epigenetic progenitor origin of human cancer. Nat Rev Genet 2006; 7:21-33.
19. Dollo L. Les lois de l'évolution. Bull Soc Belge Géol Pal Hydr 1893; 7:164-6.

Mitochondrion 10 (2010) 12–31

Contents lists available at ScienceDirect

Mitochondrion

journal homepage: www.elsevier.com/locate/mito

Review

Energetics, epigenetics, mitochondrial genetics

Douglas C. Wallace *, Weiwei Fan

Center for Molecular and Mitochondrial Medicine and Genetics (MAMMAG) and Departments of Biological Chemistry, Ecology and Evolutionary Biology, and Pediatrics. University of California, Irvine, CA 92697-3940, United States

ARTICLE INFO

Article history:
Received 2 August 2009
Received in revised form 21 September 2009
Accepted 23 September 2009
Available online 29 September 2009

Keywords:
Mitochondria
Mitochondrial disease
mtDNA
OXPHOS
Energetics
Epigenetics

ABSTRACT

The epigenome has been hypothesized to provide the interface between the environment and the nuclear DNA (nDNA) genes. Key factors in the environment are the availability of calories and demands on the organism's energetic capacity. Energy is funneled through glycolysis and mitochondrial oxidative phosphorylation (OXPHOS), the cellular bioenergetic systems. Since there are thousands of bioenergetic genes dispersed across the chromosomes and mitochondrial DNA (mtDNA), both *cis* and *trans* regulation of the nDNA genes is required. The bioenergetic systems convert environmental calories into ATP, acetyl-Coenzyme A (acetyl-CoA), S-adenosyl-methionine (SAM), and reduced NAD^+. When calories are abundant, ATP and acetyl-CoA phosphorylate and acetylate chromatin, opening the nDNA for transcription and replication. When calories are limiting, chromatin phosphorylation and acetylation are lost and gene expression is suppressed. DNA methylation via SAM can also be modulated by mitochondrial function. Phosphorylation and acetylation are also pivotal to regulating cellular signal transduction pathways. Therefore, bioenergetics provides the interface between the environment and the epigenome. Consistent with this conclusion, the clinical phenotypes of bioenergetic diseases are strikingly similar to those observed in epigenetic diseases (Angelman, Rett, Fragile X Syndromes, the laminopathies, cancer, etc.), and an increasing number of epigenetic diseases are being associated with mitochondrial dysfunction. This bioenergetic–epigenomic hypothesis has broad implications for the etiology, pathophysiology, and treatment of a wide range of common diseases.

1. Introduction

"The modern definition of epigenetics is information heritable during cell division other than the DNA sequence itself" (Feinberg, 2007). Hence, epigenetics is thought to provide a flexible interface between the organism and its environment. Until now, the DNA sequences of interest to biology and medicine have been in the chromosomal DNA, which is transmitted during meiotic and mitotic cell division according to the rules of Gregor Mendel. However, most common metabolic and degenerative diseases and multiple cancers are familial, but are not classically Mendelian in their transmission. Therefore, such "complex diseases" have been attributed to epigenetic changes in response to the environmental change (Feinberg, 2007, 2008).

However, deficiency in energy metabolism has also emerged as an alternative explanation for the etiology of complex diseases over the past 21 years. The primary limiting factor for growth and reproduction of all biological systems is energy and the first reports that mitochondrial DNA (mtDNA) mutations can cause disease (Goto et al., 1990; Holt et al., 1988, 1990; Shoffner et al., 1990; Wallace et al., 2007, 1988a,b) have been followed by reports that a broad spectrum of metabolic and degenerative diseases can have a mitochondrial etiology (Wallace et al., 2007). Moreover, environmentally adaptive mtDNA variants have been associated with predisposition to virtually the entire range of common "complex" diseases (Wallace, 2008).

However, similar symptoms imply a common pathophysiology. Therefore, epigenetic and mitochondrial genetic diseases must be interrelated through their impinging on a common function.

To understand nuclear–mitochondrial interactions, we must consider the early stages in the endosymbiontic event that created the eukaryotic cell about 2 billion years ago (Lane, 2002, 2005; Wallace, 2007). In the beginning, the proto-nucleus–cytosol was limited by energy. This limitation was alleviated by its symbiosis with an oxidative α-protobacterion, the proto-mitochondrion. Therefore, growth and replication of the nucleus became limited by mitochondrial energy production and thus calorie availability. This necessitated the regulation of nuclear replication and gene expression by calorie availability mediated by mitochondrial energetics. This was achieved by coupling modulation of nDNA chromatin structure and function by modification via high energy intermediates: phosphorylation by ATP, acetylation by acetyl-Coenzyme A (Ac-CoA), deacetylation by nicotinamide adenine

* Corresponding author. Tel.: +1 949 824 3490; fax: +1 949 824 6388.
E-mail address: dwallace@uci.edu (D.C. Wallace).

1567-7249/$ - see front matter © 2009 Elsevier B.V. and Mitochondria Research Society. All rights reserved.
doi:10.1016/j.mito.2009.09.006

dinucleotide (NAD^+), and methylation by S-adenosyl-methionine (SAM).

Conversely, the nucleus had to develop mechanisms for modulating mitochondrial growth and replication. This was additionally complicated by the successive transfer of genes from the proto-mitochondrial DNA to the nDNA, with the cytosolic translation products being directionally imported back into the mitochondrion (Wallace, 2007). This process proceeded over a billion years with the result that the nDNA-encoded genes of the mitochondrial genome are now dispersed throughout the chromosomes (Wallace, 2007). Therefore, new mechanisms had to evolve to permit the coordinate expression of the mitochondrial genes based on nuclear requirements for energy for growth and reproduction. As a result, this became one of the early driving forces for the evolution of inter-chromosomal coordinate transcriptional regulation.

Over the subsequent 1.2 billion years, the nucleus–cytosol became increasingly specialized in specifying structure while the mitochondrion became entirely dedicated to energy production. Ultimately, this subcellular specialization became sufficiently refined and efficient that it permitted the advent of multicellularity and thus plants and animals (Wallace, 2007). Still, all subsequent tissue development, species radiation, and environmental adaptation were rooted in the fundamental energetic–epigenetic cooperation.

2. Mitochondrial bioenergetics

Complex structures can only be maintained by the continual flux of energy. Life, therefore, is the interaction between structure, energy, and information, with information required for both structure and energetics (Wallace, 2007).

2.1. Mitochondrial energetics: OXPHOS

Energetics in animals is based on the availability of reducing equivalents, consumed as carbohydrates and fats. Glucose is cleaved into pyruvate via glycolysis, and the pyruvate enters the mitochondrion via pyruvate dehydrogenase (PDH) resulting in acetyl-CoA, $NADH + H^+$, and CO_2. The acetyl-CoA then enters the Tricarboxylic Acid (TCA) Cycle which strips the hydrogens from the hydrocarbons generating $NADH + H^+$. Fatty acids are oxidized within the mitochondrion by β oxidation to generate acetyl-CoA, $NADH + H^+$, and $FADH_2$, the latter contained in the electron transfer factor (ETF). Two electrons (reducing equivalents from hydrogen) are transferred from $NADH + H^+$ to the OXPHOS complex NADH dehydrogenase (complex I) or from $FADH_2$ containing enzymes such as the ETF dehydrogenase or succinate dehydrogenase (SDH, complex II) to reduce ubiquinone (coenzyme Q_{10}, CoQ) to ubiquinol $CoQH_2$. The electrons from $CoQH_2$ are transferred successively to complex III (bc_1 complex), cytochrome *c*, complex IV (cytochrome *c* oxidase, COX), and finally to oxygen ($½O_2$) to give H_2O.

The energy that is released as the electrons flow down the ETC is used to pump protons out across the mitochondrial inner membrane through complexes I, III, and IV creating a proton electrochemical gradient ($\Delta P = \Delta\Psi + \Delta\mu^{H+}$). The potential energy stored in ΔP is used for multiple purposes: to import proteins and Ca^{++} into the mitochondrion, to generate heat, and to synthesize ATP within the mitochondrial matrix. The energy to convert ADP + Pi to ATP comes from the flow of protons through the ATP synthetase (complex V) back into the matrix. Matrix ATP is then exchanged for cytosolic ADP by the inner membrane adenine nucleotide translocators (ANTs) (Wallace, 2007).

The efficiency by which dietary reducing equivalents are converted to ATP by OXPHOS is known as the coupling efficiency. This is determined by the efficiency by which protons are pumped out of the matrix by complexes I, III, and IV and the efficiency by which proton flux through complex V is converted to ATP. The uncoupler drug 2,4-dinitrophenol (DNP) and the nDNA-encoded uncoupler proteins 1, 2, and 3 (Ucp1, 2, and 3) render the mitochondrial inner membrane leaky for protons, by-passing complex V and dissipating the energy as heat (Wallace, 2007).

2.2. OXPHOS complexes and the mtDNA

OXPHOS complexes are assembled from proteins encoded in both the nDNA and the mtDNA. Complex I is composed of 45 polypeptides, seven (ND1, 2, 3, 4, 4L, 5, and 6) encoded by the mtDNA; complex II from four nDNA polypeptides; complex III from 11 polypeptides, one (cytochrome *b*, cyt *b*) encoded by the mtDNA; complex IV form 13 polypeptides, three (COI, II, III) from the mtDNA; and complex V from about 16 polypeptides, two (ATP6 and 8) from the mtDNA. The mtDNA also encodes the 22 tRNAs and 12S and 16S rRNAs for translation of the 13 mtDNA polypeptides. Of the five complexes, only complexes I, III, IV, and V transport protons, and these are the same complexes for which key polypeptides are retained on the mtDNA. Therefore, it follows that the complex I, III, IV, and V electron and proton transfer proteins have been retained on the maternally-inherited and non-recombining mtDNA to avoid mixing OXPHOS complex proteins which could be incompatible and affect the coupling efficiency (Wallace, 2007).

Each mammalian cell contains hundreds of mitochondria and thousands of mtDNAs. When a mutation arises in a mtDNA, it creates a mixed population of normal and mutant mtDNAs, a state known as heteroplasmy. When a heteroplasmic cell divides, the two types of mtDNAs are randomly distributed into the daughter cells, resulting in genetic drift toward either pure mutant or wild type. Over time this replicative segregation results in segregation of the mutant mtDNAs into pure mutant or normal populations, termed homoplasmic cells (Wallace, 2007). As the percentage of mutant mtDNAs increases, mitochondrial energetic function decreases. When energy output is insufficient for normal tissue function, a threshold is crossed, symptoms appear, and apoptosis or necrosis may be initiated and clinical symptoms ensue (Wallace, 2005b, 2007).

2.3. Reactive oxygen species (ROS)

As a by-product of OXPHOS, mitochondria generate much of the endogenous ROS of the cell. Under normal physiological conditions, ROS production is highly regulated, at least in part controlled by complex I (Evans et al., 2000; Hansen et al., 2006; Jones, 2006a; Kelley and Parsons, 2001; McCord, 2000). However, when the ETC becomes highly reduced, the excess electrons can be passed directly to O_2 to generate superoxide anion ($O_2^{\cdot-}$). The $O_2^{\cdot-}$ generated by complex I is released into the mitochondrial matrix where it is converted to hydrogen peroxide (H_2O_2) by the matrix manganese superoxide dismutase, MnSOD (*Sod2* gene). Superoxide generated from complex III is released into the mitochondrial intermembrane space where it is converted to H_2O_2 by Cu/ZnSOD (*Sod1*) which is positioned in the mitochondrial intermembrane space and cytosolic. Mitochondrial H_2O_2 can diffuse into the nucleus–cytosol. If H_2O_2 encounters a reduced transition metal or is mixed with $O_2^{\cdot-}$, the H_2O_2 can be further reduced to hydroxyl radical ($OH^{\cdot}$), the most potent oxidizing agent of the ROS (Fig. 1). ROS can damage cellular proteins, lipids, and nucleic acids. Hence, excessive mitochondrial ROS production can exceed the antioxidant defenses of the cell, and the cumulative damage can ultimately destroy the cell.

2.4. The mitochondrial permeability transition pore (mtPTP)

The mitochondria evolved a self-destruct system, the mtPTP. The mtPTP is activated when the biochemical health of the

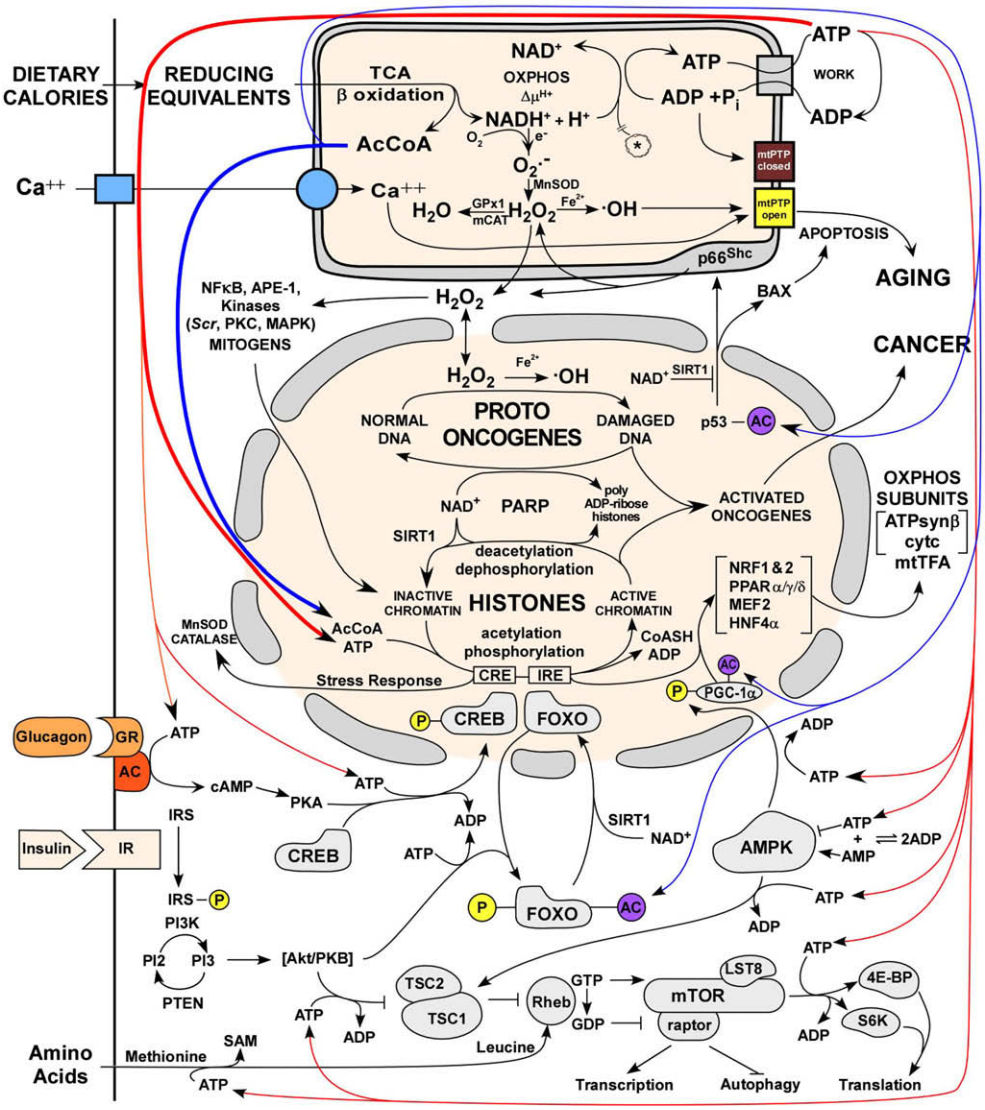

Fig. 1. Energetic regulation of the epigenome. Mitochondrial energetics links the epigenome to calorie availability through high energy intermediates and redox reactions. The mitochondrion is at the top of the figure, the nucleus in the middle, and the cytosol in the bottom. Calories as reducing equivalents enter the cell and mitochondria at the upper left resulting in generation of acetyl-CoA, reduction of NAD^+, and ATP. Energy then flows from top to bottom. ATP drives the phosphorylation of nuclear and cytosolic signal transduction proteins, acetyl-CoA acetylates chromatin and signal transduction proteins, and NAD^+ acts through the Sirtuins to deacetylate proteins. Abbreviations: AcCoA = acetyl-CoA, NAD^+ = nicotinamide adenine dinucleotide (oxidized) and NADH (reduced), mtPTP = mitochondrial permeability transition pore, GPx1 = glutathione peroxidase 1, mCAT = mitochondrially-targeted catalase, PARP = poly ADP ribose polymerase. Other abbreviations are described in the text.

mitochondria and cell decline, specifically when mitochondrial energy production declines, ROS generation increases, and excessive Ca^{++} is released into the cytosol and taken up by the mitochondrion. When the mtPTP is activated, it opens a channel in the mitochondrial inner membrane, short circuits ΔP, and initiates programmed cell death (apoptosis) (Wallace, 2005c).

2.5. Mitochondrial dynamics

The mitochondria within a mammalian cell are in constant motion and undergoing repeated rounds of fission and fusion. Mitochondrial fusion and fission not only merges the mitochondrial inner and outer membranes but also mixes mitochondria matrices and redistributes the mtDNAs. The mammalian mitochondrial fusion machinery involves three major proteins: mitofusin 1 (Mfn1), 2 (Mfn2), and the Optic Atrophy-1 Protein (Opa1) (Chen et al., 2005, 2003a; Cipolat et al., 2004), while the mitochondrial fission machinery involves dynamic-related protein 1 (Drp1), Fis1, and Mff (Gandre-Babbe and van der Bliek, 2008; James et al., 2003; Smirnova et al., 2001; Yoon et al., 2003).

3. THe energetic evolution of the epigenome

Prior to the advent of free oxygen in the biosphere, substrate-level phosphorylation was the primary mechanism for generating ATP in non-photosynthetic organisms. After the generation of free oxygen by photosystem II the redox range of biology was greatly expanded and OXPHOS became the most efficient system for generating ATP from the reducing equivalents present in organic molecules (Lane, 2002, 2005; Wallace, 2007).

3.1. The energetic evolution of the epigenome

In the proto-nucleus–cytosol cell, ATP, from glycolysis, would have provided the high energy intermediate linking calories to cellular growth and replication. Consequently, phosphorylation–

dephosphorylation must have been the first post-translational modification evoked for regulating DNA–protein interactions. When substrates were plentiful, ATP concentrations would increase, leading to increased phosphorylation of DNA-bound proteins. The resulting negative charge added to the protein by the phosphate group would then increase repulsion of the proteins from the DNA negatively charged sugar–phosphate backbone, opening chromatin for DNA transcription and replication. Phosphorylation also was used to modulate enzyme activities, signal transduction pathways, and the transcriptional apparatus in relation to energy availability.

As atmospheric oxygen became a dominant terminal electron acceptor, OXPHOS became the major source of ATP in non-photosynthetic eukaryotic cells. This cemented the symbiosis between the oxidative proto-mitochondrion and the proto-nucleus–cytosol. As a result acetyl-CoA became the metabolic intermediate that linked glycolytic pyruvate and fatty acid catabolism with the mitochondrial TCA cycle and OXPHOS and the concentration of acetyl-CoA became the cytosolic correlate for caloric availability.

Therefore, acetyl-CoA must have been the next energetic substrate to be used to couple cellular energetics with nuclear gene expression and cellular proliferation. Acetylation of lysines on DNA-binding proteins neutralizes their positive charge, reducing protein affinity for DNA. As a result, when carbohydrates and or fats were abundant, protein acetylation increased; DNA-binding proteins became acetylated and detached; and transcription, replication, and cell proliferation were stimulated. When carbohydrates and fats were limited (fasting–starvation), acetyl-CoA levels decreased; acetylation decreased; chromatin became condensed; and cellular gene expression, replication and proliferation were suppressed. In mammalian cells the carbon for acetyl-CoA destined for histone acetylation is derived from glucose through the mitochondrial TCA cycle via citrate. Glucose atoms transverse glycolysis to pyruvate and the pyruvate enters the mitochondrion where it is converted to acetyl-CoA via pyruvate dehydrogenase. The mitochondrial acetyl-CoA is condensed with oxaloacetate by citrate synthetase to generate citrate and the citrate is exported from the mitochondrion into the cytosol and nucleus by mitochondrion inner membrane citrate carrier. Cytosolic and nuclear citrate can then be converted to acetyl-CoA via ATP-citrate lyase, an enzyme found in both the nucleus and the cytosol. The nuclear acetyl-CoA is then preferentially used for histone acetylation. In the absence of glucose and the presence of supraphysiological levels of acetate, the mammalian cytosolic acetyl-CoA synthetase (AceCS1) can also generate acetyl-CoA. This can diffuse into the nucleus for use in histone acetylation (Rathmell and Newgard, 2009; Wellen et al., 2009). The facultative anaerobe, *Saccaromyces* cerevisiae, lacks ATP-citrate lyase. Therefore, it generates acetyl-CoA for histone acetylation via cytosolic and nuclear acetyl-CoA synthetases (Asc1p and Asc2p) (Takahashi et al., 2006), which might reflect its unique metabolism. The importance of acetylation as an energy surrogate is also extended to the regulation of transcription factors, enzymes, and signal transduction pathways. However, the kinetics of acetylation of histones versus other substrates differs (Rathmell and Newgard, 2009; Wellen et al., 2009).

Reduced energy supplies (fasting) would not only reduce acetyl-CoA levels but also reduce available reducing equivalents, resulting in the oxidation of NADH to NAD^+. Since NAD^+ but not NADH is a substrate for the class III histone deacetylases, the Sirtuins, starvation would activate the Sirtuins to deacetylate the DNA-binding proteins. This would increase the positive charge of the chromatin proteins, causing chromatin condensation, and suppressing transcription, replication, growth, and proliferation.

The third macromolecular modification system for modulating nuclear gene expression and replication in response to energy availability and nutrient supply is methylation by s-adenosyl-L-methionine (SAM). Methylation can increase macromolecular interactions through increased van der Waals forces. Therefore, methylation is more versatile than phosphorylation or acetylation for chromatin regulation.

SAM is produced in the cytosol by the reaction L-methionine + ATP to give SAM + Pi + PPi. Thus, SAM links energy production to the methylation of lysines and arginines in proteins and cytosines in DNA. The production of methionine from homocysteine is also regulated by mitochondrial metabolism. The single carbon metabolisms of the mitochondrion and cytosol are linked through the exchange of serine and glycine, which are interconvert within the two compartments through methylene-tetrahydrofolate via the mitochondrial and cytosolic serine hydroxymethyltransferases. The mitochondrial bifunctional enzyme converts methylene-tetrahydrofolate to formyl-tetrahydrofolate, thus diverting mitochondrial one carbon units from serine production to format, which is used in purine biosynthesis. Mitochondrial bifunctional enzyme is expressed in embryonic but not differentiated cells. When mitochondrial bifunctional enzyme is not expressed, mitochondrial serine production increases and the serine is exported to the cytosol. In the cytosol, the single carbon units of serine are transferred through methylene-tetrahydrofolate and methyl-tetrahydrofolate to convert homocystine to methionine, which can then be converted to SAM. The synthesis of serine within the mitochondrion requires NAD^+. When OXPHOS is inhibited, the mitochondrial NADH/NAD^+ ratio increases, thus inhibiting the mitochondrial production of methylene-tetrahydrofolate and thus serine. This reduces methionine and SAM production (Naviaux, 2008).

All of these macromolecular modification systems were in place prior to the advent of multicellularity 800 million years ago (Wallace, 1982, 2007). Multicellularity and terminal differentiation created two types of cell, the mortal somatic cells and the immortal germ and pluripotent stem cells. Since immortal cells predated mortal cells, it follows that immortal germ and stem cells should still utilize phosphorylation and acetylation to link energy availability with cell growth and reproduction and that stem cells should have the most open chromatin (Wen et al., 2009). However, to form tissues, the terminally differentiated cells must stop replicating. Hence, large blocks of chromatin must be shut down (Wen et al., 2009). Moreover, new genes were needed to block the cell cycle when activated by acetylation of the surrounding cellular chromatin. The p21 gene is one current example, being up-regulated when its promoter is acetylated and functioning to block replication (Glozak and Seto, 2007; Xiao et al., 2000). Cells which circumvented such replication blockades would then need to be destroyed before they could disrupt the tissue structure. This led to the development of mtPTP and pro-apoptotic proteins like Bax, which are also induced by histone acetylation at their promoters (Glozak and Seto, 2007). Additional layers of control were added once cellular proliferation became disconnected from energetics and increasingly complex structures were formed.

3.2. Energetic regulation of the epigenome

The nDNA of the modern eukaryotic cell is packaged in nucleosomes encompassing 146–147 base pairs of DNA wrapped around a complex of two copies each of histones H2A, H2B, H3, and H4. In yeast, these histones and the C-terminal domain of RNA Polymerase II (POLII) can be phosphorylated by kinases using ATP. Changes in histone serine/threonine phosphorylation in yeast are linked to changes in the extracellular environment. A change in carbon source results in the phosphorylation of serine 10 in H3 (H3-S10Pi), which is linked to acetylation of lysine 14 in H3 (H3-K14Ac). This stimulates transcription. ATP-driven phosphorylation of the POLII C-terminal domain also modulates transcription and

phosphorylation of serine 10 in H2B (H2-S10Pi) is associated with stress and cell death (Fuchs et al., 2009).

3.2.1. Energetic regulation at the chromatin level

Acetylation of histones is catalyzed by histone acetyltransferases (HATs) which catalyze the reaction of acetyl-CoA with the ε-amino group of lysines in histones. There are four classes of HATs known in eukaryotic cells, Gcn5/PCAF, MYST, p300/CBP, and Rtt109. All have structurally similar acetyl-CoA binding sites (Marmorstein and Trievel, 2009; Smith and Denu, 2009). The p300/CBP HAT complex was first characterized as an activator of cAMP responsive genes. Elevated cAMP activates protein kinase A to phosphorylate CREB at serine 133. Phospho-CREB recruits CBP to cAMP response elements (CREs) in the DNA, and CBP uses its intrinsic HAT activity to open the chromatin for transcription (Tini et al., 2002).

Histone deacetylases (HDACs) fall into four classes. Three classes have similar deacetylase mechanisms involving Zn^{2+} and include class I (HDAC1–3 and 8), class II (HDAC 4–7 and 9–10), and class IV (HDAC 11). The class III Sirtuin HDACs catalyze deacetylation by the reaction of acetyl-lysine + NAD^+ → lysine + nicotinamide + 2′-O-acetyl-ADP ribose (OAADPr) (Smith and Denu, 2009).

Methylation of chromatin, with the methyl group donated by SAM, can occur on either lysines or arginines. Lysine methylation is catalyzed by histone lysine methyltransferases and can result in mono-, di-, or tri-methylation. There are two histone lysine methyltransferase classes: the SET domain family and the DOT1 family. The SET domain class methylates both nucleosomal and free histones while the DOT1 class only methylates nucleosomal histones (Smith and Denu, 2009). Histone demethylation involves two classes of reactions. The first class includes lysine-specific demethylase 1 (LSD1) and is specific for mono- and di-methylated histones. LSD1 employs FAD to oxidize the $-N-CH_3$ bond, which is then cleaved by water to generate formaldehyde. The resulting $FADH_2$ is reoxidized by O_2 to generate H_2O_2. The second class is the Jumonj family of histone demethylases. These demethylate trimethyl-lysines in a reaction using O_2 and 2-oxoglutarate as coreactants generate succinate and CO_2 and release formaldehyde (Marmorstein and Trievel, 2009; Smith and Denu, 2009).

Arginine methylation is catalyzed by protein arginine methyltransferases (PRMT) in which the methyl group for SAM is transferred to the arginine guanidinium side chain. There are two classes of PRMTs: PRMT1 first generates monomethylarginine and then asymmetric N,N′-dimethylarginine while PRMT2 initially generates monomethylarginine but then generates symmetric N,N′-dimethylarginine. JMJD6, a homolog of he JHDM family of lysine demethylases, provides an arginine demethylase (Smith and Denu, 2009). A number of additional chromatin modifications are also known including ubiquitination; sumoylation; and protein arginine deiminase, which hydrolyzes the guanidinium side chain to generate citrulline and ammonia (Marmorstein and Trievel, 2009; Smith and Denu, 2009).

The distribution of histone modifications has been hypothesized to provide a "histone code" of gene expression (Fuchs et al., 2009; Strahl and Allis, 2000). In yeast, the 5′ coding regions of active genes have an increased density of H2A-K7Ac, H3-K9Ac, H3-K14Ac, H3-K18Ac, H4-K5Ac, and H4-K12Ac while the 3′ coding regions of active genes are enriched for H2B-K16Ac, H4-K8Ac, and H4-K16Ac (Wyrick and Parra, 2009). Furthermore, H3-K4me is associated with active transcription, H3-K4me3 is prevalent near promoters, and H3-K4me1 is more abundant in coding regions (Fuchs et al., 2009). In mammalian cells, active chromatin histones H3, H4, and H2A are acetylated including H3-K9Ac and histones H3 and H4 are methylated including H3-K4me, H3-K4me2 and H3-K4me3, the later found at the 5′ end of transcribed regions; H3-K36me3 found at the 3′ end of transcribed regions; plus H3-K9me, H3-K27me, and H4-K20me. By contrast, in inactive chromatin histones are hypoacetylated and H3 is methylated to generate H3-K9me3, H3-K27me3, and H3-K79me3. Methylated H3-K9 specifically interacts with Heterochromatin Protein 1 (HP1). H4-K16Ac and H4-K20me have also been noted in cancer cell chromatin (Glozak and Seto, 2007; Schneider and Grosschedl, 2007).

Beyond local histone modifications, the nuclear genome is organized into structural and functional chromosomal territories (Schneider and Grosschedl, 2007). In general, gene-rich chromosomes such as human chromosome 19 are located toward the interior of the nucleus while gene-poor chromosomes like 18 are located toward the periphery of the nucleus (Cremer et al., 2003). The functional genes within the nuclear interior are organized into "transcriptional factories" in which widely scattered genes can be colocalized into the same focus of active transcription. This permits positive and negative transcriptional regulatory factors bound to particular cis DNA elements to influence the expression of genes dispersed on the same of different chromosomes (Cai et al., 2006; Fraser and Bickmore, 2007; Gondor and Ohlsson, 2006; Schneider and Grosschedl, 2007; Zhao et al., 2006).

The chromatin in the central nucleus is generally gene-rich regions, more diffuse, and associated with increased gene expression (ridges). The chromatin toward the nuclear periphery is gene-poor, more compact, and has reduced gene expression (antiridges) (Goetze et al., 2007). Transcribed regions of the chromatin can form loops which can either interact with genes within the loop (Cai et al., 2006; Gondor and Ohlsson, 2006) or between chromatin loops on the same or different chromosomes (Schneider and Grosschedl, 2007; Zhao et al., 2006). In the case of the *IL3, 4, 5* gene cluster on mouse chromosome 11, activation of T helper 2 cells results in the 200 kb region becoming folded into a series of small loops through the induction and binding of the special AT-rich sequence binding protein 1 (SATB1). SABT1 binds to the base of each loop and is accompanied by the acetylation of H3-K9 and H3-K14; the binding of the regulatory factors GATA3, STAT6, c-maf, and Brg1; and the recruitment of RNA polymerase II (Cai et al., 2006). Therefore, the regional clustering of related transcriptional units plus the development of transcriptional factories between chromosomes can provide the capacity for the transcription regulation of the widely dispersed nDNA genes of the mitochondrial genome.

Transcriptionally inactive regions of the genome can be bound in large organized chromatin K9 modifications (LOCKs) blocks. These regions can range in size up to 4.9 Mb and have been identified by the immunoprecipitation of chromatin enriched for H3-K9Me2 or H3-K27me3. They are commonly demarcated by CCCTC-binding factor (CTCF) insulator sites, and are envisioned to represent relatively inactive chromatin regions associated with the periphery of the nuclear envelope. In undifferentiated mouse ES cells only about 4% of the chromatin is in LOCKs, but in differentiated ES cells this increases to 31%. In brain 10% of the chromatin is in LOCKs while in liver 46% is in LOCKs. In the human chromosome 15q11-13 imprinted region associated with Angelman and Prader-Willi syndromes, placental chromatin contains two Mb LOCKs, one encompassing the *SNRPN* gene associated with Pader-Willi and the other encompassing the *GABRB3* gene, the Angelman syndrome *UBE3A* gene lying between the two LOCKs (Wen et al., 2009). Regions of the chromatin ranging in size from 0.1 to 10 Mb have also been found to be preferentially associated with nuclear lamina, specifically lamin B1, located on the inside of the nuclear envelope. These lamina-associated domains (LADs) are generally low gene expression domains and are flanked by CTCF binding sites, CpG islands, and promoters oriented away from the LADs (Guelen et al., 2008). Approximately 82% of LOCKs correspond to LADs (Wen et al., 2009).

3.2.2. Energetic regulation at the signal transduction level

The post-translational modification of a wide spectrum of metabolic and regulatory proteins by phosphorylation and acetylation unifies the energetic regulation of chromatin with the physiological state of the cell. Phosphorylation modulates the activity of a significant portion of the cellular proteins. The great majority of receptors for environmental signals transmit these signals via tyrosine or serine–threonine phosphorylation. Most of the intermediate steps in signal transduction pathways are also mediated by kinases and phosphatases (Alberts et al., 2002).

3.2.2.1. Global energetic regulation of metabolism. A more global regulation of metabolism by energy availability can be mediated by the conversion of ATP to cAMP by adenylylcyclase. cAMP is linked to cellular energetics throughout the kingdoms of life. Classic examples include modulation of the lactose operon in *Escherichia coli*; providing the chemical gradient along which *Dictyostelium discoidum* amoebe migrate during starvation to form the fruiting body (Alberts et al., 2002); regulation of mitochondrial OXPHOS, ROS, and longevity in *Drosophila* (Tong et al., 2007); the modulation of peroxisome-proliferator-activated receptor γ-coactivator-1α (PGC-1α) transcription (Daitoku et al., 2003); and phosphorylation of complexes I and IV proteins in mammalian cells (Bellomo et al., 2006; Chen et al., 2004; Lee et al., 2005; Papa et al., 2002; Technikova-Dobrova et al., 2001).

Acetylation–deacetylation of regulatory and metabolic proteins is also ubiquitous. The p53 protein can be acetylated by p300/CBP at six lysines and by PCAK at another lysine. Acetylation at lysine 382 by p300/CBP increases its activity, while the deacetylation of lysine by Sirt1 reduces its activity. Acetylation of transcriptional co-repressor PLZF by p300 at five lysines within the Zn-finger domain increases its DNA binding and enhances its suppression of growth promoting genes. Acetylation of GATA1 by p300/CBP within its Zn-fingers is important for chromatin binding and transcriptional activation resulting in hematopoietic terminal differentiation. NFκB, which is a heterodimer of RelA/p65 and p50 or p52 subunits, is maintained in an inactive form in the cytoplasm complexed with IκB. Upon stimulation, IκB is phosphorylated by IκB kinase and degraded permitting NFκB to be translocated to the nucleus. Acetylation of p65 by p300/CBP or PCAF at K218, K221, and K310 enhances DNA binding and transcriptional activity and inhibits IκB binding. Deacetylation by HDAC3 promotes IκB binding and nuclear egress. Deacetylation of NFκB by Sirt1 at K310 decreases expression of NFκB target genes (Glozak and Seto, 2007). Acetylation of PGC-1α by GCN5 attenuates its transcriptional co-activator activity suppressing mitochondrial biogenesis. Deacetylation by Sirt1 restores PGC-1α activity and increases mitochondrial biogenesis (Gerhart-Hines et al., 2007). Acetylation of FOXO by p300/CBP causes its removal from the nucleus, while deacetylation by Sirt1 facilitates its transfer back into the nucleus (Accili and Arden, 2004).

DNA methylation, DNA repair, and transcription come together through acetylation by the association of p300/CBP HAT, thymidine DNA glycosylase (TDG), and the bifunctional protein apurinic/apyrimidinic endonuclease/redox factor-1 (APE/Ref1$^{Red/Ox}$). Methylation of cytosine in CpG dinucleotides is important in regulation of gene expression. However, deamination of cytosine and methylcytosine result in uracil and thymine, respectively, accounting for approximately 30% of all *de novo* nDNA mutations. Correction of the resulting G/T and G/U base pairs involves DNA glycosylases that recognize and excise the mispaired thymine or uracil. Mammals have two thymine DNA glycosylases, TDG and MBD4. MBD4 is concentrated in heterochromatin, but TDG is enriched in transcriptionally active euchromatin. When TDG binds to the G/T or G/U base mismatches, this leads to the additional binding of both p300/CBP and APE-1/Ref1$^{Red/Ox}$. The p300/CBP acetylates the local histones to open the chromatin while the APE-1/Ref1$^{Red/Ox}$ cleaves the apyrimidinic DNA strand for repair (Tini et al., 2002). APE-1/Ref1$^{Red/Ox}$ is a bifunctional protein that not only participates in DNA repair, but also regulates a variety of transcription factors through thiol/disulfide conversions. Since thiol–disulfide chemistry is regulated by mitochondrial and cytosolic redox state (Hansen et al., 2006; Jones, 2006b, 2008; Kemp et al., 2008; Schafer and Buettner, 2001) the p300/CBP-TDG-APE-1/Ref$^{Red/Ox}$ complex integrates all aspects of the energetic regulation of the epigenome (Fig. 1).

The coordination between cellular metabolism and transcriptional regulation is classically illustrated by the response of mammalian metabolism to the availability of carbohydrate calorie resources. When carbohydrates were abundant to our ancestors, such as during the plant growing season, consumption of plant starch resulted in increased blood glucose levels. This stimulates the pancreatic β cells to release insulin. Insulin signals the availability of carbohydrates to the rest of the tissues in the body, shifting metabolism toward glycolysis for ATP generation and the storage of excess calories as fat. When carbohydrates are scarce, glucose becomes limiting to animals, serum glucose levels fall, insulin secretion declines, and the pancreatic α cells secrete glucagon. Glucagon then signals via cAMP to mobilize stored fat and up-regulate mitochondrial OXPHOS to burn fat and generate energy to survive periods of glucose deprivation (Wallace, 2007) (Fig. 1).

When insulin is secreted due to increased serum glucose, it binds to insulin receptors of target tissue cells. This activates phosphatidyl-inositol 3 kinase (PI3K) which activates the Akt/PKB protein kinase. Akt then phosphorylates and inactivates the FOXO transcription factors. When unphosphorylated, FOXO transcription factors are active and bind to insulin response elements (IREs) in the promoters of nDNA genes. One FOXO target gene is the transcriptional co-activator, PGC-1α. PGC-1α interacts with a variety of tissue-specific transcription factors to induce key nDNA-encoded mitochondrial genes to up-regulate OXPHOS. Thus, when glucose is abundant, the FOXOs are phosphorylated and inactive, PGC-1α is down-regulated, mitochondrial OXPHOS is depressed, and metabolism shifts toward glycolysis. When blood glucose is low, insulin secretion decline, and the FOXOs are unphosphorylated and active. This induces PGC-1α and OXPHOS. Low blood glucose also stimulates glucagon secretion, which binds to the glucagon receptor of target calls and activates adenylylcyclase to produce cAMP. Elevated cAMP activates PKA to phosphorylate CREB which enters the nucleus and binds CRE cis elements, one of which is up-stream of PGC-1α. This up-regulates PGC-1α and OXPHOS expression. Therefore, when carbohydrates are limiting, the expression of PGC-1α is doubly induced by the dephosphorylation of the FOXOs and the phosphorylation of CREB, switching cellular metabolism toward OXPHOS to burn stored fats to survive periods of carbohydrate deprivation. Antioxidant defenses are also up-regulated in conjunction with OXPHOS to offset the effects of increased mitochondrial ROS production (Fig. 1).

The switch from glycolysis to OXPHOS may also be mediated by the cytosolic NAD^+/NADH levels through Sirt1. Catabolism of glucose by glycolysis reduces cytosolic NAD^+ to NADH and produces pyruvate, which is further metabolized in the mitochondrion. By contrast, fatty acid oxidation occurs exclusively in the mitochondrion, leaving cytosolic NAD^+ oxidized. Therefore, when glucose in abundant, the cytosolic NAD^+ is reduced and the NADH can not be used by Sirt1 as a co-reactant to deacetylate the FOXOs and PGC-1α. Hence, the FOXOs and PCG-1α remain inactive down-regulating mitochodntrial biogenesis. When fats are oxidized, cytosolic NAD^+ remains abundant, permitting the deacetylation of the FOXOs and PGC-1α and the up-regulation of OXPHOS.

3.2.2.2. Metabolic regulation via nuclear receptors. PGC-1α is one of three members of a gene family of transcriptional co-activators

(PGC-1α, PGC-1β, and PERC) that modulate mitochondrial function by regulating genes for energetics including mitochondrial biogenesis, thermogenesis, and fatty acid oxidation (Kelly and Scarpulla, 2004, 2002). PGC-1α was cloned through its interaction with PPARγ (Yang et al., 2006). PPARγ is a member of the nuclear receptor (NR) superfamily, a large family of ligand-dependent transcriptional factors. This superfamily consists of 48 members in human and 49 in mouse which are central to the regulation of metabolism, development, reproduction, and immune response. All members of the nuclear receptor superfamily share a common architecture containing a N-terminal ligand independent activation domain (AF-1), a DNA binding domain (DBD) consisting of two highly conserved zinc-finger motifs which interact with the hormone response elements (HRE, 5′-AGGTCA-3′), a hinge region, and the C-terminal ligand binding domain (LBD). Various members of the NR superfamily can bind to DNA as monomers, homodimers, or heterodimers. Based on their ligand binding, the NRs are divided into three major groups, "endocrine receptors" which encompass the steroid receptors and heterodimeric receptors, the "adopted orphan receptors" which include the lipid sensors and "enigmatic orphans", and the "orphan receptors" whose ligands are unknown.

The steroid receptors of the endocrine class include the estrogen receptors (ER) α and β, androgen receptor, glucocorticoid receptor and others, all of which function as homodimers. The heterodimeric endocrine receptors include the thyroid hormone receptors α and β which dimerize with RXR.

The orphan receptors bind lipids and include PPARα, γ, and δ which also heterodimerize with RXR. PPARα is expressed in liver, heart, muscle and kidney and regulates fatty acid oxidation and apolipoprotein synthesis. PPARγ is most abundant in adipose tissue and regulates adipogenesis, but it is also expressed in liver and skeletal muscle. PPARδ is ubiquitously expressed and promotes mitochondrial fatty acid oxidation, energy expenditure, and thermogenesis. Mice over expressing PPARδ in skeletal muscle exhibit a shift in their muscle fiber distribution from glycolytic type II fibers to oxidative type I fibers with an associated remarkable increase in exercise endurance (Wang et al., 2004).

The enigmatic "adopted orphan receptors" include the estrogen-related receptors (ERR) α, β, and γ. The ERRs often act as monomers binding consensus half sites found in many genes involved in mitochondrial function. Under physiological conditions, the ERRs are not regulated by ligands, but instead by binding the inducible co-activators PGC-1α and PGC-1β. The interactions of ERRs with the PGC-1s then induce mitochondrial β-oxidation and oxidative metabolism. PGC-1α and β can interact with other NRs to up-regulate mitochondrial genes. While both can interact with PPAR α and δ in muscle, heart, and white adipose tissue to induce mitochondrial fatty acid oxidation, PGC-1α can interact with FXR and HNF-4α in liver to induce gluconeogenesis during fasting, and PGC-1β can interact with SREBP-1c (steroid regulatory element binding protein-1c) and FOXA2 to promote lipogenesis. NR heterodimers involving RXR can interact with transcriptional co-repressors such as SMRT/NCOR plus HDACs in the absence of ligands to inhibit transcription, but in the presence of ligands can shift to binding transcriptional co-activators p300/CBP or SRC/p160 to activate transcription. On activation or induction of PGC-1, the ERR binds PGC-1 and this nucleates an active transcriptional complex that can include p300/CBP and SRC/p160 (Mangelsdorf and Evans, 1995; Shulman and Mangelsdorf, 2005; Sonoda et al., 2008).

While the interaction of PGC-1α and β with the NRs appear to be master regulators of oxidative metabolism, other steroid receptors also play an integral and often unexpected role in regulating mitochondrial function. It is now known that the estrogen receptors ERα and β are present not only in the nucleus–cytosol, but also in the mitochondrial matrix (Duckles et al., 2006; Pedram et al., 2006; Stirone et al., 2005). In cerebral vascular endothelial cells, estrogen induces mtDNA-encoded polypeptides such as COI and also the nDNA-encoded mitochondrial polypeptides COX subunit IV (COX14), cytochrome *c*, and the nDNA gene mitochondrial nuclear transcription factor-1 (NRF1), as well as citrate synthetase and COX activities (Duckles et al., 2006; Stirone et al., 2005). Estrogen also decreases mitochondrial ROS production in association with an increase in MnSOD specific activity without increases in protein level in both vascular endothelial cells (Razmara et al., 2007, 2008; Stirone et al., 2005) and also mammary tumor cells (Pedram et al., 2006). Therefore, the NR superfamily exerts broad control on many aspects of mitochondrial physiology in response to endogenous and exogenous environmental factors.

3.2.2.3. Metabolic regulation via TOR kinase. In addition to the transcriptional regulation of mitochondrial function, mitochondrial bioenergetics and biogenesis is modulated by post-translational modifications. One important mediator of cellular and mitochondrial energetics is AMP-activated protein kinase (AMPK). Under conditions where energy production is compromised (e.g. hypoxia, starvation, OXPHOS inhibitors) or when energy consumption accelerates (e.g. muscle contraction), the ATP/ADP ratio declines. This drives the adenylate kinase reaction (2ADP → ATP + AMP). The resulting increased AMP/ATP ratio then activates AMPK. Activated AMPK phosphorylates PGC-1α; up-regulates PGC-1α expression and OXPHOS (Jager et al., 2007); induces glucose uptake and glycolysis; activates fatty acid oxidation and suppresses fatty acid synthesis; stabilizes p53, p21, and p27 to inhibit cell growth and proliferation; and represses the target of rapamycin (TOR) kinase to inhibit protein synthesis (Hardie, 2007). When nutrients again become available, the AMP/ATP ratio declines, AMPK activity is suppressed, and TOR signaling is activated to resume protein synthesis and stimulate cell growth (Wullschleger et al., 2006) (Fig. 1).

The TOR serine/threonine kinases link nutrient availability to regulation of anabolism or catabolism. Mammalian cells have two TOR (mTOR) complexes: mTORC1 and mTORC2. mTORC1 consists of mTOR, raptor, and mLST8 and it regulates protein synthesis, metabolism, ribosomal biogenesis, transcription, and autophagy (Fig. 1). mTORC2 is composed of mTOR, rictor, and mLST8 and it regulates via Akt/PKB cell proliferation, survival, metabolism, transcription and actin organization and thus motility. Rapamycin, when complexed with FKBP12, inhibits mTORC1 but not mTORC2.

mTORC1 is regulated by the insulin signaling pathway, stress and hypoxia, cellular energy levels through AMPK, and nutrient levels. Insulin and insulin-like growth factors activate the insulin receptor which phosphorylates insulin receptor substrate (IRS), thus activating PI3K. This activates Akt/PKB to phosphorylate and inactivate the tuberous sclerosis protein complex (TSC). TSC is composed of the proteins hamartin (TSC1) and tuberin (TSC2) and TSC2 acts as a GTPase activating protein (GAP) for the small GTPase Rheb. Rheb binds to the kinase domain of mTOR. When bound to GTP Rheb activates mTOR and when bound to GDP it inhibits mTOR. Thus, when insulin and IGFs are present, TSC is inactive, and Rheb retains GTP and activates mTOR. When insulin and IGF are absent, TSC is active, Rheb GTP is converted to GDP, and mTOR is inhibited. Activated mTORC1 phosphorylates downstream proteins S6K1 and 4E-BP to increase protein synthesis, and other targets to stimulate growth related processes. The Ras/ERK pathway can also phosphorylate TSC, stimulating growth. When ATP is limiting and the AMP/ATP ratio rises, AMPK is activated and phosphorylates TSC, enhancing GAP activity, converting Rheb GTP to GDP, and thus inhibiting mTOR. Therefore, ATP deficiency inhibits protein synthesis and growth processes. Similarly, hypoxia inhibits mTORC1 signaling and limits protein synthesis and growth via activation of hypoxia inducible factors-1α and -2α (HIF-1α, HIF-2α). The HIF-1α–HIF-1β complex induces the

expression of the REDD complex (REDD1 and 2) which releases TSC2 from its association with the inhibitory 14-3-3 protein permitting TSC1/2 to inhibit mTORC1 and inhibit growth (DeYoung et al., 2008). Increased amino acids stimulate growth through mTORC1. The elevated amino acids, in particular leucine, induce an influx of Ca^{++} into the cell, which activates calmodulin. The Ca^{++}/calmodulin complex binds hVps34 which is attached to the mTORC1 complex. This activates hVps34 to generate PI(3)P which activates mTORC1 leading to phosphorylation of S6K1, 4E-BP, and other mTORC1 targets proteins and increased protein synthesis and growth (Gulati et al., 2008). Nutrient deprivation, by contrast, is associated with reduced cytosolic Ca^{++}, inhibition of mTORC1, dephosphorylation of target proteins and inhibition of protein synthesis and growth. mTORC1 also phosphorylates and inhibits the ATG1 protein kinase which mediates the early steps in autophagy. Therefore, when energy and nutrients are plentiful, mTORC1 is active, ATG1 is phosphorylated and autophagy is inhibited. When nutrients and energy are limiting, mTORC1 is inactive, ATG1 becomes dephosphorylated, and autophagy recovers nutrients from cellular macromolecules (Wullschleger et al., 2006).

3.2.2.4. Metabolic and circadian regulation via Sirtuins and NAD$^+$. Cellular energetics is also modulated by the cellular redox state through the NADH/NAD^+ ratio. Since NAD^+, but not NADH, is a substrate for many of the class III Sirtuin deacetylases, Sirtuin activity links protein deacetylation to the cellular NADH/NAD^+ ratio. Mammals possess seven Sirtuins: SIRT1, -2, -6, and -7 located in the nucleus; SIRT1 and -2 in the cytosol; and SIRT3, -4, and -5 in the mitochondrion. SIRT1 is the best studied, deacetylating proteins using NAD^+. Acetylation of FOXO transcription factors by p300/CBP reduces their activities, while deacetylation by SIRT1 increases activity. Thus, when calories are limited, NADH is oxidized to NAD^+. This activates SIRT1 to deacetylate the FOXOs, up-regulating OXPHOS to begin oxidizing stored fat. PGC-1α can also be acetylated by GCN5 reducing its activity when calories are plentiful, and deacetylation by SIRT1 and NAD^+ when reducing equivalents are scarce increasing PCG-1α activity in muscle and up-regulating mitochondrial fatty oxidation (Gerhart-Hines et al., 2007). SIRT1 also regulates mitophagy through deacetylation of members of the ATG family of proteins (Lee et al., 2008). SIRT3 deacetylation of various OXPHOS proteins also modulates mitochondrial metabolic rate (Ahn et al., 2008).

SIRT1 deacetylase activity is also linked to circadian rhythms (Asher et al., 2008; Nakahata et al., 2008). Circadian rhythms are generated by a transcriptional negative feedback loop in which two transcription factors BMAL1 and CLOCK form a heterodimeric complex that drives the expression of two negative regulators, PER and CRY. Expression of PER and CRY attenuates the activity of the heterodimeric BMAL1/CLOCK complex and turns down PER and CRY expression. The CLOCK protein has HAT activity which is enhanced by BMAL1 and is essential to maintain the circadian rhythm (Doi et al., 2006). CLOCK-driven acetylation of histones H3 and H4 and BMAL1 are all cyclical, as is PER2 acetylation (Asher et al., 2008; Doi et al., 2006). BMAL1 and PER2 are also more stable when acetylated (Asher et al., 2008; Nakahata et al., 2008). SIRT1 also binds and deacetylates CLOCK, BMAL1, and PER2. Therefore, deacetylation by SIRT1 plus NAD^+ is also regulating circadian rhythm. SIRT1 expression level is circadian in mouse liver, being maximum at Zeitgeber time (ZT) 16 during the active dark period (ZT = 0 being the beginning of a 12 h light cycle) and minimum at ZT4 during the quiescent light period. SIRT1 deacetylation is required for the oscillation of BMAL1 expression, since SIRT1 knockout cells have significantly reduced expression of the core circadian genes including *Clock*, *Bmal1*, *Per1*, and *Cry1* (Asher et al., 2008; Nakahata et al., 2008). Consistent with the SIRT1 requirement for NAD^+ for its deacetylase activity, oscillations of the circadian clock are coupled to oscillations of the cellular NAD^+ levels. The synthesis of NAD^+, in turn, is regulated by the expression of nicotinamide phosphoribosyltransferase (NAMPT), the rate-limiting step in mammalian NAD^+ synthesis. The *Nampt* gene in mouse contains an E-box (CACGTG) cis element that binds and is regulated by the CLOCK–BMAL1–SIRT1 complex. This causes the expression of NAMPT and thus NAD^+ levels to oscillate. Therefore, circadian rhythms are regulated both by the transcriptional CLOCK–BMAL1 and CRY-PER feedback loop and also by the SIRT1–CLOCK–BMAL1 and NAMPT–NAD^+ metabolic feedback loop (Nakahata et al., 2009; Ramsey et al., 2009; Wijnen, 2009). Since cellular energetics drives oxidation–reduction reactions and modulates the NAD^+/NADH redox ratio, and the redox state of NAD^+ is modulated by caloric availability, circadian rhythms, food intact, and activity must interact (Eckel-Mahan and Sassone-Corsi, 2009).

The circadian oscillations of the *Clock*, *Bmal1*, *Per2*, and *Cry1* genes are also paralleled by oscillations in the expression of 28 of the 45 nuclear receptor genes (Yang et al., 2006). The mRNA levels of the PPAR family members showed tissue-specific oscillations that correlated with those of the *Clock*, *Bmal1*, *Per2*, and *Cry1* genes in mouse white adipose tissue (WAT), brown adipose tissue (BAT), liver, and skeletal muscle (Yang et al., 2006). In BAT, all three *PPAR* genes, as well as *PGC-1α* and *UCP*-1, reach their maximal expression during ZT4, the light period when mice are at rest, and minimum at ZT16 during the dark period when mice are active. Thus, BAT thermogenesis is maximum during resting and minimum during periods of maximum activity, thus balancing heat generation by ATP hydrolysis during exercise with heat generation during rest by thermogenesis. In WAT, by contrast, *PPARγ* is maximum during the active dark period, ZT16, and minimal during the resting light period, ZT4. This parallels the expression of the *SREBP-1c*, *adiponectin*, and *leptin* and is consistent with energy production being maximal during the dark period when mice are most active (Yang et al., 2006). Since the circadian regulation of the *PPAR* genes is at the transcription level, part of the regulation must be the result of changes at the chromatin level. Therefore, calorie intake and energy metabolism directly regulate epigenomic gene expression, and reciprocally epigenomic changes regulated food intake and energy metabolism.

3.2.2.5. PGC-1α and Sirtuin mutant mice. The spectrum of phenotypic and physiological parameters regulated by energy metabolism has been demonstrated by generating mice in which the genes of the PGC-1 and Sirtuin families have been inactivated. In mice lacking *PGC-1α* (−/−) only about half of the pups survive through early postnatal period into adulthood. These animals weigh 10–15% less at 2 months of age, and have abnormal BAT with large lipid droplets, but normal liver, heart, skeletal muscle, and pancreas (Lin et al., 2004). The *PGC-1β* knockout mice show grossly normal development, growth, and fertility (Sonoda et al., 2007).

Both the *PGC-1α* and *PGC-1β* knockout mice show reduced cold tolerance, decreased mitochondrial energy metabolism, and altered circadian rhythms indicating that the two transcription coactivators have overlapping functions. However, the two knockout mice differ in their tissue specificities demonstrating that *PGC-1α* and *PGC-1β* have different roles in regulating metabolism. *PGC-1α* knockout mice accumulate large lipid droplets in BAT and up-regulate gluconeogenesis in liver under normal conditions, while *PGC-1β* knockout mice accumulate large lipid droplets in their livers after being fed a high-fat diet. *PGC-1α* −/− mice are hyperactive in both light and dark cycles while *PGC-1β*-deficient mice have decreased activity during the dark cycle. Finally, *PGC-1α*-deficient but not *PGC-1β*-deficient mice develop neuronal degeneration (Lin et al., 2004; Sonoda et al., 2007).

The activation of PGC-1α by NAD^+-linked deacetylation by SIRT1 directly ties OXPHOS induction to calorie restriction (Cheng

et al., 2003; McBurney et al., 2003) (Boily et al., 2008; Wallace, 2005c). SIRT1 is the mammalian orthologue of the yeast Sir2, and Sir2 orthologues regulate life span in association with calorie restriction in multiple species (Lin et al., 2000; Rogina and Helfand, 2004; Wallace, 2005c). Thus, longevity and mitochondrial energetics are linked.

The homozygous knockout of Sirt1 in the mouse on a 129/Sv background results in a 50% prenatal mortality, with the remaining animals being small and dying within a month. Sirt1 deficiency on a CD1 and 129/Sv mixed background results in animals which survive to adulthood, though both males and females are sterile (McBurney et al., 2003). On the 129/Sv background, the *Sirt1* −/− mutation is associated with retinal and heart defects (Cheng et al., 2003). Microarray analysis of Sirt1-silenced animals suggests that Sirt1 acts more on mammalian signal transduction pathways and transcription factors than on chromatin structure (McBurney et al., 2003).

Sirt1 −/− mice remain small and are also less active, yet their daily food intake is normal. This is because they are hypermetabolic, *Sirt1* −/− liver mitochondria being more uncoupled and thus less efficient at generating ATP. Caloric restriction of *Sirt1* −/− mice does not extend lifespan, supporting the hypothesis that life span is extended by the up-regulation of mitochondrial OXPHOS through the Sirt1-mediated deacetylation of the FOXO and PGC-1α transcription factors (Boily et al., 2008).

Mice in which the mitochondrial Sirt3 and Sirt5 genes have been inactivated are viable (Haigis et al., 2006; Lombard et al., 2007). *Sirt3* −/− mice have no histological abnormalities or marked changes in the expression of TFAM, MnSOD, COX IV, cyt c, and Ucp-1 in BAT even though mitochondrial proteins such as glutamate dehydrogenase (GDH) have markedly increased acetylated lysine levels (Lombard et al., 2007). However, the hyperacetylation of mitochondrial proteins seen in *Sirt3* −/− mouse embryo fibroblasts and *Sirt3* −/− tissues is associated with a 50% reduction in mitochondrial ATP production and complex I activity (Ahn et al., 2008). Thus, *Sirt3* appears to be regulating mitochondrial basal metabolic rate. Since Sirtuins are activated by NAD^+, an increased NAD^+/NADH ratio resulting from a starvation state would deacetylate the OXPHOS proteins increasing mitochondrial basal metabolic rate and facilitating the oxidation of stored fats to generate ATP.

Sirt4 is an ADP-ribosylase. While *Sirt4* −/− mice appear normal in development, growth, and fertility, they show increased circulating insulin levels. Exposure of *Sirt4* −/− islets to glucose significantly increases insulin secretion. Injection of glutamine into *Sirt4* −/− mice also increases plasma insulin and *Sirt4* −/− islets exposed to glutamine or leucine have increased insulin secretion. These effects are mediated by the Sirt4-regulating ADP-ribosylation of pancreatic GDH which decreases its activity thus negatively regulating amino acid stimulated insulin secretion (Haigis et al., 2006).

Therefore, the acetylation of the FOXO transcription factors and the PGC-1α and β transcriptional co-activators via acetyl-CoA depress OXPHOS, shifting metabolism toward glycolysis in the fed state. However, during fasting the shift of the NADH/NAD^+ ratio toward NAD^+ results in the Sirt1-mediated deacetylation of these factors. Similarly, during fasting when NAD^+ is prevalent, GDH is ADP-ribosylated and inactivated, suppressing amino acid stimulated insulin secretion. This inhibits the storage of calories as fat, activates the FOXOs and induces and activates PGC-1α, thus inducing mitochondrial OXPHOS to oxidize fatty acids and amino acids to provide energy during fasting. Therefore, regulation of energetic gene expression and metabolism is directly linked to the availability and nature of the calories for the animal, intimately linking mitochondrial energy metabolism and the epigenome.

4. Mitochondrial genetic disease

The elucidation of a broad spectrum of mtDNA and nDNA mitochondrial gene mutation diseases has revealed that mitochondrial dysfunction can result in the entire range of clinical phenotypes associated with metabolic and degenerative diseases as well as cancer and aging (Wallace et al., 2007). Mitochondrial diseases have been shown to affect the highly oxidative tissues including the brain, heart, muscle, kidney, and endocrine systems; as well as the metabolic systems resulting in diabetes, obesity, and influence a range of age-related disorders. Thus, the symptoms of mitochondrial diseases correspond to those attributed to epigenomic changes.

4.1. Recent mtDNA mutations and diseases

Clinically relevant mtDNA variants fall into three classes: recent deleterious mutations resulting in maternally transmitted disease, ancient adaptive variants that predispose individuals to disease in different environments, and the age-related accumulation of somatic mtDNA mutations that erode function and provide the aging clock. The extraordinary clinical variability of mtDNA diseases results from different mutations in the same gene causing different phenotypes and from the same mutation at different levels of heteroplasmy causing different phenotypes (Wallace, 2005c).

Pathogenic mtDNA mutations include both rearrangement mutations and base substitution mutations. Rearrangement mutations can either be *de novo* deletion mutations or maternally transmitted insertion mutations which are unstable and generate deletion mutations in post-mitotic cells. Most deletion mutations remove at least one tRNA and thus affect protein synthesis (Wallace et al., 2001). mtDNA rearrangement syndromes are invariably heteroplasmic and have been associated with maternally-inherited diabetes and deafness, Chronic Progressive External Ophthalmoplegia (CPEO), the Kearns–Sayre Syndrome (KSS), and the Pearson marrow/pancreas syndrome. Differences in mtDNA rearrangement phenotypes appear to stem from differences between insertions and deletions, the diversity of tissues that contain the rearrangement, and the percentage of mtDNAs harboring the rearrangement in each tissue (Wallace et al., 2007).

Base substitution mutations can alter either polypeptide genes (polypeptide mutations) or rRNAs and tRNAs (protein synthesis mutations). Pathogenic polypeptide mutations encompass a broad spectrum of multisystem diseases including LHON (Wallace et al., 1988a), Leigh syndrome (Holt et al., 1990), and mitochondrial myopathy (Andreu et al., 1999a,b, 1998). Mitochondrial tRNA and rRNA protein synthesis mutations can result in multisystem diseases including Myoclonic Epilepsy and Ragged Red Fiber Disease (MERRF) (Shoffner et al., 1990; Wallace et al., 1988b); Mitochondrial Encephalomyopathy, Lactic Acidosis, and Stroke-Like Episodes (MELAS) (Goto et al., 1990); encephalomyopathy; mitochondrial myopathy and exercise intolerance; CPEO and KSS; gastrointestinal syndrome; dystonia; diabetes; deafness; cardiomyopathy; renal failure, Alzheimer Disease (AD); Parkinson Disease (PD) (Wallace et al., 2007).

4.2. Ancient mtDNA mutations and disease

As modern humans migrated out of Africa, mtDNA mutations accumulated along radiating maternal lineages. When a mtDNA acquired a functional mutation beneficial in a particular environment, then that mtDNA became enriched by selection and radiated within that environment to give a cluster of related mtDNA haplotypes, known as a haplogroup. Hence, haplogroups correlate with the geographic origin of the indigenous population

being studied and are designated by sequential alphabetical letters (Mishmar et al., 2003; Ruiz-Pesini et al., 2004; Ruiz-Pesini and Wallace, 2006; Wallace, 2005c; Wallace et al., 1999, 2003).

These same ancient adaptive mtDNA mutations influence individual predisposition to a wide spectrum of common diseases today. Various mtDNA haplogroups have been associated with neurodegenerative diseases (Brown et al., 2002, 1997, 1995; Carrieri et al., 2001; Chagnon et al., 1999; Ghezzi et al., 2005; Jones et al., 2007; Khusnutdinova et al., 2008; Shoffner et al., 1993; Torroni et al., 1997; Udar et al., 2009; van der Walt et al., 2004, 2003), diabetes and metabolic syndrome (Crispim et al., 2006; Fuku et al., 2007; Mohlke et al., 2005; Nishigaki et al., 2007; Saxena et al., 2006), infectious disease including AIDS progression (Baudouin et al., 2005; Hendrickson et al., 2008, 2009; Raby et al., 2007), longevity (De Benedictis et al., 1999; Ivanova et al., 1998; Niemi et al., 2003; Rose et al., 2001; Tanaka et al., 2000, 1998), and cancer (Bai et al., 2007; Booker et al., 2006; Brandon et al., 2006; Darvishi et al., 2007; Gottlieb and Tomlinson, 2005; Wallace, 2005a). From these reports, it is clear that mtDNA functional variation modulates predisposition to a wide range of metabolic and degenerative diseases as well as influencing cancer risk and longevity.

4.3. Somatic mtDNA mutations in aging and cancer

Mutations in the mtDNA have been observed to accumulate with age in a variety of post-mitotic tissues in a wide range of species, and in a spectrum of complex of age-related diseases (Wallace, 2005c). Increasing the mtDNA mutation rate in mice increases their aging rate (Kujoth et al., 2005; Trifunovic et al., 2004) while decreasing the somatic mtDNA mutation rate by introducing catalase into the mitochondrial matrix extends mouse life span (Schriner et al., 2005). Therefore, the accumulation of somatic mtDNA mutations provides an aging clock that helps define an animal's life span and contributes to the delayed-onset and progressive course of complex diseases (Wallace, 2005c). Moreover, both somatic and germline mtDNA mutations have been associated with cancer (Brandon et al., 2006; Ishikawa et al., 2008; Petros et al., 2005; Wallace, 2005a).

4.4. Mitochondrial diseases of nDNA–mtDNA interaction

Mutations in nDNA-encoded OXPHOS genes have also been linked to a variety of multisystem disorders (Wallace et al., 2007). These include mutations that inactivate OXPHOS complex structural and assembly genes (Procaccio and Wallace, 2004; Zhu et al., 1998), mutations that destabilize the mtDNA (Carrozzo et al., 2007; Kaukonen et al., 2000; Mandel et al., 2001; Nishino et al., 1999; Palmieri et al., 2005; Saada et al., 2001; Spelbrink et al., 2001; Van Goethem et al., 2001), and mutations that perturb mitochondrial fusion and fission (Delettre et al., 2000; Zuchner et al., 2004).

5. Mitochondrial explanations for epigenetic diseases

Therefore, mitochondrial gene defects can result in virtually all of the symptoms associated with the common "complex" diseases, confirming the importance of mitochondrial bioenergetics in health. Since mitochondrial metabolism also regulates the substrates for epigenomic regulation, it follows that changes in mitochondrial metabolism may also perturb the epigenomic state. Furthermore, in cells and animals in which the epigenomic elements NRs, PGC-1α and β, and the Sirtuins are inactivated, mitochondrial function is also perturbed. Similarly, compounds such as resveratrol and its derivatives, which activate SIRT1, can up-regulate mitochondrial energy production and have been found to ameliorate metabolic and age-related phenotypes (Baur et al., 2006; Baur and Sinclair, 2006; Feige et al., 2008; Figarella-Branger et al., 1992; Lagouge et al., 2006; Milne and Denu, 2008; Milne et al., 2007; Pearson et al., 2008; Wood et al., 2004). It therefore follows that alterations in the epigenome should also perturb mitochondrial function. Epigenetic alteration in mitochondrial function could occur at either the local intra-chromosomal domain level to suppress mitochondrial regulatory or maintenance genes or at the inter-chromosomal level to disrupt transcriptional factories resulting in the loss of coordinate regulation of energetic genes.

5.1. Altered intra-chromosomal domains and energetics

Evidence that mitochondrial dysfunction is associated with epigenomic changes can be found for a wide range of classical epigenomic diseases. In cancer, a genetic disease, changes in the epigenome such as "Loss of Imprinting" (LOI) and hypomethylation are common. LOI of the insulin-like growth factor II (IGF2) provides one example of how changes in the cancer epigenome might affect mitochondrial function. Half of Wilms tumors as well as lung cancer, breast cancer, ovarian cancer, and glioma show LOI of the IGF2 locus. IGF2 is an imprinted locus normally expressed only from the paternal allele. Hence, LOI increases IGF2 expression (Bjornsson et al., 2007; Feinberg, 2007). In the mouse, LOI of Igf2 is associated with enhanced Igf2 signaling due to augmentation of Akt/PKB signaling (Kaneda et al., 2007). Activation of the Akt/PKB pathway suppresses mitochondrial OXPHOS and drives the cell toward glycolysis (Fig. 1). Glycolysis is also enhanced in liver cancer by reversing the hypermethylation of the promoter of hexokinase II. Following epigenomic activation, hexokinase II transcription is further regulated by glucose; hypoxia via HIF-1α, cAMP via CREB, insulin and glucagon, and mutated p53 (Goel et al., 2003; Wallace, 2005a). Hexokinase II binds glucose and ATP, converting them into glucose-6-phosphate, the commitment step of glycolysis. Akt/PKB also phosphorylates hexokinase II causing it to bind to the mitochondrial outer membrane pore protein porin (voltage dependent anion channel, VDAC) with high affinity. The binding of hexokinase II to VDAC also antagonizes the pro-apoptotic action of Bax and Bak. The expression profile of the ANT isoforms is also altered in transformed cells (Torroni et al., 1990) and the ANTs export the mitochondrial ATP from the matrix to the intermembrane space so that VDAC can export ATP into the cytosol. Thus the binding of hexokinase II to VDAC means that ATP leaving the mitochondria binds preferentially to hexokinase II. This co-opts mitochondrial ATP production to drive glycolysis. Therefore, epigenetic changes in cancer specifically suppress mitochondrial function in favor of glycolysis.

The chromatin modifications of cancer cells can be directly modulated by mitochondrial OXPHOS. Cancer cells which have been cured of their mtDNA but either chemical or genetic treatments have been found to have altered methylation patterns in 2–9% of the CpG islands surveyed. This is comparable to the 2–5% alteration in methylation regions associated with epigenomic changes during differentiation. In three out of four cases, removal of the mtDNA leads to the hypomethylation commonly associated with LOI in cultured cancer cells. When mtDNAs were reintroduced to the mtDNA-deficient cancer cells, 30% of the hypomethylated sites become remethylated. Thus, there is a direct cause and effect relationship between mitochondrial function and epigenomic methylation in cancer cells (Naviaux, 2008; Smiraglia et al., 2008).

The p53 protein also regulates OXPHOS through induction of the complex IV chaperone protein "Synthesis of Cytochrome *c* Oxidase 2" (SCO2) which is responsible for inserting Cu into COX. By contrast, p53 negatively regulates phosphoglycerate mutase of glycolysis and Akt. Therefore, mutational inactivation of p53 in cancer

cells suppresses OXPHOS and induces glycolysis (Matoba et al., 2006).

Epigenetic alteration in genomic methylation in association and in part because of mitochondrial OXPHOS deficiency acts in concert with alterations in the expression of IGF2, hexokinase II, the ANTs, and the inactivation of p53, to shift cancer cell energy production of toward glycolysis. This helps to explain Otto Warburg's observation over 70 years ago that cancer cells generate excess lactate indicating hyperactive glycolysis, in the presence of oxygen, "aerobic glycolysis" (Wallace, 2005a).

LOI in the IGF2 gene region on chromosome 11q15.5 can also result in the dymorphology condition, Beckwith–Wiedemann Syndrome (BWS). About 15% of BWS of patients show LOI at the IGF2 locus reactivating the maternal allele and resulting in the overproduction of IGF2. IGF2 overproduction leads to prenatal overgrowth, midline abdominal wall defects, ear creases and pits, and neonatal hypoglycemia. BWS cases associated with IGF2 LOI are also prone to Wilm's tumor (Bjornsson et al., 2007; Feinberg, 2007, 2008). Again, over-expression of IGF2, acting via the PI3K-Akt-FOXO-PGC-1α pathway, would suppress mitochondrial OXPHOS (Fig. 1).

In the mouse, the BWS locus is located on chromosome 7. The expression of the paternally expressed *Igf2* gene and the maternally expressed *H19* are regulated by the surrounding chromatin loop structure. The *Igf2* and *H19* genes are encompassed in an approximately 100 kb imprinted region, separated by a CTCF insulator site with an enhancer down stream of *H19*. The paternal and maternal transcription of the *Igf2* and *H19* genes is regulated by the interaction of differentially methylated regions (DMRs), three in *Igf2* and one at the CTCF insulator site. On the maternal chromosome, the DMR of *H19* associates with DMR1 near the 5′ end of *Igf2*. This places *H19* in the active chromatin domain with the enhancer and the *Igf2* gene on the other side of the CTCF site in an inactive chromatin domain shutting off *Igf2*. On the paternal chromosome, the *H19* DMR interacts with the 3′ *Igf2* DMR2 domain. This creates a loop which brings the *Igf2* gene adjacent to the *H19* enhancer on the same side as the enhancer, thus permitting its transcription. The *H19* gene on this chromosome is methylated and silenced (Murrell et al., 2004). Therefore, LOI in both cancer and BWS link epigenomic alterations to mitochondrial dysfunction.

Prader–Willi syndrome (PWS) and Angelman syndrome (AS) are classical examples of epigenomic diseases resulting from genetic errors in imprinted loci on chromosome 15q11-13. Preliminary evidence is implicating mitochondrial dysfunction in AS as well. PWS is associated with hypotonia, hyperphagia, and obesity while AS is associated with hyperactivity, thinness, and autism. PWS involves a paternal deficiency in 15q11-13 while AS involves a maternal deficiency. Current evidence suggests that the expression of the small nuclear ribonuclear polypeptide N (*SNRPN*) and the adjacent imprinting control region (ICR) and the expression of the ubiquitin-protein ligase E3A (*UBE3A*) are reciprocally imprinted on the maternal and paternal chromosomes. Therefore, genetic inactivation of the expressed *UBE3A* gene is responsible for AS and inactivation of the expressed *SNRPN* and ICR loci are associated with the PWS phenotype (Feinberg, 2007). In an analysis of mice mutated at the *UBE3A* locus, we have found that the brain mitochondria are small and dense and that the activity of the combined respiratory complex III is reduced (Su et al., 2009). Therefore, mitochondrial dysfunction may contribute to the etiology of AS. While the mechanism by which *UBE3A* deficiency causes mitochondrial dysfunction is unknown, *UBE3A* is an E3 ubiquitin ligase and ubiquination is important in maintaining the structural and functional integrity of the mitochondrion (Escobar-Henriques et al., 2006; Neutzner and Youle, 2005). The mitochondrial ubiquitin ligase MARCH-V is important in regulating the mitochondrial fusion and fission dynamics through Drp1 and Fis1 (Karbowski et al., 2007; Nakamura et al., 2006) and the human deubiquitinating enzyme ubiquitin-specific protease 30 (USP30) is embedded in the mitochondrial outer membrane and important in maintaining mitochondrial morphology (Nakamura and Hirose, 2008). Therefore, loss of the 15q11-13 loci could perturb mitochondrial function and explain some of the pathophysiology of these diseases.

Tuberous sclerosis complex (TSC) is another cell over-growth disorder, which affects virtually every organ of the body. Clinical features include cutaneous hypomelanotic macules, facial angiofibromas, etc.; central nervous system subependymal nodules, and cortical tubers, learning difficulties, and seizures; renal angiomyolipomas and cysts; cardiac rhabdomyomas; and retinal hamartoma. TSC is caused by mutations in either the hamartin TSC1 gene or the tuberin TSC2 gene. TSC1 + 2 act through Rheb to regulate TORC1, and TOR is implicated in regulation of mitochondrial OXPHOS (Chen et al., 2008; Shadel, 2008)(Fig. 1).

About 25–50% of TSC subjects manifest autistic traits. Autism has been associated with alteration in neurite growth and synaptic plasticity and there is growing evidence that the mitochondria play a central role in these processes (Kang et al., 2008; Li et al., 2004; Mattson and Liu, 2002; Schuman and Chan, 2004). Therefore, TSC forms a connection between cell over-growth syndromes, neurological disorders such as autism, and mitochondrial energy metabolism.

The Fragile X Mental Retardation (FMR) Syndrome is also associated with mental retardation and autism. The FMR protein (FMRP) is an RNA binding protein that has recently been shown to be required for the expression of the mitochondrial and cytosolic Cu/Zn superoxide dismutase (SOD1) (Bechara et al., 2009). Since SOD1 functions to eliminate mitochondrial intermembrane space superoxide, its suppression could increase mitochondrial oxidative stress and thus cause symptoms through mitochondrial dysfunction (Wallace, 2005c).

Rett syndrome is an autism spectrum disorder caused by mutations in the X-linked *MeCP2* gene (Amir et al., 1999; Loat et al., 2008). Rett patients have been reported to harbor mitochondrial structural aberrations and reductions in skeletal muscle OXPHOS complexes I, III, IV, though not II. Furthermore, mice in which MeCP2 is inactivated have increased complex III and core protein 1 gene (*Ugcrc1*) expression, together with reduced OXPHOS coupling (Eeg-Olofsson et al., 1989; Heilstedt et al., 2002; Kriaucionis et al., 2006). The MeCP2 protein binds to methyl CpG nDNA domains and modulates gene expression, either activation or repression, in part by recruiting histone-modifying enzymes such as deacetylases and methyltransferases (Chen et al., 2003b; Klein et al., 2007). MeCP2 can impart long-term silencing by binding to CpG rich domains and stimulating the deacetylation of histones H3 and H4 resulting in chromatin condensation. MeCP2 can also perform histone deacetylase-independent repression which is relevant to X chromosome inactivation and genomic imprinting (Matijevic et al., 2009). One of the targets of MeCP2 is promoter III of the neurotrophin gene, *BDNF* (Brain-Derived Neurotrophic Factor). It was first thought the MeCP2 repressed BDNF expression (Chen et al., 2003b), but MeCP2 was subsequently reported to enhance BDNF expression (Klein et al., 2007). Neurotrophic factors such as BDNF as well as cAMP stimulate the phosphorylation of CREB, which is important in neuronal plasticity and neurite outgrowth. Furthermore, the translation of *BDNF* mRNA and *p250GAP* mRNA are inhibited by the microRNA, miR132, and both BDNF and p250GAP regulate neuronal morphogenesis. The expression of miR132 is also induced by phospho-CREB demonstrating a feedback loop for regulating neuronal morphogenesis (Klein et al., 2007; Vo et al., 2005). Neurotrophic factors such as BDNF and NGF, bind and activate the tropomyosin-related kinase (Trk) receptor B (TrkB). Major downstream pathways of the neurotrophic factors are the PI3K-Akt- and MAPK pathways and PKC. These in turn

regulate AP1, NFκB, and the FOXOs to regulate energy production pathways, antioxidant enzymes, and anti-apoptotic proteins (Mattson, 2008).

In a rat brain preparation of mitochondria plus synaptosomal membranes, BDNF was found to act through the MAPK pathway to increase OXPHOS coupling efficiency, presumably increasing ATP production. This modulation occurs through complex I, not complex II, and occurs when glutamate and malate are used as the mitochondrial NADH generators, but not when pyruvate and malate were used. Thus, the BDNF regulation of mitochondrial respiration is specific for glutamate as a substrate, and glutamate along with γ-aminobutyric acid (GABA) are coupled through the TCA cycle to neuronal metabolism and transmission. BDNF can also modulate the stimulation of oxygen consumption by calcium, which is also consistent with increasing coupling efficiency (Markham et al., 2004). Surprisingly, the BDNF receptor, TrkB, has been localized to the mitochondrion, as well as to the plasma and endoplasmic reticulum membranes, in both muscle and nerve cells. The TrkB receptor has three isoforms, full length TrkB with tyrosine kinase activity, and two truncated forms (TrkB-T1 and TrkB-T2) without the tyrosine kinase domain. The truncated forms of TrkB appear to predominate in the mitochondrion, and preliminary studies suggest that they are localized to the mitochondrial inner membrane (Wiedemann et al., 2006). Since TrkB1 has been reported to mediate BDNF-evoked calcium signaling in glial cells, it is possible that TrkB-T1 is directly regulating mitochondrial ATP production and mitochondrial calcium homeostasis through modulating the mitochondrial membrane potential. Therefore, inactivation of MeCP2 could selectively repress the expression of the nDNA-encoded mitochondrial genes, providing a coherent argument that at least part of the pathophysiology of Rett syndrome involves mitochondrial dysfunction.

MeCP2 also binds to the PWS imprinting control region (ICR) and down-regulates *Ube3a* and the adjacent Gaba receptor gene (*Gabrb3*). MeCP2 also binds to the *H19* imprinted region altering regulation of the adjacent *Igf2* expression (Samaco et al., 2005). This co-regulation of the dispersed genes within a chromosomal region suggests that MeCP2 might regulate chromatin transcriptional loop domains (Murrell et al., 2004) and perhaps disrupts a mitochondrial gene transcriptional factory. Therefore, Rett Syndrome provides a strong case for how perturbation of the epigenome could reduce mitochondrial function.

Timothy syndrome, which presents with autism and Long QT syndrome, provides further evidence for connecting neurodegenerative disease with Ca^{++} regulation and thus mitochondrial function. Timothy Syndrome has been linked to mutations in the T-type voltage-gated $Ca_v1.2$ channel encoded by the *CACNA1C* gene, most commonly involving the G406R allele (Gargus, 2009). $Ca_v1.2$ shows its highest expression in the hippocampus, amygdale, and putamen. A survey of the *CACNA1H* gene, a close paralog of the Timothy syndrome Ca^{++} channel, in 461 autism DNAs revealed six new mutations. Functional studies of two of these mutant proteins, R212C and R902W, revealed extended Ca^{++} influx into the cytosol (Splawski et al., 2006). Cytosolic Ca^{++} levels are regulated by mitochondrial Ca^{++} uptake, driven by the mitochondrial inner membrane potential (ΔP). Excessive Ca^{++} uptake would limit ATP production, increase oxidative stress, and activate the mtPTP causing cell death.

Evidence is also accumulating implicating mitochondrial dysfunction in some forms of autism spectrum disorder (ASD), in addition to AS, TSC, Rett syndrome, FMR and Timothy syndrome. A subset of ASD patients is associated with chromosomal gene copy number variants (CNV). Ten percent of sporadic autism patients have CNVs, as compared to 3% of multiplex families and 1% of controls (Sebat et al., 2007; Zhao et al., 2007). A subset of these variants may coincide with important nDNA mitochondrial gene loci (Smith et al., 2008). Alterations in mitochondrial structure and function have been repeatedly observed in autistic patients (Correia et al., 2006; Filipek, 2005; Gargus and Imtiaz, 2008; Haas et al., 1996; Holtzman, 2008; Lombard, 1998; Oliveira et al., 2007; Poling et al., 2006), and alterations in the mtDNA have been observed in some cases of ASD (Fillano et al., 2002; Graf et al., 2000; Pons et al., 2004). The activity of the mitochondrial inner membrane Ca-regulated aspartate/glutamate carrier (AGC) gene, *SLC25A12*, and/or its expression have been reported to be increased in autistic patients, at least in part due to elevated brain calcium levels (Lepagnol-Bestel et al., 2008; Palmieri et al., 2008; Ramoz et al., 2004). *SLC25A12*-deficient mice show impaired myelination, confirming that alterations in AGC activity can affect neurological function (Hong et al., 2007). Since AGC regulates the increased flux of reducing equivalents into the mitochondrion, increased AGC activity would initially increase ATP production, but ultimately overload the ETC with electrons increasing oxidative stress and causing the loss of neuronal spines and synapses characteristic of autism pathology (Lepagnol-Bestel et al., 2008; Palmieri et al., 2008; Ramoz et al., 2004). Therefore, mitochondrial dysfunction may account for some forms of ASD.

The importance of mitochondrial ROS production in cell function and stem cell biology has been demonstrated in studies of mice in which the Bmi1 member of the Polycomb family has been inactivated. The Polycomb family of transcription repressors mediates gene silencing by regulating chromatin structure. Bim1 is essential for the maintenance and self-renewal of both the hematopoietic and neuronal stem cells, and *Bim1* −/− mice have severe neurological abnormalities, alterations in hematopoietic cells, growth retardation, and shortened life span. Bone marrow cells from Bim1-deficient mice show an inhibition of mitochondrial ETC, reduced O_2 consumption, reduced ATP production, and increase mitochondrial ROS production. The increased mitochondrial ROS is a major factor for the reduced stem cell function. The reduction of the *Bim1*−/− induced ROS using N-acetylcysteine antioxidant is associated with the recovery of the bone marrow derived cells and partial restoration of thymic atrophy. In part, the effects of the increased mitochondrial ROS are due to activation of the DNA damage response pathway. This was confirmed by inactivation of the Chk2 gene which partially restored the normal phenotype (Liu et al., 2009). Therefore, genes central to stem cell function and thus development can be directly regulated by mitochondrial ROS signaling.

The mitochondrion also plays an important role in calcium homeostasis. In mice, neuronal spine formation and maintenance can be modulated by the inactivation of the mitochondrial anti-apoptotic protein, Bcl-w, and the glutamate receptor δ (Grid2), an excitatory Ca^{++} channel expressed in Purkinje cells. Bcl-w and Grid2-deficient mice develop enormously elongated mitochondria in their Purkinje dendrites indicating blocked mitochondrial fission. This is associated with aberrant dendrites, spines, and synapses and results in severe ataxia. Therefore, mitochondrial calcium not only regulates mitochondrial metabolism but also mitochondrial fission, directly affecting synapse formation, learning, and memory (Liu and Shio, 2008).

5.2. Altered transcriptional factories and energy deficits

While the above examples suggest the inhibition of mitochondrial function through alterations in the transcriptional regulation of individual chromosomal domains, the maintenance of the mitochondria likely also requires the coordinate expression of many mitochondrial loci dispersed across multiple chromosomes. These dispersed mitochondrial genes might require inter-chromosomal factories for coordinate expression. Therefore, we might expect that epigenomic defects that disrupt transcriptional factories

might also be associated with mitochondrial dysfunction. The laminopathies could represent this class of epigenomic defect.

The laminopathies are caused by mutations in the *LMNA* gene, the product of which is involved in the production of the type V intermediate filament lamina that line the inside of the nuclear envelope, but are also found in the nucleoplasm. The lamina are produced from three genes: lamins A and C produced by alternative splicing from the *LMNA* gene, lamin B1 produced by the *LMNB1* gene, and lamins B2 + B3 produced from the *LMNB2* gene. The B-type lamins are ancient and constitutive and remain associated with the nuclear envelope at interphase and during mitosis. The A-type lamins (A/C) arose along with the metazoans, are expressed in association with differentiation, dissociate from the nuclear envelope during mitosis (Liu and Zhou, 2008), and a substantial portion are found centrally within the nucleus (Galiova et al., 2008).

The lamin A protein consists of a globular N-terminus domain, followed by an α-helical rod-like domain containing four coiled-coil repeats (1A, 1B, 2A, 2B), a nuclear localization sequence, an Ig-like domain, and a C-terminal domain which includes the end of the mature lamin A followed by a C-terminal pre-peptide extension ending in the sequence Cys-Ser-Ile-Met. In newly synthesized normal prelamin A, the Cys in the Cys-Ser-Ile-Met peptide is farnesylated by farnesyltransferase (FT) resulting in binding to the endoplasmic reticulum (ER). The ER metalloprotease, ZMPSTE24, then cleaves off the terminal Ser-Ile-Met peptide, and the free Cys carboxyl group is methylated. ZMPSTE24 again cleaves prelamin A 15 amino acids N-terminal from the farnesylated Cys. This releases soluble lamin A to be imported into the nucleus where it is assembled with lamin B into the nuclear lamina as well as being located in the nucleoplasm. Lamin C encompasses the N-terminal 2/3 of the lamin A protein (Liu and Zhou, 2008). The lamin B proteins are also farnesylated, but not proteolytically processed. Hence, they remain membrane bound and diffuse along the ER into the nuclear envelope where they nucleate the assembly of the soluble lamin A and C polypeptides into the nuclear lamina.

Over 200 pathogenic mutations have been identified in the *LMNA* gene yielding a plethora of clinical phenotypes. These phenotypes can be recapitulated by the introduction of *Lmna* and *Zmpste24* gene mutations into the mouse, thus proving that lamin A and C defects cause these diseases (Stewart et al., 2007).

The pathophysiology of these diseases remains a mystery. A common finding among the *LMNA* mutations is the presence of highly distorted nuclei and marked repositioning of heterochromatin within the nucleus (Liu and Zhou, 2008; Park et al., 2009; Worman and Bonne, 2007). The nuclear lamina binds the Sun 1 and 2 proteins, which extend through the inner nuclear membrane, interact with the Nesprin-2 Giant and Nesprin-3 proteins that extend through the outer nuclear membrane, and which bind to the cytosolic actin cytoskeleton. Emerin, which interacts with lamin A, also links the nuclear envelope to the microtubule network and anchors the centrosome (Hale et al., 2008; Lee et al., 2007). LMNA-induced alterations in the cytoskeleton should alter the distribution and movement of mitochondria which are tethered to the cytoskeleton. Since treatment of cells with microtubule inhibitors alters mitochondrial OXPHOS activity and increases ROS production (Wagner et al., 2008), *LMNA* mutations could contribute to reduced mitochondrial function and increased ROS production.

Lamin A deficiency also results in redistribution of chromatin within the nucleus. In immortalized mouse embryo fibroblasts, 50% of the nuclear periphery is occupied by heterochromatin, but in *Lmna* −/− cells, the level of peripheral heterochromatin is significantly reduced. Moreover, the number of chromocenters is reduced in the nuclear interior of *Lmna* −/− cells and the heterochromatin clusters in larger internal nuclear aggregates. *Lmna* −/− cells also have smaller chromosomal domain areas than *Lmna* +/+ cells. Among the HP1α, β, and γ proteins important in heterochromatization, the HP1β develops chain-like aggregates. Treatment of *Lmna* +/+ or −/− cells with the HDAC inhibitor, Trichostatin (TSA), causes the areas of the chromosomal domains of *Lmna* −/− cell to increase and approach the size and distribution as those of *Lmna* +/+ cells and also restores the distribution of the HP1β and SC-35 foci (Galiova et al., 2008). Therefore, *Lmna* mutations that disorganize the chromatin domain structure and could result in loss of coordinate transcriptional control of the dispersed energy genes.

Consistent with this conjecture, lamin A mutations have been associated with an altered distribution and function of key transcription factors (e.g., c-fos, β-catenin, etc.) (Liu and Zhou, 2008; Pekovic et al., 2007; Pekovic and Hutchison, 2008), activation of the MAPK stress pathway (Muchir et al., 2007), and the Notch pathway (Scaffidi and Misteli, 2008). Lamin A alterations have also been associated with suppression of the Wnt and Mitf signaling pathways in epidermal stem cells (Espada et al., 2008) and of myogenin (*Myog*) expression in muscle cells. Increases in H3-K9me2 and failures to hypertrimethylate H3-K4 around *Myog* and the redistribution of H3-K27me3 away from the pericentric heterochromatin have also been observed (Hakelien et al., 2008). Therefore, lamin A appears to be important in maintaining an open chromatin conformation and thus the sustaining of transcription, perhaps within transcriptional factories important for coordinate mitochondrial gene expression.

Patients with *LMNA* mutations have been classified into four classes based on clinical phenotypes (Liu and Zhou, 2008). However, *LMNA* mutations frequently exhibit pleiotropic phenotypes and variable familial expressivity (Mercuri et al., 2005; Rankin et al., 2008). Class I laminopathies encompasses diseases of skeletal muscle and heart, including autosomal dominant (AD)-Emery-Dreifuss muscular dystrophy (EDMD), autosomal recessive (AR)-EDMD, AD-dilated cardiomyopathy 1A, and AD-limb girdle muscular dystrophy (LGMD). EDMD and LGMD *LMNA* mutations present with variable degrees of muscle weakness, cardiomyopathy, and contractures (Park et al., 2009). Cardiomyopathy patients are subject to cardiac conduction defects, sudden death, and dilated cardiomyopathy, with or without skeletal muscle weakness (Perrot et al., 2009; Wolf et al., 2008). EDMD mutations are distributed in lamin A from the N-terminal end through the Ig-like domain, but can be found elsewhere. DCM1A and LGMD1A mutations are found primarily in the coiled-coil protein domain (Liu and Zhou, 2008). Suggestive evidence that heart-muscle lamin A diseases are associated with mitochondria dysfunction comes for a boy who presented at six with delayed motor milestones, and proximal and truncal weakness. This progressed by 9 years to severe, progressive cardiomyopathy necessitating heart transplant. His mother and brother had died at 31 and 8 years, respectively, of cardiomyopathy. Mitochondrial respiratory chain analysis of heart and skeletal muscle revealed a complex IV activity of 0.005 (normal being 0.014–0.034). Molecular studies failed to detect any of the known common pathogenic mtDNA mutations. However, nDNA studies revealed that the family harbored the common *LMNA* p.R644C missense mutation (Mercuri et al., 2005).

The Class II laminopathies involve Charcot-Marie-Tooth (CMT) type 2B1, a peripheral neuropathy. The two *LMNA* mutations linked with AD-CMT2B1 are associated with mildly reduced nerve conduction, neuron demyelination, and axonal degeneration (Liu and Zhou, 2008), and both are adjacent to each other in the 2A coiled-coil domain (Liu and Zhou, 2008). Charcot-Marie-Tooth, Type 2A can also be caused by mutations in the nDNA-encoded mitochondrial fusion gene, mitofusin 2 (Zuchner et al., 2004).

Class III laminopathies encompass the lipodystrophy syndromes and include AD-familial partial lipodystrophy, Dunnigan-type (FPLD2); AD-congenital generalized lipodystrophy type 2

(CGL2); and AR-mandibuloacral dysplasia. FPLD2 *LMNA* mutations are associated with loss of subcutaneous white adipose tissue (WAT) in limbs and the accumulation of WAT in the face, neck, and abdominal areas. The CGL2 *LMNA* mutations lead to diabetes with glucose intolerance, hepatic stenosis, hyperpigmentation, muscular atrophy, and hypertrophic cardiomyopathy (Araujo-Vilar et al., 2008; Liu and Zhou, 2008; Worman and Bonne, 2007). Women with FPLD2 from *LMNA* mutations can develop an array of fertility problems including polycystic ovaries, infertility, gestational diabetes, and preeclampsia (Vantyghem et al., 2008). Population variants in *LMNA* have also been associated with increased risk of diabetes (Duesing et al., 2008), and alterations in *LMNA* mRNA levels are observed in patients with diabetes and obesity (Miranda et al., 2008). FLPD mutations are often found in the Ig-like domain and the C-terminal region of the mature lamin A protein (Liu and Zhou, 2008).

A mitochondrial association with Class III laminopathies is supported by a study of cultured human fibroblast cell lines harboring six different heterozygous *LMNA* mutations (D47Y, L92F, L387V, R399H, L421P, and R482W) all derived from patients with insulin resistance and/or lipodystrophy. All of these cell lines were found by western blot to have a marked deficiency in the level of the mtDNA COII (COX2) protein but not the nDNA COX4 protein. These cell lines also showed increased ROS production which colocalized with the mitochondria (Caron et al., 2007).

All of these cells exhibit distorted nuclei have reduced proliferative capacity, increased tendency to generate senescent SA-β-galactosidase positive cells, and elevated prelamin A protein levels. Treatment of normal fibroblast cultures with the HIV anti-retroviral protease inhibitors indinavir and nelfinavir, which cause chemically-induced lipodystrophy syndromes, generated the same mitochondrial defects and cellular phenotypes as seen in the laminopathies (Caron et al., 2007). Furthermore, AIDS progression and drug-induced lipodystrophy have also been shown to be modulate mtDNA haplogroups (Hendrickson et al., 2008, 2009).

Class IV laminopathies encompasses the accelerated aging syndromes, AD-Hutchinson–Gilford progeria syndrome (HGPS), AD-Werner Syndrome (WS), and AD-restrictive lethal dermopathy (Worman and Bonne, 2007). AD-HGPS individuals only live into their mid teens and exhibit an array of premature aging manifestations including ischemic heart disease, central nervous system problems, hearing loss, and insulin unresponsiveness (Korf, 2008; Merideth et al., 2008). *LMNA* mutations can also result in the later-onset Werner premature aging syndrome (Kudlow et al., 2007). Class IV *LMNA* mutations are primarily confined to the C-terminal end of the protein. The most common HGPS mutation is a synonymous mutation, p.G608G (Liu and Zhou, 2008), which exposes a cryptic splice site leading to a 150 nucleotide deletion in the transcript. As a result, 50 amino acids of the mature protein are deleted which eliminates the ZMPSTE24 proteolytic processing site for removal of the C-terminal prelamin A domain, while still retaining the C-terminal end of the lamin A protein with the Cys-Ser-Ile-Met sequence. The p.G608G mutation thus generates a novel protein, progerin, which remains attached to the ER and nuclear envelope membranes by its farnesyl group. This results in faulty assembly of the nuclear lamina, distortion of the nuclear shape, and a dominant negative gene action (Caron et al., 2007; Liu and Zhou, 2008; Scaffidi and Misteli, 2008). Since, the level of progerin has been found to correlate with the level of mitochondrial dysfunction in cells (Caron et al., 2007), the progeric laminopathies could also have a mitochondrial etiology.

In HGPS, the expression of progerin is also associated with reduced proliferative life span in cultured cells and increased telomere shortening rate. Telomeres, consist of thousands of copies of the TTAGGG repeat. They cap the ends of chromosomes and are maintained by the RNA–protein reverse transcriptase telomerase. The limited proliferative life span and rapid telomere decay of progeria and WS cells expressing porgerin can be ameliorated by introduction into these cells of the apoprotein of telomerase, TERT (Huang et al., 2008; Kudlow et al., 2008). Furthermore, lamin A has intrinsic affinities for binding DNA containing telomeric repeats (Shoeman and Traub, 1990) and telomeres are generally centrally localized within the nucleus of interphase cells (Scherthan, 2003).

WS can also be caused by mutations in the WRN helicase gene. The WRN helicase facilitates the opening of the ordered structure of the G-rich telomere sequences making it important in telomere maintenance and suppression of telomere sister-chromatid exchanges (Kudlow et al., 2007). Since *LMNA* mutations also cause WS, lamin A must be important in telomere decay. This creates a direct link between progeria and the mitochondrion. It is now clear that telomere decay is primarily due to mitochondrially-generated ROS which causes the oxidation and loss of telomere repeats (Parrinello et al., 2003; Passos et al., 2007; Passos and von Zglinicki, 2005; Richter et al., 2007; Richter and von Zglinicki, 2007; Saretzki et al., 2003, 2008; von Zglinicki, 2002; Yang et al., 2008). In cells expressing telomerase, increased ROS production activates a SRC family tyrosine kinase located in the nuclear periphery which phosphorylates TERT. This causes TERT to be exported from the nucleus and imported into the mitochondrion where it reduces ROS production, protects mtDNA from damage, and regulates apoptosis in a Bcl-2 dependent fashion (Ahmed et al., 2008; Del Bufalo et al., 2005; Haendeler et al., 2003, 2004; Santos et al., 2004). Since non-stem cells do not express TERT, the increased telomere shortening of progeria cells must be due to increased ROS production due to mitochondrial dysfunction.

6. Perspective

The similarity in symptoms between mitochondrial and epigenomic diseases suggests that they have a common pathophysiology. Is so, alterations in mitochondrial function will have important effects on the epigenome and alterations in the epigenome will have significant effects on mitochondrial function (Borrelli et al., 2008).

The epigenome has been hypothesized to provide the interface between the environment and the regulation of nDNA gene expression (Feinberg, 2007, 2008). The most important factors in an organism's environment are the availability of calories and the demands made on the organism for the use of those calories. The mitochondrion lies between availability of environmental calories and their conversion to usable energy. This occurs by the conversion by the mitochondrion and glycolysis of energy rich compounds such as carbohydrates and fats into ATP, acetyl-CoA, SAM, and NADH. ATP, acetyl-CoA, SAM, and the NADH/NAD^+ ratio, in turn, are the high-energy substrates that drive the modification of the epigenome. Prevalent calories increase the ATP, acetyl-CoA, SAM and NADH, causing the modification of histones, the opening of the chromatin, increased gene expression, and the stimulation of growth and reproduction. Reduced calorie levels deplete ATP, acetyl-CoA, SAM, and increase NAD^+, reducing histone modification, compacting the chromatin, and reducing gene expression, growth and reproduction.

The mitochondrial genome encompasses over 1500 nDNA genes plus the mtDNA genes. The nDNA mitochondrial genes plus the glycolysis genes are dispersed throughout the chromosomes. Therefore, the efficient exploitation of environmental calories requires the coordinate expression of the bioenergetic genes according to the availability of calories and the energy requirements of the organism. Procedures must then exist for regulating the expression of the nDNA bioenergetic genes in relation to calorie

availability. The large number and random distribution of the bioenergetic genes would require both *cis* and *trans* regulation. The *cis* regulation of nDNA bioenergetic genes could occur within chromatin loops and be influenced by imprinting. The *trans* regulation of nDNA bioenergetic genes would require inter-chromosomal regulation by diffusible transcription factors or by the interaction of related genes through tertiary chromatin structures such as transcriptional islands and lamin A associated interactions.

Mutations in mtDNA or nDNA mitochondrial genes diminish energy production causing energy deficiency diseases. These preferentially affect the tissues most reliant on high energy flux: brain, heart, muscle, renal, and endocrine systems. Severe alterations of mitochondrial energy production should alter ATP, acetyl-CoA, SAM, and NADH levels and thus perturb the epigenome and the coordinate expression of bioenergetic genes.

Similarly, certain alterations in the epigenome should alter the coordinate expression of nDNA bioenergetic genes, thus diminishing bioenergetics and resulting in symptoms in the high energy flux tissues. Coordinate expression of bioenergetic genes could be perturbed through either *cis* or *trans* regulation systems. Alterations in the structure of chromatin loop domains should cause aberrant *cis* gene expression and are most apparent in imprinting diseases such as BWS, AS, PWS, etc. Alterations in the epigenome that affect *trans* interactions include mutations in *trans* acting factors such a PGC-1α, FOXOs, MeCP2, but also could be affected by alterations in the overall chromatin arrangement in the nucleus as seen in the laminopathies.

Therefore, mitochondrial diseases and many epigenomic diseases may have a common pathophysiology, bioenergetic failure. If this continues to be shown to be true, then it will have major implications for the diagnosis and treatment of the common complex diseases associated with mitochondrial and epigenomic dysfunction.

Acknowledgments

The authors would like to thank Ms. Marie T. Lott for her assistance in assembling this document. The work has been supported by NIH Grants NS21328, AG24373, DK73691, AG13154, AG16573, a CIRM Comprehensive Grant RC1-00353-1, a Doris Duke Clinical Interfaces Award 2005, and an Autism Speaks High Impact Grant awarded to DCW and a CIRM Predoctoral Fellowship awarded to WF.

References

Accili, D., Arden, K.C., 2004. FoxOs at the crossroads of cellular metabolism, differentiation, and transformation. Cell 117, 421–426.

Ahmed, S., Passos, J.F., Birket, M.J., Beckmann, T., Brings, S., Peters, H., Birch-Machin, M.A., von Zglinicki, T., Saretzki, G., 2008. Telomerase does not counteract telomere shortening but protects mitochondrial function under oxidative stress. Journal of Cell Science 121, 1046–1053.

Ahn, B.H., Kim, H.S., Song, S., Lee, I.H., Liu, J., Vassilopoulos, A., Deng, C.X., Finkel, T., 2008. A role for the mitochondrial deacetylase Sirt3 in regulating energy homeostasis. Proceedings of the National Academy of Sciences of the United States of America 105, 14447–14452.

Alberts, B., Johnson, A., Lewis, J., Raff, M., Roberts, K., Walter, P., 2002. Molecular Biology of the Cell. Garland Science, New York and London.

Amir, R.E., Van den Veyver, I.B., Wan, M., Tran, C.Q., Francke, U., Zoghbi, H.Y., 1999. Rett syndrome is caused by mutations in X-linked MECP2, encoding methyl-CpG-binding protein 2. Nature Genetics 23, 185–188.

Andreu, A.L., Bruno, C., Dunne, T.C., Tanji, K., Shanske, S., Sue, C.M., Krishna, S., Hadjigeorgiou, G.M., Shtilbans, A., Bonilla, E., DiMauro, S., 1999a. A nonsense mutation (G15059A) in the cytochrome b gene in a patient with exercise intolerance and myoglobinuria. Annals of Neurology 45, 127–130.

Andreu, A.L., Bruno, C., Shanske, S., Shtilbans, A., Hirano, M., Krishna, S., Hayward, L., Systrom, D.S., Brown Jr., R.H., DiMauro, S., 1998. Missense mutation in the mtDNA cytochrome b gene in a patient with myopathy. Neurology 51, 1444–1447.

Andreu, A.L., Hanna, M.G., Reichmann, H., Bruno, C., Penn, A.S., Tanji, K., Pallotti, F., Iwata, S., Bonilla, E., Lach, B., Morgan-Hughes, J., DiMauro, S., 1999b. Exercise intolerance due to mutations in the cytochrome b gene of mitochondrial DNA. New England Journal of Medicine 341, 1037–1044.

Araujo-Vilar, D., Lado-Abeal, J., Palos-Paz, F., Lattanzi, G., Bandin, M.A., Bellido, D., Dominguez-Gerpe, L., Calvo, C., Perez, O., Ramazanova, A., Martinez-Sanchez, N., Victoria, B., Costa-Freitas, A.T., 2008. A novel phenotypic expression associated with a new mutation in LMNA gene, characterized by partial lipodystrophy, insulin resistance, aortic stenosis and hypertrophic cardiomyopathy. Clinical Endocrinology (Oxford) 69, 61–68.

Asher, G., Gatfield, D., Stratmann, M., Reinke, H., Dibner, C., Kreppel, F., Mostoslavsky, R., Alt, F.W., Schibler, U., 2008. SIRT1 regulates circadian clock gene expression through PER2 deacetylation. Cell 134, 317–328.

Bai, R.K., Leal, S.M., Covarrubias, D., Liu, A., Wong, L.J., 2007. Mitochondrial genetic background modifies breast cancer risk. Cancer Research 67, 4687–4694.

Baudouin, S.V., Saunders, D., Tiangyou, W., Elson, J.L., Poynter, J., Pyle, A., Keers, S., Turnbull, D.M., Howell, N., Chinnery, P.F., 2005. Mitochondrial DNA and survival after sepsis: a prospective study. Lancet 366, 2118–2121.

Baur, J.A., Pearson, K.J., Price, N.L., Jamieson, H.A., Lerin, C., Kalra, A., Prabhu, V.V., Allard, J.S., Lopez-Lluch, G., Lewis, K., Pistell, P.J., Poosala, S., Becker, K.G., Boss, O., Gwinn, D., Wang, M.D., Ramaswamy, S., Fishbein, K.W., Spencer, R.G., Lakatta, E.G., Le Couteur, D., Shaw, R.J., Navas, P., Puigserver, P., Ingram, D.K., de Cabo, R., Sinclair, D.A., 2006. Resveratrol improves health and survival of mice on a high-calorie diet. Nature 444, 337–342.

Baur, J.A., Sinclair, D.A., 2006. Therapeutic potential of resveratrol: the in vivo evidence. Nature Reviews Drug Discovery 5, 493–506.

Bechara, E.G., Didiot, M.C., Melko, M., Davidovic, L., Bensaid, M., Martin, P., Castets, M., Pognonec, P., Khandjian, E.W., Moine, H., Bardoni, B., 2009. A novel function for fragile X mental retardation protein in translational activation. PLoS Biology 7, e16.

Bellomo, F., Piccoli, C., Cocco, T., Scacco, S., Papa, F., Gaballo, A., Boffoli, D., Signorile, A., D'Aprile, A., Scrima, R., Sardanelli, A.M., Capitanio, N., Papa, S., 2006. Regulation by the cAMP cascade of oxygen free radical balance in mammalian cells. Antioxidants and Redox Signaling 8, 495–502.

Bjornsson, H.T., Brown, L.J., Fallin, M.D., Rongione, M.A., Bibikova, M., Wickham, E., Fan, J.B., Feinberg, A.P., 2007. Epigenetic specificity of loss of imprinting of the IGF2 gene in Wilms tumors. Journal of the National Cancer Institute 99, 1270–1273.

Boily, G., Seifert, E.L., Bevilacqua, L., He, X.H., Sabourin, G., Estey, C., Moffat, C., Crawford, S., Saliba, S., Jardine, K., Xuan, J., Evans, M., Harper, M.E., McBurney, M.W., 2008. SirT1 regulates energy metabolism and response to caloric restriction in mice. PLoS One 3, e1759.

Booker, L.M., Habermacher, G.M., Jessie, B.C., Sun, Q.C., Baumann, A.K., Amin, M., Lim, S.D., Fernandez-Golarz, C., Lyles, R.H., Brown, M.D., Marshall, F.F., Petros, J.A., 2006. North American white mitochondrial haplogroups in prostate and renal cancer. Journal of Urology 175, 468–472. discussion 472-473.

Borrelli, E., Nestler, E.J., Allis, C.D., Sassone-Corsi, P., 2008. Decoding the epigenetic language of neuronal plasticity. Neuron 60, 961–974.

Brandon, M., Baldi, P., Wallace, D.C., 2006. Mitochondrial mutations in cancer. Oncogene 25, 4647–4662.

Brown, M.D., Starikovskaya, E., Derbeneva, O., Hosseini, S., Allen, J.C., Mikhailovskaya, I.E., Sukernik, R.I., Wallace, D.C., 2002. The role of mtDNA background in disease expression: a new primary LHON mutation associated with Western Eurasian haplogroup. J Human Genetics 110, 130–138.

Brown, M.D., Sun, F., Wallace, D.C., 1997. Clustering of Caucasian Leber hereditary optic neuropathy patients containing the 11778 or 14484 mutations on an mtDNA lineage. American Journal of Human Genetics 60, 381–387.

Brown, M.D., Torroni, A., Reckord, C.L., Wallace, D.C., 1995. Phylogenetic analysis of Leber's hereditary optic neuropathy mitochondrial DNA's indicates multiple independent occurrences of the common mutations. Human Mutation 6, 311–325.

Cai, S., Lee, C.C., Kohwi-Shigematsu, T., 2006. SATB1 packages densely looped, transcriptionally active chromatin for coordinated expression of cytokine genes. Nature Genetics 38, 1278–1288.

Caron, M., Auclair, M., Donadille, B., Bereziat, V., Guerci, B., Laville, M., Narbonne, H., Bodemer, C., Lascols, O., Capeau, J., Vigouroux, C., 2007. Human lipodystrophies linked to mutations in A-type lamins and to HIV protease inhibitor therapy are both associated with prelamin A accumulation, oxidative stress and premature cellular senescence. Cell Death and Differentiation 14, 1759–1767.

Carrieri, G., Bonafe, M., De Luca, M., Rose, G., Varcasia, O., Bruni, A., Maletta, R., Nacmias, B., Sorbi, S., Corsonello, F., Feraco, E., Andreev, K.F., Yashin, A.I., Franceschi, C., De Benedictis, G., 2001. Mitochondrial DNA haplogroups and APOE4 allele are non-independent variables in sporadic Alzheimer's disease. Human Genetics 108, 194–198.

Carrozzo, R., Dionisi-Vici, C., Steuerwald, U., Lucioli, S., Deodato, F., Di Giandomenico, S., Bertini, E., Franke, B., Kluijtmans, L.A., Meschini, M.C., Rizzo, C., Piemonte, F., Rodenburg, R., Santer, R., Santorelli, F.M., van Rooij, A., Vermunt-de Koning, D., Morava, E., Wevers, R.A., 2007. SUCLA2 mutations are associated with mild methylmalonic aciduria, Leigh-like encephalomyopathy, dystonia and deafness. Brain 130, 862–874.

Chagnon, P., Gee, M., Filion, M., Robitaille, Y., Belouchi, M., Gauvreau, D., 1999. Phylogenetic analysis of the mitochondrial genome indicates significant differences between patients with Alzheimer disease and controls in a French–Canadian founder population. American Journal of Medical Genetics 85, 20–30.

Chen, C., Liu, Y., Liu, R., Ikenoue, T., Guan, K.L., Liu, Y., Zheng, P., 2008. TSC-mTOR maintains quiescence and function of hematopoietic stem cells by repressing

mitochondrial biogenesis and reactive oxygen species. The Journal of Experimental Medicine 205, 2397–2408.
Chen, H., Chomyn, A., Chan, D.C., 2005. Disruption of fusion results in mitochondrial heterogeneity and dysfunction. The Journal of Biological Chemistry 280, 26185–26192.
Chen, H., Detmer, S.A., Ewald, A.J., Griffin, E.E., Fraser, S.E., Chan, D.C., 2003a. Mitofusins Mfn1 and Mfn2 coordinately regulate mitochondrial fusion and are essential for embryonic development. Journal of Cell Biology 160, 189–200.
Chen, R., Fearnley, I.M., Peak-Chew, S.Y., Walker, J.E., 2004. The phosphorylation of subunits of complex I from bovine heart mitochondria. The Journal of Biological Chemistry 279, 26036–26045.
Chen, W.G., Chang, Q., Lin, Y., Meissner, A., West, A.E., Griffith, E.C., Jaenisch, R., Greenberg, M.E., 2003b. Derepression of BDNF transcription involves calcium-dependent phosphorylation of MeCP2. Science 302, 885–889.
Cheng, H.L., Mostoslavsky, R., Saito, S., Manis, J.P., Gu, Y., Patel, P., Bronson, R., Appella, E., Alt, F.W., Chua, K.F., 2003. Developmental defects and p53 hyperacetylation in Sir2 homolog (SIRT1)-deficient mice. Proceedings of the National Academy of Sciences of the United States of America 100, 10794–10799.
Cipolat, S., Martins de Brito, O., Dal Zilio, B., Scorrano, L., 2004. OPA1 requires mitofusin 1 to promote mitochondrial fusion. Proceedings of the National Academy of Sciences of the United States of America 101, 15927–15932.
Correia, C., Coutinho, A.M., Diogo, L., Grazina, M., Marques, C., Miguel, T., Ataide, A., Almeida, J., Borges, L., Oliveira, C., Oliveira, G., Vicente, A.M., 2006. Brief report: high frequency of biochemical markers for mitochondrial dysfunction in autism: no association with the mitochondrial aspartate/glutamate carrier SLC25A12 gene. Journal of Autism and Developmental Disorders 36, 1137–1140.
Cremer, M., Kupper, K., Wagler, B., Wizelman, L., von Hase, J., Weiland, Y., Kreja, L., Diebold, J., Speicher, M.R., Cremer, T., 2003. Inheritance of gene density-related higher order chromatin arrangements in normal and tumor cell nuclei. The Journal of Cell Biology 162, 809–820.
Crispim, D., Canani, L.H., Gross, J.L., Tschiedel, B., Souto, K.E., Roisenberg, I., 2006. The European-specific mitochondrial cluster J/T could confer an increased risk of insulin-resistance and type 2 diabetes: an analysis of the m.4216T > C and m.4917A > G variants. Annals of Human Genetics 70, 488–495.
Daitoku, H., Yamagata, K., Matsuzaki, H., Hatta, M., Fukamizu, A., 2003. Regulation of PGC-1 promoter activity by protein kinase B and the forkhead transcription factor FKHR. Diabetes 52, 642–649.
Darvishi, K., Sharma, S., Bhat, A.K., Rai, E., Bamezai, R.N., 2007. Mitochondrial DNA G10398A polymorphism imparts maternal Haplogroup N a risk for breast and esophageal cancer. Cancer Letters 249, 249–255.
De Benedictis, G., Rose, G., Carrieri, G., De Luca, M., Falcone, E., Passarino, G., Bonafe, M., Monti, D., Baggio, G., Bertolini, S., Mari, D., Mattace, R., Franceschi, C., 1999. Mitochondrial DNA inherited variants are associated with successful aging and longevity in humans. FASEB Journal 13, 1532–1536.
Del Bufalo, D., Rizzo, A., Trisciuoglio, D., Cardinali, G., Torrisi, M.R., Zangemeister-Wittke, U., Zupi, G., Biroccio, A., 2005. Involvement of hTERT in apoptosis induced by interference with Bcl-2 expression and function. Cell Death and Differentiation 12, 1429–1438.
Delettre, C., Lenaers, G., Griffoin, J.M., Gigarel, N., Lorenzo, C., Belenguer, P., Pelloquin, L., Grosgeorge, J., Turc-Carel, C., Perret, E., Astarie-Dequeker, C., Lasquellec, L., Arnaud, B., Ducommun, B., Kaplan, J., Hamel, C.P., 2000. Nuclear gene OPA1, encoding a mitochondrial dynamin-related protein, is mutated in dominant optic atrophy. Nature Genetics 26, 207–210.
DeYoung, M.P., Horak, P., Sofer, A., Sgroi, D., Ellisen, L.W., 2008. Hypoxia regulates TSC1/2-mTOR signaling and tumor suppression through REDD1-mediated 14-3-3 shuttling. Genes and Development 22, 239–251.
Doi, M., Hirayama, J., Sassone-Corsi, P., 2006. Circadian regulator CLOCK is a histone acetyltransferase. Cell 125, 497–508.
Duckles, S.P., Krause, D.N., Stirone, C., Procaccio, V., 2006. Estrogen and mitochondria: a new paradigm for vascular protection? Molecular Interventions 6, 26–35.
Duesing, K., Charpentier, G., Marre, M., Tichet, J., Hercberg, S., Froguel, P., Gibson, F., 2008. Evaluating the association of common LMNA variants with type 2 diabetes and quantitative metabolic phenotypes in French Europids. Diabetologia 51, 76–81.
Eckel-Mahan, K., Sassone-Corsi, P., 2009. Metabolism control by the circadian clock and vice versa. Nature Structural and Molecular Biology 16, 462–467.
Eeg-Olofsson, O., al-Zuhair, A.G., Teebi, A.S., al-Essa, M.M., 1989. Rett syndrome: genetic clues based on mitochondrial changes in muscle. American Journal of Medical Genetics 32, 142–144.
Escobar-Henriques, M., Westermann, B., Langer, T., 2006. Regulation of mitochondrial fusion by the F-box protein Mdm30 involves proteasome-independent turnover of Fzo1. The Journal of Cell Biology 173, 645–650.
Espada, J., Varela, I., Flores, I., Ugalde, A.P., Cadinanos, J., Pendas, A.M., Stewart, C.L., Tryggvason, K., Blasco, M.A., Freije, J.M., Lopez-Otin, C., 2008. Nuclear envelope defects cause stem cell dysfunction in premature-aging mice. Journal of Cell Biology 181, 27–35.
Evans, A.R., Limp-Foster, M., Kelley, M.R., 2000. Going APE over ref-1. Mutation Research 461, 83–108.
Feige, J.N., Lagouge, M., Canto, C., Strehle, A., Houten, S.M., Milne, J.C., Lambert, P.D., Mataki, C., Elliott, P.J., Auwerx, J., 2008. Specific SIRT1 activation mimics low energy levels and protects against diet-induced metabolic disorders by enhancing fat oxidation. Cell Metabolism 8, 347–358.
Feinberg, A.P., 2007. Phenotypic plasticity and the epigenetics of human disease. Nature 447, 433–440.
Feinberg, A.P., 2008. Epigenetics at the epicenter of modern medicine. JAMA 299, 1345–1350.
Figarella-Branger, D., Pellissier, J.F., Scheiner, C., Wernert, F., Desnuelle, C., 1992. Defects of the mitochondrial respiratory chain complexes in three pediatric cases with hypotonia and cardiac involvement. Journal of the Neurological Sciences 108, 105–113.
Filipek, P.A., 2005. Medical aspects of autism. In: Volkmar, F.R., Klin, A., Paul, R., Cohen, D.J. (Eds.), Handbook of Autism and Pervasive Developmental Disorders. John Wiley and Sons, New York, pp. 534–578 (Chapter 520).
Fillano, J.J., Goldenthal, M.J., Rhodes, C.H., Marin-Garcia, J., 2002. Mitochondrial dysfunction in patients with hypotonia, epilepsy, autism, and developmental delay: HEADD syndrome. Journal of Child Neurology 17, 435–439.
Fraser, P., Bickmore, W., 2007. Nuclear organization of the genome and the potential for gene regulation. Nature 447, 413–417.
Fuchs, S.M., Laribee, R.N., Strahl, B.D., 2009. Protein modifications in transcription elongation. Biochimica et Biophysica Acta 1789, 26–36.
Fuku, N., Park, K.S., Yamada, Y., Nishigaki, Y., Cho, Y.M., Matsuo, H., Segawa, T., Watanabe, S., Kato, K., Yokoi, K., Nozawa, Y., Lee, H.K., Tanaka, M., 2007. Mitochondrial haplogroup N9a confers resistance against type 2 diabetes in Asians. American Journal of Human Genetics 80, 407–415.
Galiova, G., Bartova, E., Raska, I., Krejci, J., Kozubek, S., 2008. Chromatin changes induced by lamin A/C deficiency and the histone deacetylase inhibitor trichostatin A. European Journal of Cell Biology 87, 291–303.
Gandre-Babbe, S., van der Bliek, A.M., 2008. The novel tail-anchored membrane protein Mff controls mitochondrial and peroxisomal fission in mammalian cells. Molecular Biology of the Cell 19, 2402–2412.
Gargus, J.J., 2009. Genetic calcium signaling abnormalities in the central nervous system: seizures, migraine, and autism. Annals of the New York Academy of Sciences 1151, 133–156.
Gargus, J.J., Imtiaz, F., 2008. Mitochondrial energy-deficient endophenotype in autism. American Journal of Biochemistry and Biotechnology 4, 198–207.
Gerhart-Hines, Z., Rodgers, J.T., Bare, O., Lerin, C., Kim, S.H., Mostoslavsky, R., Alt, F.W., Wu, Z., Puigserver, P., 2007. Metabolic control of muscle mitochondrial function and fatty acid oxidation through SIRT1/PGC-1alpha. EMBO Journal 26, 1913–1923.
Ghezzi, D., Marelli, C., Achilli, A., Goldwurm, S., Pezzoli, G., Barone, P., Pellecchia, M.T., Stanzione, P., Brusa, L., Bentivoglio, A.R., Bonuccelli, U., Petrozzi, L., Abbruzzese, G., Marchese, R., Cortelli, P., Grimaldi, D., Martinelli, P., Ferrarese, C., Garavaglia, B., Sangiorgi, S., Carelli, V., Torroni, A., Albanese, A., Zeviani, M., 2005. Mitochondrial DNA haplogroup K is associated with a lower risk of Parkinson's disease in Italians. European Journal of Human Genetics 13, 748–752.
Glozak, M.A., Seto, E., 2007. Histone deacetylases and cancer. Oncogene 26, 5420–5432.
Goel, A., Mathupala, S.P., Pedersen, P.L., 2003. Glucose metabolism in cancer. Evidence that demethylation events play a role in activating type II hexokinase gene expression. The Journal of Biological Chemistry 278, 15333–15340.
Goetze, S., Mateos-Langerak, J., Gierman, H.J., de Leeuw, W., Giromus, O., Indemans, M.H., Koster, J., Ondrej, V., Versteeg, R., van Driel, R., 2007. The three-dimensional structure of human interphase chromosomes is related to the transcriptome map. Molecular and Cellular Biology 27, 4475–4487.
Gondor, A., Ohlsson, R., 2006. Transcription in the loop. Nature Genetics 38, 1229–1230.
Goto, Y., Nonaka, I., Horai, S., 1990. A mutation in the $tRNA^{Leu(UUR)}$ gene associated with the MELAS subgroup of mitochondrial encephalomyopathies. Nature 348, 651–653.
Gottlieb, E., Tomlinson, I.P., 2005. Mitochondrial tumour suppressors: a genetic and biochemical update. Nature Reviews Cancer 5, 857–866.
Graf, W.D., Marin-Garcia, J., Gao, H.G., Pizzo, S., Naviaux, R.K., Markusic, D., Barshop, B.A., Courchesne, E., Haas, R.H., 2000. Autism associated with the mitochondrial DNA G8363A transfer RNA(Lys) mutation. Journal of Child Neurology 15, 357–361.
Guelen, L., Pagie, L., Brasset, E., Meuleman, W., Faza, M.B., Talhout, W., Eussen, B.H., de Klein, A., Wessels, L., de Laat, W., van Steensel, B., 2008. Domain organization of human chromosomes revealed by mapping of nuclear lamina interactions. Nature 453, 948–951.
Gulati, P., Gaspers, L.D., Dann, S.G., Joaquin, M., Nobukuni, T., Natt, F., Kozma, S.C., Thomas, A.P., Thomas, G., 2008. Amino acids activate mTOR complex 1 via Ca^{2+}/CaM signaling to hVps34. Cell Metabolism 7, 456–465.
Haas, R.H., Townsend, J., Courchesne, E., Lincoln, A.J., Schreibman, L., Yeung-Courchesne, R., 1996. Neurologic abnormalities in infantile autism. Journal of Child Neurology 11, 84–92.
Haendeler, J., Hoffmann, J., Brandes, R.P., Zeiher, A.M., Dimmeler, S., 2003. Hydrogen peroxide triggers nuclear export of telomerase reverse transcriptase via SRC kinase family-dependent phosphorylation of tyrosine 707. Molecular and Cellular Biology 23, 4598–4610.
Haendeler, J., Hoffmann, J., Diehl, J.F., Vasa, M., Spyridopoulos, I., Zeiher, A.M., Dimmeler, S., 2004. Antioxidants inhibit nuclear export of telomerase reverse transcriptase and delay replicative senescence of endothelial cells. Circulation Research 94, 768–775.
Haigis, M.C., Mostoslavsky, R., Haigis, K.M., Fahie, K., Christodoulou, D.C., Murphy, A.J., Valenzuela, D.M., Yancopoulos, G.D., Karow, M., Blander, G., Wolberger, C., Prolla, T.A., Weindruch, R., Alt, F.W., Guarente, L., 2006. SIRT4 inhibits glutamate

dehydrogenase and opposes the effects of calorie restriction in pancreatic beta cells. Cell 126, 941–954.
Hakelien, A.M., Delbarre, E., Gaustad, K.G., Buendia, B., Collas, P., 2008. Expression of the myodystrophic R453W mutation of lamin A in C2C12 myoblasts causes promoter-specific and global epigenetic defects. Experimental Cell Research 314, 1869–1880.
Hale, C.M., Shrestha, A.L., Khatau, S.B., Stewart-Hutchinson, P.J., Hernandez, L., Stewart, C.L., Hodzic, D., Wirtz, D., 2008. Dysfunctional connections between the nucleus and the actin and microtubule networks in laminopathic models. Biophysical Journal 95, 5462–5475.
Hansen, J.M., Go, Y.M., Jones, D.P., 2006. Nuclear and mitochondrial compartmentation of oxidative stress and redox signaling. Annual Review of Pharmacology and Toxicology 46, 215–234.
Hardie, D.G., 2007. AMP-activated/SNF1 protein kinases: conserved guardians of cellular energy. Nature Reviews Molecular Cell Biology 8, 774–785.
Heilstedt, H.A., Shahbazian, M.D., Lee, B., 2002. Infantile hypotonia as a presentation of Rett syndrome. American Journal of Medical Genetics 111, 238–242.
Hendrickson, S.L., Hutcheson, H.B., Ruiz-Pesini, E., Poole, J.C., Lautenberger, J., Sezgin, E., Kingsley, L., Goedert, J.J., Vlahov, D., Donfield, S., Wallace, D.C., O'Brien, S.J., 2008. Mitochondrial DNA haplogroups influence AIDS progression. AIDS 22, 2429–2439.
Hendrickson, S.L., Kingsley, L.A., Ruiz-Pesini, E., Poole, J.C., Jacobson, L.P., Palella, F.J., Bream, J.H., Wallace, D.C., O'Brien, S.J., 2009. Mitochondrial DNA haplogroups influence lipoatrophy after highly active anti-retroviral therapy. Journal of Acquired Immune Deficiency Syndromes 51, 111–116.
Holt, I.J., Harding, A.E., Morgan-Hughes, J.A., 1988. Deletions of muscle mitochondrial DNA in patients with mitochondrial myopathies. Nature 331, 717–719.
Holt, I.J., Harding, A.E., Petty, R.K., Morgan-Hughes, J.A., 1990. A new mitochondrial disease associated with mitochondrial DNA heteroplasmy. American Journal of Human Genetics 46, 428–433.
Holtzman, D., 2008. Autistic spectrum disorders and mitochondrial encephalopathies. Acta Paediatrica 97, 859–860.
Hong, C.J., Liou, Y.J., Liao, D.L., Hou, S.J., Yen, F.C., Tsai, S.J., 2007. Association study of polymorphisms in the mitochondrial aspartate/glutamate carrier SLC25A12 (aralar) gene with schizophrenia. Progress in Neuro-Psychopharmacology and Biological Psychiatry 31, 1510–1513.
Huang, S., Risques, R.A., Martin, G.M., Rabinovitch, P.S., Oshima, J., 2008. Accelerated telomere shortening and replicative senescence in human fibroblasts overexpressing mutant and wild-type lamin A. Experimental Cell Research 314, 82–91.
Ishikawa, K., Takenaga, K., Akimoto, M., Koshikawa, N., Yamaguchi, A., Imanishi, H., Nakada, K., Honma, Y., Hayashi, J., 2008. ROS-generating mitochondrial DNA mutations can regulate tumor cell metastasis. Science 320, 661–664.
Ivanova, R., Lepage, V., Charron, D., Schachter, F., 1998. Mitochondrial genotype associated with French Caucasian centenarians. Gerontology 44, 349.
Jager, S., Handschin, C., St-Pierre, J., Spiegelman, B.M., 2007. AMP-activated protein kinase (AMPK) action in skeletal muscle via direct phosphorylation of PGC-1alpha. Proceedings of the National Academy of Sciences of the United States of America 104, 12017–12022.
James, D.I., Parone, P.A., Mattenberger, Y., Martinou, J.C., 2003. HFis1, a novel component of the mammalian mitochondrial fission machinery. The Journal of Biological Chemistry 278, 36373–36379.
Jones, D.P., 2006a. Disruption of mitochondrial redox circuitry in oxidative stress. Chemico-Biological Interactions 163, 38–53.
Jones, D.P., 2006b. Redefining oxidative stress. Antioxidants and Redox Signaling 8, 1865–1879.
Jones, D.P., 2008. Radical-free biology of oxidative stress. American Journal of Physiology – Cell Physiology 295, C849–C868.
Jones, M.M., Manwaring, N., Wang, J.J., Rochtchina, E., Mitchell, P., Sue, C.M., 2007. Mitochondrial DNA haplogroups and age-related maculopathy. Archives of Ophthalmology 125, 1235–1240.
Kaneda, A., Wang, C.J., Cheong, R., Timp, W., Onyango, P., Wen, B., Iacobuzio-Donahue, C.A., Ohlsson, R., Andraos, R., Pearson, M.A., Sharov, A.A., Longo, D.L., Ko, M.S., Levchenko, A., Feinberg, A.P., 2007. Enhanced sensitivity to IGF-II signaling links loss of imprinting of IGF2 to increased cell proliferation and tumor risk. Proceedings of the National Academy of Sciences of the United States of America 104, 20926–20931.
Kang, J.S., Tian, J.H., Pan, P.Y., Zald, P., Li, C., Deng, C., Sheng, Z.H., 2008. Docking of axonal mitochondria by syntaphilin controls their mobility and affects short-term facilitation. Cell 132, 137–148.
Karbowski, M., Neutzner, A., Youle, R.J., 2007. The mitochondrial E3 ubiquitin ligase MARCH5 is required for Drp1 dependent mitochondrial division. The Journal of Cell Biology 178, 71–84.
Kaukonen, J., Juselius, J.K., Tiranti, V., Kyttala, A., Zeviani, M., Comi, G.P., Keranen, S., Peltonen, L., Suomalainen, A., 2000. Role of adenine nucleotide translocator 1 in mtDNA maintenance. Science 289, 782–785.
Kelley, M.R., Parsons, S.H., 2001. Redox regulation of the DNA repair function of the human AP endonuclease Ape1/ref-1. Antioxidants and Redox Signaling 3, 671–683.
Kelly, D.P., Scarpulla, R.C., 2004. Transcriptional regulatory circuits controlling mitochondrial biogenesis and function. Genes and Development 18, 357–368.
Kemp, M., Go, Y.M., Jones, D.P., 2008. Nonequilibrium thermodynamics of thiol/disulfide redox systems: a perspective on redox systems biology. Free Radical Biology and Medicine 44, 921–937.
Khusnutdinova, E., Gilyazova, I., Ruiz-Pesini, E., Derbeneva, O., Khusainova, R., Khidiyatova, I., Magzhanov, R., Wallace, D.C., 2008. A mitochondrial etiology of neurodegenerative diseases: evidence from Parkinson's disease. Annals of the New York Academy of Sciences 1147, 1–20.
Klein, M.E., Lioy, D.T., Ma, L., Impey, S., Mandel, G., Goodman, R.H., 2007. Homeostatic regulation of MeCP2 expression by a CREB-induced microRNA. Nature Neuroscience 10, 1513–1514.
Korf, B., 2008. Hutchinson–Gilford progeria syndrome, aging, and the nuclear lamina. New England Journal of Medicine 358, 552–555.
Kriaucionis, S., Paterson, A., Curtis, J., Guy, J., Macleod, N., Bird, A., 2006. Gene expression analysis exposes mitochondrial abnormalities in a mouse model of Rett syndrome. Molecular and Cellular Biology 26, 5033–5042.
Kudlow, B.A., Kennedy, B.K., Monnat Jr., R.J., 2007. Werner and Hutchinson–Gilford progeria syndromes: mechanistic basis of human progeroid diseases. Nature Reviews Molecular Cell Biology 8, 394–404.
Kudlow, B.A., Stanfel, M.N., Burtner, C.R., Johnston, E.D., Kennedy, B.K., 2008. Suppression of proliferative defects associated with processing-defective lamin A mutants by hTERT or inactivation of p53. Molecular Biology of the Cell 19, 5238–5248.
Kujoth, G.C., Hiona, A., Pugh, T.D., Someya, S., Panzer, K., Wohlgemuth, S.E., Hofer, T., Seo, A.Y., Sullivan, R., Jobling, W.A., Morrow, J.D., Van Remmen, H., Sedivy, J.M., Yamasoba, T., Tanokura, M., Weindruch, R., Leeuwenburgh, C., Prolla, T.A., 2005. Mitochondrial DNA mutations, oxidative stress, and apoptosis in mammalian aging. Science 309, 481–484.
Lagouge, M., Argmann, C., Gerhart-Hines, Z., Meziane, H., Lerin, C., Daussin, F., Messadeq, N., Milne, J., Lambert, P., Elliott, P., Geny, B., Laakso, M., Puigserver, P., Auwerx, J., 2006. Resveratrol improves mitochondrial function and protects against metabolic disease by activating SIRT1 and PGC-1alpha. Cell 127, 1109–1122.
Lane, N., 2002. Oxygen: The Molecule that made the World. Oxford University Press, Oxford.
Lane, N., 2005. Power, Sex, Suicide: Mitochondria and the Meaning of Life. Oxford University Press, Oxford.
Lee, I., Salomon, A.R., Ficarro, S., Mathes, I., Lottspeich, F., Grossman, L.I., Huttemann, M., 2005. cAMP-dependent tyrosine phosphorylation of subunit I inhibits cytochrome c oxidase activity. The Journal of Biological Chemistry 280, 6094–6100.
Lee, I.H., Cao, L., Mostoslavsky, R., Lombard, D.B., Liu, J., Bruns, N.E., Tsokos, M., Alt, F.W., Finkel, T., 2008. A role for the NAD-dependent deacetylase Sirt1 in the regulation of autophagy. Proceedings of the National Academy of Sciences of the United States of America 105, 3374–3379.
Lee, J.S., Hale, C.M., Panorchan, P., Khatau, S.B., George, J.P., Tseng, Y., Stewart, C.L., Hodzic, D., Wirtz, D., 2007. Nuclear lamin A/C deficiency induces defects in cell mechanics, polarization, and migration. Biophysical Journal 93, 2542–2552.
Lepagnol-Bestel, A.M., Maussion, G., Boda, B., Cardona, A., Iwayama, Y., Delezoide, A.L., Moalic, J.M., Muller, D., Dean, B., Yoshikawa, T., Gorwood, P., Buxbaum, J.D., Ramoz, N., Simonneau, M., 2008. SLC25A12 expression is associated with neurite outgrowth and is upregulated in the prefrontal cortex of autistic subjects. Molecular Psychiatry 13, 385–397.
Li, Z., Okamoto, K., Hayashi, Y., Sheng, M., 2004. The importance of dendritic mitochondria in the morphogenesis and plasticity of spines and synapses. Cell 119, 873–887.
Lin, J., Wu, P.H., Tarr, P.T., Lindenberg, K.S., St-Pierre, J., Zhang, C.Y., Mootha, V.K., Jager, S., Vianna, C.R., Reznick, R.M., Cui, L., Manieri, M., Donovan, M.X., Wu, Z., Cooper, M.P., Fan, M.C., Rohas, L.M., Zavacki, A.M., Cinti, S., Shulman, G.I., Lowell, B.B., Krainc, D., Spiegelman, B.M., 2004. Defects in adaptive energy metabolism with CNS-linked hyperactivity in PGC-1alpha null mice. Cell 119, 121–135.
Lin, S.J., Defossez, P.A., Guarente, L., 2000. Requirement of NAD and SIR2 for life-span extension by calorie restriction in *Saccharomyces cerevisiae*. Science 289, 2126–2128.
Liu, B., Zhou, Z., 2008. Lamin A/C, laminopathies and premature ageing. Histology and Histopathology 23, 747–763.
Liu, J., Cao, L., Chen, J., Song, S., Lee, I.H., Quijano, C., Liu, H., Keyvanfar, K., Chen, H., Cao, L.Y., Ahn, B.H., Kumar, N.G., Rovira, I.I., Xu, X.L., van Lohuizen, M., Motoyama, N., Deng, C.X., Finkel, T., 2009. Bmi1 regulates mitochondrial function and the DNA damage response pathway. Nature 459, 387–392.
Liu, Q.A., Shio, H., 2008. Mitochondrial morphogenesis, dendrite development, and synapse formation in cerebellum require both Bcl-w and the glutamate receptor delta2. PLoS Genetics 4, e1000097.
Loat, C.S., Curran, S., Lewis, C.M., Duvall, J., Geschwind, D., Bolton, P., Craig, I.W., 2008. Methyl-CpG-binding protein 2 polymorphisms and vulnerability to autism. Genes, Brain, and Behavior 7, 754–760.
Lombard, D.B., Alt, F.W., Cheng, H.L., Bunkenborg, J., Streeper, R.S., Mostoslavsky, R., Kim, J., Yancopoulos, G., Valenzuela, D., Murphy, A., Yang, Y., Chen, Y., Hirschey, M.D., Bronson, R.T., Haigis, M., Guarente, L.P., Farese Jr., R.V., Weissman, S., Verdin, E., Schwer, B., 2007. Mammalian Sir2 homolog SIRT3 regulates global mitochondrial lysine acetylation. Molecular and Cellular Biology 27, 8807–8814.
Lombard, J., 1998. Autism: a mitochondrial disorder? Medical Hypotheses 50, 497–500.
Mandel, H., Szargel, R., Labay, V., Elpeleg, O., Saada, A., Shalata, A., Anbinder, Y., Berkowitz, D., Hartman, C., Barak, M., Eriksson, S., Cohen, N., 2001. The deoxyguanosine kinase gene is mutated in individuals with depleted hepatocerebral mitochondrial DNA. Nature Genetics 29, 337–341.
Mangelsdorf, D.J., Evans, R.M., 1995. The RXR heterodimers and orphan receptors. Cell 83, 841–850.

Markham, A., Cameron, I., Franklin, P., Spedding, M., 2004. BDNF increases rat brain mitochondrial respiratory coupling at complex I, but not complex II. European Journal of Neuroscience 20, 1189–1196.

Marmorstein, R., Trievel, R.C., 2009. Histone modifying enzymes: structures, mechanisms, and specificities. Biochimica et Biophysica Acta 1789, 58–68.

Matijevic, T., Knezevic, J., Slavica, M., Pavelic, J., 2009. Rett syndrome: from the gene to the disease. European Neurology 61, 3–10.

Matoba, S., Kang, J.G., Patino, W.D., Wragg, A., Boehm, M., Gavrilova, O., Hurley, P.J., Bunz, F., Hwang, P.M., 2006. P53 regulates mitochondrial respiration. Science 312, 1650–1653.

Mattson, M.P., 2008. Glutamate and neurotrophic factors in neuronal plasticity and disease. Annals of the New York Academy of Sciences 1144, 97–112.

Mattson, M.P., Liu, D., 2002. Energetics and oxidative stress in synaptic plasticity and neurodegenerative disorders. Neuromolecular Medicine 2, 215–231.

McBurney, M.W., Yang, X., Jardine, K., Hixon, M., Boekelheide, K., Webb, J.R., Lansdorp, P.M., Lemieux, M., 2003. The mammalian SIR2alpha protein has a role in embryogenesis and gametogenesis. Molecular and Cellular Biology 23, 38–54.

McCord, J.M., 2000. The evolution of free radicals and oxidative stress. American Journal of Medical Genetics 108, 652–659.

Mercuri, E., Brown, S.C., Nihoyannopoulos, P., Poulton, J., Kinali, M., Richard, P., Piercy, R.J., Messina, S., Sewry, C., Burke, M.M., McKenna, W., Bonne, G., Muntoni, F., 2005. Extreme variability of skeletal and cardiac muscle involvement in patients with mutations in exon 11 of the lamin A/C gene. Muscle and Nerve 31, 602–609.

Merideth, M.A., Gordon, L.B., Clauss, S., Sachdev, V., Smith, A.C., Perry, M.B., Brewer, C.C., Zalewski, C., Kim, H.J., Solomon, B., Brooks, B.P., Gerber, L.H., Turner, M.L., Domingo, D.L., Hart, T.C., Graf, J., Reynolds, J.C., Gropman, A., Yanovski, J.A., Gerhard-Herman, M., Collins, F.S., Nabel, E.G., Cannon 3rd., R.O., Gahl, W.A., Introne, W.J., 2008. Phenotype and course of Hutchinson–Gilford progeria syndrome. New England Journal of Medicine 358, 592–604.

Milne, J.C., Denu, J.M., 2008. The Sirtuin family: therapeutic targets to treat diseases of aging. Current Opinion in Chemical Biology 12, 11–17.

Milne, J.C., Lambert, P.D., Schenk, S., Carney, D.P., Smith, J.J., Gagne, D.J., Jin, L., Boss, O., Perni, R.B., Vu, C.B., Bemis, J.E., Xie, R., Disch, J.S., Ng, P.Y., Nunes, J.J., Lynch, A.V., Yang, H., Galonek, H., Israelian, K., Choy, W., Iffland, A., Lavu, S., Medvedik, O., Sinclair, D.A., Olefsky, J.M., Jirousek, M.R., Elliott, P.J., Westphal, C.H., 2007. Small molecule activators of SIRT1 as therapeutics for the treatment of type 2 diabetes. Nature 450, 712–716.

Miranda, M., Chacon, M.R., Gutierrez, C., Vilarrasa, N., Gomez, J.M., Caubet, E., Megia, A., Vendrell, J., 2008. LMNA mRNA expression is altered in human obesity and type 2 diabetes. Obesity 16, 1742–1748.

Mishmar, D., Ruiz-Pesini, E.E., Golik, P., Macaulay, V., Clark, A.G., Hosseini, S., Brandon, M., Easley, K., Chen, E., Brown, M.D., Sukernik, R.I., Olckers, A., Wallace, D.C., 2003. Natural selection shaped regional mtDNA variation in humans. Proceedings of the National Academy of Sciences of the United States of America 100, 171–176.

Mohlke, K.L., Jackson, A.U., Scott, L.J., Peck, E.C., Suh, Y.D., Chines, P.S., Watanabe, R.M., Buchanan, T.A., Conneely, K.N., Erdos, M.R., Narisu, N., Enloe, S., Valle, T.T., Tuomilehto, J., Bergman, R.N., Boehnke, M., Collins, F.S., 2005. Mitochondrial polymorphisms and susceptibility to type 2 diabetes-related traits in Finns. Human Genetics 118, 245–254.

Muchir, A., Pavlidis, P., Decostre, V., Herron, A.J., Arimura, T., Bonne, G., Worman, H.J., 2007. Activation of MAPK pathways links LMNA mutations to cardiomyopathy in Emery-Dreifuss muscular dystrophy. Journal of Clinical Investigation 117, 1282–1293.

Murrell, A., Heeson, S., Reik, W., 2004. Interaction between differentially methylated regions partitions the imprinted genes Igf2 and H19 into parent-specific chromatin loops. Nature Genetics 36, 889–893.

Nakahata, Y., Kaluzova, M., Grimaldi, B., Sahar, S., Hirayama, J., Chen, D., Guarente, L.P., Sassone-Corsi, P., 2008. The NAD$^+$-dependent deacetylase SIRT1 modulates CLOCK-mediated chromatin remodeling and circadian control. Cell 134, 329–340.

Nakahata, Y., Sahar, S., Astarita, G., Kaluzova, M., Sassone-Corsi, P., 2009. Circadian control of the NAD$^+$ salvage pathway by CLOCK-SIRT1. Science 324, 654–657.

Nakamura, N., Hirose, S., 2008. Regulation of mitochondrial morphology by USP30, a deubiquitinating enzyme present in the mitochondrial outer membrane. Molecular Biology of the Cell 19, 1903–1911.

Nakamura, N., Kimura, Y., Tokuda, M., Honda, S., Hirose, S., 2006. MARCH-V is a novel mitofusin 2- and Drp1-binding protein able to change mitochondrial morphology. EMBO Reports 7, 1019–1022.

Naviaux, R.K., 2008. Mitochondrial control of epigenetics. Cancer Biology and Therapy 7, 1191–1193.

Neutzner, A., Youle, R.J., 2005. Instability of the mitofusin Fzo1 regulates mitochondrial morphology during the mating response of the yeast *Saccharomyces cerevisiae*. The Journal of Biological Chemistry 280, 18598–18603.

Niemi, A.K., Hervonen, A., Hurme, M., Karhunen, P.J., Jylha, M., Majamaa, K., 2003. Mitochondrial DNA polymorphisms associated with longevity in a Finnish population. Human Genetics 112, 29–33.

Nishigaki, Y., Yamada, Y., Fuku, N., Matsuo, H., Segawa, T., Watanabe, S., Kato, K., Yokoi, K., Yamaguchi, S., Nozawa, Y., Tanaka, M., 2007. Mitochondrial haplogroup N9b is protective against myocardial infarction in Japanese males. Human Genetics 120, 827–836.

Nishino, I., Spinazzola, A., Hirano, M., 1999. Thymidine phosphorylase gene mutations in MNGIE, a human mitochondrial disorder. Science 283, 689–692.

Oliveira, G., Ataide, A., Marques, C., Miguel, T.S., Coutinho, A.M., Mota-Vieira, L., Goncalves, E., Lopes, N.M., Rodrigues, V., Carmona da Mota, H., Vicente, A.M., 2007. Epidemiology of autism spectrum disorder in Portugal: prevalence, clinical characterization, and medical conditions. Developmental Medicine and Child Neurology (London) 49, 726–733.

Palmieri, L., Alberio, S., Pisano, I., Lodi, T., Meznaric-Petrusa, M., Zidar, J., Santoro, A., Scarcia, P., Fontanesi, F., Lamantea, E., Ferrero, I., Zeviani, M., 2005. Complete loss-of-function of the heart/muscle-specific adenine nucleotide translocator is associated with mitochondrial myopathy and cardiomyopathy. Human Molecular Genetics 14, 3079–3088.

Palmieri, L., Papaleo, V., Porcelli, V., Scarcia, P., Gaita, L., Sacco, R., Hager, J., Rousseau, F., Curatolo, P., Manzi, B., Militerni, R., Bravaccio, C., Trillo, S., Schneider, C., Melmed, R., Elia, M., Lenti, C., Saccani, M., Pascucci, T., Puglisi-Allegra, S., Reichelt, K.L., Persico, A.M., 2008. Altered calcium homeostasis in autism-spectrum disorders: evidence from biochemical and genetic studies of the mitochondrial aspartate/glutamate carrier AGC1. Molecular Psychiatry ePub ahead of print http://dx.doi.org/10.1038/mp.2008.1063.

Papa, S., Scacco, S., Sardanelli, A.M., Petruzzella, V., Vergari, R., Signorile, A., Technikova-Dobrova, Z., 2002. Complex I and the cAMP cascade in human physiopathology. Bioscience Reports 22, 3–16.

Park, Y.E., Hayashi, Y.K., Goto, K., Komaki, H., Hayashi, Y., Inuzuka, T., Noguchi, S., Nonaka, I., Nishino, I., 2009. Nuclear changes in skeletal muscle extend to satellite cells in autosomal dominant Emery-Dreifuss muscular dystrophy/limb-girdle muscular dystrophy 1B. Neuromuscular Disorders 19, 29–36.

Parrinello, S., Samper, E., Krtolica, A., Goldstein, J., Melov, S., Campisi, J., 2003. Oxygen sensitivity severely limits the replicative lifespan of murine fibroblasts. Nature Cell Biology 5, 741–747.

Passos, J.F., Saretzki, G., Ahmed, S., Nelson, G., Richter, T., Peters, H., Wappler, I., Birket, M.J., Harold, G., Schaeuble, K., Birch-Machin, M.A., Kirkwood, T.B., von Zglinicki, T., 2007. Mitochondrial dysfunction accounts for the stochastic heterogeneity in telomere-dependent senescence. PLoS Biology 5, e110.

Passos, J.F., von Zglinicki, T., 2005. Mitochondria, telomeres and cell senescence. Experimental Gerontology 40, 466–472.

Pearson, K.J., Baur, J.A., Lewis, K.N., Peshkin, L., Price, N.L., Labinskyy, N., Swindell, W.R., Kamara, D., Minor, R.K., Perez, E., Jamieson, H.A., Zhang, Y., Dunn, S.R., Sharma, K., Pleshko, N., Woollett, L.A., Csiszar, A., Ikeno, Y., Le Couteur, D., Elliott, P.J., Becker, K.G., Navas, P., Ingram, D.K., Wolf, N.S., Ungvari, Z., Sinclair, D.A., de Cabo, R., 2008. Resveratrol delays age-related deterioration and mimics transcriptional aspects of dietary restriction without extending life span. Cell Metabolism 8, 157–168.

Pedram, A., Razandi, M., Wallace, D.C., Levin, E.R., 2006. Functional estrogen receptors in the mitochondria of breast cancer cells. Molecular Biology of the Cell 17, 2125–2137.

Pekovic, V., Harborth, J., Broers, J.L., Ramaekers, F.C., van Engelen, B., Lammens, M., von Zglinicki, T., Foisner, R., Hutchison, C., Markiewicz, E., 2007. Nucleoplasmic LAP2alpha-lamin A complexes are required to maintain a proliferative state in human fibroblasts. Journal of Cell Biology 176, 163–172.

Pekovic, V., Hutchison, C.J., 2008. Adult stem cell maintenance and tissue regeneration in the ageing context: the role for A-type lamins as intrinsic modulators of ageing in adult stem cells and their niches. Journal of Anatomy 213, 5–25.

Perrot, A., Hussein, S., Ruppert, V., Schmidt, H.H., Wehnert, M.S., Duong, N.T., Posch, M.G., Panek, A., Dietz, R., Kindermann, I., Bohm, M., Michalewska-Wludarczyk, A., Richter, A., Maisch, B., Pankuweit, S., Ozcelik, C., 2009. Identification of mutational hot spots in LMNA encoding lamin A/C in patients with familial dilated cardiomyopathy. Basic Research in Cardiology 104, 90–99.

Petros, J.A., Baumann, A.K., Ruiz-Pesini, E., Amin, M.B., Sun, C.Q., Hall, J., Lim, S., Issa, M.M., Flanders, W.D., Hosseini, S.H., Marshall, F.F., Wallace, D.C., 2005. MtDNA mutations increase tumorigenicity in prostate cancer. Proceedings of the National Academy of Sciences of the United States of America 102, 719–724.

Poling, J.S., Frye, R.E., Shoffner, J., Zimmerman, A.W., 2006. Developmental regression and mitochondrial dysfunction in a child with autism. Journal of Child Neurology 21, 170–172.

Pons, R., Andreu, A.L., Checcarelli, N., Vila, M.R., Engelstad, K., Sue, C.M., Shungu, D., Haggerty, R., de Vivo, D.C., DiMauro, S., 2004. Mitochondrial DNA abnormalities and autistic spectrum disorders. Journal of Pediatrics 144, 81–85.

Procaccio, V., Wallace, D.C., 2004. Late-onset Leigh syndrome in a patient with mitochondrial complex I NDUFS8 mutations. Neurology 62, 1899–1901.

Raby, B.A., Klanderman, B., Murphy, A., Mazza, S., Camargo Jr., C.A., Silverman, E.K., Weiss, S.T., 2007. A common mitochondrial haplogroup is associated with elevated total serum IgE levels. The Journal of Allergy and Clinical Immunology 120, 351–358.

Ramoz, N., Reichert, J.G., Smith, C.J., Silverman, J.M., Bespalova, I.N., Davis, K.L., Buxbaum, J.D., 2004. Linkage and association of the mitochondrial aspartate/glutamate carrier SLC25A12 gene with autism. American Journal of Psychiatry 161, 662–669.

Ramsey, K.M., Yoshino, J., Brace, C.S., Abrassart, D., Kobayashi, Y., Marcheva, B., Hong, H.K., Chong, J.L., Buhr, E.D., Lee, C., Takahashi, J.S., Imai, S., Bass, J., 2009. Circadian clock feedback cycle through NAMPT-mediated NAD$^+$ biosynthesis. Science 324, 651–654.

Rankin, J., Auer-Grumbach, M., Bagg, W., Colclough, K., Nguyen, T.D., Fenton-May, J., Hattersley, A., Hudson, J., Jardine, P., Josifova, D., Longman, C., McWilliam, R., Owen, K., Walker, M., Wehnert, M., Ellard, S., 2008. Extreme phenotypic diversity and nonpenetrance in families with the LMNA gene mutation R644C. American Journal of Medical Genetics. Part A 146A, 1530–1542.

Rathmell, J.C., Newgard, C.B., 2009. Biochemistry. A glucose-to-gene link. Science 324, 1021–1022.
Razmara, A., Duckles, S.P., Krause, D.N., Procaccio, V., 2007. Estrogen suppresses brain mitochondrial oxidative stress in female and male rats. Brain Research 1176, 71–81.
Razmara, A., Sunday, L., Stirone, C., Wang, X.B., Krause, D.N., Duckles, S.P., Procaccio, V., 2008. Mitochondrial effects of estrogen are mediated by estrogen receptor alpha in brain endothelial cells. Journal of Pharmacology and Experimental Therapeutics 325, 782–790.
Richter, T., Saretzki, G., Nelson, G., Melcher, M., Olijslagers, S., von Zglinicki, T., 2007. TRF2 overexpression diminishes repair of telomeric single-strand breaks and accelerates telomere shortening in human fibroblasts. Mechanisms of Ageing and Development 128, 340–345.
Richter, T., von Zglinicki, T., 2007. A continuous correlation between oxidative stress and telomere shortening in fibroblasts. Experimental Gerontology 42, 1039–1042.
Rogina, B., Helfand, S.L., 2004. Sir2 mediates longevity in the fly through a pathway related to calorie restriction. Proceedings of the National Academy of Sciences of the United States of America 101, 15998–16003.
Rose, G., Passarino, G., Carrieri, G., Altomare, K., Greco, V., Bertolini, S., Bonafe, M., Franceschi, C., De Benedictis, G., 2001. Paradoxes in longevity: sequence analysis of mtDNA haplogroup J in centenarians. European Journal of Human Genetics 9, 701–707.
Ruiz-Pesini, E., Mishmar, D., Brandon, M., Procaccio, V., Wallace, D.C., 2004. Effects of purifying and adaptive selection on regional variation in human mtDNA. Science 303, 223–226.
Ruiz-Pesini, E., Wallace, D.C., 2006. Evidence for adaptive selection acting on the tRNA and rRNA genes of the human mitochondrial DNA. Human Mutation 27, 1072–1081.
Saada, A., Shaag, A., Mandel, H., Nevo, Y., Eriksson, S., Elpeleg, O., 2001. Mutant mitochondrial thymidine kinase in mitochondrial DNA depletion myopathy. Nature Genetics 29, 342–344.
Samaco, R.C., Hogart, A., LaSalle, J.M., 2005. Epigenetic overlap in autism-spectrum neurodevelopmental disorders: MECP2 deficiency causes reduced expression of UBE3A and GABRB3. Human Molecular Genetics 14, 483–492.
Santos, J.H., Meyer, J.N., Skorvaga, M., Annab, L.A., Van Houten, B., 2004. Mitochondrial hTERT exacerbates free-radical-mediated mtDNA damage. Aging Cell 3, 399–411.
Saretzki, G., Murphy, M.P., von Zglinicki, T., 2003. MitoQ counteracts telomere shortening and elongates lifespan of fibroblasts under mild oxidative stress. Aging Cell 2, 141–143.
Saretzki, G., Walter, T., Atkinson, S., Passos, J.F., Bareth, B., Keith, W.N., Stewart, R., Hoare, S., Stojkovic, M., Armstrong, L., von Zglinicki, T., Lako, M., 2008. Downregulation of multiple stress defense mechanisms during differentiation of human embryonic stem cells. Stem Cells 26, 455–464.
Saxena, R., de Bakker, P.I., Singer, K., Mootha, V., Burtt, N., Hirschhorn, J.N., Gaudet, D., Isomaa, B., Daly, M.J., Groop, L., Ardlie, K.G., Altshuler, D., 2006. Comprehensive association testing of common mitochondrial DNA variation in metabolic disease. American Journal of Human Genetics 79, 54–61.
Scaffidi, P., Misteli, T., 2008. Lamin A-dependent misregulation of adult stem cells associated with accelerated ageing. Nature Cell Biology 10, 452–459.
Scarpulla, R.C., 2002. Nuclear activators and coactivators in mammalian mitochondrial biogenesis. Biochimica et Biophysica Acta 1576, 1–14.
Schafer, F.Q., Buettner, G.R., 2001. Redox environment of the cell as viewed through the redox state of the glutathione disulfide/glutathione couple. Free Radical Biology and Medicine 30, 1191–1212.
Scherthan, H., 2003. Knockout mice provide novel insights into meiotic chromosome and telomere dynamics. Cytogenetic and Genome Research 103, 235–244.
Schneider, R., Grosschedl, R., 2007. Dynamics and interplay of nuclear architecture, genome organization, and gene expression. Genes and Development 21, 3027–3043.
Schriner, S.E., Linford, N.J., Martin, G.M., Treuting, P., Ogburn, C.E., Emond, M., Coskun, P.E., Ladiges, W., Wolf, N., Van Remmen, H., Wallace, D.C., Rabinovitch, P.S., 2005. Extension of murine life span by overexpression of catalase targeted to mitochondria. Science 308, 1909–1911.
Schuman, E., Chan, D., 2004. Fueling synapses. Cell 119, 738–740.
Sebat, J., Lakshmi, B., Malhotra, D., Troge, J., Lese-Martin, C., Walsh, T., Yamrom, B., Yoon, S., Krasnitz, A., Kendall, J., Leotta, A., Pai, D., Zhang, R., Lee, Y.H., Hicks, J., Spence, S.J., Lee, A.T., Puura, K., Lehtimaki, T., Ledbetter, D., Gregersen, P.K., Bregman, J., Sutcliffe, J.S., Jobanputra, V., Chung, W., Warburton, D., King, M.C., Skuse, D., Geschwind, D.H., Gilliam, T.C., Ye, K., Wigler, M., 2007. Strong association of de novo copy number mutations with autism. Science 316, 445–449.
Shadel, G.S., 2008. Expression and maintenance of mitochondrial DNA: new insights into human disease pathology. American Journal of Pathology 172, 1445–1456.
Shoeman, R.L., Traub, P., 1990. The in vitro DNA-binding properties of purified nuclear lamin proteins and vimentin. The Journal of Biological Chemistry 265, 9055–9061.
Shoffner, J.M., Brown, M.D., Torroni, A., Lott, M.T., Cabell, M.R., Mirra, S.S., Beal, M.F., Yang, C., Gearing, M., Salvo, R., Watts, R.L., Juncos, J.L., Hansen, L.A., Crain, B.J., Fayad, M., Reckord, C.L., Wallace, D.C., 1993. Mitochondrial DNA variants observed in Alzheimer disease and Parkinson disease patients. Genomics 17, 171–184.
Shoffner, J.M., Lott, M.T., Lezza, A.M., Seibel, P., Ballinger, S.W., Wallace, D.C., 1990. Myoclonic epilepsy and ragged-red fiber disease (MERRF) is associated with a mitochondrial DNA $tRNA^{Lys}$ mutation. Cell 61, 931–937.
Shulman, A.I., Mangelsdorf, D.J., 2005. Retinoid x receptor heterodimers in the metabolic syndrome. New England Journal of Medicine 353, 604–615.
Smiraglia, D.J., Kulawiec, M., Bistulfi, G.L., Gupta, S.G., Singh, K.K., 2008. A novel role for mitochondria in regulating epigenetic modification in the nucleus. Cancer Biology and Therapy 7, 1182–1190.
Smirnova, E., Griparic, L., Shurland, D.L., van der Bliek, A.M., 2001. Dynamin-related protein Drp1 is required for mitochondrial division in mammalian cells. Molecular Biology of the Cell 12, 2245–2256.
Smith, B.C., Denu, J.M., 2009. Chemical mechanisms of histone lysine and arginine modifications. Biochimica et Biophysica Acta 1789, 45–57.
Smith, M., Spence, M.A., Flodman, P., 2008. Nuclear and mitochondrial genome defects in autisms. Annals of the New York Academy of Science 1151, 102–132.
Sonoda, J., Mehl, I.R., Chong, L.W., Nofsinger, R.R., Evans, R.M., 2007. PGC-1beta controls mitochondrial metabolism to modulate circadian activity, adaptive thermogenesis, and hepatic steatosis. Proceedings of the National Academy of Sciences of the United States of America 104, 5223–5228.
Sonoda, J., Pei, L., Evans, R.M., 2008. Nuclear receptors: decoding metabolic disease. FEBS Letters 582, 2–9.
Spelbrink, J.N., Li, F.Y., Tiranti, V., Nikali, K., Yuan, Q.P., Tariq, M., Wanrooij, S., Garrido, N., Comi, G., Morandi, L., Santoro, L., Toscano, A., Fabrizi, G.M., Somer, H., Croxen, R., Beeson, D., Poulton, J., Suomalainen, A., Jacobs, H.T., Zeviani, M., Larsson, C., 2001. Human mitochondrial DNA deletions associated with mutations in the gene encoding Twinkle, a phage T7 gene 4-like protein localized in mitochondria. Nature Genetics 28, 223–231.
Splawski, I., Yoo, D.S., Stotz, S.C., Cherry, A., Clapham, D.E., Keating, M.T., 2006. CACNA1H mutations in autism spectrum disorders. The Journal of Biological Chemistry 281, 22085–22091.
Stewart, C.L., Kozlov, S., Fong, L.G., Young, S.G., 2007. Mouse models of the laminopathies. Experimental Cell Research 313, 2144–2156.
Stirone, C., Duckles, S.P., Krause, D.N., Procaccio, V., 2005. Estrogen increases mitochondrial efficiency and reduces oxidative stress in cerebral blood vessels. Molecular Pharmacology 68, 959–965.
Strahl, B.D., Allis, C.D., 2000. The language of covalent histone modifications. Nature 403, 41–45.
Su, H., Fan, W., Coskun, P.E., Vesa, J., Gold, J.A., Jiang, Y.H., Potluri, P., Procaccio, V., Acab, A., Weiss, J.H., Wallace, D.C., Kimonis, V.E., 2009. Mitochondrial dysfunction in CA1 hippocampal neurons of the *UBE3A* deficient mouse model for Angelman syndrome. Neuroscience Letters ePub ahead of print <http://dx.doi.org/10.1016/j.neulet.2009.1006.1079>.
Takahashi, H., McCaffery, J.M., Irizarry, R.A., Boeke, J.D., 2006. Nucleocytosolic acetyl-coenzyme a synthetase is required for histone acetylation and global transcription. Molecular Cell 23, 207–217.
Tanaka, M., Gong, J., Zhang, J., Yamada, Y., Borgeld, H.J., Yagi, K., 2000. Mitochondrial genotype associated with longevity and its inhibitory effect on mutagenesis. Mechanisms of Ageing and Development 116, 65–76.
Tanaka, M., Gong, J.S., Zhang, J., Yoneda, M., Yagi, K., 1998. Mitochondrial genotype associated with longevity. Lancet 351, 185–186.
Technikova-Dobrova, Z., Sardanelli, A.M., Speranza, F., Scacco, S., Signorile, A., Lorusso, V., Papa, S., 2001. Cyclic adenosine monophosphate-dependent phosphorylation of mammalian mitochondrial proteins: enzyme and substrate characterization and functional role. Biochemistry 40, 13941–13947.
Tini, M., Benecke, A., Um, S.J., Torchia, J., Evans, R.M., Chambon, P., 2002. Association of CBP/p300 acetylase and thymine DNA glycosylase links DNA repair and transcription. Molecular Cell 9, 265–277.
Tong, J., Schriner, S.E., McCleary, D., Day, B.J., Wallace, D.C., 2007. Life extension through neurofibromin mitochondrial regulation and antioxidant therapy for Neurofibromatosis-1 in Drosophila melanogaster. Nature Genetics 39, 476–485.
Torroni, A., Petrozzi, M., D'Urbano, L., Sellitto, D., Zeviani, M., Carrara, F., Carducci, C., Leuzzi, V., Carelli, V., Barboni, P., De Negri, A., Scozzari, R., 1997. Haplotype and phylogenetic analyses suggest that one European-specific mtDNA background plays a role in the expression of Leber hereditary optic neuropathy by increasing the penetrance of the primary mutations 11778 and 14484. American Journal of Human Genetics 60, 1107–1121.
Torroni, A., Stepien, G., Hodge, J.A., Wallace, D.C., 1990. Neoplastic transformation is associated with coordinate induction of nuclear and cytoplasmic oxidative phosphorylation genes. The Journal of Biological Chemistry 265, 20589–20593.
Trifunovic, A., Wredenberg, A., Falkenberg, M., Spelbrink, J.N., Rovio, A.T., Bruder, C.E., Bohlooly, Y.M., Gidlof, S., Oldfors, A., Wibom, R., Tornell, J., Jacobs, H.T., Larsson, N.G., 2004. Premature ageing in mice expressing defective mitochondrial DNA polymerase. Nature 429, 417–423.
Udar, N., Atilano, S.R., Memarzadeh, M., Boyer, D.S., Chwa, M., Lu, S., Maguen, B., Langberg, J., Coskun, P., Wallace, D.C., Nesburn, A.B., Khatibi, N., Hertzog, D., Le, K., Hwang, D., Kenney, M.C., 2009. Mitochondrial DNA haplogroups associated with age-related macular degeneration. Investigative Ophthalmology and Visual Science 50, 2966–2974.
van der Walt, J.M., Dementieva, Y.A., Martin, E.R., Scott, W.K., Nicodemus, K.K., Kroner, C.C., Welsh-Bohmer, K.A., Saunders, A.M., Roses, A.D., Small, G.W., Schmechel, D.E., Murali Doraiswamy, P., Gilbert, J.R., Haines, J.L., Vance, J.M., Pericak-Vance, M.A., 2004. Analysis of European mitochondrial haplogroups with Alzheimer disease risk. Neuroscience Letters 365, 28–32.
van der Walt, J.M., Nicodemus, K.K., Martin, E.R., Scott, W.K., Nance, M.A., Watts, R.L., Hubble, J.P., Haines, J.L., Koller, W.C., Lyons, K., Pahwa, R., Stern, M.B., Colcher, A., Hiner, B.C., Jankovic, J., Ondo, W.G., Allen Jr., F.H., Goetz, C.G., Small, G.W., Mastaglia, F., Stajich, J.M., McLaurin, A.C., Middleton, L.T., Scott, B.L., Schmechel, D.E., Pericak-Vance, M.A., Vance, J.M., 2003. Mitochondrial

polymorphisms significantly reduce the risk of Parkinson disease. American Journal of Human Genetics 72, 804–811.
Van Goethem, G., Dermaut, B., Lofgren, A., Martin, J.J., Van Broeckhoven, C., 2001. Mutation of POLG is associated with progressive external ophthalmoplegia characterized by mtDNA deletions. Nature Genetics 28, 211–212.
Vantyghem, M.C., Vincent-Desplanques, D., Defrance-Faivre, F., Capeau, J., Fermon, C., Valat, A.S., Lascols, O., Hecart, A.C., Pigny, P., Delemer, B., Vigouroux, C., Wemeau, J.L., 2008. Fertility and obstetrical complications in women with LMNA-related familial partial lipodystrophy. The Journal of Clinical Endocrinology and Metabolism 93, 2223–2229.
Vo, N., Klein, M.E., Varlamova, O., Keller, D.M., Yamamoto, T., Goodman, R.H., Impey, S., 2005. A cAMP-response element binding protein-induced microRNA regulates neuronal morphogenesis. Proceedings of the National Academy of Sciences of the United States of America 102, 16426–16431.
von Zglinicki, T., 2002. Oxidative stress shortens telomeres. Trends in Biochemical Sciences 27, 339–344.
Wagner, B.K., Kitami, T., Gilbert, T.J., Peck, D., Ramanathan, A., Schreiber, S.L., Golub, T.R., Mootha, V.K., 2008. Large-scale chemical dissection of mitochondrial function (Erratum in Nat Biotechnol 2008 Jul 26(7):831; comment in Nat Biotechnol 2008 Mar 26(3):294–6). Nature Biotechnology 26, 343–351.
Wallace, D.C., 1982. Structure and evolution of organelle genomes. Microbiological Reviews 46, 208–240.
Wallace, D.C., 2005a. Mitochondria and cancer: Warburg Address. Cold Spring Harbor Symposia on Quantitative Biology 70, 363–374.
Wallace, D.C., 2005b. The mitochondrial genome in human adaptive radiation and disease: on the road to therapeutics and performance enhancement. Gene 354, 169–180.
Wallace, D.C., 2005c. A mitochondrial paradigm of metabolic and degenerative diseases, aging, and cancer: a dawn for evolutionary medicine. Annual Review of Genetics 39, 359–407.
Wallace, D.C., 2007. Why do we have a maternally inherited mitochondrial DNA? Insights from evolutionary medicine. Annual Review of Biochemistry 76, 781–821.
Wallace, D.C., 2008. Mitochondria as chi. Genetics 179, 727–735.
Wallace, D.C., Brown, M.D., Lott, M.T., 1999. Mitochondrial DNA variation in human evolution and disease. Gene 238, 211–230.
Wallace, D.C., Lott, M.T., Brown, M.D., Kerstann, K., 2001. Mitochondria and neuro-ophthalmological diseases. In: Scriver, C.R., Beaudet, A.L., Sly, W.S., Valle, D. (Eds.), The Metabolic and Molecular Basis of Inherited Disease, vol. 2. McGraw-Hill, New York, pp. 2425–2512.
Wallace, D.C., Lott, M.T., Procaccio, V., 2007. Mitochondrial genes in degenerative diseases, cancer and aging, 5th ed.. In: Rimoin, D.L., Connor, J.M., Pyeritz, R.E., Korf, B.R. (Eds.), Emery and Rimoin's Principles and Practice of Medical Genetics, vol. 1 Churchill Livingstone Elsevier, Philadelphia, PA, pp. 194–298 (Chapter 13).
Wallace, D.C., Ruiz-Pesini, E., Mishmar, D., 2003. MtDNA variation, climatic adaptation, degenerative diseases, and longevity. Cold Spring Harbor Symposia on Quantitative Biology 68, 479–486.
Wallace, D.C., Singh, G., Lott, M.T., Hodge, J.A., Schurr, T.G., Lezza, A.M., Elsas, L.J., Nikoskelainen, E.K., 1988a. Mitochondrial DNA mutation associated with Leber's hereditary optic neuropathy. Science 242, 1427–1430.
Wallace, D.C., Zheng, X., Lott, M.T., Shoffner, J.M., Hodge, J.A., Kelley, R.I., Epstein, C.M., Hopkins, L.C., 1988b. Familial mitochondrial encephalomyopathy (MERRF): genetic, pathophysiological, and biochemical characterization of a mitochondrial DNA disease. Cell 55, 601–610.
Wang, Y.X., Zhang, C.L., Yu, R.T., Cho, H.K., Nelson, M.C., Bayuga-Ocampo, C.R., Ham, J., Kang, H., Evans, R.M., 2004. Regulation of muscle fiber type and running endurance by PPARdelta. PLoS Biology 2, e294.
Wellen, K.E., Hatzivassiliou, G., Sachdeva, U.M., Bui, T.V., Cross, J.R., Thompson, C.B., 2009. ATP-citrate lyase links cellular metabolism to histone acetylation. Science 324, 1076–1080.
Wen, B., Wu, H., Shinkai, Y., Irizarry, R.A., Feinberg, A.P., 2009. Large histone H3 lysine 9 dimethylated chromatin blocks distinguish differentiated from embryonic stem cells. Nature Genetics 49, 246–250.
Wiedemann, F.R., Siemen, D., Mawrin, C., Horn, T.F., Dietzmann, K., 2006. The neurotrophin receptor TrkB is colocalized to mitochondrial membranes. International Journal of Biochemistry and Cell Biology 38, 610–620.
Wijnen, H., 2009. Circadian rhythms. A circadian loop asSIRTs itself. Science 324, 598–599.
Wolf, C.M., Wang, L., Alcalai, R., Pizard, A., Burgon, P.G., Ahmad, F., Sherwood, M., Branco, D.M., Wakimoto, H., Fishman, G.I., See, V., Stewart, C.L., Conner, D.A., Berul, C.I., Seidman, C.E., Seidman, J.G., 2008. Lamin A/C haploinsufficiency causes dilated cardiomyopathy and apoptosis-triggered cardiac conduction system disease. Journal of Molecular and Cellular Cardiology 44, 293–303.
Wood, J.G., Rogina, B., Lavu, S., Howitz, K., Helfand, S.L., Tatar, M., Sinclair, D., 2004. Sirtuin activators mimic caloric restriction and delay ageing in metazoans. Nature 430, 686–689.
Worman, H.J., Bonne, G., 2007. "Laminopathies": a wide spectrum of human diseases. Experimental Cell Research 313, 2121–2133.
Wullschleger, S., Loewith, R., Hall, M.N., 2006. TOR signaling in growth and metabolism. Cell 124, 471–484.
Wyrick, J.J., Parra, M.A., 2009. The role of histone H2A and H2B post-translational modifications in transcription: A genomic perspective. Biochimica et Biophysica Acta 1789, 37–44.
Xiao, H., Hasegawa, T., Isobe, K., 2000. P300 collaborates with Sp1 and Sp3 in p21(waf1/cip1) promoter activation induced by histone deacetylase inhibitor. The Journal of Biological Chemistry 275, 1371–1376.
Yang, C., Przyborski, S., Cooke, M.J., Zhang, X., Stewart, R., Anyfantis, G., Atkinson, S.P., Saretzki, G., Armstrong, L., Lako, M., 2008. A key role for telomerase reverse transcriptase unit in modulating human embryonic stem cell proliferation, cell cycle dynamics, and in vitro differentiation. Stem Cells 26, 850–863.
Yang, X., Downes, M., Yu, R.T., Bookout, A.L., He, W., Straume, M., Mangelsdorf, D.J., Evans, R.M., 2006. Nuclear receptor expression links the circadian clock to metabolism. Cell 126, 801–810.
Yoon, Y., Krueger, E.W., Oswald, B.J., McNiven, M.A., 2003. The mitochondrial protein hFis1 regulates mitochondrial fission in mammalian cells through an interaction with the dynamin-like protein DLP1. Molecular and Cellular Biochemistry 23, 5409–5420.
Zhao, X., Leotta, A., Kustanovich, V., Lajonchere, C., Geschwind, D.H., Law, K., Law, P., Qiu, S., Lord, C., Sebat, J., Ye, K., Wigler, M., 2007. A unified genetic theory for sporadic and inherited autism. Proceedings of the National Academy of Sciences of the United States of America 104, 12831–12836.
Zhao, Z., Tavoosidana, G., Sjolinder, M., Gondor, A., Mariano, P., Wang, S., Kanduri, C., Lezcano, M., Sandhu, K.S., Singh, U., Pant, V., Tiwari, V., Kurukuti, S., Ohlsson, R., 2006. Circular chromosome conformation capture (4C) uncovers extensive networks of epigenetically regulated intra- and interchromosomal interactions. Nature Genetics 38, 1341–1347.
Zhu, Z., Yao, J., Johns, T., Fu, K., De Bie, I., Macmillan, C., Cuthbert, A.P., Newbold, R.F., Wang, J., Chevrette, M., Brown, G.K., Brown, R.M., Shoubridge, E.A., 1998. SURF1, encoding a factor involved in the biogenesis of cytochrome c oxidase, is mutated in Leigh syndrome. Nature Genetics 20, 337–343.
Zuchner, S., Mersiyanova, I.V., Muglia, M., Bissar-Tadmouri, N., Rochelle, J., Dadali, E.L., Zappia, M., Nelis, E., Patitucci, A., Senderek, J., Parman, Y., Evgrafov, O., Jonghe, P.D., Takahashi, Y., Tsuji, S., Pericak-Vance, M.A., Quattrone, A., Battaloglu, E., Polyakov, A.V., Timmerman, V., Schroder, J.M., Vance, J.M., 2004. Mutations in the mitochondrial GTPase mitofusin 2 cause Charcot-Marie-Tooth neuropathy type 2A. Nature Genetics 36, 449–451.

Trends in Cell Biology

CellPress

Special Series: Mitochondria

Review

Mitochondria and Epigenetics – Crosstalk in Homeostasis and Stress

Olli Matilainen,[1,2] Pedro M. Quirós,[1,2] and Johan Auwerx[1,*]

Through epigenetic mechanisms cells integrate environmental stimuli to fine-tune gene expression levels. Mitochondrial function is essential to provide the intermediate metabolites necessary to generate and modify epigenetic marks in the nucleus, which in turn can regulate the expression of mitochondrial proteins. In this review we summarize the function of mitochondria in the regulation of epigenetic mechanisms as a new aspect of mitonuclear communication. We focus in particular on the most common epigenetic modifications – histone acetylation and histone and DNA methylation. We also discuss the emerging field of mitochondrial DNA (mtDNA) methylation, whose physiological role remains unknown. Finally, we describe the essential role of some histone modifications in regulating the mitochondrial unfolded protein response (UPR^{mt}) and the mitochondrial stress-dependent lifespan extension.

Trends

Crosstalk between mitochondria and the nuclear epigenome represents bidirectional mitonuclear communication: mitochondria are essential mediators of epigenetic processes and, conversely, changes in epigenome regulate mitochondrial function.

Mitochondrial DNA can be methylated, although its biological significance remains unknown.

Mitochondria-mediated changes in the epigenome affect stress responses and longevity.

Mitochondrial Genetics and Function

Mitochondria are the central core of energy metabolism within the cell, producing ATP through oxidative phosphorylation (OXPHOS) and an intricate system that coordinates fatty acid and glucose oxidation. In addition, mitochondria regulate intermediate metabolism, controlling the levels of many different metabolites essential for diverse cellular functions [1]. Mitochondria have their own independent genome – the mtDNA – a relic from their bacterial origin, which has been significantly reduced in size as a result of millions of years of coevolution within eukaryotic cells. Mammalian mtDNA encodes only 37 genes: two ribosomal RNAs, 22 transfer RNAs, and 13 proteins that are part of the mitochondrial OXPHOS complexes [2]. The remainder of the mitochondrial proteome, comprising more than 1000 proteins, is encoded in the nucleus. Whereas circular mtDNA exists in multiples copies in each mitochondrion, and is maternally inherited and redundant [3], nuclear DNA (nDNA) is wrapped around nucleosomes consisting of eight histone protein cores.

Mitochondrial function depends on the coordination of nuclear and mitochondrial genomes, and therefore the transcription and translation of both genomes are coregulated. This coregulation is especially evident for the OXPHOS complexes which are composed of protein subunits encoded in both genomes, and thereby must be assembled in a stoichiometric manner [4,5]. The function of mitochondria is controlled by the nucleus through a mechanism termed 'anterograde regulation' (signaling from the nucleus to the mitochondria) that promotes biogenesis and regulates mitochondrial activity to meet the cellular needs. On the other hand, mitochondria can control the expression of nuclear genes through a 'retrograde response' (signaling from mitochondria to the nucleus), thus modifying cellular function by reprogramming its metabolism. This bidirectional regulation, which we have defined as mitonuclear

[1]Laboratory for Integrative and Systems Physiology, Ecole Polytechnique Fédérale de Lausanne (EPFL), 1015 Lausanne, Switzerland
[2]These authors contributed equally

*Correspondence:
admin.auwerx@epfl.ch (J. Auwerx).

communication, constitutes a robust network maintaining cellular homeostasis and regulating the adaptation to a variety of stressors [6]. In addition to this bidirectional regulation, environmental changes and cellular metabolism can modify gene expression by regulating the epigenome. In this review we discuss the epigenetic regulation of mitochondrial function, and the mechanisms controlling both nuclear and mitochondrial epigenome. In addition, we discuss the impact of the interplay between the nuclear epigenome and mitochondria on physiology and traits such as lifespan.

Interplay Between Mitochondrial Function and Chromatin Dynamics

Changes in the environment, such as nutritional fluctuations and stress conditions, are translated into adjustments of gene expression through the modification of the epigenome. Epigenetic changes regulate the expression of specific genes without altering the underlying DNA sequence. These changes are mediated by modifications in the dynamics of chromatin structure that varies between an open and transcriptionally active state, euchromatin, and a condensed and transcriptionally repressed state, heterochromatin [7]. The main epigenetic mechanisms involved in this transition are post-translational histone modifications and DNA methylation. Histone N-terminal tails are targets of multiple covalent modifications, including acetylation, methylation, ubiquitylation, phosphorylation, and *O*-GlcNAcylation, which together form the 'histone code' [8,9]. Specific histone-tail modifications can regulate gene expression by influencing chromatin condensation and by providing binding sites for regulatory proteins. Furthermore, histone modifications can be either activating or repressing depending on the target residues. Within the histone code, acetylation and methylation are the best-studied post-translational modifications. Histone acetylation uses acetyl-CoA, whereas *S*-adenosyl methionine (SAM) is needed for both histone and DNA methylation. Therefore, these modifications are strictly dependent on the cellular energy status, noting that the levels of aforementioned metabolites are regulated by intermediate metabolism and mitochondrial function [10–12]. We briefly describe here how mitochondrial metabolism affects the dynamics of acetylation and methylation, and also how these two mechanisms can regulate mitochondrial function.

Histone Acetylation

Histone acetylation is one of the best-studied forms of chromatin modification and is associated with transcriptional activation. Histone acetyltransferases (HATs) and histone deacetylases (HDACs) are the enzymes responsible for adding and removing, respectively, acetyl groups on histone tails. These enzymes regulate gene expression by modulating chromatin packaging. HATs transfer an acetyl group from acetyl-CoA to the ε-amino group of lysine residues, which relaxes the chromatin by masking the positive charge of the lysine, thereby increasing accessibility to transcriptional activators. Conversely, HDACs promote the removal of these acetyl groups, resulting in chromatin compaction and silencing of gene transcription [13]. HATs and HDACs are classified into different families that are partially conserved from yeast to mammals [14,15]. Importantly, their activity requires specific metabolic coenzymes whose biosynthesis depends on intracellular ATP levels and mitochondrial function.

As described above, the levels of acetyl-CoA are crucial for the function of HATs. Acetyl-CoA can be generated from different metabolic pathways and intermediates including glycolysis and pyruvate, fatty acid oxidation, acetate, ketone bodies, and amino acids [12,16]. In mitochondria, acetyl-CoA and oxaloacetate are converted into citrate by citrate synthase within the tricarboxylic acid (TCA) cycle. Subsequently, citrate is exported to the cytosol where it is converted, in an inverse reaction, into acetyl-CoA and oxaloacetate by ATP-citrate lyase (ACLY) (Figure 1) [17]. Cellular levels of acetyl-CoA are strictly dependent on energy status: when energy production is high, acetyl-CoA is upregulated, promoting histone acetylation and gene expression. On the other hand, when cellular metabolism is slow, decreases in acetyl-CoA levels reduce histone acetylation, suppressing gene expression through chromatin

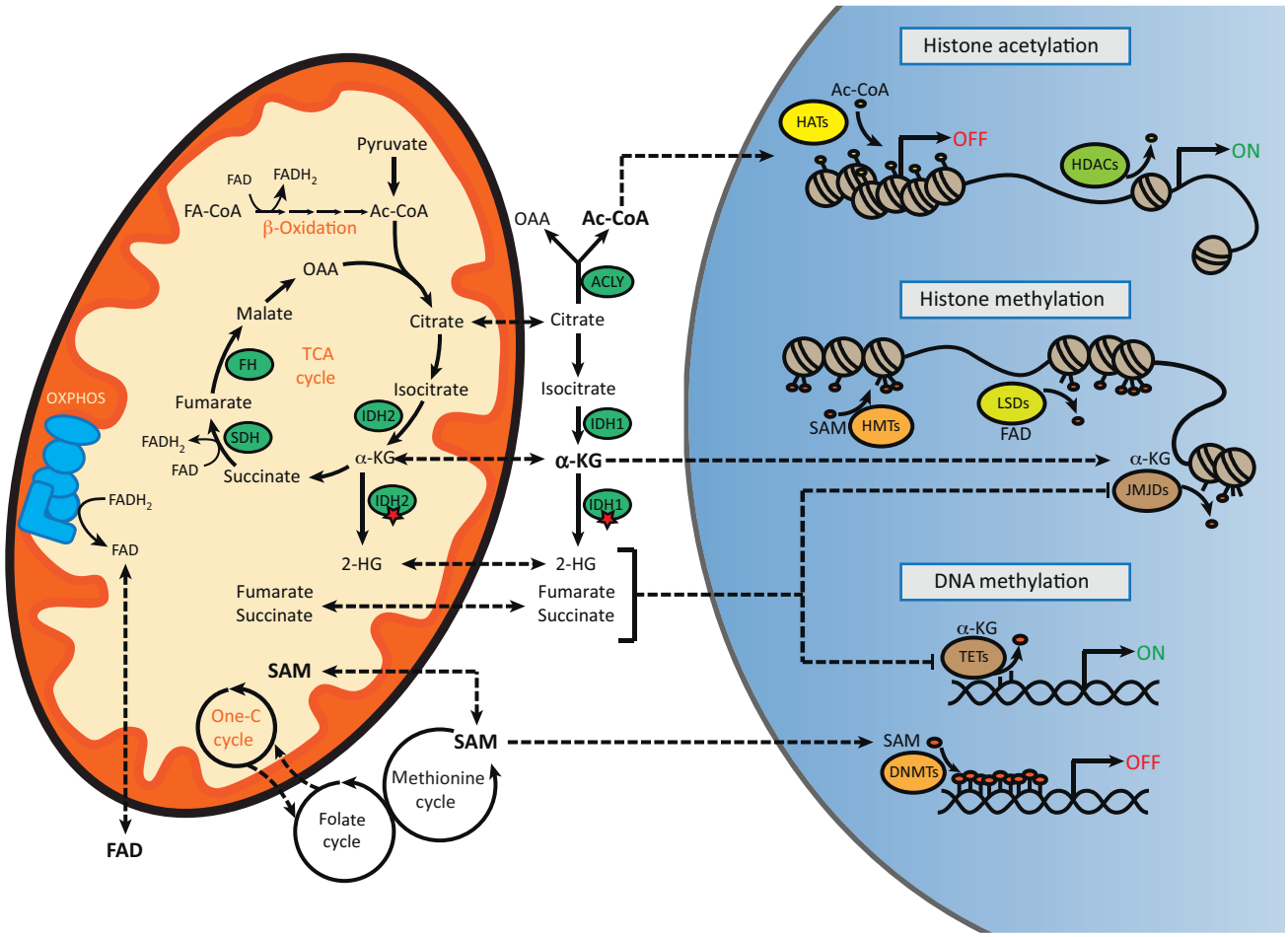

Trends in Cell Biology

Figure 1. Mitochondrial Function and Epigenetic Regulation. Mitochondrial function is essential to provide intermediate metabolites required to generate and modify epigenetic marks, especially histone acetylation and methylation, and also DNA methylation. Acetyl-CoA, the source of acetyl groups used by histone acetyltransferases (HATS), is generated in the cytosol by the ACLY using citrate which can be generated from TCA cycle in mitochondria. α-Ketoglutarate (α-KG) generated in the TCA cycle both in mitochondria and the cytosol is an essential cofactor of the histone demethylases (HDMs), JMJDs, and TET DNA methylases. On the other hand, fumarate and succinate, as well as the oncometabolite 2-hydroxyglutarate (2-HG), inhibit both JMJDs and TETs. Fumarate and succinate accumulate in mitochondria as a result of mutations affecting the succinate dehydrogenase complex (SDH) and fumarate hydratase (FH). 2-HG is generated by gain-of-function mutations in either cytosolic or mitochondrial isocitrate dehydrogenase enzymes, IDH1 and IDH2, respectively. Mitochondria also play essential role regulating the levels and redox state of flavin adenine dinucleotide (FAD), an essential cofactor of the LSDs, a class of HDMs. FAD is reduced, during the TCA cycle and β-oxidation, to $FADH_2$ and then oxidized during oxidative phosphorylation (OXPHOS). Finally, *S*-adenosyl methionine (SAM) is the source of methyl groups used by histone and DNA methytransferases (HMTs and DNMTs), respectively, in the nucleus. SAM is generated through the coupling of the folate and methionine cycles in the cytosol, which in turn are sustained by the one-carbon (one-C) metabolism in mitochondria. SAM can also enter into mitochondria where it is used by DNMTs to methylate the mtDNA. Abbreviations: Ac-CoA, acetyl-CoA; ACLY, ATP-citrate lyase; FA-CoA, fatty acyl CoA; LSD, Lys-specific demethylase; OFF, transcriptional inhibition; ON, transcriptional activation; OAA, oxaloacetic acid; TCA cycle, tricarboxylic acid cycle.

condensation [12]. In addition to acetyl-CoA-mediated histone acetylation, mitochondrial dysfunction caused by the loss of mtDNA decreases site-specific histone acetylation marks [18], adding another mitochondrion-related mechanism controlling the histone acetylation. Together, mitochondrial function, and in particular the TCA cycle, is an essential regulator of histone acetylation, and hence of global gene expression.

Given their well-established role as epigenetic regulators of mitochondrial metabolism, the sirtuin family of HDACs, which use NAD^+ as a cofactor to remove acetyl groups from the lysine residues of their substrates, has been extensively covered in the literature [19–22]. Although

sirtuin activity is known to be sensitive to the cellular NAD^+ pools [23], and hence to cellular metabolism in general, direct evidence that mitochondrial NAD^+ levels control sirtuin activity is currently lacking, and will require detailed analysis of subcellular NAD^+ pools – which at present is technically challenging.

Histone Methylation

In addition to histone acetylation, methylation is a further well-characterized histone modification. Unlike acetylation, histone methylation can activate or repress transcription by modifying a single lysine (K) or arginine (R) amino acid residue on a histone protein. In the methylation step, lysine can be mono-, di-, or trimethylated, while arginine can be mono- or dimethylated. Although these modifications can occur on any histone, the most frequent methylations are described on lysine residues of histone 3 (H3) and histone 4 (H4) [10,24]. Lysine methylation is implicated in both activation and repression, depending on the particular residue and the level of methylation. For instance, methylation marks on H3K4, H3K48, H3K36, or H3K79 are associated with activation, whereas H3K9, H3K27, and H4K20 methylation is associated with silencing of transcription [24]. Furthermore, as illustrated by H3K27 and H4K20, the number of attached methyl groups can determine the consequence of methylation, shifting methylated lysine from an activating to a repressing mark or vice versa [25].

The enzymes responsible for histone methylation are histone methyltransferases (HMTs), while histone demethylases (HDMs) remove methyl marks. The HMTs are grouped into different classes: SET domain lysine methyltransferases, non-SET domain lysine methyltransferases, and arginine methyltransferases. All aforementioned classes use SAM as a precursor in methyl group transfer [10,26]. Therefore, mitochondrial function can regulate histone methylation by controlling the synthesis of SAM. Although SAM is generated through the methionine–homocysteine cycle in the cytosol, this cycle depends on the folate cycle and ATP, which both are reliant on mitochondrial metabolism [10,27]. Whereas mitochondria are involved in controlling histone methylation, there is also regulation in the reverse direction because some HMTs can modulate mitochondrial function. This is exemplified by lysine methyltransferase SETD7 (SET7/9), whose inhibition promotes mitochondrial biogenesis and activates an antioxidant response through PGC1α and NFE2L2, respectively [28].

Based on the catalytic domain and their mechanism of demethylation, the HDMs, and in particular the lysine demethylases (KDMs), can be classified into two different families: Lys-specific demethylases (LSD) and Jumonji C (JmjC) domain demethylases (JMJD). LSDs are flavin adenine dinucleotide (FAD)-dependent amine oxidases composed of two domains: a FAD-binding and a substrate-binding domain. LSDs can demethylate mono- and dimethylated H3K9 or H3K4, leading to transcriptional activation or repression. LSD1 (KDM1A) was the first histone demethylase discovered [29,30]. It can be recruited by different multiprotein complexes, such as the NuRD (nucleosome remodeling and deacetylase) or CoREST (corepressor of REST) that participate in H3K4me2 and H3K4me1 demethylation [31,32], or form complexes with androgen or estrogen nuclear receptors, demethylating H3K9 [30,33]. Several reports have described an important role of LSD1 in regulating of mitochondrial gene expression, especially in adipose tissue, although there are some contradictory opinions regarding its activity. Transgenic overexpression of LSD1 has been reported to promote oxidative metabolism of white adipose tissue (WAT) by activating mitochondrial and thermogenic genes [34]. However, another group reported that LSD1 decreases mitochondrial respiration and energy expenditure [35]. In brown adipose tissue (BAT), LSD1 promotes mitochondrial fatty acid oxidation and brown adipogenesis, increasing thermogenesis and energy expenditure in mice [36–38]. Conversely, it has also been described that inhibition of LSD1 reduces glycolysis and activates mitochondrial respiration in human hepatocellular carcinoma cells [39].

The JMJD family encompasses most of the KDMs and, depending on their chromatin-interacting domains and substrate specificity, six different groups (KDM2–7) have been identified [40]. JMJDs belong to the α-ketoglutarate (α-KG; also known as 2-oxoglutarate, 2OG)-dependent dioxygenase (2OGDD) enzymes. Their function is activated by Fe(II) and α-KG cofactors used by the JmjC domain, and inhibited by succinate and fumarate [41]. KDMs contain a variety of domains which serve to bind to histones, recognize substrates, and remove methyl groups. Furthermore, in addition to histone methylation, KDMs can also act on other substrates playing diverse roles in cellular function [40]. Several KDMs have been reported to regulate mitochondrial function, especially those associated with H3K4 marks. In this regard, Lid, an ortholog of KDM5 in flies, is reported to be a direct regulator of genes required for mitochondrial structure and function [42]. In mammalian cells it has been shown that KDM5A, which demethylates H3K4, acts as a direct repressor of metabolic regulatory genes, and that the loss of KDM5A activates mitochondrial biogenesis and affects mitochondrial morphology [43,44].

Similarly to HATs/HDACs, HMTs/HDMs also require specific metabolic coenzymes whose biosynthesis depends on intracellular ATP levels and mitochondrial function [10]. The redox cofactor FAD, which is required for LSDs, is synthesized *de novo* from riboflavin that generates flavin mononucleotide and then FAD by the ATP-dependent enzymes riboflavin kinase and FAD-synthase, respectively. In mitochondria, FAD is used as a cofactor by the succinate dehydrogenase (SDH) complex in the TCA cycle and by acyl-CoA dehydrogenase in β-oxidation where it is reduced to $FADH_2$. The two high-energy electrons of $FADH_2$ are used through the electron transport chain (ETC) to produce ATP by OXPHOS, reverting FAD to its oxidized form (Figure 1). α-KG, the cofactor of JMJDs, is a key intermediate of the TCA cycle that is generated from isocitrate by the isocitrate dehydrogenases 2 and 3 (IDH2 and IDH3) in mitochondria and by IDH1 in cytosol (Figure 1). Therefore, it is evident that mitochondrial dysfunction or deregulation of the TCA cycle affect histone methylation, and can therefore cause changes in gene expression. Mitochondrial dysfunction can induce histone hypermethylation by increasing the levels of reactive oxygen species (ROS) [45], succinate, or fumarate [46] which inhibit histone demethylases. This is especially relevant in several cancers caused by mutations in components of the SDH complex and fumarate hydratase (FH) that lead to the accumulation of succinate and fumarate, thus inhibiting the function of HDMs [41]. It has been shown that *in vitro* inhibition of SDH increases H3 methylation, which is reversed by overexpression of the JMJD3 histone demethylase (KDM6B) [47]. Succinate also inhibits the activity of KDM2A, preventing the starvation-induced reduction of ribosomal RNA transcription; KDM2A represses the transcription of rRNA by binding to ribosomal DNA promoters and demethylating H3K36me1/2 [48]. Moreover, JMJDs and TET demethylases can be inhibited by 2-hydroxyglutarate (2-HG), an oncometabolite generated from α-KG by gain-of-function mutations in IDH1 and IDH2 (Figure 1) [49,50]. Finally, because oxygen is required for the catalytic reactions mediated by JMJDs, oxygen deficiency (as observed in hypoxia or ischemic conditions) regulates histone methylation and the gene expression [51].

DNA Methylation

DNA methylation is a fundamental epigenetic process that modifies chromatin structure and regulates gene expression by changing the structure of a single nucleotide. In eukaryotes, the most common DNA modification is 5-methylcytosine (5mC), although other DNA modifications such as N^6-methyladenine (6mA) have recently been described in both invertebrates and mammals [52,53].

Especially in mammals, DNA methylation studies have mainly focused on 5mC because it is widely distributed across the genome, and pleiotropic functions, such as X-chromosome

inactivation, genomic imprinting, gene regulation, epigenetic memory maintenance, and tumorigenesis, have been attributed to this particular type of methylation [54]. DNA methylation levels are furthermore changed over the lifetime of an animal, and serve as an estimate of the chronological age of cell types, tissues, and organs, defined as the epigenetic clock [55]. DNA methylation occurs typically on CpG sites that are often clustered in regions, known as CpG islands, that contain a high frequency of CpG dinucleotides. However, non-CpG methylation can also be detected in mammals, in particular in stem cells and in the brain, as well as in some pathological conditions such as cancer [56]. DNA and histone methylation show a close interrelationship and have a converging impact on the regulation of gene expression, affecting particularly the promoter and enhancer regions of target genes. In mammals, three DNA methyltransferases (DNMT1, DNMT3A, and DNMT3B) generating 5mC methylation have been identified. DNMT1 is the main DNA methyltransferase, and it maintains genomic DNA methylation patterns following DNA replication, while DNMT3A and DNMT3B are mainly responsible for *de novo* DNA methylation. In addition, a paralog of DNMT3A and DNMT3B, DNMT3L, is a catalytically inactive enzyme that interacts with these enzymes and with H3 to promote DNA methylation [57]. DNMTs use also SAM as a methyl donor, and therefore (similarly to histone methylation) dysregulation of the methionine and folate cycles also affects DNA methylation (Figure 1).

Many mitochondrial genes, such as those encoding the two key enzymes of lipid oxidation, CPT1a and ACACA [58,59], are regulated by DNA methylation either on their promoter or on intronic regions. Interestingly, the mitochondrial uncoupling protein UCP1 can be regulated by both DNA and histone methylation [60]. Regarding this, the nuclear corepressor RIP140, which inhibits mitochondrial biogenesis, is a key player regulating histone and DNA methylation to silence UCP1 expression in white adipocytes [61]. Non-CpG methylation has also been associated with mitochondrial function, especially in pathological conditions. For instance, non-CpG hypermethylation at the promoters of the genes encoding PGC-1α and PDK4 have been associated with obesity in humans, and the methylation pattern of these genes can be restored following gastric bypass surgery and weight loss [62]. Exercise also reduces non-CpG methylation at the promoters of genes encoding PGC-1α, PDK4 and PPAR-δ, promoting their expression in human skeletal muscle [63]. In addition, the activity of the PGC-1α (*PPARGC1A*) gene promoter is reduced by non-CpG methylation in the skeletal muscle of type 2 diabetic patients, and this depends on DNMT3B and is triggered by TNF-α or free fatty acids [64].

There are different mechanisms of DNA demethylation, and these can act either passively, by decreasing the activity of DNMTs on newly synthesized DNA strands, or actively by specific enzymes removing methyl groups independently of DNA replication. The active processes require the oxidation of the methyl residues on cytosines, generating 5-hydroxymethylcytosine (5hmC). This mark functions as an intermediate between methylated and demethylated cytosine, and has different biological functions [57]. Ten-eleven translocation (TET) enzymes are responsible for oxidizing 5mC to 5hmC. The generation of 5hmC by TETs triggers a demethylation process involving the base excision repair (BER) mechanism. Family of TET enzymes, which contains three members (TET1–3), comprises methylcytosine dioxygenases that also belong to the 2-OGDO family [65]. Therefore, similarly to JMJDs, TETs require α-KG, Fe(II), and oxygen for the hydroxylation of 5mC, and they are also inhibited by succinate, fumarate and 2-HG [66]. Likewise, mitochondrial dysfunction or TCA cycle deregulation affects their activity and consequently DNA methylation. This is exemplified by the hypermethylator phenotype observed in paragangliomas and gastrointestinal stromal tumors triggered by mutations in SDH and FH, in which the concomitant accumulation of succinate and fumarate inhibits both TETs and JMJDs [67,68].

Packaging and Methylation of mtDNA

Although there are no histones in mitochondria, mtDNA does not exist in a 'naked' form. It is packaged into nucleoids, which are DNA–protein assemblies composed of mtDNA surrounded by core and peripheral nucleoid factors [69]. Core nucleoid factors including the mitochondrial transcription factor A (TFAM, the central mtDNA packaging factor), mitochondrial single-strand binding protein (mtSSB), POLG, mtRNA polymerase (POLRMT), and Lon protease are involved in mtDNA maintenance and transcription [69–72]. Peripheral nucleoid factors, such as ATPase AAA domain-containing protein 3 (ATAD3), prohibitins 1 and 2 (PHB1 and PHB2), and mitochondrial nucleoid factor 1 (MNF1), which interact with core nucleoid factors but not directly with mtDNA, are components of signaling pathways regulating mitochondrial biogenesis, apoptosis, and mitonuclear communication [69].

Although containing CpG sites and non-CpG sites (435 and 4747 in humans, respectively), methylation of mtDNA has been a matter of debate since the 1970s [73–76]. Multiple methods have been developed to detect mtDNA methylation, but all have drawbacks [77]. However, it is generally accepted that mtDNA methylation adds a potential epigenetic layer of regulation to the control of mtDNA transcription. Related to this, it has been reported that a transcript variant of human and mouse DNMT1 translocates to the mitochondria, where it presumably modifies 5mC and 5hmC levels and hence influences the transcription of mitochondrial genes [78]. In addition to DNMT1, TET1 and TET2 have also been found in mitochondria [79]. Although the physiological role of mtDNA methylation is still unknown, it has been found that aging decreases mtDNA 5hmC in the mouse frontal cortex [79]. In the same tissue, the expression of mitochondrion-encoded genes is upregulated upon aging [79], suggesting that epigenetic regulation of mtDNA transcription is also involved in the aging process. In addition, mtDNA methylation status has been proposed as a biomarker for the detection and diagnosis of diseases [80], indicating that changes in mtDNA methylation may be involved in the onset or progression of pathological conditions.

Mitochondrial Stress Response and Epigenetic Regulation As Determinants of Lifespan in Invertebrates and Yeast

Inhibition of mitochondrial function extends lifespan in many organisms, and work with *C. elegans* has shown that the timing of the lifespan-extending mitochondrial stress is a crucial determinant of longevity. For example, to promote lifespan, inhibition of the mitochondrial ETC or disruption of mitochondrial ribosome function by *cco-1* and *mrps-5* RNAi, respectively, must take place during development [81–83]. Knockdown of either *cco-1* or *mrps-5* perturbs mitochondrial function, activating an organelle-specific proteostatic stress response – the mitochondrial unfolded protein response (UPR^{mt}). In the UPR^{mt}, the compromised protein-folding environment in mitochondria leads to ClpP-mediated generation of peptides, which are transported to the cytoplasm through the ATP-binding cassette protein HAF-1 [84]. These peptides activate the transcription factor ATFS-1, which under normal conditions is degraded in the mitochondria, but is translocated into the nucleus upon mitochondrial stress [85]. In the nucleus, together with the homeobox transcription factor DVE-1 and the ubiquitin-like protein UBL-5, ATFS-1 drives the expression of mitochondrial chaperones and proteases to restore mitochondrial protein homeostasis [85–87]. The UPR^{mt} is required for the extended longevity upon mitochondrial stress [83]; similarly to mitochondria-mediated longevity, the UPR^{mt} can be induced only during the developmental stages [83,88]. This suggests that the UPR^{mt} and mitochondria-mediated longevity share an epigenetic label which programs organismal survival during adulthood.

Mitochondrial stress modifies the epigenome through extensive chromatin reorganization manifested by histone methyltransferase MET-2- and nuclear cofactor LIN-65-mediated changes in the pattern of H3K9me2 methylation. H3K9me2 methylation enhances chromatin

compaction, thus preventing the transcriptional machinery from initiating transcription. During this mitochondrial stress-mediated chromatin condensation and downregulation of global transcription, loci harboring UPR^{mt} genes are opened and bound by the transcriptional regulators ATFS-1 and DVE-1. These factors activate the UPR^{mt} to balance mitochondrial proteostasis and to promote mitochondria-derived longevity. Importantly, the nuclear translocation of LIN-65 and DVE-1 are dependent on each other, indicating that mitochondrial stress-mediated chromatin reorganization and transcriptional activation of the UPR^{mt} are finely tuned and interconnected processes [89] (Figure 2). In addition to H3K9 methylation, H3K27 methylation also regulates the responses to mitochondrial stress. In non-stressed conditions, the UPR^{mt} gene loci are silenced by H3K27me2 and H3K27me3 methylation. During mitochondrial stress, JMJD-1.2 and JMJD-3.1, H3K27me2 and H3K27me3 demethylases and orthologs of mammalian PHF8 and JMJD3, respectively, remove the silencing marks, thus allowing the

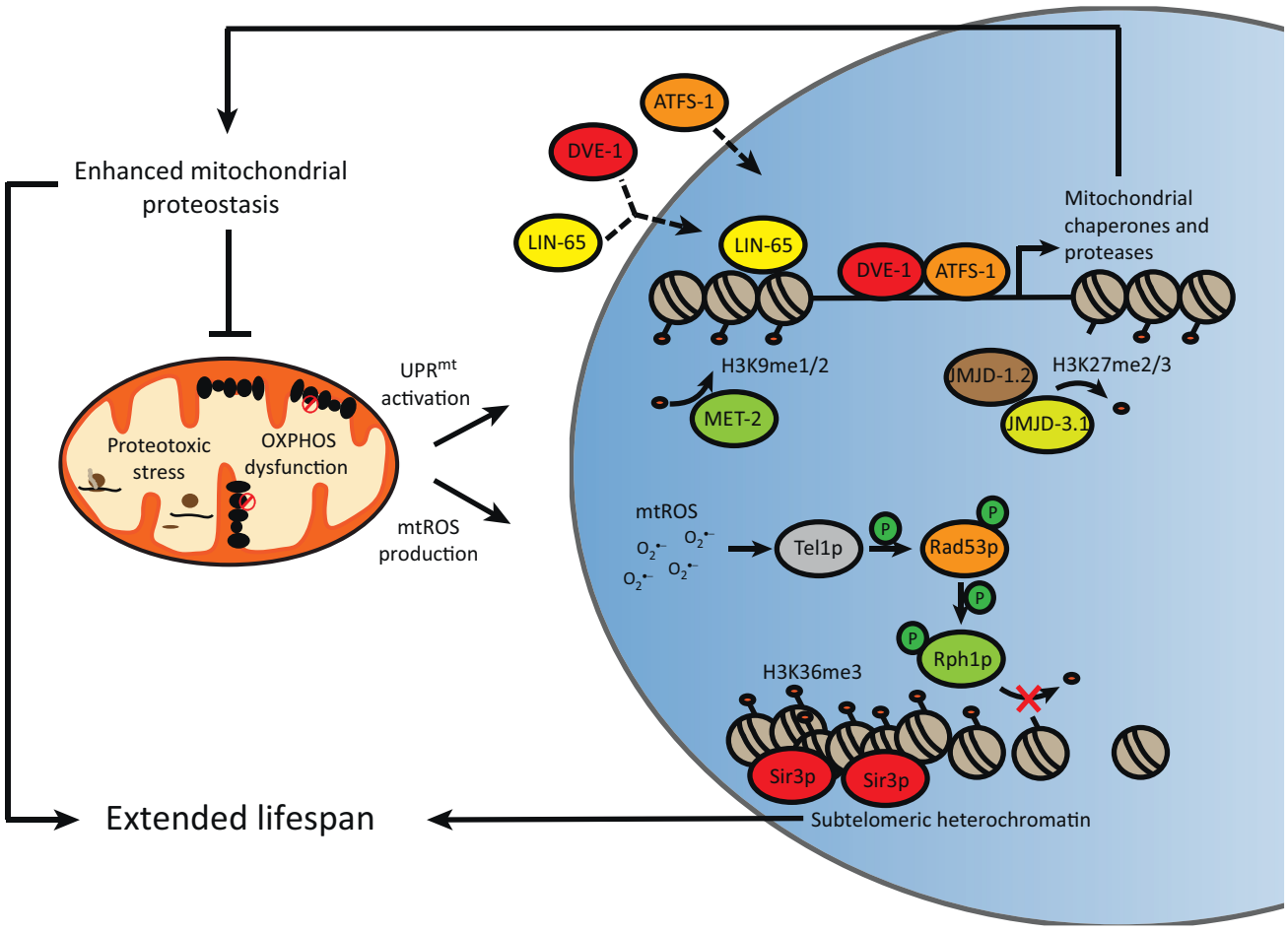

Figure 2. Interplay Between Mitochondria and the Nuclear Epigenome in Lifespan Regulation. Work with *C. elegans* has shown that mitochondrial stress reorganizes the chromatin through MET-2- and LIN-65-mediated changes in histone H3 lysine 9 (H3K9) methylation. While H3K9 methylation silences the chromatin, specific loci open up to allow DVE-1 and ATFS-1 to activate transcription of genes involved in the mitochondrial unfolded protein response (UPR^{mt}). In addition, modification of H3K27 methylation is also involved in the UPR^{mt}. The H3K27me2 and H3K27me3 demethylases, JMJD-1.2 and JMJD-3.1, respectively, remove the silencing histone marks during mitochondrial stress to activate the UPR^{mt}. In both mechanisms, epigenetically regulated UPR^{mt} activation is required for lifespan extension following mitochondrial stress. Work with yeast has shown that the mitochondrial reactive oxygen species (mtROS) activate Tel1p and Rad53p, homologs of the mammalian DNA damage response kinases ATM and Chk2, which then phosphorylate (P) and inactivate the histone H3K36 demethylase Rph1p specifically at subtelomeric heterochromatin. This leads to enhanced binding of Sir3p, and thus repression of subtelomeric transcription and increased longevity. Abbreviations: OXPHOS, oxidative phosphorylation.

activation of the UPR^{mt}. Importantly, JMJD-1.2- and JMJD-3.1-mediated H3K27 demethylation is required both to promote mitochondrial proteostasis and to induce lifespan extension upon mitochondrial stress [90] (Figure 2). Moreover, ectopic JMJD-1.2 and JMJD-3.1 expression is sufficient to activate the UPR^{mt} and to promote longevity, as well as to regulate the expression of mitochondrial genes [90]. This demonstrates that H3K27 methylation acts as an epigenetic switch controlling mitochondrial function and homeostasis during stress that is conserved across species [90]. Notably, JMJD-3.1 also activates in a cross-modal fashion genes involved in another stress response, the cytosolic heat-shock response [91], further highlighting the importance of dynamic H3K27 methylation in governing global cellular stress responses.

The UPR^{mt} is not the only pathway that exploits mitochondria-mediated epigenetic modifications to regulate lifespan. In yeast, hormetic mitochondrial ROS (mtROS) activates Tel1p and Rad53p, orthologs of the mammalian DNA damage response kinases ATM and Chk2, which in turn inactivate the H3K36 demethylating enzyme, Rph1p, at subtelomeric chromatin. This leads to increased binding of Sir3p and silencing of subtelomeric chromatin, resulting in extended chronological lifespan [92] (Figure 2).

Overall, mitochondrial function regulates longevity by modulating the epigenome, and hence links two key hallmarks of aging – mitochondrial dysfunction and epigenetic alterations [93] – in the determination of lifespan.

Outstanding Questions

How do pathological conditions affecting mitochondria influence the epigenome?

What is the function of mtDNA methylation?

Are all different mitochondrial stress responses regulated by epigenetic changes?

In addition to ROS, what signals do mitochondria generate to mediate epigenetic changes in the nucleus?

Concluding Remarks

Our review highlights that the nuclear epigenome modulates mitochondrial function in numerous ways. Conversely, metabolic signals originating from the mitochondria can initiate epigenetic modifications in the nucleus. This reciprocal relationship between mitochondria and the nuclear genome is a multilayered process that also involves an important epigenetic component. We are only beginning to understand the full complexity of this regulation. The future will show whether the crosstalk between nuclear epigenetic mechanisms and mitochondria will open the path to interventions in which mitochondrial diseases and dysfunction can be managed by targeting the epigenome, and vice versa.

Acknowledgements

The research in the laboratory of the authors is supported by grants from the École Polytechnique Fédérale de Lausanne, the Swiss National Science Foundation (31003A-140780), and the AgingX program of the Swiss Initiative for Systems Biology (51RTP0-151019), and the NIH (R01AG043930).

Supplemental Information

Supplemental information associated with this article can be found online at http://dx.doi.org/10.1016/j.tcb.2017.02.004.

References

1. Nunnari, J. and Suomalainen, A. (2012) Mitochondria: in sickness and in health. *Cell* 148, 1145–1159
2. Wallace, D.C. and Chalkia, D. (2013) Mitochondrial DNA genetics and the heteroplasmy conundrum in evolution and disease. *Cold Spring Harbor Perspect. Biol.* 5, a021220
3. Rebelo, A.P. *et al.* (2011) Mitochondrial DNA transcription regulation and nucleoid organization. *J. Inherit. Metab. Dis.* 34, 941–951
4. Couvillion, M.T. *et al.* (2016) Synchronized mitochondrial and cytosolic translation programs. *Nature* 533, 499–503
5. Richter-Dennerlein, R. (2016) Mitochondrial protein synthesis adapts to influx of nuclear-encoded protein. *Cell* 167, 471–483
6. Quiros, P.M. *et al.* (2016) Mitonuclear communication in homeostasis and stress. *Nat. Rev. Mol. Cell Biol.* 17, 213–226
7. Margueron, R. and Reinberg, D. (2010) Chromatin structure and the inheritance of epigenetic information. *Nat. Rev. Genet.* 11, 285–296
8. Zentner, G.E. and Henikoff, S. (2013) Regulation of nucleosome dynamics by histone modifications. *Nat. Struct. Mol. Biol.* 20, 259–266
9. Allis, C.D. and Jenuwein, T. (2016) The molecular hallmarks of epigenetic control. *Nat. Rev. Genet.* 17, 487–500
10. Teperino, R. *et al.* (2010) Histone methyl transferases and demethylases; can they link metabolism and transcription? *Cell Metab.* 12, 321–327
11. Mouchiroud, L. *et al.* (2014) Transcriptional coregulators: fine-tuning metabolism. *Cell Metab.* 20, 26–40
12. Menzies, K.J. *et al.* (2016) Protein acetylation in metabolism–metabolites and cofactors. *Nat. Rev. Endocrinol.* 12, 43–60
13. Tessarz, P. and Kouzarides, T. (2014) Histone core modifications regulating nucleosome structure and dynamics. *Nat. Rev. Mol. Cell Biol.* 15, 703–708
14. Seto, E. and Yoshida, M. (2014) Erasers of histone acetylation: the histone deacetylase enzymes. *Cold Spring Harbor Perspect. Biol.* 6, a018713

15. Lee, K.K. and Workman, J.L. (2007) Histone acetyltransferase complexes: one size doesn't fit all. *Nat. Rev. Mol. Cell Biol.* 8, 284–295
16. Pietrocola, F. *et al.* (2015) Acetyl coenzyme A: a central metabolite and second messenger. *Cell Metab.* 21, 805–821
17. Wellen, K.E. *et al.* (2009) ATP-citrate lyase links cellular metabolism to histone acetylation. *Science* 324, 1076–1080
18. Martinez-Reyes, I. (2016) TCA cycle and mitochondrial membrane potential are necessary for diverse biological functions. *Mol. Cell* 61, 199–209
19. Bonkowski, M.S. and Sinclair, D.A. (2016) Slowing ageing by design: the rise of NAD^+ and sirtuin-activating compounds. *Nat. Rev. Mol. Cell Biol.* 17, 679–690
20. Houtkooper, R.H. *et al.* (2012) Sirtuins as regulators of metabolism and healthspan. *Nat. Rev. Mol. Cell Biol.* 13, 225–238
21. Chalkiadaki, A. and Guarente, L. (2015) The multifaceted functions of sirtuins in cancer. *Nat. Rev. Cancer* 15, 608–624
22. German, N.J. and Haigis, M.C. (2015) Sirtuins and the metabolic hurdles in cancer. *Current biology* 25, R569–583
23. Imai, S. *et al.* (2000) Transcriptional silencing and longevity protein Sir2 is an NAD-dependent histone deacetylase. *Nature* 403, 795–800
24. Greer, E.L. and Shi, Y. (2012) Histone methylation: a dynamic mark in health, disease and inheritance. *Nat. Rev. Genet.* 13, 343–357
25. Voigt, P. *et al.* (2013) A double take on bivalent promoters. *Genes Dev.* 27, 1318–1338
26. Chiang, P.K. *et al.* (1996) S-adenosylmethionine and methylation. *FASEB J.* 10, 471–480
27. Ducker, G.S. and Rabinowitz, J.D. (2017) One-carbon metabolism in health and disease. *Cell Metab.* 25, 27–42
28. He, S. *et al.* (2015) Lysine methyltransferase SETD7 (SET7/9) regulates ROS signaling through mitochondria and NFE2L2/ARE pathway. *Sci. Rep.* 5, 14368
29. Shi, Y. *et al.* (2004) Histone demethylation mediated by the nuclear amine oxidase homolog LSD1. *Cell* 119, 941–953
30. Metzger, E. *et al.* (2005) LSD1 demethylates repressive histone marks to promote androgen-receptor-dependent transcription. *Nature* 437, 436–439
31. Wang, Y. *et al.* (2009) LSD1 is a subunit of the NuRD complex and targets the metastasis programs in breast cancer. *Cell* 138, 660–672
32. Lee, M.G. *et al.* (2005) An essential role for CoREST in nucleosomal histone 3 lysine 4 demethylation. *Nature* 437, 432–435
33. Perillo, B. *et al.* (2008) DNA oxidation as triggered by H3K9me2 demethylation drives estrogen-induced gene expression. *Science* 319, 202–206
34. Duteil, D. *et al.* (2014) LSD1 promotes oxidative metabolism of white adipose tissue. *Nat. Commun.* 5, 4093
35. Hino, S. *et al.* (2012) FAD-dependent lysine-specific demethylase-1 regulates cellular energy expenditure. *Nat. Commun.* 3, 758
36. Zeng, X. *et al.* (2016) Lysine-specific demethylase 1 promotes brown adipose tissue thermogenesis via repressing glucocorticoid activation. *Genes Dev.* 30, 1822–1836
37. Sambeat, A. *et al.* (2016) LSD1 interacts with Zfp516 to promote UCP1 transcription and brown fat program. *Cell Rep.* 15, 2536–2549
38. Duteil, D. *et al.* (2016) Lsd1 ablation triggers metabolic reprogramming of brown adipose tissue. *Cell Rep.* 17, 1008–1021
39. Sakamoto, A. *et al.* (2015) Lysine demethylase LSD1 coordinates glycolytic and mitochondrial metabolism in hepatocellular carcinoma cells. *Cancer Res.* 75, 1445–1456
40. Kooistra, S.M. and Helin, K. (2012) Molecular mechanisms and potential functions of histone demethylases. *Nat. Rev. Mol Cell Biol.* 13, 297–311
41. Xiao, M. *et al.* (2012) Inhibition of alpha-KG-dependent histone and DNA demethylases by fumarate and succinate that are accumulated in mutations of FH and SDH tumor suppressors. *Genes Dev.* 26, 1326–1338
42. Liu, X. and Secombe, J. (2015) The histone demethylase KDM5 activates gene expression by recognizing chromatin context through its PHD reader motif. *Cell Rep.* 13, 2219–2231
43. Varaljai, R. *et al.* (2015) Increased mitochondrial function downstream from KDM5A histone demethylase rescues differentiation in pRB-deficient cells. *Genes Dev.* 29, 1817–1834
44. Lopez-Bigas, N. *et al.* (2008) Genome-wide analysis of the H3K4 histone demethylase RBP2 reveals a transcriptional program controlling differentiation. *Mol. Cell* 31, 520–530
45. Sullivan, L.B. *et al.* (2013) The proto-oncometabolite fumarate binds glutathione to amplify ROS-dependent signaling. *Mol. Cell* 51, 236–248
46. Sciacovelli, M. *et al.* (2016) Fumarate is an epigenetic modifier that elicits epithelial-to-mesenchymal transition. *Nature* 537, 544–547
47. Cervera, A.M. *et al.* (2009) Inhibition of succinate dehydrogenase dysregulates histone modification in mammalian cells. *Mol. Cancer* 8, 89
48. Tanaka, Y. *et al.* (2010) JmjC enzyme KDM2A is a regulator of rRNA transcription in response to starvation. *EMBO J.* 29, 1510–1522
49. Yan, H. *et al.* (2009) IDH1 and IDH2 mutations in gliomas. *New Eng. J. Med.* 360, 765–773
50. Figueroa, M.E. *et al.* (2010) Leukemic IDH1 and IDH2 mutations result in a hypermethylation phenotype, disrupt TET2 function, and impair hematopoietic differentiation. *Cancer Cell* 18, 553–567
51. Hancock, R.L. *et al.* (2015) Epigenetic regulation by histone demethylases in hypoxia. *Epigenomics* 7, 791–811
52. Greer, E.L. *et al.* (2015) DNA methylation on N6-adenine in *C elegans*. *Cell* 161, 868–878
53. Wu, T.P. *et al.* (2016) DNA methylation on N^6-adenine in mammalian embryonic stem cells. *Nature* 532, 329–333
54. Bergman, Y. and Cedar, H. (2013) DNA methylation dynamics in health and disease. *Nat. Struct. Mol. Biol.* 20, 274–281
55. Horvath, S. (2013) DNA methylation age of human tissues and cell types. *Genome Biol.* 14, R115
56. Patil, V. *et al.* (2014) The evidence for functional non-CpG methylation in mammalian cells. *Epigenetics* 9, 823–828
57. Schubeler, D. (2015) Function and information content of DNA methylation. *Nature* 517, 321–326
58. Irvin, M.R. *et al.* (2014) Epigenome-wide association study of fasting blood lipids in the genetics of lipid-lowering drugs and diet network study. *Circulation* 130, 565–572
59. Oh, S.Y. *et al.* (2005) Alternative usages of multiple promoters of the acetyl-CoA carboxylase beta gene are related to differential transcriptional regulation in human and rodent tissues. *J. Biol. Chem.* 280, 5909–5916
60. Shore, A. *et al.* (2010) Role of Ucp1 enhancer methylation and chromatin remodelling in the control of Ucp1 expression in murine adipose tissue. *Diabetologia* 53, 1164–1173
61. Kiskinis, E. *et al.* (2007) RIP140 directs histone and DNA methylation to silence Ucp1 expression in white adipocytes. *EMBO J.* 26, 4831–4840
62. Barres, R. *et al.* (2013) Weight loss after gastric bypass surgery in human obesity remodels promoter methylation. *Cell Rep.* 3, 1020–1027
63. Barres, R. *et al.* (2012) Acute exercise remodels promoter methylation in human skeletal muscle. *Cell Metab.* 15, 405–411
64. Barres, R. *et al.* (2009) Non-CpG methylation of the PGC-1alpha promoter through DNMT3B controls mitochondrial density. *Cell Metab.* 10, 189–198
65. Pastor, W.A. *et al.* (2013) TETonic shift: biological roles of TET proteins in DNA demethylation and transcription. *Nat. Rev. Mol. Cell Biol.* 14, 341–356
66. Xu, W. *et al.* (2011) Oncometabolite 2-hydroxyglutarate is a competitive inhibitor of alpha-ketoglutarate-dependent dioxygenases. *Cancer Cell* 19, 17–30
67. Letouze, E. *et al.* (2013) SDH mutations establish a hypermethylator phenotype in paraganglioma. *Cancer cell* 23, 739–752

68. Mason, E.F. and Hornick, J.L. (2013) Succinate dehydrogenase deficiency is associated with decreased 5-hydroxymethylcytosine production in gastrointestinal stromal tumors: implications for mechanisms of tumorigenesis. *Modern Pathol.* 26, 1492–1497

69. Gilkerson, R. *et al.* (2013) The mitochondrial nucleoid: integrating mitochondrial DNA into cellular homeostasis. *Cold Spring Harbor Perspect. Biol.* 5, a011080

70. Bogenhagen, D.F. *et al.* (2008) The layered structure of human mitochondrial DNA nucleoids. *J. Biol. Chem.* 283, 3665–3675

71. Lu, B. *et al.* (2007) Roles for the human ATP-dependent Lon protease in mitochondrial DNA maintenance. *J. Biol. Chem.* 282, 17363–17374

72. Kukat, C. *et al.* (2015) Cross-strand binding of TFAM to a single mtDNA molecule forms the mitochondrial nucleoid. *Proc. Natl. Acad. Sci. U.S.A.* 112, 11288–11293

73. Groot, G.S. and Kroon, A.M. (1979) Mitochondrial DNA from various organisms does not contain internally methylated cytosine in -CCGG- sequences. *Biochim. Biophys. Acta* 564, 355–357

74. Dawid, I.B. (1974) 5-methylcytidylic acid: absence from mitochondrial DNA of frogs and HeLa cells. *Science* 184, 80–81

75. Vanyushin, B.F. and Kirnos, M.D. (1977) Structure of animal mitochondrial DNA (base composition, pyrimidine clusters, character of methylation). *Biochim. Biophys. Acta* 475, 323–336

76. Nass, M.M. (1973) Differential methylation of mitochondrial and nuclear DNA in cultured mouse, hamster and virus-transformed hamster cells. In vivo and in vitro methylation. *J. Mol. Biol.* 80, 155–175

77. van der Wijst, M.G. and Rots, M.G. (2015) Mitochondrial epigenetics: an overlooked layer of regulation? *Trends Genet.* 31, 353–356

78. Shock, L.S. *et al.* (2011) DNA methyltransferase 1, cytosine methylation, and cytosine hydroxymethylation in mammalian mitochondria. *Proc. Natl. Acad. Sci. U.S.A.* 108, 3630–3635

79. Dzitoyeva, S. *et al.* (2012) Effect of aging on 5-hydroxymethylcytosine in brain mitochondria. *Neurobiol. Aging* 33, 2881–2891

80. Iacobazzi, V. *et al.* (2013) Mitochondrial DNA methylation as a next-generation biomarker and diagnostic tool. *Mol. Genet. Metab.* 110, 25–34

81. Houtkooper, R.H. *et al.* (2013) Mitonuclear protein imbalance as a conserved longevity mechanism. *Nature* 497, 451–457

82. Dillin, A. *et al.* (2002) Rates of behavior and aging specified by mitochondrial function during development. *Science* 298, 2398–2401

83. Durieux, J. *et al.* (2011) The cell-non-autonomous nature of electron transport chain-mediated longevity. *Cell* 144, 79–91

84. Haynes, C.M. *et al.* (2010) The matrix peptide exporter HAF-1 signals a mitochondrial UPR by activating the transcription factor ZC376.7 in *C. elegans*. *Mol. cell* 37, 529–540

85. Nargund, A.M. *et al.* (2012) Mitochondrial import efficiency of ATFS-1 regulates mitochondrial UPR activation. *Science* 337, 587–590

86. Benedetti, C. *et al.* (2006) Ubiquitin-like protein 5 positively regulates chaperone gene expression in the mitochondrial unfolded protein response. *Genetics* 174, 229–239

87. Haynes, C.M. *et al.* (2007) ClpP mediates activation of a mitochondrial unfolded protein response in *C elegans*. *Dev. cell* 13, 467–480

88. Rea, S.L. *et al.* (2007) Relationship between mitochondrial electron transport chain dysfunction, development, and life extension in *Caenorhabditis elegans*. *PLoS Biol.* 5, e259

89. Tian, Y. *et al.* (2016) Mitochondrial stress induces chromatin reorganization to promote longevity and UPR(mt). *Cell* 165, 1197–1208

90. Merkwirth, C. *et al.* (2016) Two conserved histone demethylases regulate mitochondrial stress-induced longevity. *Cell* 165, 1209–1223

91. Labbadia, J. and Morimoto, R.I. (2015) Repression of the heat shock response is a programmed event at the onset of reproduction. *Mol. cell* 59, 639–650

92. Schroeder, E.A. *et al.* (2013) Epigenetic silencing mediates mitochondria stress-induced longevity. *Cell Metab.* 17, 954–964

93. Lopez-Otin, C. *et al.* (2013) The hallmarks of aging. *Cell* 153, 1194–1217

Free Radical Biology and Medicine 130 (2019) 528–541

Contents lists available at ScienceDirect

Free Radical Biology and Medicine

journal homepage: www.elsevier.com/locate/freeradbiomed

Original article

Mitochondria are a substrate of cellular memory

Amin Cheikhi[a,b], Callen Wallace[c], Claudette St Croix[c,d], Charles Cohen[b], Wan-Yee Tang[e], Peter Wipf[f], Panagiotis V. Benos[g], Fabrisia Ambrosio[b,h,i,j,*], Aaron Barchowsky[b,k,*]

[a] Division of Geriatric Medicine, Department of Medicine, University of Pittsburgh, Pittsburgh, PA 15261, USA
[b] Department of Environmental and Occupational Health, University of Pittsburgh, Pittsburgh, PA 15261, USA
[c] Center for Biological Imaging, University of Pittsburgh, Pittsburgh, PA 15261, USA
[d] Department of Cell Biology, University of Pittsburgh, Pittsburgh, PA 15261, USA
[e] Department of Environmental Health and Engineering, Johns Hopkins Bloomberg School of Public Health, Baltimore, MD 21205, USA
[f] Department of Chemistry, University of Pittsburgh, Pittsburgh, PA 15260, USA
[g] Department of Computational and Systems Biology, University of Pittsburgh, Pittsburgh, PA 15261, USA
[h] Department of Physical Medicine and Rehabilitation, University of Pittsburgh, Pittsburgh, PA, USA
[i] McGowan Institute for Regenerative Medicine, University of Pittsburgh, Pittsburgh, PA 15219, USA
[j] Department of Bioengineering, University of Pittsburgh, Pittsburgh, PA 15261, USA
[k] Department of Pharmacology and Chemical Biology, University of Pittsburgh, Pittsburgh, PA 15261, USA

ARTICLE INFO

Keywords:
Mitochondria
Cellular memory
Epigenetics
Arsenic
XJB-5-131

ABSTRACT

Cellular memory underlies cellular identity, and thus constitutes a unifying mechanism of genetic disposition, environmental influences, and cellular adaptation. Here, we demonstrate that enduring physicochemical changes of mitochondrial networks invoked by transient stress, a phenomenon we term 'mitoengrams', underlie the transgenerational persistence of epigenetically scripted cellular behavior. Using C2C12 myogenic stem-like cells, we show that stress memory elicited by transient, low-level arsenite exposure is stored within a self-renewing subpopulation of progeny cells in a mitochondrial-dependent fashion. Importantly, we demonstrate that erasure of mitoengrams by administration of mitochondria-targeted electron scavenger was sufficient to reset key epigenetic marks of cellular memory and redirect the identity of the mitoengram-harboring progeny cells to a non-stress-like state. Together, our findings indicate that mnemonic information emanating from mitochondria support the balance between the persistence and transience of cellular memory.

1. Introduction

Life-long regenerative capacity relies on a rare subpopulation of self-renewing stem cells that transition between quiescent and activated states to restore tissue homeostasis in response to stress and injury. During this process, restoration of transcriptional identity in daughter stem cells and their return to a quiescent ground state is contingent on inherited cellular memory. This memory can be impeded by stressors that trigger metabolic, transcriptional, and/or epigenetic perturbations, ultimately predisposing stem cells to dysfunction over time [1].

Previous yeast studies of synthetic cellular memory correlated mitochondrial dysfunction with transmission of transient stress memory over multiple generations [2–4]. In these studies, synthetic transcriptional circuits were used to detect a subpopulation of cells with heritable damage responses [2]. This subpopulation was shown to have a higher rate of mitochondrial activity that persisted for many generations following the transient stress event [2]. Whether mitochondrial activity is a primary cause or merely a downstream consequence of cellular memory is unclear [5]. Moreover, mechanisms by which mitochondria are involved in cellular memory during stem cell self-renewal have not been elucidated.

Neuronal memory is stored as specific pattern of synaptic networks connectivity and associated enduring cellular alterations of a specific subpopulation of neurons, referred to as memory engram cells [6]. "Engrams" is a term that defines neuronal memory allocation and persistence in the brain as a physicochemical property. In the current studies, we tested the hypothesis that enduring traces of mitochondrial networks' physicochemical alterations, or 'mitoengrams', underlie cellular memory.

To test the hypothesis, we conducted a cell population-based

* Corresponding authors at: Department of Environmental and Occupational Health, University of Pittsburgh, Public Health 4133, 130 De Soto Street, Pittsburgh, PA 15261, USA.
E-mail addresses: amc165@pitt.edu (A. Cheikhi), ctw14@pitt.edu (C. Wallace), claudette.stcroix@pitt.edu (C. St Croix), wtang10@jhu.edu (W.-Y. Tang), pwipf@pitt.edu (P. Wipf), benos@pitt.edu (P.V. Benos), ambrosio@upmc.edu, ambrosiof@upmc.edu (F. Ambrosio), aab20@pitt.edu (A. Barchowsky).

https://doi.org/10.1016/j.freeradbiomed.2018.11.028
Received 17 September 2018; Received in revised form 19 November 2018; Accepted 21 November 2018
Available online 22 November 2018

assessment of mitochondrial activity and networks status using the C2C12 culture model of myogenesis [7]. We focused on the reserve cell (RC) population of myogenic progenitors, as this population retains key properties of adult muscle stem (satellite) cells, including self-renewal [7]. Specifically, we quantified mitochondrial activity and regulation of cellular memory in RC progeny following two opposing interventions: transient exposure to a low level of the mitochondrial stressor, arsenite, and the rescue of mitochondrial phenotype using the mitochondria-targeted electron scavenger, XJB-5-131 (XJB) [8]. The results demonstrate that persistent behavioral impairment and underlying epigenetic memory of stress observed in the RC progeny are due to the inheritance of dysfunctional mitochondria. Importantly, the severity of impairment was scalable to mitochondrial activity, network connectivity pattern and subcellular localization, where 'scalability' refers to the ability of a system, network or process, to handle growing amounts of work [9]. Moreover, we demonstrate that memory of stress is stored within a subpopulation of mitoengram-harboring progeny cells. These findings suggest that cellular memory is a statistical property defined at the cell population level.

2. Materials and methods

2.1. Cell culture and isolation of reserve cells

Near confluent, proliferating C2C12 myoblasts were incubated in differentiation medium (DMEM: low pyruvate (GIBCO 1243062) containing, 10% horse serum, and 1% P/S in the absence or presence of a single dose of 20 nM sodium arsenite (Fisher Scientific). Medium was not changed throughout the 4 days of differentiation process. After 4 days, undifferentiated reserve cells (RC) were separated from the myotubes by mild trypsinization. Briefly, myotubes were specifically detached by mild trypsinization 19 (Cat#: ICN1689149, MP Biomedicals) for 3 min in Dulbecco's modified Eagle's medium, whereas undifferentiated reserve cells remained adherent to the dish. The remaining cells (reserve cells, RC) were then detached by trypsinization, and passed through a 40 μm cell strainer (Corning, Inc. 352340, ThermoFisher) to obtain a uniform single-cell suspension. The cells were and re-plated (10,000 cells/cm^2) onto a new dish in growth medium. After at least 30 min, the media was replaced with a fresh growth media (DMEM: low pyruvate containing 10% FBS, 10% horse serum, and 1% P/S) with or without the mitochondrially targeted drug XJB-5-131. The RC were left to proliferate for 3–4 days then harvested for different analyses.

2.2. Mitochondrial membrane potential

Cells were seeded and grown at 37 °C and 5% CO2 in a humidified chamber in a 96 well black culture plate at 50,000 cells/well for same day measurement (about 6 h after plating) or 10,000 cells/well 3–4 days post-plating rescue experiments with mitochondrially targeted XJB-5-131. Medium was discarded, cells were rinsed, then 200 μl per well of assay medium (140 mM NaCl, 2.5 mM KCl, 1.8 mM CaCl2, 1 mM MgCl2 and 20 mM HEPES, pH = 7.4, mOsm = 300). An excess of JC-1 (1 μM) was added and the cells were equilibrated with the dye at 37 °C and 5% CO_2 in a humidified chamber for 90 min. The ratio of the fluorescence of JC-1 aggregates formed as mitochondrial membrane ($\Delta\Psi m$) potential increases (ex 353 nm, em 595 nm) to JC-1 monomer (ex 485, em 535) was then measured every 10 min over 3 h.

2.3. Measurement of mitochondrial superoxide

Cells were stained with 250 nM of MitoSOX red (Ex: 488 nm/Em: 575 nm, cat #: M36008, ThermoFisher) for 15 min at 37 °C in the dark. The cells were then collected by trypsinization and washed with Hank's balanced salts solution (HBSS), fixed in 1.5% paraformaldehyde for 10 min, washed to remove any residual paraformaldehyde, re-suspended in 0.5 ml of phosphate buffered saline (PBS). Relative MitoSOX fluorescence intensity per cell was then quantified by flow cytometry using a Becton Dickinson FACS Canto.

2.4. FACS analysis for cell surface proteins

Quantification of cell surface protein expression was performed on non-permeablized RCs and progeny using antibodies to Alexa Fluor® 647 Rat anti-Mouse CD34 at 1:100 (cat #: 560233, BD Biosciences) and Alexa Fluor® 647 Rat anti-Mouse CD133 at 1:100 (cat #: 315-2C11, Biolegend). Cells were then collected by trypsinization, washed with free HBSS (Cat #: 14170112, ThermoFisher), resuspended in 0.5 ml of HBSS and incubated in the dark at room temperature for 15 min. Cells were then pelleted, washed and re-suspended in 0.5 ml of HBSS, fixed in 1.5% paraformaldehyde for 10 min, washed with PBS then PBS plus 0.5% BSA (PBB) to remove any residual paraformaldehyde and re-suspended in 0.5 ml of PBS. Flow cytometric analysis was performed with to quantify relative fluorescence intensity of CD34 and CD133 staining per cell.

2.5. FACS for intracellular proteins

Isolated RCs were washed, pelleted and fixed by resuspension in 2% paraformaldehyde for 10 min at room temperature. The cells were washed three times with PBS, then permeabilized with 0.1% Triton X-100 made in PBS solution for 15 min. Pelleted cells were then washed three times with PBS followed by a second round of washing using PBS plus 0.5% BSA (PBB). Cells were then blocked with 2% BSA for 45 min, washed with three times in PBB and incubated with the following primary antibodies; rabbit monoclonal Cyclin D1((92G2 (Cat #: 2978), Cell Signaling) at 1:50, rabbit monoclonal Caveolin-1(D46G3) (Cat #: Cat #: 3267, Cell Signaling) at 1:50 and rabbit anti-Ki67 (Cat #: ab15580, Abcam).

2.6. Replicative age assay

The replicative age of the isolated RC was traced through the assessment of CFSE fluorescent intensity decay as the RC divide. Cells were trypsinized and stained with 1 μM (CellTrace™ CFSE Cell Proliferation Kit, for flow cytometry, Cat#: C34554). Cells were stained for 20 min at room temperature with gentle agitation. A brief wash with complete medium was then used to quench any dye remaining in solution. The cells were then incubated in growth medium at 37 °C under 5% CO_2 for four days. RC progeny were trypsinized, fixed and CFSE fluorescent intensity per cell was quantified by flow cytometry.

2.7. Cellular thiol status (reductive potential)

Cellular thiol status was used as an index of the degree of cellular oxidative stress. Glutathione (GSH) levels were quantified using ThioGlo®-1 (SigmaAldrich, St. Louis, MO). The content of total low molecular weight thiols (LMWT) was estimated by an immediate fluorescence response registered upon addition of ThioGlo-1 to cell lysate (25 μg) with glutathione (GSH) peroxidase (1 U) and cumene hydroperoxide (100 μmol/l) for 30 min. Levels of total protein sulfhydryls were determined as fluorescence response after adding 4 mM SDS to each LMWT sample. Fluorescence was measured using a Fusion alpha plate reader (PerkinElmer) with excitation filter A (360 ± 40 nm) and emission filter B (530 ± 25 nm). The difference between the fluorescence response of the original sample and the GSH peroxidase-treated sample corresponds to the amount of reduced GSH. All values were normalized to total protein concentration as measured by modified Bradford assay (BioRad).

2.8. Transmission electron microscopy

Cells grown on tissue culture plastic ware were fixed in 2.5% glutaraldehyde in 100 mM PBS (8 gm/l NaCl, 0.2 gm/l KCl, 1.15 gm/l $Na_2HPO_4{\cdot}7H_2O$, 0.2 gm/l KH_2PO_4, pH 7.4) overnight at 4 °C. Monolayers were then washed in PBS three times then post-fixed in aqueous 1% osmium tetroxide, 1% Fe_6CN_3 for 1 h. Cells were washed three times in PBS then dehydrated through a 30–100% ethanol series then several changes of Polybed 812 embedding resin (Polysciences, Warrington, PA). Cultures were embedded in by inverting Polybed 812-filled BEEM capsules on top of the cells. Blocks were cured overnight at 37 °C, and then cured for two days at 65 °C. Monolayers were pulled off the coverslips and re-embedded for cross section. Ultrathin cross sections (60 nm) of the cells were obtained on a Riechart Ultracut E microtome, post-stained in 4% uranyl acetate for 10 min and 1% lead citrate for 7 min. Sections were imaged using a JEM 1011 TEM (JEOL, Peabody, MA) at 80 kV. Images were taken using a side-mount AMT 2k digital camera (Advanced Microscopy Techniques, Danvers, MA).

2.9. Immunofluorescence imaging

Cells were grown on coverslips in 24 well-plate washed three times with HBSS, fixed with 2% paraformaldehyde for 10 min at room temperature, and permeabilized with 0.1% Triton X-100 made in PBS solution for 15 min. The cell monolayer was then washed with PBS. A second round of washing was done using PBS plus 0.5% BSA (PBB). Cells were then blocked with 2% BSA for 45 min, washed with PBB and incubated with rabbit-anti Histone H2A.Z at 1:100 (Cat #: 2718S, Cell Signaling) or anti-mouse Tom20 at 1:100 (Cat #: sc-17764, Santa-Cruz) overnight. The cell monolayers were washed with PBB and incubated with Goat anti-mouse Alexa Fluor 488 Dye and Goat anti-rabbit Cy3. Cell monolayers were washed with PBB, stained with DAPI for 30 s, and washed again with PBS. Coverslips were adhered with gelvatol to a slide and stored at 4 Celsius with minimal exposure to light until imaged.

2.10. 3D imaging and image processing

Samples were imaged using a 1.40 numeric aperture 60x objective on a Nikon Ti microscope equipped with a Nikon A1 point scanning confocal scan head. Optical sections were acquired at 200 nm intervals in Z and reconstructed in three dimensions and subsequent image processing was performed with Nikon Elements software (see also Supplementary information).

2.11. Gene transcripts and ChIP analysis

RNA isolated from RC using the AllPrep DNA/RNA/miRNA Universal Kit (Qiagen, Germantown, MD) was treated with DNaseI and reverse transcribed using iScript™ gDNA Clear cDNA Synthesis Kit (BIO-RAD, Hercules, CA). The mRNA levels of *Dnmt1* and *Dnmt3a* were quantified by SYBR Green-based real-time PCR (qPCR) using SsoAdvanced™ Universal SYBR® Green Supermix (BIO-RAD, Hercules, CA). Transcript levels of *Dnmt1* and *Dnmt3a* were normalized to the expression level of Rpl44, and the fold changes of *Dnmt1* or *Dnmt3a* relative to universal mouse reference RNA was calculated using 2-ΔΔ Ct method. Each sample was measured in duplicates. Primers sequence: Rpl44 (Forward: 5′-AGATGAGGCAGAGGTCCAA-3′ and Reverse: 5′-GTTGTAAGAAAGGCGGTCA-3′); Dnmt1 (Forward:5′-GTCGGACAGT GACACCCTTT-3′, Reverse: 5′-TTTAGTGGGGCCCTTCGTG-3′), Dnmt3a (Forward: 5′-GGGCCACACGGCAGAG-3′ and Reverse 5′-TGCCGTGGTC TTTGTAAGCA-3′). For ChIP analysis, RC were fixed with 1% formaldehyde for 15 min followed by quenching with 125 mM glycine solution. Crosslinked cells were pelleted and washed with PBS containing protease inhibitor cocktail. Chromatin isolation and immunoprecipitation was performed using ChIP-IT kit (Active Motif, Carlsbad, CA), following the manufacturer's instructions. One to two μg of ChIP-validated antibodies against RNA Polymerase II (A2032, Epigentek, Farmingdale, NY), DNMT1 (A1001, Epigentek, Farmingdale, NY), DNMT3A (39206, Active Motif, Carlsbad, CA), H3K9M2 (ab1220, Abcam, Cambridge, MA), H3K27M3 (ab6002, Abcam, Cambridge, MA), H2A.Zac (ab18262, Abcam, Cambridge, MA), EZH2 (39876, Active Motif, Carlsbad, CA) or nonspecific negative control mouse IgG (Active Motif, Carlsbad, CA) were used for immunoprecipitation of each sample. Non-immunoprecipitated chromatin was used as input. Following reverse cross-linking and elution of chromatin, DNA from each sample was purified with QIAquick PCR purification kit (Qiagen, Germantown, MD). Purified DNA sample concentrations were quantified by QubitiT DNA HS assay kit (Thermo Fisher Scientific, Waltham, MA). Ten ng of purified DNA was used for PCR of *Dnmt1* or *Dnmt3a* promoters. The primers were designed for *Dnmt1* and *Dnmt3a* promoter regions: *Dnmt1* (Forward: 5′-ATGGTCTTCCCCCACTCTCT-3′ and Reverse: 5′-TGCAGACGACAGAACAGCTC-3′), *Dnmt3a* (Forward: 5′-ACTGAGGGAGCCAGGTCTAGT-3′ and Reverse: 5′-TGTCCAAAAAGA GTTGGATGC-3′). The percent of immunoprecipitated DNA relative to the input was calculated.

2.12. Methylation-specific PCR

200 ng of RC genomic DNA (gDNA) was subjected to bisulfite conversion with the EZ DNA Methylation Kit (Zymo Research, Irvine, CA) followed by PCR using primers specific for methylated DNA in the *Dnmt3a* promoter (Dnmt3a-MSP: Forward: 5′-TTTTTTTGGATATTTTA AGGTACGG-3′ and Reverse: 5′- ACACTAAAACTAAAAACAACAA CGC-3′). PCR was conducted on the bisulfite-modified DNA with GoTaq (Promega, Madison, WI) using the following conditions: 5 min at 95 °C; 1 min at 95 °C, 1 min at 58 °C, 2 min at 72 °C for 35 cycles; 12 min at 72 °C (final extension). PCR amplicons were separated by electrophoresis on 2% agarose gel. Bands were quantified by densitometry using GelQuant.NET software provided by biochemlabsolutions.com. Fully methylated control DNA (Zymo Research, Irvine, CA) was used as a reference to calculate the percentage methylation of DNA samples.

2.13. Statistical analysis

Data in bar graphs are expressed as mean ± SEM. Significance between groups was determined by Student's *t*-tests or two-way ANOVA. *A priori*, differences were considered to be significantly different at $p < 0.05$. Statistical analysis was performed using Graphpad Prizm v7 software. The fitting to the tails of the investigated distributions was performed using Mathematica and MathStatica packages (see also statistical appendices).

3. Results

3.1. Environmental stress impairs RC mitochondrial physiochemical properties and enhances self-renewal

To stimulate a protracted mitochondrial phenotype *in vitro*, we differentiated C2C12 myogenic progenitor cells for 4 days in absence or presence of a non-cytotoxic, trace amount of arsenite (20 nM, Fig. 1A), an inducer of a total cell integrated stress response. Undifferentiated mononuclear RC were then separated from differentiated myotubes and collected for analysis (Fig. 1A–B). We chose arsenite because it is rapidly effluxed from cells and intracellular residual traces are barely detectable, even with exposures 1000-fold greater than used in these experiments [10,11]. We previously found that mitochondrial morphology was disrupted and mitochondrial oxygen consumption, as well as proton leak and ROS generation, were increased in satellite cells and myofibers of mice exposed to 100 ppb arsenite in their drinking water [12].

RC isolated from arsenite-exposed cultures (RC^{primed}) had elevated

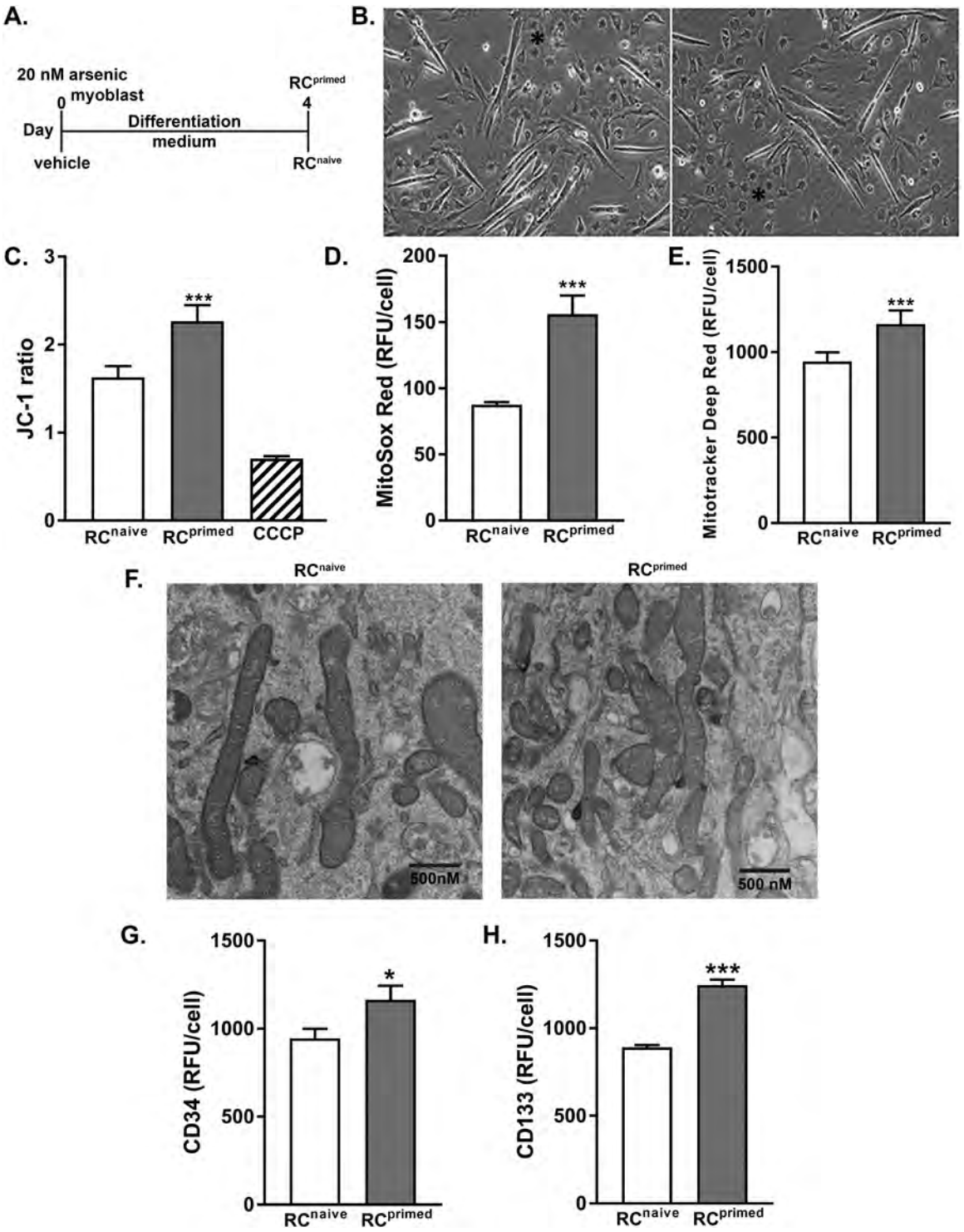

Fig. 1. The phenotype of RC exposed to transient stress. (A) Schematic of the experimental design. C2C12 cells were cultured in the presence or absence of 20 nM of sodium arsenite for four days in differentiation medium. **(B)** Representative images of C2C12 myogenesis. The resulting heterogeneous culture contained fused multinucleated myotubes and mononucleated RC in an undifferentiated state (asterisks). **(C)** Control (RC^{naive}) or arsenite-exposed RC (RC^{primed}) RC were isolated and analyzed for mitochondrial membrane potential using the ratiometric probe JC-1 (1 μM; emission of monomeric JC-1 at 535 ± 10 nm/emission of JC-1 aggregates at 595 ± 10 nm). The proton ionophore, carbonyl cyanide m-chlorophenyl hydrazone (CCCP; 20 μM) was used as a positive control for JC-1 measured membrane potential. Flow cytometric analysis of the two RC populations (10,000 cells each) indicated a concomitant increase of **(D)** mitochondrial superoxide generation and **(E)** mitochondrial mass in RC^{primed} relative to their naïve counterparts, as quantified by of mitochondrial superoxide indicator MitoSOX Red (250 nM; Ex: 488 nm/Em: 575 nm) and the mitochondrial mass dye mitotracker deep red (MTDR, 100 nM, Ex: 644 nm/Em: 665 nm), respectively. **(F)** Electron microscopy showed that mitochondria in RC^{primed} are more abundant, relatively larger, and display increased cristae remodeling relative to $RC^{naïve}$. Flow cytometric analysis revealed upregulation of self-renewal markers, **(G)** CD34-APC and **(H)** CD133-APC in RC^{primed}. All results represent three independent experiments (n = 3) and are presented as means ± SEM of microplate or single cell fluorescence intensity. Differences from $RC^{naïve}$ are designated by *$p < 0.05$ and ***$p < 0.001$ as determined by Student's *t*-test.

mitochondrial membrane potential, increased mitochondrial superoxide generation, and increased mitochondrial mass relative to their non-stressed counterparts ($RC^{naïve}$; Fig. 1C–E, Fig. S1A–C). In keeping with our earlier observations in vascular cells exposed to low levels of arsenite and the progenitor cells isolated from arsenite-exposed mice [12,13], assessment of the redox state in RC^{primed} showed adaptive increases in reduced glutathione levels, low-molecular-weight thiol (LMWTs) levels, and protein sulfhydryl levels, rather than toxic oxidative stress (Fig. S1D). Qualitative electron microscopic examination of RC showed that both $RC^{naïve}$ and RC^{primed} exhibited a mixture of orthodox and condensed mitochondrial configurations with no evidence of mitophagy. However, RC^{primed} appeared to have slightly larger and more tubular mitochondria (Fig. 1F).

The RC presumably exist in a dormant state in which the cells retain self-renewal properties and are not actively cycling [7]. To determine whether RC with different mitochondrial phenotypes resolve to different cell behaviors, we used flow cytometry to quantify levels of two surface markers of self-renewal, CD34 and CD133 [14,15]. In accordance with previous reports of CD34 and CD133 upregulation with increased mitochondrial mass and activity [16,17], expression of self-renewal markers increased in RC^{primed} cells compared to $RC^{naïve}$ cells (Fig. 1G, H and Fig. S1E, F).

3.2. Transgenerational memory of RC behavior is linked to mitochondrial inheritance

We previously found that satellite cells isolated from mice exposed to 100 ppb arsenite in their drinking water and cultured in arsenite-free medium retained evidence of a protracted stress response [12]. The cells retained altered mitochondrial morphology, enhanced mitochondrial oxygen consumption, and increased ROS generation [12], reflecting a form of cellular memory [18]. To determine whether this stress memory was recapitulated in the RC^{primed} phenotype, we collected the $RC^{naïve}$ and RC^{primed} after the four-day differentiation protocol, and re-plated the cells in arsenite-free growth medium to mimic activation (Fig. 2A) [21]. The cells were allowed to undergo several generations of expansion over four days, and the resulting RC progenies were collected for analysis. To determine replicative age (number of generations), RC were labeled with CFSE at the time of replating. CFSE dye dilution decreases with each cell division [20], as quantified by fluorescent flow cytometric analysis. Unlike $RC^{naïve}$ progeny, analysis of CFSE univariate histograms of RC^{primed} progeny on the first (*i.e.* Day 0) and fourth (*i.e.* Day 3) days of culture revealed greater cycling and cell division (Fig. 2B–C). This enhanced cycling within the RC^{primed} progeny was corroborated by increased levels of Ki67, a cell cycle marker (Fig. 2D, Fig. S2A). Further characterization of RC^{primed} progeny showed excessive cyclin D1 (Fig. 2E, Fig. S2B) and caveolin-1 levels (Fig. 2F, Fig. S2C), indicating self-renewal [21,22] and replicative stress [23,24].

We next assessed the replicative age-classes of RC progeny subpopulations with Gaussian mixture models (ModFit LT, VSH) of replicative CFSE fluorescence dilution. The models are probabilistic models that assume all the data points are generated from a mixture of a finite number of Gaussian distributions with unknown parameters. These models can be thought of as generalizing k-means clustering to incorporate information about the covariance structure of the data as well as the centers of the latent Gaussians. The modeling confirmed a greater number of subpopulations with advanced replicative age (*i.e.* populations with -2^n dye content) within the RC^{primed} progeny, relative to control. These findings suggest accelerated replicative aging in RC^{primed} progeny relative to naïve counterparts (Fig. 2G).

To determine the biological significance of the mitochondrial physicochemical alterations within RC^{primed} progeny, we co-stained the isolated CFSE-labeled RC with an antibody to CD34 or the mitochondrial mass dye, Mitotracker (Fig. 2H, I). Flow cytometry linked the accelerated replicative aging RC^{primed} progeny subpopulations to their enhanced propensity for self-renewal and increased mitochondrial content (Fig. 2H, I). Taken together, these findings support the hypothesis that inherited mitochondria contain remnants of memory that transmit the stress response from ancestral RC.

3.3. "Mitoengrams" underlie the memory of stress

To interrogate whether inheritable mitochondrial remnants of transient stress memory serve as substrate of transmissible memory, we assessed whether reversion of the RC^{primed} mitochondrial phenotype to a naïve state impacts nuclear epigenetic regulation of gene transcription. To decrease stress promoted ROS generation, we added XJB to the RC when they were replated after the stress exposure. XJB catalyzes ROS turnover and concentrates more than 1000-fold in the mitochondria, and its primary effect in improving skeletal muscle health is through mitochondrial electron scavenging [8]. We found that adding XJB to the RC^{primed} progeny restored mitochondrial physicochemical properties and enhanced propensity for self-renewal to a naïve-like state (Fig. 3A–F, Fig. S3A–E). Of note, XJB administration to $RC^{naïve}$ progeny reduced membrane potential and mitochondrial mass to below control levels, but importantly also returned arsenite-promoted membrane potential and mass to these same low levels (Fig. 3A and C). Mitochondrial ROS generation in RC^{primed} progeny returned to control levels, but there was no effect of XJB in reducing ROS to below control levels in $RC^{naïve}$ (Fig. 3B). In addition, XJB returned arsenite-driven cell self-renewal to basal levels, but had no effect on self-renewal in $RC^{naïve}$ cells (Fig. 3E–F).

As proof-of-principle that a mitochondrial functional state underlies the cellular memory of stress in RC progeny, we investigated the epigenetic regulation of DNA methyltransferases, *Dnmt3a* and *Dnmt1* [25]. Treatment with XJB reverted RC^{primed} progeny transcript levels of *Dnmt3a* (Fig. 3G) and *Dnmt1* (Fig. S4A) to levels resembling $RC^{naïve}$ progeny. There was small effect of XJB on transcript expression in the control $RC^{naïve}$ cells (Fig. 3A and C), perhaps indicating that the effect of XJB on mitochondrial membrane potential or mass contributes influences mitochondrial-nuclear communication through pathways outside of those affected by arsenite.

The epigenetic regulation of methyltransferase expression caused by arsenite or XJB were confirmed by chromatin immunoprecipitation (ChIP) of RNA polymerase II (Pol II) with qPCR of the respective promoters (Fig. 3H, Fig. S4B). ChIP analysis with antibody to DNMT3a and methylation sequencing showed that loss of DNMT3a binding and decreased promoter methylation increased transactivation of *Dnmt3a* in RC^{primed} progeny (Fig. 3I–J). Restoration of mitochondrial integrity by XJB treatment effectively returned both DNMT3a binding to the *Dnmt3a* promoter and the *Dnmt3a* promoter methylation status to naïve-like levels (Fig. 3I–J). In contrast, binding of both DNMT3a and DNMT1 to the *Dnmt1* promoter was not sensitive to XJB (Fig. S4C–D). These results suggest that inherited mitochondrial alterations in RC^{primed} progeny are upstream of epigenetic memory of stress.

DNA methyltransferase transcriptional changes are coupled with chromatin remodeling and an imbalance of activating and repressive histone modifications [26]. The histone variant, H2A.Z, is an epigenetic regulator of adult muscle stem cell function [27], stress memory [28,29], and self-renewal [30]. ChIP analysis with antibodies to H2A.Z or acetylated H2A.Z (H2A.Zac) showed that increased transcription of *Dnmt3a* and *Dnmt1* in RC^{primed} progeny was associated with increased promoter-bound H2A.Zac (Fig. 3K–L; Fig. S4E). H2A.Zac is particularly enriched at bivalent promoters that bind facilitating histone 3 dimethylated on lysine 4 ($H3K4me^2$), or repressive histone 3 trimethylated on lysine 27 ($H3K27me^3$) [31]. The increased H2A.Zac binding to the RC^{primed} *Dnmt1* promoter was concomitant with increased binding of facilitating $H3K4me^2$ (Fig. S4F). XJB intervention in RC^{primed} progeny reverted the transcriptional status of *Dnmt3a* by reducing H2A.Zac binding to a naïve-like state (Fig. 3L). The major effect of XJB in restoring *Dnmt1* transcription appeared to be reduced binding of

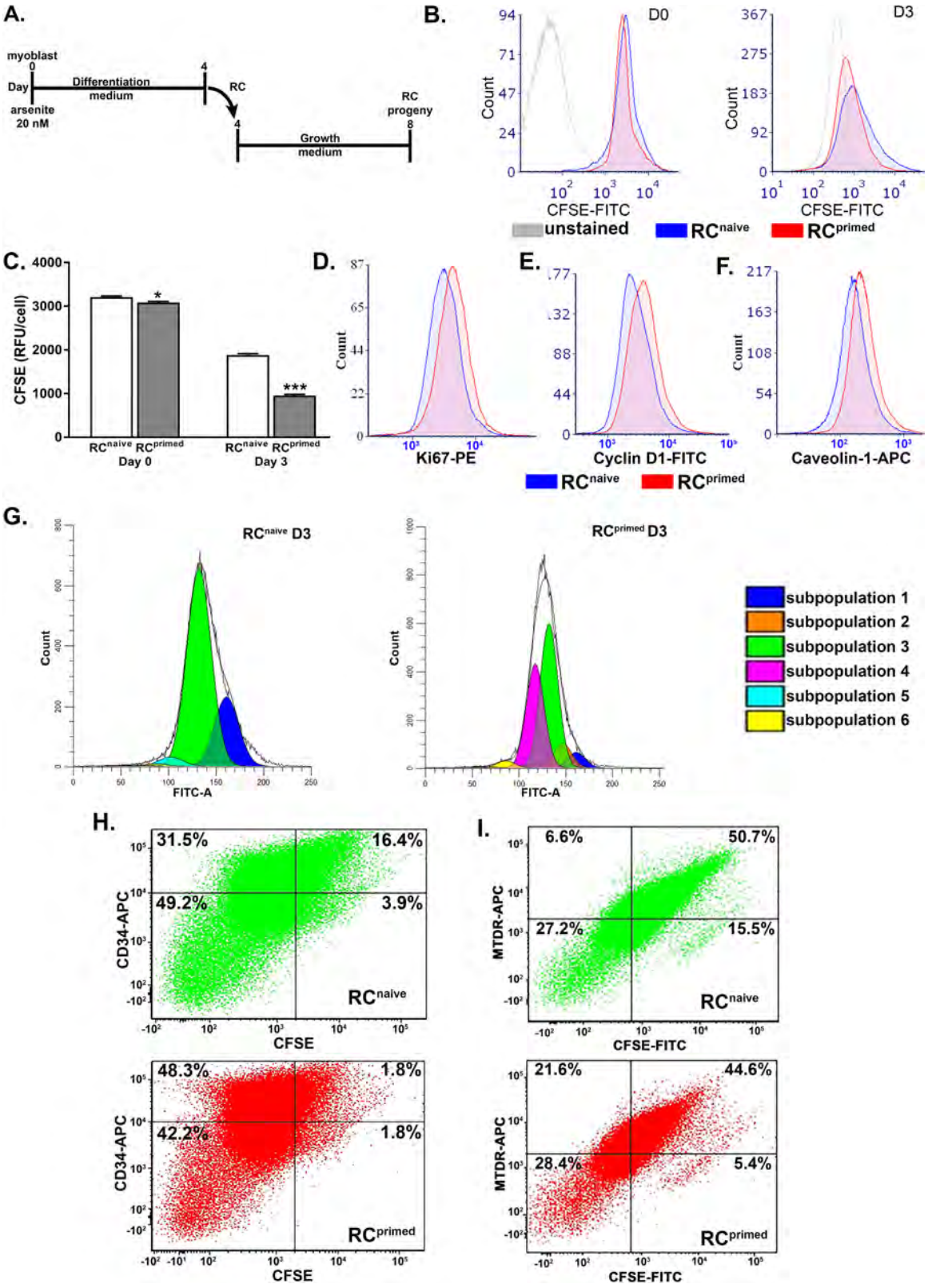

(caption on next page)

Fig. 2. Transgenerational transmission of altered mitochondria and RC behavior. (A) Schematic of the experimental design. **(B)** Flow cytometric tracking of RC progeny replicative history using CFSE fluorescence; representative histograms illustrated the dilution profile of CFSE-labeled RC and RC progeny between Day 0 and Day 3 of expansion in stressor-free growth media. **(C.)** Quantitative comparison of the data in **B** showing mean and SEM of CFSE fluorescence per cell (10,000 cells counted on D0 and 30,000 on D3). Statistical significance is designated by *($p < 0.05$) and ***($p < 0.001$) as determined by two-way ANOVA. **(D–F)** Increased RC^{primed} population cycling demonstrated by increased expression of Ki67 **(D)**, cyclin D1 **(E)**, and caveolin-1 **(F). (GF)** Analysis of CFSE dilution in replicating subpopulations by ModFit® software (Verity Software House, USA) showing CFSE dilution in RC generations after 3 days expansion in stressor-free growth media. The software drew approximative peaks within the CFSE-histogram centered on halving intensity values from the parental peak CFSE-intensity. The resolved RC generational ages range from non-dividing RC progeny subpopulations (blue) to RC populations with more advanced replicative age (pink, cyan and yellow). **(H–I)** Bivariate dot plot histograms indicated fast-replicatively aging RC^{primed} progeny subpopulations corresponding to subpopulations that **(H)** exhibited dysregulated self-renewal **(I)** and that harbor larger mitochondrial mass. Results are representative fluorescent intensity per cell of at least 10,000 cells counted, in each of three independent experiments (n = 3).

$H3K4m^2$, despite the lack of an effect on H2A.Zac promoter binding (Fig. S4E, F). These results suggest that the inherited mitochondrial state is coupled to regulation of *de novo* DNA methylation-dependent dynamic cellular memory [32,33]. Moreover, these findings suggest that cell population history is captured through enduring mitochondrial physicochemical alterations, or "mitoengrams", that define identity and behavior of the population progeny.

3.4. Storage of cellular memory involves a preferential pattern of mitochondrial connectivity and subcellular localization

Considering the parallel with brain synaptic networks topology as a locus of retrievable memory information storage or "engrams" [34], we tested the hypothesis that storage of cellular memory is associated with a specific architecture of mitochondrial connectivity. We identified the morphological branch points and endpoints of mitochondrial networks using a graph theory model of 2D images of mitochondria [35,36]. Graphical abstraction based on this model revealed heterogeneity in network topology ranging from small clusters of linear or branched tree-like segments to massive subnetworks with branching nodes, predominantly of degree 3 (*i.e.* three edges per node) (Fig. 4A, S5A–D, S6A–B). Intriguingly, we found that RC^{primed} networks had more branching points of degree 3 than $RC^{naïve}$ progeny, implying increased mitochondrial connectivity (Fig. 4B).

Mitochondrial perinuclear clustering influences transcriptional identity and behavior of stem cells [37,38]. Graph theory predicts that the emergence of cyclic patterns at and above a threshold edge to node ratio (E/N) of 1.0 is linked to the coalescence of small tree-like clusters into large connected networks [39,40]. Thus, the "hypercyclic" topological appearance of RC^{primed} progeny mitochondrial networks might be due to a higher E/N ratio. Indeed, E/N probability plots showed that the subnetworks in RC^{primed} progeny exhibited an E/N ratio above the theoretical threshold of 1.0 (Fig. 4C), indicating a stronger propensity for cyclicity. This also resulted in a higher frequency of perinuclear networks (*i.e.* full cycle around the nuclear localization) (Fig. 4A). However, XJB reinstated the RC^{primed} E/N to a naïve-like ratio, with reduced cyclicity and lower perinuclear clustering of mitochondrial networks (Fig. 4A–C).

Most naturally occurring biological networks, including physical and functional neuronal connections *in vivo* and *in vitro*, share intrinsic topological properties described as 'small-world' behavior [41–43]. Specifically, any two nodes in the network can be connected through a small number of intermediate edges (also termed 'short path length'), and when two nodes are connected to a third they also tend to be connected, or highly clustered, themselves. Computation of the average path length and average clustering coefficient using the graphical representations of mitochondrial networks revealed the existence of two topologically distinct mitochondrial networks subpopulations (Fig. S7A–C). $RC^{naïve}$ progeny contained networks having both dense and sparse topologies (Fig. S7B, C), whereas RC^{primed} progeny networks were predominantly sparse due to increased average path length (*i.e.* network "diameter") (Fig. S7A and C). Intervention with XJB, however, restored dense topology networks (Fig. S7A). We posit that regulation of mitochondrial connectivity and perinuclear clustering may afford mitochondrial control over the nucleus following a stress event.

3.5. "Mitoengrams" cells are a repository for memory in the cell population

In the brain, memory of an experience is captured by only a subpopulation of activated engrams-bearing neurons [44]. Likewise, mitochondrial networks topology may be intrinsically linked to total mitochondrial mass [45], and both mitochondrial mass and functionality may exhibit a cell size-dependent scaling behavior at the cell population level [46]. Scalability is one of the more important qualities of mitochondrial networks. As cells grow and/or differentiate, the mitochondrial networks that support their functions also need to remodel their size and architecture to maintain performance and support increased cellular energy demand. Thus, we tested the hypothesis that the cellular memory of stress is discriminately stored in a subpopulation of RC^{primed} progeny, and that the stored memory is scalable to mitoengrams. We considered mitochondrial volume (*i.e.* mass) and nuclear H2A.Z expression levels as proof-of-principle surrogate markers for mitoengrams and epigenetic memory, respectively. 3D imaging and volume rendering of mitochondrial networks revealed that, contrary to naïve counterparts, RC^{primed} progeny mitochondrial networks were more voluminous with extensive connectivity surrounding the nucleus (Figs. 5A–B; S8A–E). In keeping with its effects on mitochondrial potential, mass, and ROS production, XJB reverted the RC^{primed} mitochondrial networks to a naïve-like state (Fig. 5A–B). Concomitantly, H2A.Z protein quantification through 2D confocal imaging of RC nuclei was the highest in RC^{primed} progeny, consistent with the upregulation of H2A.Z in CD34+/CD133+ progenitor cells [47]. Intervention with XJB restored RC^{primed} nuclear H2A.Z levels to a naïve-like state (Fig. 5D–E, Fig. S9A).

At the population level, complementary cumulative density function (CCDF) models based on the empirical means and standard deviations of RC distributions showed that memory state changes of progeny resulted in a simple rescaling of the probability distribution of mitoengrams and epigenetic marks. These changes were driven by the subpopulation of RCs with high mitochondrial mass and H2A.Z expression levels, which map to the right tail of RC probability distributions (Fig. S9B–C). On the other hand, the probabilities of such RC behavior occurring with normal Gaussian distribution are extremely low and incompatible with experimental data. This implies that RC progeny populations are not normally distributed.

Indeed, empirical CCDFs of mitochondrial mass and H2A.Z expression revealed that the subpopulation of RC^{primed} progeny at the tail extreme of the distribution exhibited higher probabilities of forming voluminous networks and expressing elevated nuclear H2A.Z. These data suggest that RC^{primed} subpopulations follow heavy-tailed distributions, as opposed to thin-tailed distributions that would be modeled exponentially (Fig. 5C and F). This heavy or "fat" tail behavior means that there is a larger probability of having large values for mitochondrial mass and H2A.Z protein expression. However, these heavy tailed subpopulations disappeared with XJB intervention, which restored the distribution of mitochondrial mass and nuclear H2A.Z expression to that similar to naïve progeny (Fig. 5C and F). Goodness of fit tests suggested a power law model with exponential cut-off best fit the

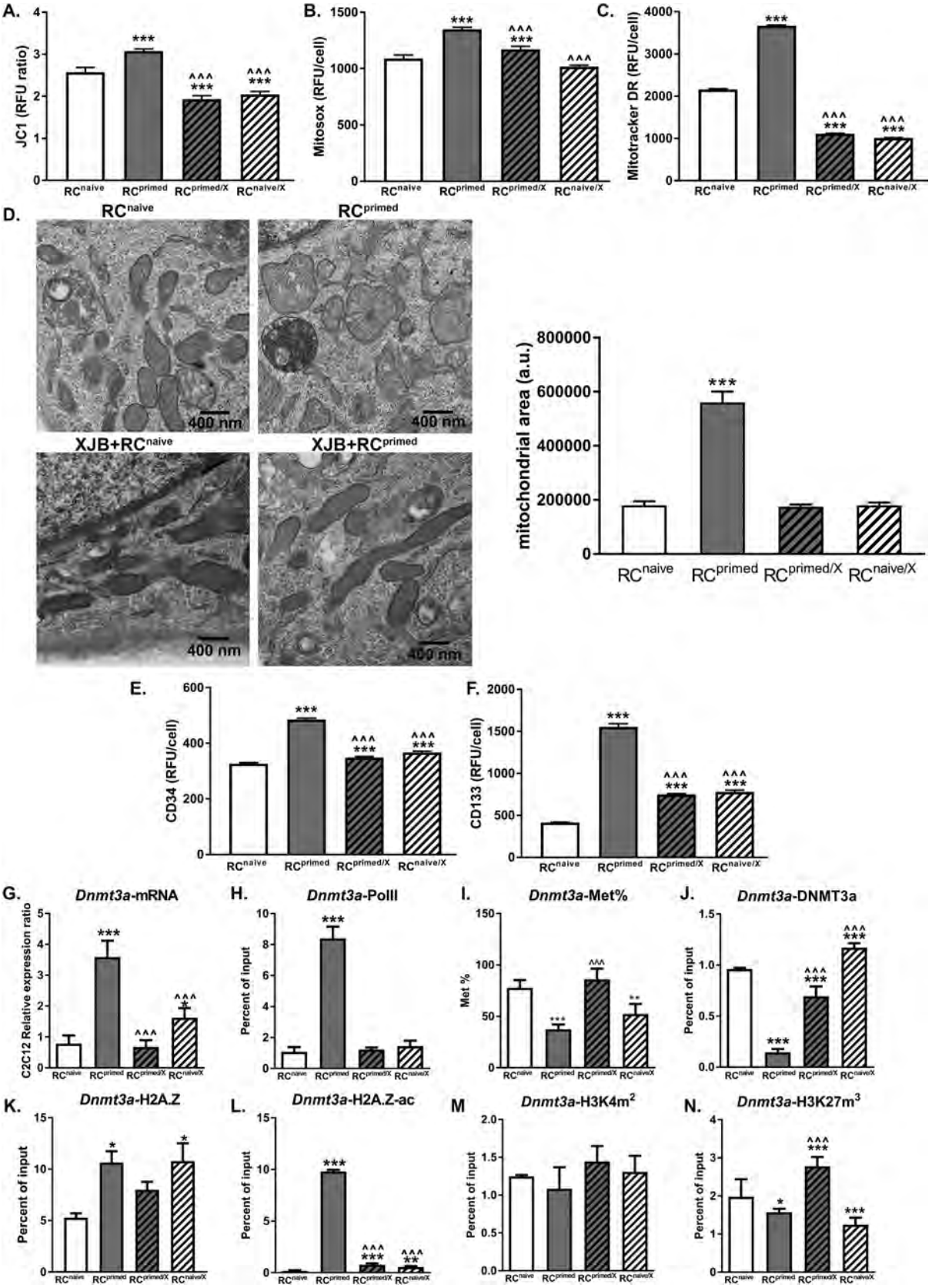

Fig. 3. Cellular memory is promoted by mitoengrams. (A–D) Addition of XJB (100 nM) decreased RC^{primed} progeny mitochondrial membrane potential **(A)** and superoxide generation **(B),** as mitochondrial abundance **(C)** and cristae ultrastructure **(D)** normalized and mitochondrial area (measured from TEM images) returned to non-stressed levels **(D). (E–F)** XJB reverted RC^{primed} progeny to naïve-like behavior indicated by normalized CD34 and CD133 levels. **(G–N)** RT-PCR and ChIP-qPCR analysis of DNA methyltransferase, Dnmt3a, and modified histones bound to the *Dnmt3a* promoter. ChIP protein targets are designated by non-italicized abbreviations in the graph titles. Data are presented as mean ± SEM, and results are representative of three independent experiments (n = 4 each). Differences from $RC^{naïve}$ progeny and RC^{primed} progeny are designated by * $p < 0.05$, ** $p < 0.01$, *** $p < 0.001$ and ^^^ $p < 0.001$, respectively, as determined using two-way ANOVA.

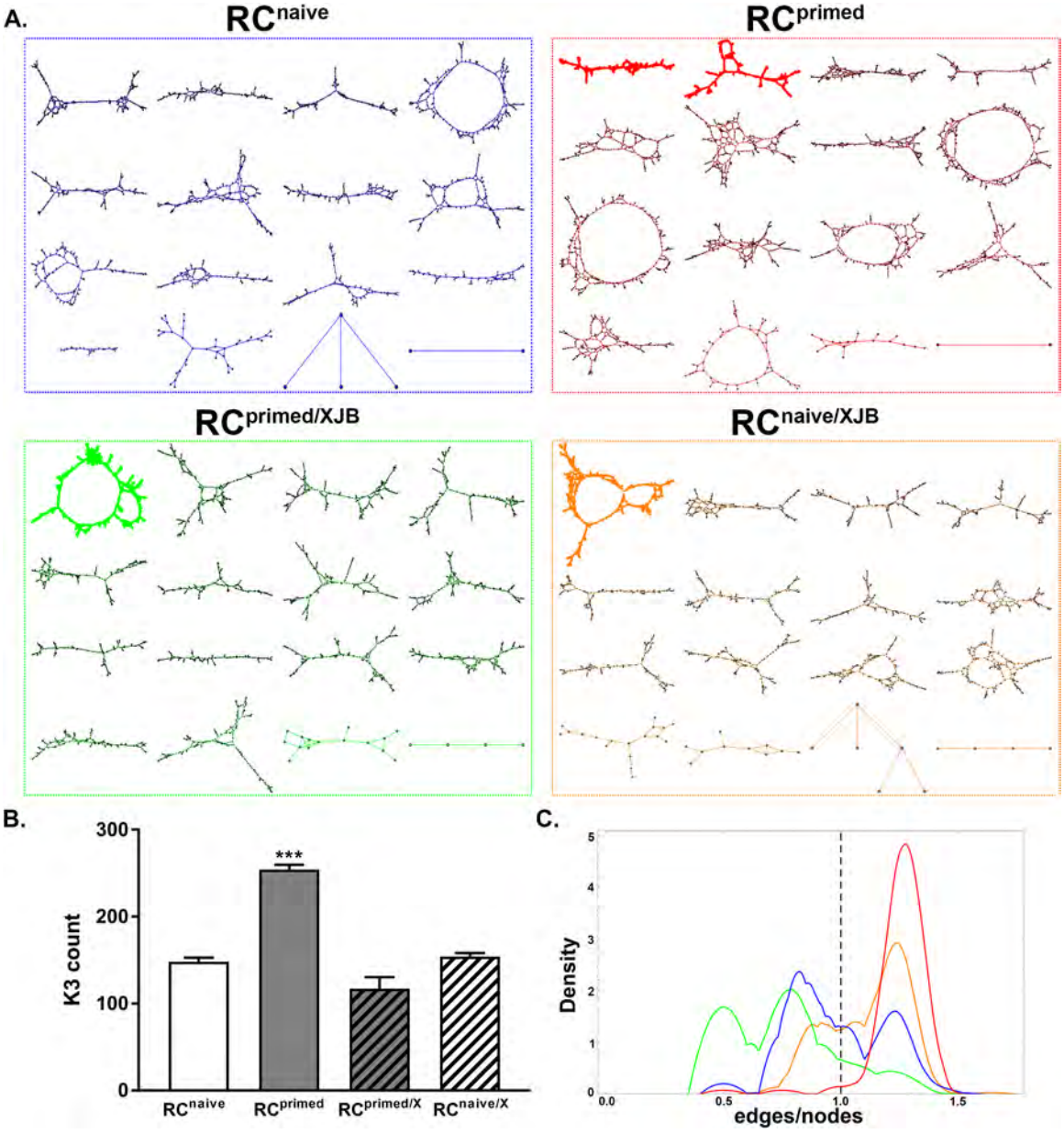

Fig. 4. Cyclicity and perinuclear clustering propensity of mitochondrial networks in RC progeny with memory of stress. (A) Graph theory modeling of 2D mitochondrial networks' topology with mitochondrial tubules defined by one or more network edge connected through nodes of degree k = 2. Isolated clusters were defined by the connectivity of a small number of mitochondrial tubules through nodes of degree k = 2 and 3 with or without cycles. Large subnetworks exhibited greater connectivity and cyclicity, including perinuclear full cycle around the nuclei. **(B–C)** Quantitative analysis of branching-points of degree k = 3 indicates increased connectivity in RC^{primed} progeny. Network density compared to edges to nodes ratio (E/N) indicated increased connectivity and a higher density of networks with E/N above the 1.0 theoretical threshold in RC^{primed} progeny. These connectivity and subcellular partitioning patterns were reverted to a naïve-like state following addition of XJB. Results are representative of pooled data of three independent experiments (n = 3) and are presented as means ± SEM. Differences from $RC^{naïve}$ are designated by ***p < 0.001 as determined by two-way ANOVA.

tail of RC progeny populations. This means that the probability of measuring a particular value of some mitochondrial or nuclear metric varies inversely as a power of that value. Comparison of the power law model to alternative heavy-tail distributions indicates that the power law model provided significantly better fits to the mitochondrial mass and H2A.Z in the tail RC^{primed} progeny subpopulations (Fig. S10, statistical appendix I and II).

Scalability is one of the most important qualities of mitochondrial networks. As cells grow and/or differentiate, the mitochondrial networks that support their functions also need to remodel their size and architecture to maintain their performance (responsiveness or throughput) and support increased cellular energy demand. As RC^{primed} progeny divide, mitochondrial mass and H2A.Z expression obeyed a scaling relationship that was extracted from the power law fittings. This was illustrated by the near-linear relationship between the experimental averages of mitochondrial mass and nuclear H2A.Z, as well as these experimental averages and their respective scaling factors (Tables 1–2, Fig. 6A–C). Most significantly, we found a linear relationship by scaling mitochondrial mass and H2A.Z (Fig. 6D).

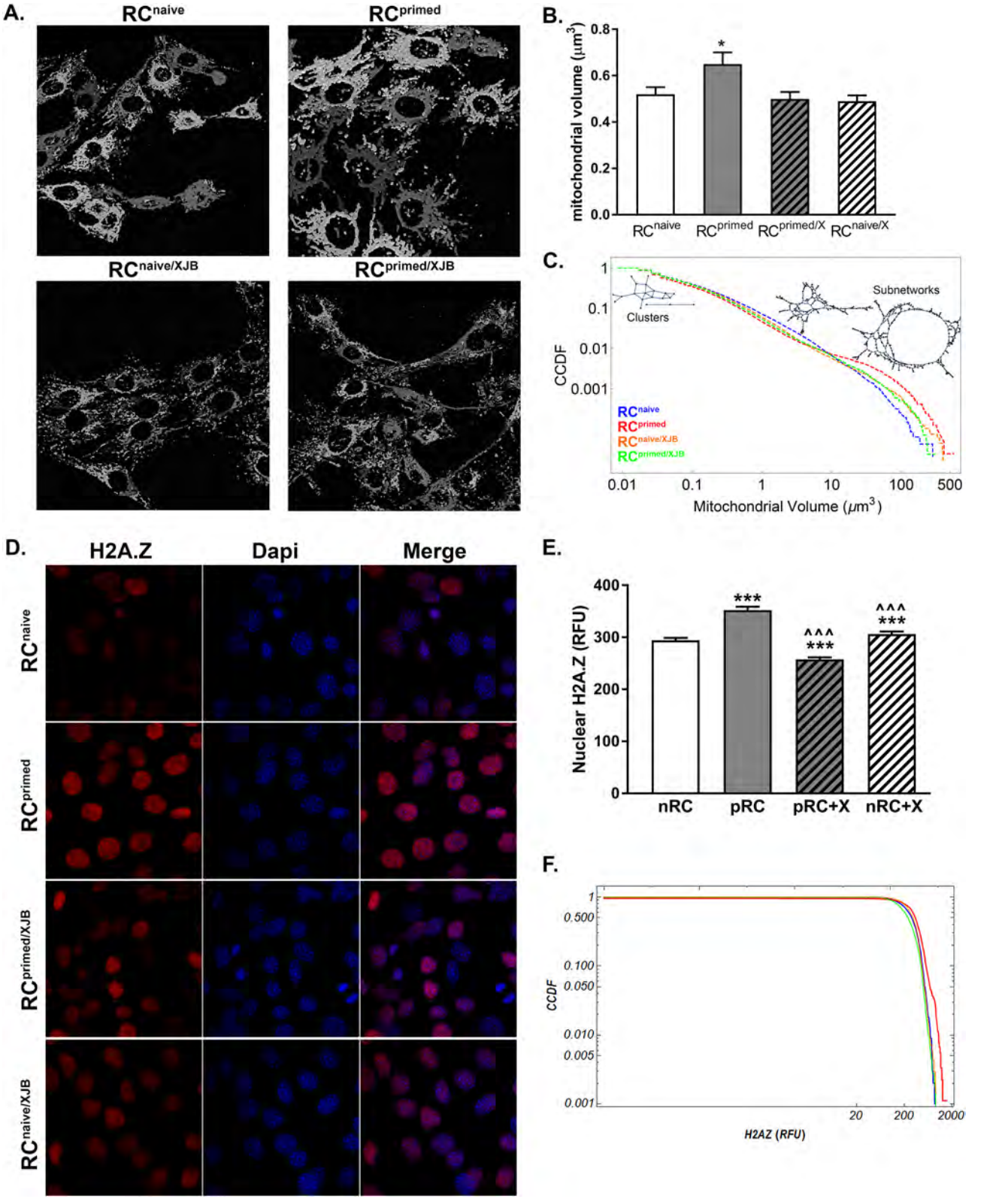

(caption on next page)

Fig. 5. Mitoengrams underlie cell population memory. (A–B) Representative 3D confocal microscopy images of RC Tom20-labeled mitochondria. 3D rendering of the deconvolved z-stacks shows the distribution of mitochondrial networks subpopulations and mitochondrial connectivity. **(B)** Mitochondrial volumes were quantified in the 3D images and compared. **(C)** Complementary cumulative density function (CCDF) modeling of empirical population-level mitochondrial volume measurements revealed their right heavy-tailed behavior. **(D–E)** Imaging and quantification of nuclear H2A.Z protein levels across the cell population indicated subpopulations of nuclei with enhanced H2A.Z in RC^{primed}. CCDF modeling of H2A.Z content confirmed the extreme nature of the subpopulation of the RC^{primed} that was reverted to a naïve-like state by XJB addition. Gaussian results are representative of three independent experiments (n = 3) and are presented as means ± SEM of mitochondrial volume. Difference designated by * < 0.05 with regard to $RC^{naïve}$, was determined using one-way ANOVA with Tukey's post hoc test. CCDF of mitochondrial volume was constructed from the total number of mitochondrial voxels by pooling imaging data of three independent experiments (n = 3): $RC^{naïve}$ progeny (n = 47,387 voxels), RC^{primed} progeny (n = 41,009 voxels), $RC^{naïve/XJB}$ progeny (n = 67,676 voxels) and $RC^{primed/XJB}$ progeny (n = 42,301 voxels). Likewise, CCDF of nuclear H2A.Z expression was constructed from the total number of nuclei by pooling imaging data from another independent set of three independent experiments (n = 3): $RC^{naïve}$ progeny (n = 996 nuclei), RC^{primed} progeny (n = 907 nuclei), $RC^{naïve/XJB}$ progeny (n = 688 nuclei) and $RC^{primed/XJB}$ progeny (n = 1091 nuclei). See also Figs. S9–10.

4. Discussion

It is increasingly evident that many identity-defining cellular decisions are contingent on mitochondria. Here, we report that mitochondria contribute to the upstream regulation of transient of storage environmental information in the cellular memory over many cell generations. We show that lasting memories of a remote cellular experience are discriminately encoded in a subset of a cell population progeny as enduring mitochondrial alterations, or mitoengrams. These mitoengrams map to programmatic histone modifications and DNA methylation that define genomic memory. We reveal that mitochondria provide mnemonic information that underlie the transmission, storage and retrieval of cellular memory across generations after removal of an environmental stress. This memory stored within subpopulations of progenitor cells likely contributes to the resilience of the total cell population and adaptation to environmental stressors.

The stress response to the low level of arsenite exposure likely represents an integrated whole cell response instead of a direct action of the metalloid within the mitochondria. Arsenicals are well-established mitochondrial toxicants that, in high concentrations, can compete with phosphate in ATP-generating phosphotransfer reactions, destroy electron gradients, and impair lipoic acid co-factors for dehydrogenase activities [48–50]. However, at lower, more environmentally relevant levels, arsenite impairs mitochondrial dehydrogenase activities indirectly through oxidant-dependent signal transduction [48]. At 20 nM, as was used in these studies, it is stoichiometrically improbable that arsenite would directly affect the mitochondria. Moreover, it likely requires extra-mitochondrial signaling, such as receptor-mediated oxidant generating cascades [51], to alter mitochondrial dynamics and function. In addition, we observed increase mitochondrial membrane potential, electron flux, and increased mitochondrial mass at this low-level exposure.

While identifying the specific mechanisms for arsenite-promoted mitochondrial adaptation and mitoengram formation is beyond the scope of the current work, the reversal of this adaptation and the mitoengrams held in mitochondrial dynamic and network change by XJB place the mitoengrams central to arsenite-induced epigenetic memory. It is possible that some extra-mitochondrial effects of XJB that block arsenite-signaling will contribute to restoration of the basal state of the progenitor cells. However, the fact that this nitroxide/gramicidin conjugate concentrates more than 1000-fold in skeletal muscle mitochondria [8] strongly supports the centrality of the mitochondrial in dictating the cellular memory of stress over multiple cell generations.

Mitochondria are dynamic organelles that undergo morphological changes through fission and fusion. Although the assumption is often made that stem cell self-renewal capacity is dependent on mitochondrial fission [52,53], genetic studies in the mouse brain links the regulation of cortical neural stem cell self-renewal to mitochondrial fusion [54]. This implies a more complex relationship between mitochondrial dynamics and stem cell identity than originally anticipated [55]. A major distinction of our study from earlier studies is that we used a cell population-based approach. This is important given that mitochondrial networks morphology and stem cells fates are notoriously heterogeneous within the same stem cell population [56]. Previous studies which have shown that mitochondrial age and the peripheral location of mitochondrial networks dictates inheritance of self-renewal determination did not consider the contribution of heterogeneity of the populations, as small cell numbers were considered [52,53]. Although, these studies often implemented a thymidine synchronization of self-renewing cells, which may have altered mitochondrial connectivity [53]. Clearly, more in depth studies are needed to understand the molecular mechanisms linking mitochondrial dynamics to retention of cellular memory.

In the current studies, we provide empirically-based mathematical evidence that, beyond absolute length of mitochondrial tubules, patterning of mitochondrial connectivity may serve as a functional regulatory factor. We quantified the connectivity patterns that promote perinuclear localizations of RC mitochondrial networks to control persistence or transience of cellular memory. Although much is known of the role of changes in mitochondrial content, potential, reactive oxygen species, and/or dynamics in defining the identity of different stem cell types, the global strategies by which these mitochondrial factors combine to systematically regulate stem cell population dynamics are largely unknown. Deciphering these strategies is critical to understanding functional decline of stem cells linked to many age-related conditions and diseases. Here, we identify small-world behavior of mitochondrial networks as a mechanism that enables power law scaling between mitochondrial-derived outputs and epigenetic marks regulating genomic memory. Biological networks are known to exhibit small-world architecture [57], characterized by small path lengths that can enable more efficient exchange of mass and/or information within a network [58]. In the context of metabolic networks, small-world properties were suggested to minimize transition times between metabolic states [59]. Significantly, it has been proposed that an increase in average path lengths of small-world networks, such as we observed in mitoengram-associated networks, may reflect a tradeoff between network efficiency and multi-functionality; robustness and/or evolvability [60].

Stem cells rapidly acclimate to transient local and systemic fluctuations. The memory of acclimation embodied in epigenetic adaptation enhances spatiotemporal plasticity to better adapt to recurring environmental stressors. However, a clear understanding of cellular memory transience and persistence in epigenetic regulation is still lacking. In the light of the scaling of mitoengrams and epigenetic marks, the emergence of such properties of multi-functionality and robustness in mitoengram cells is consistent with the preferential H2A.Z binding to active and bivalent promoters, notably during self-renewal and myogenic differentiation [61,62]. H2A.Z is a highly specific biomarker for discriminating cells undergoing asymmetric (low levels of H2A.Z expression) *versus* symmetric (high levels of H2A.Z expression) division, including in human skeletal muscle satellite stem cells [63]. Furthermore, H2A.Z expression levels increase with age at genes involved in transcriptional regulation [64]. We propose a model whereby mitoengrams serve as a physiological substrate for control of stem cell division symmetry and ensuing discriminative storage of transgenerational cellular memories through an H2A.Z-mediated retrograde mito-nuclear mechanism. The scalable relationship between mitoengrams and

Table I. Statistics for Mitochondrial Volume (mass)

mitochondrial volume distribution	Naïve Progeny	Primed Progeny	XJB/Primed Progeny	XJB/Naïve Progeny
mean	0.499	0.644	0.504	0.49
Standard Deviation	3.624	7.798	5.294	4.662
variance	13.135	60.812	28.029	21.74
skewness	35.583	32.094	40.859	31.456
kurtosis	2008.24	1446.22	2310.26	1313.6
median	0.06	0.0519	0.06	0.06
interquantile range	0.181	0.138	0.173	0.164
min	0.017	0.008	0.017	0.008
Max	282.202	563.219	397.717	303.402

Table II. Statistics for Nuclear H2A.Z Protein Levels

Nuclear H2A.Z distribution	Naïve Progeny	Primed Progeny	XJB/Primed Progeny	XJB/Naïve Progeny
mean	294.329	350.494	257.523	306.077
Standard Deviation	140.461	200.628	133.781	129.558
variance	19729.3	40251.8	17897.4	16785.4
skewness	0.622532	1.12597	0.883461	0.702524
kurtosis	3.45132	6.26006	4.06078	4.45465
median	282.588	336.302	236.702	303.773
interquantile range	202.594	219.792	187.953	171.786
min	17.0863	0	0.	25.7569
Max	876.604	1542.44	891.725	932.31

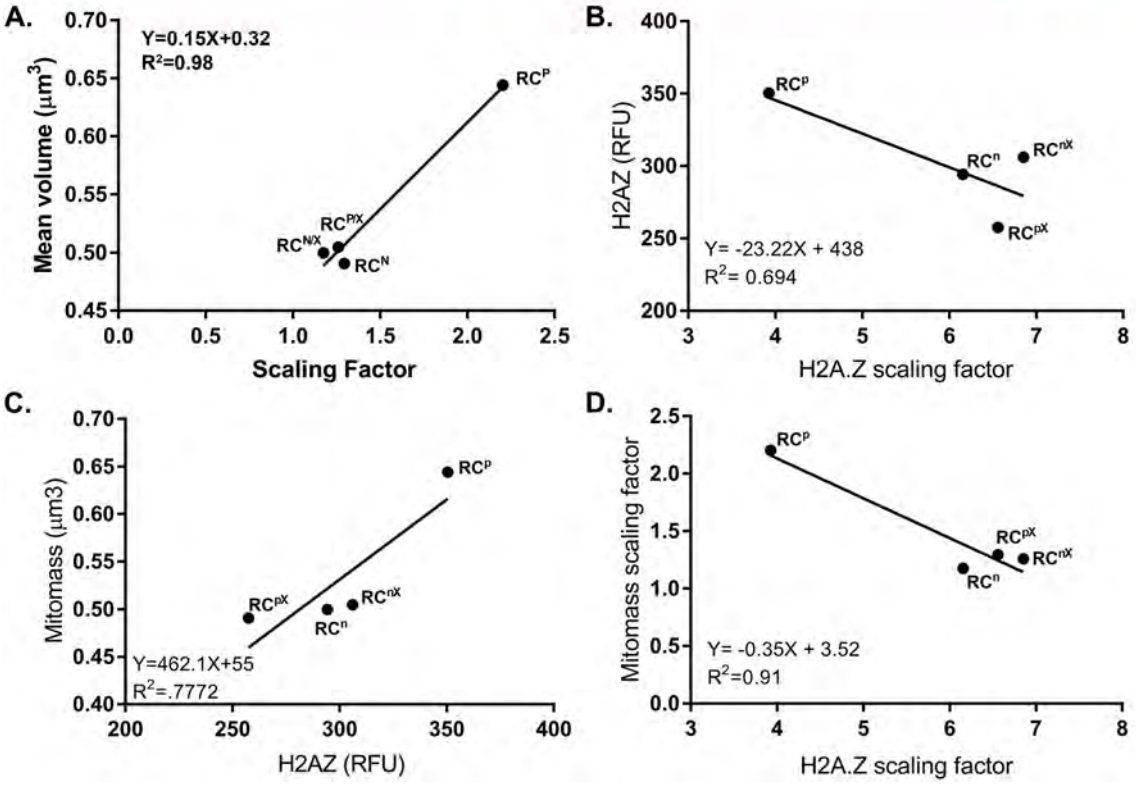

Fig. 6. Cellular memory scalability to mitochondria at the population level. (Tables I and II) Descriptive statistics of overall cell population mitochondrial volume (i.e mass) and nuclear H2A.Z protein expression as surrogate markers for mitoengrams and epigenetic memory respectively. **(A–D)** Persistence or transience of cellular memory involves scaling of **(A–C)** mitochondrial mass and nuclear H2A.Z distributions. **(D)** Power law nature of cellular memory scalability to mitochondrial mass. Mitochondrial targeting by XJB restored the RC^{primed} progeny population mitochondrial content and H2A.Z expression by a simple rescaling of probability distributions and associated statistics **(Tables I and II).**

cellular memory is consistent with a power-law model of behavior in self-renewing cells and a cell autonomous mechanism of epigenetic memory [65,66]. The power law or "scaling law" is a statistical equation in the form: $a = kb^{\alpha}$, where k is a proportionality constant and α is the power or scaling factor.

More broadly, the decryption of stem cell state-specific mitoengrams is essential not only to understanding stem cell fate, but also to ascertain whether compromised allocation of cellular memories heralds the degeneration of stem cell function and constitutes the mechanistic basis of the multiple long-term trajectories of disease and aging. Indeed, these memories may be maladaptive, hindering the maintenance of a reliable stem cell pool and affecting the regenerative capacity of a given organ. In some circumstances, it may be advantageous for the stem cell to "learn to forget". Accordingly, the integrity of the stem cell functionality entails a balancing act between transience and persistence of cellular memories. Optimization of mitochondria-targeted nitroxide/gramicidin conjugates, such as XJB or alternative chemistry-based approaches to target mitochondria, could lead to a new generation of

effective mitochondrial-targeted therapeutics that promote stem cell resilience over time.

Acknowledgements

We thank Dr. Donna Stolz and Mara Sullivan at the Center for Biological Imaging for assistance with imaging and. This work was supported by the NIH NIA National Institute on Aging, USA grant AG052978-01 (FA), the Pittsburgh Claude D. Pepper Older Americans Independence Center, USA P30 AG024827 (AC), and NIEHS National Institute of Environmental Health Sciences, USA grants R01ES023696 and R01ES025529 (FA and AB). Finally, we acknowledge the NIH National Institutes of Health supported microscopy resources in the Center for Biologic Imaging (Grant #1S10OD019973-01).

Appendix A. Supplementary material

Supplementary data associated with this article can be found in the online version at doi:10.1016/j.freeradbiomed.2018.11.028.

References

[1] F. Chen, Y. Liu, N.K. Wong, J. Xiao, K.F. So, Oxidative stress in stem cell aging, Cell Transplant. 26 (2017) 1483–1495.
[2] D.R. Burrill, P.A. Silver, Synthetic circuit identifies subpopulations with sustained memory of DNA damage, Genes Dev. 25 (2011) 434–439.
[3] D.R. Burrill, M.C. Inniss, P.M. Boyle, P.A. Silver, Synthetic memory circuits for tracking human cell fate, Genes Dev. 26 (2012) 1486–1497.
[4] M.C. Inniss, P.A. Silver, Building synthetic memory, Curr. Biol. 23 (2013) R812–R816.
[5] D.R. Burrill, P.A. Silver, Recording cellular experiences of DNA damage, Cell Cycle 10 (2011) 2410–2411.
[6] S.A. Josselyn, S. Kohler, P.W. Frankland, Finding the engram, Nat. Rev. Neurosci. 16 (2015) 521–534.
[7] N. Yoshida, S. Yoshida, K. Koishi, K. Masuda, Y. Nabeshima, Cell heterogeneity upon myogenic differentiation: down-regulation of MyoD and Myf-5 generates 'reserve cells', J. Cell Sci. 111 (Pt 6) (1998) 769–779.
[8] S. Javadov, S. Jang, N. Rodriguez-Reyes, A.E. Rodriguez-Zayas, J. Soto Hernandez, T. Krainz, P. Wipf, W. Frontera, Mitochondria-targeted antioxidant preserves contractile properties and mitochondrial function of skeletal muscle in aged rats, Oncotarget 6 (2015) 39469–39481.
[9] A.B. Bondi, Characteristics of scalability and their impact on performance, in: Proceedings of the Second International Workshop on Software and Performance, Ottawa, Ontario, Canada, 2000, pp. 195–2013.
[10] L.M. Del Razo, M. Styblo, W.R. Cullen, D.J. Thomas, Determination of trivalent methylated arsenicals in biological matrices, Toxicol. Appl. Pharmacol. 174 (2001) 282–293.
[11] E. Dopp, U. von Recklinghausen, R. Diaz-Bone, A.V. Hirner, A.W. Rettenmeier, Cellular uptake, subcellular distribution and toxicity of arsenic compounds in methylating and non-methylating cells, Environ. Res. 110 (2010) 435–442.
[12] F. Ambrosio, E. Brown, D. Stolz, R. Ferrari, B. Goodpaster, B. Deasy, G. Distefano, A. Roperti, A. Cheikhi, Y. Garciafigueroa, A. Barchowsky, Arsenic induces sustained impairment of skeletal muscle and muscle progenitor cell ultrastructure and bioenergetics, Free Radic. Biol. Med. 74 (2014) 64–73.
[13] A. Barchowsky, E.J. Dudek, M.D. Treadwell, K.E. Wetterhahn, Arsenic induces oxidant stress and NF-kappa B activation in cultured aortic endothelial cells, Free Radic. Biol. Med. 21 (1996) 783–790.
[14] N. Ieronimakis, G. Balasundaram, S. Rainey, K. Srirangam, Z. Yablonka-Reuveni, M. Reyes, Absence of CD34 on murine skeletal muscle satellite cells marks a reversible state of activation during acute injury, PLoS One 5 (2010) e10920.
[15] J. Meng, S. Chun, R. Asfahani, H. Lochmuller, F. Muntoni, J. Morgan, Human skeletal muscle-derived CD133(+) cells form functional satellite cells after intramuscular transplantation in immunodeficient host mice, Mol. Ther. 22 (2014) 1008–1017.
[16] D. Romero-Moya, C. Bueno, R. Montes, O. Navarro-Montero, F.J. Iborra, L.C. Lopez, M. Martin, P. Menendez, Cord blood-derived CD34+ hematopoietic cells with low mitochondrial mass are enriched in hematopoietic repopulating stem cell function, Haematologica 98 (2013) 1022–1029.
[17] I.S. Song, Y.J. Jeong, S.H. Jeong, H.J. Heo, H.K. Kim, K.B. Bae, Y.H. Park, S.U. Kim, J.M. Kim, N. Kim, K.S. Ko, B.D. Rhee, J. Han, FOXM1-induced PRX3 regulates stemness and survival of colon cancer cells via maintenance of mitochondrial function (1006–1016 e1009), Gastroenterology 149 (2015).
[18] D.R. Burrill, P.A. Silver, Making cellular memories, Cell 140 (2010) 13–18.
[19] Y. Nagata, K. Ohashi, E. Wada, Y. Yuasa, M. Shiozuka, Y. Nonomura, R. Matsuda, Sphingosine-1-phosphate mediates epidermal growth factor-induced muscle satellite cell activation, Exp. Cell Res. 326 (2014) 112–124.
[20] T. Sathiyaseelan, C.L. Baldwin, Evaluation of cell replication by bovine T cells in polyclonally activated cultures using carboxyfluorescein succinimidyl ester (CFSE) loading and flow cytometric analysis, Res. Vet. Sci. 69 (2000) 275–281.
[21] N. Baker, R.S. Tuan, The less-often-traveled surface of stem cells: caveolin-1 and caveolae in stem cells, tissue repair and regeneration, Stem Cell Res. Ther. 4 (2013) 90.
[22] S. Jash, G. Dhar, U. Ghosh, S. Adhya, Role of the mTORC1 complex in satellite cell activation by RNA-induced mitochondrial restoration: dual control of cyclin D1 through microRNAs, Mol. Cell. Biol. 34 (2014) 3594–3606.
[23] T. Shimura, Y. Ochiai, N. Noma, T. Oikawa, Y. Sano, M. Fukumoto, Cyclin D1 overexpression perturbs DNA replication and induces replication-associated DNA double-strand breaks in acquired radioresistant cells, Cell Cycle 12 (2013) 773–782.
[24] D. Volonte, H. Zou, J.N. Bartholomew, Z. Liu, P.A. Morel, F. Galbiati, Oxidative stress-induced inhibition of Sirt1 by caveolin-1 promotes p53-dependent premature senescence and stimulates the secretion of interleukin 6 (IL-6), J. Biol. Chem. 290 (2015) 4202–4214.
[25] T. Vaissiere, C.A. Miller, DNA methylation: dynamic and stable regulation of memory, Biomol. Concepts 2 (2011) 459–467.
[26] W.A. Burgers, F. Fuks, T. Kouzarides, DNA methyltransferases get connected to chromatin, Trends Genet.: TIG 18 (2002) 275–277.
[27] J. Segales, E. Perdiguero, P. Munoz-Canoves, Epigenetic control of adult skeletal muscle stem cell functions, FEBS J. 282 (2015) 1571–1588.
[28] Z. Avramova, Transcriptional 'memory' of a stress: transient chromatin and memory (epigenetic) marks at stress-response genes, Plant J. 83 (2015) 149–159.
[29] I.B. Zovkic, B.J. Walters, H2A.Z helps genes remember their history so we can remember ours, Bioessays 37 (2015) 596–601.
[30] R. Pandey, Y. Dou, H2A.Z sets the stage in ESCs, Cell Stem Cell 12 (2013) 143–144.
[31] T. Kouzarides, Chromatin modifications and their function, Cell 128 (2007) 693–705.
[32] Z. Gong, Q. Zhou, Dnmt3a in the dorsal dentate gyrus is a key regulator of fear renewal, Sci. Rep. 8 (2018) 5093.
[33] M.J. Morris, M. Adachi, E.S. Na, L.M. Monteggia, Selective role for DNMT3a in learning and memory, Neurobiol. Learn. Mem. 115 (2014) 30–37.
[34] D.S. Roy, S. Muralidhar, L.M. Smith, S. Tonegawa, Silent memory engrams as the basis for retrograde amnesia, Proc. Natl. Acad. Sci. USA 114 (2017) E9972–E9979.
[35] V.M. Sukhorukov, D. Dikov, A.S. Reichert, M. Meyer-Hermann, Emergence of the mitochondrial reticulum from fission and fusion dynamics, PLoS Comput. Biol. 8 (2012) e1002745.
[36] N. Zamponi, E. Zamponi, S.A. Cannas, O.V. Billoni, P.R. Helguera, D.R. Chialvo, Mitochondrial network complexity emerges from fission/fusion dynamics, Sci. Rep. 8 (2018) 363.
[37] A.B. Al-Mehdi, V.M. Pastukh, B.M. Swiger, D.J. Reed, M.R. Patel, G.C. Bardwell, V.V. Pastukh, M.F. Alexeyev, M.N. Gillespie, Perinuclear mitochondrial clustering creates an oxidant-rich nuclear domain required for hypoxia-induced transcription, Sci. Signal. 5 (2012) ra47.
[38] T. Lonergan, C. Brenner, B. Bavister, Differentiation-related changes in mitochondrial properties as indicators of stem cell competence, J. Cell Physiol. 208 (2006) 149–153.
[39] S.A. Kauffman, The origins of order: self-organization and selection in evolution, Spin Glass. Biol. (1992) 61–100.
[40] M.E. Newman, D.J. Watts, S.H. Strogatz, Random graph models of social networks, Proc. Natl. Acad. Sci. USA 99 (Suppl.1) (2002) S2566–S2572.
[41] D. Poli, V.P. Pastore, P. Massobrio, Functional connectivity in in vitro neuronal assemblies, Front. Neural Circuits 9 (2015) 57.
[42] O. Sporns, D.R. Chialvo, M. Kaiser, C.C. Hilgetag, Organization, development and function of complex brain networks, Trends Cogn. Sci. 8 (2004) 418–425.
[43] S. Yu, D. Huang, W. Singer, D. Nikolic, A small world of neuronal synchrony, Cereb. Cortex 18 (2008) 2891–2901.
[44] T.F. Liu, V. Vachharajani, P. Millet, M.S. Bharadwaj, A.J. Molina, C.E. McCall, Sequential actions of SIRT1-RelB-SIRT3 coordinate nuclear-mitochondrial communication during immunometabolic adaptation to acute inflammation and sepsis, J. Biol. Chem. 290 (2014) 396–408.
[45] G. Dalmasso, P.A. Marin Zapata, N.R. Brady, A. Hamacher-Brady, Agent-based modeling of mitochondria links sub-cellular dynamics to cellular homeostasis and heterogeneity, PLoS One 12 (2017) e0168198.
[46] T.P. Miettinen, M. Bjorklund, Mitochondrial function and cell size: an allometric relationship, Trends Cell Biol. 27 (2017) 393–402.
[47] B.J. Abraham, K. Cui, Q. Tang, K. Zhao, Dynamic regulation of epigenomic landscapes during hematopoiesis, BMC Genom. 14 (2013) 193.
[48] T. Samikkannu, C.H. Chen, L.H. Yih, A.S. Wang, S.Y. Lin, T.C. Chen, K.Y. Jan, Reactive oxygen species are involved in arsenic trioxide inhibition of pyruvate dehydrogenase activity, Chem. Res. Toxicol. 16 (2003) 409–414.
[49] K.A. Rein, B. Borrebaek, J. Bremer, Arsenite inhibits beta-oxidation in isolated rat liver mitochondria, Biochim. Biophys. Acta 574 (1979) 487–494.
[50] C. Bhuvaneswaran, C.H. Ho, C.L. Wadkins, Inactivation of coupled respiration of mitochondria by inorganic arsenate and partial restoration by ATP, Biochem. Biophys. Res. Commun. 49 (1972) 690–697.
[51] A.C. Straub, L.R. Klei, D.B. Stolz, A. Barchowsky, Arsenic requires sphingosine-1-phosphate type 1 receptors to induce angiogenic genes and endothelial cell remodeling, Am. J. Pathol. 174 (2009) 1949–1958.
[52] K. Ito, R. Turcotte, J. Cui, S.E. Zimmerman, S. Pinho, T. Mizoguchi, F. Arai, J.M. Runnels, C. Alt, J. Teruya-Feldstein, J.C. Mar, R. Singh, T. Suda, C.P. Lin, P.S. Frenette, K. Ito, Self-renewal of a purified Tie2+ hematopoietic stem cell population relies on mitochondrial clearance, Science 354 (2016) 1156–1160.
[53] P. Katajisto, J. Dohla, C.L. Chaffer, N. Pentinmikko, N. Marjanovic, S. Iqbal, R. Zoncu, W. Chen, R.A. Weinberg, D.M. Sabatini, Stem cells. Asymmetric apportioning of aged mitochondria between daughter cells is required for stemness, Science 348 (2015) 340–343.
[54] M. Khacho, A. Clark, D.S. Svoboda, J. Azzi, J.G. MacLaurin, C. Meghaizel, H. Sesaki,

D.C. Lagace, M. Germain, M.E. Harper, D.S. Park, R.S. Slack, Mitochondrial dynamics impacts stem cell identity and fate decisions by regulating a nuclear transcriptional program, Cell Stem Cell 19 (2016) 232–247.
[55] H. Chen, D.C. Chan, Mitochondrial dynamics in regulating the unique phenotypes of cancer and stem cells, Cell Metab. 26 (2017) 39–48.
[56] D.C. Woods, Mitochondrial heterogeneity: evaluating mitochondrial subpopulation dynamics in stem cells, Stem Cells Int. 2017 (2017) 7068567.
[57] D.J. Watts, S.H. Strogatz, Collective dynamics of 'small-world' networks, Nature 393 (1998) 440–442.
[58] V. Latora, M. Marchiori, Efficient behavior of small-world networks, Phys. Rev. Let. 87 (2001) 198701.
[59] A. Wagner, D.A. Fell, The small world inside large metabolic networks, Proc. Biol. Sci. 268 (2001) 1803–1810.
[60] Z. Zhang, J. Zhang, A big world inside small-world networks, PLoS One 4 (2009) e5686.
[61] G. Hu, K. Cui, D. Northrup, C. Liu, C. Wang, Q. Tang, K. Ge, D. Levens, C. Crane-Robinson, K. Zhao, H2A.Z facilitates access of active and repressive complexes to chromatin in embryonic stem cell self-renewal and differentiation, Cell Stem Cell 12 (2013) 180–192.
[62] C. Law, P. Cheung, Expression of non-acetylatable H2A.Z in myoblast cells blocks myoblast differentiation through disruption of MyoD expression, J. Biol. Chem. 290 (2015) 13234–13249.
[63] Y.H. Huh, M. Noh, F.R. Burden, J.C. Chen, D.A. Winkler, J.L. Sherley, Sparse feature selection identifies H2A.Z as a novel, pattern-specific biomarker for asymmetrically self-renewing distributed stem cells, Stem Cell Res. 14 (2015) 144–154.
[64] G. Stefanelli, A.B. Azam, B.J. Walters, M.A. Brimble, C.P. Gettens, P. Bouchard-Cannon, H.M. Cheng, A.M. Davidoff, K. Narkaj, J.J. Day, A.J. Kennedy, I.B. Zovkic, Learning and age-related changes in genome-wide H2A.Z binding in the mouse hippocampus, Cell Rep. 22 (2018) 1124–1131.
[65] M. Sugimori, Y. Hayakawa, B.M. Boman, J.Z. Fields, M. Awaji, H. Kozano, R. Tamura, S. Yamamoto, T. Ogata, M. Yamada, S. Endo, M. Kurimoto, S. Kuroda, Discovery of power-law growth in the self-renewal of heterogeneous glioma stem cell populations, PLoS One 10 (2015) e0135760.
[66] V.W.C. Yu, R.Z. Yusuf, T. Oki, J. Wu, B. Saez, X. Wang, C. Cook, N. Baryawno, M.J. Ziller, E. Lee, H. Gu, A. Meissner, C.P. Lin, P.V. Kharchenko, D.T. Scadden, Epigenetic memory underlies cell-autonomous heterogeneous behavior of hematopoietic stem cells (1310–1322 e1317), Cell 167 (2016).

SUPPLEMENTAL INFORMATION

SUPPLEMENTARY FIGURE LEGENDS

Figure S1. Reserve cells stress response

(A) JC-1 microplate assay for mitochondrial membrane potential: Fluorescence of JC-1 emitted at 535+/-10 nm (green fluorescence) and 595+/-10 nm (red fluorescence) with 488 nm excitation is monitored at 5 min intervals over 180 minutes at 37°C to produce stable kinetic traces. **(B-C)** Representative histograms of FACS analysis and corresponding descriptive statistics depicting the increase in **(B)** mitochondrial superoxide (MitoSox fluorescence) and **(C)** mass (Mitotracker Deep Red fluorescence) in RC^{primed} as compared to their naïve counterparts. The histograms shift to the right (higher fluorescence intensity) is reflective of an increase of the overall central tendency (i.e. mean and median) and variability (i.e. standard deviation, variance, range, IQ range) in the RC^{primed} population due to the emergence of a subset of RC with elevated superoxide production and mitochondrial mass. **(D)** Assessment of RC redox state: Glutathione (GSH), total protein thiols (TPT), and low-molecular-weight thiols (LMWT) contents are increased in RC^{primed} relative to their $RC^{naïve}$ counterparts, indicating an antioxidant stress-response. Concentrations of GSH, TPT and LMWT were normalized to total protein concentration measured using Bradford protein assay (Bio-Rad). **(E-F)** Representative histograms of FACS analysis (10^4-2.10^4 cells) and corresponding descriptive statistics portraying the dysregulation of self-renewal capacity as reflected by the excessive expression of surface markers **(E)** CD34 and **(F)** CD133. Results are representative of three independent experiments (n=3) and are presented as mean ± SEM of microplate or single cell fluorescence intensity. Differences from $RC^{naïve}$ are designated by ***$p<0.001$ as determined by Student's t-test.

Figure S2. Altered divisional history of RC^{primed} progeny. **(A-D)** Flow cytometric analysis indicated an abnormal increase in the cycling propensity of RC^{primed} relative to their naïve counterparts as demonstrated by **(A)** quantifying CFSE dye dilution profiles and quantifying cell proliferation using **(B)** Ki67 and cell progression and self-regulators and self-renewal regulators **(C)** Cyclin D1 and **(D)** Caveolin-1. Results are representative of three independent experiments (n=3) and are presented as mean ± SEM of single cell fluorescence intensity. Differences from $RC^{naïve}$ are designated by *$p<0.05$ and ***$p < 0.0001$, as determined by Student's t-test.

Figure S3: Mitochondrial targeting restores RC progeny behavior. (A) Change of mitochondrial membrane potential overtime was measured as the ratio between fluorescent intensities for both J-aggregates and monomeric forms. Increasing ratios indicate increased mitochondrial membrane potential. **(B-C)** Representative histograms of FACS analysis and corresponding descriptive statistics depicting the restoration by XJB tratment of **(B)** mitochondrial superoxide generation and **(C)** mass in RC^{primed} to RC^{naive} levels.**(D-E)** Representative histograms of FACS analysis and corresponding descriptive statistics portray the reversal by XJB of the self-renewal behavior in RC^{primed} to naïve-like state as shown by the expression of **(D)** CD34 and **(E)** CD133 progeny. Results are representative of three independent experiments (n=3).

Figure S4 Epigenetic effects of mitoengrams. (A.) RT-PCR measure of DNA methyltransferase, *Dnmt1*, expression in RC^{primed} and RC^{naive} cells plated in the absence of XJB (100 nM). (B-G) ChIP-qPCR analysis of *Dnmt1* promoter binding of polymerase II (Pol II), DNA methyltransferasesm and modified histones. ChIP protein targets are designated by non-italicized abbreviations in the graph titles. Data are presented as mean ± SEM, and results are representative of three independent experiments (n=4 each). Differences from $RC^{naïve}$ progeny are designated by * $p < 0.05$, ** $p < 0.01$, *** $p < 0.001$. Difference from RC^{primed} progeny is designated by ^^^ $p < 0.001$. All differences were determined using one-way ANOVA with Tukey's post hoc test.

Figure 5. Extracting 2D mitochondrial networks architecture and properties from confocal z-stacks. (A) Extracting a 2D network architecture of a toy image using Wolfram / Mathematica routine functions. **(Left)** Images are binarized into grayscale images in which all values above an automatically determined global threshold (that partitions the intensity values in image into two intervals by means of cluster variance maximization-Otsu's algorithm-) are replaced with 1 and others with 0. **(Middle)** the skeletonization of the binarized image object effectively gives the medial axis of its foreground multiplied with the distance transform, whereby the value of each nonzero pixel is the absolute Euclidean distance in pixels to the nearest pixel of background. (Right) The corresponding graph object that represents the connectivity of the morphological branch points and endpoints of the objects in image is obtained by applying morphological thinning. The morphological branch points and endpoints of the image skeleton are converted into nodes. The graph exhibits an undirected edge between two vertices if the corresponding branch points or endpoints are 8-connected by the skeleton and the weight of each edge is set to the number of pixels in the corresponding skeleton connection. **(B-D)** Extracting a 2D mitochondrial network architecture from 3D confocal z-stacks. (B) Projections of multiple z-stack sections into one 2D image were performed either by generating a maximum intensity composite, thresholded, binarized, skeletonized and (C) converted to a graph amenable to standard conceptual tools of graph theory and computational tools of network science. **(D)** Networks can be defined by a collection of nodes (vertices), and edges (links) between pairs of nodes. Nodes in mitochondrial networks represent branching points and endpoints of mitochondrial tubules, while edges represent the tubules themselves.

Figure S6. Branch-pointd of mitochondrial networks are dominated by node degree k=3. (A-B) Computational graphic analysis revealed an exclusive presence of node degrees $1 < k < 4$. (A) Probability density functions of node degrees. (B) Branch-points are dominated by node degree k=3.

Figure S7. Mitoengrams are associated with sparse small-world mitochondrial networks topology. (A-C) Average clustering coefficient and average path length are global measures that provide valuable information regarding the topology of a network. In graph theory, clustering reflects the functional topology of a network by quantifying the degree to which a set of network nodes resembles a clique (i.e. tendency to be highly clustered). A clustering coefficient is the fraction of triangles present around a node and average clustering coefficient is the average of the clustering coefficients of all nodes. A path length is the average distance from a node to all other nodes and the average path length is the average of the path lengths of all nodes. Nodes with a short average path length in the network can be connected through a small number of intermediate edges (i.e higher efficiency of connectivity). **(A)** Regardless of the experimental condition, mitochondrial networks exhibit a small-world topology characterized by a high clustering and short average path length between any two nodes (as compared to a random graph model with the same number of edges and nodes - data not shown-); whereas the naïve RC progeny exhibit two subpopulations of networks: **(B)** dense small-world networks exhibit a small network diameter (which is the shortest distance between the two most distant nodes in the network); and **(C)** sparse small-world networks (increased diameter). The topology of RC^{primed} progeny mitochondrial networks collapse to the second topology, indicating that persistence of cellular memory is contingent on a specific mitochondrial network connectivity. However, **(A)** XJB intervention restored the architectural balance of mitochondrial networks along with the other mitoengrams properties.

Figure S8. RC population-level mitochondrial volume distribution. (A-E) RC were imaged using a 1.40 numeric aperture 60x objective on a Nikon Ti microscope equipped with a Nikon A1 point scanning confocal scan head. Optical sections were acquired at 200 nm intervals in Z and reconstructed in 3 dimensions and subsequent image processing was performed with Nikon Elements software. **(A)** The 3D volumes were pre-processed using a 3D Blind deconvolution algorithm (Nikolaisen et al., 2014) to remove systemic disturbances (e.g. haze), to improve image contrast and object segmentation (Biggs, 2010), and to maintain the linear relationship in object intensities and their relative intensity changes, thus validating the use in quantitative analysis (Lee et al., 2014). **(B)** 3D Thresholding; binary masks defining positive mitochondrial signal were generated to define the morphology of the network. **(C)** Using an object classifier, each object was classified by size in 0.5 μm increments and 2D binary masks were generated. Binary masks were then converted into a skeletonized 3D network such that the length of all mitochondria in the field maintain a uniform thickness in order to eliminate volume related bias unrelated to branching or network length and connectivity. **(D)** Binary planes were reconnected into 3D binary objects that were categorized by color-coded classes in 3D object measurement. **(E)** Mitochondrial subpopulations /3D Binary objects classified as continuous groups of adjacent positive voxels, were measured and classified into size categories in order to gain information related to cell population-level mitochondrial heterogeneity. Nine classes were defined corresponding to; class1 [0.01 μm - 0.05 μm], class2 [0.5 μm - 1 μm], class3 [1 μm – 1.5 μm], class4 [1.5 μm - 2 μm], class5 [2 μm – 2.5 μm], class6 [2.5 μm – 3 μm], class7 [3 μm – 3.5 μm], class8 [3.5 μm – 4 μm] and class9 of objects greater than 4 μm.

Figure S9. Heterogeneous nuclear expression of H2A.Z protein. (A) Representative immunofluorescence micrographs of total nuclear H2A.Z (red) and nuclear counterstaining (DAPI) at 20X magnification. **(B)** Gaussian model complementary cumulative distribution functions of mitochondrial mass and nuclear H2A.Z protein expression simulating their presumable normal distributions based on their empirical means and standard deviations of mitochondrial content. However, the extremely low exceedance probabilities are incompatible with the empirical observations and suggest that they are not normally distributed normally within the RC populations.

Figure S10. Power-law scaling behavior of the tail cell subpopulation. **(A-B)** Empirical complementary cumulative distribution functions of mitochondrial mass and nuclear H2A.Z expression levels and their maximum likelihood fitted power-law (exponential cut-off -Pareto-) and alternative distribution models (see also statistical appendix I&II). Both mitochondrial content and nuclear H2A.Z expression scale up or down respectively with a rate corresponding to the power law scaling exponent α. This suggests a large population-level variance of mitochondrial content and H2A.Z expression, with only a minor subset of the RC population having a high mitochondrial mass and levels of nuclear RC. The fat tail behavior is more pronounced in the primed RC progeny with memory of stress compared to their naïve counterparts. However, XJB intervention reverts the primed RC progeny both mitochondrial mass and nuclear H2A.Z expression levels to naïve-like distribution. Fitting results correspond to the pooled mitochondrial and nuclear data of two independent sets of three independent experiments (n=3).

A.

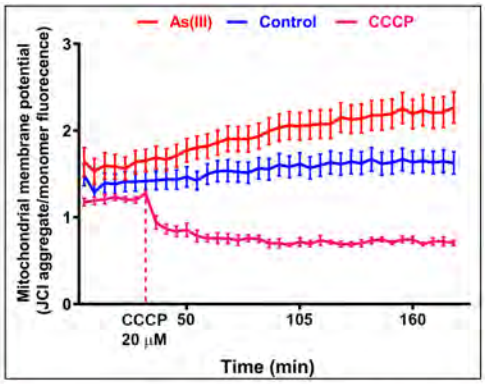

B.

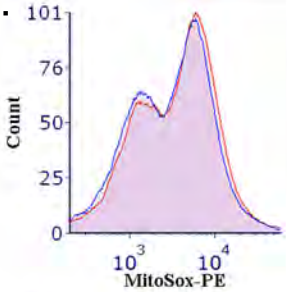

Mitochodrial superoxide $O_2^{-\cdot}$ (RFU)	$RC^{naïve}$	RC^{primed}
mean	4640.32	5280.34
standard deviation	9727.25	11621.3
median	2770.01	3243.99
interquantile range	4446.33	4921.88
variance	9.46194×10^7	1.35055×10^8
skewness	14.0755	13.6171
kurtosis	301.991	256.896
min	0.254866	0.00188
Max	262144.	262144

C.

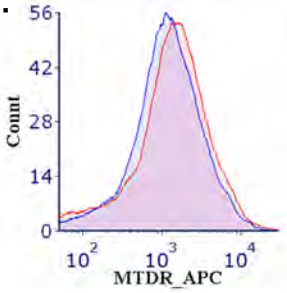

Mitochodrial mass (RFU)	$RC^{naïve}$	RC^{primed}
mean	1525.17	1791.79
standard deviation	1874.51	2116.65
median	1003.05	1204.62
interquantile range	1275.52	1548.92
variance	3.51379×10^6	4.48019×10^6
skewness	5.86742	4.41977
kurtosis	78.7182	41.4903
min	0.024435	0.531991
Max	45866.6	40227.7

D.

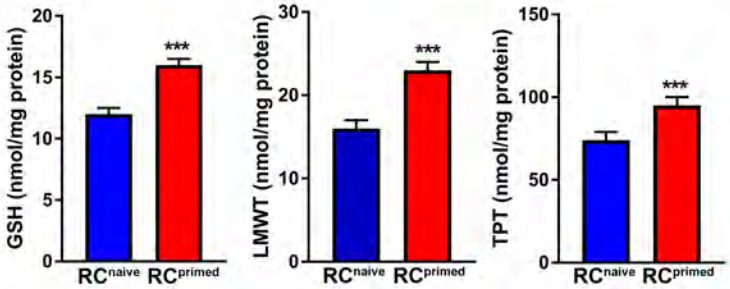

E.

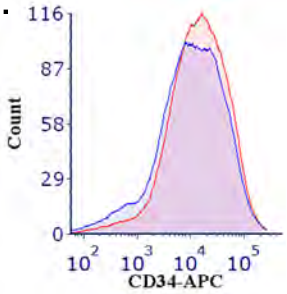

CD34–APC (RFU)	$RC^{naïve}$	RC^{primed}
mean	6034.29	6567.78
standard deviation	14748.1	17304.7
median	3552.16	3819.22
interquantile range	4255.16	4440.98
variance	2.17505×10^8	2.99453×10^8
skewness	13.0766	12.0532
kurtosis	208.361	168.595
min	0.082052	0.046519
Max	262144	262144

F.

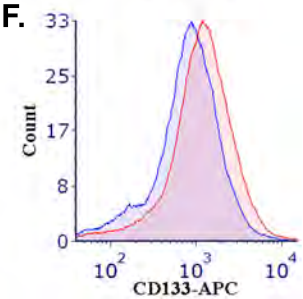

CD133–APC (RFU)	$RC^{naïve}$	RC^{primed}
mean	923.044	1238.37
standard deviation	1156.81	2308.13
median	712.647	944.728
interquantile range	695.564	908.673
variance	1.33821×10^6	5.32744×10^6
skewness	13.1362	56.6655
kurtosis	339.903	4282.97
min	0.0576395	0.152513
Max	41227.7	178361.

Supplemental Figure 1

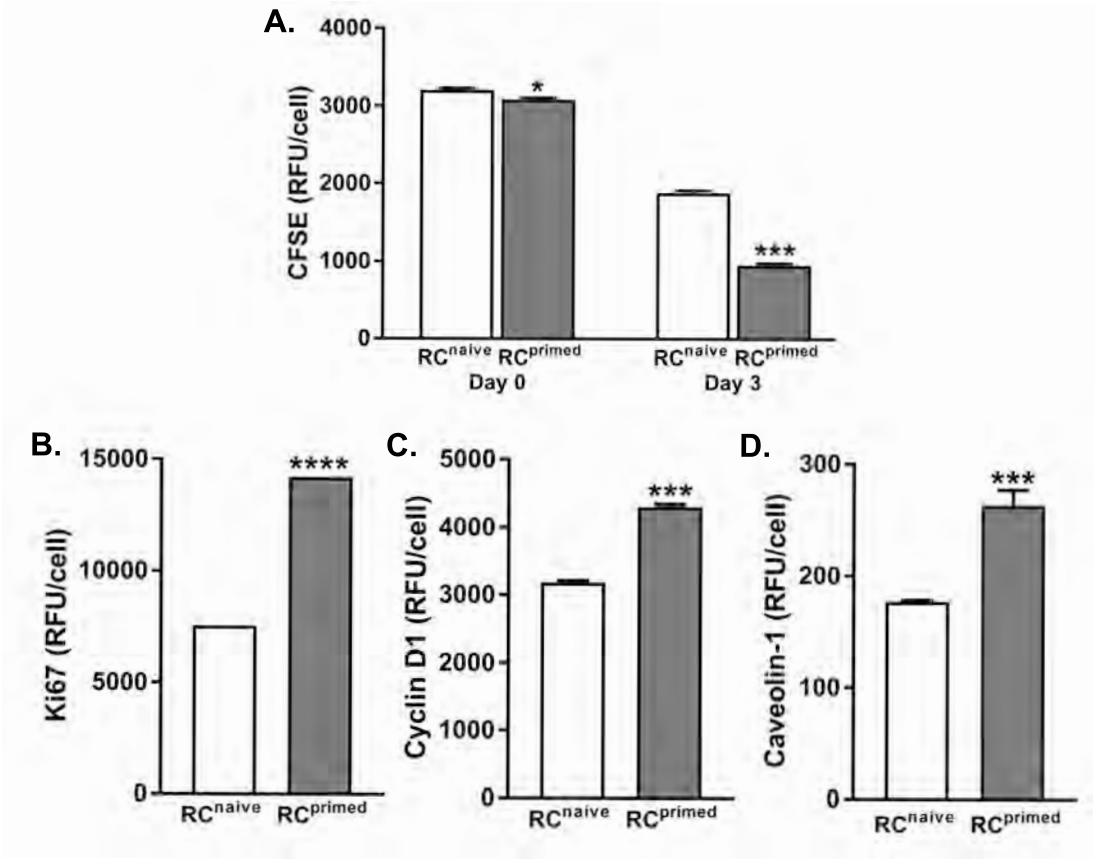

Supplemental Figure 2

A.

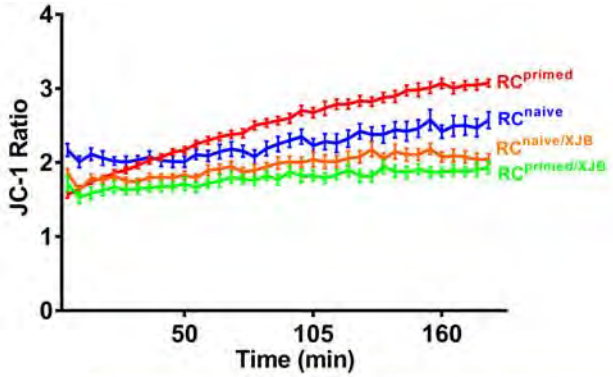

B.

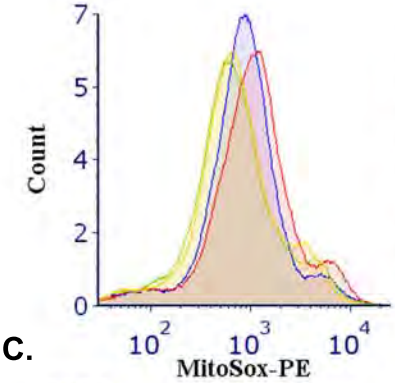

Mitochodrial superoxide O_2^- (RFU)	$RC^{naïve}$	RC^{primed}	$RC^{XJB/naïve}$	$RC^{XJB/primed}$
mean	1058.07	1344.89	1085.15	1008.35
standard deviation	1564.55	1815.22	1884.28	1453.46
median	704.263	861.341	554.905	579.306
interquantile range	644.614	915.647	677.489	680.835
variance	2.44781×10^6	3.29502×10^6	3.55051×10^6	2.11254×10^6
skewness	9.0947	6.51078	8.33281	8.81814
kurtosis	161.065	90.6641	127.06	185.244
min	0.265749	0.011999	0.016715	0.48234
Max	45868.7	43542.7	42952.9	47809.8

C.

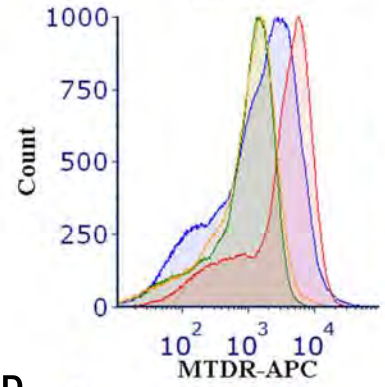

Mitochodrial mass (RFU)	$RC^{naïve}$	RC^{primed}	$RC^{XJB/naïve}$	$RC^{XJB/primed}$
mean	1734.86	2060.38	969.49	876.812
standard deviation	2394.8	2726.28	1042.91	797.344
median	1016.75	1246.15	646.558	642.94
interquantile range	1705.22	2111.27	974.02	894.127
variance	5.73508×10^6	7.4326×10^6	1.08767×10^6	635757.
skewness	5.54081	5.60847	5.2925	4.43455
kurtosis	67.4863	77.6971	78.2049	77.1274
min	0.00188	0.048733	0.034535	0.137535
Max	61550.9	76532.3	30955.2	24603.6

D.

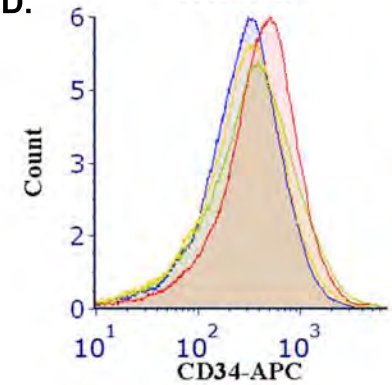

CD34–APC (RFU)	$RC^{naïve}$	RC^{primed}	$RC^{XJB/naïve}$	$RC^{XJB/primed}$
mean	321.861	449.564	475.049	348.307
standard deviation	316.057	492.436	775.795	373.347
median	248.829	345.489	306.603	253.857
interquantile range	266.227	361.76	404.879	300.594
variance	99892.1	242493.	601858.	139388.
skewness	5.55133	7.66161	20.431	4.63598
kurtosis	81.9803	126.075	889.731	47.912
min	0.011999	0.131169	0.030318	0.072161
Max	8938.6	14192.9	45448.4	8769.71

E.

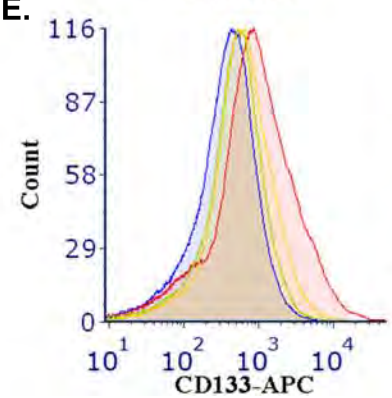

CD133–APC (RFU)	$RC^{naïve}$	RC^{primed}	$RC^{XJB/naïve}$	$RC^{XJB/primed}$
mean	492.682	1586.26	781.295	676.976
standard deviation	1893.96	4924.52	1978.43	1292.03
median	346.841	740.175	507.963	453.936
interquantile range	387.897	1190.53	596.985	501.062
variance	3.58708×10^6	2.42509×10^7	3.91419×10^6	1.66934×10^6
skewness	101.957	29.1255	84.4188	29.5354
kurtosis	12866.7	1258.11	10183.4	1876.21
min	0.012687	0.00188	0.012687	0.018865
Max	262144.	262144.	262144.	114608.

Supplemental Figure 3

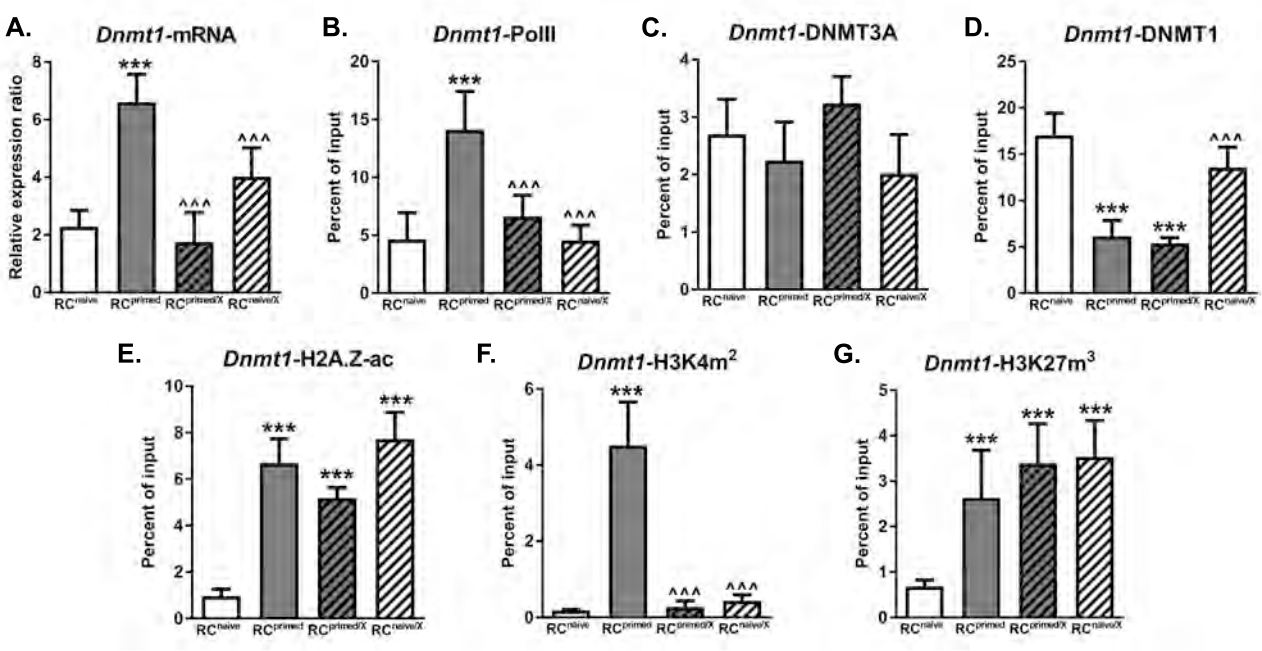

Supplemental Figure 4

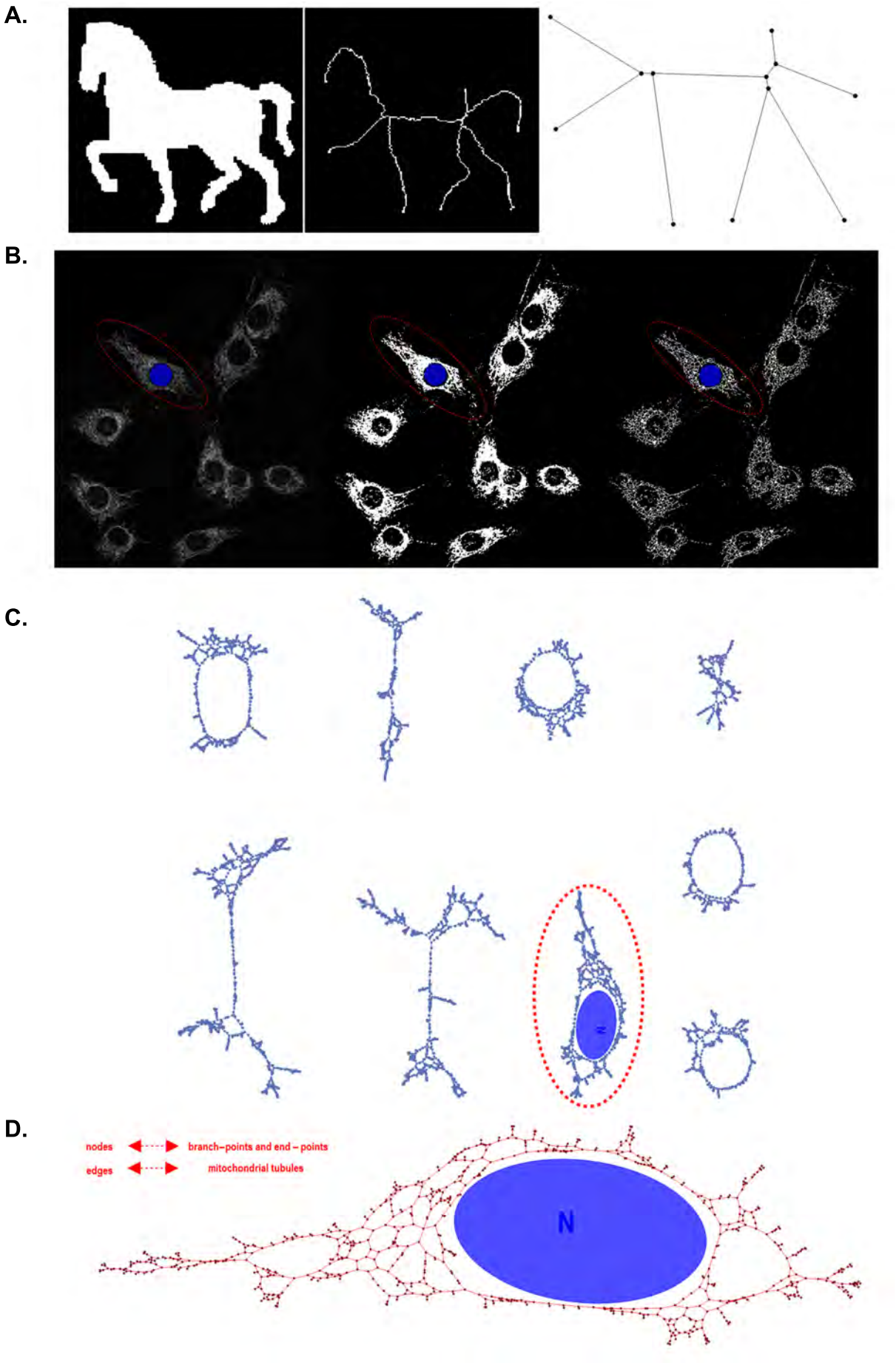

Supplemental Figure 5

A.

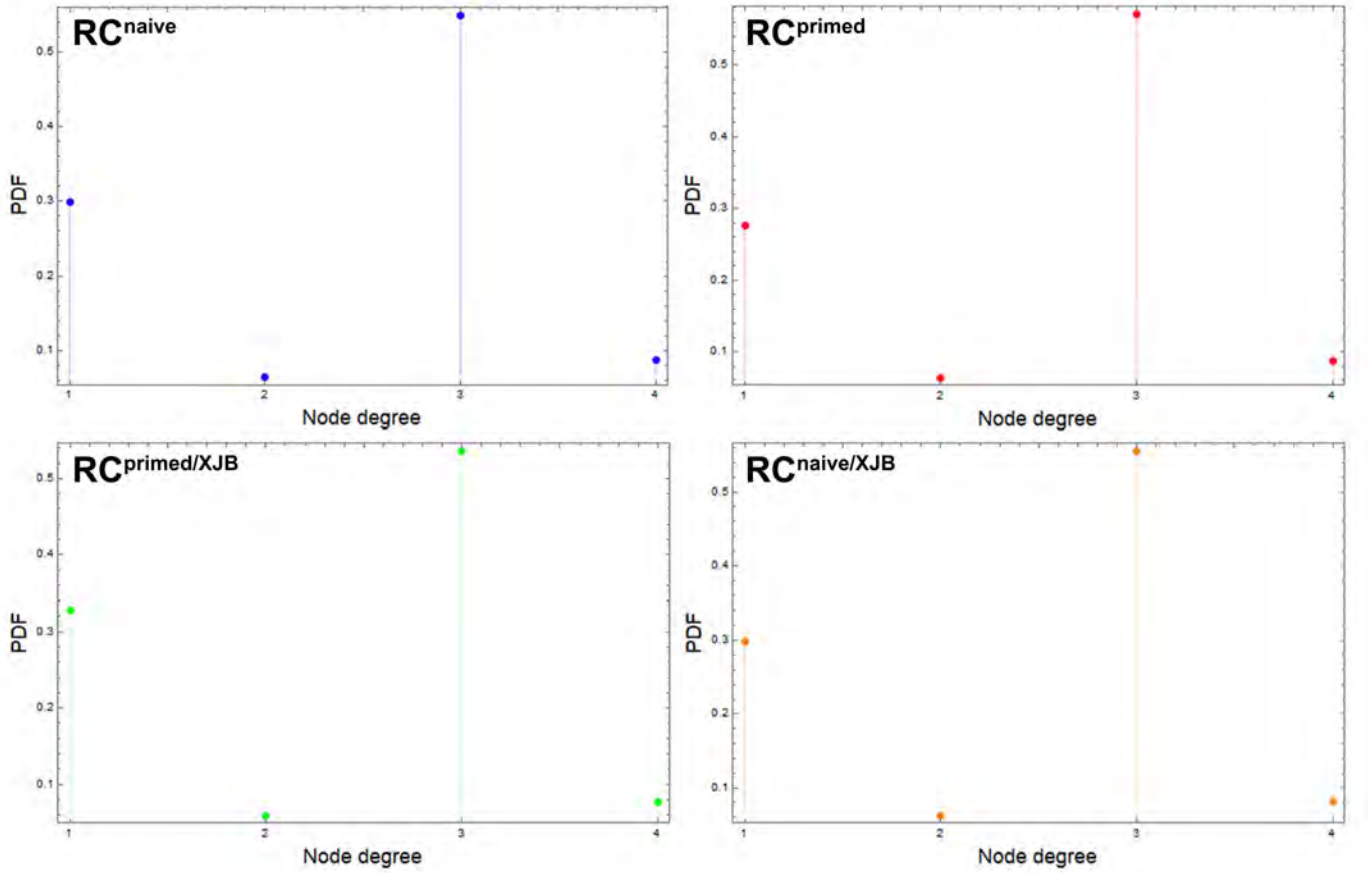

B.

Condition	% (k = 4)	% (k = 3)
RC^{Naive}	13.7178	86.2822
RC^{Primed}	13.0013	86.9987
$RC^{XJB/Naive}$	13.4103	86.5897
$RC^{XJB/Primed}$	12.4994	85.3979

Supplementary Figure 6

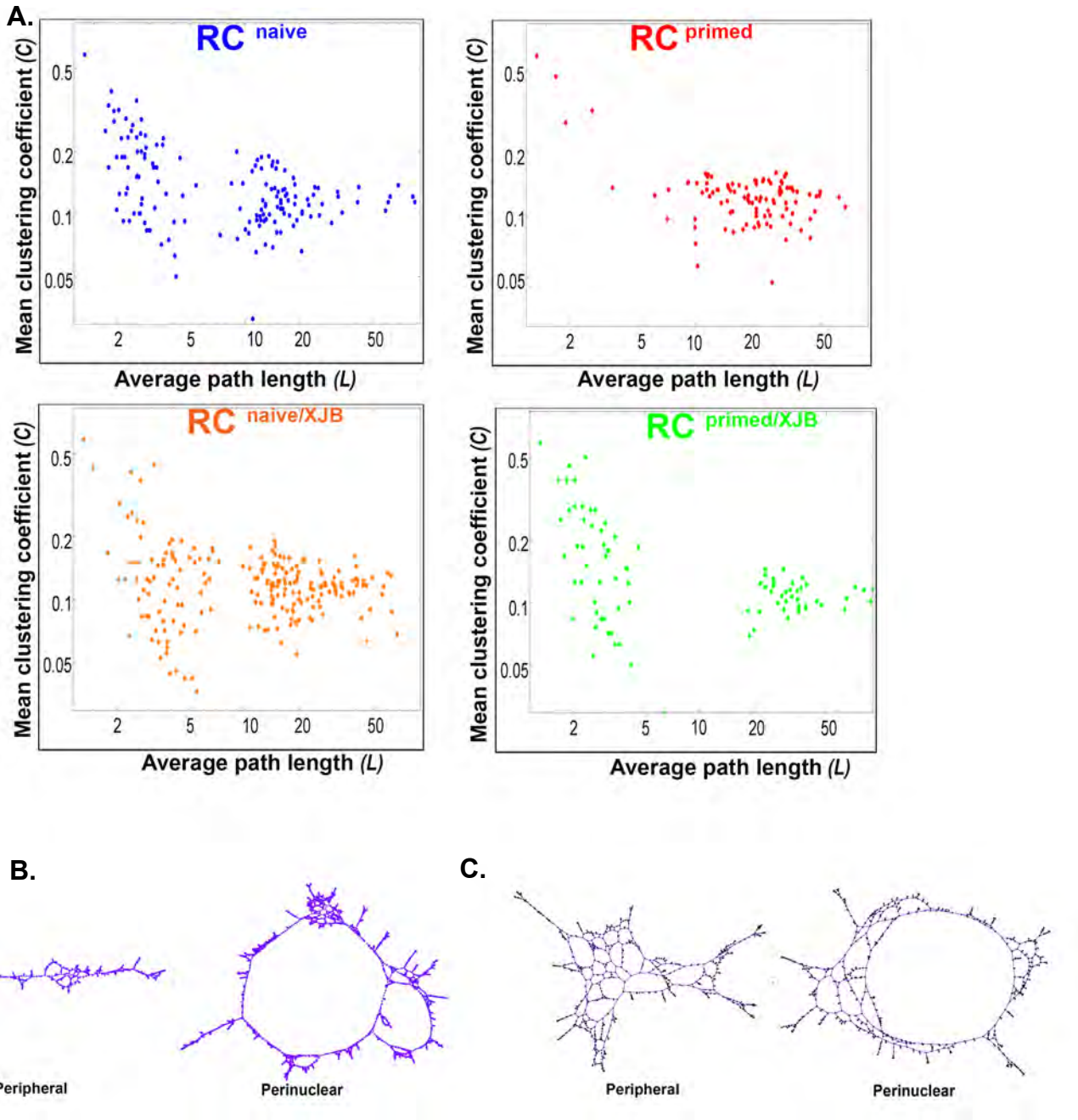

Dense small-world networks

Sparse small-world networks

Supplemental Figure 7

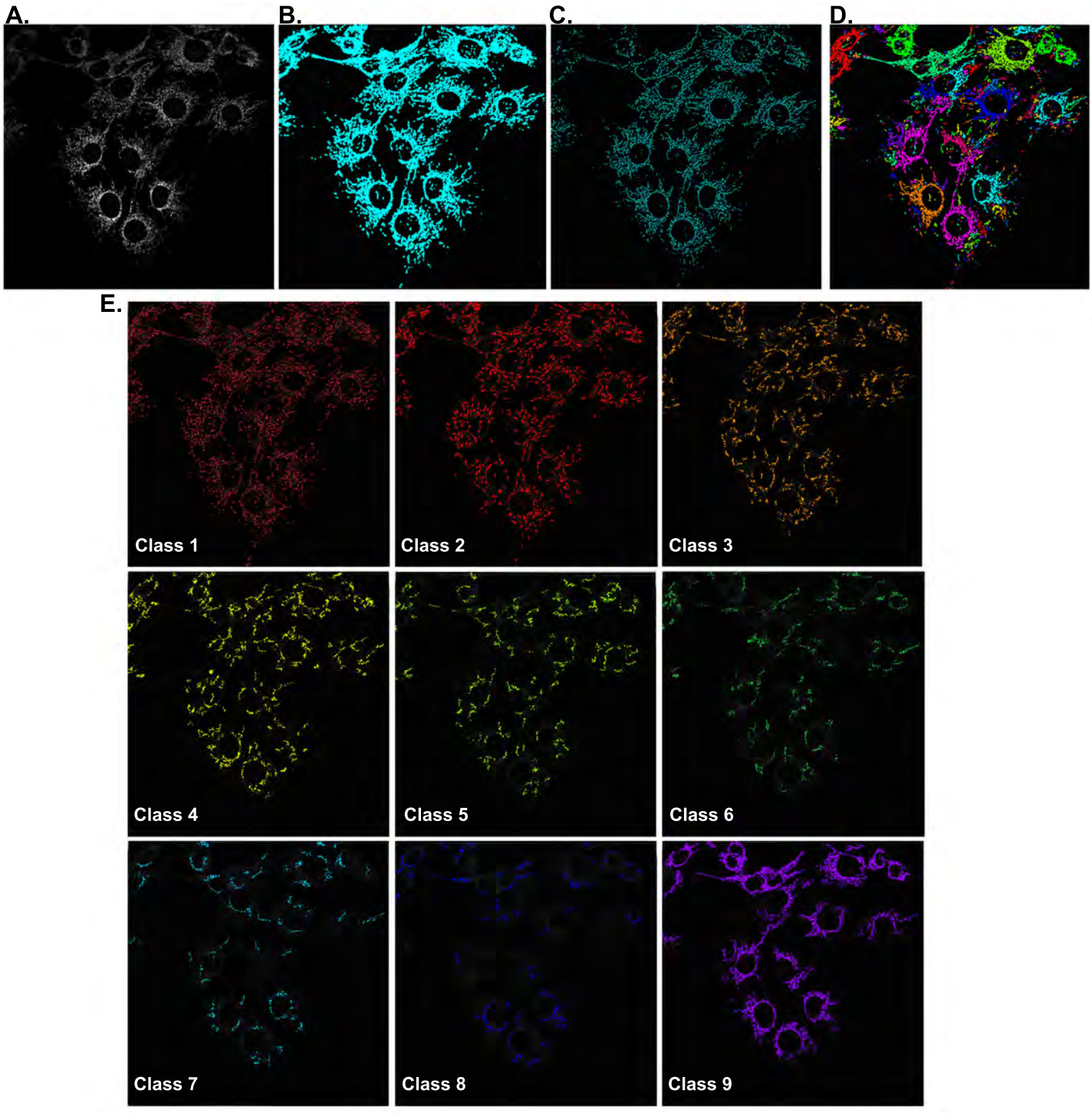

Supplemental Figure 8

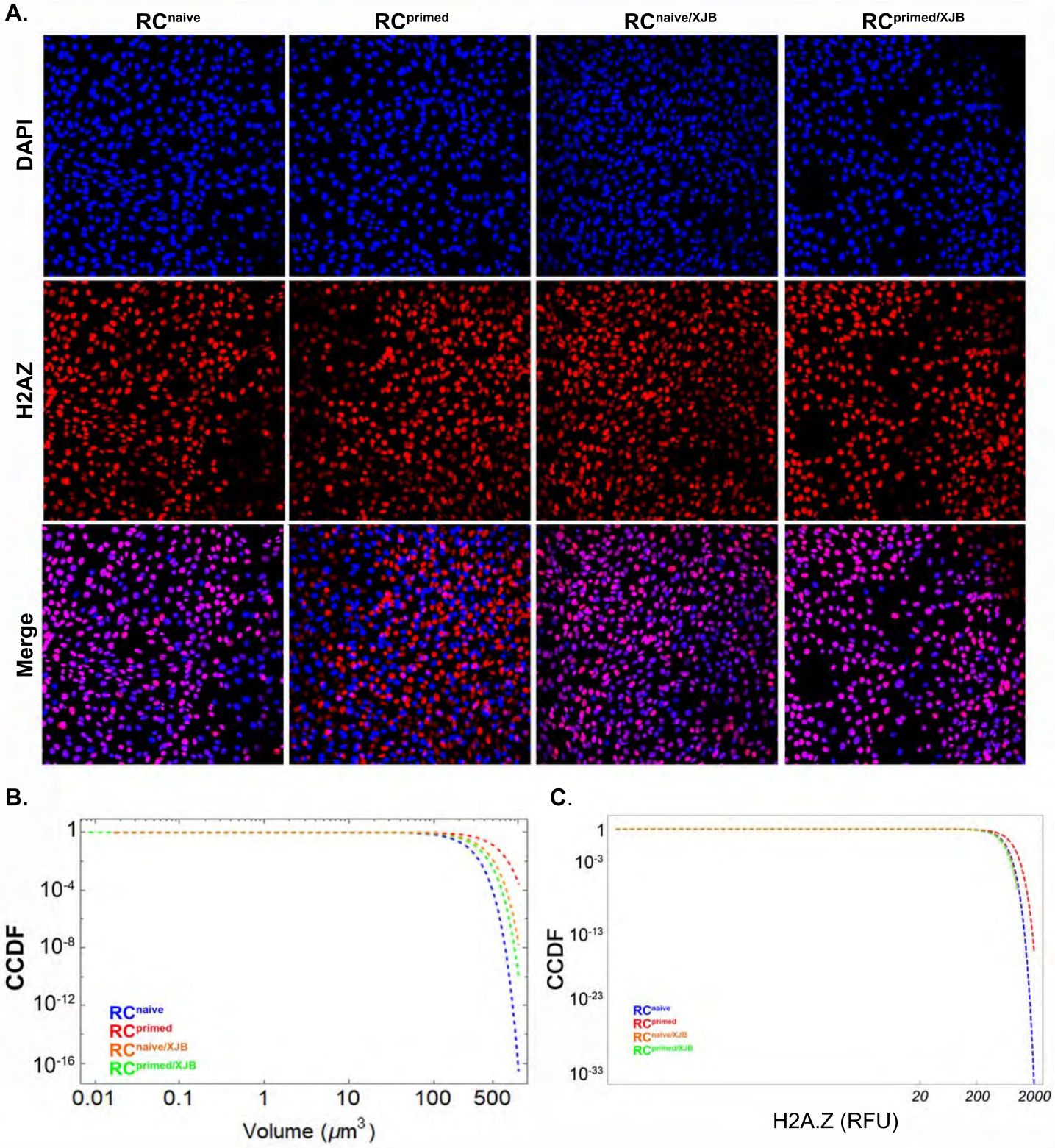

Supplemental Figure 9

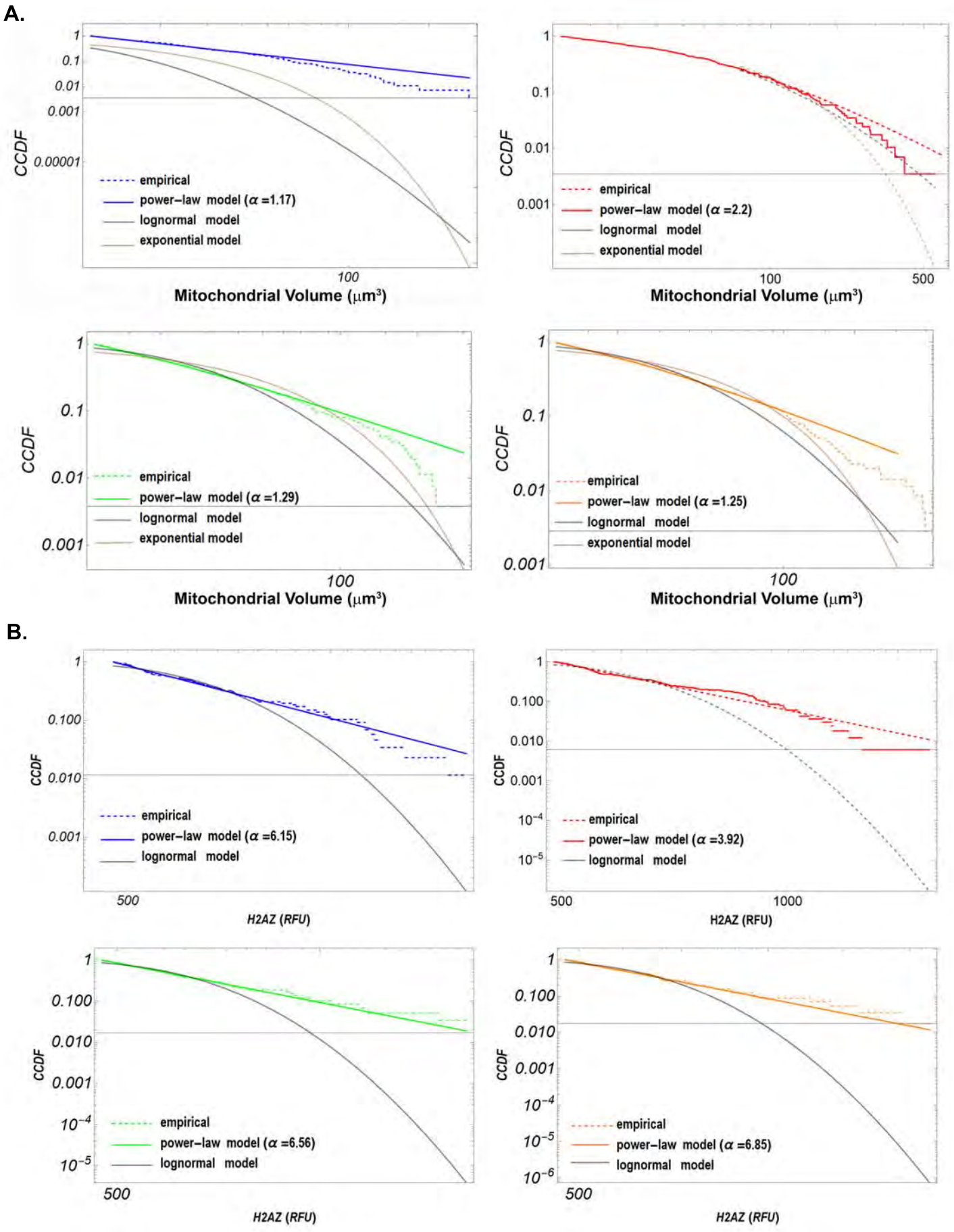

Supplemental Figure 10

CCDF of the empirical data:

The reliability function is equivalent to 1-CDF[dist,x] and gives the probability that an observed value is greater than x.

Distribution Estimation:

A maximum likelihood method attempts to maximize the log-likelihood function $\sum_i log(f(x_i;\theta))$, where θ are the distribution parameters and $f(x;\theta)$ is the PDF of the symbolic distribution. In practice, however, ML problems rarely yield closed form solutions. Consequently, ML estimation generally requires numerical methods that iterate progressively from one potential solution to the next, designed to terminate (at some pre-specified tolerance) at the point that maximizes the likelihood. Mathematica uses the function FindMaximum[f,x] which searches for a local maximum in f,starting from an automatically selected point.

Goodness-of-Fit Testing:

1) The goodness of fit (GOF) indices for assessing relative fit and model selection:

The GOF indices that were utilized are Akaike's information criterion (AIC),
$AIC = -2L + 2k$
and Schwarz Bayesian information criterion (BIC),
$BIC = -2L + k\ ln\ (N)$
where L denotes the maximized value of the likelihood function of the model and k being the numbers of parameters .

Given a data set, the AIC or BIC are computed for all models under consideration. Then,under the assumption, that both models have the same log likelihood, the model with less parameters ,and thus the lowest index, is selected (the least information loss relative to the true model).

Both AIC and BIC combine absolute fit with model parsimony. That is, they penalize by adding parameters to the model. However, the BIC penalizes by adding parameters to the model more strongly than the AIC.

2) The goodness of fit (GOF) statistics for assessing overall fit :

To determine the discrepancy between the empirical data and a specified statistical model, we performed goodness-of-fit hypothesis test with null hypothesis H_0 All distributions are equally far from the true distribution *dist* and alternative hypothesis H_a that one of the test distributions is closer to the true distribution. By default, a probability value or p-value is returned. If the asymptotic p-value is large, than any difference between the empirical data and the model can be explained with statistical fluctuations. If $p \approx 0$, then the model does not provide a plausible fit to the data and another distribution may be more appropriate.

The tests use the *CDF F(x)* of the test distribution *dist* and the empirical *CDF* $\hat{F}(x)$ of the data as well as their difference $d(x)=F(x)-\hat{F}(x)$ and $\bar{d}=Expectation[d(x),\ldots]$. The *CDFs F(x)* and $\hat{F}(x)$ should be the same under the null hypothesis H_0 .

GOF statistics are GOF indices with known sampling distributions, usually obtained using asymptotic methods, that are used in statistical hypothesis testing. The following tests, with different powers against the fat tail, were used:

- Anderson-Darling effectively uses a test statistic based on **Expectation** $\pi \frac{(d(x))^2}{F(x)(1-F(x))}, \ldots$ where $\hat{F}$ is the empirical CDF of data and *F(x)* is the CDF of distribution. For univariate data, the test statistic is given by $-\sum_{k=1}^{n} \frac{(2k-1)(\log(1-F(y_{-k+n+1}))+\log(F(y_k)))}{n} - n$ where $y_1 < \ldots < y_n$ is the sorted data.
- Cramer Von Mises effectively uses a test statistic based on the expectation value of $(d(x))^2$ where $\hat{F}$ is the empirical CDF of data and F(x) is the CDF of distribution. For univariate data, the test statistic is given by $\frac{1}{12n} + \sum_{i=1}^{n} \left(\frac{2i-1}{2n} - F(x)_i\right)^2$
- Pearson Chi Square χ^2 test effectively compares a histogram of data to a theoretical histogram based on distribution. The bins are chosen to have equal probability in distribution. For univariate data, the test statistic is given by $\sum_{i=1}^{n}(o_i - e_i)^2 / e_i$, where o_i and e_i are the observed and expected counts for the i^{th} histogram bin, respectively.
- Kolmogorov Smirnov effectively uses a test statistic based on $\mathrm{Sup}_x |\hat{F}(x)-F(x)|$ where $\hat{F}(x)$ is the empirical CDF of data and F(x) is the CDF of dist.
- Kuiper effectively uses a test statistic based on $\mathrm{Sup}_{d(x)>0}(\hat{F}(x)-F(x)) - \mathrm{inf}_{d(x)<0}(\hat{F}(x)-F(x))$ where $\hat{F}$ is the empirical CDF of data and F(x) is the CDF of distribution.
- Watson effectively uses a test statistic based on $E((d(x)-\bar{d})^2)$ where $d(x)=\hat{F}(x)-F(x)$ and $\bar{d}=E(d(x),\ldots)$, $\hat{F}$ is the empirical CDF of data and F(x) is the CDF of distribution.

Appendix I: Mitochondrial Volume

Naïve RC progeny:

The goodness of fit (GOF) indices for assessing relative fit and model selection:

	AIC	BIC	Adj-R^2	R^2
Pareto	-1409.1	-1398.17	0.998815	0.998823
LogNormal	-914.314	-903.377	0.993192	0.99324
Exponential	-438.939	-431.648	0.963352	0.963482

The goodnessof fit (GOF) statistics for assessing overall fit :

Pareto :

```
PDF[ParetoDistribution[a, b], x]
```

$$\begin{cases} a^b\, b\, x^{-1-b} & x \geq a \\ 0 & \text{True} \end{cases}$$

	Estimate	Standard Error	Confidence Interval
a	10.9221	0.0265948	{10.8698, 10.9745}
b	1.17524	0.00694437	{1.16157, 1.18891}

	Statistic	P-Value
Anderson-Darling	0.968452	0.374098
Cramér-von Mises	0.109634	0.53968
Pearson x^2	24.3498	0.183074

Lognormal:

```
PDF[LogNormalDistribution[a, b], x]
```

$$\begin{cases} \dfrac{e^{-\frac{(-a+\text{Log}[x])^2}{2\,b^2}}}{b\,\sqrt{2\,\pi}\,x} & x > 0 \\ 0 & \text{True} \end{cases}$$

	Estimate	Standard Error	Confidence Interval
a	2.13215	0.00420557	{2.1239, 2.14041}
b	0.618353	0.007244	{0.604135, 0.632571}

	Statistic	P-Value
Anderson-Darling	41.2429	0.
Cramér-von Mises	2.86993	1.46896×10^{-7}
Pearson x^2	514.837	2.55852×10^{-90}

Exponential:

```
PDF[ExponentialDistribution[a], x]
```

$$\begin{cases} a e^{-a x} & x \geq 0 \\ 0 & \text{True} \end{cases}$$

	Estimate	Standard Error	Confidence Interval
a	0.0747081	0.000963239	{0.0728176, 0.0765987}

	Statistic	P-Value
Anderson-Darling	592.737	0.
Cramér-von Mises	114.483	2.10942×10^{-15}
Pearson x^2	3944.95	$3.064844253836299 \times 10^{-823}$

Primed RC progeny:

The goodness of fit (GOF) indices for assessing relative fit and model selection:

	AIC	BIC	Adj-R^2	R^2
Pareto	-1750.35	-1735.74	0.999631	0.999634
LogNormal	-1300.89	-1289.93	0.998206	0.998218
Exponential	-830.965	-823.66	0.990635	0.990668

The goodnessof fit (GOF) statistics for assessing overall fit :

Pareto :

PDF[ParetoDistribution[a, b, c], x]

$$\begin{cases} \frac{b\left(\frac{a-c+x}{a}\right)^{-1-b}}{a} & x \geq c \\ 0 & \text{True} \end{cases}$$

	Estimate	Standard Error	Confidence Interval
a	72.9787	2.51256	{68.0329, 77.9244}
b	2.2034	0.0581784	{2.08888, 2.31792}
c	10.0186	0.0718415	{9.87717, 10.16}

	Statistic	P-Value
Anderson-Darling	0.509312	0.737157
Cramér-von Mises	0.0354075	0.955221
Pearson x^2	25.5263	0.143937

Lognormal:

PDF[LogNormalDistribution[a, b], x]

$$\begin{cases} \frac{e^{-\frac{(-a+\text{Log}[x])^2}{2b^2}}}{b\sqrt{2\pi}\,x} & x > 0 \\ 0 & \text{True} \end{cases}$$

	Estimate	Standard Error	Confidence Interval
a	3.65205	0.00449374	{3.6432, 3.66089}
b	0.932627	0.00736501	{0.91813, 0.947125}

	Statistic	P-Value
Anderson-Darling	2.12901	0.0781382
Cramér-von Mises	0.175789	0.31973
Pearson x^2	53.7368	0.0000362118

Exponential:

```
PDF[ExponentialDistribution[a], x]
```

$$\begin{cases} a\, e^{-a\,x} & x \geq 0 \\ 0 & \text{True} \end{cases}$$

	Estimate	Standard Error	Confidence Interval
a	0.0169559	0.00020003	{0.0165622, 0.0173496}

	Statistic	P-Value
Anderson-Darling	7.36557	0.000225935
Cramér-von Mises	0.904282	0.00413348
Pearson x^2	87.4211	9.46806×10^{-11}

XJB-5-131 / Primed RC progeny:

The goodness of fit (GOF) indices for assessing relative fit and model selection:

	AIC	BIC
Pareto	−1877.86	−1862.43
LogNormal	−769.387	−761.671
Exponential	−1168.12	−1156.55

The goodnessof fit (GOF) statistics for assessing overall fit :

Pareto :

PDF[ParetoDistribution[a, b, c], x]

$$\begin{cases} \dfrac{b\left(\dfrac{a-c+x}{a}\right)^{-1-b}}{a} & x \geq c \\ 0 & \text{True} \end{cases}$$

	Estimate	Standard Error	Confidence Interval
a	17.38	0.786041	{15.8321, 18.9279}
b	1.29449	0.0384062	{1.21886, 1.37013}
c	10.7543	0.0542201	{10.6476, 10.8611}

	Statistic	P-Value
Anderson-Darling	0.930363	0.395777
Cramér-von Mises	0.0861263	0.657209
Pearson x^2	28.9462	0.0490411

Lognormal:

PDF[LogNormalDistribution[a, b], x]

$$\begin{cases} \dfrac{e^{-\frac{(-a+\text{Log}[x])^2}{2b^2}}}{b\sqrt{2\pi}\,x} & x > 0 \\ 0 & \text{True} \end{cases}$$

	Estimate	Standard Error	Confidence Interval
a	3.23517	0.00751585	{3.22037, 3.24997}
b	0.757022	0.0123496	{0.732703, 0.781341}

	Statistic	P-Value
Anderson-Darling	6.11464	0.000858584
Cramér-von Mises	0.593212	0.0232648
Pearson x^2	106.846	1.21287×10^{-14}

Exponential:

```
PDF[ExponentialDistribution[a], x]
```

$$\begin{cases} a e^{-a x} & x \geq 0 \\ 0 & \text{True} \end{cases}$$

	Estimate	Standard Error	Confidence Interval
a	0.0254941	0.000491737	{0.0245258, 0.0264624}

	Statistic	P-Value
Anderson-Darling	13.8654	2.55487×10^{-6}
Cramér-von Mises	2.1493	5.91119×10^{-6}
Pearson x^2	203.454	2.04038×10^{-33}

XJB-5-131 / Naïve RC progeny:

The goodness of fit (GOF) indices for assessing relative fit and model selection:

	AIC	BIC	Adj-R^2	R^2
Pareto	-1877.86	-1862.43	0.999194	0.999201
LogNormal	-1168.12	-1156.55	0.993859	0.993894
Exponential	-769.387	-761.671	0.98076	0.980815

The goodnessof fit (GOF) statistics for assessing overall fit :

Pareto :

PDF[ParetoDistribution[a, b, c], x]

$$\begin{cases} \frac{b\left(\frac{a-c+x}{a}\right)^{-1-b}}{a} & x \geq c \\ 0 & \text{True} \end{cases}$$

	Estimate	Standard Error	Confidence Interval
a	20.0633	0.675275	{18.7351, 21.3914}
b	1.25996	0.0276616	{1.20555, 1.31436}
c	10.6484	0.048747	{10.5525, 10.7443}

	Statistic	P-Value
Anderson-Darling	1.03154	0.341003
Cramér-von Mises	0.0939613	0.615296
Pearson x^2	30.4	0.0636263

Lognormal:

PDF[LogNormalDistribution[a, b], x]

$$\begin{cases} \frac{e^{-\frac{(-a+\text{Log}[x])^2}{2b^2}}}{b\sqrt{2\pi}x} & x > 0 \\ 0 & \text{True} \end{cases}$$

	Estimate	Standard Error	Confidence Interval
a	3.33025	0.00677209	{3.31693, 3.34357}
b	0.829185	0.0111493	{0.807256, 0.851113}

	Statistic	P-Value
Anderson-Darling	7.17626	0.000275563
Cramér-von Mises	0.727832	0.0109071
Pearson x^2	136.6	2.22847×10^{-19}

Exponential:

```
PDF[ExponentialDistribution[a], x]
```

$$\begin{cases} a\, e^{-a x} & x \geq 0 \\ 0 & \text{True} \end{cases}$$

	Estimate	Standard Error	Confidence Interval
a	0.023095	0.000348083	{0.0224103, 0.0237796}

	Statistic	P-Value
Anderson-Darling	15.4875	1.7605×10^{-6}
Cramér-von Mises	2.26607	3.23928×10^{-6}
Pearson x^2	245.32	1.00185×10^{-40}

Naïve RC progeny:

The goodness of fit (GOF) indices for assessing relative fit and model selection:

	AIC	BIC	Adj-R^2	R^2
Pareto	-410.554	-403.156	0.998528	0.998562
LogNormal	-234.08	-226.683	0.98881	0.989067
Exponential	153.809	158.741	0.0226623	0.0338961

The goodnessof fit (GOF) statistics for assessing overall fit :

Pareto :

PDF[ParetoDistribution[a, b], x]

$$\begin{cases} a^b\, b\, x^{-1-b} & x \geq a \\ 0 & \text{True} \end{cases}$$

	Estimate	Standard Error	Confidence Interval
a	487.533	0.477047	{486.585, 488.482}
b	6.15623	0.0782246	{6.0007, 6.31176}

	Statistic	P-Value
Anderson-Darling	0.361693	0.885374
Cramér-von Mises	0.0459403	0.900431
Kolmogorov-Smirnov	0.0581415	0.913625
Kuiper	0.102175	0.694193
Pearson x^2	11.069	0.437504
Watson U^2	0.0433771	0.79337

Lognormal:

PDF[LogNormalDistribution[a, b], x]

$$\begin{cases} \frac{e^{-\frac{(-a+\text{Log}[x])^2}{2b^2}}}{b\sqrt{2\pi}\,x} & x > 0 \\ 0 & \text{True} \end{cases}$$

	Estimate	Standard Error	Confidence Interval
a	6.31982	0.00283405	{6.31419, 6.32546}
b	0.124143	0.00486301	{0.114474, 0.133812}

	Statistic	P-Value
Anderson-Darling	2111.35	0.
Cramér-von Mises	29.	6.66134×10^{-16}
Kolmogorov-Smirnov	1.	5.6783×10^{-78}
Kuiper	0.988506	6.66134×10^{-16}
Pearson x^2	957.	3.42608×10^{-198}
Watson U^2	7.25	0.

Exponential:

PDF[ExponentialDistribution[a], x]

$$\begin{cases} a e^{-a x} & x \geq 0 \\ 0 & \text{True} \end{cases}$$

	Estimate	Standard Error	Confidence Interval
a	1.	1.9937×10^{209}	$\{-3.96335 \times 10^{209}, 3.96335 \times 10^{209}\}$

	Statistic	P-Value
Anderson-Darling	-87.	1.
Cramér-von Mises	29.	8.88178×10^{-16}
Kolmogorov-Smirnov	1.	5.6783×10^{-78}
Kuiper	0.988506	6.66134×10^{-16}
Pearson x^2	87.	6.43789×10^{-14}
Watson U^2	7.25	0.

Primed RC progeny:

The goodness of fit (GOF) indices for assessing relative fit and model selection:

	AIC	BIC	Adj-R^2	R^2
Pareto	-693.269	-683.952	0.997456	0.997487
LogNormal	-376.985	-367.667	0.982704	0.982913
Exponential	289.475	295.687	0.01203	0.0180177

The goodness of fit (GOF) statistics for assessing overall fit :

Pareto :

PDF[ParetoDistribution[a, b], x]

$$\begin{cases} a^b\, b\, x^{-1-b} & x \geq a \\ 0 & \text{True} \end{cases}$$

	Estimate	Standard Error	Confidence Interval
a	488.022	0.727643	{486.585, 489.459}
b	3.92573	0.0498941	{3.82721, 4.02425}

	Statistic	P-Value
Anderson-Darling	1.00163	0.356151
Cramér-von Mises	0.144333	0.407314
Kolmogorov-Smirnov	0.0774679	0.261547
Kuiper	0.133908	0.0314744
Pearson x^2	37.1818	0.00119037
Watson U^2	0.138635	0.129521

Lognormal:

PDF[LogNormalDistribution[a, b], x]

$$\begin{cases} \frac{e^{-\frac{-a+\text{Log}[x]^2}{2b^2}}}{b\sqrt{2\pi}\,x} & x > 0 \\ 0 & \text{True} \end{cases}$$

	Estimate	Standard Error	Confidence Interval
a	6.39441	0.00431178	{6.3859, 6.40293}
b	0.203471	0.00757065	{0.188522, 0.218421}

	Statistic	P-Value
Anderson-Darling	11.3244	7.10408×10^{-6}
Cramér-von Mises	0.970364	0.00288781
Kolmogorov-Smirnov	0.15821	0.000447628
Kuiper	0.277452	1.44569×10^{-10}
Pearson x^2	134.927	2.29616×10^{-21}
Watson U^2	0.882758	0.

Exponential:

```
PDF[ExponentialDistribution[a], x]
```

$$\begin{cases} a\, e^{-a\,x} & x \geq 0 \\ 0 & \text{True} \end{cases}$$

	Estimate	Standard Error	Confidence Interval
a	1.	1.00467×10^{209}	$\{-1.98376 \times 10^{209}, 1.98376 \times 10^{209}\}$

	Statistic	P-Value
Anderson-Darling	3056.22	0.
Cramér-von Mises	249.168	7.10543×10^{-15}
Pearson x^2	17 131.3	$5.257711437476852 \times 10^{-3678}$

XJB-5-131 / Primed RC progeny:

The goodness of fit (GOF) indices for assessing relative fit and model selection:

	AIC	BIC	Adj-R^2	R^2
Pareto	-323.507	-317.175	0.999175	0.999202
LogNormal	-161.387	-155.054	0.988226	0.988612
Exponential	9.14413	13.3659	0.804132	0.807343

The goodnessof fit (GOF) statistics for assessing overall fit :

Pareto :

PDF[ParetoDistribution[a, b], x]

$$\begin{cases} a^b\, b\, x^{-1-b} & x \geq a \\ 0 & \text{True} \end{cases}$$

	Estimate	Standard Error	Confidence Interval
a	486.877	0.402248	{486.072, 487.681}
b	6.56047	0.0744754	{6.41144, 6.70949}

	Statistic	P-Value
Anderson-Darling	0.164319	0.99728
Cramér-von Mises	0.0219054	0.994844
Kolmogorov-Smirnov	0.0589929	0.978861
Kuiper	0.0795788	0.984433
Pearson x^2	3.83051	0.954669
Watson U^2	0.0175139	0.997279

Lognormal:

PDF[LogNormalDistribution[a, b], x]

$$\begin{cases} \frac{e^{-\frac{(-a+\text{Log}[x])^2}{2b^2}}}{b\sqrt{2\pi}\,x} & x > 0 \\ 0 & \text{True} \end{cases}$$

	Estimate	Standard Error	Confidence Interval
a	6.30244	0.00283164	{6.29677, 6.3081}
b	0.109718	0.00496635	{0.0997799, 0.119655}

	Statistic	P-Value
Anderson-Darling	4.68127	0.00412394
Cramér-von Mises	0.241895	0.1991
Kolmogorov-Smirnov	0.155477	0.103492
Kuiper	0.188605	0.0979824
Pearson x^2	21.7288	0.0165473
Watson U^2	0.155535	0.0920677

Exponential:

```
PDF[ExponentialDistribution[a], x]
```

$$\begin{cases} a\, e^{-a x} & x \geq 0 \\ 0 & \text{True} \end{cases}$$

	Estimate	Standard Error	Confidence Interval
a	1.	1.22299×10^{208}	$\{-2.44635 \times 10^{208}, 2.44635 \times 10^{208}\}$

	Statistic	P-Value
Anderson-Darling	-59.	1.
Cramér-von Mises	19.6667	1.11022×10^{-16}
Kolmogorov-Smirnov	1.	2.08926×10^{-53}
Kuiper	0.983051	4.44089×10^{-16}
Pearson x^2	59.	5.6004×10^{-9}
Watson U^2	4.91667	0.

XJB-5-131 / Naïve RC progeny:

The goodness of fit (GOF) indices for assessing relative fit and model selection:

	AIC	BIC	Adj-R^2	R^2
Pareto	-285.725	-279.596	0.998938	0.998975
LogNormal	-157.318	-151.189	0.989897	0.990251
Exponential	101.627	105.713	0.0343328	0.0512744

The goodnessof fit (GOF) statistics for assessing overall fit :

Pareto :

PDF[ParetoDistribution[a, b], x]

$$\begin{cases} a^b\, b\, x^{-1-b} & x \geq a \\ 0 & \text{True} \end{cases}$$

	Estimate	Standard Error	Confidence Interval
a	488.437	0.45654	{487.522, 489.352}
b	6.85279	0.0922498	{6.66791, 7.03766}

	Statistic	P-Value
Anderson-Darling	0.207982	0.988095
Cramér-von Mises	0.0262714	0.986754
Kolmogorov-Smirnov	0.0556341	0.990392
Kuiper	0.0772763	0.990102
Pearson x^2	6.49123	0.772444
Watson U^2	0.0214352	0.988922

Lognormal:

PDF[LogNormalDistribution[a, b], x]

$$\begin{cases} \frac{e^{-\frac{-a+\text{Log}[x]^2}{2b^2}}}{b\sqrt{2\pi}\,x} & x > 0 \\ 0 & \text{True} \end{cases}$$

	Estimate	Standard Error	Confidence Interval
a	6.30778	0.00294349	{6.30188, 6.31368}
b	0.110035	0.00503348	{0.0999473, 0.120122}

	Statistic	P-Value
Anderson-Darling	3.77693	0.0113007
Cramér-von Mises	0.210326	0.24833
Kolmogorov-Smirnov	0.152414	0.127347
Kuiper	0.215056	0.0358085
Pearson x^2	25.7895	0.00403389
Watson U^2	0.179854	0.0566257

Exponential:

PDF[ExponentialDistribution[a], x]

$$\begin{cases} a\, e^{-a x} & x \geq 0 \\ 0 & \text{True} \end{cases}$$

	Estimate	Standard Error	Confidence Interval
a	1.	8.45574×10^{209}	$\{-1.69389 \times 10^{210}, 1.69389 \times 10^{210}\}$

	Statistic	P-Value
Anderson-Darling	-57.	1.
Cramér-von Mises	19.	2.22045×10^{-16}
Kolmogorov-Smirnov	1.	1.19306×10^{-51}
Kuiper	0.982456	6.66134×10^{-16}
Pearson x^2	57.	1.33293×10^{-8}
Watson U^2	4.75	0.

OPEN ACCESS Freely available online

PLOS ONE

Antipurinergic Therapy Corrects the Autism-Like Features in the Poly(IC) Mouse Model

Robert K. Naviaux[1,2,3,4]*, Zarazuela Zolkipli[1,5], Lin Wang[1,2], Tomohiro Nakayama[1,5], Jane C. Naviaux[1,6], Thuy P. Le[1,3], Michael A. Schuchbauer[6], Mihael Rogac[1,2¤], Qingbo Tang[2], Laura L. Dugan[2], Susan B. Powell[6]

1 The Mitochondrial and Metabolic Disease Center, University of California San Diego School of Medicine, San Diego, California, United States of America, **2** Department of Medicine, University of California San Diego School of Medicine, San Diego, California, United States of America, **3** Department of Pediatrics, University of California San Diego School of Medicine, San Diego, California, United States of America, **4** Department of Pathology, University of California San Diego School of Medicine, San Diego, California, United States of America, **5** Department of Neurosciences, University of California San Diego School of Medicine, San Diego, California, United States of America, **6** Department of Psychiatry, University of California San Diego School of Medicine, San Diego, California, United States of America

Abstract

Background: Autism spectrum disorders (ASDs) are caused by both genetic and environmental factors. Mitochondria act to connect genes and environment by regulating gene-encoded metabolic networks according to changes in the chemistry of the cell and its environment. Mitochondrial ATP and other metabolites are mitokines—signaling molecules made in mitochondria—that undergo regulated release from cells to communicate cellular health and danger to neighboring cells via purinergic signaling. The role of purinergic signaling has not yet been explored in autism spectrum disorders.

Objectives and Methods: We used the maternal immune activation (MIA) mouse model of gestational poly(IC) exposure and treatment with the non-selective purinergic antagonist suramin to test the role of purinergic signaling in C57BL/6J mice.

Results: We found that antipurinergic therapy (APT) corrected 16 multisystem abnormalities that defined the ASD-like phenotype in this model. These included correction of the core social deficits and sensorimotor coordination abnormalities, prevention of cerebellar Purkinje cell loss, correction of the ultrastructural synaptic dysmorphology, and correction of the hypothermia, metabolic, mitochondrial, P2Y2 and P2X7 purinergic receptor expression, and ERK1/2 and CAMKII signal transduction abnormalities.

Conclusions: Hyperpurinergia is a fundamental and treatable feature of the multisystem abnormalities in the poly(IC) mouse model of autism spectrum disorders. Antipurinergic therapy provides a new tool for refining current concepts of pathogenesis in autism and related spectrum disorders, and represents a fresh path forward for new drug development.

Citation: Naviaux RK, Zolkipli Z, Wang L, Nakayama T, Naviaux JC, et al. (2013) Antipurinergic Therapy Corrects the Autism-Like Features in the Poly(IC) Mouse Model. PLoS ONE 8(3): e57380. doi:10.1371/journal.pone.0057380

Editor: Madepalli K. Lakshmana, Torrey Pines Institute for Molecular Studies, United States of America

Received October 29, 2012; **Accepted** January 21, 2013; **Published** March 13, 2013

Funding: This research was supported by grants from the Autism Speaks Trailblazer program, the Jane Botsford-Johnson Foundation, and the Wright Family Foundation, and MH091407, with additional support from the UCSD Christini Foundation, the Lennox Foundation, the Hailey's Wish Foundation, and the Larry L. Hillblom Foundation, and the Gerber Foundation. The funders had no role in study design, data collection and analysis, decision to publish, or preparation of the manuscript.

Competing Interests: The authors declare no competing financial interests.

* E-mail: Naviaux@ucsd.edu

¤ Current address: Department of Child, Adolescent and Developmental Neurology, Children's Hospital, University Medical Centre, Ljubljana, Slovenia.

Introduction

Autism spectrum disorders (ASDs) are complex, multisystem disorders that are defined by unifying, core abnormalities in the development of language, social behavior, and repetitive behaviors. Hundreds of single-gene causes and chromosomal copy-number variations (CNVs) are known to confer risk, but in aggregate account for less than 20% of children with ASD [1]. More than 80% of children with ASD do not have a monogenic or CNV cause. The majority of children with ASD develop disease as the result of interactions between large sets of genes and environmental factors. Common comorbidities in non-single-gene forms of ASD provide important clues to shared mechanisms of disease. Comorbidities include epilepsy [2], GI abnormalities [3], sleep disturbances [2], abnormalities in tryptophan metabolism and platelet hyperserotonemia [4], altered intracellular calcium and mitochondrial dynamics [5], hypoimmunoglobulinemia [6], hyperuricosuria [7], methylation disturbances [8], disturbances in sulfur [9] and glutathione metabolism [10], neuroinflammation [11], cerebellar vermis hypoplasia [12], and Purkinje cell loss [13]. We hypothesized that all of these clinical comorbidities can result from a single, evolutionarily conserved, metabolic state associated with a cellular danger response (CDR). Since mitochondria are located at the hub of the wheel of metabolism and play a central role in non-infectious cellular stress [14], innate immunity [15],

inflammasome activation [16], and the stereotyped antiviral response [17], we searched for a signaling system that was both traceable to mitochondria and critical for innate immunity. Purinergic signaling via extracellular nucleotides like ATP and ADP satisfied these requirements. In the following study we tested the role of purinergic signaling in the maternal immune activation mouse model of ASD and show that antipurinergic therapy reverses the abnormalities found in this model.

ATP, ADP, UTP, and UDP are mitokines—signaling molecules made by mitochondria—that act as signaling molecules when outside the cell, and have separate metabolic functions inside the cell. Outside the cell, they bind to and regulate purinergic receptors that are present on the surface of every cell in the body. ATP has been found to be a co-neurotransmitter at every type of synaptic junction studied to date [18]. Excess extracellular ATP (eATP) is an activator of innate and adaptive immunity [19], is a danger signal and damage-associated molecular pattern (DAMP) that is chemotactic for neutrophils [20], and a potent regulator of microglial activation, death, and survival [21]. The concentration of extracellular nucleotides under normal circumstances is ultimately controlled by mitochondrial function and cellular health.

Fifteen different isoforms of purinergic receptors are known that are stimulated by extracellular nucleotides [18]. These are divided into ionotropic P2X receptors and metabotropic P2Y receptors. P2Y receptors are G-protein coupled receptors (GPCRs). Together, P2X and P2Y receptors are known to control a broad range of biological characteristics that have relevance to autism. These include all the known abnormalities that occur in autism. For example, purinergic signaling modulates normal synaptogenesis and brain development [18], the PI3K/AKT pathway [22], innate and adaptive immune responses, and chronic inflammation [23], neuroinflammation, antiviral signaling [17], microglial activation, neutrophil chemotaxis, autophagy, gut motility [24], gut permeability [25], taste chemosensory transduction [26], sensitivity to food allergens [27], hearing [28], and chronic pain syndromes [18].

We hypothesized that the conserved cellular danger response (CDR) coordinates the metabolic responses to intracellular pathogens [17] and NRF2-coordinated electrophilic chemical stress [29]. In the MIA model of ASD, adult females are exposed to a simulated viral infection by injection of a synthetic, double strand RNA poly(Inosine:Cytosine) (poly(IC)) at vulnerable times during pregnancy. This produces offspring with neurodevelopmental abnormalities associated with both ASD [30] and schizophrenia [31]. Injected poly(IC) RNA is not replicated, but is recognized by the antiviral response machinery within the cell. Poly(IC) binds to TLR3, the dsRNA-activated protein kinase (PKR), and other proteins, activates the cellular danger response, inhibits the translation of cap-dependent mRNAs, and stimulates IL1β, IL6, TNFα, and the type I interferons (IFNα and IFNβ). Poly(IC) exposure produces self-limited sickness behavior that is characterized by initial fever then hypothermia, decreased activity, reduced food and water intake, weight loss, and spontaneous recovery in about 24 hours [32].

We tested the hypothesis that the cell danger response (CDR) is sustained by hyperpurinergia. Suramin is a well-known and well-studied competitive inhibitor of purinergic signaling [33]. It has been used medically for the treatment of African Sleeping Sickness (Trypanosomiasis) since shortly after it was first synthesized in 1916. Its antipurinergic actions were discovered in 1988, after a search for inhibitors of ATP-mediated P2X and P2Y signaling [34]. We used suramin to test the role of purinergic signaling in the maternal immune activation (MIA) model of autism-like behaviors in C57BL/6J mice. In this study, we report for the first time the functional correction of both the core behavioral symptoms and multi-system comorbidities of the MIA model of autism spectrum disorders using a single drug that inhibits purinergic signaling. A total of 16 multisystem features of this model were either corrected or improved by suramin treatment (summarized in Table 1).

Materials and Methods

Animals and Husbandry

All studies were conducted at the University of California, San Diego (UCSD) in facilities accredited by the Association for Assessment and Accreditation of Laboratory Animal Care International (AAALAC) under UCSD Institutional Animal Care and Use Committee (IACUC)-approved animal subjects protocols. Six to 8-week old C57BL/6J (strain# 000664) mice were obtained from Jackson Laboratories (Bar Harbor, ME) and maintained on *ad libitum* Harlan Teklad 8604 mouse chow (14% fat, 54% carbohydrate, 32% protein) and water. Animals were housed in a temperature (22–24°C) and humidity (40–55%) controlled vivarium with a 12 h light-dark cycle (lights on at 7 AM). Two different protocols were used to produce the MIA model. In the first cohort, primiparous dams (experienced mothers) were mated at 12–14 weeks of age. Experienced sires were 4 months old. Seventy-five (75) offspring were studied from cohort 1. We used a higher-dose, two-dose protocol in the second cohort. In the second cohort, nulliparous dams were mated at 9–10 weeks of age and the sires were also 9–10 weeks of age. Ninety-three (93) offspring were studied from cohort 2. Behavioral and endocrine results from cohort 2 males are reported in Figures 1, 2, and 3. Brain biochemistry and synaptosome studies from cohort 1 males are reported in Figures 4, 5, 6, 7, 8, and 9. Brain cerebellar Purkinje cell results from cohort 2 males are reported in Figure 10. Temperature data from cohort 1 males and females appears in Table S1. Females generally displayed fewer and milder abnormalities than males in the poly(IC) MIA model (Figure S4). The results from long-term temperature measurements in females are reported in Figures 2B and 2C. Additional studies in both cohorts and both sexes are reported in the supporting online material (Tables S1, S2, and S3, and Figures S1, S2, S3, and S4). A total of 168 mice (86 males and 82 females) were studied.

Poly(IC) Preparation and Gestational Exposure

To initiate the maternal immune activation (MIA) model pregnant dams received either a single intraperitoneal (ip) injection of Poly(I:C) (Potassium salt; Sigma-Aldrich Cat# P9582; >99% pure; <1% mononucleotide content) of 0.17 A260 U/g; 2 mg/kg ip on E12.5 (cohort 1), or two doses (0.25 U/g [3 mg/kg] on E12.5 and 0.125 U/g [1.5 mg/kg] on E17.5) in cohort 2. This 2-dose poly(IC) regimen resulted in reduced fecundity of 40% (8 liveborn litters in 20 pregnancies; 95% CI = 19–64%) associated with fetal resorption after E12.5. Control animals injected with saline had a fecundity of 80% (8 liveborn litters in 10 pregnancies; 95% CI = 44–97%). There were no differences in liveborn litter size between saline and poly(IC)-injected pregnancies, which was 8.3+/−1.5 for 12–14 week-old primiparous dams, and 5.6+/−0.8 for 9–10 week-old nulliparous dams. P9582 vials contained nominally 50 mg of total solids (45 mg of PBS salts) and 5 mg of K-Poly(I:C) lyophilized from 5 ml of PBS—hereafter referred to as a 50/5 vial. The contents of a 50/5 vial were reconstituted in 5 ml of sterile, nuclease-free water to yield an isotonic solution. Triplicate 5 µl samples of this solution were diluted 1:200 in 1 ml of water and measured spectrophotometrically at 260 nm and 280 nm. A typical 50/5 vial contained 450 U of Poly(IC), and

Table 1. Summary of Antipurinergic Therapy Results in the Poly(IC) Mouse Model of Autism Spectrum Disorders.

Feature	Abnormality in Males	Response to Antipurinergic Therapy
Social Preference	Decreased	Normalized ($p<0.05$)
Sensorimotor Coordination (Rotarod)	Decreased	Normalized ($p<0.001$)
Basal Body Temperature	Decreased	Normalized ($p<0.001$)
Oxygen Consumption During Sleep	Unchanged*	Increased ($p<0.001$)
Plasma Immunoglobulins	Unchanged*	Increased ($p<0.05$)
Plasma Corticosterone	Unchanged*	Increased ($p<0.03$)
Synaptosomal Structure by Electron Microscopy	Fragile and malformed post-synaptic densities; Accumulation of electron dense material	Normalized
Cerebral Mitochondrial Respiratory Chain Complex I Activity	Increased	Normalized ($p<0.02$)
Cerebral Mitochondrial Respiratory Chain Complex IV Activity	Increased	Normalized ($p<0.02$)
Synaptosomal Purinergic Receptor (P2Y2) Expression	Decreased	Normalized ($p<0.02$)
Synaptosomal Purinergic Receptor (P2X7) Expression	Decreased	Normalized ($p<0.02$)
Synaptosomal ERK1/2 Phosphorylation	Decreased	Normalized ($p<0.001$)
Synaptosomal CAMKII Phosphorylation	Decreased	Normalized ($p<0.001$)
Synaptosomal FMRP Expression	Decreased	Normalized ($p<0.02$)
Synaptosomal Nictotinic Acetylcholine Receptor subunit α7 Expression	Unchanged*	Increased ($p<0.001$)
Cerebellar Vermis Lobule VII Purkinje Cell Number	Decreased	Preserved ($p<0.05$)

*Unchanged at 4 months of age in the sham-treated poly(IC) mice, but increased therapeutically by suramin.
doi:10.1371/journal.pone.0057380.t001

had an A260/A280 ratio of 1.65. The stock solution was then further diluted with a sufficient volume of 0.15M NaCl to produce an isotonic solution that was 50 A260 Units/ml. Using this concentration, a dose of 0.25 U/g is achieved using a volume of 5 μl/g, or 125 μl in a typical 25 g pregnant female.

Postnatal Handling and Antipurinergic Therapy

Offspring of timed matings were weaned at 3–4 weeks of age into cages of 2–4 animals. No mice were housed in isolation. Littermates were identified by ear tags and distributed into different cages in order to minimize litter and dam effects. At 6-weeks of age, half the animals received a weekly injection of either saline (5 μl/g ip) or suramin (hexasodium salt, 10 or 20 mg/kg ip; Tocris Cat #1472). Beginning at 8-weeks of age all animals were evaluated by a series of test paradigms described below. At 16 weeks of age, male animals were sacrificed for synaptosome isolation, mitochondrial studies, hematology, blood chemistry, neuropathology, and immunohistochemical evaluation. Females from cohort 2 were followed for 8 months to monitor basal body temperatures and response to withdrawal of suramin treatment (Figs. 2B and 2C).

Body Temperature Measurements

A BAT-12 Microprobe digital thermometer and RET-3 mouse rectal probe (Physitemp Instruments, Clifton, New Jersey) were used to obtain rectal core temperatures to a precision of +/− 0.1°C. The probe was alcohol-cleaned, dipped in olive oil, then gently inserted 2 cm into the rectum for 10 seconds to achieve temperature and signal stability. Care was taken to avoid animal transport stress immediately prior to measurement in order to avoid stress-induced hyperthermia [35]. Temperatures were measured between 9 am to 12 noon each day.

Locomotor Activity

Locomotor activity was tested in a brief open field test for 10 min in the light to assess anxiety-like behavior and subsequently in the mouse behavioral pattern monitor (mBPM) for 30 min in the dark to assess exploratory behavior and locomotor activity. Observers were blinded to treatment groups.

Social Preference

Social preference was tested using a three-chambered box similar to what has been previously described [36]. Briefly, a Plexiglas box (60 cm L×60 cm W×30 cm H) was divided into 3 equal compartments by Plexiglas partitions containing an opening through which the mice could freely enter the 3 chambers. All testing was performed between the hours of 8 am and 1 pm. The test was conducted in two 10-minute phases. In phase I, the test mouse was first allowed to explore the chambers for 10 minutes. Each of the two outer chambers contained an empty, inverted stainless steel wire cup (Galaxy Cup, Spectrum Diversified Designs, Inc., Streetsboro, OH). In phase II, the test mouse was briefly removed, an unfamiliar mouse, age and sex matched, was placed under one of the wire cups and Lego blocks were placed under the other wire cup. The test mouse was then gently placed back in the arena and given an additional 10 minutes to explore. Room lighting for social behavior studies was 1–2 lux. An overhead camera and Ethovision v3 video tracking software (Noldus, Leesburg VA) were used to record the amount of time spent in each chamber and the number of entries into each chamber. In addition, a human observer, blinded to the treatment groups, scored time spent sniffing each wire cage, using a computer keypad. Stranger mice were used up to 4 times before new strangers were cycled in. The location (left or right) of the novel object and novel mouse alternated across subjects. Hand-

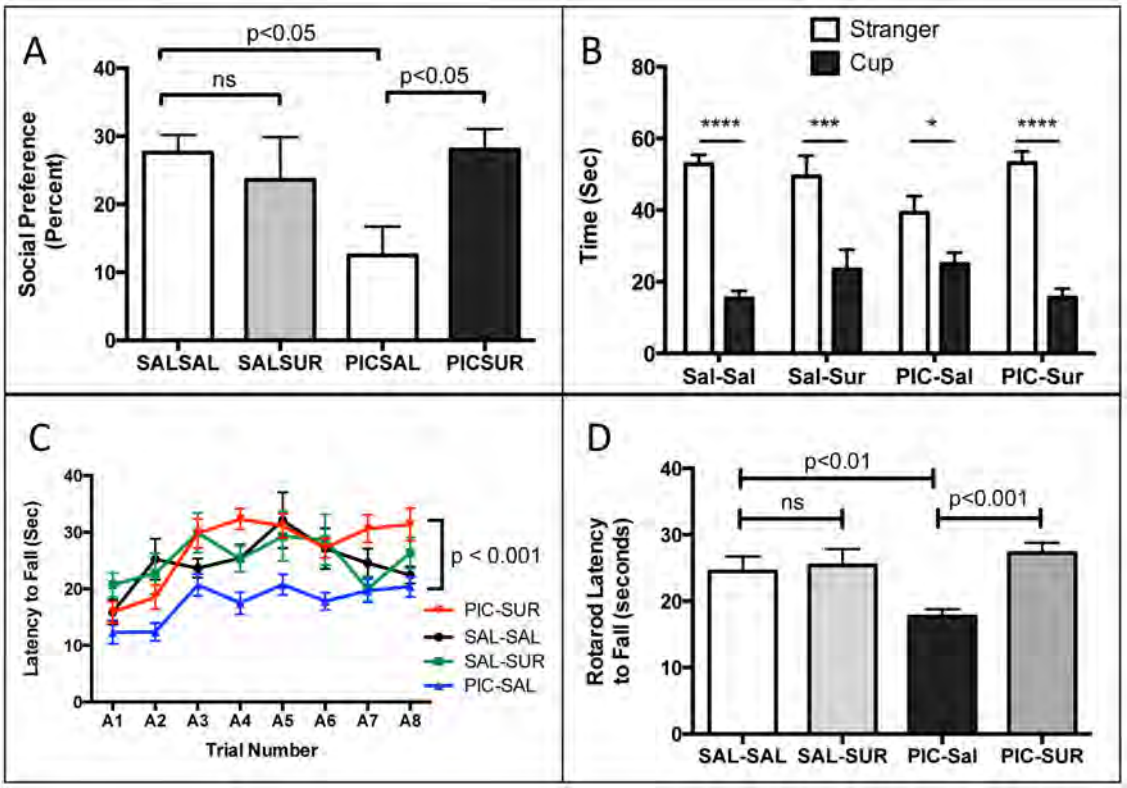

Figure 1. Correction of the Core Behavioral Features of the Maternal Immune Activation (MIA) Mouse Model of Autism Spectrum Disorders (ASD). (A) Social Preference. MIA males had a 54% decrease in social preference compared to controls (PIC-Sal 12.5+/−4.2% vs Sal-Sal 27.6+/−2.6%; one-way ANOVA $F(3,42) = 3.74$; with Newman-Keuls post-hoc testing; n = 9–15 males per group; age = 10-weeks; $p<0.02$). This was corrected by suramin treatment (PIC-Sur 28.1% vs Sal-Sal 27.6%; p = ns). (B) Social Preference as the time spent with stranger mouse vs. inanimate cup from 0–5 minutes. Analyzed by 2-Way ANOVA with Bonferroni pair-wise post testing (*$p<0.05$; ***$p<0.001$; ****$p<0.0001$). Treatment with suramin had little effect on normal behavior (Sal-Sal vs Sal-Sur), but a strong effect in improving social behavior in the MIA group (PIC-Sal vs. PIC-Sur). Zone x treatment interaction $F(3,43) = 3.72$; $p<0.05$; n = 9–15 males per group; age = 10-weeks. (C) Rotarod Training Curves. MIA (PIC-Sal) animals displayed deficits that were corrected by suramin treatment. Analyzed by repeated measures ANOVA with Tukey post testing: Sal-Sal vs. PIC-Sal $q = 6.749$, $p<0.01$; PIC-Sal vs PIC-Sur $q = 11.13$, $p<0.001$; n = 9–16 males per group; age = 11-weeks. (D) Rotarod Sensorimotor Coordination. MIA animals had a 28% decrease in sensorimotor coordination as measured by latency to fall by rotarod testing (PIC-Sal = 17.7+/−1.6 sec vs Sal-Sal = 24.5+/−2.2 sec; one-way ANOVA $F(3,46) = 7.08$; n = 9–16 males per group; age = 11-weeks; $p<0.001$). This was corrected by suramin treatment (PIC-Sur 27.2+/−1.6 sec vs Sal-Sal 24.5+/−2.2 sec; p = ns). Values are expressed as mean +/− SEM.
doi:10.1371/journal.pone.0057380.g001

scored times (seconds) with stranger and object were more sensitive than computer-calculated zone times (data not shown). Social preference (SP) in percent was calculated as 100 multiplied by the hand-scored time spent interacting with the stranger mouse (t_M) divided by the sum of the time with stranger plus time with object (t_M+t_L) minus 50: $SP = 100\times[t_M/(t_M+t_L)]-50$. Total times spent interacting with stranger and Lego cup, as quantified by blinded observer, are presented in Figure 1B. Hand-scored and machine-scored results were similar (Figure S3).

Rotarod

Training and testing were performed between the hours of 8 am and 1 pm using an accelerating rotarod protocol (Economex Rotarod, Columbus Instruments fitted with a 4 cm diameter spindle fitted with gray plastic, grooved walking surface) as previously described [37], with the following modifications. Prior to testing on an accelerating rod, mice were first trained at a fixed speed of 4 rpm. Each mouse was given up to 3 consecutive trials to achieve the endpoint of maintaining balance on the rotarod for at least 30 seconds. If a mouse was unsuccessful in the first 3 attempts, it was rested for 30 minutes, and then given another 3 attempts. Using this training protocol, all of the mice successfully maintained balance for 30 seconds within 2 training sessions. The acceleration phase testing was conducted over the subsequent 2 days, with 4 trials per day. Each mouse was individually placed on the rotarod at 4 rpm, which was then accelerated from 4 to 40 rpm over 5 minutes. The inter-trial time between repeat tests was 45 minutes. Latency to fall was recorded in seconds. Rotarod room lighting was 20–22 lux.

Plasma Immunoglobulins, and Corticosterone

Whole blood (100–200 µl) was collected at 15 weeks of age, for immunoglobulin and corticosterone measurements by submandibular venous lancet (Goldenrod 5 mm) into heparinized or EDTA anticoagulated 0.3 ml Microtainer tubes (Becton-Dickinson). Blood draws were performed between the hours of 9 am and 1 pm to avoid known circadian variations in corticosterone and certain cytokines such as IL6. Plasma was separated by centrifugation at 1500 g×5 min and frozen at −80°C until use. Plasma immunoglobulins, albumin, and total protein were performed by the UCSD Animal Care Program Diagnostic Laboratory. Plasma concentrations of corticosterone were measured by ^{125}I double antibody radioimmunoassay using 10 µl of plasma diluted 1:200 with assay buffer (MP Biomedicals LLC,

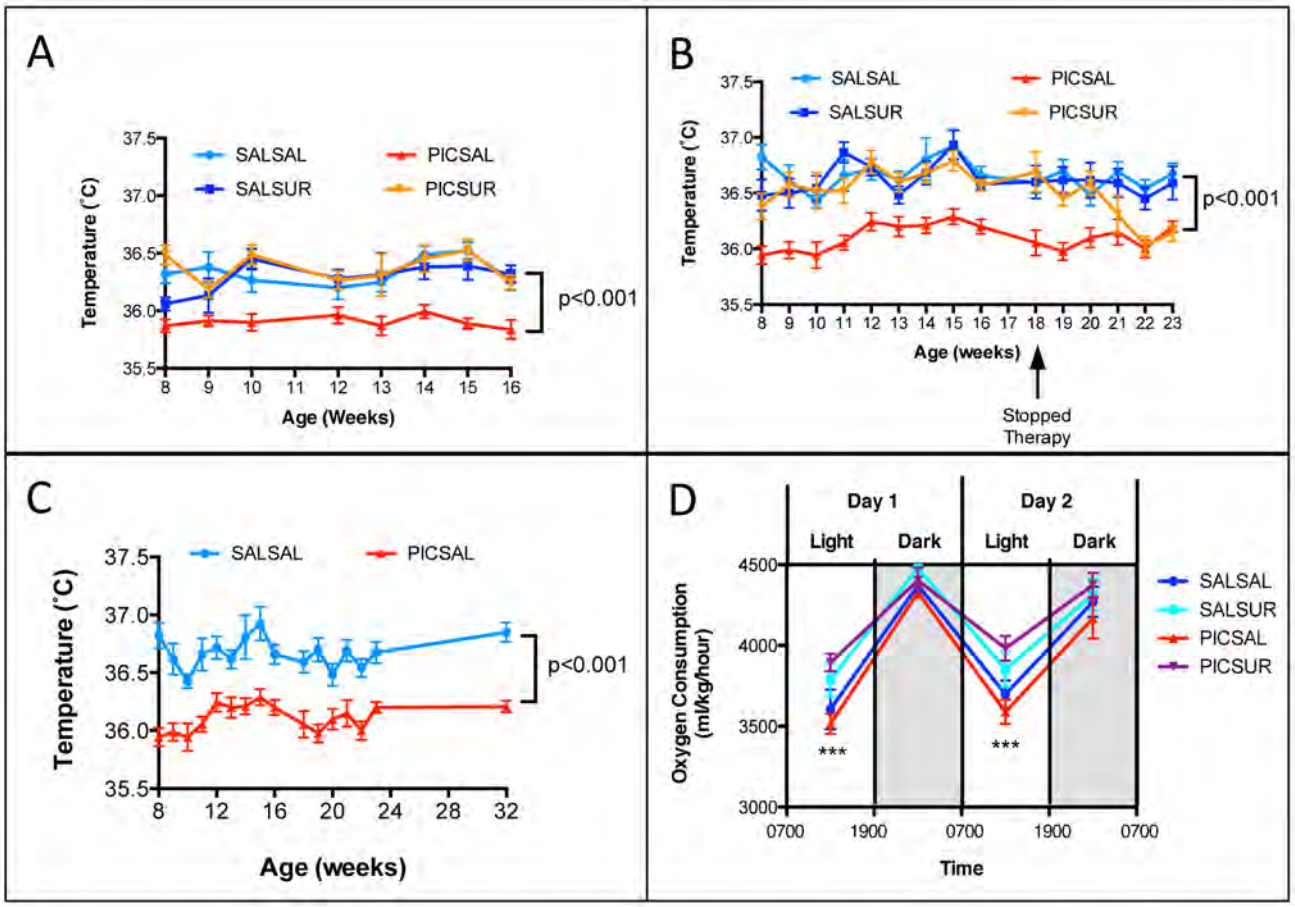

Figure 2. Relative Hypothermia Was Corrected, and Aerobic Metabolism was Increased by Antipurinergic Therapy. (A) Relative Hypothermia in the MIA Model was Corrected by Antipurinergic Therapy. (Linear mixed effects model analysis; F(1,47) = 25.3; n = 9–16 males per group; ages 8–16 weeks; $p<0.001$) (B) Correction of the Relative Hypothermia Was Lost After Discontinuing Antipurinergic Therapy. Weekly injections of suramin were discontinued in females at 18 weeks of age (PIC-SUR group; orange line, inverted triangles). By 22 weeks, hypothermia in the MIA animals returned to the untreated level approximately 0.5° below normal. (F(1,39) = 43.7; n = 9–16 females per group; $p<0.001$). (C) Relative Hypothermia is a Long-term Feature of the Poly(IC) MIA Model. Hypothermia persisted for at least 8 months of age (linear mixed effects model analysis F(1,19) = 114; n = 9–12 females per group; $p<0.001$). (D) Aerobic Metabolism. Oxygen consumption in the MIA animals showed a trend toward being decreased in both sleep (light) and active (dark) cycles. Suramin treatment increased sleep cycle oxygen consumption by 11%; MIA = PIC-Sal VO_2 = 3552+/−47.6 ml/kg/hour; Treated MIA = PIC-Sur = 3938+/−45.9 (one-way ANOVA F(3,44) = 8.0; n = 6 males per group; age = 14 weeks; p = 0.0002). Antipurinergic therapy had no significant effect on oxygen consumption in the control animals; Saline-treated Controls = Sal-Sal VO_2 = 3652+/−72.8; Treated Controls = Sal-Sur = 3821+/−71.5 (n = 6 males per group; p = 0.11). Values are expressed as mean +/− SEM.
doi:10.1371/journal.pone.0057380.g002

Orangeburg, NY). The intraassay coefficient of variation (CV) was 4% with an interassay CV of 7%.

Comprehensive Metabolic Evaluations

Comprehensive Lab Animal Monitoring System (CLAMS, Columbus Instruments) cages were used to measure individual consumption rates of oxygen (VO_2) and production rates of carbon dioxide (VCO_2). The ratio of VCO_2/VO_2 is the Respiratory Exchange Ratio (RER). The RER was used to estimate the relative proportions of fat and carbohydrate utilized by each mouse provided the same diet of ad libitum Teklad 8604 mouse chow. The RER was then applied to the volume of gases exchanged to calculate energy expenditure in calories. In addition to gas measurements, feeding, drinking and total locomotor activity were also simultaneously measured. All of these measurements were made every 13 minutes for 48 hours starting after a 12-hour acclimatization period. Results were analyzed for each 12-hour interval of active (dark) and inactive/sleep (light) phases. Weights were measured prior to, and on completion of the experiment. Experimental data were exported from Oxymax (Windows) to Microsoft Excel and analyzed in GraphPad Prism.

Synaptosome Isolation

Animals were sacrificed by cervical dislocation to prevent artifactual inhibition of mitochondrial function by all the known inhaled and injectable anesthetic agents. The brain was collected within 1 minute of sacrifice in 5 ml of ice cold BIOPS (K-MES 50 mM pH 7.1, Taurine 20 mM, Imidazole 20 mM, ATP 5.8 mM, $MgCl_2$ 6.6 mM, Na_2-Phosphocreatine 15 mM, DTT 0.5 mM K_2-EGTA 10 mM, $CaCO_3$ 2.8 mM; adjusted to pH 7.1). The wet weight was recorded to the nearest 0.1 mg. The right cerebri from two animals in the same treatment group were typically pooled and processed together. Nine volumes of BBG (0.32 M Sucrose, 1 mM K_2-EDTA, 10 mM Tris pH 7.4, 10 mM glucose) were added and the brain was homogenized in a cold Glass-Glass Dounce (Kontes) homogenizer with 7–10 strokes. The homogenate was centrifuged at 3100 g×3 min at 4°C in a fixed angle SS34 rotor. The supernatant (S1) was collected and the

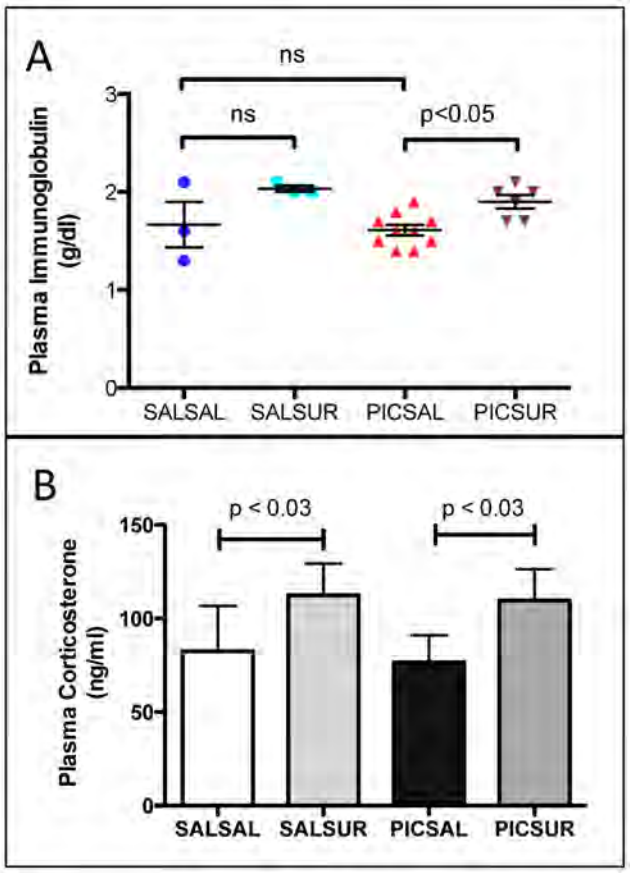

Figure 3. Plasma Immunoglobulins and Corticosterone. (A) Plasma immunoglobulins were increased 18% by antipurinergic therapy. (PIC-Sal = 1.6+/−0.05 mg/dl; PIC-Sur = 1.9+/−0.07 mg/dl; n = 6–10 males per group; age = 12 weeks; one-way ANOVA $F(3,37) = 5.72$; $p<0.05$) (B) Plasma corticosterone levels were increased 50% by weekly suramin treatment (PIC-Sal = 77+/−14 ng/ml; PIC-Sur = 117+/−16 ng/ml; two-way ANOVA $F(1,37) = 5.16$; $p = 0.03$; n = 8–12 males per group; age = 12 weeks). Values are expressed as mean +/− SEM.
doi:10.1371/journal.pone.0057380.g003

pellet (P1) was homogenized again in 5 volumes of BBG. The homogenate was centrifuged at 1000 g×3 min. The supernatant (S2) was pooled with S1 and centrifuged at 16,000 g×10 min. The resulting pellet was resuspended in 4 ml of 15% Percoll in BB (0.32 M Sucrose, 1 mM K_2-EDTA, 10 mM Tris pH 7.4). This suspension was carefully layered on a step gradient of 25% and 40% Percoll in BB (3.5 ml/each). The step gradient was centrifuged at 31,000 g×5 minutes at 4°C in a SS-34. Synaptosomes in band #2 at the 15%/25% Percoll interface were diluted with 10 volumes BB and centrifuged at 16,000 g×10 min. The pellet contained the synaptosomes. The synaptosomal pellet was resuspended in 5 volumes of SB (120 mM NaCl, 4.7 mM KCl, 2.2 mM $CaCl_2$, 1.2 mM $MgCl_2$, 25 mM HEPES, 1.2 mM $MgSO_4$, 1.2 mM KH_2PO_4, 10 mM glucose) and centrifuged at 16,000 g×10 min. This removed sucrose and EDTA, which can interfere with many mitochondrial assays. The washed synaptosomal pellet was resuspended in 2 tissue volumes of SB.

Synaptosome Electron Microscopy

Cerebral synaptosomes were drop dialyzed against water for 15 minutes, and 100 µg was pelleted by centrifugation at 16,000 g×10 minutes. Pellets were fixed in 3% glutaraldehyde in 0.1M cacodylate buffer, and after a brief wash, post fixed in 1% osmium tetroxide and subsequently dehydrated in graded ethanol series, treated in propylene oxide and embedded in EMbed 812/Araldite (Electron Microscopy Sciences, Hatfield PA). Thick sections (2 µm) were cut, mounted on glass slides and stained in toluidine blue for general assessment in the light microscope. Subsequently, 70 nm thin sections along the centrifugal gradient (from top to bottom of the pellet to assess for sedimentational sorting) were mounted on copper slot grids coated with parlodion and stained with uranyl acetate and lead citrate for examination at 80 kV on a Philips CM100 electron microscope (FEI, Hillsbrough OR). Images in tif format were documented using a Megaview III CCD camera (Olympus Soft Imaging Solutions, Lakewood CO).

Brain Neuropathology and Confocal Microscopy

Brains were removed after 4% paraformaldehyde (PFA) perfusion-fixation of 4–5 randomly selected animals per group, and post-fixed for 6–24 hours in 4% PFA in PBS. Para-sagittal sections of the cerebellar vermis (50 µm) were cut with a Vibratome (The Vibrotome Company, St. Louis). Floating sections were blocked in PBS containing 5% horse serum, 1% BSA, and 0.3% Triton X-100 for 1 hour at room temperature, and incubated overnight at 4°C with antibodies against calbindin (Swant, PO Box 327, CH-1723 Marly, Switzland CB-38a, 1:3000), and NeuN (Millipore,Temecula, MAB377, 1:1000). Sections were then washed and stained with secondary antibodies for 2 hour at room temperature (Alex488-conjugated antibody against rabbit and Alex568-conjugated antibody against mouse, Invitrogen). Immunostained slices were mounted on coverslips, and imaged on a dedicated Zeiss LSM510 confocal imaging system. Cerebellar Purkinje cells were identified by calbindin staining in green at the interface of the molecular and granular layers of the cerebellar folia. Granular layer neurons were identified by NeuN staining in red.

Western Blot Analysis

Ten µg of cerebral synaptosomal, or 2 µg of isolated mitochondrial protein was loaded in SDS-polyacrylamide gels (Bis-Tris Gels) and transferred to PVDF membranes. Blots were probed with primary antibodies overnight in cold room using anti-P2Y2 (#APR-010) and anti-P2X7 (#APR-004) antibodies from Alomone Labs (Jerusalem, Israel), anti-ERK1/2 (#4695), anti-phospho-Erk1/2 (Thr202/Tyr204) (#4370), anti-CAMKII (pan) (#4436), anti-phospho-CaMKII-Thr286 (#3361), anti-PSD95 (#3450) and anti-FMRP (#4317) antibodies from Cell Signaling (Danvers, MA, U.S.A.). Mitochondrial total OXPHOS antibody cocktail (#MS604) antibodies were purchased from MitoSciences (Eugene, Oregon, U.S.A.), anti-Citrate Synthetase (CS) (#ab96600) and anti-Nicotinic Acetylcholine Receptor α7 subunit (nAchRα7) (#ab23832) antibodies were purchased from Abcam (Cambridge, MA). After washing, the membranes were blotted with 1:5000 diluted second antibodies in 5% milk/PBST for 1 hour at room temperature (goat anti-rabbit (#31460) and anti-mouse (#31430) second antibodies from Pierce (Rockford, IL USA). The proteins of interest were visualized by ECL reagent (Pierce, Cat#32109) or Pierce SuperSignalTM West Femto Maximum Sensitivity Substrate (Cat #PI-34095) and the immunoblots were exposed to X-Omat Blue films (Kodak) and scanned (Epson Perfection 2450 scanner). Bands were quantified using ImageJ 1.43u software.

Respiratory Chain Enzymology

The enzymatic activity of mitochondrial complex I was measured as NADH:CoQ_1 oxidoreductase activity by the method

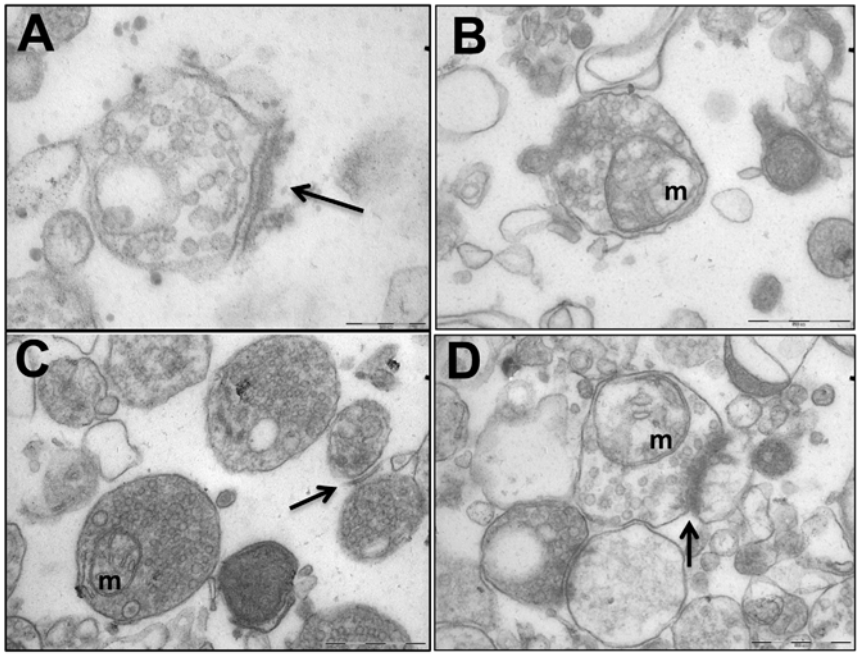

Figure 4. Cerebral Synaptosomal Ultrastructural Abnormalities Were Corrected by Antipurinergic Therapy. (A) Control (Sal-Sal) synaptosome illustrating normal post-synaptic density (PSD) morphology (arrow), and normal electron lucency of the matrix (92,000× magnification; scale bar = 200 μm). (B) Treated controls (Sal-Sur) with an included mitochondrion (''m''; scale bar = 500 μm). (C) Untreated MIA (PIC-Sal) with an included mitochondrion (''m'') and malformed, hypomorphic PSD (arrow; scale bar = 500 μm). Note the abnormal accumulation of electron-dense matrix material. (D) Treated MIA (PIC-Sur) with restoration of near-normal PSD morphology (arrow), an included mitochondrion (''m''), and reduction in abnormal accumulations of electron-dense matrix material within the synaptosomes (scale bar = 500 μm). Representative fields from n = 3–4 males per group; age = 16 weeks.
doi:10.1371/journal.pone.0057380.g004

of Hatefi [38]. Complex II was measured as succinate:CoQ_1 oxidoreductase activity by the method of Barrientos [39]. Complex II/III was measured as succinate: cytochrome c reductase activity by the method of Stumpf and Parks [40]. Complex III was measured as decyl-CoQ:cytochrome c reductase activity by the method of Barrientos [39] and expressed as a first order rate constant. Complex IV was measured as cytochrome c oxidase activity by the method of Wharton and Tzagoloff [41] and expressed as an apparent first order rate constant. Citrate synthase activity was used as a marker of mitochondrial mass and was measured by the method of Shepherd and Garland [42]. Rates were expressed as the ratio of respiratory chain enzyme activity to citrate synthase activity.

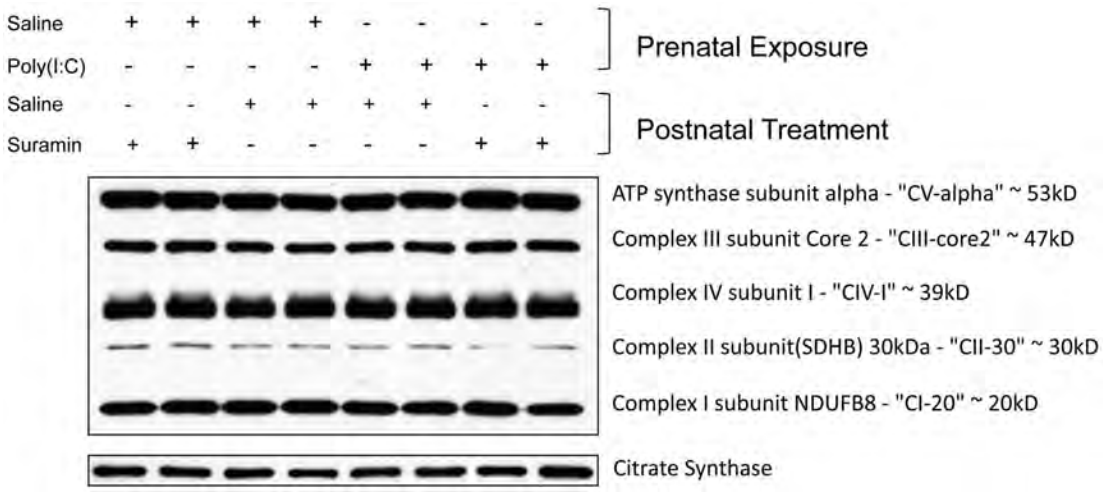

Figure 5. Cerebral Mitochondrial Respiratory Chain Subunit Mass was Unchanged in the MIA Model. Cerebral mitochondria were isolated by Percoll gradient centrifugation and quantified by Western Analysis. Each lane contains the mitochondria from 2–3 males isolated at 16-weeks of age (n = 4–5 per group).
doi:10.1371/journal.pone.0057380.g005

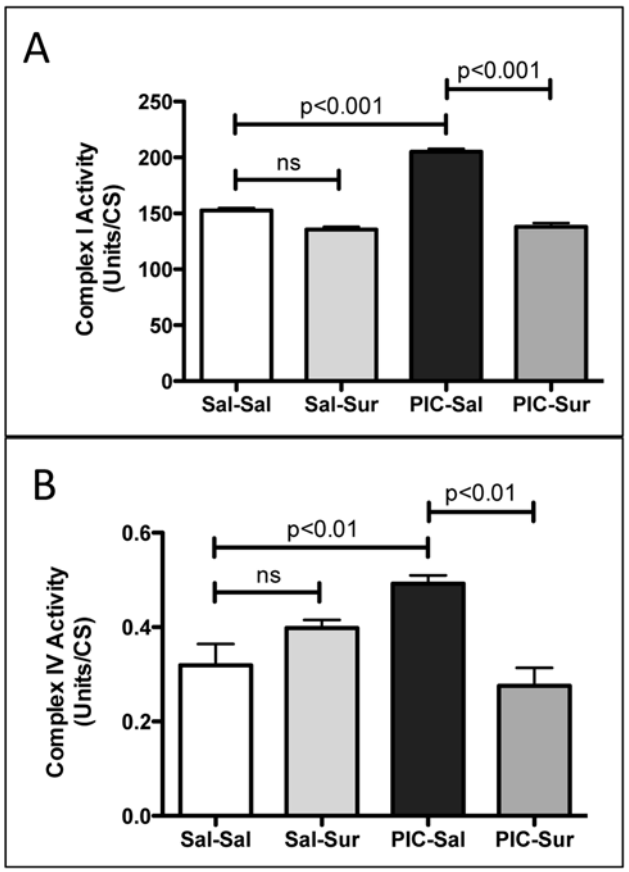

Figure 6. Cerebral Mitochondrial Respiratory Chain Hyperfunction Abnormalities Were Corrected by Antipurinergic Therapy. (A) Mitochondrial Respiratory Chain Complex I Enzymatic Activity was Increased 34% by gestational poly(IC) exposure and corrected by suramin treatment (Sal-Sal = 152+/−2.3 U/CS; PIC-Sal = 205+/−2.9 U/CS; one-way ANOVA F(3,12) = 137; $p<0.0001$; n = 4–5 males per group; age = 16 weeks). (B) Complex IV Activity was increased 53% by gestational poly(IC) exposure and corrected by suramin treatment (Sal-Sal = 0.319+/−0.045 U/CS; PIC-Sal = 0.492+/−0.018; one-way ANOVA F(3,12) = 8.9; p = 0.0022; n = 4–5 males per group; age = 16 weeks). Values are expressed as mean +/− SEM.
doi:10.1371/journal.pone.0057380.g006

Statistical analysis

Animals were randomized into active (suramin) and mock (saline) treatment groups upon weaning. Group means and standard error of the means (SEM) are reported. Data were analyzed using one-way ANOVA with treatment group as a between subject factor. One-way ANOVAs were used to test combined drug treatment and prenatal exposure effects on oxygen consumption and CO_2 production (GraphPad Prism 5.0 d). Specific post hoc comparisons between selected groups were done using Newman-Keuls method. Body temperatures were analyzed using a linear mixed effects model with time as a within subject factor (SPSS Version 20). Significance was set at $p<0.05$ and indicated numerically.

Results

Social Behavior

Male offspring exposed to poly(IC) *in utero* showed 54% reduction in social preference. This was corrected by antipurinergic therapy (Fig. 1A). Social deficits in the MIA females were milder and more variable than males in the two cohorts studied (Figure S4A). We focused on male ASD-like phenotypes in the remainder of this study. There were no effects of poly(IC) or suramin treatment on locomotor activity (data not shown).

Sensorimotor Coordination Deficits

Males also showed a 28% decrease in sensorimotor coordination as measured by latency to fall on rotarod testing. This was corrected by antipurinergic therapy (Fig. 1B). Female offspring born after the 2-dose poly(IC) protocol did not show significant rotarod abnormalities (Figure S4C).

Relative Hypothermia

Both male and female MIA animals showed relative hypothermia of about 0.5°C below the basal body temperature of controls that persisted for the life of the animals (Figs. 2A–C). The magnitude of this effect was similar in both males and females (Fig. 2A, 2B), and both cohorts (Tables S1 and S2). Normal basal body temperature was restored by antipurinergic therapy within as little as two weeks of starting therapy at 6 weeks of age in both males (Fig. 2A) and females (Fig. 2B; Tables S1 and S2). Antipurinergic therapy had no effect on the body temperature of control animals (Sal-Sur). When antipurinergic therapy was stopped at 18 weeks of age, MIA (PIC-Sur) animals reverted to their previous level of relative hypothermia (36.1°C+/−0.1°) within 1 month, while control animals maintained normothermia (36.6°C+/−0.1°) (Fig. 2B). Hypothermia resulting from gestational exposure to poly(IC) appears to be permanent unless treated with a purinergic antagonist. It has lasted for at least 8 months—the age of our oldest animals available for study (Fig. 2C).

Aerobic Metabolism

During the 12-hour period of light (7 am to 7 pm), during which the animals sleep, antipurinergic therapy increased the oxygen consumption of the MIA animals by 11% (Fig. 2D; Table S2). Antipurinergic therapy had no significant effect on oxygen consumption in the control animals (Fig. 2D). The CO_2 production rates were proportionately increased so that the respiratory exchange ratios were unchanged between groups within sleep and active cycles (Table S2). There were no differences between groups in body mass index (BMI = mass in grams ÷ anal-snout distance in cm^2), locomotor activity, weight gain, food, or water consumption during either light or dark phases. These results support the notion that antipurinergic therapy selectively increased aerobic (mitochondrial) metabolism and basal body temperature in MIA animals, and that these effects were greatest during sleep.

Plasma Immunoglobulins and Corticosterone

We measured plasma immunoglobulins because these are reduced in children with autism, and increased levels correlate with decreased symptom severity [6]. Plasma immunoglobulins were not different between control and MIA animals, although our statistical power was limited by having only 3 control (Sal-Sal) animals available for blood chemistries in this experiment. On the other hand, antipurinergic therapy increased plasma immunoglobulins by about 20% (Fig. 3A) and the ratio of globulin to total protein (Figure S1).

We measured plasma corticosterone levels because high-dose suramin (up to 200 mg/kg) used in cancer clinical trials can produce adrenocortical insufficiency [43]. Plasma corticosterone levels were increased in males by about 50% by the weekly, low-dose (10–20 mg/kg ip) suramin treatment used in our study

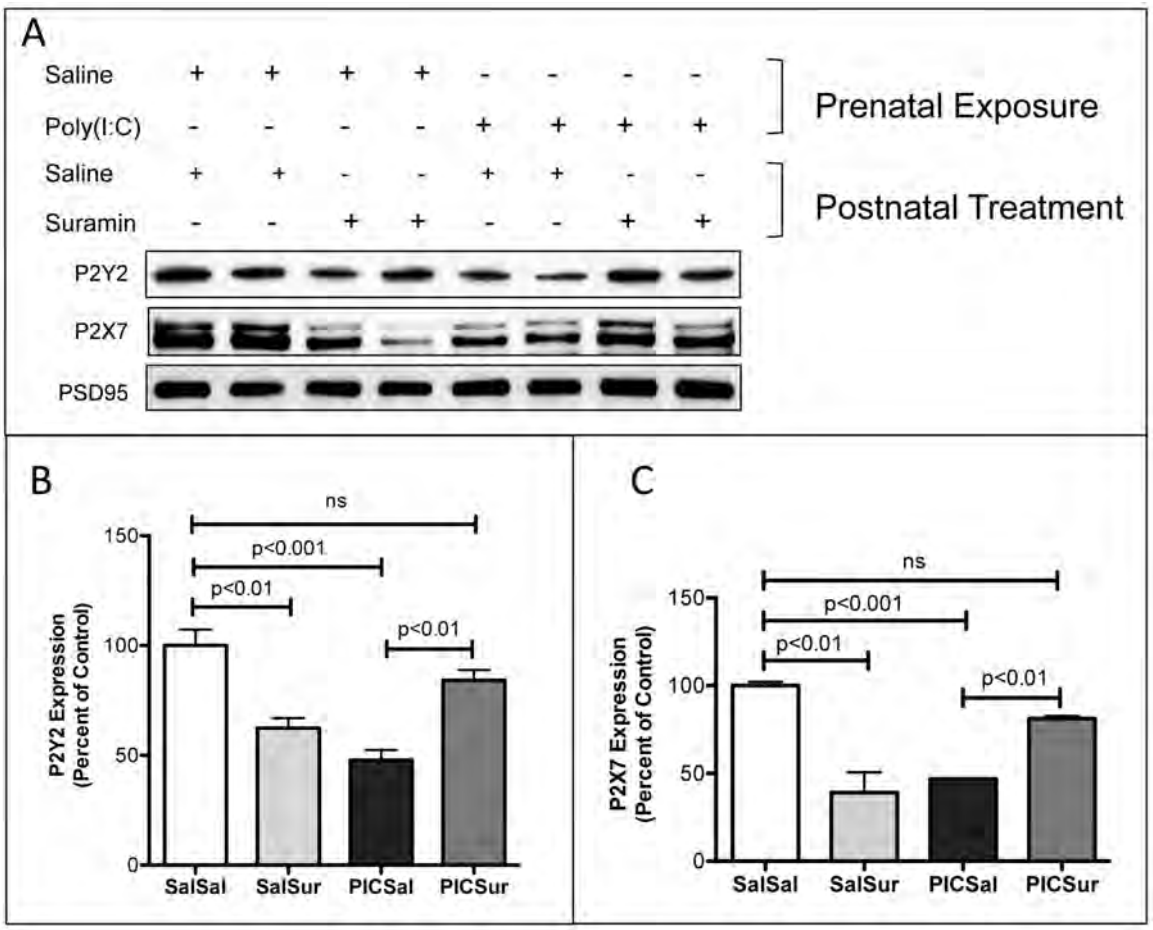

Figure 7. Cerebral Synaptosomal Purinergic Receptors were Downregulated in the MIA Model and Restored to Normal by Antipurinergic Therapy. (A) Western Analysis of Metabotropic P2Y2 and Ionotropic P2X7 receptors. Each lane contains the synaptosomes from 2–3 males isolated at 16-weeks of age (n = 4–5 per group). (B) P2Y2 receptor expression was decreased by over 50% by gestational poly(IC) exposure and normalized by suramin treatment (Sal-Sal = 100+/−7.3%; Sal-Sur = 62+/−4.6%; PIC-Sal = 48+/−4.7%; PIC-Sur = 84+/−4.7%; one-way ANOVA $F(3,12) = 18.1$; $p<0.0001$; n = 4–5 males per group). (C) P2X7 receptor expression was decreased over 50% by gestational poly(IC) exposure and normalized by suramin treatment (Sal-Sal = 100+/−2.2%; Sal-Sur = 39+/−12%; PIC-Sal = 47+/−0.5%; PIC-Sur = 81+/−1.5%; one-way ANOVA $F(3,12) = 23.2$; $p<0.0001$; n = 4–5 males per group). Post-synaptic density 95 (PSD95) protein was used as a loading control. Values are expressed as mean +/− SEM.
doi:10.1371/journal.pone.0057380.g007

(Fig. 3B). Basal plasma corticosterone levels were 2–3 fold higher in females (Figure S2A), but were not changed by suramin treatment (Figure S2B).

Synaptosomal Ultrastructural Abnormalities

Transmission electron microscopy of cerebral synaptosomes revealed significant differences between groups (Fig. 4). Control animals exhibited normally formed post-synaptic densities (PSDs) (arrow; Fig. 4A) and an electron-lucent synaptosomal matrix (Fig. 4A). Control animals receiving antipurinergic therapy were qualitatively similar to saline-treated controls (Fig. 4B). Striking differences were observed in the synaptosomes of the MIA animals. The large majority of synaptosomes contained an unidentified electron-dense matrix material (Fig. 4C) and the post-synaptic densities were fragile (easily disrupted during preparation), malformed, or both (arrow; Fig. 4C). Antipurinergic therapy of the MIA animals decreased the electron dense matrix material and restored more normal PSD architecture (arrow; Fig. 4D).

Cerebral Mitochondrial Respiratory Chain Biochemistry

Respiratory chain complexes I, III, and IV assemble to form a supercomplex in the brain and other tissues [44]. We purified cerebral mitochondria and found no change in the protein mass of the core subunits of complexes I, II, III, IV, and V measured by immunoblot analysis, or of the mass of the mitochondrial matrix marker citrate synthase (Fig. 5). In contrast, we found a 34% increase in the enzymatic activity of respiratory chain Complex I activity (NADH:CoQ1 oxidoreductase) (Fig. 6A) and a 53% increase in Complex IV activity (Cytochrome c Oxidase) (Fig. 6B). These mitochondrial respiratory chain hyperactivity abnormalities were corrected by antipurinergic therapy (Fig. 6A, 6B).

Synaptosomal Purinergic Receptors

Testing the hypothesis that purinergic signaling is chronically increased in the MIA model of ASD cannot be achieved by measuring tissue or plasma concentrations of nucleotides like ATP and ADP. The relevant concentration of nucleotides is confined to a thin shell, or pericellular halo, that defines the unstirred water layer (UWL) around the effector cells where receptors and their

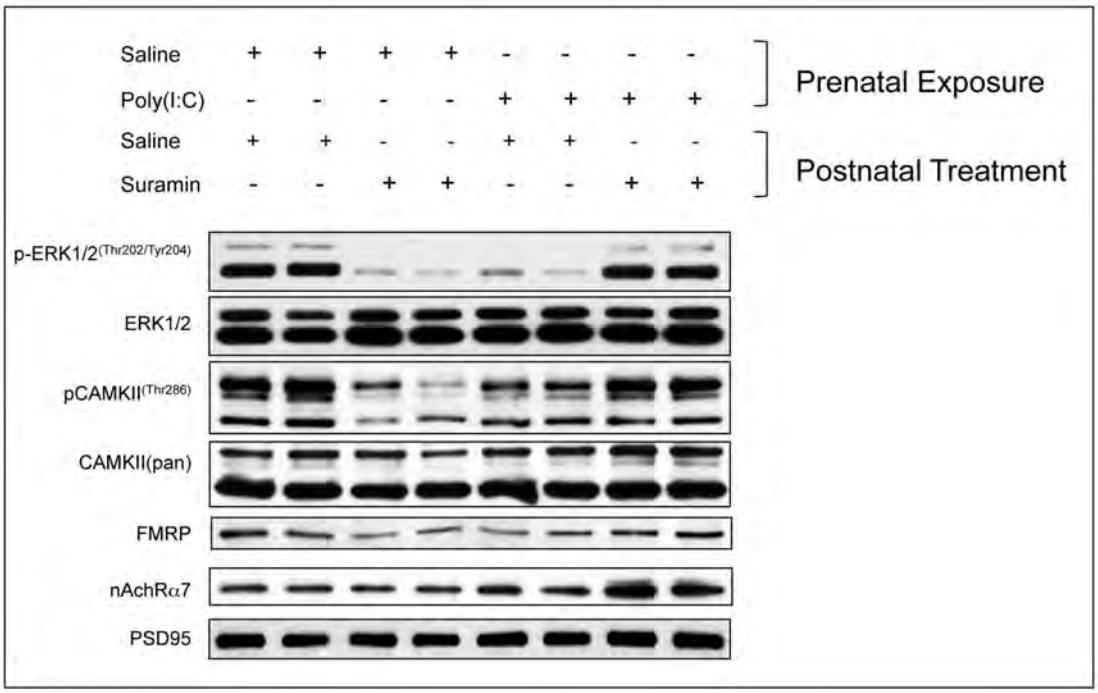

Figure 8. Cerebral Synaptosomal Hypophosphorylation of Extracellular Response Kinase 1 and 2 (ERK1/2), Calcium-Calmodulin Kinase II (CAMKII), and Downregulation Fragile X Protein (FMRP) in the MIA Model Were Corrected, and Nicotinic Acetylcholine Receptor subunit α7 (nAchRα7) Expression was Increased by Antipurinergic Therapy. (A) Western analysis of phosphorylated ERK1/2 (pERK1/2$^{Thr202/Tyr204}$), total ERK1/2, phosphorylated CAMKII (pCAMKII^{Thr286}), total CAMKII (CAMKIIpan), FMRP (Fragile X Syndrome protein), Nicotinic Acetylcholine Receptor subunit α7 (nAchRα7), and PSD95 (post-synaptic density protein 95) was used as a loading control for synaptosomes. Each lane contains the synaptosomes from 2–3 males isolated at 16-weeks of age (n = 4–5 per group).
doi:10.1371/journal.pone.0057380.g008

ligands meet. Concentrations of metabolites in the UWL can be 1000-fold higher than in plasma or interstitial fluid [45]. Hence, we selected purinergic receptor downregulation as a surrogate for chronic hyperpurinergia. Immunoblot analysis of cerebral synaptosomes showed 50–60% reduction in the expression of P2Y2, and P2X7 receptors in the MIA animals. These abnormalities were corrected by antipurinergic therapy (Fig. 7A–C).

We also noted downregulation of purinergic receptors in the synaptosomes of non-MIA control animals treated with suramin (SalSur; Fig. 7A–C). However, downregulation by chronic inhibition of purinergic signaling by suramin treatment alone did not produce any behavioral abnormalities in these control animals. The finding that antipurinergic therapy had opposite biochemical effects in healthy and ASD-like animals, and no behavioral effects in healthy animals, emphasizes the importance of more distal steps in the purinergic signaling cascade that are not addressed in this study. P2Y6 and the P1 adenosine receptors (A1, A2A, A2B, and A3) were not expressed at levels detectable by femto-ECL in cerebral synaptosomes (data not shown).

Synaptosomal ERK1/2 and CAMKII Signaling

We next quantified ERK1 and 2 and CAMKII phosphorylation because they are known effectors of P2Y2- and P2X7-mediated purinergic signaling [22,46]. We found a 90% reduction in the phosphorylation of ERK1 (MAPK3) and 2 (MAPK1), and a 50% reduction in the phosphorylation of calcium/calmodulin-dependent protein kinase II (CAMKII) (Fig. 8, 9A, 9B). These abnormalities were corrected by antipurinergic therapy. Treatment of non-MIA control animals with suramin also resulted in hypophosphorylation (SalSur; Fig. 8, 9A, 9B). This effect is opposite of the effect of suramin in MIA (PIC-Sur) animals. No behavioral changes or toxicities were observed in the control animals treated with suramin. This suggests that both the behavioral and biochemical responses to antipurinergic therapy were dependent on the physiologic state of the animal being treated.

Synaptosomal FMRP Deficits

We next tested our hypothesis that chronic innate immune activation by hyperpurinergia would result in the downregulation of the Fragile X Mental Retardation Protein (FMRP) to facilitate inflammatory cytokine expression. This occurs because FMRP inhibits the translation of many inflammatory cytokines through AU-rich elements (AREs) in the 3′-untranslated regions of their respective mRNAs [47], and must be downregulated to permit increased cytokine translation. We found that FMRP expression was decreased by nearly 50% in the MIA males and restored to normal with antipurinergic therapy (Fig. 8, 9C). Treatment of non-MIA control animals also decreased synaptosomal FMRP expression (SalSur; Fig. 8, 9C).

Synaptosomal nAchRα7 Expression

We tested the expression of the nicotinic acetylcholine receptor subunit α7 (nAchRα7) because of its role as an anti-inflammatory regulator of innate immunity [48] and its promise as a therapeutic target in schizophrenia and other disorders [49]. We found that nAchRα7 expression was not changed in untreated MIA animals (PIC-Sal; Fig. 8, 9D). However, suramin treatment of these animals increased the expression of this cholinergic receptor by over 75% (PIC-Sur; Fig. 9D).

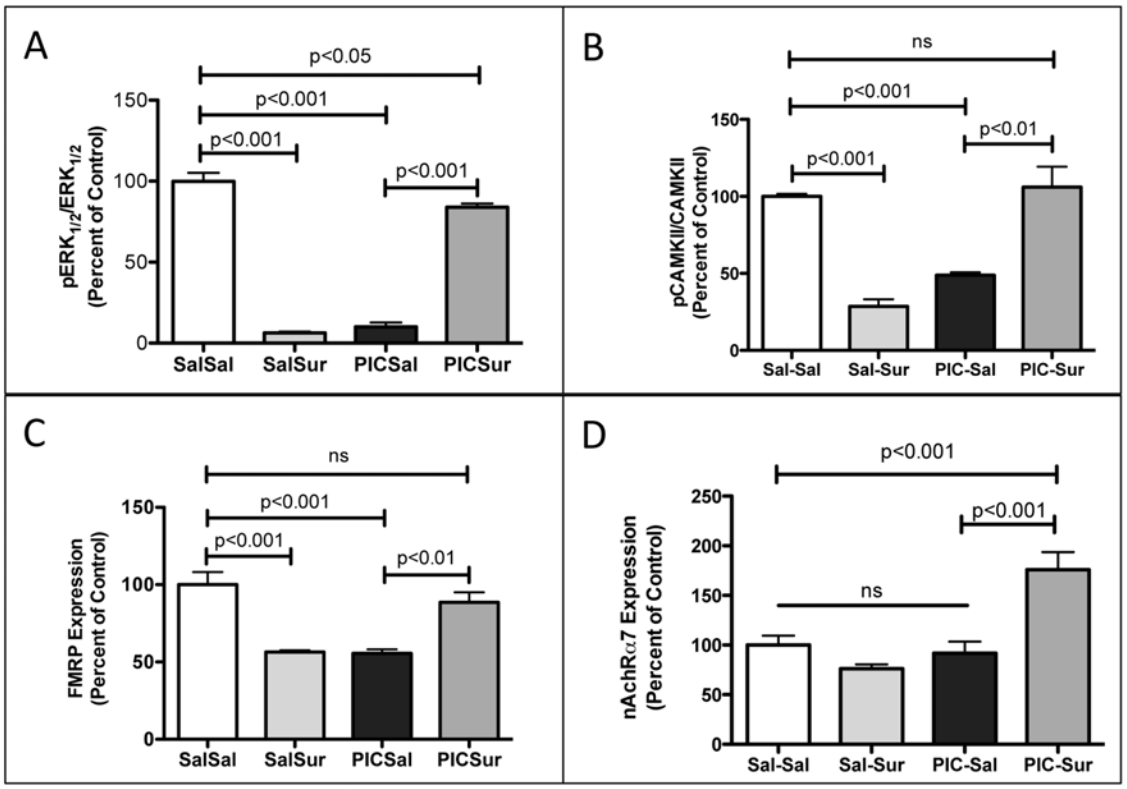

Figure 9. Quantitative Analysis of the Extracellular Response Kinase 1 and 2 (ERK1/2), Calcium-Calmodulin Kinase II (CAMKII), Fragile X Protein (FMRP), and the Nicotinic Acetylcholine Receptor subunit α7 (nAchRα7) in Cerebral Synaptosomes in the MIA Model. (A) ERK1 (MAPK3) and ERK2 (MAPK1) phosphorylation was decreased by over 90% by gestational poly(IC) exposure and normalized by suramin treatment (Sal-Sal = 100+/−5%; Sal-Sur = 6.2+/−0.8%; PIC-Sal = 9.9+/−2.6%; PIC-Sur = 84+/−2.3%; one-way ANOVA $F(3,12) = 241$; $p<0.0001$; n = 4–5 males per group; age = 16 weeks). (B) CAMKII phosphorylation was decreased by over 50% by gestational poly(IC) exposure and normalized by suramin treatment (Sal-Sal = 100+/−3%; Sal-Sur = 29+/−4.5%; PIC-Sal = 49+/−1.9%; PIC-Sur = 106+/−13%; one-way ANOVA $F(3,12) = 25$; $p<0.0001$; n = 4–5 males per group; age = 16 weeks). (C) Fragile X Mental Retardation Protein (FMRP) expression was decreased by over 40% by gestational poly(IC) exposure and normalized by suramin treatment (Sal-Sal = 100+/−8%; Sal-Sur = 56+/−1.2%; PIC-Sal = 55+/−2.5%; PIC-Sur = 89+/−6.5%; one-way ANOVA $F(3,12) = 17.7$; $p<0.0001$; n = 4–5 males per group; age = 16 weeks). (D) Nicotinic Acetylcholine Receptor subunit α7 (nAchRα7) expression was increased by over 75% by suramin treatment. (one-way ANOVA $F(3,12) = 14.1$; Sal-Sal = 100+/−9%; PIC-Sur = 176+/−18%; $p<0.001$; n = 4–5 males per group; age = 16 weeks; Newman-Keuls post test). Values are expressed as mean +/− SEM.
doi:10.1371/journal.pone.0057380.g009

Cerebellar Purkinje Cell Dropout

Some of the first structural brain abnormalities to be reported in autism were examples of volume loss in the brainstem and cerebellar vermis that was most significant in lobules VI and VII [12,50]. We wished to quantify cerebellar Purkinje cells in the MIA model because Purkinje cell dropout is a characteristic feature of certain primary mitochondrial disorders such as Alpers syndrome [51] and because Purkinje cell dropout in lobule VII of the cerebellar vermis is also a feature of decreased FMRP expression in Fragile X Syndrome [52] and in the MIA mouse model [53]. We found evidence of patchy Purkinje cell loss (Fig. 10A) that was marked in Lobule VII (Fig. 10B–D). Quantitative analysis showed a 63% loss of Purkinje cells in the MIA (PIC-Sal) ASD animals by 16-weeks of age (PIC-Sal; Fig. 10D). Antipurinergic therapy, starting at 6-weeks of age, prevented Purkinje cell loss measured at 4 months of age (PIC-Sur; Fig. 10D). This is consistent with the hypothesis that Purkinje cell survival and loss are occurring dynamically throughout the first few months of life in the MIA mouse model and that suramin treatment slows the rate of Purkinje cell loss.

Discussion

The purpose of our study was to test the role of purinergic signaling abnormalities in a mouse model of ASD, and to test a new approach to treatment that targeted these abnormalities. We did not start treatment until 6-weeks of age, near the onset of reproductive maturity in the mouse, because we wished to test the hypothesis that many of the autism-like features of the MIA model were treatable after they appear, and are not fixed. No animal model is a perfect surrogate for human autism. However, the maternal immune activation (MIA) model, using poly(IC) exposure to simulate a viral infection during pregnancy, has been used extensively over the past decade to study the detailed neurodevelopmental abnormalities associated with both ASD [30] and schizophrenia [31]. Maternal fever in humans is a known risk factor for ASD [54]. This mouse model can be adjusted in severity and character according to the dose of poly(IC) used, and the timing of exposure during pregnancy. In this report we used either one or two gestational exposures to poly(IC). The one-exposure paradigm of poly(IC) given on E12.5 produced biochemical and metabolic abnormalities, but weaker behavioral and sensorimotor coordination abnormalities. The two-exposure paradigm on E12.5 and E17.5 magnified these effects and permitted more in-depth

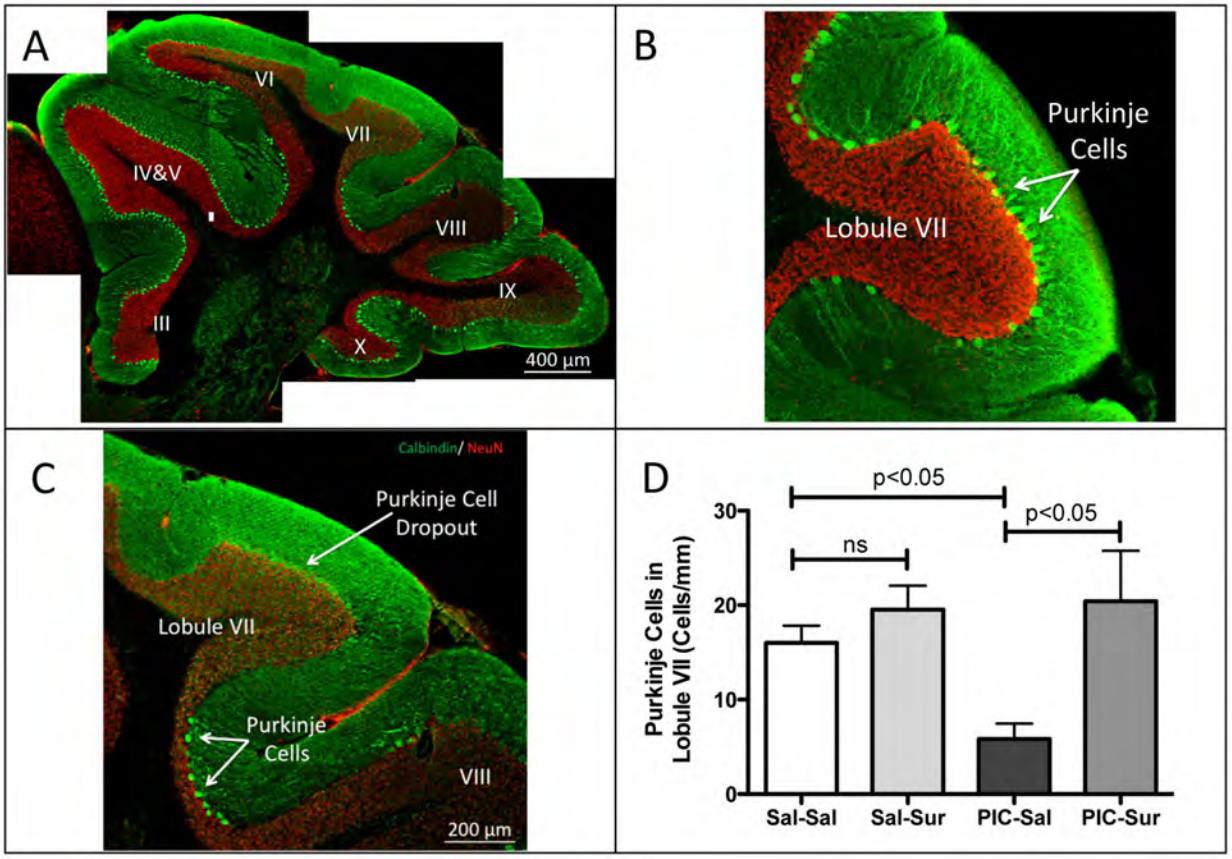

Figure 10. Purkinje Cell Dropout Was Prevented by Antipurinergic Therapy. (A) Mosaic reconstruction of a representative parasagittal section of the cerebellar vermis in an untreated MIA animal (PIC-Sal). Sections were stained for calbindin (green) and neuN (red). Purkinje cells are the bright, large neurons located at the margins of the molecular (green) and granular (red) layers of the cerebellum. Lobules III though X are indicated. MIA animals at 16 weeks of age, showed patchy loss of Purkinje cells that was most striking in lobules VI and VII. (B) Higher magnification of lobule VII in a control (Sal-Sal) animal illustrating normal Purkinje cell numbers. (C) Higher magnification of lobule VII in MIA illustrating nearly complete Purkinje cell dropout, with scattered cells at the boundary between lobules VII and VIII in an animal exposed to poly(IC) during gestation. (D) Quantitation of Lobule VII Purkinje Cells. Animals exposed to poly(IC) during gestation had a 63% reduction in Purkinje cell numbers. This was prevented by suramin treatment (10–20 mg/kg ip qWeek) started at 6 weeks of age (Sal-Sal = 16.0+/−1.8 cells/mm; Sal-Sur = 19.6+/−2.5; PIC-Sal = 5.8+/−1.6, PIC-Sur = 20.4+/−5.4; one-way ANOVA $F(3,13) = 5.3$; $p = 0.013$; Newman-Keuls post hoc test; n = 4–5 males per group; age = 16 weeks). Values are expressed as mean +/− SEM.
doi:10.1371/journal.pone.0057380.g010

analysis of the ASD-like features of the MIA model. We found that all the abnormalities that were produced by poly(IC) were corrected by treatment with suramin (Table 1).

Perhaps our most striking observation was the preservation of cerebellar Purkinje cells in lobule VII with antipurinergic therapy (Fig. 10). It has been shown that Purkinje cell loss is a consistent feature of the MIA mouse model of autism [53]. This is especially prominent in lobules VI and VII of the cerebellar vermis [53], and represents a strong point of shared biology between human ASD and the MIA model. One of the first structural brain abnormalities found in children with ASD was hypoplasia of the cerebellar vermis that preferentially affected lobules VI and VII [12]. This has also been documented in adults with Fragile X Syndrome [52]. Cerebellar Purkinje cells are large, fast-spiking (ca. 50 Hz), GABAergic, inhibitory neurons that are particularly sensitive to bioenergetic supply and demand problems, and to toxic exposures [55]. Our finding of preserved cerebellar Purkinje cell numbers at 16 weeks of age in the MIA model with antipurinergic therapy supports the notion that the rate of postnatal Purkinje cell loss is dynamic and can be regulated by environmental factors. In the MIA mouse model, antipurinergic therapy slows the rate of Purkinje cell loss from 6 to 16 weeks of age.

Like human autism spectrum disorders, the MIA mouse model of ASD has both core behavioral abnormalities, and multisystem comorbidities that emerge as a consequence of underlying metabolic disturbances. Our results support the paradigm that all of the observed metabolic disturbances in this model are a manifestation of the conserved cell danger response (CDR). The CDR therefore lies at or near the root cause of the neurodevelopmental and biochemical abnormalities that characterize the ASD-like features in this model. Extracellular ATP is a mitokine and well-known danger signal [19] that we hypothesized initiates and sustains the cellular danger response in autism spectrum disorders. In related studies we found that direct systemic injection of nucleotides like ATP and ADP caused rapid hypothermia by decreasing mitochondrial oxygen consumption and tissue oxygen demand (VO_2, data not shown). Hypothermia from systemic nucleotide injection has been studied in the fields of torpor and hibernation physiology [56]. We found that a convenient marker of the persistent cellular danger response in the poly(IC) model is relative hypothermia of about 0.5°C. Hypothermia was associated

with an increase in the maximal enzymatic rates, but not the mass, of brain mitochondrial respiratory chain complexes I and IV. Treatment with suramin decreased brain mitochondrial activity to normal, increased the whole body oxygen consumption (metabolic rate, VO_2) in the MIA animals, and increased the body temperature to normal (Fig. 2). The combination of higher mitochondrial electron transport activities measured *in vitro* and decreased basal oxygen consumption measured *in vivo* implies a novel increase in mitochondrial coupling efficiency and increased reserve capacity in ASD that is similar to that seen with exercise training [57]. We did not further investigate this phenomenon in this study.

Purinergic P2Y2 receptors and their phosphorylated effectors, ERK1/2 and CAMKII, are downregulated by chronic nucleotide stimulation in a process that leads to desensitization [58]. Our finding of downregulation of these purinergic receptors and their effectors is strong evidence for chronically elevated purinergic signaling in the poly(IC) model. Together, these findings are consistent with the notion that hyperpurinergia is a causal factor that initiates and maintains the cellular danger response in the MIA model of ASD. Suramin treatment corrected both the hyperpurinergia and the multisystem abnormalities in this model (Table 1).

We quantified the expression of the Fragile X protein (FMRP) in cerebral synaptosomes because deficiency is a cause of autism spectrum disorders, and normal expression inhibits the translation of several cytokines induced by innate immune activation [47]. Since innate immunity is persistently activated in the MIA model, we expected to find FMRP to be downregulated. We found that synaptosomal FMRP was decreased by about 50% in the MIA model and that antipurinergic therapy restored normal levels (Fig. 9C). This supports the notion that FMRP is downregulated as part of the multi-system abnormalities found in the MIA model even though the animals are not genetically deficient in the Fragile X (*FMR1*) gene. These observations are consistent with the hypothesis that FMRP down-regulation is part of the generalized cellular danger response produced by hyperpurinergia in this model of autism spectrum disorders.

Suramin treatment strongly increased the expression of the nicotinic acetylcholine receptor subunit α7 (nAchRα7) in cerebral synaptosomes of MIA animals, but had no effect on control animals (PIC-Sur v Sal-Sur; Figs. 8 and 9D). Since nAchRα7 expression was not diminished in sham-treated MIA animals, we concluded that a structural decrease in is not a core feature of pathogenesis in this model. However, since expression was increased nearly 100% by antipurinergic therapy, it appears that increased cholinergic signaling through the nAchRα7 receptor may be therapeutic in the MIA model of autism spectrum disorders. Cholinergic signaling through these receptors is a well-established antiinflammatory regulator of innate immunity in both the CNS [48] and periphery [59], and is dysregulated in human autism [60]. Antipurinergic therapy appears to provide a novel means for upregulating the expression of this receptor pharmacologically in disorders associated with innate immune dysregulation and inflammation.

Conclusions

Antipurinergic therapy with suramin corrected all of the core behavioral abnormalities and multisystem comorbidities that we observed in the MIA mouse model of autism spectrum disorders. The weight of the evidence from our study supports the notion that the efficacy of suramin springs from its antipurinergic properties, but additional studies will be required to prove this point. This study did not test the generality of purinergic signaling abnormalities in other animal models or in human ASD. Although our results are encouraging, we urge caution before extending our results to humans. Long-term therapy with suramin in children with autism is not an FDA-approved usage, and is not recommended because of potentially toxic side effects that can occur with prolonged treatment [61]. However, antipurinergic therapy in general offers a fresh new direction for research into the pathogenesis, and new drug development for the treatment of human autism and related spectrum disorders.

See *Supporting Information* for additional Tables and Figures.

Supporting Information

Figure S1 Plasma immunoglobulin to total protein ratios were increased by suramin treatment in males (Sal-Sal = 0.34+/−0.016; Sal-Sur = 0.40+/−0.01; PIC-Sal = 0.31+/−0.008; PIC-Sur = 0.38+/−0.01; one-way ANOVA $F(2,16) = 21.9$; $p<0.001$ Newman-Keuls post hoc test; n = 3–10 males per group). Values are expressed as mean +/− SEM.
(TIF)

Figure S2 Plasma Corticosterone. (A) Basal plasma corticosterone levels were higher in females than males ($Sal\text{-}Sal_{Males} = 73+/-23$ ng/ml; $Sal\text{-}Sal_{Females} = 245+/-29$ ng/ml; two-way ANOVA $F(1,1,1,34) = 40.21$; n = 7–12 males or females per group; $p<0.001$). (B) Corticosterone was unchanged in females by either poly(IC) exposure or suramin treatment (two-way ANOVA $F(1,37) = 0.11$ (interaction), 0.16 (suramin treatment), and 0.48 (poly(IC) exposure); $p = 0.74$; n = 7–11 females per group). Values are expressed as mean +/− SEM.
(TIF)

Figure S3 Comparison of Social Preference Methods. (A) Hand-Scored Social Preference was measured by a blinded human observer. Hand-scoring was more specific than machine (Ethovision 3) scoring because actual social interactions of nose-to-nose and nose-to-tail encounters can be distinguished from non-social, center-of-mass proximity to both stranger mouse and inanimate cup. Results are in time spent with stranger mouse vs. inanimate cup from 0–5 minutes. Analyzed by 2-Way ANOVA with Bonferroni pair-wise post testing (*$p<0.05$; ***$p<0.001$; ****$p<0.0001$). Treatment with suramin had little effect on normal behavior (Sal-Sal vs Sal-Sur), but a strong effect in improving social behavior in the MIA group (PIC-Sal vs. PIC-Sur). Zone x treatment interaction $F(3,43) = 3.72$; $p<0.05$; n = 9–15 males per group; age = 10-weeks. (B) Ethovision-Scored Zone Time. These results are in general agreement with the hand-scored results. However, the apparent variations are greater, limiting the statistical power of the machine-scored results. Zone x treatment interaction $F(3,43) = 1.96$; $p = 0.13$; N = 9–15 males per group; age = 10 weeks.
(TIF)

Figure S4 Females in the Poly(IC) MIA Model Showed Fewer and Milder Behavioral Symptoms than Males. (A) Social Preference. Females were less social and more variable in their behavior than age-matched males. The greater behavioral variability decreased statistical power in females, although the trends were similar to males. N = 9–16 males and 9–12 females per group; age = 10 weeks. (B) Rotarod Latency to Fall was decreased in Poly(IC) Males. N = 9–16 males per group; age = 11 weeks. (C) Rotarod Latency to Fall was Unchanged in Poly(IC) Females. N = 9–12 females per group; age = 11 weeks. Analysis was by 1-way ANOVA with Tukey post testing.
(TIF)

Table S1 Cohort 1 Basal Body Temperature at 16 weeks was Decreased in the MIA Model and Restored to Normal by Antipurinergic Therapy.
(TIF)

Table S2 Cohort 2 Basal Body Temperature from 8 to 16 weeks was Decreased in the MIA Model and Restored to Normal by Antipurinergic Therapy.
(TIF)

Table S3 Circadian Analysis of Basal Metabolic Rates, Motor Activity, and Feeding.
(TIF)

Acknowledgments

We thank Alan Turken and Richard Hauger for the plasma corticosterone assays, Malcolm Wood and the Core Microscopy Facility at The Scripps Research Institute, La Jolla CA, for performing the electron microscopy, and Cheryl Yost and Kent Osborn at the UCSD Animal Care Program Diagnostic Laboratory for performing the blood chemistries and CBCs. We thank Maya Shetreat-Klein, Leanne Chukoskie, Jeanne Townsend, William Nyhan, Richard Haas, Vickie Risbrough, Sophia Colamarino, and Steve Edelson for helpful discussions and comments on the manuscript. We thank Jung-Hyun Lee, Diana Lui, and Kamran Jamil for technical assistance.

Author Contributions

Conceived and designed the experiments: RKN JCN LLD SBP. Performed the experiments: RKN SBP ZZ LW TN JCN TPL MS MR QT. Analyzed the data: RKN SBP LLD ZZ LW TN JCN TPL MR QT. Contributed reagents/materials/analysis tools: RKN LLD SBP. Wrote the paper: RKN.

References

1. Kou Y, Betancur C, Xu H, Buxbaum JD, Ma'ayan A (2012) Network- and attribute-based classifiers can prioritize genes and pathways for autism spectrum disorders and intellectual disability. Am J Med Genet C Semin Med Genet 160C: 130–142.
2. Kohane IS, McMurry A, Weber G, Macfadden D, Rappaport L, et al. (2012) The co-morbidity burden of children and young adults with autism spectrum disorders. PLoS One 7: e33224.
3. Buie T, Fuchs GJ III, Furuta GT, Kooros K, Levy J, et al. (2010) Recommendations for evaluation and treatment of common gastrointestinal problems in children with ASDs. Pediatrics 125 Suppl 1: S19–29.
4. Mulder EJ, Anderson GM, Kema IP, de Bildt A, van Lang ND, et al. (2004) Platelet serotonin levels in pervasive developmental disorders and mental retardation: diagnostic group differences, within-group distribution, and behavioral correlates. J Am Acad Child Adolesc Psychiatry 43: 491–499.
5. Palmieri L, Papaleo V, Porcelli V, Scarcia P, Gaita L, et al. (2010) Altered calcium homeostasis in autism-spectrum disorders: evidence from biochemical and genetic studies of the mitochondrial aspartate/glutamate carrier AGC1. Mol Psychiatry 15: 38–52.
6. Heuer L, Ashwood P, Schauer J, Goines P, Krakowiak P, et al. (2008) Reduced levels of immunoglobulin in children with autism correlates with behavioral symptoms. Autism Res 1: 275–283.
7. Page T, Coleman M (2000) Purine metabolism abnormalities in a hyperuricosuric subclass of autism. Biochim Biophys Acta 1500: 291–296.
8. James SJ, Melnyk S, Jernigan S, Hubanks A, Rose S, et al. (2008) Abnormal transmethylation/transsulfuration metabolism and DNA hypomethylation among parents of children with autism. J Autism Dev Disord 38: 1966–1975.
9. Waring RH, Klovrza LV (2000) Sulphur metabolism in autism. Journal of Nutritional and Environmental Medicine (Abingdon) 10: 25–32.
10. James SJ, Melnyk S, Jernigan S, Hubanks A, Rose S, et al. (2008) Abnormal Transmethylation/transsulfuration Metabolism and DNA Hypomethylation Among Parents of Children with Autism. J Autism Dev Disord 38: 1976.
11. Vargas DL, Nascimbene C, Krishnan C, Zimmerman AW, Pardo CA (2005) Neuroglial activation and neuroinflammation in the brain of patients with autism. Ann Neurol 57: 67–81.
12. Courchesne E, Saitoh O, Yeung-Courchesne R, Press GA, Lincoln AJ, et al. (1994) Abnormality of cerebellar vermian lobules VI and VII in patients with infantile autism: identification of hypoplastic and hyperplastic subgroups with MR imaging. AJR Am J Roentgenol 162: 123–130.
13. Bailey A, Luthert P, Dean A, Harding B, Janota I, et al. (1998) A clinicopathological study of autism. Brain 121 (Pt 5): 889–905.
14. Jaeschke H, McGill MR, Ramachandran A (2012) Oxidant stress, mitochondria, and cell death mechanisms in drug-induced liver injury: lessons learned from acetaminophen hepatotoxicity. Drug Metab Rev 44: 88–106.
15. West AP, Shadel GS, Ghosh S (2011) Mitochondria in innate immune responses. Nat Rev Immunol 11: 389–402.
16. Zhou R, Yazdi AS, Menu P, Tschopp J (2011) A role for mitochondria in NLRP3 inflammasome activation. Nature 469: 221–225.
17. Tal MC, Iwasaki A (2011) Mitoxosome: a mitochondrial platform for cross-talk between cellular stress and antiviral signaling. Immunol Rev 243: 215–234.
18. Abbracchio MP, Burnstock G, Verkhratsky A, Zimmermann H (2009) Purinergic signalling in the nervous system: an overview. Trends Neurosci 32: 19–29.
19. Junger WG (2011) Immune cell regulation by autocrine purinergic signalling. Nat Rev Immunol 11: 201–212.
20. Zhang Q, Raoof M, Chen Y, Sumi Y, Sursal T, et al. (2010) Circulating mitochondrial DAMPs cause inflammatory responses to injury. Nature 464: 104–107.
21. Harada K, Hide I, Seki T, Tanaka S, Nakata Y, et al. (2011) Extracellular ATP differentially modulates Toll-like receptor 4-mediated cell survival and death of microglia. J Neurochem 116: 1138–1147.
22. Franke H, Sauer C, Rudolph C, Krugel U, Hengstler JG, et al. (2009) P2 receptor-mediated stimulation of the PI3-K/Akt-pathway in vivo. Glia 57: 1031–1045.
23. Pelegrin P (2008) Targeting interleukin-1 signaling in chronic inflammation: focus on P2X(7) receptor and Pannexin-1. Drug News Perspect 21: 424–433.
24. Gallego D, Vanden Berghe P, Farre R, Tack J, Jimenez M (2008) P2Y1 receptors mediate inhibitory neuromuscular transmission and enteric neuronal activation in small intestine. Neurogastroenterol Motil 20: 159–168.
25. Matos JE, Sorensen MV, Geyti CS, Robaye B, Boeynaems JM, et al. (2007) Distal colonic Na(+) absorption inhibited by luminal P2Y(2) receptors. Pflugers Arch 454: 977–987.
26. Surprenant A, North RA (2009) Signaling at purinergic P2X receptors. Annu Rev Physiol 71: 333–359.
27. Leng Y, Yamamoto T, Kadowaki M (2008) Alteration of cholinergic, purinergic and sensory neurotransmission in the mouse colon of food allergy model. Neurosci Lett 445: 195–198.
28. Housley GD, Jagger DJ, Greenwood D, Raybould NP, Salih SG, et al. (2002) Purinergic regulation of sound transduction and auditory neurotransmission. Audiol Neurootol 7: 55–61.
29. Speciale A, Chirafisi J, Saija A, Cimino F (2011) Nutritional antioxidants and adaptive cell responses: an update. Curr Mol Med 11: 770–789.
30. Patterson PH (2011) Modeling autistic features in animals. Pediatr Res 69: 34R–40R.
31. Bitanihirwe BK, Peleg-Raibstein D, Mouttet F, Feldon J, Meyer U (2010) Late prenatal immune activation in mice leads to behavioral and neurochemical abnormalities relevant to the negative symptoms of schizophrenia. Neuropsychopharmacology 35: 2462–2478.
32. Traynor TR, Majde JA, Bohnet SG, Krueger JM (2004) Intratracheal double-stranded RNA plus interferon-gamma: a model for analysis of the acute phase response to respiratory viral infections. Life Sci 74: 2563–2576.
33. Light AR, Wu Y, Hughen RW, Guthrie PB (2006) Purinergic receptors activating rapid intracellular Ca increases in microglia. Neuron Glia Biol 2: 125–138.
34. Dunn PM, Blakeley AG (1988) Suramin: a reversible P2-purinoceptor antagonist in the mouse vas deferens. Br J Pharmacol 93: 243–245.
35. Adriaan Bouwknecht J, Olivier B, Paylor RE (2007) The stress-induced hyperthermia paradigm as a physiological animal model for anxiety: a review of pharmacological and genetic studies in the mouse. Neurosci Biobehav Rev 31: 41–59.
36. Moy SS, Nadler JJ, Young NB, Nonneman RJ, Segall SK, et al. (2008) Social approach and repetitive behavior in eleven inbred mouse strains. Behav Brain Res 191: 118–129.
37. Pallier PN, Drew CJ, Morton AJ (2009) The detection and measurement of locomotor deficits in a transgenic mouse model of Huntington's disease are task- and protocol-dependent: influence of non-motor factors on locomotor function. Brain Res Bull 78: 347–355.
38. Hatefi Y (1978) Reconstitution of the electron-transport system of bovine heart mitochondria. Methods Enzymol 53: 48–54.
39. Barrientos A (2002) In vivo and in organello assessment of OXPHOS activities. Methods 26: 307–316.
40. Stumpf DA, Parks JK (1981) Human mitochondrial electron transport chain: assay of succinate: cytochrome c reductase in leukocytes, platelets and cultured fibroblasts. Biochem Med 25: 234–238.
41. Wharton DC, Tzagoloff A (1967) Cytochrome oxidase from beef heart. Methods Enzymol 10: 245–250.

42. Shepherd D, Garland PB (1969) Citrate synthase from rat liver. Methods in Enzymology 13: 11–16.
43. Kobayashi K, Weiss RE, Vogelzang NJ, Vokes EE, Janisch L, et al. (1996) Mineralocorticoid insufficiency due to suramin therapy. Cancer 78: 2411–2420.
44. Frenzel M, Rommelspacher H, Sugawa MD, Dencher NA (2010) Ageing alters the supramolecular architecture of OxPhos complexes in rat brain cortex. Exp Gerontol 45: 563–572.
45. Korjamo T, Heikkinen AT, Monkkonen J (2009) Analysis of unstirred water layer in in vitro permeability experiments. J Pharm Sci 98: 4469–4479.
46. Leon D, Hervas C, Miras-Portugal MT (2006) P2Y1 and P2X7 receptors induce calcium/calmodulin-dependent protein kinase II phosphorylation in cerebellar granule neurons. Eur J Neurosci 23: 2999–3013.
47. Khera TK, Dick AD, Nicholson LB (2010) Fragile X-related protein FXR1 controls post-transcriptional suppression of lipopolysaccharide-induced tumour necrosis factor-alpha production by transforming growth factor-beta1. FEBS J 277: 2754–2765.
48. Tracey KJ (2009) Reflex control of immunity. Nat Rev Immunol 9: 418–428.
49. Jones CK, Byun N, Bubser M (2012) Muscarinic and nicotinic acetylcholine receptor agonists and allosteric modulators for the treatment of schizophrenia. Neuropsychopharmacology 37: 16–42.
50. Hashimoto T, Tayama M, Murakawa K, Yoshimoto T, Miyazaki M, et al. (1995) Development of the brainstem and cerebellum in autistic patients. J Autism Dev Disord 25: 1–18.
51. Naviaux RK, Nyhan WL, Barshop BA, Poulton J, Markusic D, et al. (1999) Mitochondrial DNA polymerase gamma deficiency and mtDNA depletion in a child with Alpers' syndrome. Ann Neurol 45: 54–58.
52. Greco CM, Navarro CS, Hunsaker MR, Maezawa I, Shuler JF, et al. (2011) Neuropathologic features in the hippocampus and cerebellum of three older men with fragile X syndrome. Mol Autism 2: 2.
53. Shi L, Smith SE, Malkova N, Tse D, Su Y, et al. (2009) Activation of the maternal immune system alters cerebellar development in the offspring. Brain Behav Immun 23: 116–123.
54. Zerbo O, Iosif AM, Walker C, Ozonoff S, Hansen RL, et al. (2012) Is Maternal Influenza or Fever During Pregnancy Associated with Autism or Developmental Delays? Results from the CHARGE (CHildhood Autism Risks from Genetics and Environment) Study. J Autism Dev Disord.
55. Yang D, Kim KH, Phimister A, Bachstetter AD, Ward TR, et al. (2009) Developmental exposure to polychlorinated biphenyls interferes with experience-dependent dendritic plasticity and ryanodine receptor expression in weanling rats. Environ Health Perspect 117: 426–435.
56. Bouma HR, Verhaag EM, Otis JP, Heldmaier G, Swoap SJ, et al. (2012) Induction of torpor: mimicking natural metabolic suppression for biomedical applications. J Cell Physiol 227: 1285–1290.
57. Pesta D, Hoppel F, Macek C, Messner H, Faulhaber M, et al. (2011) Similar qualitative and quantitative changes of mitochondrial respiration following strength and endurance training in normoxia and hypoxia in sedentary humans. Am J Physiol Regul Integr Comp Physiol 301: R1078–1087.
58. Tulapurkar ME, Schafer R, Hanck T, Flores RV, Weisman GA, et al. (2005) Endocytosis mechanism of P2Y2 nucleotide receptor tagged with green fluorescent protein: clathrin and actin cytoskeleton dependence. Cell Mol Life Sci 62: 1388–1399.
59. Rosas-Ballina M, Olofsson PS, Ochani M, Valdes-Ferrer SI, Levine YA, et al. (2011) Acetylcholine-synthesizing T cells relay neural signals in a vagus nerve circuit. Science 334: 98–101.
60. Galassetti PR, Novak B, Nemet D, Rose-Gottron C, Cooper DM, et al. (2005) Breath ethanol and acetone as indicators of serum glucose levels: an initial report. Diabetes Technol Ther 7: 115–123.
61. Voogd TE, Vansterkenburg EL, Wilting J, Janssen LH (1993) Recent research on the biological activity of suramin. Pharmacol Rev 45: 177–203.

SOM Table 1. Cohort 1 Basal Body Temperature at 16 weeks was Decreased in the MIA Model and Restored to Normal by Antipurinergic Therapy.

Males	Mean Temperature ± SEM	95% CI	Mean Temperature difference from control (°C)	One-way ANOVA & Neuman-Keuls post-hoc	p-value
SALSAL (n=9)	37.3 ± 0.1	37.2 – 37.5	Reference	Overall ANOVA	p<0.05
SALSUR (n=10)	37.2 ± 0.1	36.9 – 37.5	- 0.1	SALSAL vs SALSUR	ns
PICSAL (n=9)	36.9 ± 0.1	36.6 – 37.2	- 0.4	SALSAL vs PICSAL	p<0.05
PICSUR (n=8)	37.2 ± 0.1	37.0 – 37.5	- 0.1	SALSAL vs. PICSUR ns	ns

Females	Mean Temperature ± SEM	95% CI	Mean Temperature difference from control (°C)	One-way ANOVA & Neuman-Keuls post-hoc	p-value
SALSAL (n=10)	37.8 ± 0.1	37.7 – 38.0	Reference	Overall ANOVA	p<0.005
SALSUR (n=9)	37.9 ± 0.1	37.8 – 38.1	+ 0.1	SALSAL vs SALSUR	ns
PICSAL (n=10)	37.4 ± 0.1	37.1 – 37.7	- 0.4	SALSAL vs PICSAL	p<0.01
PICSUR (n=10)	37.7 ± 0.1	37.5 – 37.9	- 0.1	SALSAL vs PICSUR	ns

SOM Table 2. Cohort 2 Basal Body Temperature from 8 to 16 weeks was Decreased in the MIA Model and Restored to Normal by Antipurinergic Therapy.

Males	Mean Temperature ± SEM	95% CI	Mean Temperature difference from control (°C)	df	Linear Mixed Models, p-value
SALSAL (n=9)	36.3 ± 0.1	36.2 - 36.4	Reference	Reference	Reference
SALSUR (n=10)	36.2 ± 0.1	36.2 - 36.4	- 0.1	301.6	p=0.71, ns
PICSAL (n=16)	35.8 ± 0.1	35.8 – 35.9	- 0.5	301.6	p < 0.001
PICSUR (n=15)	36.3 ± 0.1	36.2 – 36.4	0	301.6	p=0.88, ns

Poly IC exposure and Suramin treatment interaction F(1,47)=25.3, p<0.001

Females	Mean Temperature ± SEM	95% CI	Mean Temperature difference from control (°C)	df	Linear Mixed Models, p-value
SALSAL (n=12)	36.7 ± 0.1	36.6 – 36.8	Reference	Reference	Reference
SALSUR (n=12)	36.6 ± 0.1	36.5 - 36.7	- 0.1	348.9	p=0.61, ns
PICSAL (n=9)	36.1 ± 0.1	36.0 – 36.2	- 0.6	348.9	p < 0.001
PICSUR (n=10)	36.6 ± 0.1	36.5 - 36.7	- 0.1	348.9	p=0.56, ns

Poly IC exposure and Suramin treatment interaction F(1,39)=43.7, p<0.001

SOM Table 3. Circadian Analysis of Basal Metabolic Rates, Motor Activity, and Feeding.

	LIGHT PERIODS (Mean ± SEM)					DARK PERIODS (Mean ± SEM)				
BMR	**SALSAL**	**SALSUR**	**PICSAL**	**PICSUR**	**One-way ANOVA**	**SALSAL**	**SALSUR**	**PICSAL**	**PICSUR**	**One-way ANOVA**
VO_2 ml/kg/ hour	3652 ± 72.8	3821 ± 71.5	3552 ± 47.6	3938 ± 46.0***	p=0.0002 F(3,44)=8.0	4321 ± 52.3	4396 ± 59.2	4249 ± 67.2	4388 ±52.1	p=0.25, ns
VCO_2 ml/kg/ hour	3174 ± 62.7	3277 ± 61.4	3104 ± 56.1	3433 ± 44.9***	p=0.001 F(3,44)=6.4	4175 ± 26.2	4186 ± 64.3	4106 ± 53.1	4224 ± 56.8	p=0.45, ns
VCO_2/ VO_2	0.87 ± 0.007	0.85 ± 0.01	0.87 ± 0.008	0.87 ± 0.008	p=0.52, ns	0.97 ± 0.009	0.95 ± 0.009	0.97 ± 0.01	0.96 ± 0.008	p=0.46, ns
Activity (Counts)	368.9 ± 28.7	438.4 ± 58.8	382.1 ± 58.9	372.4 ± 45.2	p=0.74, ns	1298 ± 220.3	1335 ± 254.6	1385 ± 269	1177 ± 203.5	p=0.94, ns
VO_2 /Activity	20.35 ± 1.16	18.91 ± 2.29	20.63 ± 2.70	22.51 ± 2.29	p=0.73, ns	7.59 ± 1.13	7.60 ± 1.17	7.22 ± 1.17	8.46 ± 1.19	p=0.89, ns
Feed (Kcal)	363.4 ± 18.7	357.6 ± 16.9	359.3 ± 18.4	360.4 ± 16.8	p=0.51, ns	363.4 ± 18.7	357.6 ± 16.9	359.3 ± 18.4	360.4 ± 16.8	p=1.0, ns
Feed (calories)/ Activity (counts)	0.46 ± 0.03	0.36 ± 0.03	0.43 ± 0.06	0.44 ± 0.05	p=0.37, ns	0.32 ± 0.05	0.32 ± 0.06	0.31 ± 0.05	0.36 ± 0.06	p=0.93, ns

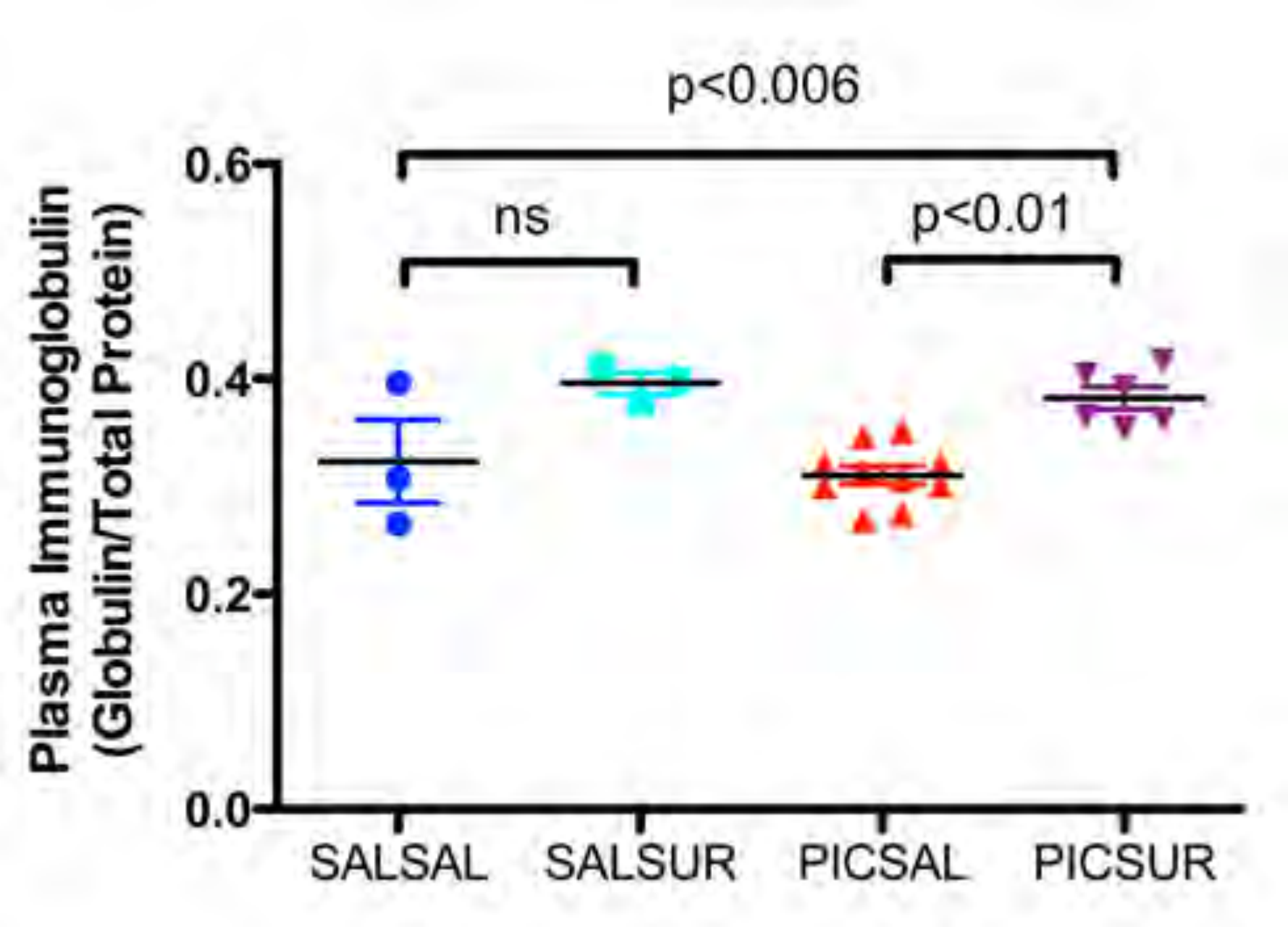
p<0.006
ns
p<0.01
Plasma Immunoglobulin
(Globulin/Total Protein)
0.6
0.4
0.2
0.0
SALSAL
SALSUR
PICSAL
PICSUR

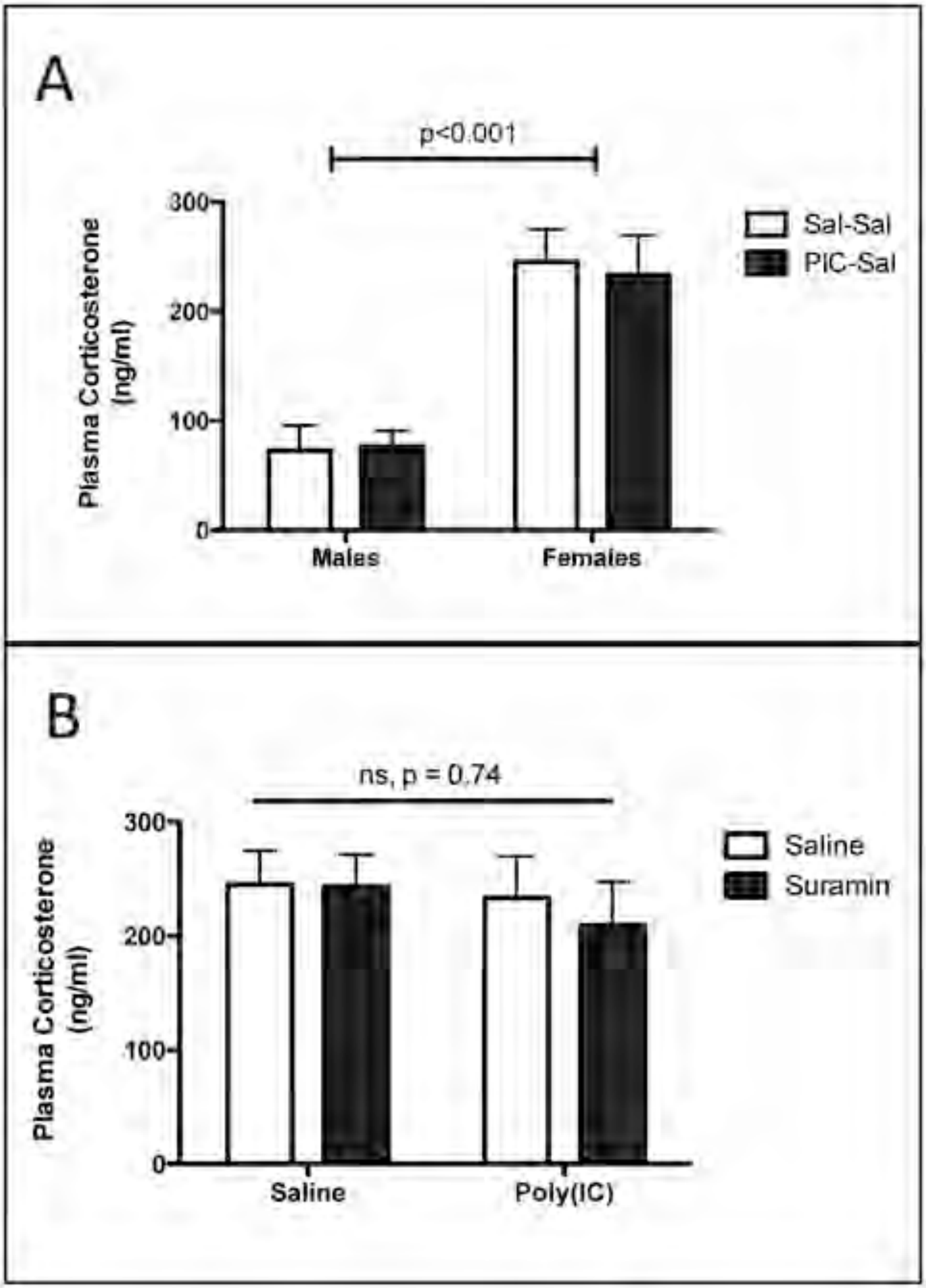
A
p<0.001
300
200
100
0
Plasma Corticosterone (ng/ml)
Sal-Sal
PIC-Sal
Males
Females
B
ns, p = 0.74
300
200
100
0
Plasma Corticosterone (ng/ml)
Saline
Suramin
Saline
Poly(IC)

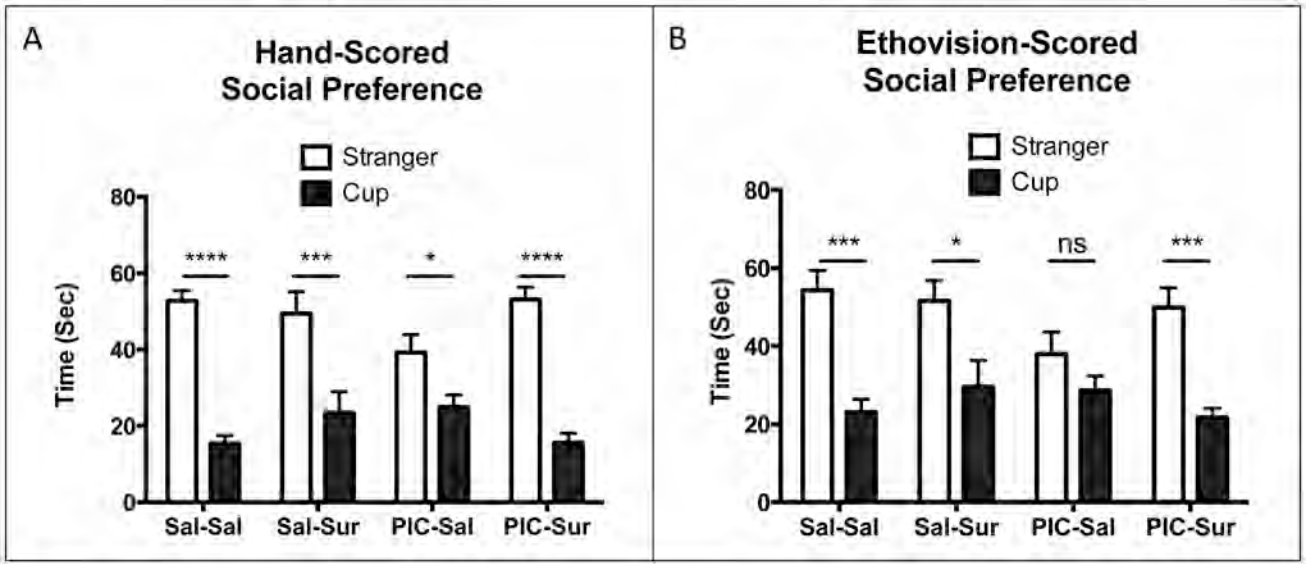
A
Hand-Scored
Social Preference
Stranger
Cup
Time (Sec)
80
60
40
20
0
****
***
*
****
Sal-Sal
Sal-Sur
PIC-Sal
PIC-Sur
B
Ethovision-Scored
Social Preference
Stranger
Cup
Time (Sec)
80
60
40
20
0
***
*
ns
***
Sal-Sal
Sal-Sur
PIC-Sal
PIC-Sur

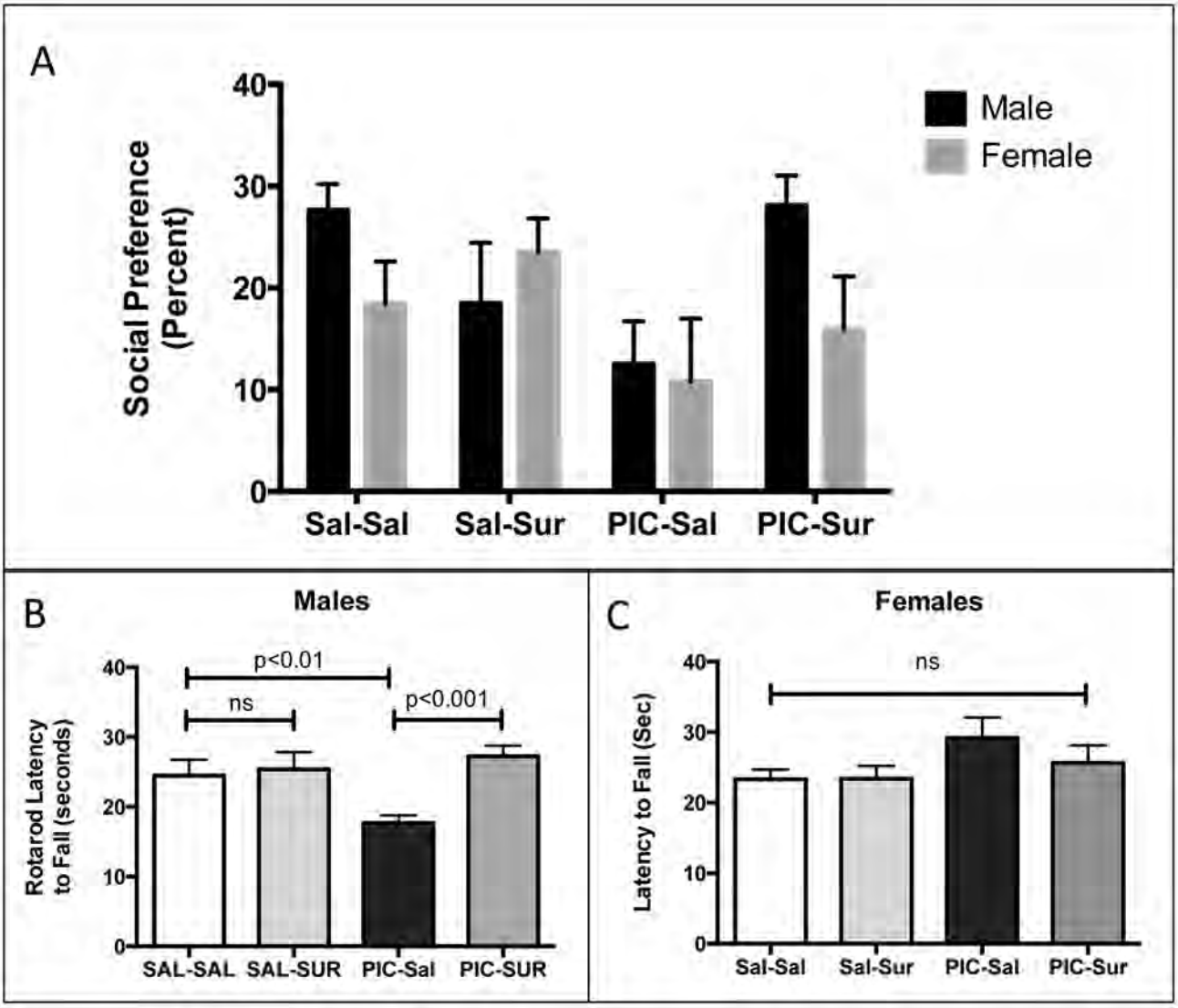
A
Social Preference (Percent)
40
30
20
10
0
Male
Female
Sal-Sal
Sal-Sur
PIC-Sal
PIC-Sur
B
Males
Rotarod Latency to Fall (seconds)
p<0.01
ns
p<0.001
SAL-SAL
SAL-SUR
PIC-Sal
PIC-SUR
C
Females
Latency to Fall (Sec)
ns
Sal-Sal
Sal-Sur
PIC-Sal
PIC-Sur

OPEN

Citation: Transl Psychiatry (2014) 4, e●●; doi:10.1038/tp.2014.33

www.nature.com/tp

ORIGINAL ARTICLE

Reversal of autism-like behaviors and metabolism in adult mice with single-dose antipurinergic therapy

JC Naviaux[1], MA Schuchbauer[1], K Li[2,3], L Wang[2,3], VB Risbrough[1,4], SB Powell[1] and RK Naviaux[2,3,4,5,6]

Autism spectrum disorders (ASDs) now affect 1–2% of the children born in the United States. Hundreds of genetic, metabolic and environmental factors are known to increase the risk of ASD. Similar factors are known to influence the risk of schizophrenia and bipolar disorder; however, a unifying mechanistic explanation has remained elusive. Here we used the maternal immune activation (MIA) mouse model of neurodevelopmental and neuropsychiatric disorders to study the effects of a single dose of the antipurinergic drug suramin on the behavior and metabolism of adult animals. We found that disturbances in social behavior, novelty preference and metabolism are not permanent but are treatable with antipurinergic therapy (APT) in this model of ASD and schizophrenia. A single dose of suramin (20 mg kg^{-1} intraperitoneally (i.p.)) given to 6-month-old adults restored normal social behavior, novelty preference and metabolism. Comprehensive metabolomic analysis identified purine metabolism as the key regulatory pathway. Correction of purine metabolism normalized 17 of 18 metabolic pathways that were disturbed in the MIA model. Two days after treatment, the suramin concentration in the plasma and brainstem was 7.64 μM pmol μl^{-1} (±0.50) and 5.15 pmol mg^{-1} (±0.49), respectively. These data show good uptake of suramin into the central nervous system at the level of the brainstem. Most of the improvements associated with APT were lost after 5 weeks of drug washout, consistent with the 1-week plasma half-life of suramin in mice. Our results show that purine metabolism is a master regulator of behavior and metabolism in the MIA model, and that single-dose APT with suramin acutely reverses these abnormalities, even in adults.

Translational Psychiatry (2014) **4,** e●●; doi:10.1038/tp.2014.33; published online xx xxx 2014

INTRODUCTION

Genetic,[1–3] environmental[4,5] and metabolic[6] factors can contribute to the risk of autism to different extents in each affected child. Despite this etiologic heterogeneity, and the well-known clinical variations that make each child unique, clinical studies suggest that a common denominator may underlie the shared behavioral and cognitive features that define autism spectrum disorders (ASDs) as a group. For example, in a prospective study conducted by the Zimmerman group at the Kennedy Krieger Institute in 2007, 83% of children with autism spectrum disorders were found to improve transiently in association with fever.[7] Improvements were lost with the resolution of the fever. This study showed that, despite the many different causes of ASD, the symptoms were not permanent and could be improved in a substantial fraction of children.

Transient improvements with fever have also been found in patients with certain forms of post-infection brain syndromes, movement disorders, dementia and schizophrenia in the early 1900s, although those early studies were made complicated by the use of live malarial parasites to produce the fevers.[8,9] In contrast to these beneficial effects, when the exposure to serious infection happens before the onset of disease—during early development, and particularly during pregnancy—the metabolic changes associated with significant fever or infection are known to increase the risk of neurodevelopmental disorders in the offspring. These disorders include schizophrenia,[10] ASDs,[11] attention deficit/hyperactivity disorder,[12] bipolar disorder,[13] epilepsy[14] and cerebral palsy.[15] The nature and developmental timing of the exposure are important. Metabolism and mitochondrial function change adaptively during and after infection, and are well-known regulators of neurotransmission[16] and synaptic plasticity.[17] Collectively, these studies suggest that, despite many different causes, the symptoms of several neurodevelopmental disorders such as ASD, schizophrenia and bipolar disorder may have a metabolic basis and be acutely responsive to treatment using the right metabolic intervention.

The maternal immune activation (MIA) mouse model of neurodevelopmental disorders produces symptoms that are biologically similar to those of ASD[18] and schizophrenia.[19] Pregnant females that are exposed to a simulated viral infection by injection of the double-stranded RNA poly(Inosine:Cytosine) produce offspring with features of ASD[20] and schizophrenia.[21] Exposure to poly(IC) activates an evolutionarily conserved metabolic response to a threat called the cell danger response (CDR).[22] Pathological persistence of the CDR, beyond the physical presence of the threat, has been observed in a variety of chronic disorders including ASDs.[22] Purinergic signaling has been hypothesized to be a key regulator of the CDR;[22] however, this has not yet been proven. In support of this hypothesis, we recently showed that antipurinergic therapy (APT) in the MIA mouse model corrected all of the behavioral, molecular and neuropathological abnormalities when weekly treatment with the antipurinergic drug suramin was

[1]Department of Psychiatry, University of California San Diego School of Medicine, La Jolla, CA, USA; [2]The Mitochondrial and Metabolic Disease Center, University of California San Diego School of Medicine, San Diego, CA, USA; [3]Department of Medicine, University of California San Diego School of Medicine, La Jolla, CA, USA; [4]Veterans Affairs Center for Excellence in Stress and Mental Health (CESAMH), La Jolla, CA, USA; [5]Department of Pediatrics, University of California San Diego School of Medicine, La Jolla, CA, USA and [6]Department of Pathology, University of California San Diego School of Medicine, La Jolla, CA, USA. Correspondence: Professor RK Naviaux, Departments of Medicine, Pediatrics, and Pathology, University of California San Diego School of Medicine, 214 Dickinson Street, Building CTF, Room C102, San Diego, CA 92103-8467, USA.
E-mail: naviaux@ucsd.edu
Received 13 November 2013 revised 14 March 2014 accepted 16 April 2014

begun at 1.5 months of age, near the age of reproductive maturity for mice.[23] Significant reductions in mitochondrial oxygen consumption and body temperature were also found. However, comprehensive metabolomic analysis was not reported in that study.[23]

In the present study, we tested the hypothesis that the behavioral manifestations of the MIA model are a consequence of pathological persistence of the evolutionarily conserved CDR,[22] and that the CDR is maintained by dysregulated purine metabolism and secondary abnormalities in purinergic signaling. We found that a single dose of the antipurinergic drug suramin given to adult animals about 6 months of age (21–27 weeks) produced the concerted correction of over 90% of the metabolic pathway disturbances, and all of the behavioral abnormalities that we tested in the MIA model. Six-month-old mice are the human biological age equivalents of about 30 years[24] (see Materials and methods). After washout of the drug, these improvements were lost and the former abnormalities returned. These data show that purine metabolism and purinergic signaling represent a novel neurochemical switch that regulates both behavior and metabolism in the MIA model of neurodevelopmental disorders such as ASD and schizophrenia.

MATERIALS AND METHODS

Animals and husbandry

All studies were conducted at the University of California, San Diego (UCSD) in facilities accredited by the Association for Assessment and Accreditation of Laboratory Animal Care International (AAALAC) under the UCSD Institutional Animal Care and Use Committee-approved animal subjects protocols, and followed the National Institutes of Health Guidelines for the use of animals in research. Six- to eight-week-old C57BL/6J (strain no. 000664) mice were obtained from Jackson Laboratories (Bar Harbor, ME, USA), given food and water *ad libitum*, identified by ear tags, and used to produce the timed matings. Animals were housed in a temperature- (22–24 °C) and humidity (40–55%)-controlled vivarium with a 12-h light–dark cycle (lights on at 0700 hours). Nulliparous dams were mated at 9–10 weeks of age. The sires were also 9–10 weeks of age. The human biological age equivalent for the C57BL/6J strain of laboratory mouse (*Mus musculus*) can be estimated from the following equation: 12 years for the first month, 6 years for the second month, 3 years for months 3–6 and 2.5 years for each month thereafter.[24] Therefore, a 6-month-old mouse would be the biological equivalent of 30 years old ($=12+6+3\times4$) on a human timeline.

Poly(IC) preparation and gestational exposure

To initiate the MIA model, pregnant dams were given two intraperitoneal injections of Poly(I:C) (Potassium salt; Sigma-Aldrich, St. Louis, MO, USA, Cat no. P9582; >99% pure; < 1% mononucleotide content). These were quantified by UV spectrophotometry. One unit (U) of poly(IC) was defined as 1 absorbance unit at 260 nm. Typically, 1U = 12 μg of RNA. 0.25 U/g [3 mg kg^{-1}] of poly(IC) was given on E12.5 and 0.125 U g^{-1} (1.5 mg kg^{-1}) on E17.5 as previously described.[23] Contemporaneous control pregnancies were produced by timed matings and randomized assignment of pregnant dams to saline injection (5 μl g^{-1} intraperitoneally (i.p.)) on E12.5 and E17.5.

Postnatal handling and antipurinergic therapy (APT)

Offspring of timed matings were weaned at 3–4 weeks of age into cages of two to four animals. No mice were housed in isolation. Only males were evaluated in these studies. Littermates were identified by ear tags and distributed into different cages in order to minimize litter and dam effects. To avoid chance differences in groups selected for single-dose treatment, the saline and poly(IC) exposure groups were each balanced according to their social approach scores at 2.25 months. At 5.25 or 6.5 months of age, half the animals received a single injection of either saline (5 μl g^{-1} i.p.) or suramin (hexasodium salt, 20 mg kg^{-1} i.p.; Tocris Bioscience, Bristol, UK, Cat no. 1472). Beginning 2 days later, behaviors were evaluated as described below. After completing the behavioral measurements, half of the subjects were killed after a 5-week-washout period for measurement of suramin tissue levels. For acute suramin levels, the other half was injected at 7.75 months of age and killed 2 days later for tissue level determinations.

Behavioral testing

Behavioral testing began at 2.25 months (9 weeks) of age. Mice were tested in social approach, rotarod, t-maze test of spontaneous alternation and light–dark box test. If abnormalities were found, treatment with suramin or saline was given at 5.25 months (21 weeks) or 6.5–6.75 months (26–27 weeks) and the testing was repeated. Only male animals were tested.

Social approach. Social behavior was tested as social preference as previously described[23] with minor modifications (see Full Methods in Supplementary Information; $N=19$–25, 2.25-month-old males per group before adult treatment with suramin. $N=8$–13, 6.5-month-old males per group).

T-Maze. Novelty preference was tested as spontaneous alternation behavior in the T-maze by a modification of the methods of Frye and Walf[25] (see Full Methods Supplementary Information). $N=19$–25, 4-month-old males per group before adult treatment with suramin. $N=8$–13, 5.25-month-old males per group.

Rotarod. Sensorimotor coordination was tested as latency to fall on the rotarod as previously described[23] (see Full Methods Supplementary Information; $N=19$–25, 2.5-month-old males per group before adult treatment with suramin. $N=8$–13, 6.75-month-old males per group).

Light–dark box. Certain anxiety-related and light-avoidance behaviors were tested in the light–dark box paradigm as previously described[26] (see Full Methods Supplementary Information; $N=19$–25, 3.5-month-old males per group).

Absence of abnormal behaviors produced by suramin. This was assessed in the non-MIA control animals (indicated as the 'Saline' group in the pretreatment figures) that were injected with suramin as adults (indicated as the 'Sal-Sur' groups in the single-dose treatment figures) using each of the above behavioral paradigms.

Suramin quantitation

Tissue samples (brainstem, cerebrum and cerebellum) were ground into powder under liquid nitrogen in a pre-cooled mortar. Powdered tissue (15–50 mg) was weighed and mixed with the internal standard trypan blue to a final concentration of 5 μM (pmol mg^{-1}) and incubated at room temperature for 10 min to permit metabolite interaction with binding proteins. Nine volumes of methanol:acetonitrile:H2O (43:43:16) pre-chilled to −20 °C was added to produce a final solvent ratio of 40:40:20, and the samples were deproteinated and macromolecules removed by precipitation on crushed ice for 30 min. The mixture was centrifuged at 16 000 *g* for 10 min at 4 °C and the supernatant was transferred to a new tube and kept at −80 °C for further LC-MS/MS (liquid chromatography-tandem mass spectrometry) analysis. For plasma, 90 μl was used, to which 10 μl of 50 μM stock of trypan blue was added to achieve an internal standard concentration of 5 μM. This was incubated at room temperature for 10 min to permit metabolite interaction with binding proteins, then extracted with 4 volumes (400 μl) of pre-chilled methanol:acetonitrile (50:50) to produce a final concentration of 40:40:20 (methanol:acetonitrile:H2O) and precipitated on ice for 10 min. Other steps were the same as for solid tissue extraction.

Suramin was analyzed on an AB SCIEX QTRAP 5500 triple quadrupole mass spectrometer equipped with a Turbo V electrospray ionization source, Shimadzu LC-20A UHPLC system, and a PAL CTC autosampler (AB SCIEX, Framingham, MA, USA). Ten microliters of extract were injected onto a Kinetix pentafluorophenyl column (150 × 2.1 mm, 2.6 μm; Phenomenex, Torrence, CA, USA) held at 30 °C for chromatographic separation. The mobile phase A was water with 20 mM ammonium acetate (NH4OAC; pH 7) and mobile phase B was methanol with 20 mM NH4OAC (pH 7). Elution was performed using the following gradient: 0 min—0% B, 15 min—100% B, 18 min—100% B, 18.1 min—0% B, 23 min—end. The flow rate was 300 μl min^{-1}. All the samples were kept at 4 °C during analysis. Suramin and trypan blue were detected using scheduled multiple reaction monitoring (MRM) with a dwell time of 30 ms in negative mode and retention time

window of 7.5–8.5 min for suramin and 8.4–9.4 min for trypan blue. MRM transitions for the doubly charged form of suramin were 647.0 m z^{-1} (Q1) precursor and 382.0 m z^{-1} (Q3) product. MRM transitions for trypan blue were 435.2 (Q1) and 185.0 (Q3). Absolute concentrations of suramin were determined for each tissue using a tissue-specific standard curve to account for matrix effects, and the peak area ratio of suramin to the internal standard trypan blue. The declustering potential, collision energy, entrance potential and collision exit potential were −104, −9.5, −32 and −16.9, and −144.58, −7, −57.8 and −20.94 for suramin and trypan blue, respectively. The electrospray ionization source parameters were set as follows: source temperature 500 °C; curtain gas 30; ion source gas 1, 35; ion source gas 2 35; spray voltage −4500 V. Analyst 1.6.1 was used for data acquisition and analysis. $N = 4$–6 per tissue. Results are reported as means ± s.e.m. in absolute μM (pmol μl^{-1}) concentration for plasma, and pmol mg^{-1} wet weight for tissues.

Metabolomics

Broad-spectrum analysis of 478 targeted metabolites from 44 biochemical pathways in the plasma was performed by a modification of the methods described by Bajad and Shulaev.[27] Only male animals that had been behaviorally evaluated were tested. Samples were analyzed on an AB SCIEX QTRAP 5500 triple quadrupole mass spectrometer equipped with a Turbo V electrospray ionization source, Shimadzu LC-20A UHPLC system and a PAL CTC autosampler (AB SCIEX). Whole blood was collected 2 days after a single dose of suramin (20 mg kg^{-1} i.p.) or saline (5 μl g^{-1} i.p.) from animals that were lightly anesthetized with isoflurane (Med-Vet International, Mettawa, IL, USA, Cat no. RXISO-250) in a drop jar into BD Microtainer tubes containing lithium heparin (Becton Dickinson, San Diego, CA USA, Ref no. 365971) by submandibular vein lancet.[28] Plasma was separated by centrifugation at 600 $g \times 5$ min at 20 °C within 1 h of collection. Fresh lithium–heparin plasma was transferred to labeled tubes for storage at −80 °C for analysis. Typically, 45 μl of plasma was thawed on ice and transferred to a 1.7-ml Eppendorf tube. Two and one-half (2.5) microliters of a cocktail containing 35 commercial stable isotope internal standards (Supplementary Table S3) and 2.5 μl of 310 stable isotope internal standards that were custom-synthesized in *Escherichia coli* and *Saccharomyces cerevisiae* by metabolic labeling with ^{13}C-glucose and ^{13}C-bicarbonate were added, mixed and incubated for 10 min at 20 °C to permit small molecules and vitamins in the internal standards to associate with plasma-binding proteins. Macromolecules (protein, DNA, RNA and so on) were precipitated by extraction with 4 volumes (200 μl) of cold (−20 °C), acetonitrile:methanol (50:50) (LCMS grade, Cat no. LC015-2.5 and GC230-4, Burdick & Jackson, Honeywell, Muskegon, MI, USA), vortexed vigorously and incubated on crushed ice for 10 min, and then removed with centrifugation at 16 000 $g \times 10$ min at 4 °C. The supernatants containing the extracted metabolites and internal standards in the resulting 40:40:20 solvent mix of acetonitrile:methanol:water were transferred to labeled cryotubes and stored at −80 °C for LC-MS/MS (liquid chromatography-tandem mass spectrometry) analysis.

LC-MS/MS analysis was performed by MRM under the Analyst v1.6.1 software control in both negative and positive modes with rapid polarity switching (50 ms). Nitrogen was used for curtain gas (set to 30), collision gas (set to high) and ion source gases 1 and 2 (set to 35). The source temperature was 500 °C. Spray voltage was set to −4500 V in negative mode and to 5500 V in positive mode. The values for Q1 and Q3 mass-to-charge ratios (m z^{-1}), declustering potential, entrance potential, collision energy and collision cell exit potential were determined and optimized for each MRM for each metabolite. Ten microliters of extract were injected with PAL CTC autosampler into a 250 mm × 2.1 mm, 5-μm Luna NH2 aminopropyl HPLC column (Phenomenex) held at 25 °C for chromatographic separation. The mobile phase was solvent A: 95% water with 23.18 mM NH4OH (Sigma, Fluka Cat no. 17837-100ML), 20 mM formic acid (Sigma, Fluka Cat no. 09676-100ML) and 5% acetonitrile (pH 9.44); solvent B: 100% acetonitrile. Separation was achieved using the following gradient: 0 min—95% B, 4 min—B, 19min—2% B, 22 min—2% B, 23 min—95% B, 28 min—end. The flow rate was 300 μl min^{-1}. All the samples were kept at 4 °C during analysis. The chromatographic peaks were identified using MultiQuant v2.1.1 (AB Sciex), confirmed by manual inspection and the peak areas were integrated. The median of the peak area of stable isotope internal standards was calculated and used for the normalization of metabolite concentration across the samples and batches. $N = 6$, 6.5-month-old males per group. Metabolite data were log-transformed before multivariate and univariate analyses.

Data analysis

Animals were randomized into active (suramin) and mock (saline) treatment groups at ~6 months of age. Group means and s.e.m. are reported. Behavioral data involving more than two groups were analyzed by two-way analysis of variance (ANOVA) and one-way ANOVAs (GraphPad Prism 5.0d, GraphPad Software Inc., La Jolla, CA USA). Pair-wise *post hoc* testing was performed by the method of Tukey. Repeated measures ANOVA with prenatal treatment and drug as between subject factors and stimulus (mouse/cup) on time spent with mouse or cup was used as an additional test of social preference. Student's *t*-test was used for comparisons involving the two groups. Significance was set at $P < 0.05$. Bonferroni *post hoc* correction was used to control for multiple hypothesis testing when *t*-tests were used to test social preference in two or more experimental groups. Metabolomic data were analyzed using multivariate partial least squares discriminant analysis, Ward hierarchical clustering and univariate one-way ANOVA with pairwise comparisons and *post hoc* correction by Fisher's least significant difference test in MetaboAnalyst.[29]

RESULTS

Restoration of normal social behavior

Social behavior in mice can be quantified as the time spent interacting with a novel ('stranger') mouse compared with the total time spent interacting with either a mouse or a novel inanimate object.[30] MIA animals showed social deficits from an early age (Figure 1a, Supplementary Figure S1a). Single-dose APT with suramin completely reversed the social abnormalities in 6.5-month-old adults (Figure 1b, Supplementary Figure S1b). Five weeks (5 half-lives) after suramin washout, a small residual benefit to social behavior was still detectable (Figure 1c, Supplementary Figure S1c). The residual social benefit of APT even after 5 weeks following suramin was correlated with retained metabolomic benefits (see below). This phenomenon was not investigated further but may be related to the development of metabolic memory and/or somatic epigenetic DNA changes that lasted longer than the physical presence of the drug.[31]

Restoration of spontaneous alternation in the T-maze

Novelty preference is an innate feature of normal rodent[32] and human[33] behavior and a predictor of socialization and communication growth in children with ASD.[34] The loss or suppression of novelty preference in children with ASD is associated with the phenomenon known as insistence on sameness.[35] We estimated preference for novelty as spontaneous alternation behavior in the T-maze.[25] The T-maze can also be used to estimate spatial working memory, especially when food-motivated.[36] We did not use the food-motivated variation in our study. We found that MIA animals showed deficient novelty preference as reflected by chance (near 50%) spontaneous alternation behavior (Figure 1d). These deficits were normalized after a single dose of suramin (Figure 1e). Five weeks after suramin washout, no residual benefit remained (Figure 1f).

Failure to restore rotarod performance in adult animals

Previous studies have shown age-dependent, postnatal loss of cerebellar Purkinje cells in the MIA model. This can reach up to 60% of Purkinje cells lost by 4 months (16 weeks) of age.[23,37] Motor coordination measured by rotarod performance is deficient in the MIA model[23] (and Figure 1g) and is critically dependent on the integrity of Purkinje cell circuits in the cerebellum.[38] We hypothesized that since Purkinje cells are known to be lost in MIA animals by 4 months (16 weeks) of age, that APT given later in life would have no effect. Our results confirmed this. We found that a single injection of suramin given to 6-month-old adults failed to restore normal motor coordination (Figures 1g and h). Although cerebellar Purkinje cell density was not quantified in this study, our results are consistent with the notion that once Purkinje cells are lost, their function cannot be restored by APT in adult animals.

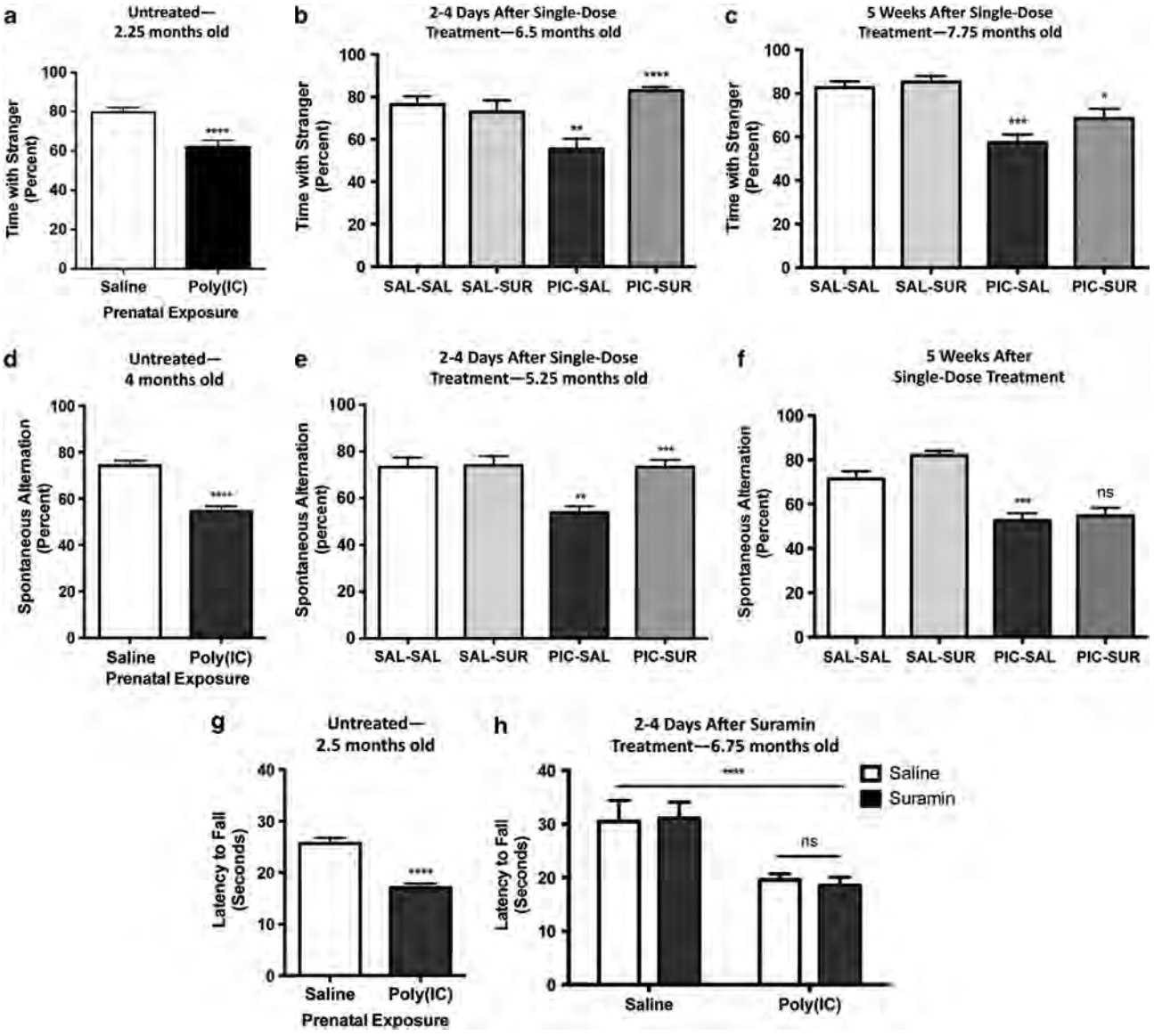

Figure 1. Single-dose correction of behavioral abnormalities. (**a**) Social abnormalities in male MIA animals were found at the earliest ages of testing at 2.25 months of age. (Student's *t*-test ****$P < 0.0002$; $N = 19$ Saline and 25 Poly(IC)). (**b**) A single dose of suramin given to adult MIA mice restored normal social behavior (PIC-Sur). two-way ANOVA was first used to test for the presence of interaction between drug treatment and experimental groups. This revealed an interaction consistent with the observation that suramin benefited social behavior in the MIA animals but had no effect on normal controls ($F(1,39) = 13.48$); $P = 0.0007$). We then performed one-way ANOVA to test for suramin effects. A single treatment with suramin (20 mg kg^{-1} i.p.) given 2–4 days before testing restored normal social behavior (one-way ANOVA $F(3,40) = 8.95$; $P < 0.0001$; Tukey *post hoc* PIC-Sal versus PIC-Sur ****$P < 0.0001$; $N = 8$–13 per group). (**c**) After 5 weeks of suramin washout, the social behavior remained improved compared with saline-treated animals but was decreased from the first week after treatment. ($F(3,40) = 10.5$; Tukey *post hoc* PIC-Sal versus PIC-Sur *$P < 0.05$; $N = 8$–13 per group). Values are expressed as means ± s.e.m. (**d**) We estimated the strength of novelty preference[32] as spontaneous alternation in the T-maze. MIA mice showed deficits in spontaneous alternation from the age of earliest testing at 4 months of age (Student's *t*-test; ****$P < 0.0001$; $N = 19$ Saline and 25 PIC). (**e**) Two-way ANOVA was first used to test for the presence of interaction between drug treatment and experimental groups. This revealed an interaction consistent with the observation that suramin restored spontaneous alternation in the MIA animals but had no effect on normal controls ($F(1,40) = 7.609$; $P = 0.0087$). We then performed one-way ANOVA to test for suramin effects. A single dose of suramin (20 mg kg^{-1} i.p.) injected 2–4 days before testing corrected the deficits in young adult animals that were 5.25 months of age. ($F(3,40) = 9.46$; ; Tukey *post hoc* Sal-Sal versus PIC-Sal **$P < 0.01$; PIC-Sal versus PIC-Sur ***$P < 0.001$); $N = 8$–13 per group). (**f**) This benefit was lost after a drug washout period of 5 weeks, leaving a significant difference between control (Sal) and MIA (PIC) groups ($F(3,39) = 18.05$; $P < 0.0001$), but no remaining effect of suramin by *post hoc* testing. (Tukey *post hoc* PIC-Sal versus PIC-Sur P = ns; $N = 8$–13 per group). Values are expressed as means ± s.e.m. (**g**) Motor coordination abnormalities were quantified on the rotarod as latency to fall. Performance was abnormal from the earliest age of testing at 2.5 months of age (Student's *t*-test ****$P < 0.0001$; $N = 19$ Saline and 25 Poly(IC)). (**h**) Suramin did not improve performance after two doses (20 mg kg^{-1} i.p.) given at 6.5 and 6.75 months of age and tested 2–4 days after the second dose. (two-way ANOVA interaction $F(1,39) = 0.1227$; $P = 0.728$ (ns); Poly(IC) effect $F(1,39) = 25.06$; ****$P < 0.0001$; treatment effect $F(1,39) = 0.01$; $P = 0.908$ (ns)). Values are expressed as means ± s.e.m.

Other behaviors

Certain features of ASD and schizophrenia were not captured by our studies of the MIA model and therefore could not be interrogated for pharmacologic response to APT. For example, we did not find any abnormalities in the MIA mouse model using our protocol when we looked for certain types of anxiety-related behavior in the light–dark box paradigm (Supplementary Figure S2). Likewise, our earlier studies showed no stereotypic repetitive movements in the C57BL/6J mouse strain either by clinical observation or by testing in the hole board exploration beam break mouse behavioral pattern monitor.[23] Finally, no abnormal behaviors were produced by suramin treatment itself. This was shown by the absence of behavioral differences between control mice treated with saline ('Sal-Sal') and those treated with suramin ('Sal-Sur') in Figures 1b, e and h.

Brainstem uptake of suramin

Suramin is known not to pass the blood–brain barrier;[39] however, no studies have looked at suramin concentrations in areas of the brain similar to the area postrema in the brainstem that lack a blood–brain barrier.[40] After completing the behavioral studies described above, we used mass spectrometry to measure drug levels in plasma, cerebrum, cerebellum and brainstem following a 5-week period of drug washout. The plasma half-life of suramin after a single dose in mice is 1 week.[41] No suramin was detected in any tissue after 5 weeks of drug washout (data not shown). We next gave an acute injection of suramin (20 mg kg^{-1} i.p.) to the remaining subjects. After 2 days, plasma suramin was 7.64 μM ± 0.50, and brainstem suramin was 5.15 pmol mg^{-1} ± 0.49 (Figure 2). No drug was detectable in the cerebrum or cerebellum (< 0.10 pmol mg^{-1} wet weight) in either control (Sal-Sur) or MIA (PIC-Sur) animals, consistent with an intact blood–brain barrier that excluded suramin from these tissues. In contrast to the cerebrum and cerebellum, the brainstem showed significant suramin uptake (Figure 2). These results are consistent with the notion that nuclei in brainstem, or their projection targets in distant sites of the brain, may mediate the dramatic behavioral effects of acute and chronic APT in this model.[23]

Restoration of normal purine metabolism rescues other metabolic disturbances

We analyzed the acute metabolomic effects in plasma 2 days after single-dose treatment with suramin or saline in the same animals studied behaviorally. We measured 478 metabolites from 44 pathways using mass spectrometry, analyzed the data by partial least squares discriminant analysis and visualized the results by projection in two dimensions (Figures 3a and b). This revealed sharp differences between control and MIA animals that were substantially normalized by a single treatment with suramin (Figure 3a). Figure 3b shows a similar analysis that illustrates the gradual return to disease-associated metabolism after 5 weeks of drug washout. Using hierarchical cluster analysis we found that the metabolic profiles of controls (Sal-Sal; light blue) and MIA animals that were treated with one dose of suramin (PIC-Sur; green) were more similar (major branch on the left of Figure 3c) than the metabolic profiles of saline-treated MIA animals (PIC-Sal; red) and the MIA animals tested 5 weeks after suramin washout (PIC-Sur W/O; dark blue; major branch on the right of Figure 3c). The reason that the metabolic profile had not returned completely to pretreatment conditions (to the position of the red triangles in Figure 3b) even after 5 weeks following a dose of suramin was not investigated but could be due to the development of metabolic memory and/or somatic epigenetic DNA changes that lasted longer than the physical presence of the drug.[31]

Figure 3d shows the top 48 significant metabolites found in the untreated MIA animals, ranked according to their impact by variable importance in projection (VIP) score. The color-coded columns on the right of the figure indicate the direction of the change. In 43 of the 48 (90%) discriminating metabolites, suramin treatment (PIC-Sur) resulted in a metabolic shift in concentration that was either intermediate (coded yellow or light green) or in the direction of and beyond that found in control animals (Sal-Sal). The biochemical pathways represented by each metabolite are indicated on the left of Figure 3d.

Metabolic pathway analysis

The most influenced biochemical pathway in the MIA mouse was purine metabolism (Table 1). Eleven (23%) of the 48 discriminant metabolites were purines. Nine (82%) of the 11 purine metabolites were increased in the untreated MIA mice, consistent with hyperpurinergia. Only ATP and allantoin, the end product of purine metabolism in mice, were decreased in the plasma. A limitation of plasma metabolomics is that it cannot measure the effective concentration of nucleotides in the pericellular halo that defines the unstirred water layer near the cell surface where receptors and ligands meet.[23] The concentration of ATP in the unstirred water layer is regulated according to conditions of cell health and danger[22] in the range of 1–10 μM, which is near the EC50 of most purinergic receptors.[42] This is up to 1000-fold more concentrated than the 10–20 nM levels of ATP in compartments removed from the cell surface such as the plasma.[43] In the plasma we found that suramin restored 9 (82%) of the 11 purine metabolites to more normal levels, including ATP and allantoin

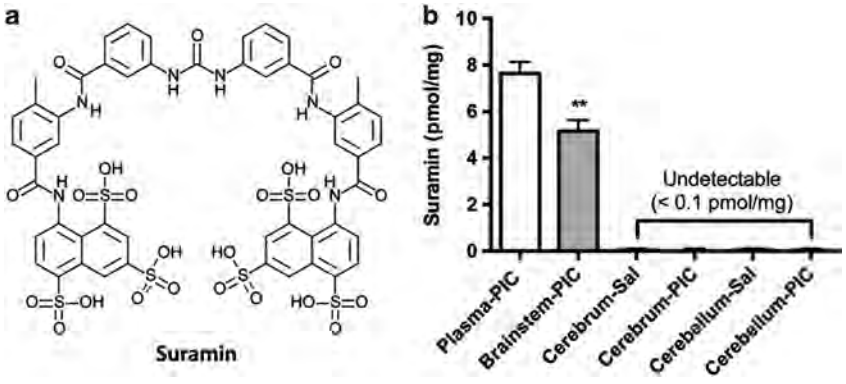

Figure 2. Plasma and brainstem suramin quantitation. (**a**) Suramin is a polysulphonated napthylurea with a molecular weight of 1297 g mol^{-1}. (**b**) Suramin was present in the plasma and brainstem but was not detectable in the cerebrum or cerebellum. Two days after a single 20 mg kg^{-1} i.p. dose of suramin, drug levels were measured in plasma (7.64 μM ± 0.50), brainstem (5.15 pmol mg^{-1} ± 0.49), cerebrum (< 0.1 pmol mg^{-1}) and cerebellum (< 0.1 pmol mg^{-1}) in both controls (Sal) and maternal immune activation (PIC) animals. ($N = 4–6$ per tissue). Values are expressed as means ± s.e.m.

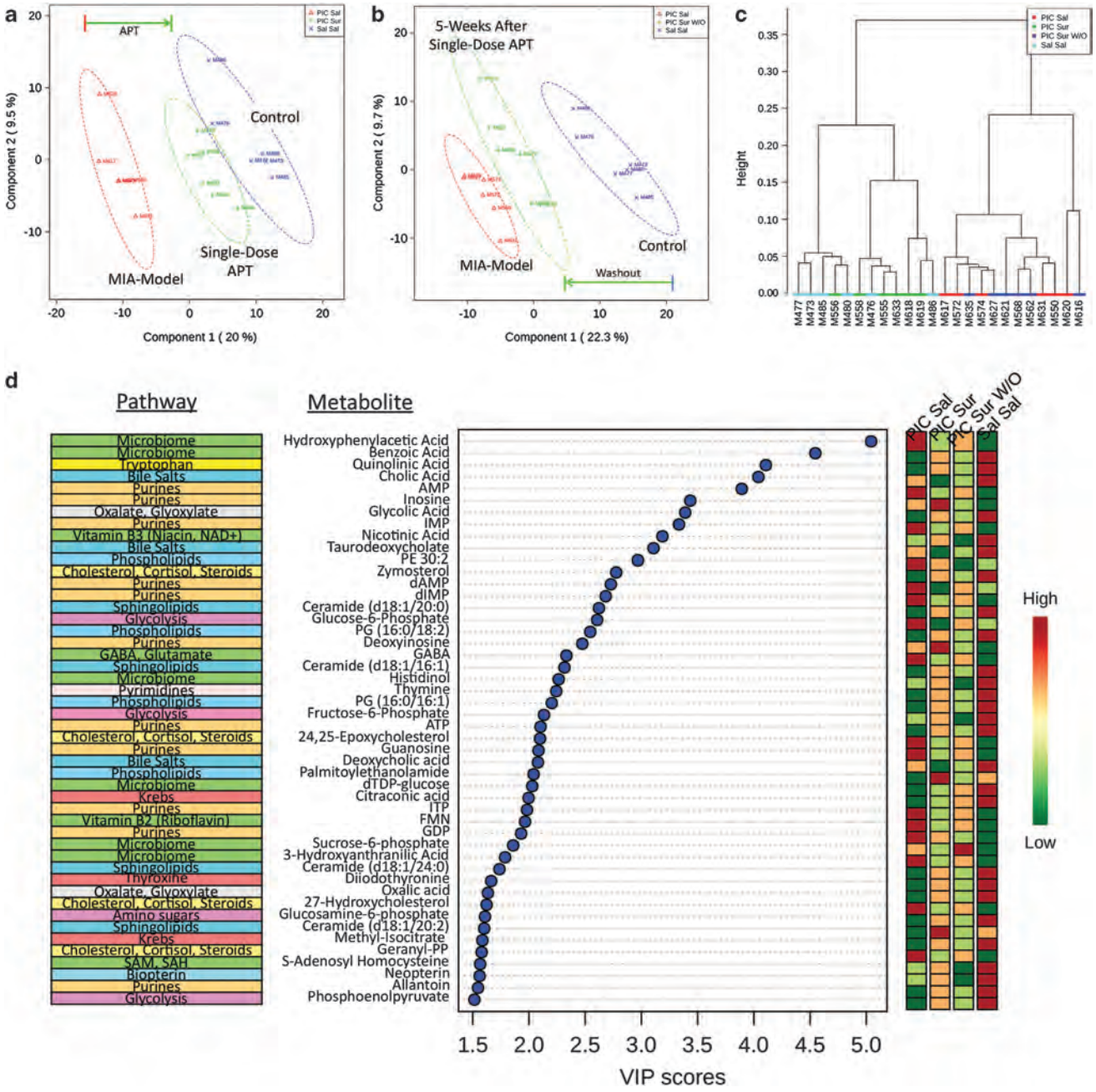

Figure 3. Metabolomic analysis. (**a**) APT rescues widespread metabolic abnormalities. Plasma samples were collected 2 days after a single dose of suramin (20 mg kg^{-1} i.p.) or saline (5 µl g^{-1} i.p.). This analysis shows that a single dose of suramin (PIC-Sur; green) drives the metabolism of MIA animals (PIC-Sal; red) strongly in the direction of controls (Sal-Sal; blue). Metabolomic profiles consisted of 478 metabolites from 44 biochemical pathways measured with LC-MS/MS. $N = 6$, 6.5-month-old males per group. (**b**) Metabolic memory preserves metabolic rescue by APT. This analysis shows that 5 weeks after a single dose of suramin (PIC-Sur W/O; green) the metabolism of treated animals has drifted back toward that of untreated, MIA animals (PIC-Sal; red; $N = 6$ males per group). (**c**) Hierarchical clustering of suramin-treated and suramin-washout metabotypes. This analysis illustrates the metabolic similarity of control (Sal-Sal; light blue) and MIA animals treated with one dose of suramin (PIC-Sur; green) compared with saline-treated MIA animals (PIC-Sal; red) and ASD-like animals tested 5 weeks after suramin washout (PIC-Sur W/O; dark blue). The numbers listed along the *x* axis are animal ID numbers. (**d**) Rank Order of metabolites disturbed in the MIA model. Multivariate analysis across the four treatment groups (PIC-Sal = MIA; PIC-Sur = acute suramin treatment; PIC-Sur w/o = 5 weeks post-suramin washout; Sal-Sal = Controls). Biochemical pathway assignments are listed on the left. Relative magnitudes of each metabolite disturbance are listed on the right as high (red), intermediate (yellow or light green) and low (dark green). Variable importance in projection (VIP) scores are a multivariate statistic that reflects the impact of each metabolite on the partial least squares discriminant analysis model. VIP scores above 1.5 are significant.

(Figure 3d, right PIC-Sur column, coded yellow or light green) and increased inosine and deoxyinosine to above normal.

Additional pathway analysis revealed a pattern of disturbances that was remarkably similar to metabolic disturbances that have been found in children with ASDs (Table 1). Eighteen of the 44 pathways were disturbed in the MIA model. The 44 pathways interrogated by this analysis are reported in Supplementary Table S1. After purine metabolism, the next most influenced pathway

Table 1. Biochemical pathways with metabolites altered in the MIA mouse model of neurodevelopmental disorders

No.	Pathway	Measured metabolites in the pathway (N)	Expected pathway proportion (P = N/478)	Expected hits in a sample of 48 (P*48)	Observed hits in the top 48 metabolites	Fold- enrichment (Obs/Exp)	Impact (Σvip)	Fraction of VIP explained (% of 116.16)	Pathway normalized by single-dose suramin treatment
1	Purine metabolism	48	0.1004	4.8201	11	2.3	28.19	24.3%	Yes (9/11)
2	Microbiome metabolism	32	0.0669	3.2134	6	1.9	17.53	15.1%	Yes (6/6)
3	Phospholipid metabolism	88	0.1841	8.8368	4	0.5	9.76	8.4%	Yes (4/4)
4	Bile salt metabolism	4	0.0084	0.4017	3	7.5	9.23	7.9%	No (0/3)
5	Sphingolipid metabolism	72	0.1506	7.2301	4	0.6	8.28	7.1%	Yes (4/4)
6	Cholesterol, cortisol, steroid metabolism	19	0.0397	1.9079	4	2.1	8.08	7.0%	Yes (4/4)
7	Glycolysis and gluconeogenesis	17	0.0356	1.7071	3	1.8	6.25	5.4%	Yes (3/3)
8	Oxalate, glyxoylate metabolism	3	0.0063	0.3013	2	6.6	5.02	4.3%	Yes (2/2)
9	Tryptophan metabolism	11	0.0230	1.1046	1	0.9	4.11	3.5%	Yes (1/1)
10	Krebs cycle	18	0.0377	1.8075	2	1.1	3.58	3.1%	Yes (2/2)
11	Vitamin B3 (niacin/NAD) metabolism	7	0.0146	0.7029	1	1.4	3.19	2.7%	Yes (1/1)
12	GABA, glutamate, arginine, ornithine, proline metabolism	6	0.0126	0.6025	1	1.7	2.33	2.0%	Yes (1/1)
13	Pyrimidine metabolism	35	0.0732	3.5146	1	0.3	2.24	1.9%	Yes (1/1)
14	Vitamin B2 (riboflavin) metabolism	4	0.0084	0.4017	1	2.5	1.97	1.7%	Yes (1/1)
15	Thyroxine metabolism	1	0.0021	0.1004	1	10.0	1.66	1.4%	Yes (1/1)
16	Amino-sugar and galactose metabolism	10	0.0209	1.0042	1	1.0	1.61	1.4%	Yes (1/1)
17	SAM, SAH, methionine, cysteine, glutathione metabolism	22	0.0460	2.2092	1	0.5	1.57	1.3%	Yes (1/1)
18	Biopterin, neopterin, molybdopterin metabolism	1	0.0021	0.1004	1	10.0	1.56	1.3%	Yes (1/1)
		398 (0.8326 × 478)	0.8326	40 (0.8326 × 48)	48		116.16	100%	94% (17/18)

Abbreviation: VIP, variable importance in projection. Pathways were ranked by their impact measured by summed VIP (ΣVIP) scores. A total of 48 metabolites were found to discriminate treatment, control, washout and MIA groups by multivariate partial least squares discriminant analysis (PLSDA). Significant metabolites had VIP scores of $\geqslant 1.5$. Eighteen (41%) of the 44 pathways interrogated had at least one metabolite with VIP scores $\geqslant 1.5$. The total impact of these 48 metabolites corresponded to a summed VIP score of 116.16. The fractional impact of each pathway is quantified as the percent of the summed VIP score and displayed in the final column on the right in the table. Single dose APT with suramin not only corrected purine metabolism but also normalized 17 (94%) of 18 metabolic pathway abnormalities that defined the MIA model of neurodevelopmental disorders.

was the microbiome. Microbiome metabolites are molecules that are produced by biochemical pathways that are absent in mammalian cells but are present in bacteria that reside in the gut microbiome.[44] Together, purine and microbiome metabolism accounted for nearly 40% (ΣVIP = 39.4%) of the impact measured by VIP scores. The two top discriminant metabolites were products of the microbiome (Figure 3d). A total of seven pathways each contributed 5% or more to the VIP pathway impact scores (Table 1). These top seven pathways were purines, microbiome metabolism, phospholipids, bile salt metabolism, sphingolipids, cholesterol, cortisol, and steroid metabolism and glycolysis. Seventy-five percent (75%) of the metabolite VIP score impact was accounted for by metabolites in these seven pathways (Table 1). Univariate statistical analysis was conducted by one-way ANOVA and pairwise group comparisons with *post hoc* correction (Supplementary Table S2). Forty-six (46) metabolites satisfied a false discovery rate threshold of less than 10% in this analysis. These were rank ordered by *P*-values. This univariate analysis identified 16 (35% of 46) metabolites (shaded yellow, Supplementary Table S3) that were also found by multivariate analysis across the four groups, and 30 (65%) additional metabolites (unshaded in Supplementary Table S2) that were discriminating only in pairwise group comparisons.

Restoration of normal purine metabolism by APT led to the concerted normalization of 17 (94%) of the 18 biochemical pathway disturbances that characterized the MIA model (Table 1; far right column). Only the bile salt pathway was not restored by suramin (Table 1,Figure 3d). The three bile salt metabolites were highest in the plasma of control animals (Figure 3d; Sal-Sal coded red in the columns on the right), lower in MIA animals (Figure 3d; PIC-Sal coded yellow) and made even lower by suramin (Figure 3d; PIC-Sur, coded dark green). Overall, we found that restoration of normal purine metabolism with APT led to the concerted improvement in both the behavioral and metabolic abnormalities in this model.

DISCUSSION

Children with inborn errors in purine and pyrimidine metabolism have long been known to have neurodevelopmental and behavioral abnormalities.[45] However, the neurochemical basis for the brain and behavioral manifestations of these classic disorders such as Lesch-Nyhan syndrome[46] and adenosine deaminase deficiency[45] is not yet understood. Genetic disorders of purine metabolism were some of the first single-gene disorders found to be associated with ASD behaviors. In 1969, William Nyhan described a 3-year-old boy with autistic behavior and hearing impairment caused by a defect in the first committed step in purine biosynthesis, phosphoribosyl pyrophosphate synthase.[47] This mutation created an enzyme that was resistant to feedback inhibition by ATP, resulting in phosphoribosyl pyrophosphate synthase superactivity, and excess purine biosynthesis.[47–49] Other reports of purine[50] and pyrimidine[51] disorders linked to autism soon followed.

The discovery of ATP signaling by Geoffrey Burnstock just a few years later in 1972 showed for the first time that extracellular nucleotides could act as neurotransmitters.[52] However, the fields of inborn errors in purine and pyrimidine metabolism and purinergic signaling developed independently for the next 40 years. Our work in autism lies at the confluence of these two rivers of investigation. A large number of other single gene disorders,[53] genetic variants, chromosomal and copy number variations[2,54] and environmental factors[6,55] are known to increase the risk of ASD. Most of these have no apparent ties to purine and pyrimidine metabolism. Our results are consistent with the unifying hypothesis that each factor, or mixture of factors, that causes ASD, does so by triggering a conserved cellular response to stress that we have called the CDR.[22] In the MIA mouse model, the CDR is maintained by abnormalities in purinergic signaling that can be treated with antipurinergic drugs such as suramin.

It is well known that ATP inside the cell acts as an energy carrier. It is less well known that ATP and other nucleotides located outside the cell can bind to cell surface receptors and act as signaling molecules and neuromodulators that are important in inflammation,[56] neurotransmission[57] and many other biological processes. As such, ATP, other nucleotides and certain metabolites have been collectively considered as mitokines—signaling molecules traceable to mitochondrial function.[23] Fifteen different isoforms of phosphorylated purinergic nucleotide receptors are now known.[58] Four additional purinergic receptors are responsive to the unphosphorylated nucleoside adenosine, and called the P1, or adenosine receptors.[59] The 15 phosphorylated nucleotide receptors are divided into seven ionotropic P2X1-7 receptors, and eight metabotropic, P2Y G-protein-coupled receptors numbered 1–14. Six former P2Y receptors (nos 3, 5 and 7–10) have been reclassified. Purinergic receptors are expressed in tissue-specific patterns on every cell type in the body. Together, the 19 P1, P2X and P2Y receptors control a broad range of biological functions that have relevance to a number of neurodevelopmental disorders, including autism, schizophrenia, attention deficit/hyperactivity and bipolar disorder. These include synaptogenesis and brain development,[58] neuronal plasticity,[60,61] sleep,[62] regulation of the PI3K/AKT/GSK3β (glycogen synthase kinase-3β) pathway,[63] control of immune responses and chronic inflammation,[64] gut motility,[65] gut permeability,[66] taste chemosensory transduction,[67] sensitivity to food allergies,[68] hearing,[69] innate immune signaling,[70] neuroinflammation, antiviral signaling, microglial activation, neutrophil chemotaxis, autophagy, chronic pain syndromes,[58] cerebellar Purkinje cell signaling and motor coordination,[71] and the regulation of autonomic parasympathetic control of heart rate variability.[72] The importance of metabolism in regulating behavior has recently been highlighted by the discovery that acute inhibition of the metabolic control protein GSK3β restores normal spontaneous alternation in the Y-maze in the MIA model.[73]

Our results show that purine metabolism is a master regulatory pathway in the MIA model (Table 1,Figure 3d,Supplementary Table S1). Correction of purine metabolism with APT restored normal social behavior (Figure 1b) and novelty preference (Figure 1e). Comprehensive metabolomic analysis revealed disturbances in several other metabolic pathways relevant to children with ASDs. These included disturbances in microbiome, phospholipid, cholesterol/sterol, sphingolipid, glycolytic and bile salt metabolism (Table 1). The top, non-microbiome-associated metabolite was quinolinic acid (Figure 3d), which was decreased in the MIA model. Quinolinic acid is a product of the indoleamine 2,3-dioxygenase pathway of tryptophan metabolism.[74] Interestingly, abnormalities in purine,[47,75] tryptophan,[76,77] microbiome,[78,79] phospholipid,[80] cholesterol/sterol[81] and sphingolipid[82,83] metabolism have each been reported in children with ASDs. Abnormalities in purine metabolism,[84] tryptophan,[85] cholesterol/sterol,[86] sphingolipid[87] and phospholipid[88] metabolism have also been described in schizophrenia. Although the detailed metabolic features of ASD and schizophrenia are different, these disorders share biochemical pathway disturbances that reveal the persistent activation of the evolutionarily conserved CDR[22] in both ASD and schizophrenia. These data show that the metabolic disturbances in the MIA model and human ASD and schizophrenia are similar and provide strong support for the biochemical validity of this animal model.

Our results also reveal a novel mechanism by which drugs that cannot penetrate the blood–brain barrier can still have central nervous system effects. We show that suramin is taken up into the brainstem (Figure 2b), an area of the brain known to contain critical collections of chemosensory neurons such as the area postrema that is not protected by the blood–brain barrier.[40]

Purinergic neurons in the area postrema are known to integrate blood-borne signals that activate the hypothalamic–pituitary–-adrenal axis during stress,[89] coordinate parasympathetic and sympathetic autonomic balance[90] and regulate whole-body metabolism and sickness behavior during inflammation[91] in response to the evolutionarily conserved CDR associated with ASDs and other disorders.[22] These data provide a plausible new mechanism that could apply to many drugs that have central nervous system effects but are known not to pass the blood–brain barrier.

Although our results of single-dose correction of abnormal behaviors in an animal model of autism and schizophrenia are encouraging, there are several caveats that must be considered before extending the results to humans. First, while the MIA mouse model captures several features of ASD and schizophrenia, no animal model can fully capture the complexities of human behavior. Second, suramin is a poor drug choice for chronic use because of potentially toxic side effects that can occur with prolonged treatment.[92] Third, human forms of ASD and schizophrenia may occur by mechanisms not captured by the MIA model. Mechanisms that do not involve the CDR[22] may not be amenable to APT. Human clinical trials will be necessary to answer these questions.

In summary, this study identifies purinergic signaling as a novel neurochemical switch that regulates both behavior and metabolism in the MIA mouse model. Our results provide new tools for refining current concepts of pathogenesis in autism, schizophrenia and several other neurodevelopmental disorders, and create a fresh path forward for the development of newer and safer drugs. The data provide preclinical support for the hypothesis that some of this new class of antipurinergic medicines need not be given chronically. Rather, new drugs might be given only once, or intermittently, during sensitive windows to unblock metabolism, restore more normal neural network function, improve resilience and plasticity, and permit improved development in response to behavioral and interdisciplinary therapies, and to natural play.

CONFLICT OF INTEREST

The authors declare no conflict of interest.

ACKNOWLEDGMENTS

We thank Dewleen Baker, Sophia Colamarino, Richard Haas, William Nyhan, Maya Shetreat-Klein, Leanne Chukoskie, Jeanne Townsend, Will Alaynick, Andrea Chiba, Ben Murrell, Jim Adams and Steve Edelson for helpful discussions and comments on the manuscript. We thank Laura Dugan for providing the rotarod and comments on the manuscript. We thank two anonymous reviewers for helpful comments. This research was supported by grants from the Jane Botsford Johnson Foundation (RKN) and National Institute of Health grant MH091407 (SBP), with additional support from the UCSD Christini Foundation, the Wright Family Foundation and the It Takes Guts Foundation to RKN. The funders had no role in the study design, data collection and analysis, decision to publish or preparation of the manuscript.

AUTHOR CONTRIBUTIONS

JCN coordinated the study, conducted the experiments, analyzed the data and wrote parts of the manuscript. MAS conducted some of the mouse behavioral studies and helped with coordination and injections. KL conducted the tissue suramin quantitations and metabolomics. LW helped with brain dissections. VBR established the T-maze task. SBP directed the behavioral studies and their analysis and contributed funding. RKN assembled the team, funded and directed the project, analyzed the data and wrote the manuscript.

REFERENCES

1 Anney R, Klei L, Pinto D, Almeida J, Bacchelli E, Baird G *et al.* Individual common variants exert weak effects on the risk for autism spectrum disorderspi. *Hum Mol Genet* 2012; **21**: 4781–4792.
2 Pinto D, Pagnamenta AT, Klei L, Anney R, Merico D, Regan R *et al.* Functional impact of global rare copy number variation in autism spectrum disorders. *Nature* 2010; **466**: 368–372.
3 Casey JP, Magalhaes T, Conroy JM, Regan R, Shah N, Anney R *et al.* A novel approach of homozygous haplotype sharing identifies candidate genes in autism spectrum disorder. *Hum Genet* 2012; **131**: 565–579.
4 Volk HE, Lurmann F, Penfold B, Hertz-Picciotto I, McConnell R. Traffic-related air pollution, particulate matter, and autism. *JAMA Psychiatry* 2013; **70**: 71–77.
5 Hallmayer J, Cleveland S, Torres A, Phillips J, Cohen B, Torigoe T *et al.* Genetic heritability and shared environmental factors among twin pairs with autism. *Arch Gen Psychiatry* 2011; **68**: 1095–1102.
6 Krakowiak P, Walker CK, Bremer AA, Baker AS, Ozonoff S, Hansen RL *et al.* Maternal metabolic conditions and risk for autism and other neurodevelopmental disorders. *Pediatrics* 2012; **129**: e1121–e1128.
7 Curran LK, Newschaffer CJ, Lee LC, Crawford SO, Johnston MV, Zimmerman AW. Behaviors associated with fever in children with autism spectrum disorders. *Pediatrics* 2007; **120**: e1386–e1392.
8 Vogel G. Malaria as lifesaving therapy. *Science* 2013; **342**: 686.
9 Patterson PH. *Infectious Behavior--Brain-Immune Connections in Autism, Schizophrenia, and Depression*. The MIT Press,Cambridge, MA, USA, 2011, p 162.
10 Mednick SA, Machon RA, Huttunen MO, Bonett D. Adult schizophrenia following prenatal exposure to an influenza epidemic. *Arch Gen Psychiatry* 1988; **45**: 189–192.
11 Zerbo O, Iosif AM, Walker C, Ozonoff S, Hansen RL, Hertz-Picciotto I. Is maternal influenza or fever during pregnancy associated with autism or developmental delays? Results from the CHARGE (CHildhood Autism Risks from Genetics and Environment) Study. *J Autism Dev Disord* 2013; **43**: 25–33.
12 Pineda DA, Palacio LG, Puerta IC, Merchan V, Arango CP, Galvis AY *et al.* Environmental influences that affect attention deficit/hyperactivity disorder: study of a genetic isolate. *Eur Child Adolesc Psychiatry* 2007; **16**: 337–346.
13 Parboosing R, Bao Y, Shen L, Schaefer CA, Brown AS. Gestational influenza and bipolar disorder in adult offspring. *JAMA Psychiatry* 2013; **70**: 677–685.
14 Sun Y, Vestergaard M, Christensen J, Nahmias AJ, Olsen J. Prenatal exposure to maternal infections and epilepsy in childhood: a population-based cohort study. *Pediatrics* 2008; **121**: e1100–e1107.
15 Harvey L, Boksa P. Prenatal and postnatal animal models of immune activation: relevance to a range of neurodevelopmental disorders. *Dev Neurobiol* 2012; **72**: 1335–1348.
16 Accardi MV, Daniels BA, Brown PM, Fritschy JM, Tyagarajan SK, Bowie D. Mitochondrial reactive oxygen species regulate the strength of inhibitory GABA-mediated synaptic transmission. *Nat Commun* 2014; **5**: 3168.
17 Pascual O, Casper KB, Kubera C, Zhang J, Revilla-Sanchez R, Sul JY *et al.* Astrocytic purinergic signaling coordinates synaptic networks. *Science* 2005; **310**: 113–116.
18 Malkova NV, Yu CZ, Hsiao EY, Moore MJ, Patterson PH. Maternal immune activation yields offspring displaying mouse versions of the three core symptoms of autism. *Brain Behav Immun* 2012; **26**: 607–616.
19 Pacheco-Lopez G, Giovanoli S, Langhans W, Meyer U. Priming of metabolic dysfunctions by prenatal immune activation in mice: relevance to schizophrenia. *Schizophr Bull* 2013; **39**: 319–329.
20 Patterson PH. Modeling autistic features in animals. *Pediatr Res* 2011; **69**: 34R–40R.
21 Bitanihirwe BK, Peleg-Raibstein D, Mouttet F, Feldon J, Meyer U. Late prenatal immune activation in mice leads to behavioral and neurochemical abnormalities relevant to the negative symptoms of schizophrenia. *Neuropsychopharmacology* 2010; **35**: 2462–2478.
22 Naviaux RK. Metabolic features of the cell danger response. *Mitochondrion* advance online publication, 24 August 2013; PMID: 23981537.
23 Naviaux RK, Zolkipli Z, Wang L, Nakayama T, Naviaux JC, Le TP *et al.* Antipurinergic therapy corrects the autism-like features in the poly(IC) mouse model. *PLoS ONE* 2013; **8**: e57380.
24 Flurkey K, Currer JM, Harrison DE. Mouse models in aging research. In: Fox JG ea (ed) *The Mouse in Biomedical Research*, 2nd edn, vol. 3. Academic Press: San Diego, CA, USA, 2007 pp 637–672.
25 Frye CA, Walf AA. Effects of progesterone administration and APPswe+PSEN1-Deltae9 mutation for cognitive performance of mid-aged mice. *Neurobiol Learn Memory* 2008; **89**: 17–26.
26 Toth M, Gresack JE, Bangasser DA, Plona Z, Valentino RJ, Flandreau EI *et al.* Forebrain-specific CRF over-production during development is sufficient to induce enduring anxiety and startle abnormalities in adult mice. *Neuropsychopharmacology* 2014; **39**: 1409–1419.
27 Bajad S, Shulaev V. LC-MS-based metabolomics. *Methods Mol Biol* 2011; **708**: 213–228.
28 Golde WT, Gollobin P, Rodriguez LL. A rapid, simple, and humane method for submandibular bleeding of mice using a lancet. *Lab Anim* 2005; **34**: 39–43.

29 Xia J, Mandal R, Sinelnikov IV, Broadhurst D, Wishart DS. MetaboAnalyst 2.0--a comprehensive server for metabolomic data analysis. *Nucleic Acids Res* 2012; **40**: W127–W133.
30 Moy SS, Nadler JJ, Young NB, Nonneman RJ, Segall SK, Andrade GM *et al.* Social approach and repetitive behavior in eleven inbred mouse strains. *Behav Brain Res* 2008; **191**: 118–129.
31 Intine RV, Sarras MP Jr. Metabolic memory and chronic diabetes complications: potential role for epigenetic mechanisms. *Curr Diabetes Rep* 2012; **12**: 551–559.
32 Hughes RN. Neotic preferences in laboratory rodents: issues, assessment and substrates. *Neurosci Biobehav Rev* 2007; **31**: 441–464.
33 Vecera SP, Rothbart MK, Posner MI. Development of spontaneous alternation in infancy. *J Cogn Neurosci* 1991; **3**: 351–354.
34 Munson J, Faja S, Meltzoff A, Abbott R, Dawson G. Neurocognitive predictors of social and communicative developmental trajectories in preschoolers with autism spectrum disorders. *J Int Neuropsychol Soc* 2008; **14**: 956–966.
35 Gotham K, Bishop SL, Hus V, Huerta M, Lund S, Buja A *et al.* Exploring the relationship between anxiety and insistence on sameness in autism spectrum disorders. *Autism res* 2013; **6**: 33–41.
36 Moy SS, Nadler JJ, Young NB, Perez A, Holloway LP, Barbaro RP *et al.* Mouse behavioral tasks relevant to autism: phenotypes of 10 inbred strains. *Behav Brain Res* 2007; **176**: 4–20.
37 Shi L, Smith SE, Malkova N, Tse D, Su Y, Patterson PH. Activation of the maternal immune system alters cerebellar development in the offspring. *Brain Behav Immun* 2009; **23**: 116–123.
38 Tsai PT, Hull C, Chu Y, Greene-Colozzi E, Sadowski AR, Leech JM *et al.* Autistic-like behaviour and cerebellar dysfunction in Purkinje cell Tsc1 mutant mice. *Nature* 2012; **488**: 647–651.
39 Hawking F. Concentration of Bayer 205 (Germanin) in human blood and cerebrospinal fluid after treatment. *Trans R Soc Trop Med Hyg* 1940; **34**: 37–52.
40 Siso S, Jeffrey M, Gonzalez L. Sensory circumventricular organs in health and disease. *Acta Neuropathol*2010; **120**: 689–705.
41 Sola F, Farao M, Pesenti E, Marsiglio A, Mongelli N, Grandi M. Antitumor activity of FCE 26644 a new growth-factor complexing molecule. *Cancer Chemother Pharmacol* 1995; **36**: 217–222.
42 Jacobson KA, Balasubramanian R, Deflorian F, Gao ZG. G protein-coupled adenosine (P1) and P2Y receptors: ligand design and receptor interactions. *Purinergic Signal* 2012; **8**: 419–436.
43 Adams JB, Audhya T, McDonough-Means S, Rubin RA, Quig D, Geis E *et al.* Nutritional and metabolic status of children with autism vs neurotypical children, and the association with autism severity. *Nutr Metab* 2011; **8**: 34.
44 Wikoff WR, Anfora AT, Liu J, Schultz PG, Lesley SA, Peters EC *et al.* Metabolomics analysis reveals large effects of gut microflora on mammalian blood metabolites. *Proc Natl Acad Sci USA* 2009; **106**: 3698–3703.
45 Micheli V, Camici M, Tozzi MG, Ipata PL, Sestini S, Bertelli M *et al.* Neurological disorders of purine and pyrimidine metabolism. *Curr Top Med Chem* 2011; **11**: 923–947.
46 Nyhan WL. Disorders of purine and pyrimidine metabolism. *Mol Genet Metab* 2005; **86**: 25–33.
47 Nyhan WL, James JA, Teberg AJ, Sweetman L, Nelson LG. A new disorder of purine metabolism with behavioral manifestations. *J Pediatr* 1969; **74**: 20–27.
48 Becker MA, Raivio KO, Bakay B, Adams WB, Nyhan WL. Variant human phosphoribosylpyrophosphate synthetase altered in regulatory and catalytic functions. *J Clin Invest* 1980; **65**: 109–120.
49 Nyhan WL. Phosphoribosylpyrophosphate synthetase and its abnormalities. *Atlas of Inherited Metabolic Disorders*. 3rd edn Hodder Arnold: London, UK, 2012, 503–506.
50 Ciardo F, Salerno C, Curatolo P. Neurologic aspects of adenylosuccinate lyase deficiency. *J Child Neurol* 2001; **16**: 301–308.
51 Berger R, Stoker-de Vries SA, Wadman SK, Duran M, Beemer FA, de Bree PK *et al.* Dihydropyrimidine dehydrogenase deficiency leading to thymine-uraciluria. An inborn error of pyrimidine metabolism. *Clin Chim Acta* 1984; **141**: 227–234.
52 Burnstock G, Satchell DG, Smythe A. A comparison of the excitatory and inhibitory effects of non-adrenergic, non-cholinergic nerve stimulation and exogenously applied ATP on a variety of smooth muscle preparations from different vertebrate species. *Br J Pharmacol* 1972; **46**: 234–242.
53 Miles JH. Autism spectrum disorders--a genetics review. *Genet Med* 2011; **13**: 278–294.
54 Betancur C. Etiological heterogeneity in autism spectrum disorders: more than 100 genetic and genomic disorders and still counting. *Brain Res* 2011; **1380**: 42–77.
55 McDonald ME, Paul JF. Timing of increased autistic disorder cumulative incidence. *Environ Sci Technol* 2010; **44**: 2112–2118.
56 Eltzschig HK, Sitkovsky MV, Robson SC. Purinergic signaling during inflammation. *New Engl J Med* 2012; **367**: 2322–2333.
57 Burnstock G. Introduction to purinergic signalling in the brain. *Adv Exp Med Biol* 2013; **986**: 1–12.
58 Abbracchio MP, Burnstock G, Verkhratsky A, Zimmermann H. Purinergic signalling in the nervous system: an overview. *Trends Neurosci* 2009; **32**: 19–29.
59 Chen JF, Eltzschig HK, Fredholm BB. Adenosine receptors as drug targets--what are the challenges? *Nat Rev Drug Discov* 2013; **12**: 265–286.
60 Chen J, Tan Z, Zeng L, Zhang X, He Y, Gao W *et al.* Heterosynaptic long-term depression mediated by ATP released from astrocytes. *Glia* 2013; **61**: 178–191.
61 Dias RB, Rombo DM, Ribeiro JA, Henley JM, Sebastiao AM. Adenosine: setting the stage for plasticity. *Trends Neurosci* 2013; **36**: 248–257.
62 Halassa MM. Thalamocortical dynamics of sleep: roles of purinergic neuromodulation. *Semin Cell Dev Biol* 2011; **22**: 245–251.
63 Franke H, Sauer C, Rudolph C, Krugel U, Hengstler JG, Illes P. P2 receptor-mediated stimulation of the PI3-K/Akt-pathway *in vivo*. *Glia* 2009; **57**: 1031–1045.
64 Pelegrin P. Targeting interleukin-1 signaling in chronic inflammation: focus on P2X(7) receptor and Pannexin-1. *Drug News Perspect* 2008; **21**: 424–433.
65 Gallego D, Vanden Berghe P, Farre R, Tack J, Jimenez M. P2Y1 receptors mediate inhibitory neuromuscular transmission and enteric neuronal activation in small intestine. *Neurogastroenterol Motil* 2008; **20**: 159–168.
66 Matos JE, Sorensen MV, Geyti CS, Robaye B, Boeynaems JM, Leipziger J. Distal colonic Na(+) absorption inhibited by luminal P2Y(2) receptors. *Pflugers Arch Eur J Physiol* 2007; **454**: 977–987.
67 Surprenant A, North RA. Signaling at purinergic P2X receptors. *Annu Rev Physiol* 2009; **71**: 333–359.
68 Leng Y, Yamamoto T, Kadowaki M. Alteration of cholinergic, purinergic and sensory neurotransmission in the mouse colon of food allergy model. *Neurosci Lett* 2008; **445**: 195–198.
69 Housley GD, Jagger DJ, Greenwood D, Raybould NP, Salih SG, Jarlebark LE *et al.* Purinergic regulation of sound transduction and auditory neurotransmission. *Audiol Neurootol* 2002; **7**: 55–61.
70 Zhang Q, Raoof M, Chen Y, Sumi Y, Sursal T, Junger W *et al.* Circulating mitochondrial DAMPs cause inflammatory responses to injury. *Nature* 2010; **464**: 104–107.
71 Brockhaus J, Dressel D, Herold S, Deitmer JW. Purinergic modulation of synaptic input to Purkinje neurons in rat cerebellar brain slices. *Eur J Neurosci* 2004; **19**: 2221–2230.
72 Kirchhof P, Fabritz L, Fortmuller L, Matherne GP, Lankford A, Baba HA *et al.* Altered sinus nodal and atrioventricular nodal function in freely moving mice overexpressing the A1 adenosine receptor. *Am J Physiol Heart Circ Physiol* 2003; **285**: H145–H153.
73 Willi R, Harmeier A, Giovanoli S, Meyer U. Altered GSK3beta signaling in an infection- based mouse model of developmental neuropsychiatric disease. *Neuropharmacology* 2013; **73**: 56–65.
74 Takikawa O. Biochemical and medical aspects of the indoleamine 2,3-dioxygenase- initiated L-tryptophan metabolism. *Biochem Biophys Res Commun* 2005; **338**: 12–19.
75 Page T, Coleman M. Purine metabolism abnormalities in a hyperuricosuric subclass of autism. *Biochim Biophys Acta* 2000; **1500**: 291–296.
76 Schain RJ, Freedman DX. Studies on 5-hydroxyindole metabolism in autistic and other mentally retarded children. *J Pediatr* 1961; **58**: 315–320.
77 Mulder EJ, Anderson GM, Kema IP, de Bildt A, van Lang ND, den Boer JA *et al.* Platelet serotonin levels in pervasive developmental disorders and mental retardation: diagnostic group differences, within-group distribution, and behavioral correlates. *J Am Acad Child Adolesc Psychiatry* 2004; **43**: 491–499.
78 Mulle JG, Sharp WG, Cubells JF. The gut microbiome: a new frontier in autism research. *Curr Psychiatry Rep* 2013; **15**: 337.
79 Williams BL, Hornig M, Buie T, Bauman ML, Cho Paik M, Wick I *et al.* Impaired carbohydrate digestion and transport and mucosal dysbiosis in the intestines of children with autism and gastrointestinal disturbances. *PLoS ONE* 2011; **6**: e24585.
80 Pastural E, Ritchie S, Lu Y, Jin W, Kavianpour A, Khine Su-Myat K *et al.* Novel plasma phospholipid biomarkers of autism: mitochondrial dysfunction as a putative causative mechanism. *Prostaglandins Leukot Essen Fatty Acids* 2009; **81**: 253–264.
81 Tierney E, Bukelis I, Thompson RE, Ahmed K, Aneja A, Kratz L *et al.* Abnormalities of cholesterol metabolism in autism spectrum disorders. *Am J Med Genet* 2006; **141B**: 666–668.
82 Schengrund CL, Ali-Rahmani F, Ramer JC. Cholesterol, GM1, and autism. *Neurochem Res* 2012; **37**: 1201–1207.
83 Nordin V, Lekman A, Johansson M, Fredman P, Gillberg C. Gangliosides in cerebrospinal fluid in children with autism spectrum disorders. *Dev Med Child Neurol* 1998; **40**: 587–594.
84 Yao JK, Dougherty GG, Reddy RD, Matson WR, Kaddurah-Daouk R, Keshavan MS. Associations between purine metabolites and monoamine neurotransmitters in first- episode psychosis. *Front Cell Neurosci* 2013; **7**: 90.

85 Yao JK, Dougherty GG Jr., Reddy RD, Keshavan MS, Montrose DM, Matson WR *et al*. Altered interactions of tryptophan metabolites in first-episode neuroleptic-naive patients with schizophrenia. *Mol Psychiatry* 2010; **15**: 938–953.
86 Bicikova M, Hill M, Ripova D, Mohr P, Hampl R. Determination of steroid metabolome as a possible tool for laboratory diagnosis of schizophrenia. *J Steroid Biochem Mol Biol* 2013; **133**: 77–83.
87 Smesny S, Schmelzer CE, Hinder A, Kohler A, Schneider C, Rudzok M *et al*. Skin ceramide alterations in first-episode schizophrenia indicate abnormal sphingolipid metabolism. *Schizophr Bull* 2013; **39**: 933–941.
88 Kaddurah-Daouk R, McEvoy J, Baillie R, Zhu H, K Yao J, Nimgaonkar VL *et al*. Impaired plasmalogens in patients with schizophrenia. *Psychiatry Res* 2012; **198**: 347–352.
89 Lee HY, Whiteside MB, Herkenham M. Area postrema removal abolishes stimulatory effects of intravenous interleukin-1beta on hypothalamic-pituitary-adrenal axis activity and c-fos mRNA in the hypothalamic paraventricular nucleus. *Brain Res Bull* 1998; **46**: 495–503.
90 Price CJ, Hoyda TD, Ferguson AV. The area postrema: a brain monitor and integrator of systemic autonomic state. *Neuroscientist* 2008; **14**: 182–194.
91 McCusker RH, Kelley KW. Immune-neural connections: how the immune system's response to infectious agents influences behavior. *J Exp Biol* 2013; **216**: 84–98.
92 Voogd TE, Vansterkenburg EL, Wilting J, Janssen LH. Recent research on the biological activity of suramin. *Pharmacol Rev* 1993; **45**: 177–203.

Supplementary Information accompanies the paper on the Translational Psychiatry website (http://www.nature.com/tp)

SUPPLEMENTARY ONLINE MATERIAL

FULL METHODS ONLINE

Social Preference

Social preference was tested using a three-chambered box similar to what has been previously described[1]. Briefly, a Plexiglas box (60cm L x 60cm W x 30cm H) was divided into 3 equal compartments by Plexiglas partitions containing an opening through which the mice could freely enter the 3 chambers. All testing was performed between the hours of 8 am and 1 pm. The test was conducted in two 10-minute phases. In phase I, the test mouse was allowed to explore the chambers for 10 minutes. Pilot experiments showed that mice did most of their chamber exploration and zone interaction in the first half of each block. Therefore, we report social preference as the time spent interacting socially (sniffing) in first 5 minutes of each phase. Each of the two outer chambers contained an empty, inverted stainless steel wire cup (Galaxy Cup, Spectrum Diversified Designs, Inc., Streetsboro, OH). Stranger mice were habituated to a wire cup for at least 30 minutes before use. In phase II, the test mouse was briefly removed, an unfamiliar mouse, age and sex matched, was placed under one of the wire cups and Lego blocks were placed under the other wire cup. The test mouse was then gently placed back in the arena and given an additional 10 minutes to explore. Room lighting for social behavior studies was 1-2 lux, measured using a Minolta IV F light meter. An overhead camera (Sony CCD Digital Ultra Pro Series, able to detect images down to 0.05 lux). and Ethovision v3 video tracking software (Noldus, Leesburg VA) were used to record the amount of time spent in each chamber and the number of entries into each chamber. In addition, a human observer, blinded to the treatment groups, scored time spent sniffing each wire cage, using Ethovision Observer software. Only male mice were tested. Stranger mice were used up to 4 times before new strangers were cycled in. The location (left or right) of the novel object and novel mouse alternated across subjects. To avoid chance differences in groups selected for single-dose treatment, the saline and poly(IC) exposure groups were each balanced according to their social

approach scores at 2.25 months of age prior to single-dose treatment with saline or suramin at 6.5 months. Results of social behavior testing are reported as the percent of time spent interacting with a stranger mouse (vs Lego blocks) in the first five minutes (mean +/- SEM). Social behaviors were evaluated at 2-4 days, and 5 weeks after suramin injection.

T-Maze

The T-maze apparatus is constructed of black plexiglass. The protocol is adapted from Frye and Walf[2]. The main stem is 45 cm long, 10 cm wide, and 24 cm high. Each side arm is 35 cm long, 10 cm wide, and 24 cm high. The side arms are separated from the stem by horizontal sliding doors. A start box, 8 cm in length, is also separated by a horizontal sliding door. Testing was conducted by an examiner that was blinded to the experimental groups, under low illumination, between 8 am and 1 pm. Only male animals were tested. Each mouse was tested in a session of 11 successive trials. The mice were not habituated to the maze. For the first trial only, one goal arm was closed off, forcing the mouse to choose the only open arm. Subsequent trials were by free choice. The chosen arm, and the time it takes for the mouse to choose (latency) were recorded. There was no confinement time in the chosen arm or in the start box. We confirmed that the saline and poly(IC) exposure groups had equivalent pre-treatment T-maze scores prior to single-dose treatment with saline or suramin. The percentage of alternated choices (mean +/- SEM) is reported. Spontaneous alternation was evaluated at 2-4 days, and 5 weeks after suramin injection.

Rotarod

Training and testing were performed between the hours of 8 am and 1 pm using an accelerating rotarod protocol[3] (Economex Rotarod, Columbus Instruments fitted with a 4 cm diameter grooved plastic (not steel) spindle) as previously described[4] _ENREF_85. The plastic spindle is more slippery than grooved steel and results in shorter, but highly reproducible latencies. Only

male animals were tested. Prior to testing on an accelerating rod, mice were first trained at a fixed speed of 4 rpm. Each mouse was given up to 3 consecutive trials to achieve the endpoint of maintaining balance on the rotarod for at least 30 seconds. If a mouse was unsuccessful in the first 3 attempts, it was rested for 30 minutes, and then given another 3 attempts. Using this training protocol, all of the mice successfully maintained balance for 30 seconds within 2 training sessions. The acceleration phase testing was conducted over the subsequent 2 days, with 4 trials per day. Each mouse was individually placed on the rotarod at 4 rpm, which was then accelerated from 4 to 40 rpm over 5 minutes. The inter-trial time between repeat tests was 45 minutes. Latency to fall was recorded in seconds. Observers were blinded to treatment groups. Rotarod room lighting was 20-22 lux.

Light-Dark Box

Anxiety-related and light-avoidance behaviors were tested in the light-dark box paradigm as previously described[5]. Briefly, the light-dark box consisted of two 18 × 20 × 18 cm chambers joined by a 6 × 6 cm door, with one side well-lit (850 lux) and the other side enclosed and darkened (≤ 5 lux). At the start of the test, mice were placed in the light compartment and activity was recorded for 10 min. Percent time in the light chamber was analyzed by Ethovision Tracking Software (Noldus, Leesburg, VA, USA).

SOM TABLES AND LEGENDS

SOM Table S1. Biochemical Pathways Interrogated by Metabolomic Analysis.

SOM Table S2. Rank Ordered Metabolites by Univariate Analysis.

SOM Table S2 Legend. Univariate analysis by 1-way ANOVA and a false discovery rate (FDR) threshold of 10% were used with pair-wise comparison and post hoc testing by Fisher's least significant difference method to identify metabolites that could discriminate between pairs of experimental groups. Metabolites shaded yellow were also identified by multivariate analysis (Figure 3d).

SOM Table S3. Stable Isotope Internal Standards for LC-MS/MS.

SOM FIGURE LEGENDS

SOM Figure S1. Single-Dose Correction of Behavioral Abnormalities. (a) Social abnormalities in male MIA animals were found at the earliest ages of testing at 2.25 months of age. The four groups were balanced before treatment with saline or suramin. 2-way ANOVA followed by student's t-test with Bonferroni post-hoc correction was used to compare the time spent with mouse and cup in each experimental group. There was an interaction between prenatal exposure (Saline/Poly(IC)) and stimulus (mouse/cup); ($F(3,39) = 9.28$; $p < 0.0001$; N = 9-13 per group). Student's t-test showed a social preference (mouse > cup) for the control (Saline) animals ($p < 0.0001$ = ****) and no significant preference for the MIA (Poly(IC)) animals (p = ns). **(b)** Single dose treatment of 6.5-month old MIA mice with suramin (PIC-Sur) restored normal social behavior ($p < 0.0001$ = ****). Repeated measures ANOVA was used to test for the presence of interaction between prenatal exposure, drug treatment, and stimulus (mouse/cup). There was a prenatal exposure x drug treatment x stimulus interaction ($F(1,39) = 9.34$; $p < 0.01$) consistent with the observation that suramin benefited social behavior in the MIA animals, but had no effect on normal controls. Student's t-test with Bonferroni post-hoc correction was used to compare the time spent with mouse and cup in each experimental group. Saline treatment of MIA mice (PIC-Sal) had no effect; the time with mouse and cup were not significantly different (p = ns). (N = 8-13 per group). **(c)** After 5 weeks of suramin washout, the social behavior remained improved compared to saline-treated animals, but was decreased from the first week after treatment. Repeated measures ANOVA revealed an interaction between prenatal exposure and stimulus ($F(1,39) = 6.35$; $p < 0.05$) but no 3-way interaction between prenatal exposure, drug treatment, and zone. Student's t-test with Bonferroni post-hoc correction was used to compare the time spent with mouse and cup in each experimental group. This showed persistent absence of social preference in the saline-treated MIA animals (PIC-Sal; p = ns), but still some residual social benefit of suramin 5-weeks after drug washout (PIC-Sur

mouse vs cup time; $p < 0.01$ = **). (N = 8-13 per group). Values are expressed as means +/- SEM.

SOM Figure S2. Light-Dark Box Behavior. MIA and control animals were given a choice between spending time in the dark or exploring in the light. The percent time spent in the dark, measured over 10 minutes, was used as an index of avoidance or anxiety. No differences were found in the MIA model using our protocol ($p = 0.96$ (ns); Student's t-test; Saline = 59.2 +/- 3.8%; Poly(IC) = 58.9 +/- 3.8%). Animals were 3.5-month old C57BL/6J MIA (poly(IC)-exposed) or control (saline-exposed) males. N = 19 Saline exposed and 25 Poly(IC).

Online Supplementary References

1. Moy SS, Nadler JJ, Young NB, Nonneman RJ, Segall SK, Andrade GM *et al.* Social approach and repetitive behavior in eleven inbred mouse strains. *Behavioural brain research* 2008; **191**(1)**:** 118-129.

2. Frye CA, Walf AA. Effects of progesterone administration and APPswe+PSEN1Deltae9 mutation for cognitive performance of mid-aged mice. *Neurobiology of learning and memory* 2008; **89**(1)**:** 17-26.

3. Pallier PN, Drew CJ, Morton AJ. The detection and measurement of locomotor deficits in a transgenic mouse model of Huntington's disease are task- and protocol-dependent: influence of non-motor factors on locomotor function. *Brain research bulletin* 2009; **78**(6)**:** 347-355.

4. Naviaux RK, Zolkipli Z, Wang L, Nakayama T, Naviaux JC, Le TP *et al.* Antipurinergic Therapy Corrects the Autism-Like Features in the Poly(IC) Mouse Model. *PloS one* 2013; **8**(3)**:** e57380.

5. Toth M, Gresack JE, Bangasser DA, Plona Z, Valentino RJ, Flandreau EI *et al.* Forebrain-Specific CRF Over-Production During Development is Sufficient to Induce Enduring Anxiety and Startle Abnormalities in Adult Mice. *Neuropsychopharmacology : official publication of the American College of Neuropsychopharmacology* 2013.

SOM Table S1. Biochemical Pathways Interrogated by Metabolomic Analysis.

Pathway	Metabolites	Pathway	Metabolites
1-Carbon, Folate, Formate, Glycine	6	Oxalate, Glyxoylate Metabolism	3
Amino acid metabolism not otherwise covered	6	Pentose Phosphate, Gluconate Metabolism	11
Amino-Sugar and Galactose Metabolism	10	Phosphate and Pyrophosphate Metabolism	1
Bile Salt Metabolism	4	Phospholipid Metabolism	88
Bioamines and Neurotransmitter Metabolism	3	Phytanic, Branch, Odd Chain Fatty Acids	1
Biopterin, Neopterin, Molybdopterin Metabolism	1	Polyamine Metabolism	4
Biotin (Vitamin B7) Metabolism	1	Purine Metabolism	48
Branch Chain Amino Acid Metabolism	7	Pyrimidine Metabolism	35
Cholesterol, Cortisol, Steroid Metabolism	19	SAM, SAH, Methionine, Cysteine, Glutathione Metabolism	22
Endocannabinoid Metabolism	1	Sphingolipid Metabolism	72
Fatty Acid Oxidation and Synthesis	7	Taurine, Hypotaurine Metabolism	2
Food Sources, Additives, Preservatives, Colorings, and Dyes	2	Thyroxine Metabolism	1
GABA, Glutamate, Arginine, Ornithine, Proline Metabolism	6	Tryptophan, Kynurenine, Serotonin, Melatonin Metabolism	6
Glycolysis and Gluconeogenesis	17	Tyrosine and Phenylalanine Metabolism	2
Histidine, Histamine Metabolism	2	Urea Cycle	5
Isoleucine, Valine, Threonine, or Methionine Metabolism	3	Vitamin B1 (Thiamine) Metabolism	4
Ketone Body Metabolism	2	Vitamin B12 (Cobalamin) Metabolism	1
Krebs Cycle	18	Vitamin B2 (Riboflavin) Metabolism	4
Lysine Metabolism	2	Vitamin B3 (Niacin/NAD) Metabolism	7
Microbiome Metabolism	32	Vitamin B5 (Pantothenate) Metabolism	1
Nitric Oxide, Superoxide, Peroxide Metabolism	1	Vitamin B6 (Pyridoxine) Metabolism	6
OTC and Prescription Pharmaceutical Metabolism	2	Vitamin C (Ascorbate) Metabolism	2
Subtotal	152	Subtotal	326
TOTAL Pathways and Chemical Sources	**44**	**TOTAL Metabolites**	**478**

SOM Table S2. Rank Ordered Metabolites by Univariate Analysis.

No.	Pathway	Metabolite	p-value	-Log10(p)	FDR	Fisher's LSD
1	Phospholipid Metabolism	Glycerophosphocholine	2.47E-07	6.6078	7.70E-05	PIC Sur - PIC Sal; Sal Sal - PIC Sal; PIC Sur - PIC Sur W/O; Sal Sal - PIC Sur W/O
2	Cholesterol, Cortisol, Steroid Metabolism	24,25-Epoxycholesterol	3.22E-07	6.4917	7.70E-05	PIC Sal - PIC Sur; PIC Sal - Sal Sal; PIC Sur W/O - PIC Sur; PIC Sur W/O - Sal Sal
3	Purine Metabolism	dAMP	5.11E-07	6.2918	7.88E-05	PIC Sal - PIC Sur; PIC Sal - Sal Sal; PIC Sur W/O - PIC Sur; PIC Sur W/O - Sal Sal
4	Microbiome Metabolism	Hydroxyphenylacetic acid	6.59E-07	6.1808	7.88E-05	PIC Sal - PIC Sur; PIC Sal - Sal Sal; PIC Sur W/O - PIC Sur; PIC Sur W/O - Sal Sal
5	Krebs Cycle	Oxaloacetic acid	0.00018264	3.7384	0.01746	PIC Sur - PIC Sal; Sal Sal - PIC Sal; PIC Sur - PIC Sur W/O; Sal Sal - PIC Sur W/O
6	Phospholipid Metabolism	Palmitoylethanolamide	0.00024171	3.6167	0.018301	PIC Sur - PIC Sal; Sal Sal - PIC Sal; PIC Sur - PIC Sur W/O; Sal Sal - PIC Sur W/O
7	Pyrimidine Metabolism	Deoxyuridine	0.00029313	3.5329	0.018301	PIC Sal - PIC Sur; PIC Sal - Sal Sal; PIC Sur W/O - PIC Sur; PIC Sur W/O - Sal Sal
8	Tryptophan Metabolism	Kynurenic acid	0.00032056	3.4941	0.018301	PIC Sur - PIC Sal; Sal Sal - PIC Sal; PIC Sur - PIC Sur W/O; PIC Sur - Sal Sal
9	Pyrimidine Metabolism	Uridine	0.00034459	3.4627	0.018301	PIC Sur - PIC Sal; Sal Sal - PIC Sal; PIC Sur - PIC Sur W/O; Sal Sal - PIC Sur W/O
10	Purine Metabolism	ATP	0.00043906	3.3575	0.020987	PIC Sur - PIC Sal; Sal Sal - PIC Sal; PIC Sur - PIC Sur W/O; Sal Sal - PIC Sur W/O
11	Purine Metabolism	Adenine	0.00060284	3.2198	0.025208	PIC Sur - PIC Sal; Sal Sal - PIC Sal; PIC Sur - PIC Sur W/O; Sal Sal - PIC Sur W/O
12	Microbiome Metabolism	2,3-Dihydroxybenzoate	0.00063285	3.1987	0.025208	PIC Sur - PIC Sal; Sal Sal - PIC Sal; PIC Sur - PIC Sur W/O; Sal Sal - PIC Sur W/O
13	Microbiome Metabolism	2-oxo-4-methylthiobutanoate	0.00071951	3.143	0.025357	PIC Sur - PIC Sal; Sal Sal - PIC Sal; PIC Sur - PIC Sur W/O; Sal Sal - PIC Sur W/O
14	Pyrimidine Metabolism	Thymine	0.00074269	3.1292	0.025357	PIC Sur - PIC Sal; Sal Sal - PIC Sal; PIC Sur - PIC Sur W/O; Sal Sal - PIC Sur W/O
15	Vitamin B6 (Pyridoxine) Metabolism	Nicotinate	0.0010241	2.9897	0.032629	Sal Sal - PIC Sal; PIC Sur - PIC Sur W/O; Sal Sal - PIC Sur W/O
16	Sphingolipid Metabolism	Ceramide 22:0	0.0010922	2.9617	0.032629	PIC Sur - PIC Sal; Sal Sal - PIC Sal; PIC Sur - PIC Sur W/O; Sal Sal - PIC Sur W/O
17	Phospholipid Metabolism	PC(18:0/20:3)	0.0014321	2.844	0.037644	PIC Sur - PIC Sal; Sal Sal - PIC Sal; PIC Sur - PIC Sur W/O; Sal Sal - PIC Sur W/O
18	Tryptophan Metabolism	Quinolinic Acid	0.0014598	2.8357	0.037644	Sal Sal - PIC Sal; Sal Sal - PIC Sur; Sal Sal - PIC Sur W/O
19	Glycolysis, Gluconeogenesis, Galactose Metabolism	D-Fructose 6-phosphate	0.0017065	2.7679	0.037644	PIC Sur - PIC Sal; Sal Sal - PIC Sal; PIC Sur - PIC Sur W/O; Sal Sal - PIC Sur W/O
20	Fatty Acid Oxidation and Synthesis	Oleic acid	0.0017085	2.7674	0.037644	PIC Sur - PIC Sal; PIC Sur - PIC Sur W/O; Sal Sal - PIC Sur W/O
21	Microbiome Metabolism	Benzoic acid	0.0017142	2.7659	0.037644	Sal Sal - PIC Sal; Sal Sal - PIC Sur; Sal Sal - PIC Sur W/O
22	Pyrimidine Metabolism	Carbamoyl-phosphate	0.0018628	2.7298	0.037644	PIC Sal - PIC Sur W/O; PIC Sur - PIC Sur W/O; Sal Sal - PIC Sur W/O
23	Vitamin B5 (Pantothenate) Metabolism	Pantothenic acid	0.0018832	2.7251	0.037644	PIC Sal - PIC Sur; PIC Sal - Sal Sal; PIC Sur W/O - PIC Sur; PIC Sur W/O - Sal Sal
24	SAM, SAH, Methionine, Cysteine, Glutathione Metabolism	Dimethylglycine	0.0018901	2.7235	0.037644	PIC Sur - PIC Sal; PIC Sur - PIC Sur W/O; PIC Sur - Sal Sal
25	Phospholipid Metabolism	N-oleoylethanolamine	0.0029363	2.5322	0.052436	PIC Sur - PIC Sal; Sal Sal - PIC Sal; PIC Sur - PIC Sur W/O
26	Microbiome Metabolism	Xanthosine	0.0029631	2.5283	0.052436	PIC Sur - PIC Sal; PIC Sur - PIC Sur W/O
27	Phospholipid Metabolism	Ethanolamine	0.003045	2.5164	0.052436	PIC Sur - PIC Sal; PIC Sur - PIC Sur W/O; Sal Sal - PIC Sur W/O
28	Cholesterol, Cortisol, Steroid Metabolism	24-Dihydrolanosterol	0.0030716	2.5126	0.052436	PIC Sur - PIC Sal; Sal Sal - PIC Sal; PIC Sur - PIC Sur W/O; Sal Sal - PIC Sur W/O
29	Vitamin B6 (Pyridoxine) Metabolism	4-Pyridoxic acid	0.0032599	2.4868	0.053732	PIC Sur - PIC Sal; Sal Sal - PIC Sal; PIC Sur - PIC Sur W/O; Sal Sal - PIC Sur W/O
30	Purine Metabolism	7-methylguanosine	0.0035257	2.4528	0.056176	PIC Sal - PIC Sur; PIC Sal - Sal Sal; PIC Sur W/O - PIC Sur; PIC Sur W/O - Sal Sal
31	Krebs Cycle	Succinic acid	0.0039805	2.4001	0.059459	PIC Sur - PIC Sal; Sal Sal - PIC Sal; PIC Sur - PIC Sur W/O; Sal Sal - PIC Sur W/O
32	Microbiome Metabolism	3-methylphenylacetic acid	0.0039805	2.4001	0.059459	Sal Sal - PIC Sal; PIC Sur - PIC Sur W/O; Sal Sal - PIC Sur W/O
33	Tyrosine and Phenylalanine Metabolism	Tyrosine	0.0043104	2.3655	0.062053	PIC Sur - PIC Sal; Sal Sal - PIC Sal; PIC Sur - PIC Sur W/O; Sal Sal - PIC Sur W/O
34	Pentose Phosphate, Gluconate Metabolism	D-Ribose-5-phosphate	0.0044273	2.3539	0.062053	PIC Sur - PIC Sal; PIC Sur - PIC Sur W/O; Sal Sal - PIC Sur W/O
35	Krebs Cycle	2-Hydroxyglutarate	0.0045436	2.3426	0.062053	PIC Sur - PIC Sal; Sal Sal - PIC Sal; PIC Sur - PIC Sur W/O
36	Microbiome Metabolism	3-Hydroxyanthranilic acid	0.0047418	2.3241	0.06296	PIC Sal - PIC Sur; PIC Sal - Sal Sal; PIC Sur W/O - PIC Sur; PIC Sur W/O - Sal Sal
37	Branch Chain Amino Acid Metabolism	4-methyl-2-oxopentanoic acid	0.0050399	2.2976	0.065109	PIC Sal - Sal Sal; PIC Sur - Sal Sal; PIC Sur W/O - Sal Sal
38	Bile Salt Metabolism	Deoxycholic acid	0.0053945	2.268	0.067857	Sal Sal - PIC Sal; Sal Sal - PIC Sur; Sal Sal - PIC Sur W/O
39	Fatty Acid Oxidation and Synthesis	Carnitine	0.005777	2.2383	0.070579	PIC Sal - PIC Sur; PIC Sur W/O - PIC Sur; Sal Sal - PIC Sur
40	Thyroxine Metabolism	Diiodothyronine	0.0059062	2.2287	0.070579	PIC Sur - PIC Sal; Sal Sal - PIC Sal; Sal Sal - PIC Sur W/O
41	Purine Metabolism	Allantoin	0.0065793	2.1818	0.076705	PIC Sur - PIC Sal; Sal Sal - PIC Sal; PIC Sur - PIC Sur W/O; Sal Sal - PIC Sur W/O
42	Bile Salt Metabolism	Taurodeoxycholic acid	0.00709	2.1494	0.08069	Sal Sal - PIC Sal; Sal Sal - PIC Sur; Sal Sal - PIC Sur W/O
43	Microbiome Metabolism	p-Hydroxybenzoate	0.0081414	2.0893	0.090502	PIC Sal - PIC Sur; PIC Sal - Sal Sal
44	Branch Chain Amino Acid Metabolism	Hydroxyisocaproic acid	0.0085126	2.0699	0.091299	PIC Sur - PIC Sal; Sal Sal - PIC Sal; Sal Sal - PIC Sur W/O
45	SAM, SAH, Methionine, Cysteine, Glutathione Metabolism	Reduced glutathione	0.0085951	2.0658	0.091299	Sal Sal - PIC Sal; Sal Sal - PIC Sur W/O
46	Amino Acid Metabolism not otherwise covered	Asparagine	0.0088664	2.0523	0.092133	Sal Sal - PIC Sal; PIC Sur - PIC Sur W/O; Sal Sal - PIC Sur W/O

SOM Table S3. Stable Isotope-Labeled Internal Standards for LC-MS/MS.

Polarity	Isotope Standards	Stock Concentration (μM)	Q1	Q3	DP	EP	CE	CXP
Positive	L-Alanine (2,3,3,3-D4)	10.102	94.05	48.1	54.45	10	11.08	11.16
Positive	L-Phenylalanine (ring-13C6)	10.000	172.08	126	78.1	10	21	26.93
Positive	L-Leucine (5,5,5,-D3)	10.450	135.1	89.2	70.93	10	10.87	20.1
Positive	L-Valine (D8)	10.184	126.05	77.2	70.93	10	18.64	20.1
Negative	L-Arginine:HCl (5-13C,4,4,5,5-D4)	11.145	178.11	145.18	-49.74	-11.19	-13.93	-20.65
Negative	L-Citrulline (5,5,-D2)	10.164	176.1	133.1	-88.095	-9.95	-21.1	-21.95
Positive	DL-Glutamic acid (2,4,4-D3)	10.409	151.06	115	115.4	9.04	9.97	12.93
Positive	L-Tyrosine (ring-13C6)	10.204	188.08	142	43.25	10.68	16.06	18.2
Positive	L-Ornithine:HCl (5,5-D2)	9.980	135.09	72	43.82	10.8	33.58	17.29
Positive	L-Methionine (methyl-D3)	10.409	153.05	63.9	59.88	10	29.18	26.11
Negative	L-Aspartic Acid (2,3,3-D3)	10.061	135.04	91.1	-50.16	-8.32	-21.11	-38.99
Positive	Glycine (2-13C, 15N)	51.125	79.03	61.6	78	12	5	11.4
Positive	L-Glutamine-amide-15N	10.000	148.07	84.1	35.59	7.29	26.53	15.19
Negative	D-Glucose-13C6	10.000	185.07	61	-36.2	-10	-23.1	-5.8
Negative	D-Fructose-13C6	10.000	185.07	61.01	-36.2	-10	-23.1	-5.8
Negative	Alpha-Ketoisocaproic acid (1-13C, 99%)	10.000	130.06	85	-47.37	-10.18	-10.21	-19.32
Negative	Uric acid-1,3-15N2	10.000	169.03	125	-95	-10	-20	-4
Positive	Creatinine-(methyl-13C)	10.000	115.06	87.1	31	10	15	4
Negative	Sucrose-13C12	10.000	353.12	92.02	-127.19	-12.3	-29.8	-15.05
Positive	Glycerol-13C3	10.000	96.05	59.2	99.65	10.93	20.86	11.89
Positive	L-carnitine (N-trimethyl-D9)	20.905	171.11	103.03	72.37	10	27.29	15
Positive	L-Acetylcarnitine(N-methyl-D3)	5.216	207.12	85.02	61.16	8.33	42.38	12.56
Positive	L-Propionylcarnitine (N-methyl-D3)	1.041	221.13	159	65.61	13.02	18.6	29.67
Positive	L-Butyrylcarnitine (N-methyl-D3)	1.041	235.15	173.1	51.3	9.69	17.1	8.8
Positive	L-Isovalerylcarnitine (N-trimethyl-D9)	1.081	255.17	187.1	81.73	10.65	20.49	24.89
Positive	L-Octanoylcarnitine (N-methyl-D3)	1.000	291.22	85.1	85.23	10.1	29.52	15.12
Positive	L-Myristoylcarnitine (N-trimethyl-D9)	1.027	381.31	84.9	87.75	10.08	29.38	14.5
Positive	L-Palmitoylcarnitine (N-methyl-D3)	2.054	403.34	85	49.64	10.22	35.83	16.99
Positive	L-carnitine (mono):ClO4, O-Glutaryl (N-methyl-D3)	1.889	279.14	85.1	55.82	11.71	29.35	14.83
Positive	L-carnitine:ClO4, 3-Hydroxyisovaleryl (N-methyl-D3)	1.028	265.16	85.2	76.11	10.98	34.09	20
Positive	L-carnitinie:HCl, O-Dodecanoyl(N,N,N-Trimethyl-D9)	1.000	353.28	84.8	92.11	9.53	56.38	17.6
Positive	L-carnitinie:HCl, O-Octadecanoyl(N-methyl-D3)	2.042	431.37	369.4	69.18	10.36	29.04	17.27
Positive	Cholesterol-d7	50.000	376.36	161.1	110	10	30.7	14
Positive	PC (16:0/16:0)-d62	20.000	796.58	184	32.85	10.11	43.27	27.02
Negative	Trypan blue	20.000	435.03	185	-144.58	-8.67	-57.8	-20.94

SOM Figure S1. Single-Dose Correction of Behavioral Abnormalities.

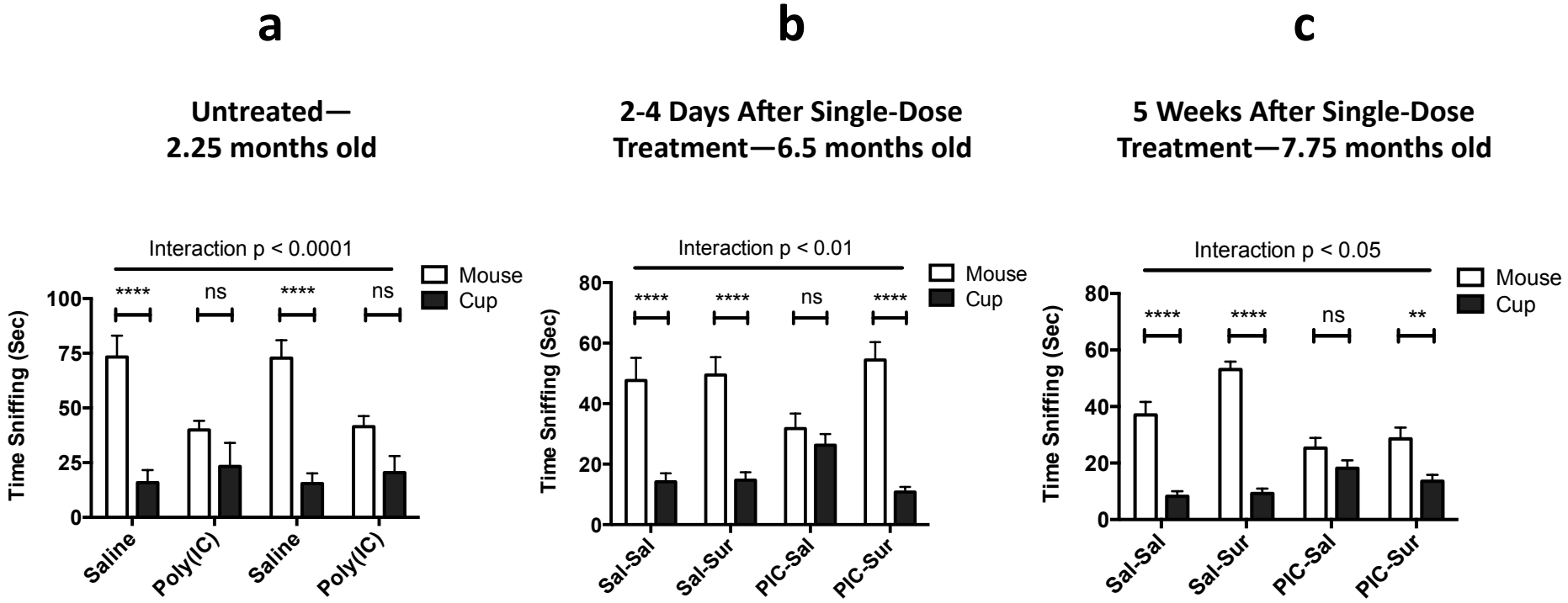

SOM Figure S2

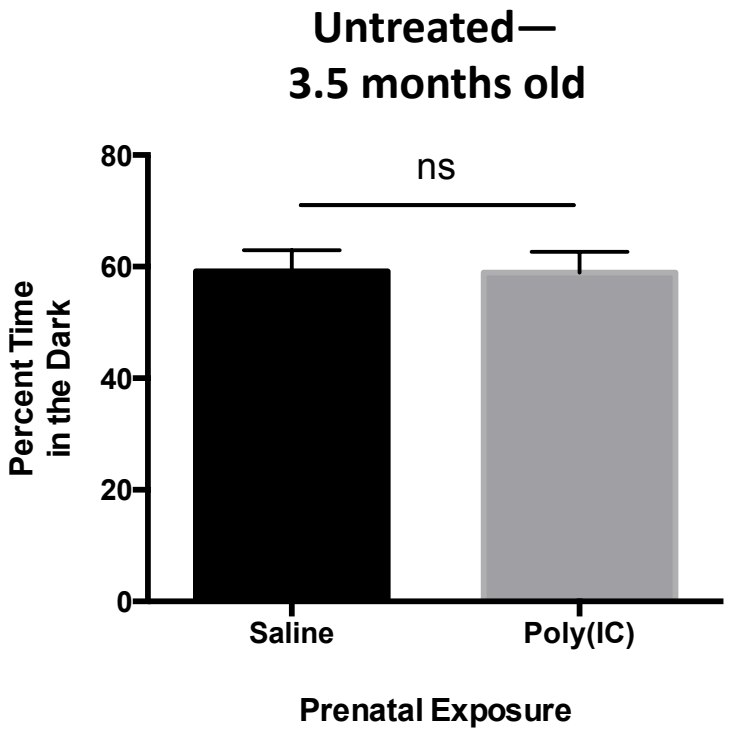

Molecular Autism

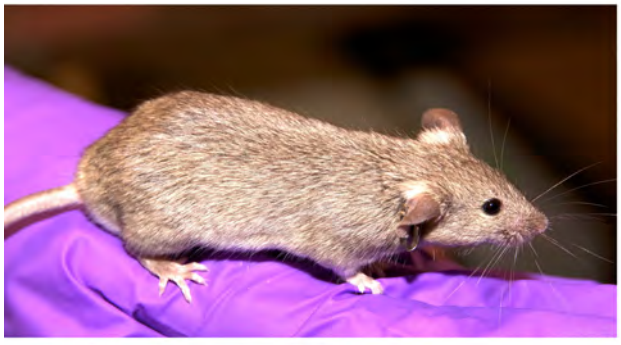

Fragile X (*Fmr1* knockout) Model

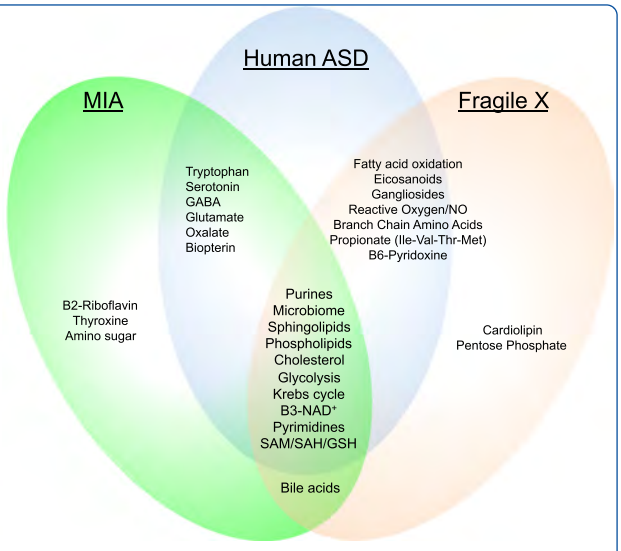

Metabolomics of Autism

Antipurinergic therapy corrects the autism-like features in the Fragile X (*Fmr1* knockout) mouse model

Naviaux *et al.*

BioMed Central

Naviaux *et al. Molecular Autism* 2015, **6**:1
http://www.molecularautism.com/content/6/1/1

Molecular Autism

RESEARCH Open Access

Antipurinergic therapy corrects the autism-like features in the Fragile X (*Fmr1* knockout) mouse model

Jane C Naviaux[5], Lin Wang[1,2], Kefeng Li[1,2], A Taylor Bright[1,2], William A Alaynick[1,2], Kenneth R Williams[1,2,8], Susan B Powell[5,6] and Robert K Naviaux[1,2,3,4,7*]

Abstract

Background: This study was designed to test a new approach to drug treatment of autism spectrum disorders (ASDs) in the Fragile X (*Fmr1*) knockout mouse model.

Methods: We used behavioral analysis, mass spectrometry, metabolomics, electron microscopy, and western analysis to test the hypothesis that the disturbances in social behavior, novelty preference, metabolism, and synapse structure are treatable with antipurinergic therapy (APT).

Results: Weekly treatment with the purinergic antagonist suramin (20 mg/kg intraperitoneally), started at 9 weeks of age, restored normal social behavior, and improved metabolism, and brain synaptosomal structure. Abnormalities in synaptosomal glutamate, endocannabinoid, purinergic, and IP3 receptor expression, complement C1q, TDP43, and amyloid β precursor protein (APP) were corrected. Comprehensive metabolomic analysis identified 20 biochemical pathways associated with symptom improvements. Seventeen pathways were shared with human ASD, and 11 were shared with the maternal immune activation (MIA) model of ASD. These metabolic pathways were previously identified as functionally related mediators of the evolutionarily conserved cell danger response (CDR).

Conclusions: The data show that antipurinergic therapy improves the multisystem, ASD-like features of both the environmental MIA, and the genetic Fragile X models. These abnormalities appeared to be traceable to mitochondria and regulated by purinergic signaling.

Keywords: Autism spectrum disorders, Purinergic signaling, Antipurinergic therapy (APT), Mitochondria, Metabolism, Metabolomics, Fragile X syndrome, Genetics, Environment, Maternal immune activation (MIA), Cell danger response (CDR)

Background

Autism spectrum disorders (ASDs) now affect 1% to 2% of children in the United States [1]. Genetic [2-4], environmental [5,6], and metabolic [7] factors can contribute to the risk of ASD to different extents in each affected child. We have previously shown that antipurinergic therapy reverses the behavioral and metabolic abnormalities in the maternal immune activation (MIA) mouse model of ASD in juveniles [8] and adults [9]. The MIA and Fragile X models have been considered to be mechanistically distinct examples of environmental and genetic causes of ASD, respectively. However, in our MIA study we found the first of several emerging connections. The *Fmr1* protein (FMRP) was downregulated by 50%, and antipurinergic therapy with suramin restored normal FMRP and normal behaviors in the MIA model [8]. FMRP is an mRNA and ribosome [10] binding protein that inhibits the expression of several key inflammatory proteins and cytokines, and binds to several DNA repair proteins involved in cell stress and defense [11]. Genetic loss of FMRP expression leads to Fragile X Syndrome, the most common

* Correspondence: naviaux@ucsd.edu
[1]The Mitochondrial and Metabolic Disease Center, University of California, San Diego School of Medicine, 214 Dickinson St., Bldg CTF, Rm C102, San Diego, CA 92103-8467, USA
[2]Department of Medicine, University of California, San Diego School of Medicine, 214 Dickinson St., Bldg CTF, Rm C102, San Diego, CA 92103-8467, USA
Full list of author information is available at the end of the article

single-gene cause of intellectual disability [12]. The *Fmr1* knockout is the oldest, and one of the most studied genetic mouse models used in autism research [13]. In our previous work we found that disturbances in purine metabolism and purinergic signaling were robust features and effective targets for treatment in the environmental MIA mouse model of autism [8,9]. Interestingly, the first genetic causes of autism identified were traced to abnormalities in purine and pyrimidine metabolism [14,15]. These observations led us to test the role of purinergic signaling in a genetic mouse model of ASD. We selected the Fragile X model to test the hypothesis that abnormalities in purinergic signaling might underlie both the environmental MIA and genetic Fragile X models.

Suramin is a well-known and well-studied competitive inhibitor of purinergic signaling [16]. It has been used medically for the treatment of African sleeping sickness (trypanosomiasis) since shortly after it was first synthesized in 1916. Its antipurinergic actions were discovered in 1988, after a search for inhibitors of ATP-mediated P2X and P2Y signaling [17]. Suramin has many other actions [18], however, metabolomic studies have shown that the expression of purinergic receptors is altered [8], and purine metabolism is the top ranked biochemical pathway that is changed by treatment in the MIA model of ASD [9]. We refer to the use of suramin and related purinergic antagonists as antipurinergic therapy (APT). In the present work, we tested the hypothesis that APT will improve behavior, metabolism, and synaptic abnormalities in the Fragile X mouse model, even in the face of a permanent, gene-coded absence of the Fragile X protein.

Methods

Mouse strains

We evaluated the Fragile X (*Fmr1*) knockout on the FVB strain background. It has the genotype: FVB.129P2-*Pde6b*$^{+}$ *Tyr*$^{c\text{-}ch}$ *Fmr1*^{tm1Cgr}/J (Jackson Stock # 004624). The *Fmr1*^{tm1Cgr} allele contains a neomycin resistance cassette replacing exon 5 that results in a null allele that makes no FMR mRNA or protein. The control strain used has the genotype: FVB.129P2-*Pde6b*$^{+}$ *Tyr*$^{c\text{-}ch}$/AntJ (Jackson Stock # 004828). In contrast to the white coat color of wild-type FVB mice, these animals had a chinchilla (*Tyr*$^{c\text{-}ch}$) gray coat color. The wild-type *Pde6b* locus from the 129P2 ES cells corrects the retinal degeneration phenotype that produces blindness by 5 weeks of age in typical FVB mice. The *Fmr1* locus is X-linked, so males are hemizygous and females are homozygous for the knockout. We also performed metabolomic analysis on *Fmr1* knockout mice on the C57BL/6J (B6) background to refine our understanding of which metabolic disturbances were directly related to the *Fmr1* knockout, and which were the result of changes in genetic background. For these studies we studied the same *Fmr1*^{tm1Cgr} knockout allele bred on the C57BL6/J background. These animals had the genotype: B6.129P2-*Fmr1*^{tm1Cgr}/J (Jackson Stock# 003025). The standard C57BL6/J strain (Jackson Stock# 000664) was used as a control for the B6 metabolic studies.

Animals, husbandry, and drug treatment

All studies were conducted at the University of California, San Diego (UCSD) in facilities accredited by the Association for Assessment and Accreditation of Laboratory Animal Care International (AAALAC) under UCSD Institutional Animal Care and Use Committee (IACUC)-approved animal subjects protocols, and followed the National Institutes of Health (NIH) Guidelines for the use of animals in research. Five-week-old male mice were obtained from Jackson Laboratories (Bar Harbor, ME), identified by ear tags, placed in cages of two to four animals, and maintained on *ad libitum* Harlan Teklad 8604 mouse chow (14% fat, 54% carbohydrate, 32% protein) and water. Animals were housed in a temperature (22°C to 24°C) and humidity (40% to 55%) controlled vivarium with a 12-h light-dark cycle (lights on at 07:00). No mice were housed in isolation. Beginning at 9 weeks of age, animals received weekly injections of either saline (5 μL/g ip) or suramin (hexasodium salt, 20 mg/kg ip; Tocris Cat #1472).

Behavioral analysis

Behavioral testing began at 13 weeks of age, after 1 month of weekly antipurinergic therapy with suramin. Mice were tested in social approach, T-maze, locomomtor activity, marble burying, acoustic startle, and prepulse inhibition paradigms as follows. The ages at the time of testing are noted in the figure legends. For a complete description of the behavioral paradigms see Full Methods Online. *Social Preference and Social Novelty*. Social behavior was tested as social preference as previously described [9], with the addition of a third phase with a second novel mouse to interrogate social novelty [19]. *T-Maze*. Novelty preference was tested as spontaneous alternation behavior in the T-maze as previously described [9]. *Marble Burying*. Marble burying behavior was measured over 30 min by a modification of methods used by Thomas *et al.* [20]. *Locomotor Activity*. Locomotor activity, hyperactivity (total distance traveled), center entries, holepoke exploration, and vertical investigation (rearing) behaviors were quantified by automated beam break analysis in the mouse behavioral pattern monitor (mBPM) as previously described [21]. *Acoustic Startle and Prepulse Inhibition*. Sensitivity to acoustic startle and prepulse inhibition of the startle reflex were measured by automated testing in commercial startle chambers as previously described [22].

Body temperature measurements

A BAT-12 Microprobe digital thermometer and RET-3 mouse rectal probe (Physitemp Instruments, Clifton, NJ, USA) were used to obtain rectal core temperatures to a precision of +/-0.1°C, as previously described [8]. Care was taken to measure temperatures ≥2 days after cage bedding changes, and to avoid animal transport stress immediately prior to measurement in order to avoid stress-induced hyperthermia [23]. Temperatures were measured between 09:00 and 12:00 each day.

Synaptosome isolation and ultrastructure

Animals were sacrificed at 25 weeks of age, after receiving 16 weeks of treatment with suramin or saline. Cerebral samples were collected, homogenized, and synaptosomes isolated by discontinuous Percoll gradient centrifugation, drop dialyzed, glutaraldehyde fixed, post-fixed in osmium tetroxide, embedded, sectioned, and stained with uranyl acetate for transmission electron microscopy (TEM) as previously described [8]. Samples from the FVB control animals (+/- suramin) were not available for study by either electron microscopy or western analysis. Therefore, we report only the effects of suramin on the two groups of *Fmr1* knockout animals (KO-saline and KO-suramin). N = 3 animals/group. Four to six TEM images were collected from each sample. One 5,800× survey image, and three to five images of informative fields at 34,000× to 64,000× were collected with internal scale bars for dimensional control. Qualitatively representative images were reported.

Western blot analysis

Twenty micrograms of cerebral synaptosomal protein was loaded in SDS-polyacrylamide gels (NuPage 4-12% gradient, Bis-Tris Gels) and transferred to PVDF membranes as previously described [8]. The blots were first stained with 0.1% Ponceau S in 5% acetic acid for 10 min, washed, scanned, and the transfer efficiency was quantified by densitometry. Blots were then blocked with 5% skim milk in tris-buffered saline with 0.1% Tween 20 (TBST) for 1 h at room temperature with shaking. Primary antibodies were obtained commercially as 1 mg/mL stocks (see Additional file 1: Table S1 for source details). These were diluted 1:500 to 1:10,000 (final concentrations of 2000 ng/mL to 100 ng/mL; Additional file 1: Table S1) in 5% BSA or 5% skim milk in TBS with 0.1% Tween 20 and optimized for each target to achieve signals in the linear range using dilutions (5 to 20 μg/lane) of cerebral synaptosomes prepared from C57BL/6J control animals. When monoclonal antibodies to a peptide of the target protein were used, peptide was pre-incubated with primary antibody to confirm specificity. When blocking peptides were not available, signal specificity was determined by correspondence of the observed band pattern and molecular weight to the published or manufacturer values for each target protein. Only antibodies that identified specific target bands in cerebral synaptosomes from age-matched control animals were used. Blots were probed with the optimized dilution of primary antibody overnight in the cold room (4°C). Secondary antibodies conjugated to horseradish peroxidase were obtained from Pierce (Rockford, IL, USA) diluted 1:5,000 (200 ng/mL) to 1:20,000 (50 ng/mL) in 3% skim milk-TBST. The blots were probed for 1 h at room temperature prior to final wash and signal development by enhanced chemiluminescence (ECL) or SuperSignal West Femto chemiluminsescent substrate (Thermo, Cat# 34095), then quantified by densitometry. At least five animals per group were analyzed. We evaluated the cerebral synaptosome expression of 54 proteins (Additional file 1: Table S1).

Metabolomics

Broad spectrum analysis of 673 targeted metabolites from 60 biochemical pathways was performed as described [9], with minor modifications. Samples were analyzed on an AB SCIEX QTRAP 5500 triple quadrupole mass spectrometer equipped with a Turbo V electrospray ionization (ESI) source, Shimadzu LC-20A UHPLC system, and a PAL CTC autosampler (AB ACIEX, Framingham, MA, USA). Whole blood was collected 3 to 4 days after the last weekly dose of suramin (20 mg/kg ip) or saline (5 μL/g ip), after light anesthesia in an isoflurane (Med-Vet International, Mettawa, IL, USA, Cat# RXISO-250) drop jar, into BD Microtainer tubes containing lithium heparin (Becton Dickinson, San Diego, CA, USA, Ref# 365971) by submandibular vein lancet [24]. Plasma was separated by centrifugation at 600g × 5 min at 20°C within 1 h of collection. Fresh lithium-heparin plasma was transferred to labeled tubes for storage at -80°C for analysis. Typically 45 μL of plasma was thawed on ice and transferred to a 1.7 mL Eppendorf tube. A total of 2.5 μL of a cocktail containing 35 commercial stable isotope internal standards, and 2.5 μL of 310 stable isotope internal standards that were custom-synthesized in *E. coli* and *S. cerevisiae* by metabolic labeling with ^{13}C-glucose and ^{13}C-bicarbonate, were added, mixed, and incubated for 10 min at room temperature to permit small molecules and vitamins in the internal standards to associate with plasma binding proteins. Macromolecules (protein, DNA, RNA, and so on) were precipitated by extraction with 4 volumes (200 μL) of cold (-20°C), acetonitrile:methanol (50:50) (LCMS grade, Cat# LC015-2.5 and GC230-4, Burdick & Jackson, Honeywell), vortexed vigorously, and incubated on crushed ice for 10 min, then removed by centrifugation at 16,000 g × 10 min at 4°C. The supernatants containing the extracted metabolites and internal standards in the resulting 40:40:20 solvent mix of acetonitrile:methanol:

water were transferred to labeled cryotubes and stored at -80°C for LC-MS/MS (liquid chromatography-tandem mass spectrometry) analysis.

LC-MS/MS analysis was performed by multiple reaction monitoring (MRM) under Analyst v1.6.1 (AB SCIEX, Framingham, MA, USA) software control in both negative and positive mode with rapid polarity switching (50 ms). Of the 673 metabolites targeted, 477 metabolites were measured by scheduled MRM in the first injection, and 196 metabolites were measured by scanning MRM in a second injection. Nitrogen was used for curtain gas (set to 30), collision gas (set to high), ion source gas 1 and 2 (set to 35). The source temperature was 500°C. Spray voltage was set to -4,500 V in negative mode and 5,500 V in positive mode. The values for Q1 and Q3 mass-to-charge ratios (m/*z*), declustering potential (DP), entrance potential (EP), collision energy (CE), and collision cell exit potential (CXP) were determined and optimized for each MRM for each metabolite. Ten microliters of extract were injected by PAL CTC autosampler into a 250 × 2 mm, 5 μm Luna NH2 aminopropyl HPLC column (Phenomenex, Torrance, CA, USA) held at 25°C for chromatographic separation. The mobile phase was solvent A: 95% water with 23.18 mM NH_4OH (Sigma-Aldrich, St. Louis, MO, USA, Fluka Cat# 17837-100ML), 20 mM formic acid (Sigma, Fluka Cat# 09676-100ML) and 5% acetonitrile (pH 9.44); solvent B: 100% acetonitrile. Separation was achieved using the following gradient: 0 min 95% B, 3 min 95% B, 3.1 min 80% B, 6 min 80% B, 6.1 min 70% B, 10 min 70% B, 18 min 2% B, 27 min 0% B, 32 min 0% B, 33 min 100% B, 36.1 95% B, 40 min 95% B end. The flow rate was 300 μL/min. All the samples were kept at 4°C during analysis. The chromatographic peaks were identified using MultiQuant (v3.0, AB SCIEX), confirmed by manual inspection, and the peak areas integrated. The median of the peak area of stable isotope internal standards was calculated and used for the normalization of metabolites concentration across the samples and batches. Prior to multivariate and univariate analysis, the data were log-transformed.

Metabolic pathway visualization in cytoscape

We constructed a rendering of mammalian intermediary metabolism in Cytoscape v 3.1.1 (http://www.cytoscape.org/). Pathways represented in the network for Fragile X syndrome included the 20 metabolic pathways and the 58 metabolites that were altered by antipurinergic therapy with suramin (VIP scores > 1.5). Nodes in the Cytoscape network represent metabolites within the pathways and have been colored according to the z-score. The z-score was computed as the arithmetic difference between the mean concentration of each metabolite in the KO-Sur treatment group and the KO-Sal control group, divided by the standard deviation in the controls. Node colors were arranged on a red-green color scale with green representing ≤-2.00 z-score, red representing ≥+2.00 z-score, and with a zero (0) z-score represented as white. The sum of the VIP scores of those metabolites with VIP scores >1.5 for each metabolic pathway is displayed next to the pathway name.

Data analysis

Group means and standard error of the means (SEM) are reported. Behavioral data were analyzed by two-way ANOVA and one-way ANOVAs (GraphPad Prism 5.0d, GraphPad Software Inc., La Jolla, CA, USA, or Stata/SE v12.1, StataCorp, College Station, TX, USA). Pair-wise post hoc testing was performed by the method of Tukey or Newman-Keuls. Significance was set at $P < 0.05$. Metabolomic data were log-transformed and analyzed by multivariate partial least squares discriminant analysis (PLSDA) in MetaboAnalyst [25]. Metabolites with variable importance in projection (VIP) scores greater than 1.5 were considered significant.

Results

Confirmation of Fragile X protein knockout

We confirmed the absence of Fragile X protein (FMRP) expression in *Fmr1* knockout mice, and its presence in FVB and C57BL/6J controls by western blot analysis before phenotyping the *Fmr1* knockout animals used in this study (Additional file 1: Figure S1).

Restoration of normal social behavior

Altered social behavior is a key measure of autism-like features in mouse models of autism. In the Fragile X knockout genetic model of autism, it has also proven to be one of the most reproducible paradigms across different studies reported in the literature [26]. We found that *Fmr1* null males showed a 26% reduction in social preference, as measured by the time spent interacting with a stranger mouse compared to an inanimate object. There was also a 35% reduction in social novelty, as measured by the time spent interacting with a novel mouse compared to a familiar mouse. This altered social behavior was corrected by antipurinergic therapy with suramin (Figure 1A-D).

Restoration of spontaneous alternation in the T-maze

Novelty preference is an innate feature of normal rodent [27] and human [28] behavior, and a predictor of socialization and communication growth in children with ASD [29]. The loss or suppression of novelty preference in children with ASD is associated with the phenomenon known as insistence on sameness [30]. We estimated preference for novelty as spontaneous alternation behavior in the T-maze [9]. The T-maze can also be used to estimate spatial

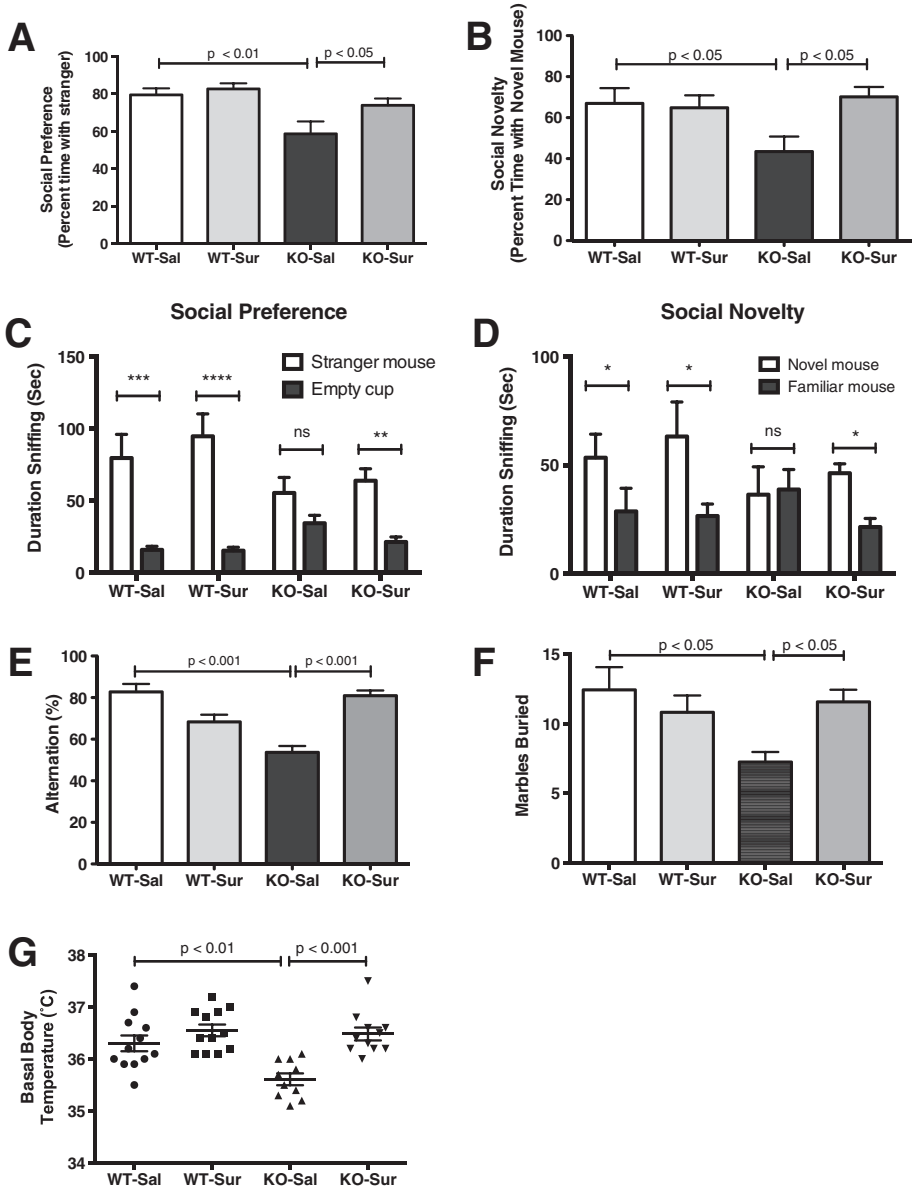

Figure 1 ASD-like symptoms were improved by antipurinergic therapy. (A) Social preference measured as percent time. *Fmr1* knockouts treated with saline showed significant deficits in social preference compared to wild-type controls ($F(3,38) = 5.94$, $P = 0.002$) and suramin corrected this ($P < 0.05$). **(B)** Social novelty measured as percent time. *Fmr1* knockouts treated with saline also showed significant deficits in social novelty. ($F(3,38) = 3.49$, $P = 0.025$) and suramin restored this ($P < 0.05$). **(C)** Social preference as absolute time spent interacting socially. *Fmr1* knockouts were less social than wild-type controls and suramin treatment corrected this (cup $F(1,76) = 56.5$, $P = 0.0001$; cup x group $F(3,76) = 3.55$, $P = 0.018$). **(D)** Social novelty as absolute time interacting with a novel mouse. *Fmr1* knockouts showed decreased novelty preference and suramin improved this (social stimulus main effect $F(1,76) = 8.6$; $P = 0.004$); social stimulus x group $F(3,76) = 3.1$, $P = 0.032$. Age 17 weeks; N = 9-12 per group for Social Preference/Social Novelty test. **(E)** Restoration of spontaneous alternation in the T-maze. Suramin improved spontaneous alternation in the *Fmr1* knockouts, but had not effect on FVB controls ($F(3,41) = 16.6$; $P < 0.0001$). Age 13 weeks; N = 11-12 per group. **(F)** Restoration of normal marble burying. *Fmr1* knockouts treated with saline buried fewer marbles compared to controls ($F(3,37) = 3.15$; $P = 0.037$) and suramin corrected this ($P < 0.05$). Age 16 weeks; N = 9-12 per group. **(G)** Relative hypothermia in the Fragile X model and correction with suramin. *Fmr1* knockout animals treated with saline had core temperatures that were 0.5-0.7°C lower than wild-type FVB controls ($F(3,41) = 10.45$, $P < 0.0001$). Suramin restored normal body temperature in *Fmr1* knockouts ($P = 0.001$). Age 15 weeks, N = 11-12 per group. Values are expressed as means +/- SEM.

working memory, especially when food motivated [31]. We did not use the food-motivated variation in our study. We found that the *Fmr1* null mice showed deficient novelty preference as reflected by chance (near 50%) spontaneous alternation behavior. These deficits were normalized by suramin treatment (Figure 1E). Fragile X knockout mice were no different from controls in latency to choice (data not shown).

Restoration of marble burying behavior

We measured marble burying as a measure of normal rodent digging behavior. Marble burying has sometimes been considered a measure of anxiety, however, comprehensive genetic and behavioral studies have shown that marble burying is a normal mouse behavior that is genetically determined [20]. We found that marble burying was diminished 38% in Fragile X knockout mice. Suramin improved this (KO-Sal v KO-Sur; Figure 1F).

Restoration of normal body temperature

Fmr1 knockout mice displayed relative hypothermia of approximately 0.5°C to 0.7°C below the basal body temperature of the FVB controls (Figure 1G). This relative hypothermia was lost in stressed animals (data not shown). The maternal immune activation (MIA) mouse model showed a similar mild reduction in body temperature [8]. Normal basal body temperature was restored by antipurinergic therapy with suramin. Suramin had no effect on the body temperature of control animals (WT-Sal vs WT-Sur, Figure 1G).

Synaptosomal ultrastructure and protein expression

Our previous studies showed synaptic ultrastructural abnormalities in the MIA mouse model that were corrected by antipurinergic therapy [8]. In that study, the animals with ASD-like behaviors were found to have abnormal synaptosomes containing an electron dense matrix and brittle or fragile and hypomorphic post-synaptic densities. In the present study of the Fragile X model, saline-treated *Fmr1* knockout mice had cerebral synaptosomes that also contained an electron dense matrix (Figure 2A, marked with an asterisk), and fragile, hypomorphic post-synaptic densities (Figure 2A, marked with an arrow). Normal appearing synaptosomes were also found in the *Fmr1* knockout animals, reflecting the well-known heterogeneity in synaptic maturation and morphology in this model. Suramin-treated mice had more cerebral synaptosomes that were near-normal in appearance, with an electron lucent matrix (Figure 2B, marked with an asterisk), and normal appearing post-synaptic densities (Figure 2B, marked with an arrow). We did not investigate dendritic spine densities in this study.

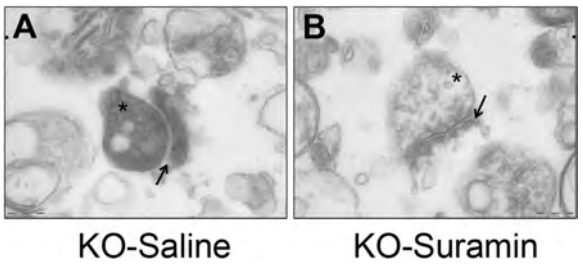

Figure 2 Cerebral synaptosome structural abnormalities were improved by antipurinergic therapy. (A) Fragile X knockout model treated with saline (KO-Saline). Note the increased electron density (dark staining) of the synaptosomal matrix (*) and the hypomorphic (thin) margins of the post-synaptic density (indicated by the arrow). Age 25 weeks, N = 3 per group. Scale bar = 200 nm. **(B)** Fragile X knockout model treated with suramin (KO-Suramin). Note the normal appearing, electron lucent synaptosomal matrix (*) and the thicker margins of the post-synaptic density (indicated by the arrow). Age 25 weeks, N = 3 per group. Scale bar = 200 nm.

Cerebral synaptosomal protein analysis

We found that 17 of 54 proteins we interrogated in cerebral synaptosomes (see Additional file 1: Table S1) were changed by antipurinergic therapy with suramin in the Fragile X model (Figures 3 and 4; KO-Sur vs. KO-Sal). As a treatment study, we focused on the effect of suramin in the *Fmr1* knockout mice only. The current study did not compare knockout brain protein levels to littermate FVB controls (see Methods).

Synaptosomal PI3K/AKT/GSK3β pathway

The PI3/AKT/GSK3β pathway is pathologically elevated in the Fragile X model [32]. Suramin inhibited this pathway at several points. Suramin decreased the expression of PI3 Kinase and AKT, and increased the inhibitory phosphorylation of the PI3K/AKT pathway protein glycogen synthase kinase 3β ($pGSK3\beta^{Ser9}$) by 47%. Suramin increased the phosphorylation of p70 S6 kinase ($pS6K^{Thr389}$) by 46% (Figures 3 and 4A-F). Phosphorylated p70 $S6K^{Thr389}$ is a negative regulator of insulin receptor substrate 1 (IRS1), and serves to oppose insulin stimulated cell growth, PI3K, and mTORC1 signaling [33]. We did not find a corresponding change in mTOR expression or phosphorylation in cerebral synaptosomes of the Fragile X model (Additional file 1: Table S1).

Synaptosomal adenomatous polyposis coli (APC) expression

APC is a tumor suppressor protein that is increased in the Fragile X knockout model [34]. APC forms a complex with, and is phosphorylated by, active GSK3β to inhibit microtubule assembly during undifferentiated cell growth of neuronal progenitors [35]. Suramin treatment returned total APC protein to control levels by decreasing expression by 29% (Figure 4G).

Synaptosomal purinergic receptors and the IP3R1 calcium channel

In earlier studies we showed the chronic hyperpurinergia associated with the MIA mouse model resulted in down-regulated expression of the P2Y2 receptor. Suramin treatment in the MIA model increased P2Y2 expression to normal levels [8]. In the Fragile X mouse model, suramin treatment increased the expression of the P2Y1 receptor 32%, and decreased P2X3 receptor expression 18%

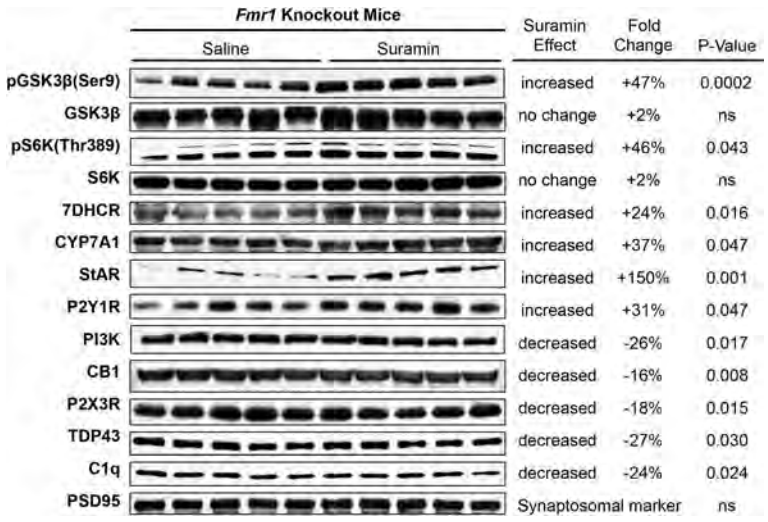

Figure 3 Western analysis of cerebral synaptosomal proteins changed by suramin treatment. Seventeen of 54 interrogated proteins were found to be changed by suramin treatment measured at 25 weeks of age. Post-synaptic density protein 95 kD (PSD95) was not influenced by suramin treatment and was used as a loading control. Protein expression data quantified by densitometry.

(Figure 4HI). There was no effect on P2Y2 expression (Additional file 1: Table S1). P2Y1 signaling is known to inhibit IP3 gated calcium release from the endoplasmic reticulum [36]. We found that suramin treatment was associated with a 101% increase in IP3R1 expression (Figure 4J).

Synaptosomal AMPA receptor (GluR1) expression

AMPA receptor (GluR1) mRNA transcription, translation, and receptor recycling are known to be pathologically dysregulated in the Fragile X model [37]. In the lateral amygdala, the Fragile X knockout results in enhanced internalization and increased internalized receptor pools, with decreased surface expression, such that the total mass of the AMPA receptor is unchanged from controls [38]. Suramin treatment decreased the overall expression of the ionotropic GluR1 in cerebral synaptosomes by 15% (Figure 4K). However, these methods were unable to distinguish between surface and internalized pools of AMPA receptors. Suramin had no effect on metabotropic glutamate receptor mGluR5 expression in this model (Additional file 1: Table S1).

Synaptosomal cannabinoid receptor expression

Cannabinoid signaling is pathologically increased in the *Fmr1* knockout model [39]. Suramin treatment decreased brain CB1 receptor expression 16% (Figure 4L). This is consistent with recent data that have shown signaling to be sharply increased in response to brain injury [40]. Pharmacologic blockade with the CB1R antagonist rimonabant has been shown to improve several symptoms in the Fragile X model [41]. CB2 expression is increased in the peripheral blood monocytes of children with autism spectrum disorders [42]. However, CB2 receptor expression in the brain synaptosomes of the Fragile X model was unchanged (Additional file 1: Table S1).

Synaptosomal PPARβ/δ expression

PPARβ (also known as PPARδ) is a widely expressed transcriptional co-activator that is correlated with the aerobic and bioenergetic capacity in a variety of tissue types [43]. Suramin treatment increased the expression of PPARβ/δ in purified brain synaptosomes by 34% (Figure 4M). Suramin treatment had no effect on synaptosomal PPARα (Additional file 1: Table S1).

Synaptosomal cholesterol and bile acid regulatory proteins

Antipurinergic therapy with suramin increased three key proteins involved in sterol and bile acid synthesis. 7-dehydrocholesterol reductase (7DHCR) was increased by 24%, cholesterol 7α-hydroxylase (CYP7A1) by 37%, and the steroidogenic acute regulatory (StAR) protein by 150% (Figure 4N-P) above saline treated control levels. The function of bile salts in the brain is unknown, although their neuroprotective effects have been shown in several models [44,45].

Synaptosomal complement C1q and TDP43

Recent studies have revealed an important role for complement proteins in tagging synapses during inflammation and remodeling [46]. Activated complement proteins have also been found in the brains of children with autism [47].

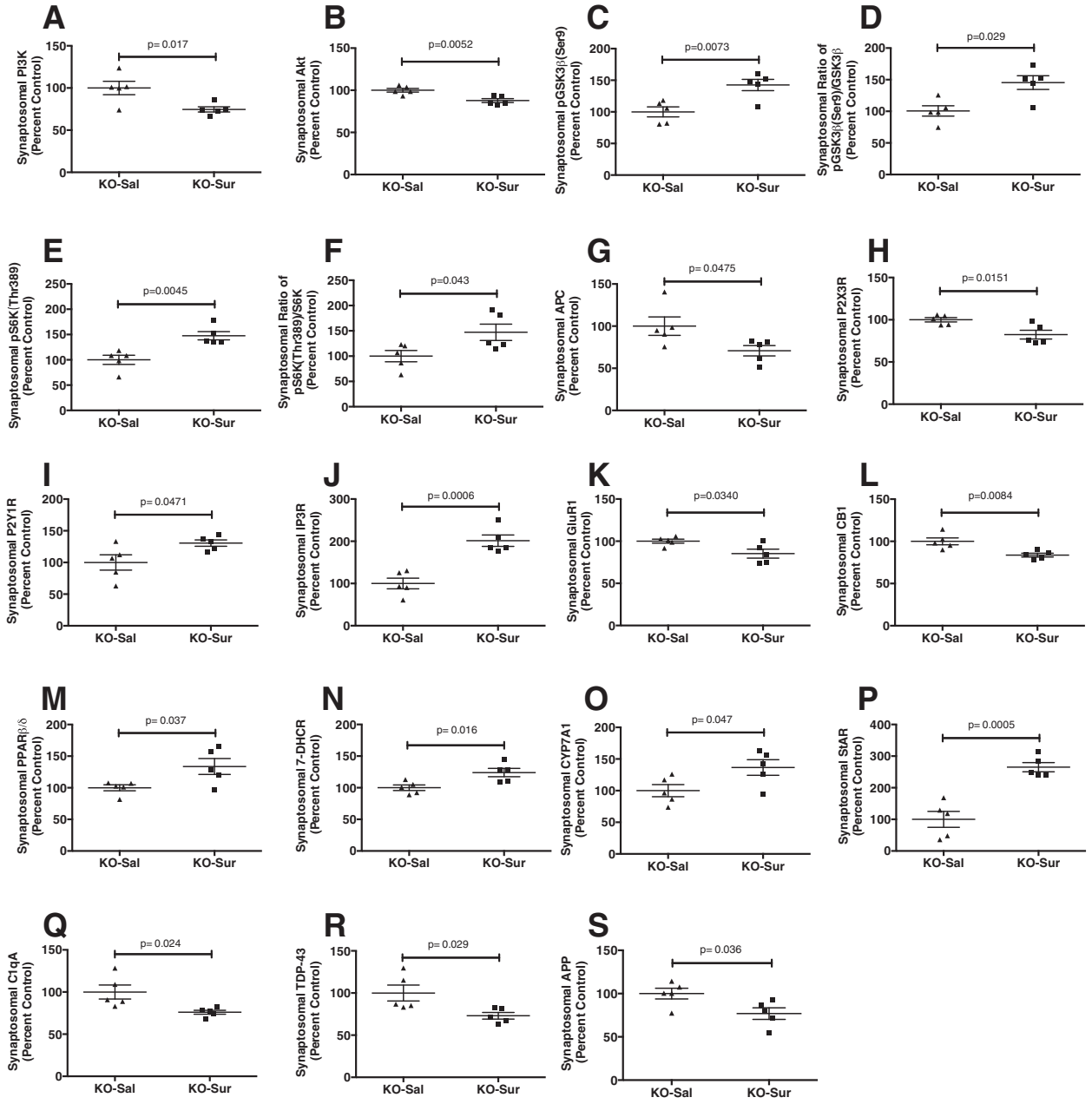

Figure 4 Cerebral synaptosomal proteins changed by antipurinergic therapy with suramin. (A) Phosphoinositol trisphosphate kinase (PI3K). **(B)** Akt (protein kinase B). **(C)** Serine 9 phosphorylation of glycogen synthase kinase (pGSK3β). **(D)** Phosphorylation ratio of glycogen synthase kinase 3β (pGSK3β/GSK3β). **(E)** Phosphorylated of ribosomal protein S6 Kinase (pS6K). **(F)** Phosphorylation ratio of pS6K/S6K. **(G)** Adenomatous polyposis coli (APC). **(H)** Purinergic receptor P2X3 (P2X3R). **(I)** Purinergic receptor P2Y1 (P2Y1R). **(J)** Inositol trisphosphate receptor (IP3R). **(K)** Glutamate receptor 1 (GluR1, also known as the AMPA receptor). **(L)** Cannabinoid receptor 1 (CB1). **(M)** Peroxisome proliferator activated receptor β (PPARβ, also known as PPARδ). **(N)** 7-Dehydrocholesterol dehydrogenase (7-DHCR). **(O)** Cholesterol 7α-hydroxylase (CYP7A1). **(P)** Steroidogenic acute response protein (StAR). **(Q)** Activated complement protein C1q (C1qA). **(R)** TAR DNA binding protein 43 (TDP43). **(S)** Amyloid-β precursor protein (APP). Age = 25 weeks, N = 5 per group. Values are expressed as means +/- SEM.

We found that suramin decreased synaptosomal C1qA by 24% (Figure 4Q).

Tar-DNA binding protein 43 (TDP43) is a single-strand DNA and RNA binding protein that disturbs mitochondrial transport and function under conditions of cell stress [48]. Mutations in TDP43 are associated with genetic forms of amyotrophic lateral sclerosis (ALS) [49]. Wild-type TDP43 protein is a component of the tau and α-synuclein inclusion bodies found in Alzheimer's and Parkinson's disease and plays a role in RNA homeostasis

and protein translation [50]. The similarities of these functions to the role of the *Fmr1* gene in RNA homeostasis prompted us to investigate TDP43 in the Fragile X model. We found that suramin treatment decreased synaptosomal TDP43 by 27% (Figure 4R).

Synaptosomal amyloid-β precursor protein expression

Amyloid-β precursor protein (APP) expression is upregulated in the brain of subjects with ASD [51]. A number of recent papers have identified the upregulation of gene networks in ASD [51] and inborn errors of purine metabolism [52] that were formerly thought to be specific for Alzheimer's and other neurodegenerative disorders. We found that antipurinergic therapy with suramin decreased synaptosomal APP levels by 23% in the Fragile X model (Figure 4S).

Synaptosomal protein pertinent negatives

We interrogated the effect of suramin on several additional proteins that were found to be dysregulated in the MIA mouse model [8]. We found no effect of suramin in the Fragile X model on ERK 1 and 2, or its phosphorylation, CAMKII or its phosphorylation, nicotinic acetylcholine receptor alpha 7 subunit (nAchRα7) expression, or the expression of the purinergic receptors P2Y2 and P2X7 (Additional file 1: Table S1). These data show that the detailed molecular effects of antipurinergic therapy with suramin are different in different genetic backgrounds and different mechanistic models of autism spectrum disorders. However, the efficacy in restoring normal behavior and brain synaptic morphology cuts across models. These data support the novel conclusion that antipurinergic therapy is operating by a metabolic mechanism that is common to, and underlies, both the environmental MIA, and the genetic Fragile X models of ASD.

Metabolomic response to suramin treatment

We analyzed the metabolomic effects in plasma of Fragile X mice after weekly treatment with suramin or saline. We measured 673 metabolites from 60 pathways by mass spectrometry (Additional file 1: Table S2), analyzed the data by partial least squares discriminant analysis (PLSDA), and visualized the results by projection in three dimensions (Figure 5), and ranked by the metabolic changes by variable importance in projection (VIP) scores (Figure 6). This analysis focused on the rank order of importance. Larger sample sizes, usually ≥15 animals per group, are required for more comprehensive metabolomic statistical analysis [53]. We found that suramin produced pharmacometabolomic changes in one-third of the biochemical pathways interrogated (20 of 60 pathways). These are summarized below.

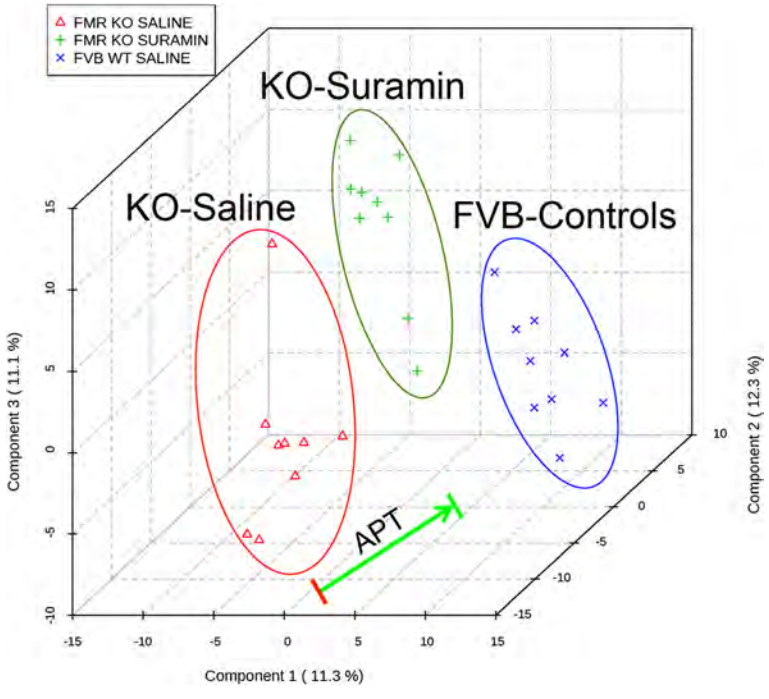

Figure 5 Antipurinergic therapy improved the widespread metabolomic abnormalities in the Fragile X mouse model. A total of 673 plasma metabolites from 60 biochemical pathways were measured by liquid chromatography tandem mass spectrometry (LC-MS/MS) and analyzed by partial least squares discriminant analysis (PLSDA). The three top multivariate components were then plotted on x, y, and z-axes, respectively. Suramin treatment shifted metabolism in the direction of wild-type controls. Age 25 weeks, N = 9-11 per group.

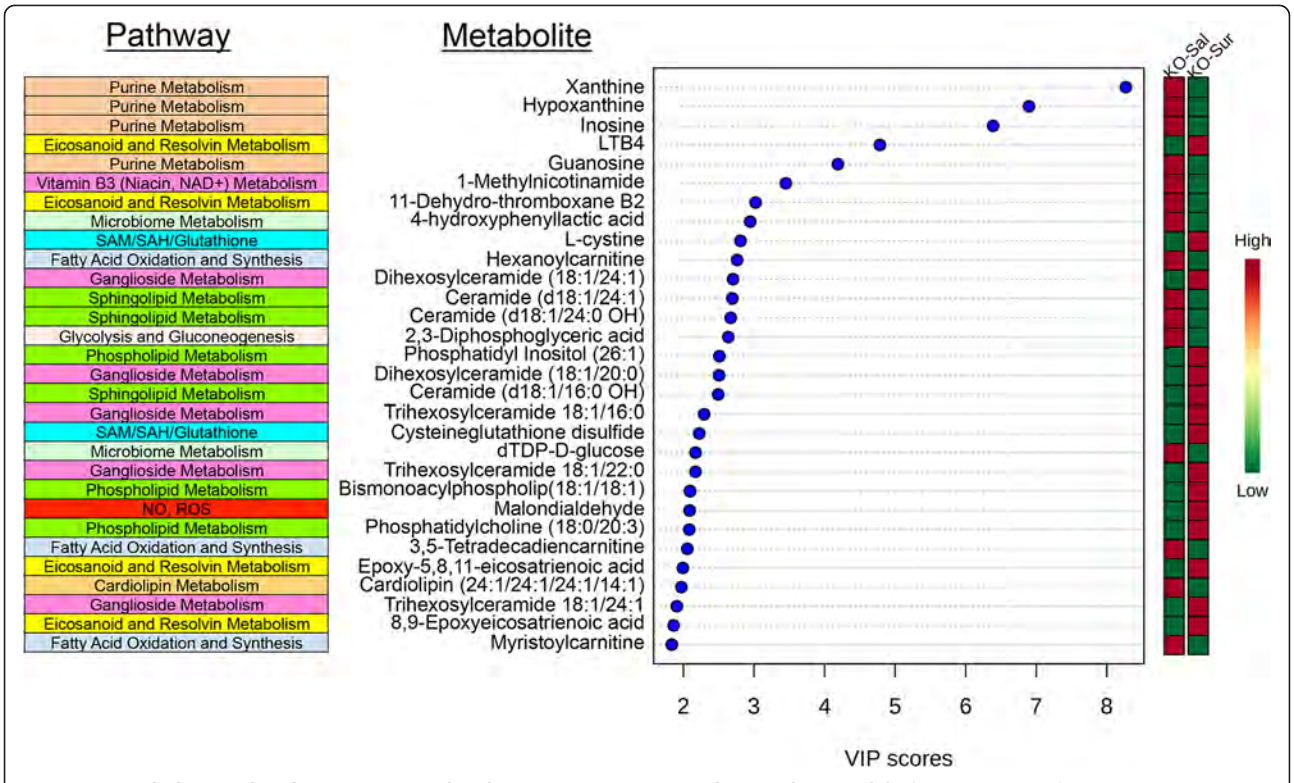

Figure 6 Metabolites and pathways associated with suramin treatment in the Fragile X model. The top 30 most discriminating metabolites and their biochemical pathways ranked by variable importance in projection (VIP) scores. See Additional file 1: Table S3 for a complete list of the top 58 discriminating metabolites. VIP scores ≥1.5 were considered statistically significant. Age 25 weeks, N = 9-11 per group.

Metabolic pathway analysis

The top 11 of 20 discriminating metabolic pathways were represented by two or more metabolites and contributed 89% of the most discriminating metabolites in the Fragile X mouse model treated with suramin (Table 1). These pathways were: purines (20%), fatty acid oxidation (12%), eicosanoids (11%), gangliosides (10%), phospholipids (9%), sphingolipids (8%), microbiome (5%), SAM/SAH glutathione (5%), NAD^+ metabolism (4%), glycolysis (3%), and cholesterol metabolism (2%) (Table 1).

A simplified map of metabolism is illustrated in the form of 26 major biochemical pathways in Figure 7. This figure shows the effect of suramin treatment on each metabolite as measured in the plasma. The magnitude of the pharmacometabolomic effect is quantified as the z-score for nearly 500 metabolites. Inspection of this figure leads to several conclusions. First, 1-carbon folate and Krebs cycle metabolism are dominated by red shading, indicating a general increase in methylation pathways, and mitochondrial oxidative phosphorylation. Next, there was a generalized increase in intermediates of the SAM/SAH and glutathione metabolism. Purine metabolism showed a mixture of upregulated precursors of adenine nucleotides and downregulated inosine and guanosine precursors. There was a generalized increase in gangliosides, phospholipids, and cholesterol metabolites needed for myelin and cell membrane synthesis. Finally, there was a generalized decrease in nine of nine acyl-carnitine species. Acyl-carnitines accumulate when fatty acid oxidation is impaired, and decline when normal mitochondrial fatty acid oxidation is restored. Each of these pathways is a known feature of the cell danger response (CDR) [54].

Lipid metabolism

Disturbances in lipid metabolism were a prominent feature of the Fragile X mouse model (Additional file 1: Figures S3A-D), and its response to treatment (Table 1, Figure 7). Treatment with suramin produced concerted effects in eight different classes of lipids that collectively explained 54% of the top ranked metabolites identified by multivariate analysis. In rank order of importance these were: fatty acid metabolism (12%), eicosanoid metabolism (11%), ganglioside metabolism (10%), phospholipid metabolism (9%), sphingolipids (8%), cholesterol/sterols (2%), cardiolipin (1%), and bile acids (1%) (Table 1). Suramin also had a significant impact on lipid metabolism in the MIA model. Four of the top six metabolic pathways were lipids, explaining 30% of the top ranked VIP scores. In rank order of importance the lipid pathways in the MIA model were: phospholipids (8%), bile acids (8%), sphingolipids (7%), and cholesterol/sterols (7%) [9].

Table 1 Biochemical pathways with metabolites changed by antipurinergic therapy in the Fragile X mouse model

No.	Pathway name	Measured metabolites in the pathway (N)	Expected pathway proportion (P = N/673)	Expected hits in sample of 58 (P * 58)	Observed hits in the top 58 metabolites	Fold enrichment (Obs/Exp)	Impact (Sum VIP score)	Fraction of impact (VIP) explained (% of 136.0)	Suramin treatment effect (KO-Sur/KO-Sal)
1	Purine metabolism	41	0.061	3.54	5	1.41	27.2	20.0%	4/5 Decreased
2	Fatty acid oxidation and synthesis	39	0.057	3.37	9	2.67	16.8	12.4%	9/9 Decreased
3	Eicosanoid and resolvin metabolism	36	0.053	3.11	6	1.93	14.7	10.8%	4/6 Increased
4	Ganglioside metabolism	12	0.018	1.04	6	5.79	13.4	9.8%	6/6 Increased
5	Phospholipid metabolism	115	0.18	9.93	6	0.60	11.5	8.5%	6/6 Increased
6	Sphingolipid metabolism	72	0.105	6.21	5	0.80	11.1	8.2%	3/5 Decreased
7	Microbiome metabolism	33	0.047	2.85	3	1.05	6.7	4.9%	2/3 Decreased
8	SAM, SAH, methionine, cysteine, glutathione metabolism	22	0.032	1.90	3	1.58	6.7	4.9%	3/3 Increased
9	Vitamin B3 (Niacin, NAD+) metabolism	8	0.012	0.69	2	2.90	5.2	3.8%	1/2 Increased
10	Glycolysis and gluconeogenesis	18	0.026	1.55	2	1.29	4.2	3.1%	2/2 Decreased
11	Cholesterol, cortisol, non-gonadal steroid metabolism	29	0.042	2.50	2	0.80	3.2	2.4%	2/2 Increased
12	Nitric oxide, superoxide, peroxide metabolism	6	0.009	0.52	1	1.93	2.1	1.5%	Increased
13	Cardiolipin metabolism	12	0.018	1.04	1	0.97	2.0	1.4%	Decreased
14	Bile salt metabolism	8	0.012	0.69	1	1.45	1.8	1.3%	Increased
15	Branch chain amino acid metabolism	13	0.019	1.12	1	0.89	1.7	1.2%	Increased
16	Isoleucine, valine, threonine, or methionine metabolism	4	0.006	0.35	1	2.90	1.7	1.2%	Increased
17	Pyrimidine metabolism	31	0.051	2.68	1	0.37	1.6	1.1%	Decreased
18	Krebs cycle	17	0.025	1.47	1	0.68	1.6	1.1%	Increased
19	Vitamin B6 (pyridoxine) metabolism	5	0.007	0.43	1	2.32	1.5	1.1%	Increased
20	Pentose phosphate, gluconate metabolism	11	0.016	0.95	1	1.05	1.5	1.1%	Increased
	20 of 60 pathways dysregulated	532 (0.79 x 673)	79% (532/673)	46 (0.79 x 58)	58		136.0	100%	33/58 Increased

Pathways were ranked by their impact measured by summed VIP (Σ_{VIP}; variable importance in projection) scores. A total of 58 metabolites were found to discriminate suramin-treated and saline-treated Fragile X knockout groups by multivariate partial least squares discriminant analysis (PLSDA). Significant metabolites had VIP scores of ≥1.5. Twenty (33%) of the 60 pathways interrogated had at least one metabolite with VIP scores ≥1.5. The total impact of these 58 metabolites corresponded to a summed VIP score of 136. The fractional impact of each pathway is quantified as the percent of the summed VIP score and displayed in the final column on the right in the table. Antipurinergic therapy with suramin not only corrected purine metabolism, but also produced changes in 19 other pathways associated with multi-system improvements in ASD-like symptoms.

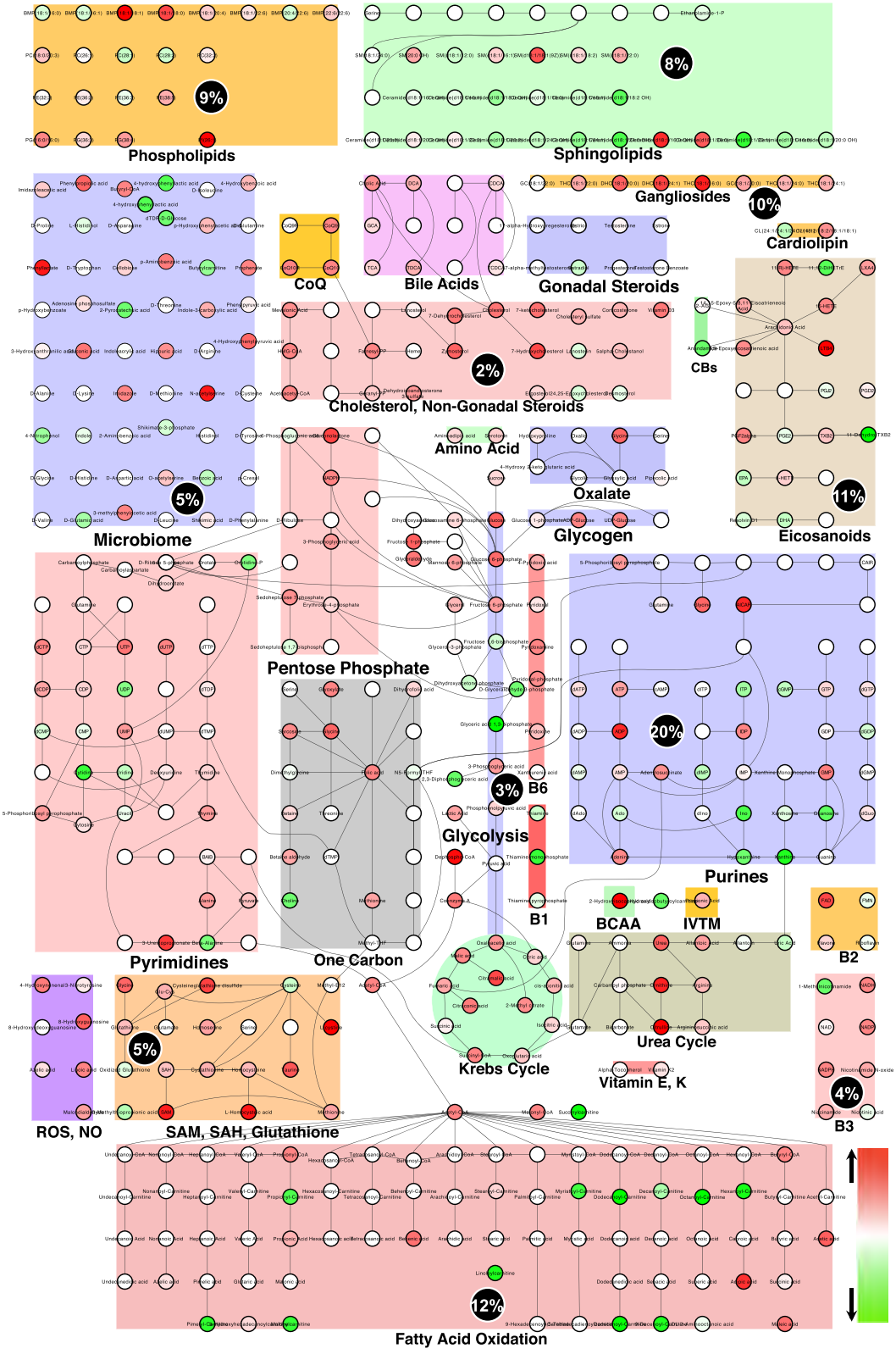

Figure 7 (See legend on next page.)

(See figure on previous page.)
Figure 7 Cytoscape visualization of the metabolic pathways altered by antipurinergic therapy in the Fragile X mouse model. Twenty-six of the 60 biochemical pathways interrogated in our metabolomic analysis are illustrated. See Additional file 1: Tables S2 and S3 for complete listing of pathways and discriminating metabolites, respectively. The fractional contribution of each of the top 20 pathways altered by suramin treatment is indicated as a percentage of the total variable importance in projection (VIP) score in the black circles. Purine metabolism contributed 20% of the top ranked VIP scores, followed by fatty acid oxidation (12%), eicosanoids (11%), gangliosides (10%), phospholipids (9%), and 15 other biochemical pathways as indicated. Smaller circles indicate the metabolites in each pathway, quantified by z-score. Metabolites in red were increased. Metabolites in green were decreased by treatment with suramin. Age 25 weeks, N = 9-11 per group.

Shared metabolic pathways in the MIA and Fragile X models

We compared the 20 pathways found to be altered in the Fragile X model (Table 1) to the 18 metabolic pathways that were altered in the maternal immune activation (MIA) model [8]. A Venn diagram of this comparison revealed 11 pathways that were shared between these two models (Figure 8). These were purines, the microbiome, phospholipid, sphingolipid, cholesterol, bile acids, glycolysis, the Krebs cycle, NAD^+, pyrimidines, and S-adenosylmethionine (SAM), S-adenosyl-homocysteine (SAH), and glutathione (GSH) metabolism.

Discussion

The Fragile X mouse model is one of the most commonly studied genetic mouse models of ASDs. Using this genetic model, we found that antipurinergic therapy (APT) with suramin improved the behavioral, metabolic, and the synaptic structural abnormalities. We previously showed that the ASD-like symptoms of the maternal immune activation (MIA) mouse model were also improved by antipurinergic therapy [8]. Regardless of the model - whether 'environmental' like the MIA model, or 'genetic' like the Fragile X knockout model - antipurinergic therapy with suramin corrected the abnormalities that characterized each model. Our results support the novel conclusion that antipurinergic therapy is operating by a mechanism that lies close to the root cause of the core behaviors and development in both the environmental MIA, and the genetic Fragile X models of ASD. This mechanism appears to be traceable to mitochondria and regulated by purinergic signaling.

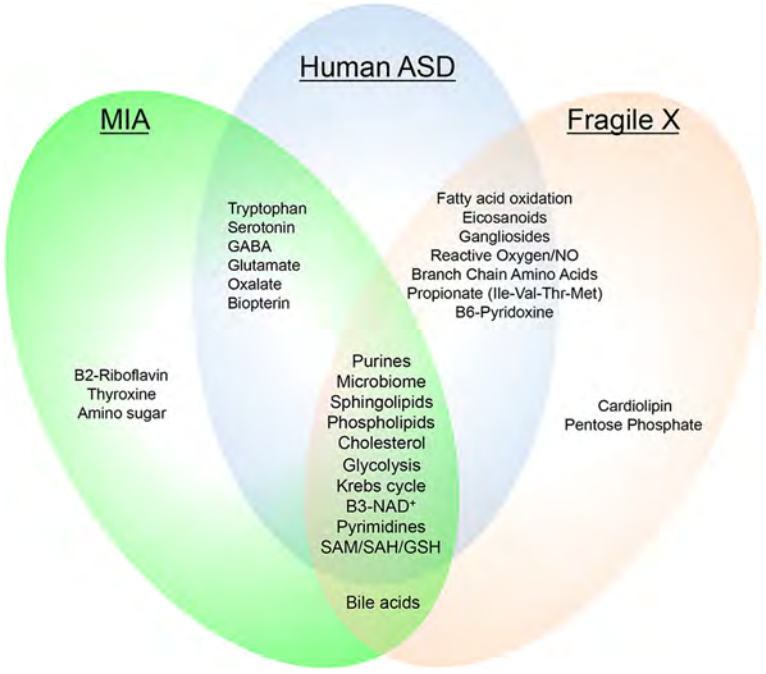

Figure 8 Metabolic pathways shared by the MIA and Fragile X mouse models and human ASD. Comprehensive metabolomic analysis identified 20 biochemical pathways associated with symptom improvements in the Fragile X (*Fmr1 knockout*) model. Seventeen pathways were shared with human ASD, and 11 were shared with the maternal immune activation (MIA) model of ASD. The 17 metabolic pathways shared with human ASD were: purines, microbiome, sphingolipids, phophoslipids, cholesterol/sterols, glycolysis, Krebs cycle, vitamin B3-NAD^+, pyrimidines, S-adenosyl methionine (SAM)/S-adenosylhomocysteine (SAH)/glutathione (GSH), fatty acid oxidation, eicosanoids, gangliosides, reactive oxygen species and nitric oxide (ROS/NO), branched chain amino acids, propionate metabolism and propiogenic amino acids (Ile, Val, Thr, and Met), and vitamin B6-pyridoxine metabolism. Bile acids were common to both the Fragile X and MIA models, but have not yet been studied in human autism.

We considered several caveats before drawing these conclusions. The Fragile X knockout mouse model is an imperfect model of human Fragile X syndrome. Human Fragile X syndrome is not the result of knockout of the gene, but rather an expansion of a CGG triplet repeat in the 5' untranslated region of the gene, and variable phenotypes have been reported in the mouse model [26]. As with many syndromic, single gene disorders, human Fragile X syndrome itself is an imperfect model of non-syndromic ASDs. At least 40% of the boys [55], and over 90% of the girls [56] with Fragile X syndrome do not meet the diagnostic criteria for ASD. We studied the most commonly reported genotype of the *Fmr1* knockout mouse model, which was backcrossed for 11 generations on the genetic background of the FVB strain of laboratory mouse. We compared the behavioral features of this *Fmr1* knockout to the FVB control strain. A potential weakness of our study is that *Fmr1* knockout and FVB control strains are not littermate controls raised by the same mothers. Some behavioral differences might be the result of differences in maternal genotype and rearing. However, the point of our study was not to reconfirm the known behavioral and molecular features of Fragile X model, but rather to ask the question, 'Are the abnormalities treatable with antipurinergic therapy (APT)?' Our data suggest that they were.

Other treatments have also been successful in mitigating the symptoms of the Fragile X mouse by addressing specific neurotransmitter or synaptic defects. These have included drug inhibition of glutamatergic signaling with mGluR5 inhibitors [57], inhibition of endocannabinoid signaling [41], and genetic inhibition of amyloid β precursor protein (APP) [58]. A number of metabolic therapies have also been successful. These have included acetyl-L-carnitine [59], omega 3 fatty acid therapy [60], and inhibition of the metabolic control enzyme glycogen synthase kinase 3β (GSK3β) [32]. Remarkably, we found that antipurinergic therapy addressed each of these abnormalities with a single intervention. Minocycline has also shown benefit in both human Fragile X syndrome [61] and mouse models [62]. Interestingly, many of the neuroprotective and anti-inflammatory effects of minocycline have been traced to its actions on mitochondrial function [63,64], and may also act to decrease hyperpurinergia by moderating mitochondrial ATP synthesis.

Purine metabolism was the most discriminating single metabolic pathway in the Fragile X mouse model treated with suramin, contributing 20% of the top ranked metabolites identified by multivariate analysis (Table 1, Figure 7). An important pharmacologic mechanism of action of suramin is as a competitive antagonist of extracellular ATP and other nucleotides, acting at purinergic receptors [9,65]. Suramin also has nearly 30 other actions [18]. Our metabolomic data show that the major functional impact of suramin in the Fragile X mouse model was on purine metabolism (Table 1). Purinergic signaling abnormalities linked to autism-like behaviors are not restricted to animal models. Several inborn errors in purine [15] and pyrimidine metabolism [14] are well known to be associated with autism-like behaviors [9]. In addition, abnormalities in purine metabolism leading to hyperuricosuria in 20% of children with non-syndromic autism have been described [66]. The specific link between purine metabolism in ASD and purinergic signaling was first made in 2012 [67], and tested in the MIA mouse model in 2013 [8]. Interestingly, brain purinergic signaling was recently identified as one of the top gene expression pathways correlated with abnormal behaviors in children with ASD [68].

We next compared the metabolomic results for both the maternal immune activation (MIA) [9] and Fragile X mouse models of ASD (Figure 8). We found 11 metabolic pathways that were common to both models. These were purines, microbiome, phospholipids, sphingolipids/gangliosides, cholesterol/sterol, bile acids, glycolysis, mitochondrial Krebs cycle, NAD^+/H, pyrimidines, and S-adenosylmethionine/homocysteine/glutathione (SAM/SAH/GSH) metabolism. Seventeen of the 20 metabolic pathway disturbances found in the Fragile X mouse model have been described in human ASD. These include purine metabolism [15,66], fatty acid oxidation [69], microbiome [70,71], phospholipid [72], eicosanoid [73-75], cholesterol/sterol [76], sphingolipids and gangliosides [77,78], glycolysis, Krebs cycle and mitochondrial metabolism [79-81], nitric oxide and reactive oxygen metabolism [82], branched chain amino acids [83], propionate and propiogenic amino acid metabolism (IVTM; Ile, Val, Thr, Met) [84], pyrimidines [14], SAM/SAH/glutathione [85], vitamin B3-NAD^+ metabolism [86], and vitamin B6-pyridoxine metabolism [87]. We found plasma cardiolipin was therapeutically downregulated by suramin. Although elevations in plasma cardiolipin species have not yet been reported in children with autism, anti-cardiolipin antibodies have [88].

The upregulation of glycolysis and downregulation of mitochondrial Krebs cycle seen in the Fragile X model of ASD are a direct consequence of the regulated decrease in mitochondrial oxidative phosphorylation (oxphos). This was corrected by suramin (Figure 7). The conditions of increased substrate supply and decreased utilization, create a poised state of mitochondrial underfunction associated with increased reserve capacity. When basal mitochondrial oxygen consumption is decreased, cellular heat production from mitochondria is reduced. This can lead to a decrease in basal body temperature. We observed a 0.7°C decrease in basal body temperature in the Fragile X mice (Figure 1G). A similar decrease was seen in the MIA mouse model [8]. A poised increase in mitochondrial reserve capacity can also produce primed mitochondria with

the capacity to respond explosively to stress. In some cases, this is manifest as a large increase in mitochondrial reactive oxygen species (ROS) production. Interestingly, an increase in mitochondrial reserve capacity and increased ROS production under stress has been documented in 32% of lymphocytoblastoid cell lines (8/25 = 32%; 95% CI 15-54%) derived from children with ASD [79]. When an explosive discharge of mitochondrial ROS occurs transiently, uncoupling can result, leading to a large increase in mitochondrial heat production and high fevers. Superfevers of 104.5° to 105.5°F have been described in occasional patients with Fragile X during infectious illness (personal communication, Randi J. Hagerman).

When cellular resources are redirected away from work, changes in activity-dependent gene expression result in a reduction in unused proteins [89]. With time these underutilized cells lose the capacity for specific kinds of work and can enter a physiologically-induced hypometabolic state that protects the cell from harsh extracellular conditions and promotes cellular persistence. This state shares metabolic similarities to the *dauer* state in *C. elegans* [90], embryonic diapause in mammals [91], plant seed development [92], and stem cells that can be recruited back into cycle after stasis or injury [93]. This latter point suggests that tissues and organs can exist as shifting mosaics of fully active cells, and hypometabolic cells that can be called into action, depending on environmental conditions. In each case, mitochondrial fatty acid oxidation is decreased to facilitate intracellular lipid accumulation needed for persistence metabolism. Fatty acid oxidation was the second most discriminating pathway in the Fragile X mouse model treated with suramin, contributing 12% of the top ranked metabolites identified by multivariate analysis (Table 1, Figure 7). Several acyl-carnitine species were elevated (Table 1, Figure 6). This is a hallmark of diminished mitochondrial fatty acid oxidation [94]. Similar elevations of acyl-carnitines have been reported in 17% of human ASD [69]. Suramin treatment decreased plasma acyl-carnitine levels in the Fragile X model (Figures 6 and 7).

Eicosanoid metabolism was the third most discriminating metabolic pathway in the Fragile X mouse model treated with suramin, contributing 11% of the top ranked metabolites identified by multivariate analysis (Table 1, Figure 7). Eicosanoid metabolism plays a crucial role in regulating the balance of inflammation and anti-inflammation after acute injury, during chronic disease [95,96], and in the antiviral and antibacterial innate immune response [97]. Upregulated lipoxygenase activity in the Fragile X mouse model was recently predicted on the basis of FMRP binding to lipoxygenase mRNA, and disinhibition in the knockout, in a medical hypothesis paper by Beaulieu [75]. The predicted increase in hydroxyeicosatetraenoic acid (HETE) species would support mGluR5-mediated long-term depression (LTD) [98], which is a well-known problem in Fragile X syndrome [99]. We found that suramin treatment increased two epoxyeicosatrienoic acids (EETs), and decreased a stable metabolite of platelet thromboxane A2 (TXA2), 11-dehydro-thromboxane B2 (Figures 6 and 7). The increase in EETs has several physiologic benefits. These include a decrease in ER stress [100], an increase in AMPK activation, and an increase in autophagy [101]. The increase in EETs and decrease in TXA2 were consistent with the anti-inflammatory action of antipurinergic therapy with suramin.

Considered as a coordinated system, these data show that the metabolic disturbances in the mouse models of ASD are similar to those found in human ASD (Figure 8). The data provide strong support for the biochemical validity of both the MIA and Fragile X mouse models. In addition, the metabolomics data revealed for the first time the surprising observation that the environmental MIA and the genetic Fragile X mouse models, and human ASD, all shared disturbances in biochemical pathways previously identified as features of the evolutionarily conserved cell danger response (CDR) (Figure 8) [54]. We found that in the mouse models, both the ASD-like symptoms and the biochemical features of the CDR were corrected by antipurinergic therapy with suramin.

Purinergic signaling begins with the regulated release of purine nucleotides like ATP, or pyrimidines like UTP, through channels in the cell membrane for autocrine and paracrine signaling, and by vesicular fusion during neurotransmission [102,103]. Purinergic (P2X and P2Y) receptors bind to extracellular ATP and other nucleotides as a means of sensing cellular health and danger [54,104]. In this usage, the word 'danger' is not an anthropomorphic construct. Danger has a chemical meaning in cells that equates to metabolic mismatches between substrate/product ratios and the gene-coded and allosterically regulated equilibrium constant (K_{eq}) of each relevant enzyme located in mitochondria, and the conductances of transporters in and out of the organelles [105]. These mismatches are coupled to mitochondrial oxygen consumption, electron flow, redox, and oxidative phosphorylation, and produce a sequence of graded metabolic responses that alter DNA methylation [106], histone modifications [107], and lead to new cellular states of gene expression and function [108]. In most differentiated cells, mitochondria make 90% of the ATP, and process 90% of the carbon skeletons and activated sulfur intermediates used to create the building blocks for cell growth, function, detoxification, and repair. Mitochondria serve as the cellular translators of real-time metabolic information, integrating it with the genetics of the cell, and providing feedback in the form of retrograde signals to the nucleus [109] used to change gene expression.

Table 2 Summary of antipurinergic therapy results in the Fragile X mouse model of autism spectrum disorders

Feature	Abnormality in Fragile X males vs. FVB controls	Response to antipurinergic therapy
Social preference	Decreased	Normalized (P <0.05)
Social novelty	Decreased	Normalized (P <0.05)
T-maze spontaneous alternation	Decreased	Normalized (P <0.001)
Marble burying	Decreased	Normalized (P <0.05)
Core body temperature	Decreased	Normalized (P <0.001)
Acoustic startle	Decreased [sic]	Unchanged (P = ns)
Metabolomics (60 pathways measured)	20 of 60 pathways disturbed	33 metabolites increased and 25 decreased of 58 changed
Synaptosomal structure by electron microscopy	Fragile and malformed post-synaptic densities; Accumulation of electron dense matrix material	Improved
Synaptosomal proteins (54 interrogated)	N/A	17 proteins were changed (for example, decreased PI3/GSK3β, GluR1, C1q, and APP; increased PPARβ/δ)
Locomotor activity - total distance (hyperactivity), center exploration, holepokes, rearing	None	N/A

When extracellular ATP binds to purinergic receptors on the cell surface it is participating in what we call a 'long-path' retrograde signaling circuit from mitochondria to the unstirred water layer on the cell surface, to neighboring cells, or back through autologous cell membrane G-protein coupled receptors and ion channels, to calcium signaling, back to mitochondria and other cellular compartments, and ultimately to the nucleus, changing gene expression. This extracellular purinergic signaling circuit is well known to regulate innate immunity, oxidative stress and shielding [110], inflammation, and cytokine production [104], sensory perception [111], in addition to sleep, cognition [112], and the autonomic nervous system [113]. Intracellular adenine nucleotides like NAD^+/H, $NADP^+$/H, cyclic-ADP-ribose (cADPR), and nicotinic acid adenine dinucleotide phosphate (NAADP) are also traceable to mitochondria, are interconverted by the enzyme CD38 [114], and play important roles in a 'short-path' retrograde signaling circuit that regulates redox, calcium release, sodium and potassium channels [115], synaptic long-term depression [116], autophagy [117], defense against intracellular pathogens [118], and social behavior by modulating oxytocin secretion [119]. These studies underscore the surprising role of extracellular and intracellular purines in regulating a diverse array of biological phenomena, ranging from innate immunity and cellular defense, to sleep, cognition, behavior, perception, affect, memory, and learning.

Although our results showing the correction of ASD-like behaviors, and improvements in metabolism and brain synaptic abnormalities in the Fragile X mouse model are encouraging, there are several caveats that must be considered before extending the results to humans. First, while the Fragile X mouse model captures several features of ASD, no animal model can fully capture the complexities of human behavior. Second, suramin is a poor drug choice for chronic use because of potentially toxic side effects that can occur with prolonged treatment [120]. Third, human forms of ASD may occur by mechanisms not captured by the Fragile X model. Mechanisms that do not involve the pathological persistence of the cell danger response (CDR) [54] may not be amenable to antipurinergic therapy. Newer, safer, more selective antipurinergic drugs, and human clinical trials will be necessary to answer these questions.

Conclusions

The data reported in this study show that the efficacy of antipurinergic therapy cuts across disease models of ASD. Both the environmental MIA [8,9] and the genetic Fragile X models (Figures 1, 2, 3, 4, 5, 6, 7, 8, Tables 1 and 2) responded with complete, or near-complete, resolution of symptoms, even when treatment was not begun until adolescence, or adulthood. The data support the hypothesis that disturbances in purinergic signaling may be a common denominator and effective therapeutic target in both the environmental MIA and genetic Fragile X mouse models of autism spectrum disorders.

Additional file

Additional file 1: This supplement includes a single PDF file with: supplementary Results, Methods, References, three tables, and four figures. Figure S1. Confirmation of Fragile X protein expression knockout in the *Fmr1*/FVB Mouse Model. **Figure S2.** Acoustic startle and prepulse inhibition. **Figure S3.** Acyl-carnitine studies in *Fmr1* knockout mouse models. **Figure S4.** Western blot assay linearity and precision analysis. **Table S1.** Synaptic proteins interrogated and antibodies used. **Table S2.** Biochemical pathways and metabolites interrogated. **Table S3.** Metabolites changed by antipurinergic therapy in the Fragile X model.

Abbreviations
APP: Amyloid β precursor protein; APT: Antipurinergic therapy; ASD: Autism spectrum disorders; C1q: Complement factor 1 subunit q; CDR: Cell danger response; *Fmr1*: Fragile X mental retardation gene locus 1; IP3: Inositol triphosphate; MIA: Maternal immune activation; P2X: Ionotropic purinergic receptors; P2Y: G-protein coupled purinergic receptors; TDP43: Tar DNA binding protein 43.

Competing interests
The authors declare that they have no competing interests.

Authors' contributions
JCN coordinated the study, conducted the experiments, analyzed the data, and wrote parts of the manuscript. KL and JCN did the metabolomics. LW helped prepare the synaptosomes, processed them for electron microscopy, and did the western studies. ATB developed the bioinformatic tools for metabolomics data processing and visualization in Cytoscape. WAA helped with the Cytoscape analysis and helped write the manuscript. KRW started the metabolic pathway renderings in Cytoscape. SBP directed the behavioral studies and their analysis. RKN assembled the team, designed, funded and directed the project, analyzed the data, and wrote the manuscript. All authors read and approved the final manuscript.

Acknowledgments
This research was supported by grants from the Jane Botsford Johnson Foundation (RKN), with additional support from the UCSD Christini Foundation, the UCSD Mitochondrial Research Fund, and the Wright Family Foundation to RKN. The funders had no role in the study design, data collection and analysis, decision to publish, or preparation of the manuscript. We thank Leanne Chukoskie, Jeanne Townsend, Sophia Colamarino, Richard Frye, John Rodakis, Ellen Heber-Katz, and Oswald Quehenberger for helpful discussions and comments. We thank Laura Dugan for providing the rotarod. We thank Dr. Malcolm Wood and the Core Microscopy Facility at The Scripps Research Institute, La Jolla, CA, for performing the electron microscopy.

Author details
[1]The Mitochondrial and Metabolic Disease Center, University of California, San Diego School of Medicine, 214 Dickinson St., Bldg CTF, Rm C102, San Diego, CA 92103-8467, USA. [2]Department of Medicine, University of California, San Diego School of Medicine, 214 Dickinson St., Bldg CTF, Rm C102, San Diego, CA 92103-8467, USA. [3]Department of Pediatrics, University of California, San Diego School of Medicine, 214 Dickinson St., Bldg CTF, Rm C102, San Diego, CA 92103-8467, USA. [4]Department of Pathology, University of California, San Diego School of Medicine, 214 Dickinson St., Bldg CTF, Rm C102, San Diego, CA 92103-8467, USA. [5]Department of Psychiatry, University of California, San Diego School of Medicine, 214 Dickinson St., Bldg CTF, Rm C102, San Diego, CA 92103-8467, USA. [6]Research Service, VA San Diego Healthcare System, La Jolla, CA, USA. [7]Veterans Affairs Center for Excellence in Stress and Mental Health (CESAMH), La Jolla, CA, USA. [8]Current Address of KRW: General Atomics, Inc, San Diego, CA, USA.

Received: 8 September 2014 Accepted: 16 December 2014
Published: 13 January 2015

References
1. Developmental Disabilities Monitoring Network Surveillance Year Principal I, Centers for Disease C, Prevention. Prevalence of autism spectrum disorder among children aged 8 years - autism and developmental disabilities monitoring network, 11 sites, United States, 2010. MMWR Surveill Summ. 2014;63:1–21.
2. Anney R, Klei L, Pinto D, Almeida J, Bacchelli E, Baird G, et al. Individual common variants exert weak effects on the risk for autism spectrum disorders. Hum Mol Genet. 2012;21:4781–4792.
3. Pinto D, Pagnamenta AT, Klei L, Anney R, Merico D, Regan R, et al. Functional impact of global rare copy number variation in autism spectrum disorders. Nature. 2010;466:368–372.
4. Casey JP, Magalhaes T, Conroy JM, Regan R, Shah N, Anney R, et al. A novel approach of homozygous haplotype sharing identifies candidate genes in autism spectrum disorder. Hum Genet. 2012;131:565–579.
5. Volk HE, Lurmann F, Penfold B, Hertz-Picciotto I, McConnell R. Traffic-related air pollution, particulate matter, and autism. JAMA Psychiatry. 2013;70:71–77.
6. Hallmayer J, Cleveland S, Torres A, Phillips J, Cohen B, Torigoe T, et al. Genetic heritability and shared environmental factors among twin pairs with autism. Arch Gen Psychiatry. 2011;68:1095–1102.
7. Krakowiak P, Walker CK, Bremer AA, Baker AS, Ozonoff S, Hansen RL, et al. Maternal metabolic conditions and risk for autism and other neurodevelopmental disorders. Pediatrics. 2012;129:e1121–1128.
8. Naviaux RK, Zolkipli-Cunningham Z, Nakayama T, Naviaux JC, Le T, Wang L, et al. Antipurinergic therapy corrects the autism-like features in the Poly(IC) mouse model. PloS One. 2013;8:e57380.
9. Naviaux JC, Schuchbauer MA, Li K, Wang L, Risbrough VB, Powell SB, et al. Reversal of autism-like behaviors and metabolism in adult mice with single-dose antipurinergic therapy. Transl Psychiatry. 2014;4:e400.
10. Chen E, Sharma MR, Shi X, Agrawal RK, Joseph S. Fragile x mental retardation protein regulates translation by binding directly to the ribosome. Mol Cell. 2014;54:407–417.
11. Alpatov R, Lesch BJ, Nakamoto-Kinoshita M, Blanco A, Chen S, Stutzer A, et al. A chromatin-dependent role of the fragile X mental retardation protein FMRP in the DNA damage response. Cell. 2014;157:869–881.
12. Bagni C, Tassone F, Neri G, Hagerman R. Fragile X syndrome: causes, diagnosis, mechanisms, and therapeutics. J Clin Invest. 2012;122:4314–4322.
13. Bakker CE, Verheij C, Willemsen R, van der Helm R, Oerlemans F, Vermey M, et al. Fmr1 knockout mice: a model to study fragile X mental retardation. The Dutch-Belgian Fragile X Consortium. Cell. 1994;78:23–33.
14. Micheli V, Camici M, Tozzi MG, Ipata PL, Sestini S, Bertelli M, et al. Neurological disorders of purine and pyrimidine metabolism. Curr Top Med Chem. 2011;11:923–947.
15. Nyhan WL, James JA, Teberg AJ, Sweetman L, Nelson LG. A new disorder of purine metabolism with behavioral manifestations. J Pediatr. 1969;74:20–27.
16. Light AR, Wu Y, Hughen RW, Guthrie PB. Purinergic receptors activating rapid intracellular Ca increases in microglia. Neuron Glia Biol. 2006;2:125–138.
17. Dunn PM, Blakeley AG. Suramin: a reversible P2-purinoceptor antagonist in the mouse vas deferens. Br J Pharmacol. 1988;93:243–245.
18. McGeary RP, Bennett AJ, Tran QB, Cosgrove KL, Ross BP. Suramin: clinical uses and structure-activity relationships. Mini Rev Med Chem. 2008;8:1384–1394.
19. Moy SS, Nadler JJ, Young NB, Nonneman RJ, Segall SK, Andrade GM, et al. Social approach and repetitive behavior in eleven inbred mouse strains. Behav Brain Res. 2008;191:118–129.
20. Thomas A, Burant A, Bui N, Graham D, Yuva-Paylor LA, Paylor R. Marble burying reflects a repetitive and perseverative behavior more than novelty-induced anxiety. Psychopharmacology (Berl). 2009;204:361–373.
21. Halberstadt AL, van der Heijden I, Ruderman MA, Risbrough VB, Gingrich JA, Geyer MA, et al. 5-HT(2A) and 5-HT(2C) receptors exert opposing effects on locomotor activity in mice. Neuropsychopharmacology. 2009;34:1958–1967.
22. Asp L, Holtze M, Powell SB, Karlsson H, Erhardt S. Neonatal infection with neurotropic influenza A virus induces the kynurenine pathway in early life and disrupts sensorimotor gating in adult Tap1-/- mice. Int J Neuropsychopharmacol. 2010;13:475–485.
23. Adriaan Bouwknecht J, Olivier B, Paylor RE. The stress-induced hyperthermia paradigm as a physiological animal model for anxiety: a review of pharmacological and genetic studies in the mouse. Neurosci Biobehav Rev. 2007;31:41–59.
24. Golde WT, Gollobin P, Rodriguez LL. A rapid, simple, and humane method for submandibular bleeding of mice using a lancet. Lab Anim. 2005;34:39–43.
25. Xia J, Mandal R, Sinelnikov IV, Broadhurst D, Wishart DS. MetaboAnalyst 2.0–a comprehensive server for metabolomic data analysis. Nucleic Acids Res. 2012;40:W127–133.
26. Budimirovic DB, Kaufmann WE. What can we learn about autism from studying fragile X syndrome? Dev Neurosci. 2011;33:379–394.
27. Hughes RN. Neotic preferences in laboratory rodents: issues, assessment and substrates. Neurosci Biobehav Rev. 2007;31:441–464.
28. Vecera SP, Rothbart MK, Posner MI. Development of spontaneous alternation in infancy. J Cogn Neurosci. 1991;3:351–354.
29. Munson J, Faja S, Meltzoff A, Abbott R, Dawson G. Neurocognitive predictors of social and communicative developmental trajectories in preschoolers with autism spectrum disorders. J Int Neuropsychol Soc. 2008;14:956–966.
30. Gotham K, Bishop SL, Hus V, Huerta M, Lund S, Buja A, et al. Exploring the relationship between anxiety and insistence on sameness in autism spectrum disorders. Autism Res. 2013;6:33–41.
31. Moy SS, Nadler JJ, Young NB, Perez A, Holloway LP, Barbaro RP, et al. Mouse behavioral tasks relevant to autism: phenotypes of 10 inbred strains. Behav Brain Res. 2007;176:4–20.

32. Franklin AV, King MK, Palomo V, Martinez A, McMahon LL, Jope RS. Glycogen synthase kinase-3 inhibitors reverse deficits in long-term potentiation and cognition in fragile X mice. Biol Psychiatry. 2014;75:198–206.
33. Fenton TR, Gout IT. Functions and regulation of the 70kDa ribosomal S6 kinases. Int J Biochem Cell Biol. 2011;43:47–59.
34. Liao L, Park SK, Xu T, Vanderklish P, Yates 3rd JR. Quantitative proteomic analysis of primary neurons reveals diverse changes in synaptic protein content in fmr1 knockout mice. Proc Natl Acad Sci U S A. 2008;105:15281–15286.
35. Arevalo JC, Chao MV. Axonal growth: where neurotrophins meet Wnts. Curr Opin Cell Biol. 2005;17:112–115.
36. MacMillan D, Kennedy C, McCarron JG. ATP inhibits Ins(1,4,5)P3-evoked Ca2+ release in smooth muscle via P2Y1 receptors. J Cell Sci. 2012;125:5151–8.
37. Muddashetty RS, Kelic S, Gross C, Xu M, Bassell GJ. Dysregulated metabotropic glutamate receptor-dependent translation of AMPA receptor and postsynaptic density-95 mRNAs at synapses in a mouse model of fragile X syndrome. J Neurosci. 2007;27:5338–5348.
38. Suvrathan A, Hoeffer CA, Wong H, Klann E, Chattarji S. Characterization and reversal of synaptic defects in the amygdala in a mouse model of fragile X syndrome. Proc Natl Acad Sci U S A. 2010;107:11591–6.
39. Straiker A, Min KT, Mackie K. Fmr1 deletion enhances and ultimately desensitizes CB(1) signaling in autaptic hippocampal neurons. Neurobiol Dis. 2013;56:1–5.
40. Shohami E, Cohen-Yeshurun A, Magid L, Algali M, Mechoulam R. Endocannabinoids and traumatic brain injury. Br J Pharmacol. 2011;163:1402–1410.
41. Busquets-Garcia A, Gomis-Gonzalez M, Guegan T, Agustin-Pavon C, Pastor A, Mato S, et al. Targeting the endocannabinoid system in the treatment of fragile X syndrome. Nat Med. 2013;19:603–7.
42. Siniscalco D, Sapone A, Giordano C, Cirillo A, de Magistris L, Rossi F, et al. Cannabinoid receptor type 2, but not type 1, is up-regulated in peripheral blood mononuclear cells of children affected by autistic disorders. J Autism Dev Disord. 2013;43:2686–2695.
43. Seedorf U, Aberle J. Emerging roles of PPARdelta in metabolism. Biochim Biophys Acta. 2007;1771:1125–1131.
44. Mortiboys H, Aasly J, Bandmann O. Ursocholanic acid rescues mitochondrial function in common forms of familial Parkinson's disease. Brain. 2013;136:3038–50.
45. Ved R, Saha S, Westlund B, Perier C, Burnam L, Sluder A, et al. Similar patterns of mitochondrial vulnerability and rescue induced by genetic modification of alpha-synuclein, parkin, and DJ-1 in Caenorhabditis elegans. J Biol Chem. 2005;280:42655–42668.
46. Stephan AH, Barres BA, Stevens B. The complement system: an unexpected role in synaptic pruning during development and disease. Annu Rev Neurosci. 2012;35:369–389.
47. Vargas DL, Nascimbene C, Krishnan C, Zimmerman AW, Pardo CA. Neuroglial activation and neuroinflammation in the brain of patients with autism. Ann Neurol. 2005;57:67–81.
48. Sasaki S, Takeda T, Shibata N, Kobayashi M. Alterations in subcellular localization of TDP-43 immunoreactivity in the anterior horns in sporadic amyotrophic lateral sclerosis. Neurosci Lett. 2010;478:72–76.
49. Wang W, Li L, Lin WL, Dickson DW, Petrucelli L, Zhang T, et al. The ALS disease-associated mutant TDP-43 impairs mitochondrial dynamics and function in motor neurons. Hum Mol Genet. 2013;22:4706–4719.
50. Toyoshima Y, Takahashi H. TDP-43 pathology in polyglutamine diseases: With reference to amyotrphic lateral sclerosis. Neuropathology. 2014;34:77–82.
51. Zeidan-Chulia F, de Oliveira BH, Salmina AB, Casanova MF, Gelain DP, Noda M, et al. Altered expression of Alzheimer's disease-related genes in the cerebellum of autistic patients: a model for disrupted brain connectome and therapy. Cell Death Dis. 2014;5:e1250.
52. Kang TH, Park Y, Bader JS, Friedmann T. The housekeeping gene hypoxanthine guanine phosphoribosyltransferase (HPRT) regulates multiple developmental and metabolic pathways of murine embryonic stem cell neuronal differentiation. PLoS One. 2013;8:e74967.
53. Grapov D, Fahrmann J, WHwang J, Poudel A, Jo J, Periwal V, et al. Diabetes associated metabolomic perturbations in NOD mice. Metabolomics. 2014;ePub:1-13.
54. Naviaux RK. Metabolic features of the cell danger response. Mitochondrion. 2014;16:7–17.
55. Harris SW, Hessl D, Goodlin-Jones B, Ferranti J, Bacalman S, Barbato I, et al. Autism profiles of males with fragile X syndrome. Am J Ment Retard. 2008;113:427–438.
56. Hatton DD, Sideris J, Skinner M, Mankowski J, Bailey Jr DB, Roberts J, et al. Autistic behavior in children with fragile X syndrome: prevalence, stability, and the impact of FMRP. Am J Med Genet A. 2006;140A:1804–1813.
57. Michalon A, Bruns A, Risterucci C, Honer M, Ballard TM, Ozmen L, et al. Chronic metabotropic glutamate receptor 5 inhibition corrects local alterations of brain activity and improves cognitive performance in fragile X mice. Biol Psychiatry. 2014;75:189–197.
58. Westmark CJ, Westmark PR, O'Riordan KJ, Ray BC, Hervey CM, Salamat MS, et al. Reversal of fragile X phenotypes by manipulation of AbetaPP/Abeta levels in Fmr1KO mice. PLoS One. 2011;6:e26549.
59. Torrioli MG, Vernacotola S, Peruzzi L, Tabolacci E, Mila M, Militerni R, et al. A double-blind, parallel, multicenter comparison of L-acetylcarnitine with placebo on the attention deficit hyperactivity disorder in fragile X syndrome boys. Am J Med Genet A. 2008;146:803–812.
60. Pietropaolo S, Goubran MG, Joffre C, Aubert A, Lemaire-Mayo V, Crusio WE, et al. Dietary supplementation of omega-3 fatty acids rescues fragile X phenotypes in Fmr1-Ko mice. Psychoneuroendocrinology. 2014;49C:119–129.
61. Leigh MJ, Nguyen DV, Mu Y, Winarni TI, Schneider A, Chechi T, et al. A randomized double-blind, placebo-controlled trial of minocycline in children and adolescents with fragile x syndrome. J Dev Behav Pediatr. 2013;34:147–155.
62. Dansie LE, Phommahaxay K, Okusanya AG, Uwadia J, Huang M, Rotschafer SE, et al. Long-lasting effects of minocycline on behavior in young but not adult fragile X mice. Neuroscience. 2013;246:186–198.
63. Kim HS, Suh YH. Minocycline and neurodegenerative diseases. Behav Brain Res. 2009;196:168–179.
64. Garcia-Martinez EM, Sanz-Blasco S, Karachitos A, Bandez MJ, Fernandez-Gomez FJ, Perez-Alvarez S, et al. Mitochondria and calcium flux as targets of neuroprotection caused by minocycline in cerebellar granule cells. Biochem Pharmacol. 2010;79:239–250.
65. Lambrecht G, Braun K, Damer M, Ganso M, Hildebrandt C, Ullmann H, et al. Structure-activity relationships of suramin and pyridoxal-5''-phosphate derivatives as P2 receptor antagonists. Curr Pharm Des. 2002;8:2371–2399.
66. Page T, Coleman M. Purine metabolism abnormalities in a hyperuricosuric subclass of autism. Biochim Biophys Acta. 2000;1500:291–296.
67. Naviaux RK. Mitochondria and Autism. In: Buxbaum JD, Hof PR, editors. The Neuroscience of Autism Spectrum Disorders. Waltham, MA: Academic Press, Elsevier; 2012. p. 179–93.
68. Ginsberg MR, Rubin RA, Falcone T, Ting AH, Natowicz MR. Brain transcriptional and epigenetic associations with autism. PLoS One. 2012;7:e44736.
69. Frye RE, Melnyk S, Macfabe DF. Unique acyl-carnitine profiles are potential biomarkers for acquired mitochondrial disease in autism spectrum disorder. Transl Psychiatry. 2013;3:e220.
70. Mulle JG, Sharp WG, Cubells JF. The gut microbiome: a new frontier in autism research. Curr Psychiatry Rep. 2013;15:337.
71. Williams BL, Hornig M, Buie T, Bauman ML, Cho Paik M, Wick I, et al. Impaired carbohydrate digestion and transport and mucosal dysbiosis in the intestines of children with autism and gastrointestinal disturbances. PLoS One. 2011;6:e24585.
72. Pastural E, Ritchie S, Lu Y, Jin W, Kavianpour A, Khine Su-Myat K, et al. Novel plasma phospholipid biomarkers of autism: mitochondrial dysfunction as a putative causative mechanism. Prostaglandins Leukot Essent Fatty Acids. 2009;81:253–264.
73. El-Ansary A, Al-Ayadhi L. Lipid mediators in plasma of autism spectrum disorders. Lipids Health Dis. 2012;11:160.
74. Gorrindo P, Lane CJ, Lee EB, McLaughlin B, Levitt P. Enrichment of elevated plasma F2t-isoprostane levels in individuals with autism who are stratified by presence of gastrointestinal dysfunction. PLoS One. 2013;8:e68444.
75. Beaulieu MA. Linking the Fragile X mental retardation protein to the lipoxygenase pathway. Med Hypotheses. 2013;80:289–291.
76. Tierney E, Bukelis I, Thompson RE, Ahmed K, Aneja A, Kratz L, et al. Abnormalities of cholesterol metabolism in autism spectrum disorders. Am J Med Genet B Neuropsychiatr Genet. 2006;141B:666–668.
77. Schengrund CL, Ali-Rahmani F, Ramer JC. Cholesterol, GM1, and autism. Neurochem Res. 2012;37:1201–7.
78. Nordin V, Lekman A, Johansson M, Fredman P, Gillberg C. Gangliosides in cerebrospinal fluid in children with autism spectrum disorders. Dev Med Child Neurol. 1998;40:587–594.
79. Rose S, Frye RE, Slattery J, Wynne R, Tippett M, Pavliv O, et al. Oxidative stress induces mitochondrial dysfunction in a subset of autism

lymphoblastoid cell lines in a well-matched case control cohort. PLoS One. 2014;9:e85436.
80. Graf WD, Marin-Garcia J, Gao HG, Pizzo S, Naviaux RK, Markusic D, et al. Autism associated with the mitochondrial DNA G8363A transfer RNA(Lys) mutation. J Child Neurol. 2000;15:357–361.
81. Smith M, Flodman PL, Gargus JJ, Simon MT, Verrell K, Haas R, et al. Mitochondrial and ion channel gene alterations in autism. Biochim Biophys Acta. 1817;2012:1796–802.
82. Frustaci A, Neri M, Cesario A, Adams JB, Domenici E, Dalla Bernardina B, et al. Oxidative stress-related biomarkers in autism: systematic review and meta-analyses. Free Radic Biol Med. 2012;52:2128–141.
83. Tirouvanziam R, Obukhanych TV, Laval J, Aronov PA, Libove R, Banerjee AG, et al. Distinct plasma profile of polar neutral amino acids, leucine, and glutamate in children with autism spectrum disorders. J Autism Dev Disord. 2012;42:827–836.
84. Al-Owain M, Kaya N, Al-Shamrani H, Al-Bakheet A, Qari A, Al-Muaigl S, et al. Autism spectrum disorder in a child with propionic acidemia. JIMD Rep. 2013;7:63–66.
85. James SJ, Melnyk S, Jernigan S, Hubanks A, Rose S, Gaylor DW. Abnormal transmethylation/transsulfuration metabolism and DNA hypomethylation among parents of children with autism. J Autism Dev Disord. 2008;38:1976.
86. Essa MM, Subash S, Braidy N, Al-Adawi S, Lim CK, Manivasagam T, et al. Role of NAD(+), oxidative stress, and tryptophan metabolism in autism spectrum disorders. Int J Tryptophan Res. 2013;6:15–28.
87. Adams JB, George F, Audhya T. Abnormally high plasma levels of vitamin B6 in children with autism not taking supplements compared to controls not taking supplements. J Altern Complement Med. 2006;12:59–63.
88. Careaga M, Hansen RL, Hertz-Piccotto I, Van de Water J, Ashwood P. Increased anti-phospholipid antibodies in autism spectrum disorders. Mediators Inflamm. 2013;2013:935608.
89. Hermey G, Mahlke C, Gutzmann JJ, Schreiber J, Bluthgen N, Kuhl D. Genome-wide profiling of the activity-dependent hippocampal transcriptome. PLoS One. 2013;8:e76903.
90. Lant B, Storey KB. An overview of stress response and hypometabolic strategies in Caenorhabditis elegans: conserved and contrasting signals with the mammalian system. Int J Biol Sci. 2010;6:9–50.
91. Storey KB, Storey JM. Metabolic rate depression in animals: transcriptional and translational controls. Biol Rev Camb Philos Soc. 2004;79:207–233.
92. Schwender J, Shachar-Hill Y, Ohlrogge JB. Mitochondrial metabolism in developing embryos of Brassica napus. J Biol Chem. 2006;281:34040–34047.
93. Naviaux RK, Le TP, Bedelbaeva K, Leferovich J, Gourevitch D, Sachadyn P, et al. Retained features of embryonic metabolism in the adult MRL mouse. Mol Genet Metab. 2009;96:133–144.
94. Vreken P, van Lint AE, Bootsma AH, Overmars H, Wanders RJ, van Gennip AH. Rapid diagnosis of organic acidemias and fatty-acid oxidation defects by quantitative electrospray tandem-MS acyl-carnitine analysis in plasma. Adv Exp Med Biol. 1999;466:327–337.
95. Weylandt KH, Chiu CY, Gomolka B, Waechter SF, Wiedenmann B. Omega-3 fatty acids and their lipid mediators: towards an understanding of resolvin and protectin formation. Prostaglandins Other Lipid Mediat. 2012;97:73–82.
96. Hammond VJ, O'Donnell VB. Esterified eicosanoids: generation, characterization and function. Biochim Biophys Acta. 1818;2012:2403–2412.
97. Le Bel M, Brunet A, Gosselin J. Leukotriene B4, an endogenous stimulator of the innate immune response against pathogens. J Innate Immun. 2014;6:159–168.
98. Feinmark SJ, Begum R, Tsvetkov E, Goussakov I, Funk CD, Siegelbaum SA, et al. 12-lipoxygenase metabolites of arachidonic acid mediate metabotropic glutamate receptor-dependent long-term depression at hippocampal CA3-CA1 synapses. J Neurosci. 2003;23:11427–11435.
99. Chen T, Lu JS, Song Q, Liu MG, Koga K, Descalzi G, et al. Pharmacological rescue of cortical synaptic and network potentiation in a mouse model for fragile x syndrome. Neuropsychopharmacology. 2014;39:1955–1967.
100. Wang X, Ni L, Yang L, Duan Q, Chen C, Edin ML, et al. CYP2J2-derived epoxyeicosatrienoic acids suppress endoplasmic reticulum stress in heart failure. Mol Pharmacol. 2014;85:105–115.
101. Samokhvalov V, Alsaleh N, El-Sikhry HE, Jamieson KL, Chen CB, Lopaschuk DG, et al. Epoxyeicosatrienoic acids protect cardiac cells during starvation by modulating an autophagic response. Cell Death Dis. 2013;4:e885.
102. Burnstock G. Introduction to purinergic signalling in the brain. Adv Exp Med Biol. 2013;986:1–12.
103. Verkhratsky A, Burnstock G. Biology of purinergic signalling: its ancient evolutionary roots, its omnipresence and its multiple functional significance. Bioessays. 2014;36:697–705.
104. Gorini S, Gatta L, Pontecorvo L, Vitiello L, la Sala A. Regulation of innate immunity by extracellular nucleotides. Am J Blood Res. 2013;3:14–28.
105. Szabo I, Zoratti M. Mitochondrial channels: ion fluxes and more. Physiol Rev. 2014;94:519–608.
106. Naviaux RK. Mitochondrial control of epigenetics. Cancer Biol Ther. 2008;7:1191–1193.
107. Bhaumik SR, Smith E, Shilatifard A. Covalent modifications of histones during development and disease pathogenesis. Nat Struct Mol Biol. 2007;14:1008–1016.
108. Picard M, Zhang J, Hancock S, Derbeneva O, Golhar R, Golik P, et al. Progressive increase in mtDNA 3243A > G Heteroplasmy causes abrupt transcriptional reprogramming. Proc Natl Acad Sci U S A. 2014;111:E4033–4042.
109. Long YC, Tan TM, Takao I, Tang BL. The biochemistry and cell biology of aging: metabolic regulation through mitochondrial signaling. Am J Physiol Endocrinol Metab. 2014;306:E581–591.
110. Naviaux RK. Oxidative shielding or oxidative stress? J Pharmacol Exp Ther. 2012;342:608–18.
111. Burnstock G. Purinergic mechanisms and pain–an update. Eur J Pharmacol. 2013;716:24–40.
112. Halassa MM. Thalamocortical dynamics of sleep: roles of purinergic neuromodulation. Semin Cell Dev Biol. 2011;22:245–251.
113. Gourine AV, Wood JD, Burnstock G. Purinergic signalling in autonomic control. Trends Neurosci. 2009;32:241–248.
114. Lee HC. Cyclic ADP-ribose and nicotinic acid adenine dinucleotide phosphate (NAADP) as messengers for calcium mobilization. J Biol Chem. 2012;287:31633–31640.
115. Kilfoil PJ, Tipparaju SM, Barski OA, Bhatnagar A. Regulation of ion channels by pyridine nucleotides. Circ Res. 2013;112:721–741.
116. Reyes-Harde M, Empson R, Potter BV, Galione A, Stanton PK. Evidence of a role for cyclic ADP-ribose in long-term synaptic depression in hippocampus. Proc Natl Acad Sci U S A. 1999;96:4061–4066.
117. Parrington J, Tunn R. Ca(2+) signals, NAADP and two-pore channels: role in cellular differentiation. Acta Physiol (Oxf). 2014;211:285–296.
118. Lischke T, Heesch K, Schumacher V, Schneider M, Haag F, Koch-Nolte F, et al. CD38 controls the innate immune response against Listeria monocytogenes. Infect Immun. 2013;81:4091–4099.
119. Liu HX, Lopatina O, Higashida C, Tsuji T, Kato I, Takasawa S, et al. Locomotor activity, ultrasonic vocalization and oxytocin levels in infant CD38 knockout mice. Neurosci Lett. 2008;448:67–70.
120. Voogd TE, Vansterkenburg EL, Wilting J, Janssen LH. Recent research on the biological activity of suramin. Pharmacol Rev. 1993;45:177–203.

doi:10.1186/2040-2392-6-1
Cite this article as: Naviaux *et al.*: Antipurinergic therapy corrects the autism-like features in the Fragile X (*Fmr1* knockout) mouse model. *Molecular Autism* 2015 **6**:1.

Additional File 1

Additional File 1. This supplement includes a single PDF file with: supplementary Results, Methods, References, three tables, and four figures.

Supplementary Results

Incidental Note of Decreased Acyl-Carnitines in FVB Wild-type Controls

In the course of our studies comparing the Fragile X knockout animals to wild-type FVB controls, we found an apparent fatty acid oxidation defect that was characterized by a 2-7 fold increase in acyl-carnitine esters in the plasma (Additional File 1: Figure S3A-D). However, when we evaluated the same *Fmr1* knockout allele on a C57BL6/J (B6) background, we discovered that the actual difference was not due to the knockout per se. Instead, we found an unusually low level of acyl-carnitines in the FVB controls compared to B6 wild-type controls (Additional File 1: Figure S3B). This created the appearance of elevated carnitines in the *Fmr1* knockout on the FVB background, even though the quantitative levels were nearly identical in all animals with Fragile X, regardless of the genetic background (Additional File 1: Figure S3A-D).

Decreased Acyl-Carnitine Levels in the FVB Wild-type Controls

Metabolomic analysis revealed a 2-7-fold increase in plasma acyl-carnitine esters in the FMR knockout when compared to the FVB background controls (Additional File 1: Figure S3A). This pattern appeared at first to be a forme fruste of Multiple Acyl-CoA Dehydrogenase Deficiency (MADD), also known as glutaric aciduria type II (GAII). MADD is an inborn error of fatty acid oxidation. It results from mutations in the proteins that transfer electrons from mitochondrial fatty acid, branched chain amino acids, and lysine and tryptophan oxidation to the mitochondrial electron transport chain (ETFQO), or from mutations in a carrier protein for the cofactor riboflavin [1]. Severe forms of MADD produce a characteristic 5-500-fold increase in plasma

acyl-carnitine esters spanning four to 20 carbons (C4-C20) in length, resulting in many acyl-carnitine concentrations greater than 100 μM. The clinical features of MADD are variable, ranging from overwhelming acidosis and death in the first few days of life [2], to riboflavin-responsive muscle weakness presenting after 25 years of age [3]. Non-monogenic, seasonal and dietary forms of MADD are known in horses [4], and can be caused by riboflavin deficiency in rodents [5]. The biochemical phenotype in the FVB/*Fmr1* knockout mice was an imperfect match to MADD, not only because it was quantitatively milder, but also because it was qualitatively different. For example, glutarylcarnitine is not elevated in the *Fmr1* knockout (Additional File 1: Figure S2a), but is elevated in authentic Glutaric Aciduria Type II (GAII; MADD). In addition, unesterified carnitine (C0), acetyl (C2), and propionyl (C3) carnitines were elevated in the FMR knockout mouse (Table 2), but are more typically decreased or normal in authentic MADD [6].

To investigate the MADD-like phenotype, we first looked for evidence of a defect in riboflavin metabolism as reflected by differences in riboflavin, FMN and FAD in the plasma. Riboflavin and FMN were normal in the *Fmr1-KO*/FVB mice (data not shown). FAD was elevated by 53% in the *Fmr1-KO*/FVB animals compared to FVB controls, and was further increased by suramin treatment. These data suggested that the increase in plasma FAD was a beneficial response to a relative deficiency in mitochondrial fatty acid oxidation caused by the *Fmr1* knockout on the FVB background, and not the cause of the MADD-like acyl-carnitine profile. We next confirmed that the *Fmr1* knockout did not produce a secondary defect in ETFQO expression by western analysis (data not shown). We next purchased *Fmr1* knockout animals bred onto the C57BL/6J background and repeated the metabolomic studies on the *Fmr1-KO*/B6 animals compared to B6 controls. The results were surprising. We found that FVB wild-type control animals have acyl-carnitine levels that are 2-60 fold lower than C57BL/6J wild-type control animals (Figure S3B). The absolute concentrations of the plasma acyl-carnitines in both *Fmr1* knockouts (FMR/FVB

and FMR/B6) were virtually indistinguishable (Figure S3C). However, because the FVB control strain has acyl-carnitine concentrations that are 2-60 fold lower than B6 controls, the *Fmr1* knockout produced an apparent forme fruste of the MADD phenotype when compared to the FVB control strain. When the *Fmr1* knockout was examined on the C57BL/6J background, there was no MADD-like phenotype (Additional File 1: Figure S3D). These data show that the same mutation (*Fmr1* knockout) produces a different metabolic phenotype on different genetic backgrounds.

Acoustic Startle Was Decreased in Knockout and Unchanged by Suramin

Fragile X mice fail to show the normal developmental increase in acoustic startle with age. When measured after 3 months of age, they are less sensitive to acoustic startle than controls despite normal hearing [7]. We found that the Fragile X mice had startle magnitudes at pulse intensities of about 100-110db that were 44% lower than wild-type. Suramin did not change the startle magnitude in *Fmr1* knockout or FVB control mice (Additional File 1: Figure S2A).

We also measured prepulse inhibition of startle (PPI) in the startle session. PPI exploits the observation that a soft sound (prepulse) delivered 50 msec or more before a loud sound will reduce the startle magnitude measured as jump force compared to the loud sound given alone. This is widely studied as a measure of sensorimotor gating, but literature reports of PPI abnormalities in the Fragile X mouse model have been mixed and age-dependent [7-10]. No consistent PPI differences were observed between *Fmr1* knockouts and controls. Suramin had no effect on PPI (Additional File 1: Figure S2B).

Locomotor Activity

Locomotor activity, hyperactivity measured as total distance traveled, hole poke exploration, and vertical investigative behavior (rearing) were quantified by automated beam break analysis in

the mouse behavioral pattern monitor (mBPM) [11]. No significant differences were found between the Fragile X knockout model and controls, or between saline treatment and suramin (data not shown).

Supplementary Methods

Social Preference and Novelty

Social preference and novelty were tested using a three-chambered box as previously described [12], with modifications designed to examine novel stranger interactions. Briefly, a Plexiglas box (60cm L x 60cm W x 30cm H) was divided into 3 equal compartments by Plexiglas partitions containing an opening through which the mice could freely enter the 3 chambers. All testing was performed between the hours of 8 am and 1 pm. The test was conducted in three 5-minute phases. In the habituation phase (phase I), the test mouse was allowed to explore the empty chambers for 5 minutes. In the social preference phase (phase II), a stainless steel wire cup (Galaxy Cup, Spectrum Diversified Designs, Inc., Streetsboro, OH) was placed into each of the two outer chambers. The test mouse was briefly removed and an unfamiliar mouse, age and sex matched, was placed under one of the wire cups. The test mouse was then gently placed back in the arena and given an additional 5 minutes to explore. In the social novelty phase (phase III), each mouse was further tested in a third 5-minute session to quantitate preference to spend time with a new stranger. The test mouse was briefly removed, and a new unfamiliar mouse was placed under the wire cage that had been previously empty. The test mouse thus chooses between the first already-investigated and now familiar mouse, and the novel unfamiliar mouse (stranger 2). Room lighting for social behavior studies was 1-2 lux, measured using a Minolta IV F light meter. An overhead camera (Sony CCD Digital Ultra Pro Series, able to detect images down to 0.05 lux) and Ethovision v3 video tracking software (Noldus, Leesburg VA) were used to record the amount of time spent in each chamber and the number of entries

into each chamber. In addition, a human observer, blinded to the treatment groups, scored time spent sniffing each wire cage, using Ethovision Observer software. Only male mice were tested. Stranger mice were habituated to a wire cup for at least 30 minutes before use. Stranger mice were used up to 4 times before new strangers were cycled into the experiment. The location (left or right) of the stranger 1 and stranger 2 mouse alternated across subjects. Results of social behavior testing are reported as the percent of time spent interacting with a stranger mouse vs empty cup in phase II (social preference), and as the percent of time spent interacting with the familiar mouse (stranger 1) vs the unfamiliar mouse (stranger 2) during phase III (social novelty).

T-Maze

The T-maze apparatus is constructed of black plexiglass. The protocol is adapted from Frye and Walf [13]. The main stem is 45 cm long, 10 cm wide, and 24 cm high. Each side arm is 35 cm long, 10 cm wide, and 24 cm high. The side arms are separated from the stem by horizontal sliding doors. A start box, 8 cm in length, is also separated by a horizontal sliding door. Testing was conducted by an examiner that was blinded to the experimental groups, under low illumination, between 8 am and 1 pm. Only male animals were tested. Each mouse was tested in a session of 11 successive trials. The mice were not habituated to the maze. For the first trial only, one goal arm was closed off, forcing the mouse to choose the only open arm. Subsequent trials were by free choice. The chosen arm, and the time it takes for the mouse to choose (latency) were recorded. There was no confinement time in the chosen arm or in the start box. The percentage of alternated choices (mean +/- SEM) is reported.

Acoustic Startle and Prepulse Inhibition

Startle and PPI testing were performed in commercial startle chambers (SRLABsystem, San Diego Instruments, San Diego, CA). Within each chamber there was a Plexiglas cylinder (3.7cm

in diameter) into which the animal was placed. Sudden movements by the mouse were detected by a piezoelectric accelerometer attached below the cylinder. A loudspeaker provided the broadband background noise and acoustic stimuli, and the whole apparatus was housed within the ventilated, sound-attenuating chamber (39cm **x** 38cm **x** 58cm). A standard computer controlled stimulus presentations and response measures. The experimental session consisted of a 5 min acclimatization period to a 65 dB background noise (continuous throughout the session). During the session, 17 trial types were presented: six 40ms startle pulses (80, 90, 100, 110, or 120db; pulse alone); a no stimulus trial (nostim); five 20ms prepulse + pulse combinations [67,69, 73, or 81 dB prepulses followed 100ms later by a P120 stimulus, or 73 dB prepulse followed 100 ms later by a P105 stimulus; prepulses + pulse]; five 20ms prepulse + pulse combinations with varying inter-stimulus intervals [73 dB prepulse followed 20, 70, 120, 360, or 1080ms later by a P120 stimulus; prepulses (vISI) + pulse]. Trial types were presented in a varied order (5 presentations of each pulse alone trial, 5 presentations of each prepulses + pulse combination, 5 presentations of each prepulses (vISI) + pulse combination, and nostim trials occurring between each trial) with an average inter-trial interval (ITI) of 15 s. In addition, 5 of the pulse alone trials, which were not included in the calculation of PPI values, were presented at the beginning of the test session to achieve a relatively stable level of startle reactivity for the reminder of the session (based on the observation that the most rapid habituation of the startle reflex occurs within the first few presentations of the startling stimulus [66]. Another 4 of the pulse alone trials, which were also not included in the calculation of PPI values, were presented at the end of the test session to assess startle habituation.

Marble Burying

Marble burying was used to quantify spontaneous digging as a measure of a normal, genetically determined trait in rodents that has been shown to be uncorrelated with classical measures of anxiety [14]. Standard polycarbonate mouse cages (7.5” x 11.5” x 5”) were used without metal

fittings. Each cage was filled with 1/8-inch sieve corncob bedding to a depth of 2.5 inches. Twenty glass marbles (1 cm diameter) were placed in 4 evenly spaced rows of 5 on top of the bedding. The mice were habituated to the testing room for 30 minutes, and then each mouse was placed individually into a marble-containing cage. Testing was conducted in a semi-dark room. After 30 minutes, the number of buried and unburied marbles was counted. Marbles that were at least 2/3 covered with bedding were counted as buried.

Mouse Behavioral Pattern Monitoring

Ten mouse BPM chambers were used to assess spontaneous exploratory behavior as described previously [15]. Each chamber was illuminated from a single source of red light above the arena. The arena had dimensions of 30.5cm×61cm×38cm and was equipped with a Plexiglas holeboard floor with 3 floor holes and 8 wall holes. Holepoking behavior was detected using an infrared photobeam. The location of the mouse was recorded every 0.1 s using a grid of 12×24 infrared photobeams that were located 1 cm above the floor. The position of the mouse was assigned to 9 unequal regions described by a tic-tac-toe pattern. Rearing behavior was recorded using an array of 16 infrared photobeams 2.5cm above the floor aligned with the long axis of the chamber. At the start of each test session, mice were placed in the bottom left hand corner of the chamber, facing the corner and the test session started immediately. Four main factors were investigated: locomotor activity as measured by transitions (calculated as a movements between the 9 regions); surface investigatory behavior as measured by holepoking; vertical investigatory activity was measured as total rearing; and center entries were quantified.

Western Blot Assay Validation

We confirmed the linearity and quantitative precision of the Western blot assays as follows. First, we selected the most abundantly expressed protein that had the highest signal intensity by Western ECL analysis, and the least abundant protein that was altered by suramin treatment.

These proteins were pGSK3β(Ser9) (Figure 3) and StAR (Figures 3, 4P), respectively. We next confirmed that these proteins were being measured within the linear dynamic range of the assay by performing serial dilutions of synaptosomes loaded in each lane from 5 µg/lane to 20 µg/lane, comparing the ECL signal intensity curves. Least squares regression analysis showed that the assays were within the linear range for both proteins (Additional File 1: Figure S4AB). We also confirmed the linear dose response of P2Y1 and P2X3, two other proteins with signal intensities that were intermediate between GSK3β and StAR (Additional File 1: Figure S4CD). Second, we repeated the assays for these proteins on 3 separate days, using independently loaded SDS-PAGE gels and blots. The ratiometric precision (coefficient of variation = SD/mean) of the observed KO-suramin/KO-saline results was +/-15% (Additional File 1: Figure S4E). Two-way analysis of variance confirmed that between-day variation contributed only 0.3-1% of the total assay variance (Additional File 1: Figure S4F).

Notes on Non-Littermate Controls

Although genetically appropriate and widely used in treatment studies [16], the use of non-littermate, wild-type background mouse strains as controls for knockout animals has significant limitations for metabolomic and behavioral studies. The commercially available FVB control strain for the Fragile X mice has been bred separately for over 8 years since the original 11 backcrosses used to transfer the *Fmr1* knockout to the FVB strain background in 2006. In addition to genetic drift, the maternal metabolic environment is different in homozygous wild-type (X^+/X^+) dams compared to homozygous *Fmr1* knockouts (X^o/X^o). The different gestational metabolic environments can have both epigenetic and metabolic effects on the offspring that can interact with the direct effects of the knockout. The use of littermate controls produced by mating heterozygous (X^+/X^o) dams with wild-type (X^+/Y) sires overcomes this problem, but adds significantly to the duration and cost of the experiments, and does not answer questions

directed at the knockout response to treatment. We report the efficacy of suramin treatment to improve social behavior, metabolism, and synapse structure in the context of the Fragile X model. Future studies will be needed to directly compare suramin effects in wild-type littermate controls.

Supplementary References

1. Yonezawa A, Inui K: **Novel riboflavin transporter family RFVT/SLC52: identification, nomenclature, functional characterization and genetic diseases of RFVT/SLC52.** *Molecular aspects of medicine* 2013, **34:**693-701.
2. Nyhan WL, Barshop BA, Al-Aqeel AI: **Multiple acyl-coA dehydrogenase deficiency/glutaric aciduria type II/ethylmalonic-adipic aciduria.** In *Atlas of Inherited Metabolic Diseases, 3rd edition.* Edited by Nyhan WL, Barshop BA, Al-Aqeel AI. London, England: Hodder Arnold; 2012: 316-324
3. Xi J, Wen B, Lin J, Zhu W, Luo S, Zhao C, Li D, Lin P, Lu J, Yan C: **Clinical features and ETFDH mutation spectrum in a cohort of 90 Chinese patients with late-onset multiple acyl-CoA dehydrogenase deficiency.** *Journal of inherited metabolic disease* 2013.
4. van der Kolk JH, Wijnberg ID, Westermann CM, Dorland L, de Sain-van der Velden MG, Kranenburg LC, Duran M, Dijkstra JA, van der Lugt JJ, Wanders RJ, Gruys E: **Equine acquired multiple acyl-CoA dehydrogenase deficiency (MADD) in 14 horses associated with ingestion of Maple leaves (Acer pseudoplatanus) covered with European tar spot (Rhytisma acerinum).** *Molecular genetics and metabolism* 2010, **101:**289-291.
5. Goodman SI: **Organic aciduria in the riboflavin-deficient rat.** *The American journal of clinical nutrition* 1981, **34:**2434-2437.
6. Sahai I, Garganta CL, Bailey J, James P, Levy HL, Martin M, Neilan E, Phornphutkul C, Sweetser DA, Zytkovicz TH, Eaton RB: **Newborn Screening for Glutaric Aciduria-II: The New England Experience.** *JIMD reports* 2013.
7. Yun SW, Platholi J, Flaherty MS, Fu W, Kottmann AH, Toth M: **Fmrp is required for the establishment of the startle response during the critical period of auditory development.** *Brain research* 2006, **1110:**159-165.
8. Chen L, Toth M: **Fragile X mice develop sensory hyperreactivity to auditory stimuli.** *Neuroscience* 2001, **103:**1043-1050.
9. Frankland PW, Wang Y, Rosner B, Shimizu T, Balleine BW, Dykens EM, Ornitz EM, Silva AJ: **Sensorimotor gating abnormalities in young males with fragile X syndrome and Fmr1-knockout mice.** *Molecular psychiatry* 2004, **9:**417-425.
10. Renoux AJ, Sala-Hamrick KJ, Carducci NM, Frazer M, Halsey KE, Sutton MA, Dolan DF, Murphy GG, Todd PK: **Impaired sensorimotor gating in Fmr1 knock out and Fragile X premutation model mice.** *Behavioural brain research* 2014, **267:**42-45.
11. Halberstadt AL, van der Heijden I, Ruderman MA, Risbrough VB, Gingrich JA, Geyer MA, Powell SB: **5-HT(2A) and 5-HT(2C) receptors exert opposing effects on locomotor activity in mice.** *Neuropsychopharmacology : official publication of the American College of Neuropsychopharmacology* 2009, **34:**1958-1967.

12. Naviaux RK, Zolkipli-Cunningham Z, Nakayama T, Naviaux JC, Le T, Wang L, Schuchbauer M, Rogac M, Li Q, Dugan LL, Powell S: **Antipurinergic Therapy Corrects the Autism-Like Features in the Poly(IC) Mouse Model.** *PloS one* 2013.
13. Frye CA, Walf AA: **Effects of progesterone administration and APPswe+PSEN1Deltae9 mutation for cognitive performance of mid-aged mice.** *Neurobiology of learning and memory* 2008, **89:**17-26.
14. Thomas A, Burant A, Bui N, Graham D, Yuva-Paylor LA, Paylor R: **Marble burying reflects a repetitive and perseverative behavior more than novelty-induced anxiety.** *Psychopharmacology* 2009, **204:**361-373.
15. Young JW, Powell SB, Scott CN, Zhou X, Geyer MA: **The effect of reduced dopamine D4 receptor expression in the 5-choice continuous performance task: Separating response inhibition from premature responding.** *Behavioural brain research* 2011, **222:**183-192.
16. Dolan BM, Duron SG, Campbell DA, Vollrath B, Shankaranarayana Rao BS, Ko HY, Lin GG, Govindarajan A, Choi SY, Tonegawa S: **Rescue of fragile X syndrome phenotypes in Fmr1 KO mice by the small-molecule PAK inhibitor FRAX486.** *Proceedings of the National Academy of Sciences of the United States of America* 2013, **110:**5671-5676.

Additional File 1: Figure Legends

Additional File 1: Figure S1. Confirmation of Fragile X Protein Expression Knockout in the *Fmr1*/FVB Mouse Model.

The results of Western immunoblot analysis are illustrated for cerebral extracts from two knockout samples (FMR/FVB KO#1 and #2), two control samples (FVB WT#1 and #2), and one C57BL/6J sample.

Additional File 1: Figure S2. Acoustic Startle and Prepulse Inhibition.

(A) Fragile X knockout had decreased acoustic startle compared to FVB controls. Pulse intensities of 120dB produced a startle magnitude of 625 +/-65 in WT-Sal, and 657 +/-70 in WT-Sur animals, and 425 +/-58 in the KO-Sal, and 431 +/-59 in the KO-Sur animals. A pulse intensity of 105 dB in FVB controls produced a startle magnitude equivalent to 120 dB in the *Fmr1* knockout animals. **(B) Prepulse Inhibition Showed No Consistent Differences Between Fragile X Knockouts and Controls.** Significant differences in PPI were observed at different pulse intensities of 120 vs 105 dB. However, there was no difference between wild-type and KO genotypes at the same pulse intensities, and suramin did not alter this. 2-way ANOVA Prepulse intensity main effect $F(1,82) = 28.46$, $p < 0.0001$. Treatment Group $F(3,82) = 0.353$, p = ns. Suramin treatment did not change PPI. N = 10-12 per group, 16-week old males.

Additional File 1: Figure S3. Acyl-Carnitine Studies in *Fmr1* Knockout Mouse Models.

(A) Acyl-Carniitine Profile in the Fragile X Model on an FVB Background. (B) Plasma Acyl-Carnitines in the FVB Background are Lower than in C57BL/6J. (C) The Biochemical of Effect *Fmr1* Knockout on Absolute Acyl-Carnitine Concentrations is Similar in Both

FVB and C57BL6/J Genetic Backgrounds. (D) *Fmr1* Knockout on the C57BL/6 Background Does Not Produce Elevated Acyl-Carnitines.

Additional File 1: Figure S4. Western Blot Assay Linearity and Precision Analysis.

Linear regression analysis showed the assays to be linear with a mean correlation coefficient of r^2 = 0.984. **(A) pGSK3β. (B) StAR. (C) P2Y1. (D) P2X3. (E) Assay Precision.** SDS-PAGE and Western blots were prepared independently on 3 separate days using brain synaptosome samples from 5 animals from each of the two treatment groups (KO-Saline, KO-Suramin). Analysis of replicate results (N = 15 KO-Sal, 15 KO-Sur) revealed a mean assay precision of +/- 15%. **(F) 2-Way ANOVA Table of Western Blot Assays.** Analysis of variance revealed that the between-day assay variation contributed 0.3-1% of the variance. Suramin treatment explained 24-78% of the variance.

Additional File 1: Tables

Additional File 1: Table S1. Synaptic Proteins Interrogated and Antibodies Used.

Additional File 1: Table S2. Biochemical Pathways and Metabolites Interrogated.

Additional File 1: Table S3. Metabolites Changed by Antipurinergic Therapy in the Fragile X Model.

Additional File 1: Table S1. Synaptic Proteins Interrogated and Antibodies Used.

No.	Protein/Antibody Target	MW (KDa)	Response to Suramin KO-Sur/KO-Sal	Vendor	Primary Ab Dilution	Cat#
1	**PI3K**	**100**	**Down**	Cell Signaling	1,000	#3811
2	**Akt**	**60**	**Down**	Cell Signaling	1,000	#9272
3	**pGSK3β (Ser9)**	**50**	**Up**	Cell Signaling	1,000	#9323
4	**pS6K(Thr389)**	**70**	**Up**	Cell signaling	3,000	#9205
5	**APC**	**310**	**Down**	Cellsignaling	1,000	#2504
6	**P2Y1R**	**48**	**Up**	Alomone Labs	1,000	#APR-009
7	**P2X3R**	**44**	**Down**	Alomone Labs	1,000	#APR-026
8	**IP3R I**	**320**	**Up**	Cellsignaling	1,000	#3763
9	**GluR1**	**106**	**Down**	Abcam	1,000	#ab172971
10	**CB1**	**53**	**Down**	Abcam	1,000	#ab172970
11	**PPAR beta/delta**	**50**	**Up**	Abcam	1,000	#ab23673
12	**7-dehydrocholesterol reductase/7DHCR**	**54**	**Up**	Abcam	1,000	#ab103296
13	**Cholesterol 7 alpha-hydroxylase/CYP7A1**	**55**	**Up**	Abcam	1,000	#ab65596
14	**Steroidogenic acute regulatory protein/StAR**	**37**	**Up**	Cell Signaling	1,000	#8449
15	**C1qA**	**25**	**Down**	Abcam	1,000	#ab155052
16	**TAR DNA-binding protein 43/TDP43**	**45**	**Down**	Cell Signaling	1,000	#3449
17	**Amyloid β (Aβ) precursor protein/APP**	**100-140**	**Down**	Cellsignaling	1,000	#2452
18	pCAMKII(Thr286)	50, 60	None	Cellsignaling	1,000	#3361
19	pERK1/2(Thr202/Tyr204)	42, 44	None	Cell Signaling	10,000	#4370
20	pSTAT3(ser727)	86	None	Cell Signaling	1,000	#9134
21	P2Y2R	42	None	Alomone Labs	1,000	#APR-010
22	P2Y4R	41	None	Alomone Labs	1,000	#APR-006
23	P2X1R	45	None	Alomone Labs	1,000	#APR-022
24	P2X2R	44	None	Alomone Labs	1,000	#APR-025
25	P2X4R	43	None	Alomone Labs	1,000	#APR-024
26	P2X5R	47	None	Alomone Labs	1,000	#APR-005
27	P2X6R	50	None	Alomone Labs	1,000	#APR-013
28	P2X7R	68	None	Alomone Labs	1,000	#APR-004
29	Metabotropic glutamate receptor 5/mGluR5	132	None	Abcam	1,000	#ab76316
30	Nicotinic Acetylcholine Receptor alpha 7 /nAchR7α	50	None	Abcam	5,000	#ab23832
31	GABA A Receptor beta 3 /GABA-β3	54	None	Abcam	1,000	#ab4046
32	Dopamine Receptor D4/D4R	42	None	Alomone Labs	1,000	#ADR-004
33	ETFQO/ETFDH	65	None	Abcam	1,000	#ab126576
34	Methionine Sulfoxide Reductase A /MSRA	30	None	Abcam	1,000	#ab16803
35	Acetyl-CoA acetyltransferase 2/ACAT2	41	None	Cellsignal	1,000	#11814
36	HMGCoA Reductase/HMOCoAR	97	None	BioVision	500	#3952-100
37	Indoleamine 2,3-dioxygenase 1/IDO-1	45	None	Millipore	1,000	#MAB5412
38	p-mTOR(ser2448)	289	None	Cell Signaling	2,000	#2971
39	mTOR	289	None	Cell Signaling	2,000	#2972
40	pPERK(Thr980)	170	None	Cell Signaling	1,000	#3179
41	p-eIF2α(Ser51)	38	None	Cell Signaling	1,000	#9721
42	Nitro Tyrosine	10-200	None	Abcam	1,000	#ab7048
43	TGFβ Receptor I	50	None	Abcam	1,000	#ab31013
44	CB2	45	None	Abcam	1,000	ab45942
45	PGC1α	115	None	Abcam	1,000	#ab54481
46	PPARα	53	None	Santa Cruz	1,000	#sc-9000
47	CYP27A1	60	None	Abcam	1,000	#ab151987
48	pAkt(Thr308)	60	None	Cell Signaling	2,000	#4056
49	pAkt(Ser473)	60	None	Cell Signaling	2,000	#9018
50	PKC	82	None	Abcam	1,000	#ab19031
51	pPKC(Ser660)	80	None	Cell Signaling	1,000	#9371
52	nAchR beta2	70	None	Alomone Labs	1,000	#ANC-012
53	Postsynaptic Density protein 95/PSD95	95	None	Cell Signaling	4,000	#3450
54	Fragile X mental retardation protein/FMRP	80	None	Cell Signaling	2,000	#4317

Additional File 1: Table S2. Biochemical Pathways and Metabolites Interrogated.

No.	Pathway	Metabolites	No.	Pathway	Metabolites
1	1-Carbon, Folate, Formate, Glycine, Serine Metabolism	9	31	Pentose Phosphate, Gluconate Metabolism	11
2	Amino Acid Metabolism (not otherwise covered)	4	32	Phosphate and Pyrophosphate Metabolism	1
3	Amino-Sugar, Galactose, & Non-Glucose Metabolism	10	33	Phospholipid Metabolism	115
4	Bile Salt Metabolism	8	34	Phytanic, Branch, Odd Chain Fatty Acid Metabolism	1
5	Bioamines and Neurotransmitter Metabolism	11	35	Phytonutrients, Bioactive Botanical Metabolites	3
6	Biopterin, Neopterin, Molybdopterin Metabolism	2	36	Plasmalogen Metabolism	4
7	Biotin (Vitamin B7) Metabolism	1	37	Polyamine Metabolism	6
8	Branch Chain Amino Acid Metabolism	13	38	Purine Metabolism	41
9	Cardiolipin Metabolism	12	39	Pyrimidine Metabolism	31
10	Cholesterol, Cortisol, Non-Gonadal Steroid Metabolism	29	40	SAM, SAH, Methionine, Cysteine, Glutathione Metabolism	22
11	Eicosanoid and Resolvin Metabolism	36	41	Sphingolipid Metabolism	72
12	Endocannabinoid Metabolism	2	42	Taurine, Hypotaurine Metabolism	2
13	Fatty Acid Oxidation and Synthesis	39	43	Thyroxine Metabolism	1
14	Food Sources, Additives, Preservatives, Colorings, and Dyes	3	44	Triacylglycerol Metabolism	1
15	Forensic Drugs	1	45	Tryptophan, Kynurenine, Serotonin, Melatonin Metabolism	10
16	GABA, Glutamate, Arginine, Ornithine, Proline Metabolism	6	46	Tyrosine and Phenylalanine Metabolism	4
17	Gamma-Glutamyl and other Dipeptides	6	47	Ubiquinone and Dolichol Metabolism	4
18	Ganglioside Metabolism	12	48	Urea Cycle	4
19	Glycolysis and Gluconeogenesis Metabolism	18	49	Very Long Chain Fatty Acid Oxidation	3
20	Gonadal Steroids	2	50	Vitamin A (Retinol), Carotenoid Metabolism	3
21	Heme and Porphyrin Metabolism	4	51	Vitamin B1 (Thiamine) Metabolism	3
22	Histidine, Histamine, Carnosine Metabolism	5	52	Vitamin B12 (Cobalamin) Metabolism	3
23	Isoleucine, Valine, Threonine, or Methionine Metabolism	4	53	Vitamin B2 (Riboflavin) Metabolism	4
24	Ketone Body Metabolism	2	54	Vitamin B3 (Niacin, NAD+) Metabolism	8
25	Krebs Cycle	17	55	Vitamin B5 (Pantothenate, CoA) Metabolism	1
26	Lysine Metabolism	3	56	Vitamin B6 (Pyridoxine) Metabolism	5
27	Microbiome Metabolism	33	57	Vitamin C (Ascorbate) Metabolism	2
28	Nitric Oxide, Superoxide, Peroxide Metabolism	6	58	Vitamin D (Calciferol) Metabolism	2
29	OTC and Prescription Pharmaceutical Metabolism	3	59	Vitamin E (Tocopherol) Metabolism	1
30	Oxalate, Glyoxylate Metabolism	3	60	Vitamin K (Menaquinone) Metabolism	1
	Subtotal	304		Subtotal	369
	TOTAL Pathways	**60**		**TOTAL Metabolites**	**673**

Additional File 1: Table S3. Metabolites Changed by Antipurinergic Therapy in the Fragile X Model.

Metabolite	VIP Score	Metabolite	VIP Score
Xanthine	8.283	Myristoylcarnitine	1.8395
Hypoxanthine	6.9083	Trihexosylceramide 18:1/24:0	1.8222
Inosine	6.3985	Cholic acid	1.8062
LTB4	4.7929	Octanoylcarnitine	1.7888
Guanosine	4.1962	Pimelylcarnitine	1.7778
1-Methylnicotinamide	3.4567	Ceramide (d18:1/26:0)	1.7619
11-Dehydro-thromboxane B2	3.0285	PG(16:0/16:0)	1.7575
4-hydroxyphenyllactic acid	2.9524	Dodecenoylcarnitine	1.7435
L-cystine	2.8156	Nicotinamide N-oxide	1.724
Hexanoylcarnitine	2.766	Dodecanoylcarnitine	1.6983
Dihexosylceramide (18:1/24:1)	2.7087	L-Homocysteic acid	1.6739
Ceramide (d18:1/24:1)	2.6984	9-Decenoylcarnitine	1.6702
Ceramide (d18:1/24:0 OH)	2.6743	Hydroxyisocaproic acid	1.6696
2,3-Diphosphoglyceric acid	2.6413	Propionic acid	1.6633
PI (26:1)	2.5143	5-alpha-Cholestanol	1.6542
Dihexosylceramide (18:1/20:0)	2.5094	Glyceric acid 1,3-biphosphate	1.6112
Ceramide (d18:1/16:0 OH)	2.4973	Bismonoacylphospholipid (18:1/18:0)	1.6108
Trihexosylceramide 18:1/16:0	2.2984	3-methylphenylacetic acid	1.6055
Cysteineglutathione disulfide	2.2284	Cytidine	1.5738
dTDP-D-glucose	2.1762	Oxaloacetic acid	1.5682
Trihexosylceramide 18:1/22:0	2.1755	9-Hexadecenoylcarnitine	1.5637
Bismonoacylphospholipid (18:1/18:1)	2.0984	Dehydroisoandrosterone 3-sulfate	1.5627
Malondialdehyde	2.0928	Ceramide (d18:1/20:1)	1.5607
PC (18:0/20:3)	2.087	11(R)-HETE	1.5384
3, 5-Tetradecadiencarnitine	2.0594	PE (38:5)	1.5338
14,15-epoxy-5,8,11-eicosatrienoic acid	1.9964	Pyridoxamine	1.5335
Cardiolipin (24:1/24:1/24:1/14:1)	1.9754	11,12-DiHETrE	1.5284
Trihexosylceramide 18:1/24:1	1.9105	Sedoheptulose 7-phosphate	1.5159
8,9-Epoxyeicosatrienoic acid	1.8643	AICAR	1.5150

Additional File 1: Figure S1

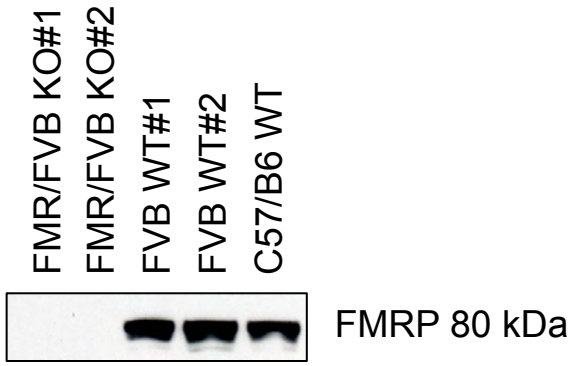

Naviaux, *et al.*, 2015

Additional File 1: Figure S2

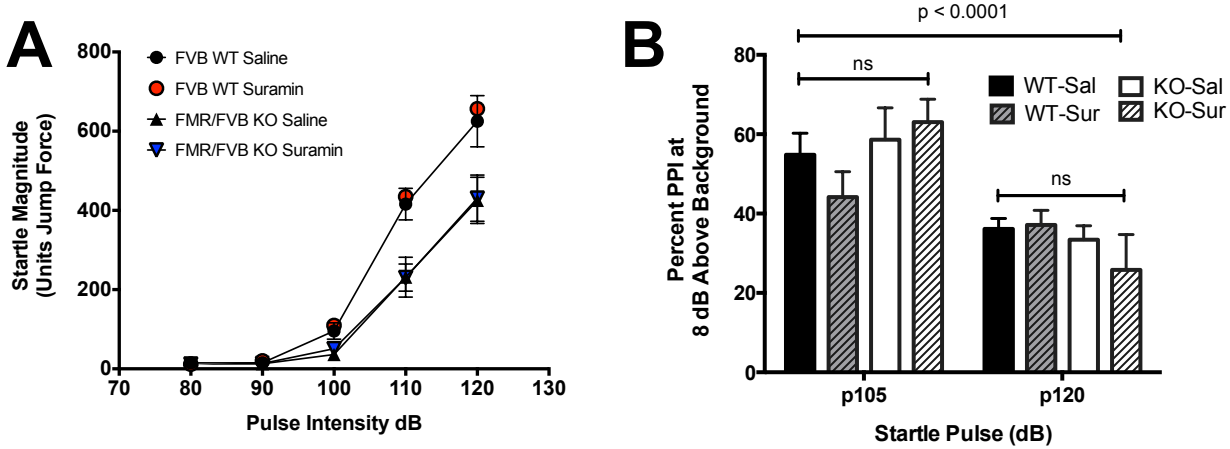

Naviaux, *et al.*, 2015

Additional File 1: Figure S3A

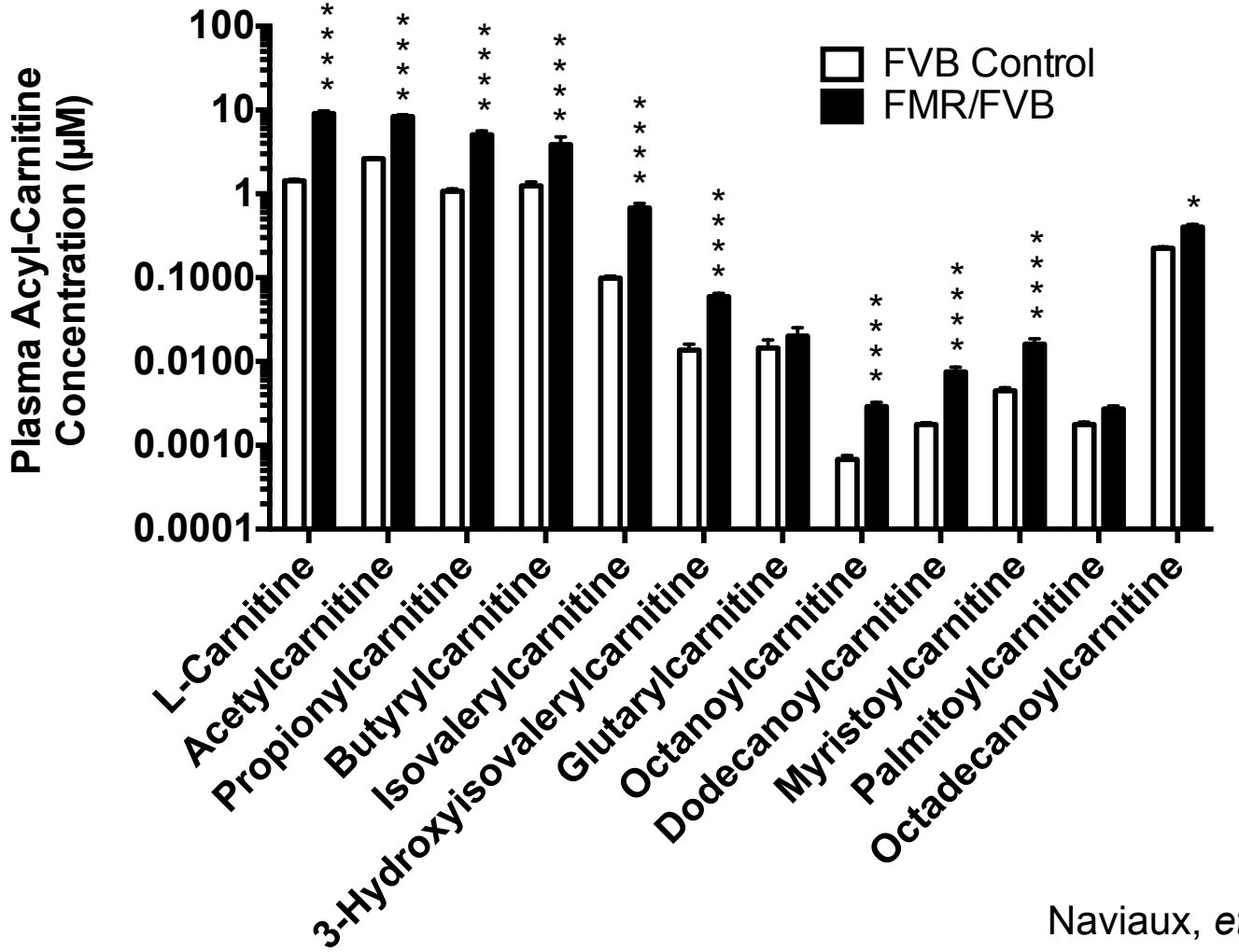

Naviaux, *et al.*, 2015

Additional File 1: Figure S3B

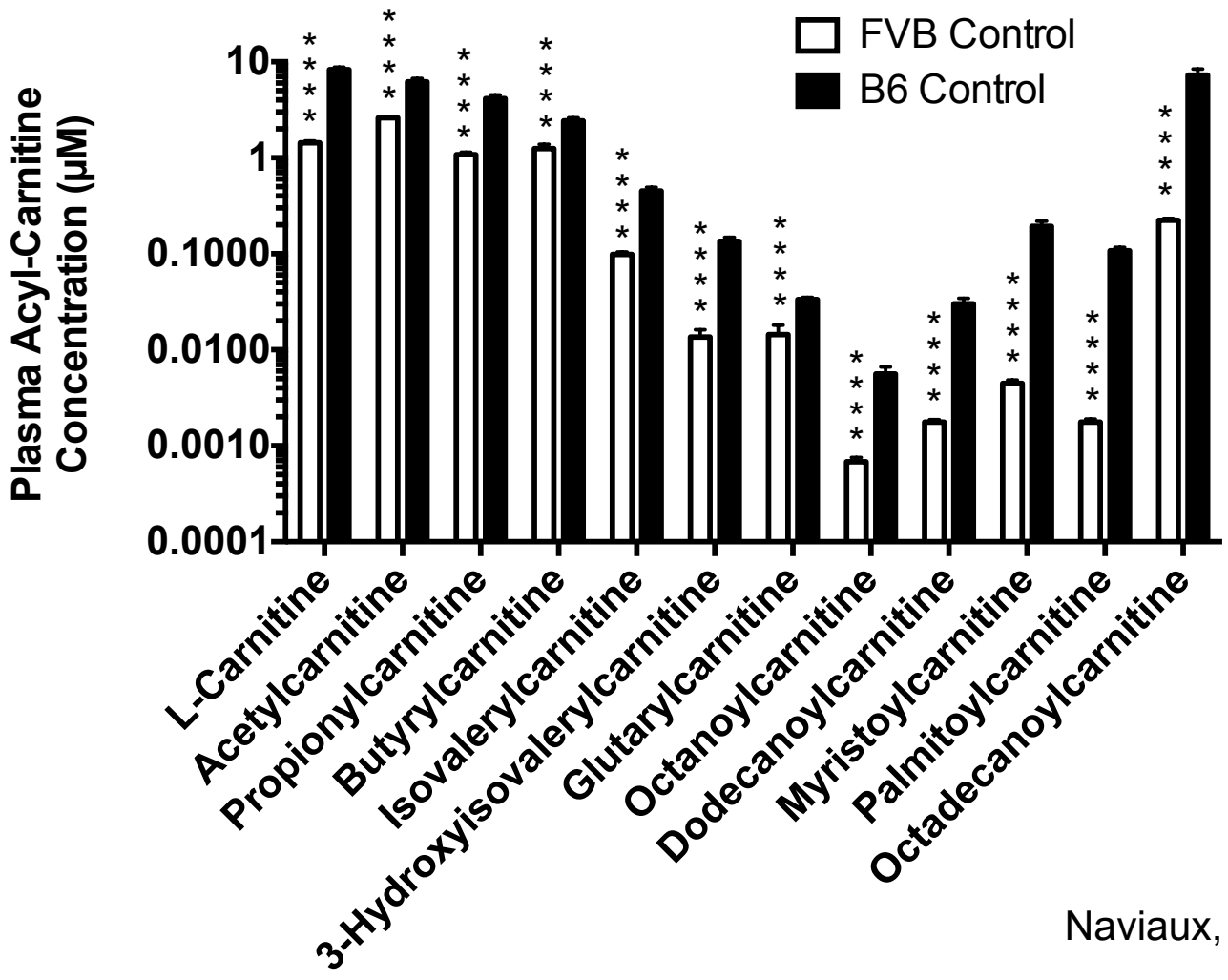

Naviaux, *et al.*, 2015

Additional File 1: Figure S3C

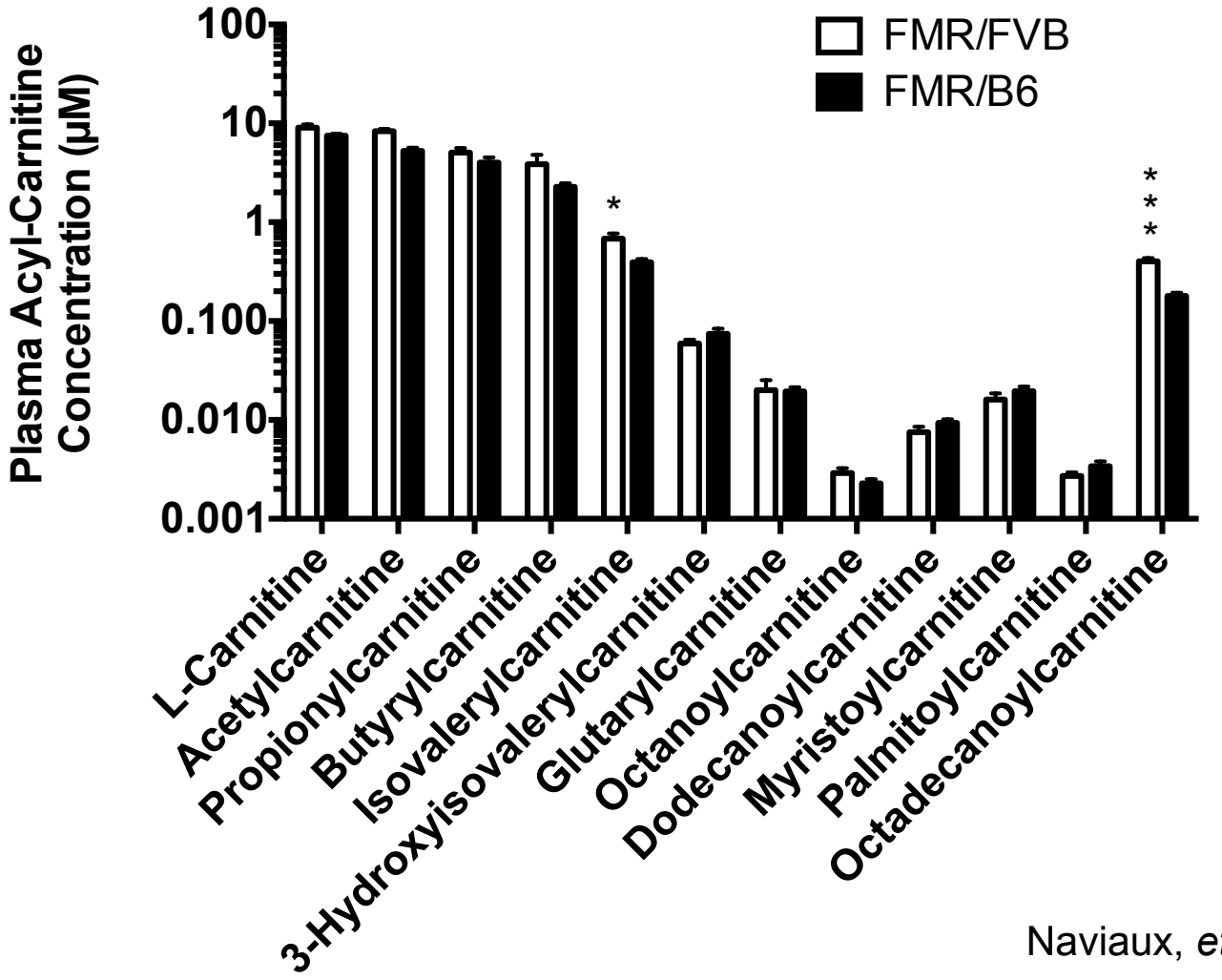

Naviaux, *et al.*, 2015

Additional File 1: Figure S3D

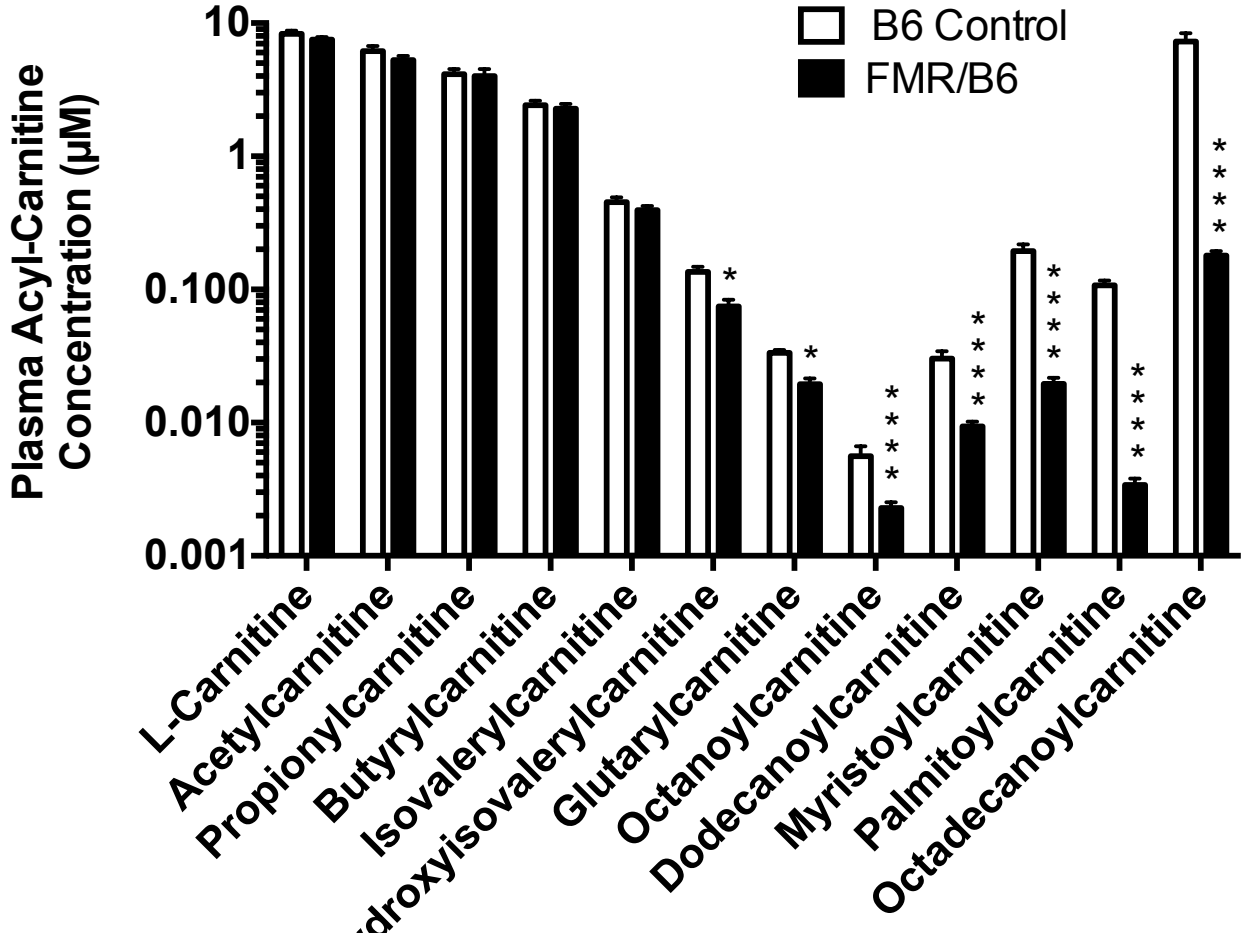

Naviaux, *et al.*, 2015

Additional File 1: Figure S4

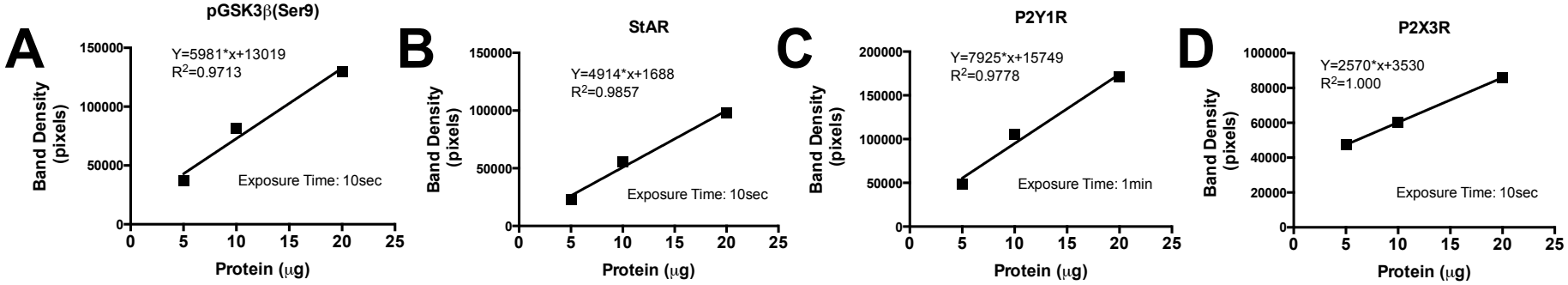

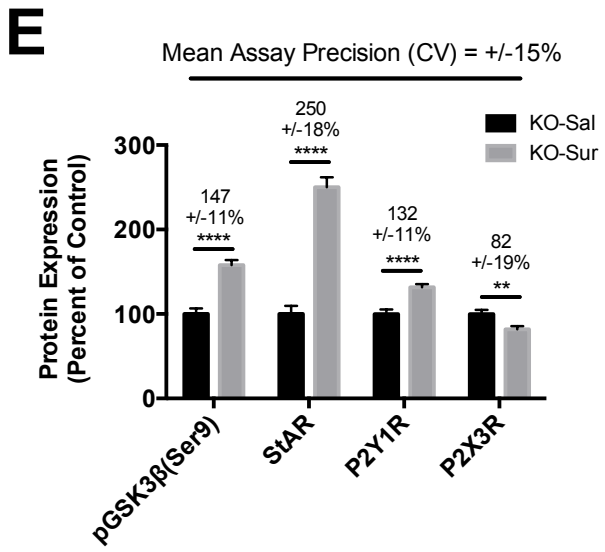

F

Protein	Samples/ Group	Replicates (Days)	Total Samples/ Group	Groups (KO-Sal v KO-Sur)	Percent of Total Variation: Day x Treatment Interaction	Day	Suramin Treatment	F	P value
pGSK	5	3	15	2	0.3%	0.3%	66.1%	(1,24) = 47.7	<0.0001
StAR	5	3	15	2	1%	1%	77.9%	(1,24) = 93.4	<0.0001
P2Y1R	5	3	15	2	0.6%	0.6%	45.5%	(1,24) = 20.5	<0.0001
P2X3R	5	3	15	2	0.4%	0.4%	23.6%	(1,24) = 7.5	<0.01

Naviaux, *et al.*, 2015

Neurobiology of Disease

P2X7 Receptors Drive Poly(I:C) Induced Autism-like Behavior in Mice

Gergely Horváth,[1,2]* Lilla Otrokocsi,[1,2]* Katinka Beko,[1,2] Mária Baranyi,[1] Ágnes Kittel,[1] Pablo Antonio Fritz-Ruenes,[1] and Beáta Sperlágh[1]

[1]Laboratory of Molecular Pharmacology, Institute of Experimental Medicine, Hungarian Academy of Sciences, 1083 Budapest, Hungary, and [2]János Szentágothai School of Neurosciences, Semmelweis University School of PhD Studies, 1085 Budapest, Hungary

Maternal immune activation (MIA) is a principal environmental risk factor contributing to autism spectrum disorder (ASD), which compromises fetal brain development at critical periods of pregnancy and might be causally linked to ASD symptoms. We report that endogenous activation of the purinergic ion channel P2X7 (P2rx7) is necessary and sufficient to transduce MIA to autistic phenotype in male offspring. MIA induced by poly(I:C) injections to P2rx7 WT mouse dams elicited an autism-like phenotype in their offspring, and these alterations were not observed in P2rx7-deficient mice, or following maternal treatment with a specific P2rx7 antagonist, JNJ47965567. Genetic deletion and pharmacological inhibition of maternal P2rx7s also counteracted the induction of IL-6 in the maternal plasma and fetal brain, and disrupted brain development, whereas postnatal P2rx7 inhibition alleviated behavioral and morphological alterations in the offspring. Administration of ATP to P2rx7 WT dams also evoked autistic phenotype, but not in KO dams, implying that P2rx7 activation by ATP is sufficient to induce autism-like features in offspring. Our results point to maternal and offspring P2rx7s as potential therapeutic targets for the early prevention and treatment of ASD.

Key words: **ASD; ATP; JNJ47965567; MIA; P2X7; poly(I:C)**

Significance Statement

Autism spectrum disorder (ASD) is a neurodevelopmental psychiatric disorder caused by genetic and environmental factors. Recent studies highlighted the importance of perinatal risks, in particular, maternal immune activation (MIA), showing strong association with the later emergence of ASD in the affected children. MIA could be mimicked in animal models via injection of a nonpathogenic agent poly(I:C) during pregnancy. This is the first report showing the key role of a ligand gated ion channel, the purinergic P2X7 receptor in MIA-induced autism-like behavioral and biochemical features. We show that genetic or pharmacological inhibition of both maternal and offspring P2X7 receptors could reverse the compromised brain development and autistic phenotype pointing to new possibilities for prevention and treatment of ASD.

Introduction

Autism spectrum disorder (ASD) is a neurodevelopmental psychiatric disorder attracting attention because of its rapidly increasing prevalence worldwide (Knuesel et al., 2014; Estes and McAllister, 2015). ASD is thought to be the result of interplay between genetic, epigenetic, and environmental factors (Ghosh et al., 2013), and recent meta-analyses indicated the role of maternal infection as a risk factor strongly associated with the later emergence of ASD in offspring (Jiang et al., 2016). Furthermore, it was suggested that immune activation of the maternal host, rather than an exogenous pathogenic microorganism, is responsible for this elevated risk because autism-like behavioral and biochemical alterations were induced in offspring by maternal treatment with nonpathogenic double-stranded RNA polyinosinic-polycytidylic acid (poly(I:C)) in rodents and nonhuman primates (Meyer, 2014; Careaga et al., 2017). In mice, maternal immune activation (MIA) by poly(I:C) at embryonic age (E12-E18) induces proinflammatory cytokine production, especially IL-6, in maternal plasma and to a lesser extent in the fetal brain, which is probably mediated through activated TLR3 expressed by circu-

Received July 24, 2018; revised Jan. 9, 2019; accepted Jan. 12, 2019.

Author contributions: B.S. designed research; G.H., L.O., K.B., M.B., A.K., and P.A.F.-R. performed research; G.H., L.O., and M.B. analyzed data; G.H., L.O., and B.S. wrote the paper.

This study was supported by Hungarian Research and Development Fund Grant K116654 to B.S., Hungarian Brain Research Program 2017-1.2.1-NKP-2017-00002 to B.S., and Gedeon Richter plc. RG-IPI-2016-TP10-0012 and the European Union's Horizon 2020 Research and Innovation Programme under the Marie Sklodowska-Curie Grant Agreement 766124. We thank Attila Köfalvi for guidance in synaptosome preparation, Flóra Gölöncsér and Bernadett Varga for technical assistance, the Nikon Microscopy Center, and Cell Biology Center (Flow Cytometry Core Facility), Institute of Experimental Medicine of the Hungarian Academy of Sciences (Budapest, Hungary) for assistance in cytometric bead array analyses.

The authors declare no competing financial interests.

*G.H. and L.O. contributed equally to this work.

Correspondence should be addressed to Beáta Sperlágh at sperlagh@koki.hu.

https://doi.org/10.1523/JNEUROSCI.1895-18.2019

 0270-6474/19/392542-20$15.00/0

lating immune cells. In turn, IL-6, directly or indirectly, influences critical steps of brain development via downstream induction of IL-17a (Choi et al., 2016; Shin Yim et al., 2017), leading to autism-like behavioral symptoms in offspring (Estes and McAllister, 2016). While these cytokines are normally downregulated during mid-pregnancy, increased levels of gestational IL-6 were associated with later emergence of ASD and correlated with intellectual disability in humans (Jones et al., 2017). Maternal cytokines profoundly affect neurogenesis, gliogenesis, neuronal migration, synapse formation, and elimination leading to aberrant cortical and cerebellar development (Meyer et al., 2006; Deverman and Patterson, 2009; Shin Yim et al., 2017). Recently, it has been found that region-specific disorganization of cortical cytoarchitecture manifested in a loss of transcription factors special AT-rich-sequence-protein 2 (SATB2), and T-brain-1 (TBR1) is the main target of maternal IL-17a produced by Th17 cells upon maternal inflammation in the developing brain (Kim et al., 2017), and these changes are causally linked to behavioral alterations in offspring (Shin Yim et al., 2017). However, the molecular signaling machinery responsible for poly(I:C) induced MIA and its conversion to abnormal brain development and an autistic phenotype in offspring is unclear.

Interestingly, in addition to compromised brain development due to MIA, human autistic subjects display a permanently altered immune status in the brain characterized by microglia activation (Suzuki et al., 2013) and elevated levels of proinflammatory cytokines (Masi et al., 2015). In addition to MIA, further postnatal factors might contribute to altered immune homeostasis and maintain dysfunctional behavior. These observations raise the possibility that interaction with molecular signaling pathways instrumental for permanently altered immune status might also be able to reverse behavioral symptoms.

The purinergic P2X7 receptor (P2rx7) is a ligand-gated ion channel sensitive to high extracellular ATP levels, expressed by immune cells and intrinsic cells of the CNS (Sperlágh and Illes, 2014). P2rx7s are activated by the elevation of extracellular ATP during cellular damage or inflammatory conditions, and its activation serves as a maturation signal for post-translational processing of proinflammatory cytokines, such as IL-1β, IL-6, or IL-18. This process requires two signals: a primary signal, termed pathogenic or danger associated molecular patterns (PAMPs and DAMPs), acting at TLR receptors, which leads to the transcription of a cytokine precursor; and a secondary stimulus triggering nucleotide-binding domain-like receptors (NLRP3) oligomerization into intracellular multiprotein complexes, forming inflammasomes. These inflammasomes then cleave proteolytically the precursor protein into mature, leaderless cytokines, which are released to the extracellular space and boost further inflammation (Bartlett et al., 2014; de Torre-Minguela et al., 2017; Adinolfi et al., 2018). P2rx7 activation is one of such secondary stimuli, which could be responsible for converting innate immune response to inflammation following MIA. Although P2rx7 activation has been recognized as a trigger or mediator of many CNS pathologies (Sperlágh and Illes, 2014; Bhattacharya, 2018; Wei et al., 2018), no such role has been demonstrated in animal models of ASD.

Materials and Methods

Animals

Animals were kept under standard laboratory conditions in 12 h light-dark cycles with food and water provided *ad libitum*. All efforts were taken to minimize animal suffering and reduce the number of animals used. All experiments followed the ARRIVE guidelines and were conducted in accordance with the principles and procedures outlined in the *Guide for the care and use of laboratory animals*, US Public Health Service. The local Animal Care Committee of the Institute of Experimental Medicine approved all experimental procedures (Permission PEI/001/778-6/2015). Experiments were performed between 9:00 and 14:00 in the animal housing room. Experiments were performed on male and female P2rx7$^{+/+}$ (C57BL/6) and P2rx7-deficient mice (weighing 25–30 g) for breeding, and their male offspring for behavior and further experiments. P2rx7$^{-/-}$ mice were obtained, bred, and genotyped as described previously (Koványi et al., 2016). Briefly, homozygous P2rx7$^{+/+}$ mice were bred on a C57BL/6J background. The original breeding pairs of P2rx7$^{-/-}$ mice were kindly supplied by Christopher Gabel from Pfizer. The animals contained the DNA construct P2X7-F1 (5′-CGGCGTGC GTTTTGACATCCT-3′) and P2X7-R2 (5′-AGGGCCCTGCGGTTC TC-3′), previously shown to delete the P2rx7 (Solle et al., 2001). Genomic DNA was isolated from the tails of P2rx7$^{+/+}$ and P2rx7$^{-/-}$ animals, and the genotypes were confirmed by PCR analysis. An overall eight backcrosses on C57BL/6 were performed for the P2rx7 KO mouse colony used in our experiments.

Experimental design

The MIA model protocol was designed and performed based on the protocol of R.K. Naviaux et al. (2013).

Primiparous dams were mated at 12–14 weeks of age. Mating trios of P2rx7$^{+/+}$ and P2rx7$^{-/-}$ mice consisted of 2 females and 1 male in each box. In Experiments 1–8, breeding partners were from the same genotype; in Experiments 9 and 10, females and males were from different genotypes. Experienced sires were 3 months old. Sires were randomly assigned as mating pairs for dams regardless of further treatment (poly(I:C) or saline). To induce MIA, a 3 mg/kg dose of poly(I:C) on E12.5 d (Experiments 1–4 and 6–10) and 1.5 mg/kg of poly(I:C) on E17.5 (Experiments 1, 3, 4, 6–9) were injected intraperitoneally to pregnant dams randomly assigned to different treatment groups. In Experiment 5, 400 μM ATP was injected intraperitoneally to pregnant dams on E12.5 d. Control mice received saline injection (100 μl) at the same time as immune-activated animals. Offspring were weaned at 4 weeks of age into cages of 3–5 animals. Behavioral experiments were performed on test-naive male mice at 8 weeks of age in the same order (social preference, self-grooming test, marble-burying test, rotarod) by an experimenter blinded to the treatments. After the behavior tests, animals were killed under light CO_2 anesthesia at an age of 80–90 d, and samples were collected for synaptosome preparation and electron microscopy (EM). In other cases (Experiment 2), experiments were terminated 2 or 48 h after the first dose of poly(I:C) injection, and maternal plasma and fetal brain samples were collected for cytometric bead array analyses, HPLC, and immunohistochemistry, respectively.

Sample size was calculated as described previously (Charan and Kantharia, 2013). A pilot study was performed to measure the basic sociability scores of MIA and saline-treated mice. We estimated sample size using G*Power 3.1.9.2 software (power: 0.8; α error probability: 0.05; direction of effect: two tails, effect size: 0.6698398; coefficient of determination ρ^2: 0.44868533; expected attrition or death of animals: 10%, sample size: ~13 animals/group) that indicated ~156 male offspring were required. Because fecundity was ~40% after poly(I:C) treatment and 80% after saline treatment, we calculated a theoretical sample size of 270 male offspring. Based on our previous experience, one pregnant dam gives birth to an average of 5 males; therefore, 54 breeding pairs were established for the experiments. Samples for *ex vivo* experiments were taken from animals used in behavioral tests.

Every experiment was performed on at least 2 or 3 independent litters; and when P2rx7$^{+/+}$ and P2rx7$^{-/-}$ animals were compared, littermate controls were used.

Drugs and treatments

The following drugs were used in our experiments: poly(I:C) potassium salt (Sigma-Aldrich, P9582, batch 086M4045V), JNJ47965567 (30 mg/kg, Tocris Bioscience), and ATP disodium salt hydrate (Sigma-Aldrich, A2383). Drugs were dissolved in sterile saline, except for JNJ47965567, which was dissolved in 30% Captisol solution (sulfobutyl ether-7

β-cyclodextrin). Controls for the experiments were saline or Captisol solutions in the same volume as the compounds. Prenatal administration of JNJ47965567/vehicle (30 mg/kg i.p.) was performed 2 h before MIA. Postnatal administration of JNJ47965567/vehicle (30 mg/kg i.p.) was a single treatment on the day of the first behavior test on mice randomly assigned to treatment groups.

Behavior tests

Social preference test. Social preference was performed according to the method described by R.K. Naviaux et al. (2013) with minor modifications. Social preference was measured by using a 3-chamber Plexiglas arena (40 × 60 cm) divided into 3 equal chambers (20 × 40 cm each) with a 4 × 4 cm square opening cut into them to allow test mice to move between chambers. Plexiglas cages were put into both of the side chambers. Sniffing zones were assigned around the cages. The experiments consisted of two phases. In Phase 1, the test mouse could explore the whole arena (habituation). In Phase 2, the test mouse was put into the center chamber briefly, the doors were closed, and one unfamiliar stranger mouse of the same age and sex was placed into one of the cages. The other cage remained empty. Then the doors were opened, and the test mouse could explore the arena for 10 min. Ethovision XT 10 system (Noldus) connected with an overhead camera was used to video track and record the time the test mouse spent in each of the sniffing zones. The location of the stranger mouse was alternated across trials. Social preference as a percentage was calculated as 100 multiplied by the time the test mouse spent interacting with the stranger mouse (t_M) divided by the total time a test mouse spent with the stranger and the empty cage (t_E) as follows:

$$SP = 100 * \frac{t_M}{t_M + t_E}$$

Rotarod test. Rotarod test was performed according to the method described by R.K. Naviaux et al. (2013) using an IITC Rotarod apparatus (4-cm-diameter rod). The instrument enables the simultaneous examination of 5 mice in separate compartments. Mice were trained at constant 4 rpm speed for three consecutive trials to achieve the ability to maintain balance on the rod for at least 30 s. Acceleration phase testing was performed on two subsequent days at four trials/d. Mice were individually placed onto the rod. The initial speed was 4 rpm, which accelerated to 40 rpm in 5 min. The intertrial interval was at least 30 min. Latency of falling down was measured in seconds.

Self-grooming test. Self-grooming test was performed by the method described by Kyzar et al. (2011) with minor modifications. Before the experiments, the mice were transported to the experimental room to acclimatize for at least 1 h. Test mice were put into clear glass observation cylinders (12 cm diameter, 20 cm height) individually for 10 min, and their spontaneous novelty-evoked grooming behavior was video recorded. The observation cylinder was cleaned using water between the tests. Behavior was manually scored using Observer XT software (Noldus), and the cumulative duration of self-grooming in seconds was counted by the software.

Marble burying test. Marble burying test was designed based on the method described by Malkova et al. (2012). Clean cages (36.7 × 14.0 × 20.7 cm) were filled with 5 cm corn cob bedding. Then, 20 blue glass marbles were gently placed onto the surface of the bedding in a 4 × 5 arrangement at the same distance from each another. At least one-fifth of the surface remained free from marbles. Testing animals were placed onto the marble free area, and the number of marbles buried was measured within a 10 min testing period. Marbles were counted as buried if they were covered by ≥60% bedding.

Open field test. Open field test was performed following the protocol of R.K. Naviaux et al. (2013). Mice were placed in the middle of a white square box (40 × 40 cm), and locomotor activity was recorded by the Ethovision XT 10 system (Noldus) for 10 min. The total distance covered during the analysis was measured in centimeters.

Brain neuropathology and confocal microscopy

After perfusion with 4% PFA and overnight postfixation of brains in 4% PFA at 4°C, 50 μm parasagittal sections of the cerebellar vermis were used for immunoreaction. Slices were permeabilized with blocking solution containing 5% normal horse serum, 1% BSA, and 0.3% Triton X-100 in 0.1 M PB for 2 h at room temperature (RT), and incubated overnight at 4°C with anti-calbindin antibody (Swant, CB-38a, 1:12,000). Sections were carefully rinsed and washed with PB and stained with fluorescent secondary antibody (Alexa-488 against rabbit, 1:3000, Invitrogen) for 2 h at RT. Purkinje cells in lobe VII of the cerebellum were imaged with a confocal Nikon C2 microscope, and counting was performed manually while the length of the lobe was measured by ImageJ.

Synaptosome preparation and EM

Synaptosome fractions were prepared following the protocol of Köfalvi et al. (2003). After decapitation, half brains were homogenized in sucrose-HEPES solution (0.32 M sucrose, 0.01 M HEPES free acid, 0.63 mM Na_2EDTA, pH 7.4) at 4°C and centrifuged at 3000 × *g* for 5 min. Supernatant was recentrifuged at 13,000 × *g* for 10 min. P2 pellets were resuspended in 45% (v/v) Percoll-Krebs solution (Krebs: 113 mM NaCl, 3 mM KCl, 1.2 mM KH_2PO_4, 1.2 mM $MgSO_4$, 2.5 mM $CaCl_2$, 25 mM $NaHCO_3$, 5.5 mM glucose, 1.5 mM HEPES, pH 7.4) and centrifuged at 13,000 × *g* at 4°C for 2 min to eliminate mitochondria. The top layer was washed twice at 4°C and centrifuged at 13,000 × *g* for 2 min in Krebs solution. Synaptosome pellets were fixed with 4% PFA in 0.1 M PBS for 60 min at RT followed by washing with PBS, and samples were postfixed in 1% OsO_4 (Taab Laboratories) for 30 min. After rinsing the intact fixed pellets within the Eppendorf tubes with distilled water, the pellets were dehydrated in graded ethanol, including block staining with 1% uranyl-acetate in 50% ethanol for 30 min, and were embedded in Taab 812 (Taab Laboratories). Overnight polymerization of samples at 60°C was followed by ultrathin sectioning and imaging by a 7100 electron microscope (Hitachi) equipped with a Megaview II digital camera (lower resolution, Soft Imaging System). Electron micrographs were taken at 20,000 or 30,000 magnifications in all investigated groups, with 4–6 animals per group. Intact and malformed synaptosomes, 45–55 for each investigated animal, were counted manually twice by an investigator blinded to the treatments.

Fetal brain immunohistochemistry

Fetal heads were collected 48 h after the intraperitoneal injection of dams with poly(I:C) (3 mg/kg) or saline, and samples were immersion fixed in 4% PFA for 24 h at 4°C. After cryoprotection in 15% sucrose (20 min) and 30% sucrose overnight at 4°C, 20 μm cryosections were cut using a cryostat (Microm HM550, Thermo Fisher Scientific) and embedded in Tissue-Tek OCT Compound (Sakura Finetek). Sections were washed in PB, permeabilized with 100 mM Na-citrate for 30 min at 65°C and 0.4% Triton X-100 for 20 min at RT, and blocked in 2% normal goat serum and 1% BSA for 1 h at RT. Primary SATB2 and TBR1 antibodies (SATB2 1:100 ab51502, TBR1 1:500 ab31940, Abcam) were applied overnight at 4°C; then slices were rinsed and washed three times in PB, incubated with fluorescent secondary antibodies (1:400 AlexaFluor-594 AffiniPure Donkey Anti-Mouse 715–585-150, Jackson ImmunoResearch Laboratories, 1:1000 Alexa-488 Anti-Rabbit, Invitrogen) containing 1:10,000 Hoechst 33342 (Tocris Bioscience) for 1 h at RT, and rinsed and washed in PB again. Slides were covered with Vectashield mounting medium (Vector), and the fetal cortex was imaged with a confocal Nikon C2 microscope at 20× magnification. TBR1 intensity was measured in the cortical plate with ImageJ software.

Maternal plasma and fetal brain cytokine analyses

Fetal brain samples and maternal plasma were collected 2 h after the intraperitoneal injection of poly(I:C) (3 mg/kg i.p.) or saline. After tissue homogenization and centrifugation, as described previously (Chapman et al., 2009; Dénes et al., 2010), supernatants were collected to measure the levels of the following inflammatory mediators: IL-1α, IL-1β, IL-6, IL-10, TNF-α and CXCL1 (KC) using BD Cytometric Bead Array Flex Sets (BD Biosciences). Measurements were performed on a BD FACSVerse flow cytometer, and data were analyzed using the FCAP Array version 5 software (Soft Flow). Cytokine concentrations of brain tissue were normalized to total protein levels measured by photometry using a BCA Protein Assay Kit (Thermo Fisher Scientific, Pierce). Absorbance was measured at 560 nm with a Victor 3V 1420 Multilabel Counter

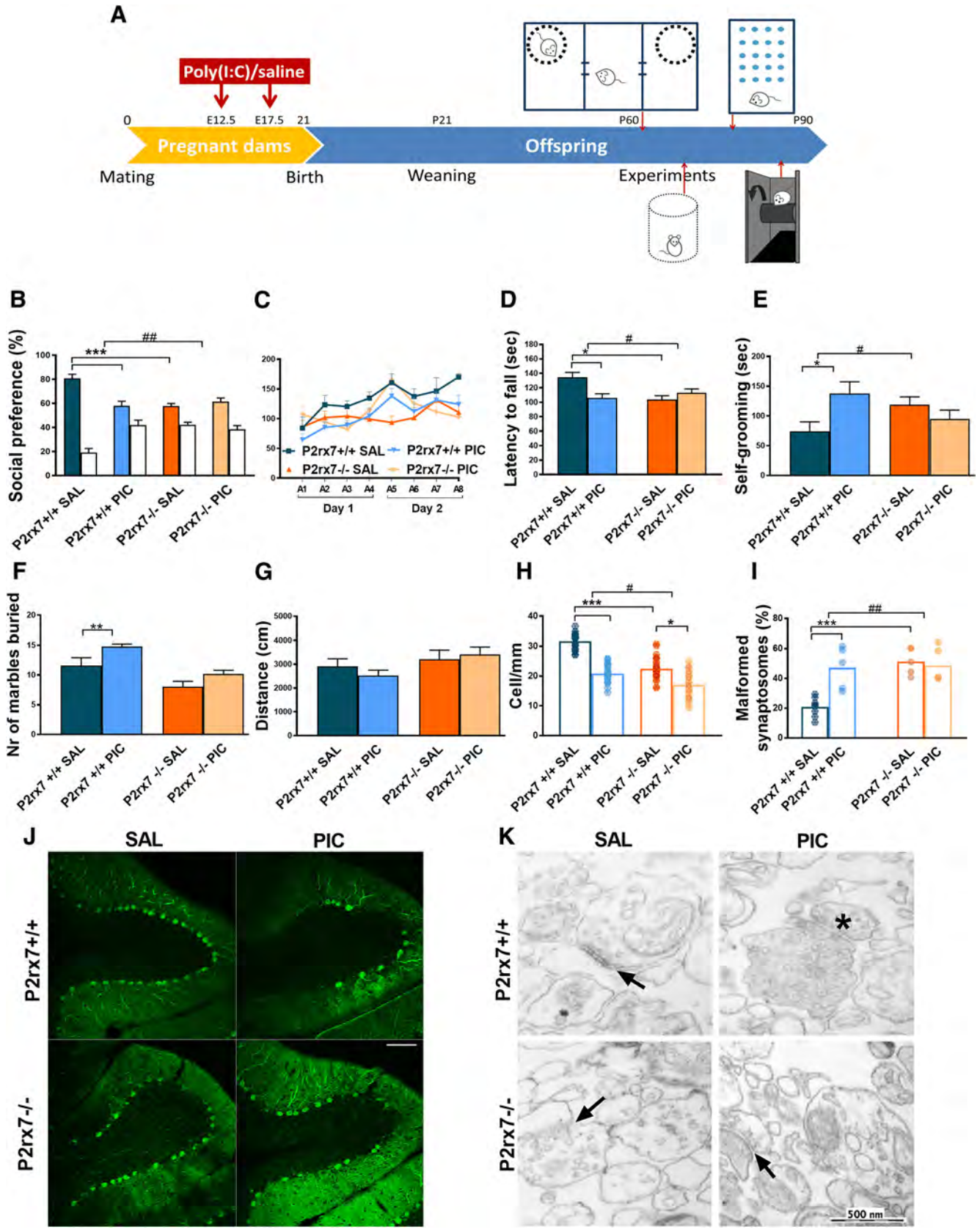

Figure 1. P2X7 receptor (P2rx7) gene deficiency disrupts MIA by poly(I:C) (PIC) on the offspring autistic phenotype. ***A***, Overview of experimental protocol (Experiment 1). ***B***, MIA elicited social deficit in P2rx7 $^{+/+}$ mice, whereas no effect of PIC was observed in P2rx7 $^{-/-}$ animals, although P2rx7 $^{-/-}$ mice displayed decreased social preference compared with P2rx7 $^{+/+}$ counterparts. White columns represent the percentage of interaction with the inanimate cages. PIC-treated P2rx7 $^{+/+}$ animals showed (***C***, ***D***) impaired motor coordination that was absent in P2rx7 $^{-/-}$ mice and (***E***, ***F***) increased repetitive behaviors (i.e., self-grooming and marble burying that were absent in P2rx7 $^{-/-}$ mice). ***G***, Basal locomotor activity was not affected by poly(I:C) administration in either WT (P2rx7 $^{+/+}$) or KO (P2rx7 $^{-/-}$) animals. ***H***, Cerebellar Purkinje cell number decreased in lobule VII by MIA in P2rx7 $^{+/+}$ offspring is ameliorated in P2rx7 $^{-/-}$ (*Figure legend continues.*)

(PerkinElmer). The cytokine levels of plasma are expressed as picograms per milliliter.

HPLC determination of monoamines, adenine nucleotides and nucleoside content

Adenine nucleotides (ATP, ADP, AMP), adenosine (Ado) in extracts from embryonic mouse brain tissue and maternal plasma were determined by using HPLC. Potassium citrate-treated maternal blood was cooled in an ice water bath for 15 min and, after that time, gently centrifuged for 10 min at 2000 rpm and 0°C. The plasma samples were centrifuged again to remove platelets and remaining cells (5000 rpm, 5 min, 0°C). The resulting plasma samples (200 μl) were treated with 20 μl of ice-cold 4 M perchloric acid solution that contained theophylline (as an internal standard) at 100 μM concentration and centrifuged at 6000 rpm for 10 min at 0°C to remove precipitated proteins. To neutralize the pH of the resulting solution, supernatant (100 μl) was treated with 4 M K_2HPO_4 (10 μl) and diluted with water (490 μl), and the centrifugation step was repeated. For analysis (500 μl) the resulting sample was injected onto the column. After the preparation of the whole embryonic mouse brain, the native tissue was frozen by liquid nitrogen. The weighed frozen tissue was homogenized in an appropriate volume of ice-cold 0.1 M perchloric acid that contained theophylline (as an internal standard) at 10 μM concentration and 0.5 mM sodium metabisulphite (antioxidant for biogenic amines). The suspension was centrifuged at 3510 × *g* for 10 min at 0°C-4°C. The perchloric anion was precipitated by addition of 3 μl of 1 M potassium hydroxide to 70 μl of the supernatant. The precipitate was then removed by centrifugation. The supernatant was kept at −20°C until analysis. The pellet was saved for protein measurement (Lowry et al., 1951). The levels of adenine nucleotides and adenosine were determined by online column switching HPLC using Discovery HS C18 50 × 2 mm and 150 × 2 mm columns (5 and 3 μm packing, respectively) with LC-20 AD (Shimadzu, Analytical & Measuring Instruments Division) and were detected (set at 253 nm) by its UV absorption (Agilent Technologies, 1100 series). The flow rate of the mobile phases (A: 10 mM potassium phosphate, 0.25 mM EDTA, 0.45 mM octane sulfonyl acid sodium salt; and B: with 6% acetonitrile (v/v), 2% methanol (v/v), pH 5.2) was 350 or 450 μl/min, respectively, in a step gradient application. The enrichment and stripping flow rate of buffer A was during 4 min, and the total run time was 55 min. Concentrations were calculated by a 2 point calibration curve using internal standard method. The data are expressed as picomol per milligrams of protein or nanomol per liter.

Statistical analysis

Data are expressed as the mean ± SEM of *n* observations, where *n* indicates biological replicates, from several independent litters. We did not exclude any sample or animal from the analyses. Data normality was tested using the Kolmogorov–Smirnov test and Shapiro–Wilk test. We used two-way ANOVA followed by Fischer LSD test for investigating treatment effects in two genotypes or investigating complex treatment effects. When data did not follow a normal distribution even after logarithmic transformation, a nonparametric test (i.e., Mann–Whitney test) was used. GraphPad Prism 7 (GraphPad Software) and Statistica 13 (Dell) software were used for statistical analysis.

Results

Genetic deficiency of P2rx7 prevents MIA-induced behavioral and histological changes in mice

At first, we examined how MIA affects an autistic-like phenotype in the absence and presence of P2rx7s in a previously established mouse poly(I:C) model (R.K. Naviaux et al., 2013). Drug and test-naive P2rx7 WT ($P2rx7^{+/+}$) and deficient ($P2rx7^{-/-}$) pregnant C57BL/6J mouse dams were injected with poly(I:C) at E12.5 (3 mg/kg i.p.) and E17.5 (1.5 mg/kg i.p.), and behavioral phenotype was examined between P60 and P90 (Experiment 1; Fig. 1*A*). Offspring of poly(I:C)-treated $P2rx7^{+/+}$ dams displayed decreased social preference in the three-chamber social interaction test (Fig. 1*B*; for exact *n*, *F*, and *p* values for all experiments, see Table 1); impairment of motor coordination in the accelerating rotarod test (Fig. 1*C*,*D*), and increased repetitive behaviors reflected in self-grooming (Fig. 1*E*) and marble burying (Fig. 1*F*), compared with offspring of saline-treated $P2rx7^{+/+}$ dams. Collectively, these observations suggested that offspring of poly(I:C)-treated $P2rx7^{+/+}$ dams have an ASD-like phenotype. These treatment-related behavioral alterations were not observed in offspring from poly(I:C)-treated $P2rx7^{-/-}$ mice (Fig. 1*B–F*). In addition, genotype-related, treatment-independent changes were also observed: lower sociability (Fig. 1*B*), decreased performance on the rotarod (Fig. 1*C*,*D*), and fewer marbles buried (Fig. 1*F*). Basal locomotor activity measured in the open field arena was not changed by either maternal poly(I:C) treatment or genotype (Fig. 1*G*). After behavior tests, offspring brains were examined for further ASD-specific morphological alterations. Lower number of Purkinje neurons was detected in cerebellar lobe VII, and the proportion of malformed synaptosomes increased after treatment (Fig. 1*H–K*). Fewer Purkinje cells were found in $P2rx7^{-/-}$ (Fig. 1*H*,*J*), whereas poly(I:C) elicited a further, but alleviated decrease. Higher proportion of malformed synaptosomes was observed after poly(I:C) treatment. P2rx7 deficiency by itself elicited a similar increase in the vulnerability of synaptosomes, yet MIA lost its effect (Fig. 1*I*,*K*). In summary, features of MIA-induced autistic-like phenotype were not observed in $P2rx7^{-/-}$ offspring. Although genetic deficiency of P2rx7s mimicked certain aspects of autistic phenotype, these changes were not replicated by either maternal or offspring P2rx7 blockade (see Figs. 3, 4). Therefore, these changes are probably due to intrinsic or developmental effect of genetic knockdown rather than acute functional P2rx7 deficiency.

Effect of MIA on maternal and fetal cytokine response, nucleotide levels and on fetal brain development

Next, we examined how MIA altered nucleotide and cytokine levels in maternal plasma and fetal brain using HPLC and multiplex fluorescent bead array analyses, respectively (Experiment 2). Fetal brain samples and maternal plasma were collected 2 h after a single intraperitoneal injection of poly(I:C) (3 mg/kg). At this time point, increased ATP and ADP levels were detected in $P2rx7^{+/+}$ maternal plasma (Fig. 2*B*), and elevated ATP levels could also be measured in fetal brains, whereas AMP decreased (Fig. 2*C*). In response to MIA, strong IL-6 induction was detected in $P2rx7^{+/+}$ mice, which was attenuated in $P2rx7^{-/-}$ mice (Fig. 2*D*). A similar, although lower, magnitude of statistically significant increase in IL-6 levels was also observed in fetal brain of $P2rx7^{+/+}$ mice, which was not detected in poly(I:C)-treated $P2rx7^{-/-}$ samples (Fig. 2*E*). There was a significant increase of IL-1α and KC in $P2rx7^{+/+}$ maternal plasma after poly(I:C) treatment, which was also attenuated in P2rx7-deficient mice (Fig. 2*D*). KC was also induced by MIA in fetal brain of $P2rx7^{+/+}$, but

←

(*Figure legend continued.*) mice; however, a genotype-related difference was also detected. Data show 20–30 technical replicates in $n = 3$ or 4 animals. ***I***, MIA increased the number of malformed synapses in $P2rx7^{+/+}$ but not in $P2rx7^{-/-}$ mice. A higher proportion of malformed synaptosomes was present in $P2rx7^{-/-}$ mice compared with saline (SAL)-treated $P2rx7^{+/+}$ mice. Exact *n*, *F*, and *p* values are provided in Table 1. ***J***, Representative image of calbindin-labeled Purkinje cells in lobule VII of the cerebellum. Scale bar, 100 μm. ***K***, Representative EM image of synaptosome preparations. Malformed synapses (asterisk) showed highly different structure (uneven membranes, irregular postsynaptic densities) from normally developed synapses (arrows). $^{*}p < 0.05$. $^{**}p < 0.01$. $^{***}p < 0.001$. ANOVA $^{\#}p < 0.05$. $^{\#\#}p < 0.01$.

Table 1. Exact *p* values for all statistical calculations and *n* = biological replicates in each experiment

Figure	Statistical analysis	*F* value	*p* value/*U* value	*Post hoc*	*p* value	*n*
1*B*	Two-way ANOVA	$F_{\text{interaction genotype} \times \text{treatment}(1,39)} = 12.044$	0.00128	P2rx7 $^{+/+}$-saline–P2rx7 $^{+/+}$-poly(I:C)	0.000054	9,16
				P2rx7 $^{-/-}$-saline–P2rx7 $^{-/-}$-poly(I:C)	0.524	8,10
				P2rx7 $^{+/+}$-saline–P2rx7 $^{-/-}$-saline	0.000358	9,8
1*C*, *D*	Two-way ANOVA	$F_{\text{interaction genotype} \times \text{treatment}(1,28)} = 5.433$	0.0272	P2rx7 $^{+/+}$-saline–P2rx7 $^{+/+}$-poly(I:C)	0.0201	5,8
				P2rx7 $^{-/-}$-saline–P2rx7 $^{-/-}$-poly(I:C)	0.412	10,10
				P2rx7 $^{+/+}$-saline–P2rx7 $^{-/-}$-saline	0.0119	5,10
1*E*	Two-way ANOVA	$F_{\text{interaction genotype} \times \text{treatment}(1,38)} = 5.1135$	0.0296	P2rx7 $^{+/+}$-saline–P2rx7 $^{+/+}$-poly(I:C)	0.0199	8,16
				P2rx7 $^{-/-}$-saline–P2rx7 $^{-/-}$-poly(I:C)	0.404	8,10
1*F*	Two-way ANOVA	$F_{\text{interaction genotype} \times \text{treatment}(1,39)} = 0.37383$	0.544	P2rx7 $^{+/+}$-saline–P2rx7 $^{+/+}$-poly(I:C)	0.0049	9,16
				P2rx7 $^{-/-}$-saline–P2rx7 $^{-/-}$-poly(I:C)	0.079	8,10
1*G*	Two-way ANOVA	$F_{\text{interaction maternal tr} \times \text{postnatal tr}(1,20)} = 0.08529$	0.36674	P2rx7 $^{+/+}$-saline–P2rx7 $^{+/+}$-poly(I:C)	0.394482	6,6
				P2rx7 $^{-/-}$-saline–P2rx7 $^{-/-}$-poly(I:C)	0.667652	6,6
1*H*	Two-way ANOVA	$F_{\text{interaction genotype} \times \text{treatment}(1,10)} = 5.162$	0.0464	P2rx7 $^{+/+}$-saline–P2rx7 $^{+/+}$-poly(I:C)	0.0000566	4,4
				P2rx7 $^{-/-}$-saline–P2rx7 $^{-/-}$-poly(I:C)	0.0201	3,3
				P2rx7 $^{+/+}$-saline–P2rx7 $^{-/-}$-saline	0.000335	4,3
1*I*	Two-way ANOVA	$F_{\text{interaction genotype} \times \text{treatment}(1,18)} = 8.9839$	0.00773	P2rx7 $^{+/+}$-saline–P2rx7 $^{+/+}$-poly(I:C)	0.00023	8,5
				P2rx7 $^{-/-}$-saline–P2rx7 $^{-/-}$-poly(I:C)	0.959	4,5
				P2rx7 $^{+/+}$-saline–P2rx7 $^{-/-}$-saline	0.000246	8,4
2*B*	Mann–Whitney		0.004329		ATP	5,6
			0.004329		ADP	5,6
			0.082251		AMP	5,6
			0.125541		Adenosine	5,6
2*C*	Mann–Whitney		0.000000		ATP	31,21
			0.459082		ADP	31,21
			0.000000		AMP	31,21
			0.234949		Adenosine	31,21
2*D*	Two-way ANOVA	$F_{\text{interaction genotype} \times \text{treatment}(1,8)} = 20.965$	0.0018		IL-1α	
				P2rx7 $^{+/+}$-saline–P2rx7 $^{+/+}$-poly(I:C)	0.000556	3,3
	Two-way ANOVA	$F_{\text{interaction genotype} \times \text{treatment}(1,8)} = 92.090$	0.00001		IL-6	
				P2rx7 $^{+/+}$-saline–P2rx7 $^{+/+}$-poly(I:C)	0.000519	3,3
				P2rx7 $^{-/-}$-saline–P2rx7 $^{-/-}$-poly(I:C)	0.000044	3,3
	Two-way ANOVA	$F_{\text{interaction genotype} \times \text{treatment}(1,8)} = 104.90$	0.00001		KC	
				P2rx7 $^{+/+}$-saline–P2rx7 $^{+/+}$-poly(I:C)	0.007849	3,3
				P2rx7 $^{-/-}$-saline–P2rx7 $^{-/-}$-poly(I:C)	0.000004	3,3
2*E*	Two-way ANOVA	$F_{\text{interaction genotype} \times \text{treatment}(1,21)} = 11.415$	0.00284		IL-6	
				P2rx7 $^{+/+}$-saline–P2rx7 $^{+/+}$-poly(I:C)	0.000719	6,6
	Two-way ANOVA	$F_{\text{interaction genotype} \times \text{treatment}(1,21)} = 3.6735$	0.06899		KC	
				P2rx7 $^{+/+}$-saline–P2rx7 $^{+/+}$-poly(I:C)	0.000236	6,6
2*F*	Two-way ANOVA	$F_{\text{interaction pretreatment} \times \text{treatment}(1,10)} = 0.24706$	0.61524		IL-6	
				vehicle-saline–vehicle-poly(I:C)	0.006896	4,3
				JNJ-saline–JNJ-poly(I:C)	0.024084	4,3
	Two-way ANOVA	$F_{\text{interaction pretreatment} \times \text{treatment}(1,10)} = 0.43155$	0.52606		IL-10	
				vehicle-saline–vehicle-poly(I:C)	0.046575	4,3
	Two-way ANOVA	$F_{\text{interaction pretreatment} \times \text{treatment}(1,10)} = 0.44738$	0.51873		KC	
				vehicle-saline–vehicle-poly(I:C)	0.003971	4,3
				JNJ-saline–JNJ-poly(I:C)	0.019628	4,3
	Two-way ANOVA	$F_{\text{interaction pretreatment} \times \text{treatment}(1,10)} = 0.06374$	0.80580		TNF-α	
				vehicle-saline–vehicle-poly(I:C)	0.046575	4,3
2*G*	Two-way ANOVA	$F_{\text{interaction pretreatment} \times \text{treatment}(1,14)} = 37.980$	0.00002		IL-6	
				vehicle-saline–vehicle-poly(I:C)	0.0000001	5,5
				JNJ-saline–JNJ-poly(I:C)	0.011356	4,4
		$F_{\text{interaction pretreatment} \times \text{treatment}(1,14)} = 17.126$	0.00100		KC	
				vehicle-saline–vehicle-poly(I:C)	0.000329	5,5
				JNJ-saline–JNJ-poly(I:C)	0.204446	4,4
2*I*	Two-way ANOVA	$F_{\text{interaction genotype} \times \text{treatment}(1,56)} = 16.578$	0.00015	P2rx7 $^{+/+}$-saline–P2rx7 $^{+/+}$-poly(I:C)	0.000001	3,3
				P2rx7 $^{+/+}$-saline–P2rx7 $^{-/-}$-saline	0.009244	3,3
2*J*	Two-way ANOVA	$F_{\text{interaction genotype} \times \text{treatment}(1,56)} = 17.348$	0.00011	vehicle-saline–vehicle-poly(I:C)	0.000001	3,3
3*B*	Two-way ANOVA	$F_{\text{interaction pretreatment} \times \text{treatment}(1,28)} = 15.4$	0.00051	vehicle-saline–vehicle-poly(I:C)	0.00076	8,8
				JNJ-saline–JNJ-poly(I:C)	0.0868	8,8
3*C*, *D*	Two-way ANOVA	$F_{\text{interaction pretreatment} \times \text{treatment}(1,28)} = 10.245$	0.00340	vehicle-saline–vehicle-poly(I:C)	0.0285	8,8
				JNJ-saline–JNJ-poly(I:C)	0.0349	8,8
3*E*	Two-way ANOVA	$F_{\text{interaction pretreatment} \times \text{treatment}(1,28)} = 2.1410$	0.155	vehicle-saline–vehicle-poly(I:C)	0.0122	8,8
				JNJ-saline–JNJ-poly(I:C)	0.547	8,8
3*F*	Two-way ANOVA	$F_{\text{interaction pretreatment} \times \text{treatment}(1,28)} = 27.917$	0.00001	vehicle-saline–vehicle-poly(I:C)	0.00000992	8,8
				JNJ-saline–JNJ-poly(I:C)	0.0452	8,8

(*Table continues.*)

Table 1. Continued

Figure	Statistical analysis	*F* value	*p* value/*U* value	*Post hoc*	*p* value	*n*
3*G*	Two-way ANOVA	$F_{\text{interaction pretreatment} \times \text{treatment}(1,45)} = 10.538$	0.00221	vehicle-saline–vehicle-poly(I:C)	0.00011	3,3
				JNJ-saline–JNJ-poly(I:C)	0.941	3,3
3*H*	Two-way ANOVA	$F_{\text{interaction pretreatment} \times \text{treatment}(1,16)} = 61.075$	0.000000750	vehicle-saline–vehicle-poly(I:C)	0.00000000055	3,8
				JNJ-saline–JNJ-poly(I:C)	0.0478	4,5
4*B*	Two-way ANOVA	$F_{\text{interactionpretreatment} \times \text{treatment}(1,28)} = 0.13636$	0.71470	vehicle-saline–vehicle-poly(I:C)	0.773	8,8
				JNJ-saline–JNJ-poly(I:C)	0.818855126	8,8
4*C*, *D*	Two-way ANOVA	$F_{\text{interactionpretreatment} \times \text{treatment}(1,28)} = 0.36544$	0.55037	vehicle-saline–vehicle-poly(I:C)	0.622871459	8,8
				JNJ-saline–JNJ-poly(I:C)	0.187131649	8,8
4*E*	Two-way ANOVA	$F_{\text{interactionpretreatment} \times \text{treatment}(1,28)} = 0.05454$	0.81704	vehicle-saline–vehicle-poly(I:C)	0.519973276	8,8
				JNJ-saline–JNJ-poly(I:C)	0.750358047	8,8
4*F*	Two-way ANOVA	$F_{\text{interactionpretreatment} \times \text{treatment}(1,28)} = 0.59189$	0.44813	vehicle-saline–vehicle-poly(I:C)	0.331080732	8,8
				JNJ-saline–JNJ-poly(I:C)	0.921913745	8,8
4*G*	Two-way ANOVA	$F_{\text{interactionpretreatment} \times \text{treatment}(1,69)} = 2.4837$	0.11961	vehicle-saline–vehicle-poly(I:C)	0.000285	3,3
				JNJ-saline–JNJ-poly(I:C)	0.161824	3,3
4*H*	Two-way ANOVA	$F_{\text{interactionpretreatment} \times \text{treatment}(1,8)} = 0.2244$	0.64836	vehicle-saline–vehicle-poly(I:C)	0.676745	3,3
				JNJ-saline–JNJ-poly(I:C)	0.3023	3,3
5*D*	Two-way ANOVA	$F_{\text{interaction genotype} \times \text{treatment}(1,41)} = 2.5759$	0.01383	P2rx7 $^{+/+}$-saline–P2rx7 $^{+/+}$-ATP	0.002692	12,15
				P2rx7 $^{-/-}$-saline–P2rx7 $^{-/-}$-ATP	0.485435	9,9
				P2rx7 $^{+/+}$-saline–P2rx7 $^{-/-}$-saline	0.002334	12,9
5*E*, *F*	Two-way ANOVA	$F_{\text{interaction genotype} \times \text{treatment}(1,28)} = 35.872$	0.0000	P2rx7 $^{+/+}$-saline–P2rx7 $^{+/+}$-ATP	0.000003	12,15
				P2rx7 $^{-/-}$-saline–P2rx7 $^{-/-}$-ATP	0.000000	9,9
				P2rx7 $^{+/+}$-saline–P2rx7 $^{-/-}$-saline	0.011589	12,9
5*G*	Two-way ANOVA	$F_{\text{interaction genotype} \times \text{treatment}(1,41)} = 2.5759$	0.11618	P2rx7 $^{+/+}$-saline–P2rx7 $^{+/+}$-ATP	0.001591	12,15
				P2rx7 $^{-/-}$-saline–P2rx7 $^{-/-}$-ATP	0.486812	9,9
				P2rx7 $^{+/+}$-saline–P2rx7 $^{-/-}$-saline	0.012792	12,9
5*H*	Two-way ANOVA	$F_{\text{interaction genotype} \times \text{treatment}(1,41)} = 0.00184$	0.96603	P2rx7 $^{+/+}$-saline–P2rx7 $^{+/+}$-ATP	0.286530	12,9
				P2rx7 $^{-/-}$-saline–P2rx7 $^{-/-}$-ATP	0.410385	9,9
5*I*	Two-way ANOVA	$F_{\text{interaction genotype} \times \text{treatment}(1,74)} = 27.482$	0.96603	P2rx7 $^{+/+}$-saline–P2rx7 $^{+/+}$-ATP	0.000000	3,3
				P2rx7 $^{-/-}$-saline–P2rx7 $^{-/-}$-ATP	0.001010	3,3
				P2rx7 $^{+/+}$-saline–P2rx7 $^{-/-}$-saline	0.830904	3,3
5*J*	Two-way ANOVA	$F_{\text{interaction genotype} \times \text{treatment}(1,9)} = 20.168$	0.00151	P2rx7 $^{+/+}$-saline–P2rx7 $^{+/+}$-ATP	0.000042	3,4
				P2rx7 $^{-/-}$-saline–P2rx7 $^{-/-}$-ATP	0.475737	3,3
				P2rx7 $^{+/+}$-saline–P2rx7 $^{-/-}$-saline	0.000934	3,3
6*B*	Two-way ANOVA	$F_{\text{interactionpretreatment} \times \text{treatment}(1,28)} = 0.13636$	0.71470	saline-vehicle–poly(I:C)-vehicle	0.773	8,8
				saline-JNJ–poly(I:C)-JNJ	0.818855126	8,8
6*C*, *D*	Two-way ANOVA	$F_{\text{interactionpretreatment} \times \text{treatment}(1,28)} = 0.36544$	0.55037	saline-vehicle–poly(I:C)-vehicle	0.622871459	8,8
				saline-JNJ–poly(I:C)-JNJ	0.187131649	8,8
6*E*	Two-way ANOVA	$F_{\text{interactionpretreatment} \times \text{treatment}(1,28)} = 0.05454$	0.81704	saline-vehicle–poly(I:C)-vehicle	0.519973276	8,8
				saline-JNJ–poly(I:C)-JNJ	0.750358047	8,8
6*F*	Two-way ANOVA	$F_{\text{interactionpretreatment} \times \text{treatment}(1,28)} = 0.59189$	0.44813	saline-vehicle–poly(I:C)-vehicle	0.331080732	8,8
				saline-JNJ–poly(I:C)-JNJ	0.921913745	8,8
6*G*	Two-way ANOVA	$F_{\text{interactionpretreatment} \times \text{treatment}(1,69)} = 2.4837$	0.11961	saline-vehicle–poly(I:C)-vehicle	0.000285	3,3
				saline-JNJ–poly(I:C)-JNJ	0.161824	3,3
6*H*	Two-way ANOVA	$F_{\text{interactionpretreatment} \times \text{treatment}(1,8)} = 0.2244$	0.64836	saline-vehicle–poly(I:C)-vehicle	0.676745	3,3
				saline-JNJ–poly(I:C)-JNJ	0.3023	3,3
7	Two-way ANOVA	$F_{\text{interaction maternal tr} \times \text{postnatal tr}(1,48)} = 12.419$	0.00094	saline-vehicle–poly(I:C)-vehicle	0.000007	3,3
				saline-JNJ–poly(I:C)-JNJ	0.617169	3,3
8*B*	Two-way ANOVA	$F_{\text{interaction maternal tr} \times \text{postnatal tr}(1,28)} = 0.00840$	0.92761	saline-vehicle–poly(I:C)-vehicle	0.493	8,8
				saline-JNJ–poly(I:C)-JNJ	0.4171	8,8
8*C*, *D*	Two-way ANOVA	$F_{\text{interaction maternal tr} \times \text{postnatal tr}(1,28)} = 0.93197$	0.34262	saline-vehicle–poly(I:C)-vehicle	0.208	8,8
				saline-JNJ–poly(I:C)-JNJ	0.937	8,8
8*E*	Two-way ANOVA	$F_{\text{interaction maternal tr} \times \text{postnatal tr}(1,28)} = 0.54089$	0.46818	saline-vehicle–poly(I:C)-vehicle	0.681	8,8
				saline-JNJ–poly(I:C)-JNJ	0.536	8,8
8*F*	Two-way ANOVA	$F_{\text{interaction maternal tr} \times \text{postnatal tr}(1,28)} = 0.02312$	0.88024	saline-vehicle–poly(I:C)-vehicle	0.776	8,8
				saline-JNJ–poly(I:C)-JNJ	0.943	8,8
8*G*	Two-way ANOVA	$F_{\text{interaction maternal tr} \times \text{postnatal tr}(1,50)} = 1.4293$	0.23753	saline-vehicle–poly(I:C)-vehicle	0.0428	3,3
				saline-JNJ–poly(I:C)-JNJ	0.742	3,3
8*H*	Two-way ANOVA	$F_{\text{interaction maternal tr} \times \text{postnatal tr}(1,8)} = 0.26085$	0.62333	saline-vehicle–poly(I:C)-vehicle	0.509306	3,3
				saline-JNJ–poly(I:C)-JNJ	0.195369	3,3
9*B*	Two-way ANOVA	$F_{\text{interaction genotype} \times \text{treatment}(1,25)} = 0.08495$	0.77310	P2rx7 $^{+/-}$-saline–P2rx7 $^{+/-}$-poly(I:C)	0.555425	7,6
				P2rx7 $^{-/+}$-saline–P2rx7 $^{-/+}$-poly(I:C)	0.823292	7,9
9*C*, *D*	Two-way ANOVA	$F_{\text{interaction genotype} \times \text{treatment}(1,28)} = 0.87193$	0.35841	P2rx7 $^{+/-}$-saline–P2rx7 $^{+/-}$-poly(I:C)	0.929087	7,6
				P2rx7 $^{-/+}$-saline–P2rx7 $^{-/+}$-poly(I:C)	0.169450	7,9
9*E*	Two-way ANOVA	$F_{\text{interaction genotype} \times \text{treatment}(1,25)} = 1.3108$	0.26309	P2rx7 $^{+/-}$-saline–P2rx7 $^{+/-}$-poly(I:C)	0.929275	7,6
				P2rx7 $^{-/+}$-saline–P2rx7 $^{-/+}$-poly(I:C)	0.083232	7,9

(*Table continues.*)

Table 1. Continued

Figure	Statistical analysis	*F* value	*p* value/*U* value	*Post hoc*	*p* value	*n*
9*F*	Two-way ANOVA	$F_{\text{interaction genotype} \times \text{treatment}(1,25)} = 0.05514$	0.81626	P2rx7 $^{+/-}$-saline–P2rx7 $^{+/-}$-poly(I:C)	0.648889	7,6
				P2rx7 $^{-/+}$-saline–P2rx7 $^{-/+}$-poly(I:C)	0.874954	7,9
9*G*	Two-way ANOVA	$F_{\text{interaction genotype} \times \text{treatment}(1,74)} = 27.482$	0.96603	P2rx7 $^{+/-}$-saline–P2rx7 $^{+/-}$-poly(I:C)	0.392272	3,3
				P2rx7 $^{-/+}$-saline–P2rx7 $^{-/+}$-poly(I:C)	0.816451	3,3
9*H*	Two-way ANOVA	$F_{\text{interaction genotype} \times \text{treatment}(1,8)} = 0.05420$	0.82176	P2rx7 $^{+/-}$-saline–P2rx7 $^{+/-}$-poly(I:C)	0.170924	3,3
				P2rx7 $^{-/+}$-saline–P2rx7 $^{-/+}$-poly(I:C)	0.104077	3,3
10*B*	Two-way ANOVA	$F_{\text{interaction genotype} \times \text{treatment}(1,12)} = 12.497$	0.00411		IL-6	
				P2rx7 $^{+/+}$-saline–P2rx7 $^{+/+}$-poly(I:C)	0.000000	4,4
				P2rx7 $^{-/-}$-saline–P2rx7 $^{-/-}$-poly(I:C)	0.000000	4,4
	Two-way ANOVA	$F_{\text{interaction genotype} \times \text{treatment}(1,12)} = 3.9123$	0.07136		IL-10	
				P2rx7 $^{+/+}$-saline–P2rx7 $^{+/+}$-poly(I:C)	0.000682	4,4
				P2rx7 $^{-/-}$-saline–P2rx7 $^{-/-}$-poly(I:C)	0.107532	4,4
	Two-way ANOVA	$F_{\text{interaction genotype} \times \text{treatment}(1,12)} = 0.23116$	0.63931		KC	
				P2rx7 $^{+/+}$-saline–P2rx7 $^{+/+}$-poly(I:C)	0.008245	4,4
				P2rx7 $^{-/-}$-saline–P2rx7 $^{-/-}$-poly(I:C)	0.029039	4,4
	Two-way ANOVA	$F_{\text{interaction genotype} \times \text{treatment}(1,12)} = 5.0053$	0.04502		TNF-α	
				P2rx7 $^{+/+}$-saline–P2rx7 $^{+/+}$-poly(I:C)	0.000003	4,4
				P2rx7 $^{-/-}$-saline–P2rx7 $^{-/-}$-poly(I:C)	0.000341	4,4
10*C*	Two-way ANOVA	$F_{\text{interaction genotype} \times \text{treatment}(1,24)} = 0.20677$	0.65340		IL-6	
				P2rx7 $^{+/-}$-saline–P2rx7 $^{+/-}$-poly(I:C)	0.000748	7,7
				P2rx7 $^{-/+}$-saline–P2rx7 $^{-/-}$-poly(I:C)	0.003678	7,7
	Two-way ANOVA	$F_{\text{interaction genotype} \times \text{treatment}(1,24)} = 0.35471$	0.55703		KC	
				P2rx7 $^{+/-}$-saline–P2rx7 $^{+/-}$-poly(I:C)	0.524458	7,7
				P2rx7 $^{-/+}$-saline–P2rx7 $^{-/+}$-poly(I:C)	0.845986	7,7

not P2rx7 $^{-/-}$ mice (Fig. 2*E*). IL-1β, TNFα, IL-10, and IL-1α remained below detection limit in maternal plasma in both genotypes (Fig. 2*D*). Likewise, only insignificant and genotype-independent changes were observed in IL-1α, IL-1β, and IL-10 levels in fetal brain and TNFα remained undetectable (Fig. 2*E*).

Next, we asked how the P2rx7 gene deletion interacted with disrupted fetal brain development and TBR1 and SATB2 expressions were examined following MIA in both genotypes. Eighteen fetal brain samples were immunostained for TBR1 and SATB2, 48 h (E14.5) after poly(I:C) treatment (3 mg/kg on E12.5). Whereas no visible change was observed in SATB2 staining, a weaker intensity of TBR1 immunofluorescence was detected in the developing cortical plate of P2rx7 $^{+/+}$ mice subjected to MIA, indicating the disruption of cortical development (Fig. 2*I*,*K*). In contrast, this change was not observed in P2rx7 $^{-/-}$ mice (Fig. 2*I*,*K*).

Maternal P2rx7 inhibition reproduces the effect of gene deficiency on MIA-induced phenotype in WT mice

In Experiment 3, we determined whether maternal P2rx7 receptors are instrumental for converting MIA to autistic phenotypic alterations in offspring. A single injection of the potent and selective P2rx7 antagonist (JNJ47965567, 30 mg/kg i.p.) or its vehicle was administered to pregnant WT dams 2 h before the respective saline/poly(I:C) administration on E12.5 and E17.5 and the experiment was continued as described for Experiment 1 (Fig. 3*A*). The effect of maternal poly(I:C) treatment was similar in vehicle-treated offspring compared with saline-treated offspring in Experiment 1, and all features of the autistic phenotype were observed: that is, social deficit (Fig. 3*B*), impairment of sensorimotor coordination (Fig. 3*C*,*D*), increase in repetitive behaviors in self-grooming (Fig. 3*E*) and marble burying tests (Fig. 3*F*), dropout of cerebellar Purkinje neurons (Fig. 3*G*,*I*), and synaptosome destruction (Fig. 3*H*,*J*). Notably, maternal JNJ47965567 treatment, by itself, did not have any significant effect on behavior. In contrast, P2rx7 antagonist treatment alleviated the poly(I:C) effect in social preference (Fig. 3*B*), rotarod (Fig. 3*C*,*D*), self-grooming (Fig. 3*E*), and marble burying tests (Fig. 3*F*) compared with an identical treatment with vehicle. Interestingly, poly(I:C)-induced loss of Purkinje cells (Fig. 3*G*, *I*) and increased synaptosome malformation (Fig. 3*H*,*J*) did not occur after JNJ47965567 treatment either.

To cross-validate the effect of genetic deficiency and maternal blockade of P2rx7s, identical P2rx7 antagonist/vehicle treatment was administered to pregnant P2rx7 $^{-/-}$ dams (Experiment 4; Fig. 4*A*). We could not observe any aspects of poly(I:C)-induced autistic phenotype under these conditions (Fig. 4*B*–*J*).

These results indicated that maternal P2rx7s are essential for autistic phenotype alterations in offspring. To identify the underlying molecular signaling machinery, we investigated whether maternal P2rx7 antagonist treatment reproduced the effect of genetic deletion on maternal plasma and fetal brain cytokine profiles (Fig. 2*F*,*G*). The significant induction of IL-6 in maternal plasma (Fig. 2*F*) and fetal brain (Fig. 2*G*) by maternal poly(I:C) treatment was attenuated by pretreatment with P2rx7 antagonist JNJ47965567 (30 mg/kg i.p. 2 h before poly(I:C)), compared with vehicle (Fig. 2*F*,*G*). Furthermore, maternal JNJ4796556 prevented the poly(I:C)-induced loss of TBR1 intensity in the developing cortical plate (Fig. 2*J*,*L*).

Endogenous activation of P2rx7 is sufficient to elicit autistic changes in WT offspring

Single administration of P2rx7 agonist ATP (400 μM) elevated the nucleotide levels in the maternal plasma (Fig. 5*B*) and fetal brain (Fig. 5*C*) after ATP administration. ATP treatment resulted in similar behavioral and morphological alterations observed in poly(I:C)-induced MIA model (Experiment 5). In the offspring of WT dams, social impairment (Fig. 5*D*), excessive self-grooming (Fig. 5*F*), and motor coordination deficit (Fig. 5*E*,*F*) appeared, accompanied by Purkinje cell loss in the cerebellum (Fig. 5*I*,*K*) and higher ratio of malformed synaptosomes in the whole brain (Fig. 5*J*,*L*). In P2rx7-deficient mice, ATP did not

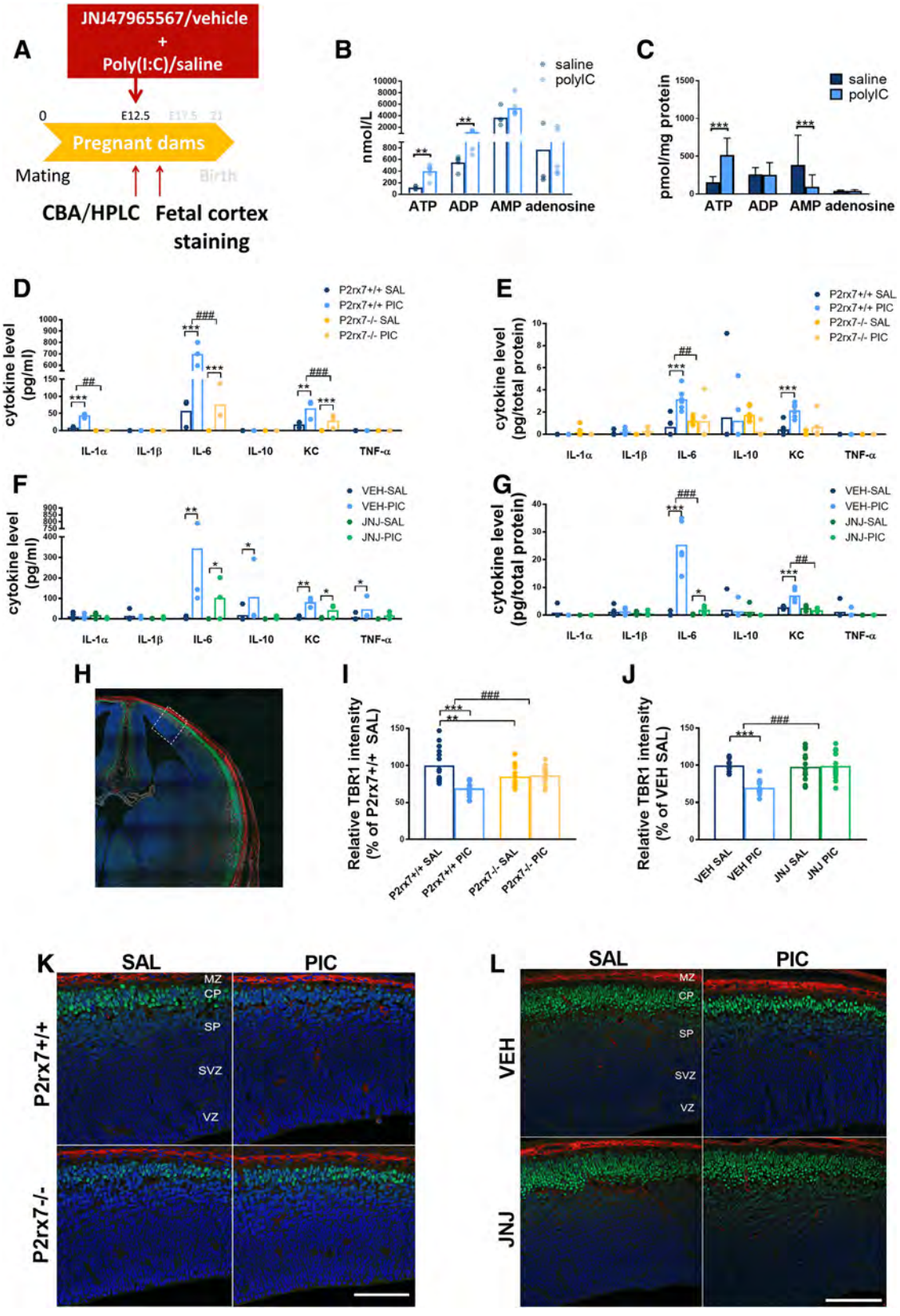

Figure 2. Poly(I:C)-induced nucleotide and cytokine levels in maternal plasma and fetal brain and effect on fetal brain development. ***A***, Experimental protocol (Experiment 2). ***B***, ***C***, MIA increased ATP and ADP levels in P2rx7 $^{+/+}$ maternal plasma, whereas in fetal brain, higher ATP, but decreased AMP levels were detected. ***D***, ***E***, IL-6 was induced in maternal blood after PIC treatment in P2rx7 $^{+/+}$ and P2rx7 $^{-/-}$ mice; however, the induction was substantially ameliorated in P2rx7 $^{-/-}$ mice. *y* axis is interrupted to increase visibility of results. IL-1α and KC levels also showed significant elevation subsequent to MIA. In fetal brain, IL-6 and KC were also induced significantly, although moderately. ***F***, ***G***, PIC induced upregulation of IL-6, and KC is attenuated in maternal plasma and fetal brain of P2rx7 $^{+/+}$ mice by pretreatment with the selective P2rx7 antagonist JNJ47965567. Cytokine values measured in the plasma are expressed in picograms per milliliter, and in the fetal brains as picograms per total protein, and they were logarithmically transformed before statistical analyses. Figures show original dataset. Exact *n*, *F*, and *p* values are provided in Table 1. ***H***, Representative stitched image of the fetal brain. White rectangle represents the location of images presented in ***I*** and ***K***. ***K***, ***L***, MIA decreased the intensity (*Figure legend continues.*)

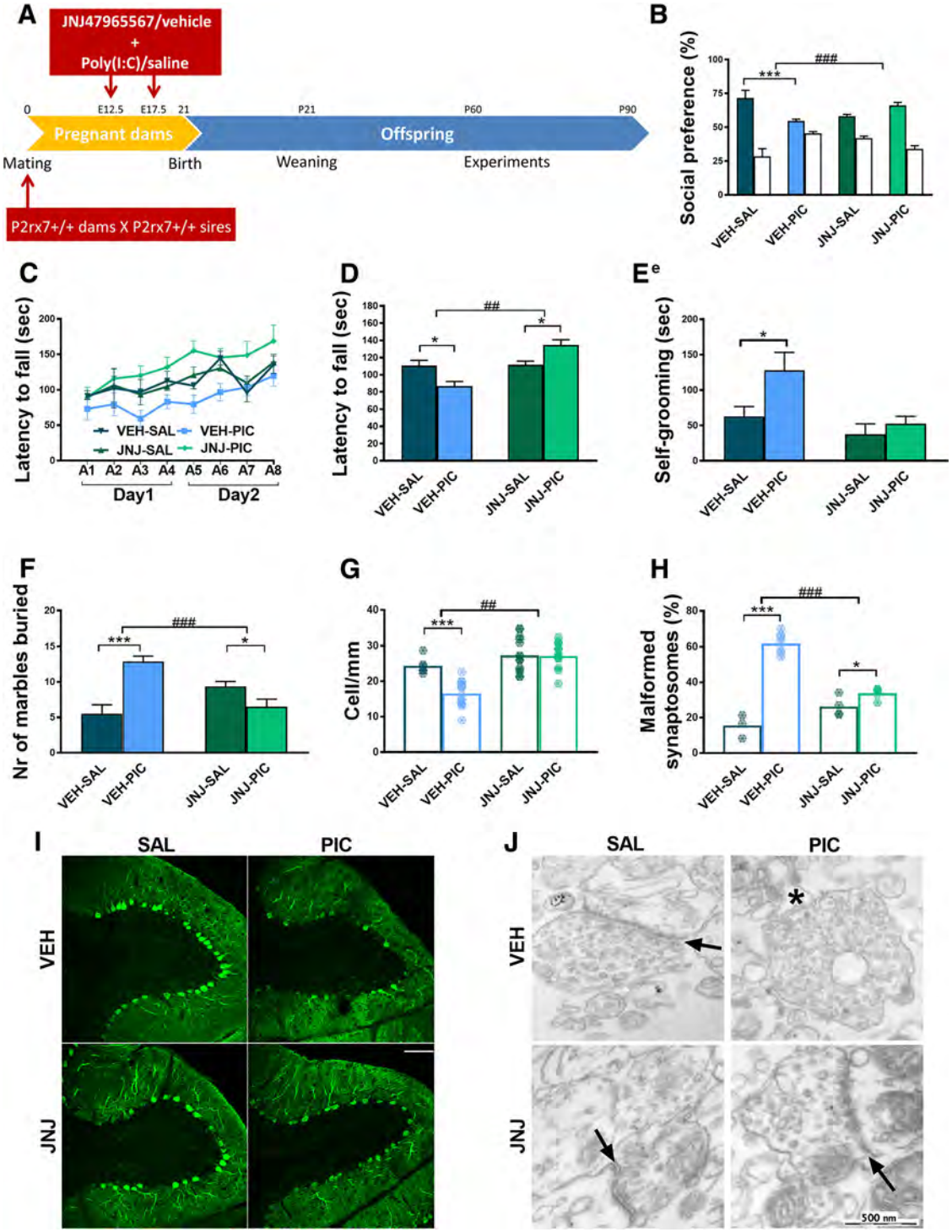

Figure 3. Maternal JNJ47965567 antagonist treatment prevented MIA-induced effects in P2rx7 $^{+/+}$ offspring. ***A***, Experimental protocol (Experiment 3). Pretreatment prevented social deficit (***B***), reversed motor coordination deficiency (***C***,***D***), and normalized repetitive behavior (***E***, ***F***). ***G***, ***I***, After pharmacological P2rx7 blockade, MIA had no influence on Purkinje cells (***G***, ***I***) or on synapses (***H***, ***J***). Scale bar, 100 μm. Asterisk indicates a malformed synaptosome. Arrows indicate intact synapses. Exact *n*, *F*, and *p* values are provided in Table 1. $^{*}p < 0.05$. $^{***}p < 0.001$. ANOVA $^{\#}p < 0.05$. $^{\#\#}p < 0.01$. $^{\#\#\#}p < 0.001$.

←

(*Figure legend continued.*) of TBR1 immunoreactivity in the developing (E14.5) cortical plate of WT mouse fetuses, but this effect was absent in KO mice. ***J***, ***L***, Maternal JNJ47965567 pretreatment prevented poly(I:C)-triggered damage of TBR1-labeled cells. MZ, Marginal zone; CP, cortical plate; SP, subplate; SVZ, subventricular zone; VZ, ventricular zone. Blue represents Hoechst 33342. Red represents SATB2. Green represents TBR1. Scale bar, 100 μm. Data show 15 technical replicates in $n = 3$ animals. $^{*}p < 0.05$. $^{**}p < 0.01$. $^{***}p < 0.001$. ANOVA $^{\#\#}p < 0.01$. $^{\#\#\#}p < 0.001$.

trigger any of these features, confirming the instrumental role of P2rx7 in the mechanism leading to an autism-like condition.

Postnatal P2rx7 inhibition reverses MIA-induced behavioral and histological alterations in WT, but not P2rx7-deficient offspring

The effect of postnatal P2rx7 antagonist treatment on maternal poly(I:C)-induced autistic phenotype in P2rx7 $^{+/+}$ offspring was

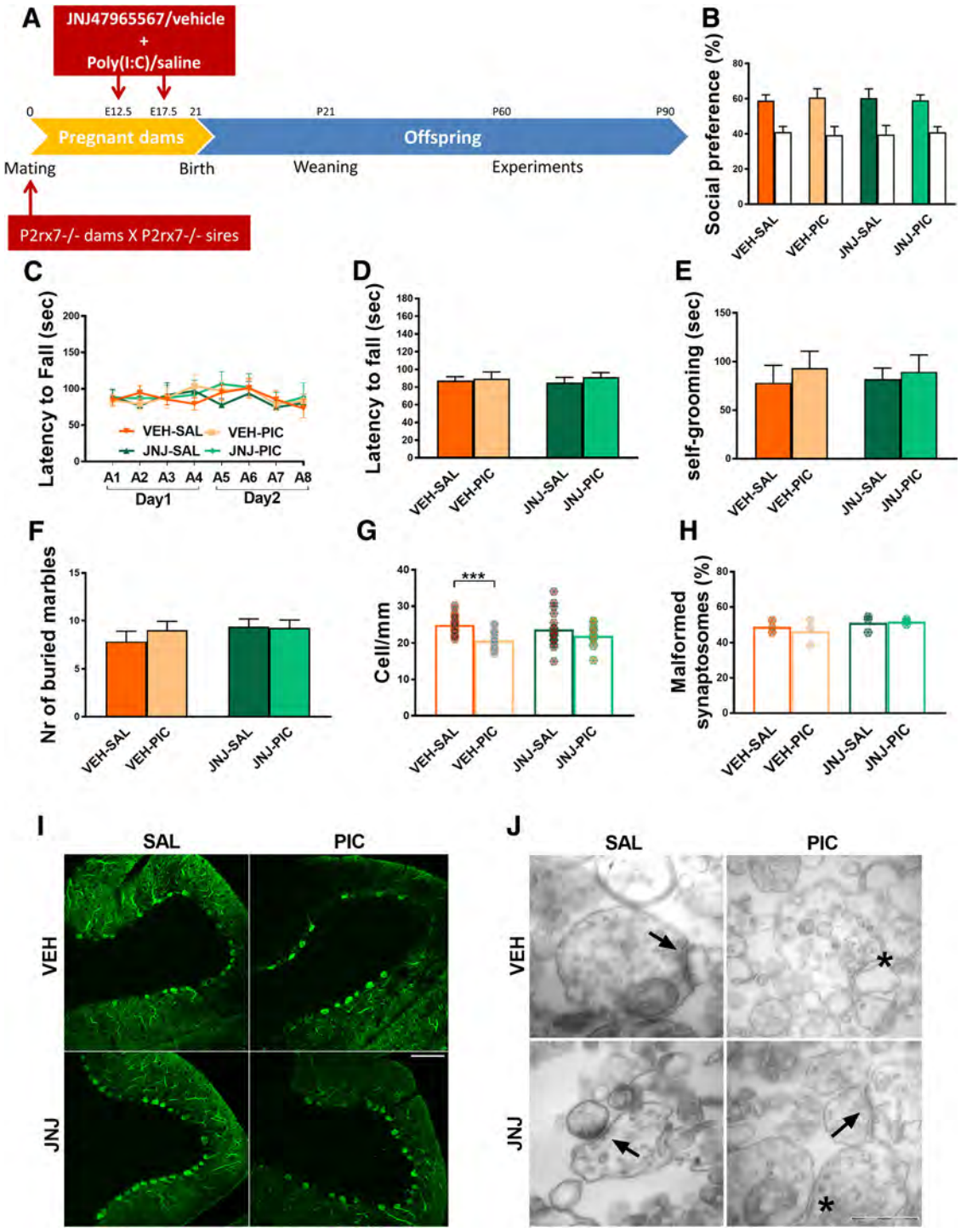

Figure 4. Maternal treatment of P2rx7-deficient dams with the P2rx7 antagonist JNJ47965567 (JNJ, 30 mg/kg i.p., 2 h before PIC injection) did not affect the phenotype of P2rx7 $^{-/-}$ offspring. ***A***, Overview of the experimental protocol (Experiment 4). JNJ pretreatment did not alter the social behavior (***B***), motor coordination deficits (***C***, ***D***), and repetitive behaviors (***E***, ***F***). ***G***, The pharmacological inhibition of maternal P2rx7s in MIA did not influence the density of Purkinje cells (***H***) or the structure of synapses in the offspring. Exact *n*, *F*, and *p* values are provided in Table 1. ***I***, Representative image of calbindin-labeled Purkinje cells in lobule VII of the cerebellum. Scale bar, 100 μm. Data show 17–20 technical replicates in $n = 3$ animals. ***J***, Representative EM image of synaptosomes. Asterisks indicate disturbed synaptosomes. Arrows indicate normal synapses. Scale bar, 500 nm. *$p < 0.05$. ***$p < 0.001$.

examined to determine whether persistent behavior changes are reversible by P2rx7s inhibition (Experiment 6). JNJ47965567 (30 mg/kg i.p.) or its vehicle was administered as a single treatment before the first behavior test (Fig. 6*A*). Postnatal vehicle treatment had no effect on social deficit (Fig. 6*B*), sensorimotor coordination (Fig. 6*C*, *D*), increase in self-grooming (Fig. 6*E*) and marble burying behaviors (Fig. 6*F*), atrophy of cerebellar Purkinje cells (Fig. 6*G*,*I*), and destruction of synapses (Fig. 6*H*,*J*) elicited by maternal poly(I:C) administration. Furthermore, postnatal P2rx7 antagonist treatment did not affect the phenotype in the lack of maternal poly(I:C) treatment (Fig. 6*B*–*J*). In contrast, all poly(I:C)-induced alterations were reversed by postnatal treatment with JNJ47965567 (Fig. 6*B*–*J*).

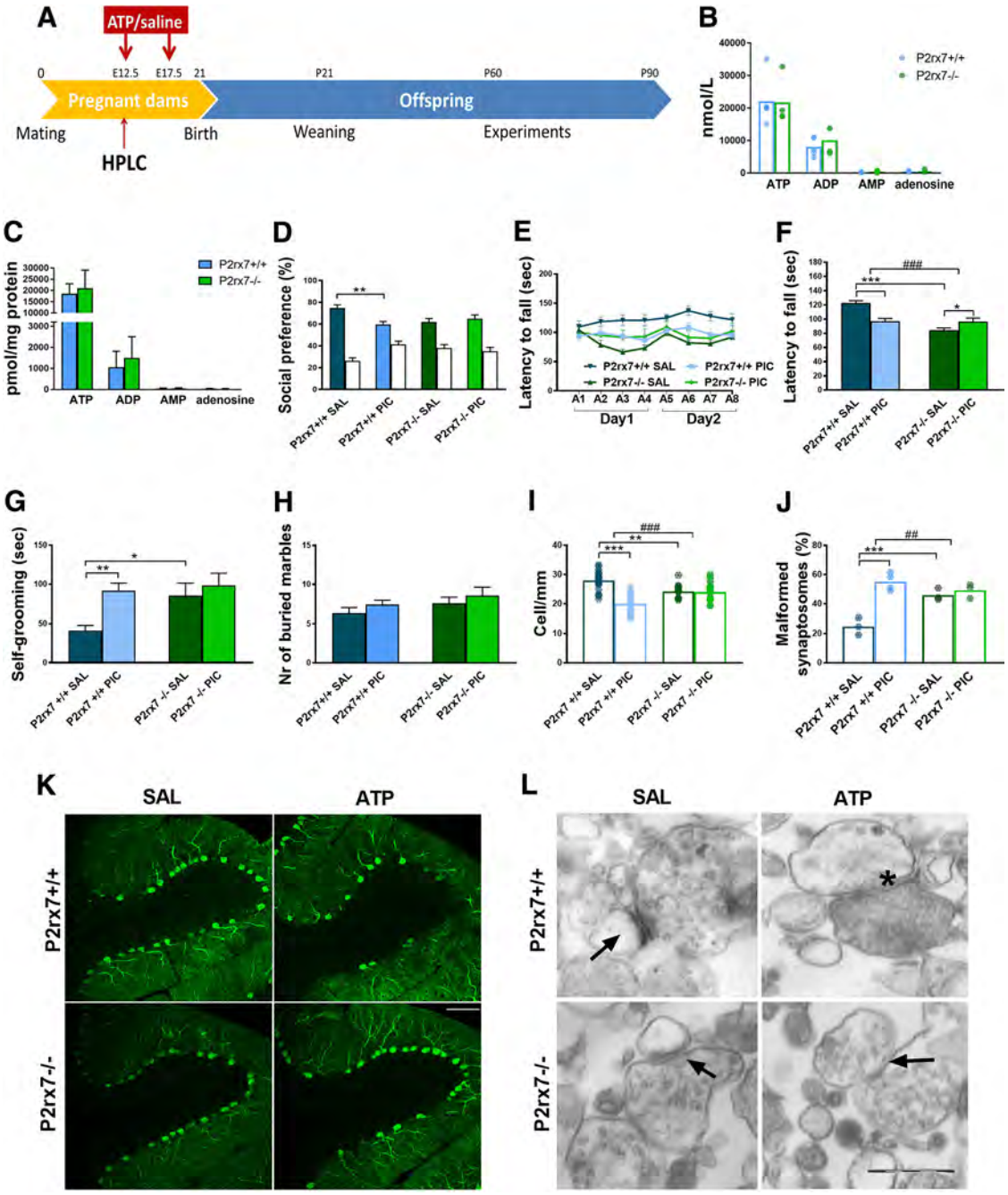

Figure 5. Endogenous activation of P2rx7 via ATP is sufficient to elicit autistic changes in WT offspring. ***A***, Experimental protocol (Experiment 8). ***B***, Elevated nucleotide levels in maternal plasma and fetal brains (***C***) after intraperitoneal injection of 400 μM ATP to mouse dams can activate P2rx7. ***D***, Single ATP injection induced behavioral alterations in WT offspring, but not in P2rx7 $^{-/-}$ offspring, in social preference test, in rotarod test (***E***, ***F***), and in the self-grooming test (***G***). ***H***, In the marble burying test, we did not find significant difference between the groups. ATP administration triggered a decrease in Purkinje cells (***I***), also visible in the representative cerebellar images (***K***). Scale bar, 100 μm. Data show 14–23 technical replicates in $n = 3$ animals. ***J***, Abnormal synaptosome structure was more typical in ATP-treated WTs. ***L***, Representative EM image of synaptosomes. Asterisk indicates malformed. Arrows indicate normal synapses. Scale bar, 500 nm. $^{*}p < 0.05$. $^{**}p < 0.01$. $^{***}p < 0.001$. ANOVA $^{\#\#}p < 0.01$. $^{\#\#\#}p < 0.001$.

The loss of cerebellar Purkinje cells and its reversal by the antagonist was not due to the alterations in subsequent behavior experiments as Purkinje cell loss was observed on young adult offspring of poly(I:C)-treated P2rx7 $^{+/+}$ dams without preceding behavior tests and JNJ47965567 (30 mg/kg i.p.) treatment reversed this change as well (Experiment 7; Fig. 7). Once again, we cross-validated the effect of gene deficiency with the effect of postnatal P2rx7 antagonist treatment, but no maternal poly (I:C)-induced autistic phenotype was observed in offspring of P2rx7 $^{-/-}$ mice either after vehicle or P2rx7 antagonist treatment (Experiment 8; Fig. 8).

P2rx7 $^{+/-}$ heterozygous offspring are not affected by poly(I:C) administration

In Experiment 9, we showed that both maternal and paternal P2rx7 $^{+/+}$ alleles are necessary to induce MIA in offspring. After cross-breeding P2rx7 $^{+/+}$ and P2rx7 $^{-/-}$ mice, the heterozygous offspring resembled the P2rx7 $^{-/-}$ phenotype regardless of ma-

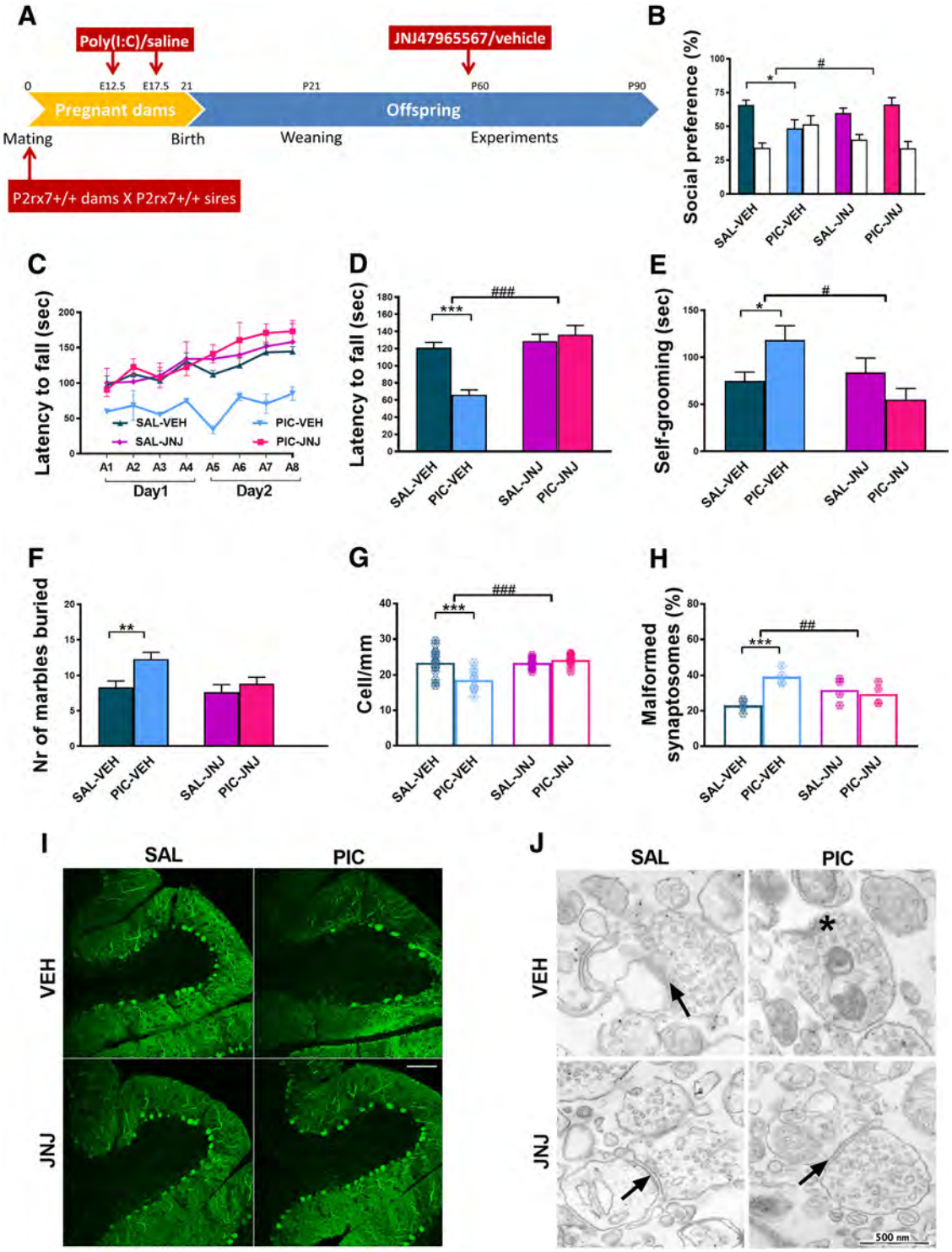

Figure 6. Postnatal inhibition of P2rx7s in the MIA model. ***A***, Experimental protocol (Experiment 5). ***B***, Postnatal antagonist treatment reversed poly(I:C) effects on social interaction, (***C***,***D***) motor coordination, and (***E***,***F***) repetitive behaviors. ***G***, ***I***, Cerebellar Purkinje cell dropout was absent in lobule VII after JNJ47965567 treatment. Scale bar, 100 μm. Data show 9–19 technical replicates in $n = 3$ animals. ***H***, ***J***, Synaptic defects were alleviated by the antagonist, malformed (asterisk) and intact (arrows) synapses indicated. $^{*}p < 0.05$. $^{**}p < 0.01$. $^{***}p < 0.001$. ANOVA $^{\#}p < 0.05$. $^{\#\#}p < 0.01$. $^{\#\#\#}p < 0.001$.

ternal or paternal origin of the allele deficiency. Social preference was not observed in any of the groups (Fig. 9*B*), neither exaggerated repetitive behaviors (Fig. 9*E*,*F*) nor impaired sensorimotor skills (Fig. 9*C*, *D*). In addition to behavioral analyses, also the morphological alterations were investigated; however, cerebellar Purkinje cell numbers (Fig. 9*G*, *I*) and condition of synaptosomes (Fig. 9*H*, *J*) were not affected by poly(I:C) administration or parental genotype.

We also examined cytokine levels in this experimental condition (Experiment 10; Fig. 10*A*), showing that in maternal plasma MIA is able to induce IL-6 and KC production (Fig. 10*B*) similarly to Experiment 2, both in P2rx7 $^{+/+}$ and P2rx7 $^{-/-}$ dams, but

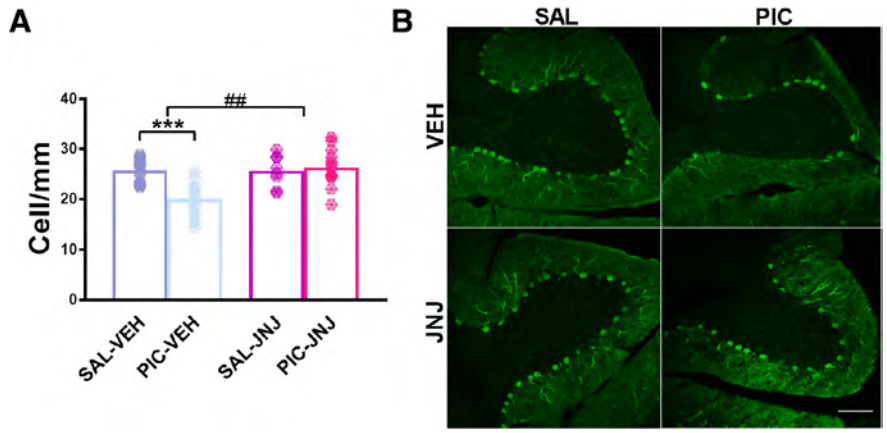

Figure 7. Postnatal treatment of P2rx7 $^{+/+}$ offspring with JNJ47965567 without behavior tests affecting cerebellar Purkinje cell dropout. Eight-week-old P2rx7 $^{+/+}$ animals received a single intraperitoneal JNJ47965567 (30 mg/kg) injection and, after 3 weeks, were killed. ***A***, Calbindin immunolabeling of Purkinje cells revealed similar cell number as in the vehicle controls; therefore, the loss of cells could not be due to subsequent behavior tests, thus supporting the findings of Figure 4*G*. ***B***, Representative images of calbindin-labeled Purkinje cells in lobule VII of the cerebellum. Scale bar, 100 μm. Data show 7–18 technical replicates in $n = 3$ animals. ***$p < 0.001$. ANOVA $^{\#\#}p < 0.01$.

less intensely in the latter group. Also, in the plasma samples, we could measure moderately elevated IL-10 level and TNF-α induction in both genotypes as well. However, in the heterozygous fetal brain samples, we could detect only a much smaller increase of IL-6, whereas other cytokine concentrations remained around the detection limit (Fig. 10*C*), again displaying the phenotype obtained in P2rx7 $^{-/-}$ offspring.

Discussion

Here we show the pivotal role of P2rx7s in the poly(I:C)-induced MIA model of ASD (Fig. 11). P2rx7s and downstream signaling pathways coupled to them are common signaling highways in the pathological nervous system; their involvement has been shown previously in animal models of psychiatric disorders (Cheffer et al., 2018), such as major depression, bipolar disorder (Basso et al., 2009; Csölle et al., 2013a, b), schizophrenia (Koványi et al., 2016), but not in ASD models. The experimental proof for endogenous P2rx7s participation in MIA-induced behavioral and morphological changes in the offspring are as follows: (1) In P2rx7 $^{-/-}$ mice, maternal poly(I:C) did not induce social deficit, sensorimotor impairment, repetitive behaviors; in addition, cerebellar Purkinje cell atrophy and synaptosome destruction were also absent or alleviated. Genetic disruption by itself elicited baseline changes in some offspring phenotypes (e.g., decreased social preference, moderate, but significant Purkinje cell loss), and increased proportion of malformed synaptosomes. However, these are probably related to permanent deficiency of P2rx7s and consequent developmental changes as we could not reproduce them acutely with either maternal or offspring P2rx7 antagonist treatment. Similar socio-communicative and sensorimotor impairment and autistic-like phenotype were observed in another genetic mouse model affecting purinergic signaling (i.e., in mice genetically deficient in P2X4 receptors) (Wyatt et al., 2013). Baseline phenotype of P2rx7 $^{-/-}$ mice has been extensively analyzed in previous studies: altered stress reactivity, but no change in basal locomotor activity, was observed in different studies (Basso et al., 2009; Csölle et al., 2013b; Bartlett et al., 2014; Otrokocsi et al., 2017) in agreement with the present study (Fig. 1*G*). These findings indicate that the lack of responsiveness of P2rx7 $^{-/-}$ offspring to MIA is probably not due to a "ceiling effect" of genetic disruption. (2) The effect of permanent knockdown of P2rx7 on poly(I:C)-induced changes could be mimicked by acute blockade of P2rx7s with specific P2rx7s antagonist on WT mice. It has been shown that JNJ47965567 has a selective action on P2rx7 *in vitro* and reaches high target engagement *in vivo* both in the systemic circulation and in the brain (Bhattacharya et al., 2013). (3) The above protective effects of JNJ47965567 could be observed in P2rx7 $^{+/+}$, but not in P2rx7 $^{-/-}$ littermates, showing that the effect of P2rx7 antagonist is specifically related to P2rx7 inhibition. (4) We demonstrated the instrumental role of P2rx7 in the process leading to autism-like condition via triggering behavioral and morphological alterations by the endogenous activation of P2rx7 during pregnancy. A single ATP injection resulted in similar autistic features observed in poly(I:C)-induced MIA model; therefore, the activation of P2rx7 is not only necessary, but sufficient, to induce autistic phenotype in WT mice. P2rx7-deficient mice were not affected by ATP administration, further strengthening our hypothesis. (5) Heterozygous offspring resemble P2rx7 $^{-/-}$ phenotype; therefore, P2rx7 needs to be present in both parents to elicit MIA-induced autistic features in offpsring.

We have examined the potential underlying mechanism of the anti-autistic effect of genetic/pharmacologic disruption of P2rx7s. At first, we demonstrated the elevation of ATP level in maternal blood and fetal brain, a prerequisite of endogenous P2rx7 activation 2 h after the first poly(I:C) treatment. Because P2rx7s are involved in regulating circulating cytokine production, such as IL-1β, IL-6, and IL-18 following primary inflammatory stimuli (Solle et al., 2001; Bartlett et al., 2014), it was also worthwhile to examine an array of cytokines at the same time point. As expected, a strong induction of IL-6 was observed in maternal circulation of P2rx7 $^{+/+}$ mice, which was attenuated by both genetic deletion and maternal inhibition of P2rx7s. Because maternal IL-6 is sufficient to induce autistic phenotype in offspring (Samuelsson et al., 2006; Hsiao and Patterson, 2011), maternal IL-6 is a likely mediator of the effect of endogenous P2rx7 activation upon maternal poly(I:C)-induced challenge. The action could be either direct, through the placenta (Wu et al., 2017), or indirect, through downstream Th17 cytokines, such as IL-17a, as described in other studies (Choi et al., 2016; Kim et al., 2017; Shin Yim et al., 2017). Interestingly, we could not detect significant change in IL-1β levels in response to MIA in either P2rx7 $^{+/+}$ or P2rx7 $^{-/-}$ animals, which argues against the activation of the canonical P2rx7-IL-1β-NLRP3 signaling pathway, at least at this early time point. Consistently, maternal P2rx7 inhibition, but not IL-1β blockade, was effective to prevent preterm birth and neonatal brain injury in a mouse model of perinatal intrauterine inflammation (Tsimis et al., 2017). Nevertheless, it cannot be excluded that at later time points other cytokines and soluble mediators also participated in maternal and fetal response to poly(I:C)-induced endogenous P2rx7 activation.

We also show here that, 48 h after poly(I:C) injection, TBR1 immunolabeling is decreased in the developing cortical plate of WTs, demonstrating compromised brain development following MIA under our experimental conditions. Importantly, in P2rx7 $^{-/-}$ mice, or after maternal P2rx7 antagonist treatment, no

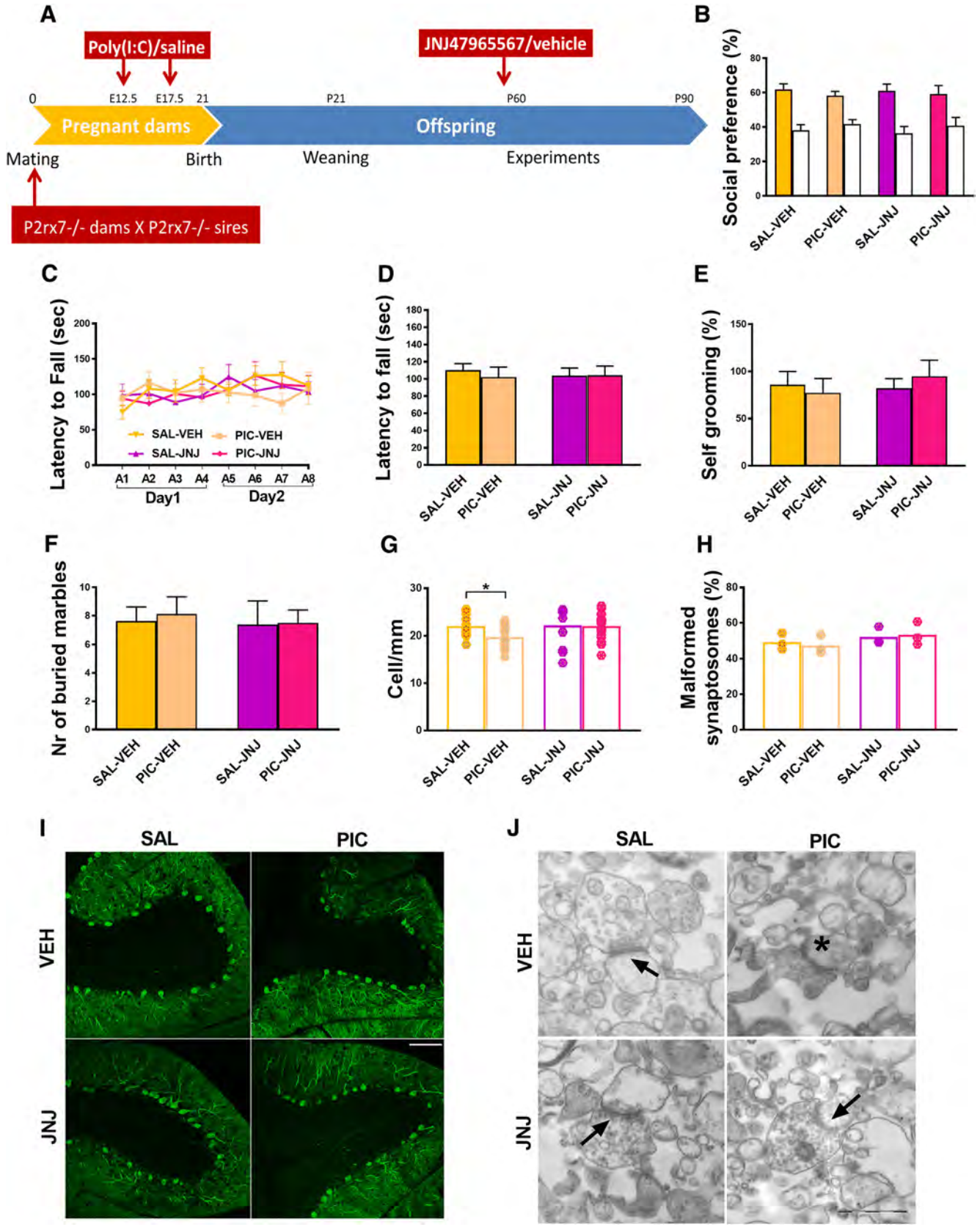

Figure 8. The P2rx7 $^{-/-}$ phenotype was not affected in the MIA model by postnatal administration of selective P2X7 antagonist JNJ47965567 (JNJ, 30 mg/kg i.p., 2 h before the first behavior test) in the offspring. ***A***, Overview of the experimental protocol (Experiment 7). JNJ pretreatment had no influence on the social behavior (***B***), motor coordination deficits (***C***, ***D***), and repetitive behaviors (***E***, ***F***). ***G***, The number of Purkinje cells was not altered in offspring after the pharmacological blockade of P2rx7s in MIA. ***H***, Synaptosome malformation was not affected by the antagonist treatment in the offspring. Exact *n* and *p* values are provided in Table 1. ***I***, Representative images of calbindin-labeled Purkinje cells in lobule VII of the cerebellum. Scale bar, 100 μm. Data show 11–15 technical replicates in $n = 3$ animals. ***J***, Representative EM image of synaptosomes. Asterisk indicates malformed synaptosome. Arrows indicate unharmed synapses. Scale bar, 500 nm. *$p < 0.05$.

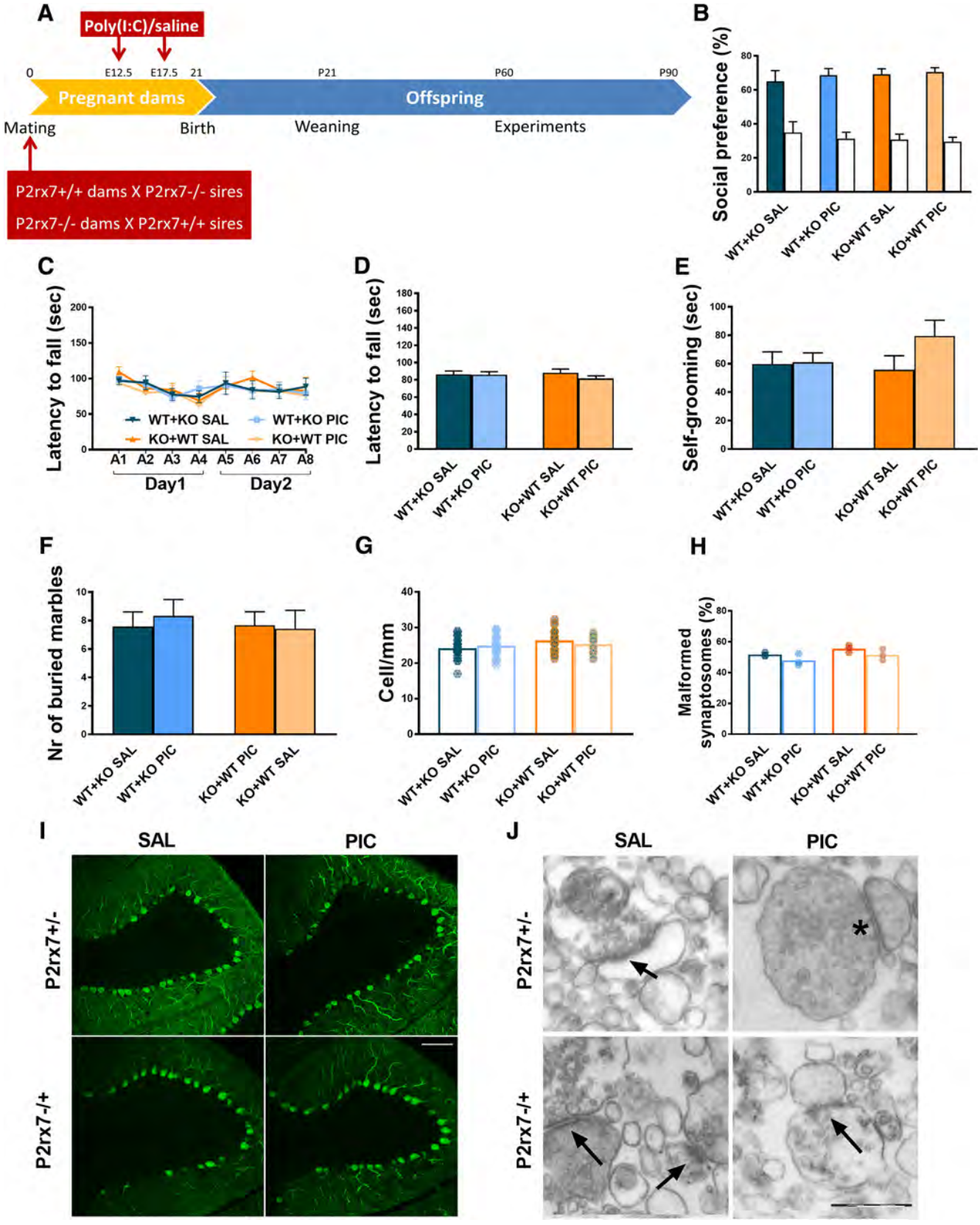

Figure 9. Heterozygous offspring are not affected by poly(I:C) administration. Cross-breeding the P2rx7 $^{+/+}$ and P2rx7 $^{-/-}$ genotypes resulted in an anti-autistic phenotype of heterozygotes, similar to the P2rx7 $^{-/-}$ phenotype. ***A***, Experimental protocol (Experiment 9). Poly(I:C) could not induce MIA and social preference (***B***), aberrant motor coordination (***C***, ***D***), or increased repetitive behaviors (***E***, ***F***) in the offspring regardless of parental origin of P2rx7. ***G***, Purkinje cells were unharmed in heterozygotes. ***I***, Representative images of calbindin-labeled cells in the cerebellum. Scale bar, 100 μm. Data show 22–24 technical replicates in $n = 3$ animals. ***H***, Synaptosome preparations did not reveal any difference in heterozygotes. ***J***, Representative EM synaptosome images. Arrows indicate intact synaptosomes. Asterisks label malformed synaptosome. Scale bar, 500 nm. *$p < 0.05$.

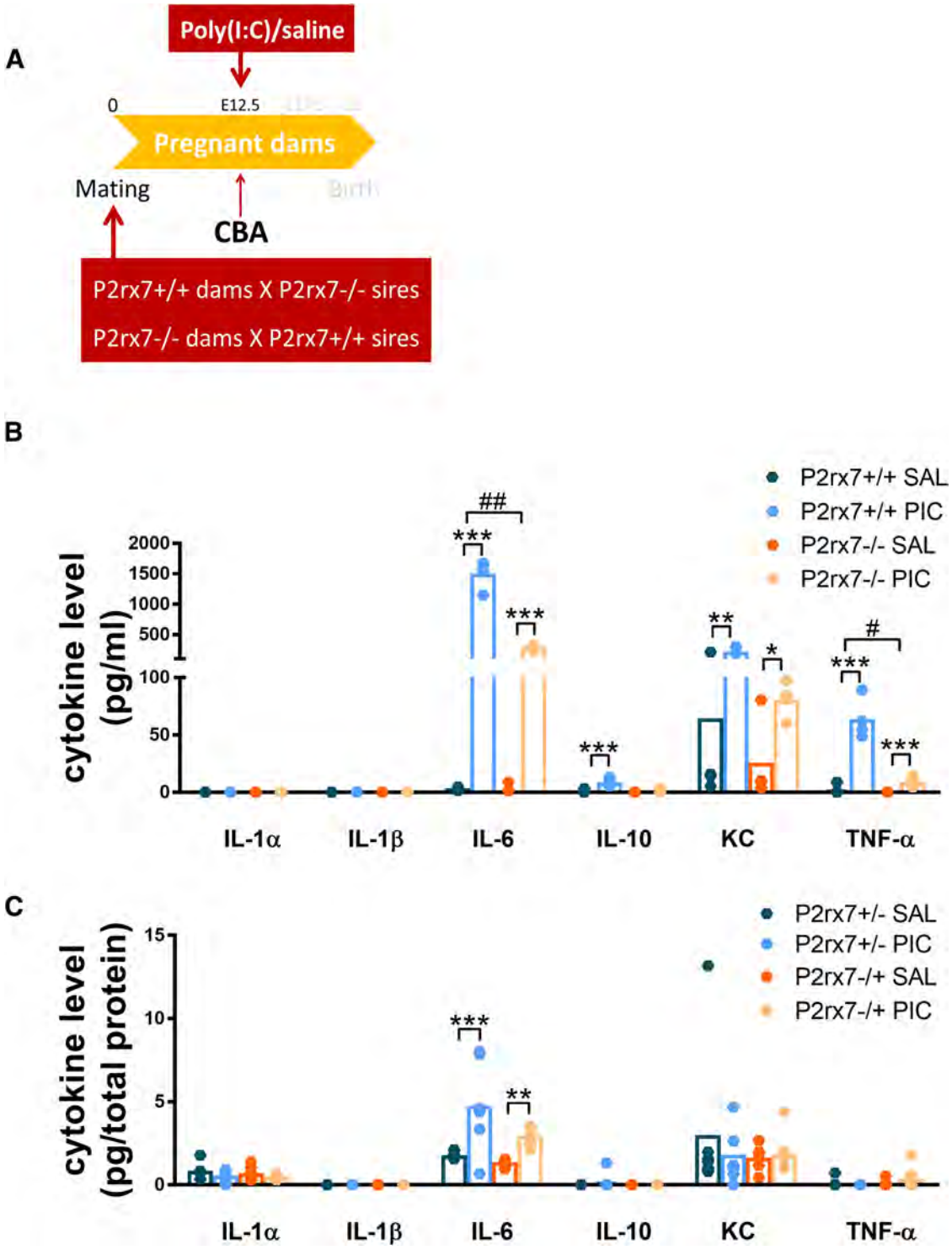

Figure 10. Cytokines are barely induced by poly(I:C) in fetal brains of homozygous offspring; only IL-6 shows a small increase, whereas maternal plasma levels are triggered as in original WT and KO comparison. ***A***, Experimental protocol (Experiment 10). ***B***, MIA triggered IL-6, KC, and TNF-α in the plasma of both P2rx7 $^{+/+}$ and P2rx7 $^{-/-}$ dams, with a more robust elevation in the WTs. IL-10 levels are significantly higher in P2rx7 $^{+/+}$ dams. *y* axis is interrupted to increase visibility of results. However, (***C***) this remarkable induction by poly(I:C) is not transferred to the fetal brains of heterozygous offspring; all values stay close to the detection limit, although in the case of IL-6 concentrations, we could find significant difference in both treated groups. Cytokine values measured in the plasma are expressed in picograms per milliliter, and in the fetal brains as picograms per total protein, and they were logarithmically transformed before statistical analyses. Figures show original dataset. Exact *n*, *F*, and *p* values are provided in Table 1. $^{*}p < 0.05$. $^{**}p < 0.01$. $^{***}p < 0.001$. ANOVA $^{\#}p < 0.05$. $^{\#\#}p < 0.01$.

significant decrease is observed in response to poly(I:C), illustrating the impact of P2rx7 inhibition on MIA-induced alterations in brain development. TBR1 is a transcription factor protein expressed by developing glutamatergic projection neurons with a critical role in neuronal migration and axonal pathfinding in the cortex, and is a high-confidence risk gene for ASD (Deriziotis et al., 2014; Huang and Hsueh, 2015). There are several mechanisms whereby TBR1 loss might influence developing neuronal circuits, and it also acts as a master gene controlling the expression of many other ASD-associated genes (Huang and Hsueh,

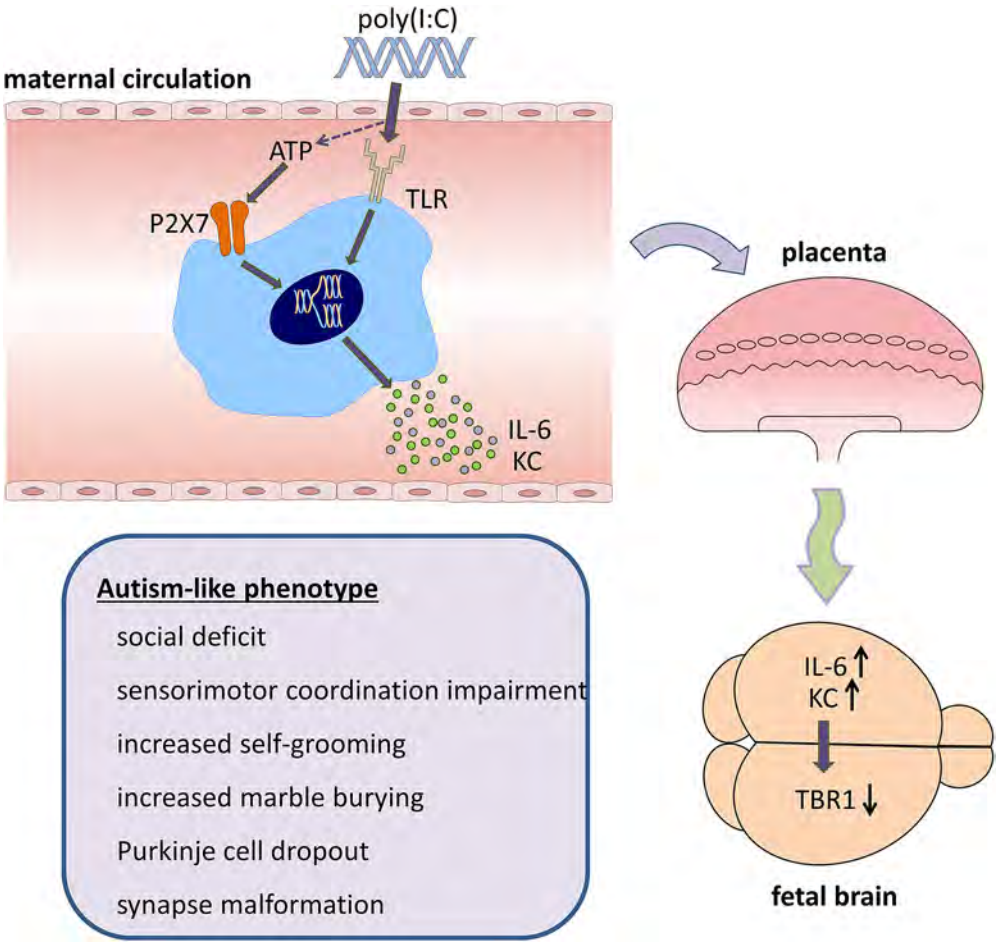

Figure 11. Autism-like phenotype develops via P2rx7-mediated MIA. Poly(I:C) injections induce maternal immune mediators, such as IL-6 and KC through increasing extracellular ATP concentrations activating P2rx7s. This triggers elevation of IL-6 and KC in the fetal brain and compromises the development of cortex reflected in the reduced level of the transcription factor TBR1 protein. Autistic features, such as social deficit, disturbed sensorimotor coordination, excessive repetitive behaviors, loss of cerebellar Purkinje neurons, and abnormal synaptosome structure, could be detected in the adult WT offspring, whereas P2rx7 $^{-/-}$ mice or WT offspring receiving maternal P2rx7 antagonist treatment did not display similar phenotype. Our hypothesis is confirmed by results of Experiment 8, where ATP administration alone could elicit autistic phenotype in offspring via P2rx7 activation.

2015). TBR1 $^{+/-}$ mice exhibit autism-like behaviors (Huang et al., 2014); therefore, it is a plausible explanation that MIA leads to similar behaviors through TBR1 depletion. In contrast, we could not observe change in SATB2 immunofluorescence, another transcription factor instrumental for normal brain development, which is the marker of postmitotic neurons in superficial cortical layers (Alcamo et al., 2008).

Finally, we demonstrated the reversal of MIA-induced behavioral and morphological phenotype by JNJ47965567 treatment in offspring. This finding implies that offspring phenotypic alterations developed as a result of the long-term impact of MIA are reversible by P2rx7 inhibition. Interestingly, there were minor differences in the effects of JNJ depending on the application protocols. This holds true for the sensorimotor coordination impairments (Figs. 3*C*, *D*, 6*C*, *D*), marble burying test (Figs. 3*F*, 6*F*), and synaptosome malformation analyses (Figs. 3*H*, *H*), where there are small, but significant, differences in case of the maternal JNJ administration, which is not detected when JNJ was administered postnatally, although P2rx7 antagonist injection to either pregnant dams or adult offspring counteracted the poly(I:C)-induced changes. Overall, the pharmacological blockade of P2rx7 with JNJ seems efficient in alleviating all of the features of poly(I:C)-induced autism in mice; however, the mechanisms following receptor inhibition could possibly be diverse, whether acting in the maternal organism or in the adult offspring, which might be responsible for differences mentioned above.

As for the potential mechanism of effect of postnatal P2rx7 blockade, it is known that the cerebellum remains plastic even after weeks/month after birth (Wang and Zoghbi, 2001). Probably prenatal poly(I:C) treatment induced such mechanisms that would have resulted in Purkinje cell loss only at the young adult age, when JNJ was administered; therefore, the antagonist could alleviate this effect. Furthermore, our observation on the reversal of Purkinje cell loss after postnatal antipurinergic treatment is not unique. J.C. Naviaux et al. (2014) demonstrated that a single-dose administration of the nonselective P2 receptor antagonist suramin corrected abnormal behaviors and Purkinje cell loss in adult mice in a similar MIA model of autism. Moreover, the alleviation of autistic symptoms by postnatal suramin administration has also been observed in a small human study (R.K. Naviaux et al., 2017).

Nevertheless, identifying the exact cell types and mechanisms responsible for the beneficial action of postnatal P2rx7 blockade awaits further investigation.

In conclusion, we discovered that activation of P2rx7s is necessary to transduce MIA to an autistic phenotype in offspring and that both behavioral and morphological alterations could be reversed by pharmacological inhibition of either maternal or off-

spring P2rx7s. In addition, direct P2rx7 activation alone is sufficient to elicit autistic phenotype in WT mice. Endogenous P2rx7 activation might disrupt cortical development and elicit phenotypic changes via proinflammatory cytokines in the ASD model. Consequently, maternal and offspring P2rx7s function as triggers to turn on and off immune activation and subsequent perinatal brain reprogramming elicited by poly(I:C), which could be used as diagnostic and/or therapeutic intervention target for the precision treatment of ASD.

References

Adinolfi E, Giuliani AL, De Marchi E, Pegoraro A, Orioli E, Di Virgilio F (2018) The P2X7 receptor: a main player in inflammation. Biochem Pharmacol 151:234–244.

Alcamo EA, Chirivella L, Dautzenberg M, Dobreva G, Fariñas I, Grosschedl R, McConnell SK (2008) Satb2 regulates callosal projection neuron identity in the developing cerebral cortex. Neuron 57:364–377.

Bartlett R, Stokes L, Sluyter R (2014) The P2X7 receptor channel: recent developments and the use of P2X7 antagonists in models of disease. Pharmacol Rev 66:638–675.

Basso AM, Bratcher NA, Harris RR, Jarvis MF, Decker MW, Rueter LE (2009) Behavioral profile of P2X7 receptor knockout mice in animal models of depression and anxiety: relevance for neuropsychiatric disorders. Behav Brain Res 198:83–90.

Bhattacharya A (2018) Recent advances in CNS P2X7 physiology and pharmacology: focus on neuropsychiatric disorders. Front Pharmacol 9:30.

Bhattacharya A, Wang Q, Ao H, Shoblock JR, Lord B, Aluisio L, Fraser I, Nepomuceno D, Neff RA, Welty N, Lovenberg TW, Bonaventure P, Wickenden AD, Letavic MA (2013) Pharmacological characterization of a novel centrally permeable P2X7 receptor antagonist: JNJ-47965567. Br J Pharmacol 170:624–640.

Careaga M, Murai T, Bauman MD (2017) Maternal immune activation and autism spectrum disorder: from rodents to nonhuman and human primates. Biol Psychiatry 81:391–401.

Chapman KZ, Dale VQ, Dénes A, Bennett G, Rothwell NJ, Allan SM, McColl BW (2009) A rapid and transient peripheral inflammatory response precedes brain inflammation after experimental stroke. J Cereb Blood Flow Metab 29:1764–1768.

Charan J, Kantharia ND (2013) How to calculate sample size in animal studies? J Pharmacol Pharmacother 4:303–306.

Cheffer A, Castillo AR, Corrêa-Velloso J, Goncalves MC, Naaldijk Y, Nascimento IC, Burnstock G, Ulrich H (2018) Purinergic system in psychiatric diseases. Mol Psychiatry 23:94–106.

Choi GB, Yim YS, Wong H, Kim S, Kim H, Kim SV, Hoeffer CA, Littman DR, Huh JR (2016) The maternal interleukin-17a pathway in mice promotes autism-like phenotypes in offspring. Science 351:933–939.

Csölle C, Baranyi M, Zsilla G, Kittel A, Gölöncsér F, Illes P, Papp E, Vizi ES, Sperlágh B (2013a) Neurochemical changes in the mouse hippocampus underlying the antidepressant effect of genetic deletion of P2X7 receptors. PLoS One 8:e66547.

Csölle C, Andó RD, Kittel Á, Gölöncsér F, Baranyi M, Soproni K, Zelena D, Haller J, Németh T, Mócsai A, Sperlágh B (2013b) The absence of P2X7 receptors (P2rx7) on non-haematopoietic cells leads to selective alteration in mood-related behaviour with dysregulated gene expression and stress reactivity in mice. Int J Neuropsychopharmacol 16:213–233.

Dénes A, Humphreys N, Lane TE, Grencis R, Rothwell N (2010) Chronic systemic infection exacerbates ischemic brain damage via a CCL5 (regulated on activation, normal T-cell expressed and secreted)-mediated proinflammatory response in mice. J Neurosci 30:10086–10095.

Deriziotis P, O'Roak BJ, Graham SA, Estruch SB, Dimitropoulou D, Bernier RA, Gerdts J, Shendure J, Eichler EE, Fisher SE (2014) De novo TBR1 mutations in sporadic autism disrupt protein functions. Nat Commun 5:4954.

de Torre-Minguela C, Mesa Del Castillo P, Pelegrín P (2017) The NLRP3 and pyrin inflammasomes: implications in the pathophysiology of autoinflammatory diseases. Front Immunol 8:43.

Deverman BE, Patterson PH (2009) Cytokines and CNS development. Neuron 64:61–78.

Estes ML, McAllister AK (2015) Immune mediators in the brain and peripheral tissues in autism spectrum disorder. Nat Rev Neurosci 16:469–486.

Estes ML, McAllister AK (2016) Maternal immune activation: implications for neuropsychiatric disorders. Science 353:772–777.

Ghosh A, Michalon A, Lindemann L, Fontoura P, Santarelli L (2013) Drug discovery for autism spectrum disorder: challenges and opportunities. Nat Rev Drug Discov 12:777–790.

Hsiao EY, Patterson PH (2011) Activation of the maternal immune system induces endocrine changes in the placenta via IL-6. Brain Behav Immun 25:604–615.

Huang TN, Hsueh YP (2015) Brain-specific transcriptional regulator T-brain-1 controls brain wiring and neuronal activity in autism spectrum disorders. Front Neurosci 9:406.

Huang TN, Chuang HC, Chou WH, Chen CY, Wang HF, Chou SJ, Hsueh YP (2014) Tbr1 haploinsufficiency impairs amygdalar axonal projections and results in cognitive abnormality. Nat Neurosci 17:240–247.

Jiang HY, Xu LL, Shao L, Xia RM, Yu ZH, Ling ZX, Yang F, Deng M, Ruan B (2016) Maternal infection during pregnancy and risk of autism spectrum disorders: a systematic review and meta-analysis. Brain Behav Immun 58:165–172.

Jones KL, Croen LA, Yoshida CK, Heuer L, Hansen R, Zerbo O, DeLorenze GN, Kharrazi M, Yolken R, Ashwood P, Van de Water J (2017) Autism with intellectual disability is associated with increased levels of maternal cytokines and chemokines during gestation. Mol Psychiatry 22:273–279.

Kim S, Kim H, Yim YS, Ha S, Atarashi K, Tan TG, Longman RS, Honda K, Littman DR, Choi GB, Huh JR (2017) Maternal gut bacteria promote neurodevelopmental abnormalities in mouse offspring. Nature 549:528–532.

Knuesel I, Chicha L, Britschgi M, Schobel SA, Bodmer M, Hellings JA, Toovey S, Prinssen EP (2014) Maternal immune activation and abnormal brain development across CNS disorders. Nat Rev Neurol 10:643–660.

Köfalvi A, Vizi ES, Ledent C, Sperlágh B (2003) Cannabinoids inhibit the release of [^{3}H]glutamate from rodent hippocampal synaptosomes via a novel CB1 receptor-independent action. Eur J Neurosci 18:1973–1978.

Koványi B, Csölle C, Calovi S, Hanuska A, Kató E, Köles L, Bhattacharya A, Haller J, Sperlágh B (2016) The role of P2X7 receptors in a rodent PCP-induced schizophrenia model. Sci Rep 6:36680.

Kyzar E, Gaikwad S, Roth A, Green J, Pham M, Stewart A, Liang Y, Kobla V, Kalueff AV (2011) Towards high-throughput phenotyping of complex patterned behaviors in rodents: focus on mouse self-grooming and its sequencing. Behav Brain Res 225:426–431.

Lowry OH, Rosebrough NJ, Farr AL, Randall RJ (1951) Protein measurement with the folin phenol reagent. J Biol Chem 193:265–275.

Malkova NV, Yu CZ, Hsiao EY, Moore MJ, Patterson PH (2012) Maternal immune activation yields offspring displaying mouse versions of the three core symptoms of autism. Brain Behav Immun 26:607–616.

Masi A, Quintana DS, Glozier N, Lloyd AR, Hickie IB, Guastella AJ (2015) Cytokine aberrations in autism spectrum disorder: a systematic review and meta-analysis. Mol Psychiatry 20:440–446.

Meyer U (2014) Prenatal poly(i:C) exposure and other developmental immune activation models in rodent systems. Biol Psychiatry 75:307–315.

Meyer U, Nyffeler M, Engler A, Urwyler A, Schedlowski M, Knuesel I, Yee BK, Feldon J (2006) The time of prenatal immune challenge determines the specificity of inflammation-mediated brain and behavioral pathology. J Neurosci 26:4752–4762.

Naviaux JC, Schuchbauer MA, Li K, Wang L, Risbrough VB, Powell SB, Naviaux RK (2014) Reversal of autism-like behaviors and metabolism in adult mice with single-dose antipurinergic therapy. Transl Psychiatry 4:e400.

Naviaux RK, Zolkipli Z, Wang L, Nakayama T, Naviaux JC, Le TP, Schuchbauer MA, Rogac M, Tang Q, Dugan LL, Powell SB (2013) Antipurinergic therapy corrects the autism-like features in the poly(IC) mouse model. PLoS One 8:e57380.

Naviaux RK, Curtis B, Li K, Naviaux JC, Bright AT, Reiner GE, Westerfield M, Goh S, Alaynick WA, Wang L, Capparelli EV, Adams C, Sun J, Jain S, He F, Arellano DA, Mash LE, Chukoskie L, Lincoln A, Townsend J (2017) Low-dose suramin in autism spectrum disorder: a small, phase I/II, randomized clinical trial. Ann Clin Transl Neurol 4:491–505.

Otrokocsi L, Kittel A, Sperlágh B (2017) P2X7 receptors drive spine synapse plasticity in the learned helplessness model of depression. Int J Neuropsychopharmacol 20:813–822.

Samuelsson AM, Jennische E, Hansson HA, Holmäng A (2006) Prenatal exposure to interleukin-6 results in inflammatory neurodegeneration in

hippocampus with NMDA/GABA(A) dysregulation and impaired spatial learning. Am J Physiol Regul Integr Comp Physiol 290:R1345–R1356.

Shin Yim Y, Park A, Berrios J, Lafourcade M, Pascual LM, Soares N, Yeon Kim J, Kim S, Kim H, Waisman A, Littman DR, Wickersham IR, Harnett MT, Huh JR, Choi GB (2017) Reversing behavioural abnormalities in mice exposed to maternal inflammation. Nature 549:482–487.

Solle M, Labasi J, Perregaux DG, Stam E, Petrushova N, Koller BH, Griffiths RJ, Gabel CA (2001) Altered cytokine production in mice lacking P2X(7) receptors. J Biol Chem 276:125–132.

Sperlágh B, Illes P (2014) P2X7 receptor: an emerging target in central nervous system diseases. Trends Pharmacol Sci 35:537–547.

Suzuki K, Sugihara G, Ouchi Y, Nakamura K, Futatsubashi M, Takebayashi K, Yoshihara Y, Omata K, Matsumoto K, Tsuchiya KJ, Iwata Y, Tsujii M, Sugiyama T, Mori N (2013) Microglial activation in young adults with autism spectrum disorder. JAMA Psychiatry 70:49–58.

Tsimis ME, Lei J, Rosenzweig JM, Arif H, Shabi Y, Alshehri W, Talbot CC, Baig-Ward KM, Segars J, Graham EM, Burd I (2017) P2X7 receptor blockade prevents preterm birth and perinatal brain injury in a mouse model of intrauterine inflammation. Biol Reprod 97:230–239.

Wang VY, Zoghbi HY (2001) Genetic regulation of cerebellar development. Nat Rev Neurosci 2:484–491.

Wei L, Syed Mortadza SA, Yan J, Zhang L, Wang L, Yin Y, Li C, Chalon S, Emond P, Belzung C, Li D, Lu C, Roger S, Jiang LH (2018) ATP-activated P2X7 receptor in the pathophysiology of mood disorders and as an emerging target for the development of novel antidepressant therapeutics. Neurosci Biobehav Rev 87:192–205.

Wu WL, Hsiao EY, Yan Z, Mazmanian SK, Patterson PH (2017) The placental interleukin-6 signaling controls fetal brain development and behavior. Brain Behav Immun 62:11–23.

Wyatt LR, Godar SC, Khoja S, Jakowec MW, Alkana RL, Bortolato M, Davies DL (2013) Sociocommunicative and sensorimotor impairments in male P2X4-deficient mice. Neuropsychopharmacology 38:1993–2002.

Article

Cell

Stress-Induced Metabolic Disorder in Peripheral CD4$^+$ T Cells Leads to Anxiety-like Behavior

Graphical Abstract

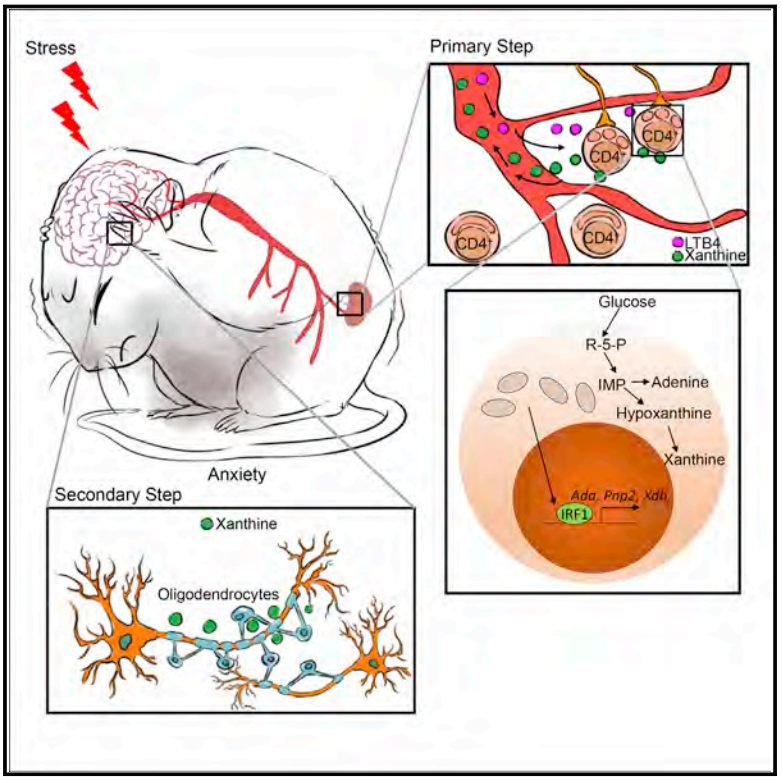

Highlights

- Peripheral CD4$^+$ T cells control stress-induced anxiety-like behavior
- Mitochondrial fission in peripheral CD4$^+$ T cell causes severe anxiety symptoms
- T cell-derived xanthine acts on the oligodendrocytes in the left amygdala
- IRF-1 controls purine synthesis in CD4$^+$ T cells and triggers the onset of anxiety

Authors

Ke-qi Fan, Yi-yuan Li, Hao-li Wang, ..., Xin-Hua Feng, Ren-jie Chai, Jin Jin

Correspondence

jjin4@zju.edu.cn (J.J.), renjiec@seu.edu.cn (R.-j.C.)

In Brief

Xanthine metabolism in CD4$^+$ T cells is found to be central to mediating the effects of stress-induced anxiety like behavior in mice through its effects on oligodendrocyte proliferation and neuronal hyperactivation.

Fan et al., 2019, Cell *179*, 864–879
October 31, 2019
https://doi.org/10.1016/j.cell.2019.10.001

CellPress

Cell

Article

Stress-Induced Metabolic Disorder in Peripheral CD4$^+$ T Cells Leads to Anxiety-like Behavior

Ke-qi Fan,[1,9] Yi-yuan Li,[1,9] Hao-li Wang,[1] Xin-tao Mao,[1] Jin-xin Guo,[1] Fei Wang,[1] Ling-jie Huang,[2] Yi-ning Li,[1] Xiang-yu Ma,[3,4,5] Zheng-jun Gao,[1] Wei Chen,[6] Dan-dan Qian,[3] Wen-jin Xue,[3] Qian Cao,[2] Lei Zhang,[2] Li Shen,[1] Long Zhang,[1] Chao Tong,[1] Jiang-yan Zhong,[1] Wei Lu,[3] Ling Lu,[7] Ke-ming Ren,[2] Guisheng Zhong,[8] Yuan Wang,[6] Mingliang Tang,[3] Xin-Hua Feng,[1] Ren-jie Chai,[3,4,5,*] and Jin Jin[1,2,10,*]

[1]MOE Laboratory of Biosystem Homeostasis and Protection and Life Sciences Institute, Zhejiang University, Hangzhou 310058, China
[2]Sir Run Run Shaw Hospital, College of Medicine, Zhejiang University, Hangzhou 310016, China
[3]Key Laboratory for Developmental Genes and Human Disease, Ministry of Education, Institute of Life Sciences, Jiangsu Province High-Tech Key Laboratory for Bio-Medical Research, Southeast University, Nanjing 210096, China
[4]Co-Innovation Center of Neuroregeneration, Nantong University, Nantong 226001, China
[5]Institute for Stem Cell and Regeneration, Chinese Academy of Science, Beijing, China
[6]Shanghai Key Laboratory of Regulatory Biology, Institute of Biomedical Sciences and School of Life Sciences, East China Normal University, 500 Dongchuan Road, Shanghai 200241, China
[7]Department of Otolaryngology Head and Neck Surgery, Nanjing Drum Tower Hospital, Nanjing University Medical School, Nanjing, 210008, Jiangsu, China
[8]iHuman Institute, ShanghaiTech University, Shanghai 201210, China
[9]These authors contributed equally
[10]Lead contact
*Correspondence: jjin4@zju.edu.cn (J.J.), renjiec@seu.edu.cn (R.-j.C.)
https://doi.org/10.1016/j.cell.2019.10.001

SUMMARY

Physical or mental stress leads to neuroplasticity in the brain and increases the risk of depression and anxiety. Stress exposure causes the dysfunction of peripheral T lymphocytes. However, the pathological role and underlying regulatory mechanism of peripheral T lymphocytes in mood disorders have not been well established. Here, we show that the lack of CD4$^+$ T cells protects mice from stress-induced anxiety-like behavior. Physical stress-induced leukotriene B4 triggers severe mitochondrial fission in CD4$^+$ T cells, which further leads to a variety of behavioral abnormalities including anxiety, depression, and social disorders. Metabolomic profiles and single-cell transcriptome reveal that CD4$^+$ T cell-derived xanthine acts on oligodendrocytes in the left amygdala via adenosine receptor A1. Mitochondrial fission promotes the *de novo* synthesis of purine via interferon regulatory factor 1 accumulation in CD4$^+$ T cells. Our study implicates a critical link between a purine metabolic disorder in CD4$^+$ T cells and stress-driven anxiety-like behavior.

INTRODUCTION

Emotional reactions, including fear and stress, are considered normal psychological and physical reactions to positive or negative situations in our lives. However, frequent acute emotional reactions referred to as chronic stress (CS) are pathological conditions that increase the risk of depression and anxiety (de Kloet et al., 2005; Krishnan and Nestler, 2008; McEwen et al., 2015). Most of the current therapeutic drugs for anxiety or depression, such as selective monoamine neurotransmitter re-uptake inhibitors, directly target the central nervous system (CNS). However, these drugs are accompanied by many side effects, including sexual dysfunction, systemic metabolic disorder, and persistent hypertension. Therefore, it is of great significance to understand the pathogenesis of mood disorders to develop nontraditional therapeutic drugs.

In addition to causing anxiety behaviors, stress can lead to disorders of the immune, metabolic, and cardiovascular systems (Dimsdale, 2008; Glaser and Kiecolt-Glaser, 2005; Reiche et al., 2004; Tamashiro et al., 2011). Acute-stress conditions appear to enhance the immune response, while CS diminishes immune responses, including decreasing leukocyte trafficking, impairing neutrophil phagocytosis, and reducing the number of peripheral lymphocytes (Glaser and Kiecolt-Glaser, 2005; Padgett and Glaser, 2003). Some recent studies have also highlighted the physiological function of various immune molecules in the onset of anxiety-like behaviors. IL-6 and IL-1β derived from innate immune cells can affect many aspects of the CNS, including neurotransmitter metabolism, neuronal endocrine function, and neuroplasticity in a mouse model (Chourbaji et al., 2006; Engler et al., 2017; McKim et al., 2018; Wakabayashi et al., 2015). Adaptive immunity is also involved in the maintenance of the CNS and is relevant to stress-triggered behaviors, including anxiety (Filiano et al., 2016). IFN-γ derived from meningeal T cells acts on neurons in the prefrontal cortex (PFC) to promote GABAergic inhibition and prevent abnormal excitability (Filiano et al., 2016). Programmed Cell Death 1 KO (*Pdcd1*$^{-/-}$) T cells exhaust tryptophan (Trp) and tyrosine, which leads to substantial deficiencies in neurotransmitters and anxiety-like behavior

(Miyajima et al., 2017). However, multiple questions regarding the effect of T cells on the onset of anxiety remain to be answered, including (1) the physiological functions of T lymphocytes in stress-induced anxiety-like behavior, (2) whether stress-induced anxiety is dependent on the activation of peripheral T cells or not, (3) the imprinting characteristics of pathological T cells in mood disorders, and (4) the molecular mechanism by which pathological T cells regulate the activity of neuronal or nonneuronal cells in the CNS.

RESULTS

$CD4^+$ T Cells Are Essential Components of Stress-Induced Anxiety Behaviors

To examine the role of the adaptive immune system in stress-induced behavioral changes, we exposed wild-type (WT) or recombination activating gene 1 (*Rag1*)$^{-/-}$ mice to electronic foot shock (ES) for 8 consecutive days to induce an anxiety model (Bourin et al., 2007; Campos et al., 2013; Steimer, 2011) (Figure 1A). In contrast to WT mice, immunodeficient *Rag1*$^{-/-}$ mice did not exhibit reduced interest in exploring the central region and locomotion in the open-field test (OFT) (Figure 1B), implying that the adaptive immunity is required for the onset of anxiety. Consistent with previous reports (Dhabhar, 2008; Dragoş and Tănăsescu, 2010), mice with acute ES exposure exhibited significantly increased frequencies and numbers of peripheral $CD4^+$ and $CD8^+$ lymphocytes compared to those of nontreated (NT) controls (Figures S1A and S1B).

To investigate which subpopulation of lymphocytes is involved in ES-induced mood disorders, we depleted $CD4^+$ or $CD8^+$ T cells by intravenous (i.v.) injection with neutralizing antibodies before inducing the ES model (Figure 1A) and verified the removal efficiencies by fluorescence-activated cell sorting (FACS) analysis (Figure S1C). Surprisingly, only $CD4^+$ T cell depletion significantly reversed the ES-induced anxiety-like behavior in the OFT and elevated plus-maze (EPM) test (Figures 1C and 1D). To further confirm the role of $CD4^+$ T cells in CS, we extended the procedures of the ES models to 30 days. As shown in Figure S1D, $CD4^+$ T cells were also required for chronic ES-induced anxiety-like behavior. In contrast to the ES model, an acute restraint stress (RS) model reduced the frequency of $CD4^+$ T cells (Figure S1E), which is consistent with observations in patients with anxiety (Figure S1F). However, $CD4^+$ T cell deficiency still prevented RS-treated mice from developing anxiety (Figure 1E), suggesting that $CD4^+$ T cells have a broad impact on physical stress-induced anxiety-like behavior.

To assess whether T cells retain anxiety imprints, NT or ES-induced splenic $CD4^+$ or $CD8^+$ T cells were adoptively transferred into *Rag1*$^{-/-}$ mice (Figure 1F). Only the *Rag1*$^{-/-}$ mice that received ES-induced $CD4^+$ T cells developed anxiety-like behavior in the OFT (Figure 1G). Surprisingly, the NT $CD4^+$ T cells induced weak anxiety-like symptoms, suggesting that some natural products derived from $CD4^+$ T cells have the ability to regulate physical reactions (Figure 1G). T cell-derived IFN-γ has also been shown to be involved in regulating neuronal connection and social behavior (Filiano et al., 2016). Without additional stimulation, the splenic $CD4^+$ T cells from ES mice exhibited a significant reduction in IFN-γ expression compared to that in NT mice (Figure S1G). However, serum IFN-γ showed no difference compared to that in NT mice, due to the increased total cell number (Figure S1H).

To elucidate whether the pathological $CD4^+$ T cells in anxiety exercise their functions in a manner dependent on their activation, we compared the abilities of naive and effector $CD4^+$ T cells to induce anxiety symptoms by adoptive transfer into *Rag1*$^{-/-}$ mice. In addition to naive $CD4^+$ T cells, we added two effector control groups including the Effector-L (from the same mice) and Effector-H groups (the same cell number). Although the transferred naive and effector $CD4^+$ T cells displayed similar activation features (Figure S1I), naive $CD4^+$ T cells triggered a more severe anxiety than did those from the two effector control groups (Figure 1H). Consequently, these data implied an important role for $CD4^+$ T cells in stress-induced anxiety independent of their activation status.

Stress Induces Mitochondrial Fission in Peripheral $CD4^+$ T Cells

To examine the distinct ability of $CD4^+$ and $CD8^+$ T cells to drive anxiety, we analyzed the transcriptome of naive ES-induced $CD4^+$ and $CD8^+$ T cells by RNA sequencing (RNA-seq). Although most of the genes in ES $CD4^+$ T cells were similar to those in the other three groups (Figure 2A and Table S1), 128 specifically differentially expressed genes (DEGs) were identified in ES-induced $CD4^+$ T cells (Figures 2B and 2C). Gene ontology (GO) analysis revealed that a large number of these DEGs encoded mitochondrial proteins (Figure 2D). Additionally, both ES- and RS-treated naive $CD4^+$ T cells exhibited severely reduced levels of glycolysis (Figure 2E) and oxidative phosphorylation (OXPHOS) (Figure 2F), as measured by the extracellular acidification rate (ECAR) and oxygen consumption rate (OCR), respectively. These data implied that stress affected the structure of mitochondria, which profoundly influences the biogenesis and function of mitochondria (Wai and Langer, 2016; Zhan et al., 2013). Confocal microscopy images demonstrated that ES-treated naive $CD4^+$ T cells predominantly exhibited punctate mitochondria (Figure 2G). Consistently, compared to those from healthy donors, naive $CD4^+$ T cells from the patients with anxiety also displayed severe mitochondrial division (Figure S2A). Immunoblotting (IB) further revealed that the outer membrane proteins that mediated mitochondrial fusion, including MFN2 and MIGA2, were significantly reduced in ES-treated naive $CD4^+$ T cells (Figure 2H and Figure S2B). Collectively, these data suggest that $CD4^+$ T cells under stress exhibit abnormal mitochondrial morphology and metabolic dysfunction.

Various neurotransmitters and hormones including dopamine, cortisol, GABA, adrenaline, L-glutamic acid and serotonin have been proven to be associated with the onset of anxiety. Surprisingly, these critical molecules in the serum did not display any consistent trends of changes between the ES- and RS-induced anxiety models (Figure S2C). Adrenal glucocorticoids appear to weaken inflammation and T-cell proliferation. Although injection of prednisone, a glucocorticoid, triggered anxiety-like behavior, $CD4^+$ T-cell depletion had no effect on these anxiety symptoms (Figure S2D), suggesting

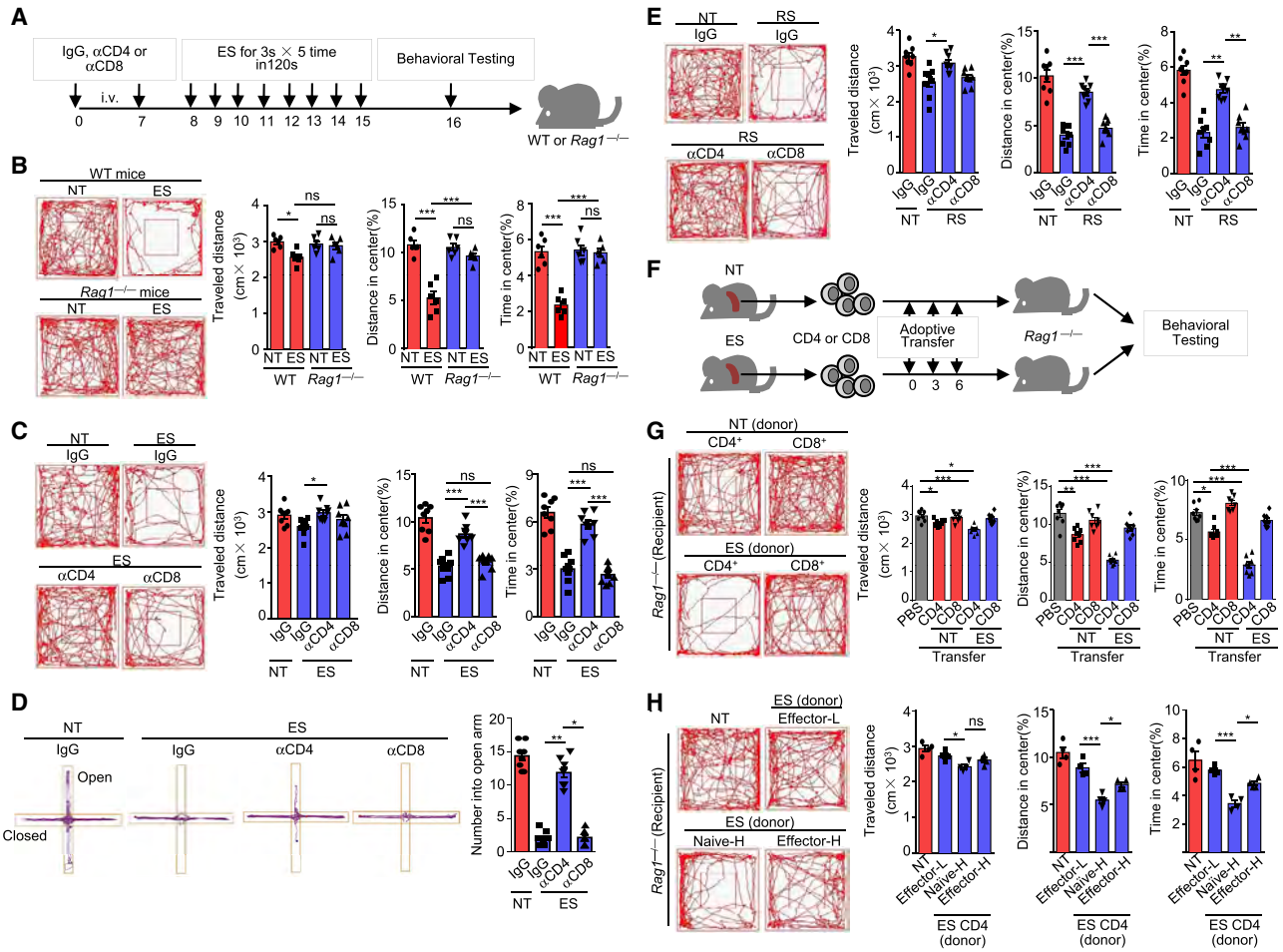

Figure 1. CD4$^+$ T Cells Play an Essential Role in Stress-Induced Anxiety-like Behavior

(A–D) Schematic of experimental design. ES, electronic foot shock; NT, nontreated; i.v., intraperitoneal injection. The treatment with indicated antibodies are only for (C) and (E).

(B) Representative tracks of wild-type (WT) or *Rag1*$^{-/-}$ mice in open-field test (OFT) (n = 6) on day 8 after inducing ES model, as well as travel distance, percentage of distance in center area and percentage of time spent in center.

(C) NT- and ES-treated mice were pretreated with indicated antibodies (500 μg/mice) twice. Representative tracks and statistic results in OFT were measured on day 16 from the first injection (n = 8).

(D) Representative tracks and statistic results in elevated plus-maze (EPM) of NT and ES mice described as (C) on day 16 (n = 8).

(E) OFT results for restraint stress (RS)-induced anxious mice pretreated with distinct antibodies (n = 8).

(F) Schematic of experimental design for T cell adoptively transfer-induced anxiety model.

(G) *Rag1*$^{-/-}$ mice were i.v. adoptively transferred with 5 × 10^6 CD4$^+$ or CD8$^+$ T cells isolated from NT or ES-treated mice (donor) for every three days. The anxiety-like behavior of recipient *Rag1*$^{-/-}$ mice was evaluated by OFT on day 8 (n = 8).

(H) *Rag1*$^{-/-}$ mice were adoptively transferred with 1.8 × 10^6 effector (CD4$^+$CD44^{hi}CD62L^{lo}, Effector-L), 6 × 10^6 naive (CD4$^+$CD44^{lo}CD62L^{hi}, Naive-H) and 6 × 10^6 effector (CD4$^+$CD44^{hi}CD62L^{lo}, Effector-H) CD4$^+$ T cells isolated from ES-treated mice for every three day. Eight days later, the anxiety-like behavior of these recipient *Rag1*$^{-/-}$ mice was evaluated by OFT (n = 4).

All data are representative of at least three independent experiments. Data are represented as means ± SEM. The significance of difference in (B–E) and (G–H) was determined by Dunnett's multiple comparisons test (Dunnett's Test). ns, no significance; *p < 0.05; **p < 0.01; ***p < 0.005.

that glucocorticoids may not be involved in CD4$^+$ T-cell-induced anxiety. Several findings have demonstrated that depressive animals exhibit increases in omega-6 fatty acids and arachidonic acid (AA) in the brain. AA is known to be a critical component of the inflammatory process via metabolism into leukotriene B4 (LTB4) and prostaglandin (PG) E2, which may further act on peripheral lymphocytes. Of all AA metabolites, only LTB4, PGB1, and 15-δ-Δ12,14-PGJ2 (15-d-PGJ2) showed a consistent increase by LC-MS (Figure 2I). In contrast to PGB1, LTB4 administration caused a severe anxiety-like behavior, which was restored by CD4$^+$ T cell removal (Figure 2J). Although 15-d-PGJ2 also led to mild anxiety symptoms, CD4$^+$ T cells were not involved in this process (Figure 2J). LTB4 significantly promoted mitochondrial fission *in vitro* (Figure 2K) and reduced MFN-2 and MIGA2 expression in naive CD4$^+$ T cells (Figure 2L). In summary, stress-induced LTB4

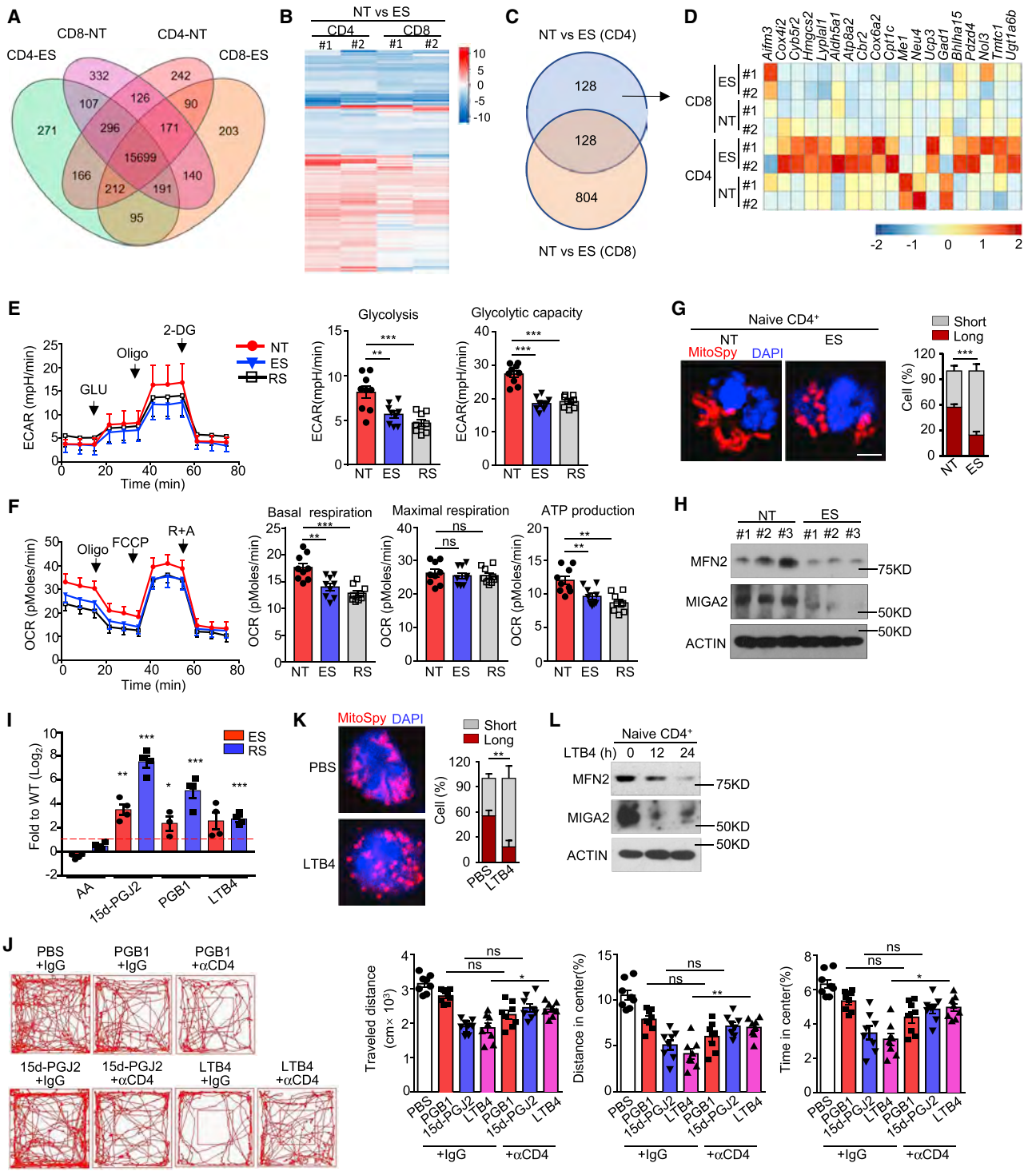

Figure 2. Stress Causes Metabolic Disorder and Mitochondrial Fission in CD4⁺ T Cells

(A) Venn diagram summarizing the expression of genes in naive T lymphocytes isolated from the spleens of NT- or ES-treated mice, as determined by RNA-seq data.

(B) Heatmap showing the differentially expressed genes (DEGs) in T lymphocytes between NT- and ES-treated mice. The DEGs were identified with a fold change of ES/NT > 2.0 or < 0.5.

(C) Comparison of the number of DEGs and gene ontology (GO) analysis of 128 specific DEGs in CD4⁺ T cells.

(D) Heatmap showing the expression of the DEGs encoding mitochondrial proteins.

(legend continued on next page)

triggers mitochondrial fission in peripheral CD4$^+$ T cells and the onset of anxiety, although the underlying mechanism remains to be further investigated.

CD4$^+$ T Cells with Diverse Mitochondria Cause Severe Anxiety-like Symptoms

To confirm the relationship between the mitochondrial morphology of T cells and anxious behavior, we generated *Mitoguardin 2* KO (*Miga2*$^{-/-}$) mice and observed highly fragmented mitochondria in naive CD4$^+$ T cells (Figure 3A). Ultrastructural analysis with electron microscopy (EM) further confirmed many small, diverse mitochondria dispersed in the cytoplasm of *Miga2*$^{-/-}$ naive CD4$^+$ T cells (Figure 3B). Interestingly, *Miga2*-deficient mice displayed decreased locomotor activity and spent much less time in the center than their WT littermates in the OFT (Figure 3C). Consistently, these *Miga2*-deficient mice were obviously afraid to enter into the open arms in the EPM test (Figure 3D). In the dark-light transition assay, *Miga2*-deficient mice exhibited fewer transitions from the dark zone to the light zone and spent less time in the light zone than WT mice (Figure S3A). Moreover, *Miga2*-deficient mice stopped struggling earlier in the tail suspension test (Figure S3B) and exhibited less social motivation and curiosity (Figure S3C), suggesting that these mice also have severe depression.

Similar to the data in the ES stress model, depletion of CD4$^+$, but not CD8$^+$, T cells restored the anxiety symptoms caused by continuous mitochondrial division (Figure 3E). Although inflammatory microglia lead to depression and anxiety by inhibiting the release of dopamine (Li et al., 2014; McKim et al., 2018; Wang et al., 2018; Wohleb et al., 2011), microglia were not involved in the onset of anxiety caused by *Miga2* deficiency, as revealed by selectively eliminating myeloid cells by liposomal clodronate (LCCA), PLX3397, or BLZ945 (Figure 3E). Recipient *Rag1*$^{-/-}$ mice adoptively transferred with *Miga2*-deficient naive CD4$^+$ T cells further confirmed the essential roles of these cells in anxiety (Figure 3F). Both integrin VLA-4 and CD6 are expressed on the T cell surface and allow these cells to penetrate the blood brain barrier (BBB) (Engelhardt et al., 2017; Lécuyer et al., 2017; Li et al., 2017; Ransohoff and Engelhardt, 2012; Theien et al., 2001; Vajkoczy et al., 2001). To clarify whether these "anxious" CD4$^+$ T cells function in the CNS, we treated *Miga2*$^{-/-}$ mice with VLA-4 or CD6 neutralizing antibodies, which disrupt T cell migration into the CNS. Surprisingly, neither the VLA-4 nor CD6 antibody had any effect on anxiety symptoms in *Miga2*-deficient mice (Figure S3D). All of these data indicate that *Miag2* deficiency-induced anxiety is independent of pathological CD4$^+$ T cell migration into the brain.

To further clarify the particular function of mitochondrial fission in peripheral CD4$^+$ T cells, we generated *Miga2* T cell-conditional knockout (KO) (*Miga*^{TKO}) mice. In contrast to another mitochondrial fusion protein *Opa1*, which is required for memory T cell characteristics (Buck et al., 2016), *Miga2*-deficient T cells did not show any obvious abnormalities in the development and homeostasis of T lymphocytes (Figures S3E and S3F). *Miga2*^{TKO} mice also displayed comparable sensitivities in models of experimental autoimmune encephalomyelitis (EAE) (Figure S3G), as revealed by comparable clinical scores, levels of immune cell infiltration in the CNS, and proliferative capacity (Figures S3H and S3I). Nevertheless, *Miga2*^{TKO} mice still displayed anxiety-like behavior similar to that of *Miga2*$^{-/-}$ mice (Figure 3G). Furthermore, *Miga2*^{TKO} mice exhibited normal extinction of fear memory in the continuous EPM test (Figure 3H), indicating that *Miga2*-deficient CD4$^+$ T cells have no effect on normal learning and memory. To eliminate a particular function of the MIGA2 protein in anxiety, we generated *Mfn1* and *Mfn2* T cell-conditional double KO (*Mfn1/2*^{TKO}) mice. Behavioral assessment indicated that the mice lacking *Mfn1/2* in T cells also exhibited anxiety-like behavior compared to their WT littermates (Figure 3I), suggesting that anxious behavior is promoted by the morphological disorder of mitochondria rather than by a specific function of certain mitochondrial proteins in CD4$^+$ T cells.

Continuous Mitochondrial Fission in T Cells Causes a Systemic Purine Metabolism Disorder

Mitochondria morphology has been intimately linked to metabolic regulation across cell types and tissues (Mishra and Chan, 2016; Wai and Langer, 2016). Consistently, partial least-squares discrimination analysis (PLS-DA) revealed that the metabolomic profile of *Miga2*^{TKO} mice was significantly different from that of their WT littermates (Figure 4A and Table S2). Some amino acids, including Trp and glutamate (Glu), account for the majority of excitatory and inhibitory neurotransmitters in the nervous system. Although various amino acids were upregulated in the serum of *Miga2*^{TKO} mice (Figure S4A), these neurotransmitter amino acids and their derivatives were not included (Figure S4B).

(E–F) Mitochondrial fitness tests were used to compare the oxygen consumption rate (OCR) (E) and extracellular acidification rate (ECAR) (F) of naive CD4$^+$ T cells isolated from NT- or ES-treated mice (n = 9). The statistical results are presented as a bar graph (right).

(G) The mitochondrial morphology of naive CD4$^+$ T cells from NT- or ES-treated mice was visualized using MitospyTM Orange CMTMRos staining. Representative confocal images are shown, as well as length quantification with 50 cells by Image-Pro. long, brown > 7 μm and short, gray < 7 μm). Bar, 5 μm.

(H) Immuno-blot (IB) analyses of indicated proteins in splenic naive CD4$^+$ T cells. #1, repeat 1; #2, repeat 2; #3, repeat 3. See also Figure S2B for the quantification of the relative density of these IB assays.

(I) LC-MS of indicated metabolites in the serum of ES-treated and RS-treated mice, presented relative to the mean value for NT mice (n = 4).

(J) WT mice were i.p. injected with indicated metabolites with αCD4 twice every three days. Anxiety-like behavior of these mice was assessed in OFT on day 8 (n = 8).

(K) Naive CD4$^+$ T cells were isolated by FACS sorter and stimulated with leukotriene B4 (LTB4) for 24 h. Mitochondrial morphology was visualized and quantified with 50 cells.

(L) IB analyses of the MFN2 and MIGA2 protein levels in naive CD4$^+$ T cells stimulated with LTB4.

All data are representative of at least three independent experiments. Data are represented as means ± SEM. The significances of difference in (E), (F), and (J) were determined by Dunnett's Test, and others were determined by two-tailed Student's t test (t test). *p < 0.05; **p < 0.01; ***p < 0.005.

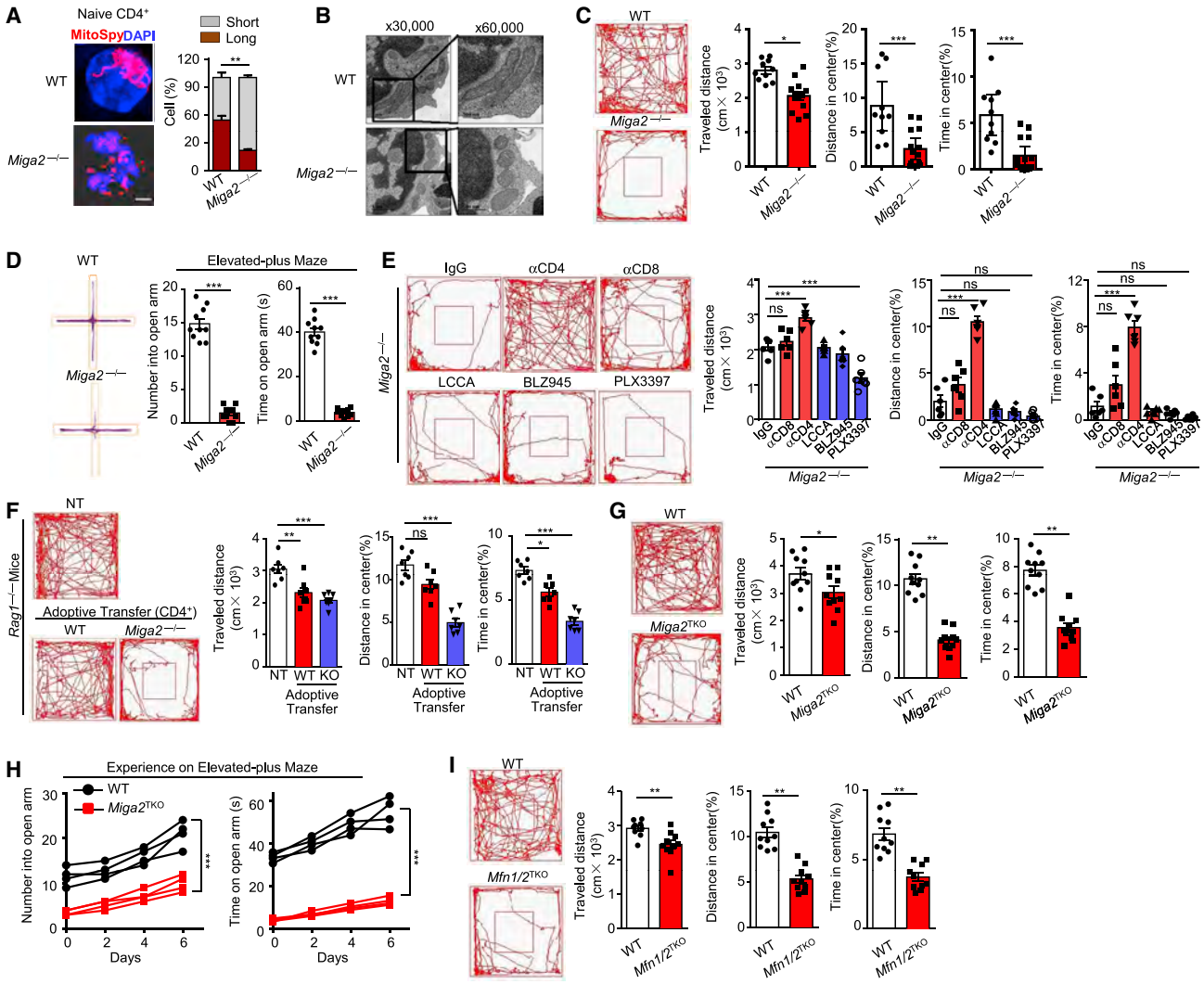

Figure 3. Sustained Mitochondrial Fission in CD4⁺ T Cells Induces the Anxiety-like Behavior

(A) Mitochondrial morphology of splenic naive CD4⁺ T cells isolated from 6-to-8-week-old WT or *Miga2*$^{-/-}$ mice was visualized and quantified with 50 cells.

(B) Mitochondrial morphology of WT and *Miga2*$^{-/-}$CD4⁺ T cells was analyzed by EM (scale bar, 500 nm or 1 μm).

(C) Representative tracks of WT and *Miga2*$^{-/-}$ mice in OFT (left, n = 10).

(D) Representative tracks in the EPM (n = 10). The number of entries into the open arms and the time spent in the open arms are presented as bar graphs (right).

(E) Some of WT and *Miga2*$^{-/-}$ mice were i.v. injected with distinct antibodies on days 0 and 7, and together i.v. injected with liposomal clodronate (LCCA, 70 mg/kg) or i.p. injected with PLX3397 (50 mg/kg) or BLZ945 (200 mg/kg) on days 0, 2, 4, and 6. The anxiety-like behavior of these mice were then evaluated in OFT on day 8 (n = 6).

(F) *Rag1*$^{-/-}$ mice were adoptively transferred with 5 × 10^6 WT or *Miga2*$^{-/-}$ splenic CD4⁺ T cells every three days. Six days later, the anxiety-like behavior of recipient *Rag1*$^{-/-}$ mice was evaluated in OFT (n = 7).

(G) OFT results for 6-to-8-week-old *Miga2*^{TKO} mice with their littermates (n = 10).

(H) The WT and *Miga2*^{TKO} mice were continuously subjected to EPM each day and measured for their responsive experience in every other day (n = 4).

(I) Representative tracks of 6-to-8-week-old WT and *Mfn1/2*^{TKO} mice in the OFT (n = 10). All data are representative of at least three independent experiments. Data are represented as means ± SEM. The significances of differences in (E) and (F) were determined by Dunnett's test, and others were determined by t test. *p < 0.05; **p < 0.01; ***p < 0.005.

Hierarchical clustering and KEGG analyses indicated that the differential metabolites in *Miga2*^{TKO} mice were mainly enriched in purine metabolism (Figures 4B and 4C). Most of the purines and their derivatives including adenine, hypoxanthine, and xanthine were 10 to 100 times more abundant in *Miga2*^{TKO} mice than in their WT littermates (Figure 4D). Interestingly, xanthine mainly accumulated in the brain but was markedly decreased in the peripheral immune organs (Figure S4C). After the removal of CD4⁺ T cells, the serum concentration of xanthine in *Miga2*^{TKO} mice was significantly decreased (Figure 4E). Current clinical evidence has revealed that patients with depression have an increased level of xanthine compared with that of healthy

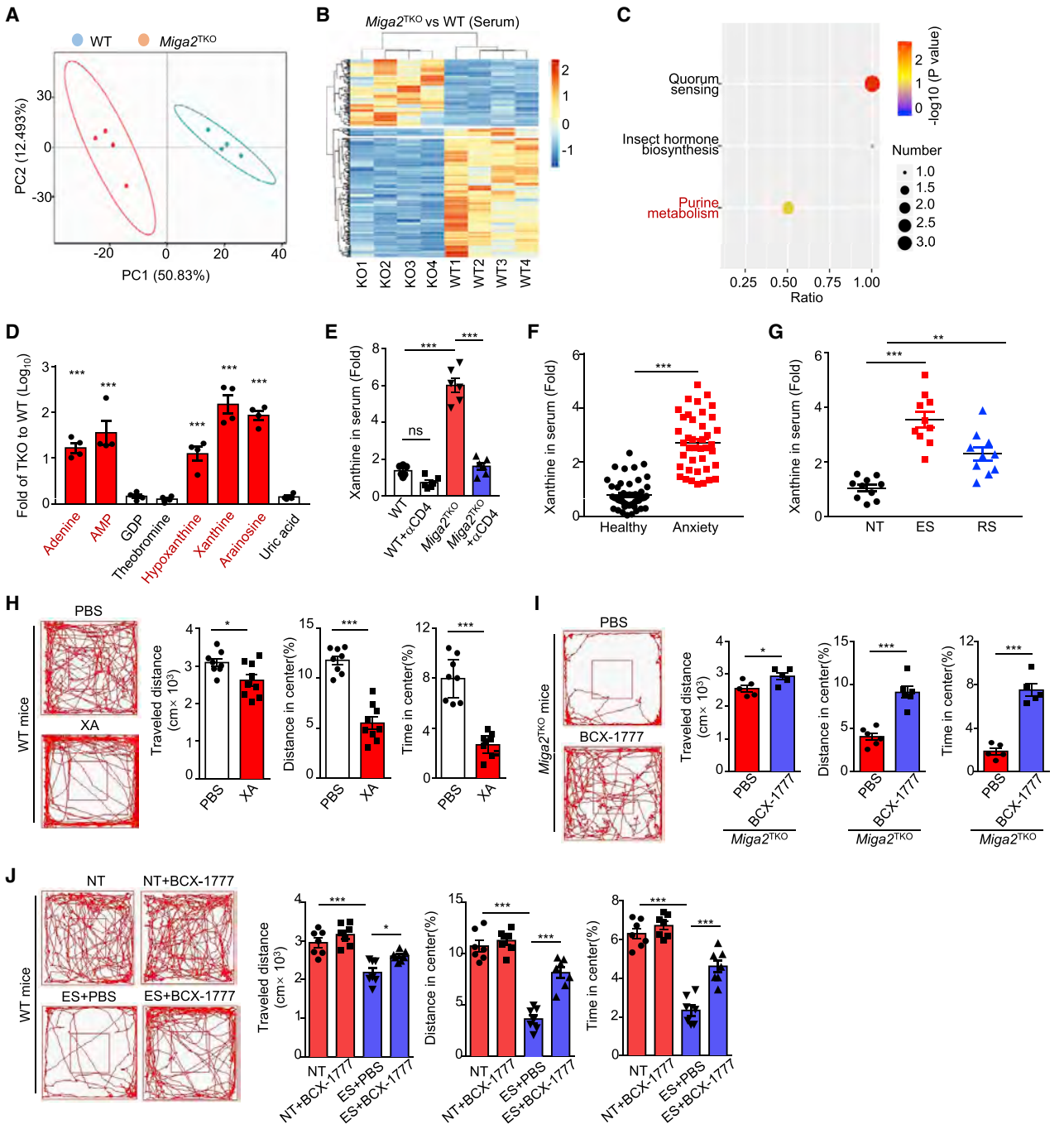

Figure 4. Mitochondrial Fission in CD4⁺ T Cells Leads to a Systemic Increase in Serum Purines

(A) Partial Least-squares discrimination analysis (PLS-DA) of the serum metabolome of WT and *Miga2*^{TKO} mice (n = 4). Each symbol represents the data of an individual mouse.

(B) Heatmap showing differential metabolic production (DMP) in the serum of WT and *Miga2*^{TKO} mice. The DMPs were identified with a fold change of *Miga2*^{TKO}/WT > 2.0 or < 0.5.

(C) KEGG analysis of these DMPs-enriched biological processes.

(D) Purine nucleotides and their derivatives in the serum were measured by PLS-DA and presented as the ratio of the abundance in *Miga2*^{TKO} mice to those in WT mice (n = 4).

(E) Xanthine in the serum of CD4⁺ T cell-depleting *Miga2*^{TKO} mice was measured by ELISA. The relative fold is to serum xanthine concentration of WT control.

(F) Dot plots showing the relative fold of xanthine in the serum of the patients with anxiety (n = 40) to those in healthy donors (n = 46).

(G) ELISA assay of the relative fold of xanthine in the serum of NT-, ES-, and RS-treated mice (n = 10).

(legend continued on next page)

controls (Ali-Sisto et al., 2016). We also found that serum xanthine was significantly higher in patients with anxiety (Figure 4F). Increased abundance of serum xanthine was also observed in two rodent anxiety models (Figure 4G) and the recipient *Rag1*$^{-/-}$mice adoptively transferred with ES CD4^{+} T cells (Figure S4D). Similar to the observation that anxiety is mainly induced by naive T cells in Figure 1H, naive CD4^{+} T cells produced a higher level of xanthine than effector T cells (Figure S4E).

To verify the direct link between excessive levels of purines and anxiety symptoms, we intraperitoneally (i.p.) injected synthetic xanthine or adenosine into WT mice. Surprisingly, xanthine, adenine, and adenine arabinoside monophosphate (Ara-AMP) all had the ability to trigger anxiety-like behavior (Figure 4H and Figure S4F). Previous reports have revealed opposite effects of adenine and xanthine on the activity of neurons (Phillis and Wu, 1982). Thus, we measured c-FOS expression on neurons, which indicates their activation after xanthine or adenosine administration. Similar to in *Miga2*$^{-/-}$ mice, xanthine treatment caused more c-FOS expression on the neurons than did PBS treatment. Oppositely, adenine led to a reduction in c-FOS^{+} neurons, which could be reversed by xanthine coinjection (Figure S4G). Therefore, xanthine plays a more dominant role when the microenvironment contains both of these purines. BCX-1777, as a purine nucleoside phosphorylase (PNP) inhibitor, has been proven to be an efficient inhibitor of purine metabolism (Li et al., 1999; Miles et al., 1998). BCX-1777 treatment significantly reduced the anxiety symptoms in *Miga2*^{TKO} and ES mice (Figures 4I and 4J) and significantly decreased the serum concentration of xanthine (Figure S4H). In summary, excessive xanthine caused by pathological CD4^{+} T cells plays a critical role in the onset of anxiety.

Xanthine Directly Acts on Oligodendrocytes in the Left Amygdala

A number of studies have suggested that the amygdala plays a critical role in generating fear and persistent anxiety (Davis, 1992; Shackman and Fox, 2016; Thomas et al., 2001). The left amygdala has been linked to social anxiety, compulsive disorders, and posttraumatic stress as well as to general anxiety (Phelps et al., 2001). Histological analysis of *Miga2*^{TKO} mice revealed that the left amygdala of *Miga2*^{TKO} mice was significantly larger and exhibited higher numbers of nonneuronal cells than the right amygdala or the amygdala of the WT control (Figure 5A and Figures S5A and S5B). The left amygdala of xanthine-treated mice displayed a pathological phenotype similar to that of *Miga2*^{TKO} mice (Figure S5C). To clarify the pathological mechanism in the amygdala, we performed single-cell RNA sequencing (scRNA-seq) by using the 10x Genomics platform in an unbiased manner (Figure S5D and Table S3). Approximately 3,000 cells passed quality control, and unsupervised clustering revealed nine clusters, which we visualized with t-distributed stochastic neighbor embedding (tSNE) (Figure S5E). We defined each population with multiple specific genes and highlighted three markers for each subset (Figure 5C). Adenine and xanthine initiate their physiological functions through four receptor subtypes, namely A1, A2A, A2B, and A3. Interestingly, the scRNA-seq data revealed that A1 is mainly expressed in oligodendrocytes and oligodendrocyte progenitor cells (OPCs), while A2B and A3 are distributed in astrocytes and microglia, respectively (Figure 5D and Table S3). FACS immunofluorescence (IF) analysis further confirmed that A1 expression was largely distributed in oligodendrocytes, but no expression of A2A, A2B, or A3 was detected (Figures 5E–5F and Figure S5F). Due to the defect of adenosine receptors on neurons, we next analyzed the transcriptome of each nonneuronal cell in the amygdala of WT-, *Miga2*$^{-/-}$–, and αCD4-treated *Miga2*$^{-/-}$ mice (Table S4). Both scRNA-seq and FACS analysis indicated a significantly increased percentage of oligodendrocytes in *Miga2*$^{-/-}$ mice, which could be reversed by depleting CD4^{+} T cells (Figures 5G and 5H). Furthermore, more A1^{+} oligodendrocytes were observed in *Miga2*$^{-/-}$ mice but not in those treated with αCD4 (Figure 5F and Figure S5G). Consistently, only DEGs in oligodendrocytes were largely restored by removing CD4^{+} T cells in *Miga2*$^{-/-}$ mice (Figure S5H). KEGG analysis showed that these DEGs in oligodendrocytes were mainly enriched in the purine metabolic process and mitotic cell cycle process (Figure S5I). As a pathogenic factor, xanthine caused a significant increase in DNA synthesis and the cell cycle in oligodendrocytes, as measured by BrdU incorporation assays, while adenine had a significant opposite effect (Figure S5J). Therefore, these data suggest that xanthine triggers the proliferation of oligodendrocytes directly.

Previous evidence has revealed that xanthine acts on A1 receptors and promotes the activity of protein kinase A (PKA)/cAMP (Darashchonak et al., 2014). Consistently, the intense bands of phospho-PKA substrates indicated that the PKA/cAMP pathway was clearly activated in oligodendrocytes of *Miga2*$^{-/-}$ mice and was downregulated by depleting CD4^{+} T cells (Figure S5K). As the only detectable adenosine receptor, A1 in oligodendrocytes was further specifically knocked down by injecting an adeno-associated virus (AAV) expressing myelin basic protein (MBP) promoter-driven *AdorA1* shRNA-GFP (AAV-MBP-sh*AdorA1*-GFP) into the left amygdala (Figure 5I). In parallel, an AAV expressing MBP promoter-driven non-silencing shRNA (AAV-MBP-NCshRNA-GFP) was used as a negative control (Figure 5I). Two weeks later, FACS analysis suggested a strong co-expression of GFP and MOG signals in the left amygdala (Figure 5J), indicating specific expression of *AdorA1* shRNA in oligodendrocytes. Without the A1 receptor in oligodendrocytes, *Miga2*-deficient mice no longer displayed anxiety-like symptoms (Figure 5K). In summary, the excessive xanthine caused by *Miga2*$^{-/-}$ T cells acts on oligodendrocytes

(H) WT mice were i.p. injected with xanthine (500mg/kg) once every three days. Anxiety-like behavior of these mice was assessed in OFT on day 8 (n = 8).
(I) *Miga2*^{TKO} mice were i.p. injected with BCX-1777 (20mg/kg) once every three days. Anxiety-like behavior was evaluated in OFT as above on day 8 (n = 5).
(J) ES-treated mice were i.p. injected with PBS or BCX-1777 (20mg/kg) every three days. The anxiety-like behavior of these mice was evaluated by OFT on day 8 (n = 7).
All data are representative of at least three independent experiments. Data are represented as means ± SEM. The significances of differences in (D), (E), (G) and (J) were determined by Dunnett's test, and others were determined by t test. *p < 0.05; ***p < 0.005.

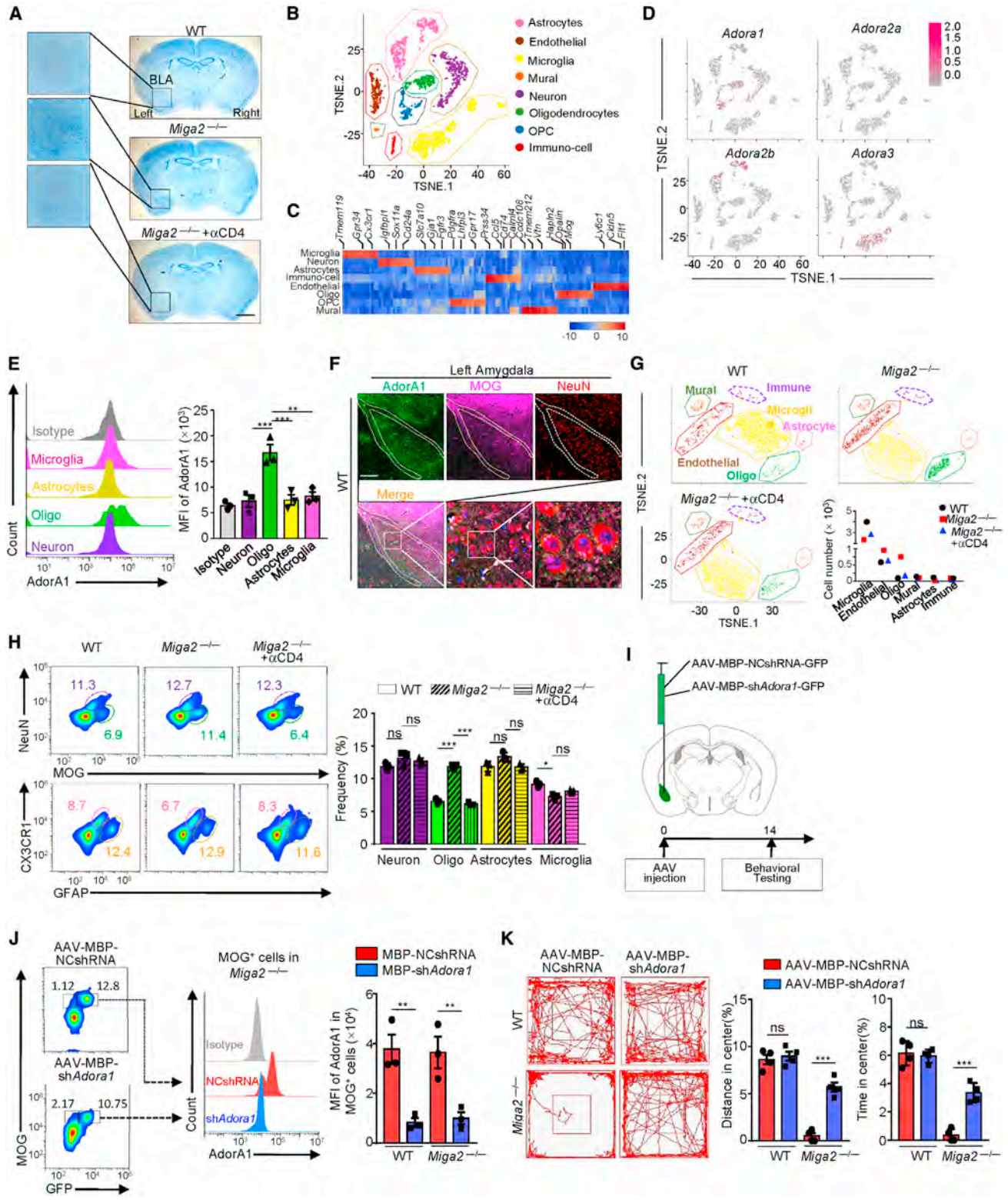

Figure 5. CD4⁺ T Cell-Derived Xanthine Acts on the Oligodendrocytes at the Amygdala via AdorA1

(A) Histological analyses of whole brains were performed by Nissl staining. Scale bar, 100 μm. See also Figure S5B for the statistical results.

(B) tSNE plots of scRNA-seq show unsupervised clusters of cells in the amygdala. 9 major clusters; OPC, oligodendrocyte progenitor cell.

(C) Heatmap of each cluster's expression of the 15 markable DEGs per cluster.

(legend continued on next page)

through the A1 receptor in the left amygdala and promotes anxiety-like behavior.

Mitochondrial Fission Promotes the *de novo* Synthesis of Xanthine in CD4$^+$ T Cells

Purine can be synthesized via two distinct pathways: the *de novo* and salvage pathways. In the *de novo* synthesis pathway, the glucose metabolic product 5-phosphoribosyl-1-pyrophosphate (PRPP) provides a backbone to form the purine ring. Similar to ES-treated T cells, *Miga2*-deficient CD4$^+$ T cells exhibited markedly reduced activities of OXPHOS and glycolysis (Figure 6A and Figures S6A and S6B). A similar metabolic pattern was observed in CD4$^+$ T cells from *Mfn1/2*^{TKO} mice (Figures S6C and S6D). A ^{13}C carbon tracing assay further revealed that *Miga2*-deficient naive CD4$^+$ T cells had lower glycolysis levels but produced more M+5 ribulose-5-p (R-5-P), CAIR, adenosine, and inosine than the WT naive CD4$^+$ T cells (Figures 6B–6C and Table S5), demonstrating that glucose flows to the pentose phosphate pathway (PPP) for *de novo* purine synthesis upon the alteration of mitochondrial morphology from fusion to fission. 2-Deoxy-D-glucose (2-DG) is a glucose analog that inhibits its catabolic pathways including glycolysis, PPP, and *de novo* purine synthesis by inhibiting hexokinase activity. The administration of 2-DG clearly normalized the anxiety-like symptoms and pathological characteristics of the left amygdala in *Miga2*^{TKO} mice (Figures S6E and S6F).

To clarify the underlying mechanism by which mitochondrial morphology regulates purine synthesis, we analyzed the transcriptome of WT and *Miga2*-deficient naive CD4$^+$ T cells. *Miga2*-deficient CD4$^+$ T cells showed reduced transcription of several critical enzymes related to the glycolytic and fatty acid β-oxidation pathway, but increases in the molecules required for purine synthesis, such as hexokinase 3 (*Hk3*), adenosine deaminase (*Ada*), purine nucleoside phosphorylase 2 (*Pnp2*), and xanthine oxidase/xanthine dehydrogenase (*Xdh*) (Table S6 and Figure 6D). Additionally, qPCR and IB analyses in *Miga2*-deficient naive CD4$^+$ T cells confirmed the elevated mRNA and protein levels of these genes (Figures 6E and 6F), which were consistent with the accumulation of the associated metabolites (Figures 4A and 6G).

PNP catalyzes the conversion of inosine and guanosine to hypoxanthine or guanine. Similar to PNP, PNP2 also functions as an enzyme regulating the purine metabolic pathway and xanthine production. Due to its low expression in primary CD4$^+$ T cells, we proposed that its deficiency may not lead to a severe immunodeficiency as *Pnp* deficiency does (Arpaia et al., 2000; Markert, 1991; Stoop et al., 1977). Thus, we generated *Pnp2*$^{-/-}$ mice with CRISPR/CAS9 by targeting exon 2 (Figure 6H and Figure S6G) and verified with qPCR analysis (Figure S6H). Consistent with our hypothesis, *Pnp2*-deficient mice did not exhibit any obvious dysfunction of T lymphocyte development or maturation (Figure S6I) and were thus further crossed with *Miga2*$^{-/-}$ mice to generate *Pnp2*$^{-/-}$*Miga2*$^{-/-}$ mice. *In vitro*, *Pnp2* deficiency partially normalized the hyperproduction of xanthine by *Miga2*$^{-/-}$ T cells (Figure 6I). After adoptive transfer into *Rag1*$^{-/-}$ mice, *Pnp2*$^{-/-}$*Miga2*$^{-/-}$ CD4$^+$ T cells did not induce anxiety symptoms as strong as those induced by *Miga2*$^{-/-}$ CD4$^+$ T cells (Figure 6J). Because *Pnp2* depletion cannot completely block the synthesis of xanthine, xanthine in the serum was still moderately increased in the recipient *Rag1*$^{-/-}$ mice transferred with *Pnp2*$^{-/-}$*Miga2*$^{-/-}$ CD4$^+$ T cells (Figure 6K). These results support the conclusion that CD4$^+$ T-cell-derived excess xanthine directly causes anxiety-like behavior.

Mitochondrial Fission Leads to Excessive Xanthine by Promoting IRF-1 Accumulation

Interferon regulatory factor-1 (IRF-1), a transcription factor, participates in various cellular processes, including cell proliferation, differentiation, apoptosis, and immunological regulation. Our previous study revealed that constitutive mitochondrial fission promoted the accumulation of IRF-1 in innate immune cells (Gao et al., 2017). We found that the stability of IRF-1 was negatively regulated via monoubiquitination by the carboxyl terminus of hsp70-interacting protein (CHIP), which was degraded by the diverse mitochondria-recruited ubiquitin E3 ligase PARKIN (Gao et al., 2017) (Figure S6J). Similar to macrophages, *Miga2* deficiency also triggered significant aggregation of IRF-1 in CD4$^+$ T cells (Figure 7A). Consistently, ES also caused severe accumulation of IRF-1 in CD4$^+$ T cells (Figure 7B). Analysis of public data regarding chromatin immunoprecipitation sequencing (CHIP-seq) of macrophages (Langlais et al., 2016) revealed that IRF-1 was enriched in the promoter regions of *Ada, Xdh*, and *Pnp2*. Thus, we analyzed the promoter sequence of these three genes and identified several potential IRF-1 binding motifs near the transcription start site (TSS) (Figure 7C). ChIP-qPCR assays further revealed that the accumulated IRF-1 in *Miga2*-deficient CD4$^+$ T cells was significantly enriched at certain binding sites in the TSSs of *Ada*, *Pnp2*, and *Xdh* compared to those in WT controls (Figure 7D). We next depleted IRF-1 in *Miga2*-deficient

(D) Dot plots showing the distributed expression of distinct adenosine receptors for each cell cluster on the t-SNE map.
(E) Flow cytometry analysis of AdorA1$^+$ expression in each cell-type at the amygdala of WT mice (n = 3). Astrocytes are defined as GFAP$^+$; Neurons are defined as NeuN$^+$; Oligodendrocytes (Oligo) are defined as MOG$^+$; Microglia are defined as CX3CR1$^+$.
(F) Representative immunofluorescence images of FITC-AdorA1 (green), APC-MOG (purple), and PE-NeuN (red) staining in sections of the amygdala from 8-week-old WT mice. Scale bar, 10 μm.
(G–H) tSNE plots of scRNA-seq (G) and flow cytometry (FACS) analysis (H) show unsupervised clustering of non-neuronal cells in the amygdala of 6-8-week-old WT, *Miga2*$^{-/-}$, and *Miga2*$^{-/-}$ mice treated with αCD4 (n = 3).
(I) Vector structure of the adeno-associated virus (AAV)-*AdorA1* shRNA under the control of myelin basic protein (MBP) promoter. The non-silencing shRNA (NCshRNA) was used as a negative control. WT or *Miga2*$^{-/-}$ mice were injected with AAV in the left amygdala.
(J) Two weeks later, FACS analyses of AdorA1 expression on the AAV-infected MOG$^+$ oligodendrocytes in the left amygdala.
(K) WT or *Miga2*$^{-/-}$ mice were injected with AAV as described above and evaluated for anxiety-like behavior by the OFT two weeks later.
All data are representative of at least three independent experiments. Data are represented as means ± SEM. The significances of differences in (E), (H), and (K) were determined by t test. ***p < 0.005.

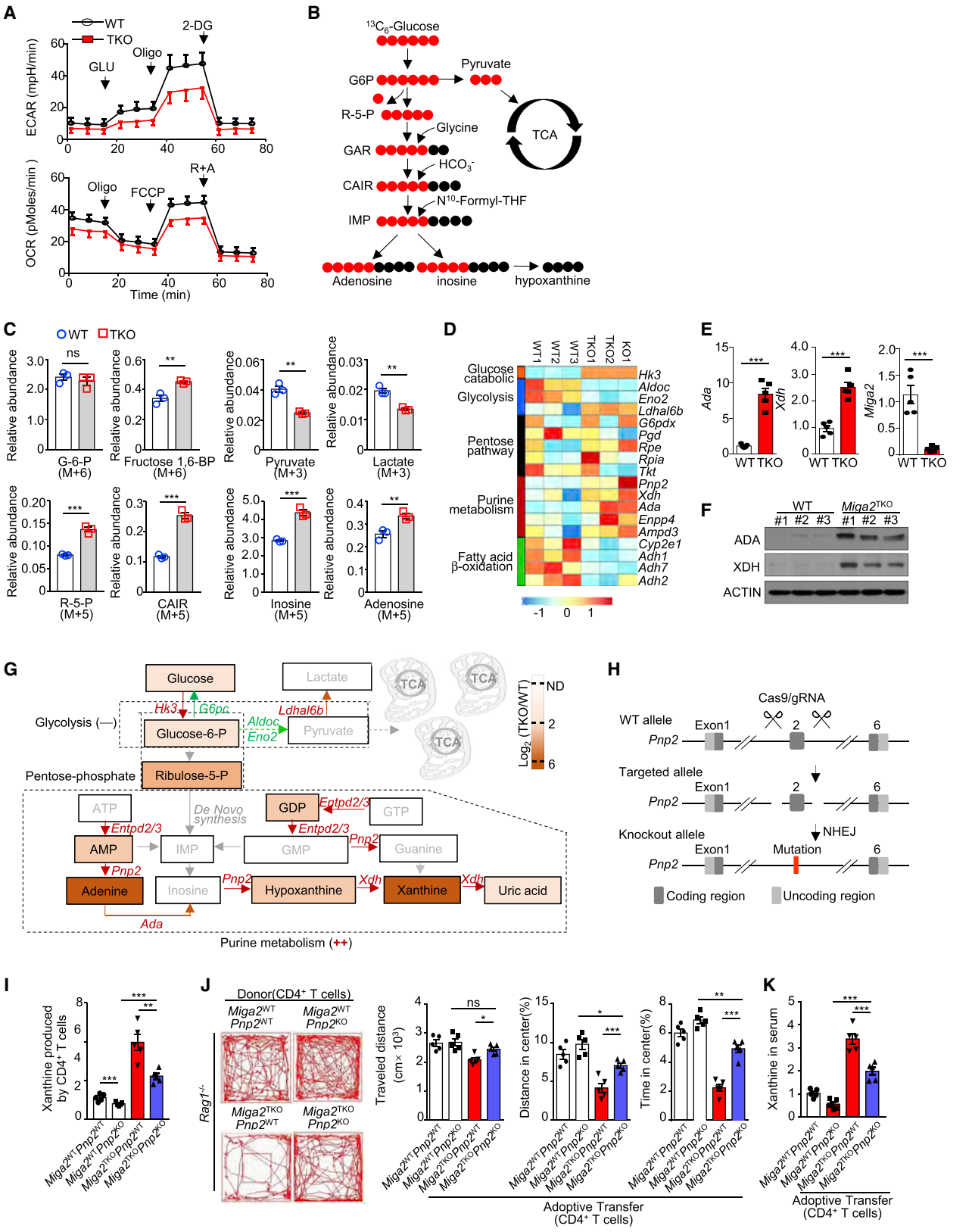

(legend on next page)

$CD4^+$ T cells by crossing with $Irf1^{-/-}$ mice. IRF-1 deficiency clearly normalized both the mRNA and protein levels of *Ada* and *Xdh* in *Miga2*-deficient $CD4^+$ T cells (Figures 7E and 7F). Additionally, the lack of IRF-1 restored most of the anxiety-like phenotypes in $Miga2^{TKO}$ mice (Figure 7G). A weak difference remained between $Miga2^{TKO}Irf1^{KO}$ and $Miga2^{WT}$ $Irf1^{KO}$ mice indicating that IRF-1 may not be the only factor contributing to T-cell-mediated anxiety-like behavior. Nonetheless, our results suggest that IRF-1 in $CD4^+$ T cells plays an essential role in mitochondrial fission-mediated purine synthesis and anxiety symptoms.

DISCUSSION

As early as 1950, Han Selye built up the concept of neuroimmunology and began to explore the crosstalk between immune cells and the nervous system. Over nearly 70 years, the function of the innate immune system in the control of mood and the onset of anxiety has been well established, but the roles of the adaptive immune system have not yet been defined. Some evidences revealed that both $Rag1^{-/-}$ and $TCR\beta^{-/-}\delta^{-/-}$ mice exhibit attenuated anxiety- and depression-like behavior (Beurel et al., 2013; Clark et al., 2015; Clark et al., 2014; Cushman et al., 2003; Rattazzi et al., 2013; Rilett et al., 2015). In contrast, some other studies showed that lymphocytes from chronically social defeated mice suppressed anxiety in recipient mice (Brachman et al., 2015; Lewitus et al., 2009). These results suggest that the controversial roles of T cells in mood disorders are largely attributed to the lack of sufficient genetic evidence.

Patients with infectious or autoimmune diseases, such as inflammatory bowel disease, displayed excessive T cell proliferation, which led to anxiety-like behavior (Gracie and Ford, 2019; Kipnis, 2016; Naidoo et al., 2015). Mice with T regulatory cell (Treg) deficiency or anti-PD-1 administration exhausted serotonin and 5-hydroxyindoleacetic acid levels in the brain because of excessively proliferative T cells. However, Trp supplementation only partially normalized behavioral symptoms and neurotransmitter levels (Miyajima et al., 2017). Surprisingly, low levels of inflammation and dysfunction of T cell responses in CS also trigger anxiety-like behavior, implying that T cells trigger anxiety in a nonconventional manner, even without traditional inflammatory characteristics. Here, our study revealed a critical association between peripheral $CD4^+$ T cell-derived xanthine and anxiety-like behavior. Miyajima et al. also demonstrated accumulated purines in the sera of anxious mice treated with anti-PD-1 (Miyajima et al., 2017). Thus, it would be interesting to investigate whether xanthine is also involved in inflammation-induced anxiety.

Purine plays an essential role in various physiological processes including the synthesis of nucleic acids, lipid metabolism, and protein glycosylation. Purines are also required for the development and maintenance of mature T lymphocytes. Defects in critical genes in the purine synthesis pathway, including *Ada* and *Pnp*, cause severe immunodeficiency (Arpaia et al., 2000; Markert, 1991; Stoop et al., 1977). However, the major source of purines *in vivo* has not been clearly identified. Our study demonstrated that $CD4^+$ T cells from NT mice produced a considerable amount of xanthine. Furthermore, we observed only weakly increased xanthine levels in the sera of recipient mice that were adoptively transferred with $Miga2^{-/-}Pnp2^{-/-}$ $CD4^+$ T cells. These results suggest that the purine required for the maturation and activation of peripheral T cells may be produced by themselves, which may explain why the $Rag1^{-/-}$ mice that received excessive NT $CD4^+$ T cells also exhibited moderate anxiety.

In summary, our data establish peripheral $CD4^+$ T cells as pivotal mediators of stress-induced mood disorders. In the future, it will be interesting to clarify whether a specific $CD4^+$ T cell subpopulation regulates emotions and behavior in anxious patients. It is also important to clarify the mechanism by which LTB4 promotes the mitochondrial morphology of $CD4^+$ T cells. Taken together, our results provide insights into the physiological function of adaptive immunity in neurodevelopment and neuropsychiatric disorders. We believe our findings have profound implications for developing a valuable therapeutic approach for various psychiatric and metabolic diseases.

Figure 6. Mitochondrial Fission Promotes Purine *de novo* Synthesis Pathway in $CD4^+$ T Cells

(A) Mitochondrial fitness tests were used to compare the OCR and ECAR of splenic $CD4^+$ T cells (n = 9).

(B) Schematic diagram of the conversion of ^{13}C–glucose into purine metabolism and the tricarboxylic acid (TCA) cycle.

(C) Naive splenic $CD4^+$ T cells were cultured in glucose-free medium for 6 h and then incubated with ^{13}C–glucose for 24 h. LC-MS was performed for M+3-, M+5-, and M+6-labeled metabolic productions.

(D) The expressions of selective regulators for distinct metabolic processes in naive $CD4^+$ T cells were analyzed by RNaseq and presented by heatmap.

(E) The mRNA of indicated genes naive $CD4^+$ T cells from WT and $Miga2^{TKO}$ mice were monitored by qRT-PCR (n = 5). These qPCR data are presented as fold change relative to the Actb mRNA level and normalized by Bio-Rad CFX Manager 3.1.

(F) The protein levels of ADA and XDH in the $CD4^+$ T cells described as (E) were measured by IB.

(G) Schematic showing purine metabolic pathways, listing representative enzymes and metabolic products, color-coded based on fold change. The genes in red characters were upregulated; those in green characters were downregulated.

(H) Schematic diagram of *Pnp2* knockout strategy.

(I) Naive $CD4^+$ T cells were isolated from the indicated mice. These $CD4^+$ T cells were cultured in glucose-free medium for 6 h and then incubated with glucose (2mg/mL) for another 24 h. Xanthine in the supernatant was measured by ELISA. The relative fold change is normalized to serum xanthine in the $Miga2^{WT}Pnp2^{WT}$ group.

(J) $Rag1^{-/-}$ mice were adoptively transferred with 5×10^6 $CD4^+$ T cells as indicated every other day. Six days later, the anxiety-like behavior of these $Rag1^{-/-}$ mice was evaluated by OFT (n = 5).

(K) Xanthine in the serum of above mice was measured by ELISA.

All data are representative of at least three independent experiments. Data are represented as means ± SEM. The significances of difference in (I–K) were determined by Dunnett's test, and others were determined by t test. *p < 0.05; **p < 0.01; ***p < 0.005.

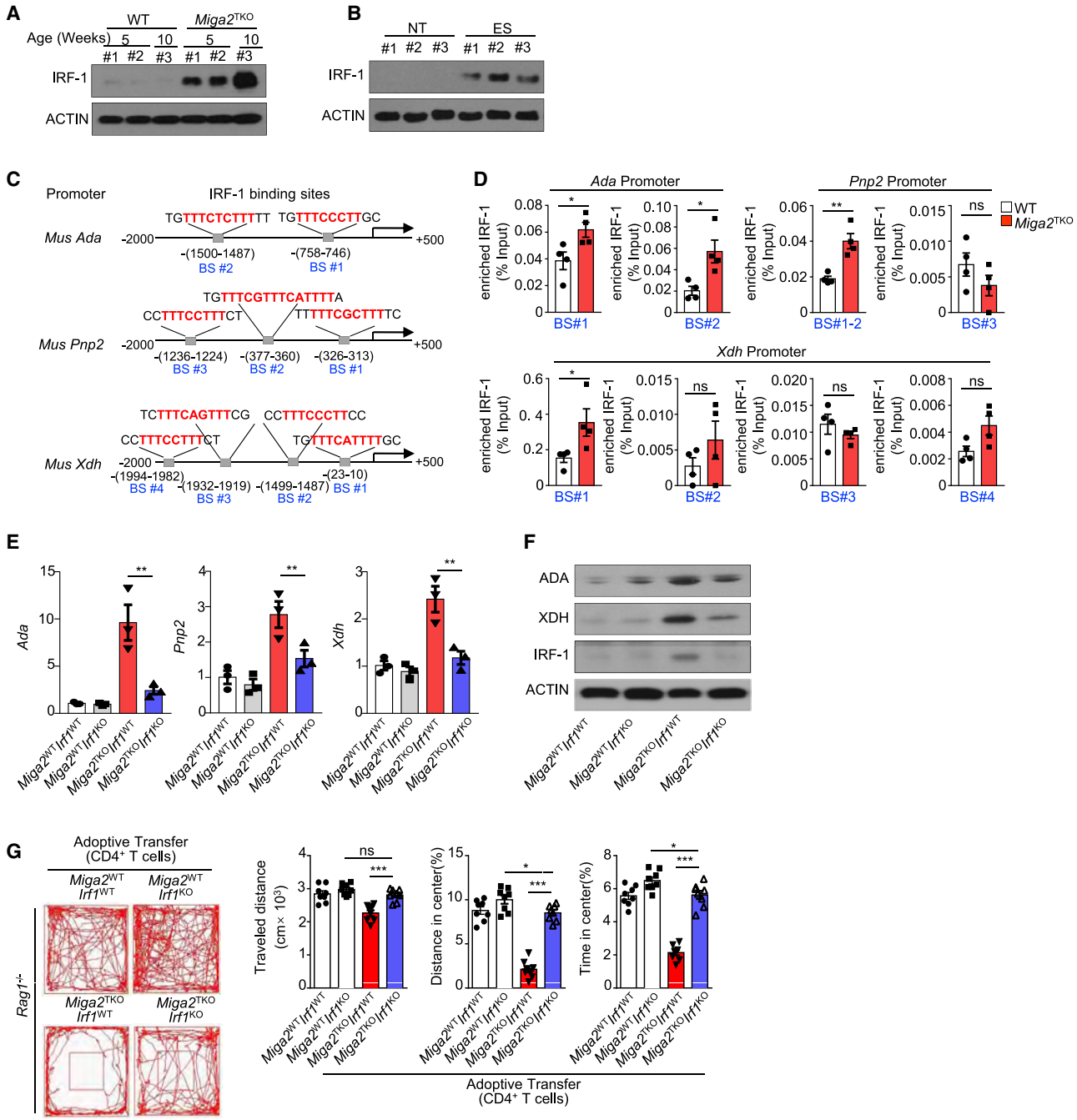

Figure 7. Accumulated IRF-1 Controls Purine Synthesis in CD4⁺ T Cells and Anxiety-like Behavior

(A) IB analysis of IRF-1 expression in naive splenic CD4⁺ T cells from WT and *Miga2*^{TKO} mice.

(B) The protein levels of IRF-1 in naive splenic CD4⁺ T cells from NT- and ES-treated mice was evaluated by IB.

(C) Schematic representation of IRF1-binding sites (BS) in the promoters of the mouse *Ada*, *Xdh*, and *Pnp2* genes. BS, binding site. The sequences in red indicate IFN-stimulated responsive elements (ISREs).

(D) ChIP-QPCR assays show the abundance of IRF-1 binding on these promoters. The results are presented relative to the total input DNA.

(E–F) The mRNA and protein levels of indicated genes in *Miga2*^{TKO} *Irf1*^{KO} naive CD4⁺ T cells were monitored by qRT-PCR (E) and IB (F).

(G) *Rag1*$^{-/-}$ mice were adoptively transferred with 5 × 10^6 *Miga2*^{TKO}*Irf1*$^{-/-}$ CD4⁺ T cells every other day. Six days later, the anxiety-like behavior of these recipient *Rag1*$^{-/-}$ mice was evaluated by the OFT (n = 8).

All data are representative of at least three independent experiments. Data are represented as means ± SEM. The significances of difference in (E) and (G) were determined by Dunnett's test, and others were determined by t test. ns, no significance; **p < 0.01; ***p < 0.005.

STAR★METHODS

Detailed methods are provided in the online version of this paper and include the following:

- KEY RESOURCES TABLE
- LEAD CONTACT AND MATERIALS AVAILABILITY
- EXPERIMENTAL MODEL AND SUBJECT DETAILS
  - Mice
  - Patients and Samples preparation
  - Study approval
- METHOD DETAILS
  - Electric shock model
  - Restraint stress model
  - Open-field test
  - Elevated plus maze test
  - Tail suspension test
  - Light–Dark box test
  - T cell depletion and drug treatment
  - Induction and assessment of EAE
  - T cell purification and adoptive transfers
  - RNA-seq analysis
  - Fluorescence microscopy
  - T cell isolation and stimulation
  - Transmission Electron Microscopy
  - $CD4^+$ T cell proliferation
  - Single cell dissociation
  - Flow cytometry and intracellular cytokine staining
  - Metabolic Assays
  - Isolation of oligodendrocytes
  - Viral injection
  - LC-MS analysis for serum metabolome
  - ^{13}C tracing by liquid-chromatography Q-exactive mass spectrometry (LC–QEMS)
  - qRT-PCR
  - Immunoblot (IB)
  - Chromatin IP (ChIP) assay
  - Tissue staining/IHC
  - *In vivo* BrdU proliferation assay
- QUANTIFICATION AND STATISTICAL ANALYSIS
- DATA AND CODE AVAILABILITY

SUPPLEMENTAL INFORMATION

Supplemental Information can be found online at https://doi.org/10.1016/j.cell.2019.10.001.

ACKNOWLEDGMENTS

We thank Bangguo Qian from PerkinElmer for the technical support. We thank Dian Wang (Hangzhou Neoline Technology Co., Ltd.) for the technical support in using Tissue Gnostics TissueFAXS6.0.123. We thank Jia-shu Yao for the clinical sample collection. Thanks also go to the Life Sciences Institute core facilities, Zhejiang University for technical assistance. This study was supported by the National Key R&D Program of China (2018YFA0800503 and 2018YFD0500100), Excellent Young Scientist Fund of NSFC (31822017), Zhejiang Provincial Natural Science Foundation of China (LR19C080001), the Strategic Priority Research Program of the Chinese Academy of Science (XDA16010302), and the National Natural Science Foundation of China (81572651, 81771675, 81622013, and 81700913).

AUTHOR CONTRIBUTIONS

Conceptualization, J.J. and Y.-Y.L.; Methodology, K.F., Y.-Y.L., and H.W.; Software, X.-T.M. and Y.-N.L.; Formal Analysis, J.G. and L.S.; Investigation, K.F., Y.-Y.L., H.W., F.W., X.-Y.M., Z.G., Lei Zhang, and K.R.; Resources, L.H., W.C., D.Q., W.X., Q.C., Long Zhang, C.T., L.L., W.L., G.Z., Y.W., M.T., and R.C.; Data Curation, J.Z.; Writing – Original Draft, J.J., K.F., Y.-Y.L., and R.C.; Writing – Review & Editing, J.J. and X.F.; Visualization, J.J., K.F., Y-Y.L., and H.W.; Supervision, J.J.; Funding Acquisition, J.J. and R.C.

DECLARATION OF INTERESTS

The authors declare no competing interests.

Received: April 15, 2019
Revised: August 15, 2019
Accepted: October 1, 2019
Published: October 31, 2019

REFERENCES

Ali-Sisto, T., Tolmunen, T., Toffol, E., Viinamäki, H., Mäntyselkä, P., Valkonen-Korhonen, M., Honkalampi, K., Ruusunen, A., Velagapudi, V., and Lehto, S.M. (2016). Purine metabolism is dysregulated in patients with major depressive disorder. Psychoneuroendocrinology *70*, 25–32.

Arpaia, E., Benveniste, P., Di Cristofano, A., Gu, Y., Dalal, I., Kelly, S., Hershfield, M., Pandolfi, P.P., Roifman, C.M., and Cohen, A. (2000). Mitochondrial basis for immune deficiency. Evidence from purine nucleoside phosphorylase-deficient mice. J. Exp. Med. *191*, 2197–2208.

Beurel, E., Harrington, L.E., and Jope, R.S. (2013). Inflammatory T helper 17 cells promote depression-like behavior in mice. Biol. Psychiatry *73*, 622–630.

Bourin, M., Petit-Demoulière, B., Dhonnchadha, B.N., and Hascöet, M. (2007). Animal models of anxiety in mice. Fundam. Clin. Pharmacol. *21*, 567–574.

Brachman, R.A., Lehmann, M.L., Maric, D., and Herkenham, M. (2015). Lymphocytes from chronically stressed mice confer antidepressant-like effects to naive mice. J. Neurosci. *35*, 1530–1538.

Buck, M.D., O'Sullivan, D., Klein Geltink, R.I., Curtis, J.D., Chang, C.H., Sanin, D.E., Qiu, J., Kretz, O., Braas, D., van der Windt, G.J., et al. (2016). Mitochondrial Dynamics Controls T Cell Fate through Metabolic Programming. Cell *166*, 63–76.

Campos, A.C., Fogaça, M.V., Aguiar, D.C., and Guimarães, F.S. (2013). Animal models of anxiety disorders and stress. Br. J. Psychiatry *35* (*Suppl 2*), S101–S111.

Chourbaji, S., Urani, A., Inta, I., Sanchis-Segura, C., Brandwein, C., Zink, M., Schwaninger, M., and Gass, P. (2006). IL-6 knockout mice exhibit resistance to stress-induced development of depression-like behaviors. Neurobiol. Dis. *23*, 587–594.

Clark, S.M., Sand, J., Francis, T.C., Nagaraju, A., Michael, K.C., Keegan, A.D., Kusnecov, A., Gould, T.D., and Tonelli, L.H. (2014). Immune status influences fear and anxiety responses in mice after acute stress exposure. Brain Behav. Immun. *38*, 192–201.

Clark, S.M., Michael, K.C., Klaus, J., Mert, A., Romano-Verthelyi, A., Sand, J., and Tonelli, L.H. (2015). Dissociation between sickness behavior and emotionality during lipopolysaccharide challenge in lymphocyte deficient Rag2(-/-) mice. Behav. Brain Res. *278*, 74–82.

Cushman, J., Lo, J., Huang, Z., Wasserfall, C., and Petitto, J.M. (2003). Neurobehavioral changes resulting from recombinase activation gene 1 deletion. Clin. Diagn. Lab. Immunol. *10*, 13–18.

Darashchonak, N., Koepsell, B., Bogdanova, N., and von Versen-Höynck, F. (2014). Adenosine A2B receptors induce proliferation, invasion and activation of cAMP response element binding protein (CREB) in trophoblast cells. BMC Pregnancy Childbirth *14*, 2.

Davis, M. (1992). The role of the amygdala in fear and anxiety. Annu. Rev. Neurosci. *15*, 353–375.

de Kloet, E.R., Joëls, M., and Holsboer, F. (2005). Stress and the brain: from adaptation to disease. Nat. Rev. Neurosci. *6*, 463–475.

Dhabhar, F.S. (2008). Enhancing versus Suppressive Effects of Stress on Immune Function: Implications for Immunoprotection versus Immunopathology. Allergy Asthma Clin. Immunol. *4*, 2–11.

Dimsdale, J.E. (2008). Psychological stress and cardiovascular disease. J. Am. Coll. Cardiol. *51*, 1237–1246.

Dragoş, D., and Tănăsescu, M.D. (2010). The effect of stress on the defense systems. J. Med. Life *3*, 10–18.

Engelhardt, B., Vajkoczy, P., and Weller, R.O. (2017). The movers and shapers in immune privilege of the CNS. Nat. Immunol. *18*, 123–131.

Engler, H., Brendt, P., Wischermann, J., Wegner, A., Röhling, R., Schoemberg, T., Meyer, U., Gold, R., Peters, J., Benson, S., and Schedlowski, M. (2017). Selective increase of cerebrospinal fluid IL-6 during experimental systemic inflammation in humans: association with depressive symptoms. Mol. Psychiatry *22*, 1448–1454.

Filiano, A.J., Xu, Y., Tustison, N.J., Marsh, R.L., Baker, W., Smirnov, I., Overall, C.C., Gadani, S.P., Turner, S.D., Weng, Z., et al. (2016). Unexpected role of interferon-γ in regulating neuronal connectivity and social behaviour. Nature *535*, 425–429.

Gao, Z., Li, Y., Wang, F., Huang, T., Fan, K., Zhang, Y., Zhong, J., Cao, Q., Chao, T., Jia, J., et al. (2017). Mitochondrial dynamics controls anti-tumour innate immunity by regulating CHIP-IRF1 axis stability. Nat. Commun. *8*, 1805.

Glaser, R., and Kiecolt-Glaser, J.K. (2005). Stress-induced immune dysfunction: implications for health. Nat. Rev. Immunol. *5*, 243–251.

Gracie, D.J., and Ford, A.C. (2019). Depression, Antidepressants, and Inflammatory Bowel Disease: Implications for Future Models of Care. Gastroenterology *156*, 2345–2347.

Kipnis, J. (2016). Multifaceted interactions between adaptive immunity and the central nervous system. Science *353*, 766–771.

Krishnan, V., and Nestler, E.J. (2008). The molecular neurobiology of depression. Nature *455*, 894–902.

Langlais, D., Barreiro, L.B., and Gros, P. (2016). The macrophage IRF8/IRF1 regulome is required for protection against infections and is associated with chronic inflammation. J. Exp. Med. *213*, 585–603.

Lécuyer, M.-A., Saint-Laurent, O., Bourbonnière, L., Larouche, S., Larochelle, C., Michel, L., Charabati, M., Abadier, M., Zandee, S., Haghayegh Jahromi, N., et al. (2017). Dual role of ALCAM in neuroinflammation and blood-brain barrier homeostasis. Proc. Natl. Acad. Sci. USA *114*, E524–E533.

Lewitus, G.M., Wilf-Yarkoni, A., Ziv, Y., Shabat-Simon, M., Gersner, R., Zangen, A., and Schwartz, M. (2009). Vaccination as a novel approach for treating depressive behavior. Biol. Psychiatry *65*, 283–288.

Li, C.M., Tyler, P.C., Furneaux, R.H., Kicska, G., Xu, Y., Grubmeyer, C., Girvin, M.E., and Schramm, V.L. (1999). Transition-state analogs as inhibitors of human and malarial hypoxanthine-guanine phosphoribosyltransferases. Nat. Struct. Biol. *6*, 582–587.

Li, Z., Ma, L., Kulesskaya, N., Võikar, V., and Tian, L. (2014). Microglia are polarized to M1 type in high-anxiety inbred mice in response to lipopolysaccharide challenge. Brain Behav. Immun. *38*, 237–248.

Li, Y., Singer, N.G., Whitbred, J., Bowen, M.A., Fox, D.A., and Lin, F. (2017). CD6 as a potential target for treating multiple sclerosis. Proc. Natl. Acad. Sci. USA *114*, 2687–2692.

Markert, M.L. (1991). Purine nucleoside phosphorylase deficiency. Immunodefic. Rev. *3*, 45–81.

McEwen, B.S., Bowles, N.P., Gray, J.D., Hill, M.N., Hunter, R.G., Karatsoreos, I.N., and Nasca, C. (2015). Mechanisms of stress in the brain. Nat. Neurosci. *18*, 1353–1363.

McKim, D.B., Weber, M.D., Niraula, A., Sawicki, C.M., Liu, X., Jarrett, B.L., Ramirez-Chan, K., Wang, Y., Roeth, R.M., Sucaldito, A.D., et al. (2018). Microglial recruitment of IL-1β-producing monocytes to brain endothelium causes stress-induced anxiety. Mol. Psychiatry *23*, 1421–1431.

Miles, R.W., Tyler, P.C., Furneaux, R.H., Bagdassarian, C.K., and Schramm, V.L. (1998). One-third-the-sites transition-state inhibitors for purine nucleoside phosphorylase. Biochemistry *37*, 8615–8621.

Mishra, P., and Chan, D.C. (2016). Metabolic regulation of mitochondrial dynamics. J. Cell Biol. *212*, 379–387.

Miyajima, M., Zhang, B., Sugiura, Y., Sonomura, K., Guerrini, M.M., Tsutsui, Y., Maruya, M., Vogelzang, A., Chamoto, K., Honda, K., et al. (2017). Metabolic shift induced by systemic activation of T cells in PD-1-deficient mice perturbs brain monoamines and emotional behavior. Nat. Immunol. *18*, 1342–1352.

Naidoo, J., Page, D.B., Li, B.T., Connell, L.C., Schindler, K., Lacouture, M.E., Postow, M.A., and Wolchok, J.D. (2015). Toxicities of the anti-PD-1 and anti-PD-L1 immune checkpoint antibodies. Ann. Oncol. *26*, 2375–2391.

Padgett, D.A., and Glaser, R. (2003). How stress influences the immune response. Trends Immunol. *24*, 444–448.

Phelps, E.A., O'Connor, K.J., Gatenby, J.C., Gore, J.C., Grillon, C., and Davis, M. (2001). Activation of the left amygdala to a cognitive representation of fear. Nat. Neurosci. *4*, 437–441.

Phillis, J.W., and Wu, P.H. (1982). Adenosine mediates sedative action of various centrally active drugs. Med. Hypotheses *9*, 361–367.

Ransohoff, R.M., and Engelhardt, B. (2012). The anatomical and cellular basis of immune surveillance in the central nervous system. Nat. Rev. Immunol. *12*, 623–635.

Rattazzi, L., Piras, G., Ono, M., Deacon, R., Pariante, C.M., and D'Acquisto, F. (2013). $CD4^+$ but not $CD8^+$ T cells revert the impaired emotional behavior of immunocompromised RAG-1-deficient mice. Transl. Psychiatry *3*, e280.

Reiche, E.M.V., Nunes, S.O.V., and Morimoto, H.K. (2004). Stress, depression, the immune system, and cancer. Lancet Oncol. *5*, 617–625.

Rilett, K.C., Friedel, M., Ellegood, J., MacKenzie, R.N., Lerch, J.P., and Foster, J.A. (2015). Loss of T cells influences sex differences in behavior and brain structure. Brain Behav. Immun. *46*, 249–260.

Shackman, A.J., and Fox, A.S. (2016). Contributions of the Central Extended Amygdala to Fear and Anxiety. J. Neurosci. *36*, 8050–8063.

Steimer, T. (2011). Animal models of anxiety disorders in rats and mice: some conceptual issues. Dialogues Clin. Neurosci. *13*, 495–506.

Stoop, J.W., Zegers, B.J.M., Hendrickx, G.F.M., van Heukelom, L.H., Staal, G.E.J., de Bree, P.K., Wadman, S.K., and Ballieux, R.E. (1977). Purine nucleoside phosphorylase deficiency associated with selective cellular immunodeficiency. N. Engl. J. Med. *296*, 651–655.

Tamashiro, K.L., Sakai, R.R., Shively, C.A., Karatsoreos, I.N., and Reagan, L.P. (2011). Chronic stress, metabolism, and metabolic syndrome. Stress *14*, 468–474.

Theien, B.E., Vanderlugt, C.L., Eagar, T.N., Nickerson-Nutter, C., Nazareno, R., Kuchroo, V.K., and Miller, S.D. (2001). Discordant effects of anti-VLA-4 treatment before and after onset of relapsing experimental autoimmune encephalomyelitis. J. Clin. Invest. *107*, 995–1006.

Thomas, K.M., Drevets, W.C., Dahl, R.E., Ryan, N.D., Birmaher, B., Eccard, C.H., Axelson, D., Whalen, P.J., and Casey, B.J. (2001). Amygdala response to fearful faces in anxious and depressed children. Arch. Gen. Psychiatry *58*, 1057–1063.

Uhlik, M., Good, L., Xiao, G., Harhaj, E.W., Zandi, E., Karin, M., and Sun, S.-C. (1998). NF-kappaB-inducing kinase and IkappaB kinase participate in human T-cell leukemia virus I Tax-mediated NF-kappaB activation. J. Biol. Chem. *273*, 21132–21136.

Vajkoczy, P., Laschinger, M., and Engelhardt, B. (2001). α4-integrin-VCAM-1 binding mediates G protein-independent capture of encephalitogenic T cell blasts to CNS white matter microvessels. J. Clin. Invest. *108*, 557–565.

Wai, T., and Langer, T. (2016). Mitochondrial Dynamics and Metabolic Regulation. Trends Endocrinol. Metab. *27*, 105–117.

Wakabayashi, C., Numakawa, T., Odaka, H., Ooshima, Y., Kiyama, Y., Manabe, T., Kunugi, H., and Iwakura, Y. (2015). IL-1 receptor-antagonist (IL-1Ra) knockout mice show anxiety-like behavior by aging. Neurosci. Lett. *599*, 20–25.

Wang, Y.-L., Han, Q.-Q., Gong, W.-Q., Pan, D.-H., Wang, L.-Z., Hu, W., Yang, M., Li, B., Yu, J., and Liu, Q. (2018). Microglial activation mediates chronic mild stress-induced depressive- and anxiety-like behavior in adult rats. J. Neuroinflammation *15*, 21.

Wohleb, E.S., Hanke, M.L., Corona, A.W., Powell, N.D., Stiner, L.M., Bailey, M.T., Nelson, R.J., Godbout, J.P., and Sheridan, J.F. (2011). β-Adrenergic receptor antagonism prevents anxiety-like behavior and microglial reactivity induced by repeated social defeat. J. Neurosci. *31*, 6277–6288.

Zhan, M., Brooks, C., Liu, F., Sun, L., and Dong, Z. (2013). Mitochondrial dynamics: regulatory mechanisms and emerging role in renal pathophysiology. Kidney Int. *83*, 568–581.

STAR★METHODS

KEY RESOURCES TABLE

REAGENT or RESOURCE	SOURCE	IDENTIFIER
Antibodies		
Rabbit monoclonal anti-Adenosine A1 Receptor(clone EPR6179), Alexa Fluor 488	Abcam	Cat# ab202949
Rabbit monoclonal anti-Myelin oligodendrocyte glycoprotein(clone EP4281), Alexa Fluor 647	Abcam	Cat# ab199472
Rabbit monoclonal anti-NeuN(clone EPR12763), Alexa Fluor 568	Abcam	Cat# ab207282
Rabbit polyclonal anti-c-Fos(clone 2H2)	Abcam	Cat# ab208942; RRID: AB_2747772
Rabbit polyclonal anti-Adenosine A2a Receptor	Abcam	Cat# ab3461; RRID: AB_303823
Rabbit polyclonal anti-Adenosine A2b Receptor	Abcam	Cat# ab222901
Rabbit polyclonal anti-Adenosine A3 Receptor	Abcam	Cat# ab203298
Rabbit monoclonal anti-IRF1(clone EPR18301)	Abcam	Cat# ab186384
Mouse monoclonal anti-Mitofusin 2(clone 6A8)	Abcam	Cat# ab56889; RRID: AB_2142629
Rabbit polyclonal anti-ADA	Abcam	Cat# ab175310
Rabbit monoclonal anti- Xanthine Oxidase [EPR4605]	Abcam	Cat# ab109235; RRID: AB_10863199
Mouse monoclonal anti-GFAP(clone 2E1.E9), Brilliant Violet 421	Biolegend	Cat# 644710; RRID: AB_2566685
Mouse monoclonal anti-CX3CR1(clone SA011F11), PE	Biolegend	Cat# 149015; RRID: AB_2565699
Mouse monoclonal anti-IRF1(clone E-4)	Santa Cruz	Cat# sc-514544
Anti-BrdU(clone 3D4), Alexa Fluor 488	BD	Cat# 558599; RRID: AB_647075
Mouse monoclonal anti-β-Actin(clone AC-74)	Sigma	Cat# A2228; RRID: AB_476697
Rat Anti-mouse B220(clone RA3-6B2), PE	BD	Cat# 553089; RRID: AB_394619
Hamster monoclonal anti-CD3e (clone 145-2C11), APC	eBioscience	Cat# 17-0031-83; RRID: AB_469316
Rat monoclonal anti-CD4(clone RM4-5), eFluor 450	eBioscience	Cat# 48-0042-82; RRID: AB_1272194
Rat monoclonal anti-CD8a(clone 53-6.7), PerCP-Cyanine5.5	eBioscience	Cat# 45-0081-82; RRID: AB_1107004
Rat anti-mouse CD44(clone IM7), FITC	BD	Cat# 561859; RRID: AB_10894581
Rat monoclonal anti-CD62L(clone MEL-14), APC	eBioscience	Cat# 17-0621-83; RRID: AB_469411
Anti-mouse CD4(clone GK 1.5)	BioXcell	Cat# BE0003-1; RRID: AB_1107636
Anti-mouse/human CD49d(clone PS/2)	BioXcell	Cat# BE0071; RRID: AB_1107657
Anti-mouse CD8a(clone 2.43)	BioXcell	Cat# BE0061; RRID: AB_1125541
Anti-O4 MicroBeads	Mitenyi	Cat# 130-094-543
Anti-CD4 MicroBeads	Mitenyi	Cat# 130-117-043
Phospho-PKA Substrate (RRXS*/T*) (100G7E)	Cell Signaling technology	Cat# 9624; RRID: AB_331817
Bacterial and Virus Strains		
AAV9-GFAP-GFP-miR30-shRNA(mAdora1)	vigenebio	N/A
AAV8-MBP-GFP-miR30-shRNA(mAdora1)	vigenebio	N/A
AAV8-MBP-GFP-miR30-shRNA(scramble)	vigenebio	N/A

(*Continued on next page*)

Continued

REAGENT or RESOURCE	SOURCE	IDENTIFIER
Biological Samples		
Patient's and healthy people's serum	Sir Run Run Shaw Hospital	http://www.srrsh-english.com
Patient's and healthy people's serum	Nanjing Drum Tower Hospital	http://www.njglyy.com
Chemicals, Peptides, and Recombinant Proteins		
Deoxycholic acid	yuanyebio	Cat# S24458
vidarabine	yuanyebio	Cat# S18122
Adenine	yuanyebio	Cat# S18009
2-DG	yuanyebio	Cat# S11070
Sodium taurochenodeoxycholate	yuanyebio	Cat# S31336
Prostaglandin B1	yuanyebio	Cat# ZC-20354
leukotriene B4	yuanyebio	Cat# ZC-22879
15-deoxy-D12,14-prostaglandin J2	yuanyebio	Cat# ZC-22860
γ-GABA	yuanyebio	Cat# S20180
DL-adrenaline	yuanyebio	Cat# S64536
Dicortol	yuanyebio	Cat# S31439
BCX-1777	MCE	Cat# HY-16209
BLZ945	Topscience	Cat# T6119
pexidartinib	Topscience	Cat# T2115
xanthine	aladdin	Cat# H108384
hypoxanthine	aladdin	Cat# X104264
papain	sigma	Cat# P4762
7-AAD (7-amino-actinomycin D)	BD	Cat# 559925
BrdU	Sangon	Cat# E607203
DAPI	Biolegend	Cat# 422801
Mitospy orange CMTMRos	Biolegend	Cat# 424803
D-Glucose-$^{13}C_6$	sigma	Cat# 389374
Critical Commercial Assays		
Mouse xanthine ELISA kit	Sangon	Cat# D720328
FITC Annexin V Apoptosis Detection Kit I	BD	Cat# 556547
Lightning-Link Kit(FITC)	Innova Biosciences	707-0010
Lightning-Link Kit(APC)	Innova Biosciences	705-0010
Lightning-Link Kit(PE)	Innova Biosciences	703-0010
Lightning-Link Kit(Percp5.5)	Innova Biosciences	763-0030
Deposited Data		
Raw and analyzed data	This paper	PRJNA528163
Experimental Models: Organisms/Strains		
Mouse: C57BL/6J	The Jackson Laboratory	CAT#000664
Mouse: B6.129S7-*Rag1*^{tm1Mom}/J	The Jackson Laboratory	CAT#002216
B6.Cg-Tg(Cd4-cre)$^{1Cwi/BfluJ}$	The Jackson Laboratory	CAT#022071
Mouse: B6-*Fam73*$^{btm1a(KOMP)Wtsi}$ (*Miga2*$^{-/-}$)	University of California, Davis Knockout Mouse Project Repository	CAT#048607-UCD
Mouse: B6.129S2-*Irf1*^{tm1Mak}/J	The Jackson Laboratory	CAT#002762
Mouse: B6-*Pnp2-eKO1*	ShanghaiModelOrganismsCenter, Inc	https://www.modelorg.com
Mouse: B6-*Mfn1*^{flox}-*Mfn2*^{flox}	Dr. Yuan Wang (East China Normal University)	N/A
Oligonucleotides		
Primers for genotyping, see Table S7	This paper	N/A
Primers for qPRC, see Table S8	This paper	N/A
Primers for CHIP-qPRC, see Table S8	This paper	N/A

(*Continued on next page*)

Continued

REAGENT or RESOURCE	SOURCE	IDENTIFIER
Software and Algorithms		
TissueFAXS6.0.123	Neoline	N/A
ImageJ		https://imagej.nih.gov/ij/
10x Cell Ranger package	10x Genomics	https://support.10xgenomics.com
FlowJo	Treestar	https://www.flowjo.com
Prism	GraphPad	https://www.graphpad.com
Other		
4-0 silk	Ethicon	Cat# W501
6-0 silk	Ethicon	Cat# W580
hemostat	Scanlan	Cat# 4635-06
needle holder	Scanlan	Cat# 6006-05

LEAD CONTACT AND MATERIALS AVAILABILITY

Further information and requests for reagents should be directed to and will be fulfilled by the Lead Contact, Jin Jin (jjin4@zju.edu.cn).

All materials generated in this study are available for requests.

EXPERIMENTAL MODEL AND SUBJECT DETAILS

Mice

Miga2 KOfirst mice (C57BL/6 background) were a gift from the Prof. Heng-Yu Fan (Zhejiang University, P. R. China). *Miga2* KOfirst mice were targeted exon 3 of *Miga2* gene using a FRT-LoxP vector. *Miga2*-floxed mice were generated by crossing the *Miga2* KOfirst mice with FLP deleter mice (Rosa26-FLPe; Jackson Laboratory). The *Miga2*-floxed mice were further crossed with *Cd4*-Cre mice (all from Jackson Laboratory, C57BL/6 background) to generate T cell conditional *Miga2* KO (*Miga2*$^{f/f}$*Cd4*-Cre, TKO) mice. *Irf1*$^{-/-}$ mice (C57BL/6 background) were provided by Prof. Shu-yu Zhang (Sichuan University, China). *Mfn1*^{flox}*Mfn2*^{flox} mice (C57BL/6 background) were provided by Prof. Yuan Wang (East China University of Science and Technology, China), and further crossed with *Cd4*-Cre mice to generate *Mfn1-Mfn2* T cell conditional double KO mice. *Pnp2*$^{-/-}$ mice in B6 background was generated by Shanghai Model Organisms Center, Inc (SMOC) by targeting of exon 2 of *Pnp2* using CRISPR/CAS9.

Heterozygous mice were bred to generate littermate controls and KO (or conditional KO) mice for experiments. In the animal studies, WT and multiple KO mice at the age of 6-8 weeks are randomly grouped. Outcomes of animal experiments were collected blindly and recorded based on ear-tag numbers of the experimental mice. The different sex did not affect the final conclusion, thus male and female mice were equally grouped in the behavior test. The Genotyping primers were performed in Table S7. Mice were maintained in specific pathogen-free (SPF) facility with room temperature, and all animal experiments were conducted in accordance with protocols approved by the Institutional Animal Care and Use Committee of Zhejiang University.

Patients and Samples preparation

Sample collection was performed at Sir Runrun Shaw Hospital and Nanjing Drum Tower Hospital between January and August 2019. Informed written consent was obtained from all participants. The Inclusion criteria were: 20 males and 20 females; age between 18 and 65 years; diagnosed with anxiety disorders according to the ICD-10 criteria; assess mood and anxiety symptoms through the Hamilton Anxiety Scale. The exclusion criteria were: using drugs targeting purine metabolism; complication with other autoimmune diseases; severe brain injuries or brain lesions have occurred. The inclusion criteria of control subjects were: age between 18 and 65 years; no psychiatric disorders according to ICD-10 criteria; no serious systemic diseases; no complications and tumor. Control group also matched the above exclusion criteria.

All blood samples of patients and healthy individuals were collected at 6:00 am, followed by centrifugation (3000 g, 10 min) to remove cells and debris, and then the serums were stored at −80°C until further analysis.

Study approval

All animal experiments were conducted in accordance with protocols (#12077) approved by the Institutional Animal Care and Use Committee of Zhejiang University.

For human studies, written informed consents were obtained from all subjects before the study protocol. All human experiments were conducted in accordance with protocols (#20190319-4) approved by the Medical Ethics Committee of Sir Run Run Shaw Hospital, Zhejiang University and Nanjing Drum Tower Hospital.

METHOD DETAILS

Electric shock model

All animals were allowed to the experimental room for 1 h before the training. Mice were individually placed in a chamber with a grid floor connected to a shock generator. Two min after being placed in the chamber, the mice were exposed to a 3 s foot shock (0.6 mA) for 5 times during 120 s randomly for 8 or 30 consecutive days. For the control group, mice were placed in the chamber at the same time without foot shock. After training, mice were placed back into their home cages. Training chambers were cleaned with 75% ethanol before and after each trial to avoid any olfactive cues.

Restraint stress model

Mice were subjected to RS by placement in a small cage (5cm × 5cm × 5cm) and subjected for 6 h restraint from 9:00 a.m. to 3:00 p.m. during 8 or 30 consecutive days. The holes along the sidewall of the cages enabled air flowing. Animals could move head and the body but were not able to jump or run. The mice had no access to food and water during the restraint. Once the restraint ended, mice were put back to their home cages immediately with access to food and water freely. For the control group, the mice were placed in the home cage at the same time without food and water.

Open-field test

Mice were gently placed in the center of a white plastic open-field arena (50cm × 50cm × 50cm) and allowed to explore freely for 5 min. A video camera positioned directly above the arena was used to track the movement of each animal, and recorded on a computer with software (Any-maze by Stoelting) to track the total distance and the amount of time spent in the center of the chamber compared to the edges. Open field test is commonly used for measuring the exploratory behavior and general activity of animals. The test room were dark and sound-insulated, tracking instrument recognized mouse central body point with infrared lasers and sensors.

More time spent in the edges of the box with less time spent in the center of the box is interpreted as anxiety-like behavior. Before the test, the mice were acclimatized to the room for 1 h, and the arena was cleaned with 70% EtOH after every trial.

Elevated plus maze test

Mice were introduced into the center quadrant of a 4-arm maze with two open arms without walls and two closed arms with walls (25cm long, 5cm wide). This structure was elevated 60 cm above the floor. The mice were placed in the center and faced to a closed arm at the start of a trial. A video camera positioned directly above the arena was used to track the movement of each animal, and recorded on a computer with software (Any-maze by Stoelting). This software tracked the amount of time the mice spent in the closed arms versus the open arms throughout a 5-min session. Higher anxiety is indicated by a lower frequency of movement into open arms and less time spent there. Before the test, mice were acclimatized to the room for 1 h, and the arena was cleaned with 70% EtOH after every trial.

Tail suspension test

Mice were suspended by their tails with tape in a position that they could not escape or hold on to nearby surfaces for 6 min. This test is based on the fact that animals subjected to a short-term inescapable stress will develop an immobile posture. The total duration of the test can be divided into periods of agitation and immobility. Video tracking data were analyzed using software to extract the resulting escape-oriented behaviors. Higher depression is indicated by less time spent trying to escape.

Light–Dark box test

Mice were gently placed in a cage (50 × 25 × 25cm) divided into a small dark compartment (one-third) and a large illuminated compartment (two-thirds) by a partition with a door. The mice were allowed to move freely between the two chambers with the door open for 5 min. Video tracking data was analyzed using software to extract the movement trail and the time spent in each compartment. Based on the innate aversion of rodents to brightly illuminated areas and spontaneous exploratory behavior of the mice, the time spent in the dark chamber could serve as an index of anxiety-like behavior.

T cell depletion and drug treatment

For the depletion of $CD4^+$ or $CD8^+$ T cells, mice were injected intravenously (i.v.) with 500 μg anti-CD4 antibody (GK 1.5) or 500 μg anti-CD8 antibody (2.43) every 7 days. To inhibit leukocyte migration into the brain, mice were injected intravenously (i.v.) with anti-VLA-4 (αVLA-4, 20 mg/kg) or anti-CD6 (αCD6, 10 mg/kg) every three days. All antibodies were stocked in fridge and diluted to their working concentrations in PBS. Mice in control group were injected with PBS of the same volume at same time intraperitoneally.

For drug treatment experiment, the solutions of drugs (2-DG/adenine/xanthine/pnp2 inhibiter) were prepared freshly each time with 0.9% saline. 8-weeks-old mice were intraperitoneally injected with drug solution depending on their working doses on day 0, day 3 and day 6. The treatment continued one week until Open-field behavior testing was performed on day 8. For control group, mice were intraperitoneally injected with 0.9% saline of the same volume at same time.

Induction and assessment of EAE

For active EAE induction, age- and sex-matched mice were immunized s.c. with MOG_{35-55} peptide (300 μg) mixed in CFA (Sigma-Aldrich) containing 5 mg/mL heat-killed Mycobacterium tuberculosis H37Ra (Difco). Pertussis toxin (200 ng, List Biological Laboratories) in PBS was administered i.v. on days 0 and 2. Mice were examined daily and scored for disease severity using the standard scale: 0, no clinical signs; 1, limp tail; 2, paraparesis (weakness, incomplete paralysis of one or two hind limbs); 3, paraplegia (complete paralysis of two hind limbs); 4, paraplegia with forelimb weakness or paralysis; 5, moribund or death. After the onset of EAE, food and water were provided on the cage floor. Mononuclear cells were prepared from the CNS (brain and spinal cord) of EAE-induced mice and analyzed by flow cytometry.

T cell purification and adoptive transfers

$CD4^+$ T cells were purified by positive magnetic cell sorting ($CD4^+$ T cell isolation kit, Miltenyi Biotec) from the spleens and lymph nodes of 6-8 weeks-old mice. For some experiments, purified $CD4^+$ T cells were further sorted on a FACS AriaII cell sorter (BD Biosciences) to obtain naive $CD4^+$ T cells ($CD4^+CD44^{lo}CD62L^{hi}$) using anti-CD44-FITC and anti-CD62L-APC antibodies. Sorted cells were spin down and washed with PBS and prepared for the following experiments.

For adoptive transfer experiments, 5×10^6 purified $CD4^+$ T cells, $CD8^+$ T cells, 3×10^6 naive $CD4^+$ T cells or 1.5×10^6 effector $CD4^+$ T cells ($CD4^+CD44^{hi}CD62L^{lo}$) were transferred by intravenous (i.v.) injection into mice grouped as indicated at day 0, 3 and 6. Control group were injected with PBS in the same time. Open-field behavior testing was taken at day 8.

RNA-seq analysis

Fresh splenic naive T cells were isolated from young WT, *Miga2*^{TKO} or *Miga2*$^{-/-}$ mice (6–8 weeks-old). In some experiment, Fresh splenic $CD4^+$ or $CD8^+$ T cells were isolated from WT, RS or ES mice. These T cells were used for total RNA isolation with Trizol (Invitrogen), and subjected to RNA-seq analysis. RNA sequencing was performed by the Life Science Institute Sequencing and Microarray Facility using an Illumina sequencer. The raw reads were aligned to the mm10 reference genome (build mm10), using Tophat2 RNA-Seq alignment software. The mapping rate was 70% overall across all the samples in the dataset. HTseq-Count was used to quantify the gene expression counts from Tophat2 alignment files. Differential expression analysis was performed on the count data using R package DESeq2. P values obtained from multiple binomial tests were adjusted using FDR (BH). Significant genes are defined by a BH corrected p value of cut-off of 0.05 and fold-change of at least two.

Fluorescence microscopy

Naive $CD4^+$ T cells ($CD44^{lo}CD62L^{hi}$, 5×10^5) were isolated and spread to 12-well plate containing 70% alcohol-pretreated slide for starvation 2 h. These $CD4^+$ T cells were stained with 250 nM of MitoSpy^{TM} Orange CMTMRos for 20 min, and fixed with 4% paraformaldehyde (PFA) for 20 min. Then the cells were washed with PBS for three times and stained with 10 ug/mL DAPI. All the samples were imaged on a confocal microscope LSM710 (Carl Zeiss) outfitted with a Plan-Apochromat 63x oil immersion objective lesnses (Carl Zeiss). Data were collected using Carl Zeiss software ZEN 2010. For quantification of mitochondrial morphology in MitoSpyTM Orange CMTMRos-stained macrophages, scoring was analyzed with Image-Pro blindly. Short were cells with a majority of mitochondria less than 7 μm; long were cells in which the majority of mitochondria were more than 7 μm.

T cell isolation and stimulation

Primary $CD4^+$ T cells were isolated from the spleen and lympho-nodes (LNs) of young adult mice (6-8 weeks old) using anti-CD4 magnetic beads (Miltenyi Biotec). Naive $CD4^+$ cells were further purified by flow cytometric cell sorting based on $CD4^+CD44^{lo}CD62L^{hi}$ surface markers, respectively (Aria II). The cells were stimulated with plate-bound anti-CD3 (1 μg/mL) and anti-CD28 (1 μg/mL) in replicate wells of 96-well plates (0.2 million cells per well) for T cell proliferation and apoptosis, 48-well plates (0.4 million cells per well) for T cell differentiation, 12-well plates (10^6 cells per well) for quantitative RT-PCR (qRT-PCR). Where indicated, the cells were acutely stimulated using an antibody cross-linking protocol.

Transmission Electron Microscopy

WT and *Miga2* KO naive $CD4^+$ T cells were washed in PBS and fixed in 2.5% GA on ice for 15 min. Then the cells were scrapped and put into a 1.5 mL EP tube. The GA solution was refreshed and the cells were suspending and incubated at 4°C overnight. Then, the cells were embedded into agarose gel. The gel was cut into small pieces, washed in PBS and post-fixed in 1% Osmic acid for 1-2 h. Then the samples were washed in PBS and dehydrated in a series of gradient ethanol (50%, 75%, 85%, 95% and 100% ethanol), each for 15 min. Then the samples were embedded in Epon resin. Embedded samples were cut into 60 nm ultrathin sections. Sections were counterstained with uranyl acetate and lead citrate. All the samples were observed using a Hitachi HT7700 electron microscope.

CD4$^+$ T cell proliferation

Naive CD4$^+$ T cells were isolated from spleens and LNs of WT or *Miga2*^{TKO} mice. For CFSE dilution assay, T cells were labeled in 5 μM CFSE (Life Technologies) in 37°C and washed with PBS for 3 times. The cells were normalized and cultured in 96-well plates with plate-coated anti-CD3 (1 μg/mL) and anti-CD28 (1 μg/mL) for 48 and 72 h. Sorted T cells were analyzed by flow-cytometry using CytoFlex (Beckman Coulter).

Single cell dissociation

Artificial cerebrospinal fluid was prepared as following: αCSF, in mM: 87 NaCl, 2.5 KCl, 1.25 NaH2PO4, 26 NaHCO3, 75 sucrose, 20 glucoses, 1 $CaCl_2$, 7 $MgSO_4$, adjusted to pH 7.4, equilibrated in 95% O2 and 5% CO2. Mice were deeply anesthetized and perfused through the heart with cold αCSF prepared previously. The amygdala was collected after the brains were removed from the skull, and dissociated using Papain diluted in αCSF followed by manual trituration using pipettes. After 30 min enzymatic digestion at 37°C with shaking of the tube every 10 min, the suspensions were filtered through a αCSF-equilibrated 35 μm cell strainer. After filtering, the suspension was diluted in a large volume (50 mL total) ice-cold αCSF, followed by centrifugation (200 g, 5 min) to reduce debris. The supernatant was removed carefully and precipitated cells were resuspended in a minimal volume ice-cold DMEM containing 1% BSA. These suspensions were then carried out with 10x Genomics Chromium Single Cell Kit for Single-Cell RNA-seq. Importantly, αCSF equilibrated in 95% O25% CO2 was used in all steps for improved cell viability, and cells were kept on ice or at 4°C at all times except for enzymatic digestion.

Flow cytometry and intracellular cytokine staining

Spleen or lymph nodes were subjected to flow cytometry using CytoFlex (Beckman Coulter) and the following fluorescence-labeled antibodies from eBioscience: PB-conjugated anti-CD4; PE-conjugated anti-B220, anti-CD45 and anti-IL-17A; PerCP5.5-conjugated anti-CD8; APC-conjugated anti-CD3 and anti-CD62L; FITC-conjugated anti-CD44, anti-IFNγ and anti-Foxp3; APC-CY7-conjugated anti-CD11b.

For intracellular cytokine staining, T cells were stimulated with PMA (0.5 ug/mL) plus ionomycin (1 ug/mL) for 3 h and monensin (eBioscience, 1000X) for another 3 h, and then subjected to intracellular IFN-γ and IL-17A by flow cytometry analysis.

Amygdala was collected and digested into single cells as ''Single cell dissociation'' section in the method. Single cells were subjected to flow cytometry and the following fluorescence-labeled antibodies from Abcam: FITC-conjugated anti-AdorA1 (EPR6179); Alexa fluor 647-conjugated anti- myelin oligodendrocyte glycoprotein (MOG, EP4281) and Alexa fluor 568-conjugated anti-NeuN (EPR12763). c-FOS (ab208942), AdorA2A (ab3461), AdorA2B (ab222901) and AdorA3 (ab203298) were purchased from Abcam plc. Some antibodies were purchased from Biolegend: Brilliant violet 421-conjugated anti-GFAP (2E1.E9) and PE-CY7-conjugated anti-CX3CR1 (SA011F11).

Metabolic Assays

Naive CD4$^+$ T cells were first purified from the spleens and lymph nodes of 6 to 8-week-old mice by positive magnetic cell sorting. These CD4$^+$ T cells were further sorted on a FACS AriaII cell sorter (BD Biosciences) to obtain naive CD4$^+$ T cells (CD4$^+$CD44^{lo}CD62L^{hi}). The oxygen consumption rate (OCR) and extracellular acidification rate (ECAR) were measured in XFp extracellular flux analyzers (EFA) (Seahorse Bioscience) by using XFp Cell Mito Stress Test Kit and XFp Glycolysis Stress Test kit, respectively. The parameters used in the assays were: 8 × 10^4 seed cells per well, 1.0 μM oligomycin, 1.0 μM FCCP, 0.5 μM rotenone/antimycin A, 10 mM glucose, and 50 mM 2-DG, as indicated.

Isolation of oligodendrocytes

6 to 8-week-old WT, *Miga2*$^{-/-}$ and *Miga2*$^{-/-}$ plus αCD4 mice were sacrificed using CO_2. The single cell dissociations of two-side amygdala are collected as described in single cell dissociation section. Oligodendrocytes from adult mouse brains were purified by positive magnetic cell sorting (Anti-O4 MicroBeads, # 130-094-543, Miltenyi Biotec). Then, the resuspended cells were incubated with anti-Mouse CD16/CD32 (553141, BD PharMingen), and stained with Alexa Fluor647-conjugated anti-MOG (Ab199472). After washing, incubated cells were further sorted on a FACS AriaII cell sorter (BD Biosciences) to obtain purified MOG$^+$ cells. The sorted cells were washed with cold PBS and prepared for the following experiments.

Viral injection

The preparation of craniotomy is referred to the standard stereotaxic coordinates of 7-week-old B6 mice. AAV-MBP-GFP-miR30-shRNA(mAdoral) or AAV-MBP-GFP-miR30-shRNA(control) was constructed by Vigene Bioscience (Shandong, China) and injected into the left amygdala at 1E+11 v.g./mouse within 600 s via a pump. After recovery of the animal, the animal was fed as usual for 2 weeks. The expression of shRNA was measured based on the GFP level by FACS. These AAV-injected mice performed the open field-test two weeks after AAV injection.

LC-MS analysis for serum metabolome

The same amount of supernatant from each treated sample used as a QC sample. The blank sample was a matrix of the experimental sample, and the pretreatment process was the same as the experimental sample.LC separation was conducted on a Accucore HILIC

column with a Vanquish UHPLC system (Thermo). The mobile phase consisted of 0.1% formic acid and 10mM ammonium acetate in 95% acetonitrile (A) and 0.1% formic acid and 10mM ammonium acetate in 50% acetonitrile (B). The gradient program was as follows: 0–1 min, 98% A+2% B; 17–17.5 min, linear gradient to 50%A+50% B; 18–20 min, 98%A+2%B; flow rate, 0.3 mL/min. The column oven temperature was maintained at 40°C. The LC system was coupled with a triple-quadruple mass spectrometer QE HF-X (Thermo).

^{13}C tracing by liquid-chromatography Q-exactive mass spectrometry (LC–QEMS)

For ^{13}C tracing experiments, splenic naive CD4^{+} T cells isolated from WT or *Miga2*^{TKO} mice were cultured with [U6]–^{13}C glucose (Sigma-Aldrich) for 24 h. The cells were washed twice in saline and lysed in extraction solvent (80% methanol/water) for 30 min at –80°C. The supernatant extracts were analyzed by LC–QE-MS after centrifugation at 12000 g, 10 min at 4°C. Liquid chromatography was performed using an HPLC (Ultimate 3000 UHPLC) system (Thermo) with an xbridge amide column (100 × 2.1 mm i.d., 3.5 μm; Waters). Mobile phase A was 20 mM ammonium acetate and 15 mM ammonium hydroxide in water with 3% acetonitrile, pH 9.0, and mobile phase B was acetonitrile. The linear gradient was as follows: 0 min, 85% B; 1.5 min, 85% B; 5.5 min, 30% B; 8 min, 30% B, 10 min, 85% B, and 12 min, 85% B. The flow rate was 0.2 mL/min. Sample volumes of 5 μL were injected for LC-MS analysis.

qRT-PCR

For qRT-PCR, total RNA was isolated using TRI reagent (Molecular Research Center, Inc.) and subjected to cDNA synthesis using RNase H-reverse transcriptase (Invitrogen) and oligo (dT) primers. qRT-PCR was performed in triplicates, using iCycler Sequence Detection System (Bio-Rad) and iQTM SYBR Green Supermix (Bio-Rad). The expression of individual genes was calculated by a standard curve method and normalized to the expression of *Actb*. The gene-specific PCR primers (all for mouse genes) are shown in Table S8.

Immunoblot (IB)

Whole-cell lysates or subcellular extracts were prepared as previous described(Uhlik et al., 1998). The samples were resolved by 8.25% SDS–PAGE. After electrophoresis, separated proteins were transferred onto polyvinylidene difluoride membrane (Millipore). For immunoblotting, the polyvinylidene difluoride membrane was blocked with 5% non-fat milk. After incubation with specific primary antibody, horseradish peroxidase-conjugated secondary antibody was applied. The positive immune reactive signal was detected by ECL (Amersham Biosciences).

Chromatin IP (ChIP) assay

ChIP assays were performed with naive T cells (5 × 10^{6}), which were fixed with 1% formaldehyde and sonicated. Lysates were subjected to IP with the IRF-1 antibodies (M-20, Santa Cruz), and the precipitated DNA was then purified by Qiaquick columns (QIAGEN) and quantified by QPCR using pairs of primers that amplify the potential target regions of the *Ada*, *Pnp2* or *Xdh* promoter. The precipitated DNA is presented as percentage of the total input DNA. The gene-specific primers are shown in Table S8.

Tissue staining/IHC

Brain were collected at the indicated time course of each figure legend. After deeply anesthetized, animals were perfused through the heart with 4% paraformaldehyde in PBS. Then brains were removed from the skull, fixed overnight in 4% PFA, and then dehydration in 30% sucrose in PBS solution for 48 h until sunk to the bottom. H&E and Nissl staining of Brain coronal section were performed by Servicebio Biotechnology Co., Ltd (China). For immunohistochemistry, the sections were pre-treated using heat mediated antigen retrieval with sodium citrate buffer and blocked with 5% bovine serum albumin. The sections were stained overnight with antibodies against following: Alexa Fluor 647-conjugated anti-Myelin oligodendrocyte glycoprotein; Alexa Fluor 488-conjugated anti-Adenosine A1 Receptor; Alexa Fluor 568-conjugated anti-NeuN. All antibodies were diluted in TBS contain 0.025% Triton X-100. Samples were further stained with DAPI for 15 min and mounted before image acquisition. Images were captured using the Vectra microscope(PerkinElmer).

In vivo BrdU proliferation assay

8-week-old C57BL/6 mice were injected intraperitoneally with 2mg BrdU (Sangon, E607203) in PBS. After 72 h, mice received an intracardiac perfusion with PBS to remove erythrocytes. The amygdala was collected and dissociated as described in in single cell dissociation section. O4^{+} cells were purified with anti-O4 microbeads (Mitenyi, 130-094-543). After that, oligodendrocytes were isolated with Aria II based on the surface marker MOG. For BrdU staining, the purified cells were fixed with 70% ethanol for 30 min, denatured for 30 min with 2M HCl, neutralized for 10 min with 0.1M borate buffer, then washed with PBS three times before anti-BrdU (1:100, BD, 558599) and 7-AAD (1:50, BD, 559925) staining. Samples were acquired using flow cytometer (Beckman CytoFLEX), and the data were analyzed with FlowJo.

QUANTIFICATION AND STATISTICAL ANALYSIS

Statistical analysis was performed using Prism software. For two-group comparison, two-tailed unpaired t tests were performed, and P values less than 0.05 were considered significant. The level of significance was indicated as $*p < 0.05$, $**p < 0.01$, $***p < 0.005$.

For multiple group comparison, Dunnett's multiple comparison test (one-way ANOVA) was performed, and P values less than 0.05 were considered significant. The Gehan-Breslow-Wilcoxon test was used for the animal survival assay. In the EAE model, the clinical scores were analyzed by Sidak's multiple comparison test (two-way ANOVA) with 90% power and a significance level of 5%. P values less than 0.05 were considered significant, and the level of significance was indicated as $*p < 0.05$, $**p < 0.01$, $***p < 0.005$.

All statistical tests are justified as appropriate, and data meet the assumptions of the tests. The groups being statistically compared show similar variance.

DATA AND CODE AVAILABILITY

The accession number for the RNAseq and single cell transcriptome data reported in this paper is [GenBank-Bioproject]: [PRJNA528163].

Supplemental Figures

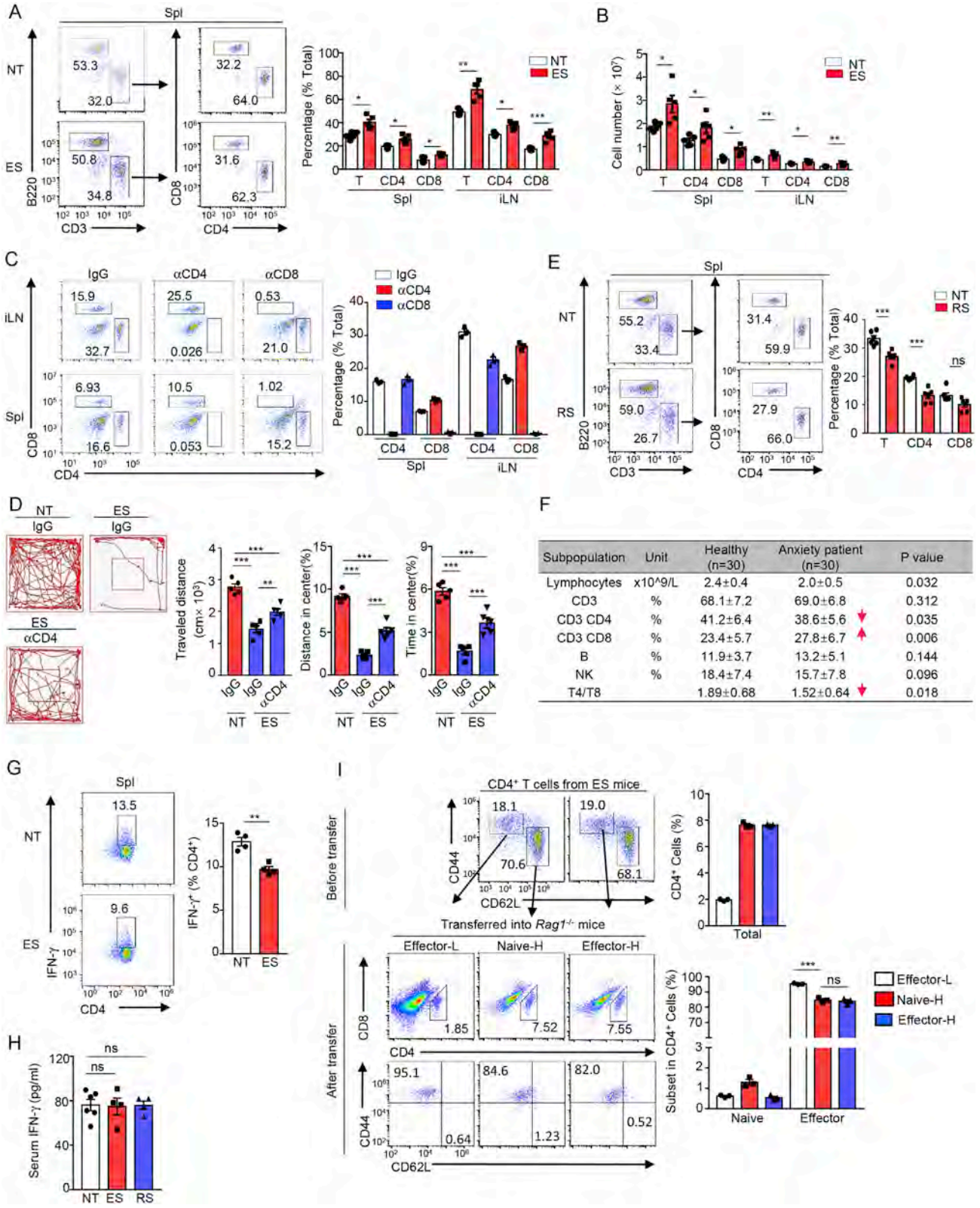

Subpopulation	Unit	Healthy (n=30)	Anxiety patient (n=30)	P value
Lymphocytes	x10^9/L	2.4±0.4	2.0±0.5	0.032
CD3	%	68.1±7.2	69.0±6.8	0.312
CD3 CD4	%	41.2±6.4	38.6±5.6 ↓	0.035
CD3 CD8	%	23.4±5.7	27.8±6.7 ↑	0.006
B	%	11.9±3.7	13.2±5.1	0.144
NK	%	18.4±7.4	15.7±7.8	0.096
T4/T8		1.89±0.68	1.52±0.64 ↓	0.018

(legend on next page)

Figure S1. $CD4^+$ T Cells are Affected by Stress-Induced Anxiety, Related to Figure 1

(**A-B**) Flow cytometry analysis of the frequency (**A**) and absolute numbers (**B**) of different T cell populations in the spleen (Spl) and inguinal lymph node (iLN) of NT or ES-treated mice (n = 5) on day 8. (**C**) Flow cytometry analysis of the frequency of different immune cells in the Spl and iLN of ES-treated mice, which were pretreated with isotype IgG, anti-CD4 (αCD4) or anti-CD8 (αCD8) as described in major Figures 1A (n = 3). (**D**) WT mice were induced anxiety by chronic ES treatment for continuous 28 days. These mice were administrated with isotype IgG or anti-CD4 (αCD4) (500 μg/mice) on day 21 and 28. Representative tracks and statistic results in open-field test (OFT) of NT and chronic ES mice on day 30 (n = 5). (**E**) Flow cytometry analysis of the frequency of T cell populations in the Spl of NT or restraint stress (RS)-treated mice on day 8 (n = 6). (**F**) The table showing the frequency of lymphocytes subpopulation in 18-65 years old patient with anxiety and healthy control by FACS analysis (n = 30). (**G**) $CD4^+$ T cells were isolated from the spleen of of 6-weeks-old NT and ES mice, and incubated with monensin (1ug/mL) for 4 h before harvest. Flow cytometric analysis of the percentage of IFN-γ- and IL-17-producing $CD4^+$ T cells (n = 4). (**H**) ELISA assay to determine the levels of IFN-γ and IL-17A in serum from NT (n = 6), ES (n = 4) and RS (n = 4) mice on day 8 after inducing anxiety models. (**I**) *Rag1*$^{-/-}$ mice were adoptively transferred with 1.8×10^6 effector (Effector-L), 6×10^6 naive (Naive-H) and 6×10^6 effector (Effector-H) $CD4^+$ T cells isolated from ES-treated mice for every three day. Flow cytometry analysis of the frequency and activated status of $CD4^+$ in the spleen of recipient *Rag1*$^{-/-}$ mice on day 8 (n = 3). All data are representative of at least three independent experiments. Data are represented as means ± SEM. The significance of difference in (**H**) was determined by Dunnett's multiple comparisons test. The significances of differences in all two group comparisons were determined by two-tailed Student's t test. *$p < 0.05$; **$p < 0.01$; ***$p < 0.005$.

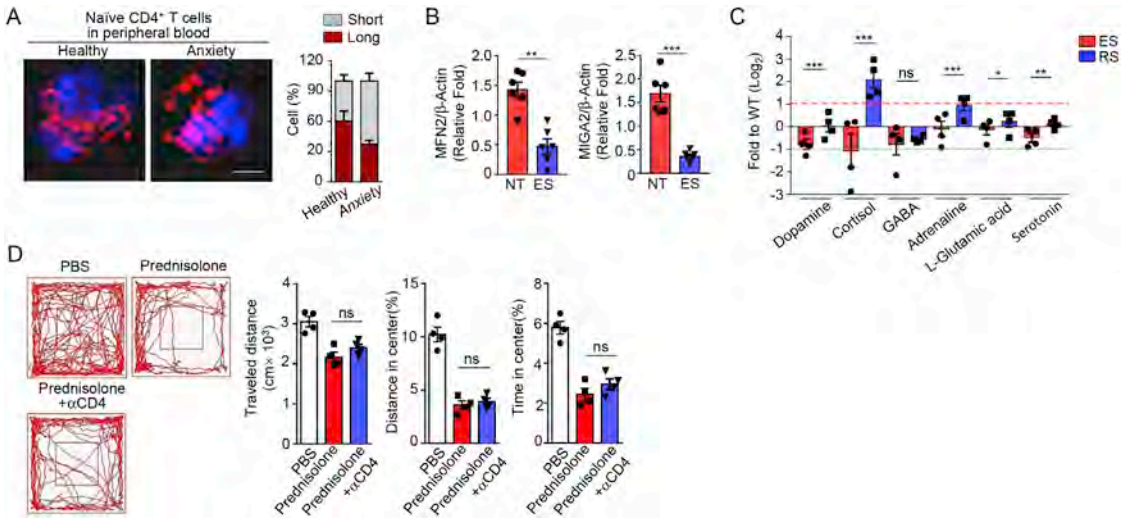

Figure S2. Mitochondrial Fission in CD4$^+$ T Cells is Associated with the Anxiety Symptom, Related to Figure 2

(**A**) Naive CD4$^+$ T cells (CD4$^+$CD44^{lo}) in peripheral blood from patients with anxiety and healthy control were isolated by FACS sorter (n = 4). Mitochondrial morphology of these naive CD4$^+$ T cells was visualized using MitospyTM Orange CMTMRos staining. Representative confocal images are shown, as well as length quantification with Image-Pro. Data are shown as the mean ± SEM of three independent experiments with 50 cells counted for each replicate; Colors indicate the morphology of the mitochondria (long, brown > 7 μm or short, gray < 7 μm). Bar, 5 μm. (**B**) Immuno-blot (IB) analyses of MIGA2 and MFN2 in the splenic naive CD4$^+$ T cells from three individual NT or ES-treated mice. #1, repeat 1; #2, repeat 2; #3, repeat 3. The relative density of these IB assay were evaluated by ImageJ. (**C**) LC-MS of indicated neurotransmitters and hormones in the serum of NT, ES-treated and RS treated mice, presented relative to the mean value for NT mice (n = 4). (**D**) WT mice were i.p. injected with prednisolone (50 mg/kg) every other day within 21 days. Anxiety-like behavior of these mice was assessed as traveled distance, percentage of distance and percentage of time spent in center area in OFT on day 22 (n = 4). All data are representative of at least three independent experiments. Data are represented as means ± SEM. The significances of differences were determined by two-tailed Student's t test. *p < 0.05; **p < 0.01; ***p < 0.005.

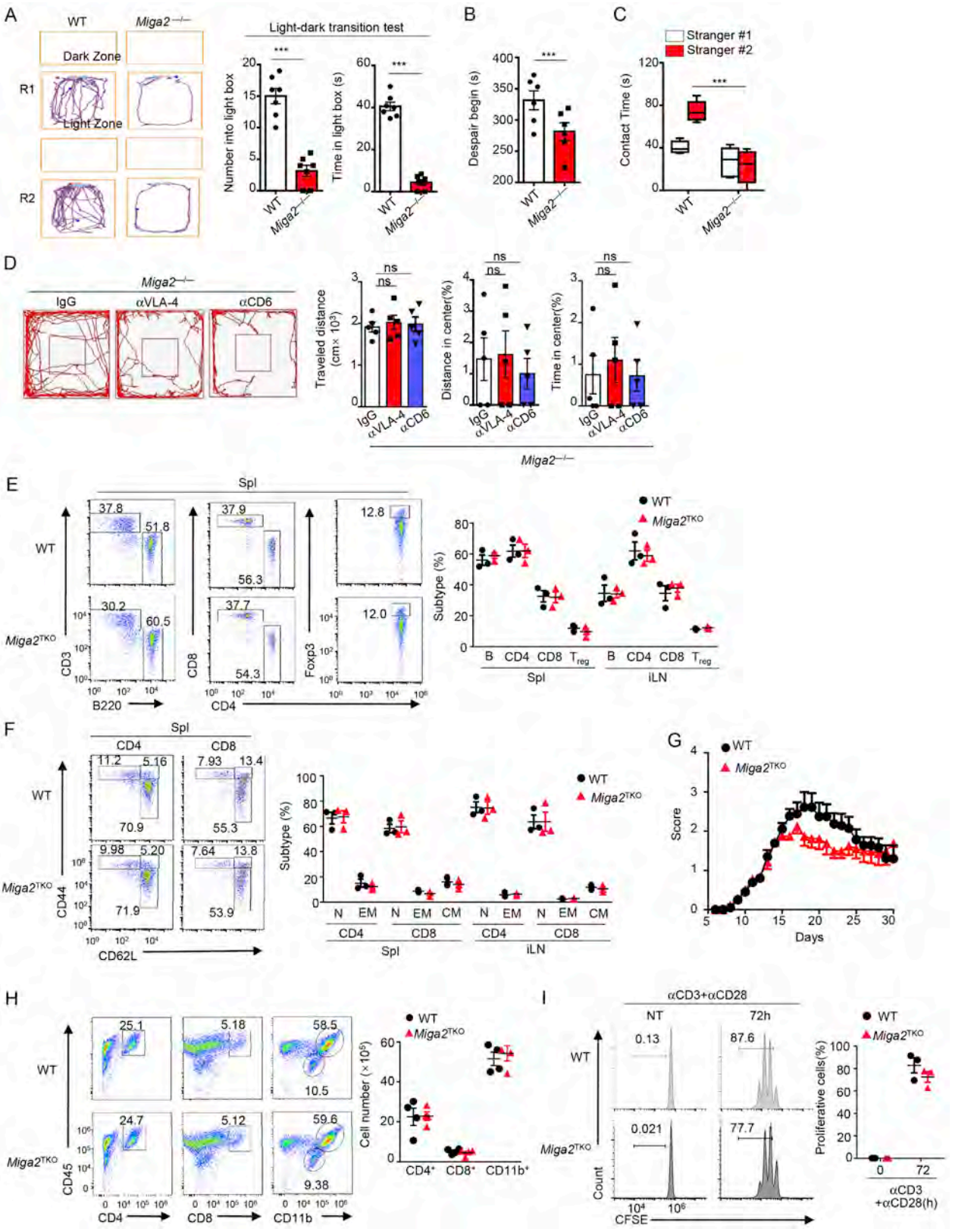

(legend on next page)

Figure S3. *Miga2*$^{-/-}$ Mice Performed Various Psychological Disorders, but Not CNS Inflammation, Related to Figure 3

(**A**) Representative tracks of 8-weeks-old WT and *Miga2*$^{-/-}$ mice in the light compartment, as well as transition numbers and the time spent in the light compartment (n = 7). (**B**) The time of immobility in the tail suspension test was record for WT and *Miga2*$^{-/-}$ mice (n = 6). (**C**) In the social novelty task, the contact time with Stranger 1 and Stranger 2 chambers of the WT and *Miga2*$^{-/-}$ mice are shown. (**D**) *Miga2*$^{-/-}$ mice were i.v. injected with anti-VLA-4 (αVLA-4, 20mg/kg) or anti-CD6 (αCD6, 10mg/kg) for every three days, and then evaluated anxiety-like behavior by open-field test on day 8 (n = 5). (**E**) Flow cytometry analysis of the frequencies of different lymphocytes in the spl of 6-8 weeks-old WT or *Miga2*^{TKO} mice (n = 3). Data all panels are presented as representative FACS plots. B cell is defined as $CD3^{-}B220^{+}$; $CD4^{+}$ T cell (CD4) is defined as $CD3^{+}B220^{-}CD4^{+}$; $CD8^{+}$ T cell (CD8) is defined as $CD3^{+}B220^{-}CD8^{+}$; regulatory T cell (Treg) is defined as $CD3^{+}B220^{-}CD4^{+}Foxp3^{+}$. (**F**) Flow cytometry analysis of naive and memory T cells in the Spl of WT or *Miga2*^{TKO} mice (n = 3). Naive T cell (N) is defined as $CD44^{lo}CD62L^{hi}$; Effector memory (EM) T cell is defined as $CD44^{lo}CD62L^{lo}$; Effector memory (EM) T cell is defined as $CD44^{hi}CD62L^{lo}$; Central memory (CM) T cell is defined as $CD44^{hi}CD62L^{hi}$. (**A**) Mean clinical scores of 6-8 weeks-old WT and *Miga2*^{TKO} mice subjected to MOG_{35-55}-induced experimental autoimmune encephalomyelitis (EAE) (n = 10/group). (**H**) Flow cytometry analysis of the immune cell infiltration into the CNS (brain and spinal cord) of EAE mice (n = 4, day 14 post-immunization). (**I**) Naive $CD4^{+}$ T cells ($CD44^{lo}CD62L^{hi}$) were isolated from the spleen of WT and *Miga2*^{TKO} mice by FACS sorter. These T cells were labeled with 5 μM Carboxyfluorescein succinimidyl ester (CFSE), and stimulated with αCD3 (1 μg/mL)/αCD28 (1 μg/mL) for 72 h. The proliferative ratio was assessed as CFSE dilution by FACS. All data are representative of at least three independent experiments. Data are represented as means ± SEM. The significances of differences in comparisons were determined by two-tailed Student's t test. ns, no significance; ***$p < 0.005$.

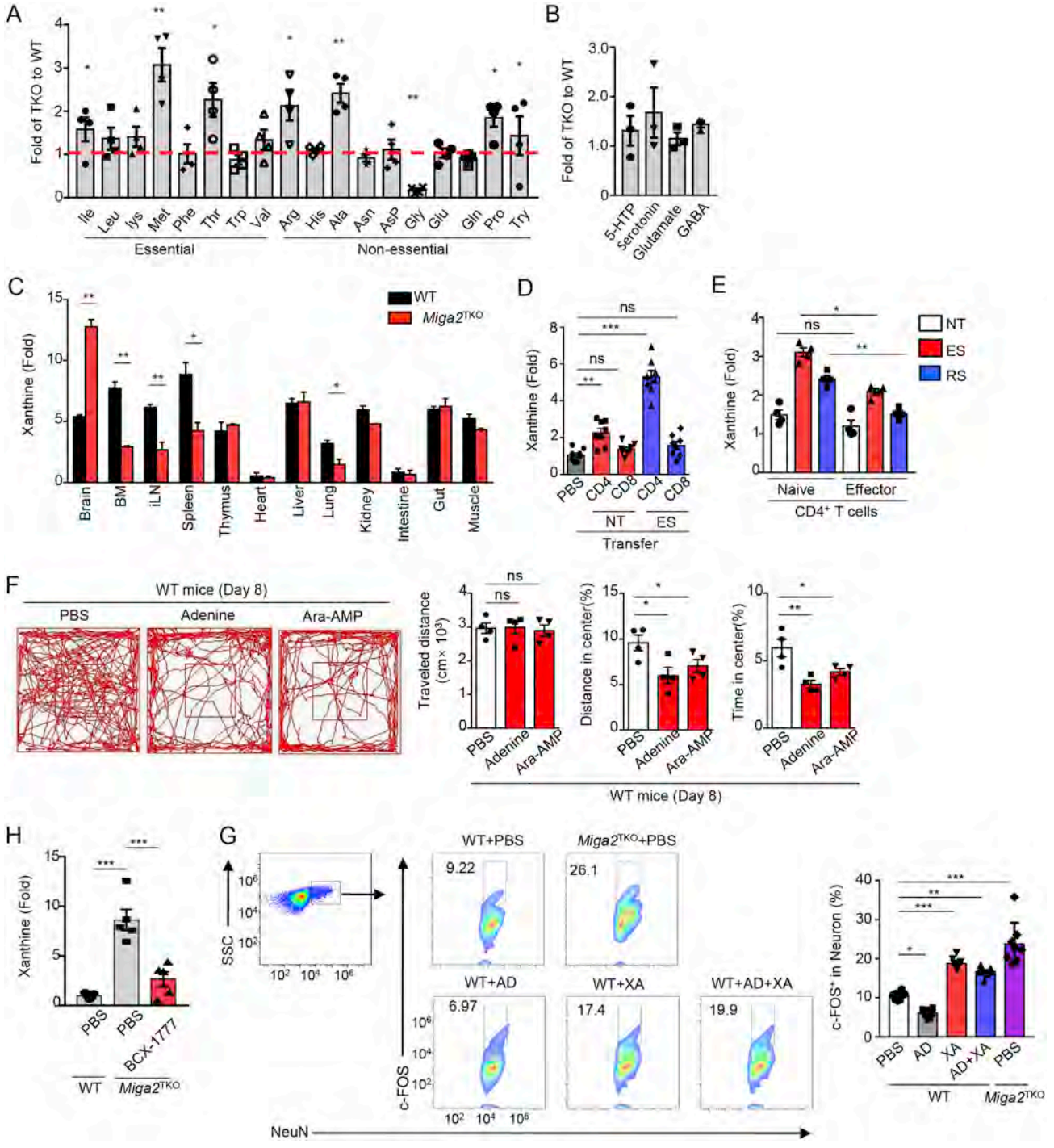

Figure S4. CNS-Enriched Xanthine Causes Anxiety-like Behavior Abnormality, Related to Figure 4

(**A-B**) The essential and non-essential amino acids (**A**) or the neurotransmitters derived from amino acids (**B**) in the serum were measured by PLS-DA and presented as the ratio of the abundance in *Miga2*^{TKO} mice to those in WT mice (n = 4). (**C**) ELISA assay of xanthine in the different organs of WT and *Miga2*^{TKO} mice are presented as relative fold to those in the heart of *Miga2*^{TKO} mice (n = 4). (**D**) *Rag1*$^{-/-}$ mice were i.v. adoptively transferred with 5 × 10^6 CD4$^+$ or CD8$^+$ T cells isolated from NT or ES-treated mice (donor) for every three days. Xanthine in the serum of recipient mice was measured by ELISA. The relative fold is to serum xanthine concentration of *Rag1*$^{-/-}$ control that treated with PBS. (**E**) 4 × 10^6 purified effector or naive CD4$^+$ T cells were isolated from ES or RS-treated mice as previous described. These CD4$^+$ T cells were cultured in 500 μL medium *in vitro*, and the supernatants were collected after 24 h. Xanthine was measured by ELISA and presented as relative folds to that of effector group from NT mice. (**F**) WT mice were i.p. injected with Adenine and its derivatives (500 mg/kg) for three times in every three days. Anxiety-like behavior of these mice was assessed as traveled distance, percentage of distance and percentage of time spent in center area in

(legend continued on next page)

OFT on day 8 (n = 4). (**G**) WT mice were injected i.p. with adenine (AD) or xanthine (XA) as indicated. *Miga2*^{TKO} mice were injected i.p. with PBS alone. Flow cytometry analysis of c-FOS^{+} cells gating with NeuN^{+} cells in the amygdala (n = 7). (**H**) *Miga2*^{TKO} mice were i.p. injected with BCX-1777 as described in major Figure 4I. The abundance of xanthine in serum of BCX-1777-treated *Miga2*^{TKO} mice was measured by ELISA and presented as the relative fold to that in PBS-treated group. All data are representative of at least three independent experiments. Data are represented as means ± SEM. The significance of difference in **D**-**G** was determined by Dunnett's multiple comparisons test. The significances of differences in all other two group comparisons were determined by two-tailed Student's t test. *$p < 0.05$; **$p < 0.01$; ***$p < 0.005$.

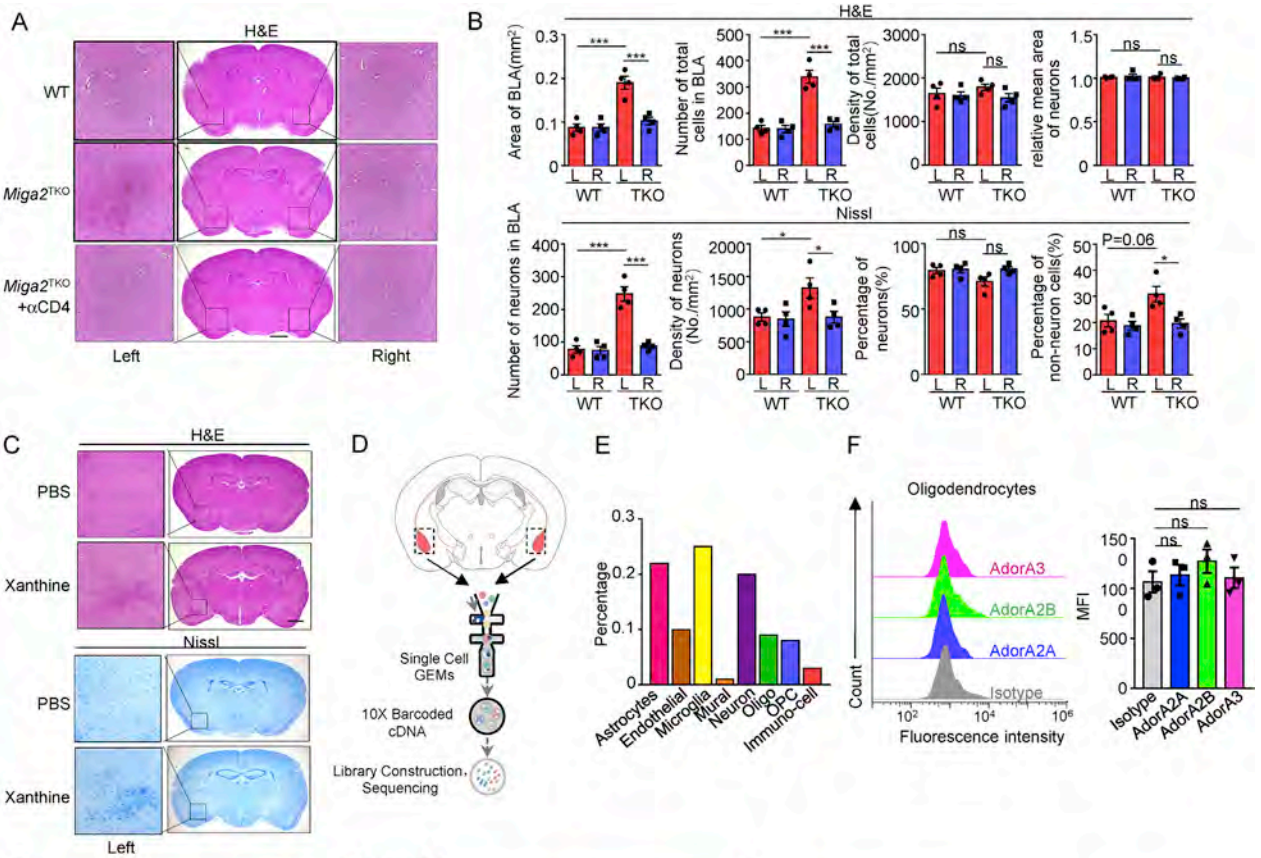

(legend continued on next page)

Figure S5. The Absence of *Miga2* or Xanthine Causes Pathological Symptoms by Directly Acting on Oligodendrocytes the Left Amygdala, Related to Figure 5

(**A**) Histological analysis of the whole brain from WT, *Miga2*^{2TKO} and CD4^{+} T cell-depleting *Miga2*^{TKO} mice was performed by H&E staining. Scale bar, 100 μm. (**B**) The statistical results of histological analysis in Figure 5A and Figure S7A were analyzed by Tissue FAXS System (TissueGnostics, AT), and presented as indication (n = 4). (**C**) Histological analysis of the amygdala was performed by H&E and nissl staining, when WT mice were injected with synthetic xanthine as described in Figure 4H. Scale bar, 100 μm. (**D**) Schematic showing the single-cell RNA sequencing (scRNA-seq) workflow. (**E**) The percentage of nine major clusters of cell types in the amygdala of WT mice revealed by scRNA-seq. (**F**) Flow cytometry analyses of AdorA2A^{+}, AdorA2B^{+} and AdorA3^{+} cells gating with MOG^{+} cells in the amygdala of WT mice (n = 3). Oligodendrocytes (Oligo) are defined as MOG^{+}. (**G**) Representative image of FITC-AdorA1 (Green), APC-MOG (Purple), PE-NeuN (Red) and DAPI (Blue) staining in mouse amygdala sections from *Miga2*$^{-/-}$ and αCD4-treated *Miga2*$^{-/-}$ mice. The scale bar is 5 μm. (**H**) The transcriptomes of astrocytes, microglia or oligodendrocytes in the amygdala were clustered among the WT, *Miga2*$^{-/-}$ (KO) and KO plus αCD4 groups. Heatmap showing the DEGs determined by scRNA-seq data. (**I**) The specific DEGs in oligodendrocytes of KO group were collected compared to those of WT and KO treated with αCD4 groups. KEGG analysis of these DEGs in indicated pathway that differ significantly (in abundance). (**J**) WT mice were injected intravenously injection of 2 mg BrdU together with AD or XA as indicated. 72 h later, purified oligodendrocytes were stained with anti-BrdU antibody and propidium iodide (PI). (**K**) Myelin oligodendrocyte glycoprotein (MOG) positive cells were isolated from the amygdala of 6-8 weeks WT, KO and KO treated with αCD4 mice by FACS sorter. PKA activity was monitored via the level of p-PKA subtracts by IB assay. Except panel D, other data are representative of at least three independent experiments. Data are represented as means ± SEM. The significances of differences were determined by Dunnett's multiple comparisons test. ns, no significance; *p < 0.05; **p < 0.01; ***p < 0.005.

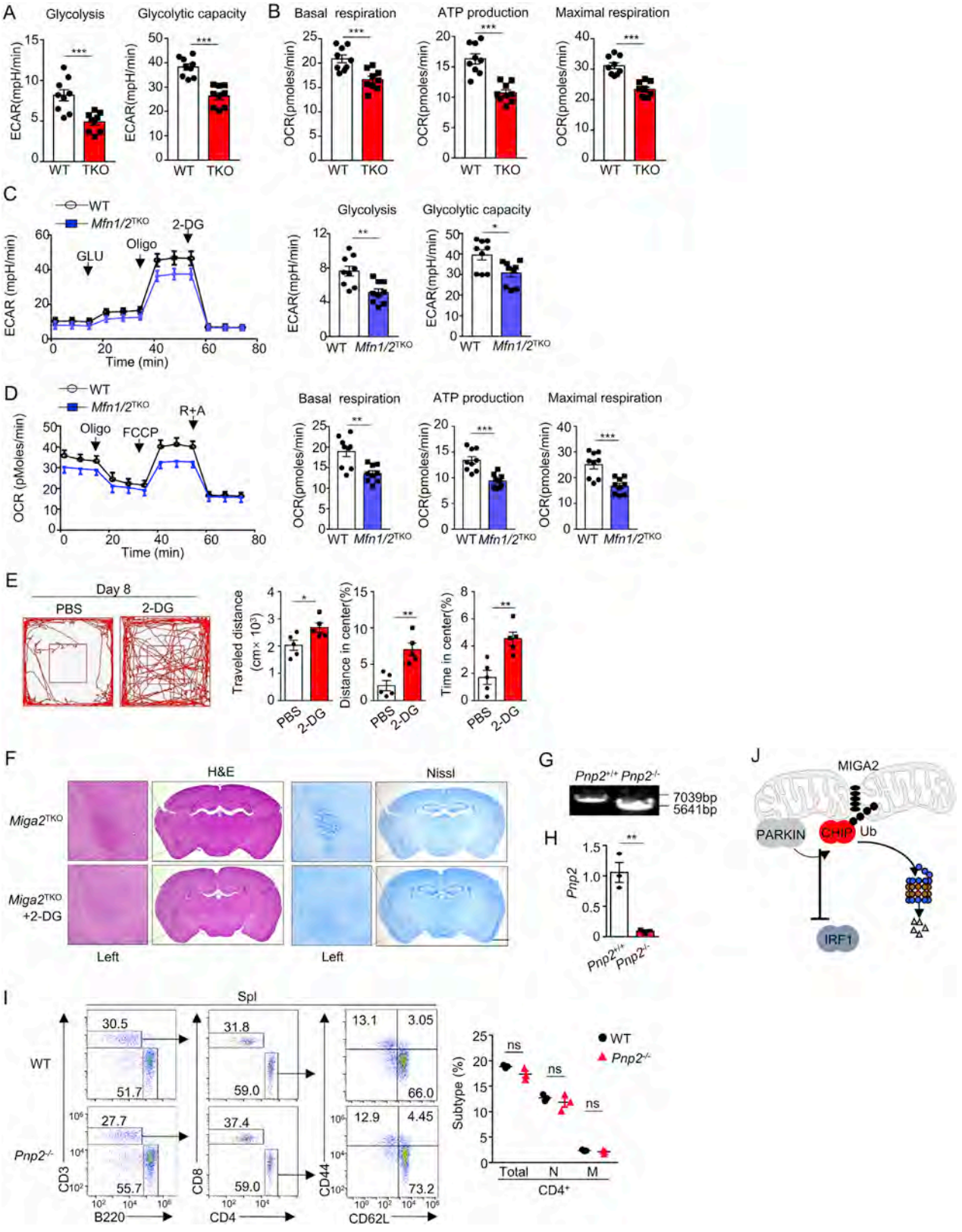

(legend on next page)

Figure S6. Mitochondrial Fission in CD4$^+$ T Cells Promotes Purine Synthesis, Related to Figure 6

(**A-B**) Mitochondrial fitness tests were used to compare ECAR (**A**) and OCR (**B**) of WT and *Miga2*^{TKO} (TKO) CD4$^+$ T cells (n = 9). The statistic results of major figure 6a were presented as bar graph. (**C-D**) Mitochondrial fitness tests were measured by ECAR (**C**) and OCR (**D**) of CD4$^+$ T cells isolated from WT and *Mfn1/2*^{TKO} mice (n = 9). The statistic results were presented as bar graph. (**E**) *Miga2*^{TKO} mice were i.p. injected with 2-Deoxy-D-glucose (2-DG) (500 mg/kg) for three times in every three days. Anxiety-like behavior of these mice was assessed as traveled distance, percentage of distance and percentage of time spent in center area in open-field test on day 8 (n = 5). (**F**) Histological analysis of the whole brain section from *Miga*^{2TKO} and 2-DG-treated *Miga2*^{TKO} mice described as above was performed by H&E and Nissl staining. Scale bar, 100 μm. (**G**) *Pnp2*$^{-/-}$ genotyping PCR. PCR was performed to detect the WT and *Pnp2* depletion alleles (with primers described in Table S7). (**H**) QPCR assay showing ablation of *Pnp2* in the CD4$^+$ T cells of *Pnp2*$^{-/-}$ mice. These qPCR data were presented as fold relative to the *Actb* mRNA level and normalized by Bio-Rad CFX Manager 3.1. (**I**) Flow cytometry analysis of the frequencies of different lymphocytes in the spl of 6-8 weeks-old WT or *Pnp2*$^{-/-}$ mice (n = 3). All panels are presented as representative FACS plots. The statics analysis was performed as plot graph. (**J**) A signal transduction model of mitochondrial fission in promoting IRF-1 stability. All data are representative of at least three independent experiments. Data are represented as means ± SEM. The significances of differences in two group comparisons were determined by two-tailed Student's t test. *$p < 0.05$; **$p < 0.01$; ***$p < 0.005$.

Neuropharmacology 167 (2020) 107930

Contents lists available at ScienceDirect

Neuropharmacology

journal homepage: www.elsevier.com/locate/neuropharm

Effects of single-dose antipurinergic therapy on behavioral and molecular alterations in the valproic acid-induced animal model of autism

Mauro Mozael Hirsch[a,b,c,**], Iohanna Deckmann[a,b,c], Júlio Santos-Terra[a,b,c], Gabriela Zanotto Staevie[a,b,c], Mellanie Fontes-Dutra[a,b,c], Giovanna Carello-Collar[a,b,c], Marília Körbes-Rockenbach[a,b,c], Gustavo Brum Schwingel[a,b,c], Guilherme Bauer-Negrini[a,b,c], Bruna Rabelo[a,b,c], Maria Carolina Bittencourt Gonçalves[d], Juliana Corrêa-Velloso[d], Yahaira Naaldijk[d], Ana Regina Geciauskas Castillo[d], Tomasz Schneider[f], Victorio Bambini-Junior[a,c,e,g], Henning Ulrich[d,g], Carmem Gottfried[a,b,c,g,*]

[a] Translational Research Group in Autism Spectrum Disorders-GETTEA, Universidade Federal do Rio Grande do Sul (UFRGS), Rua Ramiro Barcelos, 2600, 90035-003, Porto Alegre, RS, Brazil
[b] Department of Biochemistry, Universidade Federal do Rio Grande do Sul (UFRGS), Ramiro Barcelos Street, 2600, 90035-003, Porto Alegre, RS, Brazil
[c] National Institute of Science and Technology on Neuroimmunomodulation (INCT-NIM), Avenida Brasil, 4365, Manguinhos, 21045-900, Rio de Janeiro, RJ, Brazil
[d] Department of Biochemistry, Institute of Chemistry, Universidade de São Paulo (USP), Avenida Professor Lineu Prestes , 748, 05508-000, Vila Universitária, São Paulo, SP, Brazil
[e] School of Pharmacy and Biomedical Sciences, University of Central Lancashire, PR1 2HE, Lancashire, Preston, England, UK
[f] School of Medicine, Pharmacy and Health, Durham University, Durham, DH1, UK
[g] Autism Wellbeing And Research Development (AWARD) Institute, University of Central Lancashire, PR1 2HE, Lancashire, Preston, England, UK

HIGHLIGHTS

- ASD is characterized by deficits in sociability, sensory processing and by stereotypical behaviors.
- Purinergic signaling plays an important role in modulating these behaviors.
- Animals prenatally exposed to VPA showed purinergic-related molecular alterations.
- Suramin rescued ASD-like impairments in the VPA-animal model.
- Cytokine and purinergic signaling cross-talk are likely to modulate ASD features.

ARTICLE INFO

Keywords:
Autism
Animal behavior
Purinergic system
Suramin
Valproate

ABSTRACT

Autism spectrum disorder (ASD) is characterized by deficits in communication and social interaction, restricted interests, and stereotyped behavior. Environmental factors, such as prenatal exposure to valproic acid (VPA), may contribute to the increased risk of ASD. Since disturbed functioning of the purinergic signaling system has been associated with the onset of ASD and used as a potential therapeutic target for ASD in both clinical and preclinical studies, we analyzed the effects of suramin, a non-selective purinergic antagonist, on behavioral, molecular and immunological in an animal model of autism induced by prenatal exposure to VPA. Treatment with suramin (20 mg/kg, intraperitoneal) restored sociability in the three-chamber apparatus and decreased anxiety measured by elevated plus maze apparatus, but had no impact on decreased reciprocal social interactions or higher nociceptive threshold in VPA rats. Suramin treatment did not affect VPA-induced upregulation of P2X4 and P2Y2 receptor expression in the hippocampus, and P2X4 receptor expression in the medial prefrontal cortex, but normalized an increased level of interleukin 6 (IL-6). Our results suggest an important role of purinergic signaling modulation in behavioral, molecular, and immunological aberrations described in VPA model, and indicate that the purinergic signaling system might be a potential target for pharmacotherapy in preclinical studies of ASD.

* Corresponding author. Departamento de Bioquímica, ICBS, Universidade Federal do Rio Grande do Sul, Ramiro Barcelos 2600 – 21111, CEP: 90035-003, Porto Alegre, RS, Brazil.
** Corresponding author. Departamento de Bioquímica, ICBS, Universidade Federal do Rio Grande do Sul, Ramiro Barcelos 2600 – 21111, CEP: 90035-00, Porto Alegre, RS, Brazil.
E-mail addresses: mauromhirsch@gmail.com (M.M. Hirsch), cgottfried@ufrgs.br (C. Gottfried).

https://doi.org/10.1016/j.neuropharm.2019.107930
Received 3 September 2019; Received in revised form 23 December 2019; Accepted 26 December 2019
Available online 02 January 2020
0028-3908/

1. Introduction

Autism Spectrum Disorder (ASD) is a neurodevelopmental disorder characterized by impairments in communication and social interaction and repetitive or stereotyped behaviors (American Psychiatric Association, 2013). In the last years, the prevalence of ASD had a strong elevation (1:59 live births according to the most recent data from USA) (Baio et al., 2018), explained only in part by the changes in diagnostic parameters of DSM-5, demonstrating the necessity to expand studies in order to understand the pathways and possible risk factors involved in this disorder. Although the etiology is still unclear, it is already known that genetic and environmental factors are determinant for shaping the heterogeneous phenotypes exhibited by individuals with ASD (Chaste and Leboyer, 2012). The inflammatory dysregulation might appear as a potential etiological factor in neurodevelopmental disorders (Boulanger-Bertolus et al., 2018), such as ASD (Elias et al., 2015). Several studies demonstrated that the use of valproic acid (VPA) - an anticonvulsant drug widely used in the treatment of epilepsy, migraine and mood instabilities - during pregnancy, especially in the first trimester, can significantly increase the risk of developing autism (Christensen et al., 2013; Williams et al., 2001).

Prenatal exposure to VPA is one of the best characterized rodent models of autism with strong construct, face, and predictive validity (Mabunga et al., 2015; Roullet et al., 2013). Male offspring of dams injected with VPA on E12.5 show autistic-like brain abnormalities and a plethora of behavioral aberrations including decreased social behavior (Bambini-Junior et al., 2011), hyperactivity and stereotypies (Schneider and Przewłocki, 2005), increased anxiety, lower sensitivity to pain and diminished acoustic prepulse inhibition (Schneider and Przewłocki, 2005), resembling both core symptoms (Schneider and Przewłocki, 2005) and the most significant neurobehavioral derangements observed in autism (Fontes-Dutra et al., 2018; Lin et al., 2013; Markram et al., 2008). VPA offspring show also molecular and immunological aberrations including altered functioning of opioidergic (Schneider et al., 2007), serotonergic (Tsujino et al., 2007), dopaminergic (Nakasato et al., 2008), GABAergic (Robertson et al., 2016) and glutamatergic (Horder et al., 2018) signaling systems, decreased cellular immunity (Gottfried et al., 2015), electrophysiological impairments (Gogolla et al., 2009) and cytoarchitecture disruptions (Casanova et al., 2002; Fontes-Dutra et al., 2018; Hutsler and Casanova, 2016). Thus, it became necessary to understand how VPA induces developmental alterations that lead to ASD analyzing, for example, modulation of different components of synaptic transmission, like purinergic signaling.

Several studies have demonstrated mitochondrial dysfunctions in ASD (Filipek et al., 2003; Patowary et al., 2017). This impairment of mitochondrial energetic metabolism and consequent increase in extracellular ATP levels (Faas et al., 2017) leads to the onset of inflammatory processes via purinergic signaling, suggesting that this system may be involved in the etiology of ASD. Experimental evidence indicate the participation of ATP-activated P2X and P2Y purinergic receptors in embryonic brain development as well as in adult neurogenesis for maintenance of normal brain functions (Glaser et al., 2013; Oliveira and Ulrich, 2016; Ulrich et al., 2012) and alterations in this context have been already related to psychiatric disorders, like autism (Cheffer et al., 2018). Previous studies demonstrated that suramin, a non-selective inhibitor of the purinergic P2 receptors and ectonucleotidases has therapeutic effects on autistic-like behaviors in the animal model of autism through maternal immune activation (MIA) (Naviaux et al., 2014, 2013). Experimental evidence indicate that purinergic signaling could prevent behavioral changes in this animal model, which seem to be related with elevated levels of interleukin 6 (IL-6) (Smith et al., 2007). Interestingly, the Naviaux's group recently demonstrated in a small, phase I/II, randomized clinical trial that a single intravenous dose of suramin was associated with improved scores for language, social interaction, and decreased restricted or repetitive behaviors. The five children who received placebo had no improvements these parameters (Naviaux et al., 2017). However, it is still unclear how the inflammatory response and the purinergic signaling is being modulated by both prenatal effect by VPA and post-natal treatment with the anti-purinergic suramin.

Based on these previous findings, the aim of this work was to evaluate the therapeutic effects of suramin on different behavioral pattern of an animal model of autism induced by prenatal exposure to VPA and elucidate the role of purinergic signaling on inflammatory responses in the context of autism.

2. Methods

2.1. Animals and ethics

Wistar rats obtained from the local breeding colony (ICBS-Federal University of Rio Grande do Sul) were maintained under standard laboratory conditions. The animals were mated overnight, and when pregnancy was established by the presence of spermatozoa in the vaginal smear, this day was considered the zero embryonic day (E0). The offspring was weaned at postnatal day 21 (P21) and only male animals were used in this study (Bambini-Junior et al., 2011). This project was approved by the local animal ethics committee (CEUA-UFRGS 23884) and all procedures were approved by the Institutional Ethics Committee on Animal Use in accordance with Brazilian Law 11794/2008 (Arouca Law) and National Institutes of Health guide for the care and use of Laboratory animals (NIH Publications No. 8023).

2.2. Treatments

Valproic acid (sodium valproate, Sigma-Aldrich, USA) was dissolved in 0.9% saline to a final concentration of 250 mg/mL. Pregnant females received a single intraperitoneal injection of 600 mg/kg VPA or physiological saline on E12.5. Male offspring received a single intraperitoneal injection of suramin (hexasodium salt, Sigma-Aldrich, USA) at 20 mg/kg or its vehicle 0.1M PBS on P30. Thus, four experimental groups were formed: Control (only vehicles injected), suramin (SUR), VPA and VPA + SUR. The litters were split equally among the experimental groups proposed by the present work as it follows: if the litter size presented an even number, half received suramin treatment and the other half, PBS treatment. If the litter size presented an odd number, for example, the size of three, two rats received suramin treatment and one rat received PBS treatment, and vice versa, randomly.

2.3. Behavioral tests

Behavioral testing was performed in offspring, between P32-P40, starting two days after the injection of suramin. All behavioral tests were performed under light conditions of 60 LUX by experienced researchers using a double-blind approach. The following behavioral tests were performed: elevated plus maze, open field/grooming, whisker nuisance task (WNT), three-chambered test, reciprocal sociability test and tail flick test. Except for the WNT and tail flick, all tests were videotaped for later evaluations.

2.3.1. Elevated plus maze (P32)

The anxiety-like behavior was assessed in an elevated plus maze apparatus with a 10 cm × 10 cm center, connecting two opposite open arms (length: 50 cm) and two opposite arms closed with 30 cm high walls (length: 50 cm), 1 m above the floor. Rats were placed in the middle of apparatus and its movements were recorded for 5 min using a camera connected to a laptop. The time spent in the closed arms is considered a measure of anxious behavior.

2.3.2. Open field test/self-grooming (P33)

Adapted from Schneider and colleagues (Schneider and Przewłocki, 2005), the exploratory and locomotor activity and the time and number of stereotyped movements (self-grooming behavior) were assessed in an open field arena, which consists of a wooden box measuring 50 × 50 × 50 cm. Rats were placed in the center of the arena and recorded during 30 min. Using the Anymaze Software®, we performed a tracking of locomotor activity (travelled distance and average speed) and time spent and number of entries in the central during the 30 min of test.

The self-grooming behavior was evaluated considering three different time periods (0–5, 10–15 and 20–25 min). We considered grooming as number of body cleaning with paws and face-washing actions and distinguished between complete (cleaning from snout to tail) and incomplete (fast and repetitive movements on snout) self-grooming.

2.3.3. Whisker nuisance task (P34-35)

Adapted from McNamara et al. (2010) and described by Fontes-Dutra and colleagues (Fontes-Dutra et al., 2018), in this test we observed the animal response to the vibrissae stimulation. One day prior to test, animals were set to the experimenter for 5 min, in an empty housing (57.1 × 39.4 × 15.2 cm) coated with an absorbent pad. On the day of test, the vibrissae were stimulated with a wooden toothpick for three consecutive periods of 5 min (15 min in total) with a 30 s interval between them. McNamara et al. (2010) developed a nonparametric scale of 0–2 according to the response (0 = absent/typical, 1 = present/light response and 2 = profound/accentuated response), distributed in 8 categories of behavior: freezing, stance and body position, breathing, whisker position, whisking response, evading stimulation, response to stick presentation and grooming (McNamara et al., 2010). The maximum test score is 16. High scores (8–16) indicate abnormal responses to stimulation, in which the animal freezes, shakes, or is aggressive. The low scores (0–4) indicate normal responses, in which the rat is calm or indifferent to stimulation.

2.3.4. Three-chamber test (P36-37)

This test was performed as previously described by Bambini-Junior and colleagues (Bambini-Junior et al., 2011). Briefly, at the beginning, the animal was habituated in the central chamber of the apparatus for 5 min. In the Sociability Test, one object was placed in one of the side chambers and in the other an unknown interaction animal (novel rat 1). We measured the time spent in each chamber and the time of exploration of either the rat or the object for 10 min.

In the Social Novelty Test, the novel rat 1 (now known rat) remained in this place and an unknown rat (novel rat 2 – an unfamiliar and younger 21–28 days old Wistar rat) was placed in the previously empty chamber. The time spent in each chamber and the time of exploration of both the rat known or not was also evaluated for 10 min.

2.3.5. Reciprocal social behavior (P38)

Adapted from Schneider et al. (Schneider and Przewłocki, 2005), the test was performed in the same box as the open field test during 15 min. The test animal was placed in the apparatus and, after a habituation period of 5 min, an unfamiliar and younger Wistar rat (21–28 days old) interaction animal was placed with the test animal. We evaluated the social behavior of the test animal using time and number of nose to nose interaction, anogenital inspection, flank exploration and following.

2.3.6. Tail flick (P39-40)

Nociceptive thresholds were evaluated using a tail flick analgesimeter (Insight Equipments, Ribeirão Preto, Brazil). One day prior the test, the animals were gently restrained by hand for 5 min in order to habituate to apparatus. Tail flick measurements were taken three times at 30 seconds intervals.

2.4. Tissue samples

The animals were deeply anesthetized on P41 with ketamine (300 mg/kg) and xilazine (40 mg/kg). After, the animals were decapitated, and the medial prefrontal cortex and hippocampus were dissected. The tissues were immediately homogenized in TRIzol® reagent (Invitrogen, Waltham, MA) and preserved at ultra-freezer until posterior molecular analysis.

2.4.1. RNA extraction and RT-qPCR procedure

After homogenization of tissues samples, chloroform was added to perform phase separation, and RNA was precipitated from the upper aqueous layer using isopropanol. The precipitated RNA was washed with ethanol to remove impurities, resuspended in RNase-free water and stored at ultra-freezer (Hummon et al., 2007).

The mRNA transcription levels of purinergic receptors and cytokines were evaluated by reverse transcriptase followed by quantitative polymerase chain reaction (RT-qPCR). Complementary DNA (cDNA) was synthesized from mRNA using reverse transcriptase reaction containing 2 μg of total RNA, 1 μL of 10 mM dNTP mix (Invitrogen, Waltham, MA), 1 μL of oligodT primer, 4 μL M-MLV reverse transcriptase 5X reaction buffer (Invitrogen, Waltham, MA), 2 μL of 0.1 M DTT (Invitrogen, Waltham, MA), 1 μL of RNase inhibitor (Invitrogen, Waltham, MA), 1.0 μL of M-MLV reverse transcriptase (Invitrogen, Waltham, MA), and sterile distilled water to a final volume of 20 μL. The synthesis of the cDNA was completed after a sequence of three incubations at 65 °C for 5 min, 37 °C for 50 min and 70 °C for 15 min.

The quantitative PCR mix was comprised by 8 μL of cDNA (1:40) and 12 μL reaction mix containing 0.5 μL of 10 μM dNTP mix (Invitrogen, Waltham, MA), 2.0 μL of 10X PCR buffer (Invitrogen, Waltham, MA), 0.8 μL of 50 mM $MgCl_2$ (Invitrogen, Waltham, MA), 2.0 μL of 1X SYBR™ Green (Molecular Probes, USA), 0.1 μL of Platinum Taq DNA Polymerase (Invitrogen, Waltham, MA), 0.2 μL of specific forward and reverse (10 μM) primers (as specified in Supplementary Table 1) and sterile distilled water to a final volume of 20 μL. The fluorescence of SYBR™ Green was used to detect amplification, estimate Ct values, and to determine specificity after melting curve analysis. PCR cycling conditions were standardized to 95 °C for 5 min followed by 40 cycles at 95 °C for 10 s, 58 °C for 10 s, and 72 °C for 10 s. After the main amplification, sample fluorescence was measured from 60 °C to 95 °C, with an increasing ramp of 0.3 °C each, to obtain the denaturing curve of the amplified products and Tm estimation, to assure their homogeneity after peak detection. Data was obtained from an Applied Biosystems StepOne System (USA).

The RT-qPCR results were imported into Microsoft Excel and the geNorm program was used to assess the variance in expression levels of the mRNA analyzed (Vandesompele et al., 2002). This program scanned all mRNA evaluated and ranked accordingly to their stability. The more stable mRNAs were used as endogenous expression controls. PCR efficiency was calculated from the slope of the amplification curve by exponential amplification analysis using the LinRegPCR algorithm (Ramakers et al., 2003). The relative expression of mRNA was calculated considering the 100% PCR efficiency and the $-\Delta\Delta Ct$ values for each mRNA (Livak and Schmittgen, 2001) and were normalized to the endogenous genes identified by the geNorm software (Primer Design, Ltd., Southampton University, Highfield Campus, Southampton Haunts, UK)..

2.5. Statistical analysis

IBM SPSS Statistics 20.0 (IBM SPSS, Armonk, NY, USA) was used to perform the statistical analysis. Kolgomorov-Smirnov and Shapiro-Wilk tests of normality were applied to determine data distribution. For behavioral tests, we used Generalized Estimating Equations (GEE) to weight both the interventions (VPA exposure and/or suramin treatment) and the litter effect in the behavioral outcome. Considering that

GEE is a flexible method based on general linear models, allowing the analysis of data with different distribution patterns, this protocol was used to compare different correlated variables (Fontes-Dutra et al., 2019). We also divided the litter equally among the experimental groups. After a Wald Chi-Square test, we performed pairwise comparisons for the parameters that presented interaction effect between interventions (VPA-by-suramin interaction). If only main effects were observed, the individual effect of VPA or suramin was evaluated. Bonferroni's post hoc test was used as the final evaluation. Data is reported as mean ± standard error of the mean (SEM). The Poisson distribution was used for discrete variables (number), while gamma distribution was used for time variables.

The relative expressions of purinergic receptors and cytokines were compared using one-way ANOVA followed by Bonferroni. The results were expressed as mean ± SEM. All statistical analyzes were supervised by the Biostatistics Unit at the Clinical Hospital of Porto Alegre.

3. Results

3.1. Behavioral tests

3.1.1. Social behavior analysis in the three-chambered test

Rats from control and suramin groups spent significantly more time in the chamber containing a conspecific novel rat than a novel object (CON: $p < 0.001$; SUR: $p = 0.025$; Fig. 1A). In contrast, VPA animals did not present preference between spending time in the chamber with a rat or an object ($p = 0.550$). Interestingly, suramin treatment of VPA-exposed rats was able to reestablish the social feature, as the VPA + SUR group showed preference to stay in the chamber together with the novel rat ($p < 0.001$). Concerning social interaction, rats from both control and suramin groups also spent significantly more time exploring the cage containing the conspecific rather than the object (CON: $p < 0.001$ SUR: $p < 0.001$), while the VPA group showed no preference between rat and object exploration ($p = 0.131$, Fig. 1A). Suramin treatment was again able to restore this social behavior (VPA + SUR: $p < 0.001$).

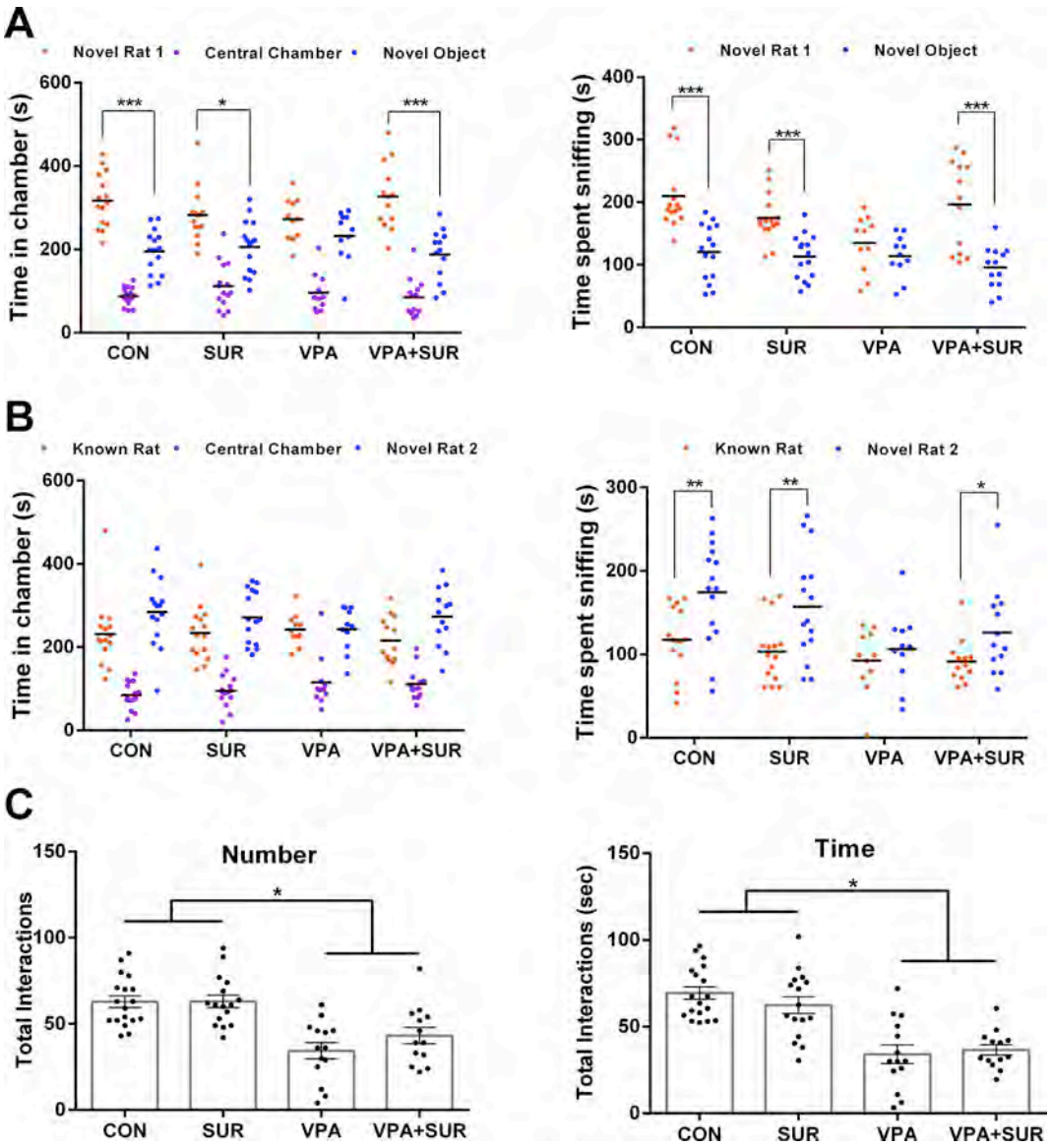

Fig. 1. Social behavior in VPA autism model. (A) Time spent in chambers and interaction time in sociability (B), social novelty tests in a three-chambered apparatus and (C) number and time of total pro-social interactions. Data expressed as means ± SEM. Asterisks indicate statistical differences with *$p < 0.05$, **$p < 0.01$, ***$p < 0.001$. Statistical analysis: Generalized Estimating Equations (GEE) followed by Bonferroni. Three-chambered test: CON ($n = 15$), SUR ($n = 15$), VPA ($n = 11$), VPA + SUR ($n = 13$). Reciprocal interactions: CON ($n = 18$), SUR ($n = 16$), VPA ($n = 14$), VPA + SUR ($n = 13$).

In the test for social novelty, all groups showed no significant difference between the time spent in the novel rat chamber and the known rat chamber (CON: $p = 0.562$; SUR: $p = 0.760$; VPA: $p = 1.000$; VPA + SUR: $p = 0.235$; Fig. 1B). However, rats from control and suramin groups spent significantly more time exploring the novel rat than the known rat (CON: $p = 0.003$; SUR: $p = 0.005$, Fig. 1B), indicating an interest in social novelty. VPA rats did not show preference in exploration time between novel and known rat (VPA: $p = 0.13$), whilst suramin treatment was able to prevent this social impairment in VPA-exposed animals (VPA + SUR: $p = 0.016$, Fig. 1B).

3.1.2. Reciprocal social behavior

Prenatal exposure to VPA significantly reduced every reciprocal social interaction parameter evaluated, except for following behavior (Supplementary Fig. S1). We observed only a VPA effect on total reciprocal social behavior, since VPA-exposed animals presented a decrease in number ($p < 0.001$) and time ($p < 0.001$) of social approaches and suramin treatment was not able to rescue these impairments (Fig. 1C).

3.1.3. Anxiety-like, exploratory and locomotor behavior

Rats from VPA group spent significantly less time exploring the open arm of the elevated plus-maze apparatus, compared to animals from control ($p = 0.001$) and suramin ($p = 0.003$) groups. VPA + SUR group spent more time exploring the open arm of the apparatus compared to the VPA group ($p < 0.001$; Fig. 2A), indicating that suramin was able to rescue the anxiety-like behaviors in rats exposed to VPA. It is worth to note that no differences were found among experimental groups in open arms entries (all $p > 0.570$; Supplementary Fig. S2A) and number of risk assessments in the elevated plus-maze apparatus (all $p > 0.210$; Supplementary Fig. S2B). In the open field arena, animals from VPA group spent significantly less time in central square compared to animals from control ($p = 0.007$) and suramin ($p < 0.001$) groups. As observed in plus maze evaluation, suramin was able to rescue this alteration, since VPA + SUR group spent more time in central square compared to VPA group ($p = 0.004$, Fig. 2B).

Concerning the *exploratory behavior*, only the VPA-exposed rats presented lower number of rearing in an open field arena ($p = 0.041$, Fig. 2C). Finally, when locomotor activity of those rats in the open field arena was evaluated, no significant differences in distance travelled (all $p > 0.910$, Fig. 2D) and average speed (all $p > 0.960$, Supplementary Fig. S2D) were found among experimental groups.

3.1.4. Self-grooming behavior

The self-grooming behavior was evaluated across three testing periods (0–5, 10–15 and 20–25 min) and distinguished between complete and incomplete self-grooming. During the second period, VPA groups spent more time performing complete self-grooming compared to control animals ($p = 0.039$), and suramin was not able to rescue from this altered behavior. Similarly, in the third period, the same pattern was observed in VPA animals ($p = 0.003$, Table 1). Taking all periods together, VPA-exposed animals spent more time doing complete self-grooming with no reversion by suramin treatment in this behavior ($p = 0.002$, Fig. 3A).

Regarding to the time spent doing incomplete self-grooming, no difference was observed among the groups (all $p > 0.100$, Table 1 or $p > 0.420$, Fig. 3C). However, the VPA group presented a trend to spend more time self-grooming in 10–15 min ($p = 0.065$), a significant increase in the third period ($p = 0.013$, Table 1), considering the three periods of test ($p = 0.002$, Fig. 3E). In all cases, postnatal treatment with suramin was not able to rescue from these alterations.

Concerning the number of self-grooming events, VPA animals presented more events of complete self-grooming only in the third period ($p = 0.002$, Table 1) with a trend to increased total complete self-grooming ($p = 0.088$, Fig. 3B). When considered the number of incomplete self-grooming and all grooming events, no differences were observed among groups in the three periods analyzed (all $p > 0.210$, Table 1) or considering three periods together (all $p > 0.553$, Fig. 3D). Finally, when considered the number of all events of self-grooming, VPA-exposed animals presented an increase only following 20–25 min ($p = 0.005$, Table 1) with no differences in the total period of test (all $p > 0.130$, Fig. 3F).

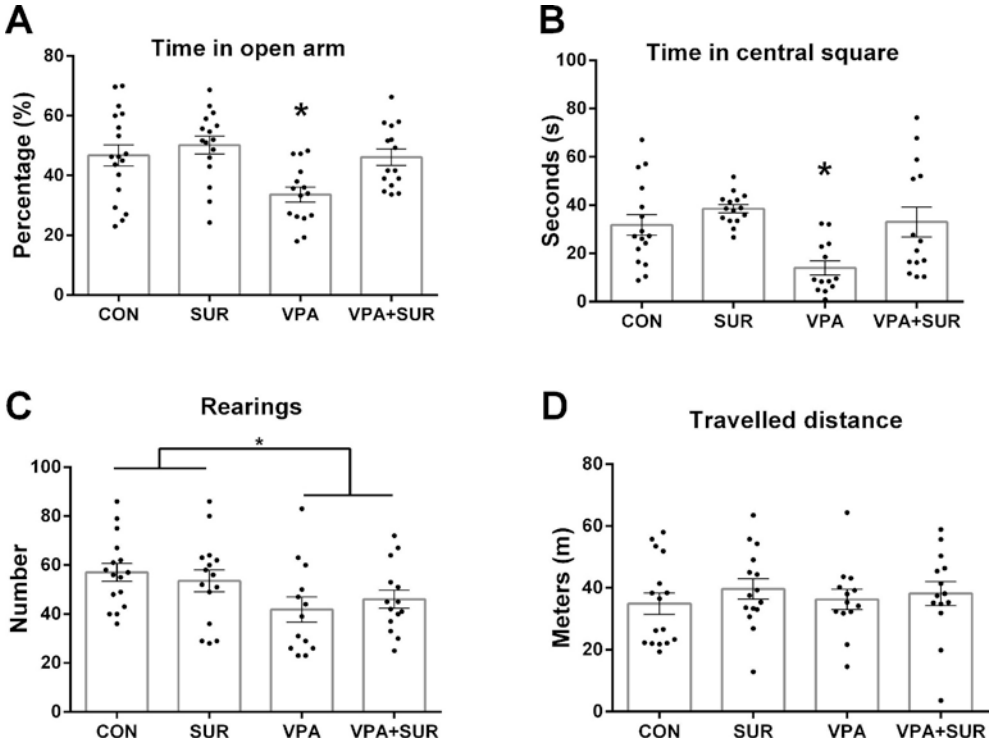

Fig. 2. Anxiety, exploratory and locomotor behavior in VPA autism model. (A) Percent of time spent in the open arms in the elevated plus-maze; (B) Time spent in central square; (C) Number of rearings and (D) distance travelled in a 50 × 50 × 50 open field arena. Data expressed as means ± SEM. Different letters indicate statistical differences with $p < 0.05$ considered significant. Statistical analysis: Generalized Estimating Equations (GEE) followed by Bonferroni. Plus Maze: CON ($n = 18$), SUR ($n = 16$), VPA ($n = 15$), VPA + SUR ($n = 15$). Open Field: CON ($n = 16$), SUR ($n = 15$), VPA ($n = 13$), VPA + SUR ($n = 14$).

Table 1
Self-grooming behavior in VPA autism model. Time and number of complete, incomplete and total grooming in three different time ranges.

			0–5 min	10–15 min	20–25 min
Time (seconds)	**Complete grooming**	CON	0.98 ± 0.66	12.67 ± 3.39 [a]	14.08 ± 5.07 [a]
		SUR	1.39 ± 0.91	11.12 ± 4.01 [a]	10.66 ± 4.21 [a]
		VPA	0.01 ± 0.00	23.57 ± 6.79 [b]	33.29 ± 7.54 [b]
		VPA + SUR	0.29 ± 0.27	21.67 ± 5.83 [b]	30.06 ± 8.06 [b]
	Incomplete grooming	CON	1.43 ± 0.55	1.52 ± 0.69	4.17 ± 1.71
		SUR	2.01 ± 1.03	2.72 ± 1.15	1.59 ± 0.86
		VPA	2.48 ± 1.12	2.26 ± 1.69	1.78 ± 0.94
		VPA + SUR	2.32 ± 0.95	0.84 ± 0.69	6.69 ± 2.85
	Total (complete + incomplete)	CON	2.41 ± 0.80	14.18 ± 3.95 [a]	18.24 ± 5.05 [a]
		SUR	3.40 ± 1.25	13.85 ± 4.33 [a]	12.25 ± 4.69 [a]
		VPA	2.49 ± 1.12	25.84 ± 7.94 [#]	35.07 ± 7.95 [b]
		VPA + SUR	2.61 ± 0.93	22.52 ± 5.90 [#]	36.76 ± 9.60 [b]
Number	**Complete grooming**	CON	0.12 ± 0.08	1.25 ± 0.34	0.69 ± 0.17 [a]
		SUR	0.20 ± 0.14	1.33 ± 0.38	0.73 ± 0.27 [a]
		VPA	0.01 ± 0.00	1.08 ± 0.29	1.77 ± 0.45 [b]
		VPA + SUR	0.08 ± 0.07	1.62 ± 0.38	1.62 ± 0.32 [b]
	Incomplete grooming	CON	0.38 ± 0.12	0.31 ± 0.12	0.44 ± 0.15
		SUR	0.27 ± 0.11	0.33 ± 0.12	0.27 ± 0.11
		VPA	0.46 ± 0.18	0.38 ± 0.23	0.31 ± 0.17
		VPA + SUR	0.38 ± 0.13	0.15 ± 0.10	0.54 ± 0.18
	Total (complete + incomplete)	CON	0.50 ± 0.15	1.56 ± 0.40	1.13 ± 0.23 [a]
		SUR	0.47 ± 0.16	1.67 ± 0.42	1.00 ± 0.36 [a]
		VPA	0.47 ± 0.16	1.46 ± 0.47	2.08 ± 0.47 [b]
		VPA + SUR	0.46 ± 0.14	1.77 ± 0.36	2.15 ± 0.37 [b]

Data expressed as means ± SEM. Different letters indicate statistical differences with $p < 0.05$ considered significant between groups that received VPA (VPA and VPA + SUR) and groups that did not receive VPA (CON and SUR), indicating the effect of prenatal exposure to VPA. #tendency of difference significant among groups that received VPA or not ($p = 0.065$). Statistical analysis: Generalized Estimating Equations (GEE) followed by Bonferroni. CON (Control, n = 16), SUR (Suramin, n = 15), VPA (valproic acid, n = 13), VPA + SUR (valproic acid treated with Suramin, n = 13).

3.1.5. Sensory behavior

In the whisker nuisance task (WNT), VPA-exposed animals presented a significant increased score when compared to control animals ($p = 0.001$, Fig. 4A), indicating higher levels of nuisance when whiskers are stimulated. The postnatal treatment with suramin was not able to rescue this alteration.

Only a VPA effect was observed in the latency to tail withdrawal in nociceptive *tail flick test*, so that VPA-exposed animals presented higher latencies compared to non-exposed animals ($p = 0.012$, Fig. 4B).

3.2. Molecular analysis

3.2.1. Expression of purinergic receptors

The relative expression of mRNA was performed in the medial prefrontal cortex. GeNorm algorithm ranked P2Y2 and P2Y4 receptor gene expression for normalization purposes (endogenous genes) and determinatino of relative expression levels of further investigated purinergic receptors. The expression rate of the ionotropic P2X4 receptor was significantly increased in the cortex of animals prenatally exposed to VPA and suramin was not able to revert this alteration ($F(3, 28) = 11{,}98$; $p < 0.0001$) (Fig. 5A). On the other hand, there were no significant differences in levels of remaining receptors (Fig. 5A).

When the receptors were evaluated in hippocampus of the young rats, P2X3 and P2Y4 were used as housekeeping genes. Curiously, the ionotropic receptor P2X4 was found significantly increased in animals from VPA and VPA + SUR groups, compared to control group also in this region ($F(3, 28) = 6020$; $p = 0.0027$). Additionally, animals presented increased mRNA levels coding for metabotropic receptor P2Y2 in VPA and VPA + SUR group compared to control group ($F(3, 28) = 6194$; $p = 0.0023$). In both cases, suramin was not able to reverse this alteration (Fig. 5B). Nevertheless, levels of remaining purinergic receptors showed no differences among experimental groups (Fig. 5B).

3.2.2. Expression of cytokine mRNA levels

In the medial prefrontal cortex, considering GAPDH and Beta3-tubulin as endogenous genes, the animals from VPA group presented an increase in relative expression of IL-6 mRNA compared to control group ($F(3, 24) = 5406$; $p = 0.005$) and the postnatal treatment with suramin rescued the levels of IL-6 of VPA-exposed rats to control levels (Fig. 6A). On the other hand, IL-1β, IFN-γ and TNF-α showed no differences between groups. Regarding to hippocampus and considering the same normalizer mRNA, no differences were found in cytokine levels among all experimental groups (Fig. 6B).

4. Discussion

An important approach in VPA model is the possibility of developing therapeutic strategies to attenuate several features observed in ASD. For instance, our group demonstrated that resveratrol (RSV), an antioxidant and anti-inflammatory molecule, prevents VPA-induced social impairments in the three-chamber test (Bambini-Junior et al., 2014) and in the number and time of reciprocal social interactions (Hirsch et al., 2018). The present results corroborate impairments in sociability and social novelty exploration in the three-chamber test, as previously demonstrated (Bambini-Junior et al., 2014, 2011). As previously shown, the postnatal treatment with a single dose of suramin was able to rescue social impairments (Naviaux et al., 2014). It is important to consider that there could be different schedules of administration of suramin, but considering its half-life and relevant clinical data, here we employed a single dose of antipurinergic treatment.

Additionally, the decrease in total reciprocal social interaction was not reversed by suramin. In fact, the reciprocal social behavior test involves complex patterns of socialization between two free animals, unlike the three-chamber test, where the conspecific animal remains trapped in a cage. Therefore, this characteristic of the test could be forcing the analyzed animal towards more complex social behavior actions, possibly causing additional impairments not reversed by suramin.

Another main finding of our study was that VPA rats presented a more anxious-like behavior compared to control animals as seen in plus maze apparatus and open field arena. Anxiety behavior is one of most

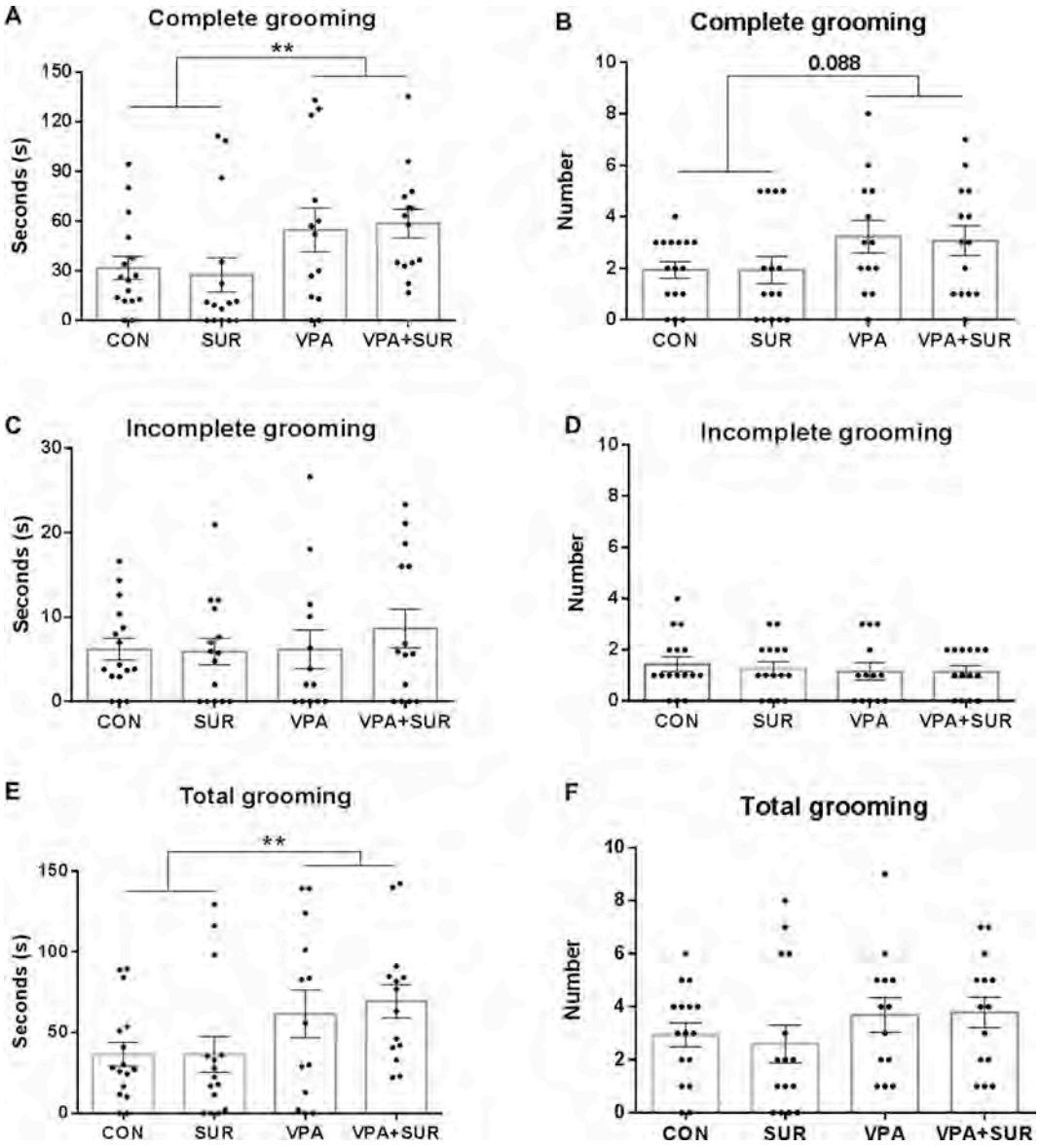

Fig. 3. Self-grooming behavior in VPA autism model. Time of (A) complete, (C) incomplete and (E) total grooming; Number of (B) complete, (D) incomplete and (F) total grooming. Data expressed as means ± SEM with **p < 0.01 considered significant. Statistical analysis: Generalized Estimating Equations (GEE) followed by Bonferroni. CON (n = 16), SUR (n = 15), VPA (n = 13), VPA + SUR (n = 14).

common comorbidities in ASD and has been reported to be present in around 50% of autistic children and adolescents (Simonoff et al., 2008; van Steensel et al., 2011). Our study corroborates previous studies that demonstrated increased anxiety-like behavior in animal models of autism (Patterson, 2011). Interestingly, the treatment with suramin was able to rescue completely this alteration, which was seen by the higher percentage of total time spent exploring the open arm of the apparatus compared to VPA group.

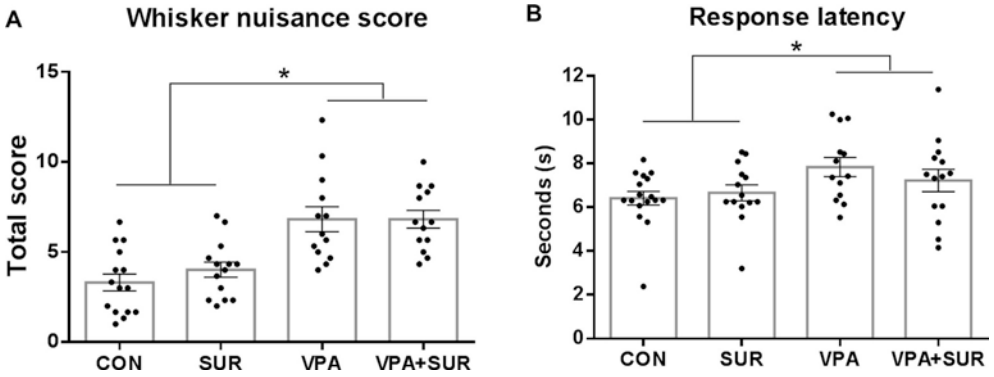

Fig. 4. Sensorial behavior in VPA autism model. (A) Total score in Whisker Nuisance Task and (B) latency to respond to thermal stimuli. Data expressed as means ± SEM with *p < 0.05. Statistical analysis: Generalized Estimating Equations (GEE) followed by Bonferroni. WNT: CON (n = 15), SUR (n = 14), VPA (n = 13), VPA + SUR (n = 13). Tail flick: CON (n = 17), SUR (n = 14), VPA (n = 13), VPA + SUR (n = 14).

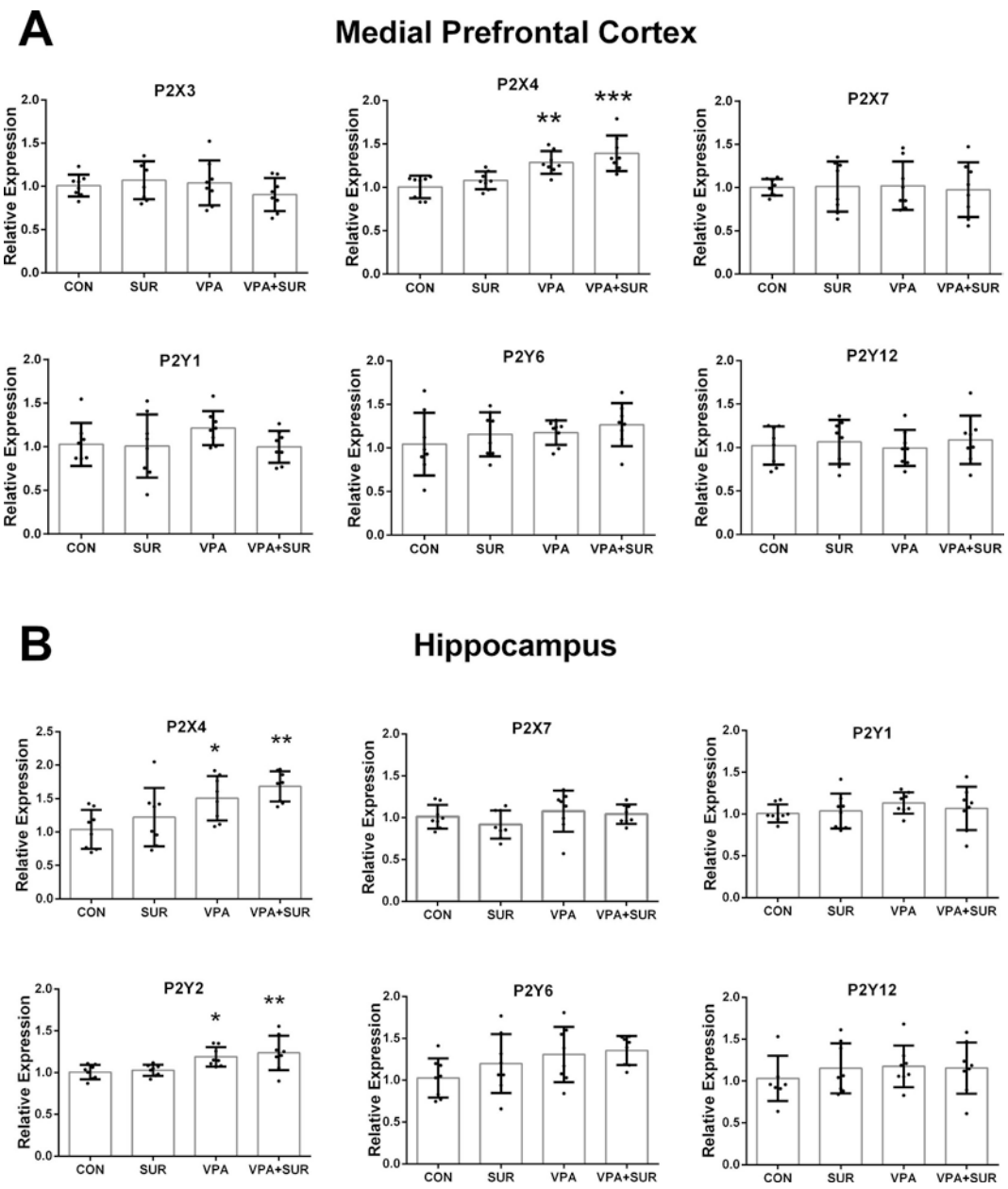

Fig. 5. Expression levels of purinergic receptors in medial prefrontal cortex (A) and hippocampus (B) of young rats from VPA autism model. Plots presented as mean ± SEM with *p < 0.05, **p < 0.01, ***p < 0.001. Statistical analysis: One-Way ANOVA followed by Tukey's test. n = 8 for all groups in both tissues.

We also observed that VPA-exposed animals do not present significant motor alterations or hyperactivity, but demonstrated a significant reduction in vertical exploratory activity, which could be related to the reduction in social interest of VPA animals described in sociability test, since animals with less exploratory tendencies possibly have impairments related to social approach. As observed in reciprocal sociability test, the postnatal treatment with suramin was not able to rescue the impairments observed in this exploratory behavior.

In addition to analyzing social behavior, the present study also assessed another core symptom of autism - the repetitive and stereotyped behavior. In animal models of autism, this feature can be measured by analyzing the repetitive self-grooming behavior. In present work, we assessed separately the self-grooming behavior as complete and incomplete events. The VPA-exposed animals showed increased time of complete self-grooming, without alteration in both number and time of incomplete grooming. Studies have demonstrated that only complete grooming is initiated by cerebellar midline or *locus coeruleus* stimulation (Strazielle et al., 2012) and that ATP can induce depolarization and increase excitability of norepinephrinergic system from *locus coeruleus*, possibly mediated by specific modulators of P2 receptors (Masaki et al., 2001; Yao and Lawrence, 2005), suggesting a putative role of the purinergic signaling system in grooming outcomes.

Previous studies already demonstrated that grooming behavior could be related to sensory components (Houghton et al., 2018). Corroborating a previous work from our group (Fontes-Dutra et al., 2018), we observed that VPA animals presented hypersensitivity to a non-harmful stimulus in WNT, suggesting a disturbance in sensory gating which could lead to increase in self-grooming behavior. Hyposensitivity to pain is also frequently observed in autistic subjects, although this feature is not a consensus, since different findings were observed depending on how the studies were conducted (Moore, 2015). In our study, VPA-exposed rats presented higher latencies to sense a thermal stimulus, indicating a lower nociceptive reactivity in accordance to previous work (Schneider et al., 2008). Postnatal treatment with

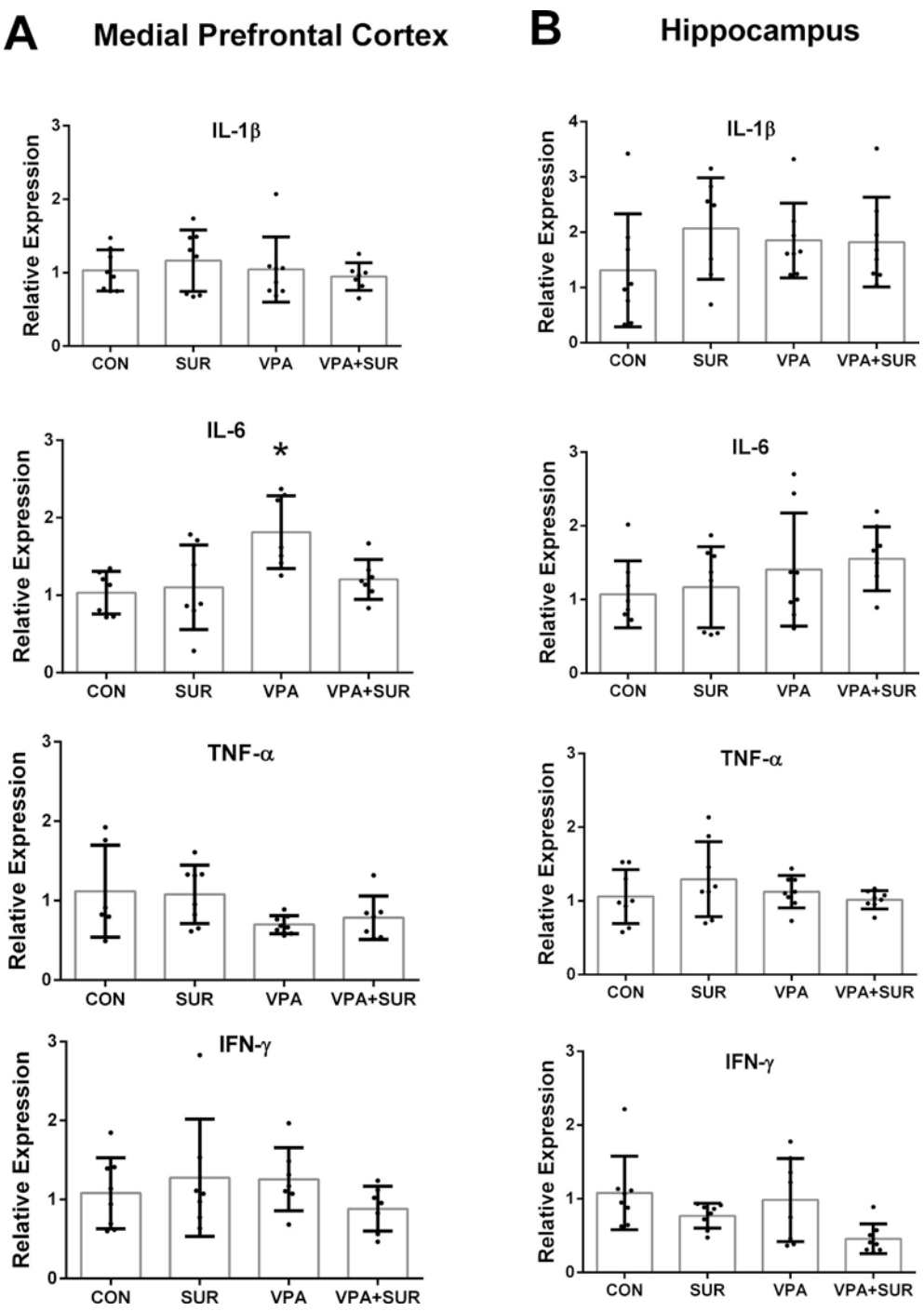

Fig. 6. Expression levels of pro-inflammatory cytokines in medial prefrontal cortex (A) and hippocampus (B) of young rats from VPA autism model. Results expressed as means ± SEM with *p < 0.05 considered significant. Statistical analysis: One-Way ANOVA followed by Tukey's test. n_{MPC} = 6–8 and n_{HIP} = 8 for all groups.

suramin was not able to rescue these sensorial impairments in VPA animals. Taking together, in the present work we demonstrated that VPA-induced alterations in behavioral components related to social and anxiety behavior in the animal model of ASD can be modulated by the anti-purinergic molecule suramin, highlighting the role of purinergic signaling system in the pathophysiology of ASD.

There are only a few studies in literature indicating the roles of purinergic system in sensory processing. Nevertheless, it is known that purinergic signaling system is important for sensory pathways (Irnich et al., 2002). Our data presented increased expression of cortical heteromeric P2X4 receptor in VPA-exposed animals. Since this receptor is involved with immunological responses in several tissues, the involvement of purinergic signaling in the ASD pathophysiology may be related to neuroimmunological alterations, as already found in patients (Gottfried et al., 2015) and animal models of autism (Wei et al., 2012; Xu et al., 2015). It is already known that suramin has therapeutic effects on social deficits (Naviaux et al., 2014, 2013), although it is poorly able to cross the blood brain barrier (Hawking, 1978; Roboz et al., 1998). Our hypothesis is that suramin could be acting only at peripheral levels modulating some characteristics of autism, possibly through a crosstalk between immunological and central nervous systems of these animals.

In our study animals from VPA group showed increased levels of

pro-inflammatory cytokine IL-6 in medial prefrontal cortex. Interestingly, a remarkable finding in the present work was the restoration IL-6 levels in this area after treatment with suramin. Since the levels of this cytokine are commonly increased in autistic patients (Gottfried et al., 2015) and in animal models of autism (Wei et al., 2012; Xu et al., 2015), the suramin-induced effect on IL-6 levels could play a role on its changes in social and anxiety-like behavior (Xu et al., 2015), which has also been rescued by suramin treatment. Therefore, the present data contribute to the understanding of how purinergic signaling is modulated in the VPA animal model of ASD, enlightening important VPA-induced alterations in ASD-related behaviors, changing both the expression pattern of purinergic receptors in medial prefrontal cortex and hippocampus, and the levels of IL-6, potentially pointing to a role of purinergic signaling system and inflammation status in VPA animal model. By contrast, postnatal treatment with suramin was capable to prevent alterations in social and anxiety-like behavior induced by VPA prenatal exposure, concomitantly reverting the high levels of IL-6.

5. Conclusion

In summary, our findings reinforce the idea of antipurinergic therapy as a novel pharmacological target in disorders associated with inflammatory dysregulation, including autism and provide new insights for the development of effective and safe treatments. Although VPA-exposed animals seem to present higher permeability in blood-brain barrier (Kumar et al., 2015; Kumar and Sharma, 2016a, Kumar and Sharma, 2016b), the limited access of suramin to CNS could explain the limitations of suramin-based therapeutic strategies. Even though suramin has been used in humans for more than 100 years as a therapeutic agent, it has plethora of important dose-dependent side effects. However, the present data provide remarkable support for the hypothesis that a drug acting through peripheral immune and inflammatory components can modulate some molecular and behavioral alterations in VPA autism model. As pointed out in a recent review (Burnstock, 2018), the development of purinergic compounds for the treatment of a wide variety of diseases is still in its infancy, but for sure, suramin studies open an important window for new drug designs and therapies. Further studies are necessary to elucidate the mechanisms of suramin action. In addition to this, the use of some specific and safer drugs could be more efficient to rescue autistic-related impairments.

Declaration of competing interest

The authors declare that there are no conflicts of interest.

Acknowledgements

We would like to thank the statistical support group of the Clinical Hospital of Porto Alegre (HCPA), Rio Grande do Sul, Brazil.

Appendix A. Supplementary data

Supplementary data to this article can be found online at https://doi.org/10.1016/j.neuropharm.2019.107930.

Funding

This work was supported by the Brazilian National Institute of Science and Technology on Neuroimmunomodulation (INCT-NIM Projec number 465489/2014-1), Rio de Janeiro, Brazil; National Council of Technological and Scientific Development (CNPq); Coordination for the Improvement of Higher Education Personnel (CAPES), São Paulo Research Foundation (FAPESP Project numbers 2012/50880-4 and 2015/14343-2) and Clinical Hospital of Porto Alegre (FIPE-HCPA).

References

American Psychiatric Association, 2013. Diagnostic and statistical manual of mental disorders. In: (DSM-5), Diagnostic and Statistical Manual of Mental Disorders fourth ed, fifth ed. TR. https://doi.org/10.1176/appi.books.9780890425596.744053.

Baio, J., Wiggins, L., Christensen, D.L., Maenner, M.J., Daniels, J., Warren, Z., Kurzius-Spencer, M., Zahorodny, W., Robinson Rosenberg, C., White, T., Durkin, M.S., Imm, P., Nikolaou, L., Yeargin-Allsopp, M., Lee, L.-C., Harrington, R., Lopez, M., Fitzgerald, R.T., Hewitt, A., Pettygrove, S., Constantino, J.N., Vehorn, A., Shenouda, J., Hall-Lande, J., Van Naarden Braun, K., Dowling, N.F., 2018. Prevalence of autism spectrum disorder among children aged 8 Years - autism and developmental disabilities monitoring network, 11 sites, United States, 2014. MMWR Surveillance Summ. 67, 1–23. https://doi.org/10.15585/mmwr.ss6706a1.

Bambini-Junior, V., Rodrigues, L., Behr, G.A., Moreira, J.C.F., Riesgo, R., Gottfried, C., 2011. Animal model of autism induced by prenatal exposure to valproate: behavioral changes and liver parameters. Brain Res. 1408, 8–15. https://doi.org/10.1016/j.brainres.2011.06.015.

Bambini-Junior, V., Zanatta, G., Della Flora Nunes, G., Mueller de Melo, G., Michels, M., Fontes-Dutra, M., Nogueira Freire, V., Riesgo, R., Gottfried, C., 2014. Resveratrol prevents social deficits in animal model of autism induced by valproic acid. Neurosci. Lett. 483, 178–181. https://doi.org/10.1016/j.neulet.2014.09.039.

Boulanger-Bertolus, J., Pancaro, C., Mashour, G.A., 2018. Increasing role of maternal immune activation in neurodevelopmental disorders. Front. Behav. Neurosci. 12, 230. https://doi.org/10.3389/fnbeh.2018.00230.

Burnstock, G., 2018. The therapeutic potential of purinergic signalling. Biochem. Pharmacol. 151, 157–165. https://doi.org/10.1016/j.bcp.2017.07.016.

Casanova, M.F., Buxhoeveden, D.P., Switala, A.E., Roy, E., 2002. Minicolumnar pathology in autism. Neurology 58, 428–432.

Chaste, P., Leboyer, M., 2012. Autism risk factors: genes, environment, and gene-environment interactions. Dialogues Clin. Neurosci. 14, 281–292.

Cheffer, A., Castillo, A.R.G., Corrêa-Velloso, J., Gonçalves, M.C.B., Naaldijk, Y., Nascimento, I.C., Burnstock, G., Ulrich, H., 2018. Purinergic system in psychiatric diseases. Mol. Psychiatry 23, 94–106. https://doi.org/10.1038/mp.2017.188.

Christensen, J., Grønborg, T.K., Sørensen, M.J., Schendel, D., Parner, E.T., Pedersen, L.H., Vestergaard, M., 2013. Prenatal valproate exposure and risk of autism spectrum disorders and childhood autism. J. Am. Med. Assoc. 309, 1696–1703. https://doi.org/10.1001/jama.2013.2270.

Elias, R., Sullivan, J.B., Lee, Y.W., White, S.W., 2015. Exploring the potential role of inflammation as an etiological process in ASD. Rev. J. Autism Dev. Disord. 2, 273–286. https://doi.org/10.1007/s40489-015-0051-z.

Faas, M.M., Sáez, T., de Vos, P., 2017. Extracellular ATP and adenosine: the Yin and Yang in immune responses? Mol. Asp. Med. 55, 9–19. https://doi.org/10.1016/j.mam.2017.01.002.

Filipek, P.A., Juranek, J., Smith, M., Mays, L.Z., Ramos, E.R., Bocian, M., Masser-Frye, D., Laulhere, T.M., Modahl, C., Spence, M.A., Gargus, J.J., 2003. Mitochondrial dysfunction in autistic patients with 15q inverted duplication. Ann. Neurol. 53, 801–804. https://doi.org/10.1002/ana.10596.

Fontes-Dutra, M., Della-Flora Nunes, G., Santos-Terra, J., Souza-Nunes, W., Bauer-Negrini, G., Hirsch, M.M., Green, L., Riesgo, R., Gottfried, C., Bambini-Junior, V., 2019. Abnormal empathy-like pro-social behaviour in the valproic acid model of autism spectrum disorder. Behav. Brain Res. 364, 11–18. https://doi.org/10.1016/J.BBR.2019.01.034.

Fontes-Dutra, M., Santos-Terra, J., Deckmann, I., Brum Schwingel, G., Della-Flora Nunes, G., Hirsch, M.M., Bauer-Negrini, G., Riesgo, R.S., Bambini-Júnior, V., Hedin-Pereira, C., Gottfried, C., 2018. Resveratrol prevents cellular and behavioral sensory alterations in the animal model of autism induced by valproic acid. Front. Synaptic Neurosci. 10, 9. https://doi.org/10.3389/fnsyn.2018.00009.

Glaser, T., Resende, R.R., Ulrich, H., 2013. Implications of purinergic receptor-mediated intracellular calcium transients in neural differentiation. Cell Commun. Signal. 11, 12. https://doi.org/10.1186/1478-811X-11-12.

Gogolla, N., LeBlanc, J.J., Quast, K.B., Südhof, T.C., Fagiolini, M., Hensch, T.K., 2009. Common circuit defect of excitatory-inhibitory balance in mouse models of autism. J. Neurodev. Disord. 1, 172–181. https://doi.org/10.1007/s11689-009-9023-x.

Gottfried, C., Bambini-Junior, V., Francis, F., Riesgo, R., Savino, W., 2015. The impact of neuroimmune alterations in autism spectrum disorder. Front. Psychiatry 6, 121. https://doi.org/10.3389/fpsyt.2015.00121.

Hawking, F., 1978. Suramin: with special reference to onchocerciasis. Adv. Pharmacol. Chemother. 15, 289–322.

Hirsch, M.M., Deckmann, I., Fontes-Dutra, M., Bauer-Negrini, G., Della-Flora Nunes, G., Nunes, W., Rabelo, B., Riesgo, R., Margis, R., Bambini-Junior, V., Gottfried, C., 2018. Behavioral alterations in autism model induced by valproic acid and translational analysis of circulating microRNA. Food Chem. Toxicol. 115, 336–343. https://doi.org/10.1016/j.fct.2018.02.061.

Horder, J., Petrinovic, M.M., Mendez, M.A., Bruns, A., Takumi, T., Spooren, W., Barker, G.J., Künnecke, B., Murphy, D.G., 2018. Glutamate and GABA in autism spectrum disorder—a translational magnetic resonance spectroscopy study in man and rodent models. Transl. Psychiatry 8, 106. https://doi.org/10.1038/s41398-018-0155-1.

Houghton, D.C., Alexander, J.R., Bauer, C.C., Woods, D.W., 2018. Abnormal perceptual sensitivity in body-focused repetitive behaviors. Compr. Psychiatr. 82, 45–52. https://doi.org/10.1016/j.comppsych.2017.12.005.

Hummon, A.B., Lim, S.R., Difilippantonio, M.J., Ried, T., 2007. Isolation and solubilization of proteins after TRIzol extraction of RNA and DNA from patient material following prolonged storage. Biotechniques 42, 467–472.

Hutsler, J.J., Casanova, M.F., 2016. Review: cortical construction in autism spectrum disorder: columns, connectivity and the subplate. Neuropathol. Appl. Neurobiol. 42,

115–134. https://doi.org/10.1111/nan.12227.
Irnich, D., Tracey, D.J., Polten, J., Burgstahler, R., Grafe, P., 2002. ATP stimulates peripheral axons in human, rat and mouse–differential involvement of A(2B) adenosine and P2X purinergic receptors. Neuroscience 110, 123–129.
Kumar, H., Sharma, B., 2016a. Memantine ameliorates autistic behavior, biochemistry & blood brain barrier impairments in rats. Brain Res. Bull. 124, 27–39. https://doi.org/10.1016/j.brainresbull.2016.03.013.
Kumar, H., Sharma, B., 2016. Minocycline ameliorates prenatal valproic acid induced autistic behaviour, biochemistry and blood brain barrier impairments in rats. Brain Res. 1630, 83–97. https://doi.org/10.1016/j.brainres.2015.10.052.
Kumar, H., Sharma, B.M., Sharma, B., 2015. Benefits of agomelatine in behavioral, neurochemical and blood brain barrier alterations in prenatal valproic acid induced autism spectrum disorder. Neurochem. Int. 91, 34–45. https://doi.org/10.1016/j.neuint.2015.10.007.
Lin, H.-C.C., Gean, P.-W.W., Wang, C.-C.C., Chan, Y.-H.H., Chen, P.S., 2013. The amygdala excitatory/inhibitory balance in a valproate-induced rat autism model. PLoS One 8, e55248. https://doi.org/10.1371/journal.pone.0055248.
Livak, K.J., Schmittgen, T.D., 2001. Analysis of relative gene expression data using real-time quantitative PCR and the $2-\Delta\Delta CT$ method. Methods 25, 402–408. https://doi.org/10.1006/meth.2001.1262.
Mabunga, D.F.N., Gonzales, E.L.T., Kim, J.-W., Kim, K.C., Shin, C.Y., 2015. Exploring the validity of valproic acid animal model of autism. Exp. Neurobiol. 24, 285–300. https://doi.org/10.5607/en.2015.24.4.285.
Markram, K., Rinaldi, T., Mendola, D. La, Sandi, C., Markram, H., 2008. Abnormal fear conditioning and amygdala processing in an animal model of autism. Neuropsychopharmacology 33, 901–912. https://doi.org/10.1038/sj.npp.1301453.
Masaki, E., Kawamura, M., Kato, F., 2001. Reduction by sevoflurane of adenosine 5'-triphosphate-activated inward current of locus coeruleus neurons in pontine slices of rats. Brain Res. 921, 226–232.
McNamara, K.C.S., Lisembee, A.M., Lifshitz, J., 2010. The whisker nuisance task identifies a late-onset, persistent sensory sensitivity in diffuse brain-injured rats. J. Neurotrauma 27, 695–706. https://doi.org/10.1089/neu.2009.1237.
Moore, D.J., 2015. Acute pain experience in individuals with autism spectrum disorders: a review. Autism 19, 387–399. https://doi.org/10.1177/1362361314527839.
Nakasato, A., Nakatani, Y., Seki, Y., Tsujino, N., Umino, M., Arita, H., 2008. Swim stress exaggerates the hyperactive mesocortical dopamine system in a rodent model of autism. Brain Res. 1193, 128–135. https://doi.org/10.1016/j.brainres.2007.11.043.
Naviaux, J., Schuchbauer, M., Li, K., Wang, L., Risbrough, V., Powell, S., Naviaux, R., 2014. Reversal of autism-like behaviors and metabolism in adult mice with single-dose antipurinergic therapy. Transl. Psychiatry 4, e400. https://doi.org/10.1038/tp.2014.33.
Naviaux, R.K., Curtis, B., Li, K., Naviaux, J.C., Bright, A.T., Reiner, G.E., Westerfield, M., Goh, S., Alaynick, W.A., Wang, L., Capparelli, E.V., Adams, C., Sun, J., Jain, S., He, F., Arellano, D.A., Mash, L.E., Chukoskie, L., Lincoln, A., Townsend, J., 2017. Low-dose suramin in autism spectrum disorder: a small, phase I/II, randomized clinical trial. Ann. Clin. Transl. Neurol. 4, 491–505. https://doi.org/10.1002/acn3.424.
Naviaux, R.K., Zolkipli, Z., Wang, L., Nakayama, T., Naviaux, J.C., Le, T.P., Schuchbauer, M.A., Rogac, M., Tang, Q., Dugan, L.L., Powell, S.B., 2013. Antipurinergic therapy corrects the autism-like features in the poly(IC) mouse model. PLoS One 8, e57380. https://doi.org/10.1371/journal.pone.0057380.
Oliveira, Á., Ulrich, H., 2016. Purinergic receptors in embryonic and adult neurogenesis. Neuropharmacology 104, 272–281. https://doi.org/10.1016/J.NEUROPHARM.2015.10.008.
Patowary, A., Nesbitt, R., Archer, M., Bernier, R., Brkanac, Z., 2017. Next generation sequencing mitochondrial DNA analysis in autism spectrum disorder. Autism Res. 10, 1338–1343. https://doi.org/10.1002/aur.1792.
Patterson, P.H., 2011. Modeling autistic features in animals. Pediatr. Res. 69, 34R–40R. https://doi.org/10.1203/PDR.0b013e318212b80f.
Ramakers, C., Ruijter, J.M., Deprez, R.H.L., Moorman, A.F.M., 2003. Assumption-free analysis of quantitative real-time polymerase chain reaction (PCR) data. Neurosci. Lett. 339, 62–66.
Robertson, C.E., Ratai, E.-M., Kanwisher, N., 2016. Reduced GABAergic action in the autistic brain. Curr. Biol. 26, 80–85. https://doi.org/10.1016/j.cub.2015.11.019.
Roboz, J., Deng, L., Ma, L., Holland, J.F., 1998. Investigation of suramin-albumin binding by electrospray mass spectrometry. Rapid Commun. Mass Spectrom. 12, 1319–1322. https://doi.org/10.1002/(SICI)1097-0231(19981015)12:19<1319::AID-RCM332>3.0.CO;2-J.
Roullet, F.I., Lai, J.K.Y., Foster, J.A., 2013. In utero exposure to valproic acid and autism - a current review of clinical and animal studies. Neurotoxicol. Teratol. 36, 47–56. https://doi.org/10.1016/j.ntt.2013.01.004.
Schneider, T., Przewłocki, R., 2005. Behavioral alterations in rats prenatally exposed to valproic acid: animal model of autism. Neuropsychopharmacology 30, 80–89. https://doi.org/10.1038/sj.npp.1300518.
Schneider, T., Roman, A., Basta-Kaim, A., Kubera, M., Budziszewska, B., Schneider, K., Przewłocki, R., 2008. Gender-specific behavioral and immunological alterations in an animal model of autism induced by prenatal exposure to valproic acid. Psychoneuroendocrinology 33, 728–740. https://doi.org/10.1016/j.psyneuen.2008.02.011.
Schneider, T., Ziółkowska, B., Gieryk, A., Tyminska, A., Przewłocki, R., 2007. Prenatal exposure to valproic acid disturbs the enkephalinergic system functioning, basal hedonic tone, and emotional responses in an animal model of autism. Psychopharmacology 193, 547–555. https://doi.org/10.1007/s00213-007-0795-y.
Simonoff, E., Pickles, A., Charman, T., Chandler, S., Loucas, T., Baird, G., 2008. Psychiatric disorders in children with autism spectrum disorders: prevalence, comorbidity, and associated factors in a population-derived sample. J. Am. Acad. Child Adolesc. Psychiatry 47, 921–929. https://doi.org/10.1097/CHI.0b013e318179964f.
Smith, S.E.P., Li, J., Garbett, K., Mirnics, K., Patterson, P.H., 2007. Maternal immune activation alters fetal brain development through interleukin-6. J. Neurosci. 27 (40), 10695–10702.
Strazielle, C., Lefevre, A., Jacquelin, C., Lalonde, R., 2012. Abnormal grooming activity in Dab1(scm) (scrambler) mutant mice. Behav. Brain Res. 233, 24–28. https://doi.org/10.1016/j.bbr.2012.04.038.
Tsujino, N., Nakatani, Y., Seki, Y., Nakasato, A., Nakamura, M., Sugawara, M., Arita, H., 2007. Abnormality of circadian rhythm accompanied by an increase in frontal cortex serotonin in animal model of autism. Neurosci. Res. 57, 289–295. https://doi.org/10.1016/J.NEURES.2006.10.018.
Ulrich, H., Abbracchio, M.P., Burnstock, G., 2012. Extrinsic purinergic regulation of neural stem/progenitor cells: implications for CNS development and repair. Stem Cell Rev. Rep. 8, 755–767. https://doi.org/10.1007/s12015-012-9372-9.
van Steensel, F.J.A., Bögels, S.M., Perrin, S., 2011. Anxiety disorders in children and adolescents with autistic spectrum disorders: a meta-analysis. Clin. Child Fam. Psychol. Rev. 14, 302–317. https://doi.org/10.1007/s10567-011-0097-0.
Vandesompele, J., De Preter, K., Pattyn, F., Poppe, B., Van Roy, N., De Paepe, A., Speleman, F., 2002. Accurate normalization of real-time quantitative RT-PCR data by geometric averaging of multiple internal control genes. Genome Biol. 3 RESEARCH0034.1-11.
Wei, H., Chadman, K.K., McCloskey, D.P., Sheikh, A.M., Malik, M., Brown, W.T., Li, X., 2012. Brain IL-6 elevation causes neuronal circuitry imbalances and mediates autism-like behaviors. Biochim. Biophys. Acta (BBA) - Mol. Basis Dis. 1822, 831–842. https://doi.org/10.1016/J.BBADIS.2012.01.011.
Williams, G., King, J., Cunningham, M., Stephan, M., Kerr, B., Hersh, J.H., 2001. Fetal valproate syndrome and autism: additional evidence of an association. Dev. Med. Child Neurol. 43, 202–206.
Xu, N., Li, X., Zhong, Y., 2015. Inflammatory cytokines: potential biomarkers of immunologic dysfunction in autism spectrum disorders. Mediat. Inflamm. 2015, 531518. https://doi.org/10.1155/2015/531518.
Yao, S.T., Lawrence, A.J., 2005. Purinergic modulation of cardiovascular function in the rat locus coeruleus. Br. J. Pharmacol. 145, 342–352. https://doi.org/10.1038/sj.bjp.0706179.

Gevi et al. Molecular Autism (2016) 7:47
DOI 10.1186/s13229-016-0109-5

Molecular Autism

RESEARCH Open Access

Urinary metabolomics of young Italian autistic children supports abnormal tryptophan and purine metabolism

Federica Gevi[1], Lello Zolla[1*], Stefano Gabriele[2] and Antonio M. Persico[3,4*]

Abstract

Background: Autism spectrum disorder (ASD) is still diagnosed through behavioral observation, due to a lack of laboratory biomarkers, which could greatly aid clinicians in providing earlier and more reliable diagnoses. Metabolomics on human biofluids provides a sensitive tool to identify metabolite profiles potentially usable as biomarkers for ASD. Initial metabolomic studies, analyzing urines and plasma of ASD and control individuals, suggested that autistic patients may share some metabolic abnormalities, despite several inconsistencies stemming from differences in technology, ethnicity, age range, and definition of "control" status.

Methods: ASD-specific urinary metabolomic patterns were explored at an early age in 30 ASD children and 30 matched controls (age range 2–7, M:F = 22:8) using hydrophilic interaction chromatography (HILIC)-UHPLC and mass spectrometry, a highly sensitive, accurate, and unbiased approach. Metabolites were then subjected to multivariate statistical analysis and grouped by metabolic pathway.

Results: Urinary metabolites displaying the largest differences between young ASD and control children belonged to the tryptophan and purine metabolic pathways. Also, vitamin B_6, riboflavin, phenylalanine-tyrosine-tryptophan biosynthesis, pantothenate and CoA, and pyrimidine metabolism differed significantly. ASD children preferentially transform tryptophan into xanthurenic acid and quinolinic acid (two catabolites of the kynurenine pathway), at the expense of kynurenic acid and especially of melatonin. Also, the gut microbiome contributes to altered tryptophan metabolism, yielding increased levels of indolyl 3-acetic acid and indolyl lactate.

Conclusions: The metabolic pathways most distinctive of young Italian autistic children largely overlap with those found in rodent models of ASD following maternal immune activation or genetic manipulations. These results are consistent with the proposal of a purine-driven cell danger response, accompanied by overproduction of epileptogenic and excitotoxic quinolinic acid, large reductions in melatonin synthesis, and gut dysbiosis. These metabolic abnormalities could underlie several comorbidities frequently associated to ASD, such as seizures, sleep disorders, and gastrointestinal symptoms, and could contribute to autism severity. Their diagnostic sensitivity, disease-specificity, and interethnic variability will merit further investigation.

Keywords: Autism, Autism spectrum disorder, Kynurenine, Melatonin, Metabolomics, Purinergic signaling, Quinolinic acid, Serotonin, Tryptophan

* Correspondence: zolla@unitus.it; apersico@unime.it
[1]Department of Ecological and Biological Sciences, University of Tuscia, Viterbo, Italy
[3]Unit of Child and Adolescent Neuropsychiatry, Interdepartmental Program "Autism 0-90", "Gaetano Martino" University Hospital, University of Messina, Messina, Italy
Full list of author information is available at the end of the article

Background

Autism spectrum disorder (ASD) represents a highly heterogeneous collection of neurodevelopmental conditions characterized by social and communication deficits, stereotypic and rigid patterns of behavior, restricted interests, and unusual sensory processing with onset in early childhood [1]. The prevalence of autism has increased significantly during the last two decades from 2–5/10,000 to 1:68 children [2, 3]. Changes in diagnostic criteria and increased attention by the medical community have certainly contributed to this trend [4]. Also, increasing parental age at conception has been shown to confer ASD risk [5], as well as some environmental factors, active especially during critical periods in prenatal/early postnatal neurodevelopment [6]. Finally, genetic susceptibility plays a prominent role in ASD pathogenesis through complex and heterogeneous underpinnings, ranging from rare variants endowed with full penetrance to common variants each explaining very small proportions of the overall phenotypic variance, either alone or through gene × environment interactions [7, 8].

Despite major advances in our understanding of the pathophysiology of ASD, this level of complexity and interindividual heterogeneity has largely hampered the translation of scientific knowledge into more effective clinical practices. ASD is still diagnosed exclusively through observation, standardized behavioral scales, and parental interviews; developmental trajectories of ASD children are periodically monitored but cannot be reliably predicted especially at an early age. Sensitive and specific quantitative biomarkers, measurable through laboratory, brain imaging, and/or electrophysiological techniques, could greatly aid clinicians in providing earlier diagnoses, more timely referrals to behavioral intervention programs, and evidence-based prognostic predictions [9].

Metabolomic technologies offer a sensitive means to search human biofluids for metabolite profiles potentially usable as biomarkers for neurodevelopmental disorders. A few studies have recently begun exploring the potential of urinary metabolomics in identifying ASD-specific metabolic patterns or in stratifying ASD patients into pathophysiologically meaningful subgroups [10–17]. Most studies have been performed on urines [10–16]; one study has explored blood plasma [17]. The analytical platforms most commonly used to identify and quantify metabolites are gas or liquid chromatography combined with mass spectroscopy (gas chromatography (GC)-mass spectroscopy (MS) and liquid chromatography (LC)-MS, respectively) [12, 16] and nuclear magnetic resonance spectroscopy (NMR) [10, 13, 14, 16, 18, 19]. In general, NMR displays greater speed and good reproducibility but also lower sensitivity compared to MS. Hence, MS- and NMR-based techniques should be viewed as complementary, not as superimposable approaches. An initial study, using 1H-NMR methods, showed an abnormal composition of urinary solutes indicative of perturbations in (a) the tryptophan/nicotinic acid metabolic pathway, (b) sulfur and amino acid metabolisms, and (c) gut microbiome, with an excess of several gut-derived co-metabolites [10]. Two other studies presumably assessing the same clinical sample with two different NMR-based technologies largely replicated these initial findings [13, 14]. Other studies using GC-MS, either alone [12, 15] or in combination with liquid chromatography [11], also identified perturbations in amino acid metabolism and gut microbial co-metabolites, as well as metabolic signatures of oxidative stress. Only one very recent study used both NMR and LC-MS, providing support for abnormalities in tryptophan metabolism, gut bacterial-derived compounds, purine and pyrimidine metabolism [16]. The only study exploring blood plasma reported metabolomic patterns compatible with (a) mitochondrial dysfunction, yielding reduced energy production and unbalanced redox status, (b) excess gut microbial co-metabolites, and (c) unbalances in various metabolic pathways, such as the Krebs cycle [17]. Collectively, metabolomic studies performed to this date suggest that autistic patients may share several metabolic abnormalities, especially involving some amino acid metabolisms, energy production, and oxidative stress, as well as the gut microbiome.

Moving from broad metabolic pathways to single compounds unveils inconsistencies between studies, which may stem from several potential confounds. Interethnic differences in the gut microbiota, stemming from differences in the nutrient composition of local diets, as well as age-related changes in both gut microbiota and human metabolism indeed require that case and control samples be tightly matched for these two variables. Age-related changes may be especially relevant to studies of ASD, where we have recently reported levels of urinary *p*-cresol to be elevated in autistic children compared to age-matched controls both in Italy and in France, but exclusively up until 8 years of age [20, 21]. Similar age-related changes in ASD have been previously described for other parameters, such as brain serotonin synthesis capacity [22, 23] and excessive head growth rates [24]. Finally, some studies have contrasted ASD patients with unrelated population controls [11, 14, 16, 17], while others have enrolled unaffected siblings as controls [15] and one study has used both [10]. These strategies are not equivalent, as first-degree relatives often fall within the broad autism spectrum (i.e., they display behavioral phenotypes intermediate between patients and population controls) [25]. In addition, siblings may carry protective gene variants with peculiar functional correlates,

possibly distinct from the metabolic patterns of unrelated typically developing children.

Taking into consideration these methodological issues, in order to maximize the probability of reliably detecting differences in urinary metabolic patterns, we focused on autistic and unrelated typically developing children 2–8 years old, tightly matched by age, sex, Italian ancestry, and city of origin within the country [20]. To ensure broad metabolite detection coverage on urine samples, which comprise molecules generated both by human cells and by the gut microbiome, we employed hydrophilic interaction chromatography (HILIC)-LC-electrospray ionization (ESI)-MS, a technology particularly suitable to separate simple and complex mixtures of carbohydrates, amino acids, glycosides, and other natural polar products in biological fluids, such as human urine and plasma [26, 27]. Applying this experimental approach, urinary metabolites most significantly distinguishing autistic from typically developing children were found to primarily fall into the tryptophan and purine metabolic pathways.

Methods

Subjects

Thirty children with idiopathic ASD and thirty typically developing controls were recruited in Central and Northern Italy. These represent the vast majority of the 64 cases and controls aged 3–7 years assessed for urinary *p*-cresol in our previous study [20]. Their demographic and clinical characteristics are summarized in Additional file 1: Table S1. Diagnostic assessments and medical screening have been previously described [20] (also see Additional file 2 with Supplementary Methods). Tight sex- and age-matching (±1 year) was applied to recruit typically developing children devoid of any overt ASD symptomatology among the offspring of clinical/academic personnel [20]. Mean age (±SEM) of cases and controls was 4.83 ± 0.30 and 5.03 ± 0.32 years, respectively (Student's $t = -0.459$, 58 *df*, $P = 0.648$, n.s.), and the M:F ratio was 22:8. All cases and controls were of Italian descent and matched by geographical area or city of origin.

Urine collection and metabolite extraction

First-morning urines were collected at home by parents using sterile containers untreated with preservatives and were brought to each clinical center the same morning in wet ice. Urine samples were then frozen, shipped in dry ice, and stored at −80 °C continuously until analysis.

Urinary specific gravity was measured by refractometry following centrifugation at 13,000*g* for 10 min) using a digital refractometer (Euromex Clinical Digital Refractometer RD.5712, NL) previously calibrated with LC-MS grade water.

Urine aliquots (200 μl) were mixed with 200 μl of methanol:acetonitrile:water (50:30:20), vortexed for 30 min at max speed at 4 °C and then centrifuged at 16,000*g* for 15 min at 4 °C. Supernatants were collected for metabolomic analysis. Quality controls (QCs) were obtained from a pooled mixture of 10 μl aliquots of all urine samples and were analyzed every 15 samples.

HILIC-UHPLC

Metabolite separation was performed as previously described [28], by hydrophilic interaction chromatography (HILIC) using the Ultimate 3000 Rapid Resolution HPLC system (Dionex, Sunnyvale, CA), featuring a binary pump and vacuum degasser, well-plate autosampler with a six-port micro-switching valve, and a thermostated column compartment. A Phenomenex Luna 3 μm HILIC 200 A (150 × 2.0 mm) column, protected by a HILIC 4 × 2.0 mm ID guard column (Phenomenex, Torrance, CA), was used to perform metabolite separation over a phase B-to-phase A gradient lasting 35 min. For the HILIC separation, mobile phase "A" consisted in 50 mM ammonium acetate mixed with acetonitrile (95:5, *v*/*v*), while eluent "B" was composed of a mixture of 50 mM ammonium acetate:water plus acetonitrile (95:5, *v*/*v*). Acetonitrile, formic acid, and HPLC-grade water were purchased from Sigma-Aldrich (St. Louis, MO).

Mass spectrometry

MS analysis was carried out on an electrospray hybrid quadrupole time-of-flight instrument MicroTOF-Q (Bruker-Daltonik, Bremen, Germany) equipped with an ESI ion source, as previously described [29]. Mass spectra for metabolite-extracted samples were acquired both in positive and in negative ion modes; only data produced in negative mode are shown, because more powerful in analyzing urinary samples. ESI capillary voltage was set at 4500 V (−) ion mode. The liquid nebulizer was set at 27 psi, and the nitrogen drying gas was set to a flow rate of 6 L/min. Dry gas temperature was maintained at 200 °C. Data were stored in centroid mode and acquired with a stored mass range of 50–1200 *m*/*z*. Instrument calibration was performed externally every day with 10 mM sodium hydroxide in 50% isopropanol: water, 0.1% formic acid. Automated internal mass scale calibration was performed through direct automated injection of the calibration solution at the beginning and at the end of each run by a six-port divert valve.

Data elaboration and statistical analysis

Data were normalized by urinary specific gravity, because creatinine excretion may be abnormally reduced in ASD children [30]. Replicates were exported as mzXML files and processed through MAVEN.52 (available at http://genomics-pubs.princeton.edu/mzroll/

index.php?show=index) [31]. Mass spectrometry chromatograms were elaborated for peak alignment, matching and comparison of parent and fragment ions, and tentative metabolite identification (within a 10-ppm mass deviation range between observed and expected results against the imported Kyoto Encyclopedia of Genes and Genomes (KEGG) database). Representative examples of mass determination and MS/MS fragmentation graphs are presented for kynurenine, melatonin, and tryptophan in Additional file 3: Figure S1. Multivariate statistical analyses were performed on the entire metabolomics data set using the MetaboAnalyst 3.0 software (http://www.metaboanalyst.ca) [32], which also overviewed data variance structure in an unsupervised manner and produced scatter plots.

Orthogonal partial least squares discriminant analysis (OPLS-DA), which defines a predictive model that describes the direction of the maximum covariance between a dataset (X) and class membership (Y), was then used to maximize the difference in metabolic profiles between cases and controls [33, 34]. OPLS-DA was performed using the Excel add-in Multibase package (Numerical Dynamics, Japan; http://www.numericaldynamics.com/) by applying orthogonal signal correction on the metabolite concentrations shifted, $\log_{10}$ transformed, centered, and scaled to unit variance.

Performance of the optimal model was tested by a receiver operating characteristic (ROC) curve analysis and the validation data set, as performed using MetaboAnalyst 3.0 software (http://www.metaboanalyst.ca) [32].

For case-control contrasts of single urinary metabolites, significance threshold was held at a nominal $P < 0.05$ with no correction for multiple testing, because (a) differences in single metabolite concentrations were tested only following significant differences in pathway enrichment were detected, (b) intra-pathway variability of single metabolites is non-independent, and (c) also different metabolic pathways are not fully independent, as some metabolites fall into more than one pathway. Detailed and summary statistics are provided in Additional files 4 and 5.

Results

The urinary metabolomes of young autistic and typically developing children are largely distinguishable on the three-dimensional OPLS-DA plot depicting the first three principal components (PC), which together explain 31.4% of the total variance (Fig. 1; accuracy, Q2 and R2 data are shown in Additional file 6). Approximately 10,000 peaks per sample were obtained referring to the KEGG database; among them, 202 metabolites were analyzed more precisely and identified. The top 25 most discriminating metabolites between cases and controls were further defined based on "variable influence on the projection" (VIP) scores >1 (Fig. 2). ROC analysis using this set of 25 metabolites yielded an AUC = 0.893 (95% CI 0.72–0.96), as shown in Additional file 7. The "metabolome overview" obtained through metabolic pathway analysis (MetPA) shows tryptophan metabolism, purine metabolism, vitamin B_6 metabolism, and phenylalanine-tyrosine-tryptophan biosynthesis as the four most perturbed metabolic pathways in ASD (Fig. 3).

Given the relevance of tryptophan-derived compounds in many neural functions, tryptophan metabolism was assessed in greater detail at the level of specific intermediates (Fig. 4):

- The kynurenine pathway displays increases in xanthurenic acid and especially in quinolinic acid, paralleled by a considerable decrease in kynurenic acid (Fig. 4, path A).
- The serotonin pathway shows a significant decrease in melatonin and its catabolite N-acetyl-5-methoxytryptamine, which have the same molecular weight and thus fall under the same MS peak (Fig. 4, path B).
- Bacterial degradation of tryptophan yields in ASD, compared to controls, prominently larger urinary concentrations of indoxyl sulfate and other indole derivatives, including indolyl-3-acetic acid and especially indolyl lactate (Fig. 4, paths C and D).

Also, purine metabolism was found to convey sizable discriminative power, because ASD cases display higher urinary concentrations of many purine metabolites compared to controls, including, among others, inosine, hypoxanthine, and xanthosine (Fig. 5).

Discussion

The present study reports significant urinary metabolomic differences between young children with idiopathic ASD and typically developing controls. At least some of the metabolic perturbations described here may reflect pathophysiologically meaningful abnormalities, possibly bearing functional consequences at the clinical level. Three strengths of the experimental design may have contributed to this positive outcome: (a) a focus on early infancy, by recruiting children within a relatively narrow age window precisely defined on the basis of previous urinary metabolic data [20, 21]; (b) the use of UHPLC-MS paired with HILIC, a very sensitive and reliable method ensuring maximum accuracy in the separation of small urinary solutes [26, 27]; (b) a pathway-centered approach, moving beyond the identification of single urinary ASD markers [10–17], as beautifully exemplified by urinary metabolomic studies of rodent models of ASD [35–37]. In particular, our recruitment strategy substantially differs from previous case-control study designs, minimizing age-dependent heterogeneity by

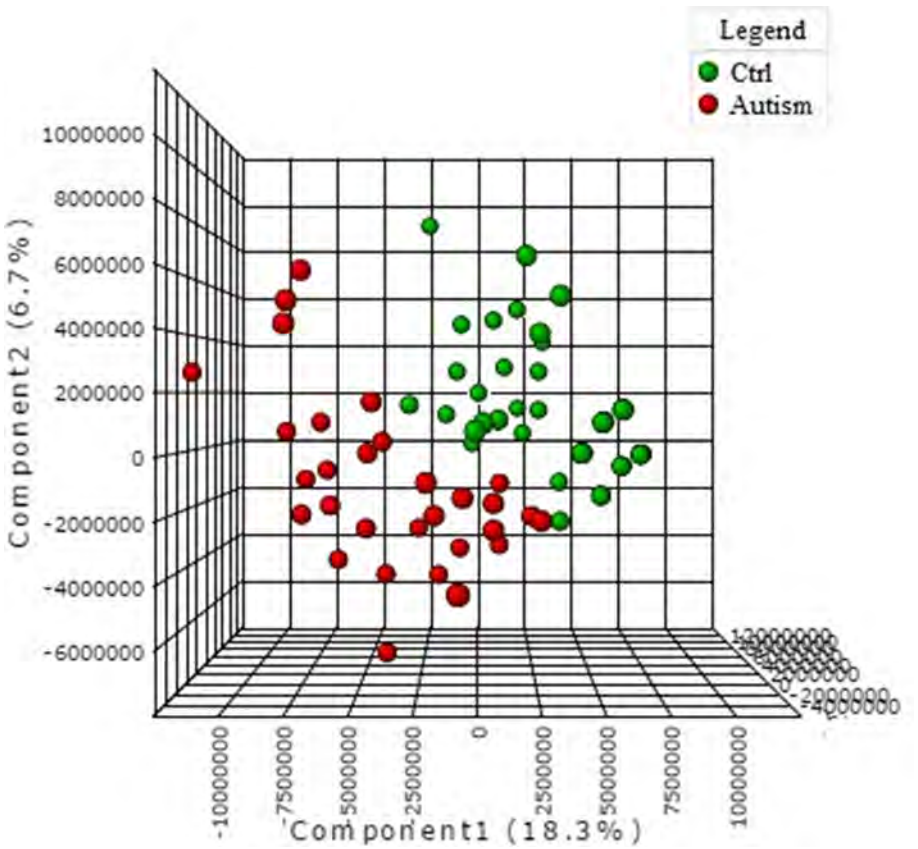

Fig. 1 OPLS-DA 3D plot based on normalized and mean-centered data. Each data point represents the metabolome of a single individual. Some data points may be superimposed to each other

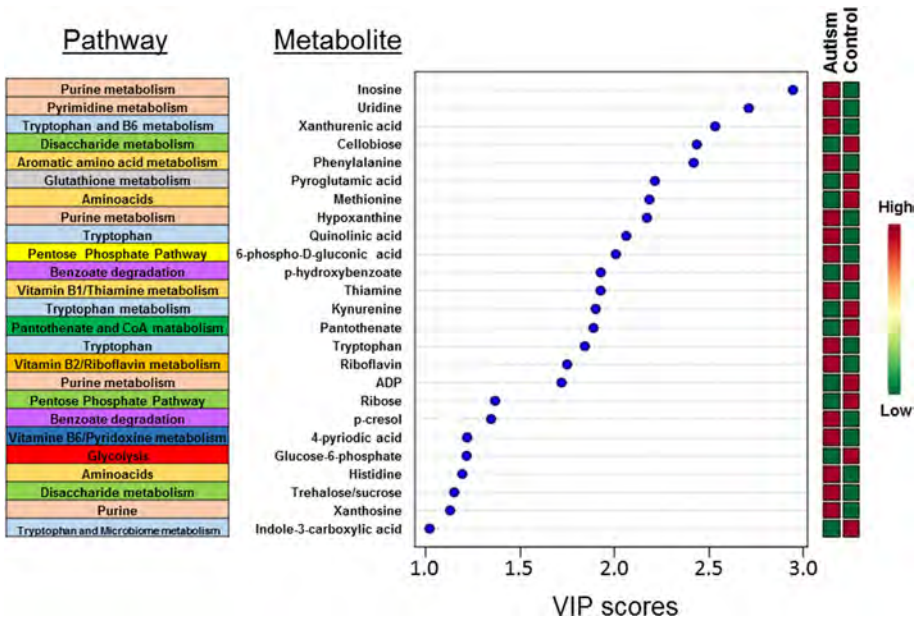

Fig. 2 The top 25 most discriminating metabolite ASD cases from controls, ranked by variable importance in projection (VIP) scores, and their KEGG biochemical pathway. VIP scores >1.0 were considered significant

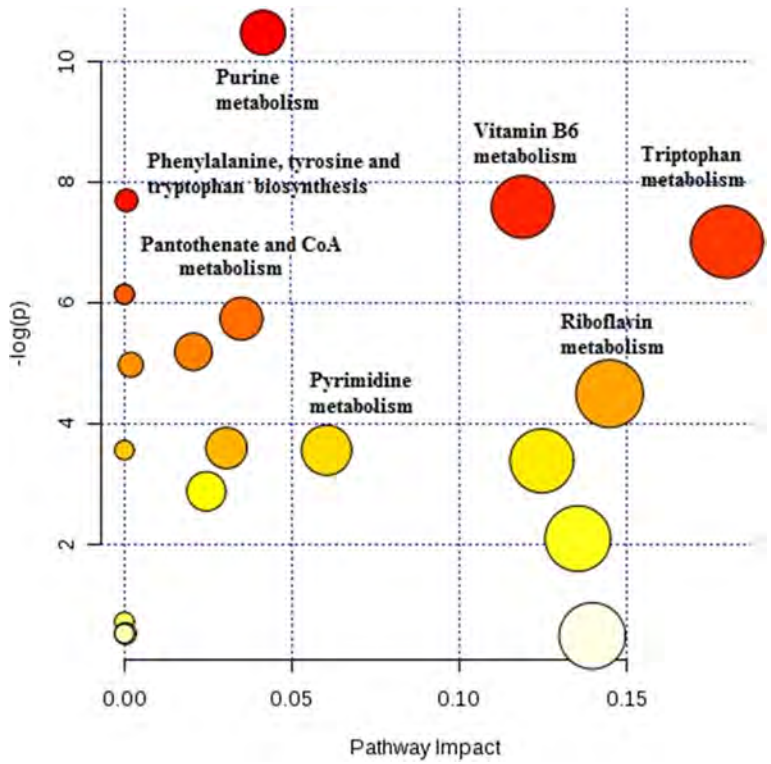

Fig. 3 Metabolic pathway analysis plot. Color intensity (*white* to *red*) reflects increasing statistical significance, while *circle diameter* covaries with pathway impact. The graph was obtained plotting on the *y-axis* the –log of *p* values from the pathway enrichment analysis and on the *x-axis* the pathway impact values derived from the pathway topology analysis

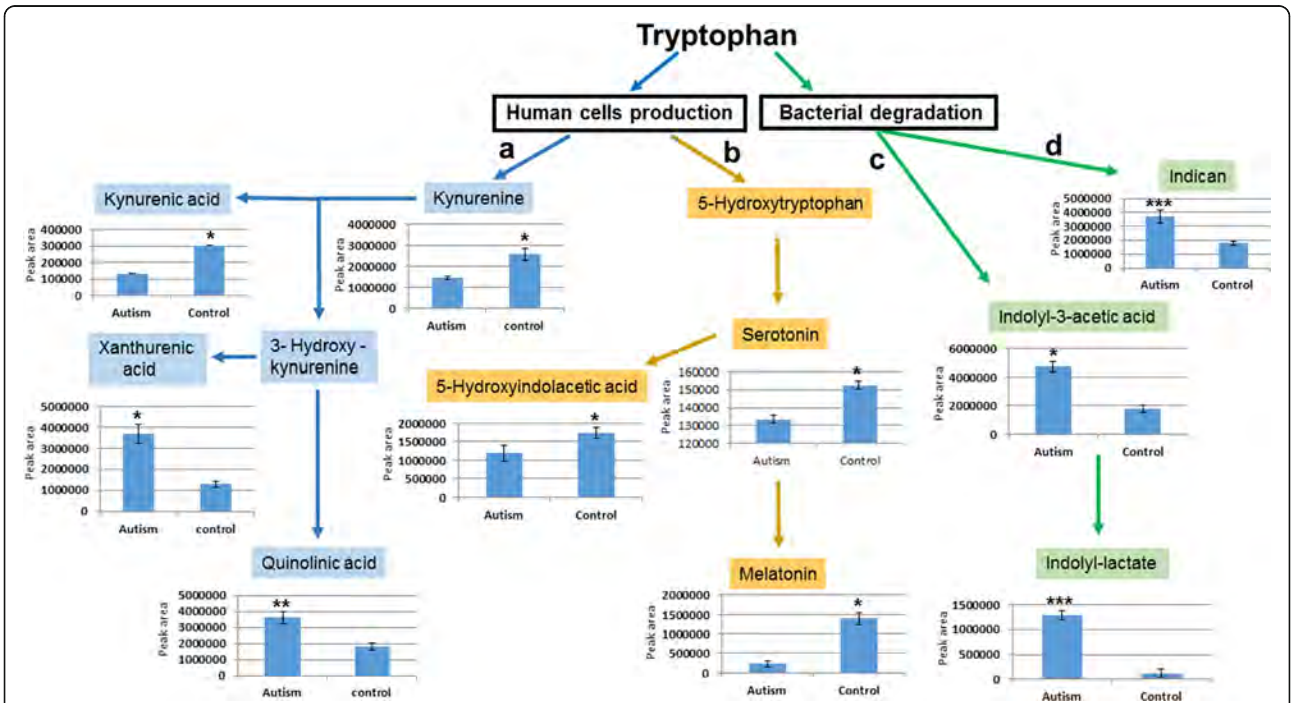

Fig. 4 Quantification of tryptophan metabolites: **a** kynurenine pathway; **b** serotonin/melatonin pathway; **c**–**d** bacterial degradation products. *Peak areas* for each metabolite were normalized by urinary specific gravity. Nominal *P* values: **P* < 0.05, ***P* < 0.0.1, ****P* < 0.001

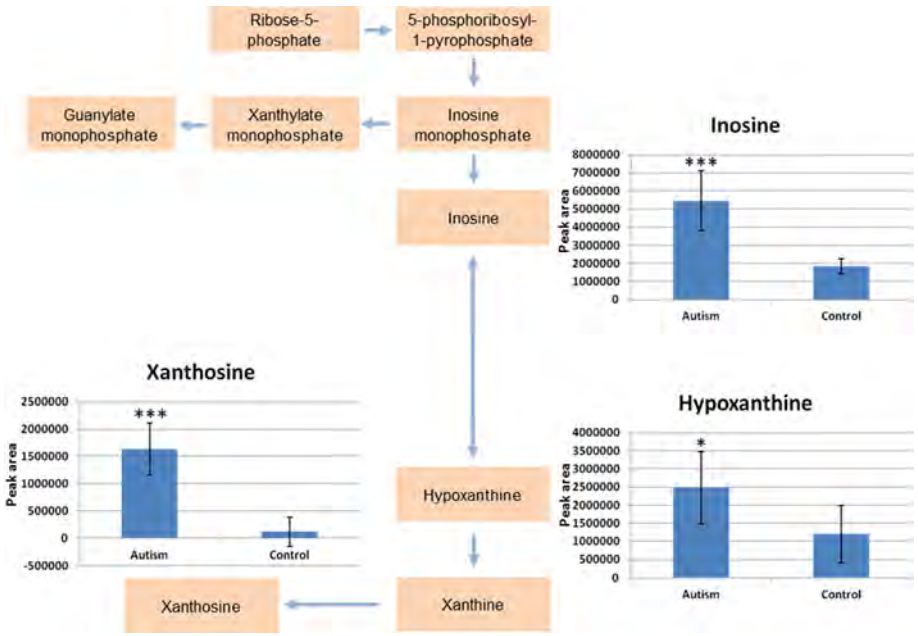

Fig. 5 Quantification of purine metabolites. *Peak areas* for each metabolite were normalized by urinary specific gravity. Nominal *P* values: **P* < 0.05, ***P* < 0.0.1, ****P* < 0.001

setting data-driven age thresholds (i.e., 2–8 years old) [20, 21], and applying tight age and sex matching between cases and controls. This strategy seemingly circumvents sample size limitations which would apply to an unfocused and unmatched case-control design. Future replications obtained applying similar recruitment criteria will enhance confidence in the pathophysiological relevance and the interethnic generalizability of our findings.

The tryptophan metabolic pathway collectively displays the largest perturbations in ASD (Fig. 3). Over 90–95% of dietary L-tryptophan is usually metabolized along the kynurenine pathway, 1–2% is converted to serotonin, and approximately 4–6% undergoes bacterial degradation prior to gut absorption through the Na^+-amino acid co-transporter B^0AT1 (Slc6a19) [38, 39]. The latter pathway yields indole derivatives not produced by mammalian metabolism, such as indoxyl sulfate [40]. Hence, changes in urinary amounts of multiple metabolites provide more reliable evidence of perturbed tryptophan metabolism, as compared to determinations of single metabolites or tryptophan itself, which also suffer from reduced statistical power due to control for multiple testing (Figs. 4 and 5). In the urines of young autistic children, we have indeed observed a substantial increase of xanthurenic acid and especially of quinolinic acid, paralleled by a decrease in kynurenine and kynurenic acid (Fig. 4, path A). This pattern is extremely interesting but must be interpreted with some caution in the absence of parallel assessments of the cerebrospinal fluid (CSF). On the one hand, the enzymes responsible for the synthesis of quinolinic acid and xanthurenic acid are primarily expressed in the microglia and in macrophages, whereas the path leading to kynurenic acid is functional in astrocytes [41]. Hence, it would be tempting to speculate that these opposite trends between cases and controls reflect an abnormal activation of microglia, which has been repeatedly seen in ASD postmortem brains [42–44], even as early as at 4 years of age [45]. On the other hand, urinary levels of quinolinic acid and kynurenic acid reflect peripheral production of these compounds, which do not pass the blood-brain barrier [41]. However, 3-hydroxykynurenine does pass the blood-brain barrier [41]. Interestingly, urinary concentrations of metabolite downstream of this compound (quinolinic acid and xanthurenic acid) are elevated in autistic children, whereas metabolite upstream of 3-hydroxykinurenine (kynurenine and kynurenic acid) are higher among controls (Fig. 4, path A). Conceivably, these trends could reflect an outflow of 3-hydroxykynurenine from the central nervous system (CNS) into the systemic circulation, where macrophage activation presumably at the level of the gut or in other peripheral organs, can transform this compound into quinolinic acid and xanthurenic acid, as well as into nicotinic acid (NAD), in agreement with previous data [10]. It will thus be important to verify this metabolomic scenario in the CSF, because it could have at least two important clinical implications: (a) quinolinic acid acts as

gliotoxin, proinflammatory mediator, and pro-oxidant molecule, boosting oxidative stress by stimulating microglia to release large amounts of NO and superoxide; (b) quinolinic acid exerts excitotoxic effects by acting as an *N*-methyl-D-aspartate (NMDA) receptor agonist, stimulating glutamate release, blocking glutamate reuptake into astrocytes, and reducing the activity of glutamine synthase; instead, kynurenic acid exerts neuroprotection via NMDA antagonism at the glycine binding site, as well as antioxidant effects [41, 46, 47]. In summary, the urinary metabolic imbalance documented here, if present also in the CNS, could favor enhanced oxidative stress and the well-known excitation>inhibition imbalance present in ASD, fostering seizures in as many as 20% of autistic individuals [48].

Another consequence of the preferential metabolization of tryptophan along the main branch of the kynurenine pathway is the relative decrease in the production of serotonin and melatonin (Fig. 4, path B). The serotonin pathway sees tryptophan being converted into 5-hydroxytryptophan (5-HTP) by tryptophan hydroxylase and onwards to 5-hydroxytryptamine (5-HT) or serotonin by 5-HTP decarboxylase. Serotonin can then be catabolized to 5-hydroxyindoleacetic acid (5-HIAA) or transformed into N-acetylserotonin by arylalkylamine N-acetyltransferase (AANAT). N-acetylserotonin is further methylated by N-acetylserotonin O-methyltransferase (ASMT) to generate the neurohormone 5-methyl-5-methoxy-N-tryptamine or melatonin. Decreases in the serotonin metabolite 5-HIAA are only modest, while urinary melatonin and its catabolite N-acetyl-5-methoxytryptamine display a more pronounced mean reduction (both share the same molecular weight and fall under the same MS peak, labeled in Fig. 4, path B, as "melatonin" only). This confirms previous assessments performed in plasma or urine [10, 49–52], while lending further support to blunted melatonin synthesis possibly due to reduced ASMT enzyme activity in ASD [53, 54]. Melatonin is synthesized and released by the pineal gland into the systemic circulation and readily passes the blood-brain barrier [55]. Its well-known role in circadian rhythmicity makes it an ideal candidate to explain the frequent occurrence, especially at the onset of ASD and during early infancy, of sleep disorders highly responsive to melatonin as a pharmacological therapy [56].

Metabolites produced by gut bacteria are well-represented also in our ASD sample, as in previous studies [10–17]. In addition to urinary *p*-cresol, found elevated in these same urine samples both here (Fig. 3) and previously using a different technology [20], we also detect a significant increase in indole derivatives of bacterial tryptophan including indolyl 3-acetic acid, indoxyl sulfate, and most prominently, indolyl lactate (Fig. 4, path C). Bacterial species expressing tryptophanase, the enzyme responsible for transforming tryptophan into indole derivatives, include *Escherichia coli*, *Proteus vulgaris*, *Paracolobactrum coliform*, *Achromobacter liquefaciens*, and *Bacteroides* spp. [40]. Once produced in the gut lumen, indole is absorbed, oxidized to indoxyl, conjugated with sulfate, and excreted as urinary indoxyl sulfate. About 3% of tryptophan entered with the diet is excreted as indoxyl sulfate [37]. Additional small amounts of tryptophan are converted into other indole derivatives found elevated here in ASD children, such as indolyl-3-acetic acid and indolyl lactate (Fig. 4, path C). The latter compound and indolyl 3-acetic acid are direct precursors of indolylacrylol glycine, found elevated in ASD by some [57] but not all studies [58, 59]. Predictably, the exact urinary bacterial compounds found elevated in ASD do differ in distinct metabolomic studies. This is not surprising since, in addition to differences in sample demographics and sensitivity of available technologies, ethnicity also exerts profound influences on the microbiome, reflecting dietary, genetic, and immunological specificities involved in the host-microbiome interactions [60]. Despite these discrepancies at the level of single compounds, urinary metabolomic studies consistently report an excess of microbiome-derived urinary metabolites, collectively supporting gut dysbiosis in ASD. These results point toward possible negative effects on CNS function exerted by microbiome-derived metabolites. At least three examples are available, albeit with different degrees of support: (a) urinary *p*-cresol amounts were found correlated with ASD severity [20] or with the intensity of stereotypic behaviors in young autistic children [21]; (b) i.c.v. injection of propionic acid, an enteric-derived short chain fatty acid, produces ASD-like behaviors in the rat [61]; (c) indoxyl sulfate is a known risk factor for cognitive impairment in chronic renal disease [62]: its influx across the blood-brain barrier using the organic anion transporter 3 significantly reduces the efflux of various neurotransmitter metabolites through the same transporter, leading to their accumulation [63]. Importantly, sizable improvements in behavioral and serum metabolome abnormalities were recorded using the maternal immune activation (MIA) rodent model of ASD following the correction of gut dysbiosis using *Bacteroides fragilis* [64].

Purine metabolites are also well represented in the urines of ASD children, which display a large excess of inosine, hypoxanthine, and xanthosine (Figs. 3 and 5). This pattern bears an interesting resemblance to the excess of urinary inosine and hypoxanthine detected in *Fmr1* knock-out mice, an animal model of fragile-X syndrome [35]. Also, mice exposed prenatally to MIA triggered by poly(I:C) injected at E12.5 and E17.5 show an excess of urinary inosine [36]. This excess of urinary

purinergic metabolites has been interpreted as part of a "cell danger metabolic response" involving mitochondrial dysfunction, adenosine triphosphate (ATP), and adenosine diphosphate (ADP) release, activation of a variety of purinergic receptors yielding microglial activation, innate, and adaptive immunity responses and leukocyte chemotactics [65]. Inborn errors of purine metabolism are associated with behavioral abnormalities including autistic features [66]. Strikingly, inhibition of purine metabolism by suramin, a competitive antagonist at P2X and P2Y purinergic receptors, reverses behavioral, neurochemical, transcriptional, and metabolomics abnormalities both in the *Fmr1* knock-out mouse and in MIA mice exposed to poly(I:C) during pregnancy [35–37]. Conceivably, this metabolic abnormality, shared between human ASD and genetic/immunological rodent models could thus represent a valuable biomarker to help guide therapeutic interventions. In addition, the cell danger response also yields relative vitamin B_6 deficiency and the enzyme kynureninase is B_6 dependent [65]; hence, a cell danger metabolic response in the presence of adequate tryptophan intake could also explain the decreased kynurenine and increased xanthurenic and quinolinic acid observed here (Fig. 4). Interestingly, these abnormalities have been sometimes overcome with vitamin B_6 supplementation [67], a therapeutic approach initially proposed for ASD in conjunction with magnesium supplementation [68]. In light of the present data, B_6-Mg^{++} supplementation in ASD may deserve further scrutiny in urinary biomarker-driven therapeutic trials, as no firm conclusion on its potential efficacy has yet been reached [69].

Conclusions

Targeting young autistic children and tightly matched controls, using the sensitive approach HILIC UHPLC-MS, and applying metabolic pathway analysis, we identified several urinary metabolic pathways significantly altered in ASD: tryptophan, purine, and vitamin B_6 metabolisms; phenylalanine, and tyrosine biosynthesis; and to a lesser extent, pantothenate and CoA, riboflavin, and pyrimidine metabolisms. Several of these same pathways, especially tryptophan, purine, and gut microbiome metabolisms, are also abnormal in animal models of ASD and provide very interesting leads toward possible pathophysiological explanations for specific symptoms present in many autistic children, such as seizures and sleep disorders. These metabolic abnormalities may apply to young children only, as suggested by studies of urinary *p*-cresol [20, 21]. It will indeed be very important to now perform a similar metabolomic assessment on ASD individuals and controls older than 8 years of age. Investigations of CSF metabolomics will be necessary to verify to what extent peripheral results reflect CNS pathophysiology. Finally, studies involving other diagnostic groups bordering with ASD, such as ADHD, intellectual disability, expressive language disorder, and obsessive-compulsive disorder, will be required to assess the disease specificity of the metabolomic abnormalities reported here and to determine their potential value as ASD-specific biomarkers, possibly able to aid clinicians in providing more reliable diagnoses in early infancy.

Additional files

Additional file 1: Table S1. Demographic and clinical characteristics of the autistic sample ($N = 30$, unless otherwise specified). Typically developing controls were tightly sex- and age-matched, with M:F = 22–8, age 5.03 ± 0.32 years, and no clinical evidence of ASD-related DSM-IV diagnoses or intellectual disability. (DOCX 21 kb)

Additional file 2: Supplementary methods and references. (DOCX 15 kb)

Additional file 3: Figure S1. Accurate mass and MS/MS fragmentation data for (a) kynurenine, (b) melatonin, and (c) tryptophan. (TIF 191 kb)

Additional file 4: Detailed and summary statistics for metabolites displayed in Figs. 4 and 5. (DOCX 17 kb)

Additional file 5: Summary statistics. (XLSX 10 kb)

Additional file 6: Figure S2. Q2 and R2 data pertaining to the PCA. $*p < 0.05$ refers to the best values of the currently selected measures (Q2). (TIF 233 kb)

Additional file 7: Figure S3. ROC curve for the top 25 most discriminating metabolites between ASD cases and controls, displayed in Fig. 2. (TIF 131 kb)

Abbreviations

5-HIAA: 5-hydroxyindoleacetic acid; 5-HT: 5-hydroxytryptamine; 5-HTTP: 5-hydroxytryptophan; AANAT: N-acetylserotonin by arylalkylamine N-acetyltransferase; ADHD: attention deficit hyperactivity disorder; ADP: adenosine diphosphate; ASD: autism spectrum disorder; ASMT: N-acetylserotonin O-methyltransferase; ATP: adenosine triphosphate; CNS: central nervous system; CSF: cerebrospinal fluid; ESI: electrospray ionization; GC: gas chromatography; HILIC: hydrophilic interaction chromatography; KEGG: Kyoto Encyclopedia of Genes and Genomes; LC: liquid chromatography; MetPA: metabolic pathway analysis; MIA: maternal immune activation; MS: mass spectroscopy; NAD: nicotinic acid; NMDA: *N*-methyl-D-aspartate; NMR: nuclear magnetic resonance; OPLS-DA: orthogonal partial least squares discriminant analysis; TOF: time of flight; VIP: variable influence on the projection

Acknowledgements

We gratefully acknowledge the patients, controls, and family members who participated in this study and the clinicians who contributed to patient recruitment within the framework of the 2011 collaborative *p*-cresol project.

Funding

This work was supported by the Italian Ministry for University, Scientific Research and Technology (PRIN n.2006058195), the Italian Ministry of Health (CCM2012), the Fondazione Gaetano e Mafalda Luce (Milan, Italy), the Autism Research Institute (San Diego, CA), and the Innovative Medicines Initiative Joint Undertaking (EU-AIMS, n. 115300). LZ and FG are supported by mobility studentship funds and post-doctoral research grant by the Interuniversity Consortium for Biotechnologies (CIB).

Availability of data and materials

Not applicable.

Authors' contributions

FG and LZ conducted the metabolomics analyses, analyzed and interpreted the biochemical data, and drafted the manuscript. SG collected the urine samples, interpreted the data, and drafted the manuscript. AMP designed

the study, was responsible for clinical assessments, interpreted the data, and wrote the manuscript. All authors read and approved the manuscript.

Competing interests
The authors declare that they have no competing interests.

Consent for publication
Not applicable.

Ethics approval and consent to participate
The Institutional Review Board of University Campus Bio-Medico (Rome, Italy) approved the study protocol (n. 50/15 PAR). All parents gave written informed consent for their children, using the approved consent form.

Author details
[1]Department of Ecological and Biological Sciences, University of Tuscia, Viterbo, Italy. [2]Unit of Child and Adolescent Neuropsychiatry, Laboratory of Molecular Psychiatry and Neurogenetics, University Campus Bio-Medico, Rome, Italy. [3]Unit of Child and Adolescent Neuropsychiatry, Interdepartmental Program "Autism 0-90", "Gaetano Martino" University Hospital, University of Messina, Messina, Italy. [4]Mafalda Luce Center for Pervasive Developmental Disorders, Milan, Italy.

Received: 25 December 2015 Accepted: 11 November 2016
Published online: 24 November 2016

References
1. American Psychiatric Association. Diagnostic and Statistical Manual of Mental Disorders. 5th ed. Washington, DC; 2013.
2. Fombonne E. Epidemiology of pervasive developmental disorders. Pediatr Res. 2009;65:591–8.
3. Developmental Disabilities Monitoring Network Surveillance Year 2010 Principal Investigators, Centers for Disease Control and Prevention (CDC). Prevalence of autism spectrum disorder among children aged 8 years—autism and developmental disabilities monitoring network, 11 sites, United States, 2010. MMWR Surveill Summ. 2014;63:1–21.
4. Rutter M. Incidence of autism spectrum disorders: changes over time and their meaning. Acta Paediatr. 2005;94:2–15.
5. Frans EM, Sandin S, Reichenberg A, Långström N, Lichtenstein P, McGrath JJ, Hultman CM. Autism risk across generations: a population-based study of advancing grandpaternal and paternal age. JAMA Psychiat. 2013;70:516–21.
6. Persico AM, Merelli S. Environmental factors and autism spectrum disorder. In: Leboyer M, Chaste P, editors. Autism spectrum disorders: phenotypes, mechanisms and treatments. vol. 180. Basilea: Karger; 2015. p. 113–34.
7. Persico AM, Napolioni V. Autism genetics. Behav Brain Res. 2013;251:95–112.
8. Berg JM, Geschwind DH. Autism genetics: searching for specificity and convergence. Genome Biol. 2012;13:247.
9. Ruggeri B, Sarkans U, Schumann G, Persico AM. Biomarkers in autism spectrum disorder: the old and the new. Psychopharmacology (Berl). 2014;231:1201–16.
10. Yap IK, Angley M, Veselkov KA, Holmes E, Lindon JC, Nicholson JK. Urinary metabolic phenotyping differentiates children with autism from their unaffected siblings and age-matched controls. J Proteome Res. 2010;9:2996–3004.
11. Ming X, Stein TP, Barnes V, Rhodes N, Guo L. Metabolic perturbance in autism spectrum disorders: a metabolomics study. J Proteome Res. 2012;11:5856–62.
12. Emond P, Mavel S, Aidoud N, Nadal-Desbarats L, Montigny F, Bonnet-Brilhault F, Barthélémy C, Merten M, Sarda P, Laumonnier F, Vourc'h P, Blasco H, Andres CR. GC-MS-based urine metabolic profiling of autism spectrum disorders. Anal Bioanal Chem. 2013;15:5291–300.
13. Mavel S, Nadal-Desbarats L, Blasco H, Bonnet-Brilhault F, Barthélémy C, Montigny F, Sarda P, Laumonnier F, Vourc'h P, Andres CR, Emond P. 1H-13C NMR-based urine metabolic profiling in autism spectrum disorders. Talanta. 2013;114:95–102.
14. Nadal-Desbarats L, Aïdoud N, Emond P, Blasco H, Filipiak I, Sarda P, Bonnet-Brilhault F, Mavel S, Andres CR. Combined 1H-NMR and 1H-13C HSQC-NMR to improve urinary screening in autism spectrum disorders. Analyst. 2014;139:3460–8.
15. Noto A, Fanos V, Barberini L, Grapov D, Fattuoni C, Zaffanello M, Casanova A, Fenu G, De Giacomo A, De Angelis M, Moretti C, Papoff P, Ditonno R, Francavilla R. The urinary metabolomics profile of an Italian autistic children population and their unaffected siblings. J Matern Fetal Neonatal Med. 2014;2:46–52.
16. Diémé B, Mavel S, Blasco H, Tripi G, Bonnet-Brilhault F, Malvy J, Bocca C, Andres CR, Nadal-Desbarats L, Emond P. Metabolomics study of urine in autism spectrum disorders using a multiplatform analytical methodology. J Proteome Res. 2015;14:5273–82.
17. West PR, Amaral DG, Bais P, Smith AM, Egnash LA, Ross ME, Palmer JA, Fontaine BR, Conard KR, Corbett BA, Cezar GG, Donley EL, Burrier RE. Metabolomics as a tool for discovery of biomarkers of autism spectrum disorder in the blood plasma of children. PLoS One. 2014;9:e112445.
18. Nicholson G, Rantalainen M, Li JV, Maher AD, Malmodin D, Ahmadi KR, Faber JH, Barrett A, Min JL, Rayner NW, Toft H, Krestyaninova M, Viksna J, Neogi SG, Dumas ME, Sarkans U, MolPAGE Consortium, Donnelly P, Illig T, Adamski J, Suhre K, Allen M, Zondervan KT, Spector TD, Nicholson JK, Lindon JC, Baunsgaard D, Holmes E, McCarthy MI, Holmes CC. A genome-wide metabolic QTL analysis in Europeans identifies functional effects of two loci shaped by recent positive selection. PLoS Genet. 2011;7:1002270.
19. Gebregiworgis T, Powers R. Application of NMR metabolomics to search for human disease biomarkers. Comb Chem High Throughput Screen. 2012;15:595–610.
20. Altieri L, Neri C, Sacco R, Curatolo P, Benvenuto A, Muratori F, Santocchi E, Bravaccio C, Lenti C, Saccani M, Rigardetto R, Gandione M, Urbani A, Persico AM. Urinary *p*-cresol is elevated in small children with autism spectrum disorder. Biomarkers. 2011;16:252–60.
21. Gabriele S, Sacco R, Cerullo S, Neri C, Urbani A, Tripi G, Malvy J, Barthelemy C, Bonnet-Brihault F, Persico AM. Urinary *p*-cresol is elevated in young French children with autism spectrum disorder: a replication study. Biomarkers. 2014;19:463–70.
22. Chugani DC, Muzik O, Behen M, Rothermel R, Janisse JJ, Lee J, Chugani HT. Developmental changes in brain serotonin synthesis capacity in autistic and nonautistic children. Ann Neurol. 1999;45:287–95.
23. Chandana SR, Behen ME, Juhász C, Muzik O, Rothermel RD, Mangner TJ, Chakraborty PK, Chugani HT, Chugani DC. Significance of abnormalities in developmental trajectory and asymmetry of cortical serotonin synthesis in autism. Int J Dev Neurosci. 2005;23:171–82.
24. Courchesne E, Pierce K, Schumann CM, Redcay E, Buckwalter JA, Kennedy DP, Morgan J. Mapping early brain development in autism. Neuron. 2007;56:399–413.
25. Piven J, Palmer P, Jacobi D, Childress D, Arndt S. Broader autism phenotype: evidence from a family history study of multiple-incidence autism families. Am J Psychiatry. 1997;154:185–90.
26. Hemstrom P, Irgum K. Hydrophilic interaction chromatography. J Sep Sci. 2006;29:1784–821.
27. Alpert AJ. Electrostatic repulsion hydrophilic interaction chromatography for isocratic separation of charged solutes and selective isolation of phosphopeptides. Anal Chem. 2008;80:62–76.
28. D'Alessandro A, Gevi F, Zolla L. A robust high resolution reversed-phase HPLC strategy to investigate various metabolic species in different biological models. Mol Biosyst. 2011;7:1024–32.
29. Gevi F, D'Alessandro A, Rinalducci S, Zolla L. Alterations of red blood cell metabolome during cold liquid storage of erythrocyte concentrates in CPD–SAGM. J Proteomics. 2012;76 Spec No:168–80.
30. Whiteley P, Waring R, Williams L, Klovrza L, Nolan F, Smith S, Farrow M, Dodou K, Lough WJ, Shattock P. Spot urinary creatinine excretion in pervasive developmental disorders. Pediatr Int. 2006;48:292–7.
31. Melamud E, Vastag L, Rabinowitz JD. Metabolomic analysis and visualization engine for LC-MS data. Anal Chem. 2010;82:9818–26.
32. Xia J, Mandal R, Sinelnikov I, Broadhurst D, Wishart DS. MetaboAnalyst 2. 0—a comprehensive server for metabolomic data analysis. Nucleic Acids Res. 2012;40:W127–33.
33. Dettmer K, Aronov PA, Hammock BD. Mass spectrometry based metabolomics. Mass Spectrom Rev. 2007;26:51–78.
34. Ellis DI, Goodacre R. Metabolic fingerprinting in disease diagnosis: biomedical applications of infrared and Raman spectroscopy. Analyst. 2006;131:875–85.
35. Naviaux JC, Wang L, Li K, Bright AT, Alaynick WA, Williams KR, Powell SB, Naviaux RK. Antipurinergic therapy corrects the autism-like features in the fragile X (Fmr1 knockout) mouse model. Mol Autism. 2015;6:1.

36. Naviaux JC, Schuchbauer MA, Li K, Wang L, Risbrough VB, Powell SB, Naviaux RK. Reversal of autism-like behaviors and metabolism in adult mice with single-dose antipurinergic therapy. Transl Psychiatry. 2014;4:e400.
37. Naviaux RK, Zolkipli Z, Wang L, Nakayama T, Naviaux JC, Le TP, Schuchbauer MA, Rogac M, Tang Q, Dugan LL, Powell SB. Antipurinergic therapy corrects the autism-like features in the poly(IC) mouse model. PLoS One. 2013;8:e57380.
38. Böhmer C, Bröer A, Munzinger M, Kowalczuk S, Rasko JE, Lang F, Bröer S. Characterization of mouse amino acid transporter B0AT1 (slc6a19). Biochem J. 2005;389(Pt 3):745–51.
39. Singer D, Camargo SM, Ramadan T, Schäfer M, Mariotta L, Herzog B, Huggel K, Wolfer D, Werner S, Penninger JM, Verrey F. Defective intestinal amino acid absorption in Ace2 null mice. Am J Physiol Gastrointest Liver Physiol. 2012;303:G686–95.
40. Keszthelyi D, Troost FJ, Masclee AA. Understanding the role of tryptophan and serotonin metabolism in gastrointestinal function. Neurogastroenterol Motil. 2009;21:1239–49.
41. Maddison DC, Giorgini F. The kynurenine pathway and neurodegenerative disease. Semin Cell Dev Biol. 2015;40:134–41.
42. Vargas DL, Nascimbene C, Krishnan C, Zimmerman AW, Pardo CA. Neuroglial activation and neuroinflammation in the brain of patients with autism. Ann Neurol. 2004;57:67–8.
43. Suzuki K, Sugihara G, Ouchi Y, Nakamura K, Futatsubashi M, Takebayashi K, Yoshihara Y, Omata K, Matsumoto K, Tsuchiya KJ, Iwata Y, Tsujii M, Sugiyama T, Mori N. Microglial activation in young adults with autism spectrum disorder. JAMA Psychiat. 2013;70:49–58.
44. Gupta S, Ellis SE, Ashar FN, Moes A, Bader JS, Zhan J, West AB, Arking DE. Transcriptome analysis reveals dysregulation of innate immune response genes and neuronal activity-dependent genes in autism. Nat Commun. 2014;5:5748.
45. Morgan JT, Chana G, Pardo CA, Achim C, Semendeferi K, Buckwalter J, Courchesne E, Everall IP. Microglial activation and increased microglial density observed in the dorsolateral prefrontal cortex in autism. Biol Psychiatry. 2010;68:368–76.
46. Guillemin G, Smith DG, Smythe GA, Armati PJ, Brew GJ. Expression of the kynurenine pathway enzymes in human microglia and macrophages. Adv Exp Med Biol. 2003;527:105–12.
47. Guillemin GJ. Quinolinic acid: neurotoxicity. FEBS J. 2012;279:1355.
48. Kohane IS, McMurry A, Weber G, MacFadden D, Rappaport L, Kunkel L, Bickel J, Wattanasin N, Spence S, Murphy S, Churchill S. The co-morbidity burden of children and young adults with autism spectrum disorders. PLoS One. 2012;7:e33224.
49. Nir I, Meir D, Zilber N, Knobler H, Hadjez J, Lerner Y. Brief report: circadian melatonin, thyroid-stimulating hormone, prolactin, and cortisol levels in serum of young adults with autism. J Autism Dev Disord. 1995;25:641–54.
50. Kulman G, Lissoni P, Rovelli F, Roselli MG, Brivio F, Sequeri P. Evidence of pineal endocrine hypofunction in autistic children. Neuroendocrinol Lett. 2000;21:31–4.
51. Tordjman S, Anderson GM, Pichard N, Charbuy H, Touitou Y. Nocturnal excretion of 6-sulphatoxymelatonin in children and adolescents with autistic disorder. Biol Psychiatry. 2005;57:134–8.
52. Tordjman S, Anderson GM, Bellissant E, Botbol M, Charbuy H, Camus F, Graignic R, Kermarrec S, Fougerou C, Cohen D, Touitou Y. Day and nighttime excretion of 6-sulphatoxymelatonin in adolescents and young adults with autistic disorder. Psychoneuroendocrinology. 2012;37:1990–7.
53. Melke J, Goubran Botros H, Chaste P, Betancur C, Nygren G, Anckarsäter H, Rastam M, Ståhlberg O, Gillberg IC, Delorme R, Chabane N, Mouren-Simeoni MC, Fauchereau F, Durand CM, Chevalier F, Drouot X, Collet C, Launay JM, Leboyer M, Gillberg C, Bourgeron T. Abnormal melatonin synthesis in autism spectrum disorders. Mol Psychiatry. 2008;13:90–8.
54. Pagan C, Delorme R, Callebert J, Goubran-Botros H, Amsellem F, Drouot X, Boudebesse C, Le Dudal K, Ngo-Nguyen N, Laouamri H, Gillberg C, Leboyer M, Bourgeron T, Launay JM. The serotonin-N-acetylserotonin–melatonin pathway as a biomarker for autism spectrum disorders. Transl Psychiatry. 2014;4:e479.
55. Vitte PA, Harthe C, Lestage P, Claustrat B, Bobillier P. Plasma, cerebrospinal fluid, and brain distribution of 14C-melatonin in rat: a biochemical and autoradiographic study. J Pineal Res. 1988;5:437–53.
56. Rossignol DA, Frye RE. Melatonin in autism spectrum disorders: a systematic review and meta-analysis. Dev Med Child Neurol. 2011;53:783–92.
57. Bull G, Shattock P, Whiteley P, Anderson R, Groundwater P, Lough JW, Lees G. Indolyl-3- acryloylglycine (IAG) is a putative diagnostic urinary marker for autism spectrum disorders. Med Sci Monit. 2003;9:CR422–5.
58. Wang L, Angley MT, Gerber JP, Young RL, Abarno DV, McKinnon RA, Sorich MJ. Is urinary indolyl-3-acryloylglycine a biomarker for autism with gastrointestinal symptoms? Biomarkers. 2009;14:596–603.
59. Wright B, Brzozowski AM, Calvert E, Farnworth H, Goodall DM, Holbrook I, Imrie G, Jordan J, Kelly A, Miles J, Smith R, Town J. Is the presence of urinary indolyl-3-acryloylglycine associated with autism spectrum disorder? Dev Med Child Neurol. 2005;47:190–2.
60. Li M, Wang B, Zhang M, Rantalainen M, Wang S, Zhou H, Zhang Y, Shen J, Pang X, Zhang M, Wei H, Chen Y, Lu H, Zuo J, Su M, Qiu Y, Jia W, Xiao C, Smith LM, Yang S, Holmes E, Tang H, Zhao G, Nicholson JK, Li L, Zhao L. Symbiotic gut microbes modulate human metabolic phenotypes. Proc Natl Acad Sci U S A. 2008;105:2117–22.
61. Thomas RH, Meeking MM, Mepham JR, Tichenoff L, Possmayer F, Liu S, MacFabe DF. The enteric bacterial metabolite propionic acid alters brain and plasma phospholipid molecular species: further development of a rodent model of autism spectrum disorders. J Neuroinflammation. 2012;9:153.
62. Watanabe K, Watanabe T, Nakayama M. Cerebro-renal interactions: impact of uremic toxins on cognitive function. Neurotoxicology. 2014;44:184–93.
63. Ohtsuki S, Asaba H, Takanaga H, Deguchi T, Hosoya K, Otagiri M, Terasaki T. Role of blood-brain barrier organic anion transporter 3 (OAT3) in the efflux of indoxyl sulfate, a uremic toxin: its involvement in neurotransmitter metabolite clearance from the brain. J Neurochem. 2002;83:57–66.
64. Hsiao EY, McBride SW, Hsien S, Sharon G, Hyde ER, McCue T, Codelli JA, Chow J, Reisman SE, Petrosino JF, Patterson PH, Mazmanian SK. Microbiota modulate behavioral and physiological abnormalities associated with neurodevelopmental disorders. Cell. 2013;155:1451–63.
65. Naviaux RK. Metabolic features of the cell danger response. Mitochondrion. 2014;16:7–17.
66. Nyhan WL, James JA, Teberg AJ, Sweetman L, Nelson LG. A new disorder of purine metabolism with behavioral manifestations. J Pediatr. 1969;74:20–7.
67. Tada K, Yokoyama Y, Nakagawa H, Yoshida T, Arakawa T. Vitamin B6 dependent xanthurenic aciduria. Tohoku J Exp Med. 1967;93:115–24.
68. Martineau J, Barthelemy C, Garreau B, Lelord G. Vitamin B6, magnesium, and combined B6-Mg: therapeutic effects in childhood autism. Biol Psychiatry. 1985;20:467–78.
69. Nye C, Brice A. Combined vitamin B6-magnesium treatment in autism spectrum disorder. Cochrane Database Syst Rev. 2005;4:CD003497.

ANNALS of Clinical and Translational Neurology
Open Access
ANA American Neurological Association since 1875

RESEARCH ARTICLE

Low-dose suramin in autism spectrum disorder: a small, phase I/II, randomized clinical trial

Robert K. Naviaux[1,2,3,4], Brooke Curtis[5], Kefeng Li[1,2], Jane C. Naviaux[1,6], A. Taylor Bright[1,2], Gail E. Reiner[1,6], Marissa Westerfield[7], Suzanne Goh[8], William A. Alaynick[1,2], Lin Wang[1,2], Edmund V. Capparelli[13], Cynthia Adams[9], Ji Sun[9], Sonia Jain[10], Feng He[10], Deyna A. Arellano[9], Lisa E. Mash[7,11], Leanne Chukoskie[7,12], Alan Lincoln[5] & Jeanne Townsend[6,7]

[1]The Mitochondrial and Metabolic Disease Center, University of California, San Diego School of Medicine, 214 Dickinson St., Bldg CTF, Rm C102, San Diego, 92103-8467, California
[2]Department of Medicine, University of California, San Diego School of Medicine, 214 Dickinson St., Bldg CTF, Rm C102, San Diego, 92103-8467, California
[3]Department of Pediatrics, University of California, San Diego School of Medicine, 214 Dickinson St., Bldg CTF, Rm C102, San Diego, 92103-8467, California
[4]Department of Pathology, University of California, San Diego School of Medicine, 214 Dickinson St., Bldg CTF, Rm C102, San Diego, 92103-8467, California
[5]Alliant International University, 10455 Pomerado Road, San Diego, California, 92131
[6]Department of Neurosciences, University of California, San Diego School of Medicine, 9500 Gilman Drive., La Jolla, CA, 92093-0662
[7]The Research in Autism and Development Laboratory (RAD Lab), University of California, 9500 Gilman Drive, La Jolla, CA, 92093-0959
[8]Pediatric Neurology Therapeutics, 7090 Miratech Dr, San Diego, CA, 92121
[9]Clinical and Translational Research Institute (CTRI), University of California, San Diego, La Jolla, CA, 92037
[10]Department of Family Medicine and Public Health, University of California, San Diego, La Jolla, CA, 92093
[11]Department of Psychology, San Diego State University, 5500 Campanile Drive, San Diego, CA, 92182
[12]Institute for Neural Computation, University of California, 9500 Gilman Drive, La Jolla, 92093-0523
[13]Department of Pediatrics, and Skaggs School of Pharmacy and Pharmaceutical Sciences, University of California, San Diego School of Medicine, 9500 Gilman Drive, La Jolla, CA, 92093-0657

Correspondence
Robert K. Naviaux, The Mitochondrial and Metabolic Disease Center, University of California, San Diego School of Medicine, 214 Dickinson St., Bldg CTF, Rm C102, San Diego, CA 92103-8467. Tel: 619-543-2904; Fax: 619-543-7868;
E-mail: Naviaux@ucsd.edu

Funding Information
All funding for this study was philanthropic. This work was supported in part by gifts from the William Wright Family Foundation, the UCSD Christini Fund, the Autism Research Institute (ARI), the Lennox Foundation, the Gupta Family and Satya Fund, the Agrawal Family, Linda Clark, the N of One Autism Research Foundation, the Rodakis Family, the It Takes Guts Foundation, the UCSD Mitochondrial Disease Research Fund, Dr. Elizabeth Mumper Cooper, and the Daniel and Kelly White Family. Funding for the mass spectrometers was provided by a gift from the Jane Botsford Johnson Foundation. The funders of the study had no role in study design, data collection or analysis, decision to publish, or preparation of the manuscript.

Abstract

Objective: No drug is yet approved to treat the core symptoms of autism spectrum disorder (ASD). Low-dose suramin was effective in the maternal immune activation and Fragile X mouse models of ASD. The Suramin Autism Treatment-1 (SAT-1) trial was a double-blind, placebo-controlled, translational pilot study to examine the safety and activity of low-dose suramin in children with ASD. **Methods**: Ten male subjects with ASD, ages 5–14 years, were matched by age, IQ, and autism severity into five pairs, then randomized to receive a single, intravenous infusion of suramin (20 mg/kg) or saline. The primary outcomes were ADOS-2 comparison scores and Expressive One-Word Picture Vocabulary Test (EOWPVT). Secondary outcomes were the aberrant behavior checklist, autism treatment evaluation checklist, repetitive behavior questionnaire, and clinical global impression questionnaire. **Results**: Blood levels of suramin were 12 ± 1.5 μmol/L (mean $\pm$ SD) at 2 days and 1.5 ± 0.5 μmol/L after 6 weeks. The terminal half-life was 14.7 ± 0.7 days. A self-limited, asymptomatic rash was seen, but there were no serious adverse events. ADOS-2 comparison scores improved by -1.6 ± 0.55 points ($n = 5$; 95% CI = -2.3 to -0.9; Cohen's $d = 2.9$; $P = 0.0028$) in the suramin group and did not change in the placebo group. EOWPVT scores did not change. Secondary outcomes also showed improvements in language, social interaction, and decreased restricted or repetitive behaviors. **Interpretation**: The safety and activity of low-dose suramin showed promise as a novel approach to treatment of ASD in this small study.

Received: 25 February 2017; Revised: 18 April 2017; Accepted: 20 April 2017

doi: 10.1002/acn3.424

Clinical Trial Registration: https://clinicaltrials.gov/ct2/show/NCT02508259

Introduction

Autism affects 1–2% of children in the United States.[1,2] Dozens of single genes and chromosomal copy number variants (CNVs)[3] increase the relative risk of autism spectrum disorder (ASD) nearly 5–50 times over the current background risk. Yet no single gene or CNV causes ASD in 100% of children who carry the mutation,[4] and no single DNA mutation accounts for more than 1–2% of all ASD.[5] Specific environmental factors have also been shown to increase the risk of ASD.[6,7] However, no single child has all of the known genetic risk factors for ASD, or is exposed to all the same environmental risks. Although the noncore symptoms of ASD are highly heterogeneous from child to child, making each child unique, the same core features used for diagnosis – abnormalities in social communication, restricted interests, repetitive behaviors, adherence to routine, and/or atypical sensory behaviors – are by definition expressed in every child. One approach to addressing the challenge of many etiologies of ASD is to define a common pathophysiology that can contribute to the core diagnostic symptoms, regardless of the initiating genetic and environmental triggers. We hypothesized that there is a conserved cellular response to metabolic perturbation or danger that is shared by all children with ASD. This is called the cell danger hypothesis.[8] Aspects of the cell danger response (CDR) are also referred to as the integrated stress response.[9–11] Preclinical studies showed that the cell danger response in mice produced a treatable metabolic syndrome that was maintained by purinergic signaling. Antipurinergic therapy with suramin corrected both the behavioral and metabolic features of these genetic and environmental mouse models of ASD.[12–14]

The formulation of the cell danger hypothesis was based on the recognition that similar metabolic pathways were coordinately regulated as an adaptive response to cellular threat regardless of whether the perturbation was caused by a virus,[15] a bacterium,[16] genetic forms of mitochondrial disease,[10] or neurodevelopmental disorders with complex gene–environment pathogenic mechanisms like autism.[17] These metabolic pathways traced to mitochondria. Mitochondria are responsible for initiating and coordinating innate immunity[18] and produce stereotyped changes in oxidative metabolism under stress[19] that lead to the regulated release of purine and pyrimidine nucleotides like ATP and UTP through cell membrane channels.[20] Inside the cell, ATP is an energy carrier. Outside the cell, extracellular ATP (eATP) is a multifunctional signaling molecule, a potent immune modulator,[21] and a damage-associated molecular pattern (DAMP) that can activate microglia, and trigger IL-1β production and inflammasome assembly.[22] Extracellular purines like ATP, ADP, and adenosine, and pyrimidines like UTP are ligands for 19 different purinergic (P2X, P2Y, and P1) receptors.[23] The intracellular concentration of ATP (iATP) in mammalian cells is typically 1–5 mmol/L,[24] but drops when ATP is released through membrane channels under stress. Typical concentrations of extracellular adenine nucleotides in the unstirred water layer at the cell surface where receptors and ligands meet are about 1–10 μmol/L, near the effective concentration for most purinergic receptors,[25] but can increase when ATP is released during cell stress. Concentrations of eATP in the blood are another 500 times lower (10–20 nmol/L).[26] Purinergic effectors like ATP are also coreleased with canonical neurotransmitters like glutamate, dopamine, and serotonin during depolarization at every synapse in which they have been studied[23] and play key roles in activity-dependent synaptic remodeling.[27] These and other features[28–30] led us to test the hypothesis that the CDR[8] was maintained by purinergic signaling.[12–14]

Suramin has many actions. One of its best-studied actions is as an inhibitor of purinergic signaling. It is the oldest member of a growing class of antipurinergic drugs (APDs) in development.[31] Suramin was first synthesized in 1916,[32] making it one of the oldest manmade drugs still in medical use. It is used to treat African sleeping sickness (trypanosomiasis), and remains on the World Health Organization list of essential medications. Concerns about the toxicity of high-dose suramin arose when the cumulative antitrypanosomal dose was increased 5 times or more over several months to treat AIDS or kill cancer cells during chemotherapy. When blood levels were maintained over 150 μmol/L for 3–6 months at a time to treat cancer, a number of dose-limiting side effects were described.[32] These included adrenal insufficiency, anemia, and peripheral neuropathy. In contrast, mouse studies suggested that high-dose suramin was not necessary to treat autism-like symptoms. These studies showed that low-dose suramin that produced blood levels

of about 5–10 μM was effective in treating ASD-like symptoms and did not produce toxicity even when used for at least 4 months.[12,14]

Here, we report the findings of the Suramin Autism Treatment-1 (SAT-1) trial, the first direct test of suramin, the cell danger hypothesis, and the relevance of abnormal purinergic signaling in children with ASD. These data help form the foundation for future studies that will test the safety and efficacy of suramin, provide fresh directions for the development of new antipurinergic drugs, and add support to the hypothesis that a potentially treatable metabolic syndrome may contribute to the pathogenesis of autism.

Materials and Methods

Study design and participants

The SAT-1 trial was an investigator-initiated, phase I/II, double-blind, placebo-controlled, randomized clinical trial to examine the safety and activity of single-dose suramin or placebo in 10 children with autism spectrum disorders (ASD). All children met DSM-5 diagnostic criteria for autism spectrum disorder, and received confirmatory testing by Autism Diagnostic Observation Schedule, 2nd edition (ADOS-2) examination. Inclusion criteria were male subjects, ages 4–17 years, living in the San Diego, California region, with a confirmed diagnosis of ASD. Exclusion criteria included children who weighed less than the 5th percentile for age, took prescription medications, or had laboratory evidence of liver, kidney, heart, or adrenal abnormalities. Children living more than a 90-min drive from the testing sites in La Jolla, CA were excluded to eliminate the possibility of aberrant behaviors resulting from extended car travel. Children with known syndromic forms of ASD caused by DNA mutation or chromosomal copy number variation (CNV) were excluded in this first study. Families were asked not to change their children's therapy (e.g., supplements, speech, and behavioral therapies) or diet throughout the study period. The study was conducted between 27 May 2015 (date of the first child to be enrolled) and 3 March 2016 (date of the last child to complete the study).

Regulatory approvals, registration, CONSORT, and informed consent

The research plan, clinical trial protocol, informed consents, advertising, and amendments were approved by the University of California, San Diego (UCSD) Institutional Review Board (IRB Project #150134) before implementation. The study was authorized by the U.S. Food and Drug Administration (IND#118212), and conformed to the World Medical Association Declaration of Helsinki–Ethical Principles for Medical Research Involving Human Subjects,[33] and the International Council for Harmonization (ICH) E6 Good Clinical Practice (GCP) guidelines. The trial was registered with clinical trials.gov (https://clinicaltrials.gov/ct2/show/NCT02508259). Reporting of the SAT-1 trial conformed to CONSORT 2010 guidelines.[34] Signed informed consent, with additional consent for video and still image photography, were obtained from the parents of all participants before enrollment and randomization. Storyboards and social stories were created to review with parents, help children visualize and prepare for the study, and create the opportunity to ask questions (Figure S1, Data S2).

Randomization and masking

Twenty male subjects with ASD were screened. Sixteen met entry criteria. Ten participants could be matched by age, nonverbal IQ, and ADOS scores into five pairs. The randomization sequence was generated electronically by the biostatistical team. Subjects within each pair were allocated to receive suramin or saline according to the prospectively determined randomization sequence. The randomization sequence was concealed from the clinical team and implemented by the UCSD investigational pharmacy, which prepared drug and placebo for infusion. The design was double blind. The mask was not broken until all subjects had completed the study and all clinical data had been collected.

Diagnostic and outcome procedures

The diagnosis of each of the enrolled participants was confirmed by ADOS-2[35] comparison scores of $\geq$7. Nonverbal IQ was tested by Leiter-3 examination.[36] The primary behavioral outcomes were ADOS scores and language assessed by standardized vocabulary testing. Expressive vocabulary was assessed by Expressive One-Word Picture Vocabulary Test (EOWPVT).[37] Primary outcomes were measured at baseline, and 2 days and 6 weeks after infusion. Secondary outcomes were the Aberrant Behavior Checklist (ABC),[38] Autism Treatment Evaluation Checklist (ATEC),[39,40] Clinical Global Impression of Improvement (CGI)[41] (Data S1), and Repetitive Behavior Questionnaire (RBQ).[42] Secondary outcomes were measured at baseline, and 7 days and 6 weeks after infusion.

Protocol deviations

The original protocol was designed to collect electroencephalography (EEG), heart rate variability (HRV), balance, gait, fine motor, and sensory motor data as secondary outcomes. However, the wide range in ages and abilities, small subject numbers, and task compliance difficulties made collection of these data incomplete and

insufficiently powered to draw any conclusions. In addition, we found that major language advances were in the form of new speech fluency and new interest in speech and social communication, and not in new vocabulary. Peabody Picture Vocabulary Testing (PPVT) did not capture this new interest in communication. These data were incomplete and insufficiently powered for analysis.

Drug and placebo administration

Suramin was provided as the hexasodium salt (MW 1429.2 g/mol) in 1 g lyophilized vials by Bayer Pharma AG (Leverkusen, Germany), under Dr. Naviaux's IND #118212. Lot #BXNOGW1, expiration date of 3 September 2018, was used in these studies. A 1 g vial was reconstituted in 10 mL of sterile water for infusion to prepare a 10% (100 mg/mL) solution. All infusions were conducted at the University of California, San Diego School of Medicine Clinical and Translational Research Institute (CTRI) in La Jolla, CA. Height and weight were recorded, vital signs and capillary oxygen saturation (pulse oximetry) measured, physical and neurological examinations were conducted, and urine and blood for safety monitoring, pharmacology, and metabolomics were collected before the infusion. Each child then received a 50 mg test dose (0.5 mL of a freshly reconstituted 10% solution) of suramin in 5 mL of saline, or 5 mL of saline only given by slow intravenous (IV) push over 3 min, followed by a 10-mL flush of saline. One hour after the test dose, vital signs were repeated and a single infusion of either suramin (20 mg/kg, minus the 50 mg test dose, in 50 mL, up to a maximum of 1 g) or saline (50 mL IV) was given over 30 min, followed by a 10-mL flush of saline. One hour after completion of the infusion, vital signs and the physical and neurological examinations were repeated, blood was collected for safety monitoring and pharmacology, and the family discharged to home. A typical infusion visit to the Clinical Translational Research Institute (CTRI) lasted about 4 h from start to finish.

Safety and adverse event monitoring

Blood and urine samples were collected for safety and toxicity monitoring at 5 times throughout the study: at baseline (32 ± 6 days before the infusion; mean ± SEM),

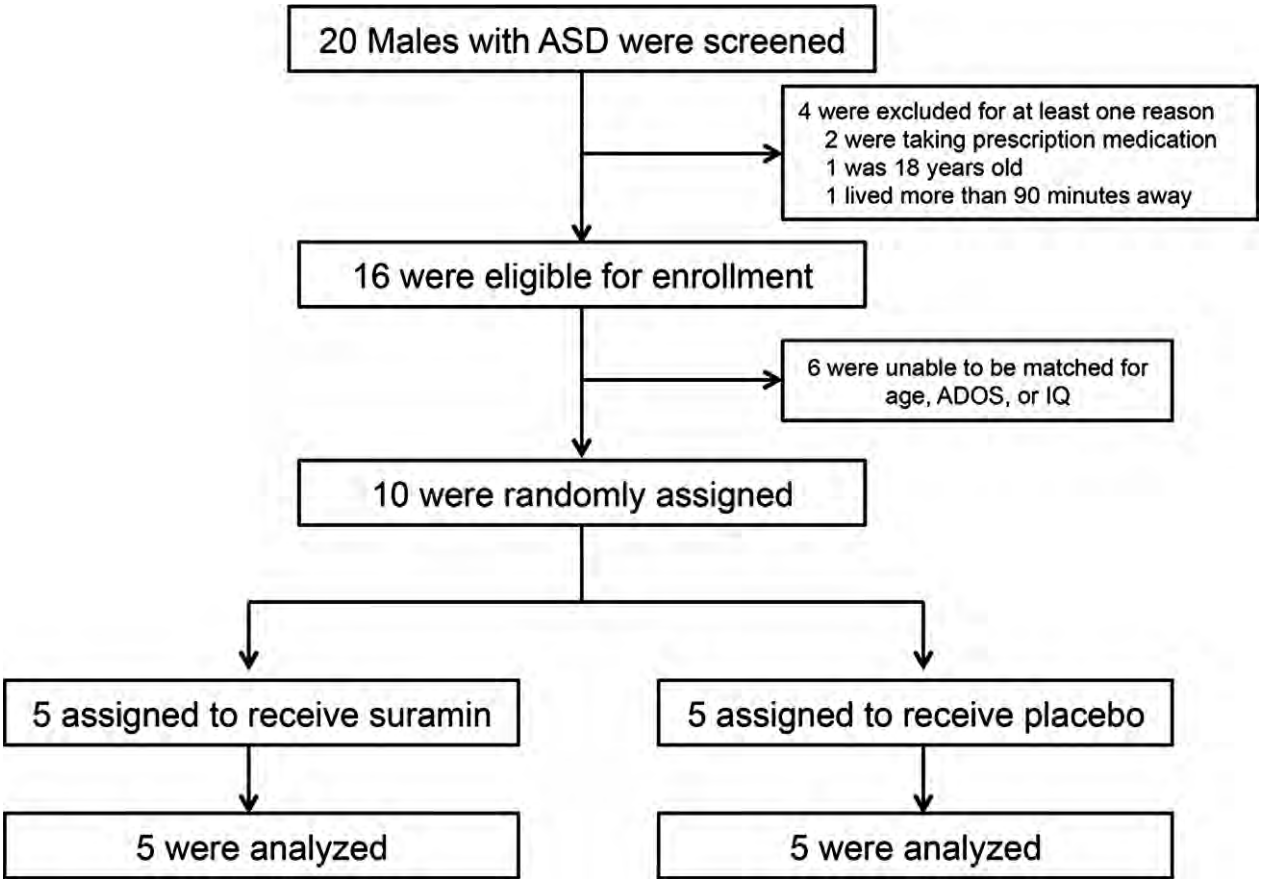

Figure 1. Trial profile.

immediately before the infusion, 1 h after the infusion, 2 days after, and 45 days after the infusion. Unexpected and adverse events were recorded as they occurred and graded in severity according to the National Cancer Institute Common Terminology Criteria for Adverse Events v4.03 (CTCAE) scale. Additional pharmacovigilence monitoring included daily scripted phone calls in the first week, then 4 weekly calls until the exit examinations at 6 weeks. Each child received a formal neurological examination by a board-certified pediatric neurologist at baseline and at the end of the study. An independent data safety monitoring board (DSMB) reviewed the data and IRB communications for the study.

Pharmacokinetics

Plasma samples were collected for suramin pharmacokinetics (PK) before the infusion, at 1 h, 2 days, and 45 days postinfusion. Suramin concentrations were measured by high-performance liquid chromatography and tandem mass spectrometry (LC-MS/MS) as described previously.[13] See Supplemental Methods for details. The small number of PK samples per subject prevented a standard, noncompartmental analysis in individual subjects. The suramin drug concentrations were analyzed using a population PK approach with post hoc empiric Bayesian estimate of PK parameters in individual subjects. The PK data were fit to a two-compartment model using the computer program NONMEM (ICON, Dublin, Ireland).[43] PK parameters were scaled allometrically with volume terms scaled to linear body weight ($kg^{1.0}$) and clearance terms scaled to weight ($kg^{0.75}$). Scaled adult suramin parameters of compartmental volumes of distribution and clearance were used as initial parameter estimates and between subject variability only estimated for clearance (CL) and the peripheral volume of distribution (V_d).

Pharmacometabolomics

Targeted, broad-spectrum, plasma metabolomic analysis, covering 63 biochemical pathways, was performed by LC-MS/MS as described previously[44] with minor modifications. In all, 431 of 610 targeted metabolites were measureable in plasma. See Supplemental Methods for details.

Table 1. Group characteristics.

Parameter	Suramin group Mean ± SD (range) or Number	Placebo group Mean ± SD (range) or Number	*P* value[2]
Number (male subjects)	5	5	N/A
Age (years)	8.9 ± 3.3 (5.7–13.6)	9.2 ± 3.8 (6.2–14.7)	0.88
Leiter IQ	82 ± 7.8 (75–92)	79 ± 8.8 (66–87)	0.69
ADOS Score	8.6 ± 0.9 (8–10)	9.4 ± 1.3 (7–10)	0.30
Weight (kg)	32 ± 14 (23–55)	40 ± 23 (24–80)	0.53
Weight percentile	64 ± 16 (42–84)	78 ± 30 (25–98)	0.40
Height (cm)	136 ± 23 (118–174)	137 ± 28 (113–180)	0.92
BSA[1] (m^2)	1.09 ± 0.32 (0.87–1.63)	1.21 ± 0.46 (0.87–1.99)	0.64
Body mass index (kg/m^2)	16.8 ± 1.1 (15.5–18.1)	19.9 ± 3.1 (16.2–24.7)	0.07
Head circumference (cm)	54.3 ± 2.8 (51.5–57.5)	54.5 ± 2.3 (51.5–57)	0.90
HC percentile	75 ± 30 (35–99)	75 ± 27 (42–97)	0.97
Age at ASD diagnosis (yrs)	3.2 ± 0.5 (2.5–3.75)	2.7 ± 0.3 (2.5–3.0)	0.10
Paternal age at birth (yrs)	37 ± 3.2 (35–41)	43 ± 12 (33–64)	0.62
Maternal age at birth (yrs)	35 ± 2.8 (32–38)	41 ± 6 (33–47)	0.053
Sibling with ASD	0	1	0.99
History of GI issues – current	0	1	0.99
Maintains a gluten-free diet	0	1	0.99
IVF conception	1	0	0.99
C-section delivery	1	1	0.99
History of premature birth	0	1	0.99
History of epilepsy[3] – current	0	0	0.99
History of developmental regression(s)	3	2	0.99
History of asthma – current	0	0	0.99
ASD symptom improvement with fever	2	1	0.99

BSA, body surface area; HC, head circumference; GI, gastrointestinal; IVF, in vitro fertilization; ASD, autism spectrum disorder.
[1]Mosteller method.
[2]Student's *t*-test for continuous data; Fisher's exact test for categorical data.
[3]Patients taking prescription drugs were excluded from the study. This included anticonvulsant medications.

Sample size calculation and statistical analysis

This was a pilot study designed to obtain activity data and effect size estimates upon which future sample size calculations could be based. No data on suramin in autism were available for sample size calculations prior to this study. Each child was used as his own control to examine before and after treatment effects in a paired *t*-test design for the analysis of the ADOS, EOWPVT, ABC, ATEC, RBQ, and blood and urine safety data. Paired, nonparametric analysis was done by Wilcoxon signed-rank sum test. Categorical data, such as the presence or absence of adverse events or historical symptoms, was analyzed by Fisher's exact test. Two-way ANOVA (treatment × time), with Sidak post hoc correction, was used to analyze the 6-week summaries captured by the ADOS, CGI, and blood and urine safety analysis. Cohen's *d* – calculated as the mean difference of the paired, within-subject scores before and after treatment, divided by the standard deviation of the differences – was used as an estimate of effect size. Metabolomic data were log-transformed, scaled by control standard deviations, and analyzed by multivariate partial least squares discriminant analysis (PLSDA), with pairwise comparisons and post hoc correction for multiple hypothesis testing using Fisher's least significant difference method in MetaboAnalyst,[45] or the false discovery rate (FDR) method of Benjamini and Hochberg. Metabolites with variable importance in projection (VIP) scores determined by PLSDA that were greater than 1.5 were considered significant. Methods were implemented in Stata (Stata/SE12.1, StataCorp, College Station, TX), Prism (Prism 6, GraphPad Software, La Jolla, CA), or R. Significant metabolites were grouped into pathways and their VIP scores summed to determine the rank-ordered significance of each biochemical pathway.

Results

Participant disposition and demographics

Figure 1 illustrates the CONSORT flow diagram for patient recruitment, allocation, and analysis in the SAT-1 study. The two treatment groups were well matched (Table 1). The mean age was 9.1 years (range = 5–14). The mean nonverbal Leiter IQ was 80 (range = 66–92). The mean ADOS-2 comparison score was 9.0 (range = 7–10).

Safety monitoring and adverse events

Extensive monitoring revealed no serious toxicities (CTCAE grades 3–5). Neurologic examinations showed there was no peripheral neuropathy (Table 2). Analysis of free cortisol, hemoglobin, white blood cell count (WBC), platelets, liver transaminases, creatinine, and urine protein showed no differences in children who received suramin and placebo (Fig. 2). Five children who received suramin

Table 2. Summary of adverse or unanticipated events.

No.	Events	Suramin (*N* = 5)	CTCAE[1] grade	Placebo (*N* = 5)	CTCAE[1] grade	*P* value[2]
1	Asymptomatic rash	5	1	0	–	0.0079
2	Uncomplicated URI[3]	2	1	2	1	0.99
3	Headache	1	1	0	–	0.99
4	Emesis × 1	1[4]	1	1[5]	1	0.99
5	Hyperactivity	2[6]	1	1	1	0.99
6	Hypoglycemia[7]	1	2	1	2	0.99
7	Leukocytosis	0	–	1[8]	1	0.99
8	Enuresis	1[9]	1	0	–	0.99
9	Peripheral neuropathy	0	–	0	–	0.99
	Total:	13	–	6	–	0.12
	Nonrash AEs:	8	–	6	–	0.77

[1]CTCAE, common terminology criteria for adverse events v4.03. Mild to moderate = Grades 1–2; Serious = Grades 3–5.
[2]Fisher's exact test.
[3]URI, upper respiratory tract infection, common cold. Infusions occurred October–February.
[4]In 7-year-old after pizza and slushee consumption after playing youth league basketball.
[5]In a 6-year-old after a car ride.
[6]In a 5- and 14-year-old intermixed with periods of calm focus in first week (the 14-year-old) or first 3 weeks (the 5-year-old).
[7]Six weeks after the infusion, after several days of a URI and fasting before lunch. Hypoglycemia was asymptomatic and corrected after a normal lunch.
[8]Leukocytosis (12.2k WBC) occurred on the day of the saline infusion and preceded a URI.
[9]In a 7-year-old briefly for a few days while sick with a cold. None of the events required medical intervention. No serious adverse events (SAEs) occurred in this study.

developed a self-limited, evanescent, asymptomatic, fine macular, patchy, morbilliform rash over 1–20% of their body (Fig. 2HI). This peaked 1 day after the infusion and disappeared spontaneously in 2–4 days. The mean number of AEs per participant was 1.9 (1.2 in the placebo group and 2.6 in the suramin group; 1.6 in the suramin group for a nonrash AE; RR = 1.3; 95% CI = 0.5–3.4; $P = 0.77$; Table 2). No serious adverse events (SAEs) occurred in this study. An independent data and safety monitoring board (DSMB) reviewed this information, as well as the clinical safety and toxicity data and IRB communications from the study, and found no safety concerns.

Pharmacokinetics

Pharmacokinetic analysis showed that at 1 h after intravenous infusion of 20 mg/kg (558 ± 41 mg/m^2; mean ± SD; Table S1), the suramin concentration was 104 ± 11.6 μmol/L (Fig. 3A). The distribution phase half-life was 7.4 ± 0.55 h. The suramin levels rapidly fell below 100 μmol/L and into the target range before day 2 in all subjects, with an average plasma level of suramin of 12.0 ± 1.5 μmol/L on day 2 (Fig. 3B, Table S1). Target concentrations of 1.5–15 μmol/L were maintained between 2 days and 6 weeks following the dose (Fig. 3). The steady-state volume of distribution was 0.83 ± 0.014 L/kg (22.7 ± 2.6 L/m^2). The clearance was 1.95 ± 0.21 mL/h/kg (0.056 ± 0.011 L/h/m^2). The terminal elimination phase half-life ($t_{1/2}$) was 14.7 ± 1.4 days (Fig. 3B,D). A two-compartment PK model showed excellent fit between measured and predicted plasma levels ($r^2 = 0.998$; Fig. 3C). These data are the first in the published literature on the pharmacokinetics of suramin in a pediatric population.

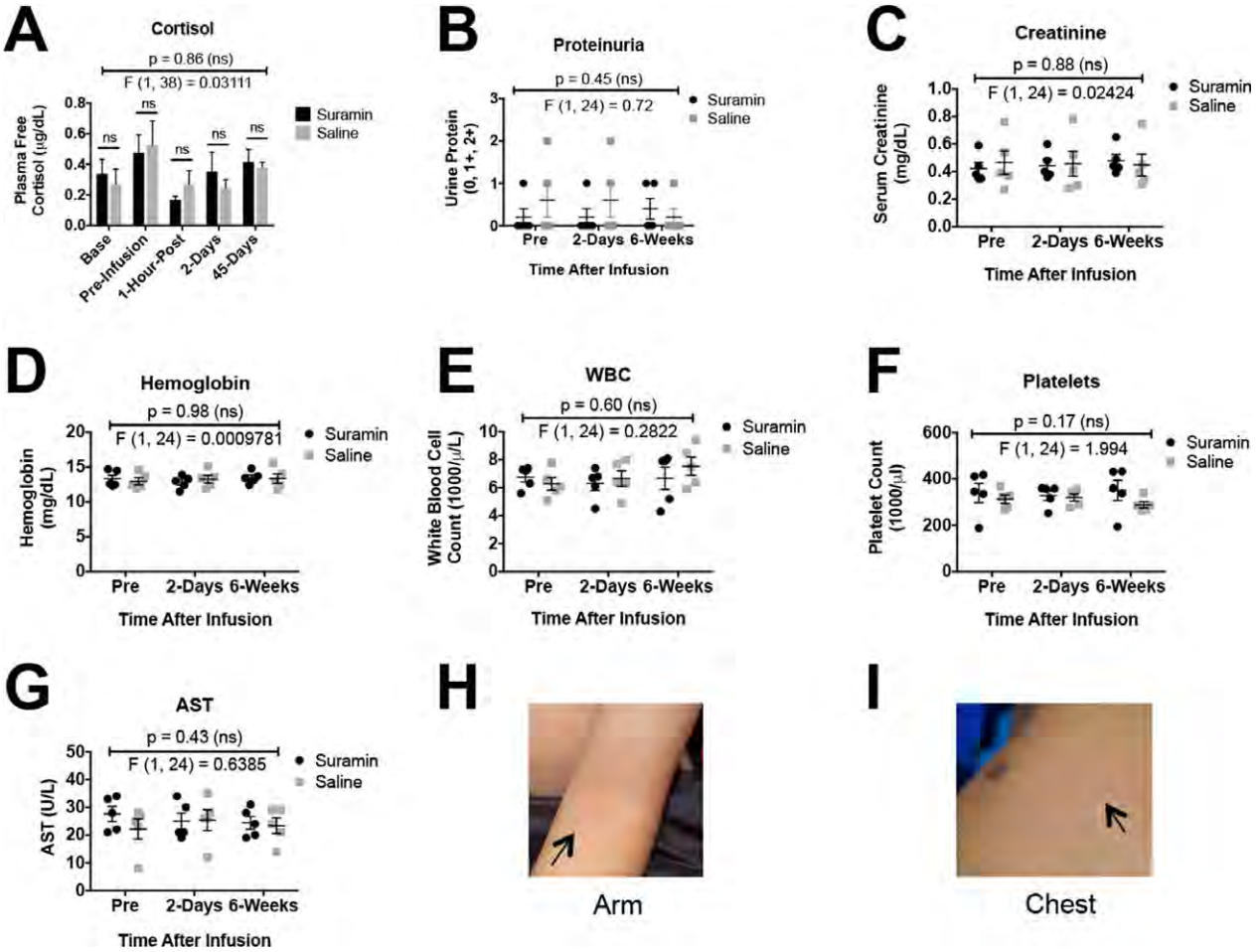

Figure 2. Safety monitoring. (A) Free cortisol, (B) proteinuria, (C) creatinine, (D) hemoglobin, (E) white blood cells (WBC), (F) platelets, (G) aspartate aminotransferase (AST), (H) rash – antecubital fossa, (I) chest. Data were analyzed by two-way ANOVA to test for treatment, time, and treatment × time interaction effects. *P* and *F* values reflect the treatment effect. Only the rash was significantly different between suramin and placebo groups.

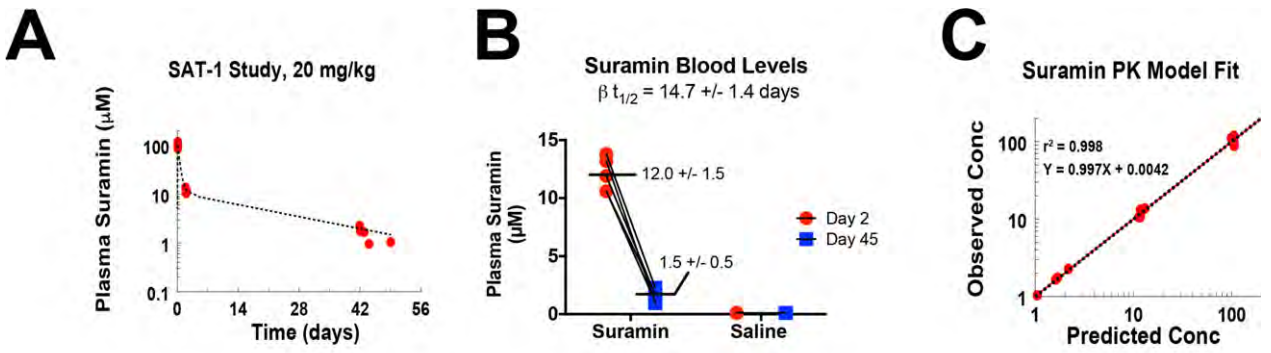

D

Parameter	Symbol	Mean ± sd
Beta elimination half-life	$t_{1/2}\,\beta$	14.7 ± 1.4 days
Alpha elimination half-life	$t_{1/2}\,\alpha$	7.41 ± 0.55 hours
Clearance	CL	1.95 ± 0.21 mL/hr/kg
Steady state volume of distribution	Vd_{ss}	0.83 ± 0.014 L/kg

Figure 3. Pharmacokinetics of single-dose suramin in children with autism spectrum disorders. (A) Two-compartment model of suramin blood concentrations. The first 48 h were dominated by the distribution phase. Over 90% of the model is described by the elimination phase. (B) Plasma suramin concentrations. (C) A two-compartment model correlated well with measured values. (D) Pediatric PK parameters of suramin.

Pharmacometabolomics

Targeted plasma metabolomics was performed immediately before infusion, at 2 days, and 6 weeks after the infusion. The rank order of the top 35 of 48 significant metabolites 6 weeks after suramin treatment is illustrated in Figure 4. The rank order after 2 days is illustrated in Figure S2. Consistent with our previously published work using mouse models, the metabolic effects of suramin resulted in a decrease of the cell danger response[8] and restored more normal metabolism.[12,13] Purine metabolism was the single most changed pathway (Table 3, Table S2). Suramin increased healthy purines such as AICAR, which is an activator of the master metabolic regulator AMP-dependent protein kinase (AMPK). 1-Methyl-adenine (1-MA) was also increased. 1-MA is derived from 1-methyl-adenosine, a recently recognized marker of new protein synthesis and cell growth. Suramin decreased other purines in the plasma such as cAMP and dGDP (Fig. 4, Tables S3 and S4). Improvements in 1-carbon, folate, methionine, and cysteine metabolism were also found (Table 3, and Figure S3). Figure 5 illustrates the similarities found in the pharmacometabolomic response to suramin in MIA[13] and Fragile X mouse models[12] and in children with ASD in this study. Twenty-one of the 28 (75%) pathways changed in ASD were also changed by suramin treatment in the mouse models of ASD (Fig. 5).

Outcomes

The primary outcome measures were ADOS-2 and Expressive One-Word Picture Vocabulary (EOWPVT) scores (Table 4). Parents reported that after suramin treatment, the rate of language, social, behavioral, and developmental improvements continued to increase for 3 weeks, then gradually decreased toward baseline over the next 3 weeks. The blood levels of suramin at 3 weeks were estimated to be 4.2 ± 0.5 μmol/L using our PK model. ADOS-2 comparison scores at 6 weeks improved by an average of −1.6 ± 0.55 points (mean ± SD; n = 5; 95% CI = −2.3 to −0.9; Cohen's d = 2.9; P = 0.0028) in the suramin treatment group and did not change in the saline group. We calculated P values by both parametric and nonparametric methods (Table 4). The mean ADOS comparison score in the suramin-treated group was 8.6 ± 0.4 at baseline and 7.0 ± 0.3 at 6 weeks. Two-way ANOVA of ADOS scores of suramin and placebo groups measured at baseline and at 6 weeks were also significant (treatment × time

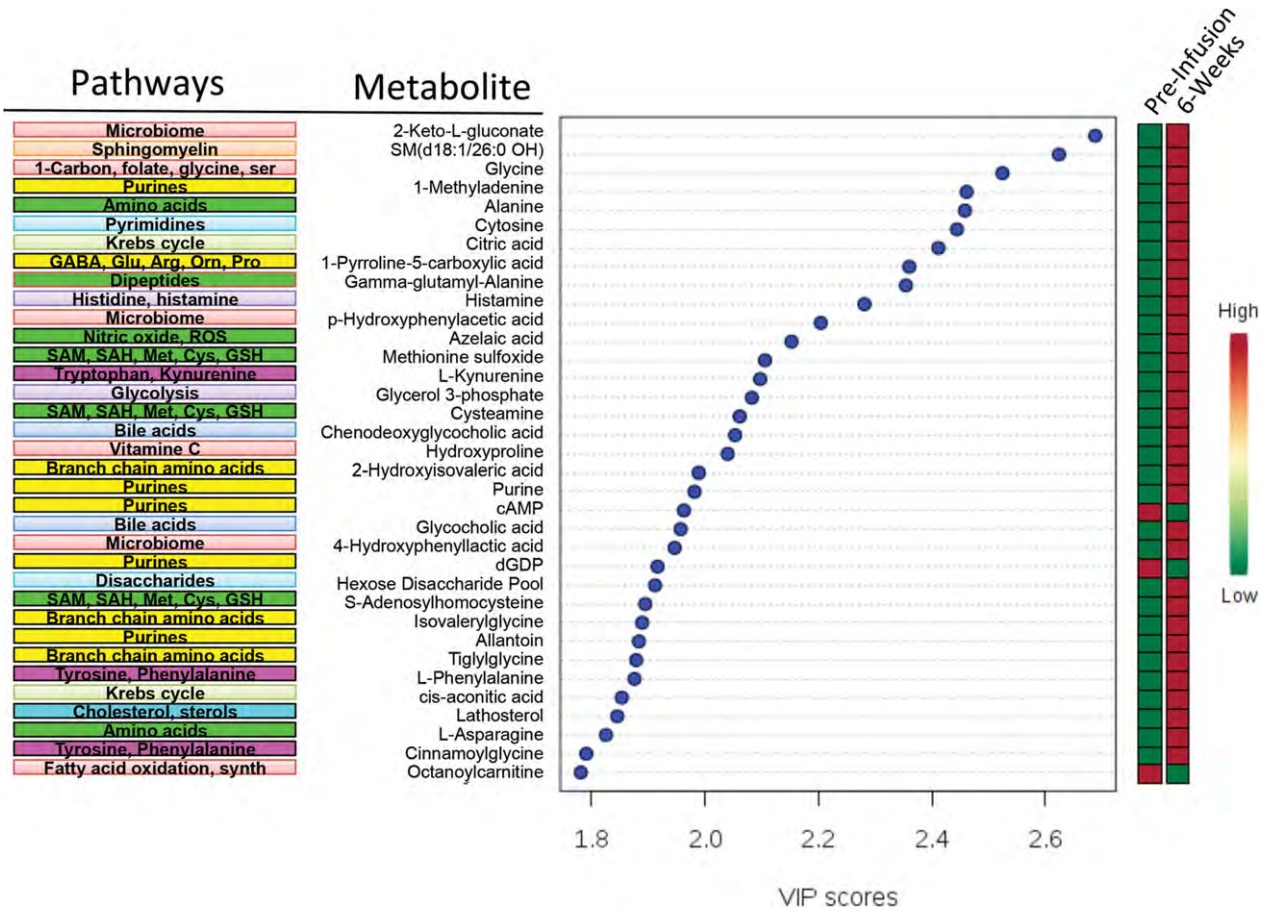

Figure 4. Suramin pharmacometabolomics. Rank order of metabolites and pathways that were changed by suramin at 6 weeks after treatment.

interaction $F(1, 8) = 12.0$; $P = 0.0085$; Figure S4A). ADOS scores were not changed in the saline-treated group (Table 4). EOWPVT scores did not change (Table 4). Several secondary outcome measures also showed improvements. These included improvements in ABC, ATEC, and CGI scores (Table 4). The Repetitive Behavior Questionnaire (RBQ) scores did not capture a change.

Discussion

The aim of the SAT-1 trial was to test the safety, pharmacokinetics, and pharmacodynamics of low-dose suramin in children with ASD. A self-limited rash was seen, but no serious adverse events occurred. Pharmacometabolomic analysis showed that the pathways changed by suramin treatment in ASD were previously known mediators of the cell danger response (CDR)[8] and that purine metabolism was changed most. Seventy-five percent of the pathways changed by suramin in children with ASD were also changed by suramin in mouse models.[12–14]

Safety

Suramin has been used safely for nearly a century to treat both children and adults with African sleeping sickness. Although side effects occurred occasionally, these could be minimized by attention to patient nutritional status, proper dose, administration procedures, and measured blood levels of suramin.[46] The low dose of suramin used in this study produced blood levels of 1.5–15 μmol/L for 6 weeks. Previous studies have never examined the side-effect profile of suramin in this low-dose range. The side-effect profile of high-dose suramin (150–270 μmol/L) is known from cancer chemotherapy studies.[32] The side-effect profile from medium-dose suramin (50–100 μmol/L) is known from African sleeping sickness studies.[46] However, the side-effect profile of low-dose suramin (5–15 μmol/L) used for antipurinergic therapy (APT) in autism is unknown. Low-dose suramin was found to be safe in five children with ASD, ages 5–14 years, in this study.

Table 3. Suramin pharmacometabolomics: biochemical pathways changed at 6-weeks.

No.	Pathway name	Measured metabolites in the pathway (*N*)	Expected pathway proportion (*P* = N/429)	Expected hits in sample of 48 (P × 48)	Observed hits in the top 48 metabolites	Fold enrichment (obs/exp)	Impact (sum VIP score)	Fraction of impact (VIP score) explained (% of 94.6)	Increased	Decreased
1	Purine metabolism	26	0.061	2.9	5	1.7	10.2	11%	3	2
2	SAM, SAH, methionine, cysteine, glutathione	15	0.035	1.7	5	3.0	9.5	10%	5	0
3	Microbiome metabolism	18	0.042	2.0	4	2.0	8.4	9%	4	0
4	Branch chain amino acid metabolism	12	0.028	1.3	4	3.0	7.4	8%	4	0
5	Bile acid metabolism	6	0.014	0.7	3	4.5	5.7	6%	3	0
6	Fatty acid oxidation and synthesis	37	0.086	4.1	3	0.7	5.0	5%	0	3
7	Amino acid metabolism (alanine)	4	0.009	0.4	2	4.5	4.3	5%	2	0
8	Krebs cycle	9	0.021	1.0	2	2.0	4.3	5%	2	0
9	Pyrimidine metabolism	9	0.021	1.0	2	2.0	4.2	4%	2	0
10	Sphingomyelin metabolism	36	0.084	4.0	2	0.5	4.1	4%	2	0
11	1-Carbon, folate, formate, glycine, serine	5	0.012	0.6	2	3.6	4.0	4%	2	0
12	GABA, glutamate, arginine, ornithine, proline	6	0.014	0.7	2	3.0	3.9	4%	2	0
13	Tyrosine and phenylalanine metabolism	3	0.007	0.3	2	6.0	3.7	4%	2	0
14	Cholesterol, cortisol, nongonadal steroid	16	0.037	1.8	2	1.1	3.5	4%	2	0
15	Gamma-glutamyl and other dipeptides	2	0.005	0.2	1	4.5	2.4	2%	1	0
16	Histidine, histamine, carnosine metabolism	4	0.009	0.4	1	2.2	2.3	2%	1	0
17	Nitric oxide, superoxide, peroxide metabolism	2	0.005	0.2	1	4.5	2.2	2%	1	0
18	Tryptophan, kynurenine, serotonin, melatonin	6	0.014	0.7	1	1.5	2.1	2%	1	0
19	Glycolysis and gluconeogenesis metabolism	7	0.016	0.8	1	1.3	2.1	2%	1	0
20	Vitamin C (ascorbate) metabolism	2	0.005	0.2	1	4.5	2.0	2%	1	0
21	Amino-sugar, hexose metabolism	5	0.012	0.6	1	1.8	1.9	2%	1	0
22	Phospholipid metabolism	73	0.170	8.2	1	0.1	1.6	2%	0	1
								Subtotal:	42	6
								Total:	48	

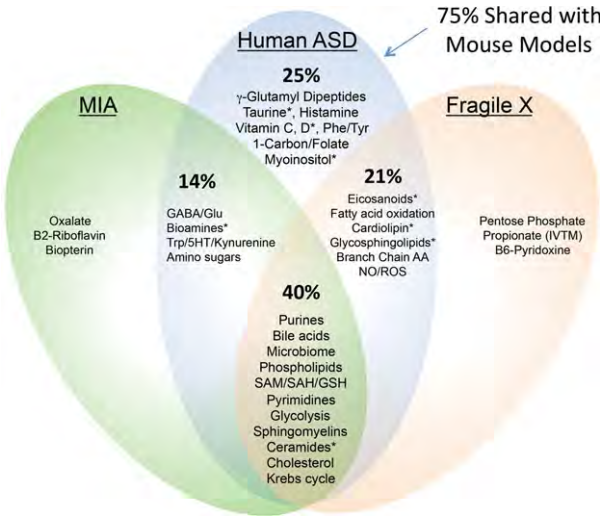

Figure 5. Shared biochemical pathways. 75% of the pathways that were altered by suramin in children with ASD were also altered in the mouse models. Asterisks (*) indicate pathways that were changed at 2 days, but not at 6 weeks after treatment.

Study limitations

Limitations of the SAT-1 study included its small size and the suboptimal timing of the outcome measurements. Parents reported that the rate of new behavioral and developmental improvements continued to increase for the first 3 weeks after the single dose of suramin, as blood levels of suramin fell from 12 to 4 μmol/L, then gradually decreased toward baseline over the next 3 weeks, as blood levels fell further from 4 to 1.5 μmol/L. This pattern of response suggested a threshold effect at about 4 μmol/L that could not have been predicted on the basis of what was known about suramin before this study, and outcomes were not measured at 3 weeks.

Another potential limitation of the trial was the self-limited rash. The rash was asymptomatic and resolved spontaneously in a few days. In theory, the rash may have biased parents in a way that caused them to either improve their scores on the ABC, ATEC, RBQ, and CGI, or to report more side-effects or adverse behaviors at both the 7-day and 6-week reports. Examiner-based ADOS scoring was more resistant to this potential bias, since the rash was not visible on exposed skin to the outcome examiners at any time. However, a design limitation of the study was that one of the two ADOS examiners was also assigned to conduct scripted phone interviews with the families, and might have been susceptible to unconscious bias even though the study remained blinded and the rash preceded any significant examiner-based outcomes by one and a half months.

Another potential weakness of this study was that ADOS scoring was not designed to be, and is not typically used as, a repeated measure of outcomes in autism treatment studies. This has occurred historically for two counterbalancing reasons: (1) because it is generally believed that ADOS scores are diagnostic and are not sensitive to change once the diagnosis is established, and (2) because training effects have the potential to produce improvements that are artifactual. With regard to the first point, under the right circumstances ADOS scores can be sensitive to change and have recently been used successfully as an outcome measure in a large autism treatment study.[47] With regard to the second point, if training effects occurred, they were asymmetric, since improvements were only observed in the suramin treatment group and were not observed in the placebo group (Table 4).

Psychopharmacology

Suramin has objective central nervous system (CNS) effects in animal models[12–14] and children with autism despite being unable to penetrate the blood–brain barrier.[48] Suramin also has a number of peripheral effects on innate immunity, metabolism, pain, gut, autonomic, inflammatory, and other pathways regulated by purinergic signaling that may contribute to the beneficial effects observed.[8,23] Previous studies have shown that suramin is taken up into the CNS at the level of the brainstem, although not appreciably into the cerebrum or cerebellum.[13] There are eight circumventricular organs (CVOs) in the brain that contain neurons that lack a blood–brain barrier.[49] The area postrema in the brainstem is one of these CVOs that monitors the chemistry of the blood and transduces this information to higher centers in the brain for neuroendocrine, affective, cognitive, and behavioral integration. Rather than being a disadvantage, the peripheral actions and indirect CNS effects of suramin may have certain advantages by minimizing the risk of CNS toxicity. While new antipurinergic drugs (APDs) may soon be developed that can pass the blood–brain barrier, this appears not to be required to produce the behavioral effects of suramin in ASD.

Conclusions

The SAT-1 trial examined the effects of low-dose suramin or placebo in 10 children with autism spectrum disorder. No safety concerns were found. A two-compartment pharmacokinetic model permitted accurate forecasting of plasma drug levels from 1 h to 6 weeks after the infusion. Metabolomic studies confirmed the importance of the cell danger response (CDR)[8] and purinergic signaling.[12–14] A single intravenous dose of suramin was associated with improved scores for language, social interaction, and

Table 4. Outcomes.

Outcome			Suramin						Placebo					
Instrument	Factor or behavior	Time after treatment (days)	Difference from baseline (mean ± SD)	95% CI	d^1	*N*	P^2	P^3	Difference from baseline (mean ± SD)	95% CI	d^1	*N*	P^2	P^3
Primary outcomes														
ADOS-2	Comparison	45	−1.6 ± 0.55	−2.3 to −0.9	2.9	5	0.0028	0.038	−0.4 ± 0.55	−1.1 to +0.28	0.7	5	0.18	0.16
	Raw	45	−4.6 ± 1.9	−7.0 to −2.2	2.4	5	0.0062	0.039	−0.4 ± 1.8	−2.7 to +1.9	0.22	5	0.65	0.58
	Social	45	−3.2 ± 1.9	−5.6 to −0.8	1.7	5	0.020	0.043	0.0 ± 1.7	−2.2 to +2.2	0	5	0.99	0.71
	Restr/Rep	45	−1.4 ± 0.89	−2.5 to −0.29	1.6	5	0.025	0.059	−0.4 ± 2.1	−3.0 to +2.2	0.19	5	0.69	0.58
EOWPVT	Vocabulary	45	−4.2 ± 8.3	−14.5 to +6.1	−0.51	5	0.32	0.50	+2.0 ± 4.6	−3.8 to +7.8	0.43	5	0.39	0.50
Secondary outcomes														
ABC	Stereotypy	7	−3.6 ± 2.1	−6.2 to −1.0	1.7	5	0.018	0.043	+0.4 ± 1.9	−2.0 to +2.8	−0.21	5	0.67	0.68
	Stereotypy	45	−4.0 ± 2.3	−6.9 to −1.1	1.7	5	0.019	0.042	+1.0 ± 4.3	−4.3 to +6.3	−0.23	5	0.63	0.69
ATEC	Total	7	−10 ± 7.7	−20 to −0.46	1.3	5	0.044	0.043	+7.2 ± 14	−10 to +25	−0.51	5	0.32	0.35
	Language	7	−2.2 ± 1.5	−4.0 to −0.36	1.4	5	0.021	0.059	0.0 ± 4.1	−5.0 to +5.0	0	5	0.99	0.89
	Sociability	7	−3.6 ± 2.6	−6.8 to −0.36	1.4	5	0.025	0.063	−0.8 ± 2.8	−4.3 to +2.6	0.29	5	0.55	0.58
	Language	45	−2.0 ± 1.4	−2.7 to −0.49	1.4	5	0.034	0.059	−0.2 ± 2.9	−3.8 to +3.4	0.07	5	0.88	0.79
CGI	Overall ASD	45	−1.8 ± 1.04	−3.4 to −0.15	1.7	5	0.05	n/a	0.0 ± 0.34	−0.55 to +0.55	0	5	0.99	n/a
	E. Language	45	−2.0 ± 1.04	−3.6 to −0.35	1.9	5	0.01	n/a	0.0 ± 0.34	−0.55 to +0.55	0	5	0.99	n/a
	Social Inter.	45	−2.0 ± 1.04	−3.6 to −0.35	1.9	5	0.01	n/a	0.0 ± 0.34	−0.55 to +0.55	0	5	0.99	n/a
RBQ	Total	45	−3.2 ± 5.8	−10.4 to +4.0	0.55	5	0.28	0.22	−0.8 ± 3.3	−4.9 to 3.3	0.24	5	0.62	0.47

ADOS-2, autism diagnostic observation schedule, 2nd edition; EOWPVT, Expressive One-Word Picture Vocabulary Test; ABC, aberrant behavior checklist; ATEC, autism treatment evaluation checklist; CGI, clinical global impression survey; RBQ, repetitive behavior questionnaire; Restr/Rep, restricted or repetitive behaviors; Overall ASD Sx, overall ASD symptoms; E. Language, expressive language; Social Inter., social interaction. *Analysis***.** ADOS, EOWPVT, ABC, ATEC, and RBQ scores were analyzed by paired analysis before and after treatment using each subject as their own control. CGI was analyzed by two-way ANOVA (symptom × time before and after treatment) with post hoc correction. Nonparametric *P* values were not calculated (n/a). *Interpretation***.** ADOS, ABC, ATEC, CGI, and RBQ are severity scores; negative differences from baseline reflect decreased severity, that is, improvement. EOWPVT is a performance score; negative differences reflect a decrease.

[1]A positive Cohen's *d* reflects improvement, and a negative *d* reflects a decrease by convention. Cohen's *d* is likely an overestimate of the actual treatment effect based on the large mean differences and small standard deviations found before and after treatment in this small study.

[2]*P* value from parametric paired *t*-test analysis.

[3]*P* value from nonparametric paired Wilcoxon signed-rank sum analysis.

decreased restricted or repetitive behaviors measured by ADOS, ABC, ATEC, and CGI scores. None of these improvements occurred in the five children who received placebo. The generalizability of these findings is unknown. Future studies will be needed to confirm these findings in larger numbers of children with ASD, and to evaluate whether a few doses of suramin given over a few months are safe and might facilitate continued improvements.

Special note from the authors

Suramin is not approved for the treatment of autism. Like many intravenous drugs, when administered improperly by untrained personnel, at the wrong dose and schedule, without careful measurement of drug levels and monitoring for toxicity, suramin can cause harm. Careful clinical trials will be needed over several years at several sites to learn how to use low-dose suramin safely in autism, and to identify drug–drug interactions and rare side effects that cannot currently be predicted. We strongly caution against the unauthorized use of suramin.

Acknowledgments

RKN thanks the patients and families who gave their time and effort in helping to make this study possible. We thank Dr. Richard Haas, Dr. Doris Trauner, and Dr. Stephen Edelson for their advice in planning the study. We thank Dr. Judy S. Reilly for critical reading of the manuscript and suggestions for improvements. RKN also thanks Jonathan Monk for assistance with the Cytoscape visualizations, Marlene Samano and Nicole Suarez, and Maeve Taaffe, Lee Vowinkel, Dennis Perpetua, Jessica Nasca, Peewee Buquing, and Patricia Moraes for their expert clinical assistance at the UCSD Clinical Translational Research Institute, and Thaine Ross and Melinda Stafford for their expert assistance in the Investigational Pharmacy. RKN extends a special thanks to graphic artists Suzanne Parlett and Qamdyn Hale for help in creating the storyboards used in the study.

Author Contributions

Dr. Robert Naviaux raised the funding, obtained the regulatory approvals, conceived, designed, and directed the trial, analyzed the data, prepared the figures, and wrote the manuscript. Dr. Curtis, Dr. Westerfield, and Ms. Mash performed the neurodevelopmental testing, provided clinical coordination, and edited the manuscript. Dr. Reiner helped design the study, coordinated patient infusions and clinical care, and edited the manuscript. Dr. Li, Dr. Jane Naviaux, and Dr. Wang performed the metabolomic and pharmacokinetic analysis, analyzed the data, prepared the figures, and wrote parts of the manuscript. Dr. Jain and Ms. He helped design the study, prepared the randomization key, performed biostatistical analyses, and edited the manuscript. Dr. Bright directed the data compilation, integrity, and completeness analysis, provided independent biostatistical analysis, and edited the manuscript. Dr. Goh helped design the study, performed neurologic examinations, and edited the manuscript. Dr. Alaynick helped design the study and edited the manuscript. Dr. Capparelli analyzed the pharmacokinetic data, prepared the figures, and wrote parts of the manuscript. Dr. Sun and Ms. Adams provided investigational pharmacy support, implemented the clinical mask, and edited the manuscript. Ms. Arellano provided clinical coordination and edited the manuscript. Dr. Chukoskie helped design the study, analyzed the data, critically reviewed and edited the manuscript. Dr. Lincoln and Dr. Townsend helped design the study, directed the neurodevelopmental studies, wrote and edited the manuscript.

Conflict of Interest

RKN has filed a provisional patent application related to antipurinergic therapy of autism and related disorders and is a scientific advisory board member for the Autism Research Institute and the Open Medicine Foundation. EVC is a DSMB member for Cempra Pharmaceuticals and The Medicines Company, and a consultant for Alexion. SG is co-owner of MitoMedical. The other authors declare no conflicts of interest.

References

1. Zablotsky B, Black LI, Maenner MJ, et al. Estimated prevalence of autism and other developmental disabilities following questionnaire changes in the 2014 National Health interview survey. Natl Health Stat Report 2015;13:1–20.
2. Christensen DL, Baio J, Van Naarden Braun K, et al. Prevalence and Characteristics of Autism Spectrum Disorder Among Children Aged 8 Years–Autism and Developmental Disabilities Monitoring Network, 11 Sites, United States, 2012. MMWR Surveill Summ 2016;65:1–23.
3. Pinto D, Pagnamenta AT, Klei L, et al. Functional impact of global rare copy number variation in autism spectrum disorders. Nature 2010;466:368–372.
4. Richards C, Jones C, Groves L, et al. Prevalence of autism spectrum disorder phenomenology in genetic disorders: a systematic review and meta-analysis. Lancet Psychiatry 2015;2:909–916.
5. Talkowski ME, Minikel EV, Gusella JF. Autism spectrum disorder genetics: diverse genes with diverse clinical outcomes. Harv Rev Psychiatry 2014;22:65–75.

6. Kalkbrenner AE, Schmidt RJ, Penlesky AC. Environmental chemical exposures and autism spectrum disorders: a review of the epidemiological evidence. Curr Probl Pediatr Adolesc Health Care 2014;44:277–318.
7. Zerbo O, Iosif AM, Walker C, et al. Is Maternal Influenza or Fever During Pregnancy Associated with Autism or Developmental Delays? Results from the CHARGE (CHildhood Autism Risks from Genetics and Environment) Study. J Autism Dev Disord 2013;43(1): 25–33.
8. Naviaux RK. Metabolic features of the cell danger response. Mitochondrion 2014;16:7–17.
9. Silva JM, Wong A, Carelli V, Cortopassi GA. Inhibition of mitochondrial function induces an integrated stress response in oligodendroglia. Neurobiol Dis 2009;34: 357–365.
10. Nikkanen J, Forsstrom S, Euro L, et al. Mitochondrial DNA Replication Defects Disturb Cellular dNTP Pools and Remodel One-Carbon Metabolism. Cell Metab 2016;23:635–648.
11. Green DR, Galluzzi L, Kroemer G. Mitochondria and the autophagy-inflammation-cell death axis in organismal aging. Science 2011;333:1109–1112.
12. Naviaux JC, Wang L, Li K, et al. Antipurinergic therapy corrects the autism-like features in the Fragile X (Fmr1 knockout) mouse model. Mol Autism 2015;6:1.
13. Naviaux JC, Schuchbauer MA, Li K, et al. Reversal of autism-like behaviors and metabolism in adult mice with single-dose antipurinergic therapy. Transl Psychiat 2014;4: e400.
14. Naviaux RK, Zolkipli-Cunningham Z, Nakayama T, et al. Antipurinergic Therapy Corrects the Autism-Like Features in the Poly(IC) Mouse Model. PLoS ONE 2013;8(3): e57380.
15. Wikoff WR, Kalisak E, Trauger S, et al. Response and recovery in the plasma metabolome tracks the acute LCMV-induced immune response. J Proteome Res 2009;8:3578–3587.
16. Degtyar E, Zusman T, Ehrlich M, Segal G. A Legionella effector acquired from protozoa is involved in sphingolipids metabolism and is targeted to the host cell mitochondria. Cell Microbiol 2009;11:1219–1235.
17. James SJ, Cutler P, Melnyk S, et al. Metabolic biomarkers of increased oxidative stress and impaired methylation capacity in children with autism. Am J Clin Nutr 2004;80:1611–1617.
18. West AP, Shadel GS, Ghosh S. Mitochondria in innate immune responses. Nat Rev Immunol 2011;11: 389–402.
19. Naviaux RK. Oxidative shielding or oxidative stress? J Pharmacol Exp Ther 2012;342:608–618.
20. Lohman AW, Isakson BE. Differentiating connexin hemichannels and pannexin channels in cellular ATP release. FEBS Lett 2014;588:1379–1388.
21. Trautmann A. Extracellular ATP in the immune system: more than just a "danger signal". Sci Signal 2009;2:pe6.
22. Riteau N, Baron L, Villeret B, et al. ATP release and purinergic signaling: a common pathway for particle-mediated inflammasome activation. Cell Death Dis 2012;3:e403.
23. Burnstock G. The Paton Lecture: Purinergic signalling: from discovery to current developments. Exp Physiol 2014;99(1):16–34.
24. Imamura H, Nhat KP, Togawa H, et al. Visualization of ATP levels inside single living cells with fluorescence resonance energy transfer-based genetically encoded indicators. Proc Natl Acad Sci USA 2009;106:15651–15656.
25. Jacobson KA, Balasubramanian R, Deflorian F, Gao ZG. G protein-coupled adenosine (P1) and P2Y receptors: ligand design and receptor interactions. Purinergic Signalling 2012;8:419–436.
26. Adams JB, Audhya T, McDonough-Means S, et al. Nutritional and metabolic status of children with autism vs. neurotypical children, and the association with autism severity. Nutr Metab 2011;8:34.
27. Jia M, Li MX, Fields RD, Nelson PG. Extracellular ATP in activity-dependent remodeling of the neuromuscular junction. Dev Neurobiol 2007;67:924–932.
28. Naviaux RK. Mitochondria and Autism. In: Buxbaum JD, Hof PR, eds. The Neuroscience of Autism Spectrum Disorders. Waltham, MA: Academic Press, Elsevier, 2012:179–193.
29. Naviaux RK. Mitochondrial control of epigenetics. Cancer Biol Ther 2008;7:1191–1193.
30. Wallace DC, Fan W. Energetics, epigenetics, mitochondrial genetics. Mitochondrion 2010;10:12–31.
31. Burnstock G. Pathophysiology and therapeutic potential of purinergic signaling. Pharmacol Rev 2006;58:58–86.
32. Stein CA. Suramin: a novel antineoplastic agent with multiple potential mechanisms of action. Can Res 1993;53 (10 Suppl):2239–2248.
33. World Medical A. World Medical Association Declaration of Helsinki: ethical principles for medical research involving human subjects. JAMA 2013;310:2191–2194.
34. Schulz KF, Altman DG, Moher D, Group C. CONSORT 2010 Statement: updated guidelines for reporting parallel group randomised trials. Trials 2010;11:32.
35. Gotham K, Risi S, Pickles A, Lord C. The Autism Diagnostic Observation Schedule: revised algorithms for improved diagnostic validity. J Autism Dev Disord 2007;37:613–627.
36. Grondhuis SN, Mulick JA. Comparison of the Leiter International Performance Scale-Revised and the Stanford-Binet Intelligence Scales, 5th Edition, in children with autism spectrum disorders. Am J Intellect Dev Disabil 2013;118:44–54.
37. Adams-Chapman I, Bann C, Carter SL, et al. Language outcomes among ELBW infants in early childhood. Early Hum Dev 2015;91:373–379.

38. Kaat AJ, Lecavalier L, Aman MG. Validity of the aberrant behavior checklist in children with autism spectrum disorder. J Autism Dev Disord 2014;44:1103–1116.
39. Geier DA, Kern JK, Geier MR. A Comparison of the Autism Treatment Evaluation Checklist (ATEC) and the Childhood Autism Rating Scale (CARS) for the quantitative evaluation of autism. J Mental Health Res Intellect Disabil 2013;6:255–267.
40. Rimland B, Edelson S. Autism treatment evaluation checklist. Autism Research Institute 2000 https://www.autism.com/ind_atec [cited 2016 June 15].
41. Busner J, Targum SD. The clinical global impressions scale: applying a research tool in clinical practice. Psychiatry (Edgmont). 2007;4:28–37.
42. Honey E, McConachie H, Turner M, Rodgers J. Validation of the repetitive behaviour questionnaire for use with children with autism spectrum disorder. Res Autism Spectr Disord 2012;6:355–364.
43. Sheiner LB, Beal SL. Evaluation of methods for estimating population pharmacokinetic parameters. II. Biexponential model and experimental pharmacokinetic data. J Pharmacokinet Biopharm 1981;9:635–651.
44. Naviaux RK, Naviaux JC, Li K, et al. Metabolic features of chronic fatigue syndrome. Proc Natl Acad Sci USA 2016;113(37):E5472–E5480.
45. Xia J, Sinelnikov IV, Han B, Wishart DS. MetaboAnalyst 3.0-making metabolomics more meaningful. Nucleic Acids Res 2015;43(W1):W251–W257.
46. Hawking F. Suramin: with special reference to onchocerciasis. Advances Pharmacol Chemother 1978;15:289–322.
47. Pickles A, Le Couteur A, Leadbitter K, et al. Parent-mediated social communication therapy for young children with autism (PACT): long-term follow-up of a randomised controlled trial. Lancet 2016;388:2501–2509.
48. Hawking F. Concentration of Bayer 205 (Germanin) in human blood and cerebrospinal fluid after treatment. Trans R Soc Trop Med Hyg 1940;34:37–52.
49. Siso S, Jeffrey M, Gonzalez L. Sensory circumventricular organs in health and disease. Acta Neuropathol 2010;120:689–705.

Supporting Information

Additional Supporting Information may be found online in the supporting information tab for this article:

Table S1. Single-dose suramin pharmacokinetics.
Table S2. Suramin pharmacometabolomics. Pathways changed at 2 days.
Table S3. Suramin pharmacometabolomics. Metabolites changed at 2 days.
Table S4. Suramin pharmacometabolomics. Metabolites changed at 6 weeks.

Figure S1. Storyboard illustration of each step of the infusion day visit.
Figure S2. Suramin pharmacometabolomics. Rank order of metabolites and pathways that were changed by suramin at 2 days after treatment.
Figure S3. Suramin pharmacometabolomics pathway visualization. (A) After 2 days. (B) After 6 weeks. Metabolites indicated in red were increased, and those in green were decreased compared to controls (see *z*-score scale in upper right).
Figure S4. Outcomes. (A) 6 Weeks ADOS comparison scores by two-way ANOVA. (B) 6 Weeks ADOS comparison score improvement after suramin. (C) 6 Weeks ADOS social affect score improvement after suramin. (D) 6 Weeks ADOS restricted and repetitive behavior score improvement after suramin. (E) 2 days ADOS comparison scores were not changed. (F) no change in 6 weeks ADOS scores in subjects receiving saline placebo. (G) no change in 6 weeks ADOS social affect scores in subjects receiving placebo. (H) no change in 6 weeks ADOS restricted and repetitive behavior scores in subjects receiving placebo. (I) no change in 6 weeks Expressive One-Word Picture Vocabulary scores. (J) 7-day improvement in ABC stereotypy scores after suramin. (K) 6-week Improvement in ABC stereotypy scores after suramin. (L) 7-day Improvement in ATEC total scores after suramin. (M) no change in 6 weeks EOWPVT scores after saline. (N) no change in 7 days ABC stereotypy scores after saline. (O) no change in 6 weeks ABC stereotypy scores after saline. (P) no change in 7 days ATEC total scores after saline. (Q) improved ATEC speech, language, and communication scores 7 days after suramin. (R) improved ATEC sociability scores 7 days after suramin. (S) improved ATEC speech, language, and communication scores 6 weeks after suramin. (T) improved ADOS comparison scores after dropping a subject who missed the 6-week visit ($N = 4$). (U) no change in 7 days ATEC speech, language, and communication after saline. (V) no change in 7 days ATEC sociability after saline. (W) no change in 6 weeks ATEC speech, language, and communication scores 6 weeks after saline (X) no change in EOWPVT scores after dropping subject who missed the 6-week visit ($N = 4$). (Y) no change in 2 days ADOS scores after suramin. (Z) no change in 6 weeks RBQ total scores after suramin. (aa) improved core symptoms of ASD and other behaviors by CGI at 6 weeks after suramin. *P* values: *0.05, **0.01, ***0.001. (bb) Top 3, most changed symptoms named by parents in the 6-week CGI. (cc) no change in 2 days ADOS scores after saline. (dd) no change in 6 weeks RBQ total scores after saline.
Data S1. Clinical Global Impression (CGI) questionnaire.
Data S2. Social Stories to Accompany the Storyboard Panels Describing Each Step of the Infusion Day Visit.

Supporting Information

Naviaux RK, Curtis B, Li K, Naviaux JC, Bright AT, Reiner G, Westerfeld M, Goh S, Alaynick WA, Wang L, Capparelli EV, Adams C, Sun J, Jain S, He F, Arellano DA, Mash L, Chukoskie L, Lincoln A, Townsend J. **Low-dose suramin in autism spectrum disorder: a small, phase I/II, randomized clinical trial**. 2017, *Annals of Clinical and Translational Neurology*.

Contents

Supplemental Materials and Methods

Diagnostic and Outcome Procedures

Examiner-based outcomes (ADOS and EOWPVT) were assessed at 2-days and 6-weeks after the infusion. Parent-based outcomes (ABC, ATEC, CGI, and RBQ) were assessed at 7-days and 6-weeks after the infusion. To minimize the effects of natural behavioral variability, the parents were instructed to mark a behavior as changed only if it was persistently changed for at least 1 week. Storyboards and accompanying social stories were created to illustrate each step of the study for parents to review with each child before the study (Figure S1, and Supplemental Data S2).

Safety and Adverse Event Monitoring

Blood and urine for safety and toxicity monitoring were collected immediately before the infusion, 1 hour after the infusion, 2 days after, and 45 days after the infusion. Vital signs and anthropomorphic measurements were also collected. Safety surveillance included 18 vital sign and anthropometric features, 19 complete blood count (CBC) parameters, 20 blood chemistry measures, 3 thyroid and cortisol measures, and 5 lipid measures at the 5 time points. 24 urinalysis features were measured at 4 times: baseline, pre-infusion, 2-days post-infusion, and 45-days post-infusion.

Verification of Data Completeness and Transcription Accuracy

Standardized questionnaire responses and the ADOS-2 and EOWPVT scores (5,490 cells of data) were compiled in spreadsheets from the original hard copy forms and from the electronic medical records. A total of 87 cells (1.6%) of the 5,490 outcome scores were either left blank,

asked about a symptom that did not apply, or were missing. One participant missed the 6-week ADOS and EOWPVT evaluations because of scheduling difficulties. His 2-day results were used as an estimate of his 6-week scores. ADOS scores remained significant when this subject was dropped from the analysis (Figure S4T). EOWPVT results were also unchanged (Figure S4X). The 4,210 cells of laboratory and vital sign data were also collected and reviewed. When specific cells of data were found to be missing, they were manually confirmed by inspection of the original questionnaire, laboratory results, and clinical data sheets. A random generator program was written that randomly selected 5% of the data. These randomly selected cells of data that were then manually checked for transcription accuracy by reviewing the hard copy responses and Red Cap electronic medical records.

Standardized Testing and Questionnaires

Two observational examinations were performed by a clinician at 3 time points: baseline (56 ± 8 days; mean ± SEM; before the infusion), 2-days post-infusion, and 6-weeks post-infusion. The two examiner-based metrics were the Autism Diagnostic Observation Schedule, 2nd edition (ADOS-2)[1, 2], with video and audio files recorded on 3 cameras, and the Expressive One Word Picture Vocabulary Testing (EOWPVT)[3]. Both of these observational metrics were administered by a trained and certified examiner using approved test materials. Three standardized questionnaires were completed by parents at 3 time points: baseline, 7-days post-infusion, and 6-weeks post-infusion. The three standardized questionnaires completed by parents were the 58-question Aberrant Behavior Checklist (ABC)[4], the 75-item Autism Treatment Evaluation Checklist (ATEC)[5, 6], and the 33-item repetitive behavior questionnaire (RBQ)[7]. Parents were asked to complete these three instruments with reference to how their child behaved in the

previous 7 days. At the end of the six weeks, we included a 24-question Clinical Global Impression (CGI)[8] questionnaire (Supplementary Data S1). In addition, parents were asked to list the 3 top behaviors or symptoms that they observed to be most changed over the previous 6-weeks. To minimize the misinterpretation of natural day-to-day variations in symptoms, parents were asked to mark a symptom as changed in the 6-week CGI only if it had lasted for at least 1 week.

Storyboards and Social Stories

We commissioned a graphic artist to prepare a storyboard of each step of the procedure (Figure S1). The panel contents and color schemes were reviewed, and revisions recommended, by a 16-year old artist with Asperger syndrome to optimize the informational value and minimize any sensory issues. Next, our developmental neuropsychologist created social stories to accompany each panel of the storyboard. The social stories are shown in Supplementary Data S2.

Phone Interviews, Parent Reports, and Clinical Observations

Scripted phone interviews were conducted daily for the first week, then weekly until the completion of the study for each child 6-weeks after the infusion. Parents also kept study journals throughout the six weeks to document their observations. These scripted and narrative observations were used to permit discovery of any changes in ASD, behavior, or constitutional symptoms such as sleep and appetite, or any adverse or unanticipated events. The parent reports also provided insight regarding the timing and pattern of the responses after the infusion that were not predicted prior to the study, and were not adequately captured by the scheduled observations.

Daily Calls. Parents were contacted by phone on days 1-7 after the infusion to ensure close follow-up and to provide the opportunity for parents to report any positive or negative observations. These calls followed the script below:

"Hi. This is _____ (state your name) at UCSD. This is our daily follow-up call to see how you and your son are doing as part of the autism study."

1. How have things been going since the infusion? Any changes since yesterday?
2. Have there been any improvements? What things are most improved?
3. Have there been any setbacks, or negative things you've noticed? What are these?
4. How is he eating?
5. How is he sleeping?
6. Are there any problems, suggestions, or concerns that I can pass on to the doctors or a nurse?

Weekly Calls. Parents were called weekly on days 14, 21, 28, and 35 after the infusion to ensure close follow-up and to provide the opportunity for parents to report any positive or negative observations. These calls followed the script below:

"Hi. This is _____ (state your name) at UCSD. This is our weekly follow-up call to see how you and your son are doing as part of the autism study."

1. How have things been going since the infusion? Any changes since last week?
2. Have there been any improvements? What things are most improved?
3. Have there been any setbacks, or negative things you've noticed? What are these?
4. How is he eating?
5. How is he sleeping?
6. Are there any problems, suggestions, or concerns that I can pass on to the doctors or a nurse?

Clinical Global Impression (CGI)

We developed a 24-question Clinical Global Impression (CGI) instrument designed to assess the core symptoms of autism spectrum disorders and some of the most common comorbid features (Supplementary Material A1). The CGI instrument scoring system was the traditional 7-point,

CGI-Improvement scale[8]. In this scale, the historian gives a score of 0 if the symptom "was never a problem", a 1 for "very much improved", a 4 for "no change", and a 7 for "very much worse". In addition to the 24 structured questions, we asked the parents to write in the top 3 symptoms or behaviors that were most changed over the 6 weeks since the suramin infusion (Supplementary Material A1). This hybrid design of structured and open-ended responses permitted us to capture a large number of clinical outcomes associated with single-dose suramin treatment.

Metabolomics

Targeted, broad-spectrum, plasma metabolomic analysis of 610 metabolites from 63 biochemical pathways was performed by high performance liquid chromatography and tandem mass spectrometry (LC-MS/MS) as described[9] with minor modifications. 431 metabolites were above the lower limit of quantitation (LLOQ) in this study. Venous blood was collected between the hours of 8 am and 5 pm, at least 3 hours after the last meal, into lithium-heparin vacutainer tubes (BD #367884). Plasma was separated by centrifugation at 900g x 10 minutes at room temperature within one hour of collection. The resulting fresh lithium-heparin plasma was transferred to labeled 1.2 ml or 2.0 ml externally threaded, cryotubes with a minimum headspace air gap for storage at -80˚C for analysis. Samples were analyzed on an AB SCIEX QTRAP 5500 triple quadrupole mass spectrometer equipped with a Turbo V electrospray ionization (ESI) source, Shimadzu LC-20A UHPLC system, and a PAL CTC autosampler. Typically, 90 µl of plasma was thawed on ice and transferred to a 1.7 ml Eppendorf tube. Five (5.0) µl of a cocktail containing 25-35 commercial stable isotope internal standards, and 5.0 µl of 57 stable isotope internal standards that were custom-synthesized in *E. coli NCM3722, Caenorhabditis elegans N2,*

and *Komagataella phaffii* (ATCC 76273; formerly known as *Pichia pastoris*) by metabolic labeling with ^{13}C-glucose and ^{13}C-bicarbonate, were added, mixed, and incubated for 10 min at 20˚C to permit small molecules and vitamins in the internal standards to associate with plasma binding proteins. Macromolecules (protein, DNA, RNA, glycans, etc.) were precipitated by extraction with 4 volumes (400 µl) of cold (-20˚C), acetonitrile:methanol (50:50) (LCMS grade, Cat# LC015-2.5 and GC230-4, Burdick & Jackson, Honeywell), vortexed vigorously, and incubated on crushed ice for 10 min, then removed by centrifugation at 16,000g x 10 min at 4˚C. The supernatants containing the extracted metabolites and internal standards in the resulting 40:40:20 solvent mix of acetonitrile:methanol:water were transferred to labeled cryotubes and stored at -80˚C for LC-MS/MS analysis.

LC-MS/MS analysis was performed by scheduled multiple reaction monitoring (sMRM) under Analyst v1.6.2 software control in both negative and positive mode with rapid polarity switching (50 ms). Nitrogen was used for curtain gas (set to 30), collision gas (set to high), ion source gas 1 and 2 (set to 35). The source temperature was 500˚C. Spray voltage was set to -4500 V in negative mode and 5500 V in positive mode. The values for Q1 and Q3 mass-to-charge ratios (m/*z*), declustering potential (DP), entrance potential (EP), collision energy (CE), and collision cell exit potential (CXP) were determined and optimized for each MRM for each metabolite. Ten microliters of extract was injected by PAL CTC autosampler via a 10 µl stainless steel loop into a 250 mm × 2.0 mm, 4µm polymer based NH2 HPLC column (Asahipak NH2P-40 2E, Showa Denko America, Inc., NY) held at 25°C for chromatographic separation. The mobile phase was solvent A: 95% water with 20 mM $(NH_4)_2CO_3$ (Sigma, Fluka Cat# 74415-250G-F), 5% acetonitrile, and 38 mM NH_4OH (Sigma, Fluka Cat# 17837-100ML), final pH 9.75; solvent B:

100% acetonitrile. Separation was achieved using the following gradient: 0-3.5 min: 95%B, 3.6-8 min: 85% B, 8.1-13 min: 75% B, 13.5–35 min: 0% B, 36–46 min: 95% B, 46.1 min: end. The flow rate was 200 µl/min. Pump pressures ranged from 920-2600 psi over the course of the gradient. All the samples were kept at 4°C during analysis. The chromatographic peaks were identified using MultiQuant (v3.0, Sciex), confirmed by manual inspection, and the peak areas integrated.

Suramin Quantitation

Suramin concentrations were measured by LC-MS/MS as previously described with modifications[10]. Plasma suramin samples were collected at 1 hour, 2 days and 42 days post-infusion. Heparinized plasma, 90 µl was used. Ten (10) µl of 50 µM stock of trypan blue was added to achieve an internal standard concentration of 5 µM. This was incubated at room temperature for 10 min to permit metabolite interaction with binding proteins, then extracted with 4 volumes (400 µl) of pre-chilled methanol-acetonitrile (50:50) to produce a final concentration of 40:40:20 (methanol:acetonitrile:H_2O), and precipitated on ice for 10 minutes. The samples were deproteinated and macromolecules removed by precipitation on crushed ice for 10 min. The mixture was centrifuged at 16,000g for 10 min at 4°C and the supernatant was transferred to a new tube and kept at -80°C for further LC-MS/MS analysis.

Suramin was analyzed on an AB SCIEX QTRAP 5500 triple quadrupole mass spectrometer equipped with a Turbo V electrospray ionization (ESI) source, Shimadzu LC-20A UHPLC system, and a PAL CTC autosampler. Ten microliters of extract were injected onto a Kinetix F5 column (100 × 2.1 mm, 2.6 µm; Phenomenex, CA) held at 30°C for chromatographic separation.

The mobile phase A was water with 20 mM ammonium acetate (NH_4OAC) (pH 7) and mobile phase B was methanol with 20 mM NH_4OAC (pH 7). Elution was performed using the following gradient: 0-1.5 min-0% B, 1.6-3 min-15% B, 3.1-7 min-60% B, 7.1-13 min-100% B, 14 min-0% B, 18 min-0% B, 18.1 minute-end. The flow rate was 400 µl/min. All the samples were kept at 4°C during analysis. Suramin and trypan blue were detected using MRM scanning mode with the dwell time of 180 ms. MRM transitions for the doubly-charged form of suramin were 647.0 m/z for the (Q1) precursor and 382.0 m/z for the (Q3) product. MRM transitions for trypan blue were 435.2 (Q1) and 185.0 (Q3). Absolute concentrations of suramin were determined using a standard curve prepared in plasma to account for matrix effects, and the peak area ratio of suramin to the internal standard trypan blue. The declustering potential (DP), collision energy (CE), entrance potential (EP) and collision exit potential (CXP) were -104, -9.5, -32 and -16.9, and -144.58, -7, -57.8 and -20.94, for suramin and trypan blue, respectively. The ESI source parameters were set as follows: source temperature 500 °C; curtain gas 30; ion source gas 1, 35; ion source gas 2 35; spray voltage -4500 V. Analyst v1.6 was used for data acquisition and analysis.

Supplemental Results

Safety Monitoring and Adverse Events

The rash caused by suramin in this study was not raised and did not itch. It was not urticarial. The children did not appear to notice it. Any residual rash was covered by clothing and not visible on exposed skin at the 2-day evaluation. Parents were instructed not to discuss it with the neuropsychology team to decrease the chance of examiner bias. Video camera records of the

ADOS testing confirmed the absence of any visible rash. The rash was a known risk of suramin treatment that was described in the informed consent documents.

Pharmacokinetics

Additional pharmacokinetic results are illustrated in Table S1. Although no behavioral outcomes were significant at 2 days after infusion, we found that 28 biochemical pathways were changed by suramin 2-days after the infusion (Table S2). Twenty-two of these (79%) remained changed at the 6-week time point (see Table 3). The rank order of metabolites most changed at day 2, and their associated metabolic pathway is illustrated in Figure S2. The full list of 61 metabolites on day 2 and 48 metabolites at 6-weeks that were significantly changed by suramin appears in Tables S3-S4. A wallchart-style biochemical pathway map was created in Cytoscape to illustrate the organization of metabolites that were increased and decreased by suramin treatment (Figure S3).

Pharmacometabolomics

The small number of subjects in this trial precluded conventional treatment group analysis because of high false discovery rates associated with measuring 431 metabolites in groups with just 5 subjects. However, by using each child as their own control in a paired analysis of pre-infusion and post-infusion results, the pharmacometabolomic effects of suramin could be characterized (see Table 3 and Figures 4-5, Table S2 and Figure S2).

Treatment Outcomes

ADOS comparison scores were improved in the suramin treatment group at 6-weeks (Figure S4AB) but were unchanged in the saline group (Supplemental Figure S4AF). ADOS scores at 2-days after treatment were not changed (Figure S4E). EOWPVT scores were not changed (Figure S4I). Secondary outcomes included Aberrant Behavior Checklist (ABC), Autism Treatment Evaluation Checklist (ATEC), the Clinical Global Impression (CGI), and the Repetitive Behavior Questionnaire (RBQ). Suramin treatment was associated with improvements in the ABC, ATEC, and CGI, but not in the RBQ (Figure S4). Three of 24 symptoms covered in the CGI were significant (Figure S4aa). Parents were also asked to specify the three top, most-changed behaviors as an unstructured component of the CGI at 6-weeks after the infusion. Five symptoms were named that achieved statistically significant results. The most-changed behaviors were social communication and play, speech and language, calm and focus, stims or stereotypies, and coping skills (Figure S4bb).

Supplemental References

1. Lord C, Risi S, Lambrecht L, et al. The Autism Diagnostic Observation Schedule—Generic: A standard measure of social and communication deficits associated with the spectrum of autism. Journal of autism and developmental disorders. 2000;30(3):205-23.
2. Lord C, Rutter M, DiLavore P, Risi S, Gotham K, Bishop S. Autism Diagnostic Observation Schedule–2nd edition (ADOS-2). Los Angeles, CA: Western Psychological Corporation. 2012.
3. Adams-Chapman I, Bann C, Carter SL, Stoll BJ, Network NNR. Language outcomes among ELBW infants in early childhood. Early Hum Dev. 2015 Jun;91(6):373-9.
4. Kaat AJ, Lecavalier L, Aman MG. Validity of the aberrant behavior checklist in children with autism spectrum disorder. Journal of autism and developmental disorders. 2014;44(5):1103-16.
5. Geier DA, Kern JK, Geier MR. A Comparison of the Autism Treatment Evaluation Checklist (ATEC) and the Childhood Autism Rating Scale (CARS) for the Quantitative Evaluation of Autism. J Mental Health Research in Intellectual Disabilities. 2013;6:255-67.
6. Rimland B, Edelson S. Autism treatment evaluation checklist: statistical analyses. Autism Research Institute. 2000.
7. Honey E, McConachie H, Turner M, Rodgers J. Validation of the repetitive behaviour questionnaire for use with children with autism spectrum disorder. Research in Autism Spectrum Disorders. 2012;6(1):355-64.
8. Busner J, Targum SD. The clinical global impressions scale: applying a research tool in clinical practice. Psychiatry (Edgmont). 2007 Jul;4(7):28-37.
9. Naviaux RK, Naviaux JC, Li K, et al. Metabolic features of chronic fatigue syndrome. Proceedings of the National Academy of Sciences of the United States of America. 2016 Sep 13;113(37):E5472-80.
10. Naviaux JC, Schuchbauer MA, Li K, et al. Reversal of autism-like behaviors and metabolism in adult mice with single-dose antipurinergic therapy. Translational psychiatry. 2014;4:e400.
11. Pickles A, Le Couteur A, Leadbitter K, et al. Parent-mediated social communication therapy for young children with autism (PACT): long-term follow-up of a randomised controlled trial. Lancet. 2016 Nov 19;388(10059):2501-9.

Supplemental Figure Legends

1. **Figure S1.** Storyboard illustration of each step of the infusion day visit.
2. **Figure S2.** Suramin pharmacometabolomics. Rank order of metabolites and pathways that were changed by suramin at 2-days after treatment.
3. **Figure S3.** Suramin pharmacometabolomics pathway visualization. (A) After 2 days. (B) After 6 weeks. Metabolites indicated in red are increased, and those in green are decreased compared to controls (see z-score scale in upper right).
4. **Figure S4.** Outcomes. (A) 6-week ADOS Comparison Scores by 2-Way ANOVA. (B) 6-Week ADOS Comparison Score Improvement after Suramin. (C) 6-Week ADOS Social Affect Score Improvement after Suramin. (D) 6-Week ADOS Restricted and Repetitive Behavior Score Improvement after Suramin. (E) 2-Day ADOS Comparison Scores were not changed. (F) No change in 6-Week ADOS Scores in subjects receiving saline placebo. (G) No change in 6-Week ADOS Social Affect Scores in subjects receiving placebo. (H) No change in 6-Week ADOS Restricted and Repetitive Behavior Scores in subjects receiving placebo. (I) No change in 6-week Expressive One Word Picture Vocabulary scores. (J) 7-Day improvement in ABC stereotypy scores after suramin. (K) 6-week Improvement in ABC stereotypy scores after suramin. (L) 7-Day Improvement in ATEC total scores after suramin. (M) No change in 6-week EOWPVT scores after saline. (N) No change in 7-day ABC stereotypy scores after saline. (O) No change in 6-week ABC stereotypy scores after saline. (P) No change in 7-day ATEC total scores after saline. (Q) Improved ATEC speech, language, and communication scores 7-days after suramin. (R) Improved ATEC sociability scores 7-days after suramin. (S) Improved ATEC speech, language, and communication scores 6-weeks after suramin. (T) Improved ADOS comparison scores after dropping a

subject who missed the 6-week visit (N = 4). (U) No change in 7-day ATEC speech, language, and communication after saline. (V) No change in 7-day ATEC sociability after saline. (W) No change in 6-week ATEC speech, language, and communication scores 6-weeks after saline (X) No change in EOWPVT scores after dropping subject who missed the 6-week visit (N = 4). (Y) No change in 2-day ADOS scores after suramin. (Z) No change in 6-week RBQ total scores after suramin. (aa) Improved core symptoms of ASD and other behaviors by CGI at 6-weeks after suramin. P values: * = 0.05; ** = 0.01; *** = 0.001. (bb) Top 3, most-changed symptoms named by parents in the 6-week CGI. (cc) No change in 2-day ADOS scores after saline. (dd) No change in 6-week RBQ total scores after saline.

Supplemental Tables

1. **Table S1.** Single-dose suramin pharmacokinetics.
2. **Table S2.** Suramin pharmacometabolomics. Pathways changed at 2-days.
3. **Table S3.** Suramin pharmacometabolomics. Metabolites changed at 2-days.
4. **Table S4.** Suramin pharmacometabolomics. Metabolites changed at 6-weeks.

Supplemental Data

1. **S1.** Clinical Global Impression (CGI) questionnaire.

2. **S2.** Social Stories to Accompany the Storyboard Panels Describing Each Step of the Infusion Day Visit.

Table S1. Single-dose suramin pharmacokinetics.

Pair Block	ID	Age (yrs)	Height (m)	Weight (kg)	BSA* (m^2)	20 mg/kg Dose (mg)	Dose (mg/m^2)	1-Hour Plasma Conc (µM)	2-Day Plasma Conc (µM)	45-Day Plasma Conc (µM)	Plasma Half-Life (days)
1	001	11	1.395	34.4	1.15	680	591	101.2	13.2	0.96	12.6
2	007	5	1.189	22.9	0.87	460	529	87.9	11.9	1.67	14.7
3	014	14	1.74	54.7	1.63	1000	613	110.9	10.6	1.04	14.9
4	012	6	1.18	23.1	0.87	460	529	118.6	13.8	2.28	16.5
5	005	7	1.271	25.1	0.95	500	526	101.8	10.6	1.76	15.0
						Mean:	558	104.1	12.0	1.54	14.7
						sd:	41	11.6	1.5	0.5	1.4

*Mosteller method. BSA: body surface area.

Table S2. Suramin pharmacometabolomics. Pathways changed at 2-days.

No.	Pathway Name	Measured Metabolites in the Pathway (N)	Expected Pathway Proportion (P = N/431)	Expected Hits in Sample of 61 (P * 61)	Observed Hits in the Top 61 Metabolites	Fold Enrichment (Obs/Exp)	Impact (Sum VIP Score)	Fraction of Impact (VIP Score) Explained (% of 119.7)	Increased	Decreased
1	Purine Metabolism	26	0.060	3.7	9	2.4	17.6	15%	4	5
2	Bile Salt Metabolism	6	0.014	0.8	4	4.7	11.9	10%	4	0
3	Microbiome Metabolism	18	0.042	2.5	4	1.6	9.3	8%	4	0
4	Branch Chain Amino Acid Metabolism	12	0.028	1.7	4	2.4	7.3	6%	4	0
5	Eicosanoid and Resolvin Metabolism	13	0.030	1.8	4	2.2	7.1	6%	0	4
6	Phospholipid Metabolism	74	0.172	10.5	3	0.3	5.7	5%	0	3
7	SAM, SAH, Methionine, Cysteine, Glutathione	15	0.035	2.1	3	1.4	5.6	5%	2	1
8	GABA, Glutamate, Arginine, Ornithine	6	0.014	0.8	3	3.5	4.7	4%	3	0
9	Pyrimidine Metabolism	9	0.021	1.3	2	1.6	4.3	4%	1	1
10	Glycolysis and Gluconeogenesis Metabolism	7	0.016	1.0	2	2.0	4.3	4%	2	0
11	Gamma-Glutamyl and other Dipeptides	2	0.005	0.3	2	7.1	3.8	3%	2	0
12	Sphingomyelin Metabolism	36	0.084	5.1	2	0.4	3.6	3%	0	2
13	Bioamines and Neurotransmitter Metabolism	9	0.021	1.3	2	1.6	3.3	3%	0	2
14	Krebs Cycle	9	0.021	1.3	2	1.6	3.3	3%	2	0
15	Vitamin D (Calciferol) Metabolism	3	0.007	0.4	1	2.4	3.1	3%	0	1
16	Cardiolipin Metabolism	7	0.016	1.0	2	2.0	3.1	3%	2	0
17	Glycosphingolipid Metabolism	12	0.028	1.7	1	0.6	2.1	2%	1	0
18	Taurine, Hypotaurine Metabolism	2	0.005	0.3	1	3.5	2.0	2%	0	1
19	Nitric Oxide, Superoxide, Peroxide	2	0.005	0.3	1	3.5	1.9	2%	0	1
20	Histidine, Histamine, Carnosine Metabolism	4	0.009	0.6	1	1.8	1.8	2%	1	0
21	Tyrosine and Phenylalanine Metabolism	3	0.007	0.4	1	2.4	1.8	2%	1	0
22	Fatty Acid Oxidation and Synthesis	37	0.086	5.2	1	0.2	1.8	2%	0	1
23	Cholesterol, Cortisol, Non-Gonadal Steroid	16	0.037	2.3	1	0.4	1.8	2%	1	0
24	Amino Acid Metabolism	4	0.009	0.6	1	1.8	1.8	1%	1	0
25	Endocannabinoid Metabolism	4	0.009	0.6	1	1.8	1.7	1%	0	1
26	Amino-Sugar, Galactose, & Non-Glucose	5	0.012	0.7	1	1.4	1.6	1%	1	0
27	Tryptophan, Kynurenine, Serotonin	6	0.014	0.8	1	1.2	1.6	1%	1	0
28	Ceramide Metabolism	34	0.079	4.8	1	0.2	1.5	1%	1	0
								Subtotals	38	23
								Totals	61	

Table S3. Suramin pharmacometabolomics. Metabolites changed at 2-days.

No.	Metabolite	Pathway Name	VIP Score	Z Score	AUC Ratio (Post/Pre)
1	Chenodeoxyglycocholic acid	Bile Salt Metabolism	3.171	1.610	2.787
2	1,25-Dihydroxyvitamin D3	Vitamin D (Calciferol) Metabolism	3.134	-1.447	0.273
3	Glycocholic acid	Bile Salt Metabolism	3.090	2.020	2.344
4	Taurodeoxycholic acid Pool	Bile Salt Metabolism	3.048	1.326	2.614
5	2-Keto-L-gluconate	Microbiome Metabolism	2.994	2.586	1.264
6	Taurocholic acid	Bile Salt Metabolism	2.615	1.102	2.183
7	2,3-Diphosphoglyceric acid	Glycolysis and Gluconeogenesis Metabolism	2.600	0.990	1.198
8	Cytosine	Pyrimidine Metabolism	2.556	2.055	1.689
9	p-Hydroxyphenylacetic acid	Microbiome Metabolism	2.546	1.464	1.192
10	11(R)-HETE	Eicosanoid and Resolvin Metabolism	2.400	-0.875	0.748
11	Hypoxanthine	Purine Metabolism	2.267	-1.000	0.745
12	Deoxyguanosine diphosphate	Purine Metabolism	2.264	-1.276	0.889
13	Glycylproline	Gamma-Glutamyl and other Dipeptides	2.205	1.212	1.773
14	Allantoin	Purine Metabolism	2.195	0.926	1.663
15	L-Isoleucine	Branch Chain Amino Acid Metabolism	2.136	0.815	1.094
16	GC(18:1/22:0)	Glycosphingolipid Metabolism	2.123	1.057	1.399
17	Cysteamine	SAM, SAH, Methionine, Cysteine, Glutathione Metabolism	2.075	1.398	1.107
18	LysoPC(16:0)	Phospholipid Metabolism	2.067	-0.908	0.777
19	Taurine	Taurine, Hypotaurine Metabolism	2.042	-0.942	0.786
20	1-Methyladenine	Purine Metabolism	2.033	1.337	1.631
21	SM(d18:1/20:1)	Sphingomyelin Metabolism	2.033	-1.250	0.745
22	PA(16:0/16:1)	Phospholipid Metabolism	1.998	-0.813	0.793
23	Cyclic adenosine monophosphate	Purine Metabolism	1.949	-0.681	0.855
24	Azelaic acid	Nitric Oxide, Superoxide, Peroxide Metabolism	1.929	-2.024	0.914
25	Shikimate-3-phosphate	Microbiome Metabolism	1.886	1.033	1.047
26	Indoxyl sulfate	Microbiome Metabolism	1.858	0.702	1.280
27	1-Methylhistidine	Histidine, Histamine, Carnosine Metabolism	1.848	0.899	1.145
28	Purine	Purine Metabolism	1.847	1.137	1.203
29	L-Phenylalanine	Tyrosine and Phenylalanine Metabolism	1.839	0.957	1.164
30	Malonic acid	Fatty Acid Oxidation and Synthesis	1.833	-0.825	0.904
31	Methionine sulfoxide	SAM, SAH, Methionine, Cysteine, Glutathione Metabolism	1.817	1.738	1.331
32	L-Valine	Branch Chain Amino Acid Metabolism	1.808	0.749	1.165
33	24,25-Epoxycholesterol	Cholesterol, Cortisol, Non-Gonadal Steroid Metabolism	1.807	1.014	1.362
34	Orotic acid	Pyrimidine Metabolism	1.787	-0.612	0.670
35	AICAR	Purine Metabolism	1.787	1.310	1.309
36	Isovalerylglycine	Branch Chain Amino Acid Metabolism	1.783	0.852	1.951
37	Alanine	Amino Acid Metabolism (not otherwise covered)	1.776	1.066	1.193
38	Xanthosine	Purine Metabolism	1.764	-1.316	0.821
39	Anandamide	Endocannabinoid Metabolism	1.713	-0.709	0.684
40	Citramalic acid	Krebs Cycle	1.704	1.229	1.121
41	Cysteine-S-sulfate	SAM, SAH, Methionine, Cysteine, Glutathione Metabolism	1.682	-0.644	0.869
42	PG(16:0/16:0)	Phospholipid Metabolism	1.664	-0.667	0.549
43	Dopamine	Bioamines and Neurotransmitter Metabolism	1.653	-0.642	0.877
44	Glycerol 3-phosphate	Glycolysis and Gluconeogenesis Metabolism	1.651	1.151	1.187
45	5-HETE	Eicosanoid and Resolvin Metabolism	1.646	-0.671	0.866
46	Myoinositol	Amino-Sugar, Galactose, & Non-Glucose Metabolism	1.645	0.785	1.286
47	L-Glutamic acid	Bioamines and Neurotransmitter Metabolism	1.641	-0.619	0.797
48	Gamma-Aminobutyric acid	GABA, Glutamate, Arginine, Ornithine, Proline Metabolism	1.626	1.101	1.068
49	L-Kynurenine	Tryptophan, Kynurenine, Serotonin, Melatonin Metabolism	1.617	0.625	1.099
50	Citric acid	Krebs Cycle	1.590	0.759	1.142
51	SM(d18:1/20:0)	Sphingomyelin Metabolism	1.576	-0.770	0.712
52	Gamma-glutamyl-Alanine	Gamma-Glutamyl and other Dipeptides	1.575	0.896	1.294
53	Tiglylglycine	Branch Chain Amino Acid Metabolism	1.562	0.657	1.141
54	L-Proline	GABA, Glutamate, Arginine, Ornithine, Proline Metabolism	1.548	0.603	1.155
55	CL(18:2/18:2/18:2/18:2)	Cardiolipin Metabolism	1.538	0.506	1.181
56	CL(18:2/18:2/18:2/18:1)	Cardiolipin Metabolism	1.535	0.474	1.102
57	11,12-Epoxyeicosatrienoic acid	Eicosanoid and Resolvin Metabolism	1.535	-0.634	0.828
58	Ceramide(d18:1/18:2)	Ceramide Metabolism	1.521	0.530	1.337
59	Guanosine	Purine Metabolism	1.519	-0.766	0.702
60	Prostaglandin J2	Eicosanoid and Resolvin Metabolism	1.509	-0.601	0.649
61	N-Acetylglutamic acid	GABA, Glutamate, Arginine, Ornithine, Proline Metabolism	1.505	0.613	1.120

Table S4. Suramin pharmacometabolomics. Metabolites changed at 6-weeks.

No.	Metabolite	Pathway Name	VIP Score	Z Score	AUC Ratio (Post/Pre)
1	2-Keto-L-gluconate	Microbiome Metabolism	2.686	2.365	1.239
2	SM(d18:1/26:0 OH)	Sphingomyelin Metabolism	2.622	2.002	1.671
3	Glycine	1-Carbon, Folate, Formate, Glycine, Serine Metabolism	2.523	1.891	1.392
4	1-Methyladenine	Purine Metabolism	2.459	2.259	2.287
5	Alanine	Amino Acid Metabolism (not otherwise covered)	2.456	1.687	1.322
6	Cytosine	Pyrimidine Metabolism	2.442	2.582	1.932
7	Citric acid	Krebs Cycle	2.410	1.772	1.363
8	1-Pyrroline-5-carboxylic acid	GABA, Glutamate, Arginine, Ornithine, Proline Metabolism	2.358	1.922	1.299
9	Gamma-glutamyl-Alanine	Gamma-Glutamyl and other Dipeptides	2.353	1.725	1.644
10	Histamine	Histidine, Histamine, Carnosine Metabolism	2.279	1.312	1.219
11	p-Hydroxyphenylacetic acid	Microbiome Metabolism	2.203	2.226	1.306
12	Azelaic acid	Nitric Oxide, Superoxide, Peroxide Metabolism	2.151	2.558	1.120
13	Methionine sulfoxide	SAM, SAH, Methionine, Cysteine, Glutathione Metabolism	2.104	2.083	1.409
14	L-Kynurenine	Tryptophan, Kynurenine, Serotonin, Melatonin Metabolism	2.096	1.751	1.303
15	Glycerol 3-phosphate	Glycolysis and Gluconeogenesis Metabolism	2.081	1.731	1.294
16	Cysteamine	SAM, SAH, Methionine, Cysteine, Glutathione Metabolism	2.060	2.007	1.157
17	Chenodeoxyglycocholic acid	Bile Salt Metabolism	2.052	1.650	2.858
18	Hydroxyproline	Vitamin C (Ascorbate) Metabolism	2.039	3.005	1.210
19	2-Hydroxyisovaleric acid	Branch Chain Amino Acid Metabolism	1.988	1.146	1.234
20	Purine	Purine Metabolism	1.980	1.650	1.307
21	Cyclic adenosine monophosphate	Purine Metabolism	1.962	-1.544	0.701
22	Glycocholic acid	Bile Salt Metabolism	1.956	1.945	2.270
23	4-Hydroxyphenyllactic acid	Microbiome Metabolism	1.945	1.172	1.294
24	Deoxyguanosine diphosphate	Purine Metabolism	1.915	-1.583	0.864
25	Hexose Disaccharide Pool	Amino-Sugar, Galactose, & Non-Glucose Metabolism	1.911	1.220	2.121
26	S-Adenosylhomocysteine	SAM, SAH, Methionine, Cysteine, Glutathione Metabolism	1.894	0.971	1.417
27	Isovalerylglycine	Branch Chain Amino Acid Metabolism	1.888	0.901	2.027
28	Allantoin	Purine Metabolism	1.882	1.068	1.798
29	Tiglylglycine	Branch Chain Amino Acid Metabolism	1.878	1.310	1.302
30	L-Phenylalanine	Tyrosine and Phenylalanine Metabolism	1.875	1.381	1.245
31	cis-aconitic acid	Krebs Cycle	1.852	0.928	1.278
32	Lathosterol	Cholesterol, Cortisol, Non-Gonadal Steroid Metabolism	1.844	1.079	1.284
33	L-Asparagine	Amino Acid Metabolism (not otherwise covered)	1.824	1.581	1.360
34	Cinnamoylglycine	Tyrosine and Phenylalanine Metabolism	1.790	2.218	1.190
35	Octanoylcarnitine	Fatty Acid Oxidation and Synthesis	1.780	-1.451	0.703
36	L-Cystine	SAM, SAH, Methionine, Cysteine, Glutathione Metabolism	1.774	1.060	1.190
37	Uridine	Pyrimidine Metabolism	1.764	0.928	1.244
38	Mevalonic acid	Cholesterol, Cortisol, Non-Gonadal Steroid Metabolism	1.673	1.036	1.386
39	Chenodeoxycholic acid	Bile Salt Metabolism	1.670	1.575	2.080
40	Guanidinoacetic acid	SAM, SAH, Methionine, Cysteine, Glutathione Metabolism	1.644	1.254	1.217
41	2-Hydroxyisocaproic acid	Branch Chain Amino Acid Metabolism	1.622	0.997	1.306
42	Decanoylcarnitine	Fatty Acid Oxidation and Synthesis	1.617	-1.157	0.644
43	3-Hydroxy-cis-5-tetradecenoylcarnitine	Fatty Acid Oxidation and Synthesis	1.612	-1.056	0.734
44	Hippuric acid	Microbiome Metabolism	1.559	0.881	1.602
45	PE (18:0/18:0)	Phospholipid Metabolism	1.555	-1.331	0.644
46	L-Proline	GABA, Glutamate, Arginine, Ornithine, Proline Metabolism	1.546	0.749	1.196
47	SM(d18:1/18:2)	Sphingomyelin Metabolism	1.508	0.750	1.424
48	L-Serine	1-Carbon, Folate, Formate, Glycine, Serine Metabolism	1.505	0.954	1.152

Supplemental Data S1. Clinical Global Impression of Improvement questionnaire

Clinical Global Impression

UCSD Suramin Autism Treatment Study

Child's Name: _____

Your Name: _____ (please print)

Date: _____

INSTRUCTIONS

Please answer the following by assessing the full 6-week period after the infusion, compared to your child's behavior before the infusion. If a symptom changed over the 6 weeks, please write in the time after the infusion for maximum change in weeks (wks) or days (d). Please note "wks" for weeks and "days" or "d" for days. For example, if a symptom started to change after 1 week, but didn't reach maximum for 2 weeks, you would write in: "2 wks".
If a symptom didn't change check box "4". If it was never a problem check box "0".

24-Point Autism Symptom Assessment

No.	Over the 6 weeks, how would you assess each of the following?	0 Never a Problem	1 Very Much Improved	2 Much Improved	3 Minimally Improved	4 No Change	5 Minimally Worse	6 Much Worse	7 Very Much Worse	Time after Infusion for maximum change (wks or days) Write-In
1	Overall symptoms of autism severity or delayed development?	☐	☐	☐	☐	☐	☐	☐	☐	
2	Receptive language?	☐	☐	☐	☐	☐	☐	☐	☐	
3	Expressive language?	☐	☐	☐	☐	☐	☐	☐	☐	
4	Difficulty following verbal commands?	☐	☐	☐	☐	☐	☐	☐	☐	
5	Flapping or self-stimulation?	☐	☐	☐	☐	☐	☐	☐	☐	
6	Sensory issues like problems with touch, texture, taste, smell, sound, light, etc.?	☐	☐	☐	☐	☐	☐	☐	☐	
7	Insistence on sameness or difficulty with transitions?	☐	☐	☐	☐	☐	☐	☐	☐	
8	Anxiety or panic attacks?	☐	☐	☐	☐	☐	☐	☐	☐	
9	Tantrums or Meltdowns?	☐	☐	☐	☐	☐	☐	☐	☐	
10	Obsessive and/or compulsive behaviors?	☐	☐	☐	☐	☐	☐	☐	☐	
11	Self-Injurious behavior?	☐	☐	☐	☐	☐	☐	☐	☐	
12	Outbursts of anger or aggression?	☐	☐	☐	☐	☐	☐	☐	☐	
13	Lack of imaginative, make-believe, or age-appropriate play?	☐	☐	☐	☐	☐	☐	☐	☐	
14	Lack of desire for social interaction?	☐	☐	☐	☐	☐	☐	☐	☐	
15	Hyperactivity?	☐	☐	☐	☐	☐	☐	☐	☐	
16	Lethargy or fatigue?	☐	☐	☐	☐	☐	☐	☐	☐	
17	Inattention?	☐	☐	☐	☐	☐	☐	☐	☐	
18	Lack of eye contact or gaze avoidance?	☐	☐	☐	☐	☐	☐	☐	☐	
19	Problems sleeping?	☐	☐	☐	☐	☐	☐	☐	☐	
20	Sound sensitivity or ear covering?	☐	☐	☐	☐	☐	☐	☐	☐	
21	Feeding problems?	☐	☐	☐	☐	☐	☐	☐	☐	
22	Gross motor problems like trouble with abnormal walking or running?	☐	☐	☐	☐	☐	☐	☐	☐	
23	Fine motor problems like trouble with buttons, zippers, snaps, or tripod grasp?	☐	☐	☐	☐	☐	☐	☐	☐	
24	Problems with bowel movements?	☐	☐	☐	☐	☐	☐	☐	☐	

Comments and recommendations:

Page 1 of 2

INSTRUCTIONS

Write down the 3 symptoms that changed the most during the 6 weeks after infusion

Child's Name: _____

Date: _____

No. Over the 6 weeks, what 3 symptoms changed the most?

		1 Very Much Improved	2 Much Improved	3 Minimally Improved	4 No Change	5 Minimally Worse	6 Much Worse	7 Very Much Worse	Write-In: Time after Infusion for maximum change (wks or days)
1		☐	☐	☐	☐	☐	☐	☐	
2		☐	☐	☐	☐	☐	☐	☐	
3		☐	☐	☐	☐	☐	☐	☐	

Pagee 2 of 2

Supplemental Data S2. Social Stories to Accompany the Storyboard Panels Describing Each Step of the Infusion Day Visit.

Check-in. "Hello again! You and your mom or dad are at our clinic today! We will do lots of different things, and meet different people. Everybody here is really nice. First, you will check in at the front desk, to let the doctor and nurses know that you are here. You might have to wait a few minutes before the nurse gets you. That's okay. You can sit in a chair and play with any toys that you brought with your today."

Numbing Medicine. "Then you will meet the nurse. She is really nice and friendly. You will sit in a chair or on the bed, and the nurse will put a special medicine on your arms, on the inside of your elbows (right where it bends.) The medicine will make your arms tingly and numb, and might tickle a little. That's okay, that's how we know that the medicine is working."

Height and Weight. "The nurse will take you to another room. You will stand on a scale and measure your weight, and you will stand tall to measure how tall you are. The nurse will also measure your blood pressure with a special bracelet that goes around your arm. She will take your temperature by touching your forehead with a fast thermometer."

Urine Sample. "If you didn't pee in a cup at home before you came to the clinic today, you will pee in a cup at the doctor's office in the bathroom. Mom or Dad will go with you if you need help."

Blood Sample. "After the bathroom, you will see the nurse again. Your arm will be nice and numb. The nurse will put a special needle in your arm, take some blood, then take out the needle and leave in a little plastic tube called an IV. Great job! That didn't hurt too much, and you sat so nice and still! The nurse will take some blood out of the tube, put some medicine in the tube, then wrap up your arm so you can go and play! We have lots of toys to play with. Or you can plan with the toys that you brought with you."

IV. "After some play time, you will sit down or lay down quietly, with no walking or jumping. A long tube called and IV will put medicine into the little tube in your arm. You can watch TV or play with your iPad, or even some Legos. Mom or Dad will sit with you the whole time."

Post-Infusion Free Time. "Next, the big tube gets put away, your arm gets wrapped up again, and you get to play some more! Or watch more TV. Have fun with your mom or dad."

Thank You Gift. "The nurse will then take the little tube out of your arm. Then you are done! Great job! You get to pick a present or have a treat, then go home with Mom or Dad. Thank you for being such a good helper today, and sitting so nicely and quietly. You had a good quiet mouth and gentle hands, and that makes Mom and Dad so happy. You did great!"

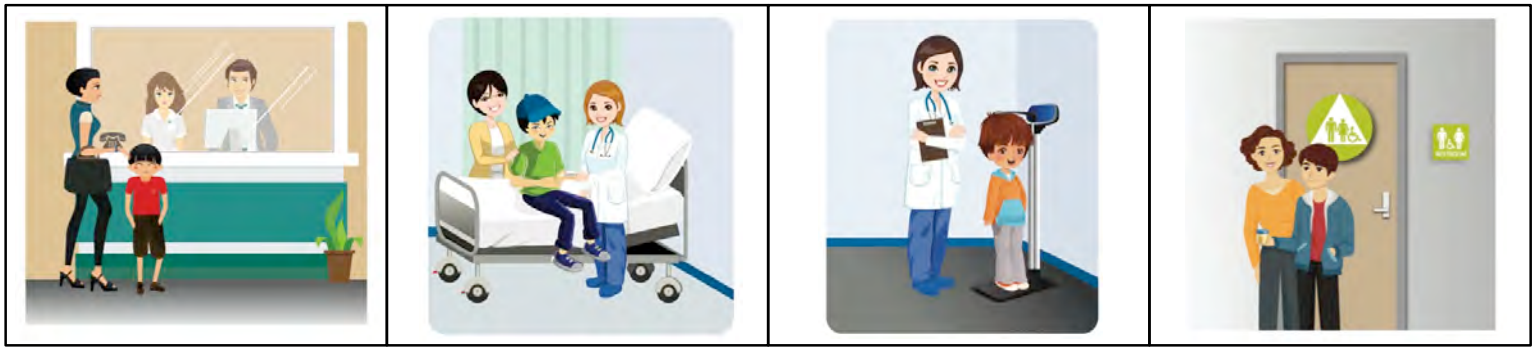

Check-in | Numbing Medicine | Height & Weight | Urine Sample

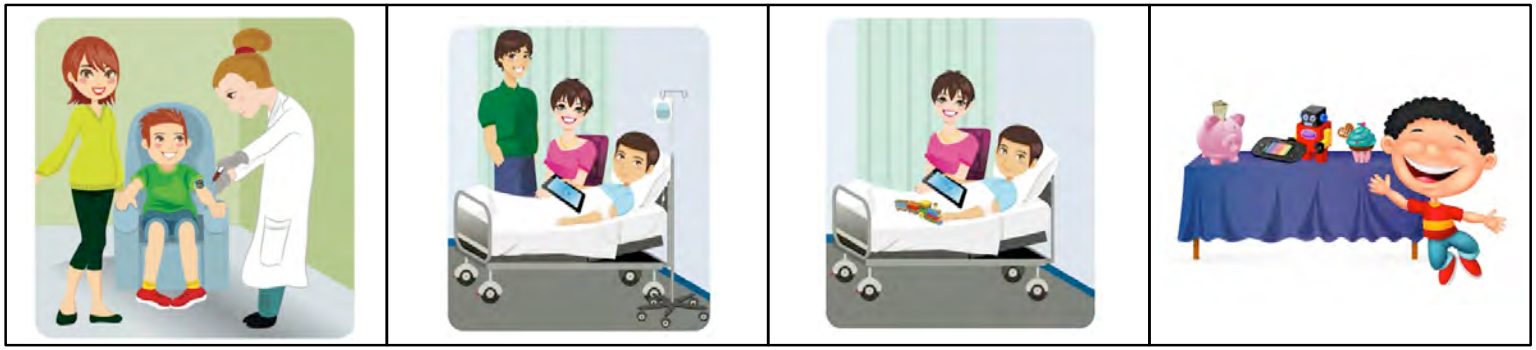

Blood Sample | IV | Post-infusion Free Time | Thank you Gift

FIGURE S1
Storyboard illustration of each step of the infusion day visit

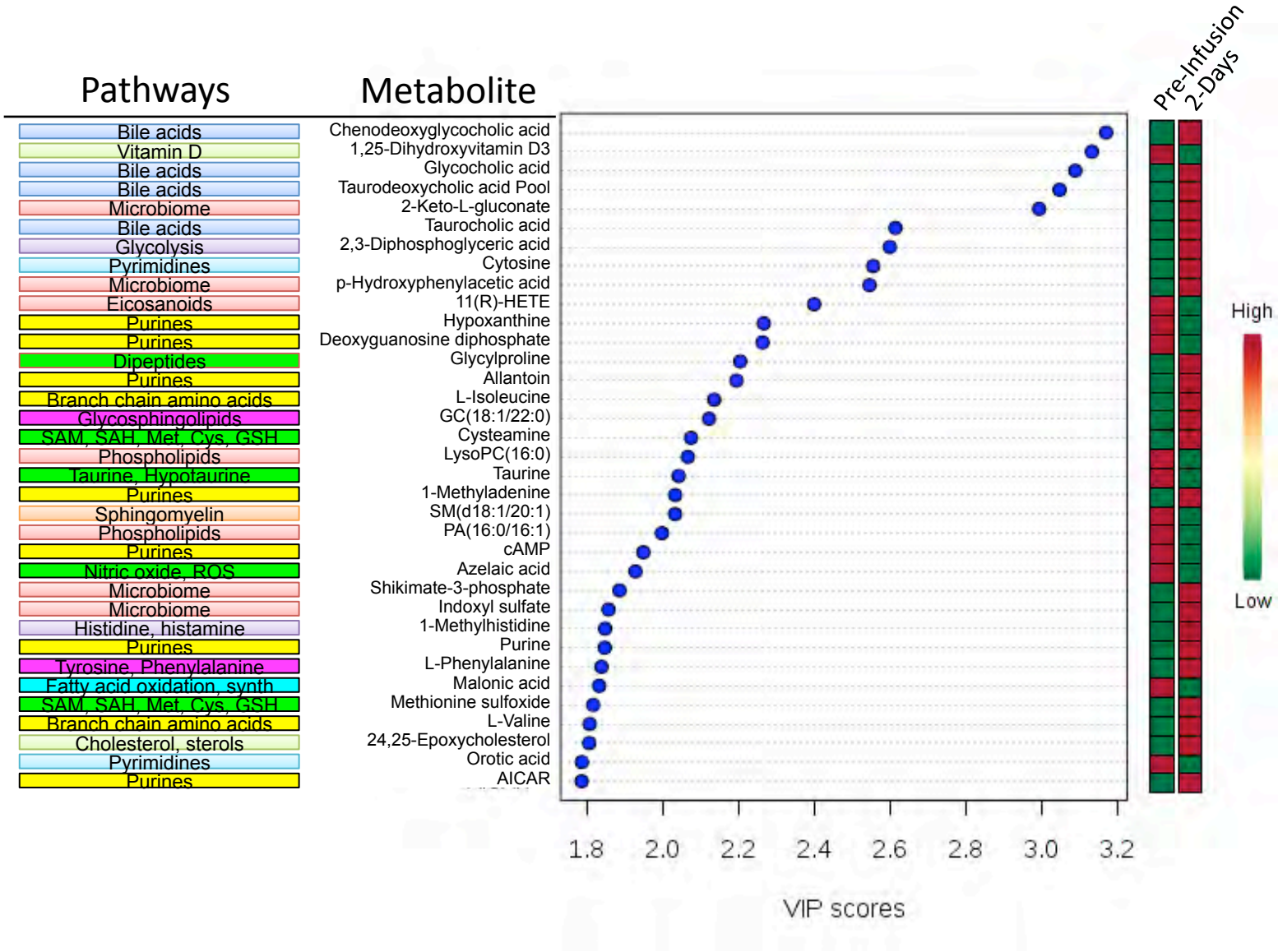

FIGURE S2

Suramin pharmacometabolomics. Metabolites and pathways changed at 2 days

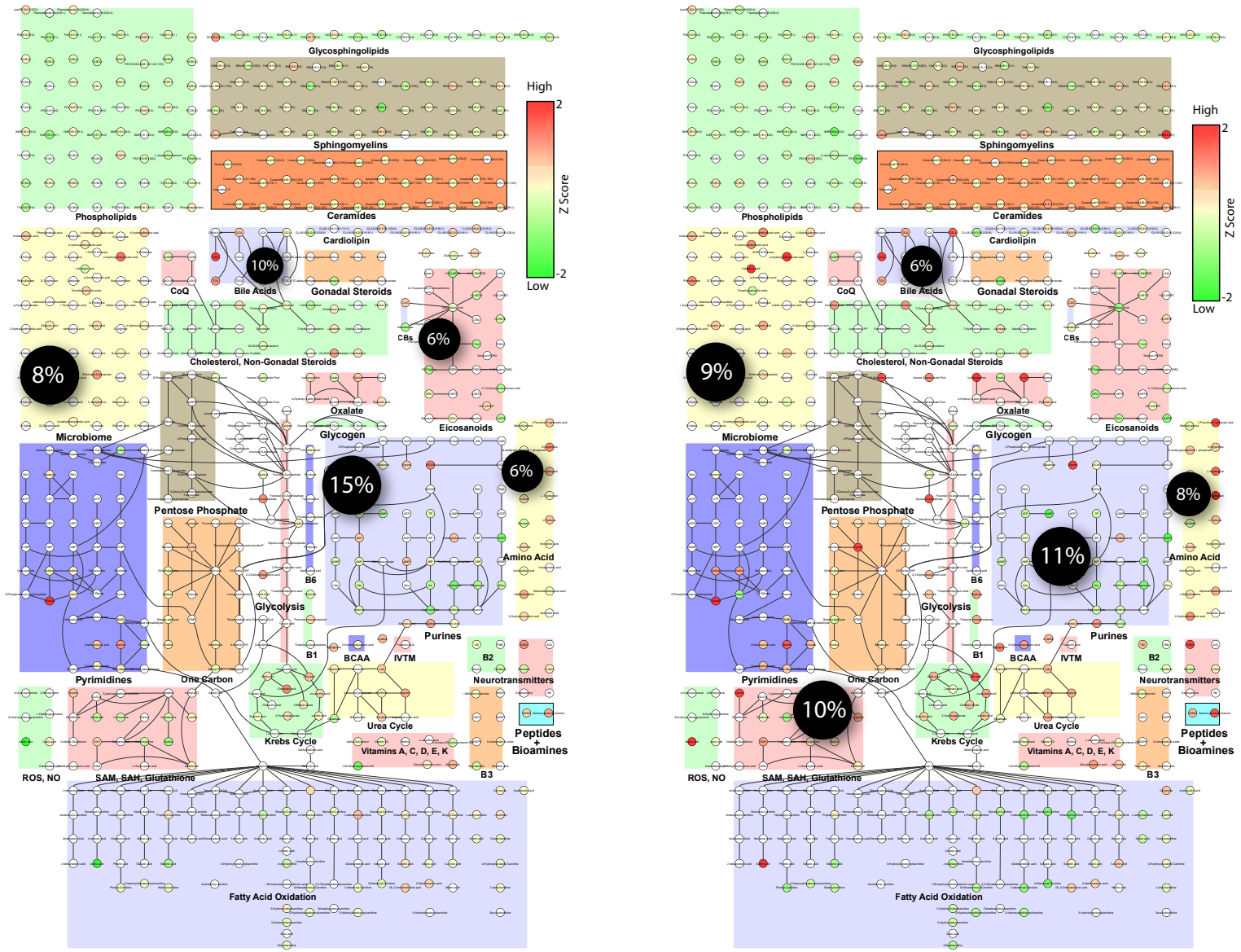

2-Days 6-Weeks

FIGURE S3. Suramin pharmacometabolomics. Pathway visualization.

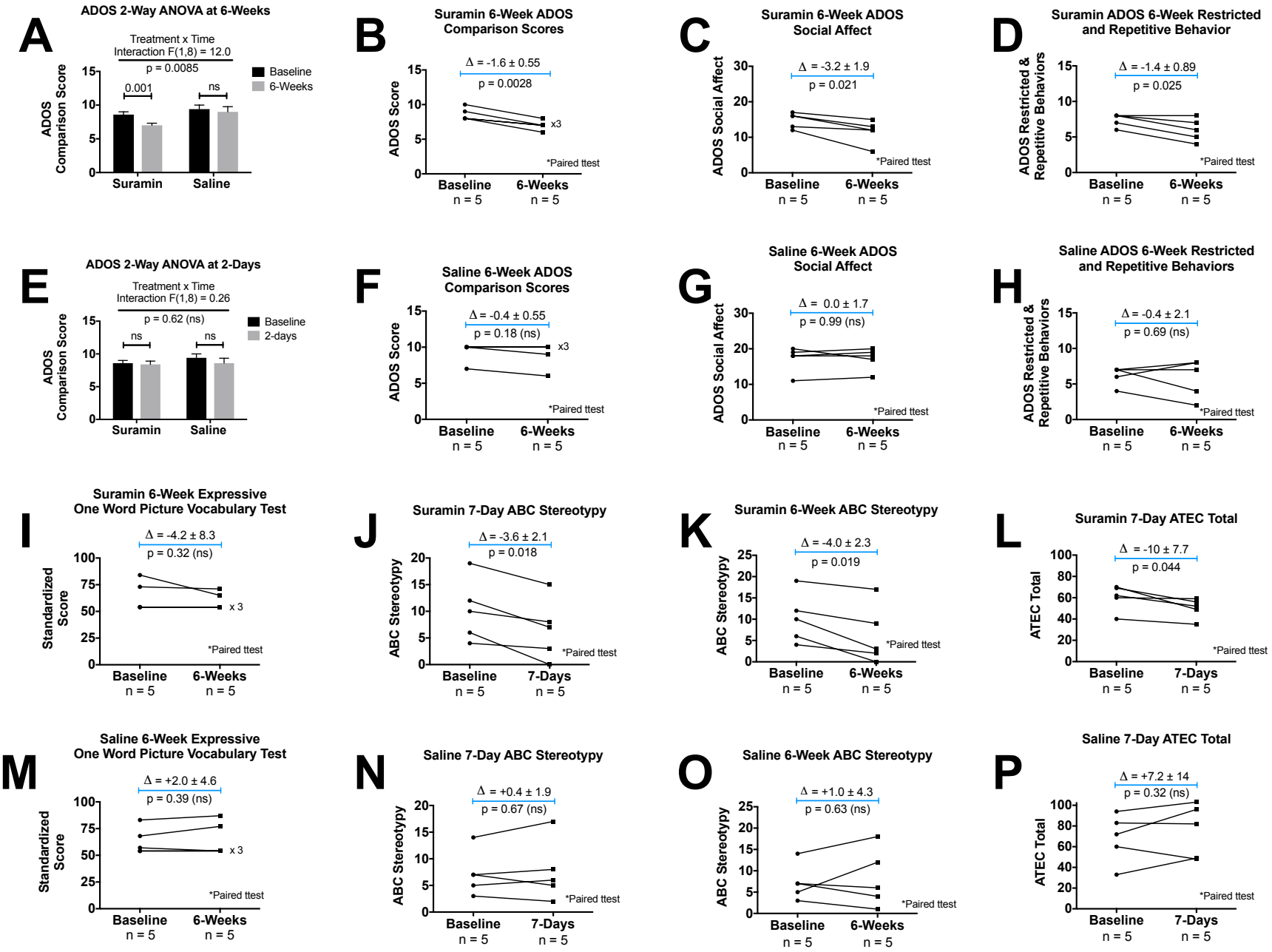

FIGURE S4 Outcomes, A-P

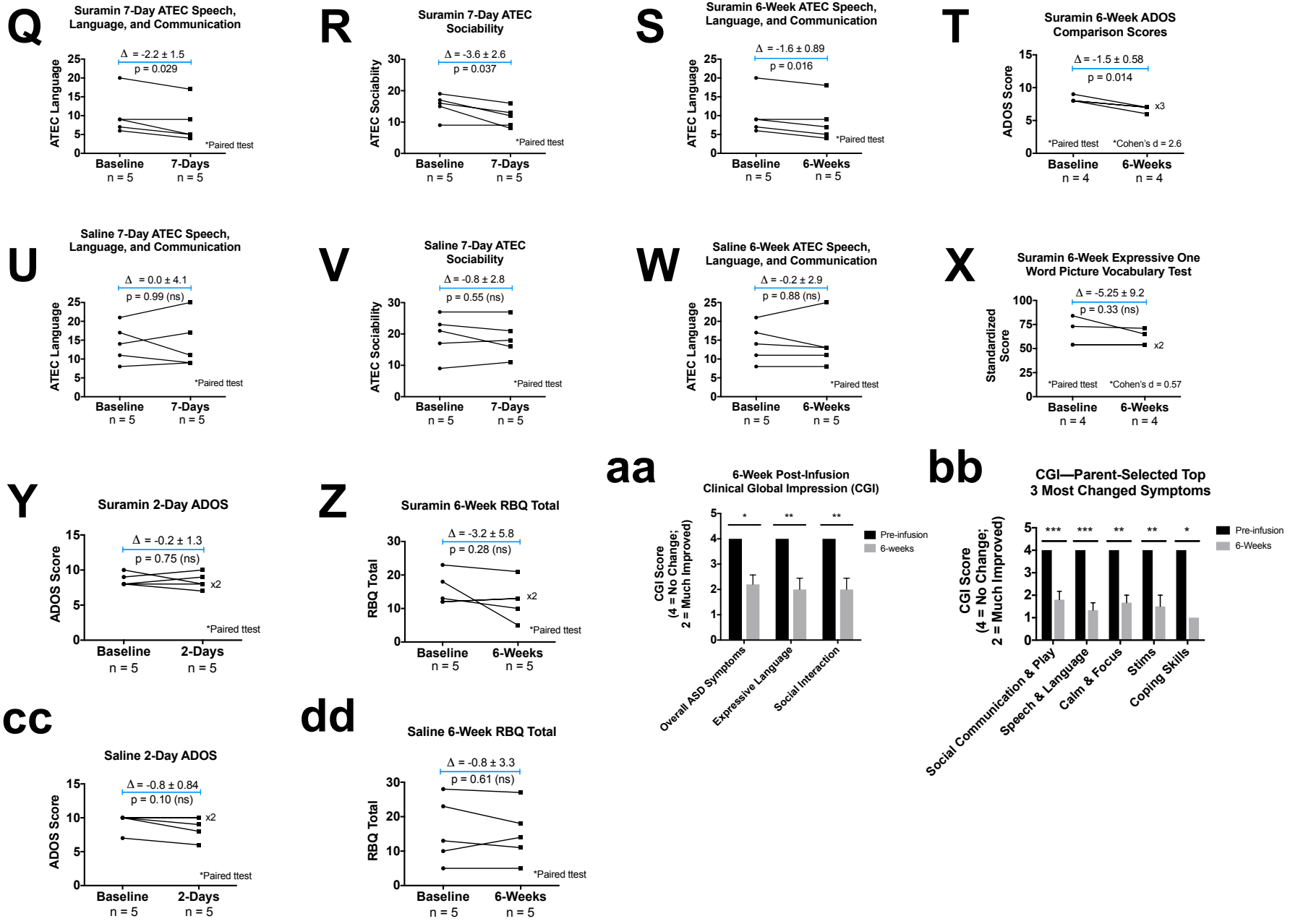

FIGURE S4 Outcomes, Q-dd

Suramin: With Special Reference to Onchocerciasis

F. HAWKING

The Commonwealth Institute of Helminthology
St. Albans, England

I. Introduction

Suramin was introduced by the Bayer workers in 1920 after more than 8 years of research on ureas of the aminonaphthalene-sulfonic type, starting from the trypanocidal activity of trypan red (discovered by Ehrlich and Shiga, 1904), of trypan blue (Mesnil and Nicolle, 1906), and of Afridol violet discovered in 1906 (for details, see Findlay, 1930, p. 259). It was tested on a few patients in Europe (1921–1922), and then extensive therapeutic trials were carried out in Africa by Kleine and Fischer (1923). The compound was found to be very valuable for the treatment of human trypanosomiasis, especially of the East African

type, which could be cured by no other drug. During recent years it has been supplanted to some extent by melarsoprol, and in the future it may be further supplanted by Berenil for human trypanosomiasis. During experiments on trypanosomiasis in volunteers in 1945, Van Hoof *et al.* (1947) discovered that it also acted upon onchocerciasis (see also Wanson, 1950) and since then it has been widely used for the treatment of this filarial infection.

Trypanosomes and onchocercal worms are very different organisms, yet the action of suramin on each of them is so remarkable that it seems that it must depend on the same active part of the suramin molecule. For experimental and historical reasons, much more is known about the action of suramin on trypanosomes than on *Onchocerca*. Accordingly, knowledge about the action on trypanosomes is cited in the following so that it may be used to illuminate the action on *Onchocerca*.

II. Chemistry

Suramin* is a trisodium salt of 8,8′-(3″,3‴-ureylenebis(3‴-benzamido-4‴-methylbenzamido))bis-1,3,5-naphthalenetrisulfonic acid:

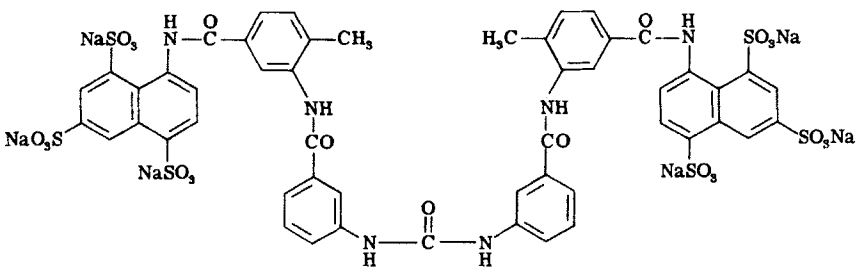

A. Physical Characteristics

Suramin is a pinkish white flocculent powder, with high solubility in water (more than 10% w/v); its solutions are stable to boiling. Suramin is hygroscopic and absorbs moisture from the atmosphere unless kept in a desiccator; the presence of this unsuspected water may cause error in quantitative experiments. It should be stored in the dark and under dry conditions.

* Synonyms: Antrypol, Germanin, Bayer 205, Fourneau 309, belganyl. Naphuride, and Naganol

B. Methods of Estimation

It can be estimated in body fluid by various methods. Following the method of Dangerfield *et al.* (1938), the suramin is hydrolyzed by boiling with hydrochloric acid for 6 hours, and the products are diazotized and coupled with methyl-α-naphthylamine to produce a purple color. This method detects concentrations down to about 5 mg/liter, which is the level where serum itself gives a blank value. A later method that depends on the action of suramin in bleaching 2-*p*-dimethylaminostyryl-6-acetamidoquinolinemethochloride was described by Gage *et al.* (1948); it is effective in the range 0.5–150 mg/liter. Another method was described by Vierthaler and Boselli (1939). More recently, a method for pharmaceutical estimation was reported by Thoma *et al.* (1967); it is based on precipitation with 2-ethoxy-6,9 diaminoacridin lactate and back titration of the excess precipitate by flocculation analysis.

C. Relation of Structure and Activity

The slightest deviation from the formula given in the preceding is accompanied by diminution of trypanocidal activity; even change of position of the sulfonic acid groups has this effect (Fourneau *et al.*, 1924; Findlay, 1930, p. 261; Findlay, 1950, p. 406). The capacity of suramin to combine with the plasma proteins depends on the naphthylamine-trisulfonic groups (Spinks, 1948). Many of the pharmacological properties of suramin, e.g., its binding to serum proteins are due to its general structure as a large molecule with many sulfonic acid groups. Many other large molecules with sulfonic acid groups have similar pharmacological properties, which need not necessarily be related to the specific action of suramin on *Onchocerca* and on trypanosomes.

III. Absorption and Distribution

When given by mouth, suramin is absorbed from the intestine only to a limited extent. When given by subcutaneous or intramuscular injection it causes intense local irritation. Consequently, it is practically always administered by intravenous injection.

After intravenous injection suramin combines with the serum proteins and much of it circulates in the blood. Some of it (probably combined with protein) is taken up by the cells of the reticuloendothelial system. In the bloodstream it persists for long periods (up to 6 months in man) and its excretion in the urine is very slow; both the persistence and the

slow excretion are due to a combination of suramin with the blood proteins. In the plasma of treated rabbits, 70–90% of the suramin is bound to plasma proteins and this serves to protect the enzymes against it. The combination is usually about 0.6 mole suramin to 1 mole protein, but it may be 2 moles suramin to 1 mole protein. Suramin combines with proteins of all kinds: serum globulins (including euglobulin and pseudoglobulin) egg albumin, casein, fibrinogen, gelatin, histones, etc. This combination with protein takes place very quickly (within a few minutes). It depends on different structures from those of the trypanocidal action, and many other large molecules with terminal napthylaminesulfonic acid groups and chondroitin sulfate combine in the same way (Spinks, 1948). The combination presumably takes place with basic groups on the protein, probably by electrostatic forces, but blockage of free amino groups by di-2-chloroethyl sulfone does not prevent combination with suramin (Wilson and Wormall, 1949). The thiol groups of proteins are not involved. Suramin does not diffuse into red blood corpuscles or into the cerebrospinal fluid except in small amounts.

The extent of the accumulation in the blood varies considerably in different subjects, with corresponding variation in the toxic and therapeutic effects (Hawking, 1940). Four days after an intravenous injection of 4.5 mg/kg into rabbits, the plasma concentration was 14 mg/liter, i.e., 11% of the dose in the plasma and 89% in tissues or elsewhere (Vierthaler and Boselli, 1939). In other rabbits, 4 days after 28 mg/kg, 36 mg/liter or 4.6% of the dose was reported in the plasma and 95% elsewhere (Dangerfield *et al.*, 1938).

Man retains the compound in the plasma less well than rabbits. In man, 1 day after 1 gm per patient intravenously the plasma concentration was 25–60 (mean 40) mg/liter, i.e., only 10% of the dose was still in the plasma (Hawking, 1940). After 5 days the plasma concentration was 8–20 mg/liter and after 10 days, 8 mg/liter. After four doses of 1 gm given over a period of a few days, the plasma concentration 1 day after the last dose is often 150 mg/liter and in 1 patient it was as high as 340 mg/liter. After three to four doses, a level of about 5 mg/liter may still be detected 150–200 days later.

According to chemical estimations (Boursnell *et al.*, 1939), no depot of suramin is formed in any tissue; but, by histological methods, suramin can be shown to be taken up as granules by cells of the reticuloendothelial system and by the epithelium of the proximal convoluted tubules of the kidney where it can be demonstrated by staining with neutral red or with Giemsa's stain (von Jancso and Jancso-Gabor, 1952). The cells of the reticuloendothelial system include those of the liver spleen and bone marrow and also the histiocytes of connective tissue all over the body.

The suramin is first bound to serum protein and then it is taken up by the phagocytic cells. It can be found as granules in the connective tissue histiocytes more than 12 days after its injection. More recent work has shown that these granules are really lysosomes in which suramin has accumulated (see Section III,C,3).

A. Excretion

Small amounts are excreted in the urine during the first few days after administration but most of the compound administered cannot be recovered. Traces have been demonstrated by biological tests in the milk of goats treated with suramin (Mayer and Zeiss, 1922).

B. Metabolism

Apparently suramin is relatively resistant to catabolism in the body, as is shown by its long persistence in the blood. Spinks (1948) could not obtain any evidence that suramin is hydrolyzed *in vivo*; and products of suramin produced by acid hydrolysis are rapidly eliminated (Dewey and Wormall, 1946). Apparently, suramin is not hydrolyzed *in vivo* or, if so, only very slowly. There is no evidence for conversion into an active metabolite, and it seems almost certain that the chemotherapeutic activity of suramin is due to the intact molecule.

(A more detailed review of suramin distribution, etc., is given by Findlay, 1950, p. 404.)

IV. Biochemistry and Pharmacology

A. Combination with Proteins and Other Large Molecules

Suramin combines well with serum proteins and with other proteins (see Section III). The combination of suramin with serum proteins may displace other drugs, e.g., chlorpromazine or sulfonamides, or anticogulants such as phenprocoumon (Huethwohl and Jahnchen, 1971).

The toxic action of crystal violet on various organisms (e.g., paramecia, miracidia, perfused toad's heart) is antagonized by suramin and by other large molecules such as Chlorazol fast pink; this action is probably another example of nonspecific combination (Riedel and El-Dakhakhny, 1964). Suramin also forms complexes with large molecules such as terephthalanilides, e.g., HSC 57133 (a compound developed to treat leukemia), and this complex formation has been used to delay the toxicity and to enhance the excretion of such anticancer agents (Yesaiv *et al.*, 1968). Suramin further forms complexes with basic trypanocidal

compounds such as pentamidine and homidium (see the following and Section VII,A,3).

B. Action on Enzymes

Suramin may destroy or inhibit many different enzymes. The most sensitive enzymes examined seem to be hyaluronidase (inhibited at 10^{-5}–10^{-6} *M*), fumarase (at 10^{-7} *M*), urease at pH 5 (at 10^{-4} *M*), hexokinase (at 10^{-4}–10^{-5} *M*) and RNA polymerase (10^{-5} *M*). In general, the strong affinity of suramin for protein suggests that it inhibits enzymes by binding to free cationic amino acid residues in the area of the active center (Williamson, 1970). This action on enzymes seems to be of two kinds: (*1*) specific action on enzymes concerned with DNA and RNA metabolism, which may be the basis of its antiparasitic action (discussed in Section VI); and (*2*) nonspecific action on enzymes of all types, probably due to its tendency to combine with proteins and large molecules. Typical examples are given by the enzymes trypsin and fumarase. Similar action is shown by many polysulfuric acid compounds, e.g., on succinic dehydrogenase (Stoppani and Brignone, 1957; Hill and Hutner, 1968). Suramin and similar compounds inhibit the calcification of rats' epiphyses *in vitro* (Harris *et al.*, 1969) and the transport of calcium in sarcoplastic reticulum, together with the ATPase enzyme related to calcium transport (Layton and Azzi, 1974).

Suramin inhibits various other ATPases (especially in membrane preparations) and enzymes requiring ATP (Fortes *et al.*, 1973). It also inhibits various enzymes concerned with phosphorylation and dephosphorylation (Rodnight, 1970). Smeesters and Jaques (1968) found that, in rat liver cells, suramin treatment markedly decreased the activities of the lysosomal enzymes β-glycerophosphatase, β-*N*-acetylaminodeoxyglucosidase, and β-glucuronidase but not of β-galactosidase, acid maltase, or the protease cathepsin D.

Suramin inhibits mitochondrial oxidative enzymes obtained from *Crithidia fasciculata* (Bacchi *et al.*, 1968), but it is not clear that this action is a specific one.

Jaffe *et al.* (1972) extracted reductases from various filarial adult worms and from schistosomes and found them to be somewhat more sensitive to the inhibitory action of suramin than mammalian reductases; on the other hand, other compounds, such as methotrexate and a related diaminoquinazoline, were more active in inhibition, and the reaction probably has little to do with the antifilarial action.

Although suramin combines with many enzymes, it is not a *general* enzyme poison. In the body, most enzymes are protected against

suramin by the strong combination that it forms with plasma proteins. Wills and Wormall (1949) distinguish two classes of enzymes affected probably in different ways: Group A is not inhibited by suramin at pH 7.0 but is inhibited at acid pH, e.g., urease (suramin probably does not combine with the active center of these enzymes but bridges over it); Group B is strongly inhibited by suramin at pH 7.0 and not so dependent on pH, e.g., hexokinase and succinic dehydrogenase (suramin probably combines with the active center of these enzymes).

C. Lysosomes

Suramin forms complexes with serum proteins and is then taken up into lysosomes where it accumulates, just as acidic vital dyes do. This accumulation occurs in the reticuloendothelial cells all over the body but particularly in the Kupffer cells of the liver and in the cells of the convoluted tubules of the kidney.

1. *Liver*

In the liver, suramin has been studied recently by Buys *et al.* (1973). With rats, about 2% of the dose injected could be found in the Kupffer cells. It stabilizes the membranes of the lysosomes. Suramin and the other compounds act on the enzymes of the lysosomes, inhibiting the acid phosphatase of the hepatocytes and the cathepsin D of the Kupffer cells. Probably this action on the enzymes involves irreversible denaturation (Davies *et al.*, 1971).

2. *Kidneys*

Suramin is filtered (in small amounts) through the capillary walls of the glomeruli and is reabsorbed by the cells of the proximal convoluted tubules where it accumulates as granules. These granules can be demonstrated by staining with neutral red or Giemsa (von Jancso and Jancso-Gabor, 1952). The effects of suramin have been studied in detail with histochemical methods by Wesolowski *et al.* (1972). They treated mice with 400 mg/kg—a high dose but one that does not cause necrosis of the tubules—and they examined the kidney 24 and 72 hours later. They found (*a*) a fall in acid phosphatase activity in the cytoplasm of the convoluted tubules and an appearance of this enzyme in the brush border; (*b*) an increase in alkaline phosphatase, ATPase, and 5-nucleotidase in the brush border of the convoluted tubules and in the endothelium of the capillaries of the glomeruli; (*c*) an increase in granules of succinic dehydrogenase and cytochrome oxidase in cells of the proximal

convoluted tubules and in the thick segments of Henle's loop. They interpret these changes as follows.

Suramin behaves like many other electronegative large molecules, such as trypan blue or horseradish peroxidase, i.e., it joins in a complex with the serum proteins, it is filtered through the renal glomeruli, and it is reabsorbed in the proximal convoluted tubules by the process of endocytosis. In the first phase of endocytosis, these substances are adsorbed to the surface of the tubule cells in conjunction with mucopolysaccharides. In the second stage of endocytosis, the proteins behave as activators; and the cell membrane (plus the accumulated substance) is invaginated to form phagosomes in the cell cytoplasm. Energy for this reaction is supplied by the enzymes of the cell membrane (alkaline phosphatase, ATPase, and 5-nucleotidase) all of which are increased after suramin treatment. Because these enzymes are also increased in the glomerulus, it may be that passage of suramin through the glomerulus is an active rather than a passive process. As succinic dehydrogenase and cytochrome oxidase become more abundant after suramin in the cells of the proximal convoluted tubules and of the thick segment of Henle's loop, it appears that the metabolism of these cells is increased during endocytosis. Later the phagosomes fuse with the primary lysosomes (rich in hydrolytic enzymes) producing secondary lysosomes. As already stated, acid vital dyes and similar compounds such as suramin stabilize lysosomal membranes and inhibit the proteolytic enzymes in them, especially acid phosphatase (thus contributing to the long persistence of suramin). In all this suramin behaves like acidic vital dyes, independent of its specific antitrypanosomal or antifilarial action.

If the accumulation of suramin in the kidney cells is too great, then they degenerate producing albuminuria and all the lesions seen by conventional histological methods. After toxic doses of suramin in animals, histological examination shows profound degeneration of the convoluted tubules with hydropic changes and sloughing of the epithelium; later, in animals that do not die, there is regenerative hyperplasia (Humphreys and Donaldson, 1941). Hyaline casts are found in the tubules; throughout the cortex there may be a few necrotic foci, minute hemorrhages, and perivascular round cell infiltration (Duncan and Manson-Bahr, 1923).

3. *Placenta*

In the same way, when suramin or trypan blue are injected into pregnant rats they are concentrated in the lysosomes of the phagocytic epithelial cells of the yolk sac but they do not penetrate into the embryo

itself. In the yolk sac they probably interfere with metabolites required by the embryo and this may well explain the teratogenic action of both these compounds (see Section V,A,1) (Lloyd and Beck, 1969).

4. *Intracellular Bacilli*

The concentration of suramin in lysosomes probably explains its action in increasing the growth of tubercle bacilli or of *Mycobacterium lepraemurium* in phagocytes, since these bacilli grow in lysosomes (Hart, 1968; Wong and Ma, 1963). This action is nonspecific since it is also shown by dextrans and by macromolecules, such as polyvinylpyrrolidone. In peritoneal macrophages cultured *in vitro*, suramin prevents phagosomes (which contain digestive enzymes) from fusing with lysosomes (which may contain foreign bodies, such as tubercle bacilli) and, thus, the digestion of the tubercle bacilli is inhibited (Hart and Young, 1975).

D. Blood Clotting and Complement

As already stated, suramin inhibits numerous enzymes including proteases, chymotrypsin, and papain. As a result of this enzyme inhibition, it interferes with the formation and hemolytic action of complement and with blood clotting. The findings vary somewhat according to the method of experimentation. In particular, at 70 μg/ml it inhibits the activation of component C1 to C1 esterase and also the activity of the C1 esterase (Eisen and Loveday, 1973). Suramin inhibits the reactions of sheep RBC with C1, C1 and 4, C14 and C2, C14 and C3–9 (Fong and Good, 1972). In connection with blood clotting, at 0.2–1.0 mg/ml (much above therapeutic concentrations), it inhibits the action of thrombin on fibrinogen, and in fibrinolysis, it inhibits the action of plasminogen. It also interferes with the formation of kinin (Eisen and Loveday, 1973). All these actions may be nonspecific due to its general tendency to bind to proteins.

1. *Hereditary Angioneurotic Edema (Quinke's Disease)*

This is a rare disease due to hereditary lack of C1-esterase inhibitors, so that in these patients the complement system is too active, leading to the release of substances that increase the permeability of capillaries. Because suramin is an inhibitor of complement and C1-esterase, it has been used, often with success, in the treatment of this condition (Brackertz, 1974; Schultz, 1974) (see Section VII,C,1).

E. Other Nonspecific Actions of Suramin

Suramin and other anionic substances, such as trypan blue, sulfobromophthalein, and lithium carmine, suppress the accumulation of iodine in the thyroid gland of rats; cationic substances do not act in this way (D'Addabbo *et al.*, 1961; Kallee and Hartenstein, 1960).

Naphthalene sulfonic acids (including suramin) dissolve fibrin clots at low concentration; this effect depends on the presence of several acidic sulfonic groups (Kaulla, 1963).

When dilute solutions of suramin (acidic) and pentamidine (basic) are mixed, a precipitate that removes part of the pentamidine from the system develops. This probably explains the observations of Guimaraes and Lourie (1951) that a previous dose of suramin inhibited some of the toxic actions of pentamidine, especially the dangerous fall in blood pressure; it also inhibited some of the actions of histamine. (It would be valuable to investigate a combination of suramin and Berenil, given simultaneously or successively for the treatment of trypanosomiasis, ultimately in man. Would the suramin diminish the dangerous action of Berenil on the blood pressure while potentiating its trypanocidal action? Or would it neutralize the trypanocidal effect?).

In summary, it is probable that most of these reactions of suramin (except those on RNA/DNA or cell division) have nothing to do with the antitrypanosomal or antifilarial actions of suramin, but they may explain some of the toxic results or nonspecific treatments such as of angioneurotic edema.

V. Toxicity

A. In Animals

The acute toxic dose (LD_{50}) for mice by intravenous injection is about 620 mg/kg. The chief toxic effect in animals is on the kidney where it causes degeneration of the convoluted tubules; there may be minute hemorrhages and degenerative changes also in the liver, lungs, and central nervous system. In some of the animals *(Mastomys natalensis)* that were treated by Lämmler *et al.* (1975) with suramin, 40 mg/kg, s.c., for 5 days, i.e., one-third of the maximum tolerated dose, edema of the nose and front feet developed 3 weeks later. These parts may have a lower temperature than the rest of the body. This happened both in uninfected animals and in those infected with *Litomosoides carinii*, and presumably it was due to a direct toxic action of the drug. It is curious that there was a delay of 16 days after the last dose of drug before these ill effects became apparent.

1. *Toxicity in a Chimpanzee*

The toxic effects of suramin have recently been studied by Gibson *et al.* (1977) in a chimpanzee which was given the excessive total dosage of 152 mg/kg during 36 days. The animal became emaciated and developed hemorrhages, chronic diarrhea, anemia, lymphocytopenia, and albuminuria. At autopsy the primary lesions were found in the intestine, kidney, spleen, and peripheral blood. The intestines were hyperemic and swollen with petechiae and ecchymoses; in the colon there was extensive ulceration and atrophy of the mucosa, and in the jejunum there was acute suppurative enteritis. The kidney tubules were degenerating. The spleen and the femoral and mesenteric lymph nodes were atrophic with few lymphocytes. There was no degeneration of the adrenal cortex. It is possible that the ulceration in the colon and the atrophy of the spleen and lymph nodes were due to the susceptibility of tissues with a high rate of cell division to an inhibitory action of suramin on DNA replication.

2. *Suramin during Pregnancy*

Suramin does not pass through the placenta into the embryo (at least in rats and mice), but it accumulates in the lysosomes of the phagocytic epithelial cells of the umbilical vesicle (which develops from the yolk sac), interfering with the nutrition of the embryo and, thus, producing ill effects (see also Section IV,C,3). Trypan blue has the same action. Rat embryos are susceptible to suramin and trypan blue only at a very restricted period before the embryo is surrounded by the yolk sac (Lloyd and Beck, 1969). The ill effects on the embryos of mice and rats have been studied by Tuchman-Duplessis and Mercier-Parot (1973) and by Mercier-Parot and Tuchman-Duplessis (1973). The action is different in mice from that in rats. Furthermore, the results obtained in these rodents cannot be assumed to occur in other animals or in humans.

a. Rats. Suramin is very toxic for pregnant rats, and 30 mg/kg (little more than the human therapeutic dose) daily from day 1 to day 12 killed 8% of the mother rats, and 75 mg/kg daily killed 14%. On the other hand, the fetuses were not affected by doses of 30 to 75 mg/kg, but they were killed and absorbed after large doses of 100 to 170 mg/kg. In rats, suramin is essentially an abortive drug and does *not* cause malformation.

b. Mice. Fetuses are most susceptible to suramin given during the middle third of pregnancy, especially on days 9–11. At this time, 25 mg/kg is tolerated, but 40–65 mg causes a 64% mortality among the fetuses; many of those which are born, die within 3 days; after that the survivors live and develop well, although some of them suffer from necroses and

amputations of limbs. In fetuses that are affected but not killed, there are developmental abnormalities, namely, cleft palate, harelip, cataracts, and abnormalities of the limbs. Those fetuses which are born may suffer from necroses of the limbs, nose, and tail which necroses later proceed to amputations.

It is fortunate that the human therapeutic use of suramin had become well-established before the thalidomide disaster, otherwise it would probably never have been permitted to proceed as far as clinical trial. Actually, suramin has now been given to many women for over 45 years and no case of infant malformation has been reported and no abortifacient action has been described. Anderson *et al.* (1976) mention a woman who must have conceived 1–2 weeks before the first of four weekly injections of 1 gm suramin and who later gave birth to a normal child. The development of the placenta in humans is different from that of rodents and the experimental results in the latter are not directly applicable to humans. Nevertheless, it is probably wise to regard pregnancy as a counterindication to suramin treatment for a chronic nonfatal condition such as onchocerciasis but not for a potentially fatal infection such as trypanosomiasis.

B. In Man

In man the toxic reactions due to suramin have been studied mostly in patients treated for trypanosomiasis. Reactions are more common in poorly nourished patients. The toxicity is cumulative owing to accumulation of the compound in the blood following repeated doses.

1. *Immediate Reactions*

1. Nausea and sometimes vomiting. This is much reduced if the intravenous injection is given very slowly; with this precaution, vomiting is rare and of little importance.

2. Collapse with nausea, vomiting, shock, sweating, and loss of consciousness. The collapse may be preceded by a short period of motor excitement and congestion of the face and body. [Fain (1942) found this occurred in 12 out of 4500 patients treated. Apted (1970) estimated it might occur in 1 in 2000–4500 cases.] It is best avoided by giving only 0.1–0.2 gm as the first dose. It is probably nonspecific, being due to the injection of a large polyanionic molecule.

3. Colic occurs rarely. There may be slight rise of temperature within half an hour, and various urticarial skin eruptions have been seen in 0.2% of patients (Harding and Hutchinson, 1948).

2. *Late Reactions (after 3 to 24 Hours)*

1. Fever may appear 2–3 hours after injection and may reach 40°C. This might be nonspecific and due to pyrogens, etc. It is probably not due to death of trypanosomes, since trypanosomes do not die until after 12 to 36 hours.

2. Intense photophobia and lachrymation, sometimes with palpebral edema have been noted after 24 hours (this must be rare).

3. Abdominal distension and constipation.

4. Cutaneous hyperesthesia of the soles or palms. The pain begins 24–48 hours after injection and may persist for a week or much longer and the skin may desquamate. In some groups of patients, this has been common (10%), e.g., Kissi people of Sierra Leone and in Venezuela, whereas in Tanzania it has been rare. Its explanation is unclear.

3. *Delayed Late Reactions (after Some Days)*

1. Irritation of the kidney is the commonest toxic reaction after suramin. Before each dose of suramin, the urine should be tested for albumin. A slight cloud can be disregarded. If it is assumed that some protein is normally filtered through the glomerulus and reabsorbed in the tubules, a slight albuminuria might be due to inhibition by suramin of reabsorption in the tubules, rather than to irritation and destruction of kidney cells. If, however, there is a heavy deposit and casts or red blood cells, further treatment with suramin should be postponed or abandoned. (For detailed description of the action on the kidney, see Section IV,C,2). Polyuria and thirst may also occur (? due to action in the kidney). It has been reported by Kennedy and Terry (1972) that 3 patients who were treated with suramin for onchocerciasis developed generalized aminoaciduria; 8 months later 1 patient still had persistent aminoaciduria, but in all 3 patients the urinary protein was normal. Apparently, the state of their urines before suramin is not known, and the significance of this report is difficult to evaluate.

2. Exfoliative dermatitis is usually a late manifestation. It is rare, but dangerous. In Venezuela, Gonzalez-Guerra *et al.* (1964) saw 2 nonfatal cases in 2037 patients; in North Cameroon, Fuglsang and Anderson (1974) saw 1 nonfatal case among 100 heavily infected patients.

3. Stomatitis may be an early complication; it may be severe and extend to the bronchi. Fuglsang and Anderson (1974) saw 1 case in 100 patients.

4. Jaundice is rare but dangerous. Jaundice may also be due to syringe transmission of virus hepatitis.

5. A certain amount of debility and weakness is common during suramin treatment. Sometimes this develops to severe prostration, which may be accompanied by chronic diarrhea and which occasionally terminates fatally after some weeks or months (Fuglsang and Anderson, 1974). The exact pathogenesis of this important and distressing syndrome is unknown. Possibly suramin interferes with the multiplication of cells with a naturally high rate of division, e.g., the epithelium of the intestine and lymphocytes. Compare the chimpanzee above (see Section V,A,1.)

Late toxic reactions to suramin seem to be more common among people who have lived on a starvation diet. In addition to those systemic reactions, there may be aggravation of ocular lesions, especially anterior uveitis, which is probably caused by the slow death of the microfilariae within the eye. In their series of 100 heavily infected patients, Fuglsang and Anderson (1974) saw posterior synechiae in 3, heavy flare or fresh keratic precipitates in 13, and fine flare or cells in 25.

4. *Allergic Reactions*

In the treatment of onchocerciasis, there may be additional reactions due to the death of adult worms and microfilariae. These come on usually after the fourth or fifth dose. They include the following:

Mild manifestations: (1) urticaria and swelling of the affected limb; (2) tenderness and swelling around nodules or impalpable worms; and (3) itching, swelling, and inflammation of the skin with papular or vesicular eruptions and desquamation (due to death of microfilariae).

More severe reactions: (1) deep abscesses around worms dying deep between muscles; and (2) painful immobilization of the hip joint due to death of worms near the hip joint capsule (Duke and Anderson, 1972).

Such severe reactions following the administration of suramin for onchocerciasis can usually be controlled by stopping the drug and giving betamethasone, 1 mg, 3 times a day, for a few days.

5. *Clinical Experiences*

Satti and Kirk (1957), working in the early days of suramin treatment for onchocerciasis, gave much too high doses, e.g., 10 gm in 19 days, and observed 4 deaths among 20 patients. The toxic reactions were those just listed as well as gingivitis leading to ulceration of the gums and mouth and persistent severe headache. These reactions were undoubtedly due to the excessively high dosage. Gonzalez-Guerra *et al.* (1964) in Venezuela gave 6.5 gm during 7 weeks to 2037 persons infected

with *Onchocerca*; 1253 (66%) had no reactions. The others (in descending order of frequency) had edema, pruritus, albuminuria, fever, headache, urticaria, and conjunctivitis. Many of those with edema and pruritus had burning pains on the soles and the feet. There was 1 death (a woman aged 40) from cerebral vascular accident probably not related to treatment, and 2 nonfatal cases of exfoliative dermatitis who recovered after some months. One man had severe prostration and great pain in the hips (? due to death of worms). These authors considered that the side effects, although rarely grave, were undoubtedly a nuisance. In a later report, Convit (1974) states that 26,963 patients had been treated in the field in Venezuela with doses of 5 to 6 gm during 5 to 6 weeks and there had been no deaths due to suramin.

Apted (1970), who has had great experience with the treatment of trypanosomiasis, concludes that, although there is a formidable list of possible reactions, none of these reactions is common except kidney damage, usually mild, and that suramin is really one of the safest drugs in use (for trypanosomiasis). It is important that the compound should be stored dry and in the dark and that the solution should be made (with pyrogen-free water) immediately before the injection and that the intravenous injection should be given slowly. The first dose should not be more than 0.2 gm for an adult to test for possible idiosyncrasy. Suramin should not be given to patients in poor general condition, or with evidence of allergy or of kidney or liver disease, or to pregnant women (especially those in early pregnancy).

Severe reactions due to onchocerciasis, as described in the foregoing, and chronic diarrhea are indications for stopping treatment and so are ulceration of the mouth and tongue. There are suggestions (Rodger, 1958; Nnochiri, 1964) that some batches of drug may cause more reactions than others. Reactions are also more severe in some countries than in others, especially in areas of intense onchocerciasis in the West African savanna. (See also Section VII,B,2.)

6. *Toxicity of Suramin for Adrenal Glands*

It was reported by Wells *et al.* (1937) and by Tomlinson and Cameron (1938) that 2 patients treated for pemphigus with large doses of suramin (16 gm in 10 months) had died and had shown degenerative changes in the cortex of the adrenal glands. Also Mahoney and Barrie (1950) described a woman who was treated for pemphigus with suramin in doses of 1 gm every 2 days for 10 doses. Five weeks later she died with acute adrenal necrosis, but it was not clear whether the necrosis was due to the suramin or to the pemphigus. In view of the earlier deaths, investigations were made in animals by Humphreys and Donaldson

(1941). They treated 100 guinea pigs and some other animals with 1–30 subtoxic doses of suramin so that 23 of the guinea pigs died and 64 out of the total had lesions in the adrenals. Histologically degenerative changes were found in the cortex, often as bands; with repeated doses there was also general atrophy of the cortex caused by disappearance of cells. On the other hand, Frisch and Gardner (1958) could find no harmful effects of suramin on the adrenals of rats given 40 mg/kg every other day for 21 days, even though 6 out of 18 died during this treatment. Moreover, Talbott *et al.* (1940) question the importance of suramin in the aforementioned human cases, since they found changes of the blood suggesting adrenal insufficiency even in untreated cases of pemphigus. Also Goldzieher (1945) reported 6 cases of death from pemphigus with histological signs of severe organic damage in the adrenal cortex, but none of these patients had received suramin.

It will be noticed that all the workers just cited were concerned with pemphigus treated with high doses of suramin and that the much more numerous workers with trypanosomiasis and onchocerciasis have not reported adrenal lesions. Consequently, it seems unlikely that toxic damage to the adrenals is a serious risk during properly conducted suramin treatment. However, Anderson *et al.* (1976) mention that 4 out of 76 patients treated with four doses of 1 gm suramin for savanna onchocerciasis died 1–2 months later with nonspecific symptoms, especially pain on swallowing. If postmortem examinations could be obtained in such cases, it might be well to pay special attention to the adrenal glands.

VI. Antiparasitic Action

The lethal effect of suramin on filariae and on trypanosomes probably depends fundamentally on a similar intracellular reaction, but for historical and experimental reasons almost all of the investigations have been made on the antitrypanosomal action.

A. Action on Trypanosomes

The mode of action of suramin on trypanosomes is still obscure. It has been reviewed by Hawking (1963a), Williamson (1970), and Williamson *et al.* (1975). Briefly, suramin is not trypanocidal *in vitro* except in unbiological concentrations of 1 mg/ml at 37°C for 24 hours (Hawking, 1939). The growth *in vitro* of *Crithidia* or *Trypanosoma rhodesiense* at 26°C was prevented by concentrations greater than 0.1 mg/ml (Hawking, 1963b). On the other hand, a minute dose of 0.03 mg/100 gm is very

effective in mice after a delay of more than 24 hours. The action is probably due to the unchanged suramin itself and not to any active metabolite. When trypanosomes are exposed to suramin *in vitro* or *in vivo*, only small (but significant) amounts of drug can subsequently be extracted from them; nevertheless, some fixation of drug must occur, because exposure of trypanosomes to suramin greatly reduces their power to infect other mice, i.e., further multiplication of the trypanosomes is diminished or abolished. Probably, suramin is initially bound to a primary site on the trypanosome from which it can be washed off up to 1 hour (reversing the loss of infectivity) and then, later, it is more firmly bound to a secondary site from which it cannot be washed and where it produced its main action (Hawking, 1939). If mice infected with *Trypanosoma evansi* are given a minimal effective dose of suramin i.p. (0.03 mg/100 mg), the trypanosomes may continue to divide 7 times during the next 35 hours; then their number remains stationary for perhaps 30 hours, after which their number rapidly diminishes to zero (Hawking and Sen, 1960). During the stationary phase, the chief morphological changes are (*a*) the percentage of dividing forms is diminished, (*b*) there are many large multinuclear forms suggesting that division of the cytoplasm has been inhibited more than that of the nucleus, and (*c*) the cytoplasm contains many basophilic inclusion bodies (which presumably are the same as the vacuolated lysosomes seen with the electron microscope, as described in Section VI,A,3).

This delayed action of suramin might be explained in general terms by an hypothesis that somehow suramin interferes slightly with the RNA–DNA replication mechanism and that each replication becomes more imperfect until the mechanism is brought to a halt by the accumulation of errors. The same delayed inhibition of cell multiplication is produced by homidium and by quinapyramine, but the site of interference with the RNA–DNA system might well be different.

It has been suggested by von Jancsó and von Jancsó (1934) that, besides its direct action, suramin also acts like an opsonin so that slightly damaged trypanosomes are removed from the circulation by the phagocytes of the reticuloendothelial system. This may well occur to some extent, but there is still a latent period of over 24 hours before phagocytosis begins; this latent period would not occur with an opsonin for bacteria.

1. *Biochemistry of RNA and DNA*

If it is explained in simple terms, the genetics of cells are determined by DNA that stores the codified information, and this information is

transferred to the rest of the cell (to make enzymes, proteins, etc.) via RNA of which these are various forms (soluble RNA, ribosome RNA, transfer RNA, messenger RNA, etc.). Ribonucleic acid is synthesized from nucleotide triphosphates, such as AMP and ATP, by enzymes (RNA polymerase) that are dependent on DNA as a template to organize the sequence in which the different nucleotides are built into the chain. The DNA can come either from the nucleus or from the kinetoplast of the trypanosome. These enzymes, polymerases, are specifically inhibited by certain trypanocidal compounds, such as homidium, suramin, and quinapyramine, that act by *preventing multiplication* of trypanosomes rather than by directly *killing* them as arsenicals do. Suramin and homidium are particularly powerful against RNA polymerases. Homidium, which has a small basic molecule, probably acts by combining with the DNA template and thus destroying its pattern for synthesis of RNA. Suramin with a large acidic molecule probably acts on the enzyme itself, perhaps combining with or covering over the "active center" (Hill and Bonilla, 1974).

2. *Experimental Evidence*

In support of the foregoing hypothesis, various pieces of experimental evidence can be quoted.

A simple biochemical system in the ribosomes of *Crithidia fasciculata* has been described by Kahan *et al.* (1968) and Lantz *et al.* (1968) who studied the incorporation of leucine-^{14}C into protein. The system required a soluble enzyme (leucyl–sRNA synthetase, M.W. 105,000) together with ATP, a regenerating system, and guanosine triphosphate. This system was inhibited by suramin, quinapyramine, and pentamidine in concentrations of 0.25 to 0.5 m*M*. (All these drugs inhibit the multiplication of trypanosomes.) They inhibited both leucyl–sRNA synthetase (pentamidine most active) and the incorporation of leucyl-^{14}C–sRNA into protein (suramin most active), i.e., they inhibited both the charging system and the transfer system. Kahan *et al.* concluded that the loss of functional activity produced by the drugs resulted from alterations in the secondary structure of the transfer RNAs.

3. *Morphology by Electron Microscope*

The early morphological changes in trypanosomes produced within 5 to 6 hours by suramin and other trypanocidal drugs have been studied with the electron microscope by Macadam and Williamson (1974). (This period may have been too short for the delayed action of suramin to

manifest itself.) During the first 6 hours, suramin produced no visible change in the nucleus, nucleolus, or kinetoplast. The main changes were in the ribosomes and the lysosomes.

a. Ribosomes. The ribosomes (which consist mostly of RNA) were reduced in number both generally and focally; in some parts they were aggregated together; and their normal aspect and normal polysomal configuration were lost. The same changes were also produced by arsenicals.

Suramin is known to inhibit RNA polymerase in high dilution, 10^{-5} *M* (Waring, 1965; Hill and Bonilla, 1974). The disruption of ribosomes (seen by electron microscopy) suggests that (*a*) ribosomal synthesis of protein must be inactivated and (*b*) this inactivation may be due to impaired synthesis of ribosomal RNA by inhibition of RNA polymerase.

Because there is no alteration of the nucleolus (which is composed largely of RNA) and no microgranules are produced during the 6-hour observation period, the ribosomal lesions may be due to suramin blocking the site on ribosomes that combines with messenger RNA. [This site for mRNA is blocked in cell-free preparations of *Escherichia coli* by large polyanionic molecules such as polyvinyl sulfate, which is analogous in many ways to the polysulfonic acid structure of suramin (Shinozawa *et al.*, 1968).] Trypanosomes made resistant to suramin become hypersensitive to puromycin, which acts on the anabolism of nucleotides, and this also suggests that a prime action of suramin is on ribosomes (Williamson, 1965).

The biochemical evidence about suramin seems to be more plentiful for RNA enzymes than for DNA ones, but this may partly be due to RNA enzymes being easier to investigate than DNA ones. The biological evidence (namely, slowing down of cell division after a latent period of up to seven divisions) points rather to DNA as the fundamental site of lesion. In any case, suramin may well interfere with the DNA–RNA system at many different places, and the demonstration of interference at one particular place does not prove that there may not be interference at other, even more important places.

b. Lysosomes. Suramin also produced large numbers of vacuolated lysosomes. Suramin is known to bind strongly to protein, and thus pinocytosis and localization in lysosomes would be facilitated. Suramin is also known to inactivate the enzymes of lysosomes, and this inactivation would explain the vacuolated lysosomes seen by electron microscopy. On the other hand, most of the compounds studied by Macadam and Williamson (1974) produced vacuolated lysosomes in trypanosomes, so this lysosome phenomenon may well be a general one with little specific significance for suramin.

4. *Note about Cell Division*

Because light microscopy shows many multinucleated trypanosomes, the inhibition by suramin of cell multiplication may act more powerfully or earlier on the cytoplasm than on the nucleus. If streptococci or clostridia are cultivated in the presence of suramin, they grow in long chains instead of breaking up into separate organisms. This happens because the subdivision of the chains into separate organisms depends on an enzyme resembling lysozyme and this enzyme (like many others) is inhibited by suramin (Lominski *et al.*, 1958; Shaikh and Lominski, 1975). It may be that division of the cytoplasm of trypanosomes is also partially dependent on a similar enzyme (liable to be inhibited by suramin). In that case, failure of cell division after suramin would be a side effect, not closely related to the specific action on the RNA and DNA metabolism leading to the death of the parasite.

5. *Other Evidence*

Further examples of suramin interfering with cell division are provided by seedlings of *Vicia faba* and by sea urchin eggs. If young roots of *V. faba* are exposed for 6 hours to 0.5% suramin they cease to show cell division, but they recover if the suramin is washed out of them. The chromosome patterns are distorted showing chromosome bridges and fragmentation, and the cells show multiple nuclei and abnormal mitotic figures (Milovidov, 1961). If sea urchin eggs, *Paracentrotus lividus* or *Sphaerechinus granularis*, are exposed to suramin at a concentration of 1/1000 just before or just after fertilization with sperms, many multipolar mitoses develop so that the eggs contain many nuclei but there is no division into single blastomeres; later the eggs die (Jirovec, 1943a,b). (If ripe eggs are mixed with sperms in seawater containing suramin 1/50–1/5000, the sperms cluster round the eggs but no fertilization occurs; this may be due to suramin stabilizing the outer cell membranes.) In both these examples, the concentrations of suramin is very high; nevertheless, they are interesting as further illustrations of suramin interfering with cell division.

By contrast, another action of suramin on *Paracentrotus* eggs is probably nonspecific, as it is stronger with dyes containing sulfonic acid groups. If fertilized eggs are soaked in suramin 1/100–1/1000, the development of ectoderm is favored against that of mesoentoderm and hatching is delayed. But this action is shown 10–100 times more strongly by Chlorazol sky blue and by Evans blue, respectively (and also by zinc). It is probably due to the polysulfonic acid structure and not to the specifically trypanocidal one (Lallier, 1958).

B. Action on Filariae

1. *Adult Worms*

a. Litomosoides carinii. It has usually been reported that suramin had no action upon *L. carinii* in cotton rats, but this conclusion was due to the period of observation being only 2 weeks, which is too short. Lämmler *et al.* (1971b) showed that, if 40 mg/kg, s.c., was given on five successive days to infected *Mastomys natalensis*, all the adult worms were killed, provided the animals were observed for 6 weeks. (The same result was achieved with double this dose in cotton rats; Lämmler and Herzog, 1974.) The worms started to die after 5 weeks, and they were all dead by 6 weeks from the beginning of treatment. In the first 28 days, squash preparations showed no change in the embryos or microfilariae of the uterus, but after this time the production of microfilariae ceased and the embryos were deformed and degenerated. After 42 days the dead worms were embedded in masses of fibrin. The antifilarial reaction of suramin is remarkable in that, although the treatment ceased after 5 days, the worms did not begin to die until 4 to 5 weeks later.

b. Onchocerca volvulus. Suramin kills the adult worms, as was first discovered by Van Hoof *et al.* (1947), this being the first indication of the antifilarial activity of the compound. When suramin is given in the usual dosage of 1 gm per week, the worms begin to die after the fourth or fifth dose at which time allergic reactions begin to appear, as described in the following. This delay of death until 5 weeks after the beginning of treatment is similar to what happens with *L. carinii*. The lethal action is exerted first on the female worms, whereas the male worms stay alive and motile much longer. This sex difference is not specific for suramin, but occurs with most antifilarial drugs, probably because male worms have a less active metabolism than females. Apparently, a plasma concentration of suramin greater than 10 mg/100 ml should be maintained for about 2 weeks in order to ensure the death of all the adult female worms (Duke, 1968a). The death of the worms is accompanied by general and local inflammatory reactions, which is discussed in detail in the following. Ashburn *et al.* (1949) made histological examinations of 34 nodules from 21 patients who had been treated with suramin in a total dose of 0.14 gm/kg or more. In nodules that were removed 60 days after treatment, the contents of the uteri had undergone necrosis or there were only normal or degenerating ova with no microfilariae. In nodules excised after longer periods, the degeneration was more complete.

c. Wuchereria bancrofti. In Tahiti, Thooris (1956) treated 20 patients and found that 1 year later the number of microfilariae was

reduced to 5% of its original number; so apparently suramin kills the adult worms and the microfilariae gradually die out (see Section VII,B,3).

d. Other Filariae. The action of suramin on *Loa loa, Dipetalonema perstans*, or *Dirofilaria immitis* is not known. It would be valuable to make observations when opportunity occurred. In particular observations should be made on patients treated with suramin for onchocerciasis who may also be infected with *Dipetalonema perstans*. *Dipetalonema witeae* is usually supposed to be insensitive, but I have found no actual references, and the period of observation might have been too short.

2. *Microfilariae*

Suramin seems to have little action on microfilariae of *Onchocerca* or other filariae, and, after 6 weeks of treatment, when the adult worms have been killed, great numbers of microfilariae remain. The natural life of *Onchocerca* is probably well over 10 months, so that even when their replenishment is cut off, it takes up to 18 months for them to dwindle and disappear. On the other hand, there is considerable evidence that, after suramin treatment, many of the microfilariae are killed much earlier than this, especially round about the sixth week after the beginning of treatment. The pronounced dermatological reactions (pruritus, urticaria, etc.) suggest that many of the microfilariae in the skin have died as a result of treatment. Duke (1968a) calculated that 2 weeks after a total dose of 9.5 gm given during 10 weeks, 92% of the microfilariae in the skin had been removed. According to the hypothesis developed in Section VI,B,5 that suramin acts by interference with cell division, such death of microfilariae would be difficult to explain, since microfilariae have no dividing cells. It may be that when suramin kills the adult worms, it provokes such a strong antifilarial immunological reaction that many of the microfilariae are also attacked by antibodies, etc., even though they have not been directly affected by the compound.

3. *Immature Worms*

a. Litomosoides carinii. Suramin has a pronounced action upon all immature stages of *L. carinii* in *M. natalensis* (Lämmler and Hertzog, 1974; Lämmler and Wolf, 1977). When given subcutaneously at 40 mg/kg/day for 5 days, beginning on the seventh, fourteenth, or twenty-eighth day after infection, it completely prevented the development of infection. A good but incomplete prophylactic action was exerted if the treatment was given for 5 days directly after the infection. Lower doses were not effective. These findings were confirmed by Wolf (1976); as

often happens, female worms were more susceptible than males. The least susceptible period was 2–6 days after infection, i.e., the third stage of the larvae.

b. Onchocerca volvulus. In 2 human volunteers, studied earlier by Duke (1968c), the results were less encouraging. The men were given 1 gm weekly for 7 or 5 weeks prior to inoculation and the suramin blood concentration at the time of inoculating infective larvae would be more than 15 mg/100 ml. Thirty-five or 50 infective larvae were inoculated intradermally, and 4–5 days later biopsies were taken at the site of inoculation. In one man, 2 live and 1 dead parasites were found (? slight prophylaxis) and in the other man, no larvae were found; apparently all the larvae had moved away and it was assumed that no prophylaxis had occurred. It may be noted that Wolf (1976) has found that after inoculation of *L. carinii* larvae the first 2–6 days are the times of least susceptibility; furthermore, since suramin acts so slowly on adult worms (6 weeks), the observation period of 4 to 5 days was too short to be significant.

In chimpanzees, however, which could be studied more exhaustively, suramin prevented the development of infection. Duke (1974) inoculated 2 chimpanzees with 750–860 infective larvae during a 12-month period. Treatment was started 2 weeks after the last inoculation and was given as 17 or 21 mg/kg, respectively, weekly for 8 weeks. In one chimpanzee, no microfilariae could be found in the skin during a 30-month period; the other chimpanzee was autopsied 4 weeks after the last treatment, and contained only two bundles of dead worms.

4. *Microfilariae Developing in Vectors*

The action of suramin on *L. carinii* developing in mites has apparently not been investigated. With *O. volvulus,* Duke (1968b) found that when *Simulium* was fed on patients with serum concentrations of 10 to 14 mg suramin per 100 ml, development of the microfilariae was not prevented. Later after the fifth to seventh dose of suramin, although some microfilariae were ingested by the vectors, they did not develop in them. Apparently, the action of suramin was exerted on the microfilariae in the man rather than in the *Simulium.*

5. *Mode of Action on Filariae*

Our knowledge of the action of suramin is incomplete, and experimentation with *Onchocerca* is difficult. Its effect is exerted only on the adult worms or on the immature forms developing in the vertebrate host. The most remarkable feature of its action is its extreme slowness. During a

course of treatment for onchocerciasis, the worms do not begin to die until after 4 to 5 weeks; and when *L. carinii* is exposed to suramin for 5 days *in vivo*, the worms do not die until 5 weeks after the end of treatment. This long delay before the death of filarial worms forms a remarkable analogy with the long delay (of seven cell divisions) before the death of trypanosomes takes place. With such a complicated chemical structure as suramin, it seems most likely that the antitrypanosomal and the antifilarial actions both depend on the same chemical configuration and, ultimately, on interference with the same biochemical processes in the parasites. Accordingly the following hypothetical account of the probable mode of antifilarial action is put forward.

1. Suramin combines with the filarial worm. Some combination is essential for any drug action. In view of the large molecular size, suramin probably penetrates by mouth and intestine rather than through the cuticle. The amount of drug fixed in this way is probably limited. It should be investigated using radioactive suramin and *L. carinii* in *Mastomys*. Estimations should be made of the concentration of drug inside the female and male worms compared with that in the plasma of the host; and radioautography should be employed to determine which part of the worm contains the most drug. It is anticipated that it will be located in the gonads.

2. By analogy with trypanosomes, suramin probably acts by interference with cell multiplication. In adult nematodes, most of the body cells do not multiply—it is only the gonad cells that continue active multiplication. Therefore special morphological study should be made of the developing oocytes and of the corresponding male cells at weekly intervals after the first day of treatment *(L. carinii* in *Mastomys)*. For this purpose the technique of examination of flattened living cells by phase contrast, as described by Taylor and Terry (1960), would be advantageous. It is postulated that suramin progressively deranges the multiplication of these cells (? by inhibition of RNA or DNA polymerase) so that after a delay the cells of the gonads are killed.

3. It would be interesting to investigate whether the action of suramin on *L. carinii* in *Mastomys* is potentiated by puromycin (see action of puromycin on drug-resistant trypanosomes, Section VI,A,3,a). If this were so, a combination of suramin plus puromycin might be valuable for human onchocerciasis.

6. *Possible Antifilarial Action of Homidium and Similar Compounds*

As described above, suramin is a very effective compound for killing the adult worms of *Onchocerca* and of *Litomosoides*, but its lethal

action is not manifested until 5 weeks after the beginning of treatment. Further, suramin is also effective in killing trypanosomes but again its lethal action is not manifested until after a latent period of seven trypanosome divisions. It seems to act not by directly killing the trypanosomes but by disrupting and ultimately preventing cell division. It may, therefore, be pointed out that certain other trypanocidal compounds, namely, phenanthridinium compounds (e.g., homidium) and quinapyramine, also have the same type of action on trypanosomes, that is, inhibition of cell division. Homidium is also known to be as active as suramin in inhibiting enzymes concerned with RNA and DNA metabolism (see Section VI,A,1). In view of all this, it is strongly recommended that further investigations should be actively undertaken on the antifilarial action of phenanthridiums (especially homidium), of quinapyramine, and of similar compounds. For the properties of these substances, see Hawking (1963a) and Williamson (1970). Two phenanthridinium compounds, namely dimidium and 7-amino-9-*p*-aminophenyl-10-methylphenanthridinium were found by Sewell and Hawking (1950) to be active on *Litomosoides*; in fact, they were much more active than suramin according to the technique used by these workers, which involved only 2 weeks of observation. Recently, preliminary experiments (not yet published) have been carried out by Dr. M. J. Worms and the author on *Litomosoides* in cotton rats: the compound is given by injection on 5 consecutive days and the rats are killed for examination after 40 to 60 days. In these circumstances, homidium, 5 mg/kg, killed all or many of the female worms but not the male ones; 10 mg/kg killed practically all the female worms but, in 1 of the 2 rats at this dose, the male worms survived. These results on the female worms are almost as good as those obtained with suramin at 40 mg/kg. Preliminary results with isometamidium (2 mg/kg, i.m.) and Berenil (20 mg/kg, s.c.) were disappointing: no antifilarial action was found. Quinapyramine, 5 mg/kg s.c., had no action in one rat but, in another, it killed 20 out of 22 female worms. Further investigation of homidium (and possibly of quinapyramine) is urgently needed.

VII. Therapeutic Use

A. Against Trypanosomes

1. *Clinical and Veterinary Use*

Clinically, suramin was long (1925–1950) the only effective treatment for Rhodesian sleeping sickness, and it is still the standard remedy

although it has been supplemented by the arsenical, melarsoprol. It is very effective in curing patients before the nervous system is involved; but after this has happened it cannot produce a permanent cure because it does not penetrate into the brain. It is used extensively for the early stages of *gambiense* sleeping sickness (in combination with arsenicals and other compounds). The course of treatment recommended by Apted (1970) for Rhodesian sleeping sickness in Tanzania is 0.2 gm, i.v., as an initial test dose and then 1 gm, i.v., on days 1, 3, 6, 14, and 21. This course quickly builds up a high concentration in the blood and enables the treatment to be completed in 3 weeks. About 10% of patients fail to maintain a high concentration in the blood, with resultant poor therapeutic results. It is desirable to check the blood concentrations by chemical estimation, when this is possible.

In veterinary practice, suramin has been used extensively for *Trypanosoma brucei* infections in horses and other animals and for *T. evansi* in camels (Sudan) or cattle.

2. *Suramin Drug Resistance of Trypanosomes*

In clinical practice, drug resistance to suramin is unknown. In the laboratory, trypanosomes can be made suramin-resistant, but the process takes much longer than with arsenicals. On repeated passage through mice, the resistance is gradually lost in about 6 months. Trypanosomes made resistant to suramin may become hypersensitive to puromycin and to the aminonucleoside of puromycin (Williamson, 1965) that interfere with nucleic acids or nucleoprotein synthesis.

3. *Suramin Complexes*

Suramin (which has six acidic groups) combines with basic compounds such as pentamidine and homidium to give insoluble complexes that are less toxic than the parent compound. They are deposited at the site of injection and are slowly absorbed, producing prophylaxis against trypanosomes over long periods. These complexes were introduced by Williamson and Desowitz (1956) and Desowitz (1957) for the prevention of infection with *Trypanosoma congolense* and *Trypanosoma vivax* in cattle. Thus, when 10 mg/kg homidium content was injected, intramuscularly, homidium suraminate gave protection for 13 months. In principle, these compounds were promising, but in actual practice they proved to have disadvantages because they caused irritation and local toxicity at the site of intramuscular injection; if sloughing occurred, the depot of drug and its protective action were lost.

B. Against Onchocerciasis

Accounts of the use of suramin for the treatment of onchocerciasis have been given by Ashburn *et al.* (1949), Burch (1949), Wanson (1950), Burch and Ashburn (1951), Sarkies (1952), Nelson (1955), Satti and Kirk (1957), and many other authors quoted below.

The problem differs according to whether it concerns individual patients under close medical supervision or whether it concerns large numbers of subjects under field conditions.

The clinical results in each case may be considered from three aspects: (1) the effect on the worms (it usually kills the adult worms but leaves many microfilariae alive); (2) the direct toxic effects of suramin on the host (these have been considered in Section V); and (3) the inflammatory reactions provoked the death of the filariae (these may be pronounced, especially in North Cameroon).

The reactions to suramin are similar to those provoked by diethylcarbamazine, but they are much later in appearing (usually about the sixth week) and they are more prolonged and less severe (in keeping with the more gradual liberation of filarial protein). After the fifth weekly dose or sometimes after the fourth dose, there may be erythematous and pruritic eruptions; there may be violent prurigo of parts of the skin that harbor microfilariae; there may be conjunctivitis and photophobia. There may be fever for a few days to 2 weeks, during which the temperature may rise to 39°–40°C. There may be pains in the joints; violent pain and stiffness sometimes develop in the hip joints, suggesting death of worms localized there (see also Sections V,B,4 and 5 and VII,B,2). One of the earliest complications is iritis, which sometimes appears after the second or third dose.

1. *Treatment of Individual Patients*

Duke and Anderson (1972) recommend an initial dose of 0.1 to 0.2 gm to test for a rare idiosyncrasy which may produce sudden collapse; then 1 gm intravenously weekly per adult of 60 kg weight to a total dose of 6 gm. Before each dose the urine should be tested for albuminuria. Light albuminuria can be disregarded, but heavy albuminuria with many casts and/or an ill-looking patient indicate postponement or cessation of treatment. Severe reactions can usually be controlled by stopping the drug and giving betamethasone, 1 mg 3 times a day, for several days and then tailing off.

At the end of this suramin treatment the adult female worms should be moribund, but there will still be microfilariae in the skin. Three weeks

after the last dose of suramin, a 3-day course of diethylcarbamazine (200 mg twice daily) should be given to destroy them. Usually this produces a mild onchocercal reaction, in which case, it should be repeated every 3 weeks until no reaction occurs.

Relation of Dosage to Effect and Toxicity. Duke (1968a) investigated the relations among the dosage schedule, the therapeutic effect, and the toxicity. Briefly, a dose of 1 gm/week, totalling 5–6 gm suramin, was sufficient to kill all the adult worms, and total doses of 7.5, 8.5, or 9.5 gm offered no therapeutic advantages, and might be more toxic. Doses totalling 4.1 gm were on the border line of effectiveness, but in some patients they did not kill all the worms. Doses of 0.5 gm/week for 7 to 8 weeks were less effective in killing all the worms, and the clinical complications were not reduced in proportion to the dose, so that this course was not recommended. Doses of 0.5 gm given daily to a total of 2.7 gm during 5 days were effective but were very poorly tolerated and could not be recommended for general use. Doses of 0.25 gm weekly for 8 weeks had very little action on the worms. Apparently, it is necessary to maintain a plasma concentration of at least 10 mg/100 ml for 1 to 2 weeks in order to kill all the adult worms.

These findings are very valuable, but it would be desirable to make further investigations to determine more closely the dosage schedule that gives the optimum ratio between therapeutic response and toxicity. For a fatal infection such as trypanosomiasis, the therapeutic response must be complete (i.e., every trypanosome must be killed); and to achieve this result, the risk of a few deaths from toxicity can be tolerated. For a nonfatal infection, such as onchocerciasis, the toxicity must be low with no risk of death but an incomplete therapeutic response (i.e. the survival of a few worms) can be tolerated. Because patients vary in the extent to which they retain suramin in their plasma, it would be desirable to supplement such investigations by estimations of the plasma concentrations. The optimum dosage schedule might well differ from one geographical area to another, according to the intensity of infection and the severity of the reactions.

Further, investigations should also be made on the optimum ratio between the intensity of treatment and its duration. The lower the intensity the less would be the toxicity. On the other hand, Duke (1968a) showed that a total dosage of 2.7 gm suramin, given in daily doses over 5 days, to patients infected with *Onchocerca* produced a more marked effect on the parasite than when the same total dose was given at weekly intervals over 5 weeks. Likewise 8 weekly doses of 0.25 gm in adult males produced little or no detectable effect on the worms.

2. *Large-Scale Treatment*

The employment of suramin on a wide scale in heavily infected areas is controversial. In Mexico it is considered too dangerous and it is not used at all. On the other hand, in Venezuela (Rivas *et al.*, 1965), Ghana (Conran and Waddy, 1959), and Uganda (Cherry, 1960), it has been used widely and successfully without significant numbers of dangerous ill effects. A pilot trial by Picq *et al.* (1974, p. 192) also gave good results with no ill effects.

In Venezuela, where onchocercal infection may be relatively light, Gonzalez Guerra *et al.* (1964) and Rivas *et al.* (1965) treated 3719 patients, mostly with a total dose of 4.5 gm (given as 0.5 gm and then 1 gm weekly per 50 kg body weight). They excluded patients with persistent albuminuria, hypertension, general bad condition, or marked anemia. Twelve to twenty-four months later, no microfilariae could be found in the skin of 96 to 100% of those patients who had received over 4.5 gm suramin. There were three grave nonfatal accidents (2 exfoliative dermatitis and 1 generalized long-lasting prostration) and one death due to cerebrovascular accident and not due to suramin. On the other hand, 34% of the patients experienced minor reactions (especially pruritus, urticaria, palmar-plantar edema, fever, headache, and pains in the joints) which were most numerous after the third and fourth injections; these reactions were not dangerous but they were troublesome and caused many patients to stop treatment. They were relieved by dexamethasone and antihistamines. In a later report, Convit (1974) states that 26,963 cases have now been treated in the field without any deaths due to treatment. The total dose was 5–6 gm during 5 to 6 weeks. Since the beginning of 1974, patients who still have microfilariae in the skin 4 weeks after finishing suramin treatment, have been given diethylcarbamazine, 200 mg daily for 3 days.

In the West Nile province of Uganda, Nelson (1955) treated 56 patients. After treatment, 8 out of 41 patients were free from microfilariae. There were many minor toxic effects especially skin eruptions after the fourth or fifth dose, and he considered that suramin treatment was not practical or acceptable unless under close medical supervision. By contrast, in the Jinja region of Uganda, Cherry (1960) treated 276 patients with apparently no ill effects. He recommended that further treatment with diethylcarbamazine should be given.

In North Cameroon, in patients heavily affected with savanna onchocerciasis, suramin (or any other effective antifilarial treatment) seems to cause many severe reactions (Anderson *et al.*, 1976). On the other hand,

from their experience in Ghana, Conran and Waddy (1956) describe the partial return of sight in many blind patients (due to improvement of corneal opacities and cataracts) and the great relief from cessation of general pruritus.

Probably suramin should be given to all heavily infected patients with considerable pruritus or with danger of ocular complications, e.g., microfilariae in the skin of the head. Marked albuminuria, pregnancy, hypertension, anemia, or poor general condition would all be counterindications. The safety and acceptability would depend largely on how well the field staff were trained to select patients and to administer the injections.

3. *Wuchereria bancrofti*

It is often stated that suramin has no action on *W. bancrofti*, but this is incorrect. Thooris (1956) in Tahiti treated 20 patients who suffered from recurrent lymphangitis (average 2.9 attacks per month). At the end of treatment, the frequency of lymphangitis was reduced by 87% and 1 year later, by 74%. By the end of the year the microfilariae were gradually reduced to 5% of their original number. Because *W. bancrofti* respond so well to diethylcarbamazine, the action of suramin is not of practical importance, but these results show that suramin does act on the adult worms of other filariae besides *Onchocerca*.

C. In Treatment of Nonparasitic Diseases

In the past, suramin has been used to treat a variety of nonparasitic diseases. In these cases the action of suramin (if any) was probably due to its large polyacidic molecule rather than to its specific antiparasitic grouping.

1. *Angioneurotic Edema (Quinke's Disease)*

This is a hereditary condition due to lack of C1-esterase inhibitors that normally inhibit the first component of complement (C1). Accordingly, the complement system is too active, and pharmacologically potent substances, such as anaphylatoxin and kinin-like C2 fragments, tend to be set free, increasing the permeability of capillaries and producing the edema. Suramin is a powerful inhibitor of C1 activators and of many other components of complement so that the use of suramin is well justified scientifically (see Section IV,D). In actual practice, some patients appear to respond well; others give a poor response to suramin but respond better to other agents such as ϵ-aminocaproic acid or

traxenic acid (Brackertz and Kueppers, 1973; Brackertz, 1974; Schulz, 1974; Eisen and Loveday, 1973; Fong and Good, 1972).

2. *Pemphigus and Other Conditions*

During the 1930s, suramin was used for treating pemphigus, frequently in very high doses, e.g., 10 gm in 19 days. According to Bolgert (1970), pemphigus can also be treated with quinacrine, Aureomycin, corticosteroids, or mercuric chloride. Mizonova (1969) treated 28 patients with suramin and corticosteroids and most of them improved. Senear Usher's syndrome is a special form of pemphigus (pemphigus foliaceus), and it has been treated with suramin in large doses (Samtsov, 1966; Terao, 1969). There seems, however, to be little scientific basis for the administration of suramin to pemphigus patients, and the multiplicity of other therapeutic agents suggests that it was not very effective and not specific. A modern "Textbook of Dermatology" (Rook *et al.*, 1968) recommends treatment with corticosteroids but does not mention suramin. Similarly, Moschella *et al.* (1975), in "Dermatology" do not mention suramin. It may be concluded that treatment of pemphigus with suramin is no longer justified. Dermatitis herpetiformis similarly has been treated with suramin in the past but the two recent textbooks of dermatology just cited do not mention it.

During the nineteen-thirties, even multiple sclerosis was treated with suramin—a treatment for which there was no justification except desperation because of the absence of any effective therapy.

ACKNOWLEDGEMENTS

This review of suramin, with special reference to its use for the treatment of onchocerciasis, was prepared in 1976 while I was holding a World Health Organization consultantship. Grateful acknowledgments are due many members of WHO for assistance, criticism, and advice; the WHO library staff for search of the literature and many other facilities; and Professor G. Lämmler for helpful comments. The opinions expressed here are the responsibility of the writer and do not involve WHO.

REFERENCES

Anderson, J., Fuglsang, H., and Marshall, T. F. de C. (1976). *Tropenmed. Parasitol.* **27**, 279.

Apted, F. I. C. (1970). *In* "The African Trypanosomiases" (H. W. Mulligan, ed.), p. 684. Allen & Unwin, London.

Ashburn, L. L., Burch, T. A., and Brady, F. J. (1949). *Bol. Of. Sanit. Panam.* **28**, 1107.

Bacchi, C. J., Hutner, S. H., Ciaccio, E. I., and Marcus, S. M. (1968). *J. Protozool.* **15**, 576.

Bolgert, M. (1970). *Ann. Med. Interne* **121**, 399.

Boursnell, J. C., Dangerfield, W. G., and Wormall, A. (1939). *Biochem. J.* **33**, 81.

Brackertz, D (1974). *Schweiz. Med. Wochenschr.* **104,** 403.
Brackertz, D., and Kueppers, F. (1973). *Klin. Wochenschr.* **51,** 620.
Burch, T. A. (1949). *Bol. Of. Sanit. Panam.* **28,** 233.
Burch, T. A., and Ashburn, L. L. (1951). *Am. J. Trop. Med.* **31,** 617.
Buys, C. H., Elferink, M. G., Bouma, J. M., Gruber, M., and Nieuwenhuis, P. (1973). *J. Reticuloendothel. Soc.* **14,** 209.
Cherry, J.K. (1960). *East Afr. Med. J.*, **37,** 550.
Conran, O., and Waddy, B. (1956). *J. Trop. Med. Hyg.* **59,** 52.
Convit, J. (1974). *Sci. Publ., Pan Am. Health Organ.* **298,** 57.
D'Addabbo, A., Kallee, E., and Heinzel, W. (1961). *Acta Isot.* **1,** 227.
Dangerfield, W. G., Gaunt, W. E., and Wormall, A. (1938). *Biochem. J.* **32,** 59.
Davies, M., Lloyd, J. B., and Beck, F. (1971). *Biochem. J.* **121,** 21.
Desowitz, R. S. (1957). *Ann. Trop. Med. Parasitol.* **51,** 457.
Dewey, H. M., and Wormall, A. (1946). *Biochem. J.* **40,** 119.
Duke, B. O. L. (1968a). *Bull. W. H. O.* **39,** 157.
Duke, B. O. L. (1968b). *Bull. W. H. O.* **39,** 169.
Duke, B. O. L. (1968c). *Bull. W. H. O.* **39,** 179.
Duke, B. O. L. (1968d). *Bull. W. H. O.* **39,** 307.
Duke, B. O. L. (1968e). *Br. Med. J.* **4,** 301.
Duke, B. O. L. (1974). *Tropenmed. Parasitol.* **25,** 84.
Duke, B. O. L., and Anderson, J. (1972). *Trop. Doctor* **2,** 107.
Duncan, J. T., and Manson-Bahr, P. H. (1923). *Trans. R. Soc. Trop. Med.* **17,** 392.
Ehrlich, P., and Shiga, K. (1904). *Berl. Klin. Wochenschr.* **41,** 329 and 362.
Eisen, V., and Loveday, C. (1973). *Br. J. Pharmacol.* **49,** 678.
Fain, A. (1942). *Rev. Trav. Sci. Med. Congo Belge* **1,** 137.
Findlay, G. M. (1930). "Recent Advances in Chemotherapy." Churchill, London.
Findlay, G. M. (1950). "Recent Advances in Chemotherapy," 3rd ed., Vol. 1. Churchill, London.
Fong, J. S., and Good, R. A. (1972). *Clin. Exp. Immunol.* **10,** 127.
Fortes, P. A., Ellory, J. C., and Lew, V. L. (1973). *Biochim. Biophys. Acta* **318,** 262.
Fourneau, E., Tréfouel, J., Tréfouel, T. B., and Vallee, J. (1924). *Ann. Inst. Pasteur, Paris* **38,** 81.
Frisch, E., and Gardner, L. I. (1958). *Endocrinology* **63,** 500.
Fuglsang, H., and Anderson, J. (1974). *Sci. Publ., Pan. Am. Health Organ.* **298,** 54.
Gage, J. C., Rose, F. C., and Scott, M. (1948). *Biochem. J.* **42,** 574.
Gibson, D. W., Duke, B. O. L., and Connor, D. H. (1977). *Tropenmed. Parasitol.* **28,** 387.
Goldzieher, J. W. (1945). *Arch. Dermatol. Syph.* **52,** 369.
Gonzalez Guerra, L., Rasi, E., and Rivas, A. (1964). *Rev. Venez. Sanid. Asist. Soc.* **29,** 90.
Guimaraes, J. L., and Lourie, E. M. (1951). *Br. J. Pharmacol. Chemother.* **6,** 514.
Harding, R. D., and Hutchinson, M. P. (1948). *Trans. R. Soc. Trop. Med. Hyg.* **41,** 481.
Harris, A. F., Cotty, V. F., Barnett, L., and Seiman, A. (1969). *Arch. Int. Pharmacodyn. Ther.* **181,** 489.
Hart, P. D. (1968). *Science* **162,** 686.
Hart, P. D., and Young, M R. (1975). *Nature (London)* **256,** 47.
Hawking, F. (1939). *Ann. Trop. Med. Parasitol.* **33,** 13.
Hawking, F. (1940). *Trans. R. Soc. Trop. Med. Hyg.* **34,** 37.
Hawking, F.(1963a). *Exp. Chemother.* **1,** 129 and 893.
Hawking, F. (1963b). *Ann. Trop. Med. Parasitol.* **57,** 255.
Hawking, F., and Sen, A. B. (1960). *Brit. J. Pharmacol. Chemother.* **15,** 567.

Hill, G. C., and Bonilla, C. A. (1974). *J. Protozool.* **21,** 632.
Hill, G. C., and Hutner, S. H. (1968). *Exp. Parasitol.* **2,** 207.
Huethwohl. B., and Jahnchen, E. (1971). *Naunyn-Schmiedeberg's Arch. Pharmacol.* **270,** Suppl. 1, R66.
Humphreys, E. M., and Donaldson, L. (1941). *Am. J. Pathol.* **17,** 767.
Jaffe, J. J., McCormack, J. J., and Meymarian, E. (1972). *Biochem. Pharmacol.* **21,** 719.
Jirovec, O. (1943a). *Biochem. Z.* **314,** 265.
Jirovec, O. (1943b). *Biochem. Z.* **315,** 69.
Kahan, D., Zahalsky, A. C., and Hutner, S. H. (1968). *J. Protozool.* **15,** 385.
Kallee, E., and Hartenstein, H. (1960). *Nucl. Med.* **1,** 273.
Kaulla, K. N. V. (1963). *Proc. Soc. Exp. Biol. Med.* **114,** 153.
Kennedy, P., and Terry, S. (1972). *Trans. R. Soc. Trop. Med. Hyg.* **66,** 27.
Kleine, F. K., and Fischer, W. (1923). *Dtsch. Med. Wochenschr.* **49,** 1039.
Lallier, R. (1958). *Publ. Stn. Zool. Napoli* **30,** 185.
Lämmler, G., and Herzog, H. (1974). *Tropenmed. Parasitol.* **25,** 78.
Lämmler, G., and Wolf, E. (1977). *Tropenmed. Parasitol.* **28,** 205.
Lämmler, G., Herzog, H., and Schütze, H. R. (1971a). *Bull. W. H. O.* **44,** 757.
Lämmler, G., Herzog, H., and Schütze, H. R. (1971b). *Bull. W. H. O.* **44,** 765.
Lämmler, G., Grüner, D., and Zahner, H. (1975). *Z. Tropenmed. Parasitol.* **26,** 97.
Lantz, M., Kahan, D., and Zahalsy, A. C. (1968). *J. Protozool.* **15,** Suppl., 23.
Layton, D., and Azzi, A. (1974). *Biochem. Biophys. Res. Commun.* **59,** 322.
Lloyd, J. B., and Beck, F. (1969). *Biochem. J.* **115,** 32P.
Lominski, I., Cameron, J., and Wyllie, G. (1958). *Nature (London)* **181,** 1477.
Macadam, R. F., and Williamson, J. (1974). *Ann. Trop. Med. Parasitol.* **68,** 301.
Mahoney, L. J., and Barrie, H. J. (1950). *Br. Med. J.* **2,** 655.
Mayer, M., and Zeiss, H. (1922). *Arch. Schiffs- Trop.-Hyg.* **26,** 237.
Mercier-Parot, L., and Tuchmann-Duplessis, H. (1973). *C. R. Seances Soc. Biol. Ses Fil.* **167,** 1518.
Mesnil, F., and Nicolle, M. (1906). *Ann. Inst. Pasteur, Paris* **20,** 513.
Milovidov, P. (1961). *Planta* **57,** 455.
Mizonova, T. P. (1969). *Vestn. Dermatol. Venerol.* **43,** 64.
Moschella, S. L., Pillsbury, D. M., and Hurley, H. S. (1975). "Dermatology," pp. 462 and 1748. Saunders, Philadelphia, Pennsylvania.
Nelson, G. S. (1955). *East Afr. Med. J.* **32,** 413.
Nnochiri, E. (1964). *Trans. R. Soc. Trop. Med. Hyg.* **58,** 413.
Picq, S. S., Rolland, A., and Roux, J. (1974). *OCCGE Conf.* p. 192.
Riedel, H., and El-Dakhakhny, M. (1964). *Arzneim.-Forsch.* **14,** 1025.
Rivas, A., Gonzales, G., Zsogon, L., Rasi, E., and Convit, J. (1965) *Acta Med. Venez., Suppl.* p. 1.
Rodger, F. C. (1958). *Trans. R. Soc. Trop. Med. Hyg.* **52,** 462.
Rodnight, R. (1970). *Biochem. J.* **120,** 1.
Rook, A., Wilkinson, D. S., and Ebling, F. J. G. (1968). "Textbook of Dermatology," p. 1178. Blackwell, Oxford.
Samtsov, V. I. (1966). *Vestn. Dermatol. Venerol.* **40,** 74.
Sarkies, J. W. R. (1952). *Trans. R. Soc. Trop. Med. Hyg.* **46,** 435.
Satti, M. H., and Kirk, R. (1957). *Bull. W. H. O.* **16,** 531.
Schulz, K. H. (1974). *Hautarzt* **25,** 12.
Sewell, P., and Hawking, F. (1950). *Br. J. Pharmacol. Chemother.* **5,** 239.
Shaikh, M. R., and Lominski, I. (1975). *Zentralbl. Bakteriol., Parasitenkd., Infektionskr. Hyg., Abt. 1: Orig., Reihe A* **230,** 237.

Shinozawa, T., Yahara, I., and Imahori, K. (1968). *J. Mol. Biol.* **36,** 305.
Smeesters, C., and Jaques, P. J. (1968). *Proc. Int. Congr. Cell Biol., 12th, 1968* Excerpta Med. Found. Int. Congr. Ser. No. 166, Abstr. No. 143, p. 82.
Spinks, A. (1948). *Biochem. J.* **42,** 109.
Stoppani, A. O. M., and Brignone, J. A. (1957). *Arch. Biochem. Biophys.* **68,** 423.
Talbott, J. H., Lever, W. F., and Conzolazio, W. V. (1940). *J. Invest. Dermatol.* **3,** 31.
Taylor, A. E. R., and Terry, R. S. (1960). *Trans. R. Soc. Trop. Med. Hyg.* **54,** 33.
Terao, T. (1969). *Jpn. J. Dermatol.* **79,** 339.
Thoma, K., Ullmann, E., and Loos, P. (1967). *Arch. Pharm. (Weinheim, Ger.)* **300,** 577.
Thooris, G. C. (1956). *Bull. Soc. Pathol. Exot.* **49,** 311.
Tomlinson, C. C., and Cameron, O. J. (1938). *Arch. Dermatol. Syph.* **38,** 555.
Tuchmann-Duplessis, H., and Mercier-Parot, L. (1973). *C. R. Seances Soc. Biol. Ses Fil.* **167,** 1717.
Van Hoof, L., Henrard, C., Peel, E., and Wanson, M. (1947). Cited by Wanson (1950).
Vierthaler, R. W., and Boselli, A. (1939). *Arch. Schiffs- Trop.-Hyg.* **43,** 149.
von Jancso, N., and Jancso-Gabor, A. (1952). *Acta Physiol. Acad. Sci. Hung.* **3,** 537.
von Jancso, N., and von Jancso, H. (1934). *Zentralbl. Bakteriol., Parasitenkd. Infektionskr. Hyg., Abt. 1: Orig.* **132,** 257.
Wanson, M. (1950). *Ann. Soc. Belge Med. Trop.* **30,** 671.
Waring, M. J. (1965). *Mol. Pharmacol.* **1,** 1.
Wells, H. G., Humphreys, E. M., and Work, E. G. (1937). *J. Am. Med. Assoc.* **109,** 490.
Wesolowski, H., Olszewska, M., and Makowski, J. (1972). *Folia Biol. (Krakow)* **20,** 395.
Williamson, J. (1965). *Proc. Int. Congr. Protozool., 2nd, 1964* Excerpta Med. Found. Int. Congr. Ser. No. 91, Abstr. No. 77, p. 81.
Williamson, J. (1970). *In* "The African Trypanosomiases" (H. W. Mulligan, ed.), p. 125. Allen & Unwin, London.
Williamson, J., and Desowitz, R. S. (1956). *Nature (London)* **177,** 1074.
Williamson, J., Macadam, R. F., and Dixon, H. (1975). *Biochem. Pharmacol.* **24,** 147.
Wills, E. D., and Wormall, A. (1949). *Biochem. J.* **44,** xxxix.
Wilson, J., and Wormall, A. (1949). *Biochem. J.* **45,** 224.
Wolf, E. (1976). Inaug.-Dissertation d. Doktorgrades, Fachbereich, Vet. med. Justus Liebig-Universität, Giessen.
Wong, P. C., and Ma, L. (1963). *J. Trop. Med. Hyg.* **66,** 99.
Yesaiv, D. W., Wodinsky, I., Rogers, W. I., and Kensler, C. J. (1968). *Biochem. Pharmacol.* **17,** 305.

Pharmaceutical Research, Vol. 23, No. 6, June 2006 (© 2006)
DOI: 10.1007/s11095-006-0165-1

Research Paper

Nontoxic Suramin as a Chemosensitizer in Patients: Dosing Nomogram Development

Danny Chen,[1] Sae Heum Song,[1] M. Guillaume Wientjes,[1,2,5] Teng Kuang Yeh,[1] Liang Zhao,[1] Miguel Villalona-Calero,[2,3] Gregory A. Otterson,[2,3] Rhonda Jensen,[1,2] Michael Grever,[2,3] Anthony J. Murgo,[4] and Jessie L-S. Au[1,2]

Received December 13, 2005; accepted January 31, 2006

Purpose. We reported that suramin produced chemosensitization at nontoxic doses. This benefit was lost at the ~10-fold higher, maximally tolerated doses (MTD). The aim of the current study was to identify in patients the chemosensitizing suramin dose that delivers 10–50 μM plasma concentrations over 48 h.
Methods. Nonsmall cell lung cancer patients were given suramin, paclitaxel, and carboplatin, every 3 weeks. The starting chemosensitizing suramin dose was estimated based on previous results on MTD suramin in patients, and adjusted by using real-time pharmacokinetic monitoring. A dosing nomogram was developed by using population-based pharmacokinetic analysis of phase I results (15 patients, 85 treatment cycles), and evaluated in phase II patients (19 females, 28 males, 196 treatment cycles).
Results. The chemosensitizing suramin dose showed a terminal half-life of 202 h and a total body clearance of 0.029 L h^{-1} m^{-2} (higher than the 0.013 L h^{-1} m^{-2} value for MTD of suramin). The dosing nomogram, incorporating body surface area as the major covariate of intersubject variability and the time elapsed since the previous dose (to account for the residual concentrations due to the slow elimination), delivered the target concentrations in >95% of treatments.
Conclusions. The present study identified and validated a dosing nomogram and schedule to deliver low and nontoxic suramin concentrations that produce chemosensitization in preclinical models.

KEY WORDS: chemosensitization; dosing nomogram; neoplasms; suramin.

INTRODUCTION

Our laboratory has shown acidic and basic fibroblast growth factors (aFGF and bFGF), expressed in solid tumors, as a cause of chemoresistance. The combined presence of these two proteins, at clinically relevant concentrations, induces an up to 10-fold resistance to drugs with diverse structures and action mechanisms, without altering drug accumulation. Inhibitors of aFGF and bFGF, including the respective monoclonal antibodies and suramin, reverse the FGF-induced resistance (1–3).

Suramin, an aromatic polysulfonated compound, has multiple, concentration-dependent effects. Targets inhibited by <50 μM suramin include reverse transcriptase, protein kinase C, transforming growth factor β, bFGF, and RNA polymerase, and targets affected by >50 μM suramin include interleukin-2, insulin-like growth factor I, topoisomerase II, epidermal growth factor, and tumor necrosis factor α (4–7). Suramin induces cell cycle arrest at the G1 phase at >50 μM (8–11), and shows appreciable cytotoxicity at >100 μM.

Suramin has been evaluated as an anticancer agent since the 1980s, and has shown activities in several malignancies, most notably in prostatic carcinoma (12,13). These earlier studies used maximally tolerated doses (MTD) yielding 100–200 μM suramin in plasma (equivalent to approximately 150–300 μg mL^{-1}) (13–15). The half-life of MTD suramin is unusually long (30–50 days), and results in significant drug accumulation upon repeated dosing. This pharmacokinetic property, together with its significant host toxicities, mandated the use of real-time pharmacokinetic analysis and adaptive control to calculate the suramin dose for individual patients. Subsequent findings of low interpatient variability in the suramin clearance and further population-based pharmacokinetic (PPK) analysis have led to the recommendation of using fixed dose schedules, consisting of series of infusions with sequentially decreasing doses or increasing intervals, to maintain plasma concentrations in the 70–200 μM range (16,17).

We reported that suramin, at a dose that delivers plasma concentration between 10 and 50 μM, significantly enhances the therapeutic efficacy of chemotherapy (doxorubicin, pacli-

[1] College of Pharmacy, The Ohio State University, 496 West 12th Avenue, Columbus, Ohio 43210, USA.
[2] James Cancer Hospital and Solove Research Institute, The Ohio State University, Columbus, Ohio, USA.
[3] Department of Internal Medicine, The Ohio State University, Columbus, Ohio, USA.
[4] National Cancer Institute, Bethesda, Maryland, USA.
[5] To whom correspondence should be addressed. (e-mail: wientjes.1@osu.edu)

taxel, docetaxel, mitomycin) against well-established subcutaneous or metastatic human xenograft tumors (breast, prostate, bladder) in immunodeficient mice, without enhancing the host toxicity (1–3,18,19). We further found that this chemosensitizing effect of suramin was diminished at higher doses/concentrations (20), presumably due to cell cycle perturbations. These findings, together with the limited clinical efficacy of MTD suramin in previous combination chemotherapy studies (13,21–23), highlight the importance of maintaining the suramin concentration within the 10–50 μM range.

The above considerations led to the initiation of several phase II clinical trials of using nontoxic suramin as a chemosensitizer (24). The goal of the present study, conducted in conjunction with the phase I/II trials in non small cell lung cancer (NSCLC), was to develop a method to identify the chemosensitizing suramin dose that delivers 10 and 50 μM plasma concentrations over the duration when the chemotherapy agents (paclitaxel and carboplatin) are present at therapeutically significant levels (i.e., 48 h). To accommodate the residual drug due to the unusually long half-life and the need to maintain the drug concentrations within the range that produces chemosensitization, we first used real-time pharmacokinetic studies to identify the suramin dose in the second or later cycles in the phase I study. This method was successful in maintaining desired suramin concentrations, but was labor-intensive and cannot be readily implemented in the community settings. Hence, we used population pharmacokinetic (PPK) analysis of the results in the first two cohorts of phase I patients to develop a dosing nomogram, which was then evaluated in an additional phase I cohort and subsequently in phase II patients.

MATERIALS AND METHODS

Patient Protocols and Treatments

Details on patient treatments had been described in a previous publication (24). The following provides the information pertinent to the present study. Briefly, a patient with pathologically or cytologically confirmed advanced (IIIB or IV) NSCLC received a 30-min infusion of suramin, followed immediately by a 3-h infusion of paclitaxel (starting at 175 mg m^{-2} and escalating to 200 mg m^{-2} after the suramin dose was established), and then a 1-h infusion of carboplatin [area under the plasma concentration–time curve (AUC) of 6 mg min mL^{-1}]. The phase I trial was open to all comers, whereas the phase II trial included two groups of patients (chemotherapy-naive or chemotherapy-refractory). For the present study, all patients with adequate samples for pharmacokinetic evaluation were included. The target suramin plasma concentration was initially set between 10 and 50 μM for 72 h and the initial dose, calculated based on the published clinical data for MTD suramin (24,25), was 240 mg m^{-2} given as a single dose. Based on the results in the first cohort of six patients, the target concentrations were amended to between 10 and 50 μM over 48 h, and suramin was administered as two split doses (two-thirds on the first day and one-third on the second day). The suramin dose for subsequent cycles (i.e., second and later cycles) was reduced to compensate for the residual plasma concentration at 72 h pretreatment. A total of 62 patients (15 in phase I and 47 in phase II) were studied for pharmacokinetics. Phase I patients received a total of 85 treatment cycles, with a median of 6 cycles. Phase II patients received a total of 198 treatment cycles, with a median of 4 cycles. All patients showed renal and hepatic function tests within the normal limits, before and after treatments.

Pharmacokinetic Studies and Data Analysis

Suramin or paclitaxel was extracted from plasma or urine, and analyzed with previously published high-performance liquid chromatography methods (26). The detection limit was 0.5 μg mL^{-1} for suramin and 15 ng mL^{-1} for paclitaxel. For carboplatin, plasma ultrafiltrates containing the free drug (not bound to plasma proteins) were obtained, diluted with deionized water, and analyzed for platinum content by using inductively coupled plasma mass spectrometry, as previously described (27).

To determine whether suramin affected the plasma protein binding of paclitaxel and vice versa, 2 mL human plasma containing nonradiolabeled paclitaxel and tritium-labeled suramin, or nonradiolabeled with tritium-labeled paclitaxel, was placed in the upper chamber of an ultrafiltration unit that was separated from the lower chamber by a cellulose membrane (molecular weight cutoff at 10,000; Amicon, Beverly, MA, USA). The unit was maintained in room temperature for 45 min, followed by centrifugation at 2,000 × *g* for 30 min. Aliquots (25 μl each) were removed from the top chamber prior to ultrafiltration (containing free plus bound drug), and from the bottom chamber after ultrafiltration (containing only the free drug), and analyzed for paclitaxel or suramin by using liquid scintillation counting. The extent of protein binding was calculated as (Total concentration − Free concentration) / (Total concentration).

Pharmacokinetic analysis was performed with WinNonlin. Phase I suramin plasma data were analyzed by using open two- and three-compartment linear models with a constant infusion input. For paclitaxel and carboplatin data and phase II suramin data, we used noncompartmental analysis. Renal clearance was calculated as the amount of suramin excreted in 24-h urine divided by the plasma AUC over the same 24-h period.

Overview of Development and Validation of Dosing Equations/Nomogram

Figure 1 outlines the schema. First, we used the pharmacokinetic results in the first cohort of six phase I patients to determine the duration that covered >90% of the paclitaxel/carboplatin AUC, with the goal of maintaining the plasma suramin concentrations at between 10 and 50 μM over this duration. This led to adjustments in the suramin regimen; administering suramin in two split doses yielded the target concentrations over 48 h in the second cohort of six patients. The pharmacokinetic results of these 12 patients were then used with PPK analysis to derive suramin dosing equations, which were then used to predict the dose in three additional phase I patients. Through retrospective and prospective analyses of the precision and accuracy of the PPK-based dosing equations, a correction factor was identified and used

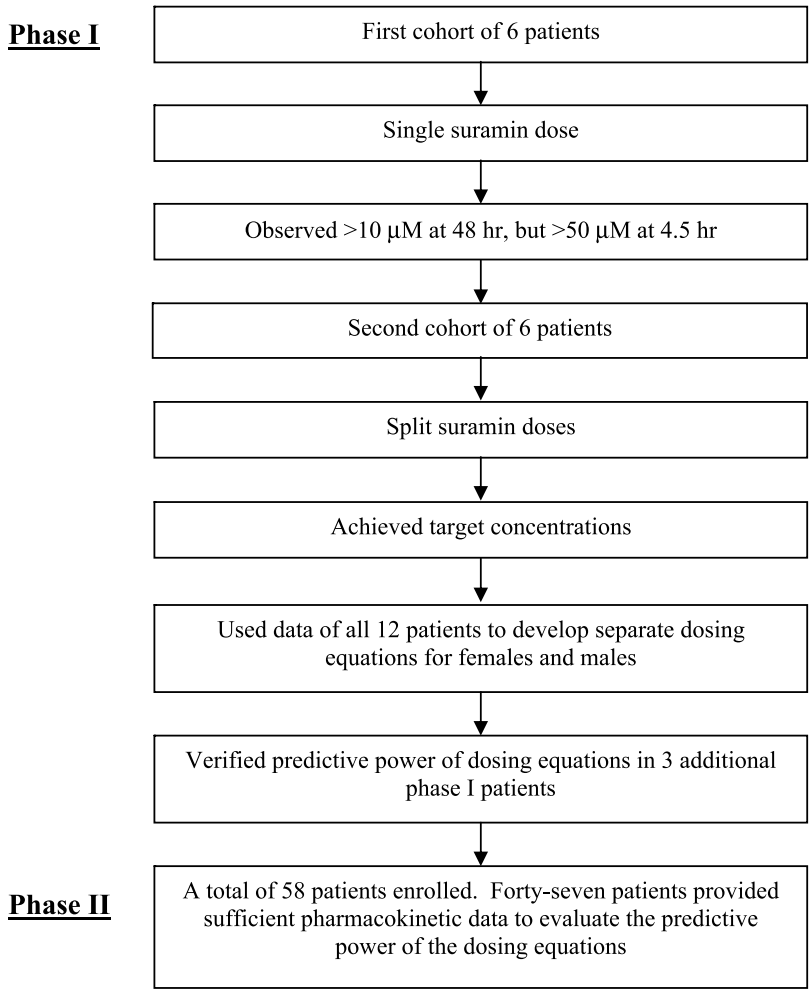

Fig. 1. Development and validation of dosing nomogram: Experimental Design.

to derive a dosing nomogram. The predictive power of the nomogram was evaluated in 47 phase II patients.

Population-Based Pharmacokinetic Analysis

Suramin data were analyzed with the nonlinear mixed-effects modeling approach (NONMEM Version V; UCSF, San Francisco, CA, USA). PPK analysis identifies the sources of interindividual variability in pharmacokinetic parameters and is performed in a stepwise manner (28,29), as follows.

The first step is to define the appropriate structural model for the pharmacokinetic parameters of interest. Because ~90% of the area under the suramin plasma concentration–time curve was accounted for by the area under one phase (i.e., terminal phase), we used a one-compartment model for PPK analysis due to its relative ease. Equation (1) describes the population-based plasma concentrations (C) as a function of clearance (CL) and volume of distribution (V), in a one-compartment model.

$$C_{ij} = \frac{\text{Dose}}{V_j} e^{-\left(\frac{CL_j}{V_j}\right) \times \text{time}_i} \quad (1)$$

where subscript i represents time and subscript j denotes a patient. For example, C_{ij} is the predicted plasma concentration at a particular time i for a patient j. The NONMEM subroutines describing this model are supplied as prewritten programming codes ADVAN1, TRAN2 in the PREDPP library of the NONMEM software.

In NONMEM analysis, error functions are used to describe the random deviations between model-predicted data and observed data, for individual pharmacokinetic parameters. Our objective was to identify the dose that can be calculated based on CL and V. Hence, the analysis focused on these two parameters. Equations (2) and (3) describe the deviation of CL (CL_j) and V (V_j) in an individual patient from the population or typical values ($CL_{\wedge typ}$ and $V_{\wedge typ}$).

$$CL_j = CL_{\wedge typ} \times (1 + \eta_{CL}) \quad (2)$$

$$V_j = V_{\wedge typ} \times (1 + \eta_V) \quad (3)$$

where η_{CL} and η_V representing the interindividual variation in CL and V are random values normally distributed around a mean of zero with a variance of ω^2.

Equation (4) describes the residual error between the predicted *vs.* the observed concentration; Y_{ij} is the observed plasma concentration of the jth individual at the ith sampling time, C_{ij} is the PPK Model-predicted values, and ε_{1ij} and ε_{2ij} are the proportional and additive errors, respectively, with a mean of zero and a variance of σ^2.

$$Y_{ij} = C_{ij} \times (1 + \varepsilon_{1ij}) + \varepsilon_{2ij} \quad (4)$$

Next, the physiological or pathological parameters of patients (referred to as covariates) that significantly contributed to the interindividual variability in CL and V were incorporated into the model (referred to as the Full Model). This was accomplished by examining the relationships between covariates and pharmacokinetic parameters in individual patients by using linear regression; covariates that showed a coefficient of determination (r^2) of greater than 0.4 with a 5% significance ($p < 0.05$) were selected as candidate covariates. A candidate covariate was incorporated into the model if its inclusion reduced the objective function value of the model by at least 3.9 (i.e., χ^2 value associated with $p < 0.05$ for 1 degree of freedom). To ascertain that the selected covariates played an important role in the model performance, the final model (referred to as PPK Model) was obtained by removing insignificant covariates from the Full Model in a more restrictive backward elimination process. In this process, a covariate was retained if its removal resulted in an increase in the objective function by at least 7.9 (χ^2 value associated with $p < 0.005$ and 1 degree of freedom).

Evaluation of Dosing Equations

The PPK Model (further described in Results), combined with individual patient parameters, yield PPK Model-based doses for each treatment cycle. The performance of the PPK Model-based dosing equations was evaluated as follows. First, we calculated the target dose (referred to as Ideal Dose) that would yield a plasma concentration of 15 μM suramin at 48 h ($C_{48\,h,target}$), using Eq. (5).

$$\text{Ideal Dose} = \frac{\text{administered dose} \times \left(C_{48h,target} - C_{pre} \times e^{-k\times 48}\right)}{\left(C_{48h,observed} - C_{pre} \times e^{-k\times 48}\right)} \quad (5)$$

where C_{pre} is observed predose suramin concentration and $C_{48h,observed}$ is the observed or fitted concentration at 48 h. The deviation of PPK Model-predicted dose from Ideal Dose for each cycle (Deviation) was calculated by using Eq. (6). The mean and standard deviation of Deviations of all cycles represent the accuracy and precision, respectively, of the PPK Model-predicted doses.

$$\text{Deviation from Ideal Dose} = \left(\frac{\text{Ideal Dose} - \text{Predicted dose}}{\text{Ideal Dose}} \times 100\%\right) \quad (6)$$

Similarly, the % deviations of the PPK Model-predicted plasma concentrations of each cycle was calculated by using Eq. (7), and the accuracy and precision of the PPK Model-predicted concentrations were calculated as described for the PPK Model-predicted doses.

$$\text{Deviation from target concentrations} = \left(\frac{(C_{predicted} - C_{observed})}{C_{predicted}} \times 100\%\right) \quad (7)$$

Validation of PPK Model-Based Dosing Method in Phase II Study

The final dosing equations and the resulting nomogram were adopted for the phase II study. A total of 58 patients were accrued to the phase II trial. The first 11 phase II patients provided only 0- and 24-h samples. We later amended the protocol and obtained additional samples (predose, 0.5, 3.5, 4.5, 6, 24, and 26 h) that enabled the determination of the 48-h concentration through pharmacokinetic data fitting (actual samples were not available). The performance of the dosing nomogram was evaluated by comparing the observed/fitted concentrations to the target range of 10–50 μM over 48 h.

Statistical Analysis

Statistical significance of the differences in pharmacokinetic parameters between groups was analyzed by using Student's *t* test. The Akaike Information Criterion and the Schwartz Criterion were used to compare the fitting of two- and three compartment pharmacokinetic models to the suramin plasma concentration–time data (30).

RESULTS

Pharmacokinetics of Paclitaxel and Carboplatin

The results show similar clearance and terminal half-lives for the two paclitaxel doses used (initially 175 mg kg^{-1}, escalating to 200 mg kg^{-1}). For carboplatin, the average dose was 679 ± 115 mg (range, 514–894; median, 654). The average AUC from time 0 to 48 h was 1.27 ± 0.24 mg min mL^{-1} for paclitaxel (200 mg kg^{-1} dose) and 6.3 ± 1.4 mg min mL^{-1} for carboplatin, and the respective AUC from time 0 to time infinity were 1.33 ± 0.27 and 6.4 ± 1.4 mg min mL^{-1}, indicating the attainment of >92% and >99% of the total AUC during the first 48 h. A comparison of the paclitaxel and carboplatin pharmacokinetics in the present trial with literature data (31–34) showed no significant changes due to the addition of suramin (not shown).

Pharmacokinetics of Chemosensitizing Suramin

The target suramin concentration range was initially set at 10–50 μM over 72 h. Results in the first six patients indicated the attainment of the target concentration of 10–20 μM at 72 h in five patients, but showed peak levels exceeding 50 μM in all patients. As >90% of the AUCs of paclitaxel and carboplatin were attained in the first 48 h, the target suramin concentrations were amended to between 10

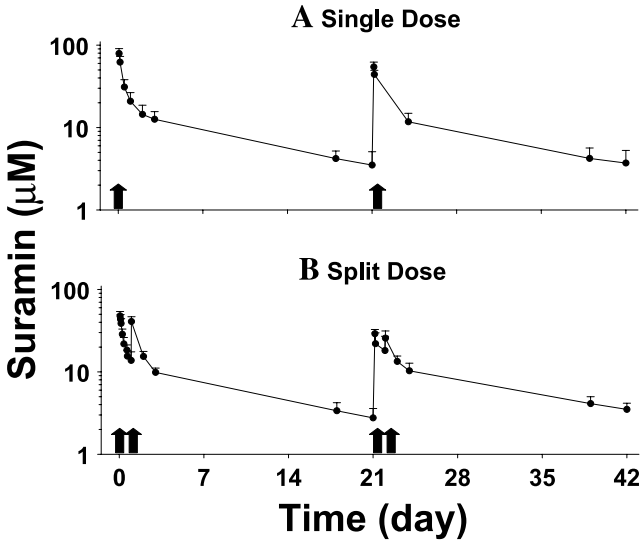

Fig. 2. Suramin plasma concentration–time profiles. Suramin was given by single doses (panel A, total of 19 treatments) or by split doses (panel B, total of 66 treatments). Arrows indicate times for the initiation of 30-min suramin infusion. Data are mean + 1 SD. Data points are connected by straight lines.

and 50 μM over 48 h. We calculated that these concentrations could be achieved by giving suramin in two split doses, with two-thirds given on the first day and the remaining one-third given 24 h later (Fig. 2). This schedule yielded the target concentration range of <50 μM immediately after the 3-h paclitaxel infusion and >10 μM at 48 h, in all of the subsequent 66 treatments administered to 13 patients (including the remaining treatments in four of the original first six patients and nine additional patients).

The suramin dose was 240 mg m^{-2} for the first cycle and 146 ± 21 mg m^{-2} for the second and later cycles. Figure 2 shows the plasma concentration–time profiles. Analysis of the data of the first cycle by using two- and three-compartment body models showed no significant difference in the goodness-of-fit ($p = 0.5$ by the Akaike Information Criterion and $p = 0.7$ by the Schwartz Criterion) and yielded nearly identical total body clearance (<10% difference, $p > 0.4$). The pretreatment suramin concentrations during the second through tenth treatment cycles remained relatively constant at about 4 μg mL^{-1} (range, 2.95–4.80 μg mL^{-1}). As the doses for these cycles were calculated by using real-time pharmacokinetics based on the parameters in individual patients (obtained by analyzing the data in the first cycle), the nearly constant pretreatment concentrations for up to 30 weeks of treatment indicate no changes in drug disposition over time.

Table I summarizes the pharmacokinetic parameters of suramin in phase I patients. The renal clearance of suramin was determined in 38 phase II patients; 1.21 ± 1.05% of the dose was excreted as unchanged drug in 24 h and the calculated renal clearance was 2.05 ± 1.69 mL h^{-1} m^{-2} (range, 0.18–8.7 mL h^{-1} m^{-1}, equal to 7.09 ± 5.76% of the total plasma clearance). The renal clearance did not show a significant correlation with the creatinine clearance ($r = 0.123$, $p = 0.46$).

In Vitro Protein Binding of Paclitaxel and Suramin

The plasma protein binding of suramin at clinically achievable concentrations (i.e., 10 and 100 μg mL^{-1}) remained constant at 99.6 ± 0.02% ($n = 3$), and was not altered by the addition of 10 μg mL^{-1} paclitaxel. The plasma protein binding of paclitaxel was 90.8 ± 0.5%, 90.8 ± 0.2%, and 88.9 ± 0.3% ($n = 3$ each) at clinically achievable concentrations of 0.1, 1, and 10 μg mL^{-1}, respectively. Addition of 100 μg mL^{-1} suramin did not affect the binding of paclitaxel at 0.1 and 1 μg mL^{-1} concentration, but significantly, albeit only slightly, decreased the paclitaxel binding at 10 μg mL^{-1}, from 88.9% to 88.3 ± 0.2%. This corresponded to a 5% increase in the free fraction of paclitaxel at 10 μg mL^{-1} (i.e., from 11.1% to 11.7%). This relative small interaction between the two drugs did not affect the disposition of paclitaxel, as in the present study its pharmacokinetics is not significantly different from previous studies where it was given only with carboplatin (35–37).

PPK-Based Pharmacokinetic Analysis

Plasma concentration–time profiles of 53 cycles obtained in the first 12 patients were analyzed by using PPK, to develop easy-to-use dosing equations. We reasoned that this task could be accomplished by using the simplest pharmacokinetic model, capable of reliably described plasma concentrations between 48 h (needed to assess maintenance of target concentrations) and the start of the next treatment cycle (determinant of the next dose). The dominance of the terminal phase (β phase half-life was 40 times the α-phase half-life, and ~90% of the total AUC was accounted for by the area under the terminal phase, calculated as B/β) led to the selection of a monoexponential model for PPK.

Table I. Pharmacokinetic Parameters of Suramin

Pharmacokinetic parameters	Literature (33)	Present study
Dose (mg m^{-2})	>2,000	240
AUC (μg h mL^{-1})	NA	8.37 ± 1.89
Alpha half-life (h)	14.8 ± 7.5	5.12 ± 1.54[b]
Beta half-life (day)	41 ± 23	8.61 ± 2.28[b]
V_1 (L m^{-2})	3.0 ± 0.6	1.94 ± 0.26[b]
V_2 (L m^{-2})	10.6 ± 3.1	6.50 ± 1.82[b]
V_{dss} (L m^{-2})	13.6 ± 3.2[a]	8.45 ± 1.88[b]
CL (L h^{-1} m^{-2})	0.013 ± 0.006	0.029 ± 0.006[b]

Results of suramin used as a chemosensitizer at low dose in 15 patients are compared to literature data obtained during Near-MTD application as a cytotoxic agent (33). As the pharmacokinetics of low dose suramin (cycle 1) was best described by a two-compartment model, this data is presented, and compared to a two-compartment analysis of high dose suramin. High dose suramin is adequately described by either a two- or a three-compartment model (33). Because the current study administered suramin every 3 weeks, whereas earlier studies administered suramin at more frequent intervals, the dose and AUC were normalized per 3-week interval. Mean ± standard deviation. NA, not available.

[a] V_{dss} was estimated as the sum of V_1 and V_2; standard deviation was calculated according to the error propagation rule $(SD1^2 + SD2^2)^{1/2}$.

[b] $p < 0.05$, unpaired two-tailed Student's t test compared to literature.

Table II. Relationship Between Suramin Clearance and Volume of Distribution and Clinical Parameters

	CL ($L\ h^{-1}$)	V (L)	Weight (kg)	IBW[a] (kg)	Height (in.)	BSA (m^2)	Age (years)	Gender	CrCL ($mL\ min^{-1}$)	Serum creatinine ($mg\ dL^{-1}$)	Serum albumin ($g\ dL^{-1}$)
						Numerical values					
Mean	50.4	18.2	79.3	68.5	68.5	1.94	60.1	8 male	88.2	0.94	4.22
SD	±11.7	±3.2	±11.1	±9.1	±3.3	±0.17	±9.2	2 female	±18.8	±0.13	±0.37
						Correlation with CL or V					
CL: *r*	1	0.577	0.789	0.710	0.632	0.789	0.569	−0.904	0.423	0.286	−0.332
CL: *p*	NA	(0.081)	(0.007)	(0.021)	(0.050)	(0.007)	(0.086)	(0.000)	(0.224)	(0.423)	(0.348)
V: *r*	0.577	1	0.854	0.511	0.498	0.773	0.117	−0.477	0.641	0.181	−0.058
V: *p*	(0.081)	NA	(0.002)	(0.131)	(0.143)	(0.009)	(0.748)	(0.164)	(0.046)	(0.618)	(0.873)

Data were taken from all cycles of 10 of the first 12 phase I patients. Two patients with samples collected for <1 terminal suramin half-life were not included. Ideal body weight (IBW) was calculated as the sum of (50 for males and 45.5 for females) and (2.3 × (height in inches − 60)). Creatinine CL was calculated using the Cockroft-Gault equation. The correlation coefficients (r) of CL and V with gender were obtained by assigning arbitrary values of 1 for male and 2 for female patients. The p values for the correlations are also indicated.

Nine potential covariates [i.e., age, body weight, ideal body weight, height, body surface area (BSA) age, gender creatinine CL, creatinine concentration, and albumin concentration] were examined. Their values and correlation coefficients with CL and V are shown in Table II. The covariates that showed statistically significant correlations with CL were body weight and BSA. In these 12 patients, the CL was significantly higher in nine male than in the three female patients. Accordingly, gender was included as a covariate. Creatinine CL showed a significant correlation by the nonparametric Spearman correlation ($r = 0.636$, $p = 0.048$). The remaining covariates did not show significant correlations in the linear regression analysis, and were not further evaluated. As body weight and BSA are strongly correlated ($r = 0.97$, $p < 0.001$), and as BSA is more widely used in dose determinations for oncology patients, only BSA (but not body weight) was used in the Full Model for $CL_{\wedge typ}$ [Eq. (8)]. V showed a significant correlation with BSA. Further testing showed improved model performance when BSA^2 was used as covariate instead of BSA. No other covariates reached statistical significance. The Full Model for $V_{\wedge typ}$ is described by Eq. (9).

$$CL_{\wedge typ} = (\theta_1 \times BSA + \theta_2 \times CrCL + \theta_3) \times (1 - \theta_4) \quad (8)$$

$$V_{\wedge typ} = \theta_5 \times BSA^2 + \theta_6 \quad (9)$$

where θ_1 and θ_2 describe the effects of BSA and CrCL on $CL_{\wedge typ}$, respectively. For males, θ_4 was set to zero. For females, θ_4 represents the difference between the clearance values for males and females. θ_5 is the proportionality constant that describes the effect of (BSA^2) on $V_{\wedge typ}$. θ_3 and θ_6 reflect the intercept values for CL and V, with the effects of the covariates removed.

Full Model was subsequently simplified by eliminating the covariates that did not significantly affect the model performance. Results are summarized in Table III. Removal of the fixed-effect parameters, θ_2, θ_3, and θ_6, from the Full Model altered the objective function value by less than 7.9,

Table III. Estimates for Population Model Parameters

	Full model				Population model				
			95% Confidence interval				95% Confidence interval		Difference in minimum values of objective function
Parameters	Mean	CV%	Low	High	Mean	CV%	Low	High	
θ_1 ($L\ h^{-1}\ m^{-2}$)	9.40	190	−1.97	20.8	26.2	2.70	24.6	27.4	15.47
θ_2	0.10	137	0.04	0.19	NA	NA	NA	NA	6.03
θ_3 ($L\ h^{-1}$)	24.8	106	8.09	41.5	NA	NA	NA	NA	2.59
θ_4	0.39	20	0.34	0.44	0.31	13.1	0.28	0.34	41.57
θ_5 ($L\ m^{-4}$)	4.30	24	3.62	4.92	5.13	4.40	4.49	5.57	29.47
θ_6 (L)	1.50	229	−0.72	3.90	NA	NA	NA	NA	1.84
$k_{\wedge typ}$ (h^{-1}, male)	NA	NA	NA	NA	0.0026	7.3	0.0023	0.0030	NA
$k_{\wedge typ}$, (h^{-1}, female)	NA	NA	NA	NA	0.0022	4.7	0.0020	0.0024	dNA

The population pharmacokinetic parameters were obtained using data from the first 12 patients (54 treatment cycles) in the phase I study. Fitted values for different fixed effect parameters [θ_1–θ_6 of Eqs. (8) and (9)] and estimates of variability of the estimates are presented. θ_2, θ_3, and θ_6 were removed from the final population model since their removal increased the objective function value by less than 7.9. NA: not applicable.

which is the value required for inclusion (29). Removal of these three parameters simultaneously altered the objective function value by 7.26. Removal of θ_2 rendered the model equations independent of the creatinine CL and simplified the model. The remaining three significant parameters were θ_1, θ_4, and θ_5. The final PPK Model is described by Eqs. (10) and (11).

$$CL_{\wedge typ} = (\theta_1 \times BSA) \times (1 - \theta_4) \quad (10)$$

$$V_{\wedge typ} = \theta_5 \times BSA^2 \quad (11)$$

Table III shows the parameter estimates and their coefficient of variations (CV) and 95% confidence intervals. The resulting final PPK Model, using only the two covariates BSA and gender, reduced the estimated interindividual variability in CL by 5-fold (from 30% to 6%) and the variability in V by 6-fold (from 20% to 3%).

Derivation of PPK Model-Based Dosing Equations

Due to the residual suramin concentration at the time of the second and later treatment cycles, separate equations are required to calculate the doses for the first treatment cycle and subsequent cycles.

The first dose was calculated by using Eq. (12), a simplified version of Eq. (1).

$$\text{Dose} = \frac{C \times V}{e^{-k \times t}} \quad (12)$$

Hence, dose calculation requires the values of V and k, the elimination rate constant. Equation (13) describes $k_{\wedge typ}$, as a function of $CL_{\wedge typ}$ and $V_{\wedge typ}$.

$$k_{\wedge typ} = \frac{CL_{\wedge typ}}{V_{\wedge typ}} \quad (13)$$

The value of k for each patient was calculated by using Eqs. (10), (11), and (13). The average k value ($k_{\wedge typ}$) was 0.0026 h^{-1} for males and 0.0022 h^{-1} for females. $k_{\wedge typ}$ showed a low variability within the same gender (CV of 7% for males and 5% for females). Substituting the values of $k_{\wedge typ}$ for each gender and the desired C of 15 μM or 21.4 μg mL^{-1} at 48 h into Eq. (12) yielded Eq. (14).

$$\begin{aligned}\text{First cycle dose (mg)} &= \frac{(21.4 \times 5.13 \times BSA^2)}{e^{-(0.0026 \text{ or } 0.0022 \times 48)}} \\ &= \text{FACTOR1} \times BSA^2\end{aligned} \quad (14)$$

The numerical values of FACTOR1 were calculated to be 124 mg m^{-4} for males and 122 mg m^{-4} for females. For ease of dose calculation in later studies, the value of FACTOR1 was set at 125 mg m^{-4} for both genders.

To attain the same target concentrations of 21.4 μg mL^{-1} at 48 h during subsequent treatment cycles, the dose administered should replace the fraction of the dose that was eliminated during the interval between treatments. This is described in Eq. (15).

$$\begin{aligned}\text{Subsequent cycle dose (mg)} &= \text{First dose} \times \left(1 - e^{-k \times t}\right) \\ &= \text{FACTOR1} \times BSA^2 \times \left(1 - e^{-k \times t}\right)\end{aligned} \quad (15)$$

Note that in contrast to the first cycle, where t = 48 h, the value of t during subsequent cycles is a variable that equals the time lapsed since the previous cycle. Furthermore, the value of t for the first cycle was relatively short (i.e., 48 h), which resulted in a <2% difference in the FACTOR values for males and females. Because of this small difference, it was not necessary to adjust for the gender-related differences in the calculation of the first cycle doses (i.e., FACTOR1 was set at 125). On the other hand, calculations of doses for subsequent cycles with time intervals of approximately 3 weeks (i.e., $t \geq 504$ h) yielded ~9% higher values for males than for females, and gender-based dose adjustments were made.

PPK Model-Based Dosing Method: Precision and Accuracy Determination, and Refinement using Phase I Results

The precision and accuracy of the PPK Model was determined by retroactive analysis of the data of the first 12 phase I patients. The precision of plasma concentration prediction by PPK Model, evaluated by using Eq. (7), was 22%. A comparison of PPK Model-predicted dose and Ideal Dose [calculated by using Eq. (5) to yield a plasma concentration of 15 μM at 48 h) indicated a 13% overestimation in the model prediction. Equation (15) was therefore further modified by multiplying FACTOR1 with 0.88 (i.e., 1 divided by 1.13), to yield Eq. (16). The overestimation is likely a result of a slight overestimation of $V_{\wedge typ}$ and consequently the calculated dose.

$$\begin{aligned}\text{Subsequent cycle dose} = 0.88 \times \text{FACTOR1} \times BSA^2 \\ \times \left(1 - e^{-k \times t}\right)\end{aligned} \quad (16)$$

This refinement yielded an accuracy of 102 (range, 51–151; median, 100; 23% standard deviation) for individual treatment cycles in individual patients, and 100 (range, 74–121; median, 97; 13% standard deviation) for all treatments in all patients. Figure 3 shows the correlation between Refined PPK Model-predicted dose and Ideal Dose.

We next performed prospective analysis by using Eqs. (14) and (16) to calculate the suramin doses during the first and subsequent cycles, respectively, for three additional phase I patients. To maintain the peak suramin concentration below 50 μM, the suramin dose was administered in two parts with two-thirds of the total dose administered prior to chemotherapy, followed by the remaining one-third of the dose given 24 h after the first dose. The plasma concentrations in all treatments in these three additional phase I patients were within the target range of 10–50 μM over the 48-h duration. The difference between the observed and target plasma concentrations of 15 μM at 48 h were <17%. Based on the above results, the Refined PPK Model-based

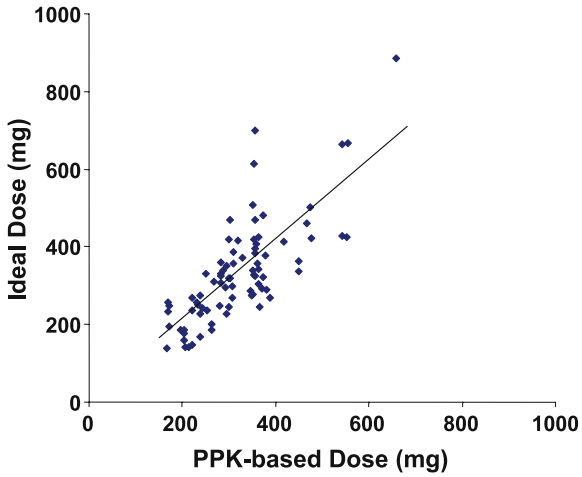

Fig. 3. Comparison of doses calculated by the PPK-based dosing method to Ideal Dose in individual patients. The first 12 patients in the phase I trial received suramin doses determined by real-time pharmacokinetics. For these patients, the Ideal Dose (mg m^{-2}) needed to obtain a plasma concentration of 15 μM at 48 h was calculated for each cycle as discussed in Materials and Methods. Diamonds represent data points and the line represents the linear regression line ($y = 1.04x$, $r^2 = 0.59$, $p < 0.0001$).

dosing equations [Eqs. (14) and (16)] were adopted and their performances were further evaluated in the subsequent phase II trial.

Validation of Refined PPK Model-Based Dosing Method in Phase II Patients

Forty-seven patients (receiving a total of 199 treatments) provided sufficiently detailed pharmacokinetic data for model validation. The suramin doses ranged from 135 to 673 mg. The target concentration range was successfully reached in >94% of administrations; suramin concentrations were below 50 μM in 194 of 199 cycles (97%) at the end of paclitaxel infusion (i.e., 4.5 h) and were at or above 10 μM at 48 h in 192 of 199 cycles (96%).

As the gender difference in suramin clearance observed in the phase I study was based on only five female patients, we extended the evaluation of the gender effect by comparing the suramin concentrations in male ($n = 28$) and female ($n = 19$) phase II patients. Note that the phase II female patients received on average 9% lower BSA-normalized doses. The results indicate no significant gender-related difference in suramin clearance (0.023 ± 0.006 L h^{-1} m^{-2} in females and 0.024 ± 0.005 L h^{-1} m^{-2} in males, $p > 0.37$).

DISCUSSION

Dose-Dependent Pharmacokinetics of Suramin

The current study showed that the dose of suramin used as a chemosensitizer is approximately 10% of MTD (38). A comparison of the pharmacokinetics of chemosensitizer suramin to the literature data on MTD suramin (38) shows a 2.5-fold higher clearance (Table I). This confirms the nonlinear suramin disposition suggested by a preliminary report on six subjects where the clearance of a 200-mg test doses was at least 2-fold lower than the clearance during MTD treatment with initial weekly administration of 2,000–2,800 mg m^{-2} [bar graph in (39)].

The processes for suramin clearance are not well understood. A study in patients with acquired immunodeficiency syndrome showed that suramin is essentially unmetabolized (40). The suggestion that renal clearance may play an important role was based on the finding that renal clearance accounted for total clearance in a single patient and the reduced total clearance in patients who received furosemide, a known inhibitor of tubular secretion (41). The present study provided an opportunity to test this hypothesized elimination; the results showed that renal clearance accounted for less than 10% of total clearance, which is in line with the value of ~20% we estimated from the published data on MTD suramin (42). The minor role of renal clearance for chemosensitizer suramin is also consistent with the exclusion of creatinine clearance as an important covariate of the PPK Model.

Several findings suggest dose-dependent tissue distribution of suramin. First, the plasma pharmacokinetics of MTD suramin was better described by a three-compartment open linear model than by a two-compartment model; the latter underestimated the plasma concentrations during the wash-

Table IV. PPK-Based Nomogram of Suramin

Suramin dose (mg) = FACTOR × BSA^2	
	FACTOR (mg/m^{-4})
Cycle 1	125
Subsequent cycles: Values of FACTOR depends on the elapsed time (days)	
Days since the administration of the first dose during previous cycle	FACTOR (mg/m^{-4})
21	80
22	82
23	84
24	86
25	87
26	88
27	90
28	91
29	92
30	93
31	94
32	95
33	96
34	97
35	98
36	98
37	99
38	100
39	100
41	102
42	102
44	103
47	104
49	105
52	106
55	106

out phase of a 12-week treatment (14,38). The existence of a slowly accumulating third compartment for MTD suramin is further supported by the slow tissue accumulation kinetics in rats receiving similar doses (43). In contrast, chemosensitizer suramin was well described by a two-compartment model. Second, chemosensitizer suramin showed a 40% smaller steady-state distribution volume. Third, progressive increases in the terminal half-life, which would be expected for significant drug accumulation in a deep, slowly equilibrating third compartment over time, was not observed during cycle 2 to cycle 10 (over 30 weeks). These findings suggest a deep compartment that is apparent only at MTD. Further studies to investigate the mechanisms of this unusual dose-dependent drug distribution and whether it contributes to the loss of the chemosensitization effect are warranted.

PPK Model-Based Dosing Nomogram

The present study used a one-compartment PPK Model (as opposed to using a two-compartment model). This approach eliminates the need of multiexponential equations and enables the derivation of an easy-to-use equation for clinical practice. The good predictive power of this equation was demonstrated in 50 patients (3 for phase I and 47 for phase II). The gender difference (14% lower clearance for 5 female patients) observed during the phase I trial led to the first dosing equations with gender-specific dose calculations. But because this difference was not observed in subsequent phase II studies in a larger group of female patients ($n = 19$), we recommend using a single dose calculation for both genders. To further facilitate clinical application, we constructed a nomogram that reduces the dosage calculation to a multiplication of the squared value of BSA with a tabulated factor to accommodate variations in treatment intervals (Table IV).

This study further showed that maintenance of patient plasma concentrations in the range of 10–50 μM for 48 h cannot be accomplished by a single intravenous short infusion starting at the beginning of the 48-h period. High peak concentrations can be avoided by using a number of approaches. In the current study, a split-dose schedule was successfully used to maintain concentrations within the desired range. An alternative approach, currently used in other phase II trials, is to administer an initial loading suramin dose, during the first treatment cycle, several hours earlier before chemotherapy.

The PPK Model-based dosing method for chemosensitizer suramin differs in several ways from the previously published fixed-dose method for MTD suramin (16,17). First, the suramin dose in earlier studies is targeted to continuously maintain plasma concentration between 100 and 200 μM, and results in a >10-fold higher dose requirement over 3 weeks compared to chemosensitizer dose used in the present study. Second, to maintain high and cytotoxic concentrations, MTD suramin regimen includes a loading dose followed by tapered follow-up doses at intervals increasing from 1 to 10 days and, in later studies, to >40 days. These types of fixed-dose schedules are not applicable for chemosensitizer suramin, where the emphasis is not on maintaining near-constant maximally tolerated concentrations, but rather on keeping plasma concentrations within the effective range (10–50 μM) for the duration when the chemotherapeutic agents are present at therapeutically significant values (e.g., 48 h for paclitaxel and carboplatin).

CONCLUSION

The present study provided a PPK Model-based nomogram to identify the chemosensitizer suramin dose in patients, to deliver the target plasma concentrations that produced chemosensitization in human xenograft models (1–3), over 48 h. This approach further eliminates the requirement of blood sampling for pharmacokinetic evaluation to guide dose adjustments. Our results further indicate nonlinear disposition of suramin in patients, and no significant pharmacokinetic interaction among suramin, paclitaxel, and carboplatin.

ACKNOWLEDGMENTS

This study was supported in part by R37CA49816, R01CA78577, R21CA91547 and U01CA76576 from the National Cancer Institute, NIH, DHHS. Patients were treated at a General Clinical Research Center (GCRC), which is supported by M01-RR00034 from the National Institutes of Health, DHHS. Analysis of carboplatin concentrations was performed by the Pharmacoanalytical Core Laboratory of The Ohio State University Comprehensive Cancer Center. Tong Shen's invaluable help in the renal clearance studies and management of clinical trial data is gratefully acknowledged.

REFERENCES

1. S. Song, M. G. Wientjes, Y. Gan, and J. L. Au. Fibroblast growth factors: an epigenetic mechanism of broad spectrum resistance to anticancer drugs. *Proc. Natl. Acad. Sci. USA* **97**:8658–8663 (2000).
2. S. Song, M. G. Wientjes, C. Walsh, and J. L. Au. Nontoxic doses of suramin enhance activity of paclitaxel against lung metastases. *Cancer Res.* **61**:6145–6150 (2001).
3. Y. Zhang, S. Song, F. Yang, J. L. Au, and M. G. Wientjes. Nontoxic doses of suramin enhance activity of doxorubicin in prostate tumors. *J. Pharmacol. Exp. Ther.* **299**:426–433 (2001).
4. C. E. Hensey, D. Boscoboinik, and A. Azzi. Suramin, an anticancer drug, inhibits protein kinase C and induces differentiation in neuroblastoma cell clone NB2A. *FEBS Lett.* **258**:156–158 (1989).
5. T. P. Wade, A. Kasid, C. A. Stein, R. V. LaRocca, E. R. Sargent, L. G. Gomella, C. E. Myers, and W. M. Linehan. Suramin interference with transforming growth factor-beta inhibition of human renal cell carcinoma in culture. *J. Surg. Res.* **53**:195–198 (1992).
6. E. De Clercq. Suramin: a potent inhibitor of the reverse transcriptase of RNA tumor viruses. *Cancer Lett.* **8**:9–22 (1979).
7. H. Nakane, J. Balzarini, E. De Clercq, and K. Ono. Differential inhibition of various deoxyribonucleic acid polymerases by Evans blue and aurintricarboxylic acid. *Eur. J. Biochem.* **177**: 91–96 (1988).
8. S. T. Palayoor, E. A. Bump, B. A. Teicher, and C. N. Coleman. Apoptosis and clonogenic cell death in PC3 human prostate cancer cells after treatment with gamma radiation and suramin. *Radiat. Res.* **148**:105–114 (1997).
9. L. Qiao, J. G. Pizzolo, and M. R. Melamed. Effects of suramin on expression of proliferation associated nuclear antigens in DU-145 carcinoma cells. *Biochem. Biophys. Res. Commun.* **201**: 581–588 (1994).

10. W. K. Evans, C. C. Earle, D. J. Stewart, S. Dahrouge, E. Tomiak, G. Goss, D. Logan, R. Goel, S. Z. Gertler, and H. Dulude. Phase II study of a one hour paclitaxel infusion in combination with carboplatin for advanced non-small cell lung cancer. *Lung Cancer* **18**:83–94 (1997).
11. J. H. Kim, E. R. Sherwood, D. M. Sutkowski, C. Lee, and J. M. Kozlowski. Inhibition of prostatic tumor cell proliferation by suramin: alterations in TGF alpha-mediated autocrine growth regulation and cell cycle distribution. *J. Urol.* **146**:171–176 (1991).
12. F. Hawking. Suramin: with special reference to onchocerciasis. *Adv. Pharmacol. Chemother.* **15**:289–322 (1978).
13. S. M. Tu, L. C. Pagliaro, M. E. Banks, R. J. Amato, R. E. Millikan, N. A. Bugazia, T. Madden, R. A. Newman, and C. J. Logothetis. Phase I study of suramin combined with doxorubicin in the treatment of androgen-independent prostate cancer. *Clin. Cancer Res.* **4**:1193–1201 (1998).
14. M. R. Cooper, R. Lieberman, R. V. La Rocca, P. R. Gernt, M. S. Weinberger, D. J. Headlee, D. R. Kohler, B. R. Goldspiel, C. C. Peck, and C. E. Myers. Adaptive control with feedback strategies for suramin dosing. *Clin. Pharmacol. Ther.* **52**:11–23 (1992).
15. M. A. Eisenberger, V. J. Sinibaldi, L. M. Reyno, R. Sridhara, D. I. Jodrell, E. G. Zuhowski, K. H. Tkaczuk, M. H. Lowitt, R. K. Hemady, and S. C. Jacobs. Phase I and clinical evaluation of a pharmacologically guided regimen of suramin in patients with hormone-refractory prostate cancer. *J. Clin. Oncol.* **13**: 2174–2186 (1995).
16. L. M. Reyno, M. J. Egorin, M. A. Eisenberger, V. J. Sinibaldi, E. G. Zuhowski, and R. Sridhara. Development and validation of a pharmacokinetically based fixed dosing scheme for suramin. *J. Clin. Oncol.* **14**:2187–2195 (1995).
17. K. Kobayashi, E. E. Vokes, N. J. Vogelzang, L. Janisch, B. Soliven, and M. J. Ratain. Phase I study of suramin administered by intermittent infusion without adaptive control to cancer patients: update of two expanded dose levels near the maximally tolerated dose. *J. Clin. Oncol.* **14**:2622–2623 (1996).
18. S. Song, B. Yu, Y. Wei, M. G. Wientjes, and J. L. Au. Low-dose suramin enhanced paclitaxel activity in chemotherapy-naive and paclitaxel-pretreated human breast xenograft tumors. *Clin. Cancer Res.* **10**:6058–6065 (2004).
19. Y. Xin, G. Lyness, D. Chen, S. Song, M. G. Wientjes, and J. L. Au. Low dose suramin as a chemosensitizer of bladder cancer to mitomycin C. *J. Urol.* **174**:322–327 (2005).
20. B. Yu, S.-H. Song, M. G. Wientjes, and J. L. Au. Suramin enhances activity of CPT-11 in human colorectal xenograft tumors. *Proc. Am. Assoc. Cancer Res.* **44**:174 (2003).
21. A. Falcone, E. Pfanner, I. Brunetti, G. Allegrini, M. Lencioni, C. Galli, G. Masi, R. Danesi, A. Antonuzzo, M. Del Tacca, and P. F. Conte. Suramin in combination with 5-fluorouracil (5-FU) and leucovorin (LV) in metastatic colorectal cancer patients resistant to 5-FU+ LV-based chemotherapy. *Tumori* **84**:666–668 (1998).
22. A. Falcone, A. Antonuzzo, R. Danesi, G. Allegrini, L. Monica, E. Pfanner, G. Masi, S. Ricci, M. Del Tacca, and P. F. Conte. Suramin in combination with weekly epirubicin for patients with advanced hormone-refractory prostate carcinoma. *Cancer* **86**: 470–476 (1999).
23. B. L. Rapoport, G. Falkson, J. I. Raats, M. de Wet, B. P. Lotz, and H. C. Potgieter. Suramin in combination with mitomycin C in hormone-resistant prostate cancer. A phase II clinical study. *Ann. Oncol.* **4**:567–573 (1993).
24. M. A. Villalona-Calero, M. G. Wientjes, G. A. Otterson, S. Kanter, D. Young, A. J. Murgo, B. Fischer, C. DeHoff, D. Chen, T. K. Yeh, S. Song, M. Grever, and J. L. Au. Phase I study of low-dose suramin as a chemosensitizer in patients with advanced non-small cell lung cancer. *Clin. Cancer Res.* **9**:3303–3311 (2003).
25. M. Kassack and P. Nickel. Rapid, highly sensitive gradient narrow-bore high-performance liquid chromatographic determination of suramin and its analogues. *J. Chromatogr. B Biomed. Appl.* **686**:275–284 (1996).
26. D. M. Ornitz and N. Itoh. Fibroblast growth factors. *Genome Biol.* **2**:3005 (2001).
27. P. Tothill, L. Matheson, J. Smyth, and K. McKay. Inductively coupled plasma mass spectrometry for the determination of platinum in animal tissues and a comparison with atomic absorption spectrometry. *J. Anal. At. Spectrom.* **5**:619–622 (1990).
28. L. B. Sheiner, B. Rosenberg, and V. V. Marathe. Estimation of population characteristics of pharmacokinetic parameters from routine clinical data. *J. Pharmacokinet. Biopharm.* **5**:445–479 (1977).
29. J. W. Mandema, D. Verotta, and L. B. Sheiner. Building population pharmacokinetic–pharmacodynamic models. I. Models for covariate effects. *J. Pharmacokinet. Biopharm.* **20**:511–528 (1992).
30. W. D. Gabrielsson J. *Pharmacokinetic/Pharmacodynamic Data Analysis: Concepts and Applications*. Swedish Pharmaceutical Press, 1994.
31. A. H. Calvert, D. R. Newell, L. A. Gumbrell, S. O'Reilly, M. Burnell, F. E. Boxall, Z. H. Siddik, I. R. Judson, M. E. Gore, and E. Wiltshaw. Carboplatin dosage: prospective evaluation of a simple formula based on renal function. *J. Clin. Oncol.* **7**: 1748–1756 (1989).
32. M. T. Huizing, A. C. Keung, H. Rosing, V. van der Kuij, W. W. Bokkel Huinink, I. M. Mandjes, A. C. Dubbelman, H. M. Pinedo, and J. H. Beijnen. Pharmacokinetics of paclitaxel and metabolites in a randomized comparative study in platinum-pretreated ovarian cancer patients. *J. Clin. Oncol.* **11**:2127–2135 (1993).
33. M. T. Huizing, L. J. Warmerdamvan, H. Rosing, M. C. Schaefers, A. Lai, T. J. Helmerhorst, C. H. Veenhof, M. J. Birkhofer, S. Rodenhuis, J. H. Beijnen, and W. W. Bokkel Huinink. Phase I and pharmacologic study of the combination paclitaxel and carboplatin as first-line chemotherapy in stage III and IV ovarian cancer. *J. Clin. Oncol.* **15**:1953–1964 (1997).
34. N. Siddiqui, A. V. Boddy, H. D. Thomas, N. P. Bailey, L. Robson, M. J. Lind, and A. H. Calvert. A clinical and pharmacokinetic study of the combination of carboplatin and paclitaxel for epithelial ovarian cancer. *Br. J. Cancer* **75**: 287–294 (1997).
35. P. R. Hoban, M. I. Walton, C. N. Robson, J. Godden, I. J. Stratford, P. Workman, A. L. Harris, and I. D. Hickson. Decreased NADPH: cytochrome P-450 reductase activity and impaired drug activation in a mammalian cell line resistant to mitomycin C under aerobic but not hypoxic conditions. *Cancer Res.* **50**:4692–4697 (1990).
36. H. F. Bligh, A. Bartoszek, C. N. Robson, I. D. Hickson, C. B. Kasper, J. D. Beggs, and C. R. Wolf. Activation of mitomycin C by NADPH:cytochrome P-450 reductase. *Cancer Res.* **50**: 7789–7792 (1990).
37. R. D. Traver, D. Siegel, H. D. Beall, R. M. Phillips, N. W. Gibson, W. A. Franklin, and D. Ross. Characterization of a polymorphism in NAD(P)H: quinone oxidoreductase (DT-diaphorase). *Br. J. Cancer* **75**:69–75 (1997).
38. D. I. Jodrell, L. M. Reyno, R. Sridhara, M. A. Eisenberger, K. H. Tkaczuk, E. G. Zuhowski, V. J. Sinibaldi, M. J. Novak, and M. J. Egorin. Suramin: development of a population pharmacokinetic model and its use with intermittent short infusions to control plasma drug concentration in patients with prostate cancer. *J. Clin. Oncol.* **12**:166–175 (1994).
39. P. R. Hutson, K. D. Tutsch, and G. Wilding. Pharmacokinetic analysis and adaptive control of suramin. In Z. D'Argenio (ed.), *Advanced Methods of Pharmacokinetic and Pharmacodynamic Systems Analysis, Volume 2*, Plenum Press, New York, 1995, pp. 177–187.
40. J. M. Collins, R. W. Klecker Jr., R. Yarchoan, H. C. Lane, A. S. Fauci, R. R. Redfield, S. Broder, and C. E. Myers. Clinical pharmacokinetics of suramin in patients with HTLV-III/LAV infection. *J. Clin. Pharmacol.* **26**:22–26 (1986).
41. S. C. Piscitelli, A. Forrest, R. M. Lush, N. Ryan, L. R. Whitfield, and D. Figg. Pharmacometric analysis of the effect of furosemide on suramin pharmacokinetics. *Pharmacotherapy* **17**: 431–437 (1997).
42. P. R. Hutson, K. D. Tutsch, R. Rago, R. Arzoomanian, D. Alberti, M. Pomplun, D. Church, R. Marnocha, A. L. Cheng, N. Kehrli, and G. Wilding. Renal clearance, tissue distribution, and CA-125 responses in a phase I trial of suramin. *Clin. Cancer Res.* **4**:1429–1436 (1998).
43. W. P. McNally, P. D. DeHart, C. Lathia, and L. R. Whitfield. Distribution of [^{14}C]suramin in tissues of male rats following a single intravenous dose. *Life Sci.* **67**:1847–1857 (2000).

Suramin: Clinical Uses and Structure-Activity Relationships

Ross P. McGeary[1,2,*,#], Andrew J. Bennett[1], Quoc B. Tran[1], Kelly L. Cosgrove[1] and Benjamin P. Ross[1,2]

[1]*School of Molecular & Microbial Sciences, The University of Queensland, Brisbane, Qld 4072, Australia;* [2]*School of Pharmacy, The University of Queensland, Brisbane, Qld 4072, Australia*

Abstract: Suramin is a polysulfonated polyaromatic symmetrical urea. It is currently used to treat African river blindness and African sleeping sickness. Suramin has also been extensively trialed recently to treat a number of other diseases, including many cancers. Here, we examine its modes of action and discuss its structure-activity relationships.

Key Words: Suramin, trypanosomiasis, onchocerciasis, FGF.

[#]**Author Profile:** Ross McGeary is a Senior Lecturer at The University of Queensland, Brisbane, Australia. He is a medical chemist with joint appointments at the Chemistry and Pharmacy Schools. Dr. McGeary's research focuses on the development of new synthetic methodologies, and the design and synthesis of enzyme inhibitors and other biologically important molecules.

INTRODUCTION

Suramin (**1**) (also known as Germanin and Bayer-205) is a symmetrical polysulfonated polyaromatic urea. The hexasodium salt ($C_{51}H_{34}N_6Na_6O_{23}S_6$, molecular weight 1429.2) is a highly water-soluble, hygroscopic pale pink powder. Its discovery in 1916 developed out of earlier observations that trypan red (**2**), and other dyes such as trypan blue (**3**) and afridol violet (**4**) [1], cured trypanosomiasis in mice [2]. The composition of suramin was kept secret by Bayer, until Fourneau and coworkers elucidated the chemical structure and published it in 1924 [3].

Suramin has been used as an early stage treatment of trypanosome-caused onchocerciasis (African river blindness) and African trypanosomiasis (African sleeping sickness) since 1920 [4]. It is currently under clinical evaluation for its potential to regress a number of cancer cell lines, including non-small cell lung cancer, advanced breast cancer, hormone refractory prostate cancer, metastatic renal cell cancer, colorectal cancer and high-grade gliomas [5-7]. Suramin's *in vitro* activity against HIV led to it being trialed in AIDS patients [8, 9]. Suramin binds to a large number of peptidic growth factors [10]. The extremely diverse range of biologically important molecules and cell lines that suramin has been reported to inhibit is, perhaps, due to its non-specific mode of binding [11]. As a result, however, its clinical applications are significantly limited because non-specific binding leads to side effects and high toxicity. Additionally, its great metabolic stability, long plasma half-life (41-78 days) and a relatively low therapeutic index are significant hurdles to overcome if members of this family of compound are to be more broadly developed as drugs [12-14].

*Address correspondence to this author at the School of Molecular & Microbial Sciences, The University of Queensland, Brisbane, Qld 4072, Australia; Tel: +61-7-3365-3955; Fax: +61-7-3346-3249;
E-mail: r.mcgeary@uq.edu.au

DISEASES TREATABLE WITH SURAMIN

Malignant Neoplasms

In 1989 suramin was trialed on 15 patients against a number of metastatic cancers, with some encouraging results [15]. Its efficacy as a treatment for metastatic adrenocortical carcinoma was examined, with the authors concluding that suramin possessed antineoplastic efficacy in the treatment of this disease, but that its toxic side effects and narrow therapeutic window required strict monitoring of serum suramin levels in patients and made it unsuitable as a first-line treatment for this carcinoma [16]. Although suramin caused significant dose-dependent growth inhibition of human breast cancer cells *in vitro* [17-19], pilot studies which examined suramin's efficacy in treating breast cancer revealed no tumor responses [20, 21]. More recent work, however, has shown a marked enhancement of the anti-cancer effects of paclitaxel when co-administered with low-dose suramin to human MCF7 breast xenograft tumors in mice, leading to the initiation of phase I/II trials of paclitaxel and low-dose suramin combination in advanced metastatic breast cancer patients [22].

Suramin has shown promise as a treatment option for hormone-refractory prostate cancer [23-30]. In 2000, a randomized phase III trial comparing suramin plus hydrocortisone to placebo plus hydrocortisone showed that moderate palliative benefit was achieved with suramin, and that time to disease progression was longer in patients who received suramin [5]. However, a later study by Rosen and coworkers was unable to confirm the previously reported high rate of activity and durability of remission achieved using suramin [31]. Kaur and coworkers [14], and Autorino and coworkers [32] have critically reviewed the phase II and phase III clinical trial outcomes of suramin in the treatment of prostate cancer. A 1992 study of the effectiveness of suramin in treating advanced platinum-resistant ovarian cancer showed that some patients experienced disease stabilization and clinical

1389-5575/08 $55.00+.00

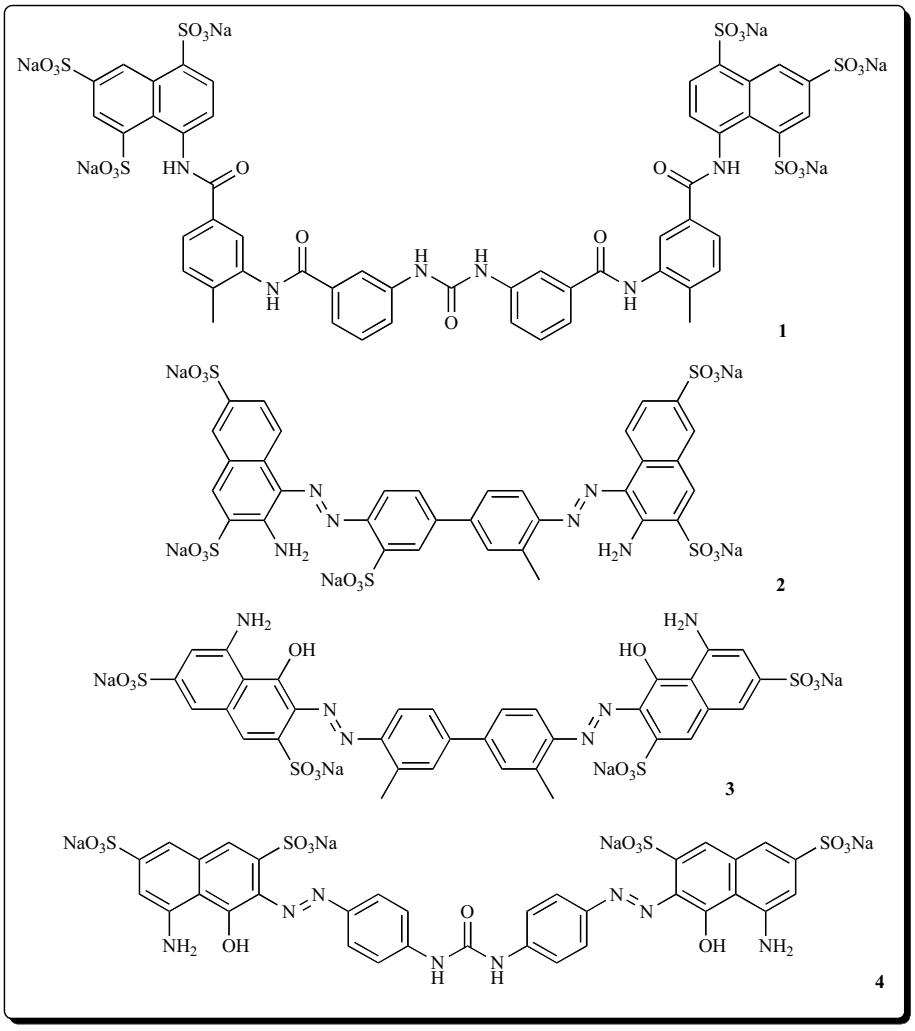

improvements [33]. Suramin caused significant dose-dependent growth inhibition of rat pancreatic tumors *in vivo* [17].

The effect of suramin on the human esophageal squamous cell carcinoma cell line KEsC-II was studied. Cell proliferation was stimulated at low concentrations of suramin, and inhibited at high concentrations, with the effects suggested to arise *via* phosphorylation of epidermal growth factor (EGF) receptors [34]. Suramin inhibits the growth of human rhabdomyosarcoma [35]. The mechanism of action in this case was determined to be the interference of the binding of insulin-like growth factor II (IGF-II) to the type I IGF receptor, thereby interrupting the IGF-II autocrine growth in these cells [35]. Similarly, suramin inhibits the growth of non-small cell lung cancer cells that express EGF receptors, and suramin was shown to inhibit, in a concentration-dependent manner, the binding of EGF to its receptors in these cells [36]. A 2000 study evaluated the activity of suramin and a number of its analogues against a panel of human tumor cell lines and in primary cultures of tumor cells from patients, in an attempt to identify the suramin pharmacophore so as to develop suramin analogs with improved therapeutic ratios. These studies suggested that the pharmacophore for cytotoxicity was different for tumor cells from patients and for cell lines. It was also shown that suramin and its analogs were insensitive to a number of drug resistance mechanisms [37].

Onchocerciasis

Onchocerciasis (African river blindness) is caused by *Onchocerca volvulus*, a parasitic worm that is transmitted by blackflies of *Simulium* species, and is very long-lived in the human body. It is endemic in many countries in Africa and Latin America. The disease results in a number of morbidities, including blindness, skin rashes, lesions, intense itching and skin depigmentation [38]. Suramin has been used since the 1920s as an anthelmintic to treat onchocerciasis [4, 39]; however, it has now been largely superseded by ivermectin (**5**) [40]. Nevertheless, suramin remains the only drug in clinical use for the treatment of onchocerciasis that is effective against adult worms.

Trypanosomiasis

Trypanosomiasis (African sleeping sickness) is a disease of humans and cattle endemic in regions of sub-Saharan Africa. It is caused by a trypanosome (a parasitic protozoon of *Trypanosoma* species) and is transmitted by the tsetse fly. Left untreated, it is invariably fatal [41, 42]; the World Health Organization estimates that there are 40,000 mortalities per year [41]. Suramin and pentamidine (**6**) have been used as an early stage treatment of trypanosomiasis (before the parasites invade the central nervous system (CNS)) since 1920 [4, 43]. Eflornithine (**7**) and the arsenic-containing

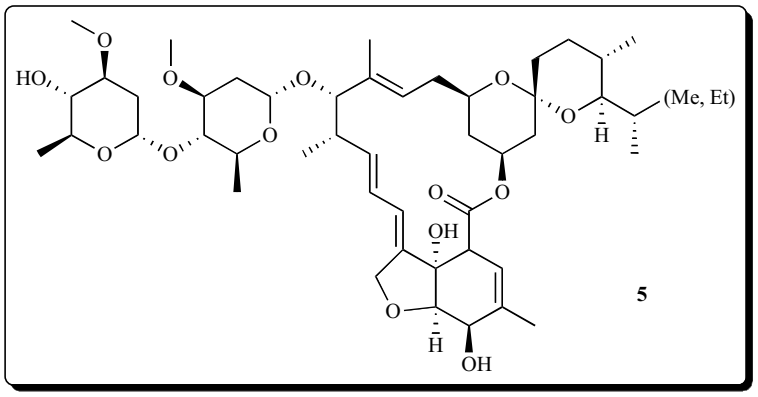

drug, melarsoprol (**8**), are used for later stages of the disease when the parasites are established in the CNS.

Suramin accumulates only slowly in trypanosomes, and it has been suggested that uptake of this drug occurs *via* endocytosis bound to low-density lipoprotein [44]. Its mode of action against trypanosomes is unknown.

Toxicity

The toxic effects of suramin are well documented [14]. Clinical trials of suramin in cancer patients have uncovered frequent toxic side effects, including proteinuria, reversible liver toxicity, cornea damage such as vortex keratopathy, adrenal insufficiency, coagulopathy, and reversible acute demyelinating polyneuropathy [15]. A trial of suramin's efficacy in treating metastatic adrenocortical carcinoma, in which the drug was administered for periods of up to 15 months, reported serious side effects in patients, including coagulopathy, thrombocytopenia, polyneuropathy and allergic skin reactions. The deaths of two patients in that trial were suggested by the authors to be possibly related to suramin therapy [16]. In a clinical trial of hormone-refractory prostate cancer, the most commonly encountered side effect was fatigue but, again, a fatality due to idiosyncratic myelosuppression (grade V) was observed in one patient [31]. Another trial of suramin's efficacy against metastatic prostate cancer reported frequent ocular symptoms such as corneal deposits and lacrymation [45]. Skin reactions to suramin are common, most usually pruritus or urticaria, but fatal toxic epidermal necrolysis has been reported [46, 47]. The most common dose-limiting toxic effects are malaise and lethargy [48], and neurotoxicity [49]. Suramin has been shown to prevent and terminate pregnancy in mice [50].

Suramin is notable for its very high (99.7%) serum protein binding, its very long half-life (41-78 days [6]), and high metabolic stability [51]. Suramin's volume of distribution is 31-46 litres and 80% of the drug is excreted renally [52].

MODES OF ACTION

Interaction of Suramin with Proteins

The anti-tumor activity of suramin [34, 53] has been proposed to stem from either its binding to essential growth factors (antagonizing the ability of these factors to stimulate the growth of tumor cells *in vitro* [15]), inhibition of protein tyrosine phosphatases, inhibition of angiogenesis, or a combination of these three processes [35, 36, 53-57]. In fact, two of these mechanisms are probably interconnected, as several reports have noted that the known angiostatic activity of suramin is at least in part related to fibroblast growth factor (FGF) binding and inhibition [58-64]. Table **1** summarizes the growth factors and enzymes that have been shown to be inhibited by, or bind to, suramin.

FGF Binding

Suramin's ability to block the binding of fibroblast growth factor (FGF) to its receptor (FGFR) is of particular interest, because this event is fundamental in the process of angiogenesis. The FGFs comprise a family of proteins which are required for a variety of biological processes including cell growth and movement, differentiation, and protection from cell death [101-103]. They function by interacting with their cognate receptor (FGFR), which is a transmembrane protein possessing an extracellular FGF/heparin ligand binding region and an intracellular tyrosine kinase domain [104]. Activation of the receptor and subsequent signal transduction occurs when two FGF:FGFR complexes dimerize [105].

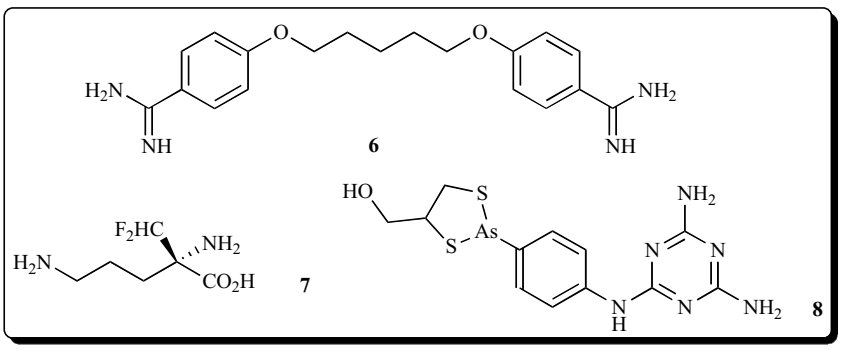

Table 1. Enzymes and Growth Factors Inhibited by Suramin

Enzyme/Growth Factor	References
DNA polymerase	[65]
Reverse transcriptase	[9, 66-68]
Topoisomerase-I and Topoisomerase-II	[69-71]
ATPase	[72, 73]
Heparanase	[74]
Protein tyrosine phosphatases (PTP)	[55, 75]
Protein kinase C	[76, 77]
Phosphoglycerate kinase	[78]
Diacylglycerol kinase	[79]
NAD^+-dependent histone deacetylases (surtuins)	[80]
Phosphatidylinositol kinase	[79]
G-Protein coupled receptor kinases	[81]
Ionotropic adenine and uracil 5′-nucleotide (P2X/P2Y) receptors	[82-84]
Bothrops asper venom phospholipase A2 (PLA2)	[85]
Fibroblast growth factors (FGFs)	[63, 86, 87]
Platelet-derived growth factor (PDGF)	[88, 86]
Epidermal growth factor (EGF)	[15, 36, 86]
Transforming growth factor-beta (TGF-β)	[15, 86]
Insulin-like growth factor II (IGF-II)	[35]
Androgen-induced growth factor (AIGF)	[89, 90]
Nerve growth factor (NGF)	[91]
Heparin-binding growth factor type-2 (HBGF-2)	[86]
Follicle-stimulating hormone (FSH)	[92]
Interleukin-2 (IL-2)	[93]
Interleukin-6 (IL-6)	[94]
Tumor necrosis factor-alpha (TNFα)	[95, 96]
Vaccinia virus complement control protein (VCP)	[97]
Plasmodium falciparum merozoite surface protein-1	[98]
Triosephosphate isomerise (TIM) reactivation	[99, 100]

Heparin is required for dimerization to occur because it is able to bind to both FGF and FGFR, thereby strengthening the ternary complex formed on the cell surface [103]. Two crystal structures of the FGF:FGFR:heparin ternary complex exist, but they differ significantly, and there is uncertainty regarding which of these structures (if either) best represent the biologically relevant structure of the complex [103].

It is clear that the inhibition of FGF activity by suramin results from the formation of a complex with FGF, not from a direct interaction with FGFR [106]. It is also highly likely that suramin binds at or near to the heparin binding site, since heparin physically disrupts suramin-FGF complexes and counteract the angiostatic effects of suramin [59, 61, 63, 107-110]. Marchetti's group has also reported that suramin inhibits heparanase, a glucuronidase whose activity correlates with the metastatic propensity of tumor cells [74].

A solution structure of FGF-1 complexed with l,3,6-naphthalenetrisulfonate (NTS) (**9**) showed that NTS weakly and heterogeneously bound to the heparin binding site of this growth factor [111]. NTS has been shown to have angiostatic activity and, according to Lozano *et al*. [111], it can be considered a minimal model for suramin action. In another study by the same group, the crystal structure of FGF-1 in complex with 5-amino-2-naphthalenesulfonate (ANS) (**10**) was solved. The solved structure revealed a 1:1 stoichiometric ratio of FGF-1 to ANS, with ANS bound to the positively-charged heparin binding site of FGF-1 [112].

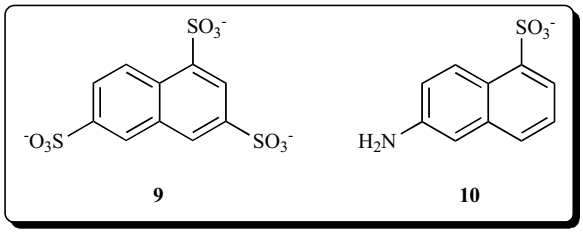

9 **10**

Two recent studies have published evidence not in concord with previous models on suramin's interactions with FGF. Ganesh *et al*. reported the crystal structure and intermolecular interactions of a 1:1 complex of suramin with the heparin-binding site in vaccinia virus complement control protein (VCP), which is geometrically similar to many heparin-binding proteins, including FGF [97]. The authors were able to compare this crystal structure with the crystal structure of the heparin-VCP complex, and so determine that suramin interacts with a single heparin-binding site in VCP [97]. This study showed significant differences in the orientations of the naphthalene rings (end groups of suramin) relative to the configuration of binding of NTS and ANS to FGF as described in previous studies [111, 112]. Ganesh and coworkers also noted that superimposition of each of the naphthalene rings in suramin, from the crystal structure [97], on the naphthalene rings in ANS and NTS complexes [111, 112] resulted in suramin either having severe steric clashes with the FGF or no interaction beyond the naphthalene ring. They concluded therefore that the structural information gained from the ANS and NTS complexes was of limited use in elucidating the mode of binding of suramin to FGF.

Using isothermal titration calorimetry, Kathir *et al*. [113] suggested that human FGF-1 (hFGF-1) binds to two molecules of suramin with nanomolar affinity. This ternary complex subsequently oligomerizes to form a stable inactive tetramer which is incapable of binding to the receptor (Fig. (**1**)). The binding of the suramin molecules to hFGF-1 was shown to occur simultaneously at specific sites on the protein, inducing a conformational change and revealing solvent-exposed hydrophobic residues at the surface. Formation of the inactive tetramer then occurs due to the hydrophobic

Fig. (1). Cartoon representing the primary mechanism by which suramin inhibits FGF-1. Reprinted with permission from Kathir, K. M. *et al*., *Biochem*., **2006**, *45*, 899-906. Copyright 2006 American Chemical Society [113].

attraction between the transiently exposed non-polar surfaces. Further NMR experiments revealed that suramin binds to residues of FGF that are involved in binding to heparin, as well as residues involved in binding to the FGFR. These two binding sites are separated by a distance of ~32 Å which suggested that a single molecule of suramin with a length of ~24 Å could not bind simultaneously to both sites [113].

Structure-Activity Relationships of FGF Binding

There have been a number of studies in which suramin analogs were prepared to determine structure-activity relationships (SARs) for suramin-FGF binding. These studies focused on a number of aspects of the structure of suramin, including the length and rigidity of the molecule, the nature of its end groups, its symmetry, the central urea group, and its methyl substituents [12, 37, 58, 62, 106, 112, 114-119]. The results of these SAR studies often differ from those directed at HIV (reverse transcriptase inhibition) [120], trypanosomiasis [121], the P2 receptor [84], or class III histone deacetylases (surtuins) [80].

The major deficiency in most of these studies is that they focused on the potential angiostatic or anti-cancer activities of suramin analogs, which are consequences of complex processes rather than the effect resulting from the direct binding of suramin to FGF or its receptor [58, 62, 106, 115-119]. Therefore, structure-activity relationships derived from these investigations do not necessarily mean that activity against proliferation and differentiation was through the inhibition of FGF by suramin. Furthermore, the SAR study summarised by Fig. (**2**) were obtained from different studies, many employing different cell lines (Table **2**), so biological activity observed for a particular functional group in one particular cell line may not necessarily confer activity in a different biological context.

Length and Symmetry of Suramin

Several SAR studies have noted that a minimum molecular length of suramin analogs was required for activity, so that compounds without at least one aromatic "spacer" positioned symmetrically either side of the central urea group had little or no biological effect compared to suramin itself [12, 58, 62, 106, 114, 117]. The spacing between the anionic binding sites in FGF is ~32 Å and thus these pockets require inhibitors in which the two anionic end-groups are similarly separated.

Molecular symmetry does not appear to be a requirement for inhibitory activity in suramin analogs, since some asymmetric compounds were found to have similar activity to suramin [106]. However, these compounds still satisfied the minimum length requirement for an inhibitor. Most analogs tested have been symmetrical due to ease of synthesis. Interestingly, some studies showed that smaller, asymmetric compounds containing a naphthalenesulfonate moiety had antiproliferative or angiostatic activity against FGF-promoted cell lines [83, 111, 112, 115, 118].

Table 2. Assays Used for Suramin and its Analogs

Type of Assay	Specific Assay	References
Cell proliferation/tumor growth inhibition	Inhibition of cell growth (various cell lines including carcinomas)	[37, 58, 112, 115-118]
	Observation of tumor colon cancer cell differentiation	[119]
	Mouse *in vivo* tumor growth inhibition	[118]
Angiogenesis inhibition	Neovascularization of the chorioallantoic membrane (CAM assay)	[12, 62, 106, 114-116, 118]
	Mouse angiogenesis assay – sponges implanted in backs of mice and evaluated for angiogenesis	[12, 58, 106, 112, 114]
	Microcarrier angiogenesis assay	[117]
FGF binding inhibition	Inhibition of FGF-2-stimulated bovine adrenalcapillary endothelial cell [^{3}H]methyl-thymidine uptake	[58]
	Inhibition of specific ^{125}I-FGF-2 binding to FGFR	[12, 58, 106, 114]

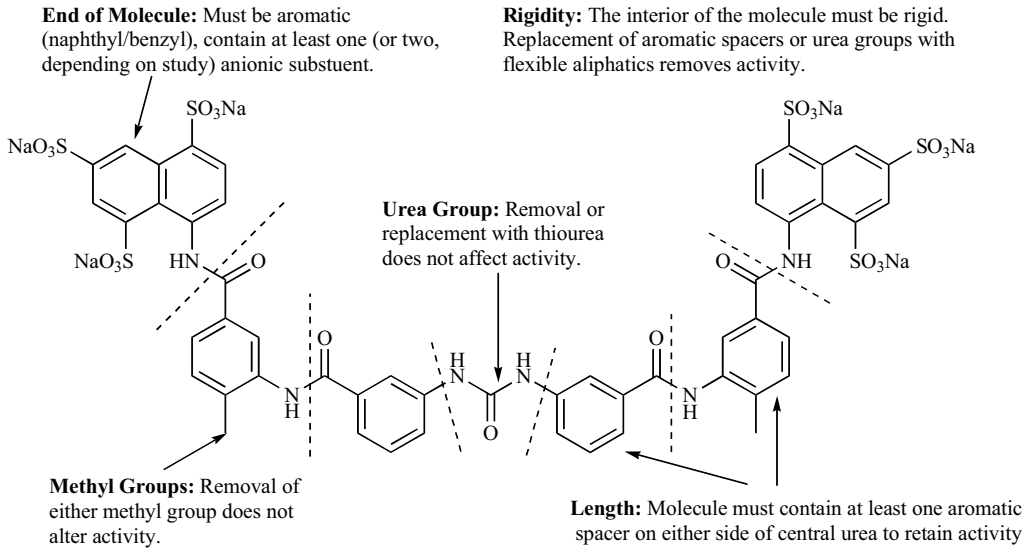

Fig. (2). Summary of the structure-activity relationships of suramin.

Rigidity

Suramin displays a high degree of rigidity due to the conjugated nature of the molecule. Modelling studies of suramin and structurally related molecules belonging to the suradista family (Fig. (**3**)) showed that in solution the compounds preferentially adopt a symmetrical, extended, quasi-planar arc shape with a distance between the two naphthalenesulfonate units of either 16-20 or 24-30 Å [12, 78, 114, 122]. Several reports have shown that the molecular rigidity of suramin is essential for inhibitory activity. Replacement of the central urea group or the aromatic spacers with more flexible aliphatic groups translated into a sharp decrease in activity [12, 62, 117]. Interestingly, Ganesh *et al*. have suggested that suramin experiences much greater conformational flexibility in solution than is generally believed, and they noted that suramin adopts a helical (non-planar) conformation in the crystal structure of the suramin-VCP complex [97].

Nature of the Aromatic Anionic Region

All SAR studies of suramin analogs agree on the necessity for anionic aromatic regions at each end of the compound [12, 37, 58, 62, 114-117]. While sulfonates have been the default choice of anionic group, a few studies at least have suggested that the aromatic portion can contain anionic groups other than sulfonates. Analogs where the sulfonates were replaced with carboxylates (e.g. **11** and **12**) were found to display activity [115], as were analogs, such as **13**, incorporating phosphonate groups [37].

The aromatic end group need not necessarily be a naphthalene derivative because several studies have found that analogs such as **11-13**, or those containing benzene monosulfonic acid groups were also active. For these compounds Gagliardi *et al*. demonstrated a reduced efficacy in the CAM assay (Table **2**, 7-26% inhibition compared to 64% inhibition for suramin) [62]. However, in studies by Firsching *et al*. [116, 117] and Kreimeyer *et al*. [115], analogs containing benzene monosulfonic acids had comparable activities to suramin in the majority of assays. Several studies altered the number of sulfonate groups (suramin contains six, three at each end) with varying results [12, 58, 62, 106, 112, 114, 116, 117]. While several benzene monosulfonic acid derivatives were found to display reasonable activity (see above), many studies argued that analogs required at least four sulfonate groups for good activity, with six required for activity comparable to that of suramin [12, 62, 106, 114, 116]. The majority of reports agreed that the actual positions of the sulfonate groups on the aromatic rings did not significantly affect activity [58, 62, 115-117].

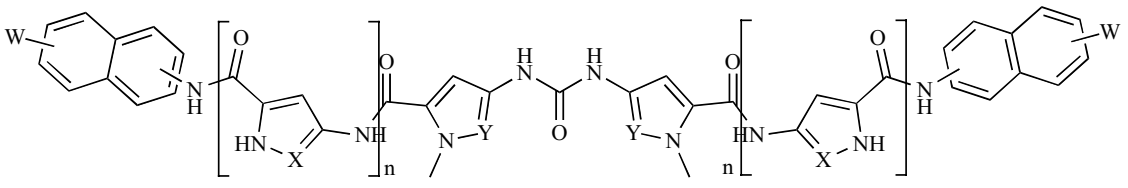

W = SO_3Na; X, Y = CH, N; n = 0-2

Fig. (3). General structure of the suradista family [123].

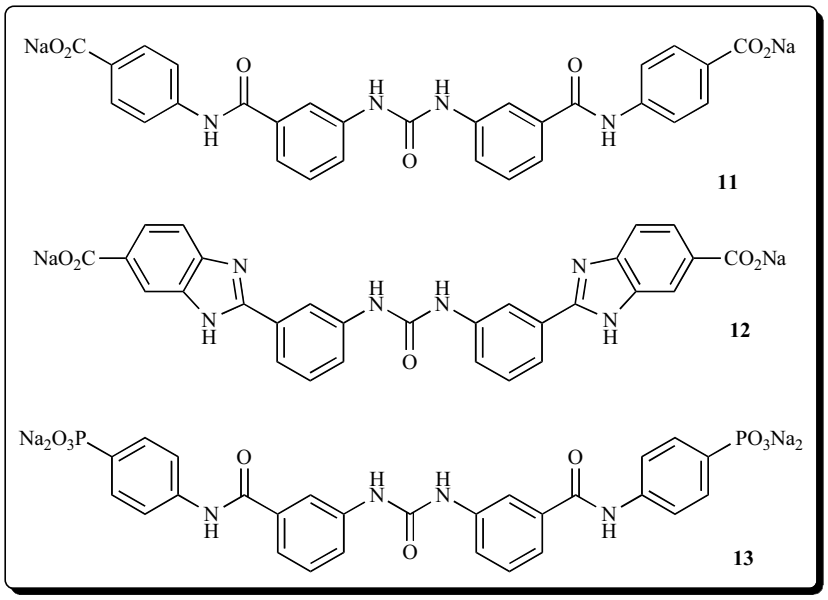

It should be noted that suramin analogs with fewer anionic groups have been shown in several studies to be significantly less toxic in mice [12, 114-117].

OTHER STRUCTURAL FEATURES

Several studies of anti-proliferative activity or FGF binding, have reported that the removal of the methyl groups of suramin did not affect inhibitory activity [12, 37, 62, 114, 116, 117, 122]. This contrasts the loss of trypanosomiasial activity when the methyl groups are omitted [3]. One study, in which the methyl groups of suramin were replaced with isopropyl groups, reported a increase in activity of the inhibition of cell growth in bovine FGF-stimulated porcine pulmonary artery endothelial cells (IC_{50} of 189 μM compared to suramin's IC_{50} of 521 μM) [4].

Amide Groups

No SAR study has systematically examined the roles of the amide groups of suramin, although one analog, NF279 (**14**), in which the amide groups were repositioned *para*- relative to the central urea group, showed high activity (the methyl groups were also removed) [37, 80, 82]. This deficiency of studies is despite the fact that amides are frequently involved in hydrogen bonding, one of the important means by which drugs can bind to their targets. It is thereby possible that one, or more, of the amide groups or the central urea group could be playing an essential role in the *in vivo* activity of suramin.

SUMMARY AND FUTURE PROSPECTS

Suramin binds to, and inhibits, a large number of enzymes and growth factors. This lack of specificity of binding limits its application as a clinical drug, and results in a broad range of toxicities and side effects. Although suramin remains useful for the treatment of onchocerciasis and trypanosomiasis, new drugs or improved analogs are needed to treat these diseases, as resistance to existing drugs increases. Suramin's promise as an anti-cancer drug has not yet been fulfilled. Suramin's role as an anti-angiogenesis agent appears to be related to its structural similarity to heparin, and its ability to inhibit the formation and dimerization of the FGF:FGF:heparin ternary complex. Structure-activity relationship studies of suramin have revealed much about its pharmacophore, but the development of suramin analogs as drugs will require candidates with much higher selectivities, and much lower toxicities.

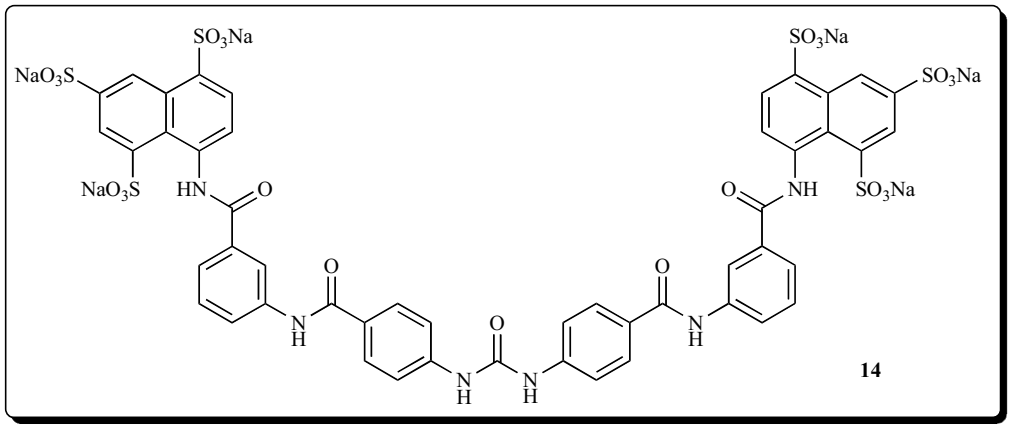

ABBREVIATIONS

AIGF	=	Androgen-induced growth factor
ANS	=	5-Amino-2-naphthalenesulfonate
CAM	=	Chorioallantoic membrane
CNS	=	Central nervous system
EGF	=	Epidermal growth factor
FGF	=	Fibroblast growth factor
FGFR	=	FGF Receptor
HBG	=	Heparin-binding growth factor
IGF	=	Insulin-like growth factor
NGF	=	Nerve growth factor
NTS	=	l,3,6-Naphthalenetrisulfonate
PDGF	=	Platelet-derived growth-factor
PTP	=	Protein-tyrosine phosphatase
SAR	=	Structure-activity relationship
TGF	=	Transforming growth factor
VCP	=	Vaccinia virus complement control protein

REFERENCES

[1] Nicolle, M.; Mesnil, F. Treatment of trypanosomiasis by benzidine colours. *Ann. Inst. Pasteur (Paris),* **1906**, *20*, 417-48.

[2] Olenick, J. G. Suramin. *Antibiotics,* **1975**, *3*, 699-703.

[3] Fourneau, E.; Trefouel, M.; Trefouel, J.; Vallee, J. Chemotherapeutic researches in the series \"Bayer 205\". Ureas of aminobenzoylaminonaphthalenesulfonic acids. *Ann. Inst. Pasteur (Paris),* **1924**, *38*, 81-114.

[4] Meyers, M. O.; Gagliardi, A. R.; Flattmann, G. J.; Su, J. L.; Wang, Y.-Z.; Woltering, E. A. Suramin Analogs Inhibit Human Angiogenesis *in Vitro*. *J. Surgical Res.,* **2000**, *91*, 130-4.

[5] Small, E. J.; Meyer, M.; Marshall, M. E.; Reyno, L. M.; Meyers, F. J.; Natale, R. B.; Lenehan, P. F.; Chen, L.; Slichenmyer, W. J.; Eisenberger, M. Suramin therapy for patients with symptomatic hormone-refractory prostate cancer: results of a randomized phase III trial comparing suramin plus hydrocortisone to placebo plus hydrocortisone. *J. Clin. Oncol.,* **2000**, *18*, 1440-50.

[6] Eisenberger, M. A.; Reyno, L. M. Suramin. *Cancer Treat. Rev.,* **1994**, *20*, 259-73.

[7] Eisenberger, M. A.; Sinibaldi, V.; Reyno, L. Suramin. *Cancer Pract.,* **1995**, *3*, 187-9.

[8] Collins, J. M.; Klecker, R. W. Jr.; Yarchoan, R.; Lane, H. C.; Fauci, A. S.; Redfield, R. R.; Broder, S.; Myers, C. E. Clinical pharmacokinetics of suramin in patients with HTLV-III/LAV infection. *J. Clin. Pharmacol.,* **1986**, *26*, 22-6.

[9] Cheson, B. D.; Levine, A. M.; Mildvan, D.; Kaplan, L. D.; Wolfe, P.; Rios, A.; Groopman, J. E.; Gill, P.; Volberding, P. A.; Poiesz, B. J. Suramin therapy in AIDS and related disorders. Report of the US Suramin Working Group. *J. Am. Med. Assoc.,* **1987**, *258*, 1347-51.

[10] Zumkeller, W.; Schofield, P. N. Growth factors, cytokines and soluble forms of receptor molecules in cancer patients. *Anticancer Res.,* **1995**, *15*, 343-8.

[11] Vakkalagadda, G. R.; Boge, T. C. Solid-phase synthesis of piperidine and cyclohexane based anti-angiogenic analogs of suramin. In *Abstracts of Papers, 223rd ACS National Meeting, Orlando, FL, United States, April 7-11, 2002*, 2002; pp MEDI-183.

[12] Manetti, F.; Cappello, V.; Botta, M.; Corelli, F.; Mongelli, N.; Biasoli, G.; Borgia, A. L.; Ciomei, M. Synthesis and binding mode of heterocyclic analogs of suramin inhibiting the human basic fibroblast growth factor. *Bioorg. Med. Chem.,* **1998**, *6*, 947-58.

[13] Bos, O. J. M.; Vansterkenburg, E. L. M.; Boon, J. P. C. I.; Fischer, M. J. E.; Wilting, J.; Janssen, L. H. M. Location and characterization of the suramin binding sites of human serum albumin. *Biochem. Pharmacol.,* **1990**, *40*, 1595-9.

[14] Kaur, M.; Reed, E.; Sartor, O.; Dahut, W.; Figg, W. D. Suramin's development: what did we learn? *Invest. New Drugs,* **2002**, *20*, 209-19.

[15] Stein, C. A.; LaRocca, R. V.; Thomas, R.; McAtee, N.; Myers, C. E. Suramin: an anticancer drug with a unique mechanism of action. *J. Clin. Oncol.,* **1989**, *7*, 499-508.

[16] Arlt, W.; Reincke, M.; Siekmann, L.; Winkelmann, W.; Allolio, B. Suramin in adrenocortical cancer: limited efficacy and serious toxicity. *Clin. Endocrinol. (Oxf).,* **1994**, *41*, 299-307.

[17] Klijn, J. G.; Setyono-Han, B.; Bakker, G. H.; van der Burg, M. E.; Bontenbal, M.; Peters, H. A.; Sieuwerts, A. M.; Berns, P. M.; Foekens, J. A. Growth factor-receptor pathway interfering treatment by somatostatin analogs and suramin: preclinical and clinical studies. *J. Steroid Biochem. Mol. Biol.,* **1990**, *37*, 1089-95.

[18] Vignon, F.; Prebois, C.; Rochefort, H. Inhibition of breast cancer growth by suramin. *J. Natl. Cancer Inst.,* **1992**, *84*, 38-42.

[19] Lindman, H.; Taube, A.; Bergh, J. C. S. Suramin inhibits the growth of human breast cancer cell lines. Studies on parental lines and corresponding sublines with acquired doxorubicin resistance with and without expression of P-glycoprotein. *Anticancer Res.,* **1994**, *14*, 363-6.

[20] Woll, P. J.; Ranson, M.; Margison, J.; Thomson, Y.; van der Water, L.; George, N.; Howell, A. Suramin for breast and prostate cancer: a pilot study of intermittent short infusions without adaptive control. *Ann. Oncol.,* **1994**, *5*, 597-600.

[21] Gradishar, W. J.; Soff, G.; Liu, J.; Cisneros, A.; French, S.; Rademaker, A.; Benson, A. B. III; Bouck, N. A pilot trial of suramin in metastatic breast cancer to assess antiangiogenic activity in individual patients. *Oncology,* **2000**, *58*, 324-33.

[22] Song, S.; Yu, B.; Wei, Y.; Wientjes, M. G.; Au, J. L. S. Low-dose suramin enhanced paclitaxel activity in chemotherapy-naive and paclitaxel-pretreated human breast xenograft tumors. *Clin. Cancer., Res.* **2004**, *10*, 6058-65.

[23] Small, E. J. Prostate cancer. *Curr. Opin. Oncol.,* **1997**, *9*, 277-86.

[24] Petrylak, D. P.; Abi-Rashid, B. Therapy for hormone-resistant prostate cancer: no longer a myth. *Cancer Treat. Res.,* **1996**, *88*, 211-8.

[25] Scher, H. I.; Steineck, G.; Kelly, W. K. Hormone-refractory (D3) prostate cancer: refining the concept. *Urology,* **1995**, *46*, 142-8.

[26] Dawson, N. A.; Figg, W. D.; Cooper, M. R.; Sartor, O.; Bergan, R. C.; Senderowicz, A. M.; Steinberg, S. M.; Tompkins, A.; Weinberger, B. Phase II trial of suramin, leuprolide, and flutamide in previously untreated metastatic prostate cancer. *J. Clin. Oncol.,* **1997**, *15*, 1470-7.

[27] Dawson, N.; Figg, W. D.; Brawley, O. W.; Bergan, R.; Cooper, M. R.; Senderowicz, A.; Headlee, D.; Steinberg, S. M.; Sutherland, M.; Patronas, N.; Sausville, E.; Linehan, W. M.; Reed, E.; Sartor, O. Phase II study of suramin plus aminoglutethimide in two cohorts of patients with androgen-independent prostate cancer: simultaneous antiandrogen withdrawal and prior antiandrogen withdrawal. *Clin. Cancer. Res.,* **1998**, *4*, 37-44.

[28] Anon, Suramin sodium: CI 1003, metaret, suramin, suramin hexasodium. *Drugs RD,* **1999**, *2*, 431-5.

[29] Knox, J. J.; Moore, M. J. Treatment of hormone refractory prostate cancer. *Semin. Urol. Oncol.,* **2001**, *19*, 202-11.

[30] Rapoport, B. L.; Falkson, G.; Raats, J. I.; de Wet, M.; Lotz, B. P.; Potgieter, H. C. Suramin in combination with mitomycin C in hormone-resistant prostate cancer. A phase II clinical study. *Ann. Oncol.,* **1993**, *4*, 567-73.

[31] Rosen, P. J.; Mendoza, E. F.; Landaw, E. M.; Mondino, B.; Graves, M. C.; McBride, J. H.; Turcillo, P.; DeKernion, J.; Belldegrun, A. Suramin in hormone-refractory metastatic prostate cancer: A drug with limited efficacy. *J. Clin. Oncol.,* **1996**, *14*, 1626-36.

[32] Autorino, R.; Di Lorenzo, G.; Damiano, R.; De Placido, S.; D'Armiento, M. Role of chemotherapy in hormone-refractory prostate cancer. Old issues, recent advances and new perspectives. *Urol. Int.,* **2003**, *70*, 1-14.

[33] Reed, E.; Cooper, M. R.; LaRocca, R. V.; Bostick-Bruton, F.; Myers, C. E. Suramin in advanced platinum-resistant ovarian cancer. *Eur. J. Cancer Clin. Oncol.,* **1992**, *28A*, 864-6.

[34] Shin, R.; Naomoto, Y.; Kamikawa, Y.; Tanaka, N.; Orita, K. Effect of suramin on human esophageal cancer cells *in vitro* and *in vivo*. *Scand. J. Gastroenterol.,* **1997**, *32*, 824-8.

[35] Minniti, C. P.; Maggi, M.; Helman, L. J. Suramin inhibits the growth of human rhabdomyosarcoma by interrupting the insulin-like growth factor II autocrine growth loop. *Cancer Res.,* **1992**, *52*, 1830-5.

[36] Fujiuchi, S.; Ohsaki, Y.; Kikuchi, K. Suramin inhibits the growth of non-small-cell lung cancer cells that express the epidermal growth factor receptor. *Oncology,* **1997**, *54*, 134-40.

[37] Dhar, S.; Gullbo, J.; Csoka, K.; Eriksson, E.; Nilsson, K.; Nickel, P.; Larsson, R.; Nygren, P. Antitumor activity of suramin analogues in human tumour cell lines and primary cultures of tumour cells from patients. *Eur. J. Cancer,* **2000**, *36*, 803-9.

[38] Thylefors, B.; Alleman, M. Towards the elimination of onchocerciasis. *Ann. Trop. Med. Parasitol.,* **2006**, *100*, 733-46.

[39] Hawking, F. Suramin: with special reference to onchocerciasis. *Adv. Pharmacol. Chemother.,* **1978**, *15*, 289-22.

[40] Mathew, N.; Kalyanasundaram, M. Antifilarial agents. *Expert Opin. Ther. Pat.,* **2007**, *17*, 767-89.

[41] D'Silva, C. Human African trypanosomiasis: future prospects for chemotherapy. *Drugs Future,* **2007**, *32*, 149-60.

[42] Nok, A. J. Effective measures for controlling trypanosomiasis. *Expert Opin. Pharmacother.,* **2005**, *6*, 2645-53.

[43] Bouteille, B.; Oukem, O.; Bisser, S.; Dumas, M. Treatment perspectives for human African trypanosomiasis. *Fundam. Clin. Pharmacol.,* **2003**, *17*, 171-81.

[44] Vansterkenburg, E. L. M.; Coppens, I.; Wilting, J.; Bos, O. J. M.; Fischer, M. J. E.; Janssen, L. H. M.; Opperdoes, F. R. The uptake of the trypanocidal drug suramin in combination with low-density lipoproteins by Trypanosoma brucei and its possible mode of action. *Acta Trop.,* **1993**, *54*, 237-50.

[45] Hemady, R. K.; Sinibaldi, V. J.; Eisenberger, M. A. Ocular symptoms and signs associated with suramin sodium treatment for metastatic cancer of the prostate. *Am. J. Ophthalmol.,* **1996**, *121*, 291-6.

[46] Falkson, G.; Rapoport, B. L. Lethal toxic epidermal necrolysis during suramin treatment. *Eur. J. Cancer,* **1992**, *28A*, 1294.

[47] May, E.; Allolio, B. Fatal toxic epidermal necrolysis during suramin therapy. *Eur. J. Cancer,* **1991**, *27*, 1338.

[48] Eisenberger, M. A.; Sinibaldi, V. J.; Reyno, L. M.; Sridhara, R.; Jodrell, D. I.; Zuhowski, E. G.; Tkaczuk, K. H.; Lowitt, M. H.; Hemady, R. K.; Jacobs, S. C.; Vanecho, D.; Egorin, M. J. Phase-I and clinical-evaluation of a pharmacologically guided regimen of suramin in patients with hormone-refractory prostate cancer. *J. Clin. Oncol.,* **1995**, *13*, 2174-86.

[49] Larocca, R. V.; Meer, J.; Gilliatt, R. W.; Stein, C. A.; Cassidy, J.; Myers, C. E.; Dalakas, M. C. Suramin-induced polyneuropathy. *Neurology,* **1990**, *40*, 954-60.

[50] Whitten, W. K. Physiological control of population growth. *Nature,* **1956**, *178*, 992.

[51] Chijioke, C. P.; Umeh, R. E.; Mbah, A. U.; Nwonu, P.; Fleckenstein, L. L.; Okonkwo, P. O. Clinical pharmacokinetics of suramin in patients with onchocerciasis. *Eur. J. Clin. Pharmacol.,* **1998**, *54*, 249-51.

[52] Cooper, M. R.; Lieberman, R.; Larocca, R. V.; Gernt, P. R.; Weinberger, M. S.; Headlee, D. J.; Kohler, D. R.; Goldspiel, B. R.; Peck, C. C.; Myers, C. E. Adaptive-control with feedback-strategies for suramin dosing. *Clin. Pharmacol. Ther.,* **1992**, *52*, 11-23.

[53] Voogd, T. E.; Vansterkenburg, L. M.; Wilting, J.; Janssen, L. H. M. Recent research on the biological activity of suramin. *Pharmacol. Rev.,* **1993**, *45*, 177-203.

[54] Bocci, G.; Danesi, R.; Benelli, U.; Innocenti, F.; Di Paolo, A.; Fogli, S.; Del Taca, M. Inhibitory effect of suramin in rat models of angiogenesis *in vitro* and *in vivo*. *Cancer Chemother. Pharmacol.,* **1999**, *43*, 205-12.

[55] Zhang, Y.-L.; Keng, Y.-F.; Zhao, Y.; Wu, L.; Zhang, Z.-Y. Suramin is an active site-directed, reversible, and tight-binding inhibitor of protein-tyrosine phosphatases. *J. Biol. Chem.,* **1998**, *273*, 12281-7.

[56] Benini, S.; Baldini, N.; Manara, M. C.; Chano, T.; Serra, M.; Rizzi, S.; Lollini, P.-L.; Picci, P.; Scotlandi, K. Redundancy of autocrine loops in human osteosarcoma cells. *Int. J. Cancer,* **1999**, *80*, 581-8.

[57] Larsen, A. K. Suramin: An anticancer drug with unique biological effects. *Cancer Chemother. Pharmacol.,* **1993**, *32*, 96-8.

[58] Braddock, P. S.; Hu, D. E.; Fan, T. P. D.; Stratford, I. J.; Harris, A. L.; Bicknell, R. A structure-activity analysis of antagonism of the growth factor and angiogenic activity of basic fibroblast growth factor by suramin and related polyanions. *Br. J. Cancer,* **1994**, *69*, 890-8.

[59] Pesenti, E.; Sola, F.; Mongelli, N.; Grandi, M.; Spreafico, F. Suramin prevents neovascularization and tumor growth through blocking of basic fibroblast growth factor activity. *Br. J. Cancer,* **1992**, *66*, 367-72.

[60] Gagliardi, A.; Hadd, H.; Collins, D. C. Inhibition of angiogenesis by suramin. *Cancer Res.,* **1992**, *52*, 5073-5.

[61] Takano, S.; Gately, S.; Neville, M. E.; Herblin, W. F.; Gross, J. L.; Engelhard, H.; Perricone, M.; Eidsvoog, K.; Brem, S. Suramin, an anticancer and angiosuppressive agent, inhibits endothelial cell binding of basic fibroblast growth factor, migration, proliferation, and induction of urokinase-type plasminogen activator. *Cancer Res.,* **1994**, *54*, 2654-60.

[62] Gagliardi, A. R. T.; Kassack, M.; Kreimeyer, A.; Muller, G.; Nickel, P.; Collins, D. C. Antiangiogenic and antiproliferative activity of suramin analogs. *Cancer Chemother. Pharmacol.,* **1998**, *41*, 117-24.

[63] Middaugh, C. R.; Mach, H.; Burke, C. J.; Volkin, D. B.; Dabora, J. M.; Tsai, P. K.; Bruner, M. W.; Ryan, J. A.; Marfia, K. E. Nature of the interaction of growth factors with suramin. *Biochemistry,* **1992**, *31*, 9016-24.

[64] Zamai, M.; Parola, A. H.; Grandi, M.; Mongeli, N.; Caiolfa, V. R. Antiangiogenic naphthalene sulfonic distamycin-A derivatives tightly interact with human basic fibroblast growth factor. *Med. Chem. Res.,* **1997**, *7*, 36-44.

[65] Jindal, H. K.; Anderson, C. W.; Davis, R.; Vishwanatha, J. K. Suramin affects DNA synthesis in HeLa cells by inhibition of DNA polymerases. *Cancer Res.,* **1990**, *50*, 7754-7.

[66] De Clercq, E. Suramin: a potent inhibitor of the reverse transcriptase of RNA tumor viruses. *Cancer Lett.,* **1979**, *8*, 9-22.

[67] Mitsuya, H.; Matsushita, S.; Yarchoan, R.; Broder, S. Protection of T cells against infectivity and cytopathic effect of HTLV-III *in vitro*. *Princess Takamatsu Symp.,* **1984**, *15*, 277-88.

[68] Chandra, P.; Vogel, A.; Gerber, T. Inhibitors of retroviral DNA polymerase: their implication in the treatment of AIDS. *Cancer Res.,* **1985**, *45*, 4677s-84s.

[69] Funayama, Y.; Nishio, K.; Takeda, Y.; Kubota, N.; Ohira, T.; Ohmori, T.; Ohta, S.; Ogasawara, H.; Hasegawa, S.; Saijo, N. suramin inhibits the phosphorylation and catalytic activity of DNA topoisomerase II in human lung cancer cells. *Anticancer Res.,* **1993**, *13*, 1981-8.

[70] Lelievre, S.; Benchokroun, Y.; Larsen, A. K. Altered topoisomerase I and II activities in suramin-resistant lung fibrosarcoma cells. *Mol. Pharmacol.,* **1995**, *47*, 898-906.

[71] Larsen, A. K.; Escargueil, A. E.; Skladanowski, A. Catalytic topoisomerase II inhibitors in cancer therapy. *Pharmacol. Ther.,* **2003**, *99*, 167-81.

[72] Fortes, P. A. G.; Ellory, J. C.; Lew, V. L. Suramin. Potent ATPase inhibitor which acts on the inside surface of the sodium pump. *Biochim. Biophys. Acta,* **1973**, *318*, 262-72.

[73] Moriyama, Y.; Nelson, N. Inhibition of vacuolar proton ATPases by fusidic acid and suramin. *FEBS Lett.,* **1988**, *234*, 383-6.

[74] Marchetti, D.; Reiland, J.; Erwin, B.; Roy, M. Inhibition of heparanase activity and heparanase-induced angiogenesis by suramin analogues. *Int. J. Cancer,* **2003**, *104*, 167-74.

[75] McCain, D. F.; Wu, L.; Nickel, P.; Kassack, M. U.; Kreimeyer, A.; Gagliardi, A.; Collins, D. C.; Zhang, Z.-Y. Suramin derivatives as inhibitors and activators of protein-tyrosine phosphatases. *J. Biol. Chem.,* **2004**, *279*, 14713-25.

[76] Hensey, C. E.; Boscoboinik, D.; Azzi, A. Suramin, an anticancer drug, inhibits protein kinase C and induces differentiation in neuroblastoma cell clone NB2A. *FEBS Lett.,* **1989**, *258*, 156-8.

[77] Khaled, Z.; Rideout, D.; O'Driscoll, K. R.; Petrylak, D.; Cacace, A.; Patel, R.; Chiang, L. C.; Rotenberg, S.; Stein, C. A. Effects of suramin-related and other clinically therapeutic polyanions on protein kinase C activity. *Clin. Cancer. Res.,* **1995**, *1*, 113-22.

[78] Polenova, T.; Iwashita, T.; Palmer, A. G. III; McDermott, A. E. Conformation of the trypanocidal pharmaceutical suramin in Its free and bound forms: transferred nuclear Overhauser studies. *Biochemistry,* **1997**, *36*, 14202-17.

[79] Kopp, R.; Pfeiffer, A. Suramin alters phosphoinositide synthesis and inhibits growth factor receptor binding in HT-29 cells. *Cancer Res.,* **1990**, *50*, 6490-6.

[80] Trapp, J.; Meier, R.; Hongwiset, D.; Kassack, M. U.; Sippl, W.; Jung, M. Structure-activity studies on suramin analogues as inhibitors of NAD+-dependent histone deacetylases (sirtuins). *ChemMedChem,* **2007**, *2*, 1419-31.

[81] Kassack, M. U. G-protein coupled receptor kinases and their inhibitors. *Expert Opin. Ther. Pat.,* **2000**, *10*, 917-28.

[82] Kassack, M. U.; Braun, K.; Ganso, M.; Ullmann, H.; Nickel, P.; Boing, B.; Muller, G.; Lambrecht, G. Structure-activity relationships of analogues of NF449 confirm NF449 as the most potent and selective known P2X1 receptor antagonist. *Eur. J. Med. Chem.,* **2004**, *39*, 345-57.

[83] Ullmann, H.; Meis, S.; Hongwiset, D.; Marzian, C.; Wiese, M.; Nickel, P.; Communi, D.; Boeynaems, J.-M.; Wolf, C.; Hausmann, R.; Schmalzing, G.; Kassack, M. U. Synthesis and structure-activity relationships of suramin-derived P2Y11 receptor antagonists with nanomolar potency. *J. Med. Chem.,* **2005**, *48*, 7040-8.

[84] Lambrecht, G.; Braun, K.; Damer, S.; Ganso, M.; Hildebrandt, C.; Ullmann, H.; Kassack, M. U.; Nickel, P. Structure-activity relaionships of suramin and pyridoxal-5'-phosphate derivatives as P2 receptor antagonists. *Curr. Pharm. Des.,* **2002**, *8*, 2371-99.

[85] Murakami, M. T.; Gava, L. M.; Zela, S. P.; Arruda, E. Z.; Melo, P. A.; Gutierrez, J. M.; Arni, R. K. Crystallization and preliminary x-ray diffraction analysis of suramin, a highly charged polysulfonated naphthylurea, complexed with a myotoxic PLA2 from Bothrops asper venom. *Biochim. Biophys. Acta,* **2004**, *1703*, 83-5.

[86] Coffey, R. J. Jr.; Leof, E. B.; Shipley, G. D.; Moses, H. L. Suramin inhibition of growth factor receptor binding and mitogenicity in AKR-2B cells. *J. Cell. Physiol.,* **1987**, *132*, 143-8.

[87] Olivier, S.; Formento, P.; Fischel, J. L.; Etienne, M. C.; Milano, G. Epidermal growth factor receptor expression and suramin cytotoxcity *in vitro*. *Eur. J. Cancer,* **1990**, *26*, 867-71.

[88] Hosang, M. Suramin binds to platelet-derived growth factor and nhibits its biological activity. *J. Cell. Biochem.,* **1985**, *29*, 265-73.

[89] Sato, B.; Kouhara, H.; Koga, M.; Kasayama, S.; Saito, H.; Sumiani, S.; Hashimoto, K.; Kishimoto, T.; Tanaka, A.; Matsumoto, K. Androgen-induced growth factor and its receptor: demonstration of he androgen-induced autocrine loop in mouse mammary carcinoma cells. *J. Steroid Biochem. Mol. Biol.,* **1993**, *47*, 91-8.

[90] Koga, M.; Kasayama, S.; Matsumoto, K.; Sato, B. Molecular mechanism of androgen-dependent growth in transformed cells. Pathway from basic science to clinical application. *J. Steroid Biochem. Mol. Biol.,* **1995**, *54*, 1-6.

[91] Gill, J. S.; Windebank, A. J. Activation of the high affinity nerve growth factor receptor by two polyanionic chemotherapeutic agents: role in drug induced neurotoxicity. *J. Neurooncol.,* **1998**, *40*, 19-27.

[92] Wrobel, J.; Green, D.; Jetter, J.; Kao, W.; Rogers, J.; Claudia Perez, M.; Hardenburg, J.; Deecher, D. C.; Lopez, F. J.; Arey, B. J.; Shen, E. S. Synthesis of (bis)sulfonic acid, (bis)benzamides as follicle-stimulating hormone (FSH) antagonists. *Bioorg. Med. Chem.,* **2002**, *10*, 639-56.

[93] Mills, G. B.; Zhang, N.; May, C.; Hill, M.; Chung, A. Suramin prevents binding of interleukin 2 to its cell surface receptor: a possible mechanism for immunosuppression. *Cancer Res.,* **1990**, *50*, 3036-42.

[94] Strassmann, G.; Kambayashi, T. Inhibition of experimental cancer cachexia by anti-cytokine and anti-cytokine-receptor therapy. *Cytokines Mol. Ther.,* **1995**, *1*, 107-13.

[95] Grazioli, L.; Alzani, R.; Ciomei, M.; Mariani, M.; Restivo, A.; Cozzi, E.; Marcucci, F. Inhibitory effect of suramin on receptor binding and cytotoxic activity of tumor necrosis factor a. *Int. J. Immunopharmacol.,* **1992**, *14*, 637-42.

[96] Mancini, F.; Toro, C. M.; Mabilia, M.; Giannangeli, M.; Pinza, M.; Milanese, C. Inhibition of tumor necrosis factor-a (TNF-a)/TNF-a receptor binding by structural analogues of suramin. *Biochem. Pharmacol.,* **1999**, *58*, 851-9.

[97] Ganesh, V. K.; Muthuvel, S. K.; Smith, S. A.; Kotwal, G. J.; Murthy, K. H. M. Structural basis for antagonism by suramin of heparin binding to vaccinia complement protein. *Biochemistry,* **2005**, *44*, 10757-65.

[98] Fleck, S. L.; Birdsall, B.; Babon, J.; Dluzewski, A. R.; Martin, S. R.; Morgan, W. D.; Angov, E.; Kettleborough, C. A.; Feeney, J.; Blackman, M. J.; Holder, A. A. Suramin and suramin analogues nhibit merozoite surface protein-1 secondary [rocessing and erythrocyte invasion by the malaria parasite Plasmodium falciparum. *J. Biol. Chem.,* **2003**, *278*, 47670-77.

[99] Gao, X.-G.; Garza-Ramos, G.; Saavedra-Lira, E.; Cabrera, N.; De Gomez-Puyou, M. T.; Perez-Montfort, R.; Gomez-Puyou, A. Reactivation of triosephosphate isomerase from three trypanosomatids and human: effect of Suramin. *Biochem. J.,* **1998**, *332*, 91-6.

[100] Opperdoes, F. R.; Wierenga, R. K.; Noble, M. E. M.; Hol, W. G. J.; Willson, M.; Kuntz, D. A.; Callens, M.; Perie, J. Unique properties of glycosomal enzymes. *UCLA Symp. Mol. Cell. Bio. New Ser.,* **1990**, *130*, 233-46.

[101] Hutley, L.; Shurety, W.; Newell, F.; McGeary, R.; Pelton, N.; Grant, J.; Herington, A.; Cameron, D.; Whitehead, J.; Prins, J. Fibroblast growth factor 1. A key regulator of human adipogenesis. *Diabetes,* **2004**, *53*, 3097-106.

[102] Murphy, P. V.; Pitt, N.; O'Brien, A.; Enright, P. M.; Dunne, A.; Wilson, S. J.; Duane, R. M.; O'Boyle, K. M. Identification of novel inhibitors of fibroblast growth factor (FGF-2) binding to heparin and endothelial cell survival from a structurally diverse carbohybrid library. *Bioorg. Med. Chem. Lett.,* **2002**, *12*, 3287-90.

[103] Harmer, N. J.; Ilag, L. L.; Mulloy, B.; Pellegrini, L.; Robinson, C. V.; Blundell, T. L. Towards a resolution of the stoichiometry of the fibroblast growth factor (FGF)-FGF receptor-heparin Complex. *J. Mol. Biol.,* **2004**, *339*, 821-34.

[104] Huhtala, M. T.; Pentikäinen, O. T.; Johnson, M. S. A dimeric ternary complex of FGFR1, heparin and FGF-1 leads to an 'electrostatic sandwich' model for heparin binding. *Structure,* **1999**, *7*, 699-709.

[105] Ornitz, D. M.; Xu, J.; Colvin, J. S.; McEwen, D. G.; MacArthur, C. A.; Coulier, F.; Gao, G.; Goldfarb, M. Receptor specificity of the fibroblast growth factor family. *J. Biol. Chem.,* **1996**, *271*, 15292-7.

[106] Ciomei, M.; Pastori, W.; Mariani, M.; Sola, F.; Grandi, M.; Mongelli, N. New sulfonated distamyin A derivatives with bFGF complexing activity. *Biochem. Pharmacol.,* **1994**, *47*, 295-302.

[107] Spivak-Kroizman, T.; Lemmon, M. A.; Dikic, I.; Ladbury, J. E.; Pinchasi, D.; Huang, J.; Jaye, M.; Crumley, G.; Schlessinger, J.; Lax, I. Heparin-induced oligomerization of FGF molecules is responsible for FGF receptor dimerization, activation, and cell proliferation. *Cell,* **1994**, *79*, 1015-24.

[108] Rapraeger, A. C.; Krufka, A.; Olwin, B. B. Requirement of heparan sulfate for bFGF-mediated fibroblast growth and myoblast differentiation. *Science,* **1991**, *252*, 1705-8.

[109] Ornitz, D. M.; Yayon, A.; Flanagan, J. G.; Svahn, C. M.; Levi, E.; Leder, P. Heparin is required for cell-free binding of basic fibroblast growth factor to a soluble receptor and for mitogenesis in whole cells. *Mol. Cell. Biol.,* **1991**, *12*, 240-7.

[110] Yayon, A.; Klagsbrun, M.; Esko, J. D.; Leder, P.; Ornitz, D. M. Cell surface, heparin-like molecules are required for binding of basic fibroblast growth factor to its high affinity receptor. *Cell,* **1991**, *64*, 841-8.

[111] Lozano, R. M.; Jimenez, M. A.; Santoro, J.; Rico, M.; Gimenez-Gallego, G. Solution structure of acidic fibroblast growth factor bound to 1,3,6-naphthalenetrisulfonate: a minimal model for the anti-tumoral action of suramins and suradistas. *J. Mol. Biol.,* **1998**, *281*, 899-915.

[112] Fernandez-Tornero, C.; Lozano, R. M.; Redondo-Horcajo, M.; Gomez, A. M.; Lopez, J. C.; Quesada, E.; Uriel, C.; Valverde, S.; Cuevas, P.; Romero, A.; Gimenez-Gallego, G. Leads for development of new naphthalenesulfonate derivatives with enhanced antiangiogenic activity: crystal structure of acidic fibroblast growth factor in complex with 5-amino-2-naphthalenesulfonate. *J. Biol. Chem.,* **2003**, *278*, 21774-81.

[113] Kathir, K. M.; Kumar, T. K. S.; Yu, C. Understanding the mechanism of the antimitogenic activity of suramin. *Biochemistry,* **2006**, *45*, 899-906.

[114] Biasoli, G.; Botta, M.; Ciomei, M.; Corelli, F.; Grandi, M.; Manetti, F.; Mongelli, N.; Paio, A. New heterocyclic analogs of suramin with bFGF inhibiting activity. synthesis, SAR and possible mode of action. *Med. Chem. Res.,* **1994**, *4*, 202-10.

[115] Kreimeyer, A.; Mueller, G.; Kassack, M.; Nickel, P.; Gagliardi, A. R. T. Suramin analogs with a 2-phenylbenzimidazole moiety as partial structure. Potential anti HIV- and angiostatic drugs. Part 2. Sulfanilic acid-, benzenedisulfonic acid-, and naphthalenetrisulfonic acid analogs. *Arch. Pharm.,* **1998**, *331*, 97-103.

[116] Firsching, A.; Nickel, P.; Mora, P.; Allolio, B. Antiproliferative and angiostatic activity of suramin analogs. *Cancer Res.,* **1995**, *55*, 4957-61.

[117] Firsching-Hauck, A.; Nickel, P.; Yahya, C.; Wandt, C.; Kulik, R.; Simon, N.; Zink, M.; Nehls, V.; Allolio, B. Angiostatic effects of suramin analogs *in vitro*. *Anti-Cancer Drugs,* **2000**, *11*, 69-77.

[118] Morris, A. D.; Leonce, S.; Guilbaud, N.; Tucker, G. C.; Perez, V.; Jan, M.; Cordi, A. A.; Pierre, A.; Atassi, G. Eriochrome Black T, structurally related to suramin, inhibits angiogenesis and tumor growth *in vivo*. *Anti-Cancer Drugs,* **1997**, *8*, 746-55.

[119] Baghdiguian, S.; Nickel, P.; Marvaldi, J.; Fantini, J. A suramin derivative induces enterocyte-like differentiation of human colon cancer cells without lysosomal storage disorder. *Anti-Cancer Drugs,* **1990**, *1*, 59-66.

[120] Mohan, P. Problems and perspectives in the design of anti-HIV-1 agents. *Drug Dev. Res.,* **1993**, *29*, 1-17.

[121] Nickel, P.; Haack, H. J.; Widjaja, H.; Ardanuy, U.; Gurgel, C.; Duewel, D.; Loewe, H.; Raether, W. Potential filaricides. Suramin analogs. *Arzneimittel-Forschung,* **1986**, *36*, 1153-7.

[122] Raj, P. A.; Marcus, E.; Rein, R. Conformational requirements of suramin to target angiogenic growth factors. *Angiogenesis,* **1998**, *2*, 183-99.

[123] Manetti, F.; Corelli, F.; Botta, M. Fibroblast growth factors and their inhibitors. *Curr. Pharm. Des.,* **2000**, *6*, 1897-924.

Received: 30 June, 2008 Revised: 02 September, 2008 Accepted: 17 September, 2008

Molecular Psychiatry (2018) 23, 94–106

www.nature.com/mp

REVIEW

Purinergic system in psychiatric diseases

A Cheffer[1], ARG Castillo[1], J Corrêa-Velloso[1], MCB Gonçalves[2], Y Naaldijk[1], IC Nascimento[1], G Burnstock[3,4] and H Ulrich[1]

Psychiatric disorders are debilitating diseases, affecting >80 million people worldwide. There are no causal cures for psychiatric disorders and available therapies only treat the symptoms. The etiology of psychiatric disorders is unknown, although it has been speculated to be a combination of environmental, stress and genetic factors. One of the neurotransmitter systems implicated in the biology of psychiatric disorders is the purinergic system. In this review, we performed a comprehensive search of the literature about the role and function of the purinergic system in the development and predisposition to psychiatric disorders, with a focus on depression, schizophrenia, bipolar disorder, autism, anxiety and attention deficit/hyperactivity disorder. We also describe how therapeutics used for psychiatric disorders act on the purinergic system.

Molecular Psychiatry (2018) **23,** 94–106; doi:10.1038/mp.2017.188; published online 26 September 2017

INTRODUCTION

The first evidence that adenosine triphosphate (ATP) and related nucleotides function as neurotransmitters was obtained in the 1970s[1–3] with the proposal of ATP cotransmitter action in subsequent years.[4–6] ATP is co-released with several neurotransmitters, such as acetylcholine, GABA, glutamate, noradrenaline and serotonin (5-hydroxy-tryptamine (5-HT)).[7,8] It acts on specific receptors in the pre- and postsynaptic neuronal and glial membrane, known as purinergic receptors.[5,9–11] Ectonucleotidases control extracellular ATP concentration, preventing prolonged agonist exposure and receptor desensitization. ATP hydrolysis generates adenosine diphosphate (ADP), adenosine monophosphate (AMP) and adenosine (ADO), involved in cell signaling.[12–14]

Purinergic receptors are classified into P1 and P2 receptors according to their biochemical and pharmacological properties.[15,16] P1 receptors are metabotropic and sensitive to ADO and subdivided into A1, A2A, A2B and A3 receptors. Whereas A1, A2A and A3 receptors have high affinities, the A2B subtype has low affinity to its ligand.[17,18] A1 and A3 receptors bind to the $G_{i/o}$ protein family, responsible for inhibition of cAMP production, whereas A2A and A2B receptors stimulate the production of cAMP via G_s protein activation.[10] A1 and A3 receptors also promote phospholipase C-β activity and consequently the formation of inositol-1,4,5-trisphosphate.[7] ADO formed from the catabolism of adenine nucleotides preferentially activates A2A receptors, whereas ADO released by specific nucleoside transporters activates A1 receptors.[19] P1 receptors are antagonized by methylxanthines and their derivatives, like caffeine, in moderate doses.[20]

P2 receptors are activated by nucleoside di- and triphosphates (ATP, ADP, uridine triphosphate (UTP), uridine diphosphate (UDP) or UDP-glucose) and classified as P2X and P2Y receptors.[10,21,22] P2X receptors are ATP-gated ion channels permeable to Na^+, K^+ and Ca^{2+} cations.[22,23] Seven subunits of these receptors (P2X1–7) expressed by different cell types are grouped either in a homomeric or heteromeric mode.[11,24,25] P2Y receptors are metabotropic and activated by purines and pyrimidines, such as ATP, ADP, UTP, UDP or UDP-glucose, and they are divided into P2Y 1, 2, 4, 6, 11, 12, 13 and 14 subtypes. P2Y1, 2, 4, 6 and 11 receptors are coupled to G_q and G_{11} proteins, leading to phospholipase C-β activation and generation of inositol-1,4,5-trisphosphate and diacylglycerol with subsequent Ca^{2+} release from endoplasmic reticulum.[22,26,27] P2Y12, 13 and 14 subtypes are coupled to G_i and G_o, inhibit adenylyl cyclase and affect intracellular calcium concentration.[11,28]

Purinergic signaling is involved in neurodevelopment and pathophysiological processes, such as cell proliferation, differentiation, neuron–glia crosstalking and inflammation.[8,29–31] P1 receptor functions appear to be better understood than those of P2 receptors in some psychiatric conditions. A1 and A2A receptors control synaptic plasticity and neurotransmitter release, for instance, glutamate, dopamine and GABA.[30,31] These neurotransmitters are targets for classical and novel drug treatment of several psychiatric conditions.[32] That is also the case for the A3 receptor regulating serotonergic and glutamatergic systems.[33,34] P2 receptors are closely related to embryonic neurodevelopment, and any disturbance of purinergic signaling may be a core process leading to psychiatric diseases in general.[35] Psychiatric disorders are explained by complex inheritance models with interplaying genes, epigenetics and environment in the etiological basis. In this review, we summarize the main findings linking the purinergic system to the most investigated psychiatric diseases.

DEPRESSION

Depression, elicited by acute and chronic stress, is related to an abnormal activation of the hypothalamic–pituitary–adrenal axis leading to increased levels of glucocorticoids (cortisol in humans, corticosterone in rodents).[36] Both hypothalamic–pituitary–adrenal axis and hormonal release are controlled by ADO receptors.[37] For instance, the activation of A2 receptors by ADO increases adrenal corticosterone synthesis, an effect that is blocked by A2 receptor

[1]Departamento de Bioquímica, Instituto de Química, Universidade de São Paulo, São Paulo, Brazil; [2]Departamento de Neurologia/Neurociência, Escola Paulista de Medicina, Universidade Federal de São Paulo, São Paulo, Brazil; [3]Autonomic Neuroscience Centre, Royal Free and University College Medical School, London, UK and [4]Department of Pharmacology and Therapeutics, The University of Melbourne, Melbourne, VIC, Australia. Correspondence: Professor H Ulrich, Departamento de Bioquímica, Instituto de Química, Universidade de São Paulo, São Paulo, SP 05508-000, Brazil.
E-mail: henning@iq.usp.br
Received 12 January 2017; revised 15 July 2017; accepted 20 July 2017; published online 26 September 2017

antagonism.[38] The particular involvement of A2A receptors in the control of hypothalamic–pituitary–adrenal axis and in regulating glucocorticoid actions is suggested by the fact that receptor overexpression promotes alterations in the levels of corticosterone and enhances synaptic plasticity and memory impairments induced by glucocorticoid. The latter effects are reversed by inhibiting the A2A receptor,[39] in agreement with previous findings.[40,41] Mostly, inhibitory A1 and excitatory A2A receptors promote pre- and postsynaptic modulatory effects on glutamatergic and monoaminergic neurotransmission[8] and are relevant for both synaptic plasticity and neuroprotection. For instance, activation of A1 receptors decreases hippocampal 5-HT release, one of the major neurotransmitters implicated in depression, whereas A2 receptor activation results in opposite effects.[42] Accordingly, A1 receptor agonists block 5-HT-mediated induction of prefrontocortical neuronal activity.[43] These data illustrate how ADO contributes to the fine control of different brain networks and how alterations in adenosinergic signaling are involved in psychiatric diseases and may be explored in the search for new treatments; this has been extensively reviewed in the literature (see, for instance, Cunha[20]).

Enhanced neuronal A1 receptor expression in transgenic mice led to pronounced acute and chronic resilience toward depressive-like behaviors.[44] Opposite effects were observed in A1 receptor knockout (KO) mice, which showed increased depressive-like behavior and were resistant to antidepressant effects of sleep deprivation.[44] The chronic unpredictable stress (CUS) model, an animal model for depression, is related to increased corticosterone levels, abnormal hippocampal circuits, altered mood and decreased memory performance.[45,46] Caffeine prevented depressive-like behavior and synaptic alterations induced by CUS.[41] Remarkably, caffeine consumption increases in stressful conditions[47] and correlates inversely with the incidence of depression in patients[48,49] and the risk of suicide.[50,51] Both blockade of A2A receptors by the selective antagonist KW6002 and its genetic deletion in CUS mice resulted not only in prophylactic, but also in therapeutically beneficial effects.[41] For instance, genetic deletion of A2A receptors prevented behavioral and synaptic alterations observed in CUS mice.[41] In agreement, A2A receptor overexpression in forebrain neurons induced depressive-like behavior in rats.[52] Similarly, A2A receptor antagonism exerts antidepressant effects in behavioral paradigms, such as the forced swimming test and tail suspension test[53,54] and also prevents maternal separation-induced long-term cognitive impacts.[40] Interestingly, alterations in the expression of A2A receptors have also been observed in platelets of patients with major depression disorder (MDD), suggesting that the receptor might be an important disease biomarker.[55] In zebrafish, A1 receptor antagonism prevents MK-801, an uncompetitive antagonist of *N*-methyl-D-aspartate receptors, from promoting antidepressant-like effects.[56] In addition, CUS decreased cell surface adenosine deaminase (ADA) activity in zebrafish brain membranes, although ectonucleotidase and soluble ADA activities did not change.[57] Reduced ADA activity could be a compensatory mechanism through which the brain normalizes ADO levels, modulating neuroprotective effects of this nucleoside in zebrafish brain.[57] Accordingly, an increased purine catabolism has been reported in MDD patients, as indicated by higher plasma levels of xanthine, one of the end products of purine degradation.[58] It is worthwhile mentioning that chronic usage of antidepressants, such as fluoxetine and nortriptyline, alters ectonucleotidase activity in the hippocampus and cortex, suggesting that alterations in purine metabolism might be involved in depression.[59]

ADO and ATP regulate microglia and astrocyte activities and their responses to damaging cues,[60–66] playing an important role by controlling glia–neuron communication. Glial cell-based synaptic dysfunction for depression characterized by hypoactivated astrocytes and hyperactivated microglia has been proposed.[67] Indeed, transgenic blockage of astrocytic ATP release resulted in depressive-like behavior in social defeated mice,[68] an animal model for depression induced by social stress.[69,70] Moreover, stimulating endogenous ATP release from astrocytes induced antidepressant-like effects mediated by P2X2 receptors in neurons of prefrontal cortex of social stressed mice.[68] Brains of depressive patients exhibit increased inflammatory cytokines,[71,72] supporting the idea that activation of microglia plays a role in depressive-like behavior, such as social withdrawal, sleep alterations and anorexia.[73–75] Altogether, as previously described,[67] (1) decreased astrocytic ATP release, resulting in deficient neuronal activation of P2X2 receptor;[68] (2) hypofunction of inhibitory A1 receptor as a consequence of a diminished astrocyte-derived ADO;[76] associated with (3) increased synaptic excitability, subsequent presynaptic ATP release and stimulation of postsynaptic A2A receptors may be related to abnormal synaptic plasticity.[39,77] Furthermore, (4) synaptic ATP release stimulates P2X7 receptors resulting in hyperactivated microglia and interleukin-1β production observed in depressive-like behaviors.[73]

P2X7 receptor KO animal models displayed higher mobility in forced swimming and tail suspension tests, a characteristic behavior of antidepressive profiles.[78–80] This observed resilience to depressive-like behavior could be related to inhibition of interleukin-1β release. Accordingly, P2X7 receptor-induced interleukin-1β release results in lower brain-derived neurotrophic factor expression in hippocampus, where this neurotrophic factor plays a key role in synaptic plasticity, neurogenesis and neuroprotection.[80,81] It is worth mentioning that uptake and bioavailability of 5-HT in the synaptic cleft is also regulated by P2X7 receptors, as, in the absence of the receptor, an elevation in 5-HT levels was observed in a lipopolysaccharide-evoked depressive behavior model.[80] Moreover, by using the same model, the P2X7 receptor antagonist Brilliant Blue G had antidepressant effects and attenuated anhedonia, a key feature of depression.[82]

In humans, the two most commonly studied P2X7 receptor single-nucleotide polymorphisms (SNPs) associated with increased susceptibility to depression, as well as to panic attack and bipolar disorder (BD), are Gln460Arg (rs2230912) and His155Tyr (rs208294).[83–86] Replacement of glutamine by arginine resulted in a receptor protein as active as the wild-type one, although the interaction of the Gln460ArgP2X7 receptor variant with wild-type P2X7 subunits impaired receptor function when both variants had been overexpressed in HEK293 cells.[87] There is no clue so far regarding the physiological importance of this finding. On the other hand, the polymorphic His155TyrP2X7 receptor is more active than the wild-type one that could explain, to some extent, its association with psychiatric disorders, given the P2X7 receptor-mediated proinflammatory effects.[88]

SCHIZOPHRENIA

ADO has emerged as an important interplayer because of its modulatory effects on glutamate and dopamine transmission, classical neurotransmitters involved in physiopathology of schizophrenia (SCZ).[89–92] A1 receptor agonists inhibit glutamate release and reduce *N*-methyl-D-aspartate receptor-induced ion currents.[93–95] In contrast, activation of A2A receptors induces release of glutamate in striatal and cortical regions.[96,97] Activation of A1 receptors should inhibit dopamine release, as receptor blockade has opposite effects.[98] Dopamine D2 receptor activation decreases glutamate release, forming A2A/D2 or even A1/A2A receptor heteromers. As ADO has a higher affinity for A1 receptors, and A2A receptor activation reduces the affinity of A1 receptors for agonists, the occurrence of A1/A2A heteromers may be a switch mechanism, by which low or high ADO concentrations inhibit or facilitate glutamate release, respectively.[96,99,100] A2A and D2 receptors are reported to exert antagonistic interactions, as A2A agonists reduce the affinity of D2 receptors for dopamine in

both rat and human striatum.[101,102] An open clinical trial demonstrated that patients treated with a combination of the antipsychotic drug haloperidol and dipyridamol (an ADO uptake inhibitor, increasing ADO availability in the synaptic cleft) had a greater improvement in positive symptoms (delusions and hallucinations) when compared with patients treated with haloperidol alone.[103] Similar results were obtained when allopurinol had been used as an adjuvant for treatment of patients with refractory positive symptoms.[104] However, neither dipyridamol nor allopurinol (inhibitor of ADO metabolic degradation) were effective in the treatment of schizophrenic patients when used as monotherapy.[105,106]

A decrease in the expression of A2A receptor protein and mRNA in striatum of schizophrenic patients has been reported, whereas no alteration in the expression of A1 receptors was observed.[107] On the other hand, the upregulation of A2A receptor expression observed in some groups of schizophrenics may represent a compensatory and adaptive mechanism to ADO hypofunction or a response to antipsychotic treatment.[108,109] A2A receptor-deficient mice showed anatomical (ventricle enlargement) as well as behavioral alterations (reduced startle habituation and prepulse inhibition) similar to those observed in schizophrenic patients.[110,111] Accordingly, specific activation of A2A receptors reversed impairments in prepulse inhibition observed in an animal model of SCZ.[112] ADO effects are not restricted to neurons as demonstrated by the fact that mice lacking specifically astrocytic A2A receptors show psychomotor and memory impairments similar to those observed in SCZ.[113] As expected, augmentation of ADO levels through pharmacological inhibition of ADO kinase resulted in improvements of the psychotic symptoms in an animal model for SCZ. Mice overexpressing ADO kinase with intrastriatally transplanted ADO-releasing cells regained their locomotor responsiveness to amphetamine. Impairment of cognitive functions was also reversed when cells releasing ADO had been grafted into the hippocampus.[114] Moreover, reduced activity of ectonucleotidases and supposedly diminished levels of ADO were observed in the post-mortem striatum of schizophrenic patients when compared with controls.[115] Although these data on ADO receptor expression point to a general hypoadenosinergic state in SCZ, we should be careful with their interpretation, as such a state might be present only in a subgroup of SCZ patients because reduction in A2A receptor expression was not observed in 50% of patients.[107] It could be postulated that SCZ, similar to other brain diseases, also results from an imbalance between A1 and A2A receptor activities.[30,31] However, more functional studies are necessary to better distinguish how A1 and A2A receptors are involved in SCZ. Even here one should be careful, as the same subtype of ADO receptor may be differently implicated in SCZ, depending on the brain area considered, as demonstrated for A2A receptors and fear conditioning/anxiety behavior.[116]

In spite of increasing evidence of ADO involvement in SCZ, studies have failed in identifying A2A receptor polymorphisms as risk factors for this illness.[117,118] However, genetic variants of the A1 receptor and ADA are likely good candidate markers for SCZ. Some SNPs are more frequent in Japanese schizophrenic populations and should be further analyzed as susceptibility factors for the disease.[119] ADA 22G/A is less active than the G/G genotype, and its expression is probably linked to higher ADO concentrations. A significantly lower frequency of this polymorphism was found in schizophrenic patients.[120] In agreement, haloperidol was found to inhibit ATP hydrolysis and ADO deamination that could, to some extent, contribute to its therapeutic effects.[121]

The fact that dopamine release in the striatum and nucleus accumbens is induced by extracellular ATP provides indirect evidence that P2X and P2Y receptors could influence SCZ

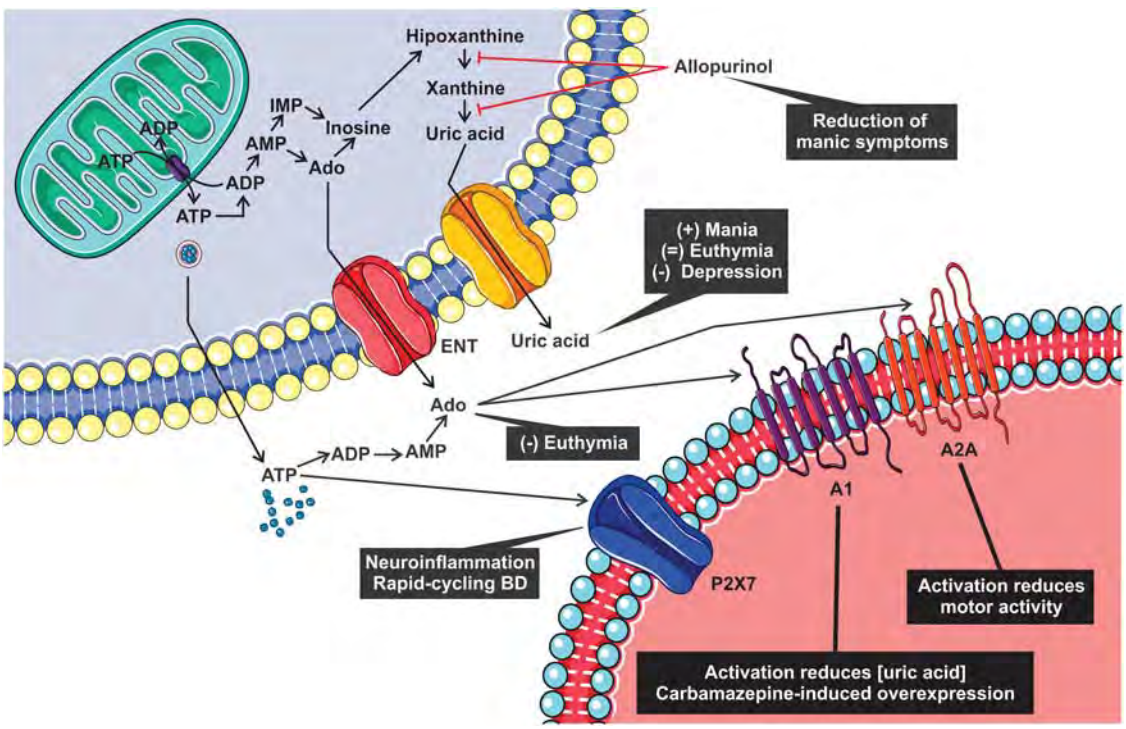

Figure 1. Purinergic pathway and dysfunction hypothesis in bipolar disorder (BD). Summary of how different components of the purinergic system are implicated in bipolar disorder. Note that this scheme does not reproduce purinergic signaling in a specific cell type or tissue. It represents a general and simplified overview of intracellular and extracellular purinergic metabolism and release related to BD. Although both intracellular and extracellular breakdown of adenosine triphosphate (ATP) to adenosine (ADO) is possible, the conversion of ADO to uric acid appears to be mainly intracellular, as shown by our scheme.

development.[122,123] ATP-induced release of dopamine was largely inhibited by Reactive Blue-2, a P2Y receptor antagonist, suggesting predominant participation of P2Y receptors.[124]

Hempel *et al.*[125] showed that the tricyclic antipsychotics prochlorperazine and trifluoperazine allosterically and negatively modulate human P2X7 receptor activity. Therefore, one may speculate that the antipsychotic-induced inhibition of the P2X7 receptor would contribute to therapeutic efficacy.[126,127] In agreement, both pharmacological blockade and genetic silencing of the P2X7 receptor alleviated schizophrenic-like behavior in an animal SCZ model.[128] In view of P2X7 receptor participation in memory control,[129] these data indicate that the P2X7 receptor might be involved in modulating SCZ symptomatology. However, polymorphisms in the gene encoding the P2X7 receptor were not associated with genesis of SCZ.[130]

BIPOLAR DISORDER

It was recognized, in the late nineteenth century, that some patients with gout or hyperuricemia experiencing abnormal mood conditions improved after lithium treatment, not only from gout or hyperuricemia but also from mood disturbances.[131,132] Since that time, the link between uric acid (UA) levels and mood disturbances has given rise to the purinergic dysfunction hypothesis for BD.[133–135] High levels of UA in bipolar patients were associated to impulsivity and excited behavior, irritated mood, hyperthymic temperament and severe manic symptoms,[135,136] whereas low levels were linked to depressive mood scores, independently of the disorder phase[137,138] (Figure 1). Lowest levels of UA were observed in MDD patients, suggesting that UA would be a useful biomarker to differentiate BD from MDD.[139] Furthermore, BD patients have increased risks of developing gout,[140] whereas allopurinol, an inhibitor of xanthine oxidase used for treating and preventing gout, reduces manic symptoms when used as an add-on therapy for treatment-resistant BD patients (Figure 1), as shown in open clinical trials.[141–144] Strikingly, allopurinol was efficient against aggressive behavior observed in dementia patients, corroborating the association between UA levels and impulsivity/aggressiveness.[145]

Peripherally, ADO levels, but not other purinergic metabolites (inosine, hypoxanthine, xanthine or UA), have been recently shown to be decreased in blood serum of euthymic bipolar patients[146] (Figure 1). This fact was associated to higher psychosocial functioning impairments and also corroborated with other hypotheses for the pathophysiology of BD, such as neuroinflammation and microglial dysfunction modulated by ADO.[146] In addition, a meta-analysis performed by Hirota and Kishi[147] showed benefits of ADO modulators for bipolar and schizophrenic patients.

In the central nervous system, ADO plays important roles in neuron and glia interactions across the excitatory responses via the glutamatergic system. Furthermore, carbamazepine, an antiepileptic drug with mood stabilizer activity and an A1 receptor antagonist, modulates ADO and receptor expression levels during chronic treatment in patients and animal models, corroborating that A1 receptor agonism may open new avenues for novel therapeutics[148,149] (Figure 1). However, the involvement of A1 receptor encoding gene polymorphisms in development of BD is still controversially discussed.[150] Still regarding P1 receptors, the A2A subunit was upregulated in platelets from bipolar patients treated with typical but not atypical antipsychotics, possibly through the heteromeric complex formed by A2A and D2 receptors.[151]

Among P2X receptors, several studies showed a contentious correlation between SNPs in P2X7 receptor gene/promoter and affective disorders, indicating a nonspecific genetic involvement in BD etiology, development or cognitive impairment.[84–86,152–159] On the other hand, animal studies demonstrated clearer correlation between P2X7 receptor targeting and emotional behavior associated with BD and MDD.[160] P2X7 receptor expression was shown to be increased by sleep deprivation; rapid cycling BD was also associated with higher expression of P2X7 receptors.[158] Thus, there is a growing interest in developing therapeutics based on targeting P2X7 receptors in BD and MDD.[161,162] Moreover, neuroinflammation linked to P2X7 receptor roles is also implicated in BD.[163,164] Figure 1 summarizes the action of diverse purinergic system components in BD.

AUTISM SPECTRUM DISORDERS

Initial studies reported increased nucleotide catabolism in patients with seizures, ataxia, neurodevelopment impairment and poor social interaction. Patients treated with oral administered pyrimidine nucleotides (UMP, CMP) showed significant improvement.[165]

Regarding extracellular purine metabolism, genotype and allele frequencies of ADA-Asn8 polymorphism were increased by a factor of two in Italian autism spectrum disorder (ASD) populations. This polymorphism is 35% less functional than the more common ADA-Asp8 allele, suggesting neuronal A1 receptor overstimulation in ASD,[166] once cell membrane surface ADA and A1 receptor expression are physically related. Otherwise, A1 receptor activity has been claimed to be neuroprotective, and some evidence points to autistic symptom improvement with ADO increase.[167,168] In general, A1 receptors show a tonic, constant low activity, preventing glutamate overrelease, interacting mainly with $G_{i/o}$ proteins and hyperpolarizing neurons by activating voltage-dependent ion channels. A2A receptors are activated by higher levels of ADO, stimulating glutamatergic signaling and promoting long-term potentiation.[20]

Notwithstanding, a balance between different levels of ADO and distinct activity profiles of P1 receptors in distinct brain areas may lead to diverse results and explain apparently controversial findings.[30] For instance, although ADA activity decreases extra- and intracellular ADO levels, ADA/A1 receptor association may facilitate signaling of this receptor.[169]

Freitag *et al.*[170] investigated the association between SNPs in the A2A receptor gene and ASD. Although rs2298383 and rs2236624 SNPs were identified as genetic risk factors for autism as suggested by decreased heterozygosity in patients, others (rs3761422-CT/TT, rs5751876-CT/TT and rs35320474-T−/−−) were associated with the occurrence and severity of autism symptoms, such as anxiety, repetitive behavior/stereotypy, impaired social interaction and verbal communication (Figure 2a),[170] demonstrating, once again, that A2A receptors modulate behavior in both healthy and disease conditions.[171–178] Indeed, A2A receptor KO mice are more anxious than wild-type controls.[172] Striatum A2A receptor KO mice have habit formation impairment and are more goal directed and flexible than the wild-type group under lever-press training,[173] whereas striatum A2A receptor activation impaired goal-directed behavior.[175] This receptor is highly expressed by striatopallidal neurons,[179] through which it regulates goal-directed behavior acquired by operant conditioning, habit formation through stimulus-response learning (goal-directed/habit formation shift)[174,175] and memory.[176] Moreover, A1 and A2A receptor agonists attenuate stereotypy in animal models of ASD symptomatology in a way that probably depends on the interaction with dopamine D2 receptors and activation of the indirect pathway.[171] Similar results were obtained by various researchers for ADO receptor pathways, mainly concerning the A2A receptor related to ASD behaviors, and are strong evidence of a direct role of the adenosinergic system on ASD.

A3 receptor agonists enhance the surface expression and activity of antidepressant-sensitive 5-HT transporters whose gain-of-function variants have been associated to both autism and obsessive–compulsive disorder.[180,181] Accordingly, the hyperfunctional L90V and V171I A3 receptor variants were identified in ASD

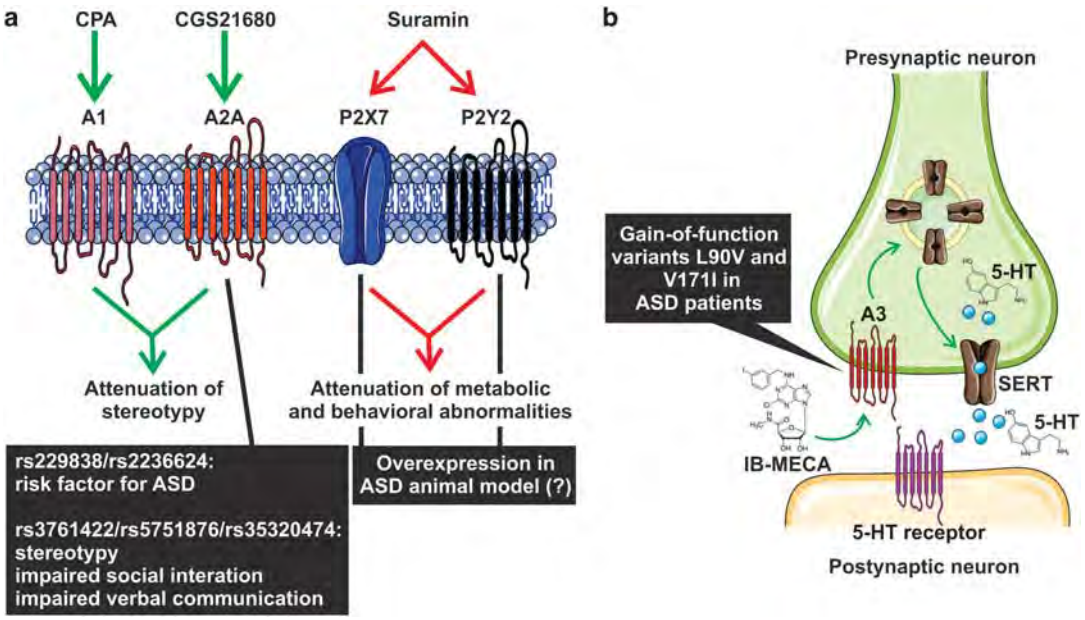

Figure 2. Involvement of the purinergic system in autism spectrum disorder (ASD). (**a**) Although the activation of P1 receptors (A1 and A2A receptors; green arrows) ameliorates ASD symptoms, such as stereotypy, inhibition of P2 receptors (mainly P2X7 and P2Y2 subtypes that are likely overexpressed in ASD animal models; red arrows) has the same effect, attenuating metabolic and behavioral alterations observed in ASD animal models. On the other hand, single-nucleotide polymorphisms (SNPs) in the gene encoding the A2A receptor have been found that increase either the susceptibility to ASD or the occurrence of symptoms usually observed in the disease. (**b**) A3 receptors and the antidepressant-sensitive 5-hydroxy-tryptamine (5-HT) transporter (SERT) are presynaptically colocalized. Selective activation of A3 receptors by IB-MECA increases the surface expression of SERT and, consequently, 5-HT reuptake into the presynaptic neuron (gain-of-function variants of SERT have been found in ASD patients). Accordingly, the hyperfunctional A3 receptor variants L90V and V171I were identified in ASD patients. Therefore, A3 receptor antagonists may be potential candidates for development of novel therapeutics against ASD.

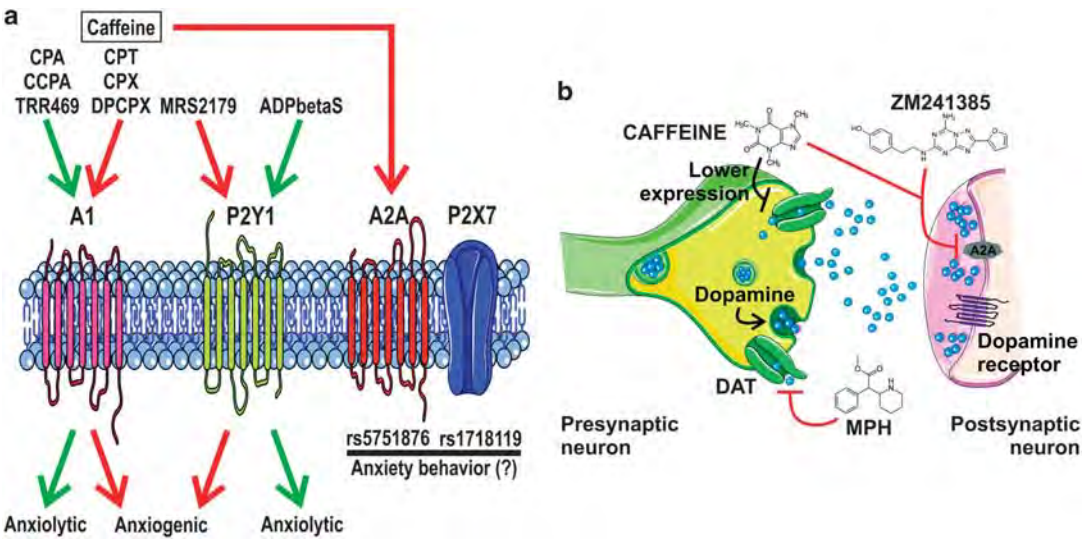

Figure 3. Purinergic system in anxiety and attention deficit/hyperactivity disorder (ADHD). (**a**) Antagonism (red arrows) of both A1 (by caffeine, CPT, CPX, and DPCPX) and P2Y1 receptors (by MRS2179) is anxiogenic, whereas anxiolytic effects have been observed with A1 receptor activation (by CPA, CCPA, and TRR469; the latter is an A1-positive allosteric modulator) and P2Y1 receptor activation by the P2Y receptor agonist ADPβS. Receptor activation is indicated by green arrows. Although polymorphisms in the genes coding for A2A (rs5751876) and P2X7 receptors (rs1718119) have been suggested to predispose to anxiety, these results are still controversial and lack corroborating evidence. (**b**) The most used therapeutic against ADHD, methylphenidate (MPH), acts by blocking the dopamine transporter (DAT) with a consequent increase in dopamine availability in the synaptic cleft. Caffeine augments responsiveness to MPH, probably by reducing DAT expression. Moreover, caffeine inhibits ADO receptors. Accordingly, the specific A2A receptor antagonist ZW241385 is capable of alleviating memory impairments observed in ADHD. CCPA, 2-chloro-N^6-cyclopentyladenosine.

patients and some nonaffected relatives, but not in controls (Figure 2b).[33,181] These residues are close to the ADO-binding site, explaining why they affect A3 receptor activity. The interactions between the adenosinegic, dopaminergic and serotoninergic systems illustrate the need of further studies in order to better explain behavior and its disorders at a molecular level.

P2 receptor actions have also been implicated in ASD. Wyatt *et al.*[182] observed, in P2X4 receptor KO mice, significant reduction

in sensory and social task performance, vocalization responses and a plausible deficit in the ability to extract and filter relevant information from the external milieu, suggesting that P2X4 receptors regulate information processing and perceptual and sociocommunicative functions. Compared with control mice, KO mice expressed less *N*-methyl-D-aspartate receptors in the prefrontal cortex, and increased expression of α-amino-3-hydroxy-5-methyl-4-isoxazole propionic acid receptors in the hippocampus.[182]

Naviaux *et al.*[183] hypothesized that autism and comorbidities can result from metabolic states associated with cellular danger response sustained by the purinergic system. Therefore, they investigated these pathways and autistic behavior in the offspring of a maternal immune activation mouse model of ASD. Compared with control animals, maternal immune activation mice showed autistic behavior, decreased synaptosomal expression of P2X7 and P2Y2 receptors as well as their effectors phospho-calmodulin-dependent protein kinase II and phospho-extracellular signal–regulated kinase-1/2 together with synaptosomal ultrastructural abnormalities. Mitochondrial responses in the maternal immune activation model led to increased purine and pyrimidine release and, consequently, to downregulation of P2X7 and P2Y2 receptor expression as a compensatory response.[183] Treatment with the P2 receptor antagonist suramin, which is more potent in inhibiting P2Y2 receptors than P2X7 receptors, normalized autism-like behavior, suggesting the involvement of a hyperactivated purinergic system in this disorder. Subsequently, a single suramin dose was enough to correct over 90% of metabolic pathway disturbance and all tested behavioral abnormalities (Figure 2a).[184] Suramin produced similar results in a genetic Fragile X syndrome model, characterized by cognitive impairments frequently associated with ASD,[185] and led to symptom improvement in autistic patients.[186] Other mechanisms rather than P2 receptor inhibition cannot be ruled out, as suramin does not only interfere with the purinergic system.[187] Moreover, results from Naviaux *et al.*[183] evidenced that the purine metabolism was strongly involved in those ASD models.[188]

Mitochondrial components, once in the extracellular medium, may function as 'pathogens' and trigger inflammatory responses, as observed in ASD patients.[189] We should highlight once again that the purinergic system is related to inflammation, and that ATP also acts as a danger signal molecule.[190,191] In fact, P2X7 receptor activation by ATP release may mediate brain inflammation as already postulated for other psychiatric diseases, such as MDD, SCZ and BD discussed here.[73,127,163]

ANXIETY DISORDERS

In anxiety-related behavior tests, both A1 and A2A receptor KO models showed increases in anxiety compared with wild-type animals.[192–194] Heterozygous mice did not develop any anxiety phenotype indicating that the complete absence of ADO receptor expression is necessary for anxiety induction. Moreover, inhibition of A1 but not of A2A receptors resulted in anxiety-like behavior in zebrafish.[195] However, a recent work showed that A2A receptor antagonism is anxiolytic in male animals pretreated with glucocorticoid.[196] In addition, A1 receptor activator TRR469 promotes anxiolytic effects comparable to diazepam without inducing sedation and motor impairment observed with diazepam (Figure 3a).[197]

Guanosine has anxiolytic effects in rats, correlating with increased ADO and reduced glutamate levels in the cerebrospinal fluid.[198] Guanosine effects on glutamate release are mimicked by the A1 receptor agonist 2-chloro-N^6-cyclopentyladenosine, but inhibited by the A1 receptor antagonist 8-cyclopentyl-1,3-dipropylxanthine, indicating that activation of A1 receptors prevents anxiety behavior.[198] In agreement, activation of A1 receptors using 2-chloro-N^6-cyclopentyladenosine or N^6-cyclopentyladenosine in mice showed anxiolytic properties, whereas the use of A1 receptor antagonists such as 8-cyclopentyl-1,3-dimethylxanthine and 8-cyclopentyltheophylline promoted anxiety behavior (Figure 3a).[199,200]

Caffeine increases panic attacks in patients suffering from panic disorder,[201] the effect being more prominent in the presence of 1976C>T and 2592C>T A2A receptor polymorphisms,[202] suggesting that A2A receptors also play a role in anxiety disorder. In agreement, deletion of A2A receptors in the forebrain augmented startle response and induced anxiety behavior in animals,[116] and this has been reproduced in patients.[203,204] Caffeine-induced increase of startle response is more pronounced in patients carrying the A2A receptor 1976C>T risk genotype.[204] In addition, A2A receptor polymorphism 1976T/C is associated with development of panic attacks and elevated anxiety.[202,205,206] This finding was partially reproduced with an European population but studies with Asian populations did not reveal any connections between A2A receptor polymorphisms and anxiety development[207] (Figure 3a). This suggests that Caucasian populations are more prone to effects of A2A receptor 1976T/C polymorphism.

Among P2 receptors, a SNP in the P2X7 receptor gene (rs1718119) is associated with an increase in anxiety-related episodes, such as agoraphobia and panic attack (Figure 3a).[208] On the other hand, P2X7 receptor KO mice did not reveal anxiety-like behavior,[78] contradicting previous findings in human subjects.[208,209] The P2Y1 subtype should be important in modulating anxiety, as anxiolytic-like responses induced by the nonspecific P2Y receptor agonist ADPβS in mice are blocked by the selective P2Y1 receptor antagonist MRS 2179 (Figure 3a). The P2Y1 receptor-evoked anxiolytic effect is likely mediated by the activation of nitric oxide synthase, as its inhibitor L-nitro-arginine methyl ester antagonized this effect. Furthermore, the natural nitric oxide synthase substrate L-arginine reversed anxiogenic properties of pyridoxal-phosphate-6-azophenyl-2',4'-disulfonic acid (PPADS), a nonspecific P2 receptor antagonist.[210]

ATTENTION DEFICIT/HYPERACTIVITY DISORDER

Higher plasma levels of UA have been found positively correlated with impulsivity and hyperactivity traits, as continual predisposition in psychiatric conditions, like attention deficit/hyperactivity disorder (ADHD). Methylphenidate (MPH), a dopamine and noradrenaline reuptake inhibitor, diminished UA plasma concentration in children.[211] Unipolar depression patients suffering from ADHD showed higher plasma UA levels when compared with patients suffering from unipolar depression alone.[212] In agreement, positive correlation exists between higher UA plasma levels and impulsiveness/excitement seeking traits in humans.[136] Similar results were obtained in a hyperuricemia mouse model.[136]

Caffeine produced positive effects in patients suffering from ADHD, providing a direct link between adenosinergic signaling and ADHD.[213] Caffeine has been used to study behavior, memory and cognitive dysfunction in ADHD. It increases arousal, as indicated by skin conductance level changes resulting from, for instance, sweating and skin blood flow increase triggered by sympathetic autonomic activation,[214] both in healthy and in ADHD children.[215,216] However, caffeine-induced augmentation in arousal of ADHD patients depends on symptom severity and is strongly associated with hyperactivity and impulsivity.[216] Moreover, rats previously and chronically treated with caffeine during adolescence augmented locomotor activity when challenged with an inactive MPH dose, suggesting a caffeine-induced cross-sensitization to MPH.[217] Besides the blockade of A2A receptor, another underlying mechanism could be caffeine-induced reduction in the expression of dopamine transporter and, consequently, in dopamine reuptake in the frontal cortex and striatum, as demonstrated with spontaneously hypertensive rats, an animal model for ADHD (Figure 3b).[218–221] In this model, chronic caffeine treatment led to attention and memory performance

Table 1. Involvement of purinergic system components in psychiatric disorders

Purinergic system	*Uric acid + metabolism*	*P1 receptors*	*P2 receptors*	*Enzymes*	*Guanosine receptors*
Psychiatric disorder					
Major depressive disorder	58	41, 44, 48–56, 76	68, 78–80, 82–86	57, 59	
Schizophrenia	104–106, 121	93, 101, 103, 107, 108–113, 117–119	125, 128, 130	115, 120	
Bipolar disorder	133, 136–138, 145	146, 148–151	84–86, 152–158, 163		
Autism spectrum disorders	165	33, 166, 167, 170, 172, 181	182–186	166	
Anxiety disorders		116, 193–197, 199–207	78, 208–210		198
Attention deficit/hyperactivity disorder	211, 212	170, 216–219, 221–226			

improvements.[221] Despite the positive effects of caffeine in ADHD patients, its efficacy as a drug for ADHD treatment has not been established.[213]

Augmented A1 receptor expression in mouse frontal cortex, a region involved in the MPH-mediated effects, occurred following acute MPH overdosage, suggesting participation of A1 receptors in ADHD pathophysiology and responses to MPH exposure.[222] The relation between A2A receptors and motor hyperactivity observed in ADHD is controversially discussed. A2A receptors may favor ADHD given their enhanced expression and colocalization with dopamine transporter in the frontal cortex of spontaneously hypertensive rats when compared with control animals.[221] In agreement, both caffeine and the selective A2A receptor antagonism reversed social memory impairments observed in spontaneously hypertensive rats (Figure 3b).[218] However, in cocaine-insensitive dopamine transporter mice, an animal model of ADHD hyperactivity, A2A receptor blockade resulted in increased motor activity, whereas A2A receptor activation led to decreased motor activity.[223] By using another ADHD animal model, a positive correlation was confirmed between A2A receptor expression and hyperactivity that was exacerbated by the treatment with psychostimulant drugs.[224]

In Tourette syndrome, a disorder that can share etiological features with ADHD, polymorphisms in the genes encoding A1 and A2A receptors have opposite effects, suggesting that such SNPs might also be involved in ADHD.[225] Although A1 SNP rs2228079 was associated with reduced Tourette syndrome severity, A2A SNP rs5751876 increases the risk of Tourette syndrome.[225] Previous work demonstrated that other A2A polymorphisms (rs3761422 and rs35320474), besides rs5751876, directly correlate with attention deficits and hyperactivity in ADHD patients.[226] As mentioned before, A2A receptor rs5751876 polymorphism has already been associated with ASD and anxiety.[170,205]

CRITICAL REVIEW: FROM NEURODEVELOPMENT TO PSYCHIATRIC DISORDERS

As one can notice, there is a large body of evidence for diverse components of the purinergic system involved in psychiatric disorders to be explored as potential therapeutic targets. As most of these works have been restricted to genetic/pharmacological approaches and to the use of postnatal animal models, a plethora of information regarding the plausible neurodevelopmental nature of psychiatric diseases may be missing. Over the past 10 years, our research group has collected many results on expression and activity patterns of P2 receptors during neurogenesis. Importantly, P2 receptors are differentially expressed during the course of proliferation, migration and differentiation into distinct neural phenotypes expressing functional cholinergic, GABAergic and glutamatergic neurotransmitter receptors.[28] Here we propose some hypotheses on how purinergic signaling could be the neurodevelopmental basis of psychiatric disorders. For instance, we have demonstrated that P2X7 receptor expression is higher in undifferentiated embryonic stem cells compared with neural-differentiated cells, and blockade of P2X7 receptor activity induces the differentiation into neurons.[227] Moreover, as stated earlier, P2X7 receptors control the hippocampal concentration of brain-derived neurotrophic factor,[80,81] and antidepressant fluoxetine is able to increase brain-derived neurotrophic factor mRNA expression in hippocampus, ventral tegmental area and nucleus accumbens.[228] Therefore, it could be hypothesized that anatomical brain alterations observed in MDD patients,[229] such as reduced gray matter volume in areas implicated in the emotional control, would have their onset in development, in which increased P2X7 receptor activity would play an important role. This hypothesis could be investigated by mimicking the neurodifferentiation process of induced pluripotent stem cells obtained from MDD patients.

A similar hypothesis could be formed and tested for SCZ that is also characterized by reduced gray matter volume and ventricle enlargement.[230] However here, besides P2X7 receptor hyperactivity, decreased A2A receptor activity would contribute to these pathological consequences.[111] Furthermore, expression and activity alterations in brain cytoarchitecture and proteins involved in neuronal migration indicate that SCZ can result from impaired cell migration during the development of the cerebral cortex.[231,232] Another hypothesis is that disturbed P2X and P2Y receptor expression during neurodevelopment might be one of the underlying mechanisms. As we have observed, these receptors follow a specific expression pattern along neural differentiation of rat embryonic telencephalon neurospheres, and ATP induces neural migration.[233]

Recent data have indicated that BD is also a neurodevelopmental disorder, and that an impaired neural network is involved in its pathogenesis. By using neurons derived from induced pluripotent stem cells obtained from BD patients, human postmortem brain samples and an animal model, Snyder and coworkers[234] shed more light on the mechanisms by which lithium acts. Their data show that lithium acts by promoting dephosphorylation of collapsin response mediator protein-2 (CRMP2) through glycogen synthase kinase-3β inhibition and, consequently, by favoring CRMP2 interaction with cytoskeleton proteins that, in turn, rescue suitable dendritic spine formation and neural network functioning.[234] We have also observed alterations in the expression of purinergic system components, mainly of ADO receptors, after treating a BD animal model (unpublished data). As the activation of A2A and P2X7 receptors triggers AKT–glycogen synthase kinase-3β signaling pathway,[235,236] controlling expression of these two most implicated purinergic receptors in BD, could be an additional mechanism, by which lithium regulates the phosphorylation state of CRMP2. Concomitantly, lithium-induced reduction in P2X7 receptor expression could protect the cells against the neuroinflammatory process implicated in BD.[163,164] CRMP2 may also be important for further psychiatric disorders, as

its expression upregulation was observed upon treatment with an antidepressant compound (see Chen *et al.*[237]).

PERSPECTIVES

Here, we discuss recent findings that together point to an important link between the purinergic system and psychiatric diseases, as summarized in Table 1. Although remarkable progress has been made regarding the participation of neurotransmitter systems and molecular mechanisms underlying the pathophysiology of psychiatric disorders, a view based only on traditional monoaminergic neurotransmission is oversimplified, and more attention should be drawn on other signaling mechanisms.

As the purinergic system plays a special and important regulatory role in brain monoaminergic pathways, increasing efforts have been undertaken in targeting it. For example, the heteromeric complex of A2A and dopamine D2 receptors is a poorly explored target involved in pathological and therapeutic mechanisms. In fact, dopaminergic dysfunction is essentially observed in many psychiatric conditions and has been recently investigated in animal models not only for ADHD but also for bipolar mania, established through the selective inhibition of dopamine transporters and subsequent overstimulation of dopamine receptors.[238] However, specific investigations of purinergic modulation under these conditions are missing and could provide a key contribution to the understanding of psycho- and motor-stimulation through dopaminergic signaling. Similarly, the glutamatergic hypothesis for the psychiatric disorders here discussed lacks specific investigations through a purinergic perspective. Notably, both P1 and P2 receptors through A2A and P2X7 subtypes prevent hyperexcitability and glutamate excitotoxicity, providing a possible target for controlling the progression and possible neurodegeneration in psychiatric conditions (for better understanding, see Parpura and Schousboe[239]). In this sense, we should also mention that the dysfunctional circuitry overlap between several psychiatric conditions could provide a clue for better understanding disease pathophysiology and etiology. Indeed, novel common mechanisms would facilitate further etiological classification of these disorders and the development of new drugs that may be used for the treatment of different psychiatric disorders at the same time.

Obtained results for the most investigated psychiatric disorders refer to ADO receptors (for all of the diseases, at least 83% of the current literature refer to involvement of ADO receptors). Few data have been published pointing at other components of the purinergic system, despite their implications in processes relevant for central nervous system development, such as cellular migration and neurodifferentiation (for instance, P2 receptor signaling is closely related to neurodevelopment, and its investigation is still at the beginning or even lacking for many psychiatric disorders). This could result, to some extent, from historical questions. ADO-induced effects were early recognized, and coffee use dates back to the tenth century. As many psychiatric diseases apparently have neurodevelopmental origins, further investigations may reveal P2 receptor functions in psychiatric conditions.

Investigation of molecular pathways of human behavior is necessarily indirect because of obvious ethical issues by employing *in vitro* and also animal models. However, researchers in this field have clear awareness of their model limitations. It is quite difficult to classify behavior disorders in humans, and we are not sure how closely they can be observed in animal models that are, at best, mimicking some behaviors of these disorders and do not reproduce a disease in its complexity. Moreover, the interpretation of results obtained with animal models will always be controversial, because psychiatric diseases share many symptoms and have similar patterns of neurotransmitters involved. Deletion or knockdown of genes or pharmacological receptor stimulation/blockade have multiple effects on the entire organism, not restricted to the brain. Consequently, some effects observed in KO models are not necessarily linked to the pathophysiology of a determined psychiatric condition.

Furthermore, our current nosological classifications are not the best ones. They are based on behavioral phenotypes because of the lack of diagnostic molecular markers, and there is overlap between supposed discrete disorders and even between disorders and normal/functional behavior. Bias could also result from population stratification, making candidate gene investigation for psychiatric disorders a challenging task. Further effort is needed for elucidating molecular mechanisms, how purinergic receptors trigger pathways, linking purinergic signaling with other neurotransmitters, neuromodulators, neuropeptides and neurotrophic factors and psychiatric diseases.

A better understanding of the cellular source of ATP release and the role of its metabolites in glial–neuron communication, as well the specific functions of purinergic receptors in neuropathological context of each psychiatric disorders, is a challenge. Despite the limitations of genetic/pharmacological approaches and animal models, progress has been made and increased our understanding of how the purinergic system and psychiatric disorders are connected, and we are more aware of the importance of this system for normal brain functioning.

In addition to genetic/pharmacological approaches, *in vitro* modulation of psychiatric conditions such as by induced pluripotent stem cells obtained from patients has arisen as an important tool for the understanding of developmental stages and progressive mechanisms of psychiatric disorders in a more specific and personalized way.[240] Furthermore, this approach can provide further insights into the action of pharmacological interventions as well on molecular mechanisms underlying purinergic signaling in those conditions. For example, induced pluripotent stem cells derived from bipolar patients were recently used as a tool for better understanding lithium-response pathways,[234] as stated earlier. We believe that different approaches leading to complementary and concordant results will allow us to get closer to a meaningful explicative theory for many of the psychiatric disorders discussed in our review.

In summary, the purinergic system represents a promising research area for future and deeper insights into the molecular basis of psychiatric diseases and may allow development of novel therapies.

CONFLICT OF INTEREST

The authors declare no conflict of interest.

ACKNOWLEDGMENTS

HU acknowledges grant support from the Brazilian funding agencies Fundação de Amparo à Pesquisa do Estado de São Paulo (São Paulo Research Foundation, FAPESP Proj. Nr. 2012/50880-4) and Conselho Nacional de Desenvolvimento Científico e Tecnológico (CNPq) for fellowship support. AC, ICN and YN thank FAPESP for post-doctoral fellowships (FAPESP Proj. Nr. 2013/02293-5, 2015/18730-0 and 2015/14343-2, respectively). JC-V thanks CNPq for fellowship support. The doctoral thesis research of ARGC and MCBG is supported by fellowships from CNPq.

REFERENCES

1 Burnstock G, Campbell G, Satchell D, Smythe A. Evidence that adenosine triphosphate or a related nucleotide is the transmitter substance released by non-adrenergic inhibitory nerves in the gut. *Br J Pharmacol* 1970; **40**: 668–688.

2 Su C, Bevan JA, Burnstock G. [3H]adenosine triphosphate: release during stimulation of enteric nerves. *Science* 1971; **173**: 336–338.

3 Nakanishi H, Takeda H. The possible role of adenosine triphosphate in chemical transmission between the hypogastric nerve terminal and seminal vesicle in the guinea-pig. *Jpn J Pharmacol* 1973; **23**: 479–490.
4 Langer SZ, Pinto JE. Possible involvement of a transmitter different from norepinephrine in the residual responses to nerve stimulation of the cat nictitating membrane after pretreatment with reserpine. *J Pharmacol Exp Ther* 1976; **196**: 697–713.
5 Burnstock G. Do some nerve cells release more than one transmitter? *Neuroscience* 1976; **1**: 239–248.
6 French AM, Scott NC. Evidence to support the hypothesis that ATP is a co-transmitter in rat vas deferens. *Experientia* 1983; **39**: 264–266.
7 Burnstock G. Physiology and pathophysiology of purinergic neurotransmission. *Physiol Rev* 2007; **87**: 659–797.
8 Burnstock G, Krügel U, Abbracchio MP, Illes P. Purinergic signalling: from normal behaviour to pathological brain function. *Prog Neurobiol* 2011; **95**: 229–274.
9 Burnstock G, Dumsday B, Smythe A. Atropine resistant excitation of the urinary bladder: the possibility of transmission via nerves releasing a purine nucleotide. *Br J Pharmacol* 1972; **44**: 451–461.
10 Ralevic V, Burnstock G. Receptors for purines and pyrimidines. *Pharmacol Rev* 1998; **50**: 413–492.
11 Abbracchio MP, Burnstock G, Boeynaems J-M, Barnard EA, Boyer JL, Kennedy C *et al.* International Union of Pharmacology LVIII: update on the P2Y G protein-coupled nucleotide receptors: from molecular mechanisms and pathophysiology to therapy. *Pharmacol Rev* 2006; **58**: 281–341.
12 Cunha RA. Regulation of the ecto-nucleotidase pathway in rat hippocampal nerve terminals. *Neurochem Res* 2001; **26**: 979–991.
13 Verkhratsky A, Burnstock G, Zimmermann H, Abbracchio MP. Purinergic signalling in the nervous system: an overview. *Trends Neurosci* 2009; **32**: 19–29.
14 Zimmermann H. Ectonucleotidases in the nervous system. *Novartis Found Symp* 2006; **276**: 113–128, 128-130, 233–237, 275–281.
15 Burnstock G. A basis for distinguishing two types of purinergic receptor. In: Straub RW, Bolis L. (eds). *Cell Membrane Receptors for Drugs and Hormones: A Multidisciplinary Approach*. Raven Press: New York, 1978, pp 107–118.
16 Fredholm BB, Abbracchio MP, Burnstock G, Dubyak GR, Harden TK, Jacobson KA *et al.* Towards a revised nomenclature for P1 and P2 receptors. *Trends Pharmacol Sci* 1997; **18**: 79–82.
17 Ciruela F, Albergaria C, Soriano A, Cuffí L, Carbonell L, Sánchez S *et al.* Adenosine receptors interacting proteins (ARIPs): behind the biology of adenosine signaling. *Biochim Biophys Acta* 2010; **1798**: 9–20.
18 Di Virgilio F. Purines, purinergic receptors, and cancer. *Cancer Res* 2012; **72**: 5441–5447.
19 Cunha RA, Correia-de-Sá P, Sebastião AM, Ribeiro JA. Preferential activation of excitatory adenosine receptors at rat hippocampal and neuromuscular synapses by adenosine formed from released adenine nucleotides. *Br J Pharmacol* 1996; **119**: 253–260.
20 Cunha RA. How does adenosine control neuronal dysfunction and neurodegeneration? *J Neurochem* 2016; **139**: 1019–1055.
21 Burnstock G, Kennedy C. Is there a basis for distinguishing two types of P2-purinoceptor? *Gen Pharmacol* 1985; **16**: 433–440.
22 Burnstock G. The past, present and future of purine nucleotides as signalling molecules. *Neuropharmacology* 1997; **36**: 1127–1139.
23 North RA. P2X receptors: a third major class of ligand-gated ion channels. *Ciba Found Symp* 1996; **198**: 91–105, 105-109.
24 Barrera NP, Ormond SJ, Henderson RM, Murrell-Lagnado RD, Edwardson JM. Atomic force microscopy imaging demonstrates that P2X2 receptors are trimers but that P2X6 receptor subunits do not oligomerize. *J Biol Chem* 2005; **280**: 10759–10765.
25 Barrera NP, Ge H, Henderson RM, Fitzgerald WJ, Edwardson JM. Automated analysis of the architecture of receptors, imaged by atomic force microscopy. *Micron* 2008; **39**: 101–110.
26 Dubyak GR, El-Moatassim C. Signal transduction via P2-purinergic receptors for extracellular ATP and other nucleotides. *Am J Physiol* 1993; **265**: C577–C606.
27 Verkhratsky A, Anderova M, Chvatal A. Differential calcium signalling in neuronal-glial networks. *Front Biosci (Landmark Ed)* 2009; **14**: 2004–2016.
28 Burnstock G, Ulrich H. Purinergic signaling in embryonic and stem cell development. *Cell Mol Life Sci* 2011; **68**: 1369–1394.
29 Burnstock G. Introductory overview of purinergic signalling. *Front Biosci (Elite Ed)* 2011; **3**: 896–900.
30 Cunha RA. Neuroprotection by adenosine in the brain: from A(1) receptor activation to A (2A) receptor blockade. *Purinergic Signal* 2005; **1**: 111–134.
31 Fredholm BB, Chen JF, Cunha RA, Svenningsson P, Vaugeois JM. Adenosine and Brain Function. *Int Rev Neurobiol* 2005; **63**: 191–270.
32 Cunha RA, Ferré S, Vaugeois J-M, Chen J-F. Potential therapeutic interest of adenosine A2A receptors in psychiatric disorders. *Curr Pharm Des* 2008; **14**: 1512–1524.
33 Campbell NG, Zhu C-B, Lindler KM, Yaspan BL, Kistner-Griffin E, NIH ARRA Consortium WA *et al.* Rare coding variants of the adenosine A3 receptor are increased in autism: on the trail of the serotonin transporter regulome. *Mol Autism* 2013; **4**: 28.
34 Dennis SH, Jaafari N, Cimarosti H, Hanley JG, Henley JM, Mellor JR. Oxygen/glucose deprivation induces a reduction in synaptic AMPA receptors on hippocampal CA3 neurons mediated by mGluR1 and adenosine A3 receptors. *J Neurosci* 2011; **31**: 11941–11952.
35 Oliveira Á, Illes P, Ulrich H. Purinergic receptors in embryonic and adult neurogenesis. *Neuropharmacology* 2016; **104**: 272–281.
36 Ströhle A, Holsboer F. Stress responsive neurohormones in depression and anxiety. *Pharmacopsychiatry* 2003; **36**(Suppl 3): S207–S214.
37 Scaccianoce S, Navarra D, Di Sciullo A, Angelucci L, Endröczi E. Adenosine and pituitary-adrenocortical axis activity in the rat. *Neuroendocrinology* 1989; **50**: 464–468.
38 Chen Y-C, Huang S-H, Wang S-M. Adenosine-stimulated adrenal steroidogenesis involves the adenosine A2A and A2B receptors and the Janus kinase 2-mitogen-activated protein kinase kinase-extracellular signal-regulated kinase signaling pathway. *Int J Biochem Cell Biol* 2008; **40**: 2815–2825.
39 Batalha VL, Ferreira DG, Coelho JE, Valadas JS, Gomes R, Temido-Ferreira M *et al.* The caffeine-binding adenosine A2A receptor induces age-like HPA-axis dysfunction by targeting glucocorticoid receptor function. *Sci Rep* 2016; **6**: 31493.
40 Batalha VL, Pego JM, Fontinha BM, Costenla AR, Valadas JS, Baqi Y *et al.* Adenosine A(2A) receptor blockade reverts hippocampal stress-induced deficits and restores corticosterone circadian oscillation. *Mol Psychiatry* 2013; **18**: 320–331.
41 Kaster MP, Machado NJ, Silva HB, Nunes A, Ardais AP, Santana M *et al.* Caffeine acts through neuronal adenosine A2A receptors to prevent mood and memory dysfunction triggered by chronic stress. *Proc Natl Acad Sci USA* 2015; **112**: 201423088.
42 Okada M, Nutt DJ, Murakami T, Zhu G, Kamata a, Kawata Y *et al.* Adenosine receptor subtypes modulate two major functional pathways for hippocampal serotonin release. *J Neurosci* 2001; **21**: 628–640.
43 Stutzmann GE, Marek GJ, Aghajanian GK. Adenosine preferentially suppresses serotonin2A receptor-enhanced excitatory postsynaptic currents in layer V neurons of the rat medial prefrontal cortex. *Neuroscience* 2001; **105**: 55–69.
44 Serchov T, Clement H-W, Schwarz MK, Iasevoli F, Tosh DK, Idzko M *et al.* Increased signaling via adenosine A1 receptors, sleep deprivation, imipramine, and ketamine inhibit depressive-like behavior via induction of Homer1a. *Neuron* 2015; **87**: 549–562.
45 Kim JJ, Diamond DM. The stressed hippocampus, synaptic plasticity and lost memories. *Nat Rev Neurosci* 2002; **3**: 453–462.
46 McEwen BS. Physiology and neurobiology of stress and adaptation: central role of the brain. *Physiol Rev* 2007; **87**: 873–904.
47 Harris A, Ursin H, Murison R, Eriksen HR. Coffee, stress and cortisol in nursing staff. *Psychoneuroendocrinology* 2007; **32**: 322–330.
48 Wang L, Shen X, Wu Y, Zhang D. Coffee and caffeine consumption and depression: a meta-analysis of observational studies. *Aust N Z J Psychiatry* 2016; **50**: 228–242.
49 Lucas M, Mirzaei F, Pan A, Okereke OI, Willett WC, O'Reilly ÉJ *et al.* Coffee, caffeine, and risk of depression among women. *Arch Intern Med* 2011; **171**: 1571–1578.
50 Lucas M, O'Reilly EJ, Pan A, Mirzaei F, Willett WC, Okereke OI *et al.* Coffee, caffeine, and risk of completed suicide: results from three prospective cohorts of American adults. *World J Biol Psychiatry* 2014; **15**: 377–386.
51 Kawachi I, Willett WC, Colditz GA, Stampfer MJ, Speizer FE. A prospective study of coffee drinking and suicide in women. *Arch Intern Med* 1996; **156**: 521–525.
52 Coelho JE, Alves P, Canas PM, Valadas JS, Shmidt T, Batalha VL *et al.* Overexpression of adenosine A2A receptors in rats: effects on depression, locomotion, and anxiety. *Front Psychiatry* 2014; **5**: 67.
53 Kaster MP, Rosa AO, Rosso MM, Goulart EC, Santos ARS, Rodrigues ALS. Adenosine administration produces an antidepressant-like effect in mice: evidence for the involvement of A1 and A2A receptors. *Neurosci Lett* 2004; **355**: 21–24.
54 Yamada K, Kobayashi M, Mori A, Jenner P, Kanda T. Antidepressant-like activity of the adenosine A(2A) receptor antagonist, istradefylline (KW-6002), in the forced swim test and the tail suspension test in rodents. *Pharmacol Biochem Behav* 2013; **114–115**: 23–30.
55 Berk M, Plein H, Ferreira D, Jersky B, Seymour PA, Koe BK *et al.* Blunted adenosine A2a receptor function in platelets in patients with major depression. *Eur Neuropsychopharmacol* 2001; **11**: 183–186.
56 da Silva RB, Siebel AM, Bonan CD. The role of purinergic and dopaminergic systems on MK-801-induced antidepressant effects in zebrafish. *Pharmacol Biochem Behav* 2015; **139 Pt B**: 149–157.
57 Zimmermann FF, Altenhofen S, Kist LW, Leite CE, Bogo MR, Cognato GP *et al.* Unpredictable chronic stress alters adenosine metabolism in zebrafish brain. *Mol Neurobiol* 2016; **53**: 2518–2528.

58 Ali-Sisto T, Tolmunen T, Toffol E, Viinamäki H, Mäntyselkä P, Valkonen-Korhonen M *et al.* Purine metabolism is dysregulated in patients with major depressive disorder. *Psychoneuroendocrinology* 2016; **70**: 25–32.
59 Pedrazza EL, Rico EP, Senger MR, Pedrazza L, Zimmermann FF, Sarkis JJF *et al.* Ecto-nucleotidase pathway is altered by different treatments with fluoxetine and nortriptyline. *Eur J Pharmacol* 2008; **583**: 18–25.
60 Bowser DN, Khakh BS. Vesicular ATP is the predominant cause of intercellular calcium waves in astrocytes. *J Gen Physiol* 2007; **129**: 485–491.
61 Rebola N, Simões AP, Canas PM, Tomé AR, Andrade GM, Barry CE *et al.* Adenosine A2A receptors control neuroinflammation and consequent hippocampal neuronal dysfunction. *J Neurochem* 2011; **117**: 100–111.
62 Gomes C, Ferreira R, George J, Sanches R, Rodrigues DI, Gonçalves N *et al.* Activation of microglial cells triggers a release of brain-derived neurotrophic factor (BDNF) inducing their proliferation in an adenosine A2A receptor-dependent manner: A2A receptor blockade prevents BDNF release and proliferation of microglia. *J Neuroinflammation* 2013; **10**: 780.
63 Gyoneva S, Shapiro L, Lazo C, Garnier-Amblard E, Smith Y, Miller GW *et al.* Adenosine A2A receptor antagonism reverses inflammation-induced impairment of microglial process extension in a model of Parkinson's disease. *Neurobiol Dis* 2014; **67**: 191–202.
64 Madeira MH, Elvas F, Boia R, Gonçalves FQ, Cunha RA, Ambrósio AF *et al.* Adenosine A2AR blockade prevents neuroinflammation-induced death of retinal ganglion cells caused by elevated pressure. *J Neuroinflammation* 2015; **12**: 115.
65 Matos M, Augusto E, Machado NJ, dos Santos-Rodrigues A, Cunha RA, Agostinho P. Astrocytic adenosine A2A receptors control the amyloid-β peptide-induced decrease of glutamate uptake. *J Alzheimers Dis* 2012; **31**: 555–567.
66 Orr AG, Hsiao EC, Wang MM, Ho K, Kim DH, Wang X *et al.* Astrocytic adenosine receptor A2A and Gs-coupled signaling regulate memory. *Nat Neurosci* 2015; **18**: 423–434.
67 Rial D, Lemos C, Pinheiro H, Duarte JM, Gonçalves FQ, Real JI *et al.* Depression as a glial-based synaptic dysfunction. *Front Cell Neurosci* 2015; **9**: 521.
68 Cao X, Li L-P, Wang Q, Wu Q, Hu H-H, Zhang M *et al.* Astrocyte-derived ATP modulates depressive-like behaviors. *Nat Med* 2013; **19**: 773–777.
69 Golden SA, Covington HE, Berton O, Russo SJ. A standardized protocol for repeated social defeat stress in mice. *Nat Protoc* 2011; **6**: 1183–1191.
70 Berton O, McClung CA, Dileone RJ, Krishnan V, Renthal W, Russo SJ *et al.* Essential role of BDNF in the mesolimbic dopamine pathway in social defeat stress. *Science* 2006; **311**: 864–868.
71 Raison CL, Capuron L, Miller AH. Cytokines sing the blues: inflammation and the pathogenesis of depression. *Trends Immunol* 2006; **27**: 24–31.
72 Howren MB, Lamkin DM, Suls J. Associations of depression with C-reactive protein, IL-1, and IL-6: a meta-analysis. *Psychosom Med* 2009; **71**: 171–186.
73 Stokes L, Spencer SJ, Jenkins TA. Understanding the role of P2X7 in affective disorders-are glial cells the major players? *Front Cell Neurosci* 2015; **9**: 258.
74 Kreisel T, Frank MG, Licht T, Reshef R, Ben-Menachem-Zidon O, Baratta MV *et al.* Dynamic microglial alterations underlie stress-induced depressive-like behavior and suppressed neurogenesis. *Mol Psychiatry* 2014; **19**: 699–709.
75 Hinwood M, Tynan RJ, Charnley JL, Beynon SB, Day TA, Walker FR. Chronic stress induced remodeling of the prefrontal cortex: structural re-organization of microglia and the inhibitory effect of minocycline. *Cereb Cortex* 2013; **23**: 1784–1797.
76 Hines DJ, Schmitt LI, Hines RM, Moss SJ, Haydon PG. Antidepressant effects of sleep deprivation require astrocyte-dependent adenosine mediated signaling. *Transl Psychiatry* 2013; **3**: e212.
77 Li P, Rial D, Canas PM, Yoo J-H, Li W, Zhou X *et al.* Optogenetic activation of intracellular adenosine A2A receptor signaling in the hippocampus is sufficient to trigger CREB phosphorylation and impair memory. *Mol Psychiatry* 2015; **20**: 1339–1349.
78 Basso AM, Bratcher NA, Harris RR, Jarvis MF, Decker MW, Rueter LE. Behavioral profile of P2X7 receptor knockout mice in animal models of depression and anxiety: relevance for neuropsychiatric disorders. *Behav Brain Res* 2009; **198**: 83–90.
79 Boucher AA, Arnold JC, Hunt GE, Spiro A, Spencer J, Brown C *et al.* Resilience and reduced c-Fos expression in P2X7 receptor knockout mice exposed to repeated forced swim test. *Neuroscience* 2011; **189**: 170–177.
80 Csölle C, Baranyi M, Zsilla G, Kittel A, Gölöncsér F, Illes P *et al.* Neurochemical Changes in the Mouse Hippocampus Underlying the Antidepressant Effect of Genetic Deletion of P2X7 Receptors. *PLoS ONE* 2013; **8**: e66547.
81 Barrientos RM, Sprunger DB, Campeau S, Higgins EA, Watkins LR, Rudy JW *et al.* Brain-derived neurotrophic factor mRNA downregulation produced by social isolation is blocked by intrahippocampal interleukin-1 receptor antagonist. *Neuroscience* 2003; **121**: 847–853.
82 Csölle C, Andó RD, Kittel Á, Gölöncsér F, Baranyi M, Soproni K *et al.* The absence of P2X7 receptors (P2rx7) on non-haematopoietic cells leads to selective alteration in mood-related behaviour with dysregulated gene expression and stress reactivity in mice. *Int J Neuropsychopharmacol* 2013; **16**: 213–233.
83 Nagy G, Ronai Z, Somogyi A, Sasvari-Szekely M, Rahman OA, Mate A *et al.* P2RX7 Gln460Arg polymorphism is associated with depression among diabetic patients. *Prog Neuropsychopharmacol Biol Psychiatry* 2008; **32**: 1884–1888.
84 Lucae S, Salyakina D, Barden N, Harvey M, Gagné B, Labbé M *et al.* P2RX7, a gene coding for a purinergic ligand-gated ion channel, is associated with major depressive disorder. *Hum Mol Genet* 2006; **15**: 2438–2445.
85 Soronen P, Mantere O, Melartin T, Suominen K, Vuorilehto M, Rytsälä H *et al.* P2RX7 gene is associated consistently with mood disorders and predicts clinical outcome in three clinical cohorts. *Am J Med Genet B Neuropsychiatr Genet* 2011; **156B**: 435–447.
86 McQuillin A, Bass NJ, Choudhury K, Puri V, Kosmin M, Lawrence J *et al.* Case-control studies show that a non-conservative amino-acid change from a glutamine to arginine in the P2RX7 purinergic receptor protein is associated with both bipolar- and unipolar-affective disorders. *Mol Psychiatry* 2009; **14**: 614–620.
87 Aprile-Garcia F, Metzger MW, Paez-Pereda M, Stadler H, Acuña M, Liberman AC *et al.* Co-expression of wild-type P2X7R with Gln460Arg variant alters receptor function. *PLoS ONE* 2016; **11**: e0151862.
88 Portales-Cervantes L, Niño-Moreno P, Salgado-Bustamante M, García-Hernández MH, Baranda-Candido L, Reynaga-Hernández E *et al.* The His155Tyr (489C>T) single nucleotide polymorphism of P2RX7 gene confers an enhanced function of P2X7 receptor in immune cells from patients with rheumatoid arthritis. *Cell Immunol* 2012; **276**: 168–175.
89 Luchins D. The dopamine hypothesis of schizophrenia. A critical analysis. *Neuropsychobiology* 1975; **1**: 365–378.
90 Seeman P, Chau-Wong M, Tedesco J, Wong K. Brain receptors for antipsychotic drugs and dopamine: direct binding assays. *Proc Natl Acad Sci USA* 1975; **72**: 4376–4380.
91 Steeds H, Carhart-Harris RL, Stone JM. Drug models of schizophrenia. *Ther Adv Psychopharmacol* 2015; **5**: 43–58.
92 Carlsson A, Waters N, Carlsson ML. Neurotransmitter interactions in schizophrenia--therapeutic implications. *Biol Psychiatry* 1999; **46**: 1388–1395.
93 de Mendonça A, Sebastião AM, Ribeiro JA. Inhibition of NMDA receptor-mediated currents in isolated rat hippocampal neurones by adenosine A1 receptor activation. *Neuroreport* 1995; **6**: 1097–1100.
94 Dolphin AC, Prestwich SA. Pertussis toxin reverses adenosine inhibition of neuronal glutamate release. *Nature* 1985; **316**: 148–150.
95 Barrie AP, Nicholls DG. Adenosine A1 receptor inhibition of glutamate exocytosis and protein kinase C-mediated decoupling. *J Neurochem* 1993; **60**: 1081–1086.
96 Ciruela F, Casadó V, Rodrigues RJ, Luján R, Burgueño J, Canals M *et al.* Presynaptic control of striatal glutamatergic neurotransmission by adenosine A1-A2A receptor heteromers. *J Neurosci* 2006; **26**: 2080–2087.
97 Marchi M, Raiteri L, Risso F, Vallarino A, Bonfanti A, Monopoli A *et al.* Effects of adenosine A1 and A2A receptor activation on the evoked release of glutamate from rat cerebrocortical synaptosomes. *Br J Pharmacol* 2002; **136**: 434–440.
98 Borycz J, Pereira MF, Melani A, Rodrigues RJ, Köfalvi A, Panlilio L *et al.* Differential glutamate-dependent and glutamate-independent adenosine A1 receptor-mediated modulation of dopamine release in different striatal compartments. *J Neurochem* 2007; **101**: 355–363.
99 Higley MJ, Sabatini BL. Competitive regulation of synaptic Ca2+ influx by D2 dopamine and A2A adenosine receptors. *Nat Neurosci* 2010; **13**: 958–966.
100 Yan L, Burbiel JC, Maass A, Müller CE. Adenosine receptor agonists: from basic medicinal chemistry to clinical development. *Expert Opin Emerg Drugs* 2003; **8**: 537–576.
101 Ferré S, O'Connor WT, Snaprud P, Ungerstedt U, Fuxe K. Antagonistic interaction between adenosine A2A receptors and dopamine D2 receptors in the ventral striopallidal system. Implications for the treatment of schizophrenia. *Neuroscience* 1994; **63**: 765–773.
102 Díaz-Cabiale Z, Hurd Y, Guidolin D, Finnman UB, Zoli M, Agnati LF *et al.* Adenosine A2A agonist CGS 21680 decreases the affinity of dopamine D2 receptors for dopamine in human striatum. *Neuroreport* 2001; **12**: 1831–1834.
103 Akhondzadeh S, Shasavand E, Jamilian H, Shabestari O, Kamalipour A. Dipyridamole in the treatment of schizophrenia: adenosine-dopamine receptor interactions. *J Clin Pharm Ther* 2000; **25**: 131–137.
104 Brunstein MG, Ghisolfi ES, Ramos FLP, Lara DR. A clinical trial of adjuvant allopurinol therapy for moderately refractory schizophrenia. *J Clin Psychiatry* 2005; **66**: 213–219.
105 Wonodi I, Gopinath HV, Liu J, Adami H, Hong LE, Allen-Emerson R *et al.* Dipyridamole monotherapy in schizophrenia: pilot of a novel treatment approach by modulation of purinergic signaling. *Psychopharmacology (Berl)* 2011; **218**: 341–345.
106 Weiser M, Gershon AA, Rubinstein K, Petcu C, Ladea M, Sima D *et al.* A randomized controlled trial of allopurinol vs. placebo added on to antipsychotics in

patients with schizophrenia or schizoaffective disorder. *Schizophr Res* 2012; **138**: 35–38.
107 Villar-Menéndez I, Díaz-Sánchez S, Blanch M, Albasanz JL, Pereira-Veiga T, Monje A *et al.* Reduced striatal adenosine A2A receptor levels define a molecular subgroup in schizophrenia. *J Psychiatr Res* 2014; **51**: 49–59.
108 Hwang Y, Kim J, Shin JY, Kim JI, Seo JS, Webster MJ *et al.* Gene expression profiling by mRNA sequencing reveals increased expression of immune/inflammation-related genes in the hippocampus of individuals with schizophrenia. *Transl Psychiatry* 2013; **3**: e321.
109 Zhang J, Abdallah CG, Wang J, Wan X, Liang C, Jiang L *et al.* Upregulation of adenosine A2A receptors induced by atypical antipsychotics and its correlation with sensory gating in schizophrenia patients. *Psychiatry Res* 2012; **200**: 126–132.
110 Wang JH, Short J, Ledent C, Lawrence AJ, van den Buuse M. Reduced startle habituation and prepulse inhibition in mice lacking the adenosine A2A receptor. *Behav Brain Res* 2003; **143**: 201–207.
111 Moscoso-Castro M, Gracia-Rubio I, Ciruela F, Valverde O. Genetic blockade of adenosine A2A receptors induces cognitive impairments and anatomical changes related to psychotic symptoms in mice. *Eur Neuropsychopharmacol* 2016; **26**: 1227–1240.
112 Hauber W, Koch M. Adenosine A2a receptors in the nucleus accumbens modulate prepulse inhibition of the startle response. *Neuroreport* 1997; **8**: 1515–1518.
113 Matos M, Shen H-Y, Augusto E, Wang Y, Wei CJ, Wang YT *et al.* Deletion of adenosine A2A receptors from astrocytes disrupts glutamate homeostasis leading to psychomotor and cognitive impairment: relevance to schizophrenia. *Biol Psychiatry* 2015; **78**: 763–774.
114 Shen H-Y, Singer P, Lytle N, Wei CJ, Lan J-Q, Williams-Karnesky RL *et al.* Adenosine augmentation ameliorates psychotic and cognitive endophenotypes of schizophrenia. *J Clin Invest* 2012; **122**: 2567–2577.
115 Aliagas E, Villar-Menéndez I, Sévigny J, Roca M, Romeu M, Ferrer I *et al.* Reduced striatal ecto-nucleotidase activity in schizophrenia patients supports the 'adenosine hypothesis'. *Purinergic Signal* 2013; **9**: 599–608.
116 Wei CJ, Augusto E, Gomes CA, Singer P, Wang Y, Boison D *et al.* Regulation of fear responses by striatal and extrastriatal adenosine A2A receptors in forebrain. *Biol Psychiatry* 2014; **75**: 855–863.
117 Deckert J, Nöthen MM, Rietschel M, Wildenauer D, Bondy B, Ertl MA *et al.* Human adenosine A2a receptor (A2aAR) gene: systematic mutation screening in patients with schizophrenia. *J Neural Transm* 1996; **103**: 1447–1455.
118 Hong CJ, Liu HC, Liu TY, Liao DL, Tsai SJ. Association studies of the adenosine A2a receptor (1976T > C) genetic polymorphism in Parkinson's disease and schizophrenia. *J Neural Transm (Vienna)* 2005; **112**: 1503–1510.
119 Gotoh L, Mitsuyasu H, Kobayashi Y, Oribe N, Takata A, Ninomiya H *et al.* Association analysis of adenosine A1 receptor gene (ADORA1) polymorphisms with schizophrenia in a Japanese population. *Psychiatr Genet* 2009; **19**: 328–335.
120 Dutra GP, Ottoni GL, Lara DR, Bogo MR. Lower frequency of the low activity adenosine deaminase allelic variant (ADA1*2) in schizophrenic patients. *Rev Bras Psiquiatr* 2010; **32**: 275–8.
121 Seibt KJ, da Luz Oliveira R, Bogo MR, Senger MR, Bonan CD. Investigation into effects of antipsychotics on ectonucleotidase and adenosine deaminase in zebrafish brain. *Fish Physiol Biochem* 2015; **41**: 1383–1392.
122 Zhang YX, Yamashita H, Ohshita T, Sawamoto N, Nakamura S. ATP induces release of newly synthesized dopamine in the rat striatum. *Neurochem Int* 1996; **28**: 395–400.
123 Krügel U, Kittner H, Illes P. Adenosine 5'-triphosphate-induced dopamine release in the rat nucleus accumbens in vivo. *Neurosci Lett* 1999; **265**: 49–52.
124 Zhang YX, Yamashita H, Ohshita T, Sawamoto N, Nakamura S. ATP increases extracellular dopamine level through stimulation of P2Y purinoceptors in the rat striatum. *Brain Res* 1995; **691**: 205–212.
125 Hempel C, Nörenberg W, Sobottka H, Urban N, Nicke A, Fischer W *et al.* The phenothiazine-class antipsychotic drugs prochlorperazine and trifluoperazine are potent allosteric modulators of the human P2X7 receptor. *Neuropharmacology* 2013; **75**: 365–379.
126 Söderlund J, Schröder J, Nordin C, Samuelsson M, Walther-Jallow L, Karlsson H *et al.* Activation of brain interleukin-1beta in schizophrenia. *Mol Psychiatry* 2009; **14**: 1069–1071.
127 Mingam R, De Smedt V, Amédée T, Bluthé R-M, Kelley KW, Dantzer R *et al.* In vitro and in vivo evidence for a role of the P2X7 receptor in the release of IL-1 beta in the murine brain. *Brain Behav Immun* 2008; **22**: 234–244.
128 Koványi B, Csölle C, Calovi S, Hanuska A, Kató E, Köles L *et al.* The role of P2X7 receptors in a rodent PCP-induced schizophrenia model. *Sci Rep* 2016; **6**: 36680.
129 Campos RC, Parfitt GM, Polese CE, Coutinho-Silva R, Morrone FB, Barros DM. Pharmacological blockage and P2X7 deletion hinder aversive memories: reversion in an enriched environment. *Neuroscience* 2014; **280**: 220–230.
130 Hansen T, Jakobsen KD, Fenger M, Nielsen J, Krane K, Fink-Jensen A *et al.* Variation in the purinergic P2RX(7) receptor gene and schizophrenia. *Schizophr Res* 2008; **104**: 146–152.
131 Barondes SH. *Mood Genes: Hunting for Origins of Mania and Depression*. Oxford University Press: New York, NY, 1999.
132 Shorter E. The history of lithium therapy. *Bipolar Disord* 2009; **11**(Suppl 2): 4–9.
133 Bartoli F, Crocamo C, Gennaro GM, Castagna G, Trotta G, Clerici M *et al.* Exploring the association between bipolar disorder and uric acid: a mediation analysis. *J Psychosom Res* 2016; **84**: 56–59.
134 Ortiz R, Ulrich H, Zarate CA, Machado-Vieira R. Purinergic system dysfunction in mood disorders: a key target for developing improved therapeutics. *Prog Neuropsychopharmacol Biol Psychiatry* 2015; **57**: 117–131.
135 Machado-Vieira R, Lara DR, Souza DO, Kapczinski F. Purinergic dysfunction in mania: an integrative model. *Med Hypotheses* 2002; **58**: 297–304.
136 Sutin AR, Cutler RG, Camandola S, Uda M, Feldman NH, Cucca F *et al.* Impulsivity is associated with uric acid: evidence from humans and mice. *Biol Psychiatry* 2014; **75**: 31–37.
137 Albert U, De Cori D, Aguglia A, Barbaro F, Bogetto F, Maina G. Increased uric acid levels in bipolar disorder subjects during different phases of illness. *J Affect Disord* 2015; **173**: 170–175.
138 Muti M, Del Grande C, Musetti L, Marazziti D, Turri M, Cirronis M *et al.* Serum uric acid levels and different phases of illness in bipolar I patients treated with lithium. *Psychiatry Res* 2015; **225**: 604–608.
139 Kesebir S, Tatlıdil Yaylacı E, Süner O, Gültekin BK. Uric acid levels may be a biological marker for the differentiation of unipolar and bipolar disorder: the role of affective temperament. *J Affect Disord* 2014; **165**: 131–134.
140 Chung K-H, Huang C-C, Lin H-C. Increased risk of gout among patients with bipolar disorder: a nationwide population-based study. *Psychiatry Res* 2010; **180**: 147–150.
141 Weiser M, Burshtein S, Gershon AA, Marian G, Vlad N, Grecu IG *et al.* Allopurinol for mania: a randomized trial of allopurinol versus placebo as add-on treatment to mood stabilizers and/or antipsychotic agents in manic patients with bipolar disorder. *Bipolar Disord* 2014; **16**: 441–447.
142 Machado-Vieira R, Soares JC, Lara DR, Luckenbaugh DA, Busnello JV, Marca G *et al.* A double-blind, randomized, placebo-controlled 4-week study on the efficacy and safety of the purinergic agents allopurinol and dipyridamole adjunctive to lithium in acute bipolar mania. *J Clin Psychiatry* 2008; **69**: 1237–1245.
143 Machado-Vieira R. Purinergic system in the treatment of bipolar disorder: uric acid levels as a screening test in mania. *J Clin Psychopharmacol* 2012; **32**: 735–736.
144 Pacher P, Nivorozhkin A, Szabó C. Therapeutic effects of xanthine oxidase inhibitors: renaissance half a century after the discovery of allopurinol. *Pharmacol Rev* 2006; **58**: 87–114.
145 Lara DR, Cruz MRS, Xavier F, Souza DO, Moriguchi EH. Allopurinol for the treatment of aggressive behaviour in patients with dementia. *Int Clin Psychopharmacol* 2003; **18**: 53–55.
146 Gubert C, Jacintho Moritz CE, Vasconcelos-Moreno MP, Quadros dos Santos BTM, Sartori J, Fijtman A *et al.* Peripheral adenosine levels in euthymic patients with bipolar disorder. *Psychiatry Res* 2016; **246**: 421–426.
147 Hirota T, Kishi T. Adenosine hypothesis in schizophrenia and bipolar disorder: a systematic review and meta-analysis of randomized controlled trial of adjuvant purinergic modulators. *Schizophr Res* 2013; **149**: 88–95.
148 Weir RL, Anderson SM, Daly JW. Inhibition of N6-[3H]cyclohexyladenosine binding by carbamazepine. *Epilepsia* **31**: 503–512.
149 Van Calker D, Steber R, Klotz KN, Greil W. Carbamazepine distinguishes between adenosine receptors that mediate different second messenger responses. *Eur J Pharmacol* 1991; **206**: 285–290.
150 Deckert J, Nöthen MM, Albus M, Franzek E, Rietschel M, Ren H *et al.* Adenosine A1 receptor and bipolar affective disorder: systematic screening of the gene and association studies. *Am J Med Genet* 1998; **81**: 18–23.
151 Martini C, Tuscano D, Trincavelli ML, Cerrai E, Bianchi M, Ciapparelli A *et al.* Upregulation of A2A adenosine receptors in platelets from patients affected by bipolar disorders under treatment with typical antipsychotics. *J Psychiatr Res* 2006; **40**: 81–88.
152 Knight J, Rochberg NS, Saccone SF, Nurnberger JI, Rice JP. An investigation of candidate regions for association with bipolar disorder. *Am J Med Genet B Neuropsychiatr Genet* 2010; **153B**: 1292–1297.
153 Backlund L, Nikamo P, Hukic DS, Ek IR, Träskman-Bendz L, Landén M *et al.* Cognitive manic symptoms associated with the P2RX7 gene in bipolar disorder. *Bipolar Disord* 2011; **13**: 500–508.
154 Barden N, Harvey M, Gagné B, Shink E, Tremblay M, Raymond C *et al.* Analysis of single nucleotide polymorphisms in genes in the chromosome 12Q24.31 region points to P2RX7 as a susceptibility gene to bipolar affective disorder. *Am J Med Genet B Neuropsychiatr Genet* 2006; **141B**: 374–382.
155 Halmai Z, Dome P, Vereczkei A, Abdul-Rahman O, Szekely A, Gonda X *et al.* Associations between depression severity and purinergic receptor P2RX7 gene polymorphisms. *J Affect Disord* 2013; **150**: 104–109.

156 Grigoroiu-Serbanescu M, Herms S, Mühleisen TW, Georgi A, Diaconu CC, Strohmaier J *et al.* Variation in P2RX7 candidate gene (rs2230912) is not associated with bipolar I disorder and unipolar major depression in four European samples. *Am J Med Genet B Neuropsychiatr Genet* 2009; **150B**: 1017–1021.
157 Green EK, Grozeva D, Raybould R, Elvidge G, Macgregor S, Craig I *et al.* P2RX7: a bipolar and unipolar disorder candidate susceptibility gene? *Am J Med Genet B Neuropsychiatr Genet* 2009; **150B**: 1063–1069.
158 Backlund L, Lavebratt C, Frisén L, Nikamo P, Hukic Sudic D, Träskman-Bendz L *et al.* P2RX7: expression responds to sleep deprivation and associates with rapid cycling in bipolar disorder type 1. *PLoS ONE* 2012; **7**: e43057.
159 Feng WP, Zhang B, Li W, Liu J. Lack of association of P2RX7 gene rs2230912 polymorphism with mood disorders: a meta-analysis. *PLoS ONE* 2014; **9**: 1–6.
160 Sperlagh B, Csolle C, Ando RD, Goloncser F, Kittel A, Baranyi M. The role of purinergic signaling in depressive disorders. *Neuropsychopharmacol Hung* 2012; **14**: 231–238.
161 Bhattacharya A, Wang Q, Ao H, Shoblock JR, Lord B, Aluisio L *et al.* Pharmacological characterization of a novel centrally permeable P2X7 receptor antagonist: JNJ-47965567. *Br J Pharmacol* 2013; **170**: 624–640.
162 Dodd S, Fernandes BS, Dean OM. Future directions for pharmacotherapies for treatment-resistant bipolar disorder. *Curr Neuropharmacol* 2015; **13**: 656–662.
163 Gubert C, Fries GR, Pfaffenseller B, Ferrari P, Coutinho-Silva R, Morrone FB *et al.* Role of P2X7 receptor in an animal model of mania induced by D-amphetamine. *Mol Neurobiol* 2016; **53**: 611–620.
164 Masuch A, Shieh C-H, van Rooijen N, van Calker D, Biber K. Mechanism of microglia neuroprotection: involvement of P2X7, TNFα, and valproic acid. *Glia* 2016; **64**: 76–89.
165 Page T, Yu A, Fontanesi J, Nyhan WL. Developmental disorder associated with increased cellular nucleotidase activity. *Proc Natl Acad Sci USA* 1997; **94**: 11601–11606.
166 Bottini N, De Luca D, Saccucci P, Fiumara A, Elia M, Porfirio MC *et al.* Autism: evidence of association with adenosine deaminase genetic polymorphism. *Neurogenetics* 2001; **3**: 111–113.
167 Masino SA, Kawamura M, Plotkin LM, Svedova J, DiMario FJ, Eigsti I-M. The relationship between the neuromodulator adenosine and behavioral symptoms of autism. *Neurosci Lett* 2011; **500**: 1–5.
168 Masino SA, Kawamura M, Cote JL, Williams RB, Ruskin DN. Adenosine and autism: a spectrum of opportunities. *Neuropharmacology* 2013; **68**: 116–121.
169 Ciruela F, Saura C, Canela EI, Mallol J, Lluis C, Franco R. Adenosine deaminase affects ligand-induced signalling by interacting with cell surface adenosine receptors. *FEBS Lett* 1996; **380**: 219–223.
170 Freitag CM, Agelopoulos K, Huy E, Rothermundt M, Krakowitzky P, Meyer J *et al.* Adenosine A2A receptor gene (ADORA2A) variants may increase autistic symptoms and anxiety in autism spectrum disorder. *Eur Child Adolesc Psychiatry* 2010; **19**: 67–74.
171 Tanimura Y, Vaziri S, Lewis MH. Indirect basal ganglia pathway mediation of repetitive behavior: attenuation by adenosine receptor agonists. *Behav Brain Res* 2010; **210**: 116–122.
172 López-Cruz L, Carbó-Gas M, Pardo M, Bayarri P, Valverde O, Ledent C *et al.* Adenosine A2A receptor deletion affects social behaviors and anxiety in mice: involvement of anterior cingulate cortex and amygdala. *Behav Brain Res* 2017; **321**: 8–17.
173 Yu C, Gupta J, Chen J-F, Yin HH. Genetic deletion of A2A adenosine receptors in the striatum selectively impairs habit formation. *J Neurosci* 2009; **29**: 15100–15103.
174 Nam HW, Hinton DJ, Kang NY, Kim T, Lee MR, Oliveros A *et al.* Adenosine transporter ENT1 regulates the acquisition of goal-directed behavior and ethanol drinking through A2A receptor in the dorsomedial striatum. *J Neurosci* 2013; **33**: 4329–4338.
175 Li Y, He Y, Chen M, Pu Z, Chen L, Li P *et al.* Optogenetic activation of adenosine A2A receptor signaling in the dorsomedial striatopallidal neurons suppresses goal-directed behavior. *Neuropsychopharmacology* 2016; **41**: 1003–1013.
176 Shen W, Flajolet M, Greengard P, Surmeier DJ. Dichotomous dopaminergic control of striatal synaptic plasticity. *Science* 2008; **321**: 848–851.
177 Squillace M, Dodero L, Federici M, Migliarini S, Errico F, Napolitano F *et al.* Dysfunctional dopaminergic neurotransmission in asocial BTBR mice. *Transl Psychiatry* 2014; **4**: e427.
178 He Y, Li Y, Chen M, Pu Z, Zhang F, Chen L *et al.* Habit formation after random interval training is associated with increased adenosine A2A receptor and dopamine D2 receptor heterodimers in the striatum. *Front Mol Neurosci* 2016; **9**: 151.
179 Fink JS, Weaver DR, Rivkees SA, Peterfreund RA, Pollack AE, Adler EM *et al.* Molecular cloning of the rat A2 adenosine receptor: selective co-expression with D2 dopamine receptors in rat striatum. *Brain Res Mol Brain Res* 1992; **14**: 186–195.
180 Prasad HC, Steiner JA, Sutcliffe JS, Blakely RD. Enhanced activity of human serotonin transporter variants associated with autism. *Philos Trans R Soc B Biol Sci* 2009; **364**: 163–173.
181 Zhu C-B, Lindler KM, Campbell NG, Sutcliffe JS, Hewlett WA, Blakely RD. Colocalization and regulated physical association of presynaptic serotonin transporters with A3 adenosine receptors. *Mol Pharmacol* 2011; **80**: 458–465.
182 Wyatt LR, Godar SC, Khoja S, Jakowec MW, Alkana RL, Bortolato M *et al.* Sociocommunicative and sensorimotor impairments in male P2X4-deficient mice. *Neuropsychopharmacology* 2013; **38**: 1993–2002.
183 Naviaux RK, Zolkipli Z, Wang L, Nakayama T, Naviaux JC, Le TP *et al.* Antipurinergic therapy corrects the autism-like features in the poly(IC) mouse model. *PLoS ONE* 2013; **8**: e57380.
184 Naviaux JC, Schuchbauer MA, Li K, Wang L, Risbrough VB, Powell SB *et al.* Reversal of autism-like behaviors and metabolism in adult mice with single-dose antipurinergic therapy. *Transl Psychiatry* 2014; **4**: e400.
185 Naviaux JC, Wang L, Li K, Bright AT, Alaynick WA, Williams KR *et al.* Antipurinergic therapy corrects the autism-like features in the Fragile X (Fmr1 knockout) mouse model. *Mol Autism* 2015; **6**: 1.
186 Naviaux RK, Curtis B, Li K, Naviaux JC, Bright AT, Gail E *et al.* Low-dose suramin in autism spectrum disorder : a small, phase I / II, randomized clinical trial. *Ann Clin Transl Neurol* 2017; **4**: 491–505.
187 Theoharides TC. Extracellular mitochondrial ATP, suramin, and autism? *Clin Ther* 2013; **35**: 1454–1456.
188 Hamidpour R, Hamidpour S, Hamidpour M, Zarabi M, Sohraby M, Shalari M. Antipurinergic therapy with suramin as a treatment for autism spectrum disorder.. *J Biomed Sci* 2016; **5**: 2:14.
189 Theoharides TC, Asadi S, Panagiotidou S, Weng Z. The 'missing link' in autoimmunity and autism: extracellular mitochondrial components secreted from activated live mast cells. *Autoimmun Rev* 2013; **12**: 1136–1142.
190 Di Virgilio F. Dr. Jekyll/Mr. Hyde: the dual role of extracellular ATP. *J Auton Nerv Syst* 2000; **81**: 59–63.
191 Rodrigues RJ, Tomé AR, Cunha RA. ATP as a multi-target danger signal in the brain. *Front Neurosci* 2015; **9**: 148.
192 Deckert J. The adenosine A2A receptor knockout mouse: a model for anxiety? *Int J Neuropsychopharmacol* 1998; **1**: 187–190.
193 Parmentier M, Ledent C, Vaugeois J-M, Schiffmann SN, Pedrazzini T, Yacoubi MEL *et al.* Aggressiveness, hypoalgesia and high blood pressure in mice lacking the adenosine A2a receptor. *Nature* 1997; **388**: 674–678.
194 Johansson B, Halldner L, Dunwiddie TV, Masino SA, Poelchen W, Giménez-Llort L *et al.* Hyperalgesia, anxiety, and decreased hypoxic neuroprotection in mice lacking the adenosine A1 receptor. *Proc Natl Acad Sci USA* 2001; **98**: 9407–9412.
195 Maximino C, Lima MG, Olivera KRM, Picanço-Diniz DLW, Herculano AM. Adenosine A1, but not A2, receptor blockade increases anxiety and arousal in zebrafish. *Basic Clin Pharmacol Toxicol* 2011; **109**: 203–207.
196 Caetano L, Pinheiro H, Patrício P, Mateus-Pinheiro A, Alves ND, Coimbra B *et al.* Adenosine A2A receptor regulation of microglia morphological remodeling-gender bias in physiology and in a model of chronic anxiety. *Mol Psychiatry* 2016; **22**: 1035–1043.
197 Vincenzi F, Ravani A, Pasquini S, Merighi S, Gessi S, Romagnoli R *et al.* Positive allosteric modulation of A1 adenosine receptors as a novel and promising therapeutic strategy for anxiety. *Neuropharmacology* 2016; **111**: 283–292.
198 Almeida RF, Comasseto DD, Ramos DB, Hansel G, Zimmer ER, Loureiro SO *et al.* Guanosine anxiolytic-like effect involves adenosinergic and glutamatergic neurotransmitter systems. *Mol Neurobiol* 2016; **54**: 423–436.
199 Jain N, Kemp N, Adeyemo O, Buchanan P, Stone W. Anxiolytic activity of adenosine receptor activation in mice. *Br J Pharmacol* 1995; **116**: 2127–2133.
200 Florio C, Prezioso A, Papaioannou A, Vertua R. Adenosine A1 receptors modulate anxiety in CD1 mice. *Psychopharmacology (Berl)* 1998; **136**: 311–319.
201 Charney DS, Heninger GR, Jatlow PI. Increased anxiogenic effects of caffeine in panic disorders. *Arch Gen Psychiatry* 1985; **42**: 233–243.
202 Alsene K, Deckert J, Sand P, de Wit H. Association between A2a receptor gene polymorphisms and caffeine-induced anxiety. *Neuropsychopharmacology* 2003; **28**: 1694–1702.
203 Gajewska A, Blumenthal TD, Winter B, Herrmann MJ, Conzelmann A, Mühlberger A *et al.* Effects of ADORA2A gene variation and caffeine on prepulse inhibition: a multi-level risk model of anxiety. *Prog Neuropsychopharmacol Biol Psychiatry* 2013; **40**: 115–121.
204 Domschke K, Gajewska A, Winter B, Herrmann MJ, Warrings B, Mühlberger A *et al.* ADORA2A gene variation, caffeine, and emotional processing: a multi-level interaction on startle reflex. *Neuropsychopharmacology* 2012; **37**: 759–769.
205 Deckert J, Nöthen MM, Franke P, Delmo C, Fritze J, Knapp M *et al.* Systematic mutation screening and association study of the A1 and A2a adenosine receptor genes in panic disorder suggest a contribution of the A2a gene to the development of disease. *Mol Psychiatry* 1998; **3**: 81–85.

206 Hohoff C, Mullings EL, Heatherley SV, Freitag CM, Neumann LC, Domschke K *et al.* Adenosine A2A receptor gene: evidence for association of risk variants with panic disorder and anxious personality. *J Psychiatr Res* 2010; **44**: 930–937.
207 Lam P, Hong C-J, Tsai S-J. Association study of A2a adenosine receptor genetic polymorphism in panic disorder. *Neurosci Lett* 2005; **378**: 98–101.
208 Erhardt A, Lucae S, Unschuld PG, Ising M, Kern N, Salyakina D *et al.* Association of polymorphisms in P2RX7 and CaMKKb with anxiety disorders. *J Affect Disord* 2007; **101**: 159–168.
209 Roger S, Mei Z-Z, Baldwin JM, Dong L, Bradley H, Baldwin SA *et al.* Single nucleotide polymorphisms that were identified in affective mood disorders affect ATP-activated P2X7 receptor functions. *J Psychiatr Res* 2010; **44**: 347–355.
210 Kittner H, Franke H, Fischer W, Schultheis N, Krugel U, Illes P. Stimulation of P2Y1 receptors causes anxiolytic-like effects in the rat elevated plus-maze: implications for the involvement of P2Y1 receptor-mediated nitric oxide production. *Neuropsychopharmacology* 2003; **28**: 435–444.
211 Barrera CM, Ruiz ZR, Dunlap WP. Uric acid: a participating factor in the symptoms of hyperactivity. *Biol Psychiatry* 1988; **24**: 344–347.
212 Özten E, Kesebir S, Eryılmaz G, Tarhan N, Karamustafalıoğlu O. Are uric acid plasma levels different between unipolar depression with and without adult attention deficit hyperactivity disorder? *J Affect Disord* 2015; **177**: 114–117.
213 Ioannidis K, Chamberlain SR, Müller U. Ostracising caffeine from the pharmacological arsenal for attention-deficit hyperactivity disorder--was this a correct decision? A literature review. *J Psychopharmacol* 2014; **28**: 830–836.
214 Critchley HD, Elliott R, Mathias CJ, Dolan RJ. Neural activity relating to generation and representation of galvanic skin conductance responses: a functional magnetic resonance imaging study. *J Neurosci* 2000; **20**: 3033–3040.
215 Barry RJ, Clarke AR, Johnstone SJ, Brown CR, Bruggemann JM, van Rijbroek I. Caffeine effects on resting-state arousal in children. *Int J Psychophysiol* 2009; **73**: 355–361.
216 Barry RJ, Clarke AR, McCarthy R, Selikowitz M, MacDonald B, Dupuy FE. Caffeine effects on resting-state electrodermal levels in AD/HD suggest an anomalous arousal mechanism. *Biol Psychol* 2012; **89**: 606–608.
217 Boeck CR, Marques VB, Valvassori SS, Constantino LC, Rosa DVF, Lima FF *et al.* Early long-term exposure with caffeine induces cross-sensitization to methylphenidate with involvement of DARPP-32 in adulthood of rats. *Neurochem Int* 2009; **55**: 318–322.
218 Prediger RDS, Fernandes D, Takahashi RN. Blockade of adenosine A2A receptors reverses short-term social memory impairments in spontaneously hypertensive rats. *Behav Brain Res* 2005; **159**: 197–205.
219 Pires VA, Pamplona FA, Pandolfo P, Fernandes D, Prediger RDS, Takahashi RN. Adenosine receptor antagonists improve short-term object-recognition ability of spontaneously hypertensive rats: a rodent model of attention-deficit hyperactivity disorder. *Behav Pharmacol* 2009; **20**: 134–145.
220 Pamplona FA, Pandolfo P, Savoldi R, Prediger RDS, Takahashi RN. Environmental enrichment improves cognitive deficits in spontaneously hypertensive rats (SHR): relevance for attention deficit/hyperactivity disorder (ADHD). *Prog Neuropsychopharmacol Biol Psychiatry* 2009; **33**: 1153–1160.
221 Pandolfo P, Machado NJ, Köfalvi A, Takahashi RN, Cunha RA. Caffeine regulates frontocorticostriatal dopamine transporter density and improves attention and cognitive deficits in an animal model of attention deficit hyperactivity disorder. *Eur Neuropsychopharmacol* 2013; **23**: 317–328.
222 Mioranzza S, Botton PHS, Costa MS, Espinosa J, Kazlauckas V, Ardais AP *et al.* Adenosine A1 receptors are modified by acute treatment with methylphenidate in adult mice. *Brain Res* 2010; **1357**: 62–69.
223 Napolitano F, Bonito-Oliva A, Federici M, Carta M, Errico F, Magara S *et al.* Role of aberrant striatal dopamine D1 receptor/cAMP/protein kinase A/DARPP32 signaling in the paradoxical calming effect of amphetamine. *J Neurosci* 2010; **30**: 11043–11056.
224 Masuo Y, Ishido M, Morita M, Sawa H, Nagashima K, Niki E. Behavioural characteristics and gene expression in the hyperactive wiggling (Wig) rat. *Eur J Neurosci* 2007; **25**: 3659–3666.
225 Janik P, Berdyński M, Safranow K, Żekanowski C. Association of ADORA1 rs2228079 and ADORA2A rs5751876 polymorphisms with Gilles de la Tourette Syndrome in the Polish population. *PLoS ONE* 2015; **10**: e0136754.
226 Molero Y, Gumpert C, Serlachius E, Lichtenstein P, Walum H, Johansson D *et al.* A study of the possible association between adenosine A2A receptor gene polymorphisms and attention-deficit hyperactivity disorder traits. *Genes Brain Behav* 2013; **12**: 305–310.
227 Glaser T, De Oliveira SLB, Cheffer A, Beco R, Martins P, Fornazari M *et al.* Modulation of mouse embryonic stem cell proliferation and neural differentiation by the P2X7 receptor. *PLoS ONE* 2014; **9**: e96281.
228 Molteni R, Calabrese F, Bedogni F, Tongiorgi E, Fumagalli F, Racagni G *et al.* Chronic treatment with fluoxetine up-regulates cellular BDNF mRNA expression in rat dopaminergic regions. *Int J Neuropsychopharmacol* 2006; **9**: 307–317.
229 Rigucci S, Serafini G, Pompili M, Kotzalidis GD, Tatarelli R. Anatomical and functional correlates in major depressive disorder: the contribution of neuroimaging studies. *World J Biol Psychiatry* 2010; **11**: 165–180.
230 van Os J, Kapur S. Schizophrenia. *Lancet* 2009; **374**: 635–645.
231 Arnold SE, Ruscheinsky DD, Han LY. Further evidence of abnormal cytoarchitecture of the entorhinal cortex in schizophrenia using spatial point pattern analyses. *Biol Psychiatry* 1997; **42**: 639–647.
232 Fukuda T, Yanagi S. Psychiatric behaviors associated with cytoskeletal defects in radial neuronal migration. *Cell Mol Life Sci* 2017; doi: 10.1007/s00018-017-2539-4; e-pub ahead of print 17 May 2017.
233 Oliveira SLB, Trujillo CA, Negraes PD, Ulrich H. Effects of ATP and NGF on proliferation and migration of neural precursor cells. *Neurochem Res* 2015; **40**: 1849–1857.
234 Tobe BTD, Crain AM, Winquist AM, Calabrese B, Makihara H, Zhao W-N *et al.* Probing the lithium-response pathway in hiPSCs implicates the phosphoregulatory set-point for a cytoskeletal modulator in bipolar pathogenesis. *Proc Natl Acad Sci USA* 2017; **114**: E4462–E4471.
235 Jeon SJ, Rhee SY, Ryu JH, Cheong JH, Kwon K, Yang S-I *et al.* Activation of adenosine A2A receptor up-regulates BDNF expression in rat primary cortical neurons. *Neurochem Res* 2011; **36**: 2259–2269.
236 Miras-Portugal MT, Gomez-Villafuertes R, Gualix J, Diaz-Hernandez JI, Artalejo AR, Ortega F *et al.* Nucleotides in neuroregeneration and neuroprotection. *Neuropharmacology* 2016; **104**: 243–254.
237 Chen W-C, Lai Y-S, Lin S-H, Lu K-H, Lin Y-E, Panyod S *et al.* Anti-depressant effects of Gastrodia elata Blume and its compounds gastrodin and 4-hydroxybenzyl alcohol, via the monoaminergic system and neuronal cytoskeletal remodeling. *J Ethnopharmacol* 2016; **182**: 190–199.
238 Queiroz AIG, de Araújo MM, da Silva Araújo T, de Souza GC, Cavalcante LM, de Jesus Souza Machado M *et al.* GBR 12909 administration as an animal model of bipolar mania: time course of behavioral, brain oxidative alterations and effect of mood stabilizing drugs. *Metab Brain Dis* 2015; **30**: 1207–1215.
239 Parpura V, Schousboe A, Verkhratsky A (eds). *Glutamate and ATP at the Interface of Metabolism and Signaling in the Brain*. Springer: New York, 2014.
240 Wen Z, Christian KM, Song sH, Ming G. Modeling psychiatric disorders with patient-derived iPSCs. *Curr Opin Neurobiol* 2016; **36**: 118–127.